

✓
Volume 21, No. 1

January-February 1959

COLLOID JOURNAL

(KOLLOIDNYI ZHURNAL)

A publication of the Academy of Sciences of the USSR

IN ENGLISH TRANSLATION

Year and issue of first translation:

Vol. 14 No. 1 Jan.-Feb. 1952

545-156
8

Annual subscription

\$80.00

Single issue

20.00

Copyright 1959

CONSULTANTS BUREAU, INC.

227 W. 17th St., NEW YORK 11, N.Y.

Editorial Board
(KOLLOIDNYI ZHURNAL)

P. N. Antipov-Karataev, B. V. Deriagin, B. A. Dogadkin
(Acting Editor), A. V. Dumanskii, V. A. Kargin,
S. M. Lipatov, P. A. Rebinder, I. P. Serdobolskii
(Secretary), M. P. Volarovich

*A complete copy of any paper in this issue may
be purchased from the publisher for \$7.50*

*Note: The sale of photostatic copies of any
portion of this copyright translation is expressly
prohibited by the copyright owners.*

Printed in the United States of America

IMPACT DEFORMATION OF RUBBER*

G. M. Bartenev and N. M. Novikova

Many rubber articles are subjected to impact stresses. It is therefore of practical importance to establish the laws and to determine the constants of impact deformation, both in relation to design calculations and for evaluation of the elastic properties of rubber articles.

The impact deformation of rubber has been studied little. In studies of impact deformation [1-4] the authors confined themselves to measurements of deformation produced by impact. Kuvshinski and Sidorovich [5] developed a method for determination of the elastic properties of rubber under impact compression and gave the theory of a method whereby two independent constants for rubber can be calculated from experimental data: dynamic modulus of elasticity and the mechanical loss angle. The theory of the method was amplified and verified [5] by careful studies of impact deformation by means of a pendulum elastometer in which the compressive deformation of a cylindrical rubber specimen and the time of impact could be measured. Close agreement between the experimental and calculated data led to the conclusion that even the simplest Maxwell and Kelvin schemes give satisfactory results in calculations of impact duration.

Below are presented the results of studies of impact deformation and details of the method used for determination of the constants, with the use of a modified pendulum tester of the Schob type. It was possible to obtain impact deformation in the pure form in this apparatus.

The instrument, the principle of which is illustrated in Fig. 1, could be used for measuring the maximum compressive deformation and the angle of impact and rebound of the pendulum. The maximum deformation of the rubber specimen was shown on the dial of the indicator 1 with the aid of a special device** consisting of the insert 2, containing a small metal rod 4 supported freely on a weak spring 3. The insert is fixed rigidly to the pendulum. The instrument stand, dial, telephone receiver (not shown in Fig. 1), and insert are connected in an electric circuit. Impact deformation is determined as follows. With the pendulum 5 in a free vertical position the cylindrical rubber specimen 6 is moved to the right by means of the support 7 until it comes into contact with the pendulum hammer 8. The pendulum hammer is flat, with a larger area than the end of the specimen. The base of the indicator dial is then moved to the right until it comes into contact with the insert rod. The instant of contact is indicated by sound in the telephone receiver. This establishes the zero point on the indicator dial.

On impact, the pendulum hammer deforms the rubber specimen. Simultaneously the spring 3 is compressed, cushioning the impact on the indicator head. The indicator base is progressively moved, with consecutive impacts of the hammer until a position is reached when there is no contact with the indicator, as shown by absence of sound in the telephone receiver. The displacement of the indicator to the left and the distance of the rod 4 and hammer 8 from the axis of rotation can be used to find the displacement of the hammer, and hence the impact deformation of the rubber specimen (as the ratio of the displacement to the original length of the specimen).

For low-temperature measurements the specimen was enclosed in a chamber, shown schematically in Fig. 2. The chamber consisted of an outer compartment 1 and an inner compartment 2, an intermediate hammer 3, and lid 4. Cooling liquid was circulated through the compartment 1. The test specimen 5 was fixed in the compartment 2. The chamber lid, made from textolite also acted as the directing sleeve for the hammer. The

*É. L. Chernyakova took part in the determinations.

**Described in another paper [1].

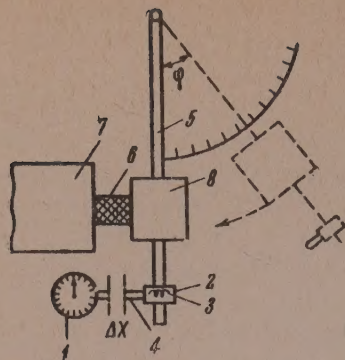


Fig. 1. Diagram of pendulum tester.

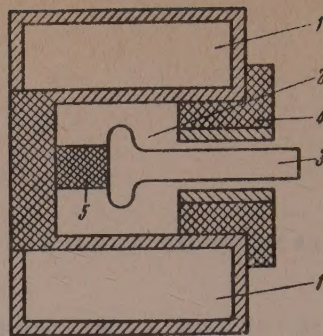


Fig. 2. Diagram of chamber for measurement of impact deformation at low temperatures.

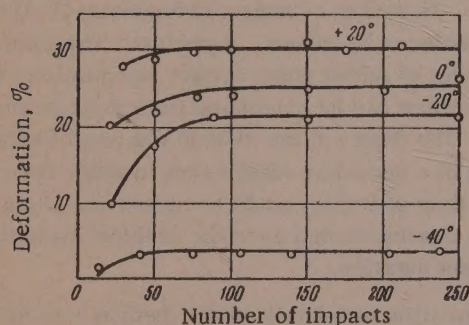


Fig. 3. Effect of the number of impacts on relative deformation of technical SKS-30 rubber vulcanizates at different temperatures (in °C).

inner surface was made of bronze. The hammer was made from Plexiglas*. The chamber was fixed to the vertical support 7 of the instrument (Fig. 1). The specimen was cemented to the back wall of the chamber made from textolite. The temperature of the specimen was measured by means of a thermocouple.

Investigations of the effect of the number of impacts on impact deformation showed that deformation becomes stabilized and independent of the number of impacts after 5-6 impacts for unfilled and after 30-50 impacts for filled rubbers. Similar results were obtained at low temperatures (Fig. 3). The frequency used was ~ 30 impacts per minute. At this impact frequency the rubber specimen recovers almost completely. The test results (magnitude of deformation) are not affected if the specimen is left to rest for five minutes after each impact. In the subsequent experiments the deformation

measurements were commenced after 5 impacts for unfilled and after 50 impacts for filled rubbers, average values for the next three impacts being taken. It follows from Fig. 3 that the subsequent impacts do not produce any appreciable temperature changes in the specimen.

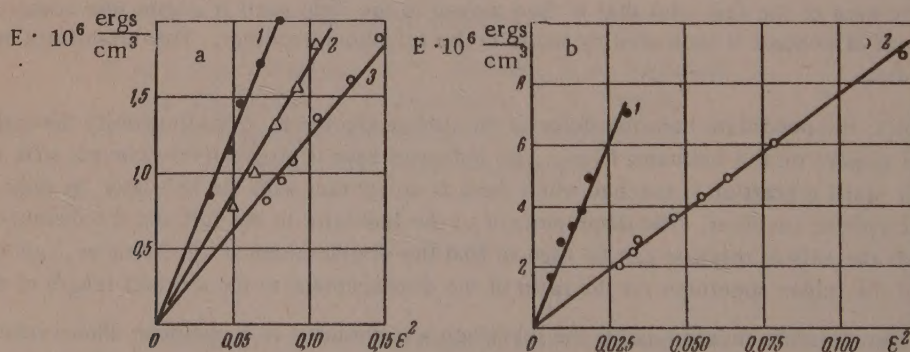


Fig. 4. Relationship between specific kinetic energy and the square of relative deformation;

a) for unfilled rubbers based on: 1) SKN-40; 2) SKN-26; 3) SKS-30;

b) for: 1) highly filler technical rubber based on SKN-40; 2) technical rubber based on SKS-30; $t = 20^\circ$; $v = 1.24$ m/second.

* The deformation of the hammer was ~ 0.5% at the maximum impact energy.

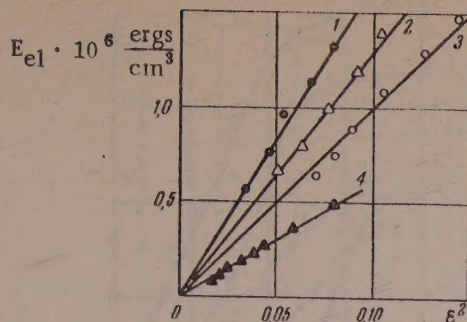


Fig. 5. Relationship between specific elastic energy and the square of relative deformation for unfilled rubbers;

- 1) based on SKN-40; $v = 0.5$ m/second;
 2) SKN-26; $v = 0.5$ m/second; 3) SKS-30;
 $v = 0.5$ m/second; 4) SKS-30; $v = 0.2$ m/second.

In distinction from static deformation ($\epsilon = \text{const}$) or extension at a constant rate ($\dot{\epsilon} = \text{const}$), which are characterized by stresses measured experimentally, impact deformation is determined by experimentally measured impact energy. Impact deformation can be regarded as a quasi-equilibrium process under the condition that the compression rate of the rubber under impact is much lower than the propagation rate of the elastic impulse ($v \ll u$). In our experiments the propagation rate of the elastic impulse was much greater than the impact velocity*. This means that the compressive deformation of the specimen on impact was virtually simultaneous along the entire length of the specimen. Therefore the equations for static deformation may be applied to impact deformation.

Deformation under impact depends both on the energy of the impact and on its initial velocity — the linear velocity of the hammer at the instant of contact with the rubber specimen. The initial impact velocity can be found from the formula.

$$v = \sqrt{2mghr^2/I}, \quad (1)$$

where m is the pendulum mass, g is the acceleration due to gravity, h is the displacement of the center of gravity of the pendulum in the vertical direction, r is the distance from the axis of rotation to the center of the pendulum hammer, and I is the moment of inertia of the pendulum. The displacement h of the center of gravity may be expressed in terms of the cosine of the angle φ (Fig. 1), the deviation of the pendulum from the equilibrium position

$$h = a(1 - \cos \varphi), \quad (2)$$

where a is the distance from the axis of rotation to the center of gravity of the pendulum.

Two test regimes are possible: 1) at constant initial impact velocity and different kinetic energies, and 2) at constant impact energy and different initial velocities. Constant initial impact velocities were used in this investigation.

For tests at constant impact velocity it must be possible to vary appropriately both the moment of inertia of the system and the height of fall of the pendulum while the impact velocity remains constant. The moment of inertia of the pendulum was varied by means of additional loads of known mass and moment of inertia. The loads were of cylindrical shape and could be screwed onto the lower end of the pendulum; the axis of such a load was a continuation of the pendulum length. For such loads the moment of inertia relative to the pendulum axis is calculated from the formula

$$I_1 = m_1 \left(\frac{3R^2 + H^2}{12} \right) + m_1 a_1^2, \quad (3)$$

where m_1 is the mass of the load, R is the radius of the cylinder base, H is the height of the cylinder and a_1 is the distance between the pendulum axis and the axis passing through the center of gravity of the cylinder. The moment of inertia of the pendulum without additional load was determined by measurements of the free oscillations of the pendulum without load, and of the pendulum with known load. The moment of inertia of the pendulum was found to be $I_0 = 1.88 \cdot 10^5 \text{ g} \cdot \text{cm}^2$.

* In our investigations the highest initial impact velocity did not exceed 2 m/second, and the modulus E of the rubber did not exceed 100 kg/cm^2 . As is known, the propagation rate of an elastic impulse is $u = \sqrt{E/\rho}$ which at $E = 10^8 \text{ dynes} \cdot \text{cm}^{-2}$ and $\rho = 1 \text{ g} \cdot \text{cm}^{-3}$ gives $u \sim 33 \text{ m} \cdot \text{sec}^{-1}$. This result is in agreement with experimental data for rubbers [6].

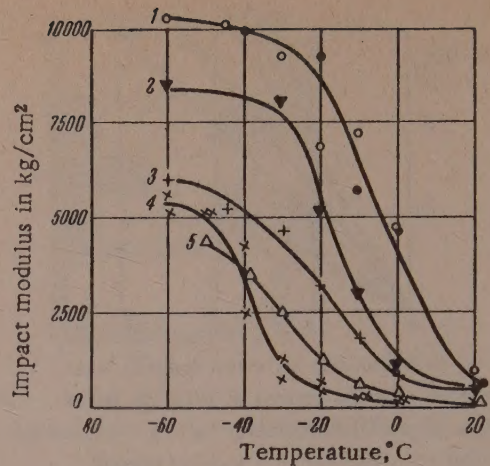
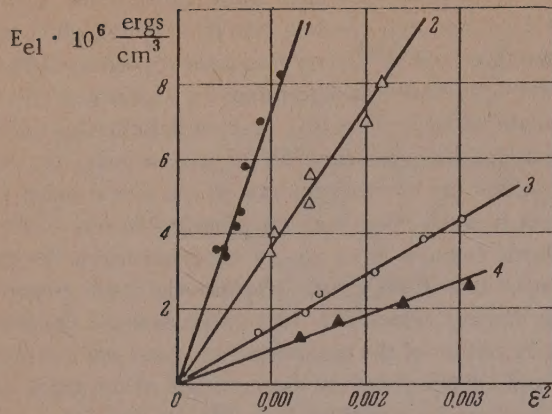


Fig. 6. Relationship between specific elastic energy and the square of relative deformation at low temperatures:

a) technical rubber based on SKS-30 (No. 73); $t = -50^\circ$; $v = 1.24$ m/second; 2) technical rubber based on SKS-30 (No. 68); $t = -40^\circ$; $v = 1.24$ m/second; 3) the same, $t = -20^\circ$, $v = 0.7$ m/second; 4) unfilled rubber from SKS-30; $t = -40^\circ$; $v = 0.9$ m/second.

Fig. 7. Effect of temperature on impact modulus for technical rubbers based on:

1) SKN-40; 2) SKN-40 (50%) and SKN-18 (50%); 3) SKS-30 (No. 42); 4) SKS-30 (No. 63); 5) SKS-30 (No. 68); $v = 0.5$ m/second.

The total kinetic energy of the pendulum at the instant of impact (E) is found from the formula:

$$E = mga(1 - \cos \varphi). \quad (4)$$

The kinetic energy after impact is:

$$E' = mga(1 - \cos \varphi'), \quad (5)$$

where φ' is the rebound angle of the pendulum after impact.

During compression of a specimen part of the kinetic energy, E_{el} , is used to do work against elasticity forces, while the rest, E_{fr} , does work against frictional forces.

The total energy at the instant of transition from compression to recovery is

$$E = E_{el} + E_{fr}. \quad (6)$$

Assuming that mechanical losses in compression and recovery of the specimen are approximately equal, and taking Equations (4) and (5) into account, we have

$$E_{fr} \cong \frac{1}{2}(E - E') = \frac{1}{2}mga[(1 - \cos \varphi) - (1 - \cos \varphi')], \quad (7)$$

$$E_{el} = E - E_{fr} = mga \left[1 - \frac{\cos \varphi + \cos \varphi'}{2} \right]. \quad (8)$$

It is more convenient to refer the impact energy to unit volume, since the elastic energy and frictional losses are proportional to the volume.

The respective specific energies are

$$E = \frac{mga}{V}(1 - \cos \varphi), \quad (9)$$

$$E_{el} = \frac{mga}{V} \left[1 - \frac{\cos \varphi + \cos \varphi'}{2} \right], \quad (10)$$

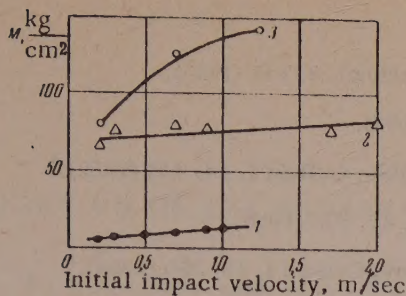


Fig. 8. Effect of the initial deformation rate on the impact modulus: 1) unfilled rubber made from SKS-30; 2) technical rubber from SKS-30 (No. 68); 3) technical rubber from SKS-30 (No. 61).

Equation (11) was subsequently confirmed for filled and unfilled vulcanizates based on natural, butadiene-styrene, and nitrile rubbers in the impact velocity range of 0.2-2 m/second. Since the deformation rate changes from its maximum value to zero during compression, the impact modulus calculated as above must be considered as the value for the average deformation rate.

Fig. 5 shows the relationship between the elastic energy, calculated from Formula (8), and the square of the deformation. It is clear from Fig. 5 that this is also a linear relationship. It follows from the results that the following expression should hold for impact deformation:

$$E_{fr} = K\varepsilon^2,$$

where K is a constant equal to one half of the friction modulus of rubber as defined by Reznikovskii [4]. This relationship was established earlier [4, 6-8] from the results of experiments on repeated deformation with free contraction.

Equation (11) remains valid at low temperatures (Fig. 6), so that it is possible to determine the impact modulus at such temperatures. Studies of the effects of low temperatures on the impact modulus are of great practical interest in relation to the problem of the experimental technique for determinations of the frost resistance of rubbers under impact deformation. Typical curves obtained in such cases are plotted in Fig. 7.

The effect of the initial deformation rate on the impact modulus of rubber at 20° is shown in Fig. 8. It is difficult to draw definite conclusions from our data concerning the influence of the rate on the impact modulus, as this relationship differs for different rubbers.

SUMMARY

1. It was shown that in impact deformation the total impact energy is proportional to the square of the compressive deformation of rubber; it is hence possible to determine a constant (the impact modulus) for a material under impact.

2. This law of impact deformation holds at low temperatures.

The Scientific Research Institute
of the Rubber Industry Moscow

Received June 10, 1957

* Above the proportionality limit there are deviations from this relationship, increasing with the compressive deformation.

LITERATURE CITED

- [1] J. Healy, Rubber Age 5, 621 (1925).
- [2] C. E. Barnett and W. C. Mathews, Rubber Chem. and Technol. 8, 159 (1935).
- [3] J. H. Fielding, Rubber Chem. and Technol. 10, 607 (1937).
- [4] M. M. Reznikovskii V. S. Yurovskaya and B. A. Dogadkin, Colloid J. 14, 444 (1952).*
- [5] E. V. Kuvshinskii and E. A. Sidorovich, J. Tech. Phys.. 26, 878 (1956).
- [6] G. M. Bartenev, M. M. Reznikovskii and M. K. Khromov, Colloid J. 18, 395 (1956).*
- [7] I. I. Trapeznikov, Trans. Automobile and Tractor Scientific Research Institute, 1, 4 (1948).
- [8] M. M. Reznikovskii and B. A. Dogadkin, Chem. Ind. 4, 227 (1954).

*Original Russian pagination. See C. B. Translation.

INVESTIGATION OF THE HYDRATION PROCESSES OF CALCIUM MONOALUMINATE

P. P. Budnikov and I. V. Kravchenko

In the modern view [1, 2], hardened hydrated aluminous cement is "microconcrete", consisting of remains of unhydrated grains of high-alumina slags, crystals of calcium hydroaluminates, and aluminum hydroxide with different water contents.

It is regarded as established [3, 4] that in accordance with the temperature conditions, the final hydration products of an aluminous cement may be: at temperatures below $+25^{\circ}$ hexagonal calcium hydroaluminates, mainly $2\text{CaO} \cdot \text{Al}_2\text{O}_3 \cdot 8\text{H}_2\text{O}$, and at temperatures above $+25^{\circ}$, tricalcium aluminate hexahydrate $3\text{CaO} \cdot \text{Al}_2\text{O}_3 \cdot 6\text{H}_2\text{O}$, crystallizing in the cubic system.

Numerous investigations [5, 6, 7] have proved that at normal and elevated temperatures the only stable calcium hydroaluminate in the $\text{CaO} - \text{Al}_2\text{O}_3 - \text{H}_2\text{O}$ system is $\text{CaO} \cdot \text{Al}_2\text{O}_3 \cdot 6\text{H}_2\text{O}$, while all the other calcium hydroaluminates are metastable and gradually pass into this compound, liberating colloidal aluminium hydroxide. This result, found by investigations of the $\text{CaO} - \text{Al}_2\text{O}_3 - \text{H}_2\text{O}$ system at concentrations of the reacting substances which are low in comparison to those found in hardening concrete, was extended by the workers cited to concretes and mortars based on aluminous cements under practical service conditions. This leads to the logical conclusion that aluminous cement is not durable and that more or less durable constructions cannot be made with such cement. Support for this conclusion was provided by the appearance of published information, mainly by French workers on the strength loss of constructions built with the use of aluminous cement. Because of such incidents the use of this cement in France has been restricted.

French workers [8, 9] consider that breakdown of this type is caused by conversion of calcium hydroaluminates crystallizing in the hexagonal system into $3\text{CaO} \cdot \text{Al}_2\text{O}_3 \cdot 6\text{H}_2\text{O}$, crystallizing in the cubic system.

The experimental data presented below show that this view is not quite correct and that the strength of hardened cement is influenced not so much by the recrystallization process itself as by the rate at which this process occurs.

In the USSR, where aluminous cement has been made on the industrial scale for over 20 years, we have no indications of any lack of durability in such cement; on the contrary, investigation of the concrete in an industrial building which had stood for 19 years showed that this cement had high strength and a stable structure. It must be pointed out, however, that the climate is much more severe in most of the industrial regions of the USSR than in France and other European countries, and aluminous cement is used less often in conditions of elevated temperatures and humidities. In view of the fact that constructions made with aluminous cement may exist under the most diverse temperature and humidity conditions in the extensive territories of our country, we undertook a deeper study of the processes taking place in hardened aluminous cements during long periods after their placement in constructions, in order to determine and prevent any possible causes of adverse effects on the durability of concrete made from aluminous cement.

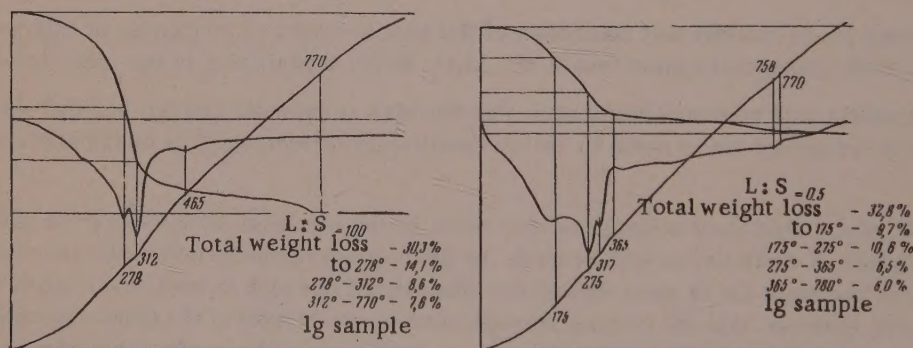
The present paper contains the results of the first stage of this study performed with synthetic calcium monoaluminate — the mineral which determines the most important constructional characteristics of aluminous cement. Calcium monoaluminate was made by fusion, in a Kryptol furnace, of a calculated mixture of pure Al_2O_3 and pure CaCO_3 , previously heated at 1100° to remove CO_2 . The melt was cooled slowly and then ground in a porcelain mill to pass completely through a No. 0085 sieve. Chemical and petrographic analysis showed that the mineral was pure, and that its optical constants were those of calcium monoaluminate.

TABLE 1

Variation of the Liquid Phase Composition Over Hydrating $\text{CaO} \cdot \text{Al}_2\text{O}_3$

Hydration time	S:L = 1:10		Molar ratio CaO:Al ₂ O ₃	S:L = 1:100		Molar ratio CaO:Al ₂ O ₃	pH of medium
	concentration mg/liter			concentration, mg/liter			
	CaO	Al ₂ O ₃		CaO	Al ₂ O ₃		
2 min	716	1236	1,06	235	332	1,09	8,5
5 "	862	1460	1,08	392	580	1,23	8,8
10 "	772	1276	1,10	403	716	1,03	9,4
20 "	918	1616	1,08	515	880	1,09	9,9
30 "	929	1664	1,02	515	812	1,16	9,9
1 hr	1008	1812	1,02	627	1068	1,07	10,0
2 "	1086	1884	1,05	683	1076	1,16	10,0
6 "	1019	1868	1,00	795	1340	1,08	10,1
14 "	358	856	0,76	862	1472	1,07	10,1
16 "	358	708	0,92	896	1604	1,02	10,2
18 "	369	728	0,92	952	1604	1,08	10,2
24 "	358	556	1,17	952	1456	1,19	10,3
2 days	179	172	1,80	952	1692	1,03	10,3
3 "	123	184	1,22	302	292	1,88	10,2
7 "	155	212	1,33	280	276	1,85	10,2
14 "	313	176	5,59	392	196	3,64	11,3
28 "	112	60	3,40	380	180	3,85	11,5
90 "	22	68	0,59	257	132	3,53	11,3

It is known that the rate of the hydration reaction and its final products depend to a considerable extent on the composition and pH of the reaction medium. Our investigation therefore commenced with a study of the composition of the liquid phase over the hydrating mineral by the usual method in which a weighed sample of the mineral was shaken with water for a definite time, and a sample of the suspension was then taken from the vessel. Half the sample was filtered, the residue was washed with alcohol, and CaO and Al_2O_3 were determined in the filtrate while the other half of the sample was used for pH determination.

Fig. 1. Thermograms of hydrated $\text{CaO} \cdot \text{Al}_2\text{O}_3$, L:S = 100 and L:S 0.5.

At the same time specimens were prepared for microscopic investigations; these were systematically examined and when necessary opened for determination of refractive indices of any new substances formed.

For determination of the significance of the solid - liquid ratio in the hydration process the composition of the liquid phase over hydrating calcium monoaluminate was studied at two ratios of the solid (S) to liquid (L) phase - S:L = 1:10, and S:L = 1:100. The results of the determinations are given in Table 1.

Table 1 shows that the pH of the medium rapidly rises from 8.5 to 10.3-11.5 during hydration of calcium monoaluminate. The reaction is more rapid and the solution supersaturation increases with decrease of the L:S ratio and increase of the temperature of the surrounding medium. The CaO and Al_2O_3 concentrations reached in 5 minutes from the start of hydration at L:S = 10 are reached in 14 hours in a suspension with L:S = 100. Rapid

TABLE 2

Strength Variations (in kg/cm²) of Hydrated CaO · Al₂O₃, Hardened Under Various Temperature and Moisture Conditions

Hardening time	Hardening temperature 15-18°			Hardening temperature 45°		
	in humid air	in water	in air	in humid air	in water	in air
6 hr	103	—	—	103	—	—
12 "	83	—	—	196	—	—
18 "	153	—	—	196	—	—
1 days	205	—	—	190	—	—
3 "	—	294	226	—	175	175
7 "	—	268	212	—	191	179
14 "	—	308	248	—	239	220
28 "	—	299	274	—	198	194
3 mo	—	297	298	—	298	157
6 "	—	332	285	—	270	218
9 "	—	354	246	—	288	209
1 yr	—	328	205	—	370	194

precipitation of new products, marked by a rapid decrease in the CaO and Al₂O₃ contents, begins after 14 hours at L : S = 10, and only after 3 days at L : S = 100. The CaO and Al₂O₃ concentrations in the liquid phase at L : S = 10 reach their maximum values, 1.086 g CaO and 1.884 g Al₂O₃ per liter, after 2 hours, whereas in a suspension with L : S = 100 the corresponding values are 0.952 and 1.692 g/liter and are reached after 2 days. The molar ratio of CaO to Al₂O₃ in both cases is close to unity for 7 days, but then rises sharply to 3 or even 4, indicating the possible formation of more highly basic calcium hydroaluminates. In suspensions with L : S = 10 the deposition of new products is almost complete after 3 months, and the CaO and Al₂O₃ concentrations in the solution become equal to the limiting concentrations of the reaction products (dicalcium hydroaluminate), whereas this process is far from complete after three months in suspensions with L : S = 100. Moreover, the persistence of high CaO and Al₂O₃ concentrations in the liquid phase for a long time may favor the formation of more highly basic calcium hydroaluminates and in particular of 3CaO · Al₂O₃ · 6H₂O, as the reaction products.

Microscopic investigation of the precipitate formed by hydration of calcium monoaluminate for 4 months at L : S = 100 showed that it consisted mainly of 3CaO · Al₂O₃ · 6H₂O with a small admixture of hexagonal calcium hydroaluminates. The thermogram of this sample (Fig. 1) shows a clear endothermic effect at 312°, characteristic of 3CaO · Al₂O₃ · 6H₂O, and a considerably smaller effect at 278°, characteristic of hexagonal calcium hydroaluminates, whereas the thermogram of calcium monoaluminate hydrated at L : S = 0.5 has pronounced effects at 175 and 275°, while the effect due to 3CaO · Al₂O₃ · 6H₂O is weak.

These experiments show that the course of the hydration process is closely associated with variations of the solution pH. The L : S ratio of the suspensions is also very significant in relation to hydration processes and therefore the aim in investigations must be to use samples hydrated under conditions as close as possible to those found in practice.

However, it is obvious that decrease of the L : S ratio introduces difficulties into the use of chemical analysis for investigation of the composition of the liquid phase over hydrating cement and therefore for comparison of the hydration of calcium aluminates of different degrees of basicity we used suspensions with low solid concentrations, and corrected the results with the aid of other analytical methods whereby these processes could be observed in cement pastes of normal consistency. Such methods are complex thermal and x-ray structural analysis. Samples of plastic consistency of 1 : 3 composition, and heat cement samples, were prepared for studies of hydration processes by these methods. The L : S ratio was 0.5 in both cases. The samples were kept under definite temperature and humidity conditions and tested at fixed intervals. The compressive strengths were determined, and the samples were subjected to complex thermal and x-ray structural analysis.

The samples were hardened under the following conditions: 1) in water at 15-18°; 2) in air at 15-18°; 3) in water at 45°; 4) in air at 45°.

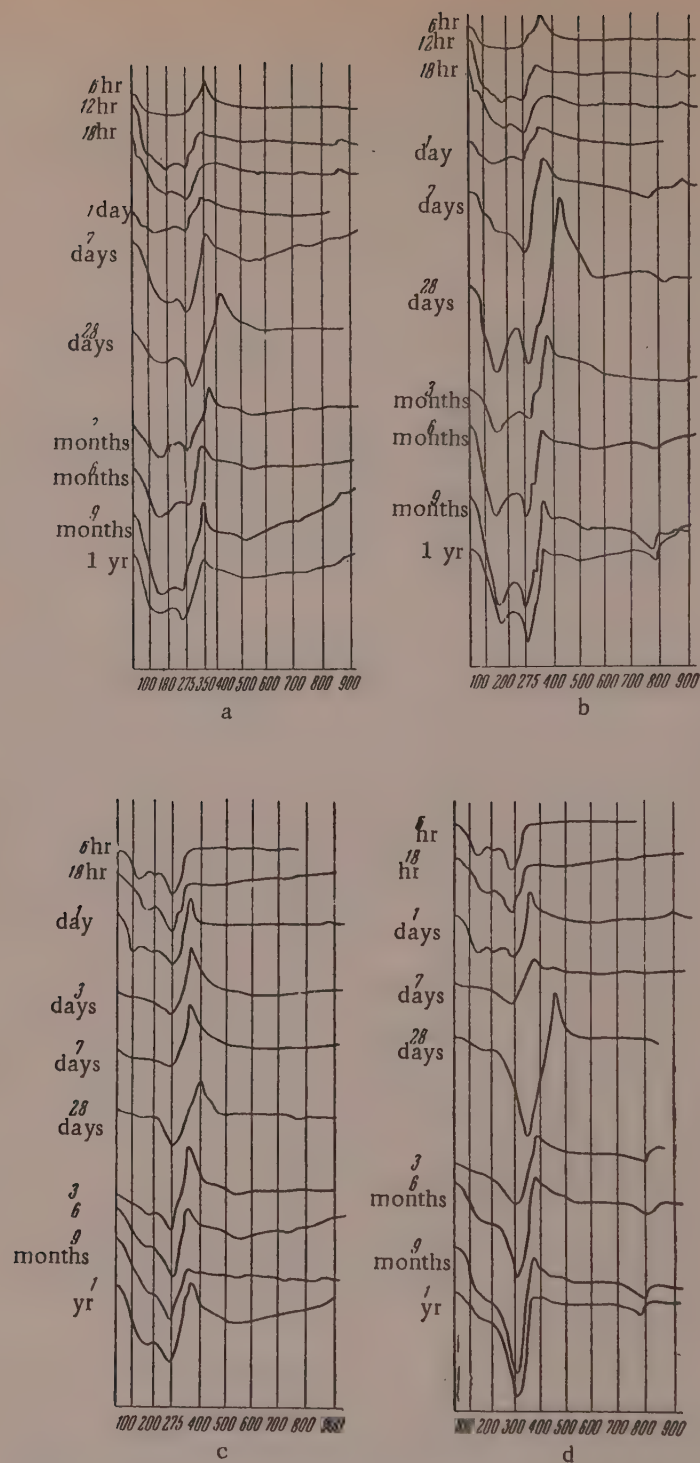


Fig. 2. Thermograms of $\text{CaO} \cdot \text{Al}_2\text{O}_3$ hardened:
a) in air at $15-18^\circ$; b) in water at $15-18^\circ$; c) in air at 45° ;
d) in water at 45°

The thermograms are reproduced in Figs. 2 and 3, and the results of the compressive strength tests are given in Table 2.

Thermograms of hydrated calcium monaluminate show that samples hardened in water and in air at $15-18^\circ$,

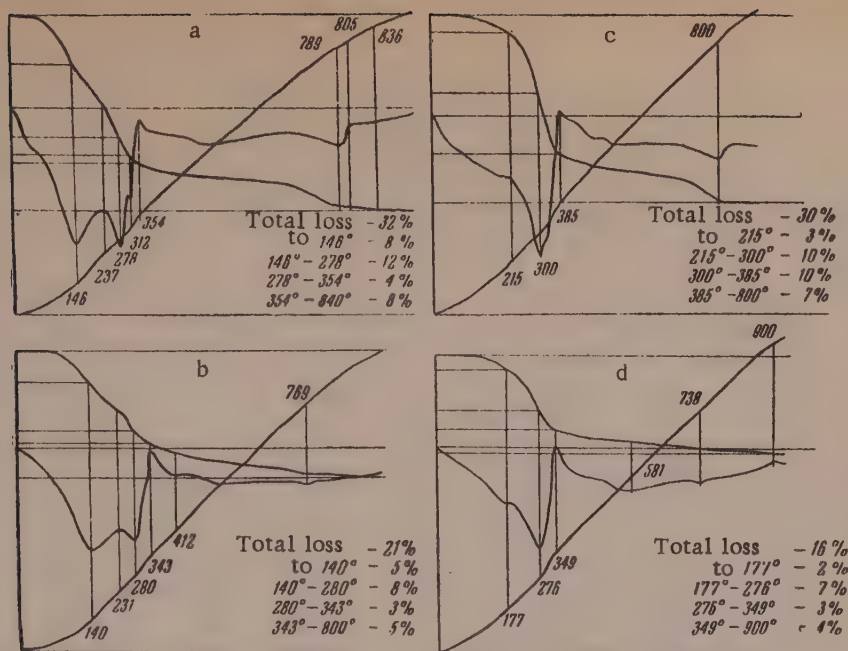


Fig. 3. Thermograms of $\text{CaO} \cdot \text{Al}_2\text{O}_3$ hydrated for 6 months:
a) in water at 15-18°; b) in air at 15-18°; c) in water at 45°; d) in air at 45°.

and in air at 45°, give two principal endothermic effects: the first, less regular at 150-200° and the second, recorded in narrower limits, at 275-295°. These two effects are characteristic of hexagonal calcium hydroaluminates, which yield water of crystallization in two stages at these temperatures.

When the mineral is hardened in water at 15-18°, on the 28th day from the start of hardening the thermograms begin to show a third weak endothermic effect at 325-330°, indicating the appearance of newly formed $3\text{CaO} \cdot \text{Al}_2\text{O}_3 \cdot 6\text{H}_2\text{O}$. Sharp endothermic effects due to hexagonal calcium hydroaluminates appear 12 hours after the start of hydration on the thermograms of the mineral hardened at 15-18°; this corresponds to a sharp strength increase of the hardened cement (see Table 2). The appearance of small amounts of $3\text{CaO} \cdot \text{Al}_2\text{O}_3 \cdot 6\text{H}_2\text{O}$ in the hardened cement is not accompanied by a strength decrease.

When the mineral is hardened in water at 45°, hexagonal calcium hydroaluminates are first formed, with their characteristic effects at 175° and 275-285°, but these effects disappear by the 14th day of hardening, and from the 3rd day the curve shows endothermic effects at 300-325°, characteristic of $3\text{CaO} \cdot \text{Al}_2\text{O}_3 \cdot 6\text{H}_2\text{O}$.

Increase of the temperature of the surrounding medium to 45° almost doubles the rate of the hydration reaction; thus, endothermic effects for hexagonal calcium hydroaluminates appear after 6 hours of hardening at this temperature while at 15-18° they appear 12 hours after the start of hydration.

The URS-501 ionization unit was used for the x-ray investigations of hardened cement. The diagrams were taken with a copper anode and a filter whereby the photographs could be taken in monochromatic C and k_α radiation. Analysis of the x-ray patterns of a sample of calcium monaluminat hardened for 3 days in water at room temperature showed that it contained considerable amounts of residual unhydrated calcium monoaluminat, as its crystal lattice is revealed quite clearly (see Table 3). Of new compounds, $2\text{CaO} \cdot \text{Al}_2\text{O}_3 \cdot 8\text{H}_2\text{O}$ is quite distinct (interference lines at 2.87, 2.53, 2.47, 1.835 and 1.667), and there are very intense lines for gibbsite, the crystallization of which was apparently only beginning.

The x-ray pattern of a monocalcium aluminate sample hardened in water at 15-18° for 5 months shows that the hydration of the mineral was complete at the end of this time. Most of the new materials consist of $3\text{CaO} \cdot \text{Al}_2\text{O}_3 \cdot 6\text{H}_2\text{O}$ and gibbsite. Small amounts of hexagonal calcium hydroaluminates are present.

In x-ray investigations of the precipitate formed when 4 g of calcium monoaluminat was shaken with 400 ml of water for 4 months it was found that crystallization of new minerals was more extensive and the con-

TABLE 3

x-Ray Data for $\text{CaO} \cdot \text{Al}_2\text{O}_3$ Hydrated Under Various Conditions

CaO·Al ₂ O ₃ , hardened in water at									
15-18°						45°			
3 days		5 months		4 months		3 days		3 months	
d	$\frac{I_x}{I_{\max}}$	d	$\frac{I_x}{I_{\max}}$	d	$\frac{I_x}{I_{\max}}$	d	$\frac{I_x}{I_{\max}}$	d	$\frac{I_x}{I_{\max}}$
4,77	10	7,27	30	7,92	10	10,64	6	8,73	10
3,23	14	5,12	35	5,16	48	6,25	4	7,63	6
2,99	100	4,91	43	4,91	14	5,54	4	6,65	10
2,88	30	4,46	30	4,46	30	4,88	6	5,16	38
2,53	51	4,05	30	3,38	39	3,72	10	4,88	62
2,47	13	3,36	51	3,16	27	3,36	8	4,46	28
2,41	40	3,03	40	2,81	70	3,19	6	3,36	62
2,34	12	2,81	50	2,58	14	2,96	10	3,21	16
2,20	14	2,48	25	2,47	41	2,52	100	3,16	30
2,03	14	2,30	63	2,30	95	2,40	40	2,82	62
1,927	31	2,04	51	2,04	100	2,96	40	2,57	14
1,843	12	1,740	24	1,814	12	2,04	14	2,47	40
1,677	5	1,710	24	1,741	44	1,922	33	2,90	100
1,657	14	1,681	51	1,710	25	1,834	33	2,04	100
1,527	25	1,306	100	1,677	58	1,745	8	1,985	10
1,459	22			1,593	15	1,681	11	1,917	12
				1,572	18	1,653	18	1,819	16
				1,404	19	1,528	27	1,814	16
						1,457	20	1,745	36
						1,406	11	1,710	26
								1,777	64
								1,593	14
								1,572	14
								1,457	14
								1,404	14
								1,198	16

* At L : S = 100; d = interplanar spacings in Å; I_x is the observed radiation intensity;

version of hexagonal calcium hydroaluminates into $3\text{CaO} \cdot \text{Al}_2\text{O}_3 \cdot 6\text{H}_2\text{O}$ was more complete than in the hardening of monoaluminate in the form of a cement paste at L : S = 0.5.

It is seen that the results of x-ray, thermographic, and petrographic analysis confirm conclusively that recrystallization processes occur in samples of hydrated $\text{CaO} \cdot \text{Al}_2\text{O}_3$ hardened at room temperature.

The x-ray patterns of calcium monoaluminate hardened in air at room temperature for 3 days and for 3 months showed that $\text{CaO} \cdot \text{Al}_2\text{O}_3$ is not hydrated completely under these conditions. Remains of the unhydrated mineral were detected in both samples. The conversion of hexagonal calcium hydroaluminates into the cubic form is simultaneously retarded, and the crystallization of gibbsite, which is probably present as a dehydrated gel, is worsened considerably. Of the hexagonal calcium hydroaluminates, the crystal lattice of $4\text{CaO} \cdot \text{Al}_2\text{O}_3 \cdot 14\text{H}_2\text{O}$ is the most pronounced.

The x-ray patterns of samples hardened in water at 45° showed that hydration is accelerated under these conditions, the conversion of hexagonal calcium hydroaluminates into the cubic form is also accelerated, and the crystallization of gibbsite is improved. Most of the new formations in a three-month sample consist of $3\text{CaO} \cdot \text{Al}_2\text{O}_3 \cdot 6\text{H}_2\text{O}$ and gibbsite. Hexagonal calcium hydroaluminates are present in small amounts and in the form of highly basic hydroaluminates — $3\text{CaO} \cdot \text{Al}_2\text{O}_3 \cdot 8\text{H}_2\text{O}$ and $4\text{CaO} \cdot \text{Al}_2\text{O}_3 \cdot 14\text{H}_2\text{O}$. Despite this, as Table 2

CaO·Al ₂ O ₃ , hardened in air at							
15-18°				45°			
3 days		3 months		3 days		3 months	
d	$\frac{I_x}{I_{max}}$	d	$\frac{I_x}{I_{max}}$	d	$\frac{I_x}{I_{max}}$	d	$\frac{I_x}{I_{max}}$
7,35	10	7,63	7	8,46	6	7,82	6
5,63	10	4,62	8	5,57	10	7,54	6
4,73	12	4,37	8	4,73	10	7,11	8
4,46	10	3,76	6	4,11	10	6,13	6
4,08	8	3,35	46	3,69	15	5,63	11
3,74	10	3,19	8	3,29	8	5,48	13
3,46	10	2,97	100	3,15	10	4,95	8
3,21	10	2,85	17	2,97	100	4,59	6
2,98	100	2,77	3	2,86	25	4,56	8
2,86	12	2,52	34	2,53	62	3,95	6
2,53	68	2,40	32	2,41	46	3,79	5
2,41	38	2,19	13	2,34	12	3,72	8
2,35*	12	2,13	10	2,18	50	3,51	5
2,20	18	2,02	12	2,09	6	3,36	8
2,14	12	1,917	34	2,02	16	3,19	8
2,03	13	1,829	8	1,922	38	2,98	100
1,928	35	1,649	17	1,749	6	2,86	20
1,834	10	1,528	24	1,685	6	2,75	6
1,657	12	1,453	19	1,657	15	2,53	38
1,582	11	1,370	10	1,579	8	2,41	36
1,526	25	1,253	10	1,528	27	2,34	8
1,457	26	1,196	8	1,457	28	2,19	16
1,409	6			1,451	15	2,14	11
				1,437	8	2,03	13
				1,405	6	1,922	25
				1,362	4	1,830	13
						1,745	8
						1,653	16
						1,579	8
						1,528	21
						1,457	20

I_{max} = maximum radiation intensity in the given x-ray pattern.

shows, the strength of the samples increases and at the end of one year it exceeds the strength of all the samples hardened under other conditions.

Hydration and recrystallization processes slow down in hardening in air at 45°. The two samples hardened in air at 45° for 3 days and 3 months respectively were found to contain the gibbsite lattice and a mixture of hexagonal calcium hydroaluminates mainly highly basic.

SUMMARY

1. When samples of calcium monoaluminate made at L:S = 0.5 are hardened in water, hexagonal calcium hydroaluminates, mainly $2\text{CaO} \cdot \text{Al}_2\text{O}_3 \cdot 8\text{H}_2\text{O}$, are first formed, and alumina gel crystallizes in the form of gibbsite. This is followed by recrystallization of $2\text{CaO} \cdot \text{Al}_2\text{O}_3 \cdot 8\text{H}_2\text{O}$ into cubic $3\text{CaO} \cdot \text{Al}_2\text{O}_3 \cdot 6\text{H}_2\text{O}$, highly basic calcium hydroaluminates appear, and the crystallization of gibbsite continues. When $\text{CaO} \cdot \text{Al}_2\text{O}_3$ is hydrated in large amounts of water, the conversion of hexagonal hydroaluminates into the cubic form is accelerated considerably. The appearance of $3\text{CaO} \cdot \text{Al}_2\text{O}_3 \cdot 6\text{H}_2\text{O}$ in the structure of the hardened cement had no adverse effects on its strength.

2. Hydration of $\text{CaO} \cdot \text{Al}_2\text{O}_3$ in water was accelerated considerably at a higher temperature, as indicated both by the amount of combined water and by the accelerated conversion of hexagonal hydroaluminates into the

cubic form. The strength of the samples, which fell at the first stages of this recrystallization, was restored, probably as the result of formation of a new crystalline structure, which now consisted of $3\text{CaO} \cdot \text{Al}_2\text{O}_3 \cdot 6\text{H}_2\text{O}$ and $\text{Al}(\text{OH})_3$ partly as a colloidal but mainly as a crystalline phase.

3. Hydration is slowed down in air hardening both at room and at elevated temperatures, owing to a deficiency of water. Remains of unhydrated $\text{CaO} \cdot \text{Al}_2\text{O}_3$, gibbsite, and a mixture of highly basic calcium hydroaluminates, mainly $4\text{CaO} \cdot \text{Al}_2\text{O}_3 \cdot 14\text{H}_2\text{O}$, continue for a long time to be the structural elements of the hardened cement.

Scientific Research Institute
of the Cement Industry Moscow

Received June 11, 1957

LITERATURE CITED

- [1] V. N. Yung, Fundamentals of Cement Technology (Moscow, Industrial Construction Press, 1951). [In Russian]
- [2] V. N. Yung, Microconcrete, in the book: Pozzolan Cements (Leningrad, 1936). [In Russian]
- [3] A. A. Baikov, Collected Works, vol. 5 (Moscow - Leningrad, Izd. AN SSSR, 1948). [In Russian]
- [4] V. N. Yung, Yu. M. Butt, V. F. Zhuravlev and S. D. Okorokov, Cement Technology (State Construction Press, 1952). [In Russian]
- [5] J. D'Ans and H. Eiek, Zement - Kalk - Gips 6, [6], 197, (1953).
- [6] J. Dreyfus, La Chemie Des Ciments, (Paris, 1950).
- [7] R. B. Peppler and L. S. Wells, J. Res. Nat. Bur. Standards 52 [2], 75, (1954).
- [8] H. Lafuma, Zement, 25, 71 (1935).
- [9] H. Lafuma, La Ciment 30 174 (1925).

THE COLLOIDAL STATE OF SOLID SOLUTIONS IN TWO-PHASE METALLIC ALLOY SYSTEMS

V. M. Glazov and V. N. Vigdorovich

In a series of investigations [1, 2] of the effects of alloy composition at a given temperature on the microhardness of solid solutions it was shown that the microhardness of crystals of a solid solution, which appear homogeneous under the microscope, increases or decreases in accordance with the microhardness of the second phase, whereas the phase diagram indicates that it should remain constant. The hypothesis that the solid solution becomes supersaturated was not confirmed by x-ray data. It was therefore suggested [1] that the crystals of a solid solution, which appear homogeneous under the microscope, in fact have a more complex structure, characterized by the presence of submicroscopic particles of a second phase which are formed in the course of dendritic crystallization and which are deposited in the interaxial dendrite spaces (second-order heterogeneity, or microheterogeneity). Since this hypothesis was put forward, we have accumulated considerable experimental data which gives more detailed information on the nature of the heterogeneous structure of real crystals in the solid solutions.

In this paper it is proposed to draw definite conclusions concerning the state of heterogeneous crystals of solid solutions in two-phase alloys.

Investigations of the microhardness of crystals of solid solutions in relation to the compositions in such systems as Al - Cu, Al - Si, Al - Zn, Al - Ti, Al - Ta, Al - Zr, Al - Mn, Al - Fe, Cu - Ti, Cu - Zr, Cu - Cr etc., showed that all the microhardness isotherms are of the form shown in Fig. 1, a, which contains data for the system Al - Cu, taken as an example. The microhardness of the crystals of the solid solution increases with the content of the second component in the two-phase region of the diagram. When the microhardness of the second phase is less than the microhardness of the homogeneous solid solution, the microhardness of the quasi-homogeneous crystals of solid solution falls instead of rising. We observed this for such systems as Cd - Bi, Cd - Sn, Al - Sn etc.

It was found that the effect of the particles present in the solid solution on its microhardness is not eliminated by relatively brief or even by fairly prolonged homogenization (up to 150 hours). However, if alloys showing increasing microhardness are subjected to very prolonged homogenization; for example, if Al - Cu alloys are homogenized to 400° for 500-600 hours, the microhardness of the crystals of solid solution in them becomes constant and equal to the microhardness of the alloy at maximum saturation at the given temperature (Fig. 1, b).

It should be pointed out that in systems in which the solubility varies substantially with temperature the microheterogenization effect is also observed in two-phase alloys with composition to the left of the point of maximum saturation, i.e., in the composition region where formation of submicroscopic particles of the second phase in the course of dendritic crystallization is impossible (for example, in the system Al - Zn, Fig. 2).

Therefore the formation of particles giving rise to microheterogeneity in the crystals of solid solutions in two-phase alloys is possible not only as the result of dendritic crystallization, but also as the result of decomposition of the solid solution with changes of solubility on decrease of temperature. Therefore two mechanisms for the occurrence of microheterogeneity, corresponding to two processes of entirely different nature, should be distinguished. The nature of these processes will be considered in detail later.

Kinetic studies of the transition of quasi-homogeneous crystals in solid solutions into the true homogeneous state, performed by means of the microhardness method, showed that the kinetic curves for different systems are strictly uniform in shape. A typical kinetic curve representing the transition of quasi-homogeneous crystals of solid solution in the alloy Al + 8% Cu (Fig. 3, a) into the true homogeneous state after 100 hours of homogenization at 400° is shown in Fig. 3, b.

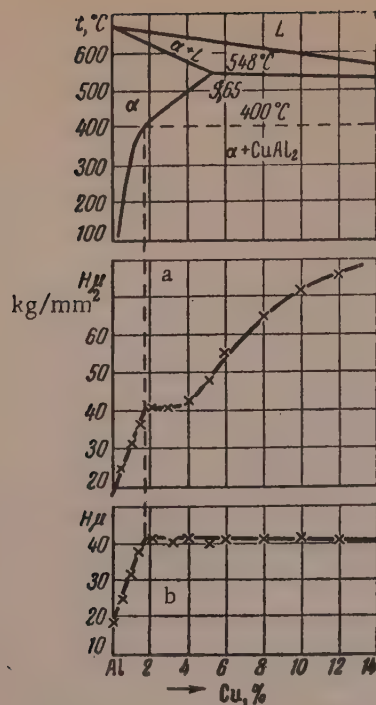


Fig. 1. Variation of microhardness with composition at 400° in the system Al - Cu after homogenization: a) for 100 hours; b) for 600 hours.

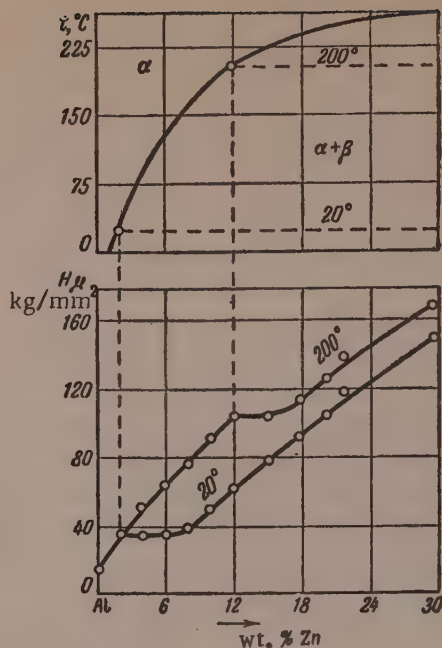


Fig. 2. Variation of microhardness with composition at 200 and 20° in the system Al - Zn.

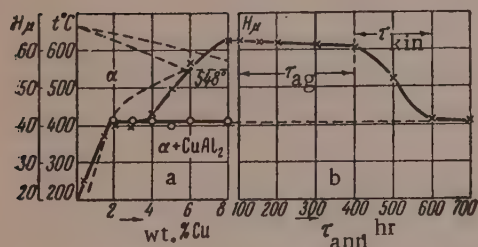


Fig. 3. Coagulation kinetics of the colloidal solution in α grains in Al + 8% Cu alloy at 400°.

The foregoing facts suggest that the microheterogeneity effect can be regarded as a colloidal state of the solid solution, by which is meant a special state primarily characterized by a definite particle size and extensive interfacial area. Another interesting fact should be mentioned, which did much to confirm our view that the heterogenized grains of a solid solution constitute a colloidal system. In microscopic examination of electropolished specimens of two-phase alloys of aluminum and copper, and aluminum and silicon, we did not observe grain heterogeneity in the solid solution in direct reflected light, even at considerable magnifications ($\times 1000$). The grains of solid solu-

tion appear absolutely homogeneous under direct reflected light. However, when the same specimens were observed in a dark field, a peculiar Tyndall effect could be seen. The reason is that transparent substances are examined in transmitted light (Fig. 4, a) whereas opaque materials, such as metals and alloys, are examined in reflected light, when the objective serves not only to produce an enlarged image, but is also a component of the illuminating system. The structure of metals and alloys is usually studied in a light field (Fig. 4, b). However, it can also be studied in a dark field (Fig. 4, c), when the boundary rays emitted by the light source are used for illumination. These rays are reflected by a plane aluminized plate onto a concave parabolic mirror condenser, which focuses them on the specimen surface. These rays are reflected, pass through the objective, and the image formed is viewed through the eyepiece. The specimen surface is illuminated from all sides by oblique rays, as in illumination by scattered daylight giving a more correct representation of the colors and the form of the specimen surface. The rays illuminating the object have a very low angle of incidence, and therefore only a small proportion of the reflected and scattered rays enters the objective. When the specimens were examined in a dark field, bright points could be observed over the whole field of the grain, the number of such points being

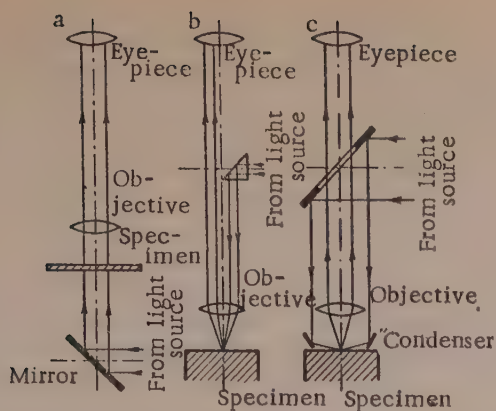


Fig. 4. Schematic representation of microstructure examination:
a) by transmitted light b) in a light field, c) in a dark field.

dispersion medium and the disperse phase is very large. It is this quantitative change of internal surface that leads to the appearance of new properties in the system and determine its colloidal character.

The two different mechanisms by which microheterogeneity arises, to which reference was made earlier, can now be considered as dispersional (due to dendritic crystallization) and condensational (due to liberation of submicroscopic particles of the second phase in the solid state) formation of a colloid solution in the solid-solution grains of two-phase alloys.

The formation of a colloid solution by the dispersional mechanism is due to the dendritic growth of the primary crystals of solid solution. As the result of dendritic crystallization regions of the as yet uncrystallized melt become trapped and surrounded on all sides by branches of the growing dendrites. Being still liquid and at the same time cut off from the main bulk of the melt, these particles of metallic liquid crystallize independently. The system remains for some time in the final crystallization stage, characterized by the existence of a solid-liquid state [3], when the dispersion medium is solid and the disperse phase is liquid. On further decrease of temperature the composition of these liquid particles alters during crystallization, up to the eutectic composition, after which particles of the second phase are formed. It is evident that, in accordance with the component interaction, the melt may ultimately reach the peritectic composition and this would also eventually lead to the appearance of particles of the second phase. Subdivision of the melt by the dendrite branches during crystallization leads to formation of particles of different sizes. Therefore a colloidal solution formed by this mechanism can be regarded as polydisperse.

Microhardness determinations of solid-solution grains, which are themselves colloidal solutions formed by the condensational mechanism, indicate that the separation and formation of particles of the second phase occurs simultaneously throughout the volume of the solid-solution grain in this case. With the aid of a somewhat simplified model of this process we may postulate that the particles of the second phase are formed in regions where the atoms of the second component tend to concentrate (local fluctuations of composition) simultaneously throughout the volume, and grow at a constant linear rate. In consequence of the equal conditions of formation and growth, the particles must then be of approximately equal size. Therefore a colloidal solution formed by the condensational mechanism may be regarded as monodisperse.

The greatest deviations from this assumption probably occur near the boundaries of the solid-solution grains, where the material has a large number of vacancies and a higher value of the isobaric - isothermal potential, which favors predominant formation of particles of the second phase.

It should be noted that in systems in which solubility is very low, it either does not change with temperature or changes very little; the condensational formation of a colloidal solution in two-phase alloys is then excluded

greater near the grain boundaries*. It should be noted this effect is not seen in dark-field examination of polished sections made from specimens subjected to prolonged homogenization, leading to loss of microheterogeneity, as shown by the microhardness method (its values correspond to the horizontal region in Fig. 1, b). Therefore prolonged homogenization results in coagulation, and the crystals of solid solution become truly homogeneous.

Thus it may be assumed that heterogenized α grains consist of a colloidal solution. As in any colloidal system, two phases are present here (there may be more than two); a heterogeneous system consists of a dispersion medium (the α solid solution) and a disperse phase (particles of the second phase distributed in the crystals of the α solid solution). The particles of the disperse phase, distributed throughout the solid solution grains, are very small, so that the interface between the

* Good photographs of polished sections cannot be obtained in a dark field.

Determinations of Alloy Solubility in the Solid State by the Microhardness Method and by x-Ray Structural Analysis

System	Temp. (°C)	Solubility, wt. %	
		microhardness method	x-ray structural analysis
Al — Cu	450	2,85	2,80
	500	4,0	4,0
Al — Zn	20	2,0	2,0
	200	12,0	12,6
Al — Si	20	0,05	0,03
	500	0,8	0,8
Al — Ti	500	0,08	0,06
Al — Ta	20	0,16	0,15

or is very weak. In such systems it is possible to observe microheterogenization of the solid-solution grains in two-phase alloys as the result of purely dendritic crystallization.

In alloys the composition of which lies to the right of the point of maximum saturation the total microheterogeneity results from both the processes in question. The relative participation of the condensational process diminishes with increase of the quenching temperature; it is then possible to observe in pure form the influence of microheterogeneity resulting from the condensational process. For this, it is first necessary to homogenize the alloy for a long time, with elimination of all microheterogeneity, and then to warm the alloy (without fusion) and cool it slowly.

It now remains to consider the stability of colloidal solutions in two-phase alloys. Investigations of solubility in the solid state for a number of binary systems, performed both by the microhardness method and by x-ray structural analysis, showed that there is complete agreement between the results given by the two methods (see table).

The table shows that the solubility data for the alloys coincide almost completely, despite the fact that in all cases when the solubility was determined by the microhardness method the microhardness isotherms for the solid-solution crystals showed an increase of microhardness in the two-phase region of the diagram.

This suggests that the composition of the solid-solution crystals themselves (with the particles of the second phase disregarded) is an equilibrium composition, and corresponds to the saturation concentration at the corresponding temperature, indicated by the line of limited solubility in the phase diagram. Hence the colloidal solution in the α grains of two-phase alloys represents the metastable state of a solid solution of stable concentration. It is implied that the composition of the dispersion medium corresponds to the composition as indicated by the phase diagram, but the isobaric — isothermal potential of such a system is very high because of the higher dispersity of the disperse phase. However, this does not change the mutual solubility of the two phases in equilibrium, as the second phase, apart from giving rise to the colloidal solution in the α grains, is also present in the alloy in a state of a definite degree of compactness.

The influence of the particle size of the segretated second phase on the limiting solubility was examined in detail by Konobeevskii [4] in the light of the general theory of phase formation. However, in the cases considered by Konobeevskii the dispersion medium did not have an equilibrium concentration (in the sense of the phase diagram), while the second phase was present only in the form of fine particles, close to the colloidal state. In the present instance the presence of the second phase in the form of compact formations, since the alloy composition corresponds to the two-phase region of the diagram, indicates that the dispersion medium has stable equilibrium concentration.

The formation of a relatively stable solution in the α grains of two-phase alloys is associated with the thermodynamic advantage of this process on cooling. However, the existence of an extensive interphase surface, the formation of which is associated with an increase of the isobaric — isothermal potential of the system, makes this state unstable. Because of this, substances in the colloidal state are particularly liable to undergo phase transformations with increase of their surface energy.

If we consider the stability of the colloidal solution in the α grains by analysis of its coagulation process (Fig. 3, b), we can distinguish two periods: the period of aggregative stability and the period of kinetic stability of the colloidal solution. The period of aggregative stability represents the time during which the dispersity of the particles of the second phase remains unchanged. During this time, under constant conditions (temperature, concentration, etc.), the system remains in a metastable state, characterized by absence of coagulation of the particles of the second phase in the solid-solution grains. The period of kinetic stability characterizes the coalescence rate of the particles of the second phase. During this period the α crystals approach a stable state.

The effects described above provide further confirmation of the common nature of the principal problems in the theories of liquid and solid solutions. If certain special properties are ascribed to the crystalline state of matter, and it is contrasted with the liquid and gaseous states, the similarity between phenomena in solid and liquid solutions generally passes unnoticed. Nevertheless, solid solutions have many of the properties of liquid solutions; in particular, as is shown in this paper, they may exist in the colloidal state.

SUMMARY

1. The microhardness of solid-solution crystals in the systems: Al - Cu, Al - Si, Al - Zn, Al - Ti, Al - Ta, Al - Zr, Al - Sn, Al - Mn, Al - Fe, Cu - Ti, Cu - Zr, Cu - Cr, Cd - Bi, Cd - Sn etc. has been studied, and it is shown that the solid-solution crystals may become microheterogeneous by two mechanisms: dispersional and condensational.

2. A technique is described for microscopic investigation of the microheterogeneity of solid-solution crystals by reflected light with the aid of a dark-field optical system whereby the presence of ultramicrocrystals in the solid-solution crystals may be detected.

3. The transition of heterogeneous solid-solution crystals from the metastable into the stable state, which occurs in two stages, has been studied from the kinetic aspect.

4. It is shown on the basis of x-ray data that microheterogeneous crystals of a solid solution represent the metastable state of a solid solution of stable concentration with regard to the equilibrium diagram.

5. The results are interpreted as indicating that the solid-solution crystals are in the colloidal state.

The A. A. Baikov Institute of Metallurgy
Academy of Sciences USSR
The M. I. Kalinin Institute of
Nonferrous Metals and Gold, Moscow

Received April 17, 1957

LITERATURE CITED

[1] A. A. Bochvar, Bull. Acad. Sci. USSR, Div. Tech. Sci. 10-11 (1945).

[2] V. M. Glazov, G. A. Korol'kov, and Yu. D. Chistyakov, Bull. Acad. Sci. USSR, Div. Tech. Sci. 10 (1955); V. M. Glazov, G. A. Korol'kov, and Yu. D. Chistyakov, Bull. Acad. Sci. USSR, Div. Tech. Sci. 12 (1955); V. M. Glazov, M. V. Zakharov, and M. V. Stepanova, Bull. Acad. Sci. USSR, Div. Tech. Sci. 1 (1956); V. M. Glazov, M. V. Mal'tsev, and Yu. D. Chistyakov, Bull. Acad. Sci. USSR, Div. Tech. Sci. 4 (1956); V. M. Glazov, V. N. Vigdorova, and G. A. Korol'kov, J. Phys. Chem. 8 (1957); V. M. Glazov, V. N. Vidorovich, and G. A. Korol'kov, Coll. Sci. Trans. Moscow Inst. Nonferrous Metals and Gold and All-Union Sci. Eng. Soc. Metallurgists 29 (1958); V. M. Glazov, V. N. Vigdorovich, and G. A. Korol'kov, Ind. Lab. 11 (1956); V. M. Glazov and G. A. Korol'kov, Metal Science and Treatment 7 (1957).

[3] A. A. Bochvar and I. I. Novikov, Coll. Sci. Trans. Moscow Inst. Nonferrous Metals and Gold and All-Union Sci. Eng. Soc. Metallurgists 23 (1952).

[4] S. T. Konobeevskii, Applications of x-Ray Analysis to Investigation of Materials [In Russian] (ONTI, People's Commissariat for the Heavy Industry, 1936); S. T. Konobeevskii, Bull. Acad. Sci. USSR, Div. Chem. Sci. 5 (1937).

INVESTIGATIONS OF THE PHYSICAL CHEMISTRY OF AGAR

3. FACTORS DETERMINING THE ELASTICOVISCOUS PROPERTIES OF AGAR GELS

S. A. Glikman and I. G. Shubtsova

The main distinction between true polymer solutions and gels is that the former have no determinable elastic limit.

In continuation of Shvedov's work [1], who showed experimentally that even very dilute gelatin solutions have rigidity at room temperature, Michaud [2] determined the minimum shearing stresses causing irreversible deformation of agar gels; for 0.05% gels this value is only 0.004 g/cm^2 , and the yield point increases very rapidly with the agar concentration: it is 0.32 g/cm^2 for 0.08% gel, 27 g/cm^2 for 0.2% gel, and 525 g/cm^2 for 0.4% gel. However, as was shown later by Duclaux and Chirata [3], even very concentrated solutions of nitrocellulose in acetone are only apparent gels, which in reality flow under any, even very small, shearing stresses.

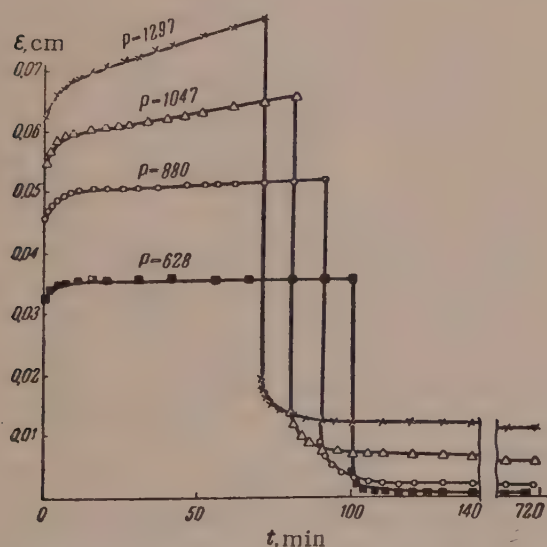


Fig. 1. Deformation kinetics of a gel from an agar fraction washed at 75°

The above values for the elastic limit of agar gels refer, of course, to one particular agar sample prepared by Michaud. Both the elastic limit and other elasto-viscous characteristics of other samples, made from different materials and by different technological processes, may differ considerably. It is known that the mechanical properties of any polymer and of systems formed by it depend primarily on the degree of polymerization if the molecules are of the same chemical nature, but if the molecules are not completely uniform in the chemical sense the number, nature, and distribution of the different monomer units in the macromolecule may have a significant influence.

The influence of sulfate ester groups and their cations in agar macromolecules was first observed by Samec and Isajevic [4]; they also found that electro-dialyzed agar is unstable to heat; this is attributed to hydrolysis of the polysaccharide in an acid medium. Fairbrother and Mastin [5] obtained free agar sulfuric acid, which had no gelating power. Hoffman and Gortner [6] showed that neutralization of agar sulfuric acid restores the gelating power, irrespective of the

cation. According to de Waele [7] and Percival [8] neither cations nor sulfate ester groups have any specific effects on the properties of agar. Pavlov and Engel'shtein [9], Gryuner and Veronyan [10], and Marshall, Newton, and Orr [11] noted that the K^+ ion gives rise to gels of higher strength than the Ca^{2+} ion. Bungenberg de Jong [12] considers that the role of sulfate ester groups in the polygalactose molecule to be that of ionogenic groups: similarly charged polymeric anions are mutually repelled, with a decrease of intermolecular cohesion; excess of cations leads to neutralization or charge reversal; the ease with which different cations are bound by the anion depends on their degree of hydration.

The data on the influence of various factors on the gelating power of agar are diverse and sometimes

TABLE 1

Elasticoviscous Characteristics of Agar Gels

Sample	Relative content of esterified units	Ratio of Ca and SO ₄ equivalents	Intrinsic viscosity $[\eta]_{\infty}$	Elasticoviscous constants				
				$E_1 \cdot 10^{-4}$ dynes/cm ²	$E_2 \cdot 10^{-4}$ dynes/cm ²	P_k dynes/cm ²	$\eta_1 \cdot 10^{-8}$ poise	$\eta_2 \cdot 10^{-8}$ poise
I. Original	1:16	0,55	1,48	3,5	16,3	1140	3,8	1,5
Fraction leached out								
at 25°	1:6	0,34	0,72	—	—	—	—	—
" 45°	1:16	0,44	0,80	—	—	—	—	—
" 60°	—	—	0,84	0,8	7,6	285	1,4	0,4
" 75°	1:34	0,68	0,96	1,9	17,2	825	1,6	1,2
" 85°	1:58	0,60	1,05	9,7	23,9	1450	4,4	1,8
" 90°	1:88	0,87	1,18	13,2	42,6	2850	4,5	2,6
II. Original	1:56	3,73	2,25	25,2	100,0	5000	22,5	7,9

contradictory; this is probably because the role of different chemical characteristics of the polymer molecules and the role of the degree of polymerization operate in conjunction. Moreover, the methods used for determination of gelating power are very diverse and usually conventional.

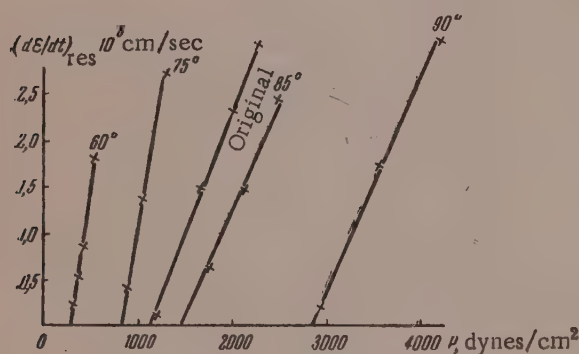


Fig. 2. Elastic limit of agar gels containing 0.5% agar and 60% sugar.

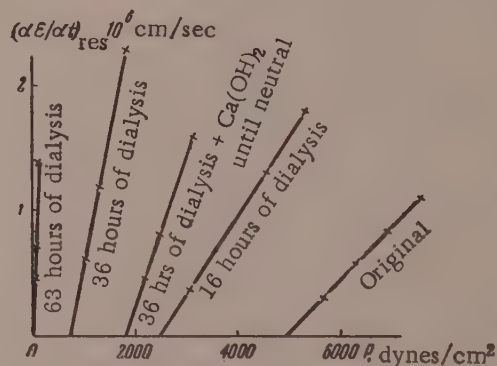


Fig. 3. Effects of dialysis and neutralization of dialyzed agar on the elastic limit of its gels.

We attempted to determine the effects of each of the three fundamental factors characterizing the nature of the agar polyelectrolyte: degree of polymerization and the relative contents of sulfate ester groups and calcium ions, on the elasticoviscous constants of agar gels which have a definite physical meaning. The materials used for the investigations were samples of Japanese agar (Sample I) [13] and Far Eastern agar (Sample II), freed from metal cations to different extents by the electrodialysis or by the action of hydrochloric acid.

The elasticoviscous constants of agar gels were determined by the method of tangential displacement of a plate, developed by Rebinder and Veiler [14]. Since aqueous agar gels are elasticobrittle bodies which readily undergo syneresis, as was noted earlier by Rebinder, Shal't, and Markovich [15], for comparison of the elastico-plastic properties of different agar samples we used gels containing sugar, so that it was possible to plot complete rheological curves at shearing stresses above the elastic limit (P_k). The experiments showed that the mechanical properties of gels containing 0.5% agar, 60% sugar, and 39.5% water remain virtually constant for several days

TABLE 2

Effects of Dialysis and Neutralization of Agar on Its Elasticoviscous Properties

Duration of dialysis, hours	% contents		η_{Sp} of 0.1% solution	$E_1 \cdot 10^{-5}$ dynes/ cm ²	$E_2 \cdot 10^{-5}$ dynes/ cm ²	P_k dynes/ cm ²	$\eta_1 \cdot 10^{-9}$ poises
	SO ₄	Ca					
0	1,060	1,640	3,50	2,5	11,1	5000	2,20
16	0,596	0,414	2,00	1,5	6,2	2500	1,50
36	0,592	0,250	1,25	0,6	1,6	750	0,45
63	0,587	0,021	0,82	0,01	0,04	18	0,02
36*	0,592	0,350	1,45	1,1	3,3	1800	0,79

* Neutralized before being dissolved.

after an initial aging period of 12 hours, if evaporation of moisture from them is prevented by a thin covering of mineral oil.

As an example, curves showing the deformation kinetics of a gel made from one of the fractions are given in Fig. 1. The constants were calculated in the usual way. However, as in the case of ethylcellulose gels [16], the deformation due to configurational elasticity in agar gels was proportional to the shearing stress only at stresses not exceeding the elastic limit, and was almost constant at stresses above P_k . The values were determined graphically by the method described by Rebinder and Segalova [17].

Fractions leached out at 25 and 45° did not give well-defined gels. Our method of investigation was not sensitive enough for determination of the elastic properties of their gelatinous solutions. However, it follows from Table 1 and Fig. 2 that the elasticoviscous constants of fractions extracted at 60° and over increase progressively with increase of intrinsic viscosity, but in contrast to $[\eta]_{\infty}$ for the original sample, which is higher than $[\eta]_{\infty}$ for any of the fractions (as was noted in our previous communication [13]), the elasticoviscous characteristics of the gel from the original samples are intermediate between the constants for fractions leached out at 75 and 85°.

The progressive increase of the elasticoviscous properties of the fractions and the higher values of the constants for Sample II as compared with Sample I are probably due to an increase of the number of intermolecular bonds and of the energy of these bonds. Both effects should occur with increase of chain length, with decrease of the number of sulfate ester groups, and with increased substitution of their hydrogens by bivalent calcium ions. These are the factors which determine the consecutive extraction of the fractions at increasing temperatures. The role of these factors consists of the following:

- the degree of polymerization has the same significance as in the fractionation of other high polymers;
- the presence of sulfate ester groups, solvated and ionized in aqueous solutions, weakens the mutual attraction of the polymer molecules, because of the repulsion of similarly charged anionic groups; the steric factor may also be significant;
- calcium ions strengthen the gel structure by formation of intermolecular bridges.

The properties of the free agar acid, without metal cations, were studied in experiments on the electro-dialysis of agar (Sample II).

It follows from the data in Table 2 and Fig. 3 that the SO₄ content which falls sharply during the first hours of dialysis (probably because of leaching of the low-molecular fractions, with high contents of sulfate ester groups and cations), remains almost constant during the subsequent dialysis. Investigation of solutions prepared from these dialyzed samples by the usual method at 100° showed that their viscosity and gelating power decrease with progressive removal of metal cations from the agar, i. e., with increasing acidity, which on heating leads to hydrolysis of the polyelectrolyte molecules. This effect is irreversible, and therefore subsequent neutralization of the free agar acid by alkali did not restore the original properties even partially.

Different results were obtained when agar samples swollen during dialysis were treated with bases and only then dissolved in the usual way on heating. In such cases, as Table 2 shows, the solution viscosities and elasticoviscous constants of the gels were considerable higher.

Since heating is required for preparation of agar solutions, it was not possible to study the properties of solutions and gels of undegraded agar acid. However, the parallel decrease of gelating power and intrinsic viscosity, which is a function of the weight-average molecular weight, at constant content of sulfate ester groups is itself a direct indication that the principal factor determining the elasticoviscous properties of agar gels is the degree of polymerization of the polyelectrolyte molecules, while the relative sulfate-ester group contents and the nature of their substitution are of additional significance.

SUMMARY

1. Higher elasticoviscous characteristics of sugar - agar gels correspond to higher intrinsic viscosities of the agar fractions, lower SO_4 contents, and higher $\text{Ca} : \text{SO}_4$ ratios.
2. In samples freed by electrodialysis from metal cations, with equal contents of sulfate ester groups, the gelating power varies in parallel with the intrinsic viscosity.
3. The principal factor determining the gelating power of agar is the degree of polymerization of the polyelectrolyte molecules. The presence of ionizable sulfate ester groups leads to some weakening of the intermolecular bonds owing to electrostatic repulsion of the anions and to steric hindrances; the calcium ions in these groups aid the formation of bridge bonds.

The N. G. Chernyshevskii State University, Saratov

Received March 6, 1958

LITERATURE CITED

- [1] F. M. Shvedov, *J. de Phys.* 8, 341 (1889).
- [2] M. Michaud, *Ann. Phys.* 19, 63 (1923).
- [3] J. Duclaux and F. Chirata, *J. Chem. Phys.* 28, 537 (1931).
- [4] M. Samec and V. Isajevic, *Kolloidchem. Beih.* 16, 285 (1922).
- [5] F. Fairbrother and H. Mastin, *J. Chem. Soc.* 123, 1412 (1923).
- [6] W. Hoffman and R. Gortner, *J. Biol. Chem.* 65, 371 (1925).
- [7] H. De Waele, *Ann. Physiol. Physicochem. Biol.* 5, 876 (1929).
- [8] E. G. V. Percival, J. C. Somerville and I. A. Forbes, *Nature*, 142, 797 (1938).
- [9] P. N. Pavlov and M. A. Éngel'shtein *Colloid J.* 2, 821 (1936).
- [10] V. P. Gryuner and L. V. Veronyan, *Colloid J.* 5, 851 (1939).
- [11] S. M. Marshall, L. Newton, and A. P. Orr, *A Study of Certain British Seaweeds* (London, 1949).
- [12] H. Bungenberg de Jong and H. Kruyt, *Colloid Sci.* 2, 259 (1949).
- [13] S. A. Glikman and I. G. Shubtsova, *Colloid J.* 19, 281 (1957).*
- [14] S. Ya. Veiler and P. A. Rebinder, *Proc. Acad. Sci. USSR* 49, 354 (1945).
- [15] P. A. Rebinder, S. Ya. Shal't and V. É. Markovich, *Bull. Moscow Chem. Tech. Inst.* (1948).
- [16] S. A. Glikman and O. G. Efremova, *Proc. Acad. Sci. USSR* 81, 1089 (1951).
- [17] P. A. Rebinder and E. E. Segalova, *Proc. Acad. Sci. USSR* 71, 85 (1950).

*Original Russian pagination. See C. B. Translation.

THERMODYNAMICS OF IRREVERSIBLE PROCESSES AND ELECTROOSMOTIC TRANSFER IN DISPERSE SYSTEMS

M. N. Gol'dshtein

The flow of heat and electricity through colloidal substances, filtration of liquids, diffusion — in fact, all processes which can be generally described as transfer phenomena — are characterized by interdependence and interaction. The interaction which has been studied most in colloid chemistry is that between electric current and liquid filtration, which lies in the field of electrokinetic effects.

Particularly important advances in studies of these effects have been achieved in recent years. The extensive experimental investigations of the Zhukov school were recently summarized in a detailed monograph [1]. A large contribution was made by Mazur and Overbeek [2], who introduced thermodynamic methods into theoretical studies of these effects.

As is known, it is assumed in the thermodynamics of irreversible processes that any effects (J_{ik}) which may be described as "generalized velocities" and which are induced by the action of a certain cause, described conventionally as a "thermodynamic force" (X_k), are linear functions of the latter

$$J_{ik} = L_{ik} \cdot X_k, \quad (1)$$

where L_{ik} is a proportionality factor [3].

The existence of this linear relationship allows of the extensive use of linear algebra and the well-known methods of the theory of linearly variable systems, in which quantities analogous to J_{ik} are termed "generalized displacements," and those analogous to X_k as "generalized forces." In the thermodynamics of Irreversible processes the term "generalized direction" is taken to mean a particular kind of effect or process caused by a given generalized force (Gol'dshtein [3]).

In presence of k different generalized forces the total generalized velocity in direction i is determined by the so-called canonical equation

$$J_i = \sum_{i,k} L_{ik} X_k. \quad (2)$$

We shall refer to the term $L_{ii}X_i$ in this sum as the principal term, and $L_{ik}X_k$ are described as the subsidiary terms. Correspondingly the coefficients L_{ii} are principal, and L_{ik} are subsidiary.

If it is assumed that in Equation (1) $X_k = 1$, it is clear that the coefficient L_{ik} is none other than the generalized velocity at a generalized unit force; we shall term these coefficients the specific velocities.

The characteristic feature of the principal velocity is that of all the kinds of effects induced by the generalized force it alone always takes place when this force acts, whereas the subsidiary velocities may be absent under particular conditions. If, for example, the generalized force is a pressure difference, then the principal generalized velocity is liquid flow, while a subsidiary velocity is electric current (streaming potential). If the generalized force is a potential difference, then the principal generalized velocity is electric current, while liquid flow (electroosmosis) is subsidiary. It is important to note that subsidiary velocities arise as the result of changes induced in the system by principal velocities.

One of the basic principles of the thermodynamics of irreversible processes, the so-called mutuality relationship established by Onsager

$$L_{ik} = L_{ki}, \quad (3)$$

can be formulated as follows in the terminology adopted here: "the specific velocity induced by the generalized force $X_k = 1$ in the direction of the generalized force X_i is equal to the specific velocity induced by the generalized force $X_i = 1$ in the direction of the generalized force X_k ."

For a nonequilibrium system in the steady state the products of the generalized forces and the velocities in the corresponding directions have the following characteristic: the sum of all these products for a given system is equal to the rate of entropy increase per unit volume of the system, multiplied by the temperature T :

$$T\theta = \sum_i J_{ik} X_i \quad (4)$$

or, with Equation (1) taken into account

$$T\theta = \sum_{i,k} L_{ik} X_k X_i, \quad (5)$$

i. e., the rate of entropy increase is a homogeneous quadratic function of the generalized forces.

It is important to bear in mind Denbigh's comment [4] that the linearity of the relationship between generalized forces and displacements should be verified experimentally in each individual case.

The very careful experiments of Manegold and Solf [5] on electroosmosis were performed with thin collodion membranes only. However, recently there has been a great increase of interest in electroosmotic effects in clay soils in connection with a number of successful industrial trials of this method for soil drying. The engineers who carried out these trials observed effects in contradiction to Equations (2) and (3). For example, B. S. Fedorov found that when an electric field is applied to a soil the filtration permeability of the latter increases significantly.

It follows that the sum of the electroosmotic and filtrational flows resulting from separate applications of current and pressure is not equal to the flow under the simultaneous action of current and pressure of the same magnitude [6].

Consider the case in which a liquid present in the pores of a diaphragm of thickness l separating two compartments of an electroosmometer is subjected simultaneously to an electric potential difference $\Delta\varphi$ and a hydraulic pressure difference ΔP . The potential difference causes flow of electric current and electroosmotic flow of the liquid. The hydraulic pressure difference causes filtrational flow of the liquid, and flow of electric current as the result of electrokinetic streaming potential (transfer current).

In this case the rate of entropy increase is the sum of the products of the filtration flow and flow of electricity, and the corresponding generalized forces.

The generalized forces are taken to be the potential gradient

$$U = \Delta\varphi/l \quad (6)$$

and the hydraulic gradient

$$H = \Delta P/l. \quad (7)$$

Accordingly, we must take the filtration rate v and the current density i as the generalized velocities.

The canonical Equations (2) then become

$$\begin{aligned} L_{11}H + L_{12}U &= v; \\ L_{21}H + L_{22}U &= i. \end{aligned} \quad (8)$$

The principal specific velocity L_{11} is known in hydraulics as the filtration coefficient, while the principal specific velocity L_{22} is none other than conductance. At $H = 0$, the first of the two Equations (8) gives

$$L_{12}U = v, \quad (9)$$

the rate of electroosmotic migration of the liquid through the diaphragm, and therefore the subsidiary specific velocity L_{12} , is the quantity of water transferred by electroosmosis through unit section of the diaphragm at unit potential gradient. This coefficient is essentially the known coefficient in the Helmholtz - Smoluchowski equation, which includes the zeta potential, the dielectric constant (D), and the viscosity of water (η). It should be

noted that there are as yet no reliable methods for direct determinations of all these quantities within the double layer and therefore the introduction in their place of the single coefficient L_{12} (known as the coefficient of electroosmosis [7], and easily determined by experiment) is very convenient in practice.

The specific subsidiary velocity L_{21} is the density of the electric current caused by filtration of water through the diaphragm at unit hydraulic gradient. It is therefore none other than the transfer-current density.

By the Onsager rule

$$L_{12} = L_{21}, \quad (10)$$

i. e., the transfer-current density at $H = 1$ is numerically equal to the electroosmotic velocity at $U = 1$.

Solving Equations (8) for H and U , we have:

$$K_{11}v + K_{12}i = H; \quad K_{21}v + K_{22}i = U, \quad (11)$$

where

$$K_{11} = \frac{L_{22}}{L_{11}L_{22} - L_{12}L_{21}}; \quad K_{22} = \frac{L_{11}}{L_{11}L_{22} - L_{12}L_{21}}; \quad K_{12} = K_{21} = -\frac{L_{12}}{L_{11}L_{22} - L_{12}L_{21}}. \quad (12)$$

When $v = 0$, i. e., when no water flows through the diaphragm, we find the pressure gradient, from the first equation in the system (11),

$$H = K_{12}i, \quad (13)$$

which can counterbalance and stop the electroosmotic flow of water produced by current of density i .

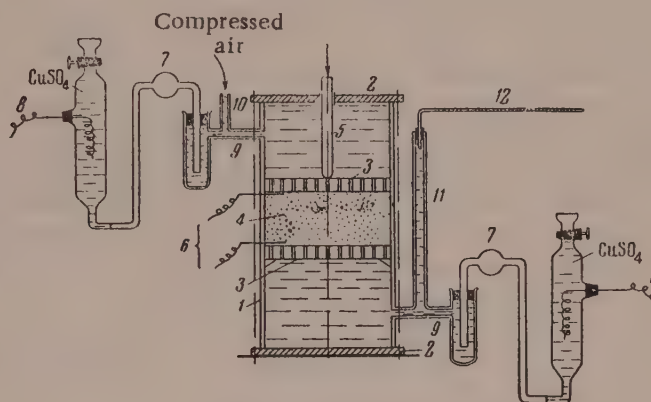


Fig. 1. Electrosmometer

This value can be conveniently described as the electroosmotic gradient. The coefficient K_{12} is unit electroosmotic gradient (when $i = 1$).

When $i = 0$, we have from the second equation in the system (11)

$$U = K_{21}v. \quad (14)$$

Therefore, $K_{21} = K_{12}$ should be regarded as the flow-potential gradient at water filtration velocity $v = 1$. Negative sign of K_{12} and K_{21} in Equation (14) indicates that the direction of the electroosmotic gradient and of the flow-potential gradient is countercurrent to the applied external generalized forces H and U .

The appearance of an electroosmotic-pressure gradient countercurrent in direction during gravitational filtration is the cause of "electrokinetic retardation" of filtration, which was formerly attributed wrongly to an increase in the viscosity of water in fine capillaries [8].

Canonical equations covering a wider range of transfer effects should be of the form:

$$\begin{aligned}
L_{11}H + L_{12}U + L_{13}C + L_{14}Q + L_{15}W + L_{16}D &= v; \\
L_{21}H + L_{22}U + L_{23}C + L_{24}Q + L_{25}W + L_{26}D &= i; \\
L_{31}H + L_{32}U + L_{33}C + L_{34}Q + L_{35}W + L_{36}D &= c; \\
L_{41}H + L_{42}U + L_{43}C + L_{44}Q + L_{45}W + L_{46}D &= q; \\
L_{51}H + L_{52}U + L_{53}C + L_{54}Q + L_{55}W + L_{56}D &= w; \\
L_{61}H + L_{62}U + L_{63}C + L_{64}Q + L_{65}W + L_{66}D &= d,
\end{aligned} \tag{15}$$

where C, Q, W, and D are the concentration, temperature, humidity, and double-layer potential gradients across the diaphragm, and c, q, w, and d are the velocities in the directions of the generalized forces represented by the corresponding capital letters.

The principal specific velocities L_{33} , L_{44} , L_{55} and L_{66} are, respectively, the coefficients of diffusion, heat conductivity, moisture conductivity, and "ionic conductivity of the diffuse layer" (we propose this last term for the rate of ion migration along the diffuse layer at unit potential gradient of the double layer across the diaphragm, i. e., the corresponding current density).

According to the Onsager rule, the subsidiary specific velocities, symmetrical about the diagonal, are respectively equal: $L_{12} = L_{21}$; $L_{31} = L_{13}$; $L_{32} = L_{23}$; $L_{14} = L_{41}$ etc.

These subsidiary coefficients take into account such phenomena as the Soret effect (thermal diffusion), the Dufour effect (the appearance of a temperature difference as the result of diffusion of the components), the thermoosmotic effect ($L_{14}Q$, displacement of water in presence of a temperature difference), etc. The term $L_{23}C$ determines the electric current which arises as the result of the concentration gradient, and $L_{13}C$ represents osmotic flow of liquid.

To test experimentally the applicability of the linear relationships of the thermodynamics of irreversible processes to electroosmosis in clay soils, we designed a special electroosmometer, shown schematically in Fig. 1. It consists of a Plexiglas cylinder 1, with detachable ends 2, attached by bolts. A lower perforated Plexiglas disk 3 can be fitted in the cylinder on special supports; this acts as a support for the diaphragm 4 of disperse material, 7 cm in diameter and 3.2 cm high. A similar upper perforated disk acts as a piston for subjecting the diaphragm to different pressures, transmitted through the rod 5. The calomel electrodes 6, marked conventionally on the diagram, are used for measurement of the streaming potential. The upper and lower compartments of the apparatus are connected to agar bridges 7. The electrodes 8 are copper, in CuSO_4 solution. The tubes 9 connecting the compartments to the bridges have side tubes 10 and 11 for removal of filtrate; they are also used for transmission of pressure to the water, by means of compressed air. The agar bridges, designed by É. M. Gutman, allow a high pressure to be set up in the system without hindrance. The liquid flow rate is measured by means of the capillary 12. Two VSA-5 selenium rectifiers in series serve as the source of potential.

Clay soils of different mineral compositions were used as the diaphragm materials: montmorillonite, illite, and kaolinite clays and a dusty loam.

The potential gradient varied from 0.1 to 1.5 v/cm, and the hydraulic-pressure gradient from 50 to 150. The latter was created either by means of compressed air, or by Argunov's vacuum method [9].

In the first series of experiments, in which the flow rate was determined from the amount of water flowing from the apparatus into a measuring vessel in 5 minutes, the results were very inconsistent; in some cases the total and simultaneous transfers were equal, while in others either one or the other was greater. Nevertheless, the simultaneous transfer was more often greater than the total (additive) transfer; this seemed to be consistent with Fedorov's observations.

However, the lack of proportionality between electroosmotic transfer and the potential gradient gave rise to considerable doubts. Thus, with a 5-fold increase of potential gradient (from 0.1 to 0.5 v/cm) the transfer increased between 1.1 and 4.6-fold, whereas with an increase of potential gradient from 0.5 to 1.0 v, i. e., a twofold increase, the transfer increased 1.2 to 4.6-fold.

A special experiment, in which the transfer was measured continuously every 15 minutes for 3 hours, and then every 30 minutes for 23 hours more, showed considerable fluctuations in the amounts of transfer, but with a consistent decrease.

All this suggests that when the current is passed the soil undergoes intensive physicochemical changes which influence its electrokinetic properties.

Soil	w %	τ^* hours	H	U v/cm	i ma/cm ²	v_f^{**} cm/sec	v_e^{***}	$v_f + v_e$	v_{f+e}^{****}
Montmorillonite clay	75,6	0	118	0,32	0,11	1,95	1,00	2,95	2,96
The same	75,6	19	122	0,60	0,26	1,69	2,04	3,73	3,72
" "	75,6	46,5	125	0,56	0,38	2,16	2,73	4,89	4,85
Illite clay	49,4	0	125	0,31	0,21	4,89	3,54	8,43	8,56
The same	49,4	49,5	125	1,0	0,78	32,90	19,0	51,9	51,1
" "	46,1	7,5	116	0,60	0,28	2,90	5,32	8,22	8,19
" "	46,1	9,5	114	0,62	0,29	3,08	5,28	8,36	8,36
Kaolinite clay	28	5	65,7	0,92	0,156	11,50	9,93	21,43	21,40
Dusty loam	23,5	7,5	106	0,59	0,22	11,80	4,33	16,13	16,21
The same	23,5	22,5	69	0,59	0,35	6,49	4,68	11,17	11,17

* τ is the time during which the current was passed through the diaphragm before the determinations were started.

** v_f is the rate of filtration through the diaphragm under hydraulic pressure in absence of current; multiplied by 10^6 .

*** v_e is the filtration rate under influence of the current in absence of pressure; multiplied by 10^6 .

**** v_{f+e} is the flow rate of the liquid through the diaphragm under the simultaneous influence of the same hydraulic pressure and electric current as in the separate determinations of v_f and v_e ; multiplied by 10^6 .

For greater accuracy, we then measured transfer by means of a capillary with divisions equivalent to 0.002 ml at 20°, so that observations could be made over short periods not exceeding 100 seconds, during which the properties of the soil could not undergo significant changes. The results are given in the table.

It is clear from the table that at any given instant the condition

$$v_f + v_e = v_{f+e} \quad (16)$$

is exactly satisfied. However, the quantities in Equation (16) vary continuously with time, but in such a way that equality is maintained.

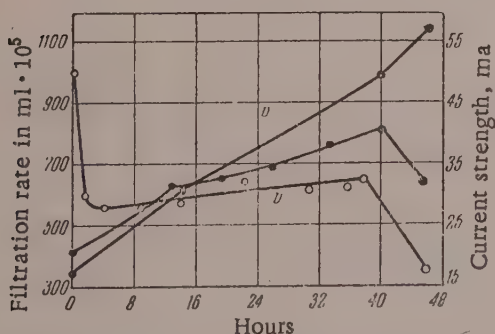


Fig. 2. Results of an experiment with montmorillonite clay.

The curves in Fig. 2 show the variations of the parameters in one experiment with a diaphragm of montmorillonite clay. It is clear from Fig. 2 that the effect of the flow of current on the properties of the clay is to increase the filtration coefficient continuously; the rate of electroosmosis also changes.

The changes taking place in the diaphragm during the experiment may be either physicochemical, or structuomechanical. The physicochemical changes include: ion-exchange and other processes taking place in the double layer and changing its potential, changes in the solution concentrations on each side of the diaphragm, effects of electrolysis processes, irregular heating of the diaphragm, the formation of a moisture gradient in the diaphragm, etc. The structuomechanical changes include: irregular packing of the diaphragm

under the influence of electrophoretic forces, particle dispersion or aggregation, the appearance of micro- and macrocracks as the result of irregular shrinkage of the diaphragm, etc.

However, despite the fact that some of these changes are nonlinear, Expressions (2) and (3) are valid at any given instant, although the specific generalized velocities change during the experiment. Expression (5) is then evidently no longer valid.

SUMMARY

1. The applicability of the principles of the thermodynamics of irreversible processes to electroosmotic effects in clays has been verified experimentally.
2. An electroosmometer of novel design is described, suitable for compression of clay soils in the course of the experiment. Pressure filtration and electroosmosis can be effected simultaneously in the instrument.
3. Despite the continuous variations of the filtration and electroosmotic coefficients caused by the flow of current, the sum of the electroosmotic and filtrational transfers at any instant is equal to the transfer caused by the simultaneous action of electric current and hydraulic pressure (of the same magnitudes).
4. The diaphragm material undergoes physicochemical and structural changes, which may lead to non-linearity of the process during electroosmosis. Despite this, the mutuality relationship continues to hold at any instant, although Onsager's law of entropy increase breaks down.

In conclusion, the author expresses his gratitude to É. M. Gutman who carried out the actual determinations, and to A. G. Kutepov for his careful construction of the electroosmometer.

The Dnepropetrovsk Institute of Transport Engineers

Received November 14, 1957

LITERATURE CITED

- [1] O. N. Grigorov (editor), *Electrokinetic Properties of Capillary Systems* (Izd. AN SSSR, 1956). [In Russian]
- [2] R. Mazur and J. Overbeek, *Recueil Trav. Chim.* 70, 83 (1951).
- [3] L. Onsager, *Phys. Rev.* 37, 405 (1931); 38, 2265 (1931); M. N. Gol'dshtein, *J. Phys. Chem.* 32, 2219 (1958).
- [4] K. Denbigh, *The Thermodynamics of the Steady State* (1951).
- [5] E. Manegold and K. Solf, *Kolloid. Z.* 55, 273 (1931).
- [6] G. M. Lomise and A. V. Netushil, *Hydrotechnical Construction* 3, 26 (1956).
- [7] B. F. Rel'tov and A. V. Novikov, *Bull. All-Union Inst. Hydrotech.* 28, 239 (1940).
- [8] G. Elton, *Proc. Roy. Soc. (London)*, A 194, 259 (1948).
- [9] P. P. Argunov, *Trans. Sci. Res. Inst. Substructures and Foundations*, 11, 63 (1948).

THE ELECTRICAL FIELD ON A MOVING DROP*

1. THE THEORY OF THE ELECTRICAL FIELD OF A DROP CONTAINING AN IONOGENIC SURFACE-ACTIVE SUBSTANCE**

S. S. Dukhin and B. V. Deryagin

There have been many studies of the electrical properties of drops, and especially of drops suspended in air. It is usually assumed that the electrical field of a drop is due to its electrification either by ions present in the air, or by ions in the liquid. It is shown in this paper that even in absence of excess charge an appreciable electrical field is formed both within and outside a drop moving relative to a surrounding medium which ensures mobility of the drop surface.

The direct cause for the formation of an electric field of a drop*** containing an ionogenic surface-active substance lies in local deviations from electroneutrality in the mobile surface of the drop****, arising because of excess surface adsorption of ions of either sign.

However, it is not necessary to examine and study quantitatively the excess surface charges in order to elucidate the causes of nonequivalence of surface concentrations of positive and negative ions, or even to calculate the electrical field. On the contrary, it is convenient to take into account the fact (confirmed below) that surface deviations from electroneutrality may be relatively small, i. e., that the fraction of adsorbed ions the electric field of which is not compensated by ions of opposite sign is small.

If this fact is taken into account, the mechanism whereby an electrical field arises near the mobile surface of a drop which has adsorbed an ionogenic surface-active substance***** is revealed by consideration of the continuity relationships for the flow of ions at the surface. Let Γ^+ and Γ^- be the adsorptions of positive and negative ions, and v_t the liquid velocity at the drop surface. The motion of the drop surface is accompanied by convective transfer of adsorbed positive and negative ions, the surface flow densities of which are Γ^+v_t and Γ^-v_t respectively. It is easy to see that the surface divergences of these flows differ from zero. Nevertheless,

*Paper presented at the IVth All-Union Conference on Colloid Chemistry in Tbilisi, May, 1958.

**The effect under consideration is observed not only in presence of characteristic ionogenic surface-active substances such as colloidal electrolytes, since, as will be shown in this paper, the magnitude of the electrical field is determined by the ratio of adsorption to volume concentration of the ions; this ratio may be fairly large even at low surface concentrations of the ions.

***In addition to the factors causing the electric field which are considered in this paper, factors examined by Natanson [1] also lead to electrification of drops. In order to examine the effects with which we are concerned separately from those considered by Natanson [1], we shall assume that the total charge of the drop is zero.

****The drop as a whole being electrically neutral.

*****The formation of an electrical field in the motion of a liquid interface was first observed by Frumkin and Levich [2, 3] in the case of a mercury drop falling through an electrolyte solution. It was necessary to take into account the adsorption of only one kind of ions, since it was possible to take into account only migration of ions in the electrical field, and diffusion had to be disregarded. In the effect under consideration adsorption of two kinds of ions must be taken into account, and the difference between the diffusion coefficients of the ions becomes the principal factor determining the magnitude and direction of the electrical field in question.

under steady-state conditions the surface ionic densities should remain constant. Therefore, the difference between the access and loss of ions in each region of the surface, caused by convective surface flow, must be balanced by the corresponding normal component of the volume flow of ions, j_n^+ or j_n^- , which in this case plays the role of a source or escape of ions in surface convective flow. It must be emphasized that equality of the flows of positive and negative ions, j_n^+ and j_n^- , ensures that the surface is close to electroneutrality. However, since the diffusion coefficients of the ions are different, j_n^+ and j_n^- can be approximately equalized only by the action of the electrical field directed in such a manner that the total flow of rapidly diffusing ions to the surface decreases, and that of slowly-diffusing ions increases, so that j_n^+ and j_n^- are equalized and the surface is approximately electroneutral. Thus, approximate electroneutrality of the surface is ensured by small deviations of the surface from electroneutrality. This effect is characterized by a peculiar interconnection of the diffusion process with the electrical field, and it can be described as diffusional-electric.

It follows from the foregoing that consideration of this effect must be based on equations which represent the ionic balance at the surface

$$\operatorname{div}_s (\Gamma^+ v_t) = j_n^+, \quad (1)$$

$$\operatorname{div}_s (\Gamma^- v_t) = j_n^-. \quad (2)$$

The normal components of the ion flows, j_n^+ and j_n^- , are due to the migration of ions in the electrical field and to their diffusion, so that writing the right-hand sides of Equations (1) and (2) in full we have

$$\left(-D^+ \frac{\partial c^+}{\partial r} + \frac{F}{RT} D^+ z^+ c^+ E_{1r} \right)_a = \operatorname{div}_s \Gamma^+ v_t; \quad (3)$$

$$\left(-D^- \frac{\partial c^-}{\partial r} - \frac{F}{RT} D^- z^- c^- E_{1r} \right)_a = \operatorname{div}_s \Gamma^- v_t, \quad (4)$$

where E_1 is the strength of the electrical field in the drop; F is the Faraday number; T is the absolute temperature; R is the universal gas constant; c^+ and c^- , D^+ and D^- , and z^+ and z^- are respectively the concentrations (in moles/cc), diffusion coefficients, and electrovalences of the positive and negative ions in a binary electrolyte; a is the drop radius.

The continuity equations determining the potential and ion distribution in the volume of a binary electrolyte during the passage of a steady current have been considered earlier [3]:

$$\vec{v} \operatorname{grad} c^+ = D^+ \Delta c^+ + \frac{F}{RT} D^+ z^+ \operatorname{div} (c^+ \vec{E}_1), \quad (5)$$

$$\vec{v} \operatorname{grad} c^- = D^- \Delta c^- - \frac{F}{RT} D^- z^- \operatorname{div} (c^- \vec{E}_1). \quad (6)$$

The principal simplifying factor is the assumption of electroneutrality

$$z^+ c^+ - z^- c^- = 0. \quad (7)$$

The same condition must hold for adsorption

$$z^+ \Gamma^+ - z^- \Gamma^- = 0. \quad (8)$$

Using equations (7) and (8), it is convenient to introduce the volume molar concentration \underline{c} and the surface molar adsorption Γ

$$c = \frac{c^+}{z^+} = \frac{c^-}{z^-}; \quad \Gamma = \frac{\Gamma^+}{z^+} = \frac{\Gamma^-}{z^-}.$$

Eliminating E_{1r} (a, θ) from Equations (3) and (4) and using Equations (7) and (8), we find the boundary conditions for determination of c (r, θ)

$$\frac{\partial c}{\partial r} (a, \theta) = \frac{1}{D_{eff}} \operatorname{div} (\Gamma v_t). \quad (9)$$

Equations (5) and (6) under Condition (7) take the form

$$\vec{v} \operatorname{grad} c = D_{eff} \Delta c. \quad (10)$$

$$\frac{F}{RT} (z^+ D^+ + z^- D^-) c \vec{E}_1 + (D^+ - D^-) \text{grad } c = \frac{\vec{i}}{F z^+ z^-}, \quad (11)$$

where $D_{\text{eff}} = \frac{D^+ D^- (z^+ + z^-)}{z^+ D^+ + z^- D^-}$; \vec{v} is the velocity distribution; \vec{i} is the total electric current. Therefore, for determination of the electrical field first within and then outside the drop it is first necessary to solve Equation (10) for convective diffusion, and then to use Equation (11) to find \vec{E}_1 ; the latter also requires a knowledge of the total current distribution $\vec{i}(r, \theta)$.

We use Equations (1) and (2) to show that with total electroneutrality of the drop surface (Equation 8) the normal component of the density of the total current at the surface is zero

$$i_n = i_n^+ - i_n^- = z^+ e j_n^+ - z^- e j_n^- = \text{div}_s [(z^+ \Gamma^+ - z^- \Gamma^-) e v_t] = 0. \quad (12)$$

To confirm that in this instance the density of the total current is everywhere zero, we transform Equation (11) into

$$\vec{i}(r, \theta) = c(r, \theta) \text{grad } \phi(r, \theta), \quad (13)$$

$$\text{where } \phi(r, \theta) = F z^+ z^- \left[\frac{F}{RT} (z^+ D^+ + z^- D^-) \varphi(r, \theta) + (D^+ - D^-) \ln c(r, \theta) \right]. \quad (14)$$

We express in terms of ψ the continuity equation for the total current $\text{div } \vec{i} = 0$ and the boundary condition at the drop surface, which is easily derived from Equations (11) and (12) if it is taken into account that $c(a, \theta) \neq 0$.

$$\text{div} [c(r, \theta) \text{grad } \phi(r, \theta)] = 0, \quad \frac{\partial \phi}{\partial r}(a, \theta) = 0.$$

The fact that the problem so formulated has only the trivial solution $\psi(r, \theta) = \text{const}$, can be demonstrated, for example, by the method of thermal analogies.

The analogous thermal problem

$$\text{div} [\lambda(r, \theta) \text{grad } T(r, \theta)] = 0, \quad \frac{\partial T}{\partial r}(a, \theta) = 0,$$

where $T(r, \theta)$ is the temperature field; $\lambda(r, \theta)$ is the coefficient of thermal conductivity varying from point to point, can be formulated as follows. It is required to find the steady-state thermal field within a sphere (or any enclosed volume) which does not contain volume sources of heat and which is ideally insulated externally. Since there are no heat sources either in the sphere or at its surface, it is clear that there are no heat flows in such a system: $T(r, \theta) = \text{const}$; this leads to Equation (14), and finally we have

$$\vec{i}(r, \theta) = 0. \quad (15)$$

Taking (15) into account, we transform Equation (11)

$$\vec{E}_1 = \frac{RT}{F} \frac{D^+ - D^-}{z^+ D^+ + z^- D^-} \frac{\text{grad } c}{c}. \quad (16)$$

It is easy to see that the potential distribution $\varphi_1(r, \theta)$ within the drop is expressed as follows:

$$\varphi_1(r, \theta) = \frac{RT}{F} \frac{D^+ - D^-}{z^+ D^+ + z^- D^-} \ln \frac{c}{c_0} + \varphi_0, \quad (17)$$

where φ_0 is the potential of the region of the drop where $c = c_0$.

In determination of the external electrical field of the drop we disregard ionization of the air, and therefore the potential distribution $\varphi_2(r, \theta)$ in the air must satisfy the Laplace equation

$$\Delta \varphi_2 = 0. \quad (18)$$

The potential difference at the drop surface is assumed to be independent of the angle δV which corresponds to fairly low values of adsorption, which do not cause appreciable variations of the potential difference*

$$\varphi_2(a, \theta) - \varphi_1(a, \theta) = \delta V. \quad (19)$$

* This theory can be easily extended to high concentrations of the surface-active substance, when changes of the potential difference along its surface, and the retarding effect of the surface-active substance on it should be taken into consideration. This case is not considered, being less interesting, as the electrical field diminishes upon retardation of the surface.

Expressing $\varphi_1(a, \theta)$ with the aid of Equation (17) and assuming $\varphi_0 = -\delta V$ which ensures zero potential at infinity

$$\varphi_2|_{r \rightarrow \infty} = 0, \quad (20)$$

we find the boundary conditions for the potential distribution in air near the drop

$$\varphi_2(a, 0) = \frac{RT}{F} \frac{D^+ - D^-}{z^+ D^+ + z^- D^-} \ln \frac{c(a, 0)}{c_0}. \quad (21)$$

We now estimate the deviations from electroneutrality within the electrolyte and at the drop surface. The deviation from electroneutrality within the volume, characterized by the quantity $z^+ c^+ - z^- c^-$, is easily estimated by means of the Poisson equation

$$\operatorname{div} \vec{E}_1 = -\frac{4\pi}{\varepsilon} (z^+ c^+ - z^- c^-) F, \quad (22)$$

and hence $\lambda = z^+ c^+ - z^- c^- = \frac{\varepsilon}{4\pi F} \operatorname{div} \vec{E}_1$.

Substitution of the value of \vec{E}_1 in accordance with Equation (16) gives:

$$z^+ c^+ - z^- c^- \sim \frac{\varepsilon}{4\pi} \frac{RT}{F^2} \frac{D^+ - D^-}{z^+ D^+ + z^- D^-} \frac{\delta c}{c_0} \frac{1}{a^2} \sim 10^{-15} \frac{\delta c}{c_0} \frac{1}{a^2} \text{ mole/liter}. \quad (23)$$

Even if we assume that $a \sim 10^{-4}$ cm $\delta c / c_0 \sim 1$, we have $z^+ c^+ - z^- c^- \sim 10^{-7}$ g · mole/liter i.e., Condition (7) holds even at every low ionic concentrations.

To estimate the deviation from electroneutrality at the drop surface, we express j_n^+ and j_n^- in terms of $\partial c^+ / \partial r$ and $\partial c^- / \partial r$ only; for this, we substitute Equation (16) into Equations (2) and (3)

$$\operatorname{div}_s (I^+ v_t) = j_n^+ = D_{\text{eff}} \frac{\partial c^+}{\partial r}; \quad (24)$$

$$\operatorname{div}_s (I^- v_t) = j_n^- = D_{\text{eff}} \frac{\partial c^-}{\partial r}. \quad (25)$$

Multiplying Equation (24) by z^+ and Equation (25) by z^- and subtracting the equations we have

$$\operatorname{div}_s [(z^+ I^+ - z^- I^-) v_t] = D_{\text{eff}} \frac{\partial}{\partial r} (z^+ c^+ - z^- c^-). \quad (26)$$

In the first approximation, assuming the solution electrically neutral (Equation (7)), we obtain Equation (8). If the deviation from electroneutrality in the volume is taken into account (Equation (22)), we obtain an estimate of the surface deviation from electroneutrality, for which we find the ratio given by Equations (26) and (24)

$$\frac{\operatorname{div} [(z^+ I^+ - z^- I^-) v_t]}{z^+ \operatorname{div} (I^+ v_t)} = \frac{\frac{\partial}{\partial r} (z^+ c^+ - z^- c^-)}{\frac{\partial}{\partial r} z^+ c^+},$$

from which it follows that

$$\frac{z^+ I^+ - z^- I^-}{z^+ I^+} \sim \frac{\lambda}{z^+ c^+} \ll 1. \quad (27)$$

This justifies the method used above for evaluation of the electrical field of a drop.

It follows from the foregoing that the electrical field of a drop should be calculated in two stages. First we solve Equation (10) for convective diffusion, and use Equation (20) to find the potential distribution at the external drop surface. We then solve the Laplace Equation (18) with boundary Conditions (20) and (21), and determine the potential distribution in the air around the falling drop. The greatest difficulties arise at the first stage. We formulate the dimensionless criteria: the Prandtl diffusion number $\operatorname{Pr}_D = \nu / D_{\text{eff}}$, where ν is the kinematic viscosity of water, and the Pe criterion, which gives the order of magnitude of the ratio of the convective and diffusional flows

$$\operatorname{Pe} = \frac{c_0}{\delta c} \frac{v_0 a}{D_{\text{eff}}}. \quad (28)$$

The concentration distribution can be determined for the two limiting cases $\operatorname{Pe} \ll 1$ and $\operatorname{Pe} \gg 1$. In the former case we can simplify the problem by neglecting the convective component of diffusion, and in the second, by using the theory of the diffusional boundary layer. The electrical field of the drop can be determined accordingly for these limiting cases.

Under the condition

$$Pe \ll 1 \quad (29)$$

convective transfer of ions can be disregarded relatively to diffusional transfer; therefore Equation (10) can be replaced by the Laplace equation

$$\Delta c = 0. \quad (30)$$

Equation (30) must be solved in conjunction with boundary Condition (9). This gives $c(r, \theta)$ to an accuracy down to a constant value, for determination of which we can in general use the fact that the average volume concentration in a moving drop must coincide with the concentration in the same drop at rest.

Consider the problem for the case when deviations of the volume and surface concentrations from the average values of c_0 and Γ_0 are not large

$$\delta c = c_0 - c(r, \theta) \ll c_0; \quad (31)$$

$$\Gamma(\theta) - \Gamma_0 \ll \Gamma_0. \quad (32)$$

In view of (32), the boundary Condition (9) can be simplified, as the relative change of $\Gamma(\theta)$, which enters (9) under the divergence sign, may be neglected. Assuming in (9) that $\Gamma(\theta) \approx \Gamma_0$, we have

$$\frac{\partial c}{\partial r}(a, \theta) = \frac{2\Gamma_0 v_0}{D_{eff} a} \cos \theta. \quad (33)$$

Solution of Equation (30) with boundary Condition (33) presents no difficulty

$$c(r, \theta) = c_0 \left(1 + \frac{\delta c}{c_0} \frac{r}{a} \cos \theta \right), \quad (34)$$

where

$$\frac{\delta c}{c_0} = 2 \frac{v_0}{D_{eff}} \frac{\Gamma_0}{c_0}, \quad (35)$$

so that Condition (31) can now be written as

$$\frac{\Gamma_0}{c_0} \ll \frac{D_{eff}}{2v_0}. \quad (36)$$

Substituting the value of $c(a, \theta)$ calculated by means of Equation (34) into Equation (21), resolving the logarithm into series, and rejecting terms higher than the first order relative to $\delta c/c_0$ we have

$$\varphi_2(a, \theta) = \frac{2RT}{F} \frac{D^+ - D^-}{z^+ D^+ - z^- D^-} \frac{v_0}{D_{eff}} \frac{\Gamma_0}{c_0} \cos \theta. \quad (37)$$

The solution of the Laplace equation in conjunction with the boundary Conditions (37) and (20) is easily found

$$\varphi_2(r, \theta) = \frac{2RT}{F} \frac{D^+ - D^-}{z^+ D^+ - z^- D^-} \frac{v_0}{D_{eff}} \frac{\Gamma_0}{c_0} \frac{a^2}{r^2} \cos \theta. \quad (38)$$

Solution of the problem is much more difficult if Condition (31) does not hold.

Without solving this problem, we reduce boundary Condition (9) to a more convenient form, which can be done for adsorptional equilibrium, and indicate a possible route to the solution. In adsorptional equilibrium $\Gamma(\theta)$ and $c(a, \theta)$ must be in the same functional relationship as c_0 and Γ_0 , where Γ_0 is the equilibrium adsorption at a stationary water - air interface at molar volume concentration c_0 . If the case when ion adsorption is close to saturation is excluded from consideration, this functional relationship can be regarded as linear

$$\Gamma(\theta)/c(a, \theta) = \Gamma_0/c_0 = \alpha, \quad (39)$$

where the constant α depends on the nature of the ionogenic substance. Expressing $\Gamma(\theta)$ in terms of $c(a, \theta)$ by means of Equation (39) and substituting it into Equation (9), and assuming that $v_t = v_0 \sin \theta$, we transform Equation (9) into

$$\frac{\partial c}{\partial r}(a, \theta) = \frac{\Gamma_0 v_0}{c_0 D_{eff} a} \frac{1}{\sin \theta} \frac{\partial}{\partial \theta} [c(a, \theta) \sin^2 \theta]. \quad (40)$$

Thus, for determination of the electrical field in this case it is first necessary to solve Equation (30) with the very complicated boundary condition (40). The function having thus been obtained in explicit form, Equation (21) is used to determine $\varphi_2(a, \theta)$. It is to be expected that the boundary conditions for solution of Equation (18) — the function $\varphi_2(a, \theta)$ — will be very complicated.

CALCULATION OF THE ELECTRICAL FIELD OF A DROP WHEN $Pe \gg 1$

Under the condition

$$Pe \gg 1 \quad (41)$$

a boundary diffusional layer is formed at the inner surface of the drop. The theory of the diffusional boundary layer has been developed mainly by Levich who considered, in particular, the diffusional layer formed at the external surface of a drop falling in a different liquid. In our case the diffusional boundary layer forms on the inner side of the drop surface, but this does not alter the problem significantly. The order of magnitude of the thickness of the diffusional boundary layer δ can be found from Equation (10).

$$\delta = \sqrt{Da/v_0}. \quad (42)$$

In reality δ is a function of the angle θ .

First we consider the case when Condition (31) is satisfied. Here c_0 is taken to be the concentration within the drop volume, and δc is the concentration difference between the drop surface and volume, so that $\delta c = c_0 - c(a, \theta)$. The potential difference is localized in the boundary layer; we denote the constant potential in the drop volume by φ_0 . For evaluation of δc we note that when (31) applies, Equation (32) holds, and the boundary Condition (9) is simplified:

$$\frac{\partial c}{\partial r}(a, \theta) \simeq \frac{2v_0 \Gamma_0}{D_{eff} a} \cos \theta.$$

Expressing $\frac{\partial c}{\partial r}$ as $\frac{\partial c}{\partial \delta}$, we have

$$\delta c \simeq \frac{2v_0 \Gamma_0 \delta}{D_{eff} a} \cos \theta. \quad (43)$$

Although δ is a function of the angle θ , we cannot solve the very complex problem involved in determination of this function, and therefore we estimate the order of magnitude of the right-hand side by means of Equation (42)

$$\delta c \sim 2 \left(\frac{v_0}{D_{eff} a} \right)^{1/2} \Gamma_0 \cos \theta. \quad (44)$$

The potential distribution on the outer drop surface can be determined by means of Equation (21), which is conveniently simplified, with the use of Condition (31), by resolution into series. Substitution of Equation (44) then gives

$$\varphi_2(a, \theta) = \frac{RT}{F} \frac{D^+ - D^-}{z^+ D^+ - z^- D^-} \frac{c_0 - c(a, \theta)}{c_0} = \frac{2RT}{F} \frac{D^+ - D^-}{z^+ D^+ - z^- D^-} \left(\frac{v_0}{D_{eff} a} \right)^{1/2} \frac{\Gamma_0}{c_0} \cos \theta. \quad (45)$$

We similarly find the potential distribution near the drop

$$\varphi_2(r, \theta) = \frac{2RT}{F} \frac{D^+ - D^-}{z^+ D^+ - z^- D^-} \left(\frac{v_0}{D_{eff} a} \right)^{1/2} \frac{\Gamma_0}{c_0} \frac{a^3}{r^3} \cos \theta. \quad (46)$$

We now determine the applicability limits of these results. With the aid of Equation (44), Condition (31) may be written as

$$\frac{\delta c}{c_0} \sim 2 \left(\frac{v_0}{D_{eff} a} \right)^{1/2} \frac{\Gamma_0}{c_0} \ll 1 \quad (47)$$

or

$$\frac{\Gamma_0}{c_0} \ll \frac{1}{2} \left(\frac{D_{eff}}{av_0} \right)^{1/2} a. \quad (48)$$

Simultaneously, the Condition $Pe = \frac{c_0}{\delta c} \frac{av_0}{D_{eff}} \gg 1$, must hold; this may be rearranged as follows with the aid of Equation (47)

$$\frac{\Gamma_0}{c_0} \ll \frac{1}{2} \left(\frac{av_0}{D_{eff}} \right)^{1/2} a. \quad (49)$$

If we introduce a_c , determined by the equation $a_c v_0 / D_{eff} = 1$, we easily see that when $a > a_c$, Condition (48) is the more rigorous, and when $a < a_c$, Condition (49) is. Therefore, these two conditions can be replaced by a single condition under which they are both satisfied

$$\frac{\Gamma_0}{c_0} \ll \begin{cases} \frac{1}{2} a \left(\frac{a v_0}{D_{eff}} \right)^{1/2}, & (a < a_c); \\ \frac{1}{2} a \left(\frac{D_{eff}}{a v_0} \right)^{1/2}, & (a > a_c), \end{cases} \quad (50)$$

We now consider the case when the solubility of the ionogenic substance is low. This problem can be considered quantitatively if the solubility of the ionogenic substance is so low that the condition directly opposite to (48) is satisfied

$$\frac{\Gamma_0}{c_0} \gg \left(\frac{D_{eff} a}{v_0} \right)^{1/2}. \quad (51)$$

The intermediate case, when

$$\frac{\Gamma_0}{c_0} \sim \left(\frac{D_{eff} a}{v_0} \right)^{1/2},$$

which is the usual situation, is the most difficult to consider theoretically.

The main simplifying factor in consideration of the problem when Condition (51) holds is the small value of adsorption on the mobile drop surface in comparison with the equilibrium adsorption Γ_0 for the same value of c_0 but with a stationary water - air interface. To demonstrate this, we estimate the order of magnitude of the left and right-hand sides of (9)

$$D_{eff} \frac{c_0 - c(a, \theta)}{\delta} \sim \frac{\Gamma v_0}{a}.$$

Division of this expression through by c_0 , and multiplication of the right-hand side by Γ_0 / c_0 , after elementary transformations based on the fact that $\delta \sim \frac{a}{V v_0 a / D_{eff}}$, reduces it conveniently to the form

$$\frac{c_0 - c(a, \theta)}{c_0} \sim \left(\frac{v_0}{D_{eff} a} \right)^{1/2} \frac{\Gamma_0}{c_0} \frac{\Gamma}{\Gamma_0}.$$

Since $\frac{c_0 - c(a, \theta)}{c_0} \ll 1$ and, by Equation (51), $\frac{c_0}{\Gamma_0} \left(\frac{D_{eff} a}{v_0} \right)^{1/2} \ll 1$, we have finally in accordance with Condition (51)

$$\frac{\Gamma}{\Gamma_0} \sim \frac{c_0}{\Gamma_0} \left(\frac{D_{eff} a}{v_0} \right)^{1/2} \frac{c_0 - c(a, \theta)}{c_0} \ll 1. \quad (52)$$

If the ratio $c(a, \theta) / c_0$ is expressed by means of Equation (39) and (52) is taken into account, it is easily seen that the ratio is much less than unity

$$\frac{c(a, \theta)}{c_0} = \frac{\Gamma(\theta)}{\Gamma_0} \ll 1, \quad (53)$$

so that (52) and therefore (53) can be conveniently simplified

$$\frac{\Gamma(\theta)}{\Gamma_0} \sim \frac{c_0}{\Gamma_0} \left(\frac{D_{eff} a}{v_0} \right)^{1/2} \ll 1 \quad (52a)$$

$$c(a, \theta) = c_0 \frac{\Gamma(\theta)}{\Gamma_0} \sim c_0 \frac{c_0}{\Gamma_0} \left(\frac{D_{eff} a}{v_0} \right)^{1/2} \ll c_0. \quad (54)$$

Since $c(a, \theta) \ll c_0$, for determination of the concentration distribution it is first convenient to adopt the approximate boundary condition

$$c(a, \theta) = 0. \quad (55)$$

The second boundary condition must reflect the fact that at the boundary of the diffusional layer the concentration approaches c_0 .

The approximate boundary Condition (55) makes the following calculation method possible. Levich [4]

found the concentration distribution under the same boundary conditions and at $Re < 1, Pe \gg 1$ for the external diffusional boundary layer of a drop falling in another liquid

$$c(r, \theta) = \int_0^N e^{-z^2} dz, \quad (56)$$

where $N = \left(\frac{v_0}{aD_{eff}} \right)^{1/2} \frac{\sqrt{3}}{2} \frac{1 + \cos \theta}{\sqrt{2 + \cos \theta}} y$, y is the distance of a given point in the external diffusional layer from the drop surface; $y = r - a$. Analysis of the original equation and of the simplifications used [4] shows that this result applies equally to the internal diffusional boundary layer of the drop. Indeed, the formation conditions of the diffusional boundary layer on the inner and outer sides of the mobile drop surface (if the different properties of the media, which are easily taken into account, are disregarded) depend only on the difference in the sign of the surface curvature, and on the fact that whereas the boundary conditions on the outer boundary of the external diffusional layer may be regarded as fixed, but the concentration in the main volume of the drop, which gives the boundary value of the concentration at the inner boundary of the internal diffusional layer, requires definition in a rigid consideration of the problem. The difference in the sign of the surface curvature is not significant if the thickness of the diffusional layer is much less than the drop radius, as when $\delta \ll a$ the boundary layer can be regarded as approximately flat. In the rear portion of the drop, where significant thickening of the diffusional layer is possible, the use of boundary-layer concepts is incorrect even apart from this factor. The concentration in the main volume of the moving drop is somewhat displaced relatively to the known homogeneous concentration in the same drop at rest, as both in the boundary diffusional layer as a whole and in the adsorption layer there may arise either an excess or a deficiency of the dissolved substance, leading to either a deficiency or, correspondingly, an excess of the dissolved substance in the main volume of the drop. Exact knowledge of the concentration distribution in the boundary layer is necessary if this effect is to be taken into account. However, if, as we assume, the thickness of the diffusional layer is small, the role of this effect is not large.

Therefore, Formula (56) can be used for describing the concentration distribution in the inner boundary layer, and c_0 must then be interpreted as the concentration in the main volume of the drop, and y as the distance of a point in the inner diffusional layer from the surface; $y = a - r$. The thickness of the inner diffusional layer is found by substitution of Formula (56) into the expression $dc/dy \approx c_0/\delta$, which gives

$$\delta = \sqrt{\frac{\pi}{3}} \left(\frac{aD_{eff}}{v_0} \right)^{1/2} \frac{\sqrt{2 + \cos \theta}}{1 + \cos \theta}. \quad (57)$$

To find the potential distribution over the drop surface, it is necessary to determine $c(a, \theta)$. Formula (56) gives a zero value for $c(a, \theta)$, because Formula (56) satisfies the approximate boundary Condition (55). Nevertheless, Formula (56) is useful because it can be used for determining $\Gamma(\theta)$, after which $c(a, \theta)$ can be found without difficulty. For this, we write Equation (9) more fully, calculating $\frac{\partial c}{\partial r}(a, \theta)$ by means of Formula (56) and assuming $v_t = v_0 \sin \theta$

$$\frac{1}{a \sin \theta} \frac{\partial}{\partial \theta} (\Gamma(\theta) v_0 \sin^2 \theta) = D_{eff} \left(\frac{v_0}{aD_{eff}} \right)^{1/2} \sqrt{\frac{3}{\pi}} c_0 \frac{1 + \cos \theta}{\sqrt{2 + \cos \theta}},$$

integration then gives

$$\Gamma(\theta) = \frac{1}{\sin^2 \theta} \left[\sqrt{\frac{3}{\pi}} \left(\frac{D_{eff} a}{v_0} \right)^{1/2} c_0 \int_0^\theta \frac{1 + \cos \theta}{\sqrt{2 + \cos \theta}} \sin \theta d\theta + \text{const} \right].$$

Since $\Gamma(\theta)$ is finite, the integration constant is zero, and we have after integration

$$\Gamma(\theta) = \frac{2}{\sqrt{3\pi}} \left(\frac{D_{eff} a}{v_0} \right)^{1/2} c_0 \frac{1 - \cos \theta}{\sin^2 \theta} \sqrt{2 + \cos \theta}, \quad (58)$$

and hence, with the aid of Condition (39), we also find $c(a, \theta)$

$$c(a, \theta) = \frac{c_0}{\Gamma_0} \Gamma(\theta) = \frac{2}{\sqrt{3\pi}} \frac{c_0}{\Gamma_0} \left(\frac{D_{eff} a}{v_0} \right)^{1/2} c_0 \frac{1 - \cos \theta}{\sin^2 \theta} \sqrt{2 + \cos \theta}. \quad (59)$$

The potential distribution on the external side of the drop surface can now be found from Equation (21)

$$\varphi_2(a, \theta) = \frac{RT}{F} \frac{D^+ - D^-}{z^+ D^+ - z^- D^-} \ln \left[\frac{2}{\sqrt{3\pi}} \frac{c_0}{\Gamma_0} \left(\frac{D_{eff} a}{v_0} \right)^{1/2} \frac{1 - \cos \theta}{\sin^2 \theta} \sqrt{2 + \cos \theta} \right]. \quad (60)$$

To determine the potential distribution $\varphi_2(r, \theta)$ in air it is necessary to solve Equation (18) in conjunction

with the boundary Conditions (60) and at infinity. Solution of this problem presents certain difficulties, not only because of the complexity of Equation (60), but also because this boundary condition becomes incorrect at the rear region of the drop. Indeed, the approximate calculation method used is based on the assumption that $\frac{c(a, \theta)}{c_0} \ll 1$. Comparison of Equation (59) and (51) soon shows that this assumption is valid for nearly all the drop surface but near the point $\theta = \pi$ $c(a, \theta)$ rises rapidly, and the condition is not observed. Thus, the potential distribution on the drop surface at θ close to π remains unknown, but this region of the surface is very small, and the more accurately Condition (51) is satisfied, the smaller it is.

DISCUSSION OF RESULTS

Let us estimate the maximum electrical fields which arise because of the diffusional electrokinetic effect in question. To do this, we first estimate the potential difference over the drop surface; for example, the potential difference between the poles of the drop. To carry out this estimation in the most general form, we use Equation (21) to find the potentials at the poles and hence their difference

$$\Delta\varphi_2 = \varphi_2(a, \pi) - \varphi_2(a, 0) = \frac{RT}{F} \frac{D^+ - D^-}{z^+ D^+ + z^- D^-} \ln \frac{c(a, \pi)}{c(a, 0)}. \quad (61)$$

Substituting the numerical values of the parameters into (61)

$$RT = 2,3 \cdot 10^{10} \text{ ergs}; F \simeq 3 \cdot 10^{14} \text{ cgsu}; \quad \frac{D^+ - D^-}{z^+ D^+ + z^- D^-} \sim 1,$$

we have

$$\Delta\varphi_2 \sim 2,5 \cdot 10^{-2} \ln \frac{c(a, \pi)}{c(a, 0)} \text{ volts}. \quad (62)$$

The electrical field strength at the external drop surface can be estimated very roughly as the potential difference divided by the drop radius

$$E_2 \sim \frac{\Delta\varphi_2}{a} \sim \frac{2 \cdot 10^{-2}}{a} \ln \frac{c(a, \pi)}{c(a, 0)} \text{ volts} \cdot \text{cm}^{-1} \quad (63)$$

If the adsorbed substance is highly soluble, when Condition (36) is satisfied, the logarithmic term in Equation (51) is much less than unity, as in this case, in accordance with (47), $c(a, 0) - c(a, \pi) \ll c_0$; at low solubilities, when Condition (51) is satisfied, the logarithmic term becomes of the order of unity or even somewhat greater. Therefore with decrease of the solubility of the adsorbed substance, or more accurately with increase of the ratio Γ_0/c_0 , and with the other factors constant, the electrical field of the drop increases and reaches values of

$$E_2 \sim 10^{-2}/a \text{ volts} \cdot \text{cm}^{-1}$$

when Condition (51) begins to be satisfied.

Thus, the effect in question produces an electrical field of the order of 100 v/cm for drops a few microns in size. Therefore, the magnitude of the electrical field due to the diffusional electrokinetic effect is in a number of instances comparable, for example, with that of a field caused by the effects considered by G. L. Natanson. More detailed consideration of this question is premature at present, as the calculated values of the electrical field may be decreased somewhat by partial retardation of the drop surface, which was not taken into consideration here. It must be pointed out that osmotic retardation of the surface, associated with the drop of surface tension over the surface, is negligible in a number of cases. The magnitude of the electrical field depends on the ratio Γ_0/c_0 and not on adsorption. This ratio, and hence the electrical field, can be large at a quite negligible value of absolute adsorption, when there is virtually no osmotic retardation. Apart from osmotic retardation, which may be disregarded in a number of cases, there should also be electrical retardation, with the following mechanism. As was noted at the beginning of this paper, the direct cause of the formation of an electrical field during the motion of a drop surface lies in local deviations of the surface from electroneutrality. Consideration of the action of the tangential component of the electrical field on these unbalanced charges readily shows that these forces tend to retard the motion of the surface and consequently to decrease the effect in question. The corrections necessary to take this effect into account will be considered in a future paper.

Electrical fields of the order of 100 v/cm near drop surfaces may influence deposition of particles about 1μ in size on the drops. This is easily shown by means of our proposed calculation method [5], according to which the flow of particles onto a moving drop is proportional to the normal component of the particle velocity at the surface. For particles of the order of 1μ the velocity in an electrical field of about 100 v/cm is close to the

sedimentation velocity. Therefore, the electrical field may have an appreciable influence on the settling of such particles onto a falling drop.

This effect may also be of interest because the derived formulas can be used for calculating ion adsorption from measurements of the potential of falling drops. Since the magnitude of the electrical field depends on the ratio Γ_0/c_0 and not on the absolute value of the adsorption, this method can be used for determining very low adsorptions, which cannot be studied by any other methods.

SUMMARY

1. The theory of a diffusional electrokinetic effect for a drop, arising in the motion of the drop surface, is presented.
2. Calculations for drops of not very large size, the fall of which is characterized by Reynolds numbers less than unity show that this effect can give rise to electrical fields up to 100 v/cm. Although electrification of drops as the result of effects the mechanism of which has been studied by G. L. Natanson may give rise to strong electrical fields, the effect in question must be taken into consideration for the usual fractions of nearly or totally electroneutral drops.
3. The diffusional electrokinetic effect offers unique opportunities for studying extremely weak adsorption.

Institute of Physical Chemistry
Academy of Sciences, USSR

Received July 11, 1958

Laboratory of Surface Phenomena, Moscow

The G. S. Skovoroda Pedagogic Institute, Khar'kov

LITERATURE CITED

- [1] G. L. Natanson, Proc. Acad. Sci. USSR 53, 119 (1946); J. Phys. Chem. 23, 304 (1949); 25, 779 (1951).
- [2] A. N. Frumkin, Bull. Acad. Sci. USSR, Chem. Ser. 223 (1945); V. G. Levich, J. Phys. Chem. 21, 689 (1947); I. N. Bagotskaya and A. N. Frumkin, J. Phys. Chem. 21, 1033 (1947).
- [3] V. G. Levich, Physicochemical Hydrodynamics (Izd. AN SSSR, 1952) 191. [In Russian]
- [4] V. G. Levich, Physicochemical Hydrodynamics (Izd. AN SSSR, 1952) 277. [In Russian]
- [5] S. S. Dukhin and B. V. Deryagin, Colloid J. 20, 326 (1958). *

*Original Russian pagination. See C. B. Translation.

RELATIONSHIP BETWEEN THE STRUCTURE OF EMULSIFIERS OF THE ALKYL ARYL SULFONATE TYPE AND THE POLYMERIZATION OF UNSATURATED COMPOUNDS

5. COLLOIDOCHEMICAL PROPERTIES OF SODIUM ALKYL ARYL SULFONATES

M. G. Zimina and N. P. Apukhtina

Alkaline alkyl aryl sulfonates are widely used as emulsifiers in the production of synthetic rubbers by the emulsion process [1]. Considerable interest therefore attaches to more detailed studies of the colloidochemical properties of individual alkyl aryl sulfonates in relation to their effects on the mechanism of emulsion polymerization.

In an earlier investigation we studied the effect of the number of alkyl groups on the solubilization of monomers [2]. It was found that the solubilization of hydrocarbons increases in the series from mono- to tri-butylaryl sulfonates. The following were determined in the present investigation: surface tension of aqueous solutions of sodium alkyl aryl sulfonates, their micellar weights, and the solubilization of α -methylstyrene in aqueous solutions of these emulsifiers.

Studies of emulsifier properties are of considerable interest because emulsifier structure influences not only the colloidochemical role of an emulsifier in the polymerization process, but also, to a certain extent, the participation of the emulsifier in the chemical reactions associated with monomer polymerization, as will be shown in the next communication.

Emulsifiers. Sodium alkylbenzene and alkylnaphthalene sulfonates were synthesized, containing alkyl chains of 4 to 6 carbon atoms, and with different numbers of such groups. The individual emulsifiers were generally made by alkylation of benzene or naphthalene by olefine obtained as by-products of synthetic-rubber production: pseudobutylene, [3], amylene, and hexylene, in presence of sulfuric acid. In the alkylation of aromatic compounds by these olefins the structure of the alkyl radical may be secondary or tertiary. It is known that in the alkylation of aromatic compounds by butylene with the double bond at the first or second carbon atom the compounds formed have only a secondary structure of the alkyl group attached to the aromatic nucleus [4]. Moreover, it is well known that most tertiary dialkyl derivatives of benzene and naphthalene are crystalline products with relatively high melting points. In our experiments alkylation always yielded liquids which as a rule had the constants of secondary alkyl aryl compounds. Di (tert-butyl) benzene was prepared by alkylation of benzene by isobutylene in presence of sulfuric acid. Di (n-butyl) benzene was prepared from n-dibromobenzene and n-butyl chloride in presence of metallic sodium [5].

The position of the alkyl groups was determined by oxidation of the alkylation products (apart from the dialkylnaphthalene derivatives) with nitric acid, yielding the corresponding carboxylic acids. Oxidation of di-butylbenzene gave terephthalic acid, the butyl groups being in the 1,4 positions [3]. Sulfonation of the alkyl derivatives by concentrated sulfuric acid gave the corresponding sulfonic acids, which were converted into the sodium salts by neutralization with caustic soda. The purity of the recrystallized emulsifiers was checked by determinations of their sulfur contents.

The butyl, amyl, and hexyl derivatives of benzene are designated as BB, AB, and HB, and the corresponding naphthalene derivatives as BN, AN, and HN respectively; the number of alkyl groups is indicated by the prefixes mono-, di-, and tri-. For example, sodium di (sec-amyl) naphthalene sulfonate is designated as di-sec-AN.

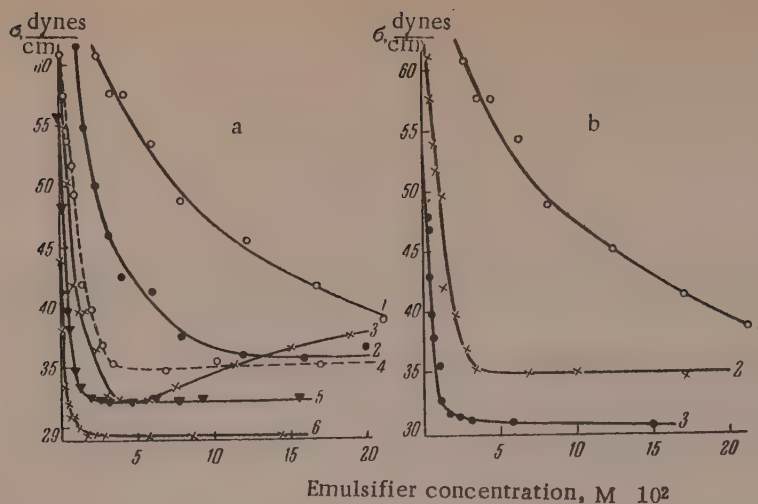


Fig. 1. Surface tension of aqueous solutions of secondary alkylbenzene sulfonates:

a): 1) mono-BB; 2) mono-AB; 3) mono-HB; 4) di-BB; 5) di-AB; 6) di-HB; b) 1) mono-BB; 2) di-BB; 3) tri-BB.

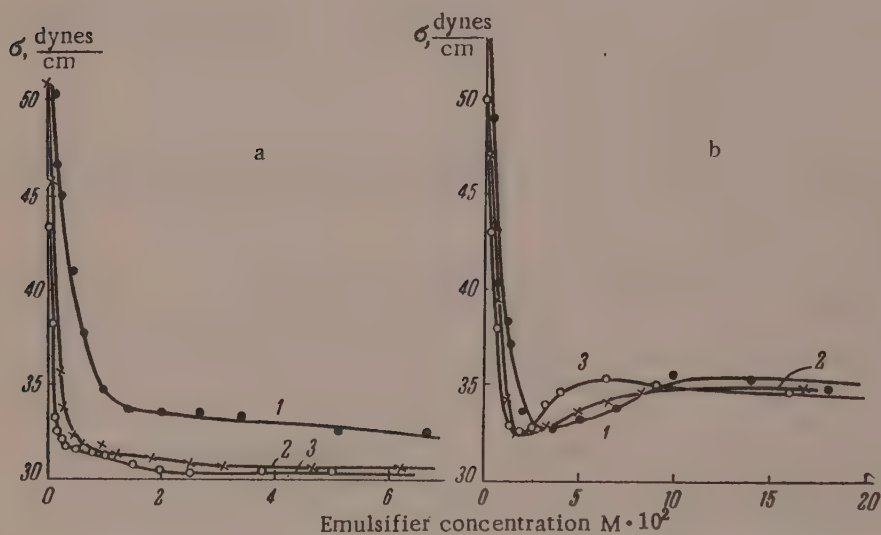


Fig. 2. Surface tension of aqueous solutions of secondary alkylnaphthalene sulfonates:

a): 1) di-BN; 2) di-AN; 3) di-HN; b): 1) mono-BN; 2) mono-AN; 3) mono-HN.

Technical α -methylstyrene was treated with 5% aqueous alkali solution to remove stabilizer, washed with water, dried over calcium chloride, and distilled. The fraction of b. p. 162-163°; n_D^{20} 1.5390 was collected.

Surface tension of aqueous emulsifier solutions was determined by the method of maximum bubble or drop pressure, developed by Rebinder and Taubman [6], at 20°. It was found that the surface tension is influenced by the number of alkyl groups attached to the aromatic nucleus in the emulsifier, by the length of the alkyl radical, and by the structural isomerism. The data in Fig. 1 show that the surface tension of aqueous emulsifier solutions decreases regularly with increase of the length of the alkyl radical and with the number of alkyl groups in the emulsifier molecule. The surface-tension curves of these emulsifiers are characteristic of typical surface-active substances: the greatest lowering of surface tension is observed at low concentrations, and with further increase

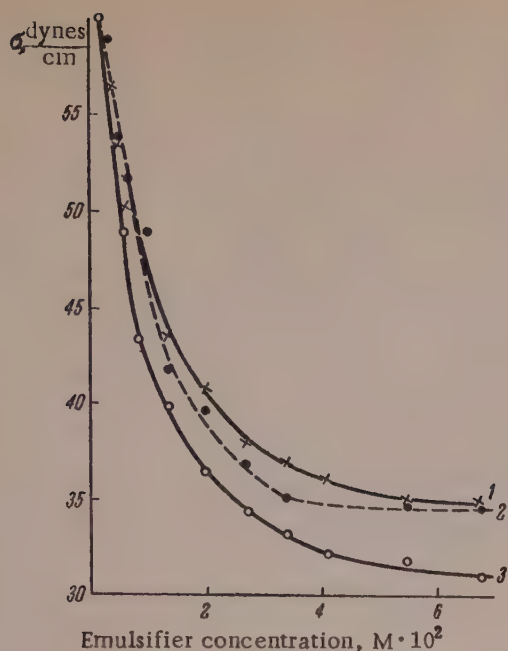


Fig. 3. Surface tension of aqueous solutions of alkylbenzene sulfonates:
1) di-n-BB; 2) di-sec-BB; 3) di-tert-BB.

of emulsifier concentration the rate of change of surface tension is sharply retarded and the curve usually becomes almost parallel to the abscissa axis. The σ concentration curves for all di (sec-alkyl) derivatives of the naphthalene series (Fig. 2,a) and for all the benzene derivatives (with the exception of mono-sec-HB) (Fig. 1,a) belong to type I, in McBain's terminology [7].

The surface tension - concentration curves for all mono derivatives of the naphthalene series (Fig. 2,b) and for sodium monohexylbenzene sulfonate (Fig. 1, a) belong to type III [7]; each passes through a minimum. The surface tension in solutions of these emulsifiers first falls very sharply with increase of concentration, passes through a minimum, then increases appreciably, and only after this the curve gradually flattens out (Fig. 2,b). Similar variations of surface tension with concentration have been reported by other workers [8]. Alexander [9] suggested that the minimum on these curves approximately corresponds to the concentration at which micelles begin to form, known as the critical concentration of micelle formation (CCM). Micelle formation lowers the volume concentration of individual surface-active molecules, and the micelles can be considered as a second dissolved component in the system. Alexander therefore

suggests that surface activity is determined by individual molecules rather than by micelles [10].

Other workers have suggested that the minima on the curves are caused by the presence of admixtures of high-molecular surface-active substances [11]. However, neither our experiments nor the observations of other workers [12] confirm this hypothesis. Thus, at the present time there is no single scientific explanation of the differences between the $\sigma - c$ (where c is the concentration) curves for different groups of surface-active substances.

The isomerism of the alkyl radical has a strong influence on the surface tension (Fig. 3). The emulsifier with the most branched (tertiary) radical has the highest surface activity. Surface tension decreases in the series di-BB > di-sec-BB > di-tert-BB.

The lowest surface tension is found in presence of the tertiary derivative. The surface tensions of solutions containing emulsifiers with normal and secondary butyl groups respectively are fairly similar. Baumgartner [13], who studied variations of detergent properties with the molecular structure of dodecylbenzenesulfonic acids with the benzene ring in different positions in the alkyl chain, also found that the surface tension decreases as the benzene ring approaches the center of the alkyl chain, i. e., that surface activity increases with branching of the alkyl radical. In our opinion, variations in surface tension must be primarily correlated with characteristics of micelle formation, which depend on the emulsifier structure.

It is known that electrolytes have a considerable influence on the surface activity of emulsifiers. Fig. 4 shows that univalent cations form the following lyotropic series in order of their influence on the surface tension of dialkyl aryl derivatives in solution: $K^+ > Na^+ > Li^+$. These cations influence surface tension in the same sequence when they are present as salts of dibutyl-naphthalenesulfonic acids [3].

Solubilization of α -methylstyrene was determined by Yurzhenko's refractometric method [14]. Despite the fact that this method involves certain difficulties, we [3] and other workers [15] have shown that it can be used for comparative evaluation of the solubilizing power of different emulsifiers.

It is known that solubilization of oleophilic substances in aqueous solutions of colloidal electrolytes depends on the molecular weight and molecular structure of the surface-active agent, the nature of the solute, electrolyte additions, and other factors.

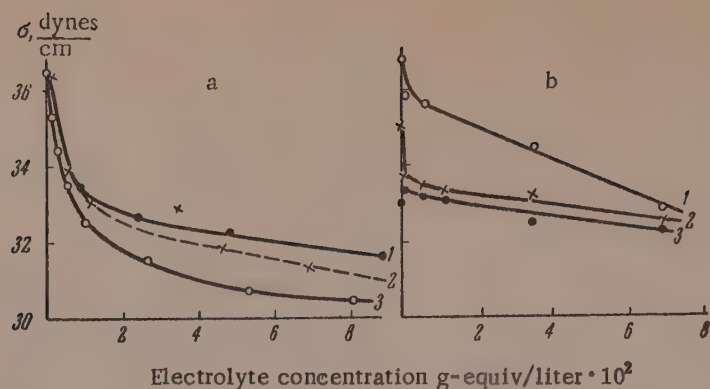


Fig. 4. Effect of electrolytes on the surface tension of aqueous solutions of dialkylbenzene sulfonates:
a) 0.2% solution of di-sec-AB; 1) LiCl; 2) NaCl; 3) KCl; b) 1% solutions of: 1) di-n-BB; 2) di-sec-BB; 3) di-tert-BB; NaCl electrolyte.

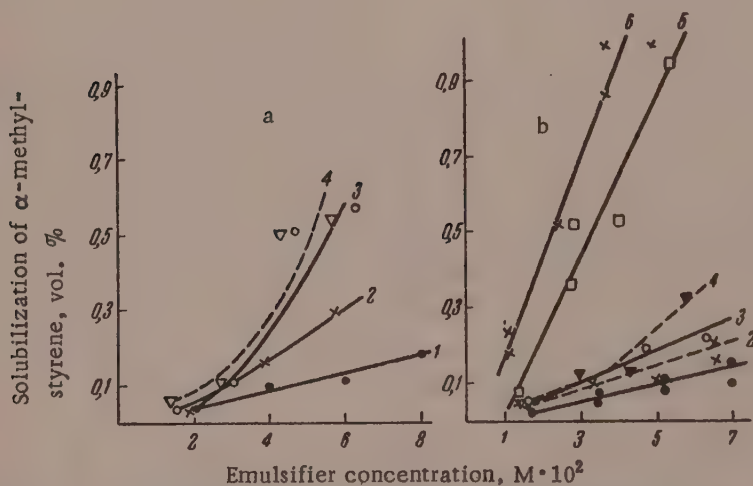


Fig. 5. Solubilization of α -methylstyrene in aqueous solutions of:
a) secondary alkylbenzene sulfonates: 1) mono-AB; 2) mono-HB; 3) di-AB; 4) di-HB; b) secondary alkyl-naphthalene sulfonates: 1) mono-BN; 2) mono-AN; 3) mono-HN; 4) di-BN; 5) di-AN; 6) di-HN.

We studied the effect of the length of the alkyl radical in alkylbenzene sulfonates, and of isomerism of the radicals, on the solubilization of α -methylstyrene at different emulsifier concentrations. As a rule, increase of the emulsifier concentration in aqueous solution increases solubilization of hydrocarbons. Yurzhenko et al. [14], who studied solubilization of monomers in aqueous emulsifier solutions in relation to the mechanism of emulsion polymerization, and McBain et al. [16], found for certain hydrocarbons that solubilization in aqueous sodium and potassium oleate solutions is a linear function of the emulsifier concentration. Other workers [17] do not consider that the relationship between the amount of hydrocarbon dissolved and the concentration of colloidal electrolyte in solution is linear. It has also been reported that for certain synthetic soaplike substances the curve for micellar solubility as a function of concentration passes through a minimum [18]. We plotted solubilization (in volume percentages) against the emulsifier concentration (in moles/liter) and found that the amount of hydrocarbon dissolved rises with the concentration of colloidal electrolyte (Fig. 5, a and 5,b).

If solubilization is expressed in moles of α -methylstyrene per mole of emulsifier, a different relationship

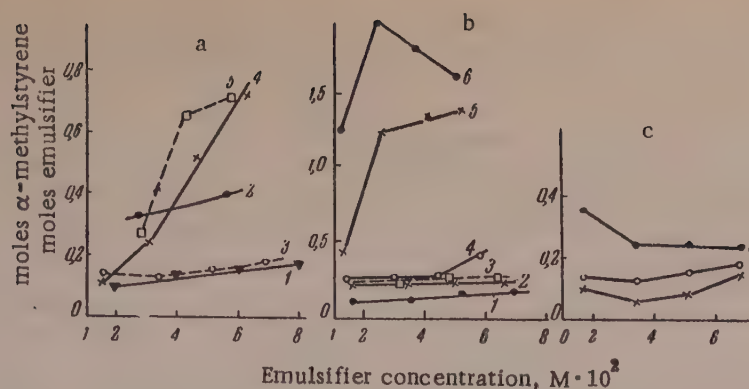


Fig. 6. Solubilization of α -methylstyrene in aqueous solutions of: a) secondary alkylbenzene sulfonates: 1) mono-AB; 2) mono-HB; 3) di-BB; 4) di-AB; 5) di-HB; b) secondary alkylnaphthalene sulfonates: 1) mono-BN; 2) mono-AN; 3) mono-HN; 4) di-BN; 5) di-AN; 6) di-HN; c) dibutylbenzene sulfonates: 1) di-n-BB; 2) di-sec-BB; 3) di-tert-BB.

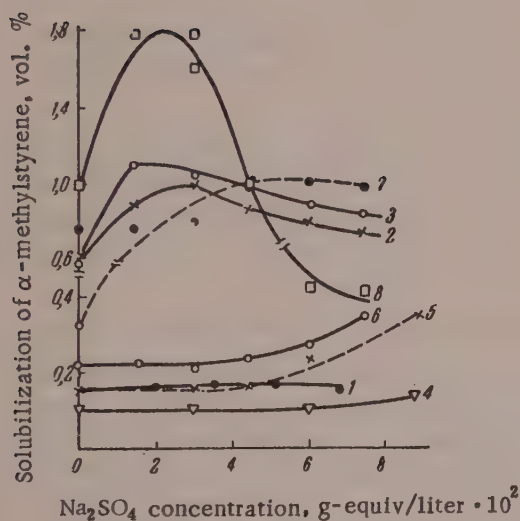


Fig. 7. Solubilization of α -methylstyrene in aqueous solutions of secondary alkyl aryl sulfonates: 1) di-BB; 2) di-AB; 3) di-HB; 4) mono-BN; 5) mono-AN; 6) mono-HN; 7) di-BN; 8) di-HN.

Values of Micellar Weights and CCM of Emulsifiers Studied

No.	Emulsifiers	Micellar weight	CCM, $M \cdot 10^4$	Degree of micellization
1	Mono-sec-BB	10000	31,8	43
2	Di-sec-BB	30000	1,7-2,5	103
3	Tri-sec-BB	125000	0,26	359
4	Di-n-BB	18200	5,3-6,5	62
5	Tri-tert-BB	28500	2,0-2,5	96
6	Mono-sec-AB	37500	1,5-2,5	151

is found between hydrocarbon solubility and emulsifier concentration (Fig. 6). With emulsifiers based on benzene and naphthalene and containing one alkyl group in the molecule, the solubilization of α -methylstyrene rises linearly with the emulsifier concentration, the rise being somewhat steeper with mono-AN and mono-HN. Solubilization increases even more steeply (Fig. 6,a) in presence of dialkylbenzene sulfonates. A similar dependence of solubilization, expressed in moles of solute per mole of emulsifier, was also found in presence of di-AN. The solubilization curve in presence of di-HN passes through a maximum (Fig. 6,b). This suggests that the relationship between solubilization

and concentration depends mainly on changes in the character of micellar structure with increase of emulsifier concentration [18].

With regard to the influence of the number of butyl groups in the emulsifier molecule on the solubilization of α -methylstyrene, it was shown earlier [3] that solubilization increases with increasing number of butyl groups.

There have been no systematic studies of the effect of the length of the alkyl radical (attached to the aromatic nucleus) on solubilization. There are data on the influence of the alkyl chain length in emulsifiers on the

solubilization or Orange OT [16], DAB (dimethylaminoazobenzene) [19], and alcohols of different chain lengths [17]. However, these investigations were performed only with sodium and potassium soaps of fatty acids. The solubilization of Sudan III in aqueous solutions of dioctyl and dihexyl esters of sodium sulfosuccinates has also been determined [14].

It is clear from Fig. 5, a and 5,b that solubilization increases with the length of the alkyl radical in the emulsifier; this is probably associated with the micellar weight of the emulsifiers, as increase in the weight of the hydrocarbon radical in surface-active substances belonging to the same homologous series increases their tendency to micelle formation [20].

Investigations of the effect of the structure of the butyl radical in emulsifiers of the benzene series on the solubilization of α -methylstyrene showed that solubilization was greatest with the most branched (tertiary) radical, i. e., that solubilization increases in the transition from normal to tertiary structure (Fig. 6,c). Winsor [21] observed a similar influence of isomerism in emulsifiers on the solubilization of organic compounds in his studies of the solubility of cyclohexane in solutions of isomeric sodium tetradecyl sulfates. He studied sulfates with hydrocarbon chains with both normal and secondary structure and found that solubilization increases as the SO_4Na group moves nearer the center of the chain, i. e., as branching increases.

Electrolytes are known to increase monomer solubilization [3, 14]. We found that in presence of sodium sulfate, in the concentration range studied (from 2 to $10 \cdot 10^2$ g-equiv/liter), solubilization is increased in the series of monosubstituted naphthalene sulfonates (Fig. 7). The solubilization curves for dialkyl aryl derivatives pass through maxima, which are more pronounced and are found at lower electrolyte concentrations for the higher alkyl derivatives.

It is well known that electrolyte additions increase the micellar weight and therefore solubilization of monomers. However, we found that electrolytes increase solubilization only up to certain limiting concentrations: further increases of mineral-salt concentrations decrease solubilization owing to the salting-out effect (Fig. 7, Curves 2, 3, 8).

Micellar weight and critical concentration* The critical concentrations of micelle formation (CCM) and molecular weights were determined by the Debye light-scattering method [20]. The calculation is based on the expression: $Hc/\Delta\tau = 1/M + 2Bc$, where M is the micellar weight, c is the solution concentration in grams per ml, H is a constant which depends on the refractive indices of the solution and solvent; B is a constant which takes into account deviations from the laws of ideal solutions.

The values found for the micellar weights and CCM of the emulsifiers studied are given in the Table.

These results show that the micellar weight increases with increase in the number of butyl groups in the emulsifier. Yurzhenko et al. [14] determined the micellar weight of an emulsifier consisting of a mixture of the three compounds (Nos. 1, 2, 3), and found it to be 66,600. The isomerism of the butyl group also influences micelle formation (see table); the micellar weight increases with increased branching of the butyl radical. The lowest micellar weight was found for sodium di(n-butyl) benzene sulfonate (di-n-BB). The micellar weight increases with the length of the alkyl chain. CCM varies in inverse proportion to the micellar weight.

SUMMARY

1. Twelve individual sodium alkylbenzene and alkyl-naphthalene sulfonates with different numbers of alkyl groups of different lengths, and three isomeric sodium dibutylbenzene sulfonates differing in the structure of their butyl groups, were synthesized.

2. The surface tension of aqueous solutions of these alkyl aryl sulfonates decreases regularly with increases in the number and length of the alkyl groups. Surface activity depends on the isomerism of the butyl group, and increases with branching of the hydrocarbon chain.

3. Solubilization of α -methylstyrene increases with the length of the alkyl chain attached to the aromatic nucleus of the emulsifier molecule.

* Micellar weights were determined in the Department of Physical Chemistry, the L'vov State University, under the guidance of Assistant Professor R. V. Kucher.

4. The effect of isomerism in butylbenzene sulfonates on the solubilization of α -methylstyrene has been studied. The emulsifier with tertiary butyl groups produced the greatest solubilization in solution, and the emulsifier with normal butyl groups, the least.

5. The micellar weights of a number of alkyl aryl sulfonates have been determined by the light-scattering method. It is shown that the micellar weight increases with the number of butyl groups in the molecule and with their degree of branching.

The S. V. Lebedev Scientific Research Institute
for Synthetic Rubber

Received May 23, 1957

LITERATURE CITED

- [1] B. A. Dolgoplosk, I. I. Radchenko, I. A. Livshits, et al. Trans. All-Union Sci. Res. Inst. Synthetic Rubber (OBTIP, Main Administration of the Rubber Industry, 1951) 3.
- [2] Ibid, 76.
- [3] N. P. Apukhtina and A. M. Lyagalova, Colloid J. 17, 337, 415 (1955).*
- [4] S. V. Lebedev, et al., Synthetic Rubber 3, 68 (1935).
- [5] K. I. Ivanov, Intermediate Products and Intermediate Reactions in the Autoxidation of Hydrocarbons (State Fuel Tech. Press, Moscow - Leningrad, 1949) 111, 116. [In Russian]
- [6] A. B. Taubman, Laboratory Manual on the Physical Chemistry of Colloids (Nonferrous Metals Press, 1932). [In Russian]
- [7] McBain, Ford, and Wilson, Kolloid-Z. 78, I (1937).
- [8] I. Masaya-Ogawa, Chem. Soc. Japan, Ind. Chem. Soc. 54, 779 (1951).
- [9] Alexander, Trans. Faraday Soc. 38, 54 (1942).
- [10] A. M. Schwartz and J. W. Perry, Surface Active Agents (Moscow, IL, 1953) 281 [Russian translation].
- [11] Miles and Shedlovsky, J. Phys. Chem. 48, 57, 1944; 49, 71 (1945).
- [12] E. E. Dreger and G. I. Keim, Ind. Eng. Chem. 36, 610 (1947).
- [13] F. N. Baumgartner, Ind. Eng. Chem. 46, 1349 (1954).
- [14] A. I. Yurzhenko and M. F. Kolehkova, Proc. Acad. Sci. USSR 47, 354 (1945); A. I. Yurzhenko, Proc. 3rd Conf. Acad. Sci. USSR on High-Molecular Compounds [In Russian] (Moscow, 1945); J. Gen. Chem. 16, 1171 (1940); A. I. Yurzhenko and R. V. Kucher, Colloid J. 13, 226 (1951).
- [15] P. A. Rebinder, et al., Colloid J. 16, 366 (1954).*
- [16] J. W. McBain and K. E. Johnson, J. Amer. Chem. Soc. 66, 9 (1944); J. W. McBain and H. H. Green, J. Amer. Chem. Soc. 68, 178 (1946).
- [17] W. D. Harkins and H. Oppenheimer, J. Amer. Chem. Soc. 71, 808 (1949).
- [18] J. W. McBain and K. I. Lissant, J. Phys. Coll. Chem. 55, 622 (1951).
- [19] J. M. Kolthoff and W. Stricks, J. Phys. Coll. Chem. 52, 1955 (1948).
- [20] P. Debye, J. Phys. Coll. Chem. 53, I (1949).
- [21] P. A. Winsor, Trans. Faraday Soc. 44, 376, 390 (1948).

*Original Russian pagination. See C. B. Translation.

THE DISPERSING ACTION OF CAVITATION

B. B. Kudryavtsev

Many different kinds of emulsions are widely used in various branches of the national economy [1], and therefore efficient methods for the production of emulsions are of undoubted interest. The use of sonic and ultrasonic vibrations for the production of emulsions has been advocated repeatedly in recent years [2-4]. It has been reported that emulsions made by means of sonic or ultrasonic vibrations have high and uniform dispersity. Although the mechanism of sonic emulsification cannot be regarded as fully understood, there is no doubt that in most cases the main role is played by intensive cavitation [5] arising in the liquid during propagation of the sonic waves. If this hypothesis is correct, it should be possible to emulsify liquids by a much simpler method, because intensive cavitation in a liquid may be produced without the use of relatively complex sonic equipment.

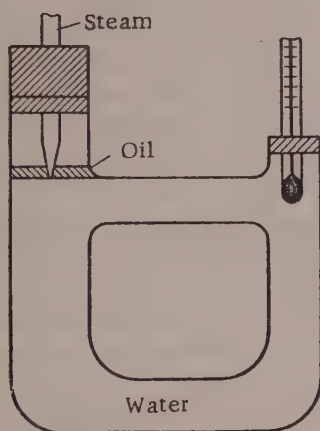


Fig. 1. Apparatus for emulsification of oil in water.

The simplest method for producing cavitation is probably by means of a jet of superheated steam passed into the liquid through a fine nozzle. The cavitation which results from this is accompanied by many of the effects which occur in the propagation of intensive ultrasonic vibration [6, 7]. It must be noted, however, that according to most recent work [8], the chemical changes induced by ultrasonic cavitation do not occur when cavitation is produced by means of a jet of superheated steam. In order to study the dispersing action of cavitation which occurs when a jet of superheated steam is passed into a liquid, we studied the emulsification of transformer oil added to water by this method. The experiments were performed in an apparatus (Fig. 1) similar to the type of vessel sometimes used as a thermostat in determinations of the melting points of organic compounds. About 15 ml of water was put into the vessel, and a drop of transformer oil (~ 0.3 ml) was floated on its surface. Steam under about 0.2

atmos excess pressure was supplied through a glass nozzle fixed in the bung, with different diameters in different experiments. The apparatus was cooled in a mixture of water and ice. The jet of steam caused rapid emulsification, together with circulation of the liquid which assisted its cooling. By the end of the experiment, which usually lasted about 30 seconds, the temperature of the liquid rose from about 5 to 40° as the result of steam condensation. The emulsions were photographed at $\times 600$ magnification, and size distribution curves were plotted, based on the results of analysis of the photographs.

Fig. 2 shows size-distribution curves of oil droplets in emulsions made with nozzles of different diameters. The nozzle diameters ranged from 0.6 to 1.3 mm, while the amount of condensed steam was kept approximately constant. It is clear from the curves in Fig. 2 that the nozzle diameter plays a subordinate role, since the distribution curves differ little from each other. The distribution curves for 1.0, 1.1, and 1.3 mm nozzles almost coincide.

Stabilizers were not used in emulsification of the oil, and therefore the emulsions separated out after 24 hours. The upper layer consisted of partially enlarged oil droplets in very close proximity to each other; the

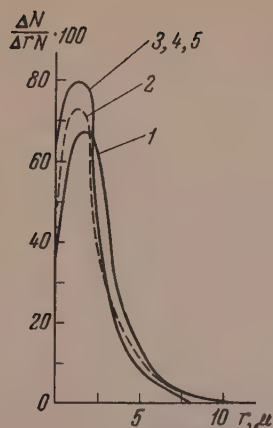


Fig. 2. Size-distribution curves of oil droplets in emulsions formed by the passage of steam through nozzles of the following diameters:

- 1) 0.6 mm; 2) 0.8 mm;
- 3) 1 mm; 4) 1.1 mm; 5) 1.3 mm.

The oil to be dispersed and the water entered the first emulsification vessel through separate tubes; superheated steam from a boiler under ~ 0.2 atmos excess pressure entered the same vessel through a nozzle with an orifice of about 1.0 mm. The coarse emulsion which formed flowed by gravity into a vessel attached to the emulsification vessel and fitted with an overflow tube. The emulsion flowed through this overflow tube from the first emulsification vessel into a second emulsification vessel, provided with the same type of superheated-steam nozzle as the first. The emulsion after the second subdivision again flowed by gravity into a third emulsification vessel of the same design as the second. The number of these vessels could be increased at will. The supply of oil, water, and steam was regulated by a system of valves. In the experiments described below the original temperature of the oil and water was 18° ; the temperature rose as the result of steam condensation to 28° in the first overflow vessel, to 38° in the second, and to 48° in the third. Special cooling was not used. The temperature rise indicated that the steam consumption in emulsification was approximately 16-18 g per kg of emulsion in each vessel.

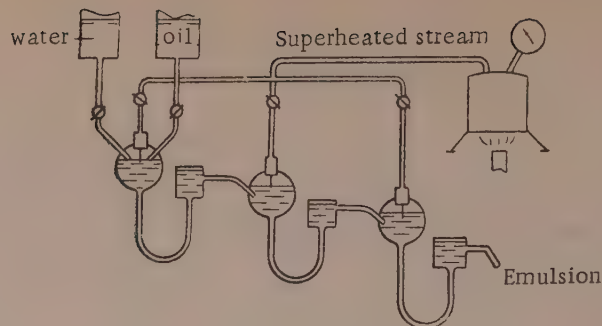


Fig. 3. Apparatus for multistage emulsification of oil in water.

lower layer contained numerous very fine oil droplets, with occasional droplets down to 5μ in diameter. This naturally raised the question of a repeated subdivision of the emulsion; this question could not be studied by means of the apparatus described because of the increase in the liquid volume as the result of steam condensation. The steam nozzle became immersed deeply in the liquid, so that there was considerable condensation of steam in the nozzle itself. The apparatus shown schematically in Fig. 3 was therefore constructed.

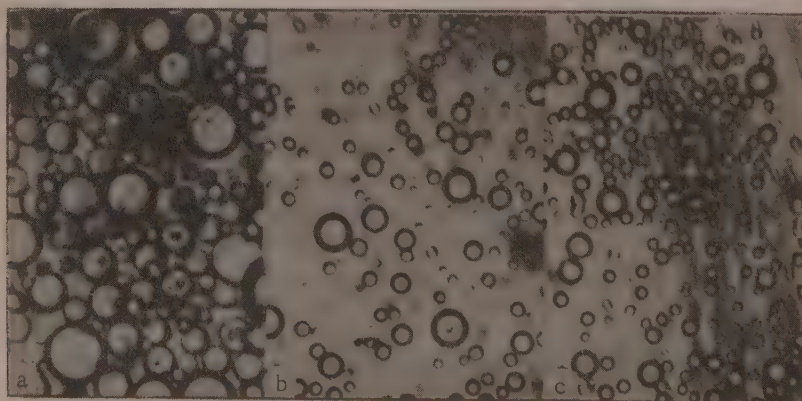


Fig. 4. Microphotographs of emulsion samples after single (a), double (b), and treble (c) subdivision.

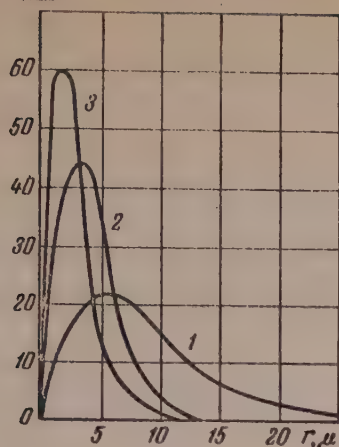
$\frac{\Delta N}{N_{AC}} \cdot 100$


Fig. 5. Size distribution curves for droplets in an emulsion after single (a), double (b), and treble (c) subdivision.

treated in the first type of apparatus. Complete dispersion of all the dye could not be achieved in these experiments, and a part of the solid settled out. The colloidal solution formed as the result of this dispersion retained its coloristic properties for a long time (over a week) without change. A disadvantage of this dispersion method is the considerable dilution of the dispersed substance with water.

From the results of this investigation it may be concluded that in most cases in which sonic emulsification methods are recommended at present the simpler cavitation method described above may be used with success. It should be stressed once again that the equipment is exceptionally simple and operating costs are low.

SUMMARY

1. The dispersing effect of cavitation produced when a jet of superheated steam is passed into water was investigated. Transformer oil is dispersed within a fraction of a minute by this method.
2. A simple apparatus has been designed for multistage dispersion of liquids, which yields finely dispersed and homogeneous emulsions.
3. Cavitation also has a dispersing effect on solids such as organic dyes, in which cohesion forces between the particles are not large.

The Moscow Regional Pedagogic Institute

Received November 28, 1957

LITERATURE CITED

- [1] W. Clayton, *Theory of Emulsions and Their Technical Treatment* (Moscow - Leningrad, IL, 1950) [Russian translation].
- [2] F. Rose, *Canad. Fisherman* 41, 8, 19, 22 (1954).
- [3] A. E. Crawford, *Ultrasonic Engineering* (1955).
- [4] S. N. Sin'kova and S. A. Puzyrev, *Colloid J.* 19, 3, 387 (1957).*
- [5] L. Bergmann, *Ultrasonics* (IL, 1956) [Russian translation].
- [6] I. G. Polotskii, *J. Gen. Chem.* 17, 1048 (1948).
- [7] I. G. Polotskii, *J. Gen. Chem.* 17, 649 (1948).
- [8] O. Lindström, *J. Acoust. Soc. America* 27, 4, 654 (1955).

*Original Russian pagination. See C. B. Translation.

Fig. 4 shows microphotographs of emulsion samples taken from the first, second, and third overflow vessels. It is seen that repeated subdivision increases the dispersity and homogeneity of the emulsions. The latter is clearly demonstrated by the distribution curves (Fig. 5) based on analysis of the microphotographs. Repeated subdivision not only lowers the average droplet size but makes the emulsion more nearly monodisperse. After threefold subdivision only a small proportion of the total number of particles exceeded 5μ in diameter. The very high efficiency of cavitation subdivision should be noted; emulsification was complete within a fraction of a minute. Among other advantages of this method are simplicity of design and absence of moving parts in the emulsification apparatus.

It was desired to study the possibility of cavitation dispersion of certain solids, including dyes used industrially in the form of highly disperse suspensions. A paste of Bright Violet vat dye (0.5 g) containing ~ 24% solid was taken, mixed with 3 ml of water, and

PROPERTIES OF THE PRODUCTS FORMED BY "MELTING OUT" OF PROTEINS FROM THE DERMA OF ANIMAL HIDES

V. A. Kut'in

The "melting out" method proposed by Küntzel [1] is sometimes used for characterization of derma proteins from animal hides and for studies of their changes under various chemical, physical, and enzymatic influences. The properties of derma proteins are estimated from their ability to pass into solution when pieces of hide are heated in water at the shrinkage temperature.

It was found in subsequent investigations that the amounts "melted out" depend on the temperature used for the process, the pH of the bath, the amounts and nature of the salts dissolved in the bath or adsorbed by the hide, the degree of shredding of the hide, the solution time, the volume ratio of water to material, and other experimental conditions. Since the amount "melted out" at 65° does not exceed 2-3%, attempts have been made to "melt out" proteins at higher temperatures [2, 3], or to use enzymes which accelerate the dissolution of the proteins. Galina [3] studied the solubility of derma proteins at 95°. At this temperature the amount of proteins dissolved from raw hides was 6.6%, and from hides limed for 12 days, 10.4%.

Higher "melting out" temperatures were not used in this or other investigations. No work has been published on the properties of the proteins which pass into solution when hides are heated in water. Neither have any methods been worked out for complete solution of derma proteins, although such a method would provide new ways for investigating the properties of proteins and their variations under various influences, and which would make it possible to effect radical changes in glue and gelatin production which, as is known, involves a lengthy multistage extraction process, with liquors of low concentration, and the extraction of proteins is incomplete.

TABLE 1

Effect of "Melting Out" Conditions on Protein Properties

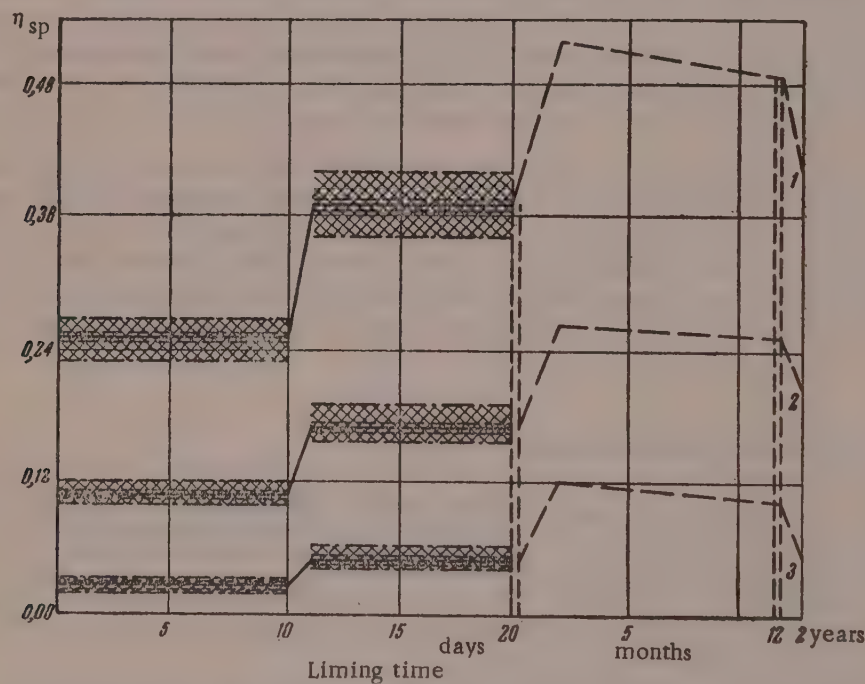
Conditions of autoclave treatment			Nitrogen content calculated as % on bone-dry protein	Results of formol titrations in ml of 0.1 N NaOH per g protein	Specific viscosity of solutions (conc. in g/100ml)	
duration, hours	pressure, atmos	temperature, (in °C)			1,0	0,5
6	8	75	17,8	—	—	0,10
6	8	90	17,8	3,3	0,28	0,12
6	8	105	17,8	3,4	0,27	0,12
6	1	100	17,6	3,4	0,31	0,14
6	2,5	120	17,5	3,4	0,30	0,14
3	8,0	120	17,4	3,4	0,27	0,12
6	15	120	17,7	3,3	0,28	0,13

The present investigation consisted of a study of the "melting out" of derma proteins under various conditions of autoclave treatment, and of the properties of the products "melted out."

TABLE 2

Analytical Data on Proteins from Hides Treated in Lime Suspensions

Characteristics	Raw hide	Liming time, days									Photo-graphic gelatin
		1	3	6	10	11	13	20	1 yr.	2 yrs.	
Moisture, %	11,6	13,6	14,3	14,6	14,2	15,2	14,4	12,3	12,2	13,0	14,5
Ash, % on bone-dry subs.	0,1	0,1	0,3	0,2	0,1	0,3	0,3	0,2	1,3	1,4	3,0
Total nitrogen, % on bone-dry subs.	17,7	17,8	17,9	17,8	17,5	17,8	17,9	17,9	16,9	16,4	17,9
Amino nitrogen, % of total nitrogen	2,2	2,1	2,5	2,5	2,6	2,6	2,6	2,5	3,7	3,6	2,7
Specific viscosity of solutions											
Concentration 1,0 g/100 ml	0,26	—	0,26	0,26	0,23	0,39	0,36	0,34	0,49	0,39	0,52
" 0,5 g/100 ml	0,11	—	0,11	0,10	0,10	0,18	0,16	0,15	0,25	0,20	0,27
" 0,2 g/100 ml	0,03	—	0,03	0,03	0,02	0,06	0,05	0,05	0,10	0,08	0,12
Axial ratio of protein particles, b/a	10	—	10	12	10	20	18	15	27	35	33



Effect of liming time on the specific viscosity of "melted out" products: concentrations: 1) 1.0; 2) 0.5; 3) 0.2 g protein per 100 ml solution.

Tongur [4] showed that the tendency of proteins to undergo heat denaturation increases in presence of oxygen, and we therefore carried out the process in an atmosphere of nitrogen containing 0.5% oxygen. Nitrogen was blown through the autoclave before the treatment. The protein material was first cut on a disk machine to a thickness of 0.5-1.0 mm. The temperature in the autoclave was measured by means of a Constantan - copper thermocouple. The pressure was measured by means of a manometer. In each experiment 100-150 g of raw or limed hide was put into a porcelain beaker and covered completely with a small amount of distilled water. The beaker was put into the autoclave, previously heated to 95-100°. The autoclave temperature was then raised to

TABLE 3

Analytical Data on Proteins From Hides Treated For Three Days In Sodium Sulfide Solutions

Characteristics	Raw hide	Sodium sulfide concentration		
		0.02 N	0.1 N	0.2 N
Moisture, %	11.6	11.5	14.5	12.5
Ash, % on bone-dry subs.	0.1	0.1	0.1	0.2
Total nitrogen, % on bone-dry subs.	17.7	17.8	17.7	17.6
Amino nitrogen, % of total nitrogen	2.3	2.4	2.1	2.0
Specific viscosity of solutions				
Concentration 1.0 g/100 ml	0.27	0.28	0.32	0.27
" 0.5 g/100 ml	0.11	0.12	0.13	0.11
" 0.2 g/100 ml	0.03	0.03	0.04	0.03
Axial ratio of protein particles, b/a	10	11	13	7

TABLE 4

Analytical Data on Proteins From Hides Treated With Sodium Sulfide Solution Containing 3.9 g/liter

Characteristics	Raw material	Treatment time, hours				
		4	8	24	72	144
Moisture, %	11.6	15.1	13.8	14.7	14.5	14.7
Ash, % on bone-dry subs.	0.1	0.02	0.02	0.1	0.1	0.1
Total nitrogen, % on bone-dry subs.	17.9	17.7	17.6	17.7	17.7	17.7
Amino nitrogen, % of total nitrogen	2.3	2.4	2.4	2.2	2.1	2.9
Specific viscosity of protein solutions						
Concentration 1.0 g/100 ml	0.27	0.32	0.24	0.28	0.32	0.24
0.5 g/100 ml	0.11	0.14	0.10	0.12	0.13	0.10
0.2 g/100 ml	0.03	0.04	0.03	0.04	0.04	0.03
Axial ratio of protein particles, b/a	10	13	13	13	13	13

120-125°. When 1.0-1.5 hours had passed after the required temperature had been reached, the autoclave was cooled to 90-95°, the nitrogen was released, and the beaker with the protein removed.

To investigate the effects of different alkalis used for liming of hides in the leather industry on the properties of the "melted out" products, three raw cowhides weighing 30-35 kg were taken. The backs of these hides were cut into 3 x 12 cm strips. These strips were grouped into asymmetrical fringes. Each group consisted of ten strips. The cut raw hides were preserved by the pickling method and stored in a cool building.

The properties of the products "melted out" of hides limed in lime suspensions, in sodium sulfide, and in caustic soda were studied. The liming time and concentrations were varied over wide limits.

After the liming the material was split, deashed (neutralized), dried with acetone free from aldehydes, cut on a disk machine, electrodialyzed, and treated in the autoclave. The dissolved proteins were precipitated and dried by means of acetone. The acetone was evaporated out of the proteins in a fan drier. The proteins could be kept for a long time in the dried state.

The protein preparations were analyzed for moisture, ash, total and amino nitrogen; the solution viscosity and asymmetry of the protein molecules were determined. Total nitrogen was determined by the Kjeldahl method, and amino nitrogen by titration of protein solutions in presence of formaldehyde.

In formol titration by the indicator method it is very difficult to obtain a distinct end point. Therefore, some fairly successful attempts have recently been made to replace the indicator method by a potentiometric method. Dunn [5] and Borsook [6] used a glass electrode. The end point was established separately for each different material. Voitsekhovskii [7] recommended the use of a simplified potentiometric circuit with platinum and calomel electrodes. We used the MOSKIP* tube potentiometer with a glass electrode. The end point in the titration was determined from a differential curve plotted in $[\Delta E/\Delta V; V]$ coordinates, where $\Delta E/\Delta V$ is the change of potential in millivolts per unit volume of alkali, and V is the volume of standard alkali solution added to the mixture. The inflection point in the curve was taken as the end point. The standard alkali solution was added from a microburet. The formaldehyde was previously neutralized by magnesium carbonate.

To 20 ml of protein solution containing 1 g per 100 ml in a 50 ml measuring flask 20 ml of neutralized commercial formalin was added. The volume was made up to the mark with distilled water, and the mixture was poured into a glass beaker for titration. The solution was stirred after each addition of alkali. The readings of the potentiometer rheochord were taken one minute after each addition of the standard alkali solution. 20 ml of the formalin solution was titrated under the same conditions in a blank experiment. The volume of alkali used in the blank experiment was subtracted from the volume used for titration of the protein solution. The amino nitrogen was then calculated as a percentage of the total nitrogen.

The specific viscosity of the solutions was measured by means of an Ostwald viscosimeter at $40 \pm 1^\circ$. The solutions measured had concentrations of 1.0, 0.5, and 0.2 g per 100 ml. The efflux time of water through the capillary was 57 seconds; the capillary length was 170 mm; the volume of the viscosimeter bulb was 2.5 cc.

The protein concentration was determined colorimetrically by the biuret reaction. Kel'zon [8] showed that when total nitrogen is determined by this method the average relative deviations of the results from those given by the Kjeldahl method are 1.97-3%. From the filtered solution 10 ml was taken by means of a pipet and transferred to a 200 ml measuring flask. The solution in the measuring flask was diluted with a tenfold volume of distilled water, and 2 ml of saturated copper sulfate solution and 20 ml of 33% caustic soda were added. The solution in the measuring flask was then made up to the mark and filtered through paper. The intensity of the violet color of the filtrate was estimated by means of the MOSKIP photocolormeter.

Since the viscosity is very much influenced by the solution pH, the determinations were always performed in the range pH 6.15-6.85.

The specific viscosity data for dilute solutions were used to calculate the intrinsic viscosity coefficient K from the equation [9]

$$K = \lim_{c \rightarrow 0} \left(\frac{\eta_{sp}}{c\varphi} \right),$$

where K is the intrinsic viscosity coefficient; c is the concentration; φ is the partial specific volume of the protein, taken as 0.75; i. e., it was assumed that the protein molecules were not hydrated.

If the intrinsic viscosity coefficient is known, Simha's table [10] can be used to find the axial ratio for the ellipsoidal protein particles. The higher this ratio, the greater is the asymmetry of the molecules.

Analytical results for the protein preparations are given in Tables 1, 2, 3, 4, and 5.

The "melting out" conditions indicated above were selected on the basis of the data in Table 1, where the properties of protein preparations obtained under different "melting out" conditions are compared. The hide specimens used were first treated for 7 days in a liquor consisting of a lime suspension (15 g/liter) and sodium sulfide (0.8 g/liter).

The results show that increase of the treatment temperature from 75 to 120° in the autoclave under excess pressure does not influence the carboxyl group content determined by formol titration, or the viscosity of protein solutions. Therefore, increase of temperature neither increases nor decreases the number of active centers in the dissolved protein, and does not change the molecular shape or dimensions.

Increase of pressure likewise has no significant influence on the proteins. The viscosity of the protein solutions varied only slightly under all the pressures investigated.

* Moscow Controls and Measuring-Instruments Plant.

Observations of the protein yields dissolved out under various conditions showed that at 75° and 8 atmos the amount of protein dissolved is only 3% of the hide weight, and at 105° it is 20%. Solution was complete at 120-125°. The solution process was accelerated if excess pressure was used. Therefore, in the subsequent experiments the process was performed at 120-125° and 6-8 atmos.

In addition to data on the protein preparations, Table 2 includes analytical data on commercial photographic gelatin for comparison.

Brief liming does not produce any appreciable changes in the total nitrogen content. Some decrease of the nitrogen content of the protein is produced after liming lasting one year.

Deliming, by electrodialysis, of material limed for more than ten days does not remove Ca^{2+} completely from the derma. A chemical compound is evidently formed between the protein and Ca^{2+} during liming. Manokhin [11] noted the possible formation of such a compound. Chernov [12] considered that the formation of a chemical compound between the alkali and collagen, the main protein in the hide, is one of the causes of the conversion of skins into hide "of definite microstructure and definite composition." Mikhailov [13] presented data confirming the formation of a stable compound of collagen with calcium ions. According to Theis and Blum [14], collagen can bind 5.81 ml of 0.1 N $\text{Ca}(\text{OH})_2$ or 0.0166 g of CaO per gram of protein during prolonged liming. This amount of bound calcium oxide corresponds to 1.66% on the bone-dry substance.

In our experiment the voltage of the direct current in electrodialysis was 110-120 v. Hides limed for one or two years were electrodialyzed for periods 4-5 times as long as those for hides limed for short times, and yet the ash content of the protein preparations obtained from them was 1.3-1.4%. The amino-nitrogen content increased with the liming time. However, this increase only becomes significant in liming lasting one or two years. In liming of up to 20 days the increase of amino nitrogen is 10-15%.

Neither the specific viscosity of protein solutions nor the axial ratio of the protein particles change as the result of treatment of hides in lime suspension for up to 10 days. Further treatment results in abrupt increases in the specific viscosity and particle asymmetry, but neither the viscosity nor the particle asymmetry reach the corresponding values for gelatin. Solutions with specific viscosities and axial ratios approaching those for gelatin are only obtained after liming lasting 2-3 months to one year. The variations of protein solution viscosity with liming time can be seen in the diagram where accuracy of the determinations is indicated by bands representing the root mean square and individual variations in duplicate determinations of the viscosity of proteins extracted from different hides.

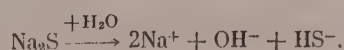
In studies of the effect of treatment of hides with sodium sulfide (which is a strong reducing agent) on the properties of the extracted proteins, the effects of different concentrations of sodium sulfide, and the effects of sodium sulfide solution containing 3.9 g per liter acting on the hide for different times, were investigated.

Tables 3 and 4 show that treatment with sodium sulfide solutions produces changes which differ from those caused by lime suspensions. The ash contents of the protein preparations are relatively low. The ash can be extracted almost completely by electrodialysis. The protein does not bind Na^+ .

Although the amino nitrogen content did not increase after treatment of the hide with sodium sulfide for three days, increase of the treatment time to six days produced a sharp rise in the carboxyl group content, determined by formol titration.

As in lime treatment, the specific viscosity of the solutions increases with concentration, but it does not reach the values obtained in lime treatment. Moreover, even six days of treatment leads to hydrolysis, accompanied by increase in the number of active centers in the protein and a decrease of solution viscosity.

Sodium sulfide is known to undergo hydrolysis:



To determine the effect of OH^- separately, in absence of HS^- , caustic soda solutions were used as sources of OH^- ions for the treatment. The analytical data for the proteins are given in Table 5.

TABLE 5

Analytical Data on Proteins From Hides Treated For Three Days with Caustic Soda

Characteristics	Raw material	Caustic soda concentration		
		0.01 N	0.05 N	0.1 N
Moisture, %	11.6	14.3	12.6	12.3
Ash, % on bone-dry subs.	0.1	0.1	0.1	0.1
Nitrogen by Kjeldahl, % on bone-dry subs.	17.7	17.5	17.7	17.8
Amino nitrogen, % of total nitrogen	2.3	2.4	2.4	2.4
Specific viscosity of protein solutions				
Concentration 1.0 g/100 ml	0.27	0.27	0.30	0.32
" 0.5 g/100 ml	0.11	0.12	0.13	0.14
" 0.2 g/100 ml	0.03	0.04	0.04	0.05
Axial ratio of protein particles, b/a	10	18	18	15

Thus, analyses of the "melted out" products showed that under ordinary liming conditions the total and amino nitrogen and ash contents of the protein change somewhat. With increase of the liming time to one year the amount of ash which cannot be removed by electrodialysis at 110-120 v reaches 1.3-1.4%. This corresponds to the amount of lime bound stably with the protein. The amino-nitrogen content increases at the same time.

The viscosity of the "melted out" products and their particle asymmetry change considerably during alkaline treatments; the action of lime produced an abrupt increase of solution viscosity. The solution viscosity and particle asymmetry decrease if the limiting period exceeds one year.

The effects of calcium hydroxide, sodium sulfide, and caustic soda on hides were investigated in this work. Each of these substances exerts its specific effects on hide. Therefore, one of them must not be replaced by another indiscriminately. The specific action of each must be taken into account. In the glue and gelatin industry, when products of high solution viscosity are required, the hides must be treated in lime suspensions.

It is shown in this paper that highly viscous and concentrated protein liquors can be obtained if the proteins are extracted in an autoclave at 120-125° during 1.0-1.5 hours in a nitrogen atmosphere.

SUMMARY

1. A method has been developed for dissolving the protein from the derma of animal hides; this may be used as a basis for extraction of proteins from derma in the glue and gelatin industry.
2. The effects of alkaline treatments on the properties of the proteins extracted from derma have been studied.

Scientific Research Institute of the
Leather and Footwear Industry, Moscow

Received June 22, 1957

LITERATURE CITED

- [1] A. Küntzel and J. Philips, *Collegium* 267 (1932).
- [2] V. G. Babakina and B. S. Kutukova, *Coll. Trans. Central Sci. Res. Inst. Leather and Footwear Ind.* 8, 18 (1935).
- [3] E. I. Galina, *Comparative Investigation of the Properties of Collagen Produced by Different Methods* (Moscow Tech. Inst. of the Light Industry, 1948). [in Russian].

- [4] V. S. Tongur, *Biochemistry* 17, 425 (1952).
- [5] M. S. Dunn and A. B. Loshakoff, *J. Biol. Chem.* 113, 389 (1936).
- [6] H. Borsook and J. Dubnoff, *J. Biol. Chem.* 131, 163 (1939).
- [7] V. L. Voitsekhovskii, *Sci. Res. Trans. Central Sci. Res. Inst. Leather and Footwear Ind.* 21 (1952).
- [8] L. F. Kel'zon, *Problems Med. Chem.* 4, 205 (1952).
- [9] R. Chernyak and A. Pasynskii, *Colloid J.* 10, 245 (1948).
- [10] A. G. Pasynskii, *Progr. Chem.* 10, 519 (1941).
- [11] I. G. Manokhin, *Raw Materials and Preparatory Operations in Leather Manufacture* (St. Petersburg, K. L. Rikker Press, 1909). [In Russian]
- [12] N. V. Chernov, *Leather Technology* (State Light Ind. Press, 1937). [In Russian]
- [13] A. N. Mikhailov, *Physicochemical Principles of Leather Technology* (State Light Ind. Press, 1949). [In Russian]
- [14] E. Theis and B. Blum, *J. Amer. Leather Chemists Assoc.* 37, 93 (1942).

KINETICS OF THE FORMATION OF CRYSTALLIZATION CENTERS OF SUPERCOOLED ORGANIC LIQUIDS ON PARTICLES OF IMPURITIES

G. L. Mikhnevich

The kinetics of the conversion of a supercooled melt into a crystalline phase has been studied experimentally by a number of workers [1-5]. The theoretical aspects of the problem have been discussed in several publications [6-9]. The problem was solved in the most general form by Kolmogorov [10] and, in another form, by Rodigin [11]. This theory relates to the spontaneous formation of crystallization centers, and has been applied with success to the crystallization of metals.

In this paper an attempt is made to determine the mechanism and kinetics of formation of crystallization centers on particles of impurities, and to correlate the kinetic law with the particle-size distribution of the impurities.

Method. The course of formation of crystallization centers can be conveniently observed in supercooled liquids with fairly low linear rates of crystallization, at least in the temperature range in which the probability of crystal formation is fairly high. Such substances include piperine, betol, aspirin, etc. Such experiments have been performed by Kondoguri [12, 13] and by the present author et al, [14, 15] on flat specimens consisting of two cover glasses with a drop of melt wetting both glasses between them. The specimen was placed on the microscope stage in such a way that a constant-temperature air stream flowed over it above and below. The centers appearing in the microscope field at $\times 60$ (or $\times 80$) magnification were counted at equal time intervals, 10 or 5 minutes. The number of centers per constant drop area was determined. The results are plotted graphically, the time (t) in minutes or days (according to the experimental temperature) being taken along the abscissa axis, and the corresponding numbers of crystallization grains (n) along the ordinate axis.

In every experiment with piperine, salol, and betol the number of visible crystallization grains reached a certain limiting value n_{∞} , which depended on the experimental temperature, and which then remained constant, although the total volume of the crystalline phase was considerably less than the volume of the melt (Figs. 1 and 2).

These results lead to the definite conclusion that the crystallization nuclei for the substances studied can only be particles of active impurities which become crystallization centers during the experiment. Since their number is limited, they gradually become exhausted and the number of crystallization centers then remains constant.

Improvement of preliminary purification by increase of the number of crystallizations or by filtration of a melt or solution of the substance through a glass filter reduces the limiting number of crystals for drops of equal volume. The limiting number also decreases appreciably on repeated crystallization of the same sample [14].

In either case the number of active impurity particles decreases as the result of deactivation [1, 16-18].

Experiments with many specimens under different conditions showed that the kinetic curves belong mainly to two types. Curves of the first type are obtained with fairly small supercooling, when the rate of appearance of visible crystallization grains decreases continuously from the appearance of the first grain and becomes zero at the limiting value (Fig. 1). Curves of the second type are obtained when the supercooling is considerable; the formation rate of crystallization centers increases at first, reaches a maximum at the inflection point of the kinetic curve, and then tends to zero (Fig 2).

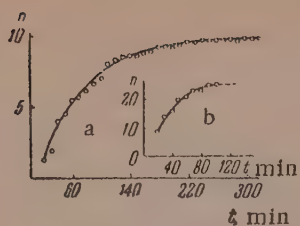


Fig. 1. Kinetics of formation of crystallization centers at high temperatures: a) betol; b) piperine; the values of \bar{n} along the ordinate axis should be multiplied by 0.15.

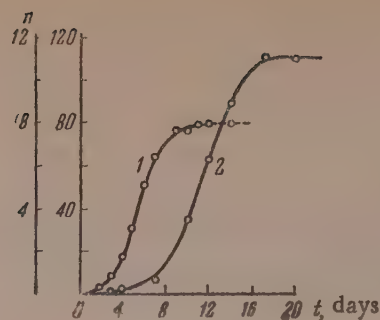


Fig. 2. Kinetics of formation of crystallization centers at moderate temperatures: 1) for salol; 2) for piperine.

The mechanism determining the kinetics of the process at various temperatures was elucidated on the hypothesis that the gradual appearance of visible crystallization grains is due to the fact that the particles of active impurities present in the melt before the start of crystallization vary in size. This view had been put forward a long time ago [1].

Suppose that the crystallization nuclei at the initial instant are solid particles coated with a crystalline layer of the substance studied, or of a substance of similar structure [16, 18]. In the course of time such nuclei become covered with a number of consecutive crystalline layers of the melt substance. When this crystalline coating becomes thick enough, it masks the influence of the surface of the foreign nucleus, so that the specific properties of the nucleus can influence only the growth rate of the first crystalline layers, and also, of course, the total number of active impurities.

Impurity "particles" may also be present in the form of micropores on the surface of a large particle, filled with a crystalline mass of the substance studied [16]. Colloidal particles can also act as such nuclei [1]. We shall regard all such particles or nuclei as solid in the sense that their dimensions remain unchanged throughout a given experiment, if the specimen is melted.

The following assumptions are made:

1. The rate \bar{c} of the conversion and subsequent steady growth of a nucleus is low over the whole temperature range studied.
2. This rate \bar{c} is constant during the latent period, and is equal to the growth rate of visible centers*.
3. The distribution of active impurities in the drop volume is uniform, and their concentration is so low that during the entire process of formation and growth to visible size the growing crystallization centers do not have time to capture and absorb active particles or nuclei present in their vicinity. In general, if impurity concentrations are high and the growth rates considerable such capture occurs, and introduces considerable complications into the effect and the associated calculations.

If the crystallization centers are formed by a spontaneous mechanism, each molecule in the bulk of the melt is capable of serving as the initial point for the formation of a nucleus which can be converted into a center as the result of fluctuations. Because of this, the effective volume in which crystallization centers can be formed decreases continuously throughout the entire process of conversion of the melt into a solid phase.

We shall show that in our earlier kinetic experiments [14, 15] (Figs. 1 and 2) there was no capture of impurity particles leading to distortion of the kinetic curves, since the distribution of the impurities could be regarded as fairly uniform. As the specimens were very thin (from 0.02 to 0.2 mm), we shall solve the plane problem,

*Constancy of the rate \bar{c} , i. e., its independence of the nucleus size, which is assumed here, was confirmed by experiments with cyclonite solutions [19].

by considering the area occupied by a crystallization center which is in the form of a lens or a plane disk thickened at the center. At low temperatures these flat formations have a thickness (in specimen drops ~ 0.2 mm thick) less than the thickness of the specimen.

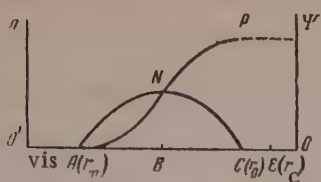


Fig. 3. Curves for the kinetics of formation of crystallization centers (ANP) and the presumed impurity particle size distribution (ANC).

We now find the condition that neighboring "disks" should not be in contact at their edges when their number reaches the limiting value n_{∞} . Let the area of the layer in the specimen, within the limits of which the crystallization grains are counted, be square in form and have the value d^2 . In this case there are n_{∞}/d^2 grains per unit area, and $\sqrt{n_{\infty}}/d$ per unit length. During the entire growth process, lasting T minutes, the greatest size of the central disk (the first to form among the others) is $\delta = 2cT$, where δ is the diameter of the disk periphery and c is the linear rate of growth.

The condition that neighboring grains are not in contact is given by the inequality

$$d/\sqrt{n_{\infty}} > \delta. \quad (1)$$

For example, with a square of ~ 3 mm side, generally used in the experiments, at the end of time T the greatest grain diameter δ was 4-5 mm, and the average true diameter was $5:60 \approx 0.083$ mm. The limiting number of crystallization centers was usually ~ 70 (compare Fig. 1, where n_{∞} is 65), and then $d/\sqrt{n_{\infty}} \approx 0.37$. Thus, Inequality (1) is satisfied. It should be noted that the inequality is increased if the average and not the maximum size of the crystallization grain is considered.

Naturally, if the distribution of the impurity particles is not uniform some of the nuclei may be absorbed by crystallization centers arising earlier; this should lead to a decrease in the limiting number of crystallization grains and some distortion of the kinetic curve at the very end of the process.

4. For simplicity of calculation we assume that the impurity particles are spherical. Other shapes can be considered by introduction of a shape factor.

If a given liquid is not capable of spontaneous nucleation of crystals, the kinetics of the process differs in different cases.

I. All the active impurity particles are "ready" centers of crystallization at the start of the process, i. e., their initial radius r is greater than the critical size r_c ($r > r_c$) at which, according to the fluctuation theory, a nucleus is in thermodynamic equilibrium with the surrounding liquid phase. In this case these particles begin to grow steadily when a constant exposure temperature has been established, become visible under the microscope, and are recorded as crystallization grains.

Hence in this case there is no formation stage as such, and the process kinetics is determined entirely by the number of active impurity particles and their size distribution.

II. All the original particles are below critical size ($r < r_c$).

It is assumed that the initial stage (formation) is statistical in character, as in the spontaneous mechanism at its later stages, and only the initial size (size of the foreign nucleus covered by a crystalline layer) is fixed. When these nuclei reach, as the result of fluctuations, the critical size (or, more correctly, a somewhat greater size), their subsequent growth becomes monotonic, as in the first case. In this case the kinetic law is only partially determined by the impurity particle size distribution.

III. Since the critical size depends on temperature, temperature conditions are possible in which some of the initial particles are smaller than r_c , while the others are equal to or greater than r_c .

Case I: $r > r_c$ (r_0, r_m), where r_0 is the least and r_m the greatest particle radius.

For visual representation of the process, we take the particle radii to the left along the abscissa axis, and

the corresponding numbers of particles along the ordinate axis; the distribution function $\psi(r)$ is then schematically represented by a certain curve ANC (Fig. 3).

In the course of time all the particles grow at a constant rate c_0 , and the distribution curve shifts steadily to the left at rate c_0 . In Fig. 3 the distance OO' represents the minimum size of a crystallization grain distinguishable under the microscope (at the given magnification), and therefore the intercept AO' represents the distance traveled by the crystallization front during the time interval known as the latent period. As the $y = \psi(r)$ curve moves further, crystallization grains begin to be detected when the curve cuts the axis $O'n$. The limiting number of grains is reached when the end C of the curve, representing the smallest size r_0 , passes through the point O' .

To show, in the same diagram, the kinetic curve (the variation of the number of visible crystallization grains with time) we take time along the abscissa axis, toward the right (with the origin at point O'), and the total number of grains visible at time t along the ordinate axis $O'n$. The particle-size distribution curve is assumed stationary while the axis $O'n$ is moved to the right at velocity c_0 . The kinetic curve ANP begins at the point A at the end of the latent period, which is represented by $O'A$, and it ends at the point C, which is the time instant at which the axis $O'n$ reaches the beginning of the distribution curve $y = \psi(r)$. At the end of time $O'C$ all the active impurity particles have been consumed and the number of crystallization grains thereafter remains at the limiting value n_{∞} . The ordinates of the kinetic curve represent the integral number of grains at the time instant corresponding to the particle size $r(t)$, i. e.,

$$n = - \int_{r_m}^{r(t)} (\psi(r) \frac{dr}{dt} dt, \quad (t_A, t). \quad (2)$$

Thus, these ordinates give the area enclosed by part of the curve $y = \psi(r)$ and the intercept $Ar(t)$ on the Or axis. The inflection point N on the kinetic curve corresponds to the maximum on the distribution curve for the impurity particles. The distribution function $\psi(r)$ can be found by graphical differentiation of the kinetic curve if the rate c_0 is known.

Case II is represented by Curve a in the schematic Fig. 4

$$r' < r_c, \quad (r_0, r_m).$$

Particles of these sizes can become crystallization centers only as the result of accidental changes of size: the particle radius may increase or decrease, but does not pass beyond the lower limit — the initial size of a nucleus covered by a crystalline layer. Only a few of them can reach the critical size, when they start to grow monotonically, as in the first case. The probability of this is calculated from the fluctuation theory [20, 21]. In this theory the probability I of spontaneous transformation of an unstable nucleus into a nucleus of critical size is determined by an expression of the form

$$I = Ce^{-\frac{U}{kT} - \frac{R(T)}{kT}}, \quad (3)$$

where T is the absolute temperature, k is the Boltzmann constant, U is the activation energy, and $R(T)$ is the work of fluctuation necessary to surmount the potential barrier.

The value of $R(T)$ is found as follows

$$R(T) = \gamma \frac{M^2 T_0^2 \sigma^3}{q^2 \rho^2 (T_0 - T)^2}, \quad (4)$$

where M is the molecular weight; T_0 is the melting point; σ is the specific interfacial energy; q is the molar heat of crystallization; ρ is the density of a crystal nucleus; γ is the shape factor, which is $4\pi/3$ for a spherical nucleus.

The critical size of a spherical nucleus is inversely proportional to the supercooling

$$r_c = \frac{2\sigma MT_0}{q\rho(T_0 - T)}. \quad (5)$$

The work $R(T)$ can be expressed, from Equations (4) and (5), as

$$R(T) = \frac{4\pi\sigma r_c^2}{3}. \quad (6)$$

For a nucleus of radius r the work is less by the quantity for the spontaneous formation of a nucleus of the same size

$$\Delta R = \frac{4\pi\sigma}{3}(r_c^2 - r^2). \quad (7)$$

Thus, the probability of transformation of a single nucleus of radius r into a crystallization center is given by the expression

$$Ae^{-\frac{4\pi\sigma}{3kT}(r_c^2 - r^2)}. \quad (8)$$

Let the impurity particle size distribution be characterized by the function $\psi(r)$ as before. The rate of transformation of all the mass of nuclei into crystallization centers is determined by the function

$$\varphi(r) = \psi(r) \left\{ Ae^{-\beta(r_c^2 - r^2)} \right\}, \quad (9)$$

where

$$\beta = 4\pi\sigma / 3kT. \quad (10)$$

This function, which we term the effective distribution function, determines the kinetic law.

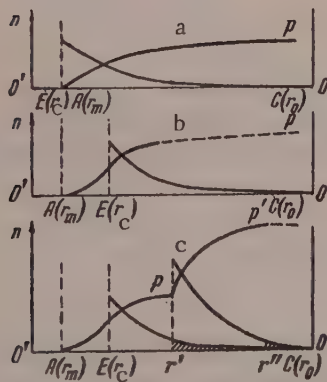


Fig. 4. Kinetics of formation of crystallization centers (Curve AP) and size distribution of nuclei arising on impurity particles as the result of fluctuations at various temperatures, in relation to the critical size r_c .

The exponential factor which includes the activation energy U depends only on the temperature T , and therefore, when we consider the process kinetics under isothermal conditions it can be incorporated in the constant A . This factor largely determines the velocity c_f of the ordinate axis $O'n$ in Fig. 3 during formation of the crystallization centers. The rate of their further growth might be characterized by another exponential factor of analogous form, contained in Volmer's or Stranskii's [22] formulas for crystal growth, derived from the fluctuation theory. This rate, denoted above by c_0 , is also determined by the activation energy, and in addition by the work of formation of a two-dimensional nucleus on the face of a three-dimensional nucleus. The process of crystal growth is in reality more complex than its description by the Volmer or Stranskii theories: the theoretically calculated dependence of the linear rate of crystallization on the temperature does not coincide with the experimental, especially at low temperatures [22].

In any event, the growth rate of crystallization centers differs from their formation rate (c_f). These

rates cannot be separated in kinetic studies, as the formation and growth processes are consecutive, and occur during the latent period.

For slowly-crystallizing substances the growth rate c_0 should predominate. In any case, we shall take a certain mean value of the rates c_0 and c_f , denoted by \underline{c} , as the rate of the over-all process.

We now assume that the process conforms to an equation for a first-order reaction

$$n = n_{\infty}(1 - e^{-\alpha t}). \quad (11)$$

We equate \underline{n} , the number of crystallization grains in Equation (11), to the integral number of crystallization centers which have reached visible size, by Formula (2) in which the function $\Psi(r)$ is replaced by the effective function $\varphi(r)$

$$-\int_{r_m}^{r(t)} \varphi(r) \frac{dr}{dt} dt = n_{\infty}(1 - e^{-\alpha t}). \quad (12)$$

We differentiate both sides of this equation with respect to time

$$-\varphi(r) \frac{dr}{dt} = \alpha n_{\infty} e^{-\alpha t}. \quad (13)$$

The derivative dr/dt is equal to the growth rate of a crystallization center or the velocity of the axis $O'n$ to the right, with the sign reversed, i. e., $-c$:

$$dr/dt = -c. \quad (14)$$

Integrating both sides of this equation

$$-t = \frac{r(t) - r_m}{c} \quad (15)$$

and substituting the value of \underline{t} from Equation (15) and dr/dt from Equation (14) into (13) we have

$$\varphi(r) = \frac{n_{\infty} \alpha}{c} e^{\frac{\alpha}{c}(r - r_m)} \quad (16)$$

or

$$\varphi(r) = \text{const} e^{\frac{\alpha}{c} r}, \quad (16a)$$

i. e., the effective distribution function is a monotonically increasing function of \underline{r} (see Fig. 4, a). To determine the nucleus size distribution function $\Psi(r)$ which can give rise to the kinetic Equation (12) as the result of fluctuations, we substitute $\varphi(r)$ from Equation (16) into (9)

$$\psi(r) = \left[\frac{\alpha n_{\infty}}{cA} e^{\beta r^2} \right] e^{-\frac{\alpha}{c}(r_m - r) - \beta r^2}. \quad (17)$$

It follows from the definition of the function $\Psi(r)$ for the initial distribution of the impurity particles that in the right-hand side of Equation (17) all the parameters should be independent of the experimental temperature.

This leads to a number of conclusions:

1. The ratio α/c should be independent of the temperature, i. e., should be proportional to the rate of the kinetic process; this can be verified experimentally.

2. The parameter β should also be independent of the temperature, i. e., the surface energy σ should be proportional to the absolute temperature. It is reasonable to suppose that σ increases and not decreases with fall of temperature. Since it is unlikely that proportionality of σ to temperature T has any physical meaning, we shall merely note that the dependence of β on temperature is slight compared with the dependence $\frac{1}{T_0 - T}^2$, which contains $1/(T_0 - T)^2$. Subsequently we shall regard β as constant. The validity of this approximation will be confirmed in a future paper.

3. The expression in brackets in Equation (17) should not vary with the temperature. For the limiting

number, Equation (9) gives

$$n_{\infty} = \frac{A}{e^{\beta r_c^2}} \int_{r_0}^{r_m} \psi(r) e^{\beta r^2} dr. \quad (18)$$

In view of the fact that the value of the integral depends relatively little on the temperature, whereas the $e^{-\beta r_c^2}$ represents strong dependence, since $r_c^2 \sim 1/(\Delta T)^2$, it may be assumed that

$$n_{\infty} \approx \text{const}/e^{\beta r_c^2}. \quad (18a)$$

Because of this the product $n_{\infty} e^{\beta r_c^2}/A$ in Equation (17) is approximately constant*.

The case described here ($r < r_c$) occurs at fairly high temperatures, in any event, if Conditions 1, 2, and 3 on pg. 62, and in particular Inequality (1), are satisfied. This is confirmed experimentally. In Fig. 1, Curve *a* refers to betol (β -naphthyl salicylate, m. p. 92.5°) for the high temperature of +13°, which is considerably higher than the abscissa of the maximum on the nucleation - temperature curve $t_m^0 = -1^\circ$; Curve *b* refers to piperine (an alkaloid derived from piperic acid, m. p. 129°, nucleation maximum $\approx 40^\circ$) for 48°. Fig. 5 shows the good fit of the curves in Fig. 1 with the logarithmic form of the first-order reaction equation (11), i. e.

$$\lg(n_{\infty} - n) = -\alpha n_{\infty} t + \lg n_{\infty}. \quad (19)$$

Case III is shown in Fig. 4:

$$r_0 < r_c < r_m. \quad (20)$$

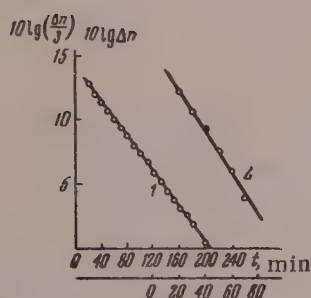


Fig. 5. Variation of $\log(n_{\infty} - n)$ with time in accordance with the first-order reaction law at high temperatures:

1) for betol; 2) for piperine.

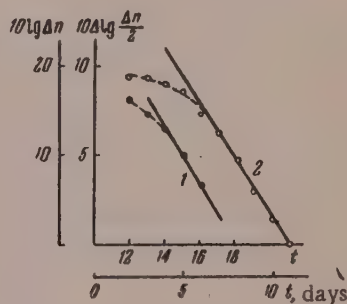


Fig. 6. Variation of $\log(n_{\infty} - n)$ with time in accordance with the first-order reaction law at moderate temperatures: 1) for salol; 2) for piperine.

It is evident that calculations relating to the fluctuation mechanism are not valid for r lying in the (r_m, r_c) range (between the points A (r_m) and E (r_c) in Fig. 4), as at $r > r_c$ crystallization centers should form on nuclei above the critical size. For $r_c < r_m$ (between the points E (r_c) and C (r_0) in Fig. 4) the effective distribution function $\varphi(r)$ is

$$\varphi(r) = \frac{\alpha}{c} n_{\infty} e^{\frac{\alpha}{c}(r-r_c)}. \quad (21)$$

*Equation (17) leads to an important conclusion: since $r < r_m$, the function $\psi(r)$ is a monotonically decreasing function of r , as β is very large relatively to α/c . Hence in the first case, when $r > r_c$, the kinetic curve (Fig. 3) should not have an inflection point, i. e., the slope of the tangent should increase continuously until either all the nuclei have been used or the whole melt has crystallized, in accordance with the total number of impurity particles and the value of r_0 for the smallest nucleus.

Thus, when $r = r_c$ one type of curve should pass into the other, and the slope of the tangent to the kinetic curve should change at the transition point. An inflection point is usually found here.

The case represented by Inequality (20) is shown in Fig. 2; the left-hand curve applies to salol, and the right-hand curve to piperine, both being plotted at room temperature. The rate of the process was so low that the crystal grains were counted at intervals of 24 hours, and not every 10 minutes as is usual at high temperatures. The same curves are plotted in logarithmic form in Fig. 6; the relationship is linear for the later times, in agreement with Equation (19), and the linearity breaks down at the instant corresponding to the inflection point. This case was verified for many samples of piperine and salol. In experiments with piperine and sulfur it was found that additional crystals appear if a lower constant temperature is used immediately after the number of crystallization centers has reached the limiting value. The number of these centers may reach a new limiting value on the new region of the kinetic curve if enough uncrystallized melt remains in the specimen [14], as shown in Fig. 4, c. This raises the question of the correlation between the increase of the limiting value of n_{∞} with the degree of utilization of all the active impurity particles.

It follows from Equation (18a) that n_{∞} should increase, as r_c decreases with fall of temperature. This conclusion has no physical meaning if it is assumed, as was done earlier, that n_{∞} is really reached with the smallest nucleus of size r_0 . This contradiction can be resolved if it can be shown that n_{∞} can be reached with particles of size $r' > r_0$, where r' can differ at different experimental temperatures.

The ordinates of the effective distribution function $\varphi(r)$ are not large at high temperatures. Therefore, the integral in Equation (18) may be represented as the sum of two integrals

$$\int_{r'}^{r_m} \varphi(r) dr + \int_{r_0}^{r'} \varphi(r) dr = n_{\infty} \quad (22)$$

or

$$\int_{r'}^{r_c} \varphi(r) dr + \int_{r_0}^{r'} \varphi(r) dr = n_{\infty} \quad (23)$$

dependent on which case, $r_m > r > r_0$ or $r_c > r > r_0$, the kinetic curve at the original high temperature represents (see Fig. 4, a and 4, b). The value of the second integral, represented by the shaded region in Fig. 4, c, may be < 1 , and then additional crystallization centers will not be found directly (during the usual interval between consecutive counts)*. After the axis O'n in Fig. 4, c has reached the abscissa $r = r'$, the number of crystallization

centers cannot increase any further, and in practice the limiting number is reached at that instant (the ordinate $r'P$ in Fig. 4).

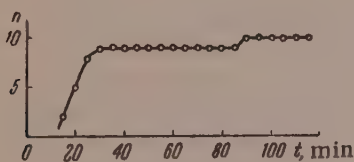


Fig. 7. Kinetics of formation of crystallization centers in betol during prolonged observation.

However, if the temperature is lowered, as shown in Fig. 4, c, new crystallization centers appear in considerable amounts, arising on nuclei of radius $r < r'$. This temperature decrease results in a new distribution, for which the ordinates of the function $\varphi(r)$ are higher than for the previous function, because of the decrease of r_c in the denominator of the limiting values of n_{∞} as given by Equations (18a) and (21). The new limiting number is

$$n'_{\infty} \cong \int_{r''}^{r'} \varphi(r) dr, \quad (24)$$

* This is confirmed by an experiment, performed several times, in which the specimen was observed for a long time after the number of centers had reached the limiting value. Fig. 7 shows that in betol subjected to repeated crystallization one center appeared after 55 minutes, after which the number of crystallization centers became constant again.

where

$$\phi_1(r) = n_{\infty} \frac{a}{c} e^{-\frac{a}{c}(r-r_c)} \quad (25)$$

This temperature lowering is difficult to effect in practice in the case of piperine, as it is necessary to have a considerable amount of the melt uncrystallized at the end of the experiment, but in the case of sulfur it is easily achieved with a large number of small drops (see [14], Fig. 2, b).

SUMMARY

1. Experimental data are presented on the kinetics of formation of crystallization centers in slowly crystallizing supercooled organic liquids which are incapable of spontaneous crystallization.
2. Crystallization centers are formed on particles on active impurities coated with a crystalline layer of the melt substance.
3. Particles larger than the critical size as determined by the fluctuation theory grow monotonically and are converted into visible crystallization grains; crystallization centers are not formed.
4. The remaining particles are converted into crystallization centers; their formation requires work, which is less than in the spontaneous mechanism. The kinetics of the process in this case can be represented by a first-order reaction equation.
5. The fluctuation mechanism operates at fairly high temperatures, at low temperatures monotonic growth takes place, while at intermediate temperatures the initial part of the kinetic curve as far as the point of inflection corresponds to growth of particles above the critical size, and the rest of the curve conforms to a first-order reaction law.

The Odessa State University
Chair of Molecular Physics

Received July 6, 1957

LITERATURE CITED

- [1] C. N. Hinshelwood and H. Hartley, *Philos. Mag.* 43, 78 (1922).
- [2] W. Rix, *Z. Kristallogr.* 96, 155 (1937).
- [3] C. Hammer, *Ann. Physik.* 33, 445 (1938).
- [4] G. Ford and V. LaMer, *J. Amer. Chem. Soc.* 72, 1959 (1950).
- [5] G. M. Pound and V. LaMer, *Ibid.* 74, 2323 (1952).
- [6] F. Göler and G. Sachs, *Z. Phys.* 77, 281 (1932).
- [7] N. N. Afanas'ev, *J. Tech. Phys.* 7, 2305 (1937).
- [8] I. L. Mirkin, *Coll. Trans. Moscow Steel Inst.* 3, 38, 65 (1938).
- [9] M. Avrami, *J. Chem. Phys.* 7, 1103 (1939).
- [10] N. A. Kolmogorov, *Bull. Acad. Sci. USSR*, 3, 335 (1937).
- [11] V. N. Rodigin, *J. Tech. Phys.* 22, 1356 (1952).
- [12] V. V. Kondoguri, *Mem. State Phys. Inst. Odessa* 5 (1928).
- [13] V. V. Kondoguri, *J. Expt. Theoret. Phys.* 2, 728 (1941).
- [14] G. L. Mikhnevich and V. P. Efimova, *Coll. Phys. - Math. Faculty, Sci. Res. Inst. Phys. Odessa Univ.* 5, 115 (1954).
- [15] G. L. Mikhnevich and V. P. Efimova, *Ibid.* 5, 123 (1954).
- [16] W. T. Richards, *J. Chem. Soc.* 54, 479 (1932); 58, 2243 (1936).

- [17] V. I. Danilov and B. M. Teverovskii, J. Expt. Theoret. Phys. 10, 1305 (1940).
- [18] V. I. Danilov, Structure and Crystallization of Liquids [In Russian] (Acad. Sci. Ukrainian SSR Press, 1956).
- [19] S. Bransom and W. Dunning, Discus. Farad. Soc. 83 (1949).
- [20] M. Volmer, Kinetik Phasenb., (1939).
- [21] Ya. I. Frenkel', Kinetic Theory of Liquids (Izd. AN SSSR, 1945). [In Russian]
- [22] I. N. Stranskii, Progr. Phys. Sci. 21, 408 (1939).

EXPERIMENTAL INVESTIGATIONS OF LAMINAR SYSTEMS

24. KINETICS OF THE FORMATION OF HYDROXIDE FILMS ON THE SURFACE OF COBALT AND NICKEL AMMINE SOLUTIONS

S. G. Mokrushin and G. A. Kitaev

In the previous communication [1] a description was given of a method for studying the growth kinetics of hydroxide films on the surface of copper ammine solutions. It was found that films of nickel and cobalt hydroxides like copper hydroxide films, are formed on solution surfaces only if monolayers of a surface-active substance are present on the surfaces; a film of more uniform thickness is formed if a surface-active substance which forms a liquid monomolecular film is applied to the solution surface. The experimental data presented below refer to the formation of hydroxide films under monolayers of oleic acid.

The ammine solutions were prepared from solutions of nickel and cobalt sulfates. The thickness of the hydroxide films was determined visually, by comparison of the interference colors of the films with the same interference colors in Newton's rings. The refractive index of $\text{Ni}(\text{OH})_2$ films was taken as 1.428 [2], and of $\text{Co}(\text{OH})_2$ films as 1.38. The increase in the thickness of nickel hydroxide films is shown graphically in Fig. 1. Comparison of the slopes of Curves 1, 2, and 3 shows that the growth rate of film thickness, which can be found from the slope of the linear portions of the curves relative to the time axis, increases with decrease of ammine concentration in the solution. The explanation of the difference between the course of Curve 2 and 3 is that in the preparation of one of the solutions (Curve 3) the amount of ammonia added was considerably in excess of the theoretical amount required for hexammine formation. During the first 20 minutes excess ammonia is removed. When the ammonia content in the solution has fallen to a level at which hydrolysis of nickel ammine is possible, the hydroxide film begins to form and grow. The relationship between the growth rate of the film and the concentration of nickel ammine is plotted in Fig. 2. It is clear from Fig. 2 that the rate of film growth diminishes in proportion to the increase of solution concentration, the decrease being greater at higher temperatures.

The growth of cobalt hydroxide films is represented by curves analogous to those shown in Fig. 1, with the difference that the slope of the linear regions (in the thickness range from 1000 to 5000 Å) increases with increase of solution concentration. Addition of excess ammonia to the solution increases the time before the start of formation of the cobalt hydroxide film and decreases its growth rate, as bivalent cobalt is easily oxidized to the trivalent state in presence of ammonia, and the trivalent cobalt ammine is considerably more stable than the bivalent, as shown by their instability constants: $K_1 = 10^{-35.16}$ (trivalent cobalt) [3] and $K_2 = 10^{-5.1}$ (bivalent cobalt) [4]. The growth rate of a film on a solution which had been left to stand for two days after preparation is very low because of oxidation of Co^{2+} to Co^{3+} . Reproducible results are obtainable only with freshly prepared solutions containing the appropriate amounts of ammonia. The solutions were prepared by additions of 5, 10, 20, and 30 ml of ammonia solution of $d = 0.91$ g/cc to cobalt sulfate solutions, to give solutions with molar concentrations of 0.025, 0.05, 0.10, and 0.15 respectively.

Fig. 3 shows the effect of the concentration of cobalt ammine solution on the growth rate of cobalt hydroxide films. The growth rate of the hydroxide film is proportional to the solution concentration and is determined by the stage of the process the kinetics of which conform to a first-order reaction equation. In this instance the process of hydrolysis and ammonia evaporation from solution conform to such an equation.

Fig. 4 shows the effects of temperature on the growth rates of nickel and cobalt hydroxide films. The experimental points lie satisfactorily on straight lines given by the equation

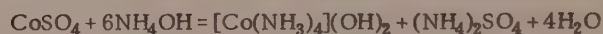
$$\lg W = A - B \frac{1}{T}.$$

To find the determining stage in the process of film growth, the kinetics of ammonia evaporation from solutions of nickel and cobalt amines was studied, as described in the previous paper. The experimental results are plotted in Fig. 5.

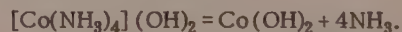
Fig. 5 shows that the initial regions of Curves 1, 2, and 3 have the same slope; the tangent of the angle is numerically equal to the rate constant for the evaporation of excess ammonia, present in solution over the theoretical amount.

The rate constant for evaporation of excess ammonia from ammine solution is $16.1 \cdot 10^{-3} \text{ min}^{-1}$ at 40° .

Fig. 6 can be used to find the ammonia content in solution at the time when intensive film growth begins. We found the ammonia contents to be 125, 64, and 26 mg per 10 ml of solutions of the following respective concentrations: 0.15, 0.10, and 0.05 mole/liter. By stoichiometric calculation, in the formation of cobaltous tetrammine by the reaction



10 ml of solutions of the above concentrations should respectively contain 102, 68, and 34 mg of ammonia, which can be removed from the solution used in the formation of the complex compound. Good agreement between experimental and calculated data was obtained only for the solution of 0.10 M concentration. The agreement between the experimental and calculated data led to the suggestion that the final linear portions of Curves 1, 2, and 3 correspond to evaporation of ammonia formed by hydrolysis of cobalt tetrammine with formation of hydroxide:



The fact that the times at which intensive growth of the hydroxide film and hydrolysis of cobalt tetrammine commence coincide confirms the above hypothesis and the equation for the hydrolysis reaction.

With the aid of the numerical value for the rate constant for evaporation of ammonia formed by the hydrolysis of cobalt tetrammine we can explain the relationship between the film growth rate and solution concentration, plotted in Fig. 3.

According to our data, the rate constant for the evaporation of ammonia liberated in hydrolysis of $[\text{Co}(\text{NH}_3)_4](\text{OH})_2$ is $K = 1.63 \cdot 10^{-3} \text{ min}^{-1}$. With the aid of the equation for the hydrolysis of cobalt tetrammine it is easily shown that the formation rate of cobalt hydroxide (in mg/minute) is given by the expression

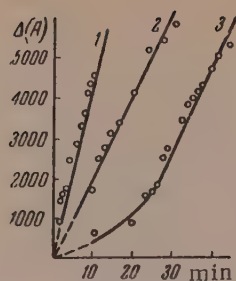


Fig. 1. Increase in the thickness of hydroxide films on nickel ammine solutions containing 0.025 mole/liter (1) and 0.20 mole/liter (2 and 3) at 30° and at an air rate of 1.0 liter/minute.

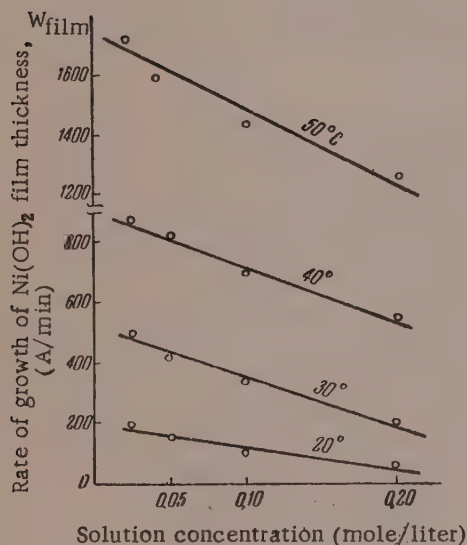


Fig. 2. Variation of the rate of film thickness growth with nickel ammine concentration.

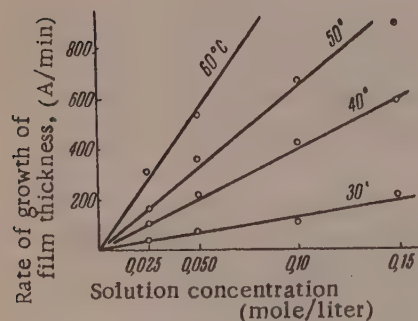


Fig. 3. Variation of the rate of film thickness growth with cobalt ammine concentration.

$$m' = \frac{93}{4 \cdot 17} k(a - x),$$

where 93 and 17 are the molecular weights of cobalt hydroxide and gaseous ammonia; a is the initial amount of ammonia in solution (this is equal to the total ammonia added to the solution less the amount combined with SO_4^{2-} ions); x is the amount of ammonia removed from solution in time τ (minutes). If we know the growth rate of film thickness W , the film area (S), and density ($d = 3.597$ [5]), we can calculate the amount of hydroxide entering the film in unit time. This is evidently

$$m'' = W \cdot Sd \cdot 10^3.$$

The calculated results are given in the table. The rates of film growth were determined graphically from Fig. 6.

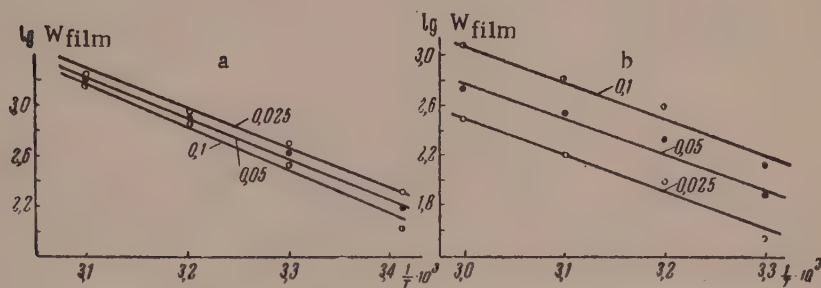


Fig. 4. Effect of temperature on the growth rate of nickel hydroxide films on solutions of 0.025, 0.05, and 0.1 M concentration: a) nickel ammine; b) cobalt ammine.

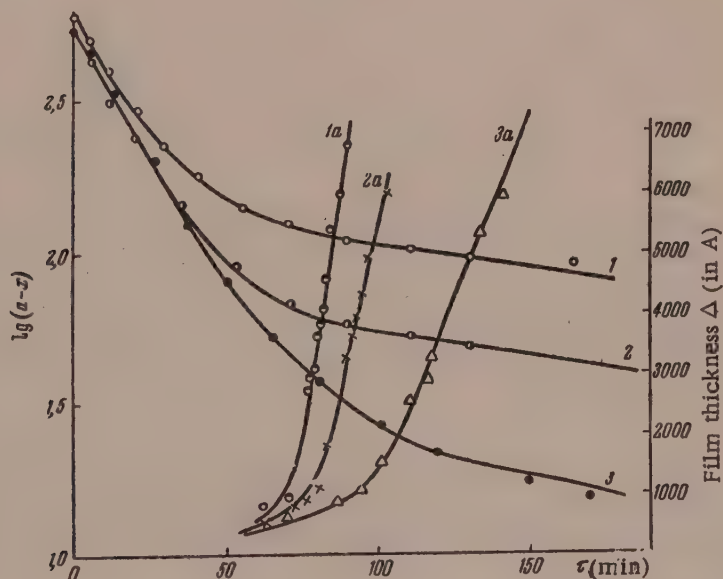


Fig. 5. Evaporation of ammonia from cobalt ammine solutions of 0.15 M (1), 0.10 M (2) and 0.05 M (3) concentration, and growth of cobalt hydroxide films (1a, 2a, 3a) on these solutions at 40° and air rate 1.0 liter/minute.

The values of m' and m'' in the table coincide; it follows that the growth rate of cobalt hydroxide film is determined by the rate of hydroxide formation resulting from hydrolysis of cobalt tetrammine.

Amounts of Hydroxide Entering the Film at Values of $(a - x)$: 34, 68, and 102 mg, for 0.05, 0.10, and 0.15 M Solutions

0.05 M		0.10 M		0.15 M	
m'	m''	m'	m''	m'	m''
$75 \cdot 10^{-3}$	$74.7 \cdot 10^{-3}$	$156.5 \cdot 10^{-3}$	$143.5 \cdot 10^{-3}$	$226 \cdot 10^{-3}$	$205 \cdot 10^{-3}$

To establish conclusively the determining stage of the process, we studied the evaporation kinetics of ammonia from a solution with a clean surface, i. e., without formation of a hydroxide film. Comparison of Curves 1 and 2 in Fig. 6 (film formation began 80 minutes after the air blow was commenced) indicates that the rate of film growth is determined by the rate of evaporation of ammonia through the film of cobalt hydroxide forming on the solution surface.

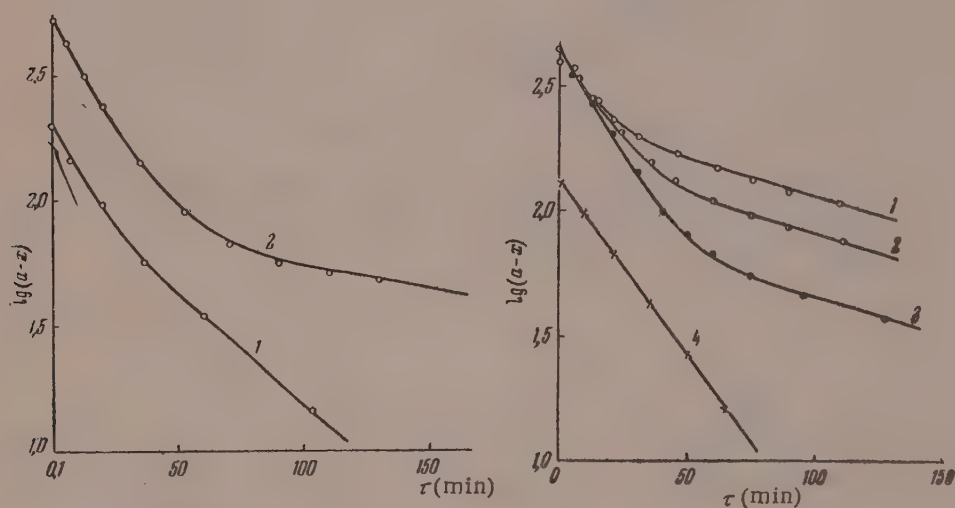


Fig. 6. Evaporation of ammonia from cobalt ammine solutions: 1) with a clean surface; 2) with surface covered by a monolayer of oleic acid.

Fig. 7. Evaporation of ammonia from nickel ammine solutions: 1) with surface covered by a monolayer of oleic acid, concentration 0.2 M; 2) the same, 0.1 M; 3) the same 0.05 M; 4) clean surface, concentration 0.1 M; at 40° and air rate 1 liter/minute.

On the basis of the above results, the process of formation and growth of cobalt hydroxide films can be represented by the following scheme: evaporation of excess ammonia (hydrolysis of cobalt tetrammine, accompanied by formation of cobalt hydroxide), and attachment of the colloidal hydroxide to the solution surface, with film formation.

Kinetic curves for the evaporation of ammonia from nickel ammine solutions are given in Fig. 7. It follows from Curves 1, 2, 3, and 4 in Fig. 7 that the evaporation rate of ammonia is determined by its rate of penetration through the nickel hydroxide film (the film begins to form 15-25 minutes after the commencement of the air blow over the solution surface). It was not possible to follow the course of film growth, as nickel hydroxide films have weak, pale interference colors, in contrast to the bright colors of copper and cobalt hydroxide films.

Determinations of solution pH by the drop method at the instant of $\text{Ni}(\text{OH})_2$ film formation showed that nickel hydroxide films are formed at pH 10-11; the formation of nickel hydroxide begins in the same pH range.

SUMMARY

1. The effects of concentration and temperature on the growth kinetics of cobalt and nickel hydroxide films on surfaces of the corresponding ammine solutions were studied.
2. A hydroxide film is formed only if a monolayer of a surface-active substance is present on the solution surface. The growth of cobalt and nickel hydroxide films under oleic acid monolayers was studied.
3. Studies of the kinetics of ammonia evaporation from ammine solutions showed that the rate of evaporation of ammonia through the hydroxide film determines the hydrolysis rates of cobalt and nickel amines.
4. The formation and growth of cobalt hydroxide films is represented by the following scheme: evaporation of excess ammonia, hydrolysis of cobalt tetrammine (with hydroxide formation), and attachment of the colloidal hydroxide to the solution surface.

The S. M. Kirov Urals Polytechnic Institute
Sverdlovsk

Received April 19, 1957

LITERATURE CITED

- [1] S. G. Mokrushin and G. A. Kitaev, *Colloid J.* 19, 93 (1957).*
- [2] S. G. Mokrushin, *Colloid J.* 10, 4, 305 (1948).
- [3] A. A. Grinberg, *Introduction to the Chemistry of Complex Compounds* (Goskhimizdat, 1945) 358. [In Russian]
- [4] A. A. Grinberg and K. B. Yatsimirskii, *Bull. Acad. Sci. USSR, Div. Chem. Sci.* 2, 211 (1952). *
- [5] *Chemist's Handbook Vol. II* (Goskhimizdat, Moscow, 1951). [In Russian]

*Original Russian pagination. See C. B. Translation.

INTERACTION OF DIRECT DYES WITH CELLOTRIOSE*

P. V. Moryganov and B. N. Mel'nikov

In thermodynamic studies of the interaction of direct dyes with cellulose fibers the method of expressing the activity of the dye in the two phases is very significant. The activity of the dye in solution can, without undue error, be taken as equal to the product of the concentrations of the ions formed from the dye molecule, as usually the dye content in solution is very low. In addition, activity coefficients for aqueous solutions of certain dyes have been found by direct experimental determination.

For example, Meggy [1] studied the distribution of a number of direct and acid dyes between amyl alcohol and water, and dye solubilities in solutions of inorganic salts, and concluded that the activity coefficients of these dyes in aqueous solutions at temperatures above 65° are very close to unity. The same is true of aqueous solutions of picric acid and methylene blue, the activity coefficients of which were also determined by direct experiment. Therefore it is sufficient to know the dye concentration in the aqueous phase in order to represent its behavior in solution. However, to express the activity of a dye in the fiber phase it is not enough to know the concentration of dye ions in the fiber. In this case it is also necessary to know the actual fiber volume in which these ions are present, and their state and behavior in it. This leads to the concept of effective fiber volume V , which is given different physical meanings and is defined in different ways by different workers. For example, Willis, Warwicker, Standing, and Urquhart [2] define V as the volume of the surface phase of the fiber in which there are forces of interaction between fiber and dye. It is assumed that within this volume the interaction force is independent of the distance between a dye particle and the surface of the cellulose phase; these forces do not operate outside the volume V .

Hanson, Neale, and Stringfellow [3] divide the dye solution into two portions – the external, and the internal with volume V – and attribute a meaning to V whereby calculated results for the dyeing process based on the Donnan theory are correlated with experimental data.

Marshall and Peters [4] regard V as a correction for dye activity in the fiber phase, and select a numerical value for V which satisfies a linear relationship between the logarithm of dye activity in the fiber ($\ln a_f$) and the logarithm of the dye activity in solution ($\ln a_o$) in accordance with the equation $\Delta\mu^0 = RT \ln \frac{a_f}{a_o}$.

Urquhart and Williams [5] correlate this quantity with the amount of moisture absorbed by the fiber at 100% relative humidity; this, of course, is not quite correct.

Therefore, the physical meaning of the quantity V is not established precisely, and methods for its determination are either very approximate or purely formal. Further work on this question is therefore needed, as the numerical value of the effective volume is needed for calculations of dye affinity and other thermodynamic characteristics. It might be possible to incorporate V in the value for affinity, but in that case it would be possible to compare affinities only of dyes which yield anions of the same charge. In reality, the valences of dye ions vary greatly, and therefore, a numerical expression for V is necessary for comparison of their affinities.

We have attempted to determine V by an essentially different method, the physical meaning of the effective fiber volume being correlated with the activity of cellulose toward the dye in its interaction with the latter. The

*Presented at the All-Union Conference on the Synthesis and Application of Dyes, held in May 1956 at the Ivanovo Institute of Chemical Technology.

TABLE 1

Thermodynamic Characteristics of Direct Dyes in Interaction with Cellotriose

Barium salt of dye	Temperature, (in °C)	Equilibrium concentration [c] · 10 ⁴ in moles/liter			Equilibrium constant K · 10 ⁻⁴	Affinity - Δμ ⁰ cal/mole	Heat of reaction - ΔH° in cal/mole	Entropy - ΔS° in cal/mole
		cello-triose	dye	dye - cello-triose complex				
Congo Red	25	0.16	3.68	0.84	14.23	7040	12700	17.6
	25	0.48	3.68	2.52	14.30			
	25	0.80	3.68	4.20	14.29			
	35	0.20	5.42	0.80	7.50	6840		
	35	0.60	5.42	2.40	7.52			
	35	1.00	5.42	4.00	7.50			
	45	0.26	7.22	0.74	3.95	6670		
	45	0.78	7.22	2.22	3.94			
	45	1.30	7.22	3.70	3.95			
Diazo Black C	25	0.30	7.10	0.70	3.28	6150	12700	20.6
	25	0.90	7.10	2.10	3.28			
	25	1.50	7.10	3.50	3.30			
	35	1.05	12.0	1.95	1.55	5900		
	35	1.75	12.0	3.25	1.56			
	45	1.30	15.4	1.70	0.85			
	45	2.20	15.4	2.80	0.825			

TABLE 2

Values of the Effective Volume (V) of Normally Bleached Cotton Fiber, Determined by Different Methods

Method for determination of V	Value of V, liters/kg
Given by Marshall and Peters	0.300
By interaction of cellotriose with Congo Red	0.306
The same, with Diazo Black C	0.288
Mean	0.297

effective fiber volume is taken to be the volume accessible to interaction between cellulose macromolecules and dye molecules or ions. In this sense we may speak of activity of cellulose toward the dye, expressing it as the ratio of the effective fiber volume to its total volume:

$$f = V_{\text{eff}} / V_{\text{tot}}$$

If every cellulose macromolecule in every part of the fiber is accessible to interaction with the dye, then $V_{\text{eff}} = V_{\text{tot}}$ and the "activity coefficient" of cellulose is unity. This would be the case if all the dye - cellulose interaction took place in a single phase, i. e., if the dyeing process was effected in homogeneous and not heterogeneous conditions. Unfortunately, such interaction between cellulose and dye cannot be effected.

We therefore decided to prepare a water-soluble cellulose preparation by degradation of cotton fiber; cellotriose was chosen as the material, on the assumption that the mechanism of its interaction with direct dyes is analogous to that of dye - cellulose interaction, i. e., that the dye forms hydrogen bonds with the hydroxyl groups of the glucose residues. When the affinity of the dye for cellotriose in a homogeneous medium, i. e., in conditions when it is not necessary to use the effective volume of the cellulose phase, has been determined, it becomes possible to calculate this effective volume from the equation for the affinity of the dye for cotton cellulose fiber

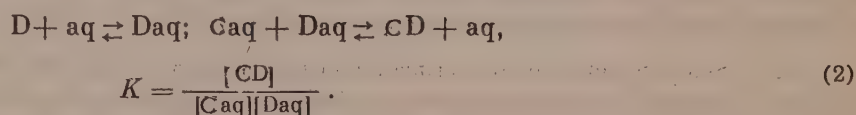
$$-\Delta\mu^{\circ} = RT \ln \frac{[Na]_f^z [D]_f}{[Na]_0^z [D]_0 V^{z+1}}, \quad (1)$$

where $\Delta\mu^\circ$ is the affinity of the dye for cellulose; $[\text{Na}]_f$ and $[\text{D}]_f$, and $[\text{Na}]_g$ and $[\text{D}]_g$ are the respective concentrations of sodium and dye ions in the fiber phase and in solution at equilibrium; z is the valence of the dye ion; R is the gas constant; and T is the absolute temperature.

By substitution of the affinity determined from experiments with cellotriose into this equation we can calculate the effective volume of the cellulose phase, taking into account the established fact that the affinity of the dye for the fiber is independent of the initial dye and electrolyte concentrations in the bath.

The affinities of direct dyes for cellulose were determined from variations of the dye solubility in presence of cellotriose. In these experiments the solubility of the pure dye $[\text{D}_{\text{aq}}]$ was first determined at a particular temperature in a thermostat. The solubility of the dye in presence of cellotriose was then determined under the same conditions. If the dye interacts with cellotriose, its solubility should increase in presence of cellotriose, and the optical density of the solution should increase until a new state of equilibrium is established. The difference between the concentrations of the pure dye solution and of the solution in presence of cellotriose gives the amount of dye which has interacted with cellotriose, and the equilibrium concentration of the latter can be found.

From known concentrations of the dye in saturated solution in water, and in presence of cellotriose, it is easy to find the equilibrium constant for the process



From the equilibrium constant we find the affinity of the dye for cellotriose

$$-\Delta\mu^\circ = RT \ln K. \quad (3)$$

Here $[\text{C}_{\text{aq}}]$, $[\text{D}_{\text{aq}}]$ and $[\text{CD}]$ are the respective equilibrium concentrations of cellotriose, dye, and cellotriose + dye complex, and K is the equilibrium constant.

Since our postulated mechanism of dye - fiber interaction assumes formation of hydrogen bonds between hydroxyl groups of cellulose or cellotriose and the auxochrome groups of the dye, it is advisable to use dyes of a low degree of dissociation, with moderate solubility in water, or to perform the experiments with fairly high contents of electrolyte in solution. The reason is that addition of dye anions to cellotriose molecules should lead to formation of charged complexes which are fairly large and therefore have low mobility. A "swarm" of sodium ions or some other positive ions should therefore be formed. Because of their high degree of hydration, these ions would tend to break the bonds between the dye and cellotriose, so that the solubility of the dye would be the same in pure water as in water with added cellotriose. If dyes of a low degree of dissociation are used, complex formation between undissociated dye molecules and cellotriose should be more pronounced. We therefore used dyes in the form of their barium salts.

Soluble cellotriose was prepared by the Hess method [6], by acetylation of purified cotton for 3 hours at 40°, the reaction mass then being held at 30° for 48 hours. The acetate was then saponified by sodium methylate in chloroform. The water-soluble saponification product consisted of cellobiose (iodine number 58.5), cellotriose (iodine number 39.7), and substances of lower iodine numbers (30-17). A cellotriose sample with iodine number ~ 40 was isolated by fractionation at a varying water - ethanol ratio, and used for experiments with direct dyes.

The experiments were performed at 25, 35, and 45°. The experimental and calculated results are given in Table 1.

On the assumption that the mechanism of dye - fiber interaction is the same whatever salt of the dye - barium or sodium - is used for dyeing the fiber, we attempted to calculate the effective volume of the cellulose phase from Equation (1). For this we used data on the equilibrium dyeing of cotton fiber by the sodium salts of Congo Red and Direct Diazo Black C, and the affinities found from the experiments with cellotriose. The results are given in Table 2, which also includes, for comparison, the data of Marshall and Peters for the effective volume of the cellulose phase.

It follows from Table 2 that the effective volume of the cellulose phase as determined by our method is

very close to the values obtained by Marshall and Peters who used a purely formal method, the selection of suitable values of V . First, this justifies the expression of dye activity in the fiber as the product of the concentrations of the corresponding ions in it, the accessible volume being restricted to the effective volume of the cellulose phase, and second, it provides convincing proof for the applicability of the thermodynamic approach in studies of dyeing processes.

For final confirmation of our results, we carried out a series of experiments on equilibrium dyeing of cotton fabrics with the barium salt of Congo Red. Congo Red barium salt dyes cellulose fibers fairly well even in absence of other neutral electrolytes, probably because of the ease of hydrogen bonding between the slightly dissociated barium salt of the dye and the charged cellulose surface. The general equation for calculation of the affinity of a direct dye for the fiber from equilibrium dyeing data is simplified in this case to

$$-\Delta\mu^{\circ} = RT \ln [D]_f^2 / [D]_G^2, \quad (4)$$

because in dyeing by the barium salt of the dye in absence of other electrolytes in the system $[Ba]_f = [D]_f$ and $[Ba]_G = [D]_G$. Moreover, the valence of the barium ion is equal to the valence of the Congo Red anion. Because of the low solubility of this barium salt at low temperatures the experiments were performed at 100°; the corresponding affinities of Congo Red barium salt for cellotriose were found by calculation from the values at 45° and the heat of reaction. Our values were 5.75 for the sodium salt and 5.91 for the barium salt at 100°. The calculated value of the affinity of the barium salt for cellotriose is 5.62.

This method for determination of the effective volume of cotton fiber from experimental data on dye affinities for cellotriose is significant, not only because it is new in principle and is based on theoretical concepts which have been confirmed by direct experiment, but also because it confirms the accepted mechanism of the interaction of direct dyes with cellulose.

SUMMARY

1. The interaction of direct dyes with cellotriose, a water-soluble degradation product of cellulose in homogeneous conditions has been effected for the first time, and the thermodynamic characteristics of the process have been determined.
2. These characteristics are shown to confirm that the mechanism of interaction of direct dyes with cellulose is a process of hydrogen bonding between the dye anions and the cellulose macromolecule.
3. A method, new in principle, is described for determination of the effective volume of cotton fiber from the affinity of dyes for cellotriose.

The Ivanovo Institute of Chemical Technology
Laboratory of the Chair of Chemical Technology of
Fibrous Materials

Received May 14, 1957

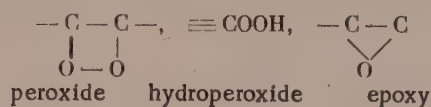
LITERATURE CITED

- [1] A. B. Meggy, Faraday Disc. on Dyeing and Tanning 16, 149 (1955).
- [2] H. F. Willis, J. O. Warwicker, H. A. Standing, and A. R. Urquhart, Trans. Faraday Soc. 41, 506 (1945).
- [3] J. Hanson, S. M. Neale, and W. A. Stringfellow, Trans. Faraday Soc. 31, 1718 (1935).
- [4] W. J. Marshall and R. H. Peters, J. Soc. Dyers Col. 63, 446 (1947).
- [5] A. R. Urquhart and Williams, J. Text Inst. 15, 559 (1924).
- [6] K. Hess and K. Dziengel, Ber. 68, 1594 (1935).

SWELLING OF VULCANIZED RUBBER IN ACETYL HYDROPEROXIDE SOLUTION

E. N. Novikova

In the autooxidation of hydrocarbons, organic hydroperoxides are intermediate oxidation products [1, 2]. Being strong oxidizing agents and compounds of low thermal stability, hydroperoxides have an initiating influence on the rate and direction of hydrocarbon autooxidation [3, 4]. Hydroperoxides oxidize unsaturated compounds to oxides; the rate and degree of oxidation of such compounds depends on their structure [5, 6]. Rubber, an unsaturated compound, is readily oxidized and yields various oxidation compounds depending on the experimental conditions; these may contain



and other oxygen-containing groups [7].

It was of interest to study the action of acetyl hydroperoxide on rubber, and to investigate the extent to which this action can be retarded by rubber-oxidation inhibitors.

Composition of Vulcanizates

Vulcanizate components, wt. parts	Vulcanizates			
	VII	VIII	III	C-2
Smoked sheet	100	100	—	—
SKB	—	—	200	—
SKN-26	—	—	—	309
Sulfur	2.75	2.75	3	4.5
Captax	0.85	0.85	3.6	2.4
Zinc oxide	5	5	10	15
Stearic acid	1.0	1.0	—	4.5
Gas black	40	—	—	—
Chalk	—	58.5	—	—
Rubberax	5	—	—	—
Vaseline oil	—	2	—	—
% content of rubber in vulcanizate	64.7	58.7	92.8	92.9

It is known that when rubber is oxidized by oxygen, degradation and structurization processes develop in it. It has been shown [8] that the degradation and structurization processes can be studied by means of kinetic curves for rubber swelling. We therefore adopted the swelling method for studying the oxidation of rubber by hydroperoxides.

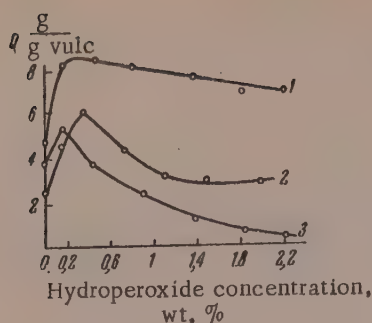


Fig. 1. Effect of acetyl hydroperoxide concentration on the degree of swelling of vulcanizates in benzene; swelling time 7 days:

1) Vulcanizate III; 2) Vulcanizate VIII; 3) Vulcanizate C-2.

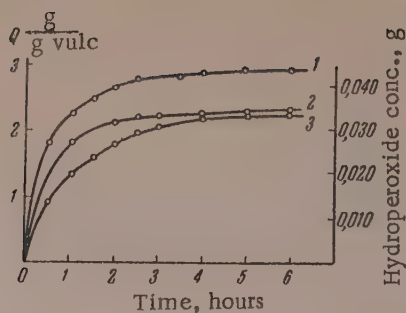


Fig. 2. Swelling kinetics of Vulcanizate VIII and consumption of acetyl hydroperoxide:

1) swelling of vulcanizate in benzene solution of acetyl hydroperoxide (0.72 wt. % of hydroperoxide); 2) swelling of vulcanizate in benzene; 3) consumption of hydroperoxide for oxidation of 0.1 g of vulcanizate during swelling.

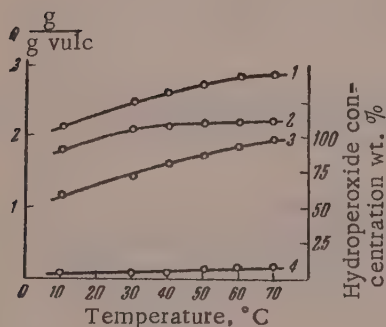


Fig. 3. Effects of temperature and acetyl hydroperoxide on the swelling of Vulcanizate VIII:

1) swelling in benzene solution of hydroperoxide; 2) swelling in benzene; 3) consumption of hydroperoxide in solution containing vulcanizate; 4) consumption of hydroperoxide in control solution.

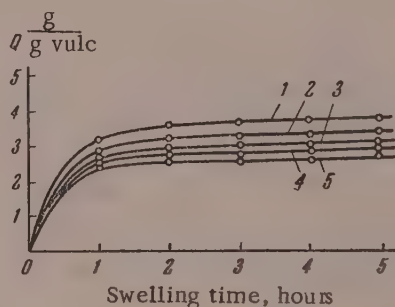


Fig. 4. Effect of phenols on the swelling of Vulcanizate VII in benzene solution of acetyl hydroperoxide at 60°:

1) hydroperoxide without inhibitors; hydroperoxide with inhibitors: 2) hydroquinone; 3) pyrocatechol; 4) pyrogallol; 5) without hydroperoxide and inhibitors.

Vulcanizates made from both natural and synthetic rubbers were used in the investigation. The composition of the vulcanized mixtures is given in the table. The vulcanized specimens were first washed alternately with acetone - benzene mixture (1:1) and acetone, and then dried in a vacuum desiccator.

The oxidizing agent was 70% acetyl hydroperoxide. Benzene or xylene was used as the swelling medium. Into beakers with ground-glass stoppers were put 5 ml lots of solvent or acetyl hydroperoxide solution with or without added inhibitors. Plates of vulcanized rubber of the same shape and weight (0.1 g) were then immersed in the solutions. The swelling was performed in the 10-80° range, the temperatures being kept constant by means of an ultrathermostat.

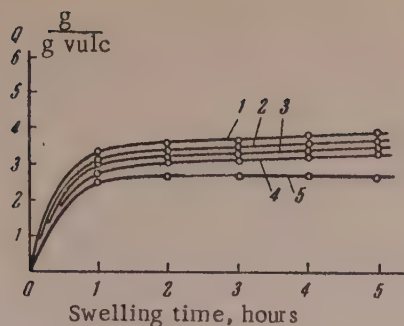


Fig. 5. Effect of naphthalene derivatives on the swelling of Vulcanizate VII in a benzene solution of acetyl hydroperoxide at 60°:

1) hydroperoxide without inhibitors; inhibitors and hydroperoxide: 2) β -naphthol; 3) α -naphthol and α -naphtholphthalein; 4) 1,7-dihydroxynaphthalene and *p*-hydroxyphenyl- β -naphthylamine; 5) without hydroperoxide and inhibitors.

Vulcanizate C-2 was not dissolved during swelling. After the solvent had been evaporated from the swollen sample, its weight had not decreased in comparison with the initial weight. All this suggests that oxidation of Vulcanizate C-2 by hydroperoxide causes structurization.

Maximum swelling of Vulcanizate VIII, based on natural rubber, is attained at a higher hydroperoxide concentration (0.37 wt. %). In solutions of higher concentrations the degree of swelling decreases and the sample goes into solution (Curve 2, Fig. 1).

The iodometric method was used to determine the consumption of acetyl hydroperoxide in the solution used for swelling of 0.1 g of Vulcanizate VIII. Curve 3 (Fig. 2) shows that the hydroperoxide is consumed gradually. Half of the hydroperoxide present in the solution (0.0361 g in 5 ml of benzene) was consumed during the first hour of swelling, and the rest during the subsequent 5-6 hours. Whereas in the original benzene solution the amount of hydroperoxide remains almost constant for 6 hours (0.0360 g in 5 ml of benzene), the degree of swelling of the vulcanized rubber (until the maximum swelling is reached) increases with the amount of hydroperoxide consumed (Curve 1). The degree of swelling of the vulcanizate is lower in benzene than in hydroperoxide solution (Curve 2).

Data on the swelling of vulcanizates in benzene solution of hydroperoxide in the 10-70° range are presented in Fig. 3.

Plates (0.1 g) of Vulcanizate VIII were immersed in ampoules containing 4 ml of benzene and 0.028 g of hydroperoxide. Swelling at each temperature was continued for one hour. The degree of swelling of the vulcanizates and the amounts of hydroperoxide in the solution after swelling and in a control solution without vulcanizate were then determined. The curves in Fig. 3 show that the degree of swelling increases with temperature. However, the higher the solution temperature, the greater is the difference between the swelling in benzene and in benzene solution of hydroperoxide. Acetyl hydroperoxide is consumed more rapidly in solutions in which the vulcanizate is swollen. In the control solution the percentage decomposition is relatively small, but it does increase from 1.5% at 30° to 10% at 70°.

This decomposition of hydroperoxide, whether it proceeds with liberation of oxygen or with formation of free radicals, must influence oxidative degradation of the vulcanizate, and therefore the degree of swelling.

The degree of swelling was determined by the gravimetric method, and was calculated per 1 g of each specimen after swelling and removal of solvent in a vacuum desiccator.

Effect of acetyl hydroperoxide concentration on the swelling of vulcanizates. As the results in Fig. 1 indicate, all three vulcanizates, made from different types of rubber (natural and synthetic), all show an initial increase of swelling, which then decreases with increasing concentration of hydroperoxide in solution.

Vulcanizate III, made from SKB, proved to be the most resistant to the action of hydroperoxide. It slowly loses its tendency to swell in benzene (Curve 1, Fig. 1).

On the other hand, Vulcanizate C-2, made from polar nitrile rubber, which contains polar groups even before oxidation, loses its capacity to swell in benzene very rapidly. The maximum swelling of Vulcanizate C-2 is found at low concentrations (0.18%) of hydroperoxide in solution. Further increase of hydroperoxide concentration leads to a sharp decrease of swelling, to far below the value for the vulcanizate in pure benzene (Curve 3, Fig. 1).

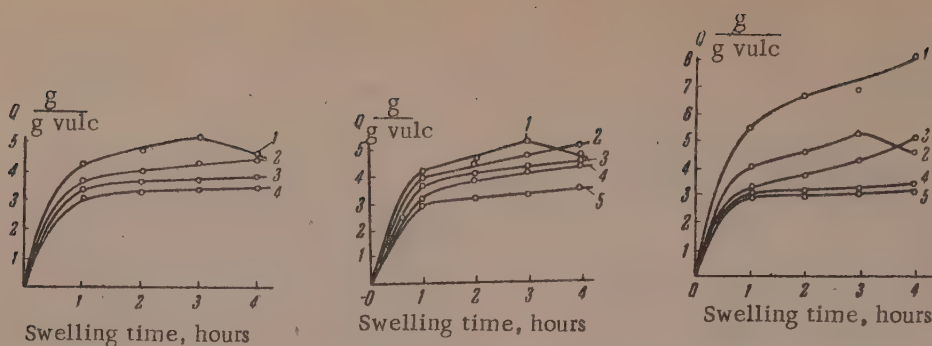


Fig. 6. Effects of phenols on swelling of Vulcanizate VII in a solution of acetyl hydroperoxide in xylene at 80°:

1) hydroperoxide without inhibitor; hydroperoxide and inhibitors; 2) pyrocatechol; 3) pyrogallol; 4) without hydroperoxide and inhibitors.

Fig. 7. Effects of naphthalene derivatives on swelling of Vulcanizate VII in a solution of acetyl hydroperoxide in xylene at 80°:

1) hydroperoxide without inhibitors; hydroperoxide and inhibitors; 2) α -naphthol and β -naphthol; 3) 1,7-dihydroxynaphthalene and phenyl- β -naphthylamine; 4) p-hydroxyphenyl- β -naphthylamine; 5) without hydroperoxide and inhibitors.

Fig. 8. Effects of inhibitors and initiators on swelling of Vulcanizate VII in solutions of acetyl hydroperoxide in xylene at 80°:

1) iron palmitate and hydroperoxide; 2) hydroperoxide; 3) iron palmitate without hydroperoxide; 4) pure xylene; 5) oxnone and chrysoidine in presence of hydroperoxide (the curves coincide).

Action of inhibitors. The effects of inhibitors on the swelling of vulcanizates in benzene and xylene in presence of acetyl hydroperoxide were studied. Addition of hydroperoxide to benzene (21.5 millimoles/liter) increases the swelling of Vulcanizate VII. Additions of 6 millimoles of phenols per liter diminish the increase produced by acetyl hydroperoxide in the degree of swelling, but, as Fig. 4 shows, they eliminate it far from completely. It seems that the action of phenols is effective in so far as hydroperoxide initiates the chain reaction of rubber oxidation at 60°; pyrogallol has the strongest retarding action on oxidative degradation during swelling, while the effect of pyrocatechol is somewhat weaker. Resorcinol retards the oxidative degradation of vulcanizates only slightly during swelling. Sample VII was found to dissolve slightly after 5 hours of swelling at 60° in benzene, and to a somewhat greater extent in a benzene solution of acetyl hydroperoxide under the same conditions. The weight of the vulcanizate sample after swelling and evaporation of the solvent indicates that vulcanizates do not dissolve under the same experimental conditions in presence of phenols.

The swelling and solubility of the samples in the solvent and in solution in presence of phenols are decreased not only because phenols terminate the chain reaction initiated by hydroperoxide and thereby decrease oxidative degradation of the vulcanizate, but also because pyrogallol and pyrocatechol can probably take part in structurization of rubber, as was shown in the case of 2,4-diaminodiphenylamine (oxnone) [9].

Fig. 5 shows data on the influence of naphthalene derivatives on the oxidative degradation of a vulcanizate during swelling. The most effective were p-hydroxyphenyl- β -naphthylamine and 1,7-dihydroxynaphthalene. These are followed by α -naphthol and β -naphthol. Triphenylphosphine and α -nitroso- β -naphthol have little effect in lowering the degree of swelling in presence of hydroperoxide.

Xylol was chosen as the solvent for investigations of the action of hydroperoxide on vulcanized rubber at higher temperatures. At higher temperatures hydroperoxide should have a stronger influence both on the vulcanizate and on the solvent, and the influence of antioxidants should be revealed more clearly.

It follows from the data in Fig. 6 and 7 that phenols and naphthalene derivatives decrease the swelling of vulcanized rubber in xylene solutions of hydroperoxide. Curve 1 (Figs. 7 and 6) shows that the degree of swelling

in xylene solution of hydroperoxide falls after some increase, due to solution of the specimen. This is confirmed by the fact that after swelling in xylene solution of hydroperoxide and evaporation of solvent the weight of the specimen fell to 0.07 g, whereas its weight before swelling was 0.1 g. If inhibitors (pyrocatechol, pyrogallol, or dihydroxynaphthalene) are added to the xylene solution of hydroperoxide, the specimens dissolve little or not at all in 4 hours.

Action of iron palmitate. It is known that salts of variable-valence metals accelerate both the oxidation of hydrocarbons and the decomposition of hydroperoxides. Our results (Fig. 8) show that iron palmitate accelerates the oxidative degradation of vulcanized rubber in xylene.

The degree of swelling of the specimen in xylene containing 0.1% of iron palmitate is greater than in pure xylene (Curves 3 and 4, Fig. 8). Iron palmitate also has an accelerating effect in presence of acetyl hydroperoxide (Curve 1, Fig. 8).

These data on the effect of iron palmitate on vulcanized rubber are in agreement with the view [10, 11] that decomposition of hydroperoxides in presence of iron proceeds by a free-radical mechanism. If so, the free radicals formed in our experiments from acetyl hydroperoxide under the influence of iron palmitate may initiate further oxidation of rubber in the vulcanizate, thus accelerating the oxidative degradation and solution of the vulcanizate.

If 6 millimoles/liter of 2,4-diaminoazobenzene (chrysoidine) or 2,4-diaminophenylamine (oxynone) is added to the xylene solution of hydroperoxide, the vulcanizate is not dissolved. Moreover, the swelling of the vulcanizate is less than in pure xylene (Curve 5, Fig. 8). This is probably because oxynone and chrysoidine are not only oxidation inhibitors, but are also involved in structurization of rubber.

Consideration of our experimental results and literature data shows that swelling of natural-rubber vulcanizates in benzene and xylene solutions of hydroperoxide is accompanied by oxidative degradation of the rubber. Acetyl hydroperoxide is decomposed by heat and accelerates the oxidative degradation of rubber, as shown by the high degree of swelling of the vulcanizate, and subsequent complete solution. This chain process of vulcanizate oxidation is retarded to various extents by oxidation inhibitors.

SUMMARY

1. Acetyl hydroperoxide influences the swelling and solution of vulcanized rubber in benzene solution.
2. Increase of temperature has a positive effect on the swelling of vulcanized rubber in benzene solutions of acetyl hydroperoxide.
3. The degree of swelling and solution of vulcanized rubber is decreased in benzene and xylene solutions of hydroperoxide at 60-80° in presence of inhibitors (pyrogallol, pyrocatechol, 1,7-dihydroxynaphthalene, p-hydroxyphenyl- β -naphthylamine, 2,4-diaminodiphenylamine, 2,4-diaminoazobenzene).
4. Iron palmitate accelerates the degradation of vulcanized rubber in xylene solutions of hydroperoxide at 80°.

The Minsk State Medical Institute

Received May 20, 1957

LITERATURE CITED

- [1] K. Ivanov and V. Savinova, Proc. Acad. Sci. USSR 48, 32 (1945); 59, 493 (1948).
- [2] B. Erofeev, A. Chirko, and L. Sorokina, Sci. Mem. V. I. Lenin Belorussian State Univ. 20, Chem. Ser. 3 (1954).
- [3] S. Medvedev and A. Podyapol'skaya, Acta Phys. Chim. URSS 2, 4, 4871 (1935); J. Phys. Chem. 13, 719 (1939).
- [4] K. Ivanov, Intermediate Products and Intermediate Reactions in the Autooxidation of Hydrocarbons (State Sci. -Tech. Press; Petroleum, Mining, and Fuel Press, 1949). [in Russian].
- [5] N. Prilezhaev, J. Russ. Phys.-Chem. Soc. 42, 1389 (1910).

- [6] I. Khvostov, Proc. Acad. Sci. USSR 93, 5, 843 (1953).
- [7] B. Dogadkin, Physics and Chemistry of Rubber (Goskhimizdat, 1947). [In Russian]
- [8] V. Gul', I. Khodzhaeva, and B. Dogadkin, Colloid J. 16, 413 (1954).*
- [9] L. Begunovskaya, V. Zhakova, B. Karmin, and V. Épshtein, Aging and Fatigue of Rubbers and Vulcanizates and Increase of Their Stability (Goskhimizdat, 1955) 31. [In Russian]
- [10] G. Razuvaev, Yu. Ol'dekop, and E. Fedorova, Progr. Chem. 21, 4, 379 (1952).
- [11] M. S. Kharasch, A. Fano, and W. Nudenberg, J. Organ. Chem. 1, 113 (1951).

*Original Russian pagination. See C. B. Translation.

FORMATION MECHANISM OF POROUS STRUCTURES

M. S. Ostrikov and G. D. Dibrov

Light porous materials are becoming increasingly important in the building materials industry and certain other branches of the national economy; in particular, foam concretes are extensively used in practice [1-3]. Methods for the production of materials with a porous structure can be divided into the following groups: a) mechanical foaming; b) formation of pores by combustion during firing; c) formation of a porous structure in an aqueous medium with subsequent removal of liquid; d) foaming of softened materials by gases liberated by one of the components of the system [4].

This classification does not cover all possible ways in which porous bodies can be formed. For example, none of the above-named groups includes our process of the formation of the system gypsum — coal-tar pitch — water, in which considerable porosity and a foam structure arise during preparation of the samples, without the use of additives or any special methods. The characteristic feature of this process is that a foamlike porous structure is formed in highly disperse heterophilic suspensions under the influence of capillary forces of a flotation character [5].

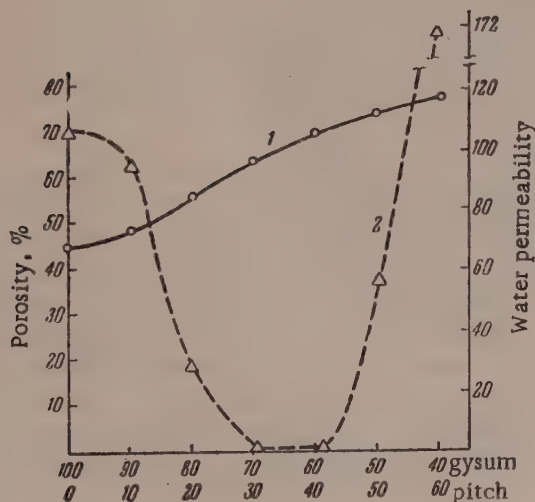


Fig. 1. Effects of the composition of gypsum pitch on its porosity (1) and water permeability (2): the abscissa axis shows weight proportions of gypsum and pitch; water permeability is expressed in ml of water penetrated into the specimens through an average surface area of 3.956 cm².

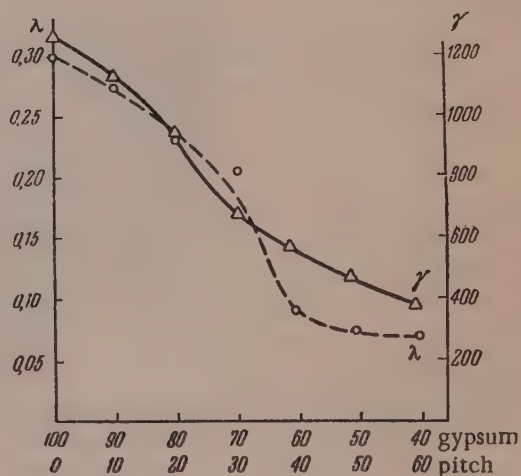


Fig. 2. Effects of composition of gypsum pitch on its heat conductivity (λ) and density (γ); the abscissa axis shows the weight proportions of gypsum and pitch in the mixtures.

The pores formed in the process are of two main types, sharply different from each other in shape, size, and origin: 1) micropores in the gypsum portion, consisting of intercrystallite spaces which lose water during drying; 2) macropores in the form of a cellular foam, easily visible with the naked eye. These pores are formed spontaneously by the action of capillary forces during the mixing process.

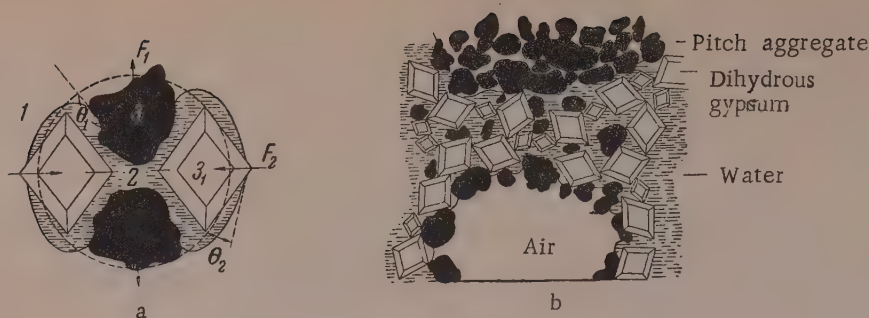


Fig. 3. a) Schematic action of capillary forces: dash lines represent the initial boundaries of a drop of water placed on an aggregate of two pitch particles (3) and two gypsum crystals (3₁); the capillary forces displaced the water (2) – air (1) interface, and the following forces arose: F₁, displacing the pitch particles, and F₂, drawing the gypsum crystals into the aqueous phase, θ is the contact angle: b) schematic distribution of pitch and gypsum particles by the action of forces F₁ and F₂.

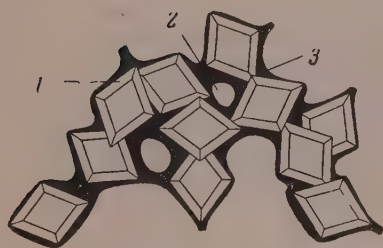


Fig. 4. Schematic structure of gypsum pitch after heat treatment: 1) gypsum crystals; 2) air bubbles; 3) melted pitch.

Specimens, in the form of disks 70 mm in diameter and 20 mm thick, were made from powdered mixtures of building gypsum and fine sand. They were mixed with pure water or water containing various additives. It was found that with increase of the amount of pitch in the mixture the amount of water required to bring the mass to normal consistency (in accordance with the GOST for gypsum) was greater. The explanation for this increase is that the hydrophobic pitch surface area, not wetted by water, becomes greater and dry friction therefore increases in the system. The mobility of the system also decreases as the result of formation and accumulation of air bubbles.

The increase in the porosity of the specimens with the pitch content is shown in Fig. 1, Curve 1. An interesting feature is that the water permeability of the system falls with decrease of gypsum content (Fig. 1, Curve 2), despite the increased porosity, and reaches zero at 30% pitch content. This remarkable property of the systems, indicative of their highly hydrophobic nature, is retained with further increase of porosity, with increase of the pitch content to 40%. After this water permeability unexpectedly returns, and rises sharply with further decrease of the gypsum content. This occurs while water repellence increases, and is due only to the fact that the capillary pressure preventing penetration of water decreases (by the Laplace law) because of the excessive increase of pore diameter. It is evident that water permeability in this region becomes of real significance when the liquid phase comes in contact with the openings of the widest pores, connected with through channels, and becomes apparent under the appropriate external pressure.

Special interest attaches to data on the heat conductivity of these systems in relation to their composition. The curve for heat conductivity (λ) in Fig. 2, as was to be expected, corresponds closely to the density (γ) curve. The linear variation of γ with porosity is evidence of the good agreement between these data, obtained independently and by different methods.

The cellular pores originate with direct participation of the powdered pitch particles. The fraction of the total volume occupied by these pores reaches 25% with 40% of pitch in the system.

The disperse pitch phase exerts its influence under the complex conditions of the interaction of four phases, where the volume of the two mobile phases is only slightly in excess of the volume of the stationary phases. The main role in the formation of cellular pores is played by capillary forces at the water – air boundary. Forces of

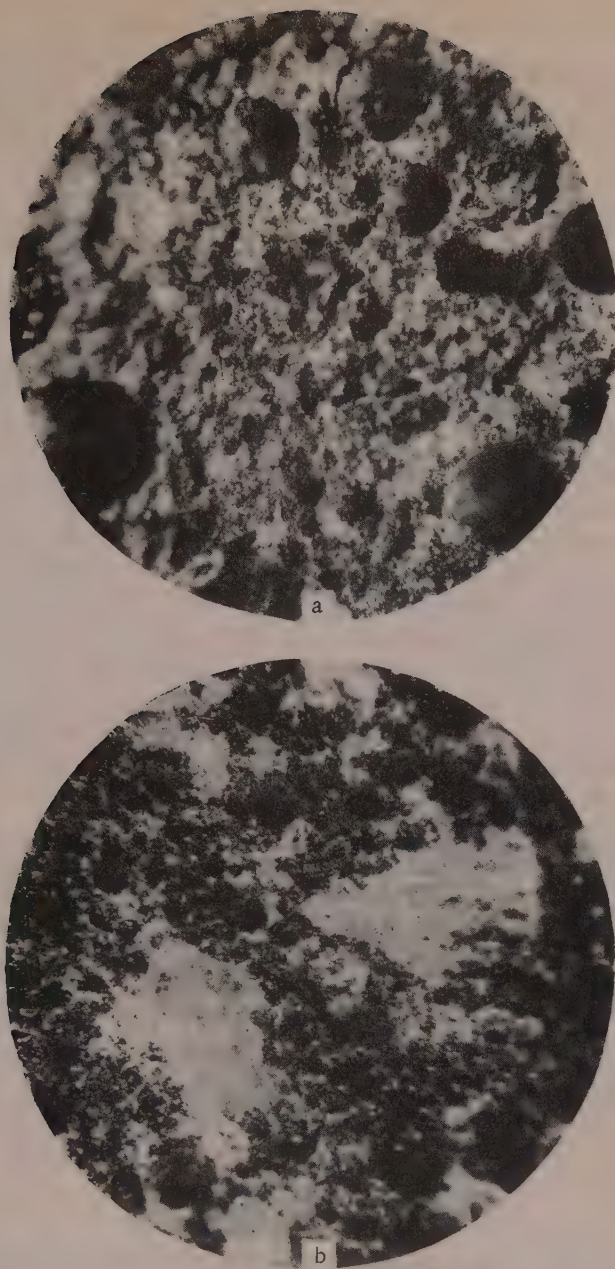


Fig. 5. Microphotographs (under low magnification) of gypsum pitch without foaming agent (a) and with a small amount of added saponin (b).

mutual attraction and friction between the solid particles also have great significance as structure-forming factors; they offer resistance to compressive forces of surface tension at the water - air interface. This resistance is an absolutely essential condition for appearance of capillary forces. The latter overcome the resistance of the structure in definite regions of the system and induce, jointly with external forces selective (dependent on wetting) and oppositely-directed displacement of the particles of the two solid phases.

The nature of the action of capillary forces in elementary regions is shown schematically in Fig. 3, a, where it is seen how the unwetted particles of the water-repellent pitch are expelled from the aqueous phase by the force F_1 . By this action of the capillary forces the hydrophobic pitch particles gradually collect in the course of stirring on the surface of the liquid phase, i. e., on the inner surfaces of the air bubbles, conferring high stability

on them (Fig. 3, b). Tangential forces of coagulative interaction between the pitch particles raise the strength and stabilizing power of the entire mineralizing layer.

In some regions there are accumulations of pitch particles, filling the whole cells. This may occur if the previous mixing of the powder is not thorough enough. However, such aggregates (visible in fractures) may also be formed by excessive stirring, as a peculiar form of flocculation — capillary separation of a hydrophobic disperse phase.

At the same time, during stirring water spreads over wetted gypsum crystals. The water — air interface therefore increases; this is favored by the stabilizing action of the highly disperse pitch particles. Later, when stirring ceases, this interface tends to contract, and levels out somewhat, forming isolated bubbles the walls of which are closely encrusted with pitch particles.

The same capillary forces cause displacement of the gypsum crystals, but in the opposite direction (Force F_2 in Fig. 3, a). The crystals are drawn into the aqueous phase, accumulate there, and interact with it, undergoing all the changes leading to formation of a rigid gypsum structure which fixes the foam structure.

The specimens in this condition are not yet strong enough for practical use, and have poor water resistance because the area of contact between gypsum and pitch is very small, and is mainly of a point character. Moreover, interphase molecular bonds between the hydrophilic gypsum phase and the hydrophobic pitch phase, as in other heterophilic systems[5], are easily disrupted by the splitting action of molecular water layers. This and other defects are eliminated to a considerable extent by heat treatment of the mixture at 150° for 2.5 hours. The melted pitch flows over the surfaces of the gypsum crystals and aggregates and forms water-repellent and water-resistant films on them. At the same time numerous bridges are formed between the crystals, strengthening the porous structure fixed during setting of the gypsum (Fig. 4). The light porous material so formed has heat-insulating properties, water repellency, and water resistance which are adequate for practical purposes. Gypsum pitch of optimum composition (40% pitch) has compressive strength $R = 25 \text{ kg/cm}^2$, bulk density $\gamma = 600 \text{ kg/m}^3$, and heat conductivity $\lambda = 0.09 \text{ kcal/m} \cdot \text{degree} \cdot \text{hr}$.

Data on the effect of surface-active foaming agents are of interest. The intensively acting surface-active substances generally used in the production of foam concrete and other porous materials [1, 2] had an antagonistic action in our systems. Additions of saponin and GK [6] dissolved in the mixing water in the amounts used in foam concrete production lowered porosity from 72 to 58.6%. The accompanying microphotographs (Fig. 5, a and 5, b) clearly reveal the difference in structure. The specimen without added surface-active substances has numerous large pores, which have disappeared completely from the specimen with added saponin.

This foam-breaking action of the foaming agent can be attributed to selective adsorption of the agent on the pitch particles, which are thereby made hydrophilic and lose their power of forming strong stabilizing layers at air-water interfaces. These results are consistent with the mechanism suggested above for the action of dispersed pitch.

SUMMARY

1. In gypsum — pitch — water disperse systems considerable porosity, exceeding 70%, arises during mixing and stirring. The foamlike structure which becomes fixed during setting and hardening of the gypsum is strengthened and its water resistance is considerably raised by heat treatment.

2. The effects of composition on porosity, density, heat conductivity, and water permeability of the systems were studied. The results show that these systems may be of practical interest as water-repellent and heat-insulating materials.

3. The surface molecular mechanism of pore structure formation in these systems was elucidated, and the role of the particles of the disperse pitch phase in the process was demonstrated.

4. The antagonistic action of surface-active substances generally used in the formation of porous bodies (saponin, GK) has been detected and explained.

The authors express their deep gratitude to Academician P. A. Rebinder for valuable guidance in this work.

The Rostov State University
The Rostov Institute of Construction Engineering

Received July 16, 1957

LITERATURE CITED

- [1] P. A. Rebinder, *Bull. Acad. Sci. USSR, Div. Tech. Sci.* 4, 293 (1937).
- [2] P. A. Rebinder, in the book: *Role of Gases and Reagents in Flotation Processes* (Izd. AN SSSR, 1950). [In Russian]
- [3] I. T. Kudryashov, *Autoclave Cellular Concretes and Their Use in Building* (Stroizdat, 1949). [In Russian]
- [4] N. A. Popov, *Artificial Porous Fillers for Light Concretes* (State Architecture and Construction Press, 1954). [In Russian]
- [5] P. A. Rebinder, *Physical Chemistry of Flotation Processes* (Metallurgy Press, Moscow — Leningrad — Sverdlovsk, 1933); M. S. Ostrikov, M. I. Kabargina, and N. T. Krivosheeva, *Proc. 2nd Conf. on Colloid Chemistry* (Acad. Sci. Ukrainian SSR Press, Kiev, 1952) 80. [In Russian]
- [6] I. T. Kudryashov et al., *Factories for Production of Cellular Concrete* (State Construction Press, 1951 73. [In Russian]

THE INFLUENCE OF ACCOMPANYING IONS ON COAGULATOR IONS*

S. G. Teletov

Our previous communication [1] contained experimental data, in the form of physicochemical analytical diagrams for colloidal systems [2], on the coagulation of ferric hydroxide sols by acetates. In the present paper we consider the influence of alkali-metal acetates on coagulation in the light of our additional experimental results and recent literature data.

In the case of ferric hydroxide sol the coagulating effect of alkali-metal acetates was found [1] to conform to the following sequence:



Hence we attempted to represent the inhibiting effects** of accompanying cations on the coagulating power of the acetate ion by the following sequence:



For studying the effect of Rb^+ as the accompanying ion, we used the nitrate and compared its effect with that of potassium nitrate. The concentrations of the original solutions used for coagulation were increased from 10 millimoles/liter for acetates to 50 millimoles/liter for nitrates. The coagulating effect of KNO_3 was found to be greater than that of RbNO_3 . This is the reverse of the sequence found for acetate, but it is consistent with the series for the coagulating action of alkali-metal chlorides on aluminum hydroxide sols, given by Dumanskii [4] as an example of the influence of accompanying cations.

The influence of accompanying ions is not yet fully understood. Peskov [5] states that "the activity of the coagulating ion changes appreciably with the nature of the ion accompanying it." At the same time it has been stated that the latter "has no appreciable influence" [6]. Subsequently Kruyt [7] admitted the existence of this influence in the case of multivalent ions, and explained it by analogy with ionic antagonism in electrolyte mixtures.

According to a number of workers, the influence of accompanying ions is quite considerable [1, 8-12]. However, some authors disregard the specific nature of the ion and attribute this influence only to the above-named cause. The same approach extends to the function for "electrolyte asymmetry" in Deryagin's expression for stability [13]. This type of explanation is not applicable to all accompanying ions, and the nature of the ions and the disperse phase must be taken into consideration.

In a number of papers the influence of organic anions is demonstrated; these include anions of monobasic [14, 15], dibasic, fatty and certain aromatic [16] acids. It has been found that the influence of the cation composition of the medium in coagulation of aluminum and ferric hydroxide sols at the instant of their formation varies [17]. The differences between the effects of accompanying ions are especially great in electrolytic foaming of sols [1, 18-21]. In the case of cations these effects are undoubtedly associated with polarizability and tendency to complex formation.

* Presented at the IVth All-Union Conference on Colloid Chemistry in Tbilisi, May 1958.

** Val'ko [3] attributed a different role to accompanying ions, and described their action as "the relieving effect."

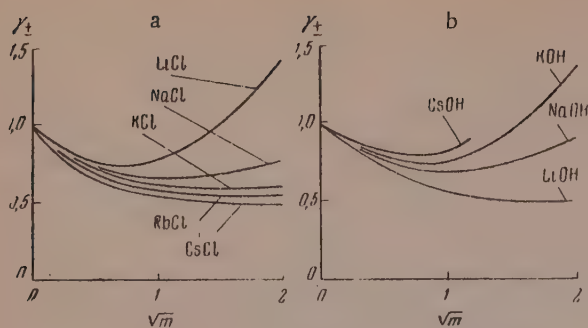


Fig. 1. Average activity coefficients at 25°C [37]: a) 1, 1 halides; b) 1, 1 hydroxides.

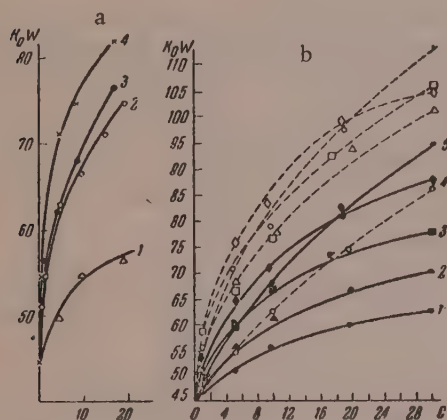


Fig. 2. Variations of k_0W for potassium ions with anion concentration in the homologous series of monobasic fatty acids [14, 15]: 1) formate, 2) acetate, 3) propionate, 4) butyrate, 5) valerate; a) without correction for hydrolysis, b) dash lines, the same; continuous lines, with correction for hydrolysis.

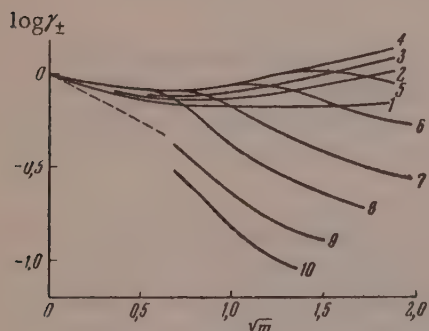


Fig. 3. Average activity coefficients of sodium salts of monobasic fatty acids in water at 25°C [37].

Glazman and his associates [22, 23] critically reviewed research into certain colloid-chemical effects in coagulation: habituation, ion antagonism, influence of accompanying ions, etc. A number of problems, including the influence of accompanying ions, were investigated in conjunction with experimental verification of concepts concerning the adsorption of ions of like charge by colloids [12, 24, 25]. The tracer atom method [26, 27] was used to demonstrate the virtual absence of adsorption of PO_4^{3-} and SO_4^{2-} ions in the case of a number of negatively charged sols [26].

However, the categorical conclusion that no accompanying ions are adsorbed [23, 26, 28] is hardly justified. Thus, the same tracer atom method has revealed: adsorption of sulfate ions, dependent on the pH of the medium, on precipitates of zinc sulfide, silver sulfide, and barium chromate [29]; chemisorption of sodium sulfate on silver [30]; adsorption of zinc ions on aluminum hydroxide films formed in presence of an electrolyte [31].

We determined the adsorption of tagged zinc ions by ferric hydroxide sols and gels. In the first case we measured the decrease of zinc concentration in an ultrafiltrate obtained with the aid of a battery unit [32], and in the second, the decrease of concentration in the equilibrium solution over the precipitate. The ratio of the adsorptions per 1 g of ferric hydroxide in the sol and gel respectively is 3:1. The adsorption was somewhat higher for ferric hydroxide than for aluminum hydroxide [31].

All this demonstrates the need for differentiated approach to the nature of the colloidal phase and of the ions adsorbed on it [25]. This applies primarily to colloidal solutions of metal hydroxides [33]. It is also probable that the influence of accompanying ions may be due to different causes, and is not always associated with their adsorption by the disperse phase.

Without going in detail into Ostwald's views [9] on coagulation, we merely note the need to draw attention to the properties of the dispersion medium and the behavior of electrolytes in it.

The activity coefficient may serve as a measure of interionic interaction [4] in the coagulant electrolyte. In that case its value characterizes the coagulating power of the electrolyte. This primarily applies to electrolytes of a related nature: the greater the force of interionic attraction the weaker apparently is the coagulating action of the electrolyte. The inhibiting effect of the accompanying ion on the coagulating ion is seen in this sense [1, 28]. This type of behavior

does not exclude possible interaction of the accompanying ion with the micelle gegenions ("relieving effect" [3]). It is evident that multivalent ions will have a stronger effect in this respect.

Published values of activity coefficients [34] were compared with series of acetates and chlorides in order of their coagulating effects, and it was observed that these values were symbatic with the coagulant action*. At electrolyte concentrations of 0.01 M the activity coefficients differ very little, but retain a sequence which is clearly pronounced at higher concentrations. There is reason to believe that in fact the electrolyte concentrations are raised considerably owing to adsorption.

It has been observed that the activity coefficients for acetates are in reverse sequence to those for chlorides. This might account for the mutually reversed sequences of alkali-metal acetates and chlorides in their coagulating effects. This has been confirmed by new data [35, 36]. The reversal of the series of activity coefficients for alkali-metal acetates relative to the normal sequence for salts of strong monobasic acids and the same metals is explained by the specific ion - solvent interaction [35, 36].

According to these views, in the case of acetates this interaction leads to "localized hydrolysis" [35, 36]. When the cations are hydrated, protons from water molecules are displaced from the forming hydration shell. These become bound by acetate ions, which are good proton acceptors. This bonding intensifies interionic interaction. Schematically this may be represented as follows:



Naturally, this effect is most pronounced for Li^+ , and weakens in the hydration series of the alkali metals:



This leads to the above-mentioned reversal of the series for acetates, hydroxides, etc.

This situation is clearly illustrated in Fig. 1 [37]. Acetates and hydroxides are good proton acceptors, behave similarly, and give rise to curves of similar configuration [35-37]. Further confirmation is provided by tabulated data for activity coefficients [36].

Our attempt to reveal differences in the influence of accompanying ions by comparison of the coagulating effects of electrolytes with activity coefficients may be extended to other substances. For example, it is possible in this way to account for the stabilizing action of monobasic fatty acid anions in the coagulation of arsenic trisulfide [14, 15]. The authors of these papers found experimentally that the coagulation threshold (k_{0w}) for potassium chloride increases with increasing concentration of the fatty acid anion (with a common cation).

The stabilizing action of the accompanying anion increases in the series from formate to butyrate (Fig. 2, [14, 15]), as shown by the definite sequence of the curves. However, the regular sequence breaks down at valerate. Curves for the activity coefficients of the sodium salts of the same acids present a completely analogous picture (Fig. 3, [37]). The same sequence in the positions of the curves is retained up to the butyrate inclusive, but it breaks down at the valerate. A similar "retardation" of the curves for formates is also characteristic (Fig. 2).

It is seen that the activity coefficients and the stabilizing effects of the anions are in a symbatic relationship. This is quite natural, as increase of the former results in an increase of the effective concentration of the stabilizing ion, and hence to weakening of the action of the coagulating ion. This relationship breaks down for valerate and the subsequent salts, probably because of the sharp increase in the role of the hydrophobic radical which influences surface activity, adsorption, and micelle formation (see curves in Fig. 3).

Thus, correlation of activity coefficients and coagulating series of electrolytes justifies our attempt for a number of independent cases. The effects of alkaline-earth acetates on coagulation should also be considered from the same standpoint, as their coagulating action has been studied [1]. It might be possible to draw an analogy with the behavior of alkali-metal acetates, but this is hindered by lack of complete data on the activity coefficients of these salts. Comparison of the coagulating effects of alkali-metal and alkaline-earth acetates is interesting in another respect. The coagulating effect of the acetate does not decrease, as might be expected, when a univalent accompanying ion is replaced by a bivalent. However, the coagulating effect of acetates is considerably lower with certain other accompanying ions. The acetates of lead, mercury, copper, and certain

* An attempt at such a comparison was reported at the Report Conference of the Chemical Faculty of Khar'kov State University in 1951.

other metals are exceptional in their effects. Solutions of mercury and copper acetates do not cause visible coagulation of ferric hydroxide sol, at strengths up to saturation. At the same time, acetates of all three above-mentioned metals mixed with various sols [1, 8-21] showed a considerable tendency to foam formation. This is probably associated with formation of coagulation structures [38] in the sols and possible formation of complexes [1, 18-21, 39] by the electrolytes.

It is interesting to note that the literature contains very few examples of salts which do not coagulate hydrophobic colloids [12]. In connection with the work of A. V. Dumanskii (1904), D. I. Mendeleev [40] refers to mercury salts, which do not coagulate colloidal ferric hydroxide.

It follows from the foregoing that the influence of accompanying ions in the coagulating power of electrolytes may be determined by various causes. Sometimes this influence is fairly great and may not be disregarded. It is possible to predict cases in which its significance should increase for all accompanying ions. For example, it is known from the literature that the influence of accompanying ions becomes more prominent with increase of the dielectric constant of the medium [11]. If this is so, then in view of the common features with biological colloidal systems [41], the significance of the influence of accompanying ions in added electrolytes should increase for blood and animal tissues with high dielectric constants [42].

Further research on these problems is clearly necessary.

SUMMARY

1. The effects of accompanying ions on the coagulating power of coagulator ions are examined. The sequences of coagulating effects of electrolytes and their activity coefficients are compared for three independent cases. A symbatic relationship was found for alkali-metal chlorides and acetates. Differences of activity coefficients of electrolytes with a common coagulator ion must be attributed to the influence of accompanying ions on the coagulator ion.

2. In addition to this increase of interionic interaction in electrolytes, another possible manifestation of the action of accompanying ions is adsorption of these ions by the colloidal phase of like charge. Data demonstrating the possibility of such adsorption of certain ions are presented.

3. The influence of accompanying ions on the coagulating power of electrolytes can be very considerable in some cases.

It is my duty to express my deep gratitude to Academician P. A. Rebinder and to Corresponding Member, Academy of Sciences Ukrainian SSR N. A. Izmailov for scrutiny of the manuscript and valuable comments.

The A. M. Gor'kii University, Khar'kov
Chair of Technical and Colloid Chemistry

Received July 2, 1957

LITERATURE CITED

- [1] V. M. Simonova and S. G. Teletov, Trans. Inst. Chem. Khar'kov State Univ. 10, 135 (1953).
- [2] A. V. Dumanskii, Progr. Chem. 1, 291 (1932).
- [3] E. Val'ko, cited through H. R. Kruyt, Colloid Science (IL, 1955) 435 [Russian translation].
- [4] A. V. Dumanskii, Colloid Science (Goskhimizdat, 1948) 259, 266. [In Russian]
- [5] N. P. Peskov, Physicochemical Principles of Colloid Science (Goskhimizdat, 1934) 299. [In Russian]
- [6] H. R. Kruyt, Progr. Chem. 9, 683 (1940).
- [7] H. R. Kruyt, Colloid Science (IL, 1955) 435 [Russian translation].
- [8] L. K. Lepin' and A. V. Bromberg, J. Phys. Chem. 13, 75 (1939).
- [9] W. Ostwald, Progr. Chem. 9, 562, 564 (1940).
- [10] I. S. Teletov and V. M. Simonova, Sci. Mem. Khar'kov State Univ. 30, 165 (1950).
- [11] Yu. M. Glazman, J. Phys. Chem. 20, 211 (1946).

- [12] A. I. Rabinerson, Koll. -Z 42, 50 (1927).
- [13] B. V. Deryagin and L. D. Landau, J. Exp. Theoret. Phys. 15, 663 (1945); B. V. Deryagin, Proc. IIIrd All-Union Conf. on Colloid Chemistry (Izd. AN SSSR) 239.
- [14] V. P. Mishin and V. P. Faidysh, Colloid J. 6, 711 (1940).
- [15] V. P. Faidysh, Colloid J. 9, 151 (1947).
- [16] V. P. Faidysh, Colloid J. 10, 317 (1948).
- [17] L. A. Kul'skii, I. T. Goronovskii, and M. I. Kaganovskii, Ukrain. Chem. J. 16, 470 (1950); I. T. Goronovskii, Dissertation (Kiev, 1955).
- [18] A. M. Shkodin and L. D. Shaposhnikova, Trans. Inst. Chem. Khar'kov State Univ. 10, 101 (1953).
- [19] A. M. Shkodin, L. D. Shaposhnikova, and S. G. Teletov, Trans. Chem. Faculty and Inst. Chem. Khar'kov State Univ. 11, 33 (1954).
- [20] A. M. Shkodin and L. D. Shaposhnikova, Ibid, 15, 9 (1956).
- [21] A. M. Shkodin and S. G. Teletov, Ibid, 17, 38 (1958).
- [22] Yu. M. Glazman and B. É. Tartakovskaya, Colloid J. 9, 241 (1947); 11, 299 (1949); Yu. M. Glazman, Colloid J. 15, 334 (1953).*
- [23] Yu. M. Glazman and I. M. Dykman, Colloid J. 18, 14 (1956).*
- [24] H. B. Weiser, J. Phys. Chem. 25, 665, (1921); K. Sen and N. Dhar, Kolloid. -Z 34, 262 (1924); S. Ghosh, N. Dhar, Zeit. Phys. Chemie 29, 435 (1925); A. V. Dumanskii and A. I. Zolin, Kolloid-Z. 59, 314 (1932); V. A. Kargin and A. I. Baibaev, J. Phys. Chem. 7, 13 (1936); V. A. Kargin and V. V. Kiseleva, J. Phys. Chem. 11, 461 (1938); V. A. Kargin and G. V. Klimovitskaya, J. Phys. Chem. 11, 467 (1938); V. A. Kargin, and Z. Ya. Berestneva, J. Phys. Chem. 13, 1625 (1939); V. A. Kargin, P. S. Vasil'ev, and O. I. Dmitrenko, J. Phys. Chem. 13, 1837 (1939); 14, 1628 (1940); V. A. Kargin, Progr. Chem. 8, 998 (1939); V. A. Kargin, O. I. Dmitrenko, and A. I. Ryabinina, Colloid J. 13, 3 (1951); O. I. Dmitrenko and A. I. Ryabinina, Colloid J. 15, 29, (1953); * T. N. Chernikova and E. N. Gapon, Colloid J. 11, 120 (1949); A. I. Brodskii, Isotope Chemistry [in Russian] (Izd. AN SSSR, 1952) p. 282.
- [25] A. I. Rabinovich, Progr. Chem. 10, 26 (1941).
- [26] D. N. Strazhesko and Yu. M. Glazman, Proc. Acad. Sci. USSR 75, 411 (1950); Proc. Acad. Sci. Ukrainian SSR 283 (1950).
- [27] Yu. M. Glazman, D. N. Strazhesko, and B. É. Tartakovskaya, Colloid J. 15, 161 (1953).*
- [28] S. G. Teletov, Summaries of Papers at the IVth All-Union Conf. on Colloid Chemistry (Izd. AN SSSR, 1958) 51. [In Russian]
- [29] G. Schweitzer and M. Bomar, Ref. Zhur. Khim. 11, 83, 32176 (1956).
- [30] B. Levy, Ref. Zhur. Khim. 1, 84, 614 (1957).
- [31] A. M. Shkodin and L. D. Shaposhnikova, Colloid J. 20, 242 (1958).*
- [32] S. G. Teletov, Ukrain. Chem. J. 20, 31 (1954).
- [33] G. Hüttig, Progr. Chem. 4, 395 (1935).
- [34] Landolt - Bornstein, Phys. Chem. Tabellen, III, 2139, Berlin (1935).
- [35] R. A. Robinson and R. H. Stokes, Ann. N. Y. Acad. Sci. 51, 4, 602 (1949).
- [36] R. A. Robinson and R. H. Stokes, Electrolyte Solutions (London, 1955) 413, 477.
- [37] H. Harned and B. Owen, Physical Chemistry of Electrolytic Solutions (IL, 1952) 362 [Russian translation].
- [38] P. A. Rebinder, J. Acad. Sci. USSR 2, 12 (1955).
- [39] K. J. Pedersen, The Complex Formation Between Cupric and Acetate Ions (Kobenhavn, 1945).

*Original Russian pagination. See C. B. Translation.

- [40] D. I. Mendeleev, Principles of Chemistry vol. 2, 593 (1947). [In Russian]
- [41] H. Freundlich, Progr. Chem. 7, 768 (1938).
- [42] I. N. Bulankin, Physical and Colloid Chemistry (Khar'kov State Univ. Press, 1957) 153. [In Russian]

A NEW INSTRUMENT (THE ELASTORELAXOMETER) FOR LARGE REVERSIBLE DEFORMATIONS, STRENGTH, AND RELAXATION OF HIGH-ELASTIC COLLOID SYSTEMS AND POLYMER SOLUTIONS

A. A. Trapeznikov

There have been numerous investigations of the elastic properties of fluid colloidal systems and polymer solutions. However, elastic deformations were measured only at low shearing stresses and low deformation rates, and the deformations obtained under such conditions could not be truly characteristic of the high elasticity of the system. The most significant in this respect should be the greatest elastic deformations, corresponding to high deformation rates in excess of the maximum relaxation rates of the systems, but these were not known or even suspected to exist in fluid colloidal systems and polymer solutions.

The significance of maximum elastic deformations was first demonstrated in our investigations [1]. Oleogels of aluminum soaps and solutions of polyisobutylene rubber in decalin were investigated. Apart from evaluation of limiting (breaking) deformations ϵ_r , corresponding to maximum $P = P_r$ on the stress - deformation $P(\epsilon)$ curves, direct determinations of large elastic (reversible) deformations and their relaxation are of great importance. We used the "silk-thread" method [2].

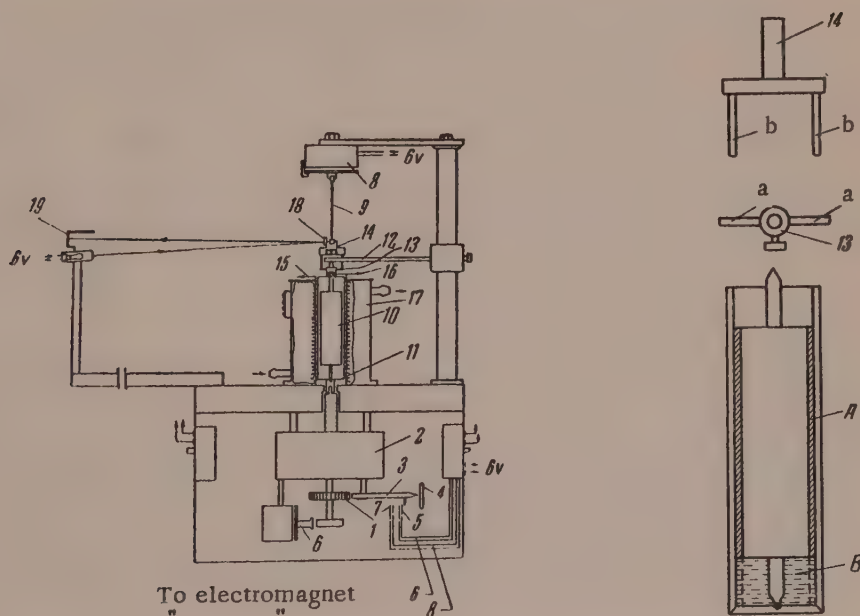


Fig. 1. Diagram and details of the instrument.

Maximum elastic deformations reflect the flexible threadlike structure of the particles, which extend at high deformation rates and are capable of coiling when not under stress. The absolute values of the maximum

TABLE 1

Angles of Rotation of Inner and Outer Cylinders in Measurement of Elastic Recoil in 2% Aluminum Naphthenate Gel ($\tau_{\text{aging}} = 64$ days)

Rotation angle of outer cylinder s°	Full rotation angle of inner cylinder s_e°	Torsion angle of inner cylinder at start of its free movement φ°	Absolute angle of rotation		Relative deformation		Shearing stress $P = C_0 \varphi / 2\pi R_1^2 L \times 10^{-2}$
			of outer cylinder relative to the inner $\theta^\circ = s - \varphi$	inner cylinder relative to its initial deviation $\theta_e^\circ = s_e - \varphi$	Predetermined $\epsilon = \theta / k'$	elastic recoil $\epsilon_e = \theta_e / k'$	
39	40	1	38.0	39.0	9.86	10.2	17.3
59	59	1.33	57.7	57.7	15.1	15.1	23.1
74	73	1.66	72.3	71.3	18.9	18.7	28.8
114	113	2.5	111.5	110.5	29.2	28.2	43.3
141	141	3.17	137.8	137.8	36.1	36.1	54.9
616	165	4.0	162.0	161.0	42.1	42.1	69.3
184	193	4.0	180.0	189.0	47.1	49.5	69.3
213	225	4.0	209.0	221.0	54.8	57.9	69.3
214	227	4.33	209.7	222.7	54.9	58.9	75.0
253	239	4.33	248.7	234.7	65.2	61.5	75.0
269	237	4.33	264.7	232.7	71.9	59.0	78.0
302	215	4.33	297.7	210.7	77.9	55.1	75.0
324	213	4.0	320.0	209.0	83.8	54.7	69.3

deformations in many colloidal systems considerably exceed the usual breaking deformations of natural rubber (1000-1200%).

The concept of maximum elastic deformations in fluid systems is also important in connection with the investigations of normal stresses by Weissenberg's method [3], which are of considerable current interest. Despite the fact that normal stresses are correlated with elastic shearing deformations, the latter are merely calculated indirectly from normal stresses, or by other methods. Until now reversible shearing deformations at high rates have not been measured directly; no instruments for the purpose have been designed.

It should also be noted that in theories of normal stresses arising in fluid systems in steady flow no account at all was taken of the transition beyond the yield value of the structure or beyond the limit of reversible deformations, accompanied by breakdown of the structure before the steady state is established.

It is clear from the foregoing that the development of methods and special instruments for direct measurements of large reversible deformation is a very important task.

We have developed a new instrument, the elastorelaxometer, based on the coaxial-cylinder principle. The idea of the instrument involves: 1) rotation of the outer cylinder at a constant rate, and the possibility of stopping it automatically at a required angle; 2) measurement of the maximum shearing stress P which develops when the outer cylinder rotates through the required angle; 3) retention of the inner cylinder in virtually its initial position during rotation of the outer cylinder until its arrest; 4) automatic release of the inner cylinder in a very short time (0.01-0.05 second) after arrest of the outer cylinder, or after different time intervals; 5) measurement of the angle of rotation of the inner cylinder after arrest of the outer cylinder, determining the elastic recoil) of the system under investigation.

To simplify the instrument, the outer cylinder is driven by a gramophone spring mechanism at a rotation rate $\Omega \approx 75$ revolutions/minute*. With an outer cylinder radius $R_2 = 1.5$ cm (height $L_2 = 12$ cm) and inner

* We have since constructed a new and more powerful model of the instrument, driven by a motor and equipped with gear boxes to give a wider range of Ω . Some of the results for rubber solutions, obtained with the new instrument, have been published [4].

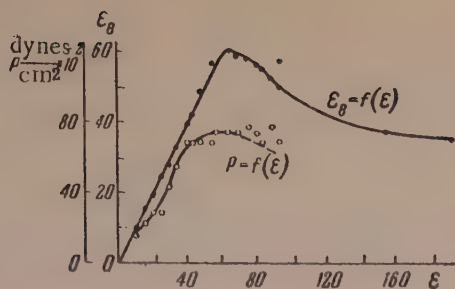


Fig. 2. $\epsilon_g(\epsilon)$ and $P(\epsilon)$ curves for 2% aluminum naphthenate gel in decalin; $\tau_{\text{aging}} = 64$ days.

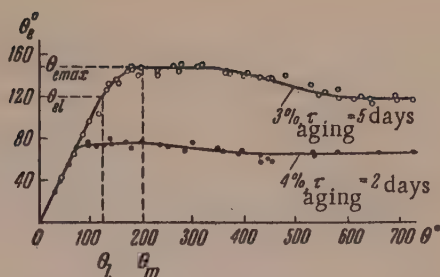


Fig. 3. $\theta_e(\theta)$ curves for 3 and 4% aluminum naphthenate gels.

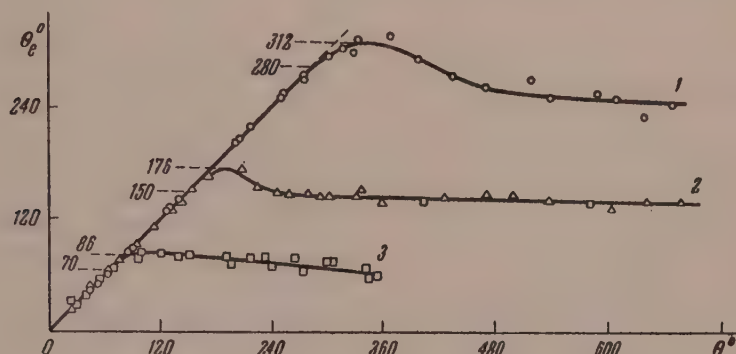


Fig. 4. $\theta_e(\theta)$ curves for 2% aluminum naphthenate gel ($\tau_{\text{aging}} = 15$ days) with three different inner cylinders of R_1 :
1) 1.300; 2) 1.396; 3) 1.450 cm.

cylinder radii R_1 from 1.3 to 1.45 cm (height $L_1 = 8.0$ cm) this gives velocity gradients $\dot{\epsilon}$ from 200 to 52.5 sec^{-1} . The instrument is shown schematically in Fig. 1. To one of the gear wheels 1 of the drive 2, situated at the lower end of the instrument, there is attached a thrust pointer 3, engaging by its inner end with a cog of the gear wheel 1, and sliding by its outer end along a circular graduated scale 4. This pointer is used to give the desired angle of rotation of the outer cylinder, from 18-20 to 720° (if the pointer is released the cylinder can be rotated continuously at a high rate). On reaching its stop, the pointer closes the contact 5 and, through a relay, switches in the electromagnetic brake 6, which eliminates the slight inertia drag of the outer cylinder. After a short time (0.01-0.05 second) the pointer, moving forward, closes the second contact 7, which switches in the electromagnet 8, situated over the upper end of the elastic measuring wire 9, through another relay.

The inner cylinder 10 has upper and lower axes with pointed ends. The lower point rests on the bottom of the outer cylinder 11, and the upper point is pressed (not too firmly) against the centering arm 12, which acts as the upper thrust bearing. Instead of the usual permanent linkage between the axis of the inner cylinder and the wire measuring the torque set up by the gel, a removable wire which is easily separated from the cylinder axis is used; it is linked with the inner cylinder by the coupling joint 13 with two projections \underline{a} , which press against the pegs \underline{b} of another coupling joint 14, fitted onto the lower end of the wire. The upper end of the wire is inserted into the lid of an electromagnetic clutch which, when the magnet is in circuit, is pulled upward and pulls the pegs \underline{b} from the projections \underline{a} , so that the inner cylinder is released. The outer and inner cylinders are fitted with pointers 15 and 16 which travel over the graduated upper lid of the thermostat 17, connected with a Hoepler ultrathermostat.

The torsion angle of the wire measuring the shearing stress is read off from the deflection of the light spot

TABLE 2

 $R_2 = 1.50$ cm, $\Omega = 6.53$ radians/sec

R_1	$1/k^*$	θ_{el}		$\theta_{e\max}$		ϵ_e		ΔR , cm	H_{el} , cm	ϵ_{el}	$H_{e\max}$, cm	$\epsilon_{e\max}$	$\frac{R_2^2 - R_1^2}{R_2^2} \cdot 100\%$
		deg	rad	deg	rad	ϵ_{el}	$\epsilon_{e\max}$						
1,450	30,52	70	1,22	86	1,5	37,2	45,7	0,050	1,83	36,6	2,25	45,0	6,55
1,396	15,00	150	2,615	176	3,07	39,2	46,1	0,104	3,92	37,7	4,60	44,2	13,3
1,300	8,04	280	4,88	341	5,45	39,2	43,8	0,200	7,32	36,6	8,18	40,8	24,9

from the mirror 18 on the scale 19. With a rigid wire (in this instance a wire of $C_0 = 99,240$ dynes · cm/radian was generally used) the rotation angle φ of the inner cylinder does not exceed 10-15°, but in most determinations it was less than 5°, so that the deformation of the system $\theta = s - \varphi$ was equal to almost the complete rotation angle s of the outer cylinder, which often exceeded 100°.

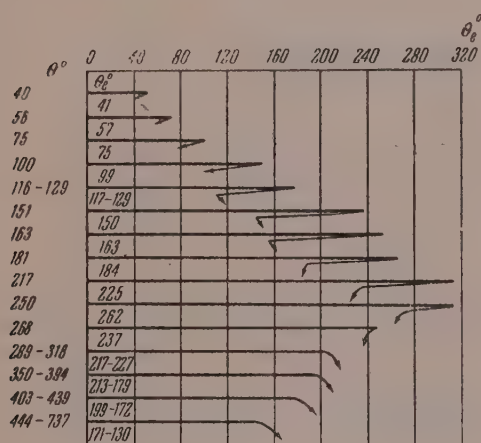


Fig. 5. Schematic curves representing the character of the motion of the inner cylinder for different predetermined deformations.

unusually high value of 62 for ϵ this is a sign of extremely high elasticity of the system.

Fig. 3 shows $\theta_e(\theta)$ curves for 3% and 4% gels; it is seen that up to a certain rotation angle $\theta = \theta_l$ of the outer cylinder the values of θ_e are equal to θ , i. e., that the given deformations are fully elastic. Subsequently the $\theta_e(\theta)$ relationship becomes nonlinear; at first θ_e increases a little, passes through a maximum $\theta_{e\max}$ and then gradually diminishes. The lag of θ_e behind θ in the $\theta > \theta_l$ range is the consequence of structural breakdown and relaxation. The fall of θ_e beyond the maximum may also be caused by both these factors, but the first is the chief one. Despite this, the elastic recoil still remains fairly large. The reason is that the disrupted structural elements, undergoing relative displacement in the deformed extended state and giving rise to irreversible deformation, are capable of rapid cohesion at new points, with recoil of their retained elastic deformation. As the deformation increases, the degree of breakdown of the structure grows and elastic recoil diminishes. Moreover, if the deformation time is greater, the relaxation which is mainly associated with contraction of the broken-down structural elements can go further.

If the system under investigation is fully elastic, the inner cylinder should turn through an angle of $\theta_e = s_e - \varphi$ (s_e is the full rotation angle of the inner cylinder), equal to the rotation angle θ of the outer cylinder; if the deformation is partially residual, then $\theta_e < \theta$. In some cases $\theta_e > \theta$, due to inertia overrun of the inner cylinder. If the medium is not elastic, the inner cylinder does not move at all after arrest of the outer cylinder; this was verified with water, mercury, and vaseline oil. The values of θ and θ_e were used to calculate the relative deformations ϵ and ϵ_e (see below). Some data are presented in Table 1.

Elastic Recoil and Shearing Stress. Fig. 2 represents $\epsilon_e(\epsilon)$ and $P(\epsilon)$ curves for 2% gel of aluminum naphthenate in decalin (Batch No. 24*), determined at $R_2 = 1.50$ cm, $R_1 = 1.396$ cm. The ratio of the values of P and ϵ_e at the curve maxima shows that the shear modulus $E \approx 130$ dynes/cm²; with the

* Aluminum naphthenate was made in the works (experimental Batch No. 24, 1954) from acidol with naphthenic acids of average molecular weight 225, by the formulation with 100% free alkali [5]. The experimental batches were prepared with the assistance of G. V. Belugina.

TABLE 3

Elastic Recoil With the Lower Part of the Cylinder Filled With Gel or Mercury; $R_2 = 1.5$

Expt. No.	Gel composition	Gel aging time, days	Lower part of outer cylinder filled with			
			radius of inner cylinder R_1 , cm	gel	radius of inner cylinder, R_1 , cm	mercury
1	2% aluminum naphthenate in decalin	~ 10	1.4	130-138	1.3	251-260
2	The same	15	1.4	160-164	—	—
	The same, another sample	26	—	—	1.3	336
3	2% aluminum naphthenate in decalin, with addition of 0.431 g of capryl alcohol	2	1.4	191	1.4	210
	The same	3	1.4	193	1.4	203
4	2% aluminum naphthenate in vaseline oil	—	1.4	133-135	1.4	136-137

Effect of Gap Width Between Cylinders on ϵ_e . Measurements of ϵ_e with different gap widths $\Delta R = R_2 - R_1$ between the cylinders, for three values of $R_1 = 1.30$; 1.396 and 1.45 cm with $R_2 = 1.5$ cm showed that the throw-back angle decreases with decrease of ΔR (Fig. 4). The values of $\epsilon = 2\theta R_2^2 / (R_2^2 - R_1^2) = 0/k'$ (Table 2) are similar for all values of ΔR .

Values of $\epsilon_{el} = H_{el}/\Delta R$ and $\epsilon_{e\max} = H_{e\max}/\Delta R$, where $H_{el} = R_2 \theta_{el}$ and $H_{e\max} = R_2 \theta_{e\max}$, calculated by the simplified formula $\epsilon_e = R_2 \theta_e / \Delta R = H / \Delta R$, as the ratio of the linear displacement of the outer cylinder to gap width, coincide (Table 2) with the preceding values for the narrowest gap and are somewhat lower with a wide gap. In general, this proves the reality of enormous elastic deformations and the validity of the formulas used. At the same time, the deformation ϵ_e is in fact the extension deformation of the gel particles.

The use of the first of the two formulas presupposes constancy of the shear modulus E over the entire range of ϵ_e and a distribution of the deformation gradient over the gap characteristic of an ideal elastic Hookian body of constant E at low ϵ_e . In reality E is not constant over the entire range of ϵ_e up to $\epsilon_{e\max}$, but this lack of constancy is probably of the same type for all gaps and the variations of E are similar at equal values of ϵ_e .

In accordance with our earlier data [1] it may be assumed that variation of the velocity gradient $\dot{\epsilon} = 2\Omega R_2^2 / (R_2^2 - R_1^2) = \Omega/k'$, as the result of changes of ΔR , at the fairly large values of $\dot{\epsilon}$ from 52.5 to 200 sec^{-1} specially used here, has almost no influence on ϵ_e for the given gel.

The agreement between the values of ϵ_e shows that the heterogeneity of the stress field $(R_2^2 - R_1^2)/R_2^2$ (Table 2), which greatly increases with increase of ΔR , has no significant influence on ϵ_{el} and $\epsilon_{e\max}$ for this gel. This is consistent with earlier measurements of E by the method of torsional vibrations for small deformations in 7% gel [1].

In calculation of ϵ_e by means of the above formulas it is assumed that the gel is deformed in the annular gap A (Fig. 1). To confirm that the elastic recoil is not due to the column of gel B under the bottom of cylinder R_1 , for which the relative deformation would be calculated from the formula for torsion of a rod as $\epsilon = R_1 \theta_e / h$ (where $R_1 = 1.4$ cm, and h is the height of the column B, 2 cm), and which at $\theta_e = 163^\circ$ would be only $\epsilon_e \approx 2.0$ instead of $\epsilon_e = 42.7$, experiments were carried out in which the lower part B between the cylinders was filled with an inelastic liquid — mercury. In this case the gel was poured on top, and was present only in the narrow annular gap A. It was found that when the volume B was filled either with the gel or with mercury the values of θ_e (Table 3) coincided, both for the same cylinder of given R_1 , and for cylinders of different R_1 (with a twofold increase of ΔR , θ_e was also doubled; see Experiments Nos. 1 and 2, Table 3). This shows that the values of θ_e determined in the instrument are in fact values for the narrow gap A between the cylinders, which justify the above formulas and confirm the existence of enormous relative shearing deformations in high-elastic bodies.

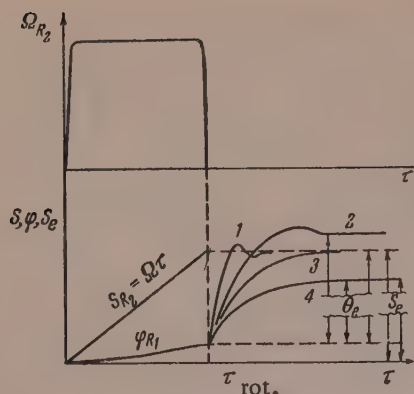


Fig. 6. Motion of the outer and inner cylinders.

Characters of the Motion of the Inner Cylinder in Elastic Recoll. The character of the motion of the inner cylinder after its release differs for different θ , and depends on transition beyond $\theta_{e \max}$.

Fig. 5 is a schematic representation of the types of motion of the inner cylinder ($M = 121.5 \text{ g} \cdot \text{cm}^2$; $R_1 = 1.396 \text{ cm}$; gel concentration 2%; $\tau_{\text{aging}} = 66 \text{ days}$) for different values of θ and corresponding final angles of rotation of the inner cylinder θ_e . The cylinder displacement θ_e is taken horizontally and the time vertically for each curve. The slope of each line is a measure of the rate of motion. Thus, at $\theta < 116^\circ$ the cylinder first travels rapidly in the forward direction, passes the new equilibrium position $\theta_e = \theta$ by inertia, and returns to it by a reverse movement. At $116^\circ < \theta < 163^\circ$ because of the large inertia over-run in the reverse direction another movement,

although slow, appears in the forward direction. In this range of θ the first inertia kicks reach $90\text{--}100^\circ$, but in all cases the final position is $\theta_e = \theta$ (within the experimental error limits of $\pm 1\text{--}2^\circ$).

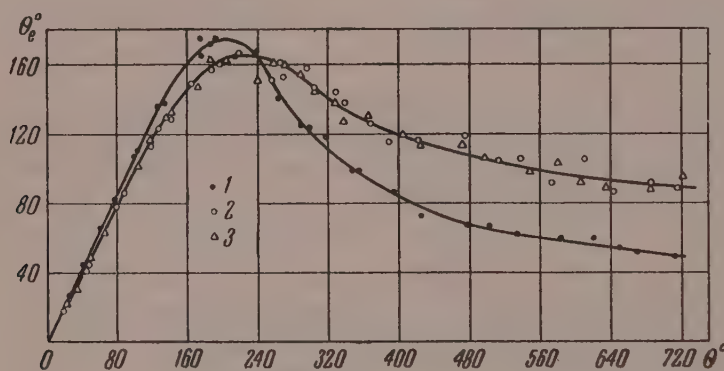


Fig. 7. $\theta_e(\theta)$ curves for 2% gel ($\tau_{\text{aging}} = 155 \text{ days}$) determined with cylinders of different moments of inertia M : 1) $376.2 \text{ g} \cdot \text{cm}^2$; 2) $121.5 \text{ g} \cdot \text{cm}^2$; 3) $26.3 \text{ g} \cdot \text{cm}^2$.

At $\theta = 181\text{--}268^\circ$ the situation changes. The inertia kicks in the forward and return direction decrease, and the motion in the reverse direction occurs in two stages: most of it is rapid, followed by a virtual halt, and then slow. At $\theta = 181\text{--}250^\circ$ the inertia kick in the forward direction decreases, and θ_e is somewhat larger than θ : thus, at $\theta = 181^\circ$, $\theta_e = 184^\circ$, and at $\theta = 217^\circ$, $\theta_e = 225^\circ$; i. e., in these cases θ_e is $3\text{--}8^\circ$ higher. At $\theta \geq 289^\circ$ the motion of the cylinder changes again; it first moves rapidly in a forward direction through a large angle, then stops, and subsequently moves slowly (through $8\text{--}15^\circ$) in the same direction. This last fact is very significant. It shows that all the deformation θ_e in this case is truly elastic, as after it has stopped the cylinder can move in the forward direction only under the influence of elastic deformation of the gel. At $\theta = 289\text{--}318^\circ$, θ_c is $217\text{--}277^\circ$, and therefore elastic deformations ϵ_e reaching 6000% , found by calculation from $\theta_{e \max}$, can in fact develop the gel. Therefore the somewhat higher values of θ in the range $\theta \geq 180^\circ$ are not inconsistent with the possibility of high values of ϵ_e .

The first rapid jump on the curves for the motion of the inner cylinder might correspond to the "instantaneous" part of the deformation, and the subsequent slow motion to creep (high-elastic part). This subdivision might be useful in a number of cases, but is very arbitrary, as it depends on the inertia of the cylinder and the time of recording of the deformation.

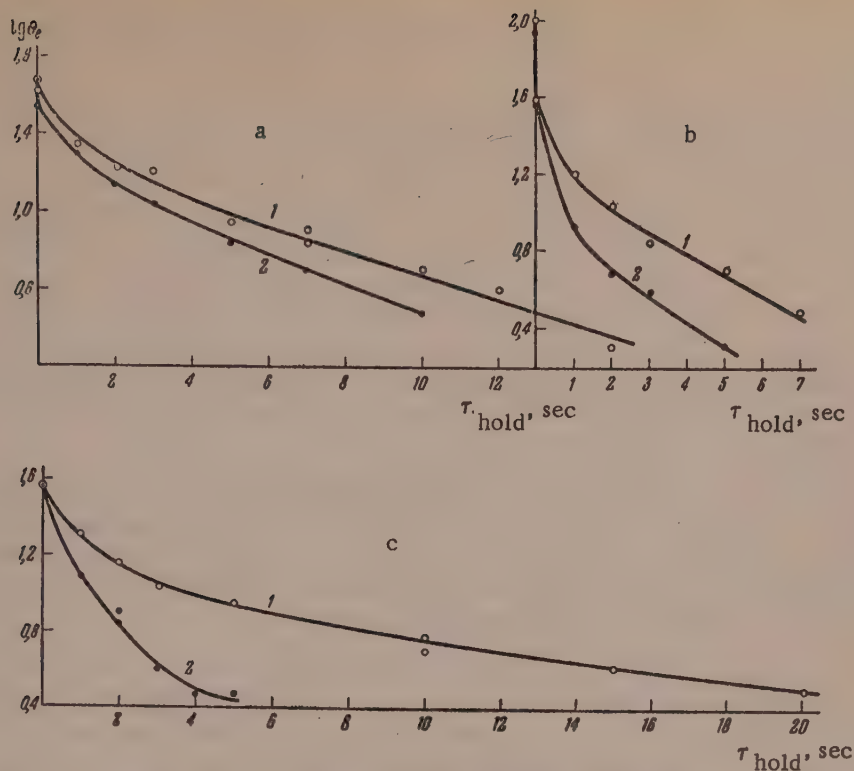


Fig. 8. Relaxation curves $\lg \theta_e = f(\tau_{\text{hold}})$: for 2% aluminum naphthenate gel with addition of 0.215% of capryl alcohol, $\tau_{\text{aging}} = 76$ days, for $\epsilon_e = 12$ (a) and $\epsilon_e = 190$ (b); for 1.5% aluminum naphthenate gel, $\tau_{\text{aging}} = 80$ days for $\epsilon_e = 12$ (c); 1) cylinder of $M_3 = 26.3 \text{ g} \cdot \text{cm}^2$; 2) cylinder of $M_2 = 121.5 \text{ g} \cdot \text{cm}^2$.

The types of cylinder motion considered here may be regarded as vibrational and aperiodic damping of a pendulum, where the elastic force is the gel elasticity and the inertia mass is the mass of the cylinder (the gel mass being disregarded*). The motion of such a pendulum might conform to the equation

$$M \frac{d^2 \theta_e}{d\tau^2} + p \frac{d\theta_e}{d\tau} + \Delta C \theta_e = 0, \quad (1)$$

under the condition that $p = f(\theta_e \theta)$ and that the gel elasticity in consequence of relaxation is $\Delta C = f(\tau, \theta_e)$; for example $\Delta C = \Delta C_0 e^{-\tau/\vartheta}$, when the relaxation time $\vartheta = f(\theta, \theta_e)$. A general scheme representing the motion of the outer and inner cylinders is shown in Fig. 6. The upper part of the diagram represents variation of Ω with time, and the lower, the angle of rotation of the outer cylinder $S_{R_2} = \Omega \tau_{\text{rot}}$ and the angle of rotation of the inner cylinder until the start of its free movement $\varphi(\tau)$, corresponding to change of the shearing stress $P(\tau)$, and also the motion of the inner cylinder after release $s_e(\tau)$. In accordance with the parameters of Equation (1), either oscillation about a new equilibrium position (when $p^2 < 4M\Delta C$) or an aperiodic approach to it (when $p^2 \gg 4M\Delta C$) is possible. The final values of s_e may be either equal to or less than the predetermined s . Therefore, high values of s_e are the consequence of inertia kicks and rapid relaxation ($\Delta C \rightarrow 0$). Values of $s_e < s$ are the consequence of structural breakdown and relaxation.

It is evident that the smaller the value of M and the slower the relaxation, the more exactly the final values of s_e correspond to true s_e . It follows from Fig. 5 that with transition through the maximum $\theta_e = \theta_{e \text{ max}}$ the nature of the motion changes from vibrational to aperiodic. This is due to the continuously increasing struc-

* If the cylinder is very light, the gel mass is comparable with the cylinder mass, and must be taken into account.

tural breakdown, accompanied by increase of the damping coefficient p , decrease of ΔC , and increase of the relaxation rate [1, 6].

The influence of the moment of inertia of the cylinder is confirmed by the curves in Fig. 7, for three cylinders of the same $R_1 = 1.40$ cm, and with $M_1 = 376.2$ g \cdot cm² (mass 398 g), $M_2 = 121.5$ g \cdot cm² (mass 81.5 g), solid and hollow stainless-steel cylinders respectively, and $M_3 = 26.3$ g \cdot cm² (mass 23.1 g), a hollow Duralumin cylinder. The experiments were performed with a low-viscosity gel (1% gel in decalin, $\tau_{\text{aging}} = 155$ days), in which relaxation is fairly rapid. It follows from Fig. 7 that in the $\theta_e < \theta_{e\text{max}}$ region $\theta_e = \theta$ for the two cylinders of smaller M , but for the heavier cylinder the values are somewhat high at all $\theta < \theta_{e\text{max}}$. In this range of θ the elastic forces are still large, because structural breakdown is still low. Therefore the system is capable of imparting a fairly high velocity at the initial moment of motion even to the heavy cylinder, and under its influence it passes by inertia through the new equilibrium position. However, the return movement is hindered and the cylinder stops without reaching the new "fixed" equilibrium position $\theta_e = \theta$, and this results in high values of θ_e (Curve 2, Fig. 6).

In the range $\theta_e < \theta_{e\text{max}}$ the values of θ_e for the heaviest cylinder are, on the contrary, least and considerably diminished. This can be attributed to a large decrease of shearing stress beyond $P = P_r$, and to decrease of the relaxation time of the system, leading to a decrease in the velocity of the heavy cylinder even in the forward direction (Curve 4, Fig. 6). Curve 1, Fig. 6 represents vibrational and Curve 3, aperiodic motion when the given value of $\theta_e = \theta$ is exactly reached (cylinders of M_2 and M_3).

The two lighter cylinders, with values of M differing 4.6-fold, give $\theta_e(\theta)$ curves which virtually coincide for all values of θ . This shows that they are suitable for determinations of ϵ_e in this gel, and that $\epsilon_e(\epsilon)$ curves are independent of M . It is obvious that at large values of E and large θ even cylinders of not very low M should give correct values of ϵ_e , but the lightest cylinders should be used in investigations of low-viscosity systems. This is also shown by the curves for relaxation of deformation $\log \epsilon_e = f(\tau_{\text{hold}})$ for 2% and 1.5% aluminate naphthenate gels (Fig. 8), the method for determination of which was described earlier [6]. The initial points, corresponding to $\tau_{\text{hold}} = 0$ second and determining the $\epsilon_e(\epsilon)$ curve, coincide for cylinders with $M_2 = 121.5$ g \cdot cm² and $M_3 = 26.3$ g \cdot cm². The curves subsequently diverge, when a part of the elastic deformations and stresses in the system disappear owing to relaxation. The small residual stress confers a lower velocity to the heavier cylinder, and the relaxation can proceed even further during this motion. The deviation is more pronounced at lower initial irreversible relaxation times; for example, at lower gel concentrations ($c = 1.5\%$) or at higher predetermined deformations ($c = 2.0\%$, $\epsilon = 190 > \epsilon_m$).

These results also lead to the conclusion that in investigations of the kinetic elastic properties of colloidal systems the moment of inertia of the cylinder (the acting body) may have an influence, especially with rapidly relaxing systems. In many investigations massive cylinders suspended from thin wires have been used in attempts to increase sensitivity. This can undoubtedly influence the form of the kinetic curves showing development of after-effects. The inertia of the acting body of the instrument should be reduced to a minimum.

The type of cylinder motion described above was observed with gels of different compositions, but in some gels of high "dynamic" viscosity (such as aluminum naphthenate in vaseline oil) the motion of the cylinder was in the forward direction only, even at $\theta < \theta_{e\text{max}}$.

The effects described have much in common with the types of motion of disks in monomolecular layers on water surfaces, such as highly elastic protein monolayers, in which an increase of the damping decrement was observed with increase of amplitude and with approach to the yield value [7].

Some Comments on Extrusion of the Gel From the Gap Between the Cylinders. It is known that elastic liquids and gels can become twisted on the rod of the inner cylinder and be extruded from the gap. This effect has been studied in detail by Weissenberg [3] and by Ward and Lord [8], and was attributed to normal stresses arising in the system in addition to tangential stresses. The methods used by these workers indicate that the steady-flow stage was investigated, and the initial deformation stage of the system as a "solid" body, with transition beyond the yield value or the maximum elastic deformation not considered at all.

It was noted in this investigation, and also in our earlier studies [1], that up to $\epsilon = \epsilon_{\text{max}}$ or up to $\epsilon = \epsilon_r$, despite the fact that the tangential stress P reaches its maximum value $P = P_r$ at which the normal stress should be greatest, extrusion of the gel does not occur; it begins only after ϵ_e has passed beyond $\epsilon_{e\text{max}}$, on the right-

hand descending branch of the $\epsilon_e(\epsilon)$ curve, i. e., in the region of extensive breakdown of the continuous network structure. Consequently, one basic condition for extrusion of the gel and its twisting around the rod is breakdown of the structure, liberation of its individual elements, and further changes of particle configuration in flow.

It should be noted that twisting around the rod occurs only in high-elastic and fluid, i. e., rapidly relaxing, gels. In brittle-elastic gels of the gelatin type when $P = P_R$ and $\epsilon_e = \epsilon_{e \max}$ is passed the gel merely cracks and is extruded from the gap in individual pieces, without twisting around the rod.

SUMMARY

1. A new instrument, the elastorelaxometer (based on the coaxial-cylinder principle) has been developed, for studies of large high-elastic deformations in relaxing colloidal gel systems and polymer solutions.

2. The effects of the following were investigated: a) width of the gap between the cylinders; b) moment of inertia of the cylinder (with rapidly relaxing colloidal systems cylinders of the minimum moment of inertia must be used); c) nature of the liquid in the bottom of the cylinder; d) nature of the motion of the inner cylinder at different ultimate deformations.

3. Values of elastic recoil ϵ_e for different predetermined deformations ϵ have been determined in dilute aluminum naphthenate gels in decalin. It is shown that ϵ_e passes through a maximum, associated with transition beyond the yield value of the structure, with increase of ϵ . It is shown that ϵ_e can reach 6000% in 2% gels.

In conclusion, the author thanks technician P. G. Glebov for help in designing and constructing the instrument, and to laboratory assistant L. S. Meshcheryakova for carrying out the determinations.

Institute of Physical Chemistry
Academy of Sciences USSR
Laboratory of Oleocolloids and Monolayers

Received September 17, 1957

LITERATURE CITED

- [1] A. A. Trapeznikov, in the book: New Methods for Physicochemical Investigation of Surface Phenomena [In Russian] 1, 20 (1950); Proc. 2nd All-Union Conf. on Colloid Chemistry, 1950 [In Russian] (Kiev, 1952); Proc. Acad. Sci. USSR 63, 57 (1948); 74, 525 (1950); A. A. Trapeznikov and E. M. Shlosberg, Proc. Acad. Sci. USSR 62, 791 (1948); in the book: New Methods for Physicochemical Investigation of Surface Phenomena [In Russian] 1, 39 (1950); A. A. Trapeznikov and V. A. Fedotova, Proc. Acad. Sci. USSR 81, 1101 (1951); 82, 97 (1952); 95, 595 (1954); Proc. 3rd All-Union Conf. on Colloid Chemistry, Minsk, 1953 [In Russian] (Izd. AN SSSR, 1956); A. A. Trapeznikov and T. G. Shalopalkina, Colloid J. 17, 471 (1955).*
- [2] A. A. Trapeznikov and T. G. Shalopalkina, Proc. Acad. Sci. USSR 111, 380 (1956).*
- [3] K. Weissenberg, Proc. 1st Intern. Congr. Rheology, Amsterdam 1, 29 (1948).
- [4] A. A. Trapeznikov and T. V. Assonova, Colloid J. 20, 398 (1958).*
- [5] A. A. Trapeznikov and G. V. Belugina, Proc. Acad. Sci. USSR 87, 825 (1952).
- [6] A. A. Trapeznikov, Colloid J. 20, 476 (1958).*
- [7] A. A. Trapeznikov, Doctorate Dissertation (Moscow, 1955). [In Russian]
- [8] A. F. H. Ward and P. Lord, 2nd Intern. Congr. Rheology, Oxford, 1953 (London, 1954) 214.

*Original Russian pagination. See C. B. Translation.

NATURE OF "DENATURATION STABILIZATION" OF GLOBULAR PROTEINS

A. S. Tsyperovich

This paper consists of a summary of some observations of false equilibria in denaturation of globular proteins, and of denaturation stabilization — effects discovered by us in studies of denaturation kinetics [1-3]. It was found that when denaturing substances of different types act on globular proteins (egg and serum albumins or edestin) in various, not excessively high, concentrations, the reaction does not proceed to completion but stops at a definite level which depends on the physicochemical conditions. Gradual retardation and cessation of the process indicate that a so-called false equilibrium is established in the system. This is quite obvious in the denaturation of egg albumin or edestin, in which reversible interconversion of native and denatured molecules does not occur, and therefore there can be no true thermodynamic equilibrium.

In a system which had reached equilibrium a definite and usually considerable part of the protein remained in the native state; this was isolated and investigated. The properties of such protein were greatly changed; it became very resistant to denaturation and several other properties were changed. An interesting fact is that the stabilizing effect can be prevented. This was demonstrated with the undenatured part of the protein isolated from the edestin — urea equilibrium system. The possibility of preventing the stabilizing effect shows that the resistant molecules did not previously exist in the protein mass, but originated as the result of modifying treatment in urea solution. This change of the protein was termed "denaturation stabilization." Detailed studies of the properties of the modified form showed that egg albumin retains its native state after stabilizing treatment with urea, but acquires a number of structural differences from ordinary native protein.

The experiments described below were conducted in order to confirm certain hypotheses concerning the mechanism of denaturation stabilization.

Molecular Weight of Protein in the Stabilized Form

The molecular weight of stabilized egg albumin was determined primarily in the light of the following considerations. It might be possible to postulate a stabilization mechanism consisting of formation of a complex between native and denatured protein molecules, in which the native molecules are protected against denaturation. This should lead to cessation of the process, i. e., to false equilibrium. This hypothesis would be consistent with the heterogeneity found experimentally (by the salting-out method [3]) for particles of the modified form. This question could be answered directly, by determination of the molecular weight of the stabilized protein. This was done by the osmotic-pressure method, which gives a direct measure of the number of molecules in solution. If complexes were formed, the molecular weight of the stabilized protein fraction would be greatly increased (the osmotic pressure of the solutions would be lower).

The determinations were performed with the purest preparations of stabilized protein, obtained by treatment of egg albumin with urea and recrystallized at least 2 or 3 times. The modified protein was isolated, as described previously [3], from equilibrium mixtures which had been left for long periods at room temperature, containing 300-400 mg of urea per ml of protein solution. The protein was carefully purified to remove decomposition products, salt ions (by prolonged dialysis), etc. We used a new variation of the compensation method for determination of osmotic pressure [4]. The determinations were performed under the following conditions: to 10 ml of 1.0-1.5% solution of the stabilized protein 0.5 ml of 2 M acetate buffer of pH 4.7 was added, to a final buffer concentration of ~ 0.1 M. 90 mg of sodium chloride was then dissolved in the mixture. The salt concentration was roughly equivalent to physiological saline. The isoelectric state of the protein and the presence

Protein preparation	pH	Temperature, (°C)	Protein concentration, %	Osmotic pressure of 1% protein solution in mm H ₂ O	Molecular weight of protein
Stabilized (modified) egg albumin, Preparation 1	4.7	21.6	1.06	58.7	42,500
The same, Preparation 2	4.75	21.5	1.55	56.7	44,200
The same, Preparation 3	4.71	22.4	0.95	51.7	48,500
Crystalline egg albumin, control	4.7	20.8	0.88	54.2	46,000

of salt ensure freedom from error due to the Donnan equilibrium effect. The protein was then put in a cellophane bag for dialysis and dialyzed in a refrigerator at 5-6° for 24 hours against 30 ml of a solution with the same buffer and salt concentration as in the protein solution (1.5 ml of 2 M acetate buffer and 270 mg of salt were added to 30 ml of water). In the course of 24 hours the buffer and sodium chloride concentrations within and outside the bag were equalized. At the end of dialysis the volume of the protein solution was measured, its concentration was determined, and both liquids were introduced into the apparatus.

The results of some of the experiments are given in the table.

It is clear from the table that modified egg albumin has the same molecular weight as the original protein. Therefore the hypothesis of complex formation between native and denatured protein must be rejected at once.

These results also prove that the molecules of modified protein are in the native state. It is known that denaturation greatly increases the ability of molecules to aggregate, especially in salt solutions. If the material isolated from the equilibrium system contained denatured molecules, then treatment at pH 4.7-4.9 in solutions containing high concentrations of ammonium sulfate at 1-1.5% protein concentrations would undoubtedly result in molecular aggregation, associated with increase of molecular weight. The fact that the molecular weight of the isolated "fraction" exactly corresponds to the molecular weight of native egg albumin (with allowance for the effects taking place during the isolation) is one important proof that the particles of the modified (highly stable) form of egg albumin formed by denaturation stabilization are in the native form.

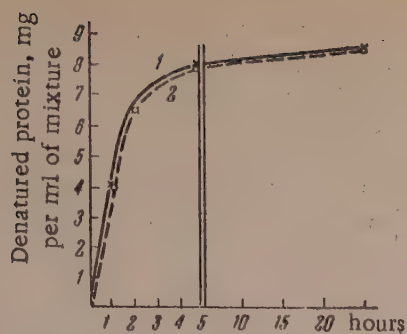
Influence of the Decomposition Products of Egg Albumin on Its Stability in Urea Solutions

It is known that protein decomposition products have a stabilizing effect on certain globular proteins [5]; literature data on this have been reported elsewhere [6]. This might naturally lead to the suggestion that "denaturation stabilization" of egg albumin (and edestin, etc.) also depends on interaction with protein decomposition products which, as has been reported [12] have been detected in considerable amounts in the equilibrium system egg albumin - urea; they were formed upon prolonged treatment of proteins with denaturing agents.

In order to determine whether these decomposition products have a stabilizing effect on the protein, we studied denaturation of egg albumin by urea, after addition of such products obtained from another mixture in which equilibrium had been reached and which had been kept for a long time.

The experiment was performed as follows. A solution of egg albumin in urea, kept for about 11 months at room temperature, was taken. It contained somewhat more urea than was used in other experiments - 400 mg per ml of protein. The original protein was recrystallized twice; its concentration was 6%, and the pH was 7 as usual. False equilibrium was reached in the system.

Protein decomposition products were obtained from this system. 30 ml of the mixture was put into a cellophane bag and dialyzed against a solution of 40 g of dry urea in 100 ml of water (i. e., 400 mg per ml of protein). The total volume of the aqueous urea solution was 130 ml. Of this, 60 ml was put in a 200 ml beaker, and the cellophane bag containing 30 ml of protein - urea mixture was immersed in this liquid. The protein decomposition products passed through the cellophane into the aqueous urea solution. The other portion of the



Denaturation of egg albumin in aqueous urea solution containing protein decomposition products: 1) with decomposition products in solution; 2) control, without decomposition products.

solution containing protein decomposition products was 1.0809, and of the control solution, 1.0766. These values correspond to 422 and 400 mg of urea per ml of water. Similar results were obtained in urea determinations from the nitrogen contents - 418 and 400 mg (a correction for the presence of protein decomposition products in one of the solutions was not applied, as such a correction would be small). It should be noted that the difference between the urea concentrations of the two solutions (~5%) is very small; it could not result in an appreciable difference in the denaturation rates. However, we eliminated the concentration difference by adding the deficient quantity of urea (~20 mg per ml) to the solution without the protein decomposition products.

Denaturation by both the aqueous urea mixtures was performed as follows. A fresh, twice-recrystallized preparation of egg albumin was used. The protein concentration of the original solution was 9.56%, and the pH was ~7. Each of two test tubes contained 10 ml of aqueous urea mixture: the one containing the protein decomposition products, and the control. To each tube 3.0 ml of protein solution was added. The final protein concentration was then 2.21%. The denaturation was effected at 35°; its course was followed by isoelectric precipitation and determinations of changes in the optical rotation.

The results are presented in the graph; it is clear that denaturation in presence and in absence of protein decomposition products proceeds at exactly the same rate. Similar results were obtained in the optical rotation determinations. The final increase of optical rotation was 0.29° in both mixtures (with optical activity of the decomposition products taken into account). Determinations of undenatured protein also gave the same contents in the two samples in all cases.

As usual, the denaturation reaction was retarded, and ceased at false equilibrium, in all experiments with and without the decomposition products. Calculations showed that the retardation commences right at the start of the denaturation process. At this stage the amount of decomposed protein is usually negligible (almost zero). The retardation of the reaction, however, is considerable.

On the basis of these results we may reject the hypothesis that egg albumin is stabilized by its decomposition products, formed in the system as the result of prolonged treatment with urea. Views on the nature of denaturation stabilization which evidently give a reasonably true explanation of the effect are presented below.

Nature of False Equilibria and Mechanism of the Denaturation

Stabilization of Globular Proteins

The Dual Action of the Denaturing Factor on the Protein

Certain conclusions may be drawn from earlier experimental data [1-3, 12, 13] in conjunction with the results of the present investigation.

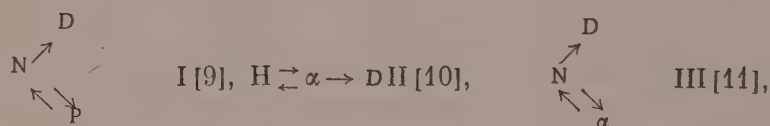
aqueous urea solution was left as a control in a similar beaker, open to free evaporation. The dialysis was continued for 4 days at +5° in a refrigerator which also contained the beaker with the control urea solution. At the end of the dialysis the presence of considerable amounts of protein decomposition products was detected in the first aqueous urea solution by the biuret reaction and by optical rotation. The control aqueous urea solution naturally did not exhibit optical activity and did not give the biuret reaction.

For quantitative comparison of the course of denaturation of fresh preparations of crystalline egg albumin in urea solutions with and without protein decomposition products after dialysis (and evaporation), their urea concentrations were checked by determinations of density and nitrogen concentration of both solutions. A 10 ml pyknometer was used for the density determinations. The density of the protein

First, it is now clear why the course of the denaturation process slows down and deviates from the monomolecular law even at the early stages, and why the reaction does not go to completion but stops at a state of false equilibrium. The cause lies in modification of some of the protein molecules ("denaturation stabilization"), as the result of which they acquire increased stability and are either denatured much more slowly, or cannot be denatured at all under given conditions. Stabilization under the influence of the denaturing agent proceeds simultaneously with the loss of the native state of the rest of the molecules, but probably more slowly. The level of false equilibrium, i. e., the extent of protein conversion, is determined by the intensity of the denaturing action, and if the latter is not very great a smaller proportion of the protein is denatured while the greater proportion is gradually (and more slowly) stabilized.

The results of a number of investigations [7], including ours [8], according to which the heat denaturation of proteins conforms to the monomolecular law, appear to be quite reliable. The absence of false equilibria (retardation of the process) in such cases may be attributed to the fact that under the usual experimental conditions in heat denaturation the action is too rapid (the temperatures being relatively high) and there is not enough time for stabilization to occur. Very similar results can be obtained in the action of urea or analogous factors on proteins if higher concentrations, higher temperatures, etc., are used. In such cases denaturation is virtually complete, and false equilibria are not established. Although the data available on the character of denaturation suggest that it is probably a characteristic first-order reaction in itself, this can be proved only in absence of conditions in which part of the protein can undergo denaturation stabilization.

Deviations of the course of denaturation from the monomolecular law have been reported in the literature several times [1]. Various explanations have been offered to account for the reaction mechanism in certain cases of irreversible and reversible denaturation (diphtheria and staphylococcus antitoxins [9], thyroglobulin [10], and luciferase [11]). These explanations are based on the assumption that denaturation, although retarded, goes to completion, and that during the process the native protein is reversibly converted into a certain intermediate form, from which it gradually returns to the native form and is then denatured (or the intermediate form may be denatured directly):



where N is native protein; D is denatured (inactive) protein; P is "protected" active protein which can be reversibly reconverted into the native form; α is an intermediate inactive form, reversibly converted into the native form.

These schemes must now be revised; corrections must be introduced into them because, as has been shown, denaturing factors can induce two processes with opposite results — denaturation and stabilization. In particular, Scheme I (to which Scheme III is similar), the purpose of which is to account for deviations of the course of denaturation from the first-order equation, becomes superfluous, as such deviations (retardation of the reaction) in fact occur because of the increased resistance of the protein in solution. The views advanced here are based on our discovery of the effect in which denaturation stops under certain conditions before reaching completion, so that the system contains denatured and native stabilized molecules. The question of the "heat stabilization" of proteins could probably be solved by subjecting a protein to prolonged heating at relatively moderate temperatures, when denaturation is not intensive. There is every reason to believe that with "gentle" heating the stability of the macromolecular protein structure would increase. Such experiments are more complicated than would seem at first sight; they are probably very lengthy. Moreover, the changes in such cases may prove of low stability, and stabilized protein would be difficult to isolate. However, this approach is attractive in the sense that clear proof of denaturation stabilization at moderate temperatures (30-40°) would extend the potentialities for interpreting this effect in the general biological aspects. Still, it may be claimed that even the results obtained so far are of general biological interest.

The character of the denaturation stabilization of protein resulting from the action of a denaturing factor can be considered in the light of the following results of earlier investigations [1-3, 12]: 1) the molecules of the modified protein form retain their fundamental type of structure; 2) the molecules undergo partial structural

changes, which distinguish the protein from the original material*. These results indicate that denaturation stabilization depends on definite changes in the macromolecular structure of the original substance, causing high stability of the native modified molecules.

The mechanism of this change of molecular structure can be represented as follows. Some of the weak bonds in the globule are broken by the action of a denaturing agent such as urea, but in such a manner as to retain the main type of chain packing characteristic of native protein. The liberated structural elements may recombine; but under denaturation conditions, in solutions of urea, etc., the formation of new bonds is difficult. Nevertheless, they can form, and the possibility is not excluded that the process requires more time. If so, stabilization would be a slower process than denaturation. The new bonds arising within the limits of the native type of chain packing should have higher stability; the stronger the denaturing action — urea concentration, temperature, etc. — the higher the stability should be. If a new bond could be formed under more "difficult" conditions, the affinity between the structural elements which it joins must be high, and the bond formed is more stable. For example, it is possible that new "local" spatial conditions favoring the formation of stronger bonds arise for individual structural elements when some of the bonds are disrupted. In all cases the modified bond network which results cements the molecules more strongly, conferring increased stability on them. Prolonged treatment (with urea or other denaturing agents) probably causes greater changes in the macromolecular structure. Denaturation then requires stronger influences than those which caused stabilization.

It may be supposed that all the protein molecules become more labile on addition of the denaturing agent to the solution. This creates possibilities for denaturative rearrangement and for stabilization of the native macrostructure. Some of the molecules then undergo abrupt denaturative changes while the rest probably undergo gradual (and slower) stabilization.

Investigation of the properties of the stabilized form of egg albumin [3] shows that modification leads to a peculiar state of the native globular protein, characterized by a number of structural differences, with a modified bond network but with the fundamental native type of molecular structure retained. It is now possible to isolate and study this form of protein. This would provide new information on the nature of its macromolecular structure, its reactivity, and its properties. The method of "strengthening" the native structure by the action of a denaturing agent is itself new and somewhat unexpected. The more customary concept is that the denaturing factor leads to breakdown of the native form of chain packing in the protein particles. Denaturation stabilization is also a special type of stabilization of the native state of globular protein, involving considerable changes in its structure. In other types of stabilization — by dehydration, action of polyhydric alcohols and carbohydrates, variations of pH, etc. — such changes do not occur.

We consider that the effect described is a very widespread and important type of protein modification. There is no doubt that modifications of this sort, which can probably be effected with minimum denaturation of the protein, open up extensive research possibilities. It seems likely that stabilizing structural changes often occur in nature in proteins under normal conditions, without special influences, at moderate temperatures, during prolonged storage, etc. The possible practical significance of this effect should also be noted. A method for the preparation of globular proteins, including biologically active proteins, in a stable form resistant to denaturation is very attractive.

SUMMARY

1. The molecular weight (determined from osmotic pressure) of egg albumin stabilized by the action of a denaturing agent does not differ from the molecular weight of the original ordinary albumin. This refutes the hypothesis whereby this "denaturation stabilization" is attributed to complex formation between native and denatured protein in the system.

2. The denaturation rate is not affected by introduction of protein decomposition products (formed by prolonged treatment with urea) into the system egg albumin — urea before the start of the reaction. This leads to rejection of the hypothesis that stabilization of the protein molecules (retardation and arrest of the denaturation process) is caused by interaction of the protein with decomposition products gradually formed by the action of urea.

*Experimental data confirming both these results are examined and summarized elsewhere [13].

3. A theory is put forward concerning the nature of this "denaturation stabilization" of globular proteins, according to which native protein molecules in solutions of denaturing agents form modified networks of hydrogen and other bonds of higher stability, formed under unfavorable conditions. These bonds cement the globules more strongly while the native type of macrostructure is retained.

Institute of Biochemistry
Academy of Sciences, Ukrainian SSR Kiev

Received June 14, 1957

LITERATURE CITED

- [1] A. S. Tsyperovich, Ukrain. Biochem. J. 24, 1, 26 (1952).
- [2] A. S. Tsyperovich, Biochemistry 21, 2, 203 (1956).
- [3] A. S. Tsyperovich and A. L. Loseva, Biochemistry, 21, 5, 546 (1956).
- [4] V. A. Belitser and E. L. Khodorova, Ukrain. Biochem. J. 22, 265 (1950).
- [5] W. M. Bayliss and E. H. Starling, J. Physiol. 30, 61 (1903); J. H. Northrop, J. Gen. Physiol. 4, 227, 245, 261 (1922).
- [6] A. S. Tsyperovich, Ukrain. Biochem. J. 29, 1 (1957).
- [7] M. Chick and C. Martin, J. Physiol. 43, 1 (1911); M. Chick and C. Martin, J. Physiol. 45, 61, 261 (1912); M. A. Lauffer, J. Amer. Chem. Soc. 65, 1793 (1943); J. H. Northrop, M. Kunitz, and R. M. Herriot, Crystalline Enzymes (IL, Moscow, 1950) [Russian translation].
- [8] A. S. Tsyperovich, Ukrain. Biochem. J. 21, 44 (1949).
- [9] G. G. Wright and V. Schomaker, J. Amer. Chem. Soc. 70, 356 (1948).
- [10] H. P. Lundgren and J. M. Williams, J. Physical Chem. 43, 989 (1939).
- [11] A. M. Chase, J. Gen. Physiol. 33, 535 (1950).
- [12] A. S. Tsyperovich, Dissertation: Study of the Denaturation and Stabilization of Globular Proteins (Kiev, Academy of Sciences, Ukrainian SSR, 1953). [In Russian]
- [13] A. S. Tsyperovich, Progr. Chem. 25, 9, 1173 (1956).

ESTIMATION OF THE AGGREGATIVE STABILITY OF SUSPENSIONS

L. I. Edel'man and D. S. Sominskiĭ

The production of stable disperse systems, including suspensions, is of great scientific and practical importance.

Aggregative stability of suspensions is especially important in sedimentometric analysis for determination of granulometric composition. It is known that correct choice of the dispersion medium, and also of surface-active stabilizers in certain cases, is decisive in determinations of true particle-size distribution.

There are several methods available for evaluation of suspension stability: investigation of sedimentation rates [1, 2], determination of complete particle-size distribution curves [1, 3], studies of the formation rate and volume of sediments [4, 5], investigations of the structural and mechanical properties of the systems [6], etc. However, these methods all require considerable time and do not always give conclusive results.

In the present investigation the optical density (D) of dilute suspensions was taken as the measure of aggregative stability of the particles. This quantity, determined photometrically, is found with the aid of the Lambert - Beer law

$$I = I_0 e^{-kcl},$$

which connects the intensity of the incident (I_0) and transmitted light (I) with the thickness of the suspension layer (l) and its concentration (c). The extinction coefficient k in the equation is the sum of the absorption and scattering coefficients. The optical density of the system (D) is then found as the negative logarithm of the I/I_0 ratio, known as the transmission coefficient, and is therefore determined by the value of kcl .

The Lambert - Beer law is valid only for dilute systems, if the particle size of the disperse phase remains constant; moreover, optical density measurements are only suitable either for sols with particles $< 0.15\mu$, or for suspensions and emulsions with particles $> 1\mu$.

We studied dilute suspensions of polydisperse mineral powders: limestone, quartz, talc, cement, sulfur, and others, with particles $> 1\mu$. A check of the applicability of the Lambert - Beer law to these suspensions showed that if the particle sizes remain unchanged the optical density over a definite region is directly proportional to the weight concentration of the system*, while if the latter is constant the optical density is directly dependent on the particle concentration: it increases regularly with increase of the specific surface of the powder (Fig. 1). Change of the dispersion medium or introduction of various surface-active additives, leading to peptization or particle aggregation, i. e. to changes in the number of particles in unit volume, influences D , so that the optical density can be used as a measure of stability of the system (at constant c and l).

Highly disperse powders should be used for evaluation of the role of the dispersion medium and surface-active additives in the aggregative stability of suspensions from determinations of optical activity. There are several reasons for this: 1) the method is more sensitive with highly disperse suspensions, as such systems have the lowest aggregative stability. The use of highly disperse powders is all the more necessary since in measurements

*At the low suspension concentrations permissible in photometric work, variations of the weight content of the solid phase do not influence stability.

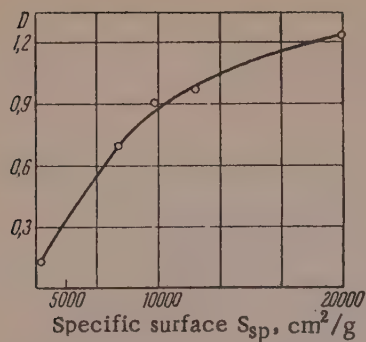


Fig. 1. Variation of optical density (D) of 0.05% aqueous quartz suspensions with dispersity (S_{sp}).

of D by the photometric method very dilute systems must be used, with concentrations of the order of 0.04-0.05%; 2) if highly disperse powders are used, rapid sedimentation of the particles in the measuring cell of the photometer is avoided, so that D is determined more accurately.

For the optical density determinations a suspension of the material was prepared of analytically accurate concentration by weight (a weighed sample being rubbed with the dispersion medium in a porcelain basin by means of a rubber-tipped rod), and the suspension was agitated thoroughly by a stirrer; the sample for determination was withdrawn immediately after the stirring. A Russian-made FMS horizontal photometer was used for determinations of D . Studies of the spectral characteristics of suspensions of the materials used showed that D can be

determined with adequate accuracy with the aid of a green light filter; $\lambda = 533 \text{ m}\mu$.

The accuracy to which the optical density can be measured directly by means of the photometer is quite high, $\pm 3\%$. Therefore for reproducible results special attention should be devoted to careful and standardized preparation of the suspensions.

TABLE 1

Optical Densities (D) of 0.05% Suspensions of Certain Materials in Various Media

Material	S_{sp}^* in cm ² /g	Dispersion medium				
		water	ethyl alcohol	ligroine	toluene	chloro-benzene
Limestone	14000	0.61	1.05	0.55	0.45	0.28
Cement	7200	—	—	0.32	0.14	0.22
Granulated slag	8500	0.46	0.64	0.35	0.20	0.19
Iron ochre	9200	1.08	0.87	0.46	0.51	0.40
Titanium dioxide	9000	1.25	0.36	0.42	0.50	0.56

* Specific surface was determined from the air permeability of a layer of compacted powder (the Kozeny - Carman method, see [7]).

For selection of a dispersion medium giving the highest particle stability for a given material, suspensions of thoroughly dried powders were made in equal concentrations, and the one which gave the suspension of the highest optical density was chosen as the best. It must be pointed out, however, that this method for selecting dispersion media is valid only with systems in which the refractive index difference between the solid and liquid phases is fairly high. Suitable dispersion media were found for sedimentometric analysis of the following fine powders: cement, limestone, granulated blast-furnace slag, iron ochre, and titanium dioxide (Table 1).

It follows from Table 1 that water is the best medium for ochre and titanium dioxide, giving the best stability; ethyl alcohol is the best medium for limestone and granulated slag. In the case of cement sedimentometric analysis is possible only in anhydrous liquid hydrocarbons, the best being ligroine.

It must be pointed out, however, that the maximum optical density of a powder suspension in a particular dispersion medium (for example, TiO_2 in water) does not always mean that the particles in the system are completely disaggregated. Therefore by the optimum dispersion medium in this case we mean relatively the best medium of those studied.

TABLE 2

Granulometric Composition of Limestone in Various Dispersion Media $S_{sp} = 10,000 \text{ cm}^2/\text{g}$

Dispersion medium	D	Contents of fractions (%) of radius ranges in μ				
		< 2 μ	2-5 μ	5-10 μ	10-20 μ	20-30 μ
Ethyl alcohol	1.05	35	24	17	17	7
Water	0.61	10	30	35	18	7
Ligroine	0.55	8	30	32	22	8
Chlorobenzene	0.28	—	41	25	19	15

The choice of the optimum dispersion medium, based on the highest optical densities of the suspensions, was checked by the results of determinations of the granulometric composition of the powders.

As an example, Table 2 contains the granulometric composition of thoroughly dried limestone, determined by sedimentometric analysis with the aid of the Figurowskii microbalance [5], in the optimum medium and in other media. For comparison, the optical densities of 0.05% suspensions are given in the same table.

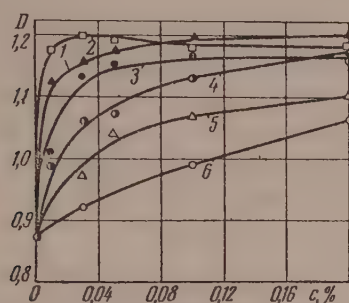


Fig. 2. Variation of optical density (D) of 0.04% aqueous suspensions of talc with stabilizer concentration:

1) tannin; 2) OP-10; 3) OP-7; 4) sulfated alcohols; 5) Nacconol; 6) Daxad.

It follows from the data in Table 2 that the highest content of fine fractions is found in the dispersion medium which gives the maximum optical density (ethyl alcohol). Moreover, changes in the optical density of limestone suspensions resulting from the use of other media are accompanied by changes of the experimentally observed granulometric composition: as D decreases, the content of the finer fractions diminishes as the result of an increase of the intermediate and coarse fractions, owing to particle aggregation.

As already stated, mere selection of a dispersion medium, even for low solid-phase concentrations, does not always ensure the formation of a stable suspension. In such cases organic surface-active agents or electrolytes must be added as stabilizers.

The comparative effectiveness of surface-active additives was also studied by determination of the optical densities of the suspensions. The method consisted of determinations of the optical densities of suspensions with various amounts of surface-active agents added to their dispersion media. The amount of stabilizer which gave the maximum D was taken as the optimum concentration. If the stabilizer itself gave an optically turbid system, not the pure solvent but a solution of the additive of the appropriate concentration was put into the second photometer cell.

Figs. 2 and 3 contain optical density - stabilizer concentration curves for 0.04% aqueous suspensions of talc (Onotsk origin) and sulfur (rhombic) in presence of various stabilizers. First, it should be noted that these curves are analogous to isotherms for stabilization of suspensions by surface-active agents, found by other methods for determination of the stability of disperse systems, such as the sedimentation rate [1]. These curves can easily be used to find the optimum amount of additive at which the adsorption layer becomes saturated.

The optical-density data (Fig. 2) show that of the additives studied the following are the most active for talc: tannin, and the wetting agents OP-7 and especially OP-10 (polyethylene glycol ethers of mono-octyl phenol).

The activity of OP-10 is regularly higher than that of OP-7; in presence of OP-10 in the suspensions the highest stability of the talc particles is reached at $c = 0.03\%$, whereas in the case of OP-7 maximum particle disaggregation is not attained even at $c = 0.1\%$ (this was confirmed by examination of a drop of the suspension under the microscope).

TABLE 3

Effect of Concentration of OP-7 Stabilizer on the Granulometric Composition of the Disperse Phase in a Talc - Water Suspension (S_{sp} of Talc = $12,000 \text{ cm}^2/\text{g}$)

Stabilizer concentration, %	Contents of fractions (%) of radius ranges in μ					D
	< 2 μ	2-5 μ	5-10 μ	10-20 μ	20-30 μ	
0	27	15	15	22	21	0.86
0.02	36	17	20	17	10	1.09
0.05	46	12	14	17	11	1.15
0.1	46	15	13	16	10	1.16

With additions of sulfated alcohols (sulfate esters) the maximum stability of the system is reached only at concentrations of the order of 0.2-0.3%. Additions of Nacconol F (alkyl aryl sulfonate) and the American wetting agent Daxad (of the Leukanol type) are even less active: even at considerable concentrations they only partially disaggregate the talc particles and do not stabilize the system completely.

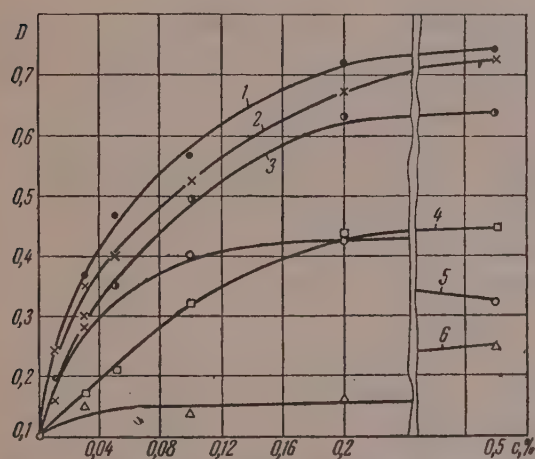


Fig. 3. Variation of optical density (D) of 0.04% aqueous suspensions of sulfur with stabilizer concentration:

1) SSB; 2) OP-10; 3) OP-7; 4) Daxad; 5) sulfated alcohols; 6) RAS.

OP-7 wetting agent, the American products Darvan and Daxad, and the anion-active wetting agent RAS (refined alkyl aryl sulfonate) - are not effective stabilizers for sulfur suspensions.

To test the accuracy to which variations of the optical density of suspensions reflect variations of the aggregative stability of the particles, the granulometric composition of the disperse phase was studied in presence of different amounts of OP-7 stabilizer (in the case of talc powder in water).

The dispersity was determined by the sedimentometric method with the aid of Figurowskii's microbalance. The results are given in Table 3, which also contains optical densities of 0.04% talc suspensions.

Comparison of the data in Table 3 with Curve 3 of Fig. 2 shows that optical-density variations give a quite reliable indication of the disaggregation of the talc particles, which is reflected in the granulometric composition found. For example, addition of 0.02% of OP-7 to the suspension appreciably increases the amount of fine fractions present, with a considerable increase of D (by 20%). If 0.1% of OP-7 is used instead of 0.05%, the granulo-

Sulfur powders are highly hydrophobic and are badly wetted by water. The optical density of sulfur suspensions is therefore extremely low. Hydrophilizing additives should therefore increase sharply the suspension stability and the optical density of the system. Since sulfur is more hydrophobic than talc, stabilizers should have a greater effect on sulfur suspensions, i. e., changes of D should also be more pronounced in sulfur suspensions.

In fact, the course of the stabilization curves for 0.04% sulfur suspensions (Fig. 3) shows that the optical density of the system increases 6 to 7-fold on addition of stabilizers, whereas in the case of talc suspensions roughly 1.3-fold changes of D are characteristic.

Of the surface-active agents studied, the best stabilizers for sulfur particles are calcium lignosulfonates (sulfite liquor, SSB) and the nonionic wetting agent OP-10. Microscopic examination of dilute sulfur suspensions stabilized by means of sulfite liquor showed their particles to be almost completely disaggregated. The other additives - sulfated alcohols,

metric composition of the talc particles remains virtually the same (Table 3), and so does the optical density.

These determinations confirm that the optical-density method can be used for estimation of suspension stability. This method differs advantageously from others by its simplicity and, in particular, by the rapidity with which the results are obtained; it provides a relatively rapid answer to the problem of the choice of the most suitable surface-active stabilizer and its optimum concentration for a given suspension, and is an aid in the choice of the dispersion medium which gives the most stable disperse system.

The effectiveness of different coagulants can also be compared by investigations of the optical properties of suspensions.

It should be noted, however, that variations of the optical density of suspensions most often result only from the so-called compact coagulation, i. e., coagulation leading to particle aggregation with changes of the particle concentration. If coagulation results in the formation of a spatial structural network in the system, additions of certain amounts of coagulants may reinforce the volume structure without change in the optical density of the system.

SUMMARY

1. A method has been developed for estimation of the stability of suspensions by measurements of their optical density.
2. Dispersion media have been found for fine powders of limestone, granulated slag, iron ocher, and cement, ensuring the highest particle stability in suspension.
3. Surface-active stabilizers for aqueous suspensions of talc and sulfur have been found.
4. It is shown that the most effective stabilizer for talc suspensions is wetting agent OP-10 at 0.03% concentration, and for sulfur suspensions, calcium lignosulfonates (sulfite liquor) at concentrations of the order of 0.3-0.5%.

All-Union Scientific Research Institute for New Problems
in the Production of Finely Ground Constructional Materials

Received March 12, 1957

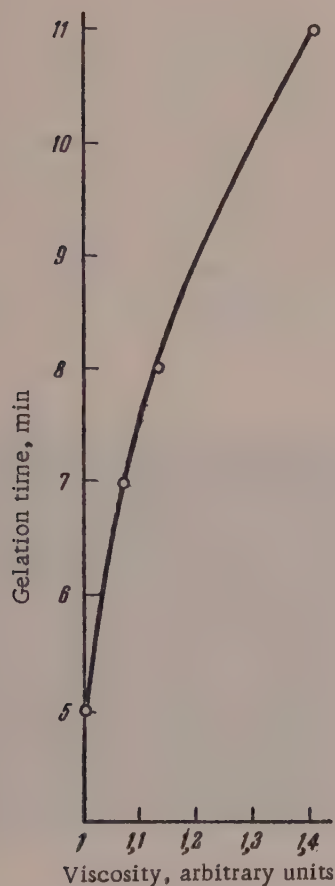
LITERATURE CITED

- [1] P. A. Rebinder (editor), Studies of the Physical Chemistry of Technical Suspensions (1933). [In Russian]
- [2] A. H. M. Andreasen, Staub 43, 5 (1956).
- [3] N. A. Figurovskii, Sedimentometric Analysis (1948). [In Russian]
- [4] L. W. Ryan, W. D. Harkins, and D. M. Gans, Ind. Eng. Chem. 24, 1288 (1932).
- [5] P. A. Rebinder, Bull. Acad. Sci. USSR, Chem. Ser. 5, 536 (1936).
- [6] L. I. Edel'man and P. A. Rebinder, Colloid J. 13, 1 (1951).
- [7] D. S. Sominskii and G. S. Khodakov, Inform. Communications of the All-Union Sci. Res. Inst. for New Problems in the Production of Finely Ground Constructional Materials, 21 (1956).

LETTERS TO THE EDITOR

EFFECT OF THE VISCOSITY OF RUBBER LATEX ON THE GELATION RATE

D. M. Sandomirskii and M. K. Vdovchenkova



Effect of latex viscosity on gelation time.

When suspensions of sodium fluosilicate or zinc oxide and solutions of ammonium salts are added to latex, gelation takes place owing to slow formation of cations which destabilize the globules [1, 2]. It is possible that among other factors (amounts of gelating agents added, latex concentration, temperature, etc.) the gelation rate is also influenced by the viscosity of the medium, as the destabilizing anions formed on the surface of the suspended particles must diffuse into the latex before they reach the globules and interact with their protective coatings. Since no data on this question are available in the literature, we performed gelation experiments with polychloroprene latex of initial concentration 52.3%, diluted to 41.8% concentration by aqueous glycerol mixtures of various compositions. This gave mixtures the viscosity of which varied from 1 to 1.4 (in arbitrary units). The gelation was effected at room temperature by additions of zinc oxide paste and ammonia and ammonium chloride solutions to the latex.

The results shown in the graph, although qualitative, clearly demonstrate the significance of diffusion processes in the gelation of latex. It appears that addition of glycerol destabilizes the latex to some extent, and the retarding effect of viscosity diminishes with increase of glycerol content.

Scientific Research Institute Received May 22, 1958
for Rubber and Latex Products

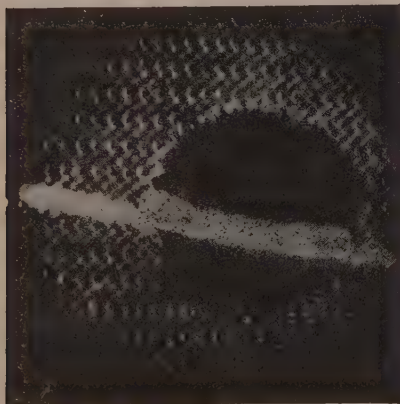
LITERATURE CITED

- [1] E. W. Madge and D. W. Pounder, *Tr. IRI* 23, 94 (1947).
- [2] S. S. Voyutskii, R. M. Panich, and K. A. Kal'yanova, *Colloid J.* 12, 50 (1950); 13, 89 (1951).

METHOD FOR PRECIPITATION OF AEROSOLS IN A THERMAL PRECIPITATOR FOR ELECTRON MICROSCOPY

N. A. Fuks and S. S. Yankovskii

It is known that the main difficulty in electron microscope investigations of aerosols is in the preparation of an aerosol precipitate which can be used for exact determinations of the number of particles in 1 cc of aerosol and of the particle-size distribution. Generally electrical or thermal precipitators are used for this purpose; in either case, because of the high electrical or thermal conductivity of the metal gauze as compared with the supporting organic film, the particles settle predominantly on the gauze wire and cannot be photographed under the electron microscope. This leads to considerable errors in counts of the settled particles. This effect is even more prominent with the use of metallic diaphragms with narrow orifices [1]. Moreover, our observations of thermal precipitation show that in certain cases the tendency to settle on the wires is somewhat more pronounced in large particles and aggregates than in fine particles, and this may lead to errors in determinations of the particle-size distribution of aerosols. The method proposed by Cartwright [2] — precipitation of aerosols on cover glasses coated with Formvar, and stripping of the latter — is very laborious and has a number of disadvantages.



We use the following method, free from the above-mentioned faults, for thermal precipitation. A circle of diameter equal to the diameter of the cylindrical thermal precipitator inserts, and with a round orifice 2.2 mm in diameter in the center, is cut from copper gauze of 180-200 mesh. The circle is straightened and flattened somewhat by pressing at 150 kg/cm², a collodion film is applied onto it by the usual method, and it is then placed on the insert end and put in the thermal precipitator. The heating is effected by a steel strip 0.1 × 1.0 mm in section (precipitators with wires are unsuitable, as in them the film bursts owing to uneven heating). Precipitation of the aerosol may be regarded as complete if the width of the band of precipitate is less than the width of the strip. The illustration shows a photograph of a

precipitate of ZnO smoke obtained by this method under the following conditions: distance between strip and film 0.15 mm, width of the open section of the strip 8 mm, heating current 1.8 amp, suction rate of aerosol 8 cc/minute; width of band 0.3 mm.

If required, the precipitate may be examined under the optical microscope, and it is then mounted for electron microscopy. For this, a circle of copper gauze (pressed as described above) 2 mm in diameter is placed on the object glass, and covered by the circle with the precipitate in such a way that the smaller circle is within the film-coated 2.2 mm orifice in the large circle. The film is then cut around the periphery of the orifice with a sharp needle, when the film with the precipitate drops onto the smaller circle; this is inserted in the chamber of the electron microscope, and then examined in the usual way. Failures with this procedure are very rare.

LITERATURE CITED

- [1] G. Zebel, Staub 39, 21 (1955).
- [2] J. Cartwright, Brit. J. Appl. Phys. Suppl. 3, 109 (1954).

BOOK REVIEW

TABLES OF LIGHT SCATTERING FUNCTIONS FOR SPHERICAL PARTICLES,
DETROIT 2, MICHIGAN, 1957, 162 pp., \$5.50

William J. Pangonis, Wilfried Heller, and Arvid Jacobson

Exact formulas of the electromagnetic theory of light diffraction by spherical particles were used for calculation, by means of electronic computers, of partial-wave amplitudes for spheres with relative refractive index \underline{m} in the 1.05-1.30 range. This includes relative refractive indices in the visible region for a number of solids and liquids in liquids (suspensions and emulsions), ice in air, etc. The tables give, to six decimal places, the real and imaginary components of the amplitudes of the electrical and magnetic partial waves for the following combinations of \underline{m} and ρ ($\rho = 2\pi a/\lambda$; a is the radius of the sphere; λ is the wave length).

TABLE 1

\underline{m}	ρ
1,05	0,2 (0,2) 7,0; 7,0 (1) 15; 22 (2) 28; 39 (1) 41
1,10	0,2 (0,2) 7,0; 7,0 (1) 21
1,15	0,2 (0,2) 7,0; 7,0 (1) 15
1,20	0,2 (0,2) 15,2
1,25	0,2 (0,2) 7,0; 7,0 (1) 15
1,30	0,2 (0,2) 7,0; 7,0 (1) 15

The usual presentation is used in Table 1 — the increments of ρ used for a particular range are given in parentheses.

In addition to partial-wave amplitudes, the tables give the relative scattering coefficient K_s for the same values of ρ and \underline{m} . The relationship between this coefficient and the "turbidity" (scattering coefficient of unit volume) is represented by the formula $\tau = \pi a^2 K_s N$. Here N is the number of particles per unit volume. In materials of considerable \underline{m} weakening of the light beam is due only to scattering (there is no absorption). Therefore the values of K_s and τ given in the tables also give a measure of weakening.

The principal data in the tables — amplitudes — are necessary for calculation of scattering indicatrices. Such calculations may be performed with the aid of tables for angular functions. These functions are expressed in terms of associated Legendre polynomials, detailed tables of which are available (Mathematical Tables Project, N. Y., 1945). Calculated tables of angular functions have been published recently. In particular, they were calculated by us and given in the book "Light Scattering in Turbid Media" (GTTI, 1951). However, it is true that calculations of intensity even from available amplitudes are extremely tedious, especially for large ρ .

The new tables form a substantial contribution to colloid optics. They supplement earlier tables published by the Bureau of Standards, which cover values of \underline{m} in the 1.33-2.00 range, and also the tables of Gumprecht and Sliepcevich. It is therefore now possible to calculate scattering for \underline{m} between 1 and 2. The value $\underline{m} = 1.20$, considered in the new tables, was also considered previously in the Gumprecht — Sliepcevich tables.

TABLE 2

Case	New tables	Gumprecht-Sliepcevich tables	Δ
$\rho=6; n=1$ Re (Bn)	-0,448656	-0,448596	60
$\rho=8; n=5$ J (Bn)	0,322014	0,321983	31
$\rho=8; n=8$ Re (Bn)	0,045921	0,045882	39
$\rho=10; n=1$ Re (Bn)	0,462686	0,462644	42
$\rho=15; n=1$ Re (Bn)	0,351772	0,351468	304

Our comparison for the 9 corresponding values of ρ showed that in most cases the difference between the amplitudes given does not exceed one unit in the last figure.

Unfortunately, there are also some instances of considerable discrepancies. Some of these are given in Table 2.

The last column gives the differences between the new and old tables, in units of the sixth decimal place.

These discrepancies are not even mentioned in the new tables. The reader can therefore only guess which of the amplitudes is correct. It is true that for applications of the theory these discrepancies are not significant, as they are beyond the limits of experimental accuracy.

The small increments of ρ ($\Delta \rho = 0.2$) used in the new tables (for $\rho \leq 7$) allows of study of a number of fine scattering characteristics which could not be investigated with the earlier tables. This is the great merit of the valuable compilation made by the three American authors.

K. S. Shifrin

ON THE SEVENTIETH BIRTHDAY OF
IVAN NIKOLAEVICH ANTIPOV-KARATAEV



The past year (1958) marked the 70th birthday and the completion of 35 years of scientific and social activity of one of the most eminent of Soviet colloid and soil scientists, distinguished scientific worker and full member of the Academy of Sciences Tadzhik SSR, Professor Ivan Nikolaevich Antipov-Karataev.

Born in the Sterlitamak district of the former Ufa province, he began his working life as a country teacher. In 1926 he graduated in pedology and agricultural chemistry at the Moscow University, and since that time he has worked in the Soil Institute of the Academy of Sciences USSR as head of the Laboratory of the Physical Chemistry of Soils and Soil Colloids. During this time he has published more than 270 papers on various aspects of soil science and agricultural and colloid chemistry. His work in the field of physics and chemistry of soil colloids has proved particularly fruitful. Together with his associates he has carried out a considerable number of observations and researches in this field, the scientific significance of which has been acknowledged both in the Russian and in foreign literature. The results of these researches were summarized in his monograph: "Soil Colloids and Methods for Their Investigation," and in numerous articles and notes published by him in the chemical and agricultural-chemical literature. He is a good experimentalist; jointly with others he has developed methods for electrolysis and electrodialysis of soils, and has devised original techniques for studying the sorption of vapors and gases by soils; he has provided a theoretical basis for methods of determination of bound water; he has made a thorough study of peptization and coagulation of soil colloids; revealed the factors determining charge reversal in soils; studied the role of the specific surface of soils and methods for its determination, etc. The most important of these methods were published in the monograph: "Modern Methods for Investigation of the Physicochemical Properties of Soils."

Broad application of the principles of colloid chemistry to soil research enabled him to carry out a number of original investigations into the nature of soil aggregates. Apart from their theoretical interest, these investi-

gations are of great practical importance, since they not only reveal the mechanism of structure formation in soils, but provide the basis for the design of agriculturally valuable soil structures.

Questions relating to the theory and applications of ion exchange occupy a prominent position in his work. These questions are closely associated with the problem of the sorptional capacity of soils and ion-exchange equilibria. Antipov-Karataev and his associates have carried out a considerable number of investigations in this field, and were the first to determine the basic criteria for ion-exchange equilibria in soils and clays and to establish the relationship between these criteria and the soil properties and nature of the ions. He was one of the first to detect the so-called hysteresis of exchange adsorption, and offered a correct explanation for the effects concerned; he devised the most successful technique for studying ion-exchange adsorption under dynamic conditions. This technique was used for studying the mechanism of exchange adsorption of anions on soils and clays, and for determination of the quantitative relationships governing the exchange of ions of different valences. On the basis of these researches, methods were developed during the war years for extensive utilization of soils as ion-exchange sorbents suitable for use as natural means of defense against chemical warfare.

An original technique was developed under his guidance for isolation and analysis of soil solutions, and a technique of x-ray thermal investigation of soils and clay minerals, which is extensively used in laboratory practice.

His scientific interests are very extensive and varied. He made investigations, conducted over many years, on amelioration of solonetz soils. These investigations are widely known not only in the Soviet Union, but also abroad. They include theoretical studies of the problem of saline soil formation, questions of their origin and geographical distribution in the USSR, development of solonetz formation in the chernozem zone and in semidesert zones, methods for determination of soil salinization, and amelioration of solonetz soils under dry and irrigated conditions.

As the result of thorough and prolonged studies of the physicochemical properties of solonetz soils, he developed methods for their radical improvement, which are being increasingly applied in collective and state farms. These methods were approved by the Council of Ministers USSR and recommended for extensive trials and use in zones of chestnut and brown soils. The results of these researches were extensively announced in the special and periodical literature, and presented in the well-known monograph "Amelioration of Solonetz Soils in the USSR," which summarizes many years of work by Antipov-Karataev and his associates.

In addition to his work on colloid and agricultural chemistry, he conducted a number of fundamental researches into problems of soil geography; his work on the soils of the Nikitskii Gardens and the Taman' peninsula, and investigations of the soils of the Volga region, Ergeni, Tebertsy, the Vakhsh Valley, Eastern Pamir, Bulgaria, and other regions and provinces are widely known in the pedological literature. In recent years he has applied considerable efforts to organization and conduct of researches involving the use of stable and radioactive isotopes in pedology. The results of these researches were reported at the Geneva International Conference on the Peaceful Uses of Atomic Energy.

He always aims to correlate his theoretical and experimental investigations with applied problems of pedology and agriculture. With this aim in view he took active part in work on soil stabilization in the Kalmyk Steppes, Tadzhikistan, Kamennaya Steppe, and other regions of the arid south-east. He is also studying, with the same purpose, the forest growth conditions of Ergeni, where experimental work on artificial afforestation of steppes is being organized on a wide scale.

He devotes much effort and attention to training new ranks of specialist chemists. Several doctorate and candidate dissertation researches were carried out under his guidance.

Antipov-Karataev does much social work. He is a member of the Higher Certification Expert Commission, a member of the editorial boards of the journals *Pedology*, *Colloid Journal*, and *Popular Literature*, a member of the agriculture section of the Lenin All-Union Academy of Agricultural Sciences, a member of the Pedological Society, and a member of the Scientific Council of the Soil Institute, Academy of Sciences USSR.

His fruitful scientific activity has been repeatedly acknowledged by government departments: he has been awarded four Orders of the Red Banner of Labor and several medals.

I. P. Serdobol'skii

INVESTIGATION OF EXCHANGE REACTIONS IN SOILS WITH THE AID OF A CALCIUM ISOTOPE

I. N. Antipov-Karataev and G. M. Kader

The V. V. Dokuchaev Soil Institute, Acad. Sci. USSR, Moscow

The science of exchange adsorption of cations has a variety of applications in soil amelioration and in particular in irrigation, where the problem of the quality of the irrigation water is extremely important.

It is known that the quality of irrigation water must conform to certain requirements: 1) It must not contain toxic organic or inorganic substances; 2) its degree of mineralization by neutral salts must not exceed 1.5-2.0 g/liter [1]; 3) to avoid development of salinization effects in the irrigated soils as the result of exchange sorption of sodium ions from the irrigation water, the content of sodium salts must not exceed a definite proportion of the contents of salts of bivalent cations (in particular, calcium).

Whereas the first two problems may be regarded as more or less solved, there is still some uncertainty with regard to the third [2, 3]. Some workers consider that, regardless of the degree of mineralization of the irrigation water, a critical equivalent ratio of sodium salts to calcium (and magnesium) salts becomes established from a value of ≥ 0.6 . However, this value can hardly be regarded as generally accepted. In determinations of the critical value at least three questions must be considered: 1) what is the amount of exchange sodium (as % of the soil exchange capacity) at which the first (initial) stage of salinization appears; i.e., at which disaggregation of the soil and peptization of the clay fractions (and humus) begins; 2) what is the equivalent ratio of sodium ions (or other univalent cations) to calcium (or other bivalent cations) in the irrigation water, at which exchange sorption of sodium ions takes place in quantities which may be regarded as critical, i.e., causing initial stages of soil salinization; 3) what is the dependence of this quantity on the degree of total mineralization of the irrigation water and on the exchange capacity of the soil. The first of these questions was answered in two ways: a) by the plotting of dispersity curves for soils saturated with exchange sodium and calcium (or a mixture of calcium and magnesium) at different equivalent ratios, with parallel determinations of zeta potential (Fig. 1); b) by determination of the threshold of irreversible coagulation of a solonetz soil suspension by means of gypsum solution ($\text{CaSO}_4 \cdot 2\text{H}_2\text{O}$) with simultaneous determination of the residual exchange sodium in the soil (Fig. 2); see also [4]. On the basis of the most recent data we take the initial salinization stage of loam soils to occur in presence of exchange sodium in an amount equivalent to 10% of the exchange capacity.

It is first necessary to determine the cation-exchange capacity of the given soil. For this is required a universal method which can be used for determination of the exchange capacity of any soil (acid, neutral, carbonate, saline). The isotope method [5] solves this problem quite satisfactorily.

To solve the principal problem — determination of the ameliorative quality of irrigation (and leaching) water — it is necessary to study the competing proportions of sodium ions and bivalent ions (mainly calcium) in the solution (irrigation water) used for treatment of the soil until adsorption equilibrium is reached.

In a series of special investigations conducted in our laboratory under conditions of strictly equivalent and reversible cation exchange in soils, the exchange constants were determined and calculated by means of the mass-action law (Table 1).

The exchange constants given in Table 1 can be used to calculate the required competing proportions of sodium ions and bivalent cations in the given systems. However, in view of the fact that the processes taking

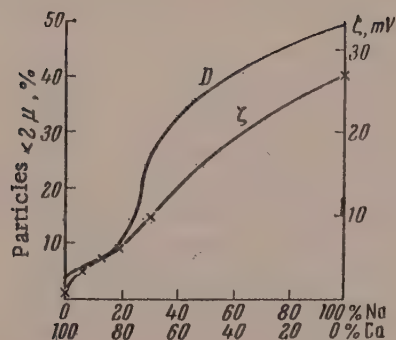


Fig. 1. Dispersivity curve for soil mass saturated with exchange sodium: D) dispersity; ζ) zeta potential.

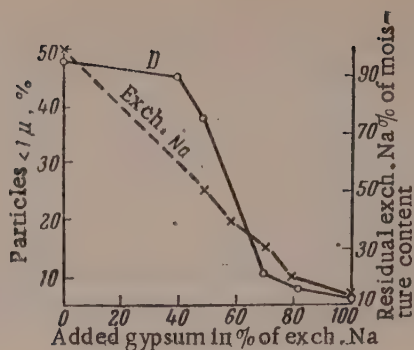


Fig. 2. Curve showing the threshold of irreversible coagulation of a solonetz soil suspension by means of gypsum solution: D) dispersity; exch. Na) residual exchange sodium in the soil.

place in competitive soil systems are sometimes complex, we recommend the use, in addition to the calculation method, of a direct experimental method which is based on our investigations of samples of chernozem soil of sorption capacity 58.15 meq/100 g, and a chestnut soil of sorption capacity 31 meq/100 g. A series of soil samples was treated with solutions of a mixture of calcium and sodium chlorides at concentrations of 1, 3, and 5 g per liter, and with different equivalent ratios of Ca^{2+} to Na^+ : 4:1, 3:2, 1:1, 2:3, 3:7 and 1:4.

The adsorbed sodium was determined by flame photometry after quantitative displacement by means of dilute HCl solution (in the case of the noncarbonate soil) or 60% ammonium chloride solution in alcohol (in the case of carbonate soils) [6]. The results of determinations of adsorbed sodium are given in Table 2.

It follows from Table 2 that the "critical" ("solonetz") content of exchange sodium depends on the degree of mineralization of the water and on the equivalent ratio of sodium to calcium ions in the solution. When the mineral content is 1 g of salts per liter of irrigation water, the "critical" ratio is shifted in the direction of higher amounts of sodium (to 75-80%); with 3 g of salts per liter, the "critical" value becomes established with 60% of sodium in the solution: when the mineralization is 5 g/liter with 50% of sodium in the solution, the soil salinity increases even more. This relationship can be represented by the linear equation:

$$x = \frac{[\text{Ca}]}{[\text{Na}]_{10}} = kc,$$

where x is the $[\text{Ca}]/[\text{Na}]$ ratio; k is the slope factor, 0.23; c is the mineral content of the solution in g/liter; the subscript 10 represents the critical $[\text{Ca}]/[\text{Na}]$ ratio at which the amount of adsorbed Na reaches 10% of the exchange capacity.

We thus propose to introduce substantial corrections into the existing standards for qualitative and quantitative evaluation of irrigation and leaching waters, based on data on the degree of mineralization of the water, and probably with the exchange capacity of the soil taken into account. The data in Table 2 suggest that the risk of solonetz formation developing under given conditions increases with decreasing cation-exchange capacity of the soil. However, further work on this is needed.

Instead of exchange sodium, exchange calcium can be determined in soil samples; this is easily done by tagging the solution (or water) by means of radioactive calcium isotope (Ca^{45}).

Table 3 contains comparative data obtained in experiments with mixed solutions of NaCl and CaCl_2 and chestnut soil.

On the basis of these results we recommend the following method for evaluation of the ameliorative quality of irrigation (and leaching) waters:

TABLE 1

Exchange Constants (K) of the Systems Studied

Samples*	Values of K in presence of salts			
	SrCl ₂	MgCl ₂	KCl	NaCl
Humus soil - Ca soil	0.8(3)*	2.04 - 2.70	4.55	15.41
Ca clay	—	1.30 - 1.37	2.85	—

* Yu. A. Polyakov's data; the remaining values of K were determined by I. N. Antipov-Karataev.

TABLE 2

Adsorbed Sodium, in Percentages of the Soil Exchange Capacities at Different Ratios of $[Ca^{2+}]$ to $[Na^+]$ in Solutions of Different Concentrations

Salt concentration, g/liter	Amount of adsorbed Na, in %, at $[Ca^{2+}]:[Na^+]$ ratios in solutions					
	4:1	3:2	1:1	2:3	3:7	1:4
Chernozem soil (noncarbonate)						
1	Traces	3.6	4.5	5.5	7.9	9.0
3	Traces	3.6	9.0	10.0	11.1	19.3
5	Traces	3.6	13.3	14.3	15.1	—
Carbonate chestnut soil						
3	7.7	—	18.3	—	28.0	—

1. A sample (from 10 to 50-100 g, according to the exchange capacity) of soil is treated in a funnel with the water under test, tagged with Ca^{45} isotope, until equilibrium is reached (as shown by the activity of the eluate).

2. The funnel with the soil sample is kept in a moist atmosphere (under a glass bell over water) and its weight is found, from which the amount of free solution of known calcium content held by the soil is calculated.

3. The exchange calcium is displaced and determined quantitatively by the isotope method. A correction is applied for the calcium content of the free solution held by the soil sample.

4. The exchange capacity of the soil is determined separately, by the isotope method.

5. The deficiency of exchange calcium as a percentage of the soil sorption capacity is found by difference. If this deficiency exceeds 50% of the exchange capacity, then the water used, containing over 2 g of salts per liter, requires improvement in the ameliorative sense.

6. A preliminary assessment of the water quality may be based on the results of direct analysis by means of the equation $[Ca]/[Na]_{10} = kc$.

SUMMARY

1. A method is proposed for amelioration assessment of irrigation (and leaching) waters, based on treatment of a soil sample with the solution (irrigation water) and subsequent determination of exchange sodium or exchange calcium. The latter can be readily effected if the solution (or water) is tagged with radioactive calcium isotope (Ca^{45}).

TABLE 3

Comparative Determinations of the Salinity of Soils Treated with Mixed $\text{CaCl}_2 + \text{NaCl}$ Solutions (total salt concentration 3 g/liter) by the Isotope Method (Ca^{45}), by Calcium Deficiency and by the Amount of Exchange Sodium

Ratio of $[\text{Ca}^{2+}]:[\text{Na}^+]$ in the original solution	Found in meq/100 g of soil		Salinity as % of soil exchange capacity*
	calcium defi- ciency by iso- tope method	exchange sodium	
4:1	2.28	2.08	7.7
1:1	5.04	5.21	18.3
3:7	9.10	8.56	28.0

* Soil exchange capacity in this experiment was 27 meq/100 g.

2. Calcium deficiency in a given soil (or, which is the same thing, "salinity" of the soil with respect to alkali cations) is found from the difference between the soil sorption capacity and the amount of exchange calcium found.

3. A relationship has been established experimentally between the critical value of exchange sodium (10% of the exchange capacity) and the total mineral content of the water (in g/liter), which can be used for preliminary qualitative assessment of waters.

LITERATURE CITED

- [1] I. N. Antipov-Karataev (editor), Amelioration of Solonetz Soils of the USSR [in Russian] (Izd. AN SSSR, 1953).
- [2] S. Arany, VI Congress International de la Sci. du Sol., Commissions IV et VI, (Paris, 1956).
- [3] D. W. Thorne and M. B. Peterson, Irrigated Soil (Philadelphia, Blakiston, 1949) p. 288.
- [4] L. Ya. Mamaeva, Trans. Soil Inst. Acad. USSR 51, 188 (1956); 51, 198 (1956).
- [5] S. G. Rydkii, F. G. Yanovskaya and K. B. Orlova, Pedology No. 7, 37 (1953).
- [6] P. Pfeffer, Z. Pflanzenernähr. Düng. Bodenkunde, B75, 17 (1956).

Received January 16, 1959

VISCOSITY OF ENAMELS FOR STEEL

K. P. Azarov and S. B. Grechanova

Enamels Laboratory, the S. Ordzhonikidze Polytechnic
Institute, Novocherkassk

Problems of boronless ground coats and borate single-coat enamels for steel and cast iron have been attracting the attention of investigators for many years. Both kinds of coatings are liable to blistering and holes, i.e., faults associated with gas evolution during firing of the coats. The main source of gases is known to be the carbon in steel, which becomes oxidized during the firing process. Since boronless ground coats and borate single-coat enamels blister on the same steel, whereas borate ground coats are free from this fault, the cause of blistering must be sought in the properties of the enamels. It is clear that degasification of the coating must depend on changes in the enamel viscosity owing to dissolution of the scale during firing. However, the very important question of the role of viscosity in formation of the coating has not been solved. The published viscosity data [1] generally apply to enamels free from iron oxide, and only three papers [2] are concerned with the influence of the latter. In all cases the investigations were performed at high temperatures, considerably above the temperatures at which the ground coats begin to form and blistering commences, and therefore they cannot form a basis for conclusions concerning the causes of these faults.

In the present investigation the viscosity in the softening region has been studied for the following industrial enamels used for coating steel: borate (b) No. 18, No. 124, No. 210; boron-free (b/f) No. 35*, No. 27*, No. 16; titanium (Ti) No. 121, 174; also ground coats, and single-coat (s/c) titanium borate enamel No. 189. On account of the interaction between the enamel melt and the oxidized steel surface, the viscosities of enamels fused with 5, 10, 15, and 20%, and in some cases with 2 and 25%, of ferric oxide were determined. The known fiber-elongation method was used for the viscosity measurements [3].

Figure 1 shows that the boron-free enamels have lower viscosities than the borate or titanium enamels. At constant temperature in the softening range, borate and titanium ground coats soften at a uniform rate, whereas retarded softening is characteristic for boron-free ground coats and single-coat titanium borate enamel (Fig. 2). This anomaly indicates that these enamels tend to crystallize, and in consequence the melt becomes a disperse system with plastic properties. This effect was first discovered by Volarovich [4] for blast-furnace slags containing titanium.

A sharp difference between borate ground coats on the one hand, and boron-free ground coats and borate single-coat enamel on the other, is also revealed on addition of ferric oxide. The viscosity isotherms (Fig. 3) show that borate ground coats are characterized by a viscosity decrease on addition of ferric oxide, whereas the viscosity is increased considerably in the case of boron-free ground coats. The viscosity of No. 189 s/c enamel decreases only with a small addition of ferric oxide (5%). Increase of ferric oxide content results in strong crystallization with a consequent sharp increase of enamel viscosity. Thus, even with 10% added ferric oxide, the viscosity could not be determined, as the fibers do not stretch. It should be noted that copper oxide, in contrast to ferric oxide, lowers the viscosity instead of raising it when added to No. 35 b/f and No. 189 s/c enamels (Fig. 4). Consistently with this, additional experiments on blistering of enamels in presence of a gas formed (graphite) showed that No. 35 b/f and No. 189 s/c enamels blister less with copper oxide than with ferric oxide (Fig. 5).

* V. P. Vaulin's compositions.

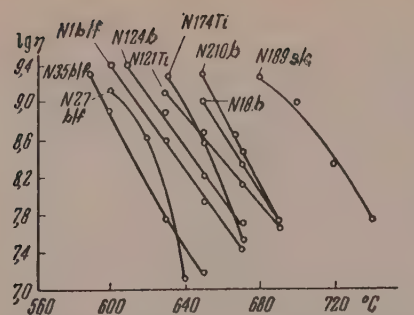


Fig. 1. Viscosities of enamels in the softening range.

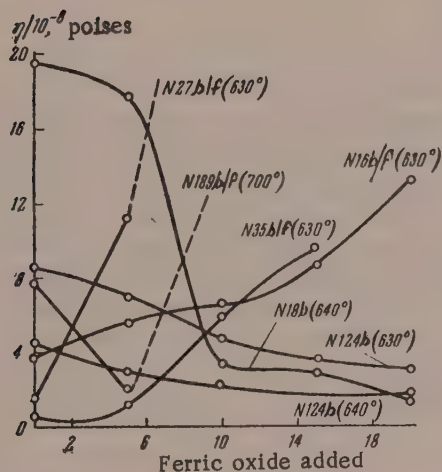


Fig. 3. Viscosity isotherms of borate and boron-free enamels fused with ferric oxide.

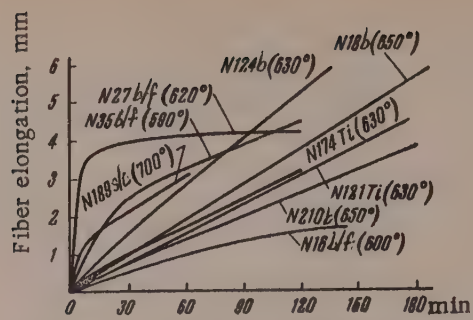


Fig. 2. Elongation rate during isothermal heating of enamels.

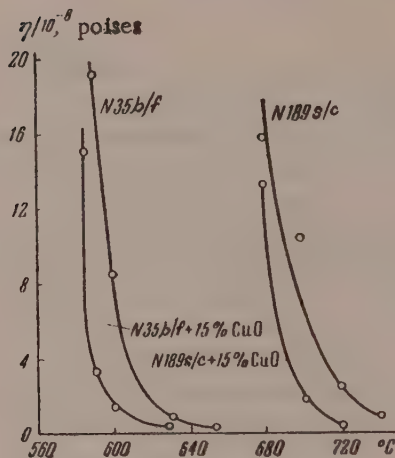


Fig. 4. Effect of copper oxide on the viscosity of No. 35 b/f and No. 189 s/c enamels.

The viscosity increase of boron-free ground coats in addition of ferric oxide may be due both to formation of FeO_4^{5-} and FeO_3^{3-} groups [5] and to crystallization of the melts. In boron-free enamels, which are more basic than borate enamels [6], the coordination number of iron is probably small, corresponding to the presence of FeO_4^{5-} and FeO_3^{3-} glass-forming groups, which strengthen the network and raise the viscosity. The sharp increase in the viscosity of No. 189 s/c enamel may be attributed to the fact that this enamel is supersaturated with crystalline formations (anatase, rutile, titanosilicates), and small additions of ferric oxide intensify crystallization.

At high temperatures iron acts as a modifier rather than as a glass former and therefore, as supplementary experiments showed, it lowers the viscosity of both borate and boron-free enamels. The increase in the solubility of ferric oxide with the temperature, demonstrated in other experiments*, in its turn diminishes the elasticoviscous properties.

In the light of these results the blistering of an enamel coating on steel may be described as follows. During the initial firing stages, ground coats and single-coat enamels come in contact with the oxidized steel surface. As the result of interaction between the coating and the scale, the viscosity of boron-free ground coats and titanium borate single-coat enamels rises sharply in the thin layers adjacent to the metal. The high viscosity of the bottom layer hinders the escape of gases formed as the result of oxidation of the carbon in steel. As a result, large blisters are formed in the coatings; these subsequently burst and leave holes. In normal borate coatings the viscosity in this thin layer decreases; this favors formation of small bubbles which can escape freely from the coating.

*Performed with the assistance of V. V. Balandina.

SUMMARY

1. High viscosity is not a characteristic feature of boron-free enamels. Under these conditions borate ground-coat enamels soften uniformly with increase of heating time, whereas the softening rate of boron-free ground coats and single-coat enamels slows down; this is evidence that boron-free and single-coat enamels have a tendency to crystallization.

2. At the softening temperature ferric oxide raises the viscosity of boron-free ground coats and single-coat borate enamels, and lowers the viscosity of borate ground coats.

3. Copper oxide lowers the viscosity of boron-free ground coats and single-coat borate enamels, and therefore these coatings do not blister on copper.

4. The blistering of enamels on steel is caused by a sharp increase in the viscosity of the coatings because of saturation with scale of the thin layer adjacent to the oxidized steel.

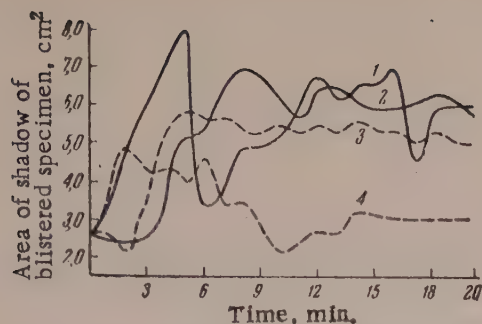


Fig. 5. Blistering, at 800°, of No. 189 s/c and No. 35 b/f enamels with additions of 15% ferric oxide + 2% graphite, and 15% copper oxide + 2% graphite: 1) No. 35 b/f + 15% Fe_2O_3 + 2% C, 2) No. 189 s/c + 15% Fe_2O_3 + 2% C, 3) No. 189 s/c + 15% CuO + 2% C, 4) No. 35 b/f + 15% CuO + 2% C.

LITERATURE CITED

- [1] W. N. Harrison, R. E. Stephens and S. M. Shelton, *J. Res. Nat. Bur. Standards* 20, 39, (1938); P. Bremond, *Bull. Soc. Franc. ceram.* April/June, 14 (1951); F. Hartmann, *Ber. Dtsch. keram. Ges.* 19, 268, (1938); J. Klarding, *Stahl und Eisen* 59, 268, (1939); B. D. Bruce and A. V. Sharon, *J. Amer. Ceram. Soc.* 32, 41, (1949).
- [2] T. B. Yce, J. S. W. Heimsoeth and F. R. Meyer, *Ibid.* 34, 366, (1951); Machin and A. J. Andrews, *J. Amer. Ceram. Soc.* 38, 378, (1955); A. Petzold, *Silikattechnik* 4, 391, 485, (1953); M. Tashiro, *J. Ceram. Assoc. Japan* 58, 51, (1950); *Ceram. Abstr.*, (February 1951), p. 23.
- [3] S. English, *J. Soc. Glass Technol.* 7, 25, (1928); H. R. Lillie, *J. Amer. Ceram. Soc.* 14, 502, (1931); 37, 111, (1954); A. S. Gorel'nik and K. S. Evstrop'ev, *Opticomechanical Ind.* No. 10, 10 (1937); M. V. Okhotin and R. I. Tsoi, *Glass and Ceramics* No. 18, 3 (1952); J. Pool, *J. Amer. Ceram. Soc.* 32, 215, (1949).
- [4] M. P. Volarovich, *J. Phys. Chem.* 4, 807 (1933).
- [5] H. Cole, *J. Soc. Glass Technol.* 35, 6T, (1951); W. Weyl, *J. Soc. Glass Technol.* 35, 448T, (1951); J. Stevels, *Verres et refractories* 4, 293, (1950); H. Moore and S. Prasad, *J. Soc. Glass Technol.* 33, 336T, (1949); 34, 173T, 193T, (1950); A. G. Dingwool and H. Moore, *J. Soc. Glass Technol.* 37, No. 179, 316T, (1953); Abd-El-Moneim Abou-El-Azm, *J. Soc. Glass Technol.* 38, No. 181, 101T, 146T, No. 182, 197T, 244T; 271T, (1954).
- [6] K. P. Azarov, *J. Appl. Chem.* 28, 33 (1954)*; K. P. Azarov, "Structure and properties of enamels," in the book: *Proceedings of Conference on the Structure of Glass* [in Russian] (Izd. AN SSSR, 1955) p. 276.*

Received July 3, 1957

*Original Russian pagination. See C.B. Translation.

THE STABILIZING ACTION OF SILVER IONS ON ALBUMIN

S. S. Vasil'ev and V. V. Yushina

The Technological Institute for Light Industries, Moscow

The interaction of protein molecules with heavy-metal ions has often been studied [1]. In particular, it is known that considerable concentrations of Ag^+ ions lead to complete coagulation of albumin. We were interested in the nature of the action of silver ions on protein solutions when each protein molecule adsorbs only a small number of these ions. For elucidation of this question, 1 N silver nitrate solution was added dropwise to a dialyzed and electro-dialyzed solution of crystalline egg albumin (prepared by Hammarsten's method). In control experiments an equal amount of silver nitrate was added to pure water of the same conductivity as the original protein solution. After addition of the silver nitrate the conductivities of the protein solution and the control solution were determined. The results are given in Fig. 1.

The adsorption can be calculated from the equation

$$n = \frac{cx}{V + x},$$

where V is the volume of protein solution, or of water in the control experiment, to which a volume x of silver nitrate solution of concentration c has been added. If any possible adsorption is disregarded, the silver concentration in the solutions obtained is $n = c \cdot x / V + x$. If there is no adsorption, the conductivity of the protein solutions obtained would be equal to the additive conductivities of the control solutions. However, it is clear from Fig. 1 that the conductivity of mixtures of protein solutions and silver nitrate solutions is appreciably lower than the conductivity of control solutions. This indicates that part of the silver is bound by the protein and, in any case, there is no exchange between the adsorbed silver ions and the more mobile hydrogen ions. It is therefore assumed that this adsorption is molecular in character, i.e., not only silver ions but also their corresponding NO_3 ions are lost from the solution by adsorption.

Suppose that as the result of addition of a volume x of silver nitrate to volume V of protein solution the conductivity of the solution formed is z . It is easily seen in Fig. 1 that a control solution formed by addition of x' volumes of silver nitrate to V volumes of water has the same conductivity z . The silver-ion concentration of this solution is $n' = c \cdot x' / V + x'$. It follows that $A = n - n'$ gram-atoms of silver is lost from a liter of the protein solution as the result of adsorption. The molecular weight of albumin $M \approx 34,000$, while a liter of the protein solution contains $G = 10c[V/(V+x)]$ g of protein. Hence the molarity of the protein is $m = G/M$. Thus we find that the number of silver ions adsorbed by each protein molecule in the experiment is

$$a = \frac{A}{m} = \frac{(n - n') M}{G}.$$

The following data are presented as an example. In the experiments indicated in Fig. 1 the protein concentration $c = 3.6\%$, the volume of the original protein solution or water $V = 15$, and $N = 0.1$ mole/liter. When $x = 2$, we have $n = 11.8 \cdot 10^{-3}$; $z = 55 \cdot 10^{-4}$ (ohm $^{-1}$). The same value is obtained when a volume $x' = 0.66$ of silver nitrate is added to water; this corresponds to $n' = 4.2 \cdot 10^{-3}$. Consequently, $A = 7.6 \cdot 10^{-3}$ mole/liter. On the other hand, $G = 32$, and then $m \approx 10^{-3}$ mole/liter. Therefore $a = 7.6$, which means that 7-8 silver ions were adsorbed on each protein molecule in this instance.

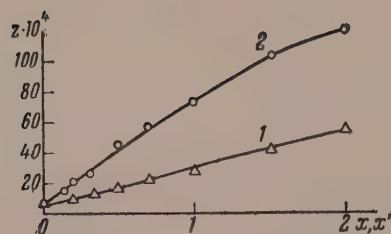


Fig. 1. Variation of conductivity with ion concentration: 1) solution of AgNO_3 in protein solution; 2) solution of AgNO_3 in water.

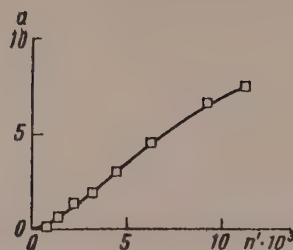


Fig. 2. Variation of adsorption \underline{a} with the equilibrium concentration n' of Ag^+ ions in solution.

V, ml	x	y	$n \cdot 10^3$	Appearance of solution
1	0.05	0.95	12.5	Clear
1	0.10	0.90	25.0	The same
1	0.20	0.80	50.0	Slightly turbid
1	0.30	0.70	75.0	Solution with protein precipitate
1	0.40	0.60	100.0	The same
1	0.50	0.50	125.0	" "
1	1.0	—	250.0	" "

The values of \underline{a} found for different values of n' are given in Fig. 2.

It should be noted that the protein solution did not undergo coagulation in these experiments. These small additions of silver nitrate even stabilized the solution, which could be heated at 60° and higher for several hours without turbidity. Coagulation occurred only after large additions of silver nitrate. This is seen in the results of the experiments given in the table. In contrast to the experiments detailed in Fig. 1, in this case \underline{x} volumes of 1 N solution of silver nitrate and \underline{y} volumes of water were added to the initial volume V of protein solution, so that $n = c \cdot x / (V + x + y)$.

Determination of silver in a solution from which protein was precipitated showed that coagulation occurs when each protein molecule has adsorbed 30 silver ions.

This leads to the conclusion that small amounts of adsorbed silver stabilize protein molecules, whereas with large amounts of adsorbed silver, coagulation replaces stabilization.

This fact is especially interesting because small doses of metal ions are known to have special biological and even therapeutic effects, opposite to the effects of large doses of ions of the same metals.

In conclusion, we may note that our preliminary experiments showed that gold ions adsorbed in small quantities on proteins also have a stabilizing effect, whereas copper and lead ions do not have this effect.

SUMMARY

1. The stability of protein solutions to the action of heat is increased by adsorption of small amounts of silver. The stabilizing effect is replaced by coagulation with increase of the amount of adsorbed silver.
2. Coagulation occurs when 30 silver ions have been adsorbed by each albumin molecule.

LITERATURE CITED

[1] E. Heymann, Koll. Z. 50, 97, (1930); H. Schorn, Biochem. Z. 199, 458, (1928); F. Haurowitz, Chemistry and Biology of Proteins (IL, Moscow, 1953) p. 226 [Russian translation].

Received December 12, 1957

INVESTIGATION OF THE VISCOPLASTIC PROPERTIES OF BUILDING MATERIALS

V. V. Vasil'eva

Moscow Institute of City Construction Engineers

Design calculations and operation of machines and mechanisms require a knowledge of the physico-mechanical and, in particular, the rheological properties of the materials (including mortars treated and conveyed in such machines). Mortars are typical disperse systems. The physico-mechanical properties of various disperse systems have been studied in considerable detail [1-5].

However, the rheological properties of building materials have been studied very little, as yet [6-10]. Plaster mortars have not been studied at all in this respect. The appropriate investigations were therefore necessary in connection with mechanization of plastering operations.

The rheological properties of building suspensions, as of many other disperse systems, are characterized by the plastic viscosity η_{pl} and the yield value Θ , in accordance with the Shvedov - Bingham equation for viscoplastic flow. These characteristics are conveniently determined under conditions of simple shear of the substance in the gap between rotating coaxial cylinders. Such conditions are obtained in rotational viscosimeters, which can be used for performing investigations in steady flow conditions. The time required for performing measurements in rotational viscosimeters is not great, and is considerably less than the time in which the structure of mortars undergoes change. Various types of rotational viscosimeters have been used for determinations of the rheological properties of disperse systems. The most convenient instrument for determination of the yield value Θ and plastic viscosity η_{pl} of mortars is the Volarovich RV-4 rotational viscosimeter [1, 11]. This instrument was used for determination of plastic viscosities and yield values of lime mortar and lime - sand, and lime - cement - sand mortars, and for studies of their variation with time from the instant of mixing, moisture content, content of filler (sand), and temperature. In all cases the pastes were stirred after being put in the viscosimeter cylinder in order to eliminate thixotropic effects.

In investigations of changes of the viscoplastic properties of lime mortar with time from the instant of mixing, all other factors which might influence these properties were excluded. The lime mortar (made with finely ground quicklime) was mixed under laboratory conditions, and variations of Θ and η_{pl} were determined at 24-hour intervals at 18-20°. The lime mortar had the same water content W , 46.7%, in all the experiments. The values of Θ and η_{pl} (average of 5-6 determinations) are given in Table 1. Values of the plasticity ψ , after Volarovich [1], such that $\psi = \Theta/\eta_{pl}$, are also given. Values of ψ have recently been used on a number of occasions for characterization of plastic disperse systems [10, 12].

It is clear from Table 1 that the yield value of lime mortar increases somewhat more rapidly than the plastic viscosity. This is because the yield value of a disperse system is highly sensitive to structural changes. In general, the variations of Θ and η_{pl} for lime mortar with time are small as compared with cement paste. It has been shown [10] that Θ for cement paste increases by a large factor in a few hours. In the case of lime mortar Θ and η_{pl} increase only 2- to 4-fold in 15-20 days. The explanation is that cement paste passes through two stages of structure formation separated by a very short time interval - formation of a coagulation structure, and structure reinforcement associated with crystallization. In the case of lime mortar a coagulation structure is formed very slowly, and if the mortar is stored without access of air the second stage may not occur at all. As Table 1 shows, the plasticity ψ of lime mortar increases somewhat with time; its absolute value was of the order of 30-40. Comparison of the value of ψ for lime mortar with the values for the plasticity of other materials (clays, peat, paints, dough, etc. [13]) shows that lime mortar has considerable plasticity.

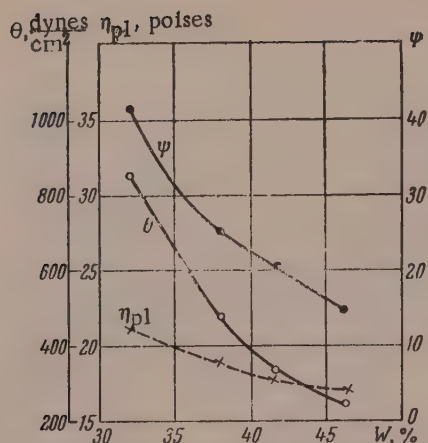


Fig. 1. Effects of moisture content W on the plastic viscosity η_{pl} , yield value Θ , and plasticity ψ of lime mortar.

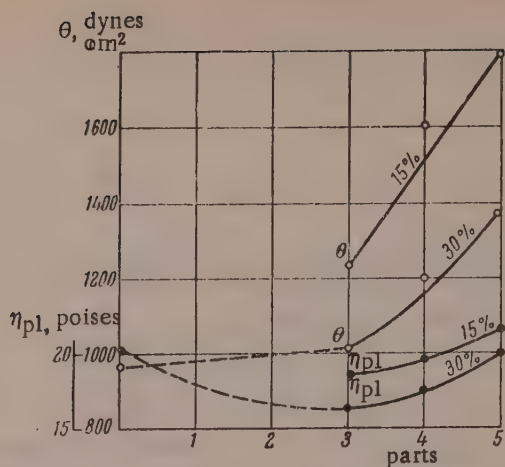


Fig. 2. Effects of sand content (c) in lime-sand mortar on the yield value Θ and plastic viscosity η_{pl} .

Variations of the rheological properties of lime mortar with the moisture content are plotted in Fig. 1. Lime mortar aged about two years was taken from a slaking pit in this case. The influence of time was therefore excluded. The determinations were performed at constant temperature ($18-20^\circ$). The experiments showed that the yield value decreases more rapidly than the plastic viscosity with increase of moisture content. With a 14% increase of the amount of water in the lime mortar, Θ decreased by a factor of 3.5, while η_{pl} decreased by only 20%. As a result, the plasticity ψ of lime mortar greatly diminishes with increase of moisture content. This is in agreement with results obtained for peat [14].

The viscoplastic properties of 1:3, 1:4, and 1:5 lime-sand mortars were also studied. The mortars were prepared under laboratory conditions. A lime mortar aged 16-17 days, the properties of which are described above, was taken in all cases. The sand was previously dried and passed through a sieve of 1.2×1.2 mm mesh. For preparation of the mortars of the above compositions, 3, 4, and 5 volumes of sand and one volume of water, respectively, was taken per volume of lime mortar; the components of each mortar were then stirred thoroughly until a homogeneous mass was obtained. A little more water was then added to the 1:4 and 1:5 mortars to give equal consistencies as measured by the cone test of the Central Scientific Research Laboratory of Constructional Materials, and the mortars were stirred again. Samples of the mortars were then dried to constant weight for determination of moisture content (Table 2).

The rheological characteristics of lime-sand mortars decrease rather more slowly than those of lime mortar with increase of water content. This is demonstrated quite well by the numerical data in Table 2. For example, when the water content of the 1:5 mortar is increased by 24.5%, Θ decreases by one-third, while η_{pl} decreases by only 7%. Therefore, the plasticity $\psi = \Theta/\eta_{pl}$ varies, on the whole, in accordance with variations of Θ , i.e., it decreases with increase of moisture content, as in the case of lime mortar.

The data in Table 2 were used to plot, in Fig. 2, the yield values and plastic viscosities of lime-sand mortars against their sand contents (at constant moisture contents of 15 and 30%). In the case of 30% moisture, points for the original lime mortar ($c = 0$), found by extrapolation of the curves in Fig. 1, are also shown. It follows from the data for 30% moisture that addition of sand increases Θ only slightly at first, and subsequently the yield value increases sharply for the 1:4 and 1:5 mortars only. Thus, on addition of the first three volumes of sand, Θ increases by about 10%, and on further addition of two volumes of sand the yield value increases by 40%. For mortars containing 15% moisture, Θ increases by 50% over the range of three to five volumes of sand. With regard to the plastic viscosity η_{pl} (see Fig. 2), this even falls somewhat at first, on addition of three volumes of sand to the lime mortar, and then rises a little on further addition of sand (1:4 and 1:5 mortars). However, it is seen that, in general, the change of η_{pl} is not large. This shows once again that plastic viscosity plays a subsidiary role in viscoplastic flow of structurized disperse systems, the principal role being played by the yield value.

TABLE 1

Variations of Yield Value (Θ), Plastic Viscosity (η_{pl}), and Plasticity (ψ) of Lime Mortar with Time After Mixing

Rheological parameters	Time after mixing			
	2 days	7 days	12 days	17 days
Θ in dynes/cm ²	244	365	609	852
η_{pl} in poises	3.03	11.8	17.6	21.6
$\psi = \Theta/\eta_{pl}$	30.4	30.9	34.0	39.4

TABLE 2

Average Yield Value (Θ), Plastic Viscosity (η_{pl}), and Plasticity (ψ) for Different Water Contents (W)

Mortar composition, volume parts	W, %	Θ , dynes/cm ²	η_{pl} , poises	$\psi = \frac{\Theta}{\eta_{pl}}$
Lime - sand mortars				
1 : 3	15,0	1218	18,8	64,7
	21,7	1096	17,0	64,4
	28,3	974	16,5	59,0
1 : 4	16,2	1583	19,5	81,0
	24,5	1340	18,8	71,0
	32,0	1156	18,1	63,0
1 : 5	10,0	1950	21,7	90,0
	31,8	1350	20,0	68,0
	34,5	1280	19,2	67,0
Lime - sand - cement mortar				
1 : 1 : 4	12	2440	26,8	91
	24	1830	24,0	74
	40	1460	20,5	71
	48	1220	19,2	63

The rheological properties of lime - cement - sand mortars were studied in relation to moisture content and temperature. Most of the experiments were performed with a 1:1:4 mortar. The mortars were prepared by the usual procedure. The determinations were initially performed at 18-20°. Table 2 contains average values (from 4-5 determinations) of yield value and plastic viscosity of 1:1:4 mortar.

The data in Table 2 show that the rheological characteristics of multicomponent mortars (lime - cement - sand) have higher values than those of lime and lime - sand mortars. This is due to the presence of a second binding component, cement. As in the earlier instances, Θ decreases more rapidly than η_{pl} with increase of moisture content.

When the moisture content is increased fourfold, Θ is halved, while η_{pl} decreases by only 25%. Because the yield value falls more rapidly than the plastic viscosity with increase of moisture content, the plasticity ψ decreases more slowly than Θ and somewhat more rapidly than η_{pl} (Table 3).

The plastic viscosity of the mortar increases considerably with fall of temperature. Thus, η_{pl} is increased by a factor of 1.8 when the temperature is lowered by 20°. The yield value of the mortars depends little on tem-

TABLE 3

Yield Value (Θ), Plastic Viscosity (η_{pl}), and Plasticity (ψ) of Lime - Cement - Sand Mortar (1:1:4) of 24% Moisture Content at Various Temperatures

Temperature, °C	Θ , $\frac{\text{dynes}}{\text{cm}^2}$	η_{pl} , poises	$\psi = \frac{\Theta}{\eta_{pl}}$
5.5	2200	35.9	61.3
10.0	1950	30.8	63.3
16.6	1830	26.1	70.1
20.0	1830	24.0	76.3
26.0	1800	20.1	89.5

perature. This is because Θ increases very little with rise of temperature, while the plastic viscosity η_{pl} increases considerably.

SUMMARY

1. In contrast to cement pastes, the yield value Θ and plastic viscosity η_{pl} of lime mortars change slowly with time.
2. As the moisture content of lime mortar increases, Θ decreases much more rapidly than η_{pl} . Therefore the Volarovich plasticity $\psi = \Theta/\eta_{pl}$ decreases.
3. The rheological characteristics Θ and η_{pl} of lime - sand mortars decrease somewhat less rapidly than those of lime mortar, with increase of moisture content. With increase of sand content, Θ increases much more rapidly than η_{pl} .
4. The values of Θ and η_{pl} for lime - cement - sand mortars are higher than for lime - sand mortars. The value of η_{pl} falls considerably while Θ remains almost unchanged with increase of temperature for these multicomponent mortars.

LITERATURE CITED

- [1] M. P. Volarovich, Trans. Inst. Appl. Mineral. No. 66, 1 (1934); Colloid J. 16, 227 (1954).
- [2] P. A. Rebinder, Proc. Conf. on Viscosity of Liquids and Colloid Solutions, 1 (1941) p. 361 [in Russian]; New Methods for Characterization of the Elastic-Plastic-Viscous Properties of Structurized Disperse Systems and Polymer Solutions, Trans. Inst. Phys. Chem. Acad. Sci. USSR [in Russian] (1950) p. 5.
- [3] D. M. Tolstoi, Colloid J. 9, No. 6, 450 (1947); Proc. 2nd All-Union Conf. on Friction and Wear in Machines, 3 [in Russian] (1949) p. 495.
- [4] G. V. Vinogradov, V. P. Pavlov, and K. I. Klimov, Petroleum Economy 2, 43 (1947).
- [5] G. I. Fuks, Viscosity and Plasticity of Petroleum Products [in Russian] (State Fuel Tech. Press, 1951).
- [6] V. P. Lobanov, Colloid J. 12, No. 5, 352 (1950).
- [7] G. I. Gorchakov, Dissertation [in Russian] (Moscow, 1949).
- [8] V. V. Stol'nikov, Dissertation [in Russian] (Moscow, 1950).
- [9] V. V. Mikhailov, Fundamentals of the Theory of Concrete Structure [in Russian] (Stroiizdat, 1941).

perature. When the temperature is lowered by 20°, Θ increases by only 18%. Most of the increase of Θ occurs in the 15-5° range, while in the 15-25° range the yield value remains almost constant. Similar results were obtained in studies of the rheological properties of clay suspensions [15].

These results indicate once again that there is an important physical distinction between these two parameters of viscoplastic flow in disperse systems. Changes of plastic viscosity in this case are primarily determined by changes in the viscosity of the dispersion medium, water, with changes of temperature. It is known [16] that the viscosity of water decreases by 40% over the 5-25° temperature range.

The yield value may be regarded as, to some extent, analogous to external friction of solids, which remains almost unchanged with temperature. The plasticity ψ of multicomponent mortars increases with rise of tem-

- [10] N. V. Mikhailov and E. E. Kalmykova, Colloid J. 16, No. 5, 350 (1954)*; Proc. Acad. Sci. USSR 99, No. 4, 573 (1954).
- [11] M. P. Volarovich, Trans. Polygraphic Inst. No. 5 (State United Press, 1937) p. 221.
- [12] T. N. Malova, Colloid J. 18, No. 4, 438 (1956)*.
- [13] M. P. Volarovich, Colloid J. 2, 557 (1936).
- [14] N. V. Lazovskaya, Trans. Moscow Peat Inst. No. 5, 141 (1957).
- [15] M. P. Volarovich and D. M. Tolstoi, J. Phys. Chem. 4, No. 6, 815 (1933).
- [16] E. Hatschek, Viscosity of Liquids, 2nd edition (State Tech. Press, 1935) p. 40 [Russian translation].

Received October 31, 1957

*Original Russian pagination. See C.B. Translation.

STUDY OF THE HYDRATION PROPERTIES AND STRUCTURE OF PEAT BY MEANS OF RADIOACTIVE ISOTOPES

1. HYDRATION PROPERTIES AND STRUCTURE OF PEAT

M. P. Volarovich and N. V. Churaev

Chair of Physics, the Moscow Peat Institute

The hydration properties and structure of peat determine the course of the principal technological processes of peat winning, processing, and drying. Solution of one of the main technological problems — removal of water from peat by natural drainage (filtration), mechanical pressing, or drying — is associated with investigations of the forms of binding between water and the solid phase of peat, and the nature of these bonds. Much attention has been, and is being, devoted to studies of the hydration properties of peat. However, because of the considerable difficulties which arise in investigations of peat, which is a complex polydisperse system, many questions are still far from a final solution.

There are several classifications of the forms in which water is bound in peat (those of Dumanskii et al. [1]); the most complete is the classification proposed by Rebinder [2]. This is based on differences in the energy of bonding between the moisture and the material, and includes chemical, physicochemical, and mechanical bonding. The amount of chemically bound water in peat is not large, not more than 10-15%* per gram of dry substance [3]. According to modern views, the adsorbed moisture of peat (physicochemical bonding) includes a water film 10-20 molecules thick on the surface of the solid phase. There is reason to believe that only these boundary layers of liquid have a number of anomalous properties, which distinguish it from the bulk of the liquid [4-6].

Let us consider, in the light of this theory, the results of determinations of bound water in peat by various methods. Korshunov [2] and Volarovich and Gusev [3] used the methods of tensimetric analysis. The amount of bound water determined by this method was from 40 to 70% for different peat samples. Somewhat similar results were obtained by Pokrovskii and Sinel'shchikov [7] by means of the freezing method, and by Kryukov and Komarova [8], who showed that after water is pressed out of peat under pressures of up to 20,000 kg/cm², up to 50-60% of moisture which cannot be removed by pressure remains in it. Somewhat lower values for bound water were obtained in experiments with dried peat, because of the irreversible structural changes which take place on drying. Thus, Apushkin [9] investigated the sorptional moisture capacity of cut peat by tensimetric methods and obtained the value 20-25%. Similar results were obtained by Naumovich [10], who used tensimetric and electrophoretic methods. Finally, calculations by means of Dumanskii's formula [11], based on the heat of wetting of dry peat powder, give the same value, 20-25% per gram of dry substance.

The most usual method for determination of bound water in peat has been the nonsolvent volume method, with sugar as the indicator substance [12]. The results of experiments carried out by Dumanskii et al. [13] and later by Dragomirova, Méli', Novikov, and Berezin [14], showed that at a sugar concentration of 30-40% the amount of firmly bound water (in Dumanskii's terminology) varies from 25 to 75% for different peat samples.

*All moisture contents of peat are given as percentages on the dry substance.

Despite the differences between these methods, they all give much the same results. Since determination of bound water by these methods depends on utilization of its special properties, it may be assumed that they determine adsorbed water, the content of which, as shown by the above data, does not exceed 50-70%. It may also be shown from the content of bound water $M_b = 0.5$ g/g, the specific surface of peat $S = 30$ m²/g, its density $\rho = 1.8$ g/cc, and the size of the water molecule $D = 3$ Å, that the thickness of the adsorbed water film on peat particles corresponds to about 30 molecular layers:

$$N = \frac{M_b}{\rho \cdot S \cdot D} = \frac{0.5}{1.8 \cdot 3 \cdot 10^5 \cdot 3 \cdot 10^{-8}} = 30. \quad (1)$$

The order of magnitude of the result confirms the above assumption.

By the existing standards, the permissible moisture content of fuel peat is 70-80%. Thus, the peat industry has not, in practice, been concerned with the removal of adsorbed water from peat. Therefore, special interest attaches to studies of other forms of bonding between water and the solid phase of peat — weaker but of greater significance in the technology of peat winning and drying.

Difficulties are met in development of methods for determination of other forms of bound water apart from adsorbed water, because these forms differ little from free water in their properties. Using low concentrations of sugar (3-5%), A. V. Dumanskii determined so-called loosely bound (film) water, which has a lower solvent power. According to Berezin [14], the water determined by this method also includes osmotic and structural water in the micelles and vegetable fragments of peat. However, at low sugar concentrations only a part of the weakly bound water in peat is determined, and even small changes of concentration produce considerable changes in the amounts of bound water found. The indefinite character of the results is an obstacle to the use of this method for quantitative studies of weakly bound water in peat.

The weakest forms of water bonding may be detected by the use of very low concentrations of the indicator substance, but this greatly decreases the accuracy of the determinations. This disadvantage can be avoided with the use of radioactive tracers. For this purpose we developed a method for determination of bound water in peat with the aid of the radioactive tracer $\text{Na}_2\text{S}^*\text{O}_4$ containing the S^{35} isotope [15]. This tracer is negatively adsorbed at the water surface [16] and is not adsorbed to any practical extent by the solid peat phase. With the use of low concentrations of the radioactive tracer (down to $10^{-10}\%$), it is also possible to avoid errors associated with changes in the properties of a disperse system produced by additions of considerable amounts of sugar or electrolyte.

A second approach to a solution of the problem of determination of weakly bound water in peat depends on consideration of mobile and immobile water. On the assumption that only the free water in peat can be moved under a pressure gradient, all the water which remains immobile can be classified as bound water. For determination of immobile water we devised a method based on filtration of water containing the same $\text{Na}_2\text{S}^*\text{O}_4$ radioactive tracer through water-saturated peat samples [17].

It is interesting to compare the results of these two methods for determination of bound water in peat. Table 1 contains the results of experiments on peat samples of different botanical composition and degree of decomposition, from which the contents of different forms of weakly bound water in peat can be estimated.

Values for the immobile water, W_i , were found from experiments on filtration of tagged water through peat samples with intact structure. The bound-water content W_b of the same peat was determined by the radioactive-tracer method. A series of check experiments showed that the relative error in determination of W_i and W_b by these methods does not exceed $\pm 5-8\%$. Since the immobile water was determined in samples retaining their natural structure, whereas bound water was determined in suspensions made from the same peat, the difference between the contents of immobile and bound water, $W_i - W_b$, may be attributed to water bound in the peat structure, W_{str} , and in particular to water trapped in enclosed fine pores which do not allow water to pass through.

As already noted, the maximum amount of bound water in peat can be determined by the use of very low concentrations of the radioactive tracer. This agrees, in particular, with Deryagin's theory [18] of nonsolvent volume. To establish what classes of bound water, apart from adsorbed water, can be determined by this method, experiments were performed on determinations of bound water in different peat fractions. The results of these experiments with two types of peat are given in Table 2.

TABLE 1

Contents of Different Forms of Bound Water in Samples of Upper and Lowland Peat

Serial No.	Peat type	Degree of decomposition R, %	Immobile water W _i , %	Bound water W _b , %	Distribution of water in peat by types of bonding				Total water capacity of peat W _t , %
					W _{ads} , %	W _{int} , %	W _{str} , %	W _{cap} , %	
1	Fuscum peat	15	570	400	40	360	170	1130	1700
2	Complex upper	20	410	300	40	260	110	1220	1630
3	Medium peat	25	430	370	50	320	60	950	1380
4	Pine - cotton grass	60	280	275	70	205	—	620	900
5	Sedge - Hypnum	35	345	345	60	285	—	715	1060
6	Sedge - bog	35	300	280	60	220	—	700	1000
7	Wood - sedge	40	280	275	60	215	—	740	750

TABLE 2

Results of Determinations of Bound Water in Individual Peat Fractions

Characteristics	Fraction size, mm				Whole peat sample, %
	> 3	3 - 1	1 - 0.25	< 0.25	

Sedge - bog peat, R = 35%

Distribution of dry mass by fractions, %	15.5	18.5	22.6	43.4	100
Bound water contents, %	296	391	369	298	331
Distribution of total bound water, %	45	72	84	130	331

Sedge peat, R = 30%

Distribution of dry mass by fractions, %	—	46.3*	17.0	36.7	100
Bound water contents, %	—	431	347	259	353
Distribution of total bound water, %	—	200	58	95	353

* Peat fraction 1 mm.

The data in Table 2 show that most of the bound water determined by the radioactive-tracer method is contained in the coarse fraction of the peat, consisting of undecomposed plant fragments. Thus, the nonsolvent volume determined by the radioactive-tracer method includes not only water of lower solvent power but also intracellular water isolated from the external solution by the plant cell walls. It should be noted that the average size of the cellular cavities in peat is $\sim 5-10\mu$. The amount of intracellular water enclosed in the cell cavities of the plant fragments can be found by subtraction of adsorption water from the total bound water:

$$W_{int} = W_b - W_{ads} \quad (2)$$

TABLE 3

Structural Characteristics m , S_0 , and δ , for Different Samples of Upper and Lowland Peat

Peat type	Degree of decomp. R , %	Hydraulic pore radius δ , μ	Active porosity, m	Kinetic spe- cific surface S_0 , m^2/g	Specific surface by dispersion analysis S_d , m^2/g
Fussum peat	15	1,25	0,31	3,3	0,25
C6mpex upper	20	1,24	0,52	5,1	0,80
Medium peat	20	0,43	0,48	11,6	0,90
Medium peat	25	0,37	0,53	13,6	1,15
Medium peat	60	0,15	0,43	28,0	3,07
Pine - cotton grass	25	0,78	0,46	6,0	1,20
Sedge	30	0,77	0,68	7,1	1,20
Sedge	35	0,70	0,56	6,1	1,29
Sedge - Hypnum	40	0,49	0,45	6,9	1,04
Wood - sedge					

The values of W_{ads} given in Table 1 are taken from earlier publications [2, 3, 7, 13, 14]. It should be remembered that calculations by Eq. (2) give all the weakly bound water in peat, including osmotic and film moisture, in addition to the intracellular water, which is the principal constituent. However, no methods for distinguishing between these forms of bound water in peat are available at present. Intracellular water is usually included with water retained by osmotic forces [1, 2]. In all probability it is more correct to consider it as structurally bound water because, as will be shown below, destruction of the cell cavities (breakdown of the structure) releases it into the free state. It may be noted that in the classification used in pedology, intracellular water is considered as an independent class of physical state of moisture in soil [19].

Intracellular water, which corresponds to one of the weakest forms of bonding between moisture and peat, can be determined by virtue of the low concentration of the radioactive tracer, and because samples of the dispersion medium are taken immediately after the tracer has been added and the mixture stirred. This minimizes diffusion of the tracer through the cell walls; incidentally, the rate of this diffusion is lower by several orders of magnitude than diffusion in solution [20]. Increase of the tracer concentration, by addition of inactive salt, leads, as in the case of sugar, to a change in the measured amount of bound water. It should be noted that the radioactive-tracer method can hardly be regarded as identical with the electrolyte-tracer method, as micro quantities of radioactive materials in solutions have a number of special properties [21].

Apart from the classes of moisture considered above, our results can be used to calculate the amount of moisture retained in peat by capillary forces (mechanical bonding):

$$W_{cap} = W_t - W_i \quad (3)$$

where W_t is the total moisture capacity of peat, values of which are taken from Grebenshchikov's paper [22].

It follows from Table 1 that most of the water in peat consists of capillary and intracellular water. Removal of this water is the main task in the technology of peat winning. As the degree of decomposition increases, the content of intracellular water falls as the result of breakdown of plant fragments during humification of the peat. The amount of capillary water also decreases; this can be attributed to increased dispersity of the peat and a decrease in the size of the capillary channels. Upper types of peat (Nos. 1-4, Table 1) bind rather more intracellular and structural water, and this makes drying of deposits composed of these types of peat difficult. Whereas in lowland types of peat the amount of immobile water does not exceed 300-350%, in upper peats its content rises to 400-600%.

As the result of experiments on filtration of tagged water it is possible not only to determine the content of immobile water, but also to calculate the active porosity m of the peat, which is the ratio of the volume of the water-conducting pores to the volume of the sample. It is then possible to use the Kozeny - Carman equation for calculation of the kinetic specific surface [23]

$$S_0 = 970 \sqrt{\frac{m^3 d^2 I}{Q}}, \text{ cm}^{-1} \quad (4)$$

where d is the diameter of the peat sample in cm; I is the pressure gradient in the filtration apparatus; Q is the filtration rate in cc/minute. In the case of peat, which is a water-saturated and water-binding disperse system, this equation could be used only after a technique had been developed [17] for determination of active porosity of peat, which differs considerably from the porosity value as usually determined. Attempts to determine active porosity by indirect methods involved complicated calculations and were based on numerous assumptions [24]. The experimental values of S_0 and m can be used to calculate the hydraulic radius of the peat pores, equal to the average thickness of the water layer over the surface of water-conducting pores:

$$\delta = m/S_0. \quad (5)$$

The values of S_0 , m , and δ , not related to any arbitrary structural scheme, may be adopted as characteristics of peat structure. The results of determinations of these values for peat samples of different botanical composition and degree of decomposition are given in Table 3; this table also contains, for comparison, values of the specific surface S_d calculated from the results of dispersion analysis [25].

It follows from the data in Table 3 that the structural characteristics so found depend on the botanical composition and the dispersity of the peat. The dimensions of water-conducting pores decrease appreciably with increasing degree of decomposition of the peat, and for a given degree of decomposition upper peats have smaller pores. Lowland peats are generally more homogeneous with regard both to dispersity (S_d) and to dimensions of water-conducting pores (δ). Variations of the kinetic specific surface S_0 in general follow the same course as the peat dispersity. The lower values of S_0 found for lowland peats are attributable to the coagulated state of their colloidal fraction [26]. The values of kinetic specific surface greatly exceed the values of S_d found by dispersion analysis, as in the latter case, shape irregularities, internal porosity, and roughness of the particles are disregarded. Similar relationships apply to a number of other disperse materials [27, 28]. It is interesting to note that the values found for S_0 are close to the value for the kinetic specific surface of peat briquets, calculated by Prokimnov by Deryagin's method [29].

The active porosity of peat is greatest for medium degrees of decomposition. Lower active porosities at lower degrees of decomposition of the peat are due to higher contents of intracellular water. As the degree of decomposition increases, the active porosity decreases, owing to a decrease in the size of water-conducting pores and closer packing of the peat particles. The active porosity of peat with natural structure varies in the range of 0.3 to 0.7, in accordance with the type of peat and its degree of decomposition.

Data on the forms of water bonding and characteristics of peat structure, obtained by the use of radioactive tracers, can be used for various technological calculations in relation to the drying of peat deposits and processing and drying of peat.

SUMMARY

1. Methods based on the use of radioactive tracers were used for studying different forms of bound water in peat. The radioactive tracer used was the S^{35} isotope in the compound Na_2SO_4 , which is not taken up by the solid phase of peat.
2. The results of determinations of bound water in different peat samples, found by the radioactive-tracer method, the nonsolvent volume method, and filtration of tagged water, were compared; it was thereby possible to estimate the contents of water bound in different forms and to distinguish between the intracellular, structurally bound, and capillary forms of water in peat.
3. Most of the bound water is present as capillary and intracellular water. The contents of different forms of bound water in peat depend on the botanical composition and degree of decomposition of the peat.
4. The method of filtration of tagged water through peat samples can be used for determinations of active porosity, kinetic specific surface, and hydraulic pore radius of the peat; these values can serve as characteristics of the peat structure.

LITERATURE CITED

- [1] N. N. Kulakov, Introduction to the Physics of Peat [in Russian] (State Power Press, 1947) p. 193.
- [2] S. S. Korchunov, "Investigation of the physicommechanical properties of peat," Trans. Sci. Res. Inst. Peat Ind. No. 12, 177 (1953).
- [3] M. P. Volarovich and K. F. Gusev, Trans. Moscow Peat Inst., No. 2, 97 (State Power Press, 1953).
- [4] A. A. Rode, Papers at the 6th Internat. Congr. Soil Science, Physics of Soils [in Russian] (Izd. AN SSSR, 1956) p. 55.
- [5] M. K. Mel'nikov and S. V. Nerpin, Papers at the 6th Internat. Congr. Soil Science, Physics of Soils, [in Russian] (Izd. AN SSSR, 1956) p. 139.
- [6] F. E. Kolyasev, Papers at the 6th Internat. Congr. Soil Science, Physics of Soils [in Russian] (Izd. AN SSSR, 1956) p. 159.
- [7] G. I. Pokrovskii and S. I. Sinel'shchikov, Pedology No. 12, 65 (1939).
- [8] P. A. Kryukov and N. A. Komarova, Papers at the 6th Internat. Congr. Soil Science, Chemistry of Soils [in Russian] (Izd. AN SSSR, 1956) p. 151.
- [9] K. K. Apushkin, Trans. Moscow Peat Inst. No. 2, 88 (State Power Press, 1953).
- [10] V. M. Naumovich, Trans. Inst. Peat Belorussian SSR, 6, 344 (Belorussian Acad. Sci. Press, 1957).
- [11] A. V. Dumanskii, Colloid J. 12, 319 (1950).
- [12] A. V. Dumanskii, Lyophily of Disperse Systems [in Russian] (Voronezh State University Press, 1940) p. 108.
- [13] A. V. Dumanskii, M. V. Chapek, et al., Colloid J. No. 2 (1936), No. 2 (1937).
- [14] A. A. Berezin and I. D. Belovidov, Trans. Moscow Peat Inst. No. 8, 167 (State Power Press, 1958).
- [15] M. P. Volarovich, F. D. Sysoeva, V. V. Chernyavskaya, and N. V. Churaev, Colloid J. 20, 122 (1958).*
- [16] A. V. Dumanskii, Colloid Science [in Russian] (Goskhimizdat, 1948) p. 127.
- [17] M. P. Volarovich, N. V. Churaev, and B. Ya. Minkov, Colloid J. 19, 159 (1957)*; Proc. Acad. Sci. USSR 114, No. 5, 964 (1957).*
- [18] B. V. Deryagin, Colloid J. 5, 257 (1939); 5, 605 (1939).
- [19] N. A. Kachinskii, Pedology No. 12, 20 (1957).
- [20] B. N. Mel'nikov and P. V. Morychanov, Colloid J. 18, 711 (1956).*
- [21] S. E. Bresler, Radioactive Elements [in Russian] (GITTL, 1957) p. 96.
- [22] A. A. Grebenshchikov, Pedology No. 9, 102 (1956).
- [23] B. V. Deryagin, M. K. Mel'nikova, and V. I. Krylova, Colloid J. 14, 423 (1952)*; B. V. Deryagin, M. K. Mel'nikova, and S. V. Nerpin, Papers at the 6th Internat. Congr. Soil Science, Physics of Soils [in Russian] (Izd. AN SSSR, 1956) p. 101.
- [24] B. P. Gorbunov, Trans. Inst. Constructions, No. 2, 166 (Acad. Sci. Uzbek SSR Press, 1951).
- [25] M. P. Volarovich and N. V. Churaev, Colloid J. 17, 200 (1955).*
- [26] S. G. Sokolov, Trans. Moscow Peat Inst. No. 8, 140 (State Power Press, 1958).
- [27] V. V. Kel'tsev and P. A. Tesner, Carbon Black [in Russian] (State Fuel Tech. Press, 1952).
- [28] V. P. Romadin, Preparation of Pulverized Coal [in Russian] (State Power Press, 1953).
- [29] V. V. Prokimnov, Candidate's Dissertation [in Russian] (Moscow Peat Inst., 1956).

*Original Russian pagination. See C.B. Translation.

Received May 29, 1958

USE OF THE RV-4 ROTATIONAL VISCOSIMETER FOR RHEOLOGICAL STUDIES OF SYSTEMS WITH RAPIDLY CHANGING STRUCTURAL PROPERTIES

M. M. Gurvich

Institute of Chemistry, Academy of Sciences,
Azerbaijan SSR, Baku

Rotational viscosimeters of the RV type, as designed by M. P. Volarovich, are widely used in rheological investigations. The range of systems studied by means of these instruments is very wide, and includes rubber [1, 2], road bitumen [3, 4], printing inks [5], mica dispersions [6], lubricating oils [7-9], mineral suspensions [10-12], greases [13], protein solutions [14], dough [15], and graphite pastes [16]. These instruments might be expected to prove useful for studies of clay suspensions used in oil-well drilling. The aim of the present investigation was to study the conditions of applicability of the RV-4 viscosimeter to these disperse systems, which are characterized by rapidly changing structural properties.

It has been shown [17] that drilling muds may be either thixotropic or nonthixotropic. Thixotropic suspensions in most cases have a high rate of structure formation, especially immediately after preparation. Nonthixotropic suspensions have a condensation — flocculation structure; their strength curves vary in form and often indicate a decrease of structural strength in time, with an increase in strength after stirring. These changes also take place fairly rapidly.

Determination of the rheological characteristics of such systems involves considerable difficulties. For conclusive results in determinations of deformation — stress relationships it is necessary to bring the system to the same initial state before each determination, and this state must not change spontaneously until the given stress is applied.

We consider the behavior of both types of drilling muds in relation to these conditions in determination of their rheological characteristics by means of the RV-4 instrument.

Thixotropic clay systems (Type II). Such systems are stirred in order to bring them to a uniform initial state of structural breakdown. In instruments of the RV type this may be effected by rotation of the pulley. However, experiments showed that despite all possible standardization of the stirring procedure, many clay systems, and especially weighted systems in which coarse particles predominate, cannot be brought to a uniform state in this way.

In the RV-4 instrument the bottoms of the outer and inner cylinders have spherical surfaces, and the linear velocity diminishes from the periphery to the center of the bottom, where it is zero. Because of this, the coarse particles may settle out under the spherical surface of the inner cylinder, and the structure may increase in strength at the same time; this was observed in the case of a thixotropic clay — hematite suspension of sp. gr. 2. After breakdown of its structure by vigorous and uniform rotation of the cylinder, the rotation rate of the inner cylinder decreased gradually under constant load. Inspection showed that a sediment accumulated on the bottom of the cylinder and a structure of a low degree of breakdown was retained.

This system was stable in the stationary state. It did not deposit a sediment when kept at rest in the instrument for 24 hours. It follows that the effect described above is caused by the distribution of velocities under the spherical surface.

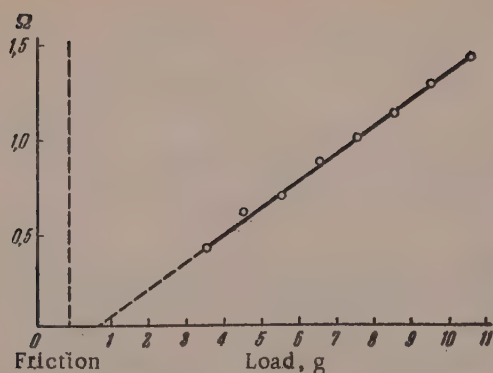


Fig. 1. Rheological curve for a thixotropic clay-hematite suspension of sp. gr. 1.6, determined by means of the RV-4 instrument.

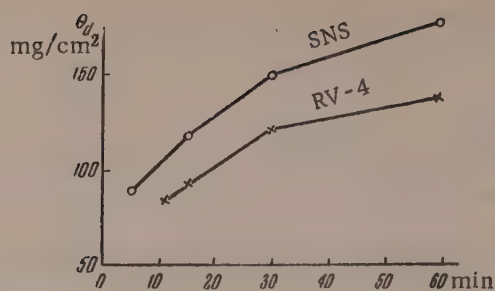


Fig. 2. Curves showing the time variations of the structural strength of a 27% suspension (by volume) of Zych clay in 2% sodium humate solution, found by parallel determinations in the RV-4 and SNS instruments.

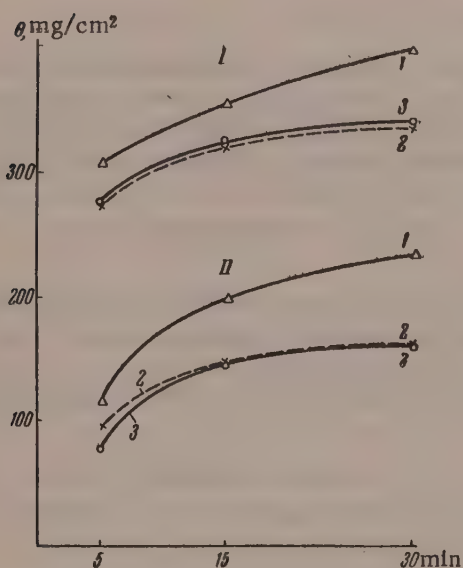


Fig. 3. Curves showing time variations of the structural strength of two thixotropic clay suspensions, found by parallel determinations with the SNS and RV-4 instruments by the old and new techniques; I and II represent different suspensions: 1) SNS instrument, usual technique; 2) the same, new technique; 3) RV-4 instrument.

This effect was eliminated when the suspension was stirred by raising and lowering of the cylinder, leading to liquefaction of the mass under the spherical surface. This method of stirring proved more suitable than stirring by rotation. The design of the RV-4 viscosimeter is more suitable than the design of the RV-8 instrument for this purpose, as stirring by axial motion of the cylinder is impossible in the latter. For work with systems of this type it might be advisable to have an inner cylinder with a lower end of a shape similar to that of the inner cylinder of the SNS instrument.

The number of points which can be determined reliably on the rheological curve for a clay suspension is relatively small; it does not exceed 8-10 with consecutive 1 g additions to the load. The velocity can be increased only up to 1.5 revolutions/second. Neither is it possible to go far in the direction of low velocities, as structure formation begins to have an effect, with irregular rotation, interruptions, and stoppages of the instrument.

Fig. 1 shows a portion of a rheological curve for a thixotropic clay-hematite suspension of sp. gr. 1.6. It is seen that the first 8 of the points which could be determined fit satisfactorily on a straight line. The yield value P_T was found to be 12.15 dynes/cm². Before determination of each point the structure was broken down by raising and lowering of the cylinder.

It is known that the static shear stress is not constant, but depends on the experimental conditions [18]; it was therefore of interest to compare curves for the structural strength of this suspension, i.e., curves for variations of the yield value with time, found by parallel determinations in the RV-4 and SNS instruments. In the SNS instrument the stress increases continuously as the result of uniform rotation of the cylinder, and there is no time for relaxation of any stress reached. In the RV-4 instrument the motion did not commence immediately after application of the load, but after some time, usually 20-40 seconds. Since this is evidently the relaxation time, each load was held for 30 seconds and increased only after this time had elapsed (if the cylinder did not begin to

TABLE 1

Variations of the Times of Consecutive Revolutions of the Pulley of the RV-4 Instrument in Free Fall and in a Thixotropic Medium (load 2 g)

Pulley revolutions	Time for one revolution, seconds	
	in free fall	in a thixotropic medium
1	6.3*	3.8
2	1.2	8.2
3	0.8	10.4
4	0.5**	13.1
5	0.5**	15.9
6	0.5**	—
7	0.5**	—

* Mean of three determinations.

** Mean time of one of the last revolutions (4-7).

Thus, if the system is allowed to relax, the static yield value decreases to an extent which increases with the relaxation time. However, in thixotropic systems with incomplete structurization, the relaxation effect is obscured by the opposite structurization process. If the determination is performed on a system of a high degree of structurization, the static shear stress depends on any arbitrary applied stress if the system is allowed enough time for relaxation [19].

The RV-4 instrument was used for determination of the static yield value for a thixotropic system with a virtually complete structure in such a way that increasingly smaller loads were arbitrarily applied and the start of the complete descent of the load was awaited. It was found that very low values of P_f could be attained in this manner. If this is the case, then the concept of static yield value becomes somewhat indefinite for thixotropic systems.

It is known that the load rotating the inner cylinder in the RV-4 instrument accelerates as it falls. This raises the question of how the acceleration changes if the instrument contains a thixotropic clay system. Breakdown of structure in thixotropic systems is accompanied by restoration. The former diminishes resistance to deformation, and the latter increases it. It is evident that the relative proportions of the two effects differ at different stages of the process, and this should influence the acceleration of the falling load.

We performed a series of experiments on thixotropic systems at different stages of structural breakdown, achieved by consecutive variations of the load and therefore of the applied stress. The following procedure was used in most cases. After breakdown of the structure by means of longitudinal movements of the inner cylinder, a given load was applied to the suspension, the first revolution of the pulley was disregarded, and the time for the second revolution (now counted as the first) and for the following five revolutions was measured. The ratio of the time for the first revolution to the average time for one of the following five may be taken as an arbitrary measure of the acceleration (positive or negative).

* However, it is necessary to distinguish between the start of motion and displacement of the pulley as the result of deformation of the mass, and only the true start of motion must be taken into consideration.

rotate)*. The determination time is increased with this procedure, and the age of the structure was calculated from the start of the motion, and not from the start of the experiment.

This procedure was used for determination of strength curves by means of both instruments. The specific characteristics of the method suggested that curves determined by means of the RV-4 instrument should lie lower than those determined with the SNS instrument; this was found to be the case (Fig. 2).

In order that the determination conditions with the two instruments should be more similar, the procedure was modified in such a way that there was time for stress relaxation in the SNS instrument. For this, the maximum rotation angle of the cylinder, corresponding to the yield value, was determined by the usual technique. The experiment was then repeated, but the motor driving the cylinder was switched off at a certain smaller angle. The cylinder was held for a short time to find whether it moved in the reverse direction. If it did, the experiment was repeated with a smaller angle until the minimum angle was found at which there is still a complete return movement of the inner cylinder. It was found that for the suspension under investigation this angle is 80-90% of the initial angle. Hence, it could be assumed that with this procedure the yield values found by parallel determinations in the RV-4 and SNS instruments should be closer together. This was found to be the case (Fig. 3).

TABLE 2

Ratios of the Time (seconds) of the First Revolution (t_1) to the Average Time of One of the Next Five Revolutions of the Pulley of the RV-4 Instrument (t_{av}) Under Different Loads

Load, g	2	3	4	5	6	7	10	16	20	30	40
t_1/t_{av}	0.43	0.84	0.94	0.94	1.0	1.1	1.1	1.1	1.43	1.80	2.0

TABLE 3

Repeated Determinations of the Rotation Rate of the Cylinder of the RV-4 Instrument in a Nonthixotropic Clay Suspension

Load, g	Rotation rate of cylinder, rev/sec		
	first determination	duplicate determination	duplicate determination after stirring by longitudinal motion of cylinder
40.5	1.240	0.965	0.868
42.5	1.389	1.136	0.020
44.5	1.479	1.330	1.208

TABLE 4

Effect of Resting Time on the Yield Value of a Nonthixotropic Clay Suspension

Resting time, minute	25	39	60	109	three days
Yield value, g of load	35.3	33.5	34.9	39.5	29.7

Determinations performed in this way (Tables 1 and 2) showed that in thixotropic clay suspensions small loads show negative accelerations, whereas large loads show positive accelerations. It follows that with a certain intermediate load the fall should be uniform.

Table 2 shows that there is a certain load for a thixotropic medium at which the fall is uniform. A possible explanation for the constant rate of fall is that the force of gravity is balanced by another force, which might be called the force of structure formation. If this is so, certain possibilities arise for quantitative characterization of thixotropy in the dynamic state, augmenting its characterization under static conditions.

Nonthixotropic clay suspensions. As noted earlier, the structure of such systems may change in different directions with time, while stirring leads to reinforcement in most cases. In such conditions it is not possible to have a definite initial state of the system, as there are no criteria for characterization of such a state. It is therefore difficult to decide how a suspension should be prepared for rheological measurements.

Certain possible methods of determination by means of the RV-4 instrument were arbitrarily chosen. By the first, the suspension was prepared by moderate stirring effected by slow rotation of the inner cylinder caused by raising of the weight. By the second method, the suspension in the instrument was stirred by longitudinal movement of the cylinder as described above. In all cases the determinations were performed immediately after the instrument had been filled, and only the average time of one of the first five revolutions of the cylinder was taken into consideration.

In most experiments a rapid change in the state of the system was recorded, leading to considerable discrepancies between duplicate determinations. Nevertheless, in some instances it proved possible to determine a portion of the rheological curve, although this only represents the state of the system during some arbitrary period of its existence.

Tables 3 and 4 contain the results of experiments with a nonthixotropic suspension the structure of which proved to be more stable than in other studied systems of this type. It is clear from the data that the rheological characteristics of this system are also very indefinite.

SUMMARY

1. The suitability of the RV-4 instrument for rheological studies of thixotropic and nonthixotropic drilling muds was investigated.
2. This instrument can be used for determination of rheological curves of thixotropic clay suspensions if more vigorous stirring is used than that achieved by rotation of the pulley (this is particularly important with weighted clay suspensions). However, even in such cases only a limited region of the rheological curve can be determined.
3. The point on the rheological curve corresponding to uniform fall of the weight rotating the cylinder of the RV-4 instrument may be of interest for characterization of thixotropy under dynamic conditions.
4. The RV-4 instrument cannot be used for the usual rheological investigations of nonthixotropic clay suspensions because of the extreme variability of such systems under dynamic conditions.
5. Parallel determinations of yield value by means of the RV-4 and SNS instruments give similar results if the determination technique with the SNS instrument is modified so as to permit relaxation of stress.

I thank Professor M. P. Volarovich for his interest and valuable advice.

LITERATURE CITED

- [1] E. P. Kheraskova and D. S. Kryukova, *Caoutchouc and Rubber* No. 1, 15 (1940).
- [2] M. P. Volarovich and L. N. Ginzburg, *Colloid J.* 14, 20 (1952).
- [3] N. N. Korotkevich, *Road Construction* No. 9, 25 (1940).
- [4] M. P. Volarovich and M. F. Nikishina, *Colloid J.* 12, 169 (1950).
- [5] M. P. Volarovich, *Trans. Inst. Polygraphic Ind. of the United State Press*, No. 5, part 3 (1937).
- [6] M. P. Volarovich and L. S. Erokhin, *J. Phys. Chem.* 12, 277 (1938).
- [7] V. L. Val'dman, *Industrial Lab.* No. 11-12, 1077 (1945).
- [8] M. P. Volarovich and V. L. Val'dman, *Friction and Wear in Machines* Vol. 2 [in Russian] (Izd. AN SSSR, Moscow - Leningrad, 1946) p. 80.
- [9] V. L. Val'dman, *Doctorate Dissertation* [in Russian] (Moscow, 1950).
- [10] M. P. Volarovich and D. M. Tolstoi, *J. Phys. Chem.* 4, 815 (1933).
- [11] M. P. Volarovich, *Trans. Inst. Appl. Mineralogy*, No. 66 (1934).
- [12] M. P. Volarovich and D. M. Tolstoi, *Colloid J.* 3, 621 (1936).
- [13] M. P. Volarovich and E. P. Loshakova, *Colloid J.* 8, 127 (1946).
- [14] P. F. D'yachenko, *Proc. Conf. on Viscosity of Liquids and Colloidal Solutions*, 1 [in Russian] (Izd. AN SSSR, 1941) p. 447.
- [15] R. A. Branopol'skaya, *Bread Industry*, No. 2 (1940).
- [16] L. V. Tolikino, *Bull. Trust for Scholastic and Stationery Materials*, No. 1, 18 (1941).

- [17] M. M. Gurchich, Colloid J. 18, 666 (1956).
- [18] N. V. Mikhailov and P. A. Rebinder, Colloid J. 17, 107 (1955).
- [19] M. M. Gurchich, B. K. Zeipalov, and R. Sh. Egieva, Proc. Acad. Sci. Azerbaidzhan SSR 14, No. 5 (1958).

Received June 19, 1957

*Original Russian pagination. See C.B. Translation.

A DIELECTRIC STUDY OF THE FORMATION OF SOAP - HYDROCARBON SOLUTIONS

Yu. F. Deinega, A. V. Dumanskii
and A. V. Lobastova

Institute of General and Inorganic Chemistry,
Academy of Sciences Ukrainian SSR, Kiev

One of the principal problems of modern colloid chemistry is determination of the general laws governing the formation of colloidal systems in the gradual transition from true solutions to two-phase lyophilic colloids, (semicolloids) and then to lyophobic stabilized suspensions or emulsions [1]. These laws can be studied with systems of the soap - solvent type. In accordance with the temperature, component concentration, and nature of the components, soap - solvent systems may exist as true solutions or isotropic melts, sols, gels, pseudogels, and suspensions [2].

In studies of the transition from true solutions to two-phase lyophilic sols, note should be taken of the concept of similarity between lyophilic disperse systems and systems in the critical state. The formation of equilibrium colloidal systems in the transition from one-phase to two-phase systems is closely associated with critical phenomena [3]. The similarity should be greatest between critical reversible thermodynamically stable systems and lyophilic disperse systems [4]. The variations of properties observed in transitions in lyophilic disperse systems may be expected to be analogous in many respects to changes of properties observed in critical effects. In accordance to the theory of the identity of critical transitions and the so-called second-order phase transitions, the dielectric constant of a binary liquid system should pass through a maximum in the critical region [5]. This was confirmed [6] in studies of the dielectric properties of three systems with limited solubility: nitrobenzene - hexane, and nitrobenzene - octane. It follows that if transitions in lyophilic disperse systems are similar to critical phenomena, the dielectric constant should pass through a maximum on formation of a colloid.

In this connection we studied micelle formation in hydrocarbon solutions of soaps, by determination of the dielectric constant. Variations of the dielectric constant with the temperature were studied for this purpose.

Solutions of sodium phenylstearate in xylene were used for the experiments. Our choice of this system was guided by the following considerations. First, hydrocarbon solutions of sodium phenylstearate are formed at lower temperatures than, say, sodium stearate solutions. Second, viscosity studies showed that the structure of benzene solutions of sodium phenylstearate can be varied considerably by means of polar additives [7].

Honing and Singleterry [8] concluded as the result of viscosimetric and optical investigations that anhydrous systems of sodium phenylstearate in benzene have a polymerlike structure, which is broken down by additions of small amounts of water or certain surface-active substances with formation of compact micelles. A secondary weakly bound spatial structure is formed in presence of excess water.

The solutions were prepared from already-prepared sodium phenylstearate (an experimental batch from the Khar'kov Chemical Reagent Factory). Oleic acid was used as the surface-active additive.

Capacities were determined in the range from 0.4 to 10 kilocycles/second by means of the Schering bridge (type MLE-1). The audio frequency source was a ZG-10 oscillator. The ÉO-7 electron oscillograph connected in a special circuit [9] was used as the indicator of bridge balance.

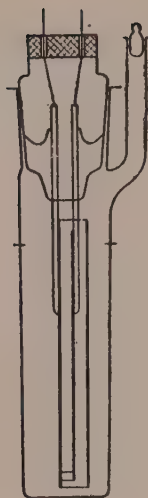


Fig. 1. Measuring condenser.

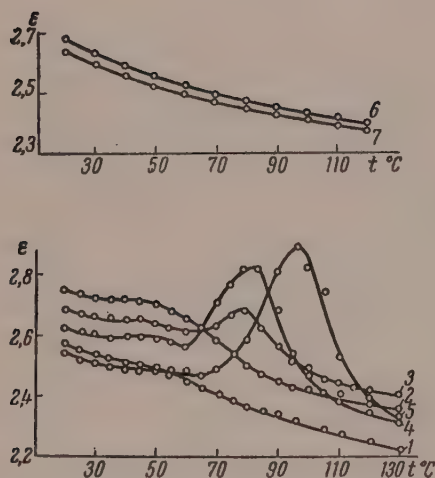


Fig. 2. Variations of DC with temperature in the system sodium phenylstearate - o-xylene (1.76 g/100 ml) containing different amounts of oleic acid: 1) without acid; 2) 0.1 ml; 3) 0.2 ml; 4) 0.3 ml; 5) 0.5 ml; 6) 3.0 ml; 7) 5.0 ml; frequency 10 kilocycles/second.

The design of the liquid condenser is shown in Fig. 1; this was equipped with removable electrodes, so that cleaning was considerably easier. The initial capacity of the condenser was $27.9 \mu\text{mf}$. The condenser was immersed in a type N ultrathermostat filled with oil. The temperature was kept constant to within $\pm 0.1^\circ$. Determinations were performed on a standard liquid (m-xylene) to allow for the capacity of the leads and to calculate the dielectric constant. The error in the dielectric-constant determinations varied with the frequency and the magnitude of the dielectric constant, and did not exceed 1%. It must be noted that the dielectric constant (DC) is appreciably influenced by the conditions of preparation of the system: heating temperature, cooling rate, aging time, and other factors. Therefore the nature of changes of DC rather than its absolute values are more significant for comparisons of different systems.

It follows from Fig. 2 that the dielectric constant of the system without acid decreases slightly on heating to 50° . As the temperature rises, there is a change in the slope of the curve, coinciding with liquefaction of the system. Small additions of acid sharply raise the DC and cause optical activity to appear. This change in the dielectric and optical properties confirms the formation of a heterogeneous system, sodium phenylstearate - hydrocarbon, in presence of the acid. The variation of the dielectric constant with temperature for a system containing >0.1 ml of oleic acid conforms to a general law: after a small decrease, the DC passes through a maximum, which is observed both on heating and on cooling of the system. The solutions lose their optical activity as the temperature corresponding to the maximum is approached.

The fact that the dielectric constant passes through a maximum with change of temperature definitely indicates that there is a connection between the changes in hydrocarbon solutions of sodium phenylstearate containing added sodium oleate, and critical phenomena. In the critical region a two-phase equilibrium system is formed on cooling, and this is converted into a one-phase system on heating. The dielectric-constant maxima are shifted in the direction of higher temperatures with increase of oleic acid concentration (Fig. 2). This indicates an increase of the critical temperature of micelle formation. However, when the oleic acid content is increased considerably (Fig. 2, Curves 5 and 6), the maxima on the $\epsilon - t$ curves disappear, probably because true solutions are formed in this temperature range (20-

120°). It is interesting to note in this connection that the structural strength of oleocolloid systems (calcium stearate in vaseline oil) also reaches a maximum and then falls with increase of oleic acid concentration [10].

In the variations of the dielectric constant of the system with small additions of acid in the 0.4-10 kilocycles/second range, some decrease of DC with increase of frequency was observed. This effect was not observed after the maximum of the $\epsilon - t$ curve had been passed, nor was it observed over the entire temperature range studied in systems containing over 3 ml of oleic acid.

The dispersion of dielectric constant at audio frequencies is apparently due to Maxwell - Wagner polarization. This type of polarization is characteristic of heterogeneous systems with phases differing in dielectric constant and conductivity, and is observed at low frequencies. In the case of homogeneous systems there is no such polarization, and consequently no dispersion of DC at audio frequencies.

For further studies of micelle formation in hydrocarbon solutions of soap, great interest attaches to measurements of dielectric constant over a wider frequency range, and also to combined investigations of the dielectric and rheological properties of such systems.

SUMMARY

1. The temperature dependence of dielectric constants for the systems sodium phenylstearate - o-xylene and sodium phenylstearate - o-xylene - oleic acid has been studied in the 20-130° range at frequencies from 400 to 10,000 cycles/second.
2. The dielectric constant of xylene solutions of sodium phenylstearate passes through a well-defined maximum at a definite temperature and concentration in presence of oleic acid. This shows that there is a connection between transitions in lyophilic disperse systems and critical phenomena. In the critical region a two-phase colloidal system is formed on cooling, while on heating it passes into a one-phase system.
3. Small additions of oleic acid cause shifts in the maxima on the $\epsilon - t$ curves, indicating an increase in the temperature of micelle formation. At considerable concentrations of the additive no transitions take place in the system (there are no maxima on the $\epsilon - t$ curves), probably because true solutions are formed in the temperature range studied.

LITERATURE CITED

- [1] P. A. Rebinder, Summaries of Papers at the 4th All-Union Conference on Colloid Chemistry [in Russian] (Izd. AN SSSR, Moscow, 1958) p. 5.
- [2] G. V. Vinogradov, Progr. Chem. 20, 533 (1951).
- [3] A. V. Dumanskii, Colloid Science [in Russian] (ONTI, Moscow, 1935) p. 235.
- [4] V. K. Semenchenko, Proc. 3rd All-Union Conference on Colloid Chemistry [in Russian] (Izd. AN SSSR, Moscow, 1956) p. 250.
- [5] V. K. Semenchenko, J. Phys. Chem. 21, 1461 (1947); Proc. Acad. Sci. USSR 92, 625 (1953); Applications of Ultrasound to Investigations of Matter, 3 [in Russian] (1956) p. 51.
- [6] V. K. Semenchenko and M. Azimov, J. Phys. Chem. 29, 1342 (1955); 30, 1821, 2228 (1956).
- [7] C. R. Singleterry, J. Amer. Oil Chemists Soc. 32, 446, (1955).
- [8] G. J. Honing, and C. R. Singleterry, J. Phys. Chem. 58, 201, (1954); 60, 1114, (1956).
- [9] The Modern Cathode-Ray Oscillograph, part 3 [in Russian] (1954) p. 127.
- [10] E. E. Segalova and P. A. Rebinder, Colloid J. 10, 223 (1948).

Received July 16, 1958

THE COMPATIBILITY OF POLYMERS IN SOLUTION*

B. A. Dogadkin, V. N. Kuleznev, and S. F. Pryakhina

The M. V. Lomonosov Institute of Fine Chemical Technology, Moscow

The growing number of applications of mixtures of polymers in various branches of the national economy justifies the attention which has been recently devoted to theoretical and experimental studies of such systems. The extensive uses of mixtures of natural and butadiene - styrene rubbers prompted us to elucidate certain facts concerning the behavior of these polymers in a common solvent. This was all the more necessary owing to the discovery that an interpolymer of these rubbers can be used as an interlayer for cementing different rubbers in laminated articles [1].

The rubbers used in the investigation - natural rubber (NR) and butadiene - styrene rubber (BSR) made by low-temperature polymerization (type SKS-30A) - were first purified by extraction with acetone (NR) or ethanol - toluene azeotrope (BSR) in a current of nitrogen to remove impurities. To dissolve the polymers, they were shaken in the solvent containing 1% of phenyl- β -naphthylamine, calculated on the rubber. The solutions were diluted to the same concentration and then mixed in various proportions. The viscosities of the mixtures were determined 24 hours after mixing by means of the Hoeppler viscosimeter, and their light scattering at an angle of 90° was measured. The relative proportions of the rubbers at various points in systems which underwent phase separation were determined refractometrically [1] after films had been made by evaporation of the corresponding solutions. The method used for preparation of rubber mixtures containing the interpolymer was described earlier [1].

Figure 1 shows the results of viscosity determinations on benzene solutions of NR, BSR, and their mixtures of various concentrations. The experimental data were used to plot viscosity against mixture composition on the assumption that the properties of the system are additive, i.e., that there is no interaction of any kind between the polymers. As Fig. 1 shows, the "additive" curve completely coincides with the experimental for mixtures of 0.5% total rubber concentration, and deviates from it for mixtures of 1% concentration. If analogous curves are plotted for mixtures of increasing concentrations, the deviations of the experimental curves from the curves plotted on the assumption of additivity become progressively greater until a concentration is reached at which the polymers in solution separate into two phases; this is generally accepted to be the sign of incompatibility of the dissolved polymers. Deviations of experimental viscosity - composition curves from additivity are the consequence of specific interaction between the molecules of the two polymers [2]. In the present instance, because of the tendency of the system to separation, the attraction forces are greater between like than between unlike molecules. As the solution concentration increases, the number of collisions between particles in solution becomes greater, and the difference between the attraction forces between like and unlike molecules has an increasing influence on the properties of the system. Thus, the deviations of the experimental values for the viscosity of polymer mixtures from the values based on the assumption of additivity of their properties characterize interaction between unlike polymer molecules; i.e., in this instance they are a measure of their incompatibility.

Rise of temperature increases the energy of thermal motion of the molecules and of their segments, and diminishes the tendency of the system to separation, as is clear from Fig. 2. Deviation of the viscosity - composition curve from additivity decreases with increase of temperature, and vanishes almost entirely at 60° for toluene solutions.

* Paper at the 4th All-Union Conference on Colloid Chemistry, May 1958.

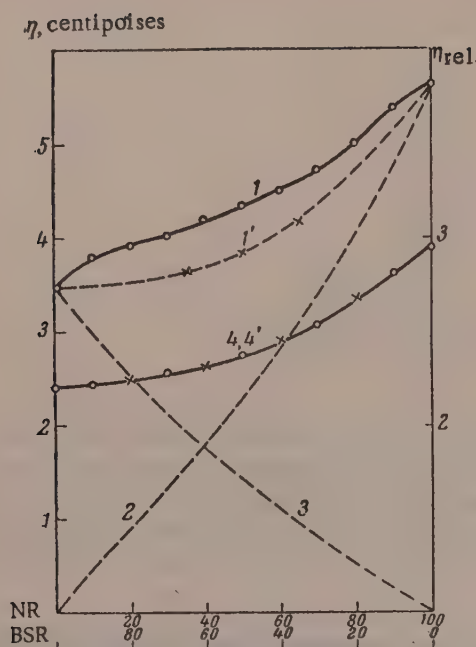


Fig. 1. Dependence of the viscosity of mixtures of benzene solutions of NR and BSR on composition: 1) viscosity of 1% solutions in centipoises; 2 and 3) variations of viscosity with concentration for NR and BSR; 4) relative viscosity of 0.5% solutions; 1', 4') the corresponding additive curves.

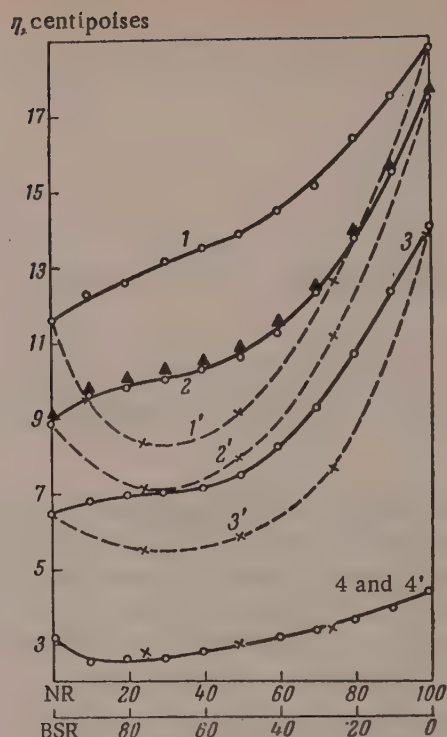


Fig. 2. Dependence of the viscosity of mixtures of 2% benzene (1, 2, 3) and toluene (4) solutions of NR and BSR on composition at various temperatures: 1) 20°; 2) 30°; 3) 50°; 4) 60°; 1', 2', 3', 4',) the corresponding additive curves; Δ) 2% solutions prepared a second time at 30°.

Voyutskii, Zaionchkovskii, and Reznikova [2] noted the great importance of the relative polarities of polymers in estimation of their compatibility, and demonstrated that small amounts of substances containing polar groups are capable of decreasing sharply the interaction between unlike polar molecules in solution, owing to shielding of groups responsible for formation of intermolecular bonds.

In view of the possible presence of a certain amount of polar (for example, oxidized) groups in NR and BSR molecules, and also of the higher polarity of BSR in comparison with NR, we studied the influence of various amounts of methanol and methyl ethyl ketone on the course of the viscosity - composition curves. Figure 3 shows, as an example, the effect of methyl ethyl ketone, with a correction for the viscosity decrease owing to dilution. A small amount (1%) of methyl ethyl ketone, which in the case of polar polymers would have produced a considerable change in the course of the viscosity - composition curve, in this instance merely lowers the curve somewhat, without causing any change in the nature of the relationship. Only if large amounts (50%) of methyl ethyl ketone are added is there a considerable change of viscosity, with convergence of the experimental and additive curves, as the result of a sharp increase in the polarity of the medium. Methanol, as a more polar substance, produces a similar effect to a greater extent.

It follows from the foregoing considerations and experimental data that signs of incompatibility appear in polymer solutions considerably before the system separates into two phases. It was reasonable to assume that these signs of incompatibility are due to the presence of microheterogeneities in solution, which grow with increase of concentration and which are nuclei of phases of different composition; if this is so, the system should have much greater turbidity than a true homogeneous solution.

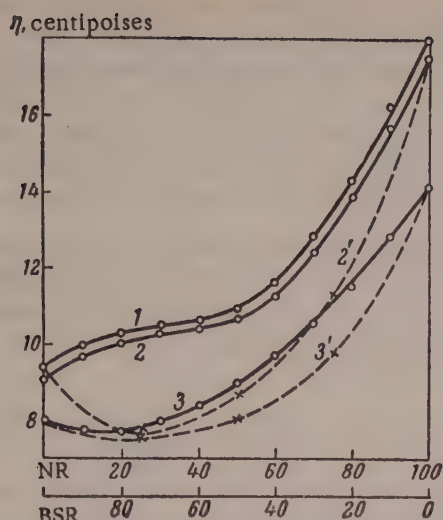


Fig. 3. Effect of methyl ethyl ketone on the viscosity of mixtures of 2% benzene solutions of NR and BSR at 30°: 1) without addition; 2) 1% of methyl ethyl ketone; 3) 50% of methyl ethyl ketone; 2' and 3') the corresponding additive curves.

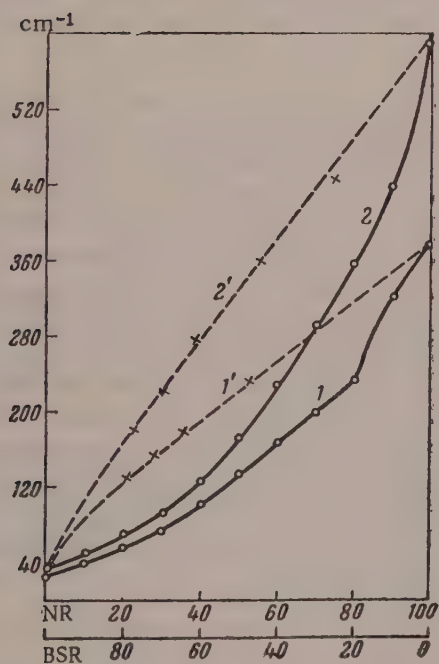


Fig. 4. Dependence of the turbidity of 2% solutions of mixtures of NR and BSR in CCl_4 on their composition: 1) after one day; 2) after one month from preparation of the solutions; 1' and 2') the corresponding additive curves.

Because the refractive indices of NR and BSR in benzene are similar, we used solutions of the rubbers in carbon tetrachloride for determinations of the turbidity τ (light scattering at an angle of 90°). The results are plotted in Fig. 4; they show that, despite the above reasoning, the experimental turbidities of the mixtures are lower than the additive values of τ for all proportions of the rubbers.

Very interesting results were also obtained in studies of phase separation in ligroin solutions of NR and BSR. The separation took place in cylindrical separating funnels, where samples could be taken from the upper and lower layers without disturbance of the interface. The total height of the mixed solutions in the funnel was 10 cm. Observations on the appearance of a boundary were continued for a month. After only two days a boundary appeared in solutions with NR:BSR ratios of 2:8, 3:7, 4:6, and 5:5; after four days a boundary appeared in the solution with a 6:4 ratio. For solutions with 7:3 and 8:2 ratios the boundary appeared after one week, and solutions with 9:1 and 1:9 ratios did not demix at all. Refractometric determinations of the rubber contents in the layers showed that the lower layers contained mainly BSR, and the upper mainly NR, although each type of layer contained about 10% of the other polymer, and 15% at NR:BSR ratios of 7:3 and 8:2.

Determinations of the concentrations in the upper part of the layer of predominant NR content (NR layer) and the lower part of the layer with predominant BSR content (BSR layer) showed that the concentrations of the NR layer at all proportions of the rubbers are lower than the concentrations of the BSR layer, and for a number of ratios the concentrations of both layers were below the original concentration (Fig. 5), although the system could by this time be regarded as being in equilibrium, as the concentrations remained constant for a considerable time (up to 1 month). A separate determination of the concentrations in the upper and lower parts of both layers showed that in a nonequilibrium system the concentration increases in a downward direction in both layers, and at the instant equilibrium is reached, the concentrations within one layer level out.

In NR, and more especially in BSR, some gel fraction is always present; this enters the solution and gives rise to some turbidity. After separation of the system both layers became quite clear, while in the BSR layer some flakes formed; these were probably remains of the gel fraction, and this could cause some decrease of the solution concentration. This kind of aggregation and floc formation in the BSR layer in systems containing rubber sol fractions probably occurs at the expense of fractions of higher molecular weight.

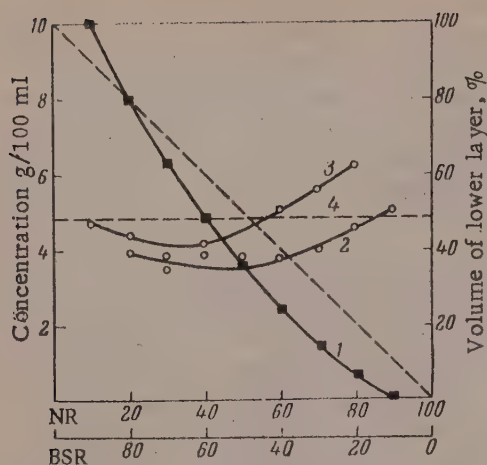


Fig. 5. Variations of concentration and volume of the layers with the composition of separated mixtures of NR and BSR solutions: 1) change in the volume of the lower layer as % of total solution volume; 2) concentration in upper layer; 3) concentration in lower layer; 4) concentrations of original solutions.

molecules, common for all condensed phases [6]. The arrangement of the molecules in a cluster must ensure maximum contact of their individual regions in order to give rise to a lattice which is sterically favorable for formation of dipole-dipole or hydrogen bonds. The force of interaction must depend on the length of the chain involved in the formation of such a lattice [7].

In a mixture of any two polymers in a common solvent, clusters are formed at a definite concentration after equilibrium has been reached; they are mainly homogeneous in composition, as this ensures the maximum close packing of the molecules, giving a gain of internal energy of the system and thereby compensating for the decrease in the entropy of mixing. Whereas in absence of a second polymer there was a definite equilibrium of aggregation-disaggregation processes and a definite ratio between the magnitudes of the intermolecular forces directed into and out of the clusters, on introduction of a second polymer the magnitude of the forces directed out of the clusters decreases; this leads both to a decrease in the number of nonassociated molecules of both polymers, and to closer packing inside the clusters themselves. The fact that the previous history of the solution has no influence on the viscosity (Fig. 2) such as is observed for the polymer pair polyvinyl chloride-butadiene nitrile copolymer [2], shows that there is no structure formation in the solution as a whole; this was to be expected at a 2% concentration of this pair of nonpolar polymers. Two or several molecules lying side by side over a definite length are evidently more rigid formations than a single molecule, and therefore the coiled clusters become more and more extended with increase of the number of molecules in them; because of the elongated shape of the clusters the viscosity of the polymer mixture is greater than the viscosity observed in absence of this tendency to formation of heterogeneous clusters. Decrease of the number of nonassociated molecules and increased packing of the clusters decrease the area of the scattering particles and therefore diminish the turbidity τ .

The clusters dissociate on increase of temperature, and the deviations of the experimental viscosity curve from additivity diminish as a result.

When a polar substance is added to a nonpolar polymer solution, the molecular coils become tighter, and the solution viscosity decreases. If the solution contains clusters, these also become more closely packed; the polymer molecules themselves occupy a smaller effective volume in solution, which is tantamount to a decrease of concentration (increase of compatibility) of the system. A significant fact is that considerable amounts of non-solvent are needed for this process. The fact that the compatibility of NR and BSR increases with addition of non-solvent to solutions of these polymers is confirmed by the results, given above, of direct determinations of the NR and BSR contents in the two layers of a separated system.

When NR and BSR separate out in a solution containing methyl ethyl ketone, more of one polymer enters the layer of the other. Thus, a 1:1 NR-BSR mixture in ligroin with 100% of methyl ethyl ketone forms two layers, with the volumes of the NR and BSR layers in 16:9 ratio; the former layer contains 35% BSR and the latter 71%, indicating that the polymer compatibility is increased in this binary solvent.

Mixtures of NR and BSR masticated in argon containing 0.1% oxygen and containing interpolymers of these rubbers do not separate out at all; this shows that the compatibility of the rubbers is increased in presence of their interpolymers.

DISCUSSION OF RESULTS

In polymer solutions at concentrations below the saturation limit there is usually a dynamic aggregation-disaggregation process involving nonpolar polymer molecules [3]; or, in the case of polar macromolecules [4], the formation of stable clusters even at very low concentrations (<0.5%). The formation of such clusters may be regarded as the first stage of gelation of the solution [5] or formation of the solid polymer phase; therefore the clusters can be expected to conform to the conditions of the closest possible packing of the

Comparison of the times required for the formation of a clear boundary in separated mixtures of NR and BSR containing different proportions of these rubbers shows that these mixtures differ in compatibility. The greatest time was required for separation of mixtures containing NR and BSR in 7:3 and 8:2 ratios; this indicates that these mixtures have a great tendency to mutual miscibility, i.e., high compatibility. It must be pointed out, however, that the concept "high compatibility" is applied here to a nonequilibrium system, although after equilibrium has been reached the amounts of one rubber in the layer of another are also greater in this case than in the other mixtures.

It should be noted that in none of the investigations of polymer compatibility in solutions was attention paid to attainment of equilibrium conditions of existence of two or more layers. In our case the appearance of a sharp boundary between the layers (after 2 days in the case of 1:1 NR - BSR mixture) was not yet a sign of equilibrium, as the concentrations in the two layers did not become constant for a month. Even the nonseparating 2% solutions of mixtures of these rubbers reach equilibrium after a certain time, showing increased values of turbidity τ one month after preparation; this indicates that breakdown of the more stable NR clusters takes place. Subsequently, the values of τ remained constant.

If two or more fragments of unlike molecules can be chemically bonded by means of interpolymerization taking place in the course of cold mastication in an inert medium [1], these molecules form looser clusters, so that conditions exist for better distribution of the molecules and separation of the system is prevented.

The foregoing observations, and the experimental results of other workers [2, 8-10] lead to a number of conclusions concerning the causes of polymer incompatibility.

If macromolecules are in contact over a considerable length of the chains, considerable interaction forces arise. Therefore, the geometric structure of the molecules, which determines the closeness of their packing in crystals, packets, or clusters, must be regarded as the principal factor determining polymer compatibility, since polarity differences [2, 10] can have an influence only on differences in the strength of bonding in such formations. Aggregation of unlike polymer molecules is relatively rare, owing to steric obstacles to contact between the appropriate groups of unlike macromolecules.

SUMMARY

1. Mixtures of 5% solutions of NR and BSR in ligroin separate into layers if the proportions of these rubbers lie between 1:9 and 9:1. The concentrations of the layers differ from the initial concentration.
2. The experimental viscosities of mixtures are higher, and turbidities lower, than the additive values for all proportions of the component rubbers.
3. Increase of temperature or addition of large amounts (50%) of methyl ethyl ketone bring the experimental and additive values of solution viscosity closer together, i.e., increase the compatibility of NR and BSR.
4. The presence of an interpolymer of the rubbers in a mixture of NR and BSR prevents separation of the solutions.
5. An explanation is put forward for the observed effects, based on the hypothesis that molecular clusters, mainly homogeneous in composition, are formed in solution.

The authors offer their deep gratitude to Professor S. S. Voyutskii for valuable comments in the course of discussion.

LITERATURE CITED

- [1] B. A. Dogadkin, V. N. Kuleznev, and Z. N. Tarasova, *Colloid J.* 20, 43 (1958).*
- [2] S. S. Voyutskii, A. D. Zaionchkovskii, and R. A. Reznikova, *Colloid J.* 18, 515 (1956).*
- [3] A. K. Doolittle, *J. Polymer Sci.* 2, 121, (1947).
- [4] N. V. Mikhailov and S. G. Zelikman, *Colloid J.* 19, 465 (1957).*
- [5] S. M. Lipatov and S. I. Meerson, *Colloid J.* 19, 390 (1957).*

*Original Russian pagination. See C.B. Translation.

- [6] V. A. Kargin, A. A. Kitaigorodskii, and G. L. Slonimskii, *Colloid J.* 19, 131 (1957).*
- [7] P. Doty, H. Wagner and S. Singer, *J. Phys. Coll. Chem.* 51, 32 (1947).
- [8] A. Dobry and F. Boyer-Kawenoki, *J. Polymer Sci.* 2, 90, (1947).
- [9] R. J. Kern and R. J. Slocum, *J. Polymer Sci.* 15, 183, (1955).
- [10] G. L. Slonimskii and N. F. Komskaia, *J. Phys. Chem.* 30, 1746 (1956).

Received May 9, 1958

*Original Russian pagination. See C.B. Translation.

RELATIONSHIP BETWEEN THE STRUCTURE OF EMULSIFIERS OF THE ALKYL ARYL SULFONATE TYPE AND POLYMERIZATION OF UNSATURATED COMPOUNDS

6. EFFECT OF SODIUM ALKYL ARYL SULFONATES ON THE POLYMERIZATION PROCESS

M. G. Zimina and N. P. Apukhtina

The S. V. Lebedev Scientific Research Institute
of Synthetic Rubber, Leningrad

Our previous communication [1] described the results of a study of certain colloidchemical properties of sodium alkyl aryl sulfonates. The effects of structure of the alkyl aryl sulfonates on the surface tension of aqueous emulsifier solutions, solubilization of α -methylstyrene, and micellar weights were studied.

Investigations were also conducted in our laboratory on the influence of the number of alkyl groups in sodium salts of individual secondary butylbenzene- and naphthalenesulfonic acids on the copolymerization of divinyl with α -methylstyrene and on solubilization of hydrocarbons [2].

The purpose of the present work was a more complete study of the relationship between colloidchemical properties of emulsifiers and the polymerization of unsaturated compounds, in relation to structural isomerism and chain length of the alkyl groups attached to the aromatic nuclei of the alkyl aryl sulfonates.

The sulfonated derivatives of butyl-, amyl-, and hexylbenzene, and of naphthalene, with different numbers of alkyl groups, synthesized and described by us earlier, were used for these investigations.

Styrene. For the experiments on bulk polymerization, the technical product was treated with 5% aqueous alkali to remove stabilizer (hydroquinone), washed with water, dried over calcium chloride, and distilled twice under vacuum in a current of nitrogen; b.p. 31-32° under 8 mm residual pressure, $n_D^{20} = 1.5451$. The second distillation was performed directly in the apparatus. The styrene content determined by the iodometric method [3] was 99.8-100%.

For emulsion polymerization, freshly distilled styrene was used after treatment with alkali solution. Its styrene content was 99.7-99.8%.

α -Methylstyrene (the technical product) was treated with 5% alkali solution to remove stabilizer, washed with water, dried over calcium chloride, and distilled. The fraction collected had b.p. 162-163°, $n_D^{20} = 1.5390$.

Divinyl (technical product). The divinyl content, determined by bromination [4], was 92%.

The catalyst — potassium persulfate (chemically pure) — contained 5.81% active oxygen [5], which corresponds to 98.2% potassium persulfate.

Emulsifiers. These were individual sodium salts of alkylbenzene and alkyl-naphthalene sulfonates, differing in the number, length, and structure of their alkyl groups. All butyl, amyl, and hexyl derivatives of benzene are denoted by the symbols BB, AB, and HB, and the corresponding naphthalene derivatives by the symbols BN, AN, and HN; the number of alkyl groups is denoted by the prefix mono, di, tri, etc. For example, sodium di(sec-amyl) benzene sulfonate is disec AB [1].

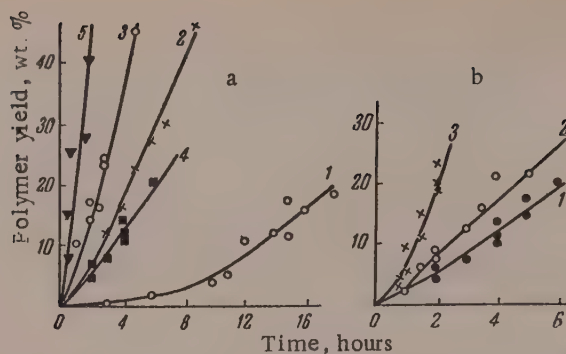


Fig. 1. Kinetics of styrene polymerization in presence of: a) secondary alkylbenzene sulfonates: 1) mono BB; 2) mono AB; 3) mono HB; 4) di BB; 5) tri BB; b) dialkylbenzene sulfonates: 1) disec BB; 2) di-n BB; 3) ditert BB.

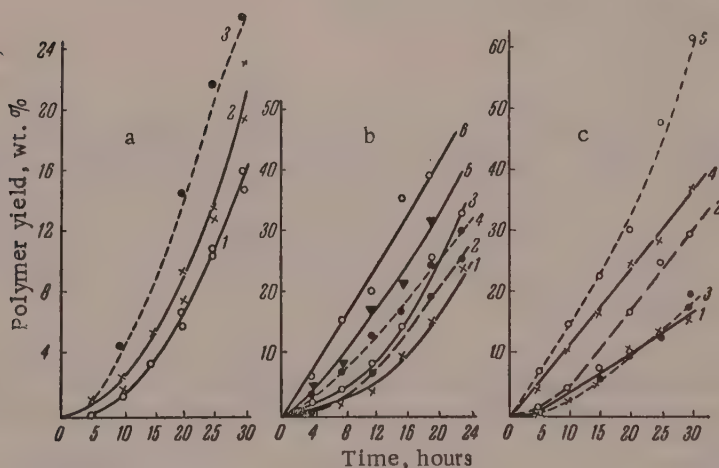


Fig. 2. Kinetics of polymerization of divinyl with α -methylstyrene in presence of: a) secondary dialkylbenzene sulfonates: 1) ditert BB; 2) disec BB; 3) di-n BB; b) secondary alkyl-naphthalene sulfonates: 1) mono BN; 2) mono AN; 3) mono HN; 4) di BN; 5) di AN; 6) di HN; c) secondary alkylbenzene sulfonates: 1) mono AB; 2) mono HB; 3) di BB; 4) di AB; 5) di HB.

Polymerization technique. The emulsion polymerization experiments were carried out in glass ampoules 50 ml in capacity; the mixtures were stirred by rotation of the ampoules in an air thermostat at 40 revolutions/minute. Before the start of polymerization, nitrogen [6] was blown through the reaction mass for 5 minutes [7]. The polystyrene latex was coagulated by means of methyl alcohol, and divinyl-methylstyrene latex by means of a solution of calcium chloride with acetic acid. The isolated polymers were washed with water, alcohol, and dried under vacuum to constant weight.

For styrene polymerization, 0.35 wt. parts of potassium persulfate, 180 wt. parts of water (per 100 wt. parts of monomer), and 0.0378 g-equivalent of emulsifier per liter were used. The polymerization temperature was 60°. For polymerization of divinyl and of divinyl-methylstyrene mixture (70:30 ratio), 0.45 wt. parts of catalyst, 100 wt. parts of water, and 0.046 g-equivalent of emulsifier per liter were used. The polymerization temperature was 50°. The bulk polymerization of styrene was effected in graduated glass ampoules with 0.01 ml divisions, sealed to the apparatus for styrene distillation. After the ampoules had been filled with styrene, nitrogen was

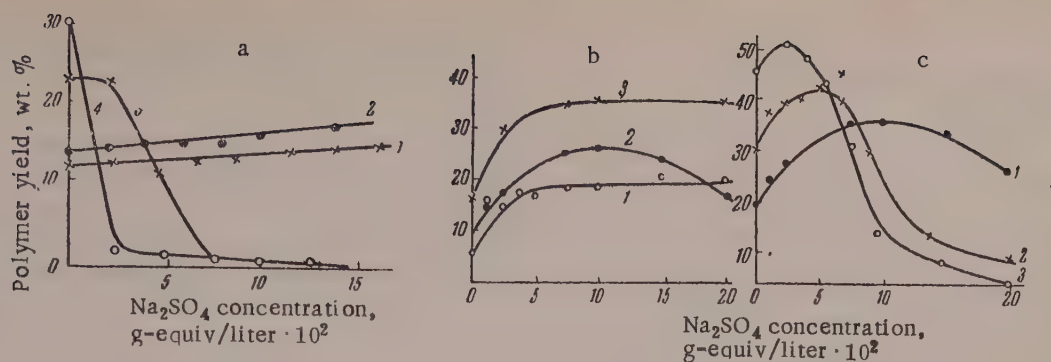


Fig. 3. Effect of Na_2SO_4 on the polymerization of divinyl with α -methylstyrene in presence of: a) secondary alkylnaphthalene sulfonates (polymerization 17 hours): 1) mono AN; 2) mono HN; 3) di AN; 4) di HN; b) alkylbenzene sulfonates (polymerization 30 hours): 1) ditert BB; 2) disec BB; 3) di-n BB; c) secondary alkylbenzene sulfonates (polymerization 25 hours): 1) di BB; 2) di AB; 3) di HB.

admitted into the vacuum system and the ampoules were sealed off in a continuous stream of nitrogen. The polymerization was performed in an oil thermostat at 100° . The volume contraction of the polymerization mixture was a measure of the course of polymerization. The yield of polystyrene was determined from the weight of polymer, precipitated by means of methyl alcohol and dried under vacuum. The molecular weights of the polymers were determined by the viscosity method; viscosities were measured at four different dilutions. The molecular weight was calculated from the formula $[\eta] = KM^a$ [8]; the chain transfer constant K_c , from the formula [9]

$$\frac{1}{p} = \frac{1}{p_0} + K_c \left(\frac{SX}{M} \right),$$

where p and p_0 are the degrees of polymerization in solution and in pure monomer, respectively; SX/M is the molecular ratio of solvent to monomer.

It was found in the emulsion polymerization of styrene in presence of alkylbenzene sulfonates with different lengths of the alkyl group attached to the aromatic ring, that the polymerization rate of styrene increases with the length of the alkyl radical in the emulsifier and with increase in the number of alkyl groups attached to the benzene ring in the emulsifier (Fig. 1).

Styrene polymerization is greatly influenced by the structure of the alkyl groups in the sulfonates studied. The highest polymerization rate is found in presence of sodium di(tert-butyl)benzene sulfonate, and the lowest in presence of the derivative with a secondary butyl group. The kinetic curves for emulsifiers with normal and secondary butyl groups are fairly similar (Fig. 1, b).

Experiments on emulsion polymerization of divinyl with α -methylstyrene showed that the polymerization rate is influenced not only by the nature and structure of the emulsifier, but also by the nature of the monomer. By their influence on the polymerization rate of the above-named monomers, the alkyl aryl sulfonates differing by the structural isomerism of their alkyl groups form a different sequence from that found for styrene polymerization. In this instance the most effective emulsifier is one with a butyl group of normal structure (di-n BB), and the least effective is the isomer with a tertiary radical (Fig. 2, a). These emulsifiers form the same sequence in relation to the emulsion polymerization of divinyl.

Increase of the length of the alkyl group and of the number of such groups attached to the aromatic ring (Fig. 2, b) has the same influence on the rate of polymerization of divinyl with α -methylstyrene as on the polymerization of styrene (Fig. 1, a, and 2, c).

It is known that electrolytes have a significant influence on the polymerization rate; the effect depends on the nature and concentration of the electrolytes and emulsifiers. We showed [2] that the polymerization rate of divinyl with α -methylstyrene increases with the number of butyl groups in the investigated series of alkyl aryl sulfonates, over a certain concentration range of strong electrolytes. In the present investigation we studied the

TABLE 1

Effect of Alkylbenzene Sulfonates on the Intrinsic Viscosity of Polystyrene

Emulsifier	$[\eta]$	Emulsifier	$[\eta]$
Monosec BB	1.36	Ditert BB	2.24
Disec BB	1.70	Monosec AB	3.15
Trisec BB	2.30	Monosec HB	3.50
Di-n BB	1.50		

influence of sodium sulfate on the polymerization of these monomers, in relation to the length and structure of the alkyl groups in the emulsifier (Fig. 3). The polymerization rate increases to some extent with increase of sodium sulfate concentration for all the mono derivatives in the naphthalene series. Addition of the electrolyte, even in small amounts (2.5-5.0 g-equiv/liter) to the diamyl and dihexyl derivatives in the naphthalene series sharply lowers the polymerization rate (Fig. 3,a). In presence of the di derivatives of the benzene series, the polymerization - sodium sulfate concentration curves pass through maxima. The maximum polymer yield is shifted to the left, i.e., occurs at lower electrolyte concentrations, with increase in the length of the alkyl chain (Fig. 3,c).

The polymerization - sodium sulfate concentration curves for divinyl with α -methylstyrene in presence of dibutyl sulfonates differing in the structural isomerism of the alkyl groups are entirely different in character (Fig. 3,b). In presence of the di(sec-butyl) derivative the monomer conversion passes through a maximum, whereas this is not found in presence of other emulsifiers, with normal or tertiary alkyl groups.

According to modern views, the influence of emulsifiers on the emulsion polymerization process is primarily associated with the colloidochemical properties of the emulsifier solutions. The principal role of the emulsifiers lies in solubilization of monomers in their micelles, and in stabilization of the monomer and latex emulsions.

We studied the solubilization of α -methylstyrene in aqueous solutions of the investigated emulsifiers, and also the micellar weights and surface tension of the latter [1]. It was found that micellar weight, solubilization, and surface activity increase with the length and the number of alkyl groups. As was shown earlier in this paper, these factors also increase the polymerization rate. The different effects of the structural isomerism of the alkyl groups in butylbenzene sulfonates on the polymerization of divinyl and divinyl - α -methylstyrene mixtures on the one hand, and on the polymerization of styrene on the other, are consistent with the differences in the solubilization of these monomers in aqueous emulsifier solutions.

The solubilization of α -methylstyrene increases with increased branching of the alkyl-group chain: solubilization was greatest in solutions of an emulsifier with a tertiary-butyl group structure, and least with the emulsifier of normal structure. Studies of the solubilization of divinyl in solutions of these emulsifiers revealed a different relationship: in this case the isomer of normal structure had the greatest effect, and the isomer with a tertiary butyl group in the alkylbenzene sulfonate had the least. These results lead to the conclusion that in presence of the same emulsifiers the nature of the monomer has the same influence both on solubilization and on the polymerization rate.

The influence of electrolytes on the polymerization rate is associated with their influence on the colloidochemical properties of emulsifier solutions. It was shown earlier [10] that the micellar weight and surface activity of emulsifiers and solubilization of monomers increase on addition of mineral salts up to a certain limit. In the same way, the effectiveness of emulsifiers in the polymerization process increases up to a certain limiting electrolyte concentration (Fig. 3,c).

Up to now it has not yet been determined whether the role of the emulsifier is confined to a purely physical influence on the polymerization mechanism or whether the emulsifier can take part in the chemical reactions involved in polymerization of the monomer. As the result of experiments on the polymerization of styrene in presence of potassium persulfate containing radioactive sulfur, Kolthoff [11] concluded that the emulsifier is not chemically involved in chain initiation, growth, or termination. Bartholome et al. [12], who studied the emulsion polymerization of styrene, state that the emulsifier molecule may take part in chain transfer.

We were also interested in the possible participation of emulsifiers in chain transfer. The effects of the number and length of the alkyl groups in alkylbenzene sulfonates and of the structural isomerism of the alkyl group on the molecular weight of polystyrene were therefore studied.

TABLE 2

Bulk Polymerization of Styrene in Presence of Alkyl Aromatic Hydrocarbons

Hydrocarbons	Polystyrene yield, wt. %	$\frac{SX}{M}$	$[\eta]$	p	$\frac{1}{p} \cdot 10^4$	$Kc \cdot 10^4$
Without hydrocarbon	9,5	—	1,90	3640,4	2,747	—
Benzene	10,5	0,1	1,80	3402,7	2,938	1,92
Monosec BB	16,8	0,098	1,58	2920,3	3,424	6,90
	10,5	0,044	1,87	3343,8	2,990	5,53
Disec BB	9,2	0,097	1,47	2641,7	3,785	10,67
	14,0	0,097	1,52	2768,0	3,612	8,92
	9,9	0,093	1,43	2552,1	3,918	12,52
Trisec BB	9,5	0,095	1,42	2534,3	2,946	12,60
	10,3	0,042	1,67	3089,0	3,237	11,70
	14,1	0,023	1,72	3219,4	3,106	15,60
Di-n BB	8,7	0,098	1,56	2845,3	3,514	7,80
	17,2	0,094	1,576	2877,0	3,476	7,75
	11,8	0,044	1,876	3343,8	2,990	5,51
Ditert BB	13,9	0,100	1,85	3541,6	2,823	1,73
	11,7	0,044	1,90	3640,4	2,747	0,0
Monosec AB	18,4	0,101	1,50	2703,0	3,699	9,43
Monosec HB	14,0	0,1	1,40	2485,4	4,024	12,76

It was found that all these factors have a considerable influence on the intrinsic viscosity of solutions of polystyrene made by emulsion polymerization (Table 1).

In the series of isomeric emulsifiers containing the butyl group, the di(tert-butyl) benzene derivative resulted in the highest viscosity of the polystyrene solutions, and the isomer with a butyl group of normal structure gave the lowest viscosity. The intrinsic viscosity of polystyrene prepared in presence of sodium di(sec-butyl) benzene sulfonate (di BB) is close to that of the polystyrene prepared with the aid of the isomer with a normal butyl-group structure (di-n BB). It follows that the molecular weight of the polymer increases with increased branching of the alkyl chain in the emulsifier.

It was shown in an investigation of the number of alkyl groups attached to the benzene ring in the emulsifier on the molecular weight of polystyrene that the intrinsic viscosity increases in the series from the mono- to the tributyl sulfonate (tri BB) (Table 1).

In our opinion the molecular weight of polystyrenes made with the use of different emulsifiers (Table 1) is influenced primarily by the micellar weight of the latter [1].

For example, the micellar weight of tri BB is considerably greater than the micellar weight of mono BB. Since all the polymerization experiments were performed at the same molar concentrations of the emulsifiers, in the case of tri BB there are roughly 9 times fewer micelles than in the case of mono BB; we may suppose that much less catalyst would enter the micelles, and the molecular weight of the polymer should be higher.

Studies of polymerization in presence of isomeric dibutylbenzene sulfonates also illustrate the influence of the micellar weight of the emulsifiers on the intrinsic viscosity of polystyrene solutions. The lowest micellar weight of the emulsifier and the lowest intrinsic viscosity of polystyrene solutions correspond to the isomer with butyl groups of normal structure (di-n BB). Approximately the same micellar weights were found for isomers with secondary (disec BB) and tertiary (ditert BB) butyl groups, although the intrinsic viscosity of polystyrene prepared in presence of ditert BB was considerably higher than that of the polymer made with the use of disec BB. In our opinion, this difference of molecular weight could be correlated with the influence of the emulsifier on chain transfer. It may be supposed that the lower viscosity of the polystyrene formed in presence of the isomer with a secondary butyl-group structure (disec BB), and also of di-n BB, is the consequence of termination of the growing

polymer chain as the result of a reaction with the emulsifier through an active α hydrogen atom. The isomer with a tertiary butyl-group structure (ditert BB) does not have such active α hydrogen atoms.

To verify the influence of the organic part of the studied emulsifier on chain transfer, we studied thermal polymerization of styrene in presence of the alkylbenzenes (Table 2) used for preparation of the emulsifiers.

The data in Table 2 lead to the conclusion that structural isomerism of the alkyl group has the greatest influence on the molecular weight, and therefore on the chain transfer constant.

The largest transfer constant is found with disec BB; the constant is somewhat smaller with the isomer of normal structure, while in the polymerization of styrene in presence of ditert BB, the chain transfer constant is of the same order as with benzene. This difference between the transfer constants should probably be attributed to the absence of active α hydrogen atoms in the tertiary isomer. Thus, the results of thermal polymerization in presence of solvents agree with the results of emulsion polymerization of styrene (Table 1) with regard to the influence of the hydrocarbon part of the emulsifier on the molecular weight of the polymer.

The influence of the number of alkyl groups and of the length of the alkyl chain attached to the benzene nucleus on the molecular weight of the thermal polymer is less appreciable (Table 2). However, there is a tendency for the chain transfer constant to increase with increase of the number and length of the alkyl groups.

Therefore, consideration of the role of emulsifiers in the polymerization process leads to the conclusion that, in agreement with modern views on the mechanism of emulsion polymerization, the colloidchemical properties of emulsifiers (solubilization, critical micelle concentration, micellar weight) are of primary significance. However, the experimental data suggest that the emulsifier is also involved in chemical reactions taking place in the polymerization process; in particular, chain transfer.

SUMMARY

1. The rates of emulsion polymerization of styrene and of a mixture of divinyl with α -methylstyrene increase with the length and the number of the alkyl groups in alkyl aryl sulfonates.

2. Structural isomerism of the alkyl groups attached to the aromatic nucleus in the emulsifier influences the polymerization rate of unsaturated compounds: in the polymerization of styrene in presence of a series of isomeric dibutylbenzene sulfonates, the most effective emulsifier is the isomer with a tertiary butyl group, and the least effective is the isomer with a secondary structure. The influence of the structural isomerism of these emulsifiers depends, in its turn, on the nature of the monomer: the emulsifiers form a different sequence in the polymerization of divinyl and of a mixture of divinyl with α -methylstyrene. The differences in the influence of isomerism of the butyl groups in alkylbenzene sulfonates on the polymerization rates of different monomers are in good agreement with differences in the solubilization of these monomers.

3. Emulsifier structure influences the molecular weight of polystyrene. The molecular weight of polystyrene prepared in presence of isomeric dibutylbenzene sulfonates increases with increased branching of the alkyl groups. The polymer of highest intrinsic viscosity in solution was obtained in presence of the isomer with a tertiary butyl-group structure, and the lowest in presence of the isomer of normal structure. The molecular weight increases with the number of alkyl groups and with increase in the length of the alkyl group.

4. Styrene was thermally polymerized in presence of alkyl aromatic hydrocarbons used for the preparation of the emulsifiers studied; the molecular weights of the polystyrenes were determined, and the chain transfer constants were calculated. With the use of isomeric dibutyl derivatives the largest transfer constant was found with the di(sec-butyl) derivative, and the smallest with the tertiary isomer. The chain transfer constants increase with increase in the length and number of alkyl groups.

5. It is suggested that the role of the emulsifier in the mechanism of emulsion polymerization is not only associated with colloidchemical factors, but that the emulsifier is also involved in chemical changes, including chain transfer.

In conclusion, the authors thank Professor B. A. Dolgoplosk for valuable advice in the course of this investigation.

LITERATURE CITED

- [1] M. G. Zimina and N. P. Apukhtina, *Colloid J.* 21, 50 (1959).*
- [2] N. P. Apukhtina and A. M. Lyagalova, *Colloid J.* 17, 338 (1955);* 17, 416 (1955).*
- [3] H. Meyer, *Analysis and Structure Determination of Organic Compounds* (ONTI, Leningrad, 1937) p. 212. [Russian translation].
- [4] A. I. Gulyaeva, V. R. Polikarpova, and Z. K. Remiz, *Analysis of the Products in the Production of Divinyl from Ethyl Alcohol by the S. V. Lebedev Process* [in Russian] (Goskhimizdat, 1950).
- [5] T. N. Kasterina and M. A. Itkina, *Collected Papers on Synthetic Resins and Plastics* [in Russian] (Goskhimizdat, 1947).
- [6] Yu. V. Karyakin and I. I. Angelov, *Pure Chemical Reagents* [in Russian] (Goskhimizdat, 1955) p. 14.
- [7] J. M. Kolthoff, and W. Dall, *J. Amer. Chem. Soc.* 69, 441, (1947).
- [8] Frank, and R. Mayo, *J. Amer. Chem. Soc.* 65, 2324 (1943).
- [9] R. A. Gregg, Frank, and R. Mayo, *Discussion of the Farad. Soc.*, No. 2, 328, (1947).
- [10] A. I. Yurzenko and R. V. Kucher, *Colloid J.* 17, 442 (1953).*
- [11] J. M. Kolthoff, R. P. O'Connor, and I. L. Hansen, *J. Polymer Sci.* 15, No. 80, 459 (1955).
- [12] E. Bartholome, H. Gerrens, R. Heibeck and H. M. Weitz, *Z. Elektrochem.* 60, No. 3, 334 (1956).

Received May 22, 1957

*Original Russian pagination. See C.B. Translation.

DETERMINATION OF THE ACTIVITY OF SODIUM IONS IN DISPERSE SYSTEMS

N. A. Komarova and P. A. Kryukov

The V. V. Dokuchaev Soil Institute, Academy of
Sciences USSR, Moscow

Determinations of the activities of different ions are of great interest in many branches of science. In pedology and agricultural chemistry, in many cases, it is extremely important to take into account the dissociated active portion of an element rather than its total content. This applies to determinations of the degree of dissociation of sorbed cations, changes of ion activity in coagulation and peptization processes, relationships between the activities of ions and the mechanism of their entry into plants and between the activities of ions in humid soil, soil solution, and plant sap, changes of ion activities during application of fertilizers, the influence of accompanying anions on cation activities, and a number of other problems.

Wide use is made in soil investigations of determinations of hydrogen-ion activity (pH); the most universal method for its determination is the potentiometric method based on emf determinations of a cell in which the indicator electrode is a glass electrode which, like a reversible metal electrode, can respond to changes of hydrogen-ion concentration in solution. However, a glass electrode may, in accordance with the chemical composition of the glass and the experimental conditions, be reversible not only with respect to hydrogen ions but also to other ions, including sodium ions.

Shul'ts [1] has demonstrated that glass electrodes made from aluminum borosilicate glasses have a sodium function. This question has been developed further [2-4].

The existence of a sodium function in glass electrodes implies that when such an electrode is immersed in a solution containing sodium ions a potential difference depending on the concentration of sodium ions in solution arises in the circuit. In accordance with the operating conditions of the glass electrode, the measured potential difference is the resultant of the potential differences arising at the following boundaries: 1) between the glass membrane and the test solution, and 2) between the membrane and the solution inside the electrode. Since the solution inside the electrode has constant concentration, the potential difference arising at the boundary between this solution and the glass membrane must also be constant, and the measured emf depends on the activity of sodium ions in the test solution. In this case the glass electrode acts as a sodium electrode, reversible with respect to sodium ions.

The necessary requirements for determination of sodium-ion activity are 1) electrodes with a stable sodium function over a definite and not too narrow concentration range; 2) a potentiometric apparatus for measurement of the electrode readings with the necessary accuracy and reliability.

Certain aluminosilicate and borosilicate glasses with different contents of Na_2O , B_2O_3 , Al_2O_3 and SiO_2 are used as electrode glasses with a sodium function. There is a definite relationship between the contents of these components and the electrode properties of the glass; in particular, with a high total content of boron and aluminum oxides, the electrode can act as a sodium electrode over a wide range of pH. If the total content of boron and aluminum oxides is 14%, the electrodes retain their sodium function in neutral and even in acid solutions. Increase of the sodium oxide content and decrease of the silica content in the glass involves a decrease of electrode resistance, while replacement of part of the boron oxide by alumina protects the glass against loss of chemical resistance. Compositions of glasses with a sodium function are given in Table 1.

TABLE 1

Characteristics of Glasses with a Sodium Function

Code mark of glass	Contents of oxides, molar %					Resistance, megohms
	Na ₂ O	B ₂ O ₃	Al ₂ O ₃	CaO	SiO ₂	
Da	11.0	11.0	3.0	—	75.0	~ 500
Di	24.0	—	11.0	3.0	61.5	~ 500
No. 11	25.0	11.0	3.0	—	61.0	~ 2
No. 13	25.0	9.0	5.0	—	61.0	~ 2

TABLE 2

Potentials of Different Electrodes in mv

NaCl concentration, N	Electrodes of Da glass			Electrodes of Di glass			Electrodes of No. 13 glass		
	I	II	III	I	II	III	I	II	III
0,0001	-113,5	-114,7	-109,5	-113,9	-119,5	-112,0	-116,5	-122,2	-121,0
0,001	-60,0	-66,1	-67,0	-73,6	-67,2	-69,5	-64,7	-70,0	-71,7
0,01	-4,0	-11,5	-9,8	-16,5	-13,8	-14,7	-12,0	-17,5	-18,2
0,10	+53,2	+43,8	+43,6	+40,4	-39,5	-39,4	+43,5	+37,7	+39,6
1,0	+113,1	+99,6	+101,5	+98,2	+95,0	+96,2	+104,0	+95,0	+101,0

TABLE 3

Variations of the Potential of Electrode From Glass No. 13 with Time

NaCl solution, N	emf, mv					
	2/11	3/6	3/27	4/19	5/22	8/7
0,0001	-109,0	-112,5	-111,7	-117,2	-117,7	-115,0
0,001	-68,0	-73,0	-73,0	-75,5	-75,1	-73,3
0,01	-20,5	-23,0	-20,5	-23,0	-22,2	-19,0
0,05	+22,0	+17,5	+18,2	+19,7	—	—
0,1	+38,5	+36,0	+34,7	—	+35,5	+39,0
1,0	+103,0	+96,5	+98,0	+98,0	+94,5	+102,2

The electrodes used were in the form of tubes 10-11 cm long. Each tube terminated in a small, fairly strong spherical bulb 8-10 mm in diameter; this was the active electrode surface. The electrodes were either made entirely from the electrode glass or, if little glass was available, fused electrodes were used with only the bulbs made of the electrode glass. The electrodes were filled with 0.1 N sodium chloride solution. To establish a stable sodium function, the prepared electrodes were first kept for 7-10 days in 0.1 N sodium chloride solution; they were placed in this solution after the experiments and permanently kept in it. If solutions of higher NaCl concentration are used for storage of the electrodes, the potential is established more rapidly; with less concentrated solutions it is established more slowly. Therefore the concentration of the solution used for storage of the electrodes may be increased if this is required by the experimental conditions.

TABLE 4

Effects of Nature and Concentration of the Anion on the Electrode Potential

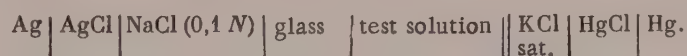
Solution concentration, N	emf, mv				
	NaCl	NaNO ₃	NaHCO ₃	Na ₂ CO ₃	Na ₂ SO ₄
0,0001	-116,2	-110,1	-114,8	-108,5	-118,3
0,0005	-88,8	-76,4	-82,4	-	-
0,001	-70,6	-65,4	-67,7	-66,0	-72,6
0,005	-35,0	-28,8	-32,2	-33,4	-32,4
0,01	-16,3	-14,1	-15,0	-13,8	-18,3
0,05	+18,1	+22,0	+18,4	+19,4	+22,4
0,10	+38,1	+36,9	+37,6	+39,8	34,7
0,50	+76,0	+78,0	+77,3	+80,1	+77,2

TABLE 5

Potential of a Glass Sodium Electrode in Different Solutions of Sodium Salts

Solution composition	Salt proportions	Electrode readings, mv	pH
0,1N NaCl + 0,1N Na ₂ SO ₄	1 : 1	+42,2	6,41
0,1N NaCl + 0,1N NaHCO ₃	1 : 1	+41,8	8,55
0,1N NaCl + 0,1N NaNO ₃	1 : 1	+43,1	6,60
0,1N NaCl + 0,1N Na ₂ SO ₄ + 0,1N NaHCO ₃	1 : 1 : 1	+42,6	8,52
0,1N NaCl + 0,1N Na ₂ SO ₄ + 0,1N NaHCO ₃ + 0,1N NaNO ₃	1 : 1 : 1 : 1	+43,2	8,37

The sodium-ion activity was determined by measurements of the e.m.f. in the following cell:



The experiments are conducted by means of a potentiometric apparatus operating on the compensation principle, with a tube amplifier containing the IP-1E electrometric tube of Russian manufacture. The amplifier was mounted in the body of the stand which carried the holders for a calomel half cell and the glass electrode. The cell used for the measurements was electrostatically shielded. The leads, especially the lead to the glass electrode, were thoroughly insulated. The purpose of all this was to avoid the effects of various kinds of electrical interference on the instrument readings and to ensure reproducible and more accurate results. The null instrument was a mirror galvanometer type MKIP with a sensitivity of $3.6 \cdot 10^{-9}$ amp/mm, connected in the anode circuit of the tube. The emf measurements were accurate to ± 0.2 mv. Galvanometer readings were taken 5 minutes after immersion of the electrode into the solution and continued until the emf became constant.

The sodium-function region of the electrodes was investigated with sodium chloride solutions varying in concentration from 1.0 to 0.0001 N at 18-20°. The experimental results show that most of the tested electrodes have a stable sodium function in the concentration range from 1.0 to 0.001 N. Some electrodes had a sodium function over a wider range of concentrations, giving satisfactory results even in 0.0001 N solutions. The potentials of glass electrodes in NaCl solutions of different concentrations are given in Table 2. A total of 65 electrodes were tested, of which 34 gave satisfactory results, while 31 were rejected as having no sodium function, or having it only a very narrow concentration range. The existence of a sodium function in the glass electrodes, which is also the criterion of their satisfactory performance, was determined from the electrode potentials plotted in emf (abscissa) - pNa (ordinate) coordinates; the linear relationship so obtained and the slope of the line were close to the theoretical.

TABLE 6

Sodium-Ion Activities in Sodium Humate Solutions

Sodium humate from sierozem			Sodium humate from chernozem		
dilution	Na ⁺ concentration, meq		dilution	Na ⁺ concentration, meq	
	flame photometry	glass electrode		flame photometry	glass electrode
Undiluted	0.82	0.80	Undiluted	2.13	1.69
1:2	0.89	0.84	1:2	2.26	1.95
1:5	0.95	0.96	1:5	2.40	2.27
1:10	1.30	1.30	1:10	2.87	2.67
1:20	1.82	1.82	1:20	3.13	2.94

TABLE 7

Sodium-Ion Activities in Soils and in Isolated Soil Solutions

Soil	Sampling depth, cm	pNa		Na ⁺ activity, meq/liter	
		in moist soil	in isolated solution	in moist soil	in isolated solution
Solonetz, R. 73	0—20	1.84	1.91	14.4	12.3
	20—40	1.74	1.78	18.2	16.6
	40—60	1.55	1.56	28.1	27.5
	180—200	1.05	1.05	89.1	89.1
Solonetz, R.112	0—20	1.68	1.68	20.8	20.8
	20—40	1.66	1.66	21.8	21.8
	40—60	1.65	1.66	22.3	21.8
	100—120	1.36	1.38	43.6	41.6
Solonetz, R.D-2	0—20	1.57	1.59	26.9	25.7
	20—40	1.60	1.60	25.1	25.1
	40—60	1.80	1.84	15.8	14.4
	140—160	1.0	1.0	100.0	100.0

For more complete characterization of the glass sodium electrodes, special experiments were performed to study their behavior in time, and their reversibility in determinations of cell emf with solutions of decreasing and increasing sodium-ion contents.

It follows from Table 3 that the electrode of No. 13 glass, less resistant chemically than Da and Di glasses, had a satisfactorily stable potential for a fairly long time. This makes work considerably easier, as the same electrode may be used with confidence for a long time. Moreover, the experiments showed that the electrodes made of the four investigated glasses operated equally satisfactorily in determinations on solutions both of increasing and of decreasing concentrations. This makes it possible to use the electrodes with solutions of different concentrations without the need for any particular sequence.

To determine the influence of the nature and concentration of the anion on the behavior of a glass sodium electrode, emf was determined in solutions of various sodium salts of different concentrations. Table 4 contains the results of sodium-ion activity determinations in solutions of NaNO₃, NaCl, NaHCO₃, Na₂CO₃, Na₂SO₄.

It is clear from Tables 4 and 5 that the nature of the anion has no specific influence on the sodium function of the glass electrode, while concentration variations result in changes of the electrode readings indicating its reversibility with respect to sodium ions present in solution. The activity coefficients of Na⁺ in solutions of the investigated sodium salts are evidently similar or equal over a fairly wide range of concentrations, from 0.5 to 0.0001 N.

For the use of glass sodium electrodes in soil investigations it is very important to have information on behavior of the electrodes in solutions containing humic acids. Sodium-ion activity was therefore determined in a solution of sodium humate isolated from sierozem. The humate solution was previously dialyzed through a cellophane membrane and filtered through a Chamberland candle. The sodium-ion activity of the resultant solution was determined by means of the glass electrode, and the concentration was determined by flame photometry. In addition, four more solutions were prepared by two-, five-, ten-, and twentyfold dilution of the original solution, and their sodium-ion activities and concentrations were also determined. The sodium-ion activities were calculated by means of calibration graphs in which the electromotive force, in millivolts, was taken along the abscissa axis and the negative logarithms of the activity along the ordinate axis. The electrode was calibrated against NaCl solutions of known concentration, taken as standard, for which the sodium-ion activity was calculated from the concentration and the activity coefficient (γ). The literature contains no data on the activity coefficient of the sodium ion separately, but there are average values of ion activities in NaCl solutions. It is therefore assumed, when the cell emf is plotted against the negative logarithm of the Na^+ activity that the activity coefficient of Na^+ in standard NaCl solutions is equal to the activity coefficient of NaCl:

$$\gamma_{\text{Na}^+} = \gamma_{\text{Cl}^-} = \gamma_{\pm\text{NaCl}}.$$

Our results show that the sodium concentration determined by flame photometry in the original solution and the solution after twofold dilution is somewhat higher than the activity as determined by the sodium glass electrode. There is some increase in the amount of sodium in solution as the result of dilution; this is indicated by both methods simultaneously (Table 6).

In view of the fact that the original Na humate solution obtained from sierozem had a low Na concentration, to confirm the observed effect we used a Na humate solution prepared as before, but from chernozem soil, and containing about twice as much Na. Four more solutions were made from it by dilution.

Table 6 shows that the amount of Na in solution increases with dilution. Moreover, there is a more pronounced difference between the amount of Na determined by flame photometry and the active Na found by means of the glass Na electrode for all solutions, and especially in the original—the most concentrated solution.

Direct determinations of Na^+ activity in moist soils and in solutions isolated from them are of considerable interest in soil science.

We determined Na^+ activities in moist soils (water: soil ratio = 1:2) and in the solutions isolated from them. Samples of solonetz soils from the Arshan'-Zel'men territory (Sarpinskii province of the Kalmyk ASSR) were studied. For most of the samples taken, equal values of Na^+ were found in the moist soil and in the isolated solutions (Table 7). In some instances there is a small difference, 0.2-0.3 pNa units, between the values for the moist samples and for the isolated solutions, the Na^+ activity being higher in the soils than in the solutions isolated from them.

When the glass sodium electrode is used for determinations of sodium concentrations in solutions and suspensions, for plotting of the calibration curve, concentrations instead of activities are taken along the ordinate axis, while emf values are taken along the abscissa axis. This construction, which assumes that activities and concentrations are equal, is permissible for dilute solutions and for approximate determinations of Na^+ concentration.

SUMMARY

1. The behavior of glass electrodes, made from aluminosilicate and borosilicate glasses, in solutions of sodium salts was studied in order to find the conditions of their applicability to determination of sodium-ion activities.

2. The investigated glass electrodes have a sodium function, and can therefore be used for determination of sodium-ion activities in soil solutions, suspensions, and moist soils.

This work was carried out under the guidance of I. N. Antipov-Karataev, to whom the authors are deeply grateful.

LITERATURE CITED

[1] M. M. Shul'ts, Sci. Mem. Leningrad Univ., Chem. Sci. Ser., No. 13, 80 (1953); M. M. Shul'ts and T. M. Ovchinnikova, J. Leningrad Univ. No. 2 (1954); M. M. Shul'ts and L. G. Aio, *ibid*, No. 8 (1955).

[2] P. A. Kryukov, M. M. Shul'ts, and V. É. Goremykin, Hydrochem. Materials 24, 23 (1955); V. É. Goremykin, *ibid*, 26, 23 (1957); V. É. Goremykin and P. A. Kryukov, Bull. Acad. Sci. USSR, Div. Chem. Sci. No. 11 (1957).*

[3] N. O. Avakyan, Bull. Acad. Sci. Armenian SSR, Biol. and Agric. Sci. 7, No. 4, 69 (1954).

[4] N. G. Zyrin and D. S. Orlov, Bull. Moscow Univ. Biol., Pedol., Geol., Geogr. Series, No. 1, 71 (1956).

Received January 16, 1959

* See C.B. Translation.

ADSORPTION OF ALIPHATIC AMINES ON BENTONITE FROM AQUEOUS SOLUTIONS

O. D. Kurilenko and R. V. Mikhalyuk

The Kiev Technological Institute of the Food Industry

Bentonite has an unbalanced crystal structure and may be classified as a colloidal electrolyte. From the point of view of its chemical composition and structure, bentonite may be considered as an aggregate of laminar molecules of an inorganic polymer capable of swelling. The laminar bentonite molecule consists of numerous unit cells. Each cell has a negative charge as the result of isomorphous replacement of Al^{3+} by Mg^{2+} and Si^{4+} by Al^{3+} in the atomic lattice. The negative charge of such a cell is balanced by means of cations, usually known as exchange cations. Thus, the bentonite anion of colloidal size is bound to cations adsorbed on it from the dispersion medium.

It has long been known that various organic cations form stable complexes with bentonites [1]. The stability of these complexes increases because cations are adsorbed on the surface of montmorillonite not only electrostatically, but also by means of van der Waals forces [2]. The practical importance of organic bentonite complexes is very great. The potentialities in the production of bentonite derivatives having a number of new properties, necessary and useful for practical purposes, cannot be overestimated. For example, it is possible to prepare bentonite derivatives with specific adsorptive capacities or catalytic activities. Organophilic bentonites can be used as active fillers in plastics and rubbers, and as thickeners in greases.

However, despite the fact that many authors have noted the specific interaction of bentonite with organic cations, the number of publications dealing with quantitative aspects of the formation of organic complexes of bentonite is rather small. Work on theoretical aspects of the production of organophilic bentonites is also backward. For these reasons quantitative investigations of the mechanism of reactions between bentonites and organic substances are of extreme topical importance.

The purpose of our work was to study adsorption of higher aliphatic amines on bentonites, in quantities several times greater than the exchange capacities of the latter.

A 2% aqueous suspension of askangel was prepared for the investigation; this material is a highly disperse, strongly swelling sodium bentonite with a cation-exchange capacity of 80 meq/g [3]. The suspension was left to settle for three days at room temperature; the nonclay sediment was then separated off, and the suspension, containing the fine fractions, was evaporated on the water bath.

The amines were previously converted into the chlorides or acetates by addition of equivalent amounts of the corresponding acids, and then dissolved in water. When dilute aqueous solutions of amine salts were added to bentonite suspensions, flocculation took place very rapidly; after thorough stirring of the suspension the precipitate was filtered off, washed with water to remove inorganic salts, and dried under vacuum (10^{-2} mm) at 65° for 12 hours. A part of the flocculated suspension was centrifuged, and the surface tension of the centrifugate determined by the method of maximum bubble pressure. The equilibrium concentration of the amine remaining in the liquid phase was estimated from the surface tension of the centrifugate, and the precipitate was analyzed for nitrogen content by the micro-Kjeldahl method.

The interaction of bentonite with solutions of amine salts was studied over a wide range of concentrations. It is clear from Fig. 1 that up to a certain concentration the adsorption of trimethyloctadecylammonium chloride proceeds irreversibly.

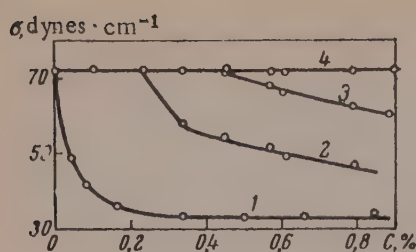


Fig. 1. Variations of surface tension (σ) of aqueous trimethyloctadecylammonium chloride solutions with concentration: 1) pure solution; 2) after addition of 0.5 g of askangel; 3) the same, 1 g of askangel; 4) the same, 2 g of askangel.

It follows from a comparison of the isotherms in Fig. 2 that aliphatic ammonium compounds with large cations are adsorbed in greater amounts. This is consistent with the fact that the attraction force between a molecule and a surface increases with the size of the molecule in inverse proportion to the cube of the distance between the center of the molecule and the surface. As a result, the molecules lie flat on the bentonite surface [4]. It was shown by Grim [5], and even earlier by Gieseking [1], that the amount of inorganic cations passing into solution in exchange reactions of organic cations with bentonites corresponds to the exchange capacity of the latter.

The considerably greater adsorption of the amine on Na bentonite as compared with Ca bentonite (Fig. 2) is partly due to the fact that the former is much more dispersible in water than the latter.

Mering [6] considered the dispersion of individual layers of montmorillonite crystallites in dilute aqueous suspensions and found that for Ca and H montmorillonites, base reflections are observed in the x-ray patterns even if large amounts of water are present. There are several signs that Na montmorillonite is dispersed down to the individual silicate layers. Mering found that the interplanar spacing of 20 kx found for Na montmorillonite in the moist state gradually vanishes as the amount of water is further increased. This effect might be attributed to instability and complete dispersion on the sheets at high water contents. However, Mering did not reach this conclusion but considered that the diffuse character of the reflections is rather the consequence of bending of the layers.

Schofield's [7] calculations based on Mattson's data on Na montmorillonite showed that the surface areas of the particles correspond to a particle thickness of 18 kx, i.e., to almost complete dispersion of the substance. Shaw [8] also interpreted electron micrographs of Na montmorillonite as evidence in favor of complete separation of the layers.

Bradley and Grim [9] concluded that Na bentonite is dispersed down to the individual silicate layers, whereas in Ca bentonite apparently a low degree of order is retained between small groups of several neighboring layers. The same number of disperse particles is obtained from 1 g of sodium bentonite as from 3 to 4 g of Ca subbentonite.

Therefore differences in the dispersity of sodium and calcium bentonites may be among the possible factors influencing the degree of adsorption of surface-active substances on montmorillonite. Another possible factor is the difference between the strength of bonding of Na and Ca ions with the montmorillonite surface; i.e., the possibility that the organic cations are exchanged more easily with Na^+ than with Ca^{2+} .

As already stated, when dilute aqueous solutions of amine salts were added to diluted bentonite suspensions, rapid flocculation took place. In the amine concentration range from 75 to 125 meq per 100 g of bentonite, the flocculated clay had the maximum sedimentation volume. The amounts of amine adsorbed (determined by the Kjeldahl method and found from surface tension determinations) in this concentration range indicated that the amines were completely bound by the bentonite.

In measurements of the heats of wetting by water of dried precipitated amine-bentonite complexes with different amine: clay ratios, it was found that the hydrophily minimum is in the same concentration range (80-120 meq) (Fig. 3).

All the foregoing is consistent with yet another property, discovered by Jordan [10] in his work on aminated bentonites. He found that the viscosity of an aqueous bentonite suspension varies with the amount of amine added, the maximum viscosity being found when the cation-exchange capacity of the bentonite is fully saturated. Thus, the minimum hydrophily found by us indicates the optimum conditions under which the most hydrophobic aminated bentonites are obtained. It seems likely that up to the concentration corresponding to the hydrophily minimum, adsorption of amines proceeds by an ion-exchange mechanism and is more stable than the second type of adsorption, which also occurs. It is supposed that the second type of adsorption (above the cation-exchange capacity of the bentonite, occurs as the result of van der Waals attraction between the bentonite surface and the amine molecules.

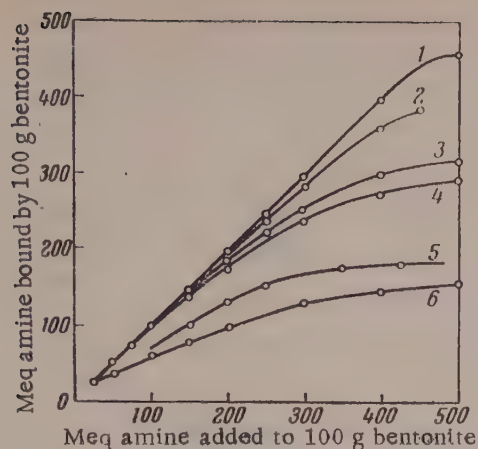


Fig. 2. Isotherms for adsorption of amines from aqueous solutions on bentonites (20°): 1) Pyzh Na bentonite and methyloctadecylamine chloride; 2) native askangel and methyloctadecylamine chloride; 3) Wyoming bentonite and dodecylamine acetate (after Grim); 4) native askangel and tridecylamine chloride; 5) Wyoming bentonite and n-butylamine acetate (after Grim); 6) Ca askangel and methyloctadecylamine chlorides.

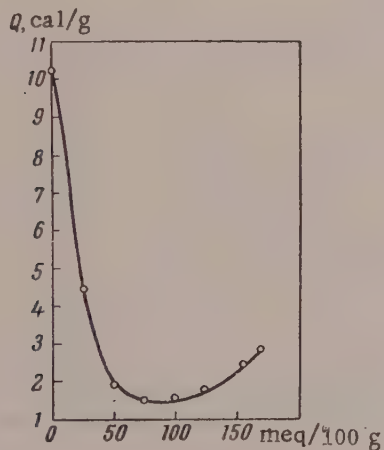


Fig. 3. Effect of different amounts of trimethyloctadecylammonium chloride bound with askangel on its heat of wetting by water.

The question arises whether the amines adsorbed in excess of the exchange capacity are held as ions or as undissociated molecules of organic electrolytes. In this connection we must first consider the state of aliphatic amine salts in aqueous solutions. Ion exchange on bentonite in solutions of inorganic electrolytes is a fairly complex effect, as a number of competing reactions occur simultaneously. This is correctly pointed out by Lewis [11]. The specific processes taking place in the interaction of bentonite with aqueous solutions of organic electrolytes are probably no simpler, and therefore there is great danger in applying the exchange laws for inorganic electrolytes to organic electrolytes.

First, it is difficult to agree with the views of a number of foreign workers (Jordan, Slabaugh, Grim and others) who, in their attempts to explain the mechanism of amine-bentonite interaction ignore the important differences between the states of lower and higher amines in aqueous solutions.

The physicochemical properties of amines dissolved in water were studied by Ralston et al. [12]; they found that whereas in aqueous solutions of lower amines a molecular mechanism applies, in the case of higher amines the possibility of micelle formation must be taken into account. Therefore the attempt of Grim and others to consider the adsorption mechanisms of, say, butylamine and octadecylamine from a common viewpoint is probably unjustified. These workers used equal solution volumes and equivalent concentrations of amines with four, twelve, and eighteen carbon atoms in the chain. However, whereas in the first case a molecularly dispersed solution may be assumed, micelle formation undoubtedly took place in the second and especially in the third case. Therefore, the latter solutions must have contained amine micelles in addition to ions and undissociated molecules.

It was noted in early publications by Rebinder and his school [13] that the hydrophobizing adsorptive action of salts of the higher fatty acids, which are very similar in their properties to amine salts, in very dilute aqueous solutions is caused mainly by the molecularly and ionically dispersed portion of the soaps. The colloidal portion of the soaps, consisting of fairly large micelles, can have only a hydrophilizing effect when adsorbed on mineral surfaces.

One cannot speak only of an ionic adsorption mechanism in relation to solutions which are known to contain micelles.

Comparison of data available in the literature with our experimental results led us to the conclusion that the following conditions are necessary for studying the interaction of bentonites with amines in an aqueous medium: 1) the bentonite should have the maximum degree of dispersion in the aqueous suspension, 2) the concentrations of higher-amine solutions must not exceed the critical concentrations of micelle formation.

It should be pointed out here that the volume critical concentration of micelle formation is very strongly influenced by the length of the hydrocarbon chain. For primary-amine acetate ions the critical concentration of micelle formation depends on the number of carbon atoms in the chain in the following manner [12]. For a chain with eighteen carbon atoms (C_{18}) the critical concentration of micelle formation is 0.0003 M; for C_{16} , 0.0008 M; for C_{14} , 0.004 M; for C_{12} , 0.013 M; for C_{10} , 0.04 M; and for C_8 it is very high.

Gaudin and Fuerstenau [14] consider that even if the volume concentration of a given amine is below the critical concentration of micelle formation, the concentration in the (Stern) double layer is higher, and micelles are adsorbed on the bentonite surface.

SUMMARY

1. Two types of amine adsorption on bentonite have been established — irreversible ionic and reversible physical.
2. The adsorption of amines on Na bentonite is several times as great as on Ca bentonite. An explanation is put forward for this effect.
3. Measurements of heats of wetting showed that inversion of the hydrophilic surface of bentonite takes place in the region of total saturation of its exchange capacity by the amine cations.
4. A mechanism for the adsorption of amines on bentonite in an aqueous medium is postulated on the basis of a number of the properties studied.

LITERATURE CITED

- [1] J. E. Giesekeing, *Soil. Sci.* 47, 1, (1939).
- [2] S. B. Hendricks, *J. Phys. Chem.* 46, 65, (1941).
- [3] F. D. Ovcharenko, Doctorate Dissertation [in Russian] (Kiev, 1955).
- [4] R. Grim, *Mineralogy of Clays* (IL, Moscow, 1956) [Russian translation].
- [5] R. E. Grim, W. H. Allaway and F. L. Cuthbert, *J. Amer. Ceram. Soc.* 30, 137, (1947).
- [6] J. Mering, *Trans. Faraday Soc.* 42B, 205, (1946).
- [7] R. K. Schofield, *Nature*, 160, 408, (1947).
- [8] B. T. Shaw, *J. Phys. Chem.*, 46, 1032, (1942).
- [9] W. F. Bradley and R. E. Grim, *J. Phys. Chem.* 52, 1404, (1948).
- [10] J. W. Jordan, *Miner Mag.* 28, 598, (1949).
- [11] D. R. Lewis, *Proc. Natl. Conf. Clays*, Bull. 169, 54, (1955).
- [12] A. W. Ralston, *Fatty Acids and Their Derivatives* (N. Y., 1948).
- [13] P. A. Rebinder, *J. Appl. Phys.* 1, 151 (1924).
- [14] A. M. Gaudin and D. W. Fuerstenau, *Trans. A. I. M. E.* 202, 958, (1955); D. W. Fuerstenau, *J. Phys. Chem.* 60, 961, (1956).

Received December 4, 1957

EFFECT OF EXCHANGE CATIONS ON THE STRUCTURAL AND MECHANICAL PROPERTIES OF SOILS

L. Ya. Mamaeva

The V. V. Dokuchaev Soil Institute, Academy of Sciences USSR, Moscow

The role of exchange bases in variations of the structural and mechanical properties of disperse systems is known to be considerable. The mechanism of such variations is not yet fully understood. It was necessary, in this connection, to determine the relationships between a number of structural and mechanical properties of humus soils and soil systems without organic matter, their moisture contents and the solubilities of their components, including humus, certain silicates, and carbonates. It was required to investigate such properties as dispersity, cohesion and strength (cohesional properties), and contraction (shrinkage).

Samples of chernozem (Kursk province) with exchange capacity of 32.3 meq, and a top loam (Moscow province) with exchange capacity of 16.2 meq, were taken for the study. The samples were saturated with Ca, Mg, K, and Na cations.

The dispersities of the soil samples saturated with various cations are given in Table 1. The highest dispersities are found for chernozem and top loam saturated with Na^+ . The dispersity is decreased by K^+ , Mg^{2+} , and Ca^{2+} exchange cations.

The increase of dispersity after destruction of the organic matter (see Table 1) is due to the fact that under the influence of K, Mg, and Ca cations introduced into the chernozem, the organic matter is coagulated first, with formation of the corresponding humates on the surfaces of the dispersed particles; these humates inhibit the coagulation of the mineral particles. Aggregation of the particles is effected in this instance by the cementing action of Mg and Ca humate films on a part of the colloid substance.

Swelling. The swelling of chernozem and top loam, saturated with exchange cations, was found from the volume increase produced by sorption of water. The swelling was determined in an apparatus in which the height of the swelling layer was measured by means of an indicator (sensitivity ± 0.01 mm). The following technique was used: the sample was placed in a crucible with a porous bottom covered with filter paper, and compacted by means of 3-4 washings with alcohol under vacuum, so that the particles were dehydrated and packed more closely. The crucible was stood on sand in a vessel into which water was poured up to the level of the crucible floor; hydrostatic upthrust due to the water was thus eliminated. The sample in the crucible was covered with a perforated plate (to allow air to escape), and the indicator tip was placed in contact with the plate. The degree of swelling was determined when the volume ceased to increase, and the amount of water taken up by the sample was a measure of its total moisture capacity (Table 2).

Comparison of the swelling of chernozem and top loam containing the same exchange cations shows that humus soils have a higher degree of swelling; this should be attributed to the high hydrophily of humates. Exchange magnesium increases somewhat the swelling of chernozem, but its action both in chernozem and in top loam approaches that of Ca^{2+} .

The amount of water in chernozem and top loam after swelling is complete and represents their total water capacity or water absorption. The total water capacity of humus soils is much higher than that of humus-free soils (Table 3). Sorption of water by soils (swelling water) involves all types of water, including: 1) free water

TABLE 1

Dispersity of Soil Samples Saturated with Different Exchange Cations

Soils	% contents of particles < 1 μ after saturation with exchange cations			
	Na ⁺	K ⁺	Mg ²⁺	Ca ²⁺
Chernozem	28.8	6.5	1.5	1.1
Chernozem with- out organic matter	27.3	7.8	9.1	7.1
Top loam	29.0	3.2	2.5	1.2

(in pores and capillaries); 2) water within the range of the molecular influence of the soil-particle surfaces, osmotically bound water; and 3) adsorbed or firmly bound water. Both in chernozem and in top loam, the water uptake depends on the nature of the adsorbed ions, and conforms to the lyotropic series: Na > K > Mg > Ca.

The maximum hygroscopicity is not in any clear relationship to the nature of the exchange cation, but it is somewhat higher in humus soils. The osmotically bound water, or molecular moisture capacity, in Lebedev's terminology, was determined by his film-equilibrium method. Even the approximate values for the amounts of this type of water show that they depend on the nature of the exchange cation. This also applies to free water (pores and capillaries, Table 3).

With Na⁺ saturation the greatest amount of osmotically bound water was found in chernozem; the amount in top loam was only one half of this. This may be attributed to the greater hydrophilicity of Na humates. Ca and Mg humates do not have these properties. Chernozem and top loam saturated with Ca²⁺ and Mg²⁺ contain equal amounts of osmotically bound water, but these are considerably less than in the corresponding samples saturated with Na⁺. The proportions of osmotic and free water in these systems should be different.

Thus, in Na chernozem the ratio of osmotic to free water is 3:1, while in Ca and Mg chernozems it is 1:2. In top loam the ratio is 1:1 for all the exchange cations. This indicates that there is less free water in Na chernozem because of the small number of pores and capillaries. In Ca and Mg chernozems there is twice as much free as osmotic water, because of the higher aggregation by the action of Ca and Mg humates, with formation of numerous pores and capillaries. Owing to the absence of organic matter, aggregation, and therefore porosity, is slight in Ca and Mg top loam, and therefore their water contents are one half that of Ca and Mg chernozems. This may serve as a measure of the packing density of soil layers free from organic matter.

Cohesiveness of moist soils. The cohesive properties were determined with the aid of the "adhesiometer" by means of tensile tests on briquets of soils and clays saturated with different cations and with different moisture contents.

The determination technique was as follows. The moistened sample was placed in a specially designed holder (consisting of two separate parts joined by means of a coupling joint) and packed down by means of a press, the pressure being 12.5 atmos in all cases. The lower end of the holder was screwed to the instrument stage, while the upper end was attached to a rod with a spring calibrated against a graduated scale. The coupling joint of the holder, with the packed sample of chernozem or loam in it, was unscrewed, and the upper and lower ends of the holder were left free. A tension was set up in the spring by a turn of a screw, and when this tension exceeded the cohesive strength of the briquet, the latter broke at the section where the two parts of the holder were joined. The work of rupture, indicated on the graduated scale by the tension of the spring, was expressed in kg/cm². The results were plotted against the moisture contents.

The cohesive properties of chernozem soils saturated with different cations are plotted against the moisture content in Fig. 1. The curves show that there are two points of maximum cohesion, at different moisture contents.

The highest cohesion is found in Na chernozem; the first cohesion maximum was found at 12-12.5% moisture content (maximum hygroscopicity 1.2). The second maximum, considerably higher than the first, occurs in the 18-20% moisture range (at double the maximum hygroscopicity). The cohesive forces in Ca and Mg chernozems are much lower than in Na chernozem, and the first cohesion maximum for these chernozems appears at 9.5-10.5% moisture, which is lower than for Na chernozem, while the second maximum, almost equal in magnitude to the first, appears at a higher moisture content (20-22.5%). The first cohesion maximum is little influenced by the nature of the adsorbed ions, whereas the influence of the exchange cations on the second maximum is quite distinct.

TABLE 2

Swelling of Soils Saturated with Different Exchange Cations

Soils	Volume increase in % of original, on saturation with exchange cations			
	Na ⁺	K ⁺	Mg ²⁺	Ca ²⁺
Chernozem	69.9	48.5	26.4	20.6
Top loam	55.4	15.2	22.1	20.0

Top loam (Fig. 3) also gives only one maximum on the cohesion curve, as in the case of chernozem free from organic matter, but the cohesive forces between the loam particles are very much greater than in chernozem with all the exchange cations. The high cohesion of loam saturated with Ca²⁺ and Mg²⁺, which differs little from the cohesion of Na loam, should be especially noted.

The considerably higher cohesion of humus-free soils, especially after saturation with bivalent cations, in comparison with the corresponding chernozems, must be attributed to closer packing of the mineral particles, and therefore to a greater contact area, than that found in Ca and Mg chernozems aggregated by means of humates.

The appearance of cohesive properties in moistened materials of different types is due to interaction of hydration layers, differing in properties and magnitude, on the surfaces of the dispersed particles. In Figs. 1-3 the cohesive properties increase on the left-hand side of the curves up to a definite maximum, beyond which further increases of moisture content alter the properties of the hydration layers and the cohesion forces begin to diminish.

The existence of cohesion under conditions of increasing humidity, when no cementing material is present as yet, must be attributed to forces of molecular interaction between the boundary surfaces of the solvation layers on the particles. If the thickness of the solvation layers is increased above a certain limit, disjoining effect begins to operate.

A characteristic feature of the cohesion properties of chernozem soils is that, beyond the first cohesion maximum, thickening of the hydration layers lowers the cohesion of the soil. The formation of a second maximum with further thickening must be ascribed to cementing of the particles by soluble humates; this effect was discussed in detail by Vershinin [1].

Strength (cohesive properties) of dry chernozem and top loam samples. The strength of dry soils depends on the nature of the surfaces by which the particles are bonded.

The strength of dry soil aggregates was measured in terms of the work required to break down the bonds between dehydrated particles; the aggregates were crushed in a special attachment to the "adhesiometer" (Table 4).

The different values obtained for the strength of the soil aggregates are due to differences in the nature of the surface layers through which the particles are joined. It must be remembered that dry aggregates are formed by the drying of highly humidified soils, so that the conditions are favorable for the maximum surface dissolution and formation of cementing substances. In chernozem soils the soil particles are cemented by humate layers. The cementing strength of the humates depends on the nature of the cations adsorbed in them, which determine differences in the solubilities of the humates; this is confirmed by the example of Na chernozem. The fact that Na chernozem has the highest strength is due not only to the cementing power of Na humates, but also to the large total surface area of contact in it, because the dispersity of Na chernozem is high, owing to its maximum peptization. In coagulated and aggregated chernozems the smaller area of contact and the lower solubility of Ca and Mg humates result in a considerable lowering of aggregate strength.

To find whether the existence of two cohesion maxima for chernozems at different moisture contents is due to the presence of organic matter or to the influence of the mineral composition, the cohesion properties of Ca and Mg chernozems from which organic matter was removed by means of H₂O₂ were determined (Fig. 2).

It is seen in Fig. 2 that the second maximum disappears from the curves; only one remains, in the same moisture range (12.5%) as the first maximum for the original chernozem. The cohesion properties of Ca and Mg chernozems are more than doubled on removal of organic matter; this effect is especially prominent in presence of exchange Mg.

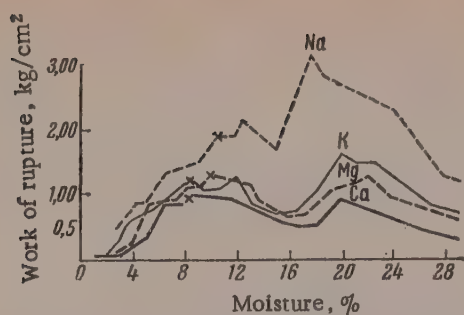


Fig. 1. Work of rupture in kg/cm^2 required to overcome cohesion forces in chernozem saturated with different cations: x) maximum hygroscopicity.

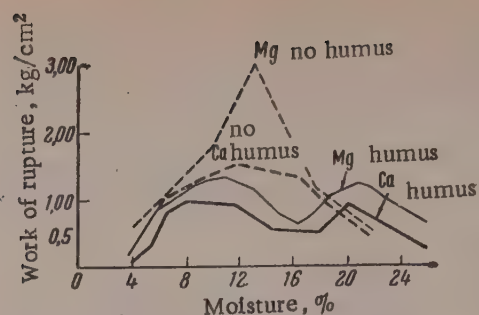


Fig. 2. Work of rupture in kg/cm^2 required to overcome cohesion forces in chernozem with and without humus, saturated with calcium and magnesium cations.

TABLE 3

Water of Swelling and Differential Moisture Contents in Chernozem and Top Loam Saturated with Different Exchange Cations, in % per 100 g of Dry Soil

Soils	Exchange cations	Water of swelling	Differential moisture contents		
			maximum hygroscopicity	osmotically bound	free (pores and capillary)
Chernozem	Na^+	101,1	10,40	72,80	17,90
	K^+	84,1	8,74	37,66	37,70
	Mg^{2+}	71,2	9,66	21,24	40,35
	Ca^{2+}	70,2	8,54	20,16	41,50
Top loam	Na^+	84,7	8,05	35,85	40,80
	K^+	46,6	7,22	17,98	21,40
	Mg^{2+}	51,8	7,72	20,18	23,90
	Ca^{2+}	47,0	7,73	17,17	22,10

In humus-free loam the nature of the surface layers of the particles is not the same as in chernozem, and the particles are bonded as the result of molecular interaction of the mineral layers. The possibility is not excluded that the products formed by surface dissolution of silicate particles, in the form of films of colloidal SiO_2 , may have a cementing action. The formation of such films on mineral particles is described by Grebenshchikov [2], who noted that, with increase of the moisture content of clay minerals, the films of colloidal SiO_2 can swell and decrease cohesion between the particles, whereas dehydration of the film results in increase of mechanical strength. Therefore, in humus-free soils the considerable strength of dry aggregates may be due not only to close packing of the particles, as in cohesion in presence of moisture, but also to the cementing action of colloidal SiO_2 .

Shrinkage (contraction) of soils on drying, or decrease of volume, is an effect which is the opposite of swelling; therefore it must be determined by the hydrophily of soils, which is in turn determined by the nature of the particle surface. The contraction mechanism is such that drying causes the particles to pack more closely, and this leads to direct contact between them. The contracting water menisci exert contracting forces and also determine the cohesion of soils at each moisture stage. Contraction of the capillary walls as moisture evaporates causes stress in the drying system; the resulting overstrain breaks down the continuity of the disperse system, with formation of cracks. This effect was used in the development of a method for determination of shrinkage during drying by measurement and summation of the cracks formed.

The following technique was used for the determinations: a suspension of the material, with excess moisture, was put in a Petri dish and dried. The dry cracked surface of the system was photographed, magnified 3-4 times in the epidiascope, and the separated portions and crack widths were outlined on thin and smooth paper. The length and width of the cracks were measured on the enlarged drawing by means of a "curvimeter." To

TABLE 4

Strength of Dry Soil Aggregates Saturated with Exchange Cations

Soils	Crushing strength in g/mg of soils saturated with exchange cations			
	Na ⁺	K ⁺	Mg ²⁺	Ca ²⁺
Chernozem	275	198	38	2
Top loam	126	94	62	46

TABLE 5

Contraction in Soils Saturated with Various Cations

Soils	Contraction in % of the area of the moist mass, saturated with exchange cations			
	Na ⁺	K ⁺	Mg ²⁺	Ca ²⁺
Chernozem	30.0	21.4	15.9	9.6
Chernozem without organic matter	14.5	14.3	15.0	12.7
Top loam	17.9	13.1	16.0	16.3

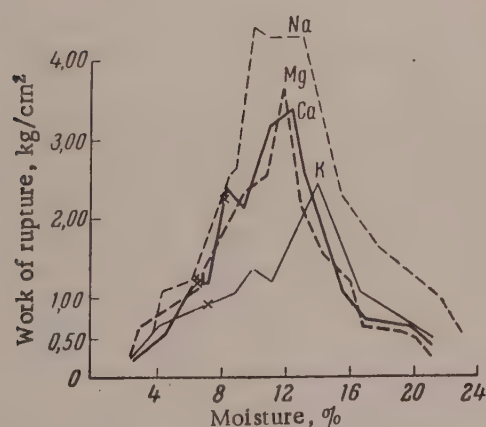


Fig. 3. Work of rupture in kg/cm² required to overcome cohesion forces in top loam saturated with different cations: x) maximum hygroscopicity.

determine the area of the cracks, which represents the shrinkage of the sample, the outlined separate portions were cut out of the enlarged drawing and the crack areas were determined by weighing (the method used by cartographers for area determination) from the weight ratios of the paper corresponding to the separated portions and the cracks.

The course of shrinkage was determined by a similar photographic method, with calculation of the area ratios of the separated portions and cracks, but at different moisture contents during drying of the disperse system.

Table 5 shows that exchange cations have a greater influence on shrinkage in chernozem soils than in humus-free soils. For example, the contraction of Na chernozem is 30%, while that of Ca chernozem is only 10%.

These results are in very good agreement with the swelling data; the swelling of Na chernozem was found to be three times that of Ca chernozem. After removal of organic matter from Na chernozem, the shrinkage decreased by nearly 50%, owing to loss of hydrophilic humates, whereas in humus-free Ca chernozem the shrinkage increases as the result of liberation of the dispersed mineral portion previously aggregated by means of the Ca humates.

After removal of organic matter from chernozem, the influence of exchange cations on the contraction of these soils, as in the case of top loam, is slight, and the contraction values differ little from each other. In these soils adsorbed Ca and Mg cause only a little less shrinkage than saturation Na⁺ (Table 5).

These results confirm once again that in chernozem soils exchange cations have a larger effect, and over wide ranges, on the shrinkage, whereas in top loam and humus-free soil the differences in the influence of different kinds of exchange cations are less pronounced.

From the standpoint of colloidomechanical effects, the most interesting aspect is packing of the particles in the course of evaporation of different types of moisture. It was shown by Kolyasev [3] that moisture evaporates in the following sequence: gravitational water, film water, solvation layers. The importance of the sequence in which different types of water evaporate is that the varying (transitional) thickness and properties of the hydration layers in the course of evaporation deter-

mine, during coalescence, not only cohesion forces, but the force of self-packing, which develops as the result of the contracting forces of the shrinking menisci. Determinations of the course of shrinkage showed that self-

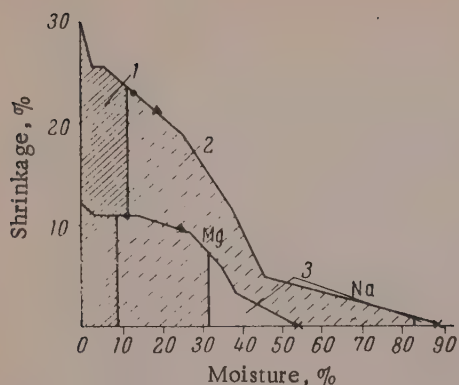


Fig. 4. Dynamics of contraction (shrinkage) in Na and Mg chernozems at different moisture contents: 1) maximum hygroscopicity; 2) osmotic water; 3) free water; x) start of contraction (shrinkage).

packing during shrinkage is influenced by the properties of the hydration layers, which are determined by the nature of the adsorbed cations. The course of shrinkage was determined for Na and Mg chernozems, in order to demonstrate the influence of univalent and bivalent cations in the sorption complex.

Shrinkage data plotted as a function of the differential moisture content (found in determinations of swelling water) (Fig. 4), show that shrinkage begins in the free-water region, but at a definite free-water content. Thus, in the case of Na chernozem, shrinkage began at 87.4% moisture content, and in the case of Mg chernozem, at 55%, despite the fact that the moisture content of the suspension when mixed was considerably greater. Terzaghi [4] and Pokrovskii [5] put forward the view that shrinkage can begin when water filling the pores is lost from the soil, and conditions of a three-phase state arise for development of meniscus forces, which is possible only in the capillary-water region. It seems likely that the start of

shrinkage in the studied materials was detected in the capillary-water region. The dynamic shrinkage curve shows that shrinkage continues as the capillary water evaporates, but the contracting forces in this case are exerted by annular menisci or film bands of osmotically bound water. This is not in agreement with the view of Terzaghi and Pokrovskii, according to whom a "shrinkage limit" is reached during evaporation of the capillary-water menisci, beyond which the residual moisture evaporates but no shrinkage takes place. This evaporation process without shrinkage of the system results in formation of air layers on the particles and disintegration of the aggregates. It is evident that the self-packing process must take place before total evaporation of the water in order to ensure direct contact between the particles which determines the strength of dry soils.

Here the influence of the exchange cations is that exchange Na not only determines the thickness of the hydration layer, which is increased by the presence of Na humate films with cementing properties, but the peptizing action of Na^+ results in the formation of a larger number of contacts, and therefore of contracting menisci, than in presence of Mg^{2+} ; this results in a higher pressure in the self-packing system, giving rise to higher strengths.

SUMMARY

1. The structural and mechanical properties of soils are determined by the nature of the interacting adsorption layers on the particle surfaces.

In humus soils, contact is effected through layers of organic substance which, according to conditions, may decrease strength in the hydrated state or increase strength in the dry state by their cementing action; the strength depends on the amount of dissolved organic substance. The degree of hydration and solution of the humates is determined by the adsorbed cations. Univalent exchange cations result in greater solubility and hydration of humates than bivalent ions, and therefore the structuromechanical values are considerably greater for the former.

2. In top loam and humus-free soil, particle interaction is effected through the surfaces of the mineral particles, which have low surface hydration; the swelling and shrinkage are therefore less. The greater cohesion of moist, and strength of dry, humus-free soils must be attributed to close packing of the particles owing to absence of humates. Another possibility is surface dissolution of silicate particles, leading to formation of colloidal SiO_2 films which, in the hydrated state, apparently have a stronger cementing effect than films of organic material, and on dehydration, result in high bonding strength even if the complex is saturated with exchange Ca^{2+} or Mg^{2+} .

I thank Academician of the Academy of Sciences, Tadzhik SSR, I. N. Antipov-Karataev for guidance and help in this work.

LITERATURE CITED

- [1] P. V. Vershinin, Doctorate Dissertation [in Russian] (Leningrad, 1953).
- [2] I. V. Grebenshchikov, Bull. Acad. Sci. USSR, Div. Tech. Sci. No. 1 (1937).
- [3] F. E. Kolyasev, Papers at the 6th International Congress of Soil Science, Physics of Soils [in Russian] (Izd. AN SSSR, Moscow, 1956).
- [4] K. Terzaghi, Theoretical Soil Mechanics (Geological Prospecting Press, 1932) [Russian translation].
- [5] G. I. Pokrovskii, Capillary Forces in Soils [in Russian] (1933).

Received January 16, 1959

APPLICATION OF THE SIMILARITY THEORY IN CALCULATIONS OF THE FLOW OF PLASTIC GREASES IN PIPES

A. A. Mamakov, N. V. Tyabin,
and G. V. Vinogradov

The S. M. Kirov Institute of Chemical Technology, Kazan'

At the present time design calculations relating to centralized feed systems for plastic greases* used in metallurgical works are based on experimental curves for the flow rate per second as a function of pressure [1, 2]. Unfortunately, the generally accepted methods of hydraulics are not used in such calculations, and no account is taken of the fact that during the past ten years considerable experimental data on the flow of greases in capillaries and pipes has been obtained by Vinogradov, Pavlov, Petrovskii, and others [3-5]. It has become necessary to generalize the extensive experimental data on the flow of greases in pipes by the methods of the similarity theory. This is all the more necessary because these methods have been widely used for generalization of experimental data on the flow in pipes of various suspensions [6], latexes [7], cement slurries [8], napalm solutions [9], clay suspensions [10, 11], peat slurry [12], and coal-oil paste [13].

Typical flow curves for a grease (solidol), determined at various temperatures by means of the rotational viscosimeter, are shown in Fig. 1. Progressive increase of the velocity gradient yields the ascending branch AB of the flow curve. Decrease of the velocity gradient gives the descending branch BC. Irreversibility of the curves is due to breakdown of the thixotropic structure of the grease. After breakdown of the structure, the flow process (descending branch of the curve) becomes reversible.

Measurements performed on the flow of greases in capillary viscosimeters yield only ascending curves, of the same type as those obtained with the rotational viscosimeter. Therefore, if the flow curves for greases have been determined by means of rotational viscosimeter, the calculations relating to the flow of these materials in ducts should be based on the ascending branches of the curves.

Repeated attempts have been made to present experimental data on the flow of greases in pipes in the form of relationships between dimensionless quantities. Arveson [14] made an early attempt to represent the viscosity properties of greases of different compositions over a wide temperature range by means of a single universal curve. However, the points on the generalized graph were very scattered, and the results could not be used for calculations.

Weltmann [15] proposed methods for calculations of pressure drop in the flow of greases through pipes on the assumption that the flow of greases conforms to the law of internal friction

$$\bar{D} \sim \bar{\tau}^N, \quad (1)$$

where N is a structure number. The relationship between the mean velocity gradient \bar{D} and the tangential stress $\bar{\tau}$ was determined by Weltmann in a rotational viscosimeter for an average gap radius between the cylinders. As, in general, N depends on \bar{D} for greases, relationship (1) plotted in logarithmic coordinates gives a curve. According

* The term "grease" will be used in this paper instead of "plastic grease."

to Weltmann, the flow of greases may be characterized by two properties: N and the effective viscosity $\eta_{\text{eff}} = \bar{\tau}/\bar{D}$. On the other hand, in Weltmann's opinion the flow curve for a grease may be replaced by its tangent, and then greases may be considered as viscoplastic materials with the following parameters: θ , the yield value and η_{pl} , plastic viscosity.

From the obvious theoretical relationships

$$\lambda = \frac{64}{\text{Re}} \frac{\text{Pl}}{8 \text{Co}}, \quad \lambda = \frac{64}{\text{Re}} \frac{N+3}{4}.$$

Weltmann [15] plotted the theoretical graph

$$\lambda = f(\text{Re}, \text{Pl}, N), \quad (2)$$

where λ is the resistance coefficient of the pipe; $\text{Re} = v d \rho / \eta$ is the Reynolds number; $\text{Pl} = \theta d / \eta_{\text{pl}} v$ is the plasticity number; v is the average velocity; d is the diameter; $\text{Co} = 4 l \theta / \Delta p d$; l is the length of the pipe; Δp is the pressure drop; η is the viscosity.

Weltmann proposes the following methods for calculation of flow in pipes.

1. For fixed values of the flow rate q and d , a plot of (1), analogous to Fig. 1, is used to find the structure number N , and the equation of Farrow, Lowe, and Neale [16] is then used to find the velocity gradient at the pipe wall

$$D_R = \frac{2v(N+3)}{d}. \quad (3)$$

The flow curve is used to find η_{eff} , and Re is calculated. The values of Re and N are used to find λ and the pressure drop from a plot of the relationship (2).

2. The flow curve is replaced by a tangent to this curve. The grease is regarded as a viscoplastic material, θ and η_{pl} for which are determined by the direction of the tangent. The values of Re and Pl are used to find λ , and the pressure drop is then found.

The calculation methods proposed by Weltmann [15] suffer from a number of serious faults and may lead to errors in determination of Δp . Having noted the existence of ascending and descending branches on the flow curves for greases, Weltmann does not indicate which branch should be used for calculations of the flow of greases in pipes. For greases $N = \varphi(D)$, and therefore determination of D_R by equation (3), derived on the assumption that $N = \text{constant}$ [16], cannot be accepted as correct. On the other hand, replacement of the flow curve (1) by a tangent is an arbitrary step. In view of the considerable slope of the flow curves for greases, especially in the region of small velocity gradients, arbitrary construction of the tangent may lead to errors in calculation. Finally, graphs for the relationship (2) were derived by Weltmann on theoretical grounds and do not correspond to experimental data on the flow of greases in pipes. These graphs are unsuitable, if only because they do not yield a universal relationship of type (2) for different greases.

Thus, up to the present, no satisfactory methods have been proposed either for generalization of experimental data or for flow calculations of greases in pipes.

In the present paper the methods of the similarity theory are used for generalization of the extensive numerical data of Vinogradov and Pavlov [4] on the flow of solidols in a capillary viscosimeter of the constant flow-rate type, and data of Vinogradov and Petrovskii [5] on the pumping of solidols through pipes in a constant-pressure unit. In these investigations the average velocity gradient was varied by seven orders of magnitude from 0.03 to $35,400 \text{ sec}^{-1}$, the temperature was varied from -45 to $+80^\circ$, the pipe lengths by a factor of 250, and their diameters by a factor of 36. This makes it possible to generalize virtually all possible cases of the flow of greases in pipes.

Two different methods were used for generalization of the experimental data: the method of variable effective viscosity, and the method of constant rheological parameters independent of the flow velocity gradients.

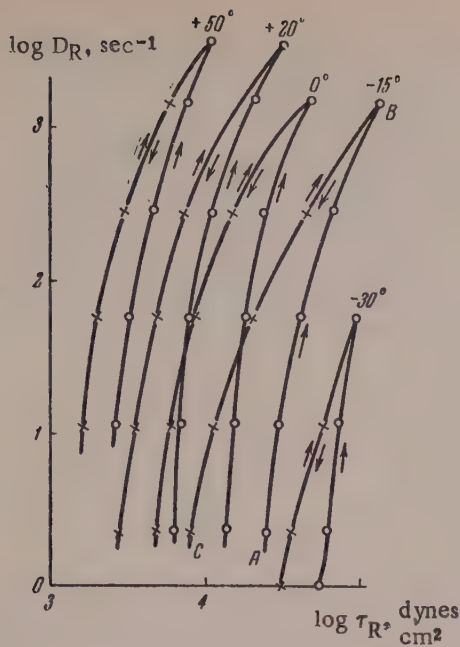


Fig. 1. $D_R = \varphi(\tau_R)$ flow curves for solidol in a rotational viscosimeter.

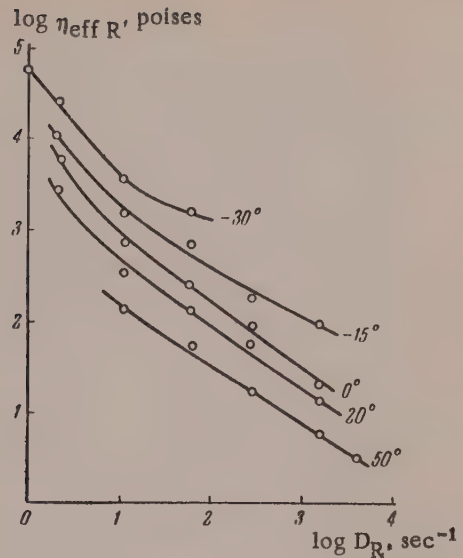


Fig. 2. Curves for the dependence of local effective viscosity of solidol on the velocity gradient in a rotational viscosimeter.

With the effective-viscosity method, the general relationship $\tau = \varphi(D)$ may be written in the form $\tau = \eta_{\text{eff}}(D) D$, where $\eta_{\text{eff}}(D)$ is the local effective viscosity, dependent on the flow velocity gradient. The equation for the flow of greases can then be written in the criterial form:

$$Eu = f(\text{Re}^*, \Gamma), \quad (4)$$

where $Eu = \Delta p / \rho v^2$ is the Euler criterion; $\text{Re}^* = v d \rho / \eta_{\text{eff}}$ is the generalized Reynolds criterion; η_{eff} is the characteristic local effective viscosity; ρ is the density; $\Gamma = d/l$ is a geometric ratio. Since

$$\lambda = 2 \Delta p d / \rho l v^2 = 2 Eu \Gamma, \quad (5)$$

the criterial relationship (4) may be written

$$\lambda = f(\text{Re}^*). \quad (6)$$

Experimental data on the flow of greases in pipes should be generalized in the form of this relationship. All the quantities in expression (6) can be readily determined from experimental data. The effective viscosity in the layer adjacent to the pipe wall $\eta_{\text{eff}} R = \tau_R / D_R$ should be chosen as the characteristic effective viscosity. This choice is justified because $\eta_{\text{eff}} R$ is determined in similar layers, and then

$$\text{Re}^* = \frac{v d \rho}{\eta_{\text{eff}} R}. \quad (7)$$

The values of $\eta_{\text{eff}} R$ were determined by experiments on the flow of solidols in a rotational viscosimeter designed by Vinogradov and Pavlov; the stress in the gap of this instrument is close to uniform. The dependence of the local effective viscosity on the velocity gradient at the viscosimeter wall, determined from the ascending branches of the flow curves in Fig. 1, is presented in Fig. 2. The effective viscosity has the same value for layers adjacent to pipe walls and to the wall of the rotational viscosimeter. The velocity gradient at the pipe wall was determined by the Weissenberg-Rabinowitsch formula [17]:

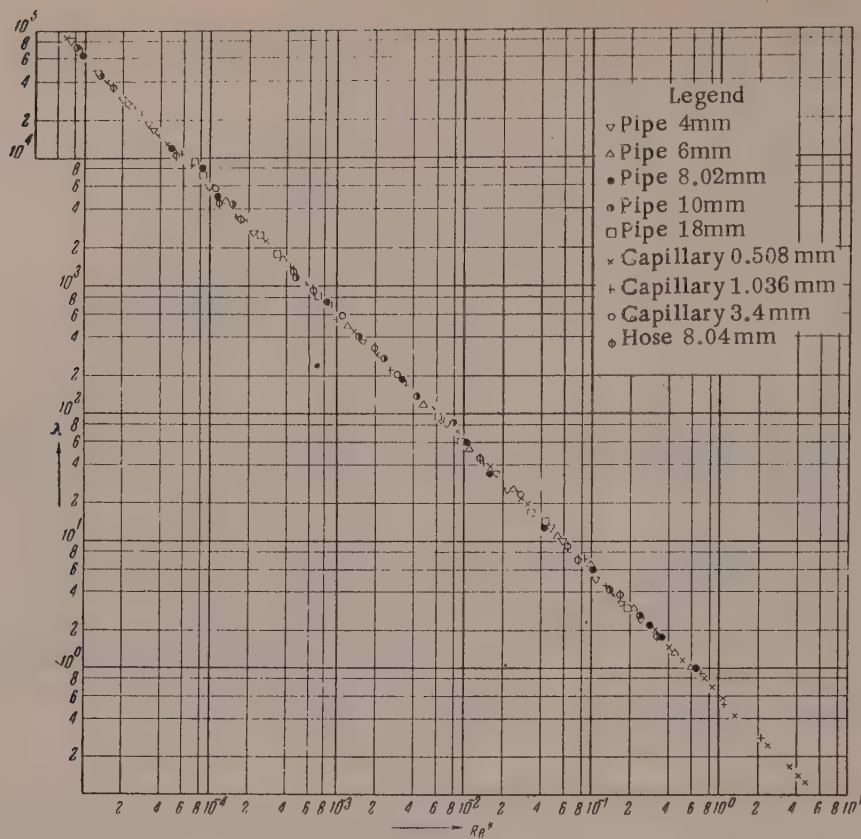


Fig. 3. Dependence of the resistance coefficient λ on the generalized Re^* criterion.

$$D_R = 6F(\tau_R) + 2\tau_R \frac{dF(\tau_R)}{d\tau_R},$$

where $F(\tau_R) = \frac{4q}{\pi d^3}$, $\tau_R = \frac{\Delta p d}{4l}$ and $\frac{dF(\tau_R)}{d\tau_R}$ were determined by graphical differentiation of the relationship $F(\tau_R) = f(\tau_R)$.

Figure 2 was used to find values of $\eta_{eff} R$ corresponding to D_R ; equations (7) and (5) were used to calculate Re^* and λ , and the relationship (6) was plotted (see Fig. 3).

For characterization of the flow of greases in terms of constant rheological parameters, Tyabin and Vinogradov [18] proposed a method for approximation of the flow curves in the form of Shvedov - Bingham linear relationships. In this case the constant rheological parameters are the plastic viscosities and yield values; the similarity theory of a viscoplastic medium can therefore be used for generalization of the experimental data [19]. If the flow curve for a grease in a given range of velocity gradients is approximately represented by a single Shvedov - Bingham equation, the Buckingham flow-rate equation for the flow of a viscoplastic medium in a circular pipe can be easily transformed into

$$\frac{\Delta p}{\gamma} = \frac{64}{Re^*} \frac{l}{d} \frac{v^2}{2g} = \lambda \frac{l}{d} \frac{v^2}{2g} k, \quad (8)$$

where

$$Re^* = \frac{vd\rho}{\eta_{pl} \left(1 + \frac{1}{6} \frac{\theta d}{v\eta_{pl}}\right)}, \quad (9)$$

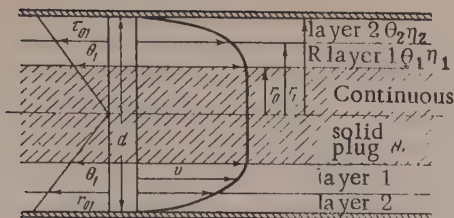


Fig. 4. Schematic flow of plastic grease in a pipe.

$$k = \frac{1}{1 + \frac{1}{3} c^4}, \quad (10)$$

$$c = \frac{r_0}{R}, \quad (11)$$

R is the pipe radius; $2R = d$; r_0 is the radius of the continuous solid plug in the pipe center; $r_0 = 2l\theta/\Delta p$. The resistance coefficient is a function of the generalized Reynolds number only, and the criterial expression for grease flow can be written in the form of equation (6).

If several straight lines are used for approximation to the flow curve, the generalization of the experimental data should be performed by means of the Tyabin and Vinogradov expression for the flow rate [18]. Approximation of flow curves for greases shows [18] that a single Shvedov - Bingham equation approximates to the flow curve roughly over the range of one tenth power variation of the velocity gradient. For technical calculations, approximation of the flow curve in the form of two Shvedov - Bingham equations is sufficient, as the magnitudes of the other approximating equations, which are several orders of magnitude less than the others, may be disregarded.

For the case in which the flow curve is approximately represented by two straight lines, Tyabin and Vinogradov [18] derived the following equation for the flow of a plastic disperse system in a circular pipe

$$q = \frac{\pi \Delta p}{8l\eta_2} (R^4 - r_1^4) + \frac{\pi \Delta p}{8l\eta_1} (r_1^4 - r_0^4) - \frac{\pi \theta_0}{3\eta_2} (R^3 - r_1^3) - \frac{\pi \theta_1}{3\eta_1} (r_1^3 - r_0^3), \quad (12)$$

where

$$r_1 = \frac{2\tau_{01}l}{\Delta p}, \quad r_0 = \frac{2\theta_1l}{\Delta p}, \quad \tau_{01} = \frac{\theta_2\eta_1 - \theta_1\eta_2}{\eta_1 - \eta_2},$$

τ_{01} is the boundary shear stress (Fig. 4); $\theta_1, \eta_1, \theta_2, \eta_2$ are the yield stresses and plastic viscosities for the zones corresponding to the approximate straight lines 1 and 2 (Figs. 4, 5); r_1 and r_0 are the radii of layer and plug (Fig. 4).

Equation (12) can be easily transformed to the form (8), where

$$Re^* = \frac{vd\rho}{\eta_2[1 + \frac{1}{6}(\theta_2d/\eta_2v)]}, \quad (13)$$

$$k_1 = \frac{1}{1 + mc_1^4},$$

$$c_1 = \frac{r_1}{R}, \quad m = \frac{4}{3} \frac{\theta_2}{\tau_{01}} - 1 + \frac{\eta_2}{\eta_1} \left[1 - \frac{4}{3} \frac{\theta_1}{\tau_{01}} + \frac{1}{3} \left(\frac{\theta_1}{\tau_{01}} \right)^4 \right]. \quad (14)$$

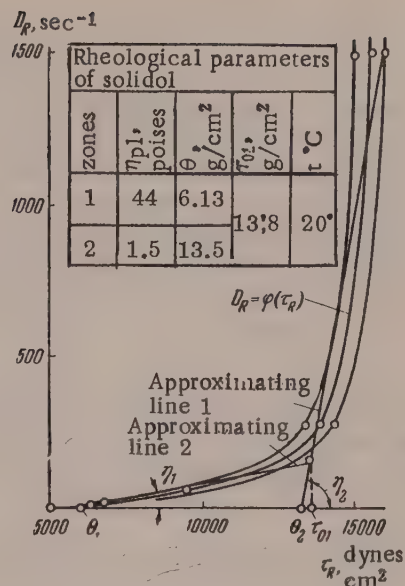


Fig. 5. Approximation to the flow curve of solidol in a rotational viscosimeter, in the form of Shvedov - Bingham equations ($t = 20^\circ$).

Therefore, experimental data may be generalized in the form of the expression (6), where λ is determined from (8), and Re^* from (9) and (13).

In generalization of the experimental data by the second method, the flow curves for solidol were approximated, on the basis of an experimental accuracy of the order of 5%. A graph in which the approximation to the flow curves was performed, such as Fig. 5, was used to find values of θ and η_{pl} , and equations (9), (13), and (5) were used to calculate Re^* and λ ; the relationship (6) was then plotted (Fig. 3), and this coincided with the similar graph obtained by the first method for generalization of the experimental data.

Experimental data on the flow of solidols in pipes fitted fairly accurately on one generalized straight line (Fig. 3), the equation for which, in logarithmic coordinates, is

$$\lambda = 64/Re^*. \quad (15)$$

Comparison of graphs for the resistance coefficient as a function of Reynolds number of viscous liquids and lubricants shows that for the latter the graph extends by 6-7 tenth powers into the region of small Reynolds numbers; this is due to the high values of the effective viscosities (Fig. 2). The experimental relationship (15) can form the basis of a method for calculating pressure drops in the flow of greases in pipes.

If the flow of a plastic grease can be represented by two constant parameters θ and η_{pl} over a given range of velocity gradients, the pressure drop is found from equation (8), which contains the unknown quantity c from equation (11).

Since $\Delta p/l = 4\theta/dc$, the Buckingham equation can be written in the form

$$\frac{c^4 - 4c + 3}{12c} = \frac{2v\eta_{pl}}{\theta d} = \alpha. \quad (16)$$

Therefore, the radius of the flow core is a function of $v\eta_{pl}/\theta d$ and of d . McMillen [20] calculated and tabulated values of α for different c from equation (16).

Values of α in Equation (16)

α	$1,25 \cdot 10^{-5}$	$5 \cdot 10^{-5}$	$2 \cdot 10^{-4}$	$8,1 \cdot 10^{-3}$	$1,8 \cdot 10^{-3}$	$3,3 \cdot 10^{-3}$	$5,1 \cdot 10^{-3}$	$1,1 \cdot 10^{-2}$	$21 \cdot 10^{-2}$
c	0,995	0,99	0,98	0,96	0,94	0,92	0,90	0,85	0,80
c	$3,5 \cdot 10^{-2}$	$5,2 \cdot 10^{-2}$	$7,4 \cdot 10^{-2}$	0,4	0,135	0,177	0,23	0,30	0,38
α	0,75	0,70	0,65	0,60	0,55	0,55	0,45	0,40	0,35
α	0,5	0,67	0,92	1,33	2,17	2,79	3,83	5,92	12,17
c	0,30	0,25	0,20	0,15	0,10	0,08	0,06	0,04	0,02

If in a given D_R range a grease is characterized by four constant parameters θ_1 , η_1 , θ_2 , η_2 , then grease ducts can be calculated with the aid of equation (8), where k is determined by equation (14), which contains the unknown quantity c_1 . Equation (12) can be reduced to the form

$$\frac{3mc_1^4 - 4 \frac{\theta_2}{\tau_{01}} c_1 + 3}{12c_1} = \frac{2v\eta_2}{\tau_{01}d}.$$

For technical calculations the term $3mc_1^4$ can be neglected in the first approximation, and then we have

$$c_1 = \frac{3}{4 \left(\frac{\theta_2}{\tau_{01}} + 6 \frac{\eta_2 v}{\tau_{01} d} \right)}.$$

If the values of \underline{c} and c_1 in (10) and (14) are known, \underline{k} and k_1 can be found, and the pressure drop can be calculated from equation (8).

SUMMARY

1. Two methods are proposed for generalization of experimental data and calculations of the flow of plastic greases in pipes in the form of a relationship between the resistance coefficient of the pipe and the generalized Reynolds number. The variable effective viscosity method consists of determination of the generalized Reynolds number from the value of the local effective viscosity for a layer adjacent to the pipe wall. The method of constant parameters consists of approximation to the flow curve by means of straight lines, corresponding to Shvedov - Bingham equations, and determination of the generalized Reynolds number from the parameters of viscoplastic flow. These methods were used to generalize experimental data on the flow of plastic greases in pipes for velocity gradients ranging from 0.03 to 35,400 sec^{-1} , 250-fold variations of pipe length, and 36-fold variations of pipe diameter.

2. An expression has been derived for the resistance coefficient of the pipe as a function of the generalized Reynolds number in the flow of plastic greases, and it is shown that for calculations of pressure drop it is possible to use the ordinary methods of hydraulics, based on application of the method of approximation to the flow curves of plastic greases in rotational viscosimeters.

The authors offer their sincere thanks to V. P. Pavlov and V. G. Petrovskii for kindly supplying the experimental data used in this paper.

LITERATURE CITED

- [1] M. P. Vavilov, Lubrication of Metallurgical Equipment [in Russian] (Mashgiz, 1954).
- [2] A. I. Shvartsman, Central Sci. Res. Inst. Heavy Machinery Report No. 2156 [in Russian] (Moscow, 1949).
- [3] G. V. Vinogradov, Doctorate Dissertation [in Russian] (Moscow, 1950).
- [4] G. V. Vinogradov and V. P. Pavlov, Proc. 2nd All-Union Conference on Friction and Wear in Machines [in Rus.] 311 (1949); Proc. Acad. Sci. USSR 58, 1391 (1947); in the book: Low-Temperature Properties of Petroleum Products [in Russian] (Moscow, 1949); V. P. Pavlov, Candidate's Dissertation [in Russian] (Moscow, 1948).
- [5] V. G. Petrovskii and G. V. Vinogradov, Petroleum Economy No. 8, 36 (1950); Trans. Stalin Military Academy No. 10 (1951).
- [6] D. H. Galwell and H. E. Babbitt, Trans. Amer. Inst. Chem. Engrs. 37, 237, (1941).
- [7] C. C. Winding, W. L. Kranich and G. P. Boumann, Chem. Eng. Progress 43, 613, (1947).
- [8] O. A. Hedstrom, Ind. Eng. Chem. 44, 651, (1952).
- [9] C. C. Winding, G. P. Boumann and W. L. Kranich, Chem. Eng. Progress 43, 527, (1947).
- [10] V. S. Filatov, Colloid J. 16, 65 (1954);* Petroleum Economy No. 2 (1954).
- [11] E. M. Solov'ev, Petroleum Economy No. 1, 40 (1957).
- [12] I. I. Orlov, Colloid J. 17, 434 (1955).*
- [13] A. D. Magomedov, Candidate's Dissertation [in Russian] (Moscow, 1955).
- [14] M. H. Arveson, Ind. Eng. Chem. 24, 71, (1932).
- [15] R. N. Weltmann, Spokesman 6, 34 (1956); Ind. Eng. Chem. 48, 386, (1956).
- [16] F. D. Farrow, G. M. Lowe and S. M. Neale, J. Text. Inst. 19, 18, (1928).
- [17] B. Rabinowitsch, J. Phys. Chem. 145, 1, (1929).
- [18] N. V. Tyabin and G. V. Vinogradov, Colloid J. 19, 352 (1957).*

*Original Russian pagination. See C.B. Translation.

[19] N. V. Tyabin, Colloid J. 14, 270 (1952).*

[20] L. McMillen, Chem. Eng. Progress 44, 537, (1948).

Received May 6, 1958

*Original Russian pagination. See C.B. Translation.

MECHANISM OF THE CONTRACTION OF COKE MATERIAL CAUSING ITS PACKING AND CRACKING

1. CONTRACTION AND SHRINKAGE OF COKE MATERIAL

B. A. Onusaitis and V. F. Kozlova

The N. P. Chizhevskii Laboratory of Metallurgical Fuel,
Institute of Combustible Minerals, Academy of Sciences, USSR

The shrinkage of coke is the result of contraction of the pores in its gel structure and of closer packing of the molecules in the aggregate forming its network structure. We consider that contraction of the pore spaces in the gel structure occurs under the action of capillary forces caused by separation and subsequent volatilization (by the action of heat) of substances filling the cells of the gel framework. The mechanism of this process has not yet been studied in coke, but it seems likely that it is analogous to the action of capillary forces in the contraction of other gels, such as silica or alumina gels [1-5].

The degree of deformation of semicoke and the nature of the porosity of the finished coke may be influenced by the action of capillary forces on the one hand, and by the compression resistance of the material on the other. As heating proceeds, the increase in the rigidity of the semicoke framework, which increases its compression resistance, is accompanied by an increase in the evaporation rate of the substances filling the pores. As the volatile substances are liberated, the capillary forces caused by them may exceed the cohesion of the particles in the material, and lead to the formation of cracks in the weaker regions. The less rigid the bonding between the coke particles, the more the coke can withstand contraction and deformation without cracking, and the more microporous will the finished coke be.

The purpose of the experimental part of this investigation was to study the presumed action of capillary forces during contraction of semicoke.

The samples used for the tests were semicoke briquets made in the plastometric test apparatus*. The heating of the apparatus was stopped when the coal charge at the bottom of the beaker reached 580-600°. Under these conditions the plastic layer stopped only 3-5 mm short of the top of the charge. The unsintered coal was scraped from the top of the briquet.

The semicoke briquets were prepared from Kuznetsk coal, GPZh grade (Zyryanovka pit, volatile yield 36.2%), K grade (Stalin pit, volatile yield 18.2%), and the production charge used in one of the coke-oven plants. The charge was composed of the following coal grades: PZh, 8%; K₂, 25%; PZh, 26%; G, SS—9%, K, 32%. The true** and apparent [6] specific gravities were first determined for all the samples, and each sample was then divided into two parts. One part was used for calcination, while the other was ground down to 5-10 mm and then boiled in anthracene oil (360-380° fraction) for 4 hours in a current of nitrogen. The semicoke was then washed during 30-35 hours with benzene in a Soxhlet apparatus until the supernatant benzene was quite colorless.

*GOST 1186-41.

** By the method recommended by the Ufa Petroleum Scientific Research Institute.

TABLE 1

Comparative Changes of Apparent and True Specific Gravities of Treated and Untreated Semicoke Samples

Original coal	Sp. gr. of untreated samples			Sp. gr. of samples treated with anthracene oil		
	before calcination	after calcination	change, %	before calcination	after calcination	change, %
Apparent specific gravity						
GPZh	0,994	1,171	17,8	0,994	1,277	28,5
	1,024	1,249	22,0	1,024	1,446	41,2
Charge	1,009	1,195	18,4	1,009	1,417	40,4
True specific gravity						
GPZh	1,499	1,658	10,6	1,499	1,779	18,7
	1,503	1,688	12,3	1,503	1,764	17,4
Charge	1,498	1,660	10,8	1,498	1,752	17,0

The samples treated with anthracene oil and washed in benzene were calcined for 4 hours at 1000° in a current of purified nitrogen. During the calcination of these samples, anthracene-oil vapor was evolved in the 200-450° range. Therefore, prolonged washing of the semicoke samples with hot benzene did not remove completely the anthracene oil from the semicoke pores. After calcination of the samples, the apparent and true specific gravities were determined again (Table 1).

Table 1 shows that treatment of semicoke with anthracene oil had a very sharp effect. After calcination, the apparent specific gravity of the treated samples increased nearly twice as much as that of the untreated samples. The smaller change of apparent specific gravity for samples of GPZh coals as compared with K coals is due to the fact that semicoke from GPZh coals has larger pores than semicoke from K coals [7].

Anthracene oil, and with it other liquid substances formed by the thermal decomposition of coal, can be washed out much more easily from semicoke with larger pores than from semicoke with finer pores. It follows that the contraction effect under the influence of capillary forces must be much less in the first case than in the second. Moreover, as was shown by one of us in an earlier paper [7], the rigidity of the framework increases on heating more rapidly and at lower temperatures in semicoke from more recent coals than in semicoke from coals of higher stages of metamorphism.

Comparison of the true specific gravities (Table 1) confirms the undoubted influence of anthracene oil on packing of the coke formed. This is also illustrated by the porosity data in Table 2.

Changes in the different pore types are especially interesting; whereas in untreated coke, the micro- and intermediate pores comprised 28.3 and 30.6% of the total pore volume, in coke treated with anthracene oil, the fraction of these pores decreased to 2.2 and 8.0%. Therefore, the shrinkage was mainly the result of a decrease in the volume of micro- and intermediate pores; this decrease was 91.5% for coke from GPZh coal, and 84.4% for coke from K coal.

Some doubt on the validity of these experiments was cast by the suggestion that anthracene oil may partially decompose and form coke during calcination of the samples. To test this suggestion, special experiments were performed with high-temperature coke (first degree of readiness)*, in which the contraction and shrinkage processes are completed. In samples of this coke, which has a rigid structure, pore contraction could not occur under the influence of capillary forces. Any decrease of porosity which might be detected could be attributed only to deposition of the pyrolysis products of anthracene oil on the pore walls.

Samples of high-temperature coke were treated and calcined as described above. The treatment was performed with anthracene oil, and also with phenanthrene, which boils at a lower temperature and distills almost without decomposition.

* As in the original Russian.

TABLE 2

Comparative Changes of Total Porosity* and Volumes of Different Pores in Coke as the Result of Treatment with Anthracene Oil and Calcination

Original coal	Total porosity of original sample, %	Samples calcined without oil treatment					Samples treated with oil and calcined						
		porosity, %	change, %	total pore volume, cc/g	volume of micro- and intermediate pores**		porosity, %	change, %	total pore volume, cc/g	change of pore volume, % on untreated coke	volume of micro- and intermediate pores**		
					cc/g	% of total volume					cc/g	% of total volume	
GFZh	33,7	29,4	12,7	0,251	0,071	28,3	28,2	16,2	0,221	12,0	0,006	2,2	91,5
KMK charge	31,9	26,0	18,5	0,209	0,064	30,6	18,1	43,3	0,125	40,2	0,010	8,0	84,4
	32,7	28,0	14,4	0,235	—	—	19,1	41,6	0,135	42,6	—	—	—

* Total porosity was calculated from the expression $[(d - \delta)/d] 100$, where d is the true, and δ the apparent, specific gravity.

** The volume of micro- and intermediate pores was calculated from data on sorption of water vapor, determined by M. V. Khvorostukhina.

Specific-gravity determinations on the original (untreated) high-temperature coke calcined at 1000° for 6 hours showed (Table 3) that its porosity remained unchanged; these determinations are therefore evidence of the rigid structure of high-temperature coke. After treatment of the calcined coke with anthracene oil and a second calcination, its apparent specific gravity increased by only 2%, and the true specific gravity by 3.7%. After treatment with phenanthrene the apparent specific gravity increased by 0.6%, and the true specific gravity by 1.9%. These values are in no way comparable to the changes, reaching 40.4%, resulting from the treatment of the nonrigid semicoke material. Phenanthrene was evidently removed completely from the coke pores.

The total porosity, calculated from the specific gravities of untreated and treated samples of production coke also changed very slightly after calcination at 1000°:

	porosity, %
Original coke	46.2
The same, after additional calcination	46.4
Coke after additional treatment with anthracene oil and calcination	43.0
Coke after additional treatment with phenanthrene and calcination	44.5

These values can be taken as being within the variability limits of porosity determinations for samples from one batch of production coke.

Thus, experiments on high-temperature coke with a rigid structure provide additional confirmation of our hypothesis of the colloidal effect in the contraction of the nonrigid structure of semicoke in the course of liberation of liquefied substances boiling at high temperatures from its pores.

SUMMARY

1. A hypothesis is put forward which accounts for the contraction of the forming coke substance (causing its shrinkage and cracking of the coke mass) mainly by the action of capillary forces which appear as the result of volatilization on heating of the substances filling the coke pores.

2. Investigations confirmed the hypothesis of the contraction mechanism of the semicoke substance and the role of the liquid phase in this process. The connection between contraction of semicokes and the colloidal structure of the original coal samples is demonstrated.

TABLE 3

Relative Changes of Apparent and True Specific Gravities of High-Temperature Coke Samples*

Sam- ples	Sp. gr. of original coke		Sp. gr. of coke after additional treatment and calcination			
	without addi- tional calci- nation	after additional calcination	with anthracene oil		with phenanthrene	
			sp. gr.	change, % of original	sp. gr.	change, % of original
Apparent specific gravity						
1	1,094	1,088	1,119	—	1,097	—
2	1,099	1,093	1,109	—	1,118	—
3	1,091	1,111	1,116	—	1,104	—
4	—	1,087	1,121	—	1,123	—
Mean	1,094	1,094	1,116	2,0	1,110	0,6
True specific gravity						
1	2,021	2,039	1,947	—	1,962	—
2	2,049	2,042	1,972	—	2,031	—
Mean	2,035	2,040	1,959	3,7	1,996	1,9

* Specific gravities of high-temperature coke determined by A. V. Kulikovskaya.

3. These results make it possible to exert an artificial influence on the granulometric composition of the coke during formation of the coke mass by utilization of capillary forces at the stage when the semicoke structure is not rigid; denser cokes can also be obtained in this way.

LITERATURE CITED

- [1] M. M. Dubinin, Physicochemical Principles of Sorption Technology, 2nd Ed. [in Russian] (ONTI, Moscow, 1935).
- [2] R. Zsigmondy, Z. anorgan. Chem. 71, 356, (1911).
- [3] V. S. Veselovskii and I. A. Selyaev, J. Phys. Chem. 6, No. 9, 1171 (1935).
- [4] I. E. Neimark and F. I. Khatset, Colloid J. 9, 289 (1947).
- [5] A. V. Kiselev, M. A. Vorms, V. V. Kiseleva, V. I. Karnaukhova and N. A. Shtokvish, J. Phys. Chem. 19, 83 (1945).
- [6] E. M. Taits, N. G. Titov, and N. V. Shishakov, Methods for Evaluation of Coals as Raw Materials for Industrial Utilization [in Russian] (Coal Tech. Press, Moscow, 1949) p. 141.
- [7] B. A. Onusaitis and N. P. Yur'evskaya, Bull. Acad. Sci. USSR, Div. Tech. Sci. No. 7, 893 (1947); No. 4, 519 (1949).

Received March 13, 1957

SORPTION OF STRONTIUM AND CALCIUM IONS BY SOILS*

Yu. A. Polyakov

The V. V. Dokuchaev Soil Institute,
Academy of Sciences USSR, Moscow

Adsorption and exchange of strontium and calcium ions in soils have been studied in great detail in recent years, because of the well-known role they play in the migration of fission products. As a result of these investigations not only has an enormous amount of factual data been accumulated, but a number of important theoretical generalizations and discoveries have been made; these rank among the latest advances of science. Nevertheless, many problems concerning the nature and mechanism of such phenomena remain controversial and incompletely solved. A particularly complex problem is that of the Sr^{90} cycle and the technique for determination of the discrimination coefficient (DC) of Sr^{**} .

If this ratio has a numerical value < 1 , this means that strontium is taken up to a smaller extent than calcium by the plant. In some papers [2] presented at the International Conference on Radioisotopes, the term "observed ratio" is used to denote the discrimination coefficient: $O. R. \text{ for plant} - \text{external medium} =$
$$= \frac{\text{Sr/Ca in plant}}{\text{Sr/Ca in external medium}}.$$

The present paper contains an examination of the principal criteria of exchange-adsorption equilibrium of Ca and Sr ions in soils, calculations of the most important thermodynamic characteristics, and an attempt to establish certain data in relation to determination of the discrimination coefficient for the soil - plant system. It may be noted that increases of the thermodynamic functions ΔH , ΔF , ΔS are always considered as positive changes (in an exothermic reaction $\Delta H < 0$).

The mechanism of sorption and exchange of radioactive and stable isotopes of calcium and strontium in soils (and other materials) has been studied by numerous authors [12, 13]. According to most of these authors, the sorption of radioisotopes by soils corresponds best to a mechanism characteristic of ion-exchange equilibria. Therefore our investigations were primarily guided by principles determining the nature of ion-exchange equilibria.

Materials and investigation methods. The experiments were performed with soils and clays from the Er-genei region. Samples of these soils were saturated with ammonium ions (by the Gedroits method), powdered, and passed through a sieve ($d = 0.4$ mm). Equal samples (2 g) were taken for all variants of the experiments. The samples were put in flasks and treated with a mixture of NH_4Cl and SrCl_2 solutions in known volume proportions. The SrCl_2 (carrier) solution was tagged with the Sr^{90} radioactive isotope. The flasks were shaken mechanically (for an hour); after 48 hours the liquids were centrifuged. The solid-liquid ratio was maintained constant in all variants of the experiments (2 g of soil to 50 ml of solution). The experiments were performed at constant ionic strength of the solutions ($I \approx 0.1$).

* Presented at the 4th All-Union Conference on Colloid Chemistry, Tbilisi, May, 1958.

** The discrimination coefficient of Sr^{90} is the term used by American authors [1] for the ratio

$$\frac{\text{Sr/Ca in plant}}{\text{Sr/Ca in the surroundings}}.$$

Determination of Equilibrium Constants

In the general form, the exchange reaction of Ca and Sr ions on soils (denoted by H) can be represented by the equation



where HCa and HSr represents soil saturated with calcium and strontium ions, respectively, and Ca and Sr are the concentrations of these ions in the liquid phase.

Let us assume that Equation (1) is stoichiometrically correct and that the state of the system corresponds to the conditions in which the law of mass action is valid. Then the thermodynamic equilibrium constant K_a for the reaction can be calculated from the following equation:

$$K_a = \frac{a_{\text{Sr}} \cdot a_{\text{Ca}}}{a_{\text{Ca}} \cdot a_{\text{Sr}}}, \quad (2)$$

where a_{Sr} and a_{Ca} are the activities of strontium and calcium ions in the equilibrium solution, and a_{Ca} and a_{Sr} are the activities of these ions in the adsorbed state.

Equation (2) is well known in the literature. Several modifications of this equation have been proposed for quantitative determination of K_a in the systems considered in this paper. We used Nikol'skii's modification [14]:

$$K = \frac{(\text{Sr}) \cdot \text{Ca}}{(\text{Ca}) \cdot \text{Sr}}, \quad (3)^*$$

where Sr, Ca, and (Sr), (Ca) are the exchange masses of strontium and calcium ions in the liquid and solid phases, expressed in milligram equivalents.

Because of the chemical similarity of strontium and calcium and of the occurrence of side processes, determination of the equilibrium constant K from Equation (1) involves great difficulties. Therefore K was found by calculation from the constant K' and K'', corresponding to two intermediate equations:



The equilibrium constant of Equation (4)

$$K' = \frac{(\text{Ca})^{1/2} \cdot \text{NH}_4}{(\text{NH}_4) \cdot \text{Ca}^{1/2}},$$

was determined earlier [15], and was found to be $K' = 5.8$.

The equilibrium constant K'' of Equation (5) was found by two independent methods: by means of the Sr^{89} radioactive isotope [15], and by the usual method (from analytical data for the NH_4 and Sr ion contents in the liquid and solid phases).

* Derivation of this equation in the form used for calculation of K is given by us elsewhere [15].

Fairly close values were obtained by the isotope method and by the usual procedure for the constant K'' . The most probable value, found as the result of repeated determinations, was

$$K'' = \frac{(\text{Sr}^{1/2}) \cdot \text{NH}_4}{(\text{NH}_4) \cdot \text{Sr}^{1/2}} = 6,5. \quad (6)$$

Therefore, the constant we require is

$$K = \left(\frac{K''}{K'} \right)^2 = 1,2.$$

Determination of the Thermodynamic Characteristics ΔH , ΔF , ΔS

The thermodynamic characteristics of exchange reactions may be determined by various methods. In this investigation they were found by calculation from the numerical value of K and its dependence on the temperature.

The change of heat content (ΔH_{298}) in ion-exchange reactions can be calculated from the van't Hoff equation

$$\frac{d \ln K}{dT} = \frac{\Delta H}{RT^2}. \quad (7)$$

Our experiments [16], and the results of other investigators [17], showed that exchange of ions of equal valence is almost independent of the temperature (at least in the 20-70° range). Therefore

$$\frac{d \ln K}{dT} = 0. \quad (8)$$

Comparison of Equations (7) and (8) readily shows that $H_{298} = 0$, i.e., the exchange reaction of strontium and calcium ions in soils proceeds without any appreciable heat effect. Determination of the change of free energy (ΔF_{298}°) is of the greatest interest, as its numerical value determines not only the direction of exchange adsorption of calcium and strontium ions under natural conditions, but also the thermodynamic stability of adsorption complexes of these elements with the soil. The change of free energy was determined from the equation

$$\Delta F^\circ = -RT \ln K. \quad (9)$$

The value of ΔF found by this method was $\Delta F_{298}^\circ = -67,2$ cal.

ΔS was found from the Gibbs-Helmholtz equation

$$\Delta F - \Delta H = \frac{T d \Delta F}{dT} = T \Delta S. \quad (10)$$

It was shown above that $\Delta H = 0$; therefore

$$\Delta S = \frac{\Delta F}{T}, \quad (11)$$

and hence (after appropriate substitution)

$$\Delta S_{298}^\circ = 0,2 \text{ cal/g.}$$

Thus, the entropy of formation of II Sr has a very low value (almost zero). From this point of view the exchange of calcium and strontium ions in soils may be regarded as an isoenergetic process. However, the positive sign of ΔS_{298}° indicates that replacement of calcium by strontium ions in soils is accompanied by an entropy increase. Therefore the adsorption compound II Sr is thermodynamically more stable than II Ca , and under natural conditions the process will go spontaneously in the direction of II Sr formation.

In conclusion, let us attempt to clarify the role which may be played by the effects discussed above in processes of assimilation of strontium and calcium ions by plants. Whether we consider this process as physico-chemical [18] or biological [19], exchange and sorption effects of Ca and Sr ions in soils undoubtedly play a very important part in it. However, there is no method whereby, by simple extraction of strontium and calcium from soil, a reliable idea could be obtained concerning the energy of assimilation of these ions by the plants themselves. Nevertheless, the thermodynamic characteristics of the exchange adsorption of Sr and Ca ions in soils (K , ΔF , ΔS) provide not merely a qualitative but also a quantitative evaluation of processes of translocation and uptake of these elements by plants; in particular, they show that, theoretically, the most probable value of $DC = (\text{Sr/Ca in plant})/(\text{Sr/Ca in soil}) = < 1$ (if the energy of absorption of Sr and Ca by plants is the same). For the conditions under consideration, DC , found in accordance with the numerical value of the equilibrium constant, was found to be 0.9. A very similar value of DC was found by us experimentally. A similar order of magnitude has been reported in the literature [2]. However, the literature also contains contradictory data, according to which $DC \gg 1$.

This shows that the processes under consideration cannot as yet be explained satisfactorily because of their complexity.

SUMMARY

1. The radioactive isotope method was used to study the exchange adsorption of strontium and calcium ions on soils and clays.
2. The basic criteria of equilibrium were determined and the principal thermodynamic functions (ΔH_{298} , ΔF_{298}° , ΔS_{298}) calculated.
3. The numerical values of H , F , and S show that the reaction is isoenergetic in character; they also indicate that the adsorption compound II Sr is thermodynamically more stable than II Ca .
4. The results were used for calculation of the most probable value of the discrimination coefficient of Sr^{90} in the soil - plant system; it was found to be < 1 in all cases, and varied from 0.8 to 0.9.

In conclusion, I thank I. N. Antipov-Karataev for help and advice in the course of this investigation.

LITERATURE CITED

- [1] C. L. Comar, R. Scott Russell, and R. H. Wasserman, *Science* 126, No. 3272, 485 (1957).
- [2] R. P. Martin, P. Newbould, and R. Scott Russell, *International Congress on Radioisotopes in Scientific Research* (1957) p. 29.
- [3] I. N. Antipov-Karataev, *Use of Isotopes in Technology, Biology, and Agriculture* [in Russian] (Izd. AN SSSR, Moscow, 1955) p. 20.
- [4] V. M. Klyuchevskii and I. V. Gulyavkin, *Pedology* No. 3, 1 (1958).
- [5] C. Amphlett, *World Crops*, 9, No. 3, 112, (1957).
- [6] A. A. Selders, J. H. Rediske, and R. F. Palmer, *The Absorption and Translocation by Plants of Radioactive Elements from "Jungle" Soil* AEC Document NW - 27620 (unclassified) (February, 1953).
- [7] K. G. Menzel, *Soil Sci.* 77, 419 (1954).
- [8] T. Harada and K. Kutsuma, *Bull. Nat. Inst. Agricul. Sci. (Japan)*, B, No. 5, 1, (1955).
- [9] L. Jacobson and R. Overstreet, *Soil. Sci.* 65, 129 (1948).
- [10] I. Vlamis and G. A. Pearson, *Science*, 111, 112, (1950).

- [11] T. Egawa, E. Limura, T. Shirai, T. Voshida, H. Kwarazaki, M. Kono, and S. Tsukahara, Food 1, No. 19, (1955).
- [12] Yu. A. Polyakov (with N. S. Germagenova), Pedology No. 8, 57 (1956).
- [13] N. V. Timofeev-Resovskii, Botanical J. 42, 161 (1957).
- [14] B. P. Nikol'skii, "Modern Methods for Investigation of the Physicochemical Properties of Soils," No. 3 [in Russian] (Izd. AN SSSR, 1948) p. 166.
- [15] Yu. A. Polyakov, Pedology No. 7, 59 (1955).
- [16] Yu. A. Polyakov, Paper at the 6th International Congress of Soil Science [in Russian] (Izd. AN SSSR, Moscow, 1956) p. 187.
- [17] H. Walton, Ion Exchange (IL, Moscow, 1957) p. 7 [Russian translation].
- [18] H. I. M. Bowen, and I. A. Dymond, J. Exptl. Bot. 7, 264, (1956).
- [19] H. I. M. Bowen, and I. A. Dymond, Proc. Roy. Soc. 144, 355, (1955).

Received January 16, 1959

CAUSES OF FORMATION, AND CERTAIN PROPERTIES, OF AIR DISPERSIONS IN VISCOSE

K. E. Perepelkin

The All-Union Scientific Research Institute
for Artificial Fibers, Mytishchi

One of the main difficulties in the spinning of viscose fibers is the presence of air in the spinning viscose, in the form of bubbles of various sizes (dispersed air) and in the dissolved state [1]. A special operation, deaeration, is needed to remove the air, and normal spinning depends on the effectiveness with which this operation is carried out [2-5].

For proper preparation of viscose for spinning, it is necessary to know the properties of the air - viscose system, which is a polydisperse dilute emulsion of the gas - liquid type. With the exception of a few investigations [6,7], systems of this type have been studied very little; nearly all the investigations deal with concentrated gas - liquid - foam systems. In real polydisperse systems, the disperse-phase particles grow, mainly as a result of coalescence or coagulation. However, apart from this, particle growth may occur by molecular transfer of the disperse-phase substance from the smaller to the larger particles; this has been demonstrated almost exclusively for only two types of disperse systems - suspensions and aerosols [8-11]. In addition, there are papers by Solomin [12] and Kurlyankin [13], who studied changes of bubble size in softened quartz glass in the course of manufacture.

Gas - liquid phase transitions play an important role in the viscose industry. However, there have been virtually no investigations in this field. It was therefore necessary to determine the principal properties of the air - viscose disperse system; in particular, the causes of its formation, its dispersity, and its variations with time.

For determination of the dispersity of air - viscose gaseous emulsions, the microscopic method was used; this was chosen because it is the most convenient, simple, and rapid. The bubbles were counted and measured by means of a long-focus microscope ($\times 10$) fitted with a micrometer eyepiece. The total amount of dispersed air in viscose was determined by dilatometric or conductovolumetric methods [14-16].

For determinations of the dispersity of air bubbles in viscose, about 30 sets of measurements were carried out on viscoses made by the "standard" method and in vacuum xanthator-mixers; the average results are plotted in Fig. 1. Curves for the volume distribution of air bubbles in viscose are shown in Fig. 2. In Figs. 1 and 2 regions corresponding to 50 and 95% of the total number of bubbles are marked by dash lines. By volume, this corresponds to roughly 1.3-1.4 and 12-13% of the total volume of the air bubbles in viscose. In the viscose samples studied, taken after mixing, the total content of dispersed air determined by the dilatometric method is on the average 29.2 ml/liter (with variations from 27 to 33 ml/liter). It follows that half of the total number of bubbles consisting of the smaller bubbles occupies 0.33-0.46 ml per liter of viscose, and 95% of the bubbles occupies 3.3-4.3 ml per liter of viscose. The smallest bubbles to be found in freshly mixed viscose have a diameter of $0.4 \cdot 10^{-3}$ cm.

Analyses showed that the air in viscose contains $\sim 8\%$ of carbon disulfide (from 4.9 to 10.2%) and virtually no oxygen, as it evidently reacts with the easily oxidized components in viscose. Therefore, the gas in viscose can be described as "air" conventionally, only.

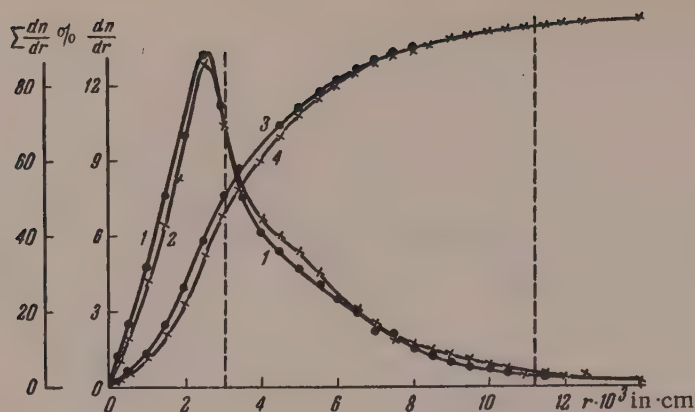


Fig. 1. Integral and differential size-distribution curves for air bubbles dispersed in viscose: 1,3) viscose from mixers; 2,4) viscose from vacuum xanthator-mixers; dash lines indicate regions corresponding to 50 and 95% of the total number of bubbles.

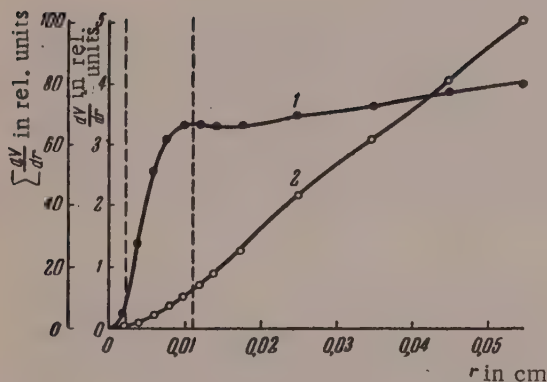


Fig. 2. Curves for the distribution of air bubbles by volume: 1) differential curve; 2) integral curve; the dash lines are as in Fig. 1.

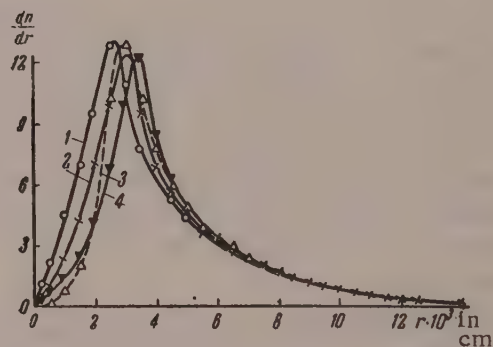


Fig. 3. Change in the dispersity of air bubbles in viscose with time: 1) original viscose; 2) viscose after 3 hours; 3) viscose kept under pressure; 4) viscose after 6 hours.

Air entering viscose during its manufacture may originate from the following sources: a) air present within the pores in the xanthate particles, and between the latter; b) air dissolved in the mixing caustic; c) air stirred in by the mixers or other mechanisms. The fact that the size-distribution curves of air bubbles in viscose are independent of the technical conditions and the dissolving equipment suggests that the main source of air in viscose is air present in the xanthate or mixing caustic, and not air stirred into the viscose in the mixers.

Experiments were performed on the stirring of air by means of mixers into viscose from which dispersed air had been removed; it was found that a disperse system with air bubbles < 0.05 mm cannot be obtained in this way, and that the content of bubbles of this size is very low. The size-distribution curve so obtained is quite different from Fig. 1, and is shifted far to the right.

Experiments on xanthate dissolving under laboratory conditions showed that the distribution curve for the air bubbles in the viscose is similar to the curves in Fig. 1. Experiments on dissolving of xanthate in mixing caustic deaerated by boiling, and also on dissolving under vacuum in the initial stages, showed that the amount of dispersed air diminishes (see table); this is in full agreement with the foregoing hypothesis.

Residual pressure, mm	Amount of air dispersed in viscose, ml/liter			
	caustic not deaerated		caustic deaerated	
	sample 1	sample 2	sample 1	sample 2
763	28.2	27.6	24.6	24.3
450	27.5	25.8	22.3	22.6
250	19.9	20.8	16.2	14.3
150	15.6	12.7	9.2	8.5
50	11.2	9.3	6.3	5.5

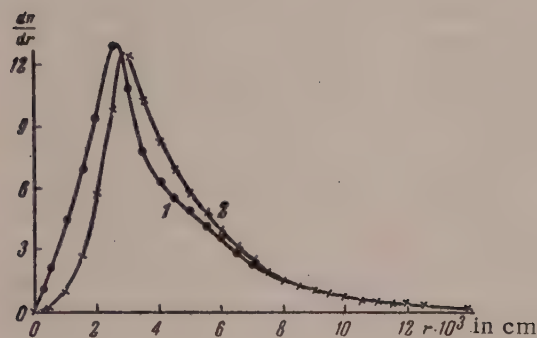


Fig. 4. Change in the dispersity of air bubbles in viscose before deaeration: 1) viscose after dissolving; 2) viscose before deaeration.

It follows from the table that in order to decrease the amount of air in viscose the dissolving should be carried out under vacuum.

The isobaric-isothermal potential of the system air bubbles - viscose, per mole of gas phase, increases with decreasing bubble radius, since the specific maximum work of surface formation increases. It follows that in the real polydisperse system air - viscose, air should pass from small to large bubbles, changing the distribution curve.

The driving force in the redistribution of bubble size is the difference of pressure due to surface tension forces (σ_{GL}) in bubbles of different radius (r)

$$\Delta P = P'_r - P''_r = \frac{2\sigma_{GL}}{r_1} - \frac{2\sigma_{GL}}{r_2} = 2\sigma_{GL} \left(\frac{1}{r_1} - \frac{1}{r_2} \right). \quad (1)$$

To simplify the picture somewhat, we may assume that the solution is in equilibrium with bubbles of radius r_x . Then this solution is undersaturated with respect to bubbles of radius $r_1 < r_x$, and supersaturated with respect to bubbles of radius $r_2 > r_x$. Accordingly, we may write the following differential equations for diffusion in the dissolution of small bubbles and growth of large bubbles:

$$\left(\frac{dm}{d\tau} \right)_1 = -2\beta S_1 \sigma_{GL} \left(\frac{1}{r_1} - \frac{1}{r_x} \right), \quad (2)$$

$$\left(\frac{dm}{d\tau} \right)_2 = -2\beta S_2 \sigma_{GL} \left(\frac{1}{r_2} - \frac{1}{r_x} \right), \quad (3)$$

where S_1 and S_2 are the bubble surface areas; β is the diffusion coefficient of the gas through the gas - liquid interface.

Assuming, as an approximation, that all the air from the dissolved small bubbles passes into the large bubbles, we have

$$\sum \left(\frac{dm}{d\tau} \right)_1 + \sum \left(\frac{dm}{d\tau} \right)_2 = 0; \quad (4)$$

$$\sum S_1 \left(\frac{1}{r_1} - \frac{1}{r_x} \right) + \sum S_2 \left(\frac{1}{r_2} - \frac{1}{r_x} \right) = 0. \quad (5)$$

After rearrangement, in view of the fact that

$$\sum S = 4\pi \sum r^2 \frac{dn}{dr}, \quad (6)$$

where \underline{n} is the number of bubbles, we have

$$r_x = \frac{\sum S}{\sum S/r} = \frac{\sum r^2 \cdot dn/dr}{\sum r \cdot dn/dr}. \quad (7)$$

Since the distribution curve changes with time, r_x increases, the maximum on the distribution curve is shifted to the right and becomes lower, and the whole curve is shifted to the right. To confirm this, a sample of viscose, containing dispersed air for which the distribution curve was known, was placed in an ampoule which was rotated slowly to avoid sedimentation of the bubbles. After 3-6 hours the distribution curve was determined again. The distribution curves in Fig. 3 fully confirm the above conclusions.

It was also of interest to see how the distribution curve changes if viscose containing dispersed air is subjected to a pressure of several atmospheres. The smallest air bubbles should dissolve, and after reduction of the pressure (to atmospheric) the dissolved air should be liberated into the remaining bubbles only; the dispersity of the bubbles in the viscose should accordingly decrease. This hypothesis was confirmed when viscose (Curve 1, Fig. 3) was kept for 30 minutes under a pressure of 5 atmos and then under atmospheric pressure for 15 minutes (see Curve 4, Fig. 3). The laboratory results were confirmed by measurements of the air-bubble distribution in viscose fed into the storage tanks immediately after the dissolving, and viscose taken for deaeration (Fig. 4).

Virtually no coalescence of air bubbles is observed in viscose; this is probably because viscose is strongly structurized. In none of the experiments concerned with air dispersed in viscose was coalescence of bubbles observed, even if the bubbles were in mutual contact for a long time. The high stability of viscose foam also confirms the high strength of the films between air bubbles in viscose. Special experiments in which viscose was forced through a filter material by means of a gear pump also demonstrated that there was no coalescence of bubbles.

SUMMARY

1. Most of the air bubbles in production viscose are $(2-6) \cdot 10^{-3}$ cm in diameter.
2. The main source of air in viscose is air present in the pores of the xanthate particles and dissolved in the caustic. The amount of air in viscose is reduced considerably if vacuum is used during dissolving.
3. It was shown in the laboratory and under production conditions that the dispersity of the air bubbles in viscose changes in course of time not as the result of bubble coalescence, but as the result of molecular transfer processes.

LITERATURE CITED

- [1] A. B. Pakshver and N. Kamyshan, *Org. Chem. Ind.* 3, No. 2, 76 (1937).
- [2] A. A. Konkin, *Artificial Fibers in Italy* [in Russian] (Moscow, Ministry of the Textile Industry Press, 1955).
- [3] A. N. Ryauzov, V. A. Gruzdev, and M. A. Artemenko, *Technology of Artificial Fibers* [in Russian] (State Light Industry Press, 1952).
- [4] Z. A. Rogovin, *Chemistry and Technology of Artificial Fibers* [in Russian] (State Light Industry Press, 1957).
- [5] K. E. Perepelkin and A. I. Meos, *Textile Ind.* No. 11, 12 (1956).
- [6] A. Krause and U. Kapitancyk, *Kolloid-Z.* 56, 50, (1931); 66, 288, (1934), 71, 55, (1935); 80, 273, (1937).

- [7] H. A. McTaggart, Trans. Roy. Soc. Can. (8) 18, 129, (1924); (3) 21, 249, (1927).
- [8] K. S. Lyalikov, in the book: Problems of Kinetics and Catalysis [in Russian], No. 7 (Izd. AN SSSR, 1949).
- [9] H. L. Frisch and F. C. Collins, J. Chem. Phys. 1797, (1952); 2158, (1953).
- [10] O. M. Todes, in the book: Problems of Kinetics and Catalysis [in Russian] No. 7 (Izd. AN SSSR, 1949).
- [11] L. Ya. Kremnev and A. A. Ravdel', Colloid J. 16, 17 (1954).*
- [12] N. V. Solomin, Proc. Acad. Sci. USSR 60, 93 (1948).
- [13] F. A. Kurlyankin, Glass and Ceramics No. 2, 27 (1936); No. 12, 13 (1951); Refractories 5, No. 8, 533 (1937).
- [14] A. I. Meos and K. E. Perepelkin, et al., Industrial Lab. No. 5, 606 (1956).
- [15] K. E. Perepelkin, Report of the Scientific and Technical Conference of the S. M. Kirov Technological Institute, Leningrad [in Russian] (1955) p. 137.
- [16] K. E. Perepelkin, in the book: Artificial Fibers, No. 16 [in Russian] BTI Light Industry Press (1958) p. 25.

Received July 27, 1958

*Original Russian pagination. See C.B. Translation.

ELECTROCHEMICAL STUDIES OF BENTONITE SUSPENSIONS

3. POTENTIOMETRIC AND CONDUCTOMETRIC TITRATION OF ELECTRODIALYZED ASKANGEL SUSPENSIONS BY ALKALI METAL HYDROXIDES

I. A. Uskov and E. T. Uskova

The T. G. Shevchenko University, Kiev;
The Ukrainian Academy of Agricultural Sciences

Despite the numerous published investigations of adsorption of cations by native aluminosilicates, there are no clear ideas concerning the influence of such properties of the ions as size, hydration, and polarizability on adsorption [1]. Questions of fixation and location of cations in the aluminosilicate crystal lattice are still controversial. There is no agreed view concerning the cation-sorption capacity of clays. The view that the sorption capacity cannot be represented by a single quantity is becoming increasingly adopted [2].

These questions are especially interesting in relation to clay minerals of the montmorillonite type which are known to have the highest sorption capacity and also a number of specific properties due to an expansible crystal lattice [1].

Potentiometric and conductometric titrations performed over a period of time were chosen as the most suitable methods for the present investigation. Electrodialyzed askangel suspensions were titrated by the hydroxides of lithium, sodium, potassium, rubidium, and cesium. The material and the determination technique are described in previous communications [3].

Potentiometric titration. The pH variations with the amounts of hydroxides added, for different times of action on electrodialyzed bentonite suspension, are plotted in Figs. 1 and 2. The curves obtained immediately after addition of the alkalis are similar to the curves for potentiometric titration of a weak acid by a strong base. All the curves except the LiOH curve have a single inflection point at pH 8-8.5. A second inflection at pH 10-10.4 appears 24 hours after the alkali addition, and in the case of LiOH after a few minutes. This inflection becomes more pronounced with time. The curves shift with time in the direction of larger amounts of bases. The amounts of the bases corresponding to the inflections on the curves are given in Table 1.

In the early stages of alkali action the nature of the cation has a considerable influence on the position of the first inflection point. The amounts of bases taken up vary as follows in the alkali-metal series: LiOH is taken up in the greatest amount; the amount of NaOH is less, and of KOH less still; the amounts increase again for rubidium and cesium hydroxide. In order of adsorbability, determined by the ability to occupy exchange sites on the clay particles, the first place is taken by lithium, followed by cesium and rubidium, then sodium, and finally potassium.

In electrodialyzed bentonite the principal exchange cations are aluminum ions [3]. When a base is added to the suspension, displacement of the exchange aluminum by the base cations is accompanied by its binding in the form of insoluble hydroxide. At first this binding favors exchange. However, the great majority of the exchange cations are contained between the silicate layers of the montmorillonite lattice [4]. These cations are available for exchange owing to the presence of intracrystalline water in the spaces between the layers [5]. Accumulation of aluminum hydroxide between the layers causes steric hindrance to further penetration of the base cations to the exchange sites.

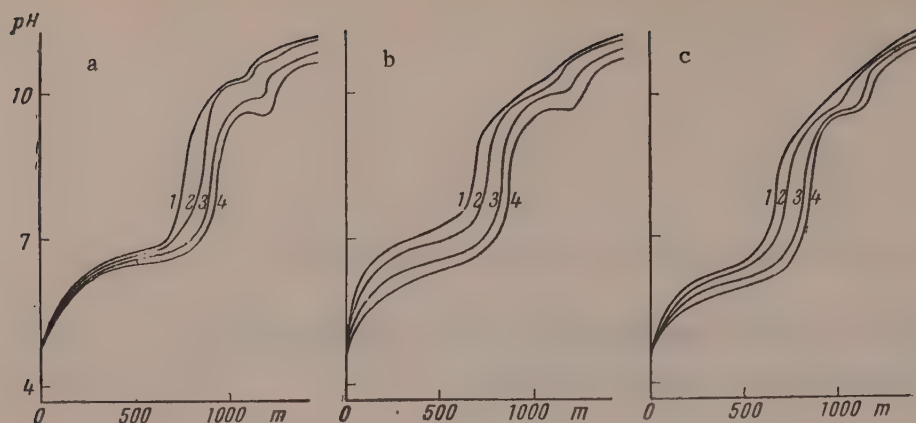


Fig. 1. pH variations of electrodyalized askangel suspension under the action of: a) LiOH for 1) 5 minutes; 2) 1 day; 3) 8 days; 4) 14 days; b) NaOH for 1) 5 minutes; 2) 1 day; 3) 8 days; 4) 15 days; c) KOH for 1) 5 minutes; 2) 2 days; 3) 10 days; 4) 16 days.

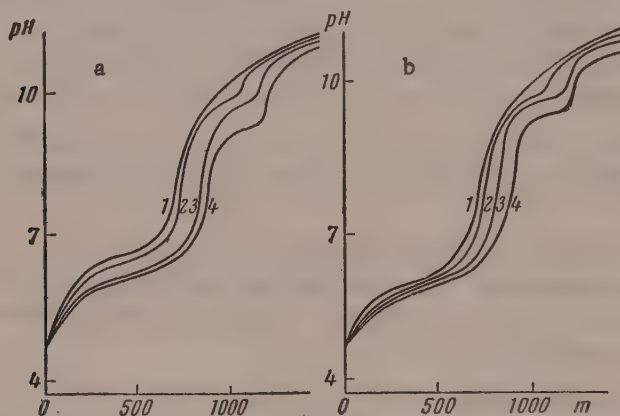


Fig. 2. pH variations of electrodyalized askangel suspension under the action of: a) RbOH for 1) 1 minute; 2) 1 day; 3) 10 days; 4) 13 days; b) CsOH for 1) 5 minutes; 2) 1 day; 3) 6 days; 4) 13 days.

Under such conditions the penetrating power of cations should diminish with increase of their size. It follows from a comparison of the action of lithium, sodium, and potassium hydroxides that the ions are adsorbed in the nonhydrated state. Indeed, the strongly hydrated lithium ion, which is very large (Table 2), should penetrate more slowly into the crystal lattice than ions of sodium and potassium, which are considerably smaller under the same conditions. The reverse is the case in practice.

The observed behavior of the cations is evidently associated with differences in the sizes of the nonhydrated ions. The hypothesis that adsorbed ions occupy exchange sites in montmorillonite in the nonhydrated state is supported by the data of numerous workers [1] on swelling, heats of wetting, dehydration, etc.; these results show poor agreement with the assumption that adsorbed cations are hydrated.

Our conclusion is not inconsistent with the observations of Wiegner [6], who showed that more highly hydrated ions have lower exchange energies. As has already been stated, when hydroxides interact with electrodyalized bentonite, what happens is not mere replacement of exchange aluminum, but also simultaneous binding of the aluminum by the hydroxyl groups of the added base, with formation of aluminum hydroxide, which is in-

TABLE 1

Sorption of Bases and Variations of Conductivity of Electrodialyzed Askangel Suspensions

Base	Time of action of base, days	First inflection		Second inflection		Relative conductivity increases in $\text{ohm}^{-1} \times 10^{-3} \text{ meq}^{-1}/\text{g}$
		pH	amount of base in meq/g	pH	amount of base in meq/g	
LiOH	0	8,4	750	10,4	1110	0,46
	1	8,45	850	10,4	1130	0,36
	8	8,3	900	10,1	1190	0,32
	14	8,2	920	9,85	1220	0,30
NaOH	0	8,4	670	(10,4)	(1080)	0,44
	1	8,4	740	10,4	1130	0,48
	8	8,15	820	10,25	1200	0,50
	14	8,1	860	10,1	1250	0,48
KOH	0	8,1	650	—	—	0,30
	2	7,8	710	10,0	1030	0,32
	10	7,9	805	10,1	1120	0,32
	16	7,7	840	10,1	1170	0,31
RbOH	0	8,0	715	—	—	0,38
	1	8,05	740	10,25	1070	0,34
	9	7,9	830	10,2	1160	0,26
	13	7,8	880	9,65	1185	0,24
CsOH	0	8,1	720	—	—	0,40
	1	8,0	750	10,2	1100	0,34
	6	7,9	815	10,2	1170	0,28
	13	7,85	890	9,75	1200	0,20

TABLE 2

Influence of Cation Size and Polarizability on the Amounts of Bases Taken Up by Electrodialyzed Askangel Suspension During 24 Hours

Cation	Ionic radius, A		Polarization coefficient $\times 10$	Sorption, meq/g
	nonhydrated	hydrated		
Lithium	0.68	10.03	0.029	750
Sodium	0.98	7.90	0.187	670
Potassium	1.33	5.32	0.888	650
Rubidium	1.48	5.09	1.49	710
Cesium	1.65	5.05	2.57	720

soluble in a weakly alkaline medium. Therefore, in our experiments on the action of bases on electrodialyzed askangel, the ability of the cations to penetrate and approach the exchange sites, their "penetrating power," is important, in addition to their replacing power.

For a graphic illustration of the influence of the size of nonhydrated ions on their penetrating power, Fig. 3 shows variations of the amounts of hydroxides taken up as functions of the nonhydrated ionic radius, for different times of action of these hydroxides. When the measurement times were different from those indicated in Fig. 3, the amounts of bases taken up were found by interpolation from "base uptake — time of base action" curves, plotted from the data in Table 1.

Each curve in Fig. 3 has a minimum, indicating the influence of two opposing factors determining the base uptake. The descending branch of the curve is satisfactorily accounted for by increase in the radii of the nonhydrated ions and the consequent difficulties in penetration to the exchange sites. However, further increase

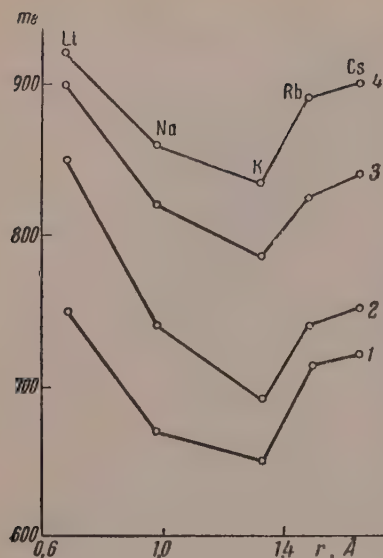


Fig. 3. Variations of the amounts of alkali metal hydroxides taken up by electrolyzed askangel suspension with the nonhydrated ionic radius, for different times of hydroxide action: 1) 5 minutes; 2) 1 day; 3) 8 days; 4) 14 days.

of the ion size from potassium to cesium is accompanied by increasing adsorption. The large size of these ions not only does not hinder their entry into the crystal lattice of the clay mineral, but even facilitates it. The better penetration of large ions may be due to their polarizability, which increases with ion size (Table 2).

It is clear from Table 2 that the polarizability of cesium and rubidium is tens of times as high as that of lithium, and several times greater than that of potassium. Bar and Tenderloo [7] showed that strongly polarized ions are retained more firmly by clay surfaces. It is likely that ionic polarizability is especially prominent in the case of rubidium and cesium, so that their adsorbability is higher.

Fig. 3 shows that the general nature of the variations of the amounts of cations adsorbed with their size remains the same over the whole time range studied. However, the minimum becomes less deep with increased action time of the bases. It is possible that in a very long experiment the difference between the amounts of bases taken up would vanish entirely. This means that the true sorption capacity would be the same for all the alkali metal hydroxides. The differences of ion-exchange capacity found in the action of different bases on electrolyzed bentonite under conditions in which equilibrium is not reached indicate that the ions approach the exchange sites at different velocities. The times required to reach equilibrium must evidently differ for the different cations studied.

Conductometric titration. The variations in the conductivity of the suspension with the amounts of added alkalies and the time of their action are similar to those found by us earlier for sodium hydroxide [3].

The absence of sharp breaks at the points where the first and third linear regions of the conductometric titration curves meet the second region, the linear nature of which is not always well defined, hinders graphical determination of the maximum amounts of bound bases. However, we are concerned not with calculation of these amounts, which are easily found potentiometrically, but with variations of the degree of dissociation of the metal-substituted bentonites from one base to another, and also with time. These variations can be estimated from conductivity changes in the region of partial substitution of the bentonite by the cation of the added base, i.e., in the first linear portion of the conductometric titration curve.

The conductivity changes are conveniently expressed per unit amount of base added to unit amount of bentonite. Table 1 contains the increases of conductivity produced by addition of a microequivalent of base to a gram of bentonite.

The data in Table 1 show that the degree of dissociation of metal-substituted bentonites decreases with time. This decrease is considerable for lithium, cesium, and rubidium askangels, and very small for sodium and potassium askangels.

According to modern views on the structure of montmorillonite, the adsorbed cations are situated mainly in the spaces between the layers, and partially (about 1/5) at the sites of disrupted bonds. Cations of the interlayer space may enter through the hexagonal openings of the oxygen network in the tetrahedron layer of montmorillonite [8]. Such cations are retained more firmly at the exchange sites than those present in the interlayer space. The observed decrease in the degree of dissociation of metal-substituted bentonites with time is evidently associated with entry of adsorbed ions into the spaces of the tetrahedron layer. Lithium ions, being small, and rubidium and cesium ions, being strongly polarized, penetrate more rapidly into these spaces than sodium and potassium ions, which are much larger than lithium ions and less polarized than rubidium and cesium ions.

The amounts of different bases taken up in a given time are different. For a comparison of the degrees of dissociation of different substituted bentonites, of equal degree of substitution by the base cations, calculations were made for times corresponding to binding of 750 meq of base per g.

The relative increases of conductivity of electrolyzed askangel suspensions at limiting saturation with 750 meq of base per g are:

Lithium	0.48	$\text{ohm}^{-1} \cdot 10^{-3} \cdot \text{meq}^{-1}$
Sodium	0.43	" "
Potassium	0.34	" "
Rubidium	0.34	" "
Cesium	0.32	" "

The relative conductivity increase is greatest for lithium hydroxide, somewhat less for sodium hydroxide, and considerably less for the other bases.

It follows that lithium bentonite is the most strongly dissociated, and sodium bentonite is somewhat less. Potassium, rubidium, and cesium bentonites are dissociated to approximately the same extent, and considerably less than lithium or sodium bentonites. Thus, potassium, rubidium, and cesium ions are retained at the exchange sites more firmly than lithium or sodium ions.

From the results of conductometric determinations it is possible to deduce how the cations penetrate to the active sites of the bentonite lattice and how they are retained there. Lithium ions penetrate easily to the exchange sites because of their small size, but can leave them easily also. In the case of sodium ions, the aluminum hydroxide formed in the interlayer space is a more serious steric obstacle which lowers their penetrating power. However, sodium ions are still smaller than the spaces of the tetrahedron layer, and therefore they are still fairly mobile. Potassium penetrates with the most difficulty to the exchange sites because of the large size and not very high polarizability of the ions; the diameter of the potassium ion exactly corresponds to the size of the spaces in the octahedron layer and when it has entered them it is firmly retained in the adsorbed state. Rubidium and cesium ions penetrate easily to the exchange sites because of their high polarizability, but, in contrast to lithium, they are firmly retained by polarization forces.

Cation adsorbability is determined by numerous factors; the most important are the ionic charge, size, hydration, and polarizability. In the interaction of acid bentonite with bases the degree of dissociation of the latter should also have an effect. In our experiments all the bases used were strong, and their cations univalent. By virtue of this we can judge the influence of cation size and hydration in the adsorbed state on adsorption from the results of potentiometric and conductometric titrations performed over a period of time.

SUMMARY

1. Potentiometric and conductometric titration of electrolyzed askangel suspensions by alkali metal hydroxides were performed over a period of time.

2. Potentiometric curves determined immediately after additions of sodium, potassium, rubidium, and cesium hydroxides each have a single inflection at pH 8-8.5. In the case of lithium hydroxide the curve has a second inflection at pH 10.4. On the second day this inflection appears on all the curves.

3. The first inflection point shifts with time toward larger amounts, which depend on the nature of the cation, of bases taken up.

4. Relative changes in the conductivity of the suspension on addition of hydroxides were calculated from the slopes of the initial region of the conductometric titration curves. This slope decreases with time for lithium, cesium, and rubidium bentonites. Its value gives an indication of the degree of dissociation of different substituted bentonites. This is highest for Li bentonite, somewhat less for Na bentonite, and much less for K, Rb, and Cs bentonites.

5. Penetration of alkali metal cations to the exchange sites in the montmorillonite lattice is influenced by the dimensions of the ions in the nonhydrated state and by their polarizability.

6. It is possible that when equilibrium is reached in the system, the sorption capacity of bentonite, determined potentiometrically, is the same for all cations.

LITERATURE CITED

- [1] R. E. Grim, *Mineralogy of Clays* (IL, Moscow, 1956) [Russian Translation].
- [2] V. I. Paramonova, O. N. Grigorov, and B. P. Nikol'skii, *Colloid J.* 6, 249 (1940); B. N. Nikol'skii and V. I. Paramonova, *Sci. Mem. Leningrad State Univ., Chem. Sci. Ser.* No. 7, 3 (1945).
- [3] I. A. Uskov and E. T. Uskova, *Colloid J.* 19, 361 (1957);* 20, 487 (1958).*
- [4] U. Hofmann, and K. Endell, D. Wilm. *Z. Kristallogr.* 86, 340, (1933); C. E. Marshall, *Z. Kristallogr.* 91, 433, (1935); S. B. Hendricks, *Z. Kristallogr.* 50, 276, (1942).
- [5] U. Hofmann, *Angew. Chemie* 68, 53, (1956).
- [6] G. Wiegner and H. Jenny, *Kolloid. Z.* 43, 268, (1927).
- [7] A. L. Bar and H. J. Tenderloo, *Kolloid. Beich.* 44, 97, (1936).
- [8] E. A. Hauser, *Chem. Revs.* 37, 287, (1945).

Received April 27, 1957

*Original Russian pagination. See C.B. Translation.

STATES OF AGGREGATION OF HIGH POLYMERS

3. SYNTHETIC POLYAMIDES

R. I. Fel'dman

The N. K. Krupskaya Moscow Regional Pedagogic Institute

The previous communications [1,2] described the influence of temperature on the states of aggregation of polymer systems, determined by the dilatometric method in the course of heating and cooling. Special attention was devoted to the behavior of anisotropic materials. It was also shown, with polyethylene and gutta percha as examples, that the behavior of crystallizing and noncrystallizing polymers is similar in many respects in investigations of this type [2].

The present paper contains data on crystallizing polymer systems, which contain, because of their affinity for water and hygroscopicity, variable amounts of a low-molecular component — water. The materials studied were certain types of polyamides, which may contain from 4 to 6% moisture under normal conditions. The effects of temperature on specimen length (l from 10 to 20 cm) were studied by the method described earlier [1]; variations of weight with the temperature, caused by sorption and loss of moisture, were investigated by means of a spring microbalance.

In order to determine the influence of specific surface on the variations of length and weight with temperature, samples of different shapes were tested: rods, films, and threads of polycaprolactam (capron), and threads of the polycondensation product of hexamethylenediamine with adipic acid (nylon). With specimens of large specific surface the total change of moisture content in the course of an experiment may be so considerable as to influence the linear dimensions of the specimens; therefore, this influence must be taken into account as an independent factor.

Polycaprolactam

Linear dilatometry*. The tests were performed on rods of average thickness 3.5 mm, and 45 mm^2 in cross-sectional area. The results of the tests, which comprised five heating — cooling cycles (total duration 14 days), are given in Fig. 1, I. The values found for the length in the first three cycles ($18^\circ \rightarrow 100^\circ \rightarrow 18^\circ$) almost coincide with the length at 100° in Cycle 4. Transition of the system into another (more stable) state is favored by heating above 100° ; this is shown by the direction of the cooling lines for Cycles 4 ($18^\circ \rightarrow 155^\circ \rightarrow 18^\circ$) and 5 ($18^\circ \rightarrow 204^\circ \rightarrow 18^\circ$), shown by a dotted line. The length change from the start (A) to the end (B) of the tests was 1%. The coefficient of linear expansion (cm/degree · cm) in the range from 18 to 197° changed from $1.2 \cdot 10^{-4}$ to $3.8 \cdot 10^{-4}$.

Films were 1 mm^2 in cross-sectional area and 0.1 mm thick. In view of the anisotropy of the films, resulting from the manufacturing process, specimens were tested in the form of strips with their long sides parallel to the direction of orientation (Type I), and strips cut at right angles to the principal orientation direction (Type II). Specimens of Type I contract when heated to a certain temperature, and lengthen on cooling. In illustration, Fig. 1, II shows the effect of temperature on length, determined under load $P = 3.5 \text{ g/mm}^2$. Specimens heated from 5 to 95° under these conditions contracted by ~3%. The hysteresis loop which commences at $50\text{--}60^\circ$ decreases on repeated heating. This relationship is somewhat more complex for Type II specimens. For $P = 3.8 \text{ g/mm}^2$ the maximum contraction when the specimens are heated from 5 to 95° is ~5%, which is more than for

* I. Shtern took part in the experimental work.

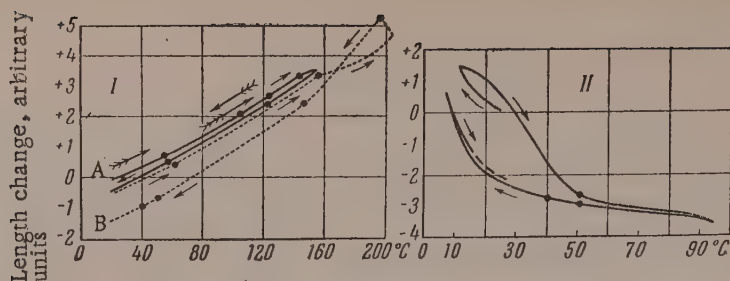


Fig. 1. Effect of temperature on length: I) capron rods, $P = 7.4 \text{ g/mm}^2$; II) capron films, $P = 3.5 \text{ g/mm}^2$.

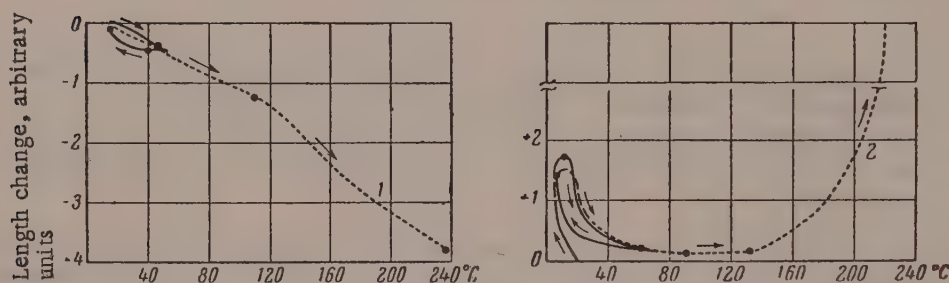


Fig. 2. Effect of temperature on length of capron threads: 1) $P = 19 \text{ g/mm}^2$; 2) $P = 371 \text{ g/mm}^2$.

Type I specimens. The $l = f(t^*)$ curves for Type 2 specimens subjected to additional extension are quite analogous to the Type I curves. Tests on specimens of Types I and II after storage under room conditions for $6\frac{1}{2}$ years showed that the form of the dilatometric curves did not change significantly. These experiments show that the properties of the films are very stable in time. The form of the $l = f(t^*)$ heating and cooling curve and the contraction (shrinkage) depends on such factors as the maximum heating temperature, the applied load in the tests, exact direction of cutting of the specimens (which involves considerable practical difficulties), and the degree of preliminary extension. For example: 1) Type II specimens additionally stretched by $\sim 250\%$ and heated to 100° shrink by $\sim 15\%$ in water; 2) Type I specimens stored for a long time and tested under a load of 5.4 g/mm^2 show the following maximum contractions: in the first cycle ($22^\circ \rightarrow 68^\circ \rightarrow 22^\circ$) 0.62% , in the second cycle ($22^\circ \rightarrow 128^\circ \rightarrow 19^\circ$) 0.5% , and in the third cycle ($19^\circ \rightarrow 148^\circ \rightarrow 19^\circ$) 1.2% , and in the fourth cycle ($19^\circ \rightarrow 186^\circ \rightarrow 18^\circ$) 2.9% . At 182° contraction ceases and is replaced by elongation. Different results are obtained when $P = 3.5 \text{ g/mm}^2$; 3) the course of $l = f(t^*)$ curves for Type I specimens, previously heated in vaseline oil to 180° and then rapidly immersed in oil at -4° , did not change significantly, but the maximum contraction found in the corresponding heating and cooling cycles decreased approximately 2-fold even under the smaller load; this may be of practical significance. For example, in the $20^\circ \rightarrow 184^\circ \rightarrow 20^\circ$ cycle, the contraction observed on heating to 181° reached 1.4% at $P = 4.2 \text{ g/mm}^2$.

The effect of temperature on the length of commercial threads of cross-sectional area $S = 2.64 \cdot 10^{-4} \text{ cm}^2$, is shown in Fig. 2. The behavior of the specimens is similar up to $\sim 90^\circ$ despite the large difference between the loads (Curves 1 and 2), but it differs above this temperature. Thus, in the examples in Fig. 2, the contraction of the specimens when heated from 8° to break at 235° is 8% (Curve 1, small load) and from 9° to 60° it is $\sim 3.5\%$ (Curve 2), while from 130° to break at 216° there is $\sim 9\%$ elongation (large load).

Weight changes of the specimens on heating and cooling. To determine the influence of hygroscopic water on the state of the specimens, their weights were determined during variations of temperature. The heating and cooling rate was the same as in the dilatometric determinations (1° in 3-5 minutes). The readings were also usually taken at intervals of 1° [1]. The extent of the hysteresis and the absolute values of the weight changes depend

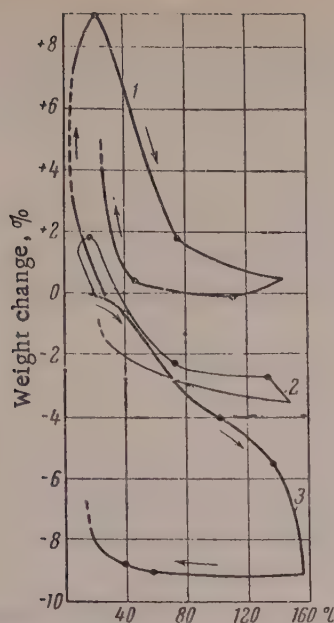


Fig. 3. Weight changes of capron specimens on heating and cooling: 1) thread ($24^{\circ} \rightarrow 4^{\circ} \rightarrow 141^{\circ} \rightarrow 23^{\circ}$); 2) film ($20^{\circ} \rightarrow 10^{\circ} \rightarrow 144^{\circ} \rightarrow 26^{\circ}$); 3) film ($16^{\circ} \rightarrow 155^{\circ} \rightarrow 18^{\circ}$).

glass transition temperature of undrawn polycaprolactam, determined from heat capacity — temperature [4] and specific volume — temperature [5] variations is $\sim 47^{\circ}$, and t_f is $210-215^{\circ}$ [6].

The following have been reported for nylon: "second-order transition temperature" at -20 and 45° [7] and 47° [8], from measurements of the dielectric properties [7] and thermal expansion [8]; a change in the course of the variation of the initial modulus with temperature, at $\sim 120^{\circ}$ [6]; change of structure at 161° [9]; and melting points at 250° [10], 264° [6, 8], and 265° [6, 11].

It should be noted that all the oriented specimens tested by us, if they did not undergo thermal degradation of flow under load in isothermal conditions at room temperature, tend to return to their initial length and moisture contents after the tests.

DISCUSSION OF RESULTS

It follows from the experimental data at our disposal, some of which are presented in this paper, that the effects observed in dilatometric temperature studies of polyamides greatly depend on the specific surface [surface area (cm^2)/volume (cm^3)] of the specimens. The length — temperature relationship determined for massive specimens (rods) of low specific surface is mainly free from anomalous regions (Fig. 1). The specimens extend when heated and contract when cooled. The behavior of specimens of large specific surface, such as the films and threads used in our experiments, is considerably more complex (Fig. 1, II). The probable cause of this discrepancy is that in the general case, the total result of the influence of temperature on the linear dimensions of the specimen, most pronounced in the behavior of thin threads and stretched films, is the aggregate effect of four different simpler phenomena:

1. Normal thermal expansion, the result of changes in the intermolecular and interatomic distances, common to all bodies; it is known that in anisotropic bodies, which include oriented films and threads, the coefficient of linear expansion may vary with direction.

on the maximum heating temperature, heating rate, and the sequence of the temperature cycles. Certain relationships illustrating this are presented in Fig. 3. The regions represented by the dash line correspond to very slow temperature changes. Comparison of Figs. 1, 2, and 3 shows that moisture has an obvious influence on the complex form of $l=f(t^{\circ})$ curves for films and threads.

Nylon

Linear dilatometry. Fig. 4 shows the effects of temperature on the length of factory-made nylon threads of $S = 1.45 \cdot 10^{-5} \text{ cm}^2$; the relationship does not differ from that for capron threads (Fig. 2). The influence of the maximum heating temperature on the behavior of the material is clear from Fig. 4 (curves 1 and 2). For the specimens studied the value of α determined above 70° varies between $0.68 \cdot 10^{-4}$ and $0.83 \cdot 10^{-4}$. The length of the specimens varied: by 2.5% from point A (13°) to point B (42°); by 1.75% from A' (16°) to B' (80°); by 1.3% from C' (15°) to D' (70°), and by 5.2% from A' to E'.

The length changes shown in Figs. 1, 2, and 4 are in arbitrary units and the different curves cannot be compared with regard to absolute values. The temperatures at which the monotonic course of the length — temperature variations breaks down may be correlated to some extent with the literature values of transition points determined by other methods.

According to thermographic data, t_f for capron varies from 206 to 233° if the heating rate is increased from 3-5 to 20-35 degrees/minute, while the glass-transition region extends from 120 to 150° if the temperature is changed at the rate of 3-5 degrees/minute [3]. The

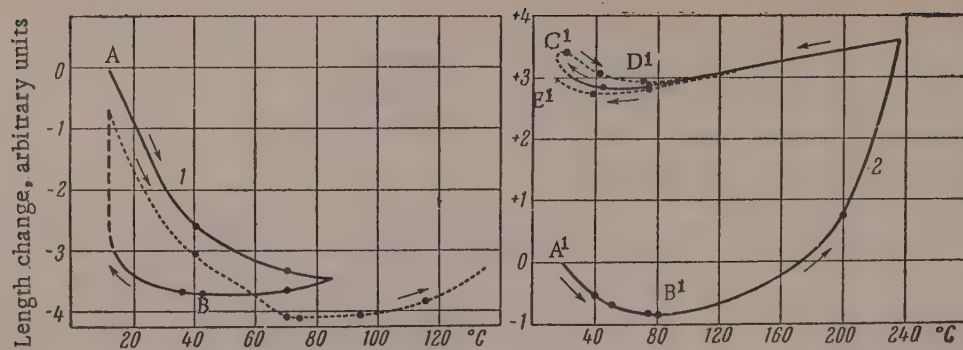


Fig. 4. Effect of temperature on length of nylon threads, $P = 178 \text{ g/mm}^2$.

2. Anomalous contraction, which may be observed in some instances with increase of temperature, not only in linear dimensions, but also in volume. The contraction is associated with transition from an unstable nonequilibrium state to a more stable state (tempering effect in quenched specimens).

3. Contraction associated with changes in the degree of orientation in anisotropic materials. In most cases such contraction is observed on partial or total loss of orientation of previously stretched specimens when heated above a certain definite temperature.

4. Incorporation of water molecules, as a rule, increases the dimensions of the specimens (perhaps unequally in different directions). Therefore, loss of moisture on increase of temperature is associated with contraction, and sorption of moisture on decrease of temperature, with elongation. If this is taken into account, the peculiarities in the behavior of the studied materials may be explained. In massive specimens sorption and loss of moisture, which occur during the experiment only in the outer layers of the material, have no effect on the dimensions of the rod as a whole, and its behavior presents a much simpler picture. Such specimens can be used for determination of the constants and transition points characteristic of the material in its normal state, such as the coefficients of linear expansion, without complications caused by moisture variations. Without discussing the physical meaning of the transition points, we must note that they are close to those reported in the literature. Our results confirm that polyamides have transition points in three temperature regions: $30\text{--}60^\circ$, $100\text{--}150^\circ$, $200\text{--}236^\circ$. The usual interpretation of these points is oversimplified. In these temperature ranges the changes taking place in the states of aggregation are more complex than mere crystallization or melting of crystals, simple vitrification, etc. Displacement of the transition points under the influence of various factors, including the kinetics of the processes, indicates that all the transitions are relaxational in character; this includes the appearance and disappearance of the crystalline portion of a polymer. Investigations of the complex behavior of threads and films with all the above factors taken into account are of great interest from the practical standpoint. Such investigations may be static or kinetic; each form is of independent significance. Our investigations were kinetic; this was in part due to practical needs. It is known that in practice, materials are often used under variable conditions (temperature fluctuations under normal atmospheric conditions) and therefore it is important to know: a) the magnitude and reversibility of contraction of the materials; b) the characteristic temperature points in the region in which the most pronounced changes associated with intensity of interaction with water, bonding strength, etc., are observed. In physicochemical analysis hydrates of definite and indefinite composition are investigated in this manner, under conditions of heating at a constant rate. The materials studied showed strong sorption of water in the temperature range from ~ 20 to $\sim 40^\circ$. It is possible that a process which is to some extent autocatalytic occurs in this region: the first portions of the sorbed moisture loosen the polymer structure and facilitate penetration of further portions.

SUMMARY

1. The method of linear dilatometry in heating and cooling cycles was used to study and compare the behavior of polyamide specimens (polycaprolactam and the polycondensation product of hexamethylenediamine with adipic acid) differing in specific surface (rods, films, threads). It is shown that the behavior of specimens with a large specific surface is influenced by variations of moisture content, load, maximum heating temperature, and the sequence of the heating and cooling cycles.

2. The aggregate result of the influence of temperature on the linear dimensions of a specimen is composed of normal thermal expansion, anomalous linear contraction as the result of loss of previous orientation, a possible volume effect in the transition from a nonequilibrium unstable state to a more stable state, and changes of moisture content.

3. The effects described, which apply in the main to nonequilibrium states, have a direct bearing on the behavior of materials in manufactured articles under the usual practical conditions.

I offer my sincere thanks to Professor S. I. Sokolov for valuable advice in discussion of the results, and to Engineer I. Shtern for assistance in the experimental work.

LITERATURE CITED

- [1] R. I. Fel'dman, Colloid J. 20, No. 2, 220 (1958).*
- [2] R. I. Fel'dman and S. I. Sokolov, Colloid J. 20, No. 3, 388 (1958);* Investigations of High-Molecular Compounds [in Russian] (Izd. AN SSSR, 1949) p. 329.
- [3] N. V. Mikhailov and V. O. Klesman, Proc. Acad. Sci. USSR 91, No. 1, 99 (1953).
- [4] M. Dole, P. Marx, R. Wilhoit and A. Worthinton, Bol. Soc. quim. Peru, No. 13, 149, (1953) (cited through Referat. Zhur. Khim. No. 9, 1955).
- [5] H. J. Kolb, and E. F. Izard, J. Appl. Phys. 20, 564, (1949).
- [6] Fibers from Synthetic Polymers (IL, 1957) [Russian translation].
- [7] R. F. Boyer, J. Appl. Phys. 25, No. 7, 825, (1955); cited through Problems of Modern Physics No. 12, 110 (1956).
- [8] R. F. Boyer and R. S. Spencer, J. Appl. Phys. 15, 398, (1944).
- [9] R. Brill, J. prakt. Chemie 161, 49, (1942).
- [10] C. W. Bunn, Chemistry of Large Molecules, Vol. 2 (IL, 1948) [Russian translation].
- [11] W. O. Baker, and C. S. Fuller, J. Amer. Chem. Soc. 64, 2399, (1942).

Received December 15, 1957

*Original Russian pagination. See C.B. Translation.

LETTERS TO THE EDITOR

THE INTERACTION OF TETRAMETHYLTHIURAM DISULFIDE AND TETRAMETHYLTHIURAM MONOSULFIDE WITH RUBBER

B. A. Dogadkin and V. A. Shershnev

The M. V. Lomonosov Institute of Fine Chemical Technology, Moscow

It has been shown by a series of investigations that tetramethylthiuram disulfide (TMTD) adds on to rubber in the course of vulcanization; the extracted vulcanizate contains sulfur and nitrogen from TMTD [1]. We have shown that at the same time TMTD is reduced to dimethyldithiocarbamic acid, which is combined in the form of zinc dithiocarbamate in mixes containing zinc oxide or stearate, or decomposes to give carbon disulfide and dimethylamine in mixes without metal oxides or containing magnesium and calcium oxides or stearates. If the acid decomposes, reversion of vulcanization takes place and the vulcanizates are mechanically inferior to those obtained with zinc oxide.

Some investigators consider that thiuram monosulfide is formed in the course of vulcanization with the disulfide [2]. It was of interest in this connection to study the interaction of tetramethylthiuram monosulfide (TMTM) with rubber. No vulcanization effect is observed when mixtures of natural or synthetic polyisoprene rubber are heated with TMTM (with or without zinc oxide) in a press at 143-175°. The products formed are completely soluble in xylene and do not have an ultimate value of the elastic modulus; this indicates absence of cross links between the rubber molecules. Qualitative tests showed that when these mixtures are heated, tetramethylthiourea (which was not detected in vulcanizates with TMTD) and carbon disulfide are formed, and in absence of zinc oxide, dimethylamine is also formed. It follows that simultaneously with its reaction with rubber, TMTM undergoes thermal decomposition, which does not occur in the case of TMTD [3]. Zinc dithiocarbamate is formed when mixtures with TMTM are heated with zinc oxide [4]. The addition kinetics of TMTM sulfur in mixtures containing zinc oxide differs from the kinetics of sulfur addition in absence of zinc oxide (Fig. 1). In the latter case up to 10% (of the sulfur introduced in the form of TMTM) becomes bound, while in mixtures with zinc oxide the amount is up to 50%, and, in addition, somewhat over 50 molar % of zinc dithiocarbamate, calculated on the TMTM introduced, is formed. In mixtures with TMTD the amounts of bound sulfur are almost the same in presence and in absence of zinc oxide. The maximum on the kinetic curves of sulfur addition, characteristic for mixtures with TMTD, is not found with TMTM.

To elucidate the nature of the interaction between rubber and TMTD and TMTM, electron paramagnetic resonance spectra were investigated in the course of heating of mixtures with TMTD and TMTM*. Four mixtures were investigated; they contained, per 100 wt. parts of acetone-extracted natural rubber: 1) 3 wt. parts TMTD; 2) 3 wt. parts TMTD and 5 wt. parts of zinc oxide; 3) 10 wt. parts TMTD; 4) 10 wt. parts TMTM. The mixtures were made in a micromill in an argon atmosphere and put into quartz ampoules which were heated directly in the resonator (in argon, vacuum, or air). All the mixtures gave essentially the same spectra on heating (140°), least pronounced for the mixture with TMTM (Fig. 2). This indicates that TMTD and TMTM probably have a common reaction mechanism in their interaction with rubber, whereas the kinetic relationships differ very considerably. This is confirmed by the reactions of TMTD and TMTM with geraniol, which can be considered as a model of the structural units in natural rubber. When mixtures of TMTD or TMTM with geraniol are heated, or exposed to ultraviolet radiation in a quartz ampoule at room temperature, they acquire a similar red-orange color, the intensity of which increases more slowly in mixtures with TMTM.

* The spectra were determined in Prof. S. E. Bresler's laboratory, the Institute of High Polymers, Acad. Sci. USSR, by E. M. Saminskii and É. N. Kazbekov.

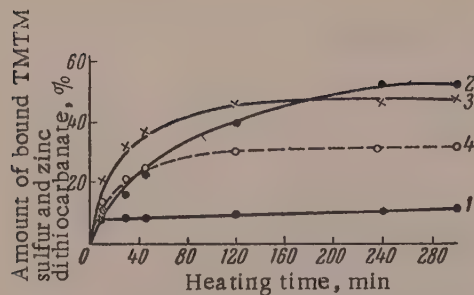


Fig. 1. Kinetics of interaction of TMTM with rubber: 1) $S_{\text{bound}}/S_{\text{intr}}$ in %, mixture: 100 wt. parts NR, 3.5 wt. parts TMTM, and 1 wt. part phenyl- β -naphthylamine; 2) $S_{\text{bound}}/S_{\text{intr}}$ in %, mixture: 100 wt. parts NR, 3.5 wt. parts TMTM, 5 wt. parts zinc oxide, and 1 wt. part phenyl- β -naphthylamine; 3) zinc dithiocarbamate in molar % of TMTM introduced (same mixture); 4) sulfur in zinc dithiocarbamate (1 mole of dithiocarbamate formed from 2 moles of TMTM, same mixture).

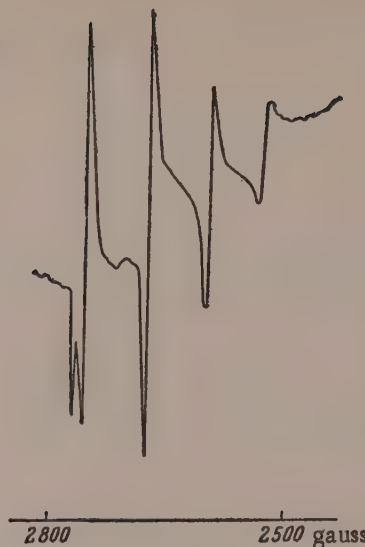


Fig. 2. Electron paramagnetic resonance spectrum of a mixture containing 100 wt. parts NR and 3 wt. parts TMTD, heated for 10 minutes at 140°.

The above facts lead to the conclusion that TMTM, like TMTD [1, 3], reacts with rubber through a free-radical stage; these compounds decompose at their C-S and S-S bonds [3, 4].

LITERATURE CITED

- [1] W. Scheele, O. Lorenz and W. Dummer, *Kautsch. u. Gummi* 7, WT 1, 273, (1954); B. A. Dogadkin and V. A. Shershnev, *Colloid J.* 20, 124 (1958)*; W. Scheele and K. Hummel, *Kautsch. u. Gummi* 11, WT-267, (1958).
- [2] G. Bruni and E. Romani, *India-Rubber J.* 62, 63 (1921); 64, 937 (1922); D. Craig, W. Davidson and A. Juve, *Rubber Chem. and Technol.* 24, 262, 275 (1951).
- [3] B. A. Dogadkin and V. A. Shershnev, *High Polymers* [in Russian] (in the press).
- [4] G. Bielstein and W. Scheele, *Colloid.-Z.* 147, 3, 152, (1956).

Received September 3, 1958

*Original Russian pagination. See C.B. Translation.

PREPARATION AND CERTAIN PROPERTIES OF LYOPHOBIC COLLOIDAL DISPERSIONS OF FIBER-FORMING POLYMERS

N. V. Mikhailov, V. I. Maiboroda, and

S. S. Nikolaeva

Scientific Research Institute of Artificial Fibers, Mytishchi

Aqueous polymer dispersions are used in various branches of technology for production of films and coatings. Despite the great practical importance of colloidal polymer solutions, theoretical studies of their nature and properties are still in their early stages. The literature contains reports of studies of the processing and properties of synthetic and natural rubber latexes [1], and on the production of polytetrafluoroethylene fibers [2] and latex from vinyl polymers [3]. The literature does not contain any publications dealing with production and investigation of aqueous dispersions of the commonest industrial fiber-forming polymers, such as polyamides and polyesters. Studies of suspensions of fiber-forming polymers in relation to production of films and fibers from them are of great theoretical and practical importance, and constitute a new problem, in the scientific sense.

We have used the condensation method to prepare, for the first time, colloidal solutions of polyethylene terephthalate (4.5% concentration) and polycaprolactam (2% concentration). True solutions were obtained when the polymers were dissolved at high temperatures; this fact is worthy of independent study. Polycaprolactam and polyethylene terephthalate solutions were prepared as follows: 1-2 g of powdered polycaprolactam crumbs was dissolved in 50 ml of glycerol previously heated to 200°. The solution was poured in a thin stream, with vigorous stirring and cooling, into an equal volume of aqueous Carbazoline C (0.5%) previously cooled to 5°.

3.5 g of powdered polyethylene terephthalate crumbs was dissolved in 40 ml of dimethylformamide at 190°. The solution was poured in a thin stream, with vigorous stirring, into an equal volume of OS-20 agent (2%) at room temperature.

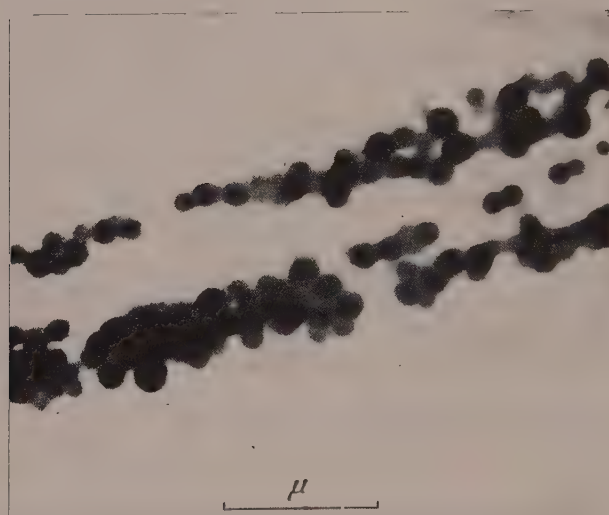
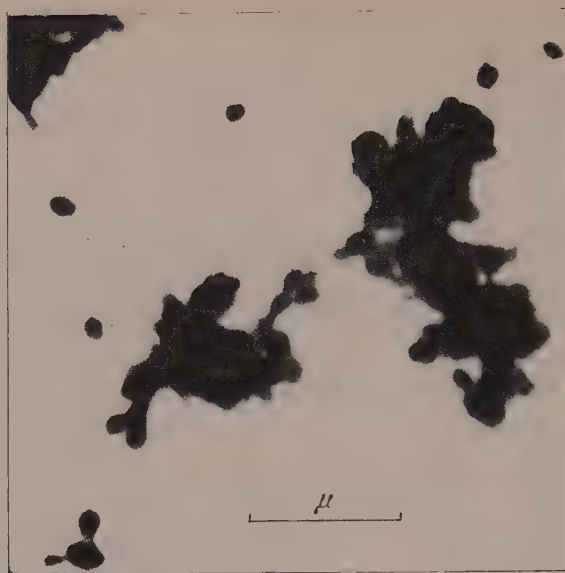
Certain physicochemical properties of the sols were investigated. The results are given in the table.

Physicochemical Properties of Polycaprolactam and Polyethylene Terephthalate Solutions

Polymers	Specific viscosity in mixed cresols (0.5%)	Relative viscosity of colloidal solution	Sign of particle charge	Particle charge in mv	Surface tension in dynes/cm	Specific conductance in $\text{ohm}^{-1} \cdot \text{cm}^{-1}$
Polycaprolactam*	0.582	1.24	+	33.3	34.7	$1.2 \cdot 10^{-5}$
Polyethylene terephthalate**	0.260	1.03	-	10.8	35.8	$7.02 \cdot 10^{-6}$

* Coagulation at pH 6.

** Isoelectric state reached at pH 3.8.



Electron micrographs of colloidal solutions ($\times 20,000$)
above) polycaprolactam; below) polyethylene terephthalate.

Investigations of the polymer sols in polarized light showed that the polymer particles exhibit birefringence.

Investigations by electron microscopy* showed that these particles are of globular form and may form chain aggregates (Figs. 1 and 2). The size of these globules reaches 500-1000 Å. Electron diffraction patterns of the particles in the polymer sols indicate an amorphous structure.

These studies will be continued by investigations of the properties and conversion of colloidal solutions of fiber-forming polymers, formed both by high-temperature polymerization and by low-temperature polymerization in a heterogeneous medium.

* This part of the work was performed jointly with junior scientific assistant V. P. Kovaleva.

SUMMARY

For the first time colloid solutions have been obtained of polyethylene terephthalate of 4.5% concentration and of polycaprolactam of 2% concentration. A study has been made of a number of physicochemical properties of the solutions obtained.

LITERATURE CITED

- [1] S. S. Voyutskii and R. M. Panich, Colloid J. 19, 268 (1957)*; D. Sandomirskii and K. Gagina, Colloid J. 15, No. 6 (1953)*; B. A. Dogadkin, J. Rubber Ind. No. 5, 547 (1936).
- [2] A. J. Hall, Fibers 18, No. 7, 239, 245, (1957).
- [3] U. S. Patent 2,737,436 (1956), Dow Chemical Co.

Received January 2, 1959

*Original Russian pagination. See C.B. Translation.

THE STRUCTURAL AND STRUCTUROMECHANICAL PROPERTIES OF INORGANIC GLASSES *

G. M. Bartenev and A. S. Ereemeeva

The State Scientific Research Institute of Glass, Moscow

The most important mechanical properties of real bodies depend significantly on the characteristics of structure, thermal motion, and interaction of their structural elements. These properties have been given the name of structuromechanical by Academician P. A. Rebinder. Studies of these properties can provide information on the structure of materials. Methods for interpretation of structural characteristics of real bodies by studies of their structuromechanical properties belong to a new branch of knowledge, physicochemical mechanics [1, 2]. Diffraction methods, which are direct methods for structural investigations of certain classes of substances, such as crystalline materials, are ineffective for studies of the structure of a number of important materials such as disperse polymeric bodies, and organic and inorganic glasses. Structuromechanical methods are of great significance in this connection.

The structure of inorganic, and in particular of silicate glasses, is still the subject of lively discussion [3]. This is primarily due to the complexity of the structure of these materials. A characteristic of inorganic glasses, in contrast to organic glasses, is their multicomponent nature, which leads to the existence of different types of bonds, chief among which are silicon-oxygen bonds and ionic bonds of different valences; it also leads to microheterogeneity and probably to processes of structure formation in melts; the consequence of all this is the formation of a very complex structure.

The existing hypotheses relating to the structure of silicate glasses reflect different aspects of this complex question: short-range order, microphase separation leading to microheterogeneity, structurization, and the chain structure of glass. These structural characteristics appear to different extents in different glasses.

Data on low-temperature heat capacity [4, 5], dielectric loss [6], mechanical properties [7], and our results [8, 9] reveal the existence of a far-reaching analogy between the structures of polymers and of silicate glasses. The mechanical behavior of glass above the softening temperature indicates the existence of high elasticity. The high-elastic properties of inorganic glasses above the vitrification temperature indicate that inorganic glasses are network polymers with flexible chains [8].

The results of our investigations showed that the spatial network has relatively low strength and is easily broken down under low loads, but is partially restored after removal of the load (the glass exhibits thixotropic properties). The main cause of hardening during cooling of a viscous glass is the vitrification process, but the structurization (aggregation) process and the thermal history of the glass play a significant role in the formation of the glass structure; this leads to variations in the mechanical behavior of different samples of the same glass.

These properties make inorganic glasses similar to organic polymer glasses on the one hand, and to thixotropic colloidal systems on the other.

Structuromechanical properties of an inorganic glass above its vitrification temperature. The principal experiments were on the torsion of glass rods at different temperatures and under different experimental condi-

* Presented at the Fourth All-Union Conference on Colloid Chemistry, Tbilisi, 1958.

TABLE 1

Structuromechanical Characteristics of Glasses

Glass type	Temperature, °C		Width of plateau, °C	Elasticity (shear) modulus G_e , kg/mm ²	High-elastic (shear) modulus G_{he} , kg/mm ²
	vitrification, T_g	flow, T_f			
White Marblit	550	680	70	2760	2.0
F-1, optical	555	675	85	1600	0.50
Black Marblit	562	740	110	2860	4.0
3S-5K	580	745	105	2180	—
VV, vertical drawing	595	745	100	2720	2.10
Continuous-rolled	605	750	90	2740	1.10
K-8, optical	615	745	80	2280	1.80
F-116, phosphate	650	905	100	3000	—
13-v	710	970	170	3720	7.20
Ts-18	715	980	140	2200	—

TABLE 2

Chemical Composition of Glasses

Glass type	Oxides, %							Other oxides, %
	SiO ₂	Al ₂ O ₃	B ₂ O ₃	CaO	MgO	Na ₂ O	K ₂ O	
White Marblit	65,4	3,5	—	6,8	0,1	12,14	—	Fe ₂ O ₃ 0,17 NaF 6,95 AlF ₃ 4,65
F-1, optical	47,38	—	—	—	—	—	6,41	PbO 45,71 As ₂ O ₃ 0,50
Black Marblit	65,0	—	—	10,3	—	14,0	—	Mn ₂ O ₃ 10,7
3S-5K	66,84	3,64	20,24	0,13	0,15	4,16	4,03	Fe ₂ O ₃ 0,13
VV, vertical drawing	71,85	—	—	7,83	3,69	14,93	—	SO ₃ 0,46
Continuous-rolled	75,06	0,24	—	8,99	0,14	15,1	—	Fe ₂ O ₃ 0,07 SO ₃ 0,6
K-8, optical	68,42	—	11,22	—	—	10,36	6,77	BaO 2,86 As ₂ O ₃ 0,36
F-116, phosphate	6,56	18,61	1,60	2,14	1,08	—	—	P ₂ O ₅ 69,82
13-v	63,76	14,98	—	12,75	3,9	3,02	—	Fe ₂ O ₃ 0,16 F 3,11
Ts-18	59,36	1,41	—	4,53	—	13,3	3,51	Fe ₂ O ₃ 0,15 ZrO ₂ 17,96

tions. The specimens (diameter 8 mm, working length 30 mm) were subjected to different loads applied through a 38 mm arm. The determinations were carried out with our modification of the apparatus designed by E. K. Keler and E. I. Kozlovskaya (Institute of Silicate Chemistry, Academy of Sciences USSR). The graphs give the torsion angles φ in scale units, where the torsion angle in radians is $\alpha = 1.93 \cdot 10^{-4} \varphi$.

When the specimens were heated under small bending or twisting loads, the glasses listed in Table 1 gave characteristic deformation curves (Fig. 1) similar to the deformation-temperature curves for organic polymers [10]. In accordance with the usual practice for polymers, we recorded two temperatures: the glass transition temperature T_g and the flow temperature T_f (Fig. 1). These data for different glasses are presented in Table 1, and the chemical composition of the glasses is given in Table 2.

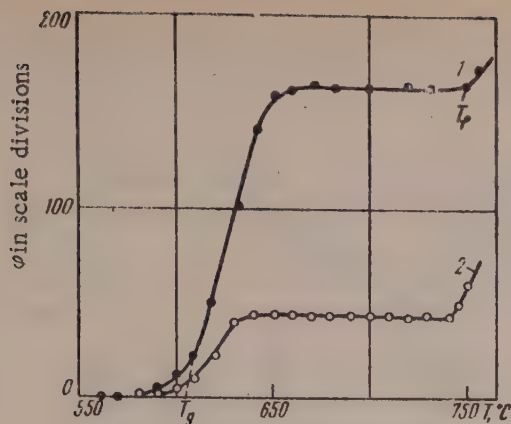


Fig. 1. Variation of the torsion angle of a glass rod with temperature at constant load and a heating rate of 3° per minute, for 1) rolled glass, 2) vertically drawn glass.

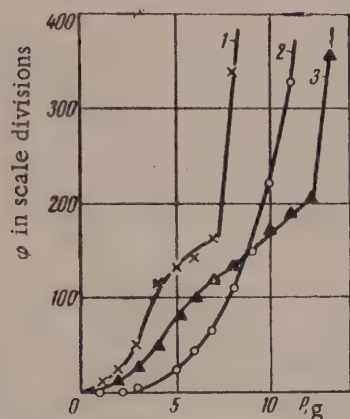


Fig. 3. Variations of torsion angle with load for VV glass at the following temperatures: 1) 705°; 2) 625°; 3) 650°.

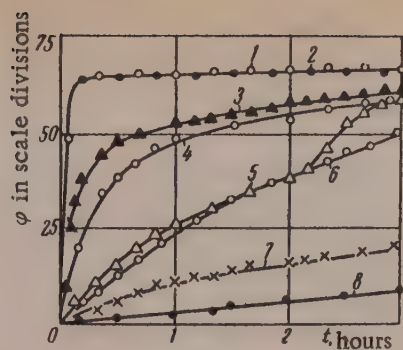


Fig. 2. Variations of torsion angle with time for VV glass at the following temperatures: 1) 670°; 2) 660°; 3) 630°; 4) 610°; 5) 600°; 6) 585°; 7) 575°; 8) 565°.

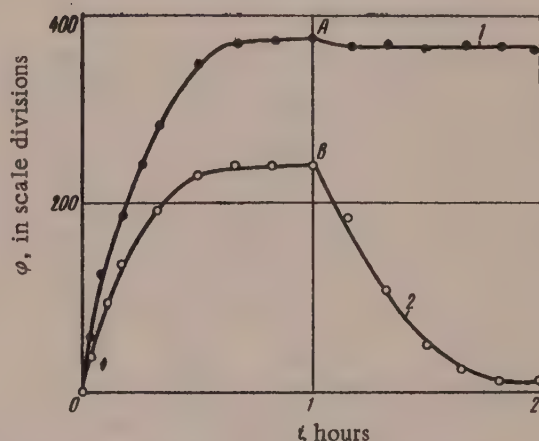


Fig. 4. Relationship between torsion angle and time at 630° under constant load (shear stress $\tau_{\max} = 0.3 \text{ kg/cm}^2$) for two specimens of rolled glass: Curves OA and OB represent deformation under load; load removed at points A and B.

Above the vitrification temperature deformation begins to develop, and it reaches its maximum value over a certain temperature range, represented by the plateau on the curve. This deformation, which we term high-elastic by analogy with polymers, is thousands of times greater than the elastic deformation measured at low temperatures. Above the flow temperature T_f , the material flows. It is clear from Table 1 that the high-elasticity range for inorganic glasses is of the order of 100°.

The course of development of high-elastic deformation in certain glasses greatly resembles that in polymers [11].

Fig. 2 shows kinetic deformation curves at different temperatures for VV glass. All the curves, at a given torque, tend to the same limit with increase of the observation time, at higher rates as the temperature increases. At temperatures corresponding to the plateau (Fig. 1) equilibrium deformation is reached very rapidly and then remains virtually unchanged.

Fig. 3 shows, for three temperatures in the high-elasticity region, the relationship between torsional deformation of glass rods and the torsional load applied through the length of arm indicated above (a new specimen was used for each experiment). The deformation curves do not conform to any simple law and vary from speci-

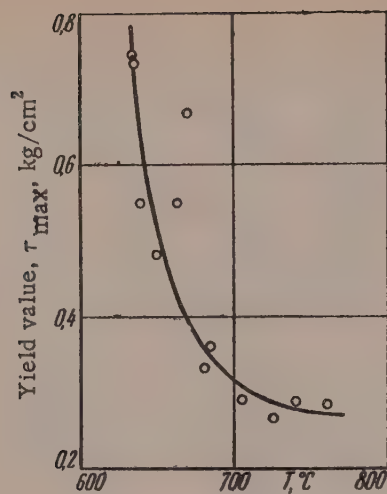


Fig. 5. Effect of temperature on the yield value of VV glass; τ_{\max} is the shear stress on the surface of the glass specimen.

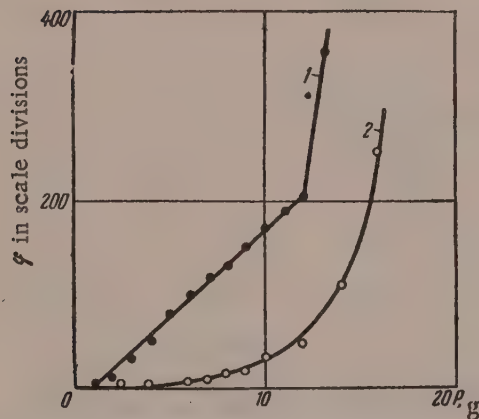


Fig. 7. Variation of torsion angle with load at 650°C for VV glass; 1) first deformation curve, 2) second deformation curve after removal of load and one hour of rest.

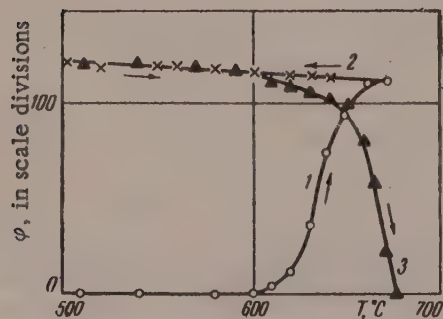


Fig. 9. Variation of torsion angle with temperature for VV glass during loading and unloading: 1) specimen heated under load; 2) specimen cooled slowly under load; 3) specimen heated without load.

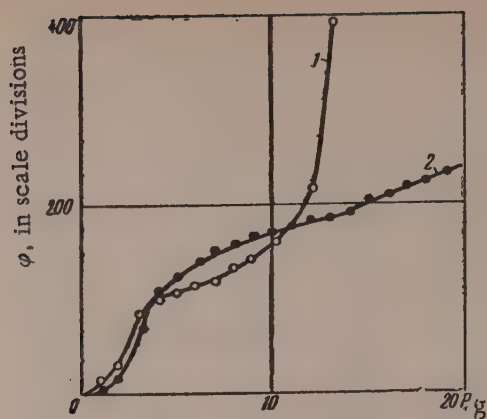


Fig. 6. Variation of torsion angle with load at 645°C for two specimens of rolled glass.

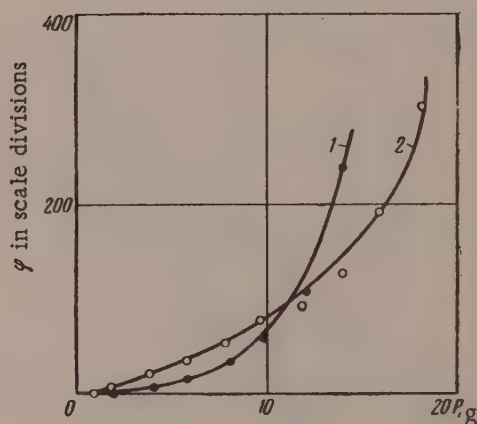


Fig. 8. Variation of torsion angle with load at 650°C for VV glass; 1) first deformation curve; 2) second deformation curve after removal of load and four hours of rest.

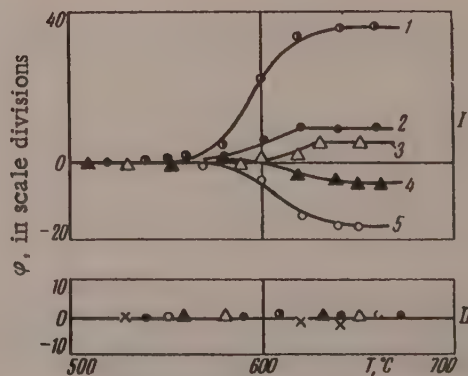


Fig. 10. I) Spontaneous torsion of 3S-5K glass rods in the softening region: 1, 5) badly annealed specimens; 2, 3, 4) well-annealed specimens; II) the same specimens heated again after being slowly cooled down from 660°C.

men to specimen; they each separate into two regions. Below a load which we shall term the yield value, deformation is completely or partially reversible (Fig. 4); above it the deformation increases sharply and does not disappear after removal of the load.

The relationship between the yield value and the temperature conforms to a quite definite law (Fig. 5). In the elasticity region the yield value reaches a minimum value ($0.2-0.3 \text{ kg/cm}^2$) and then remains almost unchanged up to the flow temperature. According to our data, the yield value, which is associated with the strength of the spatial network, is very low in the high-elasticity region (of the order of $0.2-0.3 \text{ kg/cm}^2$). Thus, low strength of the spatial network is a characteristic of inorganic glasses. Therefore, above the vitrification temperature, at loads above the yield value, these materials exhibit the behavior of viscous bodies.

A characteristic feature of all glasses is that the deformation curves for different specimens of the same glass at the same temperature do not coincide.

Test results for two specimens of rolled glass at the same temperature are plotted in Fig. 6. These results indicate that the structure of the glass is very heterogeneous. This heterogeneity is due not only to chemical heterogeneity, but also to differences in the thermal history of different regions of the glass during its formation.

Thixotropic properties of glasses. The spatial network is readily broken down at high temperatures even under small loads, and is partially restored after removal of the load. This is confirmed by the results presented below.

Test results for specimens of VV glass are presented in Fig. 7. A load was gradually applied to the specimen at constant temperature (Curve 1); the load was then removed at a large residual deformation, and the specimen was kept for one hour at the same temperature. The second deformation curve (Curve 2) was very different. Increase of the rest time after removal of the load (Fig. 8) leads to gradual restoration of the initial properties; this shows that the original structure is restored.

These results apparently indicate that inorganic glasses, like colloidal systems, have thixotropic properties.

Analogous investigations of this effect were carried out on ebonite. Similar relationships were obtained, but the thixotropic properties of ebonite are weak.

Frozen high-elastic deformations. Experiments show that inorganic glasses exhibit two kinds of mechanically reversible deformations (elastic and high-elastic), and, correspondingly, two kinds of stresses. The existence of high-elastic stresses is confirmed by freezing of high-elastic deformations.

A specimen (Fig. 9) was heated and slowly cooled under load to 20° . After removal of the load the high-elastic deformation remained, while the elastic deformation, which was a small fraction of the total, disappeared. After the specimen had been heated, the high-elastic deformation was lost and the specimen returned to its initial form. Fig. 9 illustrates a typical case. In reality, the situation is more complex, as the deformation is fully reversible in only some of the specimens, and is partial in most.

The presence of high-elastic deformations in glass accounts for a number of effects, hitherto unexplained, such as the appearance of residual birefringence [12] in glass slowly cooled under load, where quenching stresses are absent. The explanation is the cooling freezes the high-elastic deformation and therefore, molecular orientation, which is revealed by birefringence.

It has been shown [9] that above the vitrification temperature, a glass specimen undergoes spontaneous torsion in absence of external load.

Fig. 10 shows the results of control tests on glass specimens without load, carried out in a carefully balanced apparatus. The specimens were heated at the rate of 3° per minute. Starting at temperatures of $570-580^\circ$, the specimens exhibited spontaneous torsion both in the positive and in the negative direction. Specimens 2, 3, and 4 were thoroughly annealed before the tests, while Specimens 1 and 5 had been badly annealed. Thus, the better the annealing, the less is this effect.

The effect can be caused only by frozen high-elastic stresses which relax at temperatures above T_g . This was confirmed by the following experiments.

Specimens free from load were slowly cooled down from 650°, when the relaxation of high-elastic stresses was complete, and tested again (Fig. 10). As was to be expected, there was no spontaneous torsion owing to the absence of frozen high-elastic stresses. These results show that there are two types of stress in glass: residual elastic (of the toughening type), and residual high-elastic, which are network stresses. The latter evidently arise readily during formation of the glass.

In the course of formation and working of glass, elastic and high-elastic stresses (chain stresses) arise between individual regions as the result of the nonuniform temperature field. When the glass is cut (for preparation of the specimens) the elastic stresses are removed almost entirely while the high-elastic stresses remain.

It follows from the large difference between the elastic and high-elastic moduli for inorganic glasses that in massive glasses, the high-elastic stresses are small in comparison with quenching stresses*. In the case of annealed glasses, where the residual elastic stresses (stresses of the first kind) are not large, high-elastic deformation must be taken into consideration. When the specimens are cut, the birefringence does not disappear, as is the case with stresses of the first kind, such as those caused by quenching.

The structuromechanical properties of glass fibers. Our experimental data on massive glasses and glass fibers confirm the hypothesis of the chain structure of glass, advanced by Tarasov [4, 5]. This hypothesis provides a natural explanation for new experimental facts discovered during recent years. Since one of us has already developed and substantiated this theory of the structure of inorganic glasses [8], here we confine ourselves to a reference to certain new facts which confirm the chain structure of glass.

The number of facts in support of this hypothesis is increasing. Here we consider data on the mechanical properties of glass fibers and thin glass rods. It follows from the results of Bartenev and Bovkunenko [13] that strengthening of glass fibers is attributable to molecular orientation which arises under load during the drawing process; this is directly related to the chain structure of glass. Stirling [14] carried out the following experiments with rods made from glasses of different compositions. Glass rods heated above the softening temperature were drawn out under different loads and cooled. The thin rods, 1 mm in diameter, obtained in this manner were subjected to prolonged annealing; during the heat treatment their length decreased and their diameter increased. These facts have a natural explanation on the basis of chain structure. Chain orientation takes place during the drawing, and high-elastic stresses are frozen on cooling. Heat treatment results in relaxation of these stresses and is accompanied by molecular disorientation which leads to contraction of length and increase in diameter.

It is known [15, 16] that high-temperature heat treatment of glass fibers also leads to contraction and also to almost total loss of the strengthening effect. The finer a glass fiber (the higher the stretch), the greater is the strength loss during heat treatment.

Zak and Man'ko [15] heated glass fibers under load to the softening temperature and found that above 300-500° the deformation increases sharply (3 to 7-fold, according to the composition of the glass). Viscous flow is still slight in this temperature range.

The authors do not offer an explanation of this effect, which is probably due to the high-elastic properties of glass fibers. The difference between their results and ours probably lies in the fact that the plateau (Fig. 1) is not observed during extension because of the use of loads above the yield value, and of rupture of the glass fibers.

SUMMARY

1. At high temperatures and small loads inorganic glasses (massive specimens and glass fibers) exhibit high elasticity. Evidence of the high elasticity and molecular orientation is provided by strengthening of glass fibers and their behavior under heat treatment.

The elasticity modulus of inorganic glasses exceeds the high-elasticity modulus by three orders of magnitude.

2. The thixotropic properties of glass, and variations of structure from specimen to specimen, indicate that structurization processes and thermal history influence the formation of glass structure.

*Glass fibers constitute an exception, their formation causes considerable molecular orientation in consequence of the high rates of viscous deformation during drawing, and of the high stresses, which reach values of the order of 10 kg/mm².

3. The properties (high elasticity and thixotropy) found in glass show that inorganic glasses resemble organic polymer glasses on the one hand, and thixotropic colloidal systems on the other.

4. The yield value, associated with the strength of the spatial network, is very low for inorganic glasses. Therefore, above the vitrification temperature such materials behave as viscous bodies under moderate loads, and as elastic bodies under small loads.

In conclusion, it is the authors' pleasant duty to offer their deep gratitude to Academician P. A. Rebinder for his great interest and valuable advice.

LITERATURE CITED

- [1] P. A. Rebinder, J. Acad. Sci. USSR No. 2, 8 (1955); No. 10, 32 (1957); Bull. Acad. Sci. USSR, Div. Chem. Sci. No. 11, 1284 (1957);* Proc. Third All-Union Conference on Colloid Chemistry [In Russian] (Izd. AN SSSR, 1956) p. 7.
- [2] N. V. Mikhailov and P. A. Rebinder, Colloid J. 17, No. 2, 107 (1955)*
- [3] The Structure of Glass [In Russian] (Izd. AN SSSR, 1955).
- [4] V. V. Tarasov and Ya. S. Savitskaya, Proc. Acad. Sci. USSR 88, 1019 (1953).
- [5] V. V. Tarasov, Glass and Ceramics No. 2 (1954).
- [6] J. M. Stevels, Verres et refract. 7, 91 (1953); Glass Ind. 35, 657 (1954).
- [7] É. K. Keler and E. I. Kozlovskaya, Proc. Acad. Sci. USSR 116, No. 2 (1957)*
- [8] G. M. Bartenev, J. Phys. Chem. 31, No. 9, 1917 (1957).
- [9] A. S. Eremeeva, Glass, No. 3 (1958).
- [10] V. A. Kargin and T. I. Sogolova, J. Phys. Chem. 23, 530 (1949).
- [11] P. P. Kobeko, E. V. Kuvshinskii, and G. I. Gurevich, Bull. Acad. Sci. USSR, Phys. Ser., No. 3, 329 (1937).
- [12] L. N. Filon and F. C. Harris, Proc. Roy. Soc. 103, 561 (1923).
- [13] G. M. Bartenev and A. I. Bovkunenko, J. Phys. Chem., 29, 58 (1955); J. Tech. Phys. 26, 2508 (1956).
- [14] J. F. Stirling, J. Soc. Glass Techn. 39, No. 188, 134 (1955).
- [15] A. F. Zak and Yu. P. Man'ko, J. Tech. Phys. 24, No. 11, 1983 (1954); Sci. Trans. All-Union Sci. Res. Inst. Glass Fibers No. 4 (1953).
- [16] M. S. Aslanova, Sci. Trans. All-Union Sci. Res. Inst. Glass Fibers No. 7 (1953).

Received April 19, 1958

*Original Russian pagination. See C. B. Translation.

STUDY OF THE HYDRATION PROPERTIES AND STRUCTURE OF PEAT BY MEANS OF RADIOACTIVE ISOTOPES

2. CHANGES OF HYDRATION PROPERTIES AND STRUCTURE OF DISPERSION AND COMPRESSION OF PEAT*

M. P. Volarovich, N. I. Gamayunov, Z. A. Starikova and
N. V. Churaev

Chair of Physics, the Moscow Peat Institute

Processes involving dispersion and compression of peat are widely used in peat technology; they form the basis of such technological processes as mechanical working and molding of raw peat; deformation of peat deposits during drying and under loads; shrinkage of peat during drying, and artificial dehydration of peat. Despite the great importance of these processes, which ultimately determine the quality of the final product, variations of the hydration properties and structure of peat during dispersion and compression have been insufficiently studied. This applies primarily to the hydration properties of peat, in relation to variations of which experimental data are almost entirely lacking.

Kurnakov and Pospelova [1] studied the bound-water content of peat by tensimetric methods and found that the amount of bound-water in peat decreases as the result of grinding. Later, Korchunov [2] concluded that mechanical treatment of crude peat has no significant influence on the equilibrium moisture content. Thus, the available data are not only inadequate but also contradictory.

The hydration properties and structure of peat of different degrees of processing** were studied by means of radioactive tracer methods [3]. The contents of immobile water were determined in samples of the original and dispersed peat by filtration of a tagged solution, and the amounts of bound and immobilized water were found by the non-solvent volume method with the aid of the same radioactive tracer Na_2SO_4 tagged with the S^{35} isotope. As is known, these methods can be used to determine the maximum quantity of bound-water in peat, including the weakly-bound intracellular water which fills the cells cavities of the plant residues which are contained in considerable amounts (up to 50-90%) in peat.

Variations of the content of bound (immobilized) water W_b with the degree of processing of peat are plotted in Fig. 1; it is seen that the amount of bound water decreases appreciably as the result of repeated dispersion. Since processing of peat causes intensive destruction of coarsely dispersed vegetable residues [4], the decrease in the content of immobilized water can be attributed to conversion of part of the intracellular water into the free form. The possibility of such conversion was suggested earlier by Berezin and Belovidov [5], and it has now been confirmed by direct experiments. In all probability, two simultaneous processes occur during the dispersion of peat: increase of the amount of adsorbed water as a result of increase of the specific surface, and decrease of the amount of intracellular water during destruction of the cell cavities in the plant residues of peat. The results of the experiments reveal the total effect, which in the processing of coarse peats (rich in undecomposed residues) consists of a decrease of the total amount of immobilized and bound water in the peat.

* Presented at the Fourth All-Union Conference on Colloid Chemistry, Tbilisi, 1958.

** The mechanical processing of peat was carried out, as usual, under laboratory conditions in a meat grinder.

TABLE 1

Variations of Structural Characteristics of Fuscum Peat of Degree of Decomposition $R = 15\%$ During Dispersion

Peat samples	Contents of immobile water W_i , %	Active porosity, m	Kinetic specific surface S_0 , m^2/g	Hydraulic pore radius δ , μ
Original peat	570	0.31	3.3	1.250
Processed once	235	0.48	47.6	0.086
Processed five times	90	0.67	54.7	0.068

TABLE 2

Variations of the Hydration Properties and Structure of Medium Peat of $R = 25\%$ as the Result of Compression

Applied pressure p , kg/cm^2	Contents of immobile water W_i , %	Active porosity, m	Kinetic specific surface S_0 , m^2/g	Hydraulic pore radius δ , μ	Filtration coefficient K , $cm/hour$
0.14	430	0.53	13.5	0.373	0.055
0.17	350	0.53	22.1	0.228	0.020
0.18	310	0.56	20.7	0.235	0.022
0.21	295	0.61	28.5	0.195	0.016
0.29	215	0.70	40.4	0.167	0.014
0.40	180	0.66	37.9	0.115	0.007
0.45	125	0.71	78.1	0.066	0.002

The observed conversion of intracellular into free water during dispersion is a specific characteristic of peat regarded as a disperse system; in particular, it accounts for the decrease of the rheological constants of peat during dispersion [6] as the result of liberation of additional "internal lubricant" by destruction of the plant cells. In contrast to peat, in such materials as clays increase of dispersity generally increases the yield value and plastic viscosity [7].

Changes taking place in the structure of peat during mechanical processing, which have received considerably more attention, have been studied in terms of the rheological parameters [6] and plasticity and dispersity characteristics [6, 8, 9], and by methods involving qualitative descriptions of the micro and macro structure of peat [5, 10]. The results of experiments on filtration of tagged water were used to characterize the structure of peat by values of the active porosity, kinetic specific surface, and hydraulic pore radius [3]. It follows from the data in Table 1 that dispersion of raw peat produces considerable changes in its structure.

The kinetic specific surface of peat increases sharply as the result of processing, and this increases the role of surface phenomena, which determine the whole subsequent course of the technological process. The pore size decreases to the same extent. The average dimensions of water-conducting canals through which water is removed during the subsequent drying decrease to tenths of one micron. It should be noted that a considerable change of pore size and kinetic specific surface of processed peat, as compared with the original material, may influence not only the drying rate but also the mechanism by which moisture migrates in peat [11].

The decrease in the size of the water-conducting pores is accompanied by an increase in the volume occupied by them in the peat. It is easy to see that this occurs because of breakdown of the cell cavities of the plant residues. Regions previously occupied by immobile intracellular water become available for filtration of water after breakdown of the cells and this results, as Table 1 shows, in an increase of the active porosity of the peat. Thus, dispersion of peat is accompanied by a decrease in the dimensions of the water-conducting channels on the one hand, and by a considerable increase in their number on the other.

Experiments were carried out on the filtration of tagged water through samples compressed to different extents, in order to observe variations of the hydration properties and structure of peat as the result of com-

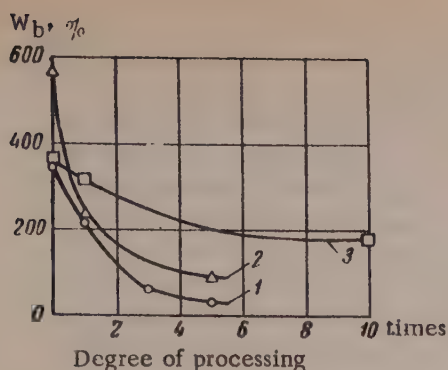


Fig. 1. Changes in the content of bound water (W_b , %) in peat at different degrees of dispersion during mechanical processing: 1) sedge - Hypnum peat, $R = 35\%$; 2) Fussum peat, $R = 15\%$; 3) sedge peat, $R = 30\%$.

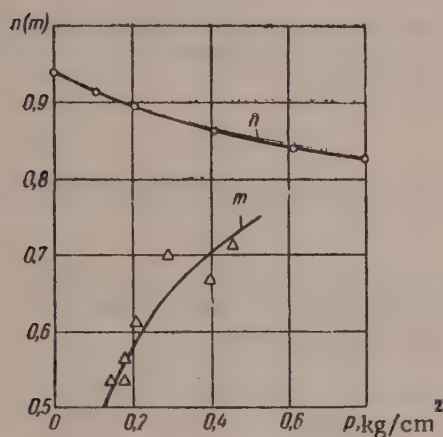


Fig. 2. Effects of compression on the porosity (n) and active porosity (m) of medium peat.

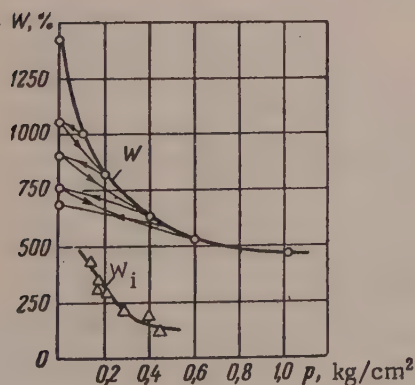


Fig. 3. Compression curve (W) for medium peat of degree of decomposition $R = 25\%$, and variations of the contents of immobile water (W_i).

pression. Upper medium peat of degree of decomposition $R = 25\%$ was used for the experiments, at pressure gradients I from 70 to 80, as compressed peat samples have poor filtration properties. Variations of the hydration properties and structure of peat are represented by the data in Table 2.

It follows from Table 2, that, as in the case of dispersed peat, increase of the degree of compression results in an increase of the kinetic specific surface S_0 and a decrease of the average radius δ of the water-conducting pores, with a consequent sharp decrease of the filtration coefficient. In strongly compressed peat samples, the dimensions of the water-conducting pores approach a limit at which free movement of the liquid under a pressure gradient becomes difficult [12]. It is known that with further increase of the degree of compression and decrease of pore radius, it becomes much more difficult to press water out of peat. It has been suggested that this may be due to the anomalous properties of thin liquid layers in the water-conducting pores in peat [13].

Compression of peat is accompanied by a decrease in the amount of immobile water. This is the consequence of deformation and partial destruction of the cell cavities in the plant residues and conversion of intracellular water into the free form. It is possible that when the load is removed there is a reverse process of imbibition of water by the plant cells. Destruction of the cell cavities leads, for the same reason as in the dispersion of peat, to an increase of active porosity. It should be noted that these effects are most pronounced in peats containing considerable amounts of intracellular water. Compression of peat of a high degree of decomposition, or of well-processed peat, is hardly likely to be accompanied by a decrease in the amount of immobilized water or by an increase of active porosity.

Variations of porosity \underline{n} and of the active porosity \underline{m} during compression of peat, determined by filtration of tagged water, are shown graphically in Fig. 2. It is clear from Fig. 2 that as intracellular water in peat is converted into the free form and the amount of immobile water decreases, the values of the active porosity \underline{m} (which differ considerably in the original peat from the porosity \underline{n} as usually determined) gradually approach the values of the porosity \underline{n} . The difference between the values of \underline{n} and \underline{m} corresponds to the immobile water in peat, which does not take part in the filtration motion. For dispersed materials which do not contain immobile (bound and immobilized) water, the values of \underline{m} and \underline{n} evidently coincide. Thus, it is particularly necessary to take the active porosity of peat into account in studies of the migration of water in samples with intact structure.

For determination of the pressure applied in compression of the samples in the filtration apparatus, parallel experiments were carried out with the same peat in Litvinov's compression apparatus [14]. The applied pressures p given in Table 2 were calculated from the compression curve and the moisture contents of compressed specimens of water-saturated peat in experiments with tagged water in the filtration apparatus. The compression curve (W) for medium peat of $R = 25\%$ is given in Fig. 3, which also shows variations in the content of immobile water (W_i) determined from experiments on filtration of tagged water. Comparison of Curves W and W_i shows that compression of water-saturated peat occurs mainly by way of deformation of the cell cavities in the plant residues and removal of immobile (intracellular) water. In all probability, this type of bonding has the lowest energy. It follows that the view that high pressure are needed to remove bound water, and in particular, water in the intracellular cavities, from peat [15, 16] is unjustified. Our experiments show that the pressures required to remove 250-300% of the intracellular water do not exceed 0.5 kg/cm^2 . A similar conclusion was reached by Bulynko [17], who showed that the water-retaining pressure in peat at 340-400% moisture content does not exceed 1 kg/cm^2 .

Since there is a certain analogy between the shrinkage processes in peat during drying and the mechanical expression of water [13], it may be assumed that a similar dehydration mechanism operates during the drying of peat. In this case, the pressure which converts intracellular water into the free form is created by shrinkage stresses.

Our results show that the investigation methods which have been developed, based on the use of radioactive isotopes, may be used both in studies of the hydration properties and structure of different types of peat, and for observing variations of these properties in the course of various technological processes.

SUMMARY

1. Variations in the hydration properties and structure of peat during dispersion and compression have been studied with the aid of radioactive-tracer methods.

2. When peat is dispersed or compressed, the immobilized water content decreases owing to conversion of part of the intracellular water into the free form by breakdown and deformation of the plant residues. This, in its turn, leads to an increase of the active porosity, especially prominent in dispersion of peat.

3. Dispersion or compression of peat results in a considerable increase of the kinetic specific surface and a decrease in the size of the water-conducting pores, which determines the character of water migration in the peat.

4. The pressure required to convert most of the intracellular water into the free state is relatively small, and does not exceed 1.0 kg/cm^2 . Thus, this form of water in peat has the lowest bonding energy.

5. The investigation methods which have been developed can be used in studies of various technological processes involving changes in the hydration properties and structure of peat.

LITERATURE CITED

- [1] N. S. Kurnakov and N. A. Pospelova, Trans. Peat Inst. No. 11 (GNTGI, 1932) p. 3.
- [2] S. S. Korchunov, Trans. Sci. Res. Inst. Peat Ind. No. 12 (State Power Press, 1953) p. 229.
- [3] M. P. Volarovich and N. V. Churaev, Colloid J. 21, 157 (1959).*
- [4] M. P. Volarovich and N. V. Churaev, Proc. 3rd All-Union Conference on Colloid Chemistry, 1953 [In Russian] (Izd. AN SSSR, 1956) p. 258; Colloid J. 17, No. 3, 200 (1955).*
- [5] A. A. Berezin and I. D. Belovidov, Trans. Moscow Peat Inst. No. 8 (State Power Press, 1958) p. 167.
- [6] M. P. Volarovich and S. N. Markov, Peat Ind. No. 10, 23 (1951).
- [7] W. K. Lewis, L. Squires and G. Broughton, Industrial Chemistry of Colloidal and Amorphous Materials (IL, 1948) p. 450 [Russian translation].
- [8] S. G. Solopov, Trans. Moscow Peat Inst. No. 8 (State Power Press, 1958) p. 140.

* Original Russian pagination. See C. B. Translation.

- [9] N. V. Churaev, Trans. Moscow Peat Inst. No. 5 (Moscow Peat Inst. Press, 1957) p. 113.
- [10] A. V. Pichugin, Trans. Moscow Peat Inst. No. 2 (State Power Press, 1953) p. 52.
- [11] B. V. Deryagin and M. K. Mel'nikova, Questions of Agricultural Physics, collection edited by A. F. Ioffe and P. P. Samoilov (The Lenin All-Union Academy of Agricultural Sciences, Leningrad, 1957) p. 30; B. V. Deryagin and F. E. Kolyasev, Hydrotechn. and Amelioration, No. 2, 3 (1950).
- [12] B. V. Deryagin and N. A. Krylov, Proc. Conference on Viscosity of Liquids and Colloidal Solutions, pt. 2 [In Russian] (Izd. AN SSSR, 1944) p. 52; B. V. Deryagin, Properties of Thin Liquid Layers and Their Role in Disperse Systems [In Russian] (All-Union Council of Scientific, Engineering and Technical Societies, Moscow, 1937).
- [13] N. A. Galybin, N. K. Rabotnov and E. P. Semenskii, Trans. Moscow Peat Inst. No. 5 (Moscow Peat Inst. Press, 1957) p. 67.
- [14] I. M. Litvinov, Investigation of Soils Under Field Conditions [In Russian] (Coal Tech. Press, 1954).
- [15] N. N. Kulakov, Introduction to the Physics of Peat [In Russian] (State Power Press, 1947).
- [16] V. G. Goryachkin, Fundamentals of Peat Production Technology [In Russian] (State Power Press, 1953).
- [17] M. G. Bulynko, Peat Ind. No. 7, 25 (1951).

Received June 19, 1958

CHANGES IN THE ADSORPTION OF POTENTIAL-DETERMINING IONS DURING COAGULATION OF LYOPHOBIC SOLS BY INDIFFERENT ELECTROLYTES*

Yu. M. Glazman, D. N. Strazhesko, E. F. Zhel'vis, and
L. L. Chervyatsova

The Technological Institute of the Light Industry, and the L. V. Pisarzhevskii
Institute of Physical Chemistry, Acad. Sci. Ukrainian SSR, Kiev

The stability of lyophobic sols is one of the central problems of modern colloid chemistry. The question which still remains least well understood concerns the role of various adsorption effects in colloidal systems on addition of electrolytes in the mechanism of coagulation [1-7].

Adsorption of counter ions has been studied repeatedly [1-3, 8, 9] and its real existence is accepted universally. It is true that different authors evaluate very differently the significance of ion adsorption of this type in the stability of lyophobic sols [1-3, 7]. Literature data relating to adsorption of similarly charged indifferent ions are extremely contradictory [9-14]. We studied this problem by the direct tagged-atom method [15-17] and reached the conclusion that such adsorption does not take place and, in any event, should not play any significant role. However, despite this conclusion, it is still uncertain whether in the coagulation of a sol by an indifferent electrolyte only the outer portion of the electric double layer is changed, or whether the inner layer is simultaneously affected to some extent. Changes in the inner layer must primarily depend on what happens to the potential-determining ions on addition of the coagulant electrolyte to the colloidal system. This question is of great importance in principle in relation to the problem of stability and coagulation of lyophobic colloids in general, and therefore, it has been frequently discussed [18-29]. Despite this, it must be acknowledged that it has not been adequately clarified in the literature; in particular, it should be noted that experimental studies of the problem were largely performed with only one substance — silver iodide.

This situation prompted the present investigation, which was concerned with the fate of the potential-determining ions during coagulation of lyophobic sols by indifferent electrolytes. The tracer-atom method was used.

The substances studied were radioactive sols of AgI^* , HgS^* , and As_2S_3^* (negatively charged), and $\text{Fe}(\text{OH})_3$ (positively charged).

Preparation of sols. Silver iodide sol was prepared, as usual, by the mixing of solutions of potassium iodide (radioactive, tagged with I^{131}) and silver nitrate, with KI in 5% excess; KI and AgNO_3 were previously purified by threefold recrystallization. The radioactive AgI^* sol so prepared was subjected to prolonged dialysis in cellophane bags. Both during preparation and during the subsequent use the sol was carefully shielded from light.

In this case, as is known, I^- ions serve as the potential-determining ions [2, 20, 30, 27].

2. For preparation of mercuric sulfide sol, hydrogen sulfide previously passed through wash bottles containing water was bubbled through $\text{Hg}(\text{CN})_2$ solution (hydrogen sulfide was prepared by the action of heat on a mix-

* Presented at the Fourth All-Union Conference on Colloid Chemistry, Tbilisi, 1958.

TABLE 1

Principal Characteristics of the Investigated Sols

Sol	Concentration of disperse phase millimoles/liter	Sign of particle charge	Probable composition of potential-determining ions	Specific activity of sol, pulses per ml per minute
AgI [*]	10.0	Negative	I ⁻	207570 ± 270
HgS [*]	19.9	The same	HgS ₂ ²⁻	117500 ± 1500
As ₂ S ₃ AsS ⁻	47.0	" "	AsS ₂ ⁻ and AsOS ⁻	652500 ± 5000
Fe(OH) ₃ [*]	70.4	Positive	FeO ⁺	900000 ± 3000

TABLE 2

Comparative Data on Activities (A) and Concentrations of Potential-Determining Ions (c) in the Intermicellar Liquids of AgI^{*}, HgS^{*}, As₂S₃^{*} and Fe(OH)₃^{*} Sols and in Solutions Formed From Them After Coagulation by Various Electrolytes

Electrolyte	Intermicellar liquid		Solutions after coagulation of sols by in-different electrolytes			
	A, pulses/ /ml · min	c · 10 ⁴ , g-ions/ /liter	CT		CT × 2	
			A, pulses/ /ml · min	c · 10 ⁴ , g-ions/liter	A, pulses/ /ml · min	c · 10 ⁴ , g-ions/liter
* AgI sol						
NaNO ₃	403±7	1,94	275±2	1,33	196±1	0,94
KNO ₃			244±1	1,18	222±2	1,07
Ca (NO ₃) ₂			197±1	0,95	176±2	0,85
Ba (NO ₃) ₂			216±1	1,04	189±1	0,91
Al (NO ₃) ₃			245±1	1,18	147±1	0,71
CeCl ₃			179±1	0,86	201±2	0,97
Th (NO ₃) ₄			224±2	1,08	205±2	0,99
* HgS sol						
KCl	719±12	6,09	527±12	4,46	495±12	4,19
BaCl ₂			690±12	5,84	645±12	5,46
CeCl ₃			637±12	5,39	582±12	4,93
Th (NO ₃) ₄			665±12	5,63	672±12	5,69
* As ₂ S ₃ sol						
KCl	898±17	12,94	432±11	6,22	396±10	5,70
BaCl ₂			438±10	6,31	404±10	6,82
CeCl ₃			669±12	9,64	614±11	8,85
Th (NO ₃) ₄			455±11	6,55	442±11	6,37
* Fe(OH) ₃ sol						
KNO ₃	281±9	2,20	2964±23	23,2	1943±19	15,2
KCl			2794±22	21,9	1814±18	14,2
K ₂ SO ₄			2470±20	19,3	3479±25	27,2
K ₃ [Fe (CN) ₆]			3500±24	27,4	4489±28	35,1
K ₄ [Fe (CN) ₆]			7625±36	59,6	10995±43	86,0

Note: Since the relative proportions of AsS₂⁻ and AsOS⁻ ions in As₂S₃ sols are uncertain, in calculation of the concentrations of potential-determining ions it was assumed for simplicity that these ions are present in equimolecular proportions. In consequence, the concentration values given are nominal, but this in no way affects their comparability.

TABLE 3

Coagulating Action of Different Electrolytes on the Investigated Sols

Electrolyte	Coagulating concentration, mM/liter	Ionic strength of solution	Radius of ionic atmosphere $1/\kappa \times 10^8$ cm
■ AgI sol			
NaNO ₃	420	0,420	4,72
KNO ₃	360	0,360	5,10
Ca (NO ₃) ₂	8,3	0,025	19,3
Ba (NO ₃) ₂	5,8	0,017	23,4
Al (NO ₃) ₃	0,37	0,0022	65,2
CeCl ₃	0,31	0,0019	70,1
Th (NO ₃) ₄	0,10	0,0010	96,7
* HgS sol			
KCl	125	0,125	8,65
BaCl ₂	1,75	0,0052	42,4
CeCl ₃	0,067	0,0004	153
■ As ₂ S ₃ sol			
KCl	75	0,075	11,2
BaCl ₂	1,50	0,0045	45,6
CeCl ₃	0,117	0,0007	116
■ Fe(OH) ₃ sol			
KNO ₃	50	0,050	13,7
KCl	50	0,050	13,7
K ₂ SO ₄	0,50	0,0015	78,9

ture of radioactive sulfur tagged with S³⁵ and paraffin wax and asbestos), and excess H₂S was then removed in a stream of hydrogen. A small amount of mercuric cyanide was then added to the sol in order to bind the residual hydrogen sulfide. Electrophoretic observations showed that particles of such sols, as of sols with excess H₂S, are negatively charged. The stabilizing ions in this case are probably HgS₂²⁻ ions [31].

3. Radioactive arsenious sulfide sol was prepared by saturation of a solution of arsenious oxide with tagged hydrogen sulfide with subsequent passage of a stream of pure hydrogen through the sol. A small excess of As₂O₃ was added to this solution. It is known that the particles in such sols are negatively charged; they are stabilized by AsS₂⁻ and AsOS⁻ ions [32]. The sol was carefully shielded from the action of light.

4. Ferric hydroxide sol was prepared by the Krecke method, by gradual addition of radioactive FeCl₃ tagged with Fe⁵⁹ to boiling water. The sol was then subjected first to hot and then to prolonged cold dialysis in cellophane bags.

The question of the nature of the stabilizer in colloidal solutions of ferric hydroxide cannot be regarded as finally settled. Whereas, most workers [1 (p. 94) 14, 33-39] are inclined to regard FeO⁺, Fe³⁺ or Fe₂O₂²⁺ ions as potential-determining, others consider [40-43] that the colloidal particles in these sols are stabilized by H⁺ ions. In view of these differences of opinion, in our experiments with Fe(OH)₃ sol we accepted as a working hypothesis the viewpoint most widely held in the literature, according to which FeO⁺ ions (or other cations containing iron) are potential-determining in this case. Accordingly, our ferric hydroxide sol was tagged with the radioactive Fe⁵⁹ isotope.

Determination of the coagulant concentrations of electrolytes. The sols were coagulated by untagged electrolytes containing coagulant ions of different valences. The coagulation thresholds were estimated visually. To definite amounts of sol variable amounts of water and electrolyte solution were added in such a way that the total volume of the mixture was always the same. The minimum electrolyte concentration sufficient for complete coagulation of the sol (coagulation was considered to be complete when a completely transparent and colorless solution formed over the precipitate) was taken to be the limiting concentration or "coagulation threshold" (CT). The observations were always made immediately after addition of the coagulant.

Investigation of changes in the concentration of potential-determining ions in solution during coagulation of sols by indifferent electrolytes. In order to establish whether any changes take place in the inner layer of the double layer on the colloidal particles during sol coagulation, it is first necessary to determine the changes in the concentration of the potential-determining ions contained in the intermicellar solution. Since in all cases the potential-determining ions were tagged (I^{131} , S^{35} , Fe^{59}), it was only necessary to compare the specific activities of the intermicellar liquid of a given sol and of the solution formed after separation of the disperse phase formed as the result of coagulation.

The intermicellar liquid was obtained by repeated alternate freezing and centrifugation of the sol [30, 32]. These operations were repeated until the radioactivity of the solution reached a constant value. The precipitate of the disperse phase after coagulation by electrolytes was also separated by centrifugation. Since it has been reported in the literature [27] that potential-determining ions are gradually desorbed from the surface of the coagulated particles, the precipitate was separated from the solution immediately after the sol had been coagulated by the electrolyte. For determination of the specific activity, 0.1 to 0.4 ml of the solution under test was placed on a filter paper (in experiments with AgI^* , HgS^* , and $As_2S_3^*$ sols the filter papers were first treated with a solution of silver nitrate, which forms nonvolatile and sparingly soluble compounds with the corresponding potential-determining ions), the filter paper was dried, and the activity was determined by means of a Geiger-Muller counter [44].

If the specific activity of the sol and its disperse-phase content are known, it is easy to calculate the concentration of potential-determining ions in the intermicellar liquid and in the solution over the precipitate after coagulation. The data required for such calculations are given in Table 1.

The disturbances in the structure of the inner layer of the double layer on the colloidal particles which are caused, as Table 2 shows, by additions of electrolytes to the systems, may be partly the consequence of the inevitable dilution of a sol during coagulation. To eliminate the influence of this factor, the intermicellar liquid was always obtained from specially-prepared sol samples, previously diluted to the appropriate extent with pure water. All the activity values in Table 2 are reduced to refer to undiluted sols of the initial concentrations.

Table 2 contains direct recalculated data which are directly indicative of changes in the concentration of the potential-determining ions of the intermicellar solutions which take place during coagulation of sols by indifferent electrolytes. Estimates of the possible error in the radiometric determinations suggest that the ion concentrations in Table 2 are accurate to at least within 2-3%.

Before a discussion of the main subject of the present investigation, we would like to draw attention to a minor fact of some interest. The intermicellar liquids of colloidal mercuric sulfide and arsenious sulfide solutions had relatively high activities (Table 2). It might be thought that these sols, which were prepared with the use of excess mercuric cyanide or arsenious oxide respectively, should not contain sulfur compounds in true solution. The results show, however, that this is not the case — despite the generally accepted view, thio- and thiooxyarsenious acids and thiomeric acid (H_2HgS_2) can evidently exist in solution if their concentrations are not too high.

From these results it can be determined quite definitely whether the coagulation process affects the inner layer of the double layer on the colloidal particles and, if so, what the nature of the changes in it is. It is clear from Table 2, that in the case of the negative sols of AgI^* , HgS^* , and $As_2S_3^*$ the concentrations of the potential-determining ions in solution after coagulation of the sols by electrolytes was lower than in the corresponding intermicellar liquids, both at CT and $CT \times 2$. This shows that in the coagulation of such sols by indifferent electrolytes, there is a certain amount of additional adsorption of potential-determining ions on the particles of the disperse phase.

A similar result was obtained earlier for silver iodide sol by Kruyt and his associates [24, 27], who used a potentiometric method. They explained the additional adsorption of potential-determining ions during coagulation from a purely electrostatic standpoint; their reasoning was roughly as follows.

The colloidal AgI particles have an electric double layer, the potential difference in which is determined by the Nernst equation:

$$\epsilon = -k \log [I] = k pI.$$

When an indifferent electrolyte is added to the system, the double layer contracts and its capacity therefore increases. If the surface charge remains the same then evidently (by definition of capacity) the potential difference ϵ decreases. However, as the potential difference ϵ is determined, in accordance with the Nernst equation, only by pI , the surface charge must increase to restore equilibrium. This is effected at the expense of the I^- ions, in the intermicellar liquid which approach the surface and are ultimately adsorbed on it.

However, it is not difficult to show in the light of our and Kruyt's results that this purely electrostatic interpretation is unsatisfactory. Even when the process corresponds qualitatively to these concepts (i.e., when additional adsorption of potential-determining ions was observed), there was no quantitative agreement with them. Indeed, it should be expected theoretically that the adsorption effect should increase simultaneously with increased contraction of the diffuse double layer which should occur with increasing ionic strength of the solution. Facts readily show that these theoretical considerations are not confirmed.

Table 3 contains calculated values of the ionic strength of the electrolytes and radii of the ionic atmospheres at electrolyte concentrations corresponding to their coagulation thresholds. Evidently, $1/\kappa$ can serve as an approximate measure of the thickness of the double layer, and therefore represents the diffuseness of its outer layer. The greatest contraction of the diffuse layer occurs, as Table 3 shows, when sols are coagulated by electrolytes with univalent counter ions. In such cases the double layer is apparently contracted almost to the limit; conversely, the higher the valence of the coagulant ions, the more diffuse it becomes. It might seem that adsorption of potential-determining ions from the intermicellar solution, if it is really caused by increase in the capacity of the double layer on addition of an electrolyte to the colloidal system, should also increase regularly in the transition from multivalent to univalent coagulant ions.

However, Kruyt and Klompe [27], in a study of the coagulation of AgI sols by potassium, barium, and lanthanum salts, reached an entirely different conclusion — they found that, despite valence differences, these ions in indifferent electrolytes have the same influence on the additional adsorption of iodide ions by the surface of the disperse phase.

In contrast to Kruyt and Klompe, we found in a study of silver iodide and other negative sols (Table 2) that the nature of the counter ion of an indifferent electrolyte alters to some extent the magnitude of additional adsorption of potential-determining ions. However, despite the purely electrostatic considerations discussed above, this effect is very weak, and, which is most important, it does not depend in any regular manner on the valence of the coagulant ion.

It must be remembered that changes in the inner layer of the electric double layer on colloidal particles are not necessarily associated only with additional adsorption of potential-determining ions from solution — they may occur in some instances as the result of orientation at the disperse phase surface of ion pairs of the indifferent electrolyte added to the sol (e.g., see [45]). Our results give an indication of the extent to which the electrolyte concentration in the boundary layers of the colloidal particles increases in such orientation, if it occurs. The negative pole of the dipole formed as the result of such orientation is apparently always directed toward the colloidal particles, regardless of the sign of its charge [46, 47]. If the colloidal particles are negatively charged, then the potential difference which arises from orientation of ion pairs in the electrolyte — the "adsorptional" potential difference (φ_a) — should evidently have the same sign as the original potential of the ionic double layer, φ_i . Since the total potential difference between the phases ($\varphi = \varphi_i + \varphi_a$) is completely determined only by the activity of the potential-determining ions in solution, then, if we assume that it is constant (i.e., independent of adsorption of the indifferent electrolyte [48]), it follows that formation of an "adsorptional" potential difference φ_a must inevitably result in a decrease of φ_i . This implies that orientation of ion pairs of the coagulant electrolyte should lead to desorption of potential-determining ions from the surface of the colloidal particles. However, no such desorption was observed in any of the investigated cases of coagulation of negatively charged

sols (Table 2); additional adsorption of potential-determining ions, due to contraction of the diffuse outer layer of the double layer, always prevailed. This evidently shows that addition of an indifferent electrolyte to a colloidal system is not, in reality, generally accompanied by any substantial increase of its concentration at the surface of the colloidal particles [15-17].

We must consider separately the results of experiments with ferric hydroxide sol (Table 2), in which there was considerable desorption of FeO^+ ions (or other similar ions containing iron) during coagulation in all cases. If, as we assumed initially, FeO^+ ions are potential-determining in $\text{Fe}(\text{OH})_3$ sols, then the results are quite inexplicable — they are in obvious and quite irreconcilable contradiction to the concepts discussed above. In fact, both the factors considered above — compression of the diffuse outer layer of the double layer and orientation of ion pairs of the coagulant electrolyte added to the sol — should act in the same direction in relation to positively-charged colloidal particles of ferric hydroxide: they cause additional adsorption of potential-determining ions from solution. However, our experimental data can be explained quite rationally if it is assumed, in accordance with Kargin's views [41, 42 see also 40] that H^+ ions are the potential-determining ions in ferric hydroxide sols. Additional adsorption of hydrogen ions which occurs when coagulant electrolytes are added to the sol samples implies an increase of their concentration in the boundary layers of the colloidal particles; it leads to intensification of chemical interaction between H^+ ions and the substance of the disperse phase, and hence to desorption of the FeO^+ ions formed in the reaction. This mechanism of FeO^+ ion desorption is probably involved in the superivalent displacement effect of Cl^- ions which had been observed by Rabinovich and Kargin [35, 49 see also 40] in the course of "rapid" potentiometric titration of ferric hydroxide sols by sodium sulfate and certain other electrolytes. This view is incidentally confirmed by the fact that this "superequivalence" effect was not observed in coagulation of $\text{Al}(\text{OH})_3$ sol, stabilized, in contrast to $\text{Fe}(\text{OH})_3$ sol, by basic aluminum salts [50].

Thus, two important conclusions may be drawn from all the results of the present investigation:

1. Coagulation of lyophobic sols by indifferent electrolytes affects not only the outer but also the inner layer of the electrical double layer on colloidal particles.
2. The changes observed in the process cannot be interpreted solely in terms of purely electrostatic compression of the double layer.

In conclusion, attention must be drawn to yet another significant fact. It follows from the numerical values of $1/\kappa$ given in Table 3, that the capacity of the double layer on the colloidal particles decreases regularly and considerably with increase of the valence of the coagulant ion. At the same time, additional adsorption of potential-determining ions in coagulation of sols by different electrolytes (Table 2) varies relatively little, and, in any event, is not in direct dependence on the valence of the counter ions. If it is taken into account that the adsorption of potential-determining ions determines the magnitude of the surface charge and that the capacity is the ratio of charge to potential, it follows that the surface potential of the disperse phase at the instant of coagulation of the sol should differ with different electrolytes; the extent of changes in the potential during coagulation evidently depends both on the valence of the counter ion and on the specific characteristics of the colloidal solution itself and of the electrolytes introduced into the system. This shows that the existing theories of coagulation [4-6] should be extended by quantitative determinations of the influence of electrolytes on the potentials of colloidal particles. It should be remembered in this connection that changes in the surface potential of colloidal particles during addition of electrolytes to sols may be due to different causes: on the one hand, to exchange adsorption of counter ions in the outer region of the double layer, and on the other, to changes taking place in the inner layer.

SUMMARY

1. A study was carried out of the coagulation of radioactive AgI^* , HgS^* , and As_2S_3^* (negative) and $\text{Fe}(\text{OH})_3^*$ (positive) sols by untagged electrolytes with coagulant ions of different valences.
2. The activities of the intermicellar liquids of these sols were compared with the activities of the corresponding solutions after coagulations; it was found that appreciable additional adsorption of potential-determining ions takes place in all cases. The desorption of iron ions observed in coagulation of $\text{Fe}(\text{OH})_3$ sols is caused by secondary effects.

Thus, coagulation of lyophobic sols by indifferent electrolytes affects not only the outer but also the inner layer of the double layer on the colloidal particles.

3. The purely electrostatic interpretation of the effects taking place within the double layer during coagulation of sols by electrolytes has been examined. There is a quantitative discrepancy between this interpretation and the experimental data.

4. The coagulation theory must be developed further, with quantitative consideration of the influence of electrolytes on the potentials of colloidal particles.

LITERATURE CITED

- [1] H. Freundlich, *Kapillarchemie* B. 2 (1932).
- [2] E. J. W. Verwey, *Progr. Chem.* 4, 1194 (1936).
- [3] A. I. Rabinovich, in the book: *Coagulation of Colloids* [In Russian] (ONTI, Moscow, 1936) p. 169.
- [4] B. V. Deryagin and L. D. Landau, *J. Exp. Theoret. Phys.* 11, 802 (1941); 15, 663 (1945).
- [5] B. V. Deryagin, *Proc. 3rd All-Union Conference on Colloid Chemistry* [In Russian] (Izd. AN SSSR, Moscow, 1956) p. 225.
- [6] E. J. W. Verwey and J. G. Overbeek, *Theory of the Stability of Lyophobic Colloids*, (Amsterdam, 1948).
- [7] H. R. Kruyt, *Colloid Science* (IL, Moscow, 1955) [Russian translation].
- [8] H. Freundlich and H. Schucht, *Z. phys. Chem.* 85, 641 (1913).
- [9] M. N. Chakravarti and N. R. Dhar, *J. Phys. Chem.* 31, 997 (1927).
- [10] K. C. Sen, *J. phys. Chem.* 29, 517 (1925).
- [11] H. B. Weiser, *J. phys. Chem.* 34, 335 (1930).
- [12] S. E. Linder and H. Picton, *J. Chem. Soc.* 67, 63 (1895).
- [13] V. N. Krestinskaya and V. S. Yakovleva, *J. Russ. Phys.-Chem. Soc.* 60, 295 (1928).
- [14] V. N. Krestinskaya and Z. V. Khakimov, *J. Gen. Chem.* 14, 70 (1944).
- [15] Yu. M. Glazman, D. N. Strazhesko and B. É. Tartakovskaya, *Colloid J.* 15, 161 (1953).*
- [16] Yu. M. Glazman, *Colloid J.* 15, 334 (1953).
- [17] Yu. M. Glazman, D. N. Strazhesko and N. A. Bisikalova, *J. Inorg. Chem.* 3, 115 (1958).
- [18] J. S. Beckley and H. S. Taylor, *J. phys. Chem.* 29, 942 (1925).
- [19] E. Lange and R. Berger, *Z. Elektrochem.* 36, 171 (1930).
- [20] E. J. W. Verwey and H. R. Kruyt, *Z. phys. Chem.* 167 (A), 149 (1933).
- [21] I. P. Protas, *J. Phys. Chem.* 10, 844 (1937).
- [22] A. Kellermann and E. Lange, *Kolloid.-Z.* 81, 88 (1937).
- [23] A. Kellermann and E. Lange, *Kolloid.-Z.* 88, 341 (1939).
- [24] H. R. Kruyt and H. de Bruyn, *Z. phys. Chem.* 168 (A), 282 (1940).
- [25] H. R. Kruyt and J. G. Overbeek, *Trans. Faraday Soc.* 36, 110 (1940).
- [26] H. de Bruyn, *Rec. trav. chim. Pays-Bas* 61, 5, 21 (1942).
- [27] H. R. Kruyt and M. A. M. Klompe, *Kolloid. Beih.* 54, 484 (1943).
- [28] E. L. Mackor, *Rec. trav. chim. Pays-Bas*, 70, 763 (1951).

* Original Russian pagination. See C. B. Translation.

- [29] M. Mirnik and B. Tezak, *Trans. Faraday Soc.* 50, 65 (1954).
- [30] V. A. Kargin and M. A. Tolstaya, *J. Phys. Chem.* 16, 115 (1942).
- [31] Yu. M. Glazman, *Proc. All-Union Conference on Colloid Chemistry [In Russian]* (Acad. Sci. Ukrainian SSR Press, Kiev, 1952) p. 349.
- [32] A. N. Kharin, *Dissertation: Colloidochemical Investigation of Sulfides and Sulfur [In Russian]* (Krasnodar, 1943).
- [33] J. Duclaux, *J. chim. phys.* 5, 29 (1907).
- [34] G. Malfitano, *Z. phys. Chem.* 68, 232 (1910).
- [35] A. I. Rabinovich and V. A. Kargin, *Z. phys. Chem.* 133, 203 (1928).
- [36] W. Pauli and E. Valkó, *Elektrochemie der Kolloide*, (1929), p. 526.
- [37] R. Zsigmondy, *Colloid Chemistry* 1, (Ukrainian Scientific Research Institute Press, Kiev, 1931), p. 191. [Russian translation].
- [38] N. P. Peskov, *Physicochemical Principles of Colloid Science [In Russian]* (State Chem. Tech. Press, Moscow-Leningrad, 1932) p. 219.
- [39] H. R. Kruyt, *Colloids* (ONTI, Leningrad, 1936) p. 95 [Russian translation].
- [40] H. B. Weiser, *J. Phys. Chem.* 35, 1 (1931).
- [41] V. A. Kargin and G. V. Klimovitskaya, *J. Phys. Chem.* 11, 467 (1938).
- [42] V. A. Kargin and V. V. Kiseleva, *J. Phys. Chem.* 11, 461 (1938).
- [43] V. F. Ust'-Kachkintsev, *Colloid J.* 15, 394 (1953).*
- [44] V. I. Spitsyn, P. N. Kodochigov, M. M. Golutvina, A.T. Kuzina and Z. A. Sokolova, *Radioactive Tracer Techniques [In Russian]* (Izd. AN SSSR, Moscow, 1955).
- [45] L. V. Yansen, *J. Phys. Chem.* 5 302 (1934).
- [46] A. Frumkin, *Z. phys. Chem.* 109, 34 (1924).
- [47] R. Burshtein, A. Frumkin and D. Lavrovskaya, *Z. phys. Chem.* 150 (A), 421 (1930).
- [48] A. Frumkin, *Z. phys. Chem.* 103, 55 (1923).
- [49] A. I. Rabinovich and E. V. Fodiman, *J. Phys. Chem.* 3, 16 (1932).
- [50] P. S. Vasil'ev and A. I. Rabinovich, *J. Phys. Chem.* 2, 354 (1931).

Received February 26, 1958

* Original Russian pagination. See C. B. Translation.

EFFECT OF A HIGH-FREQUENCY ULTRASONIC FIELD ON PLASTIC PASTES

M. N. Gol'dshtein and É. M. Gutman

The Dnepropetrovsk Institute of Transport Engineers

It is known that high-frequency mechanical vibrations often have a significant effect on the mechanical properties of disperse systems; in particular, they may break down the structure of a system and cause additional dispersion [1]. Therefore, ultrasonic vibrations may become widely used in studies of soil structure.

Golubev et al. [2] used ultrasonics to disperse soil suspensions in preparation of soil samples for mechanical analysis. The investigations were conducted at an ultrasonic oscillation frequency of $4 \cdot 10^5$ cycles per second and an acoustic output power of 75 w of the quartz oscillator. Aqueous suspensions of various soils were subjected to the action of ultrasonics, at soil-water ratios of 1:6, 1:10, and 1:20. This investigation demonstrated the disputable advantage of ultrasonic methods over other methods for dispersion of soil aggregates. Moreover, the important conclusion was reached that ultrasonics do not break up individual grains or solid particles in soils. Olmsted [3] obtained similar results.

Crouly and Wolsh [4] used ultrasonics for breaking up clay particles in 1% kaolin suspensions. Dispersion of the suspension by ultrasonics of frequency of 1 megacycle/second resulted in complete destruction of agglomerates and flakes. The observed decrease of pH was attributed to formation of nitric acid in the water under the action of ultrasound and to liberation of water-soluble adsorbed salts.

Terpilovskii and Kuznetsov-Fetisov [5] studied the effects of ultrasonics on the properties of clay suspensions used in drilling of oil wells and gas boreholes. Aqueous suspensions of clays of the Tertiary and Quaternary periods were subjected to the action of ultrasonics at a frequency of 21 kilocycles/second and intensity of 6 w/cm^2 . The viscosity, static shear strength, and caking power of the suspensions were increased by the ultrasonic treatment.

All these investigations were carried out with suspensions and gels of high moisture contents.

In this paper we present the results of an investigation of the influence of high-frequency ultrasonic vibrations on mechanical properties of various clay pastes with considerably lower moisture contents, corresponding to plastic consistency.

The soil was compacted in a metallic band 70 mm in diameter under a vertical load 2 kg/cm^2 transmitted to the soil through a porous piston. A soil sample 1 (Fig. 1) was then cut out, 56 mm in diameter and 20 mm high, inserted in a brass ring, and placed in the compression apparatus, the floor of which was the ultrasonic oscillator 2. The piezoelectric oscillator of barium titanate, 60 mm in diameter, was carefully insulated from the high-voltage electrode side.

The high-frequency field and the constant polarizing voltage were supplied to the piezoelectric oscillator from a generator constructed in the laboratory, of 300 w power (two GU-150 tubes in parallel) and frequency range of 10 kilocycles to 3 megacycles/second. The exposures were in cycles of 3 seconds each.

The acoustic power transmitted to the soil was of the order of 100 w. A filter paper 3 and a porous piston 4 were placed on top of the sample. This piston was used to apply a load of 2 kg/cm^2 in a vertical direction to the soil, lateral expansion being impossible. The vertical deformation h was measured by means of the dial 5 with 0.002 mm scale divisions.

Soil	Flow limit (moisture content, %) W_f	Rolling limit (moisture content, %) W_r	Plasticity number, $W_f - W_r$	Density, g/cc
Simferopol' clay (montmorillonite)	110.0	51.1	58.9	2.69
Chasov Yar clay (illite)	59.2	32.0	27.2	2.71
Pavlograd clay (kaolin)	32.1	21.4	10.7	2.83
Dnieper sand	17.6	—	—	2.65

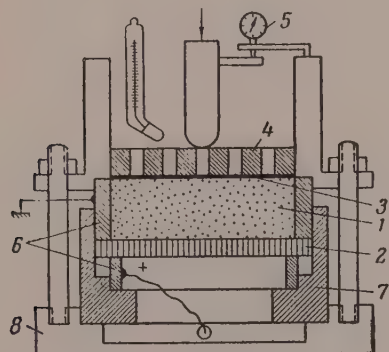


Fig. 1. Ultrasonic dilatometer: 1) soil sample; 2) barium titanate; 3) filter paper; 4) porous piston; 5) measuring dial; 6) brass rings; 7) insulator; 8) housing.

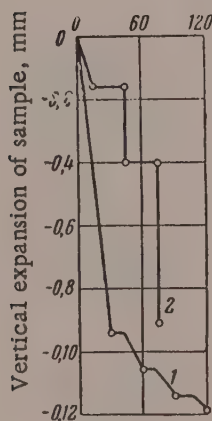


Fig. 3. Effect of ultrasonic vibrations on compaction of: 1) moist sand; 2) dry montmorillonite powder.

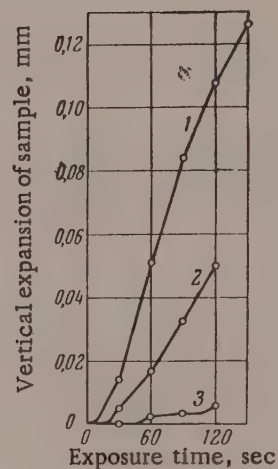


Fig. 2. Sonodilatation effect in montmorillonite pastes with different salts in the pore solution; 5% solutions of: 1) NaCl; 2) CaCl_2 ; 3) AlCl_3 .

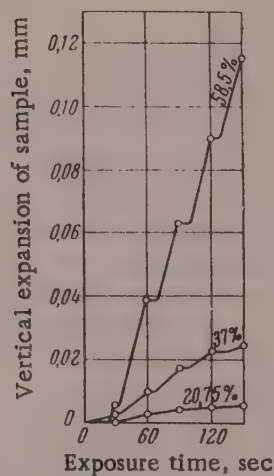


Fig. 4. Sonodilatation effect in montmorillonite pastes of different moisture contents.

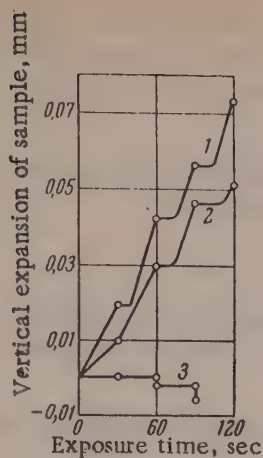


Fig. 5. Effect of mineral composition of clay pastes on the sonodilatation effect: 1) montmorillonite; 2) illite; 3) kaolinite.

Experiments with sands saturated with water showed that ultrasonic vibrations cause shrinkage which is sharp at first and then dies down asymptotically (Fig. 3, Curve 1). Dry montmorillonite powder also exhibited rapid shrinkage (Fig. 3, Curve 2). This is clearly the usual compaction under the influence of vibration, characteristic for systems in which cohesion forces are absent.

A montmorillonite sample of plastic consistency, made with distilled water and containing 58.5% moisture before the experiment, increased in volume under the influence of an ultrasonic field at a constant vertical rate of 0.001 mm/second (Fig. 4) despite the fact that it was under a load of 2 kg/cm². A 2.5-fold decrease of the anode voltage of the oscillator resulted in a 16-fold decrease of the deformation rate. The rate of volume increase was greater when water instead of oil was put in the space above the piston. The sonodilatation effect decreased sharply when the moisture content of the montmorillonite sample was lowered to 37 and 20.75% (Fig. 4).

The dilatation effect was considerably less with liquids of lower polarity. In particular, a montmorillonite sample made with transformer oil did not exhibit dilatation at all. Polar liquids (glycerol, methyl alcohol) resulted in much smaller dilatation effects than distilled water.

The nature of the cations present in the pore solution influences the magnitude of the effect to a considerable extent. The greatest effect was observed in experiments with montmorillonite samples containing 5% NaCl solution (Fig. 2, Curve 1). Montmorillonite samples with 5% CaCl₂ solution showed a somewhat smaller effect (Fig. 2, Curve 2), while in experiments with samples containing 5% AlCl₃ solution, the dilatation was considerably less (Fig. 2, Curve 3) than with samples containing Na⁺.

The effect of mineral composition on the sonodilatation effect in clay pastes is shown in Fig. 5. Illite samples exhibited somewhat smaller dilatation (Fig. 5, Curve 2) than montmorillonite (Fig. 5, Curve 1). Kaolin does not increase in volume, but even contracts somewhat (Fig. 5, Curve 3) under the influence of ultrasound. The moisture contents of the samples remained almost unchanged after the action of ultrasound in all the experiments.

We may refer in this connection to the paper by Chmutov and Alekseev [6], who studied the effect of ultrasonics on adsorption of fatty acids by microporous carbon. They found that ultrasonic treatment of microporous carbon in a solution of equilibrium concentration results in considerable additional adsorption, although the carbon does not undergo subdivision leading to an increase of surface area. The authors attributed this effect to "... increase in the mobility of the molecules of the substance, elimination of steric hindrances, and peculiar 'shaking down' of molecules in the adsorbent pores."

Pastes made from clays of different sorption capacities were studied — Simferopol' montmorillonite, Chasov Yar illite, and Pavlograd kaolinite. Experiments with fine Dnieper sand were carried out for comparison (see table).

Pastes were made with distilled water, transformed oil, glycerol, methyl alcohol, and 5% solutions of NaCl, CaCl₂, and AlCl₃. The upper piston was covered with water or oil to prevent evaporation.

When a high-frequency field (500 kilocycles/second) was applied to the oscillator, the clay samples increased appreciably in volume; the increase was approximately linear with time (Fig. 2).

When the field was removed, the deformation caused instantly and after some time slow contraction began. Since the effect was free from inertia, it follows that it is associated directly with the ultrasonic vibrations and not with the thermal action of ultrasound. Special experiments showed that the maximum temperature during the exposure did not exceed 44°.

We have given the name of the sonodilatation effect to the observed effect of expansion of clay samples under an applied ultrasonic field.

The fact that sands and kaolin do not exhibit the dilatation effect, whereas it is found in illite and to the maximum extent in montmorillonite, shows that surface activity of the mineral particles plays a dominant role in this effect. This is also shown by the considerable decrease of the effect with decreasing polarity of the liquid used (in the sequence: water, methyl alcohol, glycerol, transformer oil).

The sharp decrease of dilatation of montmorillonite with decrease of moisture content is further evidence of the role played by binding of the polar water molecules by the surfaces of the clay particles.

SUMMARY

1. High-frequency ultrasonic vibrations cause volume expansion of highly disperse pastes; the expansion is approximately linear during the exposure. In some experiments, the dilatation rate of montmorillonite paste reached 0.074 mm/minute in the vertical direction.

2. This effect is not observed in coarse-grained soil systems (sands); ultrasound causes compaction of such soils. The same is found with highly disperse dry clay powders.

3. The dilatation effect greatly increases with increases of moisture content of the clay samples and with vibration intensity. The effect is also increased in the presence of Na^+ ions in the pore solution.

4. The effect diminishes considerably with decreasing polarity of the liquid in the paste pores, and is totally absent with nonpolar liquids.

5. The probable explanation of the dilatation effect is that ultrasonic vibrations intensify binding of the polar liquid molecules, and in the case of montmorillonite they also increase the "accessible" surface area of the particles.

LITERATURE CITED

- [1] L. Bergmann, Ultrasonics (IL, Moscow, 1956) p. 469 [Russian translation].
- [2] I. F. Golubev, S. A. Manin and E. P. Ostrovskii, in the book: Problems of Soviet Pedology, 3 [In Russian] (1936).
- [3] L. B. Olmsted, J. Agr. Res., 42 (1931).
- [4] Crouly, and Wolsh, J. Amer. Ceram. Soc., 37, 433 (1954).
- [5] N. N. Terpilavskii and L. I. Kuznetsov-Fetisov, Trans. S. M. Kirov Institute of Chemical Technology, Kazan, No. 18, 100 (1954).
- [6] K. V. Chmutov and N. G. Alekseev, Proc. Acad. Sci. USSR, 67, No. 2, 321 (1949).

Received June 24, 1957

STUDY OF THE SINTERING MECHANISM OF FTOROPLAST-4 (POLYTETRAFLUOROETHYLENE) PREFORMS

1. INVESTIGATION OF THE SORPTION PROCESS

A. A. Gorina and V. A. Kargin

Scientific Research and Planning Institute of Plastics, Moscow

The aim of our study of the sintering mechanism of polytetrafluoroethylene (Ftoroplast-4) in molded preforms was to determine the nature of the process taking place in the molded preform during sintering: whether there is an increase of interparticle contact accompanied by a decrease of porosity, but with retention of the individual particles, or whether the pores are already destroyed during molding of the preform under the optimum specific pressures, while the sintering process favors denser packing of the polymer macromolecules because of their higher mobility at the high sintering temperatures, leading to total disappearance of interfaces between the particles and to radical changes in the properties of the material. Many known methods may be used for solution of this problem, such as methods for investigating permeability characteristics, electron microscopy, mechanical methods, etc.

This paper contains the results of a study of the sorption of a low-molecular substance by Ftoroplast-4 and of the diffusion of dyes in Ftoroplast-4. The direct aim of these investigations was to estimate the density of molecular packing and microporosity of the material, and changes in the latter during the sintering process.

Sorption of a Low-Molecular Substance

Sorption determinations can be used for estimating porosity of a material, including both micropores in the ordinary sense and gaps caused by loose packing of the molecular chains. This problem is simpler with polymers if the sorbed substance is not soluble in the polymer and the sorption of the substance occurs entirely in the free space of the polymer due to the presence of pores and intermolecular gaps. Therefore, ethyl alcohol was chosen as the substance for sorption experiments with polytetrafluoroethylene. The sorption capacity was estimated both by absorption from the gas phase and by immersion of specimens in liquid ethyl alcohol with subsequent estimation of sorption from permeability to diffusion.

Investigations of the penetration of aggressive liquids through high polymers have shown that in thermoplastics molecular diffusion takes place, which may be represented in terms of the change in weight of the specimen, by means of the equation derived by Kanavets [1] in his study of the effects of the contents of moisture and volatile substances on the dimensions of articles made from phenolic resins:

$$\theta_{\tau} = \theta_{\max} \left[1 - e^{-\frac{\pi^2 D \tau}{l^2}} \right], \quad (1)$$

where θ_{τ} is the weight of the specimen after time τ , in grams; θ_{\max} is the maximum weight of the specimen in grams after exposure to the sorbed medium; D is the diffusion coefficient in $\text{cm}^2/\text{second}$; τ is the time of exposure of the specimen to the medium, in seconds; l is the thickness of the specimen in centimeters.

TABLE 1

Coefficients of Diffusion (D) of Ethyl Alcohol in Ftoroplast-4

Sintering temperature of Ftoroplast-4, °C	290	300	310	from 320 to 370*	390
Diffusion coefficient $\times 10^8$, cm ² /second	4	2.13	2.04	—	0.98

*The diffusion coefficient could not be determined for these sintering temperatures owing to the inadequate sensitivity of the method. The numerical values of D are probably at least one order of magnitude less than the others given above.

TABLE 2

Effects of Heating Time and Temperature on the Depth of Penetration of Dye or Pigment into Polyethylene

Colorant	Oven temp., °C	Heating time, min	Penetration depth of colorant, mm	Colorant	Oven temp., °C	Heating time, min	Penetration depth of colorant, mm
Sudan	80	15	0,13	Sudan	110	90	1,93
	80	30	0,25		135	15	1,60
	80	45	0,47		135	30	3,83
	80	60	0,43		135	45	5,55
	80	75	1,08		135	60	8,10
	80	90	1,20		135	15	Color boundary does not move
	110	15	0,40		135	30	
	110	30	0,63		135	45	
	110	45	1,70	Iron oxides	135	60	The same » »
	110	60	1,33		135	75	
	110	75	2,33		135	90	

TABLE 3

Particular Values of Equations (5) and (7)

Heating temperature °C	Expression for the relationship $\Delta l = k\tau$	Heating time, min	Expression for the relationship $\Delta l = aT^n$
80	0.12τ	15	$0.334 \cdot 10^{-10} T^4$
110	0.27τ	30	$0.669 \cdot 10^{-10} T^5$
135	1.28τ	45	$0.124 \cdot 10^{-9} T^5$
		60	$0.132 \cdot 10^{-9} T^5$

Sorption isotherms*. Sintered and unsintered (tablet) Ftoroplast-4 films were used as the test specimens. The sorption capacity of these specimens for ethyl alcohol vapor was determined by means of a McBain spring balance (of high sensitivity) by a procedure described previously [2].

It is clear from Fig. 1 that a sintered Ftoroplast-4 film has the denser structure, and its sorption capacity is therefore lower. Limiting saturation is reached in this film at relative vapor pressures in the 40-50% range, whereas in the tablet (film not subjected to sintering) limiting saturation is not reached even at a relative vapor

*The isotherms for sorption of alcohol vapor by Ftoroplast-4 films were determined by T. V. Gatovskaya in the L. Ya. Karpov Physicochemical Institute.

TABLE 4

Effects of Sintering Temperature and Time on the Depth of Penetration of Anthraquinone Acid Green Base into Ftoroplast-4

Sintering temperature, °C	Sintering time, min	Penetration depth of dye, mm	Sintering temp., °C	Sintering time, mm	Penetration depth of dye, mm
290	30	0,3	350	90	6,0
290	60	0,7	350	120	6,5
290	75	0,7	370	30	2,5
290	90	0,8	370	60	4,3
290	120	1,0	370	75	5,0
330	30	1,0	370	90	5,3
330	60	1,3	370	120	—
330	75	1,8	390	30	3,6
330	90	2,0	390	60	4,0
330	120	2,5	390	75	6,1
350	30	1,5	390	90	6,3
350	60	4,3	390	120	—
350	75	4,1	—	—	—

TABLE 5

Particular Values of Equations (5) and (7)

Sintering temp., °C	Expression for relationship $\Delta l = k \tau$	Sintering time, min	Expression for relationship $\Delta l = aT^n$
290	0,09 τ	30	0,234 · 10 ⁻¹⁷ T ⁷
330	0,23 τ	60	0,425 · 10 ⁻¹⁷ T ⁷
350	0,62 τ	75	0,487 · 10 ⁻¹⁷ T ⁷
370	0,67 τ	90	0,172 · 10 ⁻¹⁰ T ⁸
390	0,78 τ	120	0,192 · 10 ⁻¹⁴ T ⁶

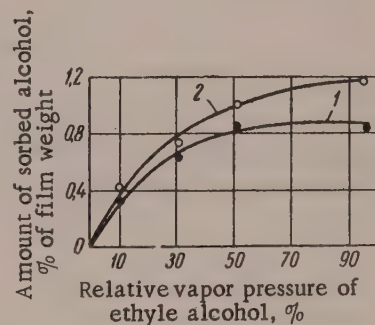


Fig. 1. Isotherms for the sorption of ethyl alcohol vapor by Ftoroplast-4: 1) sintered film; 2) unsintered film (tablet).

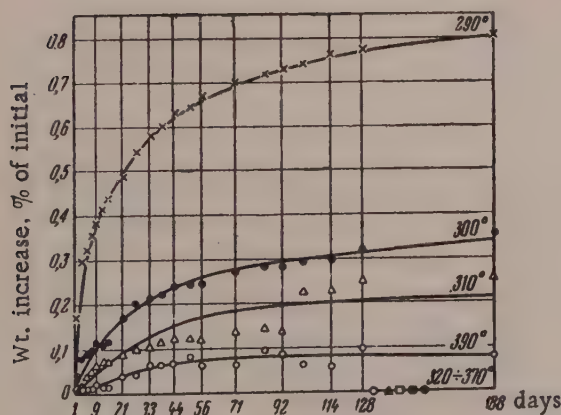


Fig. 2. Kinetic permeability curves for ethyl alcohol in Ftoroplast-4 for specimens sintered at different temperatures.

pressure of 96.2%. On the other hand, the absence of capillary condensation, even in the tablet, indicates that molded Ftoroplast-4 preforms are characterized by the absence of macropores. Therefore, the sintering process involves not only a partial increase in the packing density of the material, but also a closer packing of the macromolecules, leading to radical changes in the mechanical, dielectric, sorptional, and other properties of the material.

The kinetics of sorption of liquid ethyl alcohol by specimens of Ftoroplast-4 sintered in the form of disks 25 mm in diameter and 4 mm thick was determined for sintering temperatures from 290 to 390°, with the specimens held in alcohol for periods from 1 to 188 days. The results of the tests are plotted in Fig. 2.

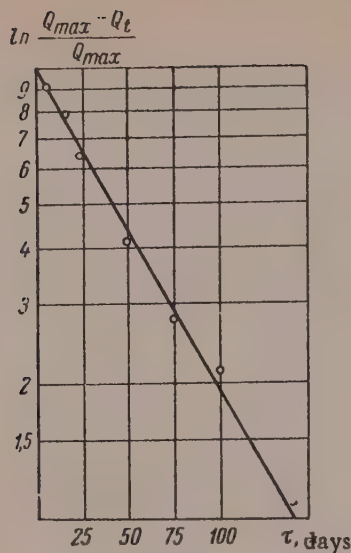


Fig. 3. The function for specimens of Ftoroplast-4 sintered at 390°

The curves in Fig. 2 and Equation (1) can be used for calculation of the coefficient of diffusion of ethyl alcohol in Ftoroplast-4, after Equation (1) has been transformed into

$$\frac{\theta_{\max} - \theta_{\tau}}{\theta_{\max}} = e^{-\pi^2 D \tau / l^2} \quad (2)$$

and in logarithmic form

$$\ln \frac{\theta_{\max} - \theta_{\tau}}{\theta_{\max}} = -\frac{\pi^2 D \tau}{l^2} \quad (3)$$

Fig. 3 shows a linear plot of the function

$$\ln \frac{\theta_{\max} - \theta_{\tau}}{\theta_{\max}} = f(\tau)$$

for a Ftoroplast-4 specimen sintered at 390°. From this straight line it is easy to find the diffusion coefficient (D), after transformation of Equation (3)

$$D = \frac{\ln \left[\frac{\theta_{\max} - \theta_{\tau}}{\theta_{\max}} \right] l^2}{\pi^2 \tau}, \text{ cm}^2/\text{sec}. \quad (4)$$

The numerical values of the diffusion coefficient of ethyl alcohol in Ftoroplast-4 specimens sintered in the 290-390° range are given in Table 1.

It follows from Table 1 that the sorption capacity of Ftoroplast-4 is halved on increase of the sintering temperature from 290 to 320°, and is decreased at least tenfold at sintering temperatures of 320-370°. At a sintering temperature of 390°, the sorption capacity of Ftoroplast-4 begins to increase again. The coefficient of diffusion increases for specimens sintered above 390° because degradation processes occur at such temperatures (especially in Ftoroplast-4 batches of low thermal stability), and relaxation processes, which also increase the polymer porosity, become more significant. This hypothesis was put forward in our earlier paper [3].

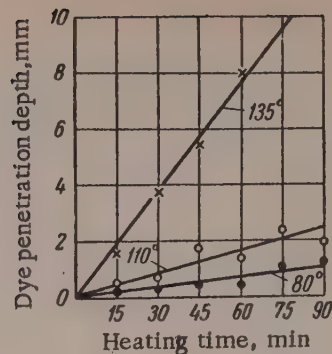


Fig. 4. Effect of the time of heating at different temperatures on penetration of Sudan dye into polyethylene.

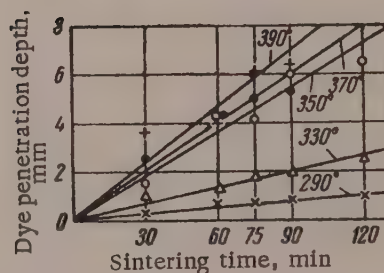


Fig. 5. Effect of the time of heating at different temperatures on penetration of Anthraquinone Acid Green Base into Ftoroplast-4.

The low values of the diffusion coefficient for specimens sintered between the transition point and 340-350° (according to the thermal stability of Ftoroplast-4) indicate that sintering also occurs at these temperatures, but, as already reported [3], the process is extremely slow.

Diffusion in Polyethylene and Ftoroplast-4

Diffusion studies consisted of determinations of the dependence of the depth of penetration of a dye on the temperature and duration of sintering; first with a model polymer (polyethylene) which has a well-defined flow temperature, and then with Ftoroplast-4 specimens. By comparison of the laws governing the diffusion of a dye in polyethylene and Ftoroplast-4 respectively, it was intended to elucidate the sintering mechanism of the latter.

In experiments with polyethylene, Sudan was used as a compatible dye and iron oxides as an incompatible pigment.

The test specimens were molded in the form of cylinders 28 mm in diameter and 25 mm high, with a colored layer in the middle, kept at room temperature for two days, and cut vertically into two equal portions. One half of each specimen was photographed. The diffusion layer was measured at three points in the photograph: at the center and at equal distances to the right and left of the center. This half of the specimen was the initial standard. The other half of the specimen was heated at 80, 110, and 135° for 15, 30, 45, 60, 75 and 90 minutes. After the required time, the specimen was removed from the oven, held for two days at room temperature, and photographed. The diffusion layer in the photograph was measured at the same points as before the heating. The results are given in Table 2.

The control experiments with iron oxides showed that, as was to be expected, there is no diffusion if an insoluble substance with very large particles is used, and therefore, the colored layer does not change in shape or size.

The linear relationship between the depth of penetration of Sudan into polyethylene and the heating time temperature from 80 to 135° (Fig. 4), is represented by the linear equation of the general form:

$$\Delta l = k\tau, \quad (5)$$

where Δl is the depth of penetration of the dye into polyethylene, in mm; k is the tangent of the angle between the line and the τ axis; τ is the time of heating, in minutes.

The power relationship between the depth of penetration of Sudan into polyethylene and the heating temperature is represented by the equation for a parabola, of the general form:

$$y = ax^n. \quad (6)$$

In this instance it is represented by an equation of the form:

$$\Delta l = aT^n, \quad (7)$$

where T is the sintering temperature in °C.

Experimental numerical values of Δl , τ , and T were used to find the particular values of Equations (5) and (7), which are given in Table 3.

Analogous experiments were carried out with Ftoroplast-4; for this, it was necessary to find colorants compatible and incompatible with Ftoroplast-4. The inorganic pigments tested were Menastral and iron oxides; the organics included vat intermediates of the aniline group, the indigo group, the anthraquinone group, etc. Of the dyes tested, only Anthraquinone Acid Green Base and dyes of the indigo group (indigotin and bromoindigo) were found to be compatible with Ftoroplast-4.

The dye used for the investigation was Anthraquinone Acid Green Base, which has the brightest color.

The experiments were performed at sintering temperatures of 290, 330, 350, 370, and 390°, and sintering times of 30, 60, 75, 90, and 120 minutes. At the end of the required sintering time, the specimen was removed from the oven and cooled in air. After two days, the specimen was cut into two equal portions. The depth of

penetration of the dye was measured at three points – in the center of the specimen and at equal distances to the right and left of the center. The results are summarized in Table 4 and Fig. 5.

The linear relationship between the depth of penetration of the dye (Anthraquinone Acid Green Base) into Ftoroplast-4 and the sintering time at temperatures from 290 to 390° is represented by the linear Equation (5). Particular values of Equation (5) are given in Table 5.

The power relationship between the migration rate of the dye boundary in Ftoroplast-4 (numerical values of K , see Table 5) and the sintering temperature is represented by the equation for a parabola, of the form $K = aT^n$. In this instances, it is represented by an equation of the form

$$K = 0,191 \cdot 10^{-20} T^8. \quad (8)$$

The power relationship between the depth of penetration of the dye and the sintering temperature is represented by Equation (7). Particular values of the equations are given in Table 5.

No diffusion was observed in analogous experiments with a pigment (iron oxides) insoluble in Ftoroplast-4.

Thus, investigations of the diffusion of soluble dyes – Sudan in polyethylene and Anthraquinone Acid Green Base in Ftoroplast-4 – showed that the penetration of dyes through these two polymers conforms to the same law. This shows that in both cases the dye diffuses into the polymer mass.

It would not be correct to regard these results as proof that the sintering mechanisms of polyethylene and Ftoroplast-4 are the same; additional investigations are needed for this.

Two processes occur simultaneously in the sintering of Ftoroplast-4 preforms: on the one hand, interdiffusion of the molecular chains or chain segments results in disappearance of interfaces between the particles; on the other hand, coalescence of the macro particles is opposed by relaxation, which tends to restore the particles to their original shapes. The optimum conditions for pressing and sintering of Ftoroplast-4 preforms were determined previously [3]. Experiments showed that specific molding pressures of the order of 500 kg/cm² result in minimum porosity, while at the optimum sintering temperatures of the preforms, 375 ± 15°, the conditions are most favorable for diffusion of the molecular chains, favoring particle coalescence.

SUMMARY

1. Macroporosity is eliminated when Ftoroplast-4 preforms are pressed at specific pressures of the order of 500 kg/cm². This facilitates coalescence of the particles when the preforms are sintered.

2. The sorption capacity of Ftoroplast-4 decreases with increase of sintering temperature, reaching a minimum at sintering temperature between the transition point and 390°. The sorption capacity increases with further increase of the sintering temperature. This shows that polytetrafluoroethylene can be sintered in the 327-390° range, but the process is very slow in the 327-360° range, which is unsuitable in practice.

When Ftoroplast-4 preforms are sintered at temperatures above 390°, degradation processes occur and relaxation effects become more significant; the latter cause increases of porosity and therefore, of the sorption capacity of the material. The optimum sintering range for Ftoroplast-4 preforms is 375±15°.

3. The fact that dye penetration in polyethylene and in Ftoroplast-4 conforms to the same laws indicates that in both cases the dye diffuses through the mass of polymer material and does not penetrate through the pores; the rate of migration is considerably higher in polyethylene than in Ftoroplast-4.

4. When pressed preforms of Ftoroplast-4 are sintered, the polymer macromolecules become more closely packed owing to their higher mobility at high temperatures, which leads to total elimination of interfaces between the particles and to considerable changes in the properties of the material.

LITERATURE CITED

- [1] I. F. Kanavets and L. F. Grigor'eva, *Org. Chem. Ind.*, No. 12, 645 (1940).
- [2] A. A. Tager and V. A. Kargin, *Colloid J.*, 10, 455 (1948).
- [3] A. A. Gorina, V. A. Kargin and P. M. Kozlov, *Chem. Ind.*, No. 2 (1959).

Received May 24, 1958

INFLUENCE OF MOLECULAR INTERACTION ON THE DIELECTRIC STRENGTH OF VULCANIZATES

V. E. Gul' and Yu. G. Lushcheikin

The M. V. Lomonosov Institute of Fine Chemical Technology, Moscow

An important characteristic of rubber as an insulating material is its dielectric strength [1]. The breakdown of a dielectric may be electronic or thermal [2-4].

Electronic breakdown occurs as the result of fusion of the dielectric by an electron avalanche which results from the interaction of an electron stream with the structural elements of the dielectric at high potentials.

In thermal breakdown, fusion of the dielectric in one direction (at a weak point) occurs because of slow removal, at this region, of the heat formed owing to dielectric loss. Thermal breakdown is more likely at high temperatures and under prolonged action of the applied voltage. Electronic breakdown is more likely in brief action of the field and at relatively low temperatures.

In electronic breakdown the material is, roughly speaking, disrupted by electrical forces. The dielectric strength then depends directly on the chemical nature of the material. In thermal breakdown, the dielectric strength depends on the chemical nature of the material only indirectly — through the magnitude of the dielectric loss, electrical conductance, and thermal conductivity.

Oakes [5] carried out a systematic study of the effects of temperature and polymer polarity on the dielectric strength of polyethylene, polyisobutylene, polystyrene, and other high polymers. The polarity of polyethylene was varied by chlorination to different degrees. The dielectric strength of nonpolar polymers (polyethylene, polystyrene, polyisobutylene) at low temperatures remained almost unchanged on heating up to a definite temperature. Subsequent heating was accompanied by a rapid decrease of dielectric strength. Chlorination of polyethylene increased its dielectric strength at low temperatures and increases it at high temperatures.

The results of these investigations are interpreted as confirming the electronic theory of breakdown. Literature data on the dielectric strength of vulcanizates made from different rubbers and of different formulations show [1, 6, 7] that the dielectric strength of rubbers in technical tests depends very little on the type of rubber, and lies mainly in the range of 20-30 kv/mm. The dielectric strength of ebonites reaches 40 and even 80 kv/mm [1, 6, 7]. Fillers, especially polar, lower the dielectric strength of vulcanizates. The dielectric strength of deformed (stretched) vulcanizates in electronic breakdown [1, 4] increases by 40%; this is attributed to orientation of the rubber molecules. The literature does not contain any descriptions of systematic studies of the influence of quantitative characteristics of the molecular structure of polymers on the dielectric strength of vulcanizates.

In an examination of the literature data on the subject we may note attempts to draw an analogy between the statistical aspects of mechanical and dielectric strength [5]. We consider that the analogy between the dielectric and mechanical strength mechanisms is reasonable, as the behavior of polymers in electrical and mechanical force fields is in many respects analogous. Attention must also be drawn to the analogy between the Debye theory relating to the orientation of molecular dipoles in an external electrical field and the theory relating to orientation of the segments of chain molecules by mechanical forces [8].

The purpose of the present investigation was to determine the relationship between the dielectric strength of unfilled vulcanizates and the intensity of intermolecular action (cohesive energy density).

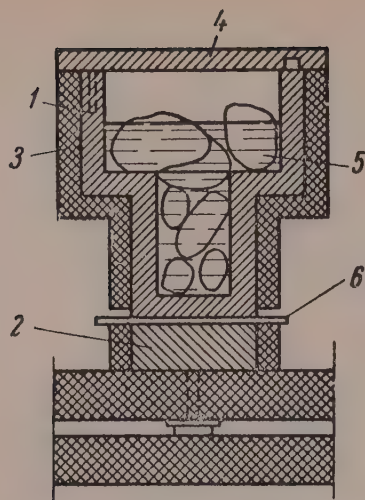


Fig. 1. Electrodes for determination of dielectric strength at low temperatures: 1) upper electrode; 2) lower electrode; 3) asbestos; 4) asbestos board; 5) acetone and solid carbon dioxide; 6) specimen.

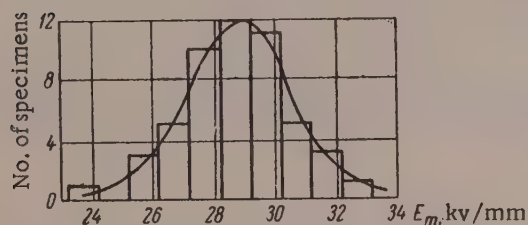


Fig. 3. Histogram representing the results of dielectric strength determinations (E_m) of SKN-18 rubber vulcanizate; interval 1 kv/mm.

reason, thin specimens were used, and the electrodes were made of brass to ensure good heat conduction; the voltage was raised rapidly to the breakdown value, so that liberation of heat in the specimen was at a minimum.

The specimens were tested by means of the apparatus the circuit of which is shown in Fig. 2. Leads from the 220 v supply were taken through a small board with a double-pole knife switch 1 and fuses 2 and 3 to the primary winding of a stepdown transformer 4 (2 kva). The secondary winding of this transformer was connected to the primary winding of the input transformer 5 of an AMI-60 oil breakdown tester (220/60 kv · 3 kva). The input transformer has variable turn ratio. The ends of the secondary winding of the input transformer were connected to the ends of the primary winding of the main step-up transformer 6. The high voltage was fed from the breakdown tester to terminals in the thermostat, and from the terminals directly to the electrodes. The thermostat was contained inside a wooden case fitted with a system of double-pole blocking contacts 7 and 8. In addition, tappings were taken from the input leads of the stepdown transformer primary winding to a neon indicator tube 9, through a 100-ohm resistance 10, which indicated that the whole system was live.

The current strength in the primary winding of the stepdown transformer was measured by the ammeter 11 connected between the panel and the input terminals of this transformer.

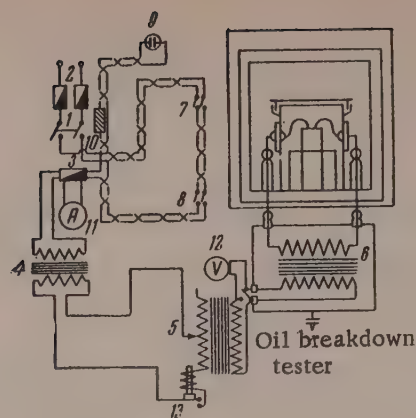


Fig. 2. Circuit of apparatus for determination of dielectric strength at high moisture contents and low temperatures.

In order to diminish nonuniformity of the field in the dielectric strength tests, specimens 0.1-0.4 mm thick were used. Reasonably good contact between the electrodes and the specimens was achieved with the use of brass electrodes. In measurements of dielectric strength at low temperatures special electrodes were used (Fig. 1). The cavity in the upper electrode was filled with a freezing mixture consisting of acetone and solid carbon dioxide. The temperature was measured by means of a thermocouple inserted through an opening in the upper electrode. Temperature equilibrium in the system became established in < 1 minute. The tests were usually performed 2 minutes after the specimen had been put in, with a previously-cooled lower electrode.

The tests were conducted in such a manner as to ensure electronic breakdown, which is influenced more fully by the nature of the polymer. For this

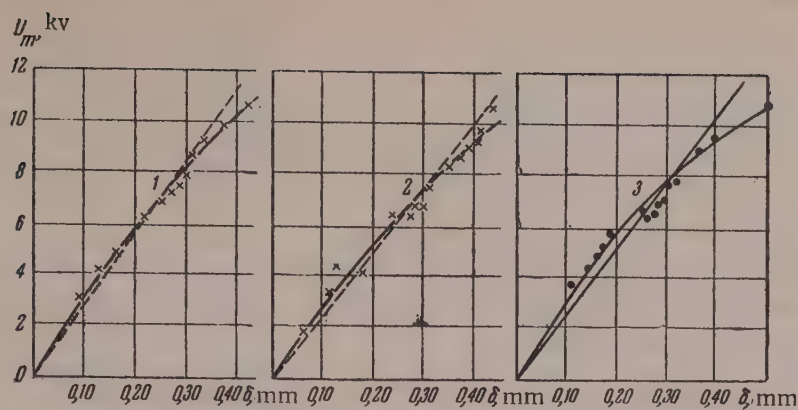


Fig. 4. Variations of breakdown voltage with specimen thickness for different rubber vulcanizates: 1) SKN-18; $E_{m \text{ av}} = 28.6 \text{ kv/mm}$; 2) SKN-26; $E_{m \text{ av}} = 25.6 \text{ kv/mm}$; 3) SKN-40; $E_{m \text{ av}} = 27.2 \text{ kv/mm}$.

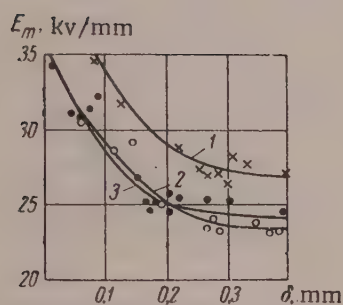


Fig. 5. Variations of dielectric strength with thickness of vulcanized-rubber specimens: 1) SKN-18; 2) SKN-26; 3) SKN-40.

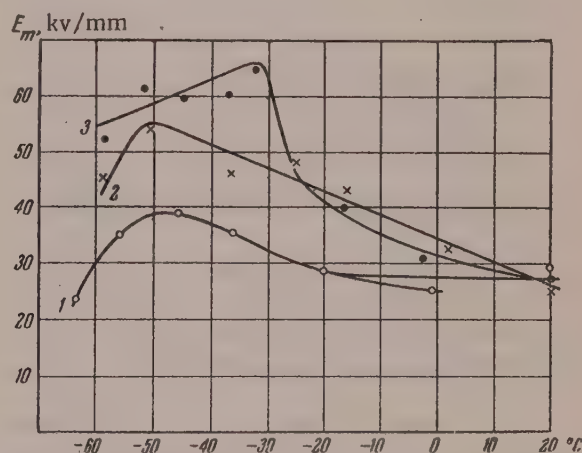


Fig. 6. Variations of dielectric strength with temperature for: 1) SKN-18; 2) SKN-26; 3) SKN-40.

It is known that if the breakdown voltage is a linear function of thickness this means that the electric field is uniform at the instant of breakdown.

A slight decrease of dielectric strength with increase of specimen thickness may be ascribed both to partial nonuniformity of the field and to the statistical character of the breakdown.

By the statistical strength theory [10] the results of mechanical strength tests depend on the probability of "weak spots" occurring in the given specimen. The probability of weak spots occurring in a specimen increases with increase of its dimensions (in particular, thickness), and its strength decreases. It is possible that in view of the statistical nature of dielectric strength these considerations also apply to dielectric breakdown. Weak spots in vulcanizates arise from small cavities, particles of polar substances including the rubber ingredients, accumulations of oxidation products, and various extraneous impurities. The statistical character of dielectric breakdown is illustrated by Fig. 3.

To determine the influence of specimen thickness on dielectric strength, tests were carried out on vulcanized acrylonitrile rubbers SKN-18, SKN-26, and SKN-40. The breakdown voltage (at which the dielectric is punctured) is plotted against specimen thickness in Figs. 4 and 5. The relationship between breakdown voltage and thickness is almost linear, while the dielectric strength decreases slightly with increasing thickness. Analogous results were obtained by Bartenev [11] in a study of the effects of specimen thickness on mechanical strength.

No conclusions concerning the effect of polymer polarity on dielectric strength can be drawn from the above results. It seems that the test temperature was not low enough for any effective manifestation of differences in molecular interaction in the polymers.

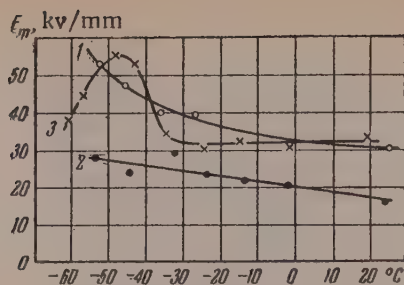


Fig. 7. Variations of dielectric strength with temperature for different rubbers: 1) natural; 2) chloroprene; 3) sodium butadiene.

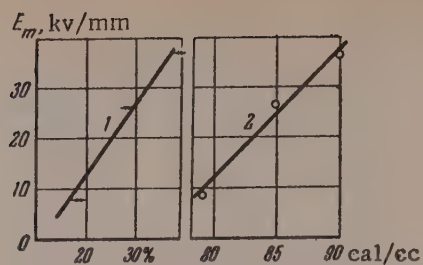


Fig. 8. Variations of maximum dielectric strength of nitrile rubbers: 1) with nitrile group contents in %; 2) with cohesive energy density.

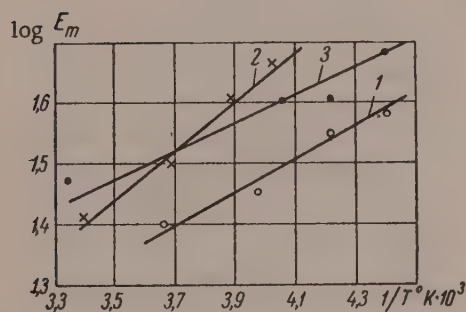


Fig. 9. Variation of the logarithm of dielectric strength with the reciprocal temperature for vulcanizates of: 1) SKN-18; 2) SKN-40; 3) smoked sheet.

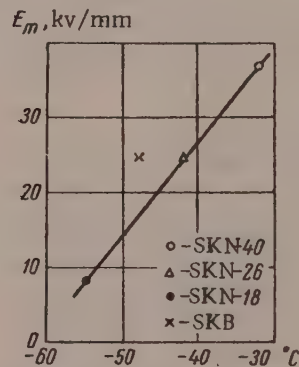


Fig. 10. Correlation between maximum values of E_m and glass-transition temperatures of rubbers.

Low-temperature experimental data for butadiene-nitrile rubbers at low temperatures are presented in

Fig. 6. The glass-transition temperatures of SKN-18, SKN-26, and SKN-40 rubbers are -55° , -42° and -32°

respectively. It was found that the temperatures corresponding to the maxima on the $E_m = f(t^\circ)$ curves and the glass-transition temperatures for these vulcanizates approximately coincide under the test conditions used.

Figure 7 (Curve 1) shows the results obtained in dielectric-strength tests on a natural-rubber vulcanizate. In this case, the glass-transition temperature was not reached and there is no maximum on the $E_m = f(t^\circ)$ curve. Chloroprene-rubber vulcanizates (Fig. 7, Curve 2) have low dielectric strength in comparison with other rubbers; it increases slightly with fall of temperature. The dielectric strength of SKB rubber (Fig. 7, Curve 3) remains almost constant down to -35° , and then increases steeply on further fall of temperature, passing through a maximum at -48° , which coincides with the glass-transition temperature of SKB (-48°). The dielectric strength of SKB falls with further decrease of temperature. It is interesting to note that the dielectric strength of nitrile rubbers at temperatures below 28° differs sharply for vulcanizates with different nitrile group contents.

It follows from Fig. 8, that the maximum values of dielectric strength increase approximately linearly with increase of molecular interaction.

The relationship between dielectric strength and temperature is also analogous to the relationship between mechanical strength and temperature (Fig. 9); both types of strength vary nonmonotonically with decrease of temperature and pass through maxima [11, 12]. The explanation offered for the nonmonotonic variation of dielectric strength at low temperatures is that when the structural elements are fixed (in the glassy state), increase of temperature is accompanied by increased scattering of the electron avalanche and an increase of dielectric strength. In the temperature region characterized by relative mobility of the structural elements, increase of temperature is accompanied by increases in the mobility of the chain segments and orientation polarization, and a decrease of dielectric strength. These views satisfactorily account for the correlation between the maximum

values of E_m (determined from the temperature relationships) and the glass-transition temperatures of the rubbers (Fig. 10).

It was of interest to investigate the effect of the time during which the voltage is applied on dielectric strength. It was found that the dielectric strength first falls sharply with increase of the time of action, and then remains approximately constant; this is probably because the breakdown mechanism changes when the time of action is increased sufficiently. Transition to thermal breakdown is possible.

SUMMARY

1. Dielectric strength is shown to be statistical in character, and to have much in common with mechanical strength, such as the character of the distribution curves and the variations of dielectric and mechanical strength with specimen thickness and temperature.

2. In the region of high elasticity, differences of molecular interaction do not have any significant influence on dielectric strength. In the transition region between the high-elastic and glassy states, the factors which determine the mobility of the molecular-chain segments have a significant influence on dielectric strength.

3. The maximum value of the dielectric strength is directly proportional to the cohesive energy density (if the other characteristics of chemical structure of the polymers are constant).

4. The dielectric strength of vulcanizates increases with fall of temperature, reaching a maximum at the glass-transition point, and decreases with further decrease of temperature.

5. There is a linear relationship between the maximum dielectric strength and the glass-transition temperature for rubbers of similar chemical structure.

6. In the transition region between the high-elastic and glassy states, the dielectric and mechanical strengths depend analogously on various factors (specimen dimensions, temperature, time of action of the mechanical or electrical field, cohesive energy density of the polymers).

LITERATURE CITED

- [1] B. A. Dogadkin, Chemistry and Physics of Rubber [In Russian] (Goskhimizdat, 1947).
- [2] S. M. Bragin, A. Val'ter and N. Semenov, Theory and Practice of Dielectric Breakdown [In Russian] (State Press Printing House, Moscow-Leningrad, 1929).
- [3] E. F. Komarkov, Science of Electrical Materials [In Russian] (ONTI, 1935).
- [4] A. A. Vorob'ev and E. K. Zavadovskaya, Dielectric Strength of Solid Dielectrics [In Russian] (State Tech. Press, Moscow, 1956).
- [5] W. G. Oakes, Proc. I. E. E. 96, 37 (1949).
- [6] S. Whitehead, Dielectric Breakdown of Solids (Gosenergoizdat, Moscow-Leningrad, 1957), [Russian translation].
- [7] I. V. Borodina and A. K. Nikitin, Technical Properties of Soviet Synthetic Rubbers [In Russian] (Goskhimizdat, Leningrad-Moscow, 1952).
- [8] A. P. Aleksandrov and Yu. S. Lazurkin, J. Tech. Phys., 9, 1249 (1939).
- [9] B. Dogadkin, K. Pechkovskaya and L. Chernikina, Colloid J., 8, 31 (1946).
- [10] A. P. Aleksandrov and S. N. Zhurkov, Brittle Fracture [In Russian] (GTTI, 1923).
- [11] G. M. Bartenev, Proc. Acad. Sci. USSR, 82, No. 1, 49 (1952); Progr. Chem., 24, 7, 815 (1955).
- [12] V. E. Gul', in the book: Advances in Polymer Chemistry and Technology [In Russian] (Goskhimizdat, Moscow, 1957) p. 220; V. E. Gul', Proc. Acad. Sci. USSR, 85, 1, 145 (1952); 96, 5, 953 (1954); V. E. Gul' and I. I. Farberova, Colloid J., 13, 6, 660 (1956).*
- [13] V. E. Gul', N. Ya. Sidnova and B. A. Dogadkin, Colloid J., 13, 6, 422 (1951).

Received December 26, 1957

* Original Russian pagination. See C. B. Translation.

PREPARATION OF HIGHLY -CONCENTRATED LITHIUM, POTASSIUM, AND SODIUM SUSPENSIONS IN AN ULTRASONIC FIELD

A. P. Kapustin

Institute of Crystallography, Academy of Sciences, USSR

The production of disperse systems with definite properties is important in various technological processes. Such properties include concentration, precipitability, viscosity, stability, etc. Disperse systems have not yet been studied sufficiently; because of this, and partly because of difficulties in preparation, their significance is not yet fully understood. Development of a method for the production of suspensions with different concentrations of the disperse phase is of interest in this connection.

It is known that one of the peculiar effects of ultrasonic vibrations on solids is to cause dispersion. Utilization of sonic and ultrasonic energy in modern dispersion technology leads to interesting practical results, important for understanding the dispersion process itself.

This paper contains the results of an experimental investigation of the dispersion of certain alkali metals, and a discussion of the conditions for effective results.

In our experiments lithium was dispersed in vacuum oil, and potassium and sodium in kerosene. Special interest attaches to the production of disperse systems of these substances by ultrasonic methods, as the use of other methods is very difficult. Moreover, to the best of our knowledge, there have been no methods proposed for production of highly concentrated suspensions by the action of ultrasonic vibrations.

The dispersion of these substances was effected in a quartz flask about 100 cc in capacity.

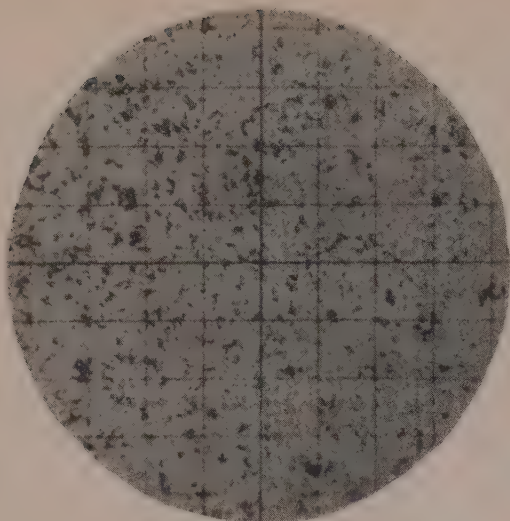
High-frequency mechanical vibrations were produced by means of a continuous-action quartz piezoelectric oscillator with a signal frequency of 700 kilocycles/second, and a magnetostrictive resonator of frequency 25 kilocycles/second. The output power was constant in all cases, the anode current being fixed. The depth of the liquid in the quartz flask was arranged so as to ensure maximum transmission of energy to the material. The energy input in the experiments did not exceed 5 w/cm^2 .

Most of the experiments were performed at an ultrasonic frequency of 700 kilocycles/second. Each exposure lasted 1-2 minutes. It was found by experience that metal present in the dispersed state in kerosene hinders further development of the process, and therefore, repeated exposure in the same liquid produces little change in the concentration of the suspension.

Four factors influencing the dispersion process were studied: time of exposure of the substance to the ultrasonic field, temperature, frequency, and ultrasonic energy.

Before the irradiation the substance to be dispersed was cut into portions of about 1 cc each and put in the flask containing the appropriate liquid.

Preliminary experiments showed that at room temperature dispersion proceeds very slowly under the influence of ultrasonic vibrations. The liquid remains transparent even after prolonged exposure (30-40 minutes). Effective results are obtained only when the substance heated to near its melting point is exposed to ultrasonic vibrations of the maximum energy.



Suspension of potassium in kerosene;
1 square represents 100 μ

melting point, but a suspension with a high sodium concentration (in the form of a mastic) cannot be obtained at once; for this, sedimentation of the disperse system is necessary. The suspension formed after the exposure is poured off into another flask, while the remaining sodium is covered with fresh kerosene and treated again. The required amount of dispersed sodium can be collected by repetition of these operations.

Potassium suspension. Because of the low melting point of potassium (63.5°), preliminary heating is not necessary, and the thermal action of ultrasonics is sufficient. Dispersion of potassium near its melting point proceeds so rapidly that a suspension with a high potassium content is obtained readily in one treatment. After settling a thick mass is formed, containing potassium particles of different sizes (see figure).

The dispersion results were not changed qualitatively by the use of low frequencies.

In all cases the dispersion rate is increased by the use of higher ultrasonic energies.

SUMMARY

1. Methods for the preparation of highly concentrated suspensions of lithium, sodium, and potassium are described.
2. The rate of dispersion of alkali metals depends on the ultrasonic energy and the temperature of the medium.
3. For a given energy, larger amounts of dispersed substance are obtained at lower frequencies.

Lithium suspension. For example, ultrasonic treatment of lithium heated in oil up to 120° has little influence on the rate of the dispersion process. The dispersion rate is increased considerably when lithium is heated to 150° (m.p. of lithium $\sim 179^{\circ}$) and exposed to ultrasonic vibrations at $\sim 5 \text{ w/cm}^2$. Ultrasonic treatment of lithium at a lower frequency (25 kilocycles/second) gives qualitatively the same results, but under comparable experimental conditions more of the substance is dispersed.

Sodium suspension. Sodium is dispersed very slowly in kerosene at 20° . To increase the degree of dispersion, the sample was subjected to repeated irradiation. As a result, the number of particles in the liquid increased, but even after one hour of treatment the concentration of the suspension changed little.

When a fresh liquid is put into the flask the rate of dispersion always increases. The rate of dispersion increases when the substance is heated to a temperature close to its

Received January 28, 1958

ADSORPTION OF ELECTROLYTES BY NICKEL HYDROXIDE

N. G. Klyukina

The N. G. Chernyshevskii State University, Saratov

The active mass of the positive plate in the alkaline cell consists of a mixture of nickel hydroxide and graphite, the latter being a conducting additive. The electrochemical properties of the nickel hydroxide-graphite electrode depend on the presence of very small amounts of impurities in the solution and in the solid phase; these may have either favorable or adverse effects on electrode performance. As the result of numerous experimental research several harmful impurities and activating additives have been discovered, but the mechanism of their action remains obscure in most cases. In the same way, not enough is known about the nature of the ion sorption processes taking place during precipitation of the hydroxide and during operation of the electrode.

Some workers regard the sorption of ions by nickel hydroxide as a chemical reaction [1-3] and others ascribe the main role in the process to adsorption effects [4, 5]. There are even greater discrepancies between the explanations offered for the action of activating additives and poisoning impurities on the nickel hydroxide electrode. An examination of literature data relating to studies of the action mechanism of a number of impurities shows that in the interaction of extraneous ions with nickel oxides, an important part is played by isomorphic substitution of ions in the crystal lattices of nickel oxides [6, 7] and by adsorption effects on the surface of the active mass [8, 9].

The aim of the present investigation was to verify the applicability of general laws determined for other substances to the sorption of ions by nickel hydroxide and to elucidate the character of this sorption, i.e., to determine whether the whole molecule is taken up or whether ion exchange takes place, and whether these processes take place on the surface of the solid phase or within it.

To solve these problems, adsorption of neutral salts of alkali and alkaline-earth metals was measured, adsorption isotherms for individual ions and alkalies were plotted, and values of the zeta potential in various media were determined. The influence of secondary structure was studied by determinations of the adsorption of certain ions of samples of nickel hydroxide differing in porosity and specific surface.

The nickel hydroxide used was prepared by addition of nickel sulfate to caustic soda solution at 40° with continuous stirring. The precipitate was filtered off, pressed, and dried.

For investigation of the influence of dispersity and structure of the powder on electrolyte sorption, additional Samples 1, 4 and 8 were taken (Table 1), which differed from each other in pore distribution, pore radii, and specific surface. The physicochemical characteristics of the samples are given in Table 1.

Before the experiments the samples were washed with distilled water until the conductivity of the wash waters became equal to that of the distilled water. The washed samples were dried at 110° and stored in a desiccator over calcium chloride.

The experimental temperature varied in the 20-25° range. These temperature variations did not have any appreciable influence on the adsorption, as the temperature coefficient in adsorption from solution is small.

In the adsorption experiments a known weight of powder was placed in an ampoule and an electrolyte solution of known concentration was added, in the proportion of 5 ml of electrolyte solution per gram of hydroxide.

TABLE 1

Physicochemical Properties of Different Samples of Nickel Hydroxide

Nickel hydroxide samples	Chemical composition		Dimensions of primary crystals, A	Specific surface, m ² /g	Pore volume, cc/100 g		
	Ni	SO ₄ ²⁻			micropores	intermediate pores	total
1	58.77	0.96	100/50	61	2.03	24.27	26.30
4	59.79	0.19	120/60	81	3.37	9.20	12.57
8	61.52	0.04	170/130	40	1.40	8.80	10.20
11	58.90	0.36	100/50	132	4.80	11.82	16.62

TABLE 2

Adsorption of Electrolytes by Nickel Hydroxide

Electrolyte	Solution concentration, meq/ml				Adsorbed, meq/100 g	
	original		equilibrium			
	cations	anions	cations	anions	cations	anions
K ₂ SO ₄	0.0953	0.0947	0.0903	0.0899	2.5	2.4
MgSO ₄	0.1090	0.1083	0.0895	0.0900	9.75	9.15
MgCl ₂	0.1167	0.1167	0.1070	0.1064	4.85	5.15
CaCl ₂	0.1480	0.1442	0.1320	0.1282	8.0	8.0
BaCl ₂	0.2422	0.2403	0.2202	0.2202	11.0	10.0
KOH	0.0919	0.0913	0.0759	0.0761	8.0	7.6

TABLE 3

Effect of Solution pH on Adsorption of Anions by Nickel Hydroxide

Salt	pH of original solution	Solution concentration, meq/ml				Adsorbed, meq/100 g	
		original		equilibrium			
		cations	anions	cations	anions	cations	anions
K ₂ SO ₄	6.8	0.25	0.206	0.195	0.195	5.0	5.5
K ₂ SO ₄ + KOH	12.6	0.245	0.213	0.230	0.210	7.5	1.5
KH ₂ PO ₄	4.4	0.082	0.241	0.076	0.115	3.0	63.0
KH ₂ PO ₄ + KOH	11.0	0.730	0.449	0.720	0.419	5.0	15.0

The ampoules were shaken in a mechanical shaker, and after a definite time, a sample of the equilibrium solution was taken for analysis.

TABLE 4

Effect of Hydrogen Ion Concentration on the Zeta Potential of Nickel Hydroxide

Electrolyte	pH	Sign and magnitude of zeta potential
0,004 N AgNO ₃	8,36	$1,36 \cdot 10^{-1}$
H ₂ O	7,1	$1,30 \cdot 10^{-2}$
0,1 N NaOH	13,0	$-6,4$

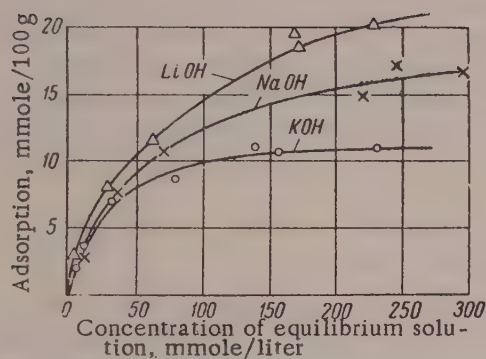


Fig. 2. Isotherms for adsorption of alkali-metal hydroxides on nickel hydroxide.

The results show that in alkaline solutions there is predominant cation adsorption, accompanied by displacement of hydrogen ions and decrease of pH of the medium. This qualitative observation of the ability of nickel hydroxide to change the sign and magnitude of the surface charge in accordance with the reaction of the medium was confirmed by direct determinations of the zeta potential in solutions with different hydrogen ion concentrations. The zeta potentials were determined by the electroosmotic method with the apparatus described by Antipov-Karataev [11]. The results are given in Table 4.

It follows that the hydrogen ion concentration of the electrolyte solution determines the adsorption properties and structure of the electric double layer at the interface between nickel hydroxide and the liquid.

Isotherms for the adsorption of individual ions and alkalies by nickel hydroxide

To determine the influence of the nature of the solute on its adsorption by nickel hydroxide, adsorption isotherms were plotted for the ions: SO_4^{2-} , CO_3^{2-} , AsO_4^{3-} and PO_4^{3-} and LiOH, NaOH, and KOH. The adsorption isotherms were plotted from 5-7 points in the concentration range from 0.005 to 0.9 N at 25°, determined by the method described above. The results of the experiments are presented in Fig. 1 and 2.

The degree of cover of the hydroxide surface by the adsorbed ions was estimated by calculation, from the values of the maximum adsorption, of the fraction of the surface occupied by the ions in the adsorption layer, by means of the Nikol'skii formula [12].

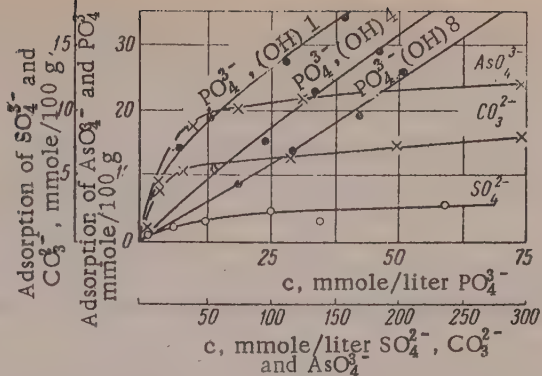


Fig. 1. Isotherms for adsorption of anions on nickel hydroxide.

Adsorption of neutral salts by nickel hydroxide

To determine the manner in which the salt is taken up, i.e., to find whether the whole molecule is taken up or whether one type of ion is adsorbed selectively, the adsorption of cations and anions from a number of alkali and alkaline-earth metal salts was investigated.

The concentrations of individual ions in the original and equilibrium solutions were determined by the usual analytical methods [10].

The results of adsorption determinations for neutral salts are given in Table 2. It is seen that cations and anions are adsorbed from solutions of neutral salts in nearly equivalent amounts. However, this equivalence breaks down with change of hydrogen ion concentration (Table 3).

Diameters of nonhydrated ions were used for the calculations and it was assumed that one end of an adsorbed electrolyte molecule is oriented toward the solid surface and the other is directed toward the diffuse region of the double layer.

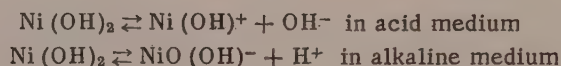
The specific surface occupied by adsorbed ions on nickel hydroxide Sample No. 11 is

$$\begin{aligned} \text{SO}_4^{2-} \dots 4,5 \text{ m}^2/\text{g} \quad \text{AsO}_4^{3-} \dots 43,7 \text{ m}^2/\text{g} \\ \text{CO}_3^{2-} \dots 12,1 \text{ m}^2/\text{g} \quad \text{PO}_4^{3-} \dots 121,0 \text{ m}^2/\text{g} \end{aligned}$$

It follows that ions are adsorbed only on certain active regions of the surface in the form of incomplete layers.

The effect of the dispersity of nickel hydroxide on its adsorption properties is illustrated by data on adsorption of PO_4^{3-} ions on different samples which differed from each other in secondary structure and specific surface (Fig. 1).

Experimental data on the adsorption of electrolytes on nickel hydroxide show that the adsorption depends on the nature of the ions in the molecule, solution concentration, and the magnitude of the surface charge. The latter is proportional to the specific surface of the powder and depends on the pH of the medium. The influence of these factors on the magnitude and mechanism of adsorption of neutral salts and alkalis by nickel hydroxide can be easily explained in the light of the theory of the structure of the electric double layer formed at the interface. Zhukov [13] and Kolthoff [14] showed that the surface charge of metal hydroxides in alkali solutions depends on the ratio of hydroxyl to metal (or hydrogen) ions in solution. In the case of amphoteric compounds, the sign of the surface charge and the nature of the dissociation of the surface molecules depend on the pH of the medium [15, 16]. Table 4 shows that nickel hydroxide can also undergo surface charge reversal in accordance with the reaction of the medium. Therefore, by analogy with iron and aluminum hydroxides, we can write



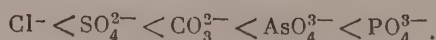
Our experimental data on adsorption of electrolytes on nickel hydroxide are in agreement with these schemes. Thus, from neutral salt solutions, cations and anions are adsorbed in nearly equivalent amounts (Table 2). Adsorption of cations increases with increase of pH of the medium. Bases in the form of whole molecules are predominantly adsorbed from mixtures of neutral salts and alkalis (Table 3).

Molecular adsorption of alkalis is also quite easily explained with the aid of the above schemes for the structure of the electric double layer on the nickel hydroxide particles.

According to the results of our determinations of electrokinetic potential, the hydroxide carries a negative surface charge in alkaline solution. The alkali-metal cations present in solution replace the hydrogen ions in the diffuse layer and displace them into solution where they combine with hydroxyl ions to form water. As the result of such exchange, whole molecules of alkali disappear from solution.

Molecular adsorption of salts can probably be regarded as the result of simultaneous adsorption of cations and anions near the isoelectric point, when the number of positive charges on the particle surface is equal to the number of negative charges.

The degree of adsorption of ions on nickel hydroxide is consistent with the electric double layer theory. Adsorption of anions from neutral salt solutions with a common cation increases with increase of the valence of the anion:



With a given anion, the adsorption of the cation increases with decreasing hydration, in the series $\text{Mg}^{2+} < \text{Ca}^{2+} < \text{Ba}^{2+}$.

An interesting fact is the reversal of the lyotropic series of alkali-metal cations in adsorption on nickel hydroxide from alkaline solutions (Fig. 2). In this case the cations form the following sequence: $\text{Li}^+ > \text{Na}^+ > \text{K}^+$.

Reversal of the lyotropic series of cations was observed by Wiegner [17] in a study of cation adsorption from aqueous alcohol mixtures, and by Mattson [18] in adsorption from concentrated solution; in general, under conditions which lead to dehydration.

Other authors associate the energy of ion adsorption with the nature of the adsorbent, such as its physical structure and swelling. For example, Walton [19] noted that differences between the degrees of adsorption of different cations disappear when strongly swelling adsorbents are used.

Our cation series, $\text{Li}^+ > \text{Na}^+ > \text{K}^+$, can probably be explained by the well-known ability of nickel hydroxide to swell in alkaline solutions, when the adsorbability of cations becomes proportional to their crystallographic radii.

SUMMARY

1. The adsorption of a number of neutral salts and alkalis has been studied on nickel hydroxide used for production of the active paste in positive plates of alkaline storage cells.

2. The proportions of cations and anions adsorbed depend on the pH of the medium and the sign of the surface charge of the hydroxide. At pH values close to the isoelectric point cations and anions are adsorbed in nearly equivalent amounts. Cation adsorption increases with decrease of hydrogen ion concentration owing to increase of the negative surface charge of the nickel hydroxide.

3. With a given anion, the adsorption of neutral salts is determined by the nature of the cation and increases with decreasing radius of the hydrated cation: $\text{Mg}^{2+} < \text{Ca}^{2+} < \text{Ba}^{2+}$. Adsorption of anions from salt solutions with a common cation conforms to the valence rule, and the anions form the following series in order of adsorbability: $\text{SO}_4^{2-} < \text{CO}_3^{2-} < \text{AsO}_4^{3-} < \text{PO}_4^{3-}$.

4. The lyotropic series of univalent alkali-metal cations is reversed in adsorption from alkaline solutions: $\text{Li}^+ > \text{Na}^+ > \text{K}^+$.

It is suggested that this sequence is determined by the structural properties of nickel hydroxide and its tendency to swelling.

5. Ion adsorption occurs only at certain active points of the surface, so that the adsorbed ions form an incomplete monolayer on the hydroxide surface.

6. The adsorption of neutral salts and alkalis on nickel hydroxide is in good agreement with the adsorption mechanism and the theory of the structure of electric double layers at interfaces.

LITERATURE CITED

- [1] A. L. Rotinyan, V. L. Kheifets, E. S. Kozil and E. S. Kolnina, *J. Gen. Chem.*, No. 8, 1294 (1954). *
- [2] A. L. Rotinyan and V. Ya. Zel'des, *J. Appl. Chem.*, 24, 604 (1951). *
- [3] W. Singley and J. T. Carriel, *J. Amer. Chem. Soc.*, 75, 778 (1953).
- [4] G. N. Kalaida and S. A. Rozentsveig, *Collected Scientific Papers on Chemical Sources of Current*, vol. I [In Russian] (1935).
- [5] I. I. Zhukov and Z. D. Pigareva, *Colloid J.*, 6, 491 (1940).
- [6] V. S. Lyzlov, *Trans. Lensoviet Technol. Inst. Leningrad*, No. 10, 71 (1941).
- [7] P. D. Lukovtsev, *Doctorate Dissertation* [In Russian] (Moscow, 1952).
- [8] B. V. Érshler, G. S. Tyurikov and A. O. Smirnova, *J. Phys. Chem.*, 14, 985 (1940).
- [9] N. I. Fedorova, *Inform. Tech. Coll. Min. Electrotech. Ind.* [In Russian] 2, 95, p. 7, (1956).
- [10] I. M. Kolthoff and E. B. Sandell, *Quantitative Analysis* (Goskhimizdat, 1948) [Russian translation].
- [11] I. N. Antipov-Karataev and G. M. Kader, *Colloid J.*, 9, 2 (1947).

* Original Russian pagination. See C. B. Translation.

- [12] B. P. Nikol'skii, J. Phys. Chem., 5, 266 (1934).
- [13] I. I. Zhukov, Selected Works [In Russian] (Izd. AN SSSR, 1955) p. 297.
- [14] I. Kolthoff and B. Moskovitz, J. phys. chem., 41, 629 (1937).
- [15] B. P. Nikol'skii and V. I. Paramonova, J. Phys. Chem., 2, 687 (1931).
- [16] I. N. Antipov-Karataev, A. P. Pryanishnikov and V. G. Sechevanov, Trans. Leningrad Section, All-Union Inst. Fertilizers and Agricultural Pedology, No. 23 (1933).
- [17] G. Wiegner, J. Soc. Chem. Ind., 65, 103, 105 (1931).
- [18] S. Mattson, Kgl. Landbruks-Högskol, Ann, 15, 308 (1942).
- [19] H. Walton, Ion Exchange [Russian translation edited by K. V. Chmutov] (IL, Moscow, 1951) p. 7.

Received March 26, 1957

EFFECT OF PRESSURE ON SWELLING ISOTHERMS AND EQUILIBRIUM CURVES

V. S. Komarov

Institute of Chemistry, Academy of Sciences, Belorussian SSR, Minsk

The purpose of the present investigation was to determine the changes of equilibrium with pressure during swelling of a polymer in mixed media, and to elucidate the affinity of the components of a mixed solution for the polymer and their state in the swollen-polymer phase.

Accordingly, we studied the swelling of vulcanized natural rubber in benzene – alcohol and benzene – chloroform mixtures under atmospheric pressure and under 1 atmosphere excess pressure.

The swelling pressure was studied with the aid of a specially designed apparatus (Fig. 1).

The diffusion partition was a No. 4 glass Schott filter which, together with a round metal plate containing a large number of perforations 1.5 mm in diameter, was inserted in the upper part of the apparatus. To avoid amalgam formation, the lower part of the apparatus was lacquered on the inside.

As shown in Fig. 1, the rubber specimen was placed under the filter and floated on the mercury surface. The solvent was introduced into the upper part of the apparatus through the orifice, A. During the first three days, the specimen was allowed to swell under atmospheric pressure. The mercury level was then raised in tube B to set up the necessary excess pressure, and the experiment was continued for 10 more days. Part of the liquid was pressed out of the swollen polymer by the action of the excess pressure; this was indicated by changes of the mercury level in tube B. When the mercury level in tube B became constant, this showed that thermodynamic equilibrium had been reached. The composition of the solution in the polymer phase was determined interferometrically by a method described earlier [1].

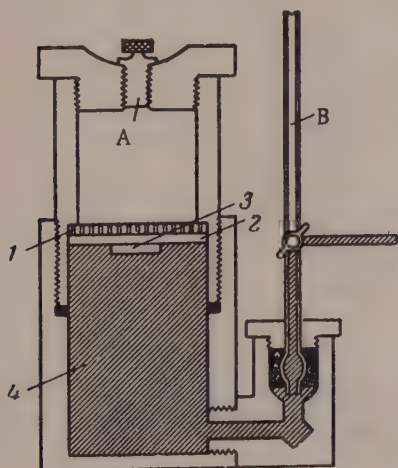


Fig. 1. Apparatus for studying swelling under pressure. 1) Metal plate; 2) Schott filter; 3) polymer; 4) mercury.

The results of the experiments are presented in Fig. 2, where the Isotherms 1, 3, and 5 represent swelling of vulcanized natural rubber under atmospheric pressure, and Isotherms 2, 4, and 6 correspond to swelling under 1 atmosphere excess pressure.

It is clear from Fig. 2 that in the region of maximum swelling the position of the isotherms depends sharply on the external pressure; this, in accordance with the Le Chatelier principle, is due to the decrease of the surface of the swollen polymer by an amount corresponding to the change of free energy.

The shift of equilibrium under the action of an external force is not only associated with a decrease of the amount of liquid absorbed per gram of polymer, but is also accompanied by changes in its composition in the polymer phase. Examination of the data in the table

Mole Fractions of Component 2 in the Polymer Phase at Atmospheric Pressure and 1 Atmos Excess Pressure

N_2^* of solution	Mole fraction of component in polymer phase (N_2^P)* *					
	Vulcanized rubber—benzene (1) — ethyl alcohol (2)		Vulcanized rubber—benzene (2) — n-butyl alcohol (2)		Vulcanized rubber—benzene (1) — chloroform (2)	
	atmospheric P	1 excess atmos	atmospheric P	1 excess atmos	atmospheric P	1 excess atmos
0,050	0,051	0,044	0,040	0,038	0,041	—
0,116	0,089	0,078	0,091	0,086	0,102	0,111
0,200	0,145	—	0,145	0,138	0,193	0,190
0,300	0,185	0,139	0,201	—	0,279	—
0,400	0,204	—	0,263	0,234	0,381	0,389
0,500	0,240	0,173	0,308	—	0,475	—
0,600	0,222	—	0,347	0,328	0,585	0,583
0,700	0,238	0,204	0,391	—	0,681	—
0,800	0,272	—	0,466	0,450	0,782	0,780
0,900	0,360	0,331	0,573	—	0,887	—

* N_2 is the mole fraction of component 2 in the solution phase.

** N_2^P is the mole fraction of component 2 in the polymer phase.

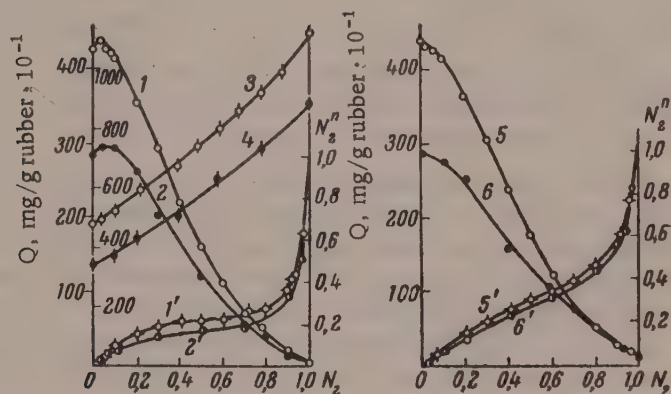


Fig. 2. Swelling isotherms and equilibrium curves: 1 and 2) swelling isotherms at atmospheric pressure and 1 atmos excess pressure; 1' and 2') equilibrium curves at atmospheric pressure and 1 atmos excess pressure for the system: vulcanized rubber — benzene— ethyl alcohol; 3 and 4) swelling isotherms at atmospheric pressure and 1 atmos excess pressure for the system: vulcanized rubber — benzene — chloroform; 5 and 6) swelling isotherms at atmospheric pressure and 1 atmos excess pressure; 5' and 6') equilibrium curves at atmospheric pressure and 1 atmos excess pressure for the system: vulcanized rubber — benzene — n-butyl alcohol.

shows that the change in the mole fraction of one component present in the polymer phase (N_2^P) under 1 atmos excess pressure is greater in the system vulcanized rubber — benzene (1) — ethyl alcohol (2) than in the system vulcanized rubber — benzene (1) — n-butyl alcohol (2).

Consideration of these results leads to the conclusion that the nature of the distribution curves depends to a considerable extent on the affinity of the components of the binary solution for the polymer. The component whose cohesive energy density is closer to the cohesive energy density of the polymer is absorbed better.

From the thermodynamic standpoint, the change of solution composition in the polymer phase under the action of external pressure will be greater, the greater the difference between the free energies of formation of a mole of the real solution and a mole of an ideal solution. As this difference decreases, the selective nature of absorption and changes in the solution composition in the polymer phase with increase of pressure tend to zero.

The decrease of the mole fraction of alcohol in the polymer phase with increase of pressure indicates that not all the alcohol molecules in the polymer phase solvate polar groups of the polymer.

SUMMARY

1. The shift of equilibrium under external pressure in vulcanized rubber – benzene – alcohol systems increases with increasing deviation of the properties of the binary solution of the low-molecular components from ideal behavior.

2. The component of the binary mixture which has the lower affinity for the polymer is pressed out preferentially from the swollen polymer.

LITERATURE CITED

- [1] G. L. Starobinets and V. S. Komarov, *Colloid J.* 15, 60 (1953).*

Received January 18, 1958

* Original Russian pagination. See C. B. Translation.

ELECTRON MICROSCOPE STUDIES OF COLLOIDS

2. MINERALS OF THE MONTMORILLONITE GROUP

M. I. Kuadzhe

Institute of Petroleum, Academy of Sciences USSR, Moscow

Many investigations, including [1-7], have been devoted to the application of electron microscopy to studies of natural formations and synthetic substances. This instrument was used by von Ardenne, Endell, and Hoffman [8] for studying fine bentonite and cement fractions, by Vikulova [5] for studying the mineral composition of clays, by Bykov and Kuadzhe [7] for investigations of bleaching earths, and by Bykov, Luk'yanovich, and Radushkevich [9] for studying natural adsorbents from the Far East. Kuadzhe [10] used the electron microscope for systematic investigations of a number of natural formations (minerals, rocks, adsorbents, and catalysts).

This paper contains certain electron micrographs* of fine fractions ($< 1 \mu$) of various natural formations, mainly of the montmorillonite group, which have been assembled in order to elucidate the composition, structure, and sorptional and catalytic properties of these formations. Fig. 1-18, 23, and 24 represent colloidal minerals of the montmorillonite group, and Fig. 19-22 represent opal, quartz, opoka, and diatomite.

Electron micrographs (Fig. 1-3) show that askangel, Askan clay, and gumbrin have close similarities both in composition and structure, and in properties. These substances consist of continuous masses of strongly swelling, extremely small and thin scales of montmorillonite with dark spots representing denser accumulations. In thinner specimens, a spongy mass can be detected, probably extended as the result of intramolecular swelling. Electron micrographs of samples of the same origin (Fig. 1 and 2) and of a sample of a different origin (Fig. 3) are very similar in appearance. However, it is found in practice that the swelling of askangel in water is several times as great as that of Askan clay or pink gumbrin. This has an appreciable influence both on the electron micrographs and on the adsorptional and catalytic properties of these clays when used in their natural state. After preliminary activation, their adsorption and catalytic properties are greatly improved owing to the removal of certain components (K, Na, Ca, Mg, and others).

Electron micrographs of light gray gumbrin, acid-activated gumbrin, and Gumbri bentonite clay (Fig. 4-6) show that these substances are very similar. It may be noticed, however, that activated gumbrin (Fig. 5) differs somewhat in structure from the native substance (Fig. 4). Similar structures were found in montmorillonite clay, Sample No. 42, from Tiofonai Kito-Kosikho in Southern Sakhalin (Fig. 7), ash tuff, Sample V (suifunite) from Terekhov in the Primor'e region (Fig. 8), and montmorillonite clay from Listvenitsa in the Transcarpathian Ukrainian SSR (Fig. 9).

Gilyabi montmorillonite clay from Khanlar in the Azerbaidzhan SSR (Fig. 10) differs hardly at all in composition, structure, and properties from Gumbri bentonite clay (Fig. 6).

Fig. 11 and 12 show montmorillonite clays from Nal'chik in the Kabardino-Balkar Autonomous SSR. Despite the fact that these clays were taken from the same source, they differ somewhat from each other in composition, structure, and properties; this is associated with their genetic origins. Two types of Nal'chik clays, B

* The author thanks V. M. Luk'yanovich, who took the electron micrographs (Fig. 1-13 and 17-22) in 1948.

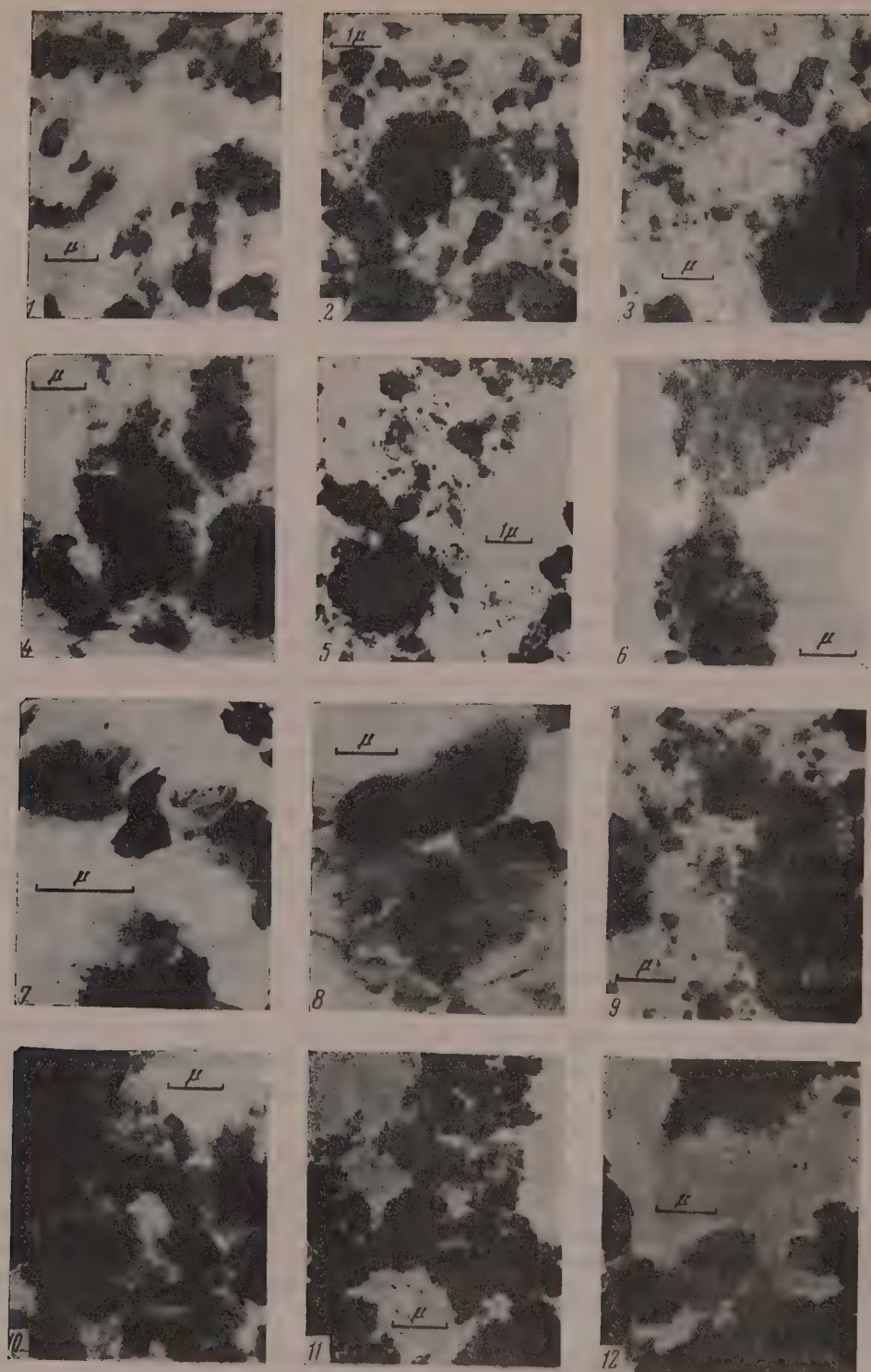


Fig. 1-12. Electron micrographs: 1) askangel, $\times 8000$; 2) Askani clay, $\times 8000$; 3) pink gumbrin, $\times 8000$; 4) light gray gumbrin, $\times 8000$; 5) activated gumbrin, $\times 8000$; 6) bentonite clay, $\times 8000$; 7) Tiofonai clay, $\times 17100$; 8) suifunite, $\times 10000$; 9) Listvennitsa clay, $\times 8000$; 10) Gilyabi clay, $\times 8000$; 11) nal'chikin B, $\times 8000$; 12) nal'chikin C, $\times 8000$.

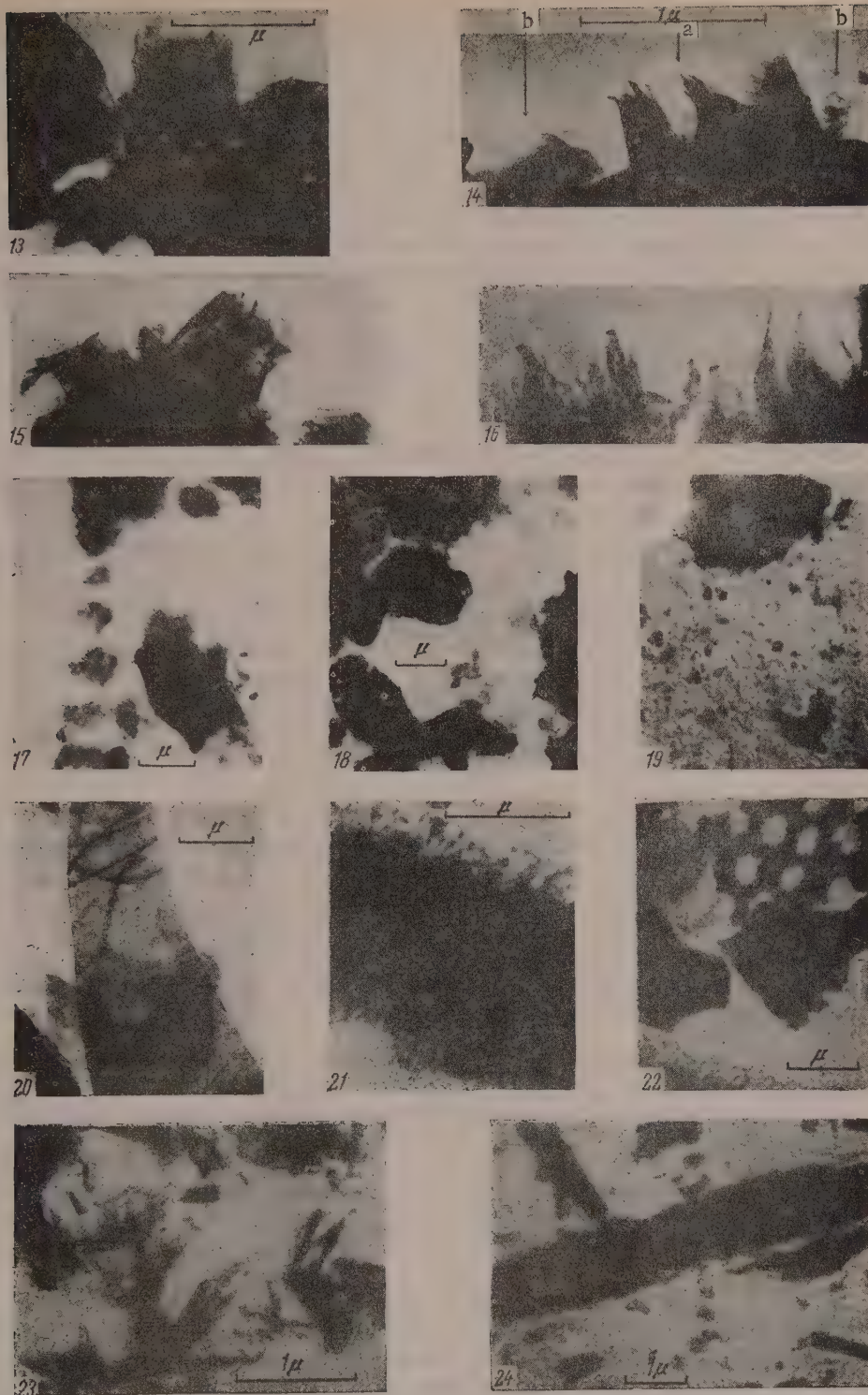


Fig. 13-24. Electron micrographs: 13) decomposed tuff No. 55, $\times 23200$; 14) German bentonite from Geisenheim, $\times 75000$; 15) American bentonite from Wyoming, $\times 75000$; 16) Californian bentonite, $\times 75000$; 17) Gorbiskii beidellite, $\times 8000$; 18) beidellite No. 37082, $\times 8000$; 19) opal from Kos-Cheku, $\times 8000$; 20) marshalite, $\times 12000$; 21) dark gray opoka, $\times 20400$; 22) diatomite with opoka, $\times 12100$; 23) nontronite, $\times 22000$; 24) nontronite, $\times 16000$.

and C*, stand out sharply by their microfauna. Nal'chikin samples type B, almost without exception, contain siliceous skeletons and shells, or skeletons and shells agglutinated from siliceous particles. This is also a feature of nal'chikin D, except that in this case foraminifera predominate, whereas radiolaria are predominant in nal'chikin type B. Nal'chikin type C, is characterized by the presence of both agglutinated and calcareous foraminifera shells. The latter represent a considerable number of different species, but the former predominate in numbers of individuals. Nal'chikin type A has the same composition.

In accordance with the alternation of these nal'chikin types B and C, variations of the microfauna fluctuate between these two types. This alternation of B and C layers, more dense and less dense, is repeated 12 times. This is due to variations in the depth of the sea and periodic unfavorable living conditions (poisoning of the seabed with H_2S) in the deeper layers, and rich development of plankton forms in upper layers [10].

Electron micrographs of nal'chikins B and C shown in Fig. 11 and 12, are very similar in appearance and differ only in detail. Whereas in the coarser fractions of nal'chikin types A, C, B, and D, there is a multitude of microfauna, this is not found in fine fractions $< 1\mu$.

Fig. 13 is an electron micrograph of tuff (decomposed) No. 55 from Kiparisov, Primor'e region, which contains rounded and angular formations in the form of large scales, partly opaque and partly semitransparent, with sharp spiny projections at the edges.

The electron micrographs of German bentonite from Geisenheim and American bentonite from Wyoming (Fig. 14 and 15) clearly show individual scales which stand out at the boundary with the medium. One part of such a scale lies in a horizontal plane, such as the part in regions indicated by the arrow at b. At these points, the thickness of the scale can be determined by comparison with the known thickness of the collodion film, in the left-hand side of the photograph (Fig. 14). Since the optical conditions are the same, this thickness is of the order of 1μ . At the point denoted by the letter a, where the plates are accidentally situated at right angles to the plane of the photograph and therefore appear as peaks, the thickness of the vertices is of the order of 3μ .

The electron micrographs show that despite the fact that the scales consist of montmorillonite crystals they have a maximum diameter of 100-300 μ . The ratio of plate diameter to thickness may reach values of about 100-300:1 for montmorillonite, and 5-25:1 for kaolinite crystals (the latter according to [1])**.

The points denoted in Fig. 14 by the letter a indicate that the distance between the scales is 15 μ . The visible accumulation of scales in this case resembles a macroscopic photograph of mica scales. The electron micrograph in Fig. 14 has much resemblance to crystals of polyoxymethylene and molecular accumulations of cellulose photographed by Von Ardenne and Boiter [12].

Such thin mineral plates as those shown in Fig. 14 at the points b cannot be photographed on a collodion film, as they are thinner than the smallest particles of the supporting film. Such plates can be photographed only by the use of the preparation method described by Von Ardenne, in which films are not used.

The scales of colloidal montmorillonite minerals are of the order of 1μ , thick. At the same time, according to the observations of Hoffmann, Endell and Wilm [13] a monatomic montmorillonite layer, which represents an aluminum silicate plane, also has a thickness of 1μ . Thus, a monomolecular crystal layer is shown for the first time in Fig. 14.

The x-ray pattern of dried montmorillonite gel clearly shows (001) interference. Consequently, within the gel there must be a large number of monomolecular parallel layers which form crystal-like scales. An accumulation of not less than 20 monomolecular layers is required in order that (001) interference may be observed. The fact that the electron microscope reveals the positions of the monomolecular layers at the edges is quite consistent with the views of Maegdefrau and Hoffmann [14], according to whom the monomolecular layers in all montmorillonite crystals, i.e., in the thicker colloid layers, cannot join and lie parallel with intervals between

* The nal'chikin samples show minor lithologic distinctions, corresponding to different varieties: A, B, C and D.

** In addition, see Fig. 11. Despite the fact that greater thicknesses are given there, a thickness of 1μ is highly probable, as the plates consist of the minimum number of layers.

them. As the result of swelling in water the distance between the monomolecular layers reaches $2\text{ m}\mu$. Thus, the crystal scales are held together by only very weak forces and it is therefore not surprising that separate layers consisting of monomolecular crystals are found at the edges.

Californian bentonite (Fig. 16)* occupies an intermediate position between Geisenheim and Wyoming bentonites.

Fig. 17 is an electron micrograph of beidellite from Gorbskii in the Transcarpathian Ukrainian SSR, and Fig. 18, represents beidellite clay No. 37082 from the Khalilova region of the Southern Urals. These clays have many features in common with minerals of the montmorillonite group. We classify them as beidellite on the basis of electron micrographs of fine fractions (diffuse particle outlines are characteristic of minerals of the montmorillonite group) and also because of the similarity of the heating curves and a number of characteristic lines in the x-ray diffraction patterns. Thus, these colloidal clay minerals from Gorbskii and the Khalilova region are intermediate between montmorillonite and hydromicas, and consists of the mineral beidellite. Some deviations from the beidellite formula $\text{RO}_2 : \text{R}_2\text{O}_3 = 3 : 1$, fluctuations of water content, variations of the endothermic and exothermic effects on thermograms, etc., are caused by the presence of iron, magnesium oxide, and other impurities in the samples. We consider beidellite in these clay samples to be a product of gradual modification of hydromicas, in accordance with the formation conditions, as the electron micrographs clearly show. Beidellite, associated with deposits at greater depths, is more diffuse. In coastal deposits, hydromicas and low-swelling beidellite usually predominate [5]. In the sample investigated by us, this mineral consists mainly of fine particles analogous in structure to fine particles of swelling beidellite, but thicker. In addition, it contains particles of irregular shape, in some instances with sharp outlines and sometimes with diffuse edges.

Examination under the electron microscope of substances often found with montmorillonite clays, such as opal from Kos-Cheku of the Aktyubinsk province, clearly shows that the main mass of the opal is diffuse, gray in color, and strongly resembles montmorillonite. Opal is similar to quartz in color but differs sharply from it in form; it consists of isometric or angular opaque grains at regions of considerable accumulation of particles or of fine aggregates with tortuous and fairly sharp outlines (Fig. 19).

Crystalline quartz sand is often met as an admixture in clays of the montmorillonite group. Fig. 20 shows quartz dust from Takubai in the Chelyabinsk province; it consists of transparent, translucent (thin), and totally opaque (thick) grains with sharp outlines of rounded isometric or irregular shape. The figure shows an extremely thin and relatively large particle with surface cracks; under it, in the lower part of the photograph, other particles smaller in size, rounded and angular in shape, may be seen. If a clay contains quartz in the form of angular grains, its particles are difficult to distinguish from particles of kaolinite, hydromica, and certain other minerals.

Fig. 21 is an electron micrograph of a fine opoka fraction with particles $1\text{ }\mu$ in size; it consists of an extremely fine fibrous material strongly resembling cotton wool, especially at the particle edges. These fibers intertwine and form a patterned fringe. The sorptional and catalytic properties of opoka are mainly due to these structural characteristics. The heating curves of fine opoka fractions are very similar to those of montmorillonite. The x-ray patterns of fine opoka fractions also contain a number of characteristic montmorillonite lines. Moreover, the chemical composition and physical properties of these opoka fractions indicate that they consist mainly of montmorillonite mineral. Opoka can be easily identified in presence of diatomites and other mineral substances by means of the electron microscope.

Fig. 22 shows a natural adsorbent, diatomite with opoka, from the Inza region in Kuibyshev province. The outlines of fossilized remains of organic formations are retained here. The diatomite can be seen at the thin regions and edges to be penetrated by fine pores. The inner surface of these pores comprises $200\text{--}300\text{ m}^3/\text{g}$. In the lower part of Fig. 22, one can see opoka of fibrous structure, especially at the grain edges. It is very similar in structure to the opoka specimen above (Fig. 21). It should be noted that heating curves of diatomites differ appreciably from those of opokas, and constitute a special type of thermogram. It should also be pointed out that opokas, tripoli earths, and diatomites quite often occur together in nature, and are apparently interrelated paragenetically. However, detailed studies of these formations show that they differ appreciably from each other in composition, structure, genesis, and properties.

* Photograph after Von Ardenne, Endell, and Hoffmann [8].

Nontronite aggregates usually consist of elongated leaflike particles (Fig. 23)*, or include elongated fibrous crystals with parallel long faces in larger specimens (Fig. 24)** . Both sharp and diffuse outlines are met in nontronite platelets.

SUMMARY

1. The genetic types of montmorillonite clays differ in particle size and shape within the limits of the same mineral group; this is associated with the conditions of their formation. In particular, in minerals of the kaolinite-halloysite and montmorillonite groups, formed as the result of crystallization of alumina and silica gels in lakes, particles larger than 0.5μ predominate, while redeposited minerals of this group are more finely dispersed.

2. Of the natural formations studied, the highest dispersity is found in strongly swelling minerals of the montmorillonite group formed by modification of volcanic ash, pumice, volcanic tuff, etc., in sea water, in an alkaline medium at a great depth.

3. Kaolinite, halloysite, montmorillonite, beidellite, nontronite, attapulgite, sepiolite, palygorskite, psilomelane, chrysotile asbestos, pyrite, goethite, boehmite, diaspore, hydrargillite, illite, sericite, glauconite, opoka, tripoli, diatomites, etc., can be identified relatively easily in the electron microscope. The electron microscope can be used for observing changes in many of these substances, in particular, increases of the sorptional capacity by the action of acids and alkalies.

LITERATURE CITED

- [1] M. von Ardenne, *Electronen Ubermikroskopie*, (Berlin, 1940).
- [2] F. Burton and W. H. Kohl, *The Electron Microscope*, (New York, 1942).
- [3] V. N. Vertsner, *Bull. Acad. Sci. USSR, Phys. Ser.*, 8, 132 (1944); *Industrial Laboratory No. 6*, 543 (1945); *No. 11*, 1364 (1947).
- [4] A. A. Lebedev, *The Soviet Model of the Electron Microscope* [In Russian] (Izd. AN SSSR, 1946) p. 31.
- [5] M. F. Vikulova, *Soviet Geology No. 39*, 79 (1949); *Trans. All-Union Geological Institute No. 2*, 3 (1950); *Electron Microscope Investigation of Clays* [In Russian] (Geology Press, 1952) p. 20.
- [6] Yu. M. Kushnir, *Electricity No. 5*, 3 and *No. 7*, 17 (1947).
- [7] V. T. Bykov and M. I. Kuadzhe, *Bull. Acad. Sci. USSR, Div. Chem. Sci. No. 5*, 487 (1951).
- [8] M. von Ardenne, K. Endell, and E. Hoffman, *Ber. Deut. Keram. Ges.* 21, 209 (1940).
- [9] V. T. Bykov, V. M. Lukyanovich and L. V. Radushkevich, *Bull. Acad. Sci. USSR, Div. Chem. Sci. No. 3*, 406 (1952).***
- [10] M. I. Kuadzhe, *Bleaching Clays from Nal'chik* [In Russian] (Peoples' Commissariat of the Local Fuel Industry RSFSR, 1938) p. 1; *Proc. Acad. Sci. USSR, new series* 74, 995 (1950); *Problems of Petrography and Mineralogy*, vol. 2 [In Russian] (Izd. AN SSSR, 1953) p. 450; *Colloid J.*, 19, 219 (1957).***
- [11] M. von Ardenne, *Naturwissenschaft* 28, 366 (1940)
- [12] M. von Ardenne and D. Boiter, *Z. Phys. Chem.*, 45, 465 (1940).
- [13] U. Hoffmann, L. Endell, and K. Wilm, *Z. Krist. (A)* 86, 340 (1933).
- [14] E. Maegdefrau and U. Hoffmann, *Z. Krist. (A)* 98, 299 (1937).
- [15] I. I. Ginzburg and I. A. Rukavishnikova, *Minerals of the Ancient Weathered Crust of the Urals* (Izd. AN SSSR, 1951).
- [16] D. W. Davies, T. G. Rochow, et al., *Electron Micrographs of Reference Clay Minerals*, American Petroleum Institute Project 49, *Clay Mineral Standards*, Preliminary Report No. 6 (1950).

Received February 4, 1958

* After Ginzburg and Rukavishnikova [15].

** After Davies, Rochow, et al. [16].

*** Original Russian pagination. See C. B. Translation.

LIGNIN AS A REINFORCING AGENT FOR SKS-30 RUBBER

Yu. F. Kurdubov, A. P. Pisarenko, S. I. Rubina and B. V. Shtarkh

Scientific Research Institute of Film Materials and Artificial Leather, Moscow

Lignin is a substance of high molecular weight, present in various amounts in all plant materials, which constitutes the major part of the incrustations in plant tissues. Lignin can be isolated from wood by a method based on hydrolysis of cellulose, when the lignin remains in undissolved form. Technical hydrolytic lignin, which is an industrial by-product in the production of ethyl alcohol from wood, is usually obtained by hydrolysis of wood by dilute acid solutions.

Rational utilization of hydrolytic lignin is hindered to a considerable extent because the structure of native lignin and of the product obtained in wood hydrolysis is not clearly understood. Hydrolytic lignin is a typical high polymer, and probably has a three-dimensional structure characteristic of highly condensed systems.

Lignin has been shown in a number of investigations [1-5] to have a reinforcing effect when used as a constituent of rubber stocks. It has been found in practice, however, that technical hydrolytic lignin is not an active filler for rubber, as it is almost devoid of active functional groups. Various activation methods are available for conversion of hydrolytic lignin into an active form.

Mechanical degradation and treatment of lignin by surface-active agents caused small increase in its reinforcing properties. A considerable reinforcement effect is obtained in rubber if lignin is used in solution form.

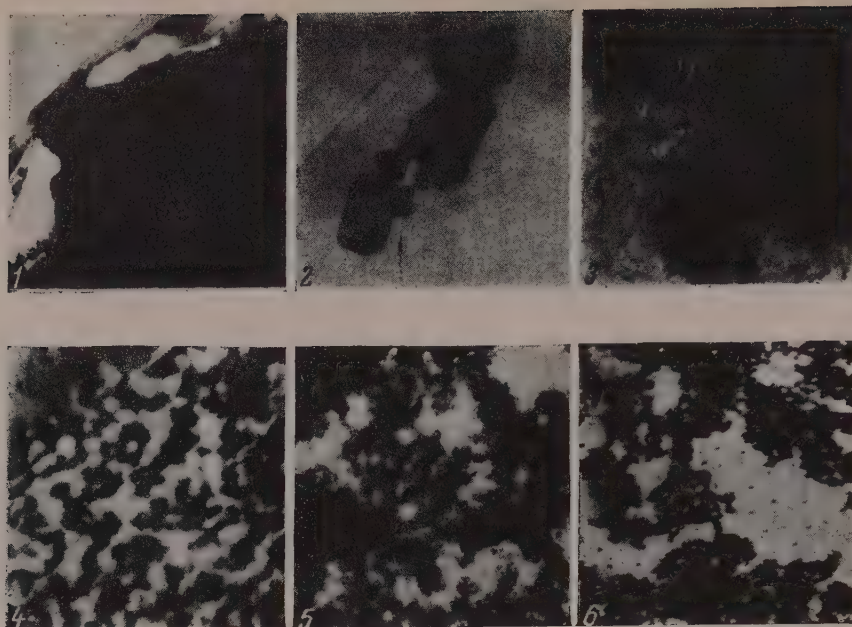
Among the available methods for conversion of hydrolytic lignin, insoluble under normal conditions, into a soluble form, mention should be made of the chlorination method developed by N. N. Shorygina, and the alkaline method, also devised under the guidance of N. N. Shorygina and developed further by Sukhanovskii and Chudakov [6].

To activate lignin by chlorination, chlorine is passed into an aqueous suspension of lignin with vigorous stirring. The process may be effected either with or without catalysts. The solubility of chlorinated lignin increases with its chlorine content. Lignin either partially or completely soluble in alkalis may be obtained by variations of the conditions used for chlorination of hydrolytic lignin. The dissolution of technical hydrolytic lignin in alkalis is accelerated considerably if the hydrolytic lignin is previously ground. In view of this, we used equipment involving vibratory treatment for grinding of materials [7] in the present investigation.

Investigations carried out by Morgulis [7] on the effectiveness of the dispersing action of mechanical forces on materials treated in vibratory mills have shown that impact, compressive, and shearing forces of various magnitudes act in different directions on all the particles of the material in all parts of the mill. The impact impulses are relatively small. However, the large number of grinding media per unit volume and the high vibration frequency (1500-3000 vibrations per minute) ensure rapid comminution of the material. Mechanical breakdown in alkaline activation of hydrolytic lignin considerably accelerates the solution process, and less caustic soda is required in such cases to dissolve the lignin.

Different samples of technical and activated hydrolytic lignins were tested as filler for rubber mixes. Chlorine- or alkali-activated lignin solutions were added in the requisite amounts to butadiene - styrene rubber latex, with subsequent coprecipitation of the mixture and isolation of the rubber in the loaded state.

Nonactivated powdered lignin was introduced directly into the rubber in a roller mill by the usual procedure of rubber production. The rubber mixes were compounded in accordance with the standard formulation, with 60 weight parts of filler to 100 of rubber.



Electron micrographs: Technical hydrolytic lignin: 1) not ground; 2) ground in a vibratory mill; 3) chlorine-activated; 4 and 5) alkali-activated; 6) channel gas black.

Physicomechanical Characteristics of Vulcanizates Made with Different Lignins

Hydrolytic lignin	Tensile strength, kg/cm ²	Relative elongation, %	Residual elongation, %
Powdered, technical, not ground	12	340	41
Powdered, technical, ground in vibratory mill	41	500	35
Chlorine-activated	124	420	57
Alkali-activated	166	684	14
The same*	200	760	20

*Lignin solution added to low-temperature polymerization latex (SKS-30A) in the proportion of 20 parts by weight to 100 parts of rubber.

The results of physicomechanical tests on vulcanizates of SKS-30 rubber loaded with different lignins are given in the table.

It is clear from the table that the strength characteristics of vulcanizates containing hydrolytic lignin, activated either by chlorine or by alkali, are considerably better than those of vulcanizates containing powdered technical lignin, either ground in the vibratory mill or not ground. Especially high strength is found for vulcanizates made by addition of alkali-activated lignin to SKS-30A latex.

It was of interest to examine the fine structure of different types of lignin and to attempt to correlate their reinforcing effect with their submicroscopic structure. This was done with the aid of the EM-3 electron microscope under magnification of $\times 7500$.

Unground hydrolytic technical lignin is a coarsely disperse system with particles 1-3 μ and larger (Photograph 1); i.e., it is a macro- and not a microscopic system, since particles of this size can be easily seen with the aid of an ordinary optical microscope.

Grinding of hydrolytic technical lignin in a vibratory mill results in an appreciable decrease of particle size (Photograph 2).

Electron micrographs of hydrolytic lignin treated with chlorine (Photograph 3) reveal diffuse edges, indicating the start of dissolution or dispersion of the particles, and very fine particles can also be seen.

Lignin of the highest degree of dispersion is obtained when technical hydrolytic lignin is activated by alkaline treatment. Micrographs of such lignin samples (4 and 5) show only network structures formed by coagulation from lignin in alkali solution. These structures resemble the fine structure found with the use of the most active carbon blacks (Photograph 6).

This fully explains the reinforcement effect observed in vulcanizates containing alkali-activated lignin.

SUMMARY

1. The properties of vulcanizates containing different types of lignin were studied.
2. The greatest reinforcement effect was found in vulcanizates containing alkali-activated hydrolytic lignin.
3. Electron microscope investigations of different lignin samples showed that alkali-activated lignin forms a network structure on coagulation; this structure resembles that of gas black, and is probably the cause of its reinforcing action.

LITERATURE CITED

- [1] A. P. Pisarenko and I. U. Mishustin, *J. Artificial Leather* No. 8-9, 10 (1955).
- [2] I. U. Mishustin, *Caoutchouc and Rubber* No. 9, 39 (1940).
- [3] A. P. Pisarenko, *J. Leather and Footwear Ind.* No. 4, 48 (1937).
- [4] I. U. Mishustin and A. P. Pisarenko. *Soviet Patent* No. 64297 (1945).
- [5] J. J. Keilen and A. Pollak, *Ind. Eng. Chem.*, 39, 4, 480 (1947).
- [6] S. I. Sukhanovskii and M. I. Chudakov, *J. Appl. Chem.*, No. 3, 410 (1956).*
- [7] M. L. Morgulis, *Vibratory Grinding of Materials* [In Russian] (Industrial Construction Press, 1957).

Received December 30, 1957

* Original Russian pagination. See C. B. Translation.

CERTAIN EMULSIFIERS AS KINETIC FACTORS IN THE OXIDATION OF CUMENE IN EMULSIONS

R. V. Kucher, A. I. Yurzhenko and M. A. Kovbuz

The University of L'vov

The main products of low-temperature liquid-phase noncatalyzed oxidation of hydrocarbons are hydroperoxides, which are initiators of many chemical processes and valuable intermediates in the production of acetone, phenol, acetophenone, certain carboxylic acids, and other oxygen compounds [1].

However, as has been shown for isopropylbenzene (cumene), the yield of hydroperoxide in liquid-phase oxidation does not exceed 50% [2]. This relatively low yield of hydroperoxide may be the consequence, according to Ivanov [3], of formation of a number of products of extensive oxidation (acids, ketones, phenols, carbon dioxide).

The rate of the oxidation reaction, considered as a chain process with degenerate branching [4] involving a free-radical stage, depends on the decomposition of the hydroperoxide (HP) formed. It is therefore important to initiate oxidation by decomposition of the products directly in the oxidation system. This course of the reaction is appreciably influenced by the reaction conditions. Thus, cumene hydroperoxide (CHP) decomposes very slowly in organic media, but its decomposition is accelerated considerably in presence of various catalysts (acids, salts of variable-valence metals) [5].

However, Emanuel* and his associates have shown that the principal products of catalytic oxidation of hydrocarbons are acids, carbonyl compounds, alcohols, and esters, and only very small amounts of hydroperoxides are formed [6].

The yields of HP may be increased by introduction of an alkaline aqueous phase into the oxidation mixture. The first experiments in this direction yielded fairly satisfactory results [7].

We showed earlier [8] that addition of 0.1 N soda solution to the oxidation system considerably increases the oxidation rate of cumene in comparison with the rate in a homogeneous liquid phase, and shortens the induction period. An interesting fact is that the yield of HP in emulsion oxidation does not stop at 50% but approaches 100%.

It seems that the alkali reacts with inhibitors (phenols, acids) formed during oxidation, and eliminates their retarding effect. We have shown [9] that the hydroperoxide decomposes very rapidly in an aqueous phase; moreover, its content in the aqueous phase is low, because of its limited solubility (1.4% at 20°), in comparison with its content in the oil phase, in which the solubility of HP is unlimited. Introduction of an emulsifier in emulsion oxidation increases the HP content of the aqueous phase because of solubilization.

The above considerations are illustrated by the results of some of our experiments on the decomposition and solubilization of CHP in an aqueous medium (Table 1).

According to our proposed topochemical scheme of hydrocarbon oxidation, the reaction develops in the aqueous phase. The hydroperoxide formed accumulates in the hydrocarbon phase, where its decomposition is slight. The role of the emulsifier is to transfer hydrocarbon and hydroperoxide into the aqueous phase by solubilization. Elucidation of this important function of emulsifiers in the oxidation process, and the wide potentialities for their use in activating this process, require systematic studies of the influence of some of the best-known and widely-used emulsifiers, such as potassium palmitate, Nekal, etc.

TABLE 1

Critical Micelle Concentrations of Emulsifiers, and Solubility and Decomposition Rate Constant of CHP in Aqueous Media

Emulsifier	Emulsifier content in aqueous phase, %	Critical micelle concentration	Solubility of CHP at 20°, %	$K \cdot 10^3$ at 98.5°
Potassium palmitate	2	—	4.87	1.96
Nekal	2	$2.9 \cdot 10^{-4}$	2.23	1.01
Leukanol	2	$2.05 \cdot 10^{-5}$	1.98	1.83

TABLE 2

Effects of Potassium Palmitate, Nekal and Leukanol on the Accumulation Rate and Final Yield of CHP

Emulsifier	Emulsifier concentration, %	Accumulation rate of CHP, % per hour	Final yield of CHP, %
Without emulsifier	0	0.8	80
Potassium palmitate	0.1	1.3	55
	0.5	7.5	72
	1.0	8.1	78
	3.0	3.5	74
	4.0	1.3	79
Nekal	0.1	1.6	75
	0.5	1.7	68
	2.0	1.2	75
	5.0	1.7	76
	5.0*	1.7	74
Leukanol	2.0	1.6	70
	5.0	1.5	69

*Solubilization.

The results of an investigation of the influence of emulsifiers on the oxidation of cumene are given below. The experimental techniques and methods for quantitative determination of CHP are given in the previous paper [9].

The experiments were performed at 90° at 1:4 ratio of hydrocarbon to aqueous phase. The aqueous phase always contained 0.1 g-equiv Na_2CO_3 per liter.

The oxidation kinetics of cumene in presence of potassium palmitate added as emulsifier to the aqueous phase is represented by the graphs in Fig. 1.

Fig. 1 shows that the CHP accumulates at the highest rate when the potassium palmitate content is 0.5-1% (Curves 2, 3). Outside these limits of emulsifier concentration the accumulation of CHP slows down. After the hydroperoxide yield has reached 70-80% on the oxidized cumene, its content decreases sharply. It is interesting to note that at potassium palmitate concentrations of 0.1% (Curve 1) and 4% (Curve 5) CHP accumulates at equal rates after a short induction period with 4% of palmitate. However, the amount of hydroperoxide formed is considerably greater in the latter case (80%) than with 0.1% of potassium palmitate (55-60%).

It follows from Fig. 1a, that in presence of 3 and 4% of potassium palmitate there is some retardation of the process at the initial stage. The rate of CHP formation is lower in absence of potassium palmitate than in its presence.

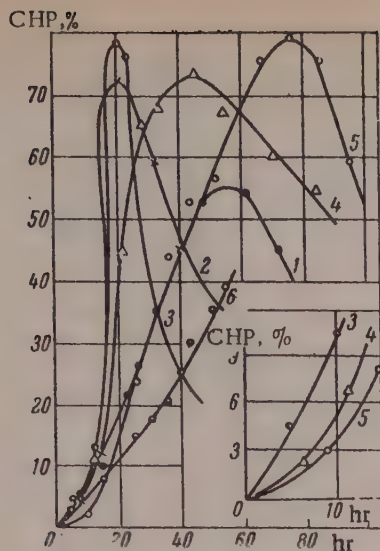


Fig. 1. Kinetic curves for accumulation of CHP in presence of different concentrations of potassium palmitate: 1) 0.1%; 2) 0.5%; 3) 1%; 4) 3%; 5) 4%; 6) in absence of potassium palmitate; initial portions of Curves 3, 4, and 5 are shown below.

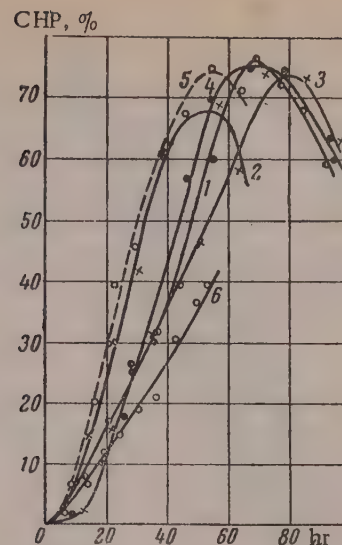


Fig. 2. Kinetic curves for accumulation of CHP in presence of Nekal: 1) 0.1%; 2) 0.5%; 3) 2%; 4) 5%; 5) 5% of Nekal after preliminary saturation of the aqueous phase with cumene; 6) in absence of Nekal.

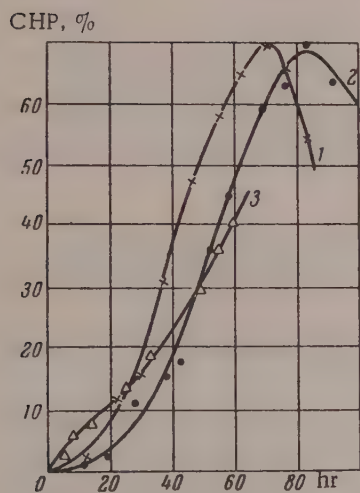


Fig. 3. Kinetic curves for accumulation of CHP in presence of Leukanol: 1) 2%; 2) 3%; 3) in absence of Leukanol.

peroxide was found after the shaking. If the oxidation is performed in a system containing previously-solubilized hydrocarbon, there is almost no induction period, while the equal slopes of Curves 5 and 6 indicate that CHP accumulates at equal rates in the two cases.

Kinetic curves for accumulation of CHP in presence of Luekanol are given in Fig. 3. In this case (Curves 1 and 2) the process is somewhat slower at the initial reaction period than it is in absence of emulsifier (Curve 3), as in the system with 5% Nekal solution. Subsequently, the rates of CHP accumulation increase considerably

A similar result is obtained with the use of Nekal (sodium dibutyl-naphthalenesulfonate) as emulsifier (Fig. 2): additions of Nekal on the whole accelerate the oxidation process, but it is less effective than potassium palmitate.

Nekal in 5% concentration has a retarding effect (Fig. 2, Curve 4). There is an induction period of approximately 15 hours, after which the reaction develops and CHP accumulates at the rate of 1.7% per hour. This can probably be attributed to suppression of the decomposition of CHP by Nekal at high concentrations [9]. However, the presence of solubilized hydrocarbon in the aqueous phase, even in small quantities, tends to accelerate the oxidation reaction. The induction period corresponds to the time required for solubilization of cumene in the Nekal micelles. When the amount of hydrocarbon solubilized in the aqueous phase is sufficient for formation and decomposition of CHP to develop in the aqueous phase, the accumulation rate of CHP begins to increase. The hypothesis was confirmed by a special experiment (Fig. 2, Curve 5) on the accumulation of CHP in a similar system of 5% Nekal solution and cumene, in which the aqueous phase was previously shaken with a small amount of cumene for 12 hours at room temperature in order to saturate it with the hydrocarbon. No hydro-

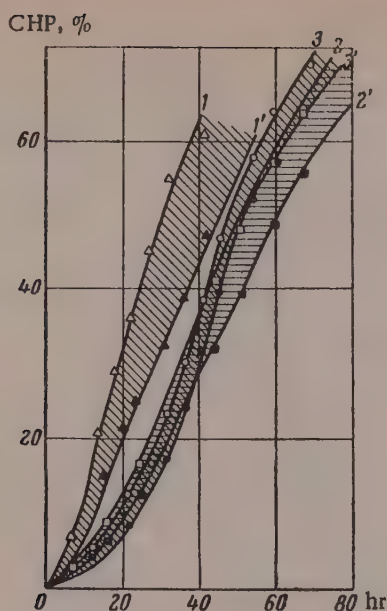


Fig. 4. Curves for the accumulation of CHP in the oil phase (1', 2', 3'), and total accumulation (1, 2, 3) in emulsion oxidation of cumene in presence of 2% of: 1) potassium palmitate; 2) Nekal; 3) Leukanol.

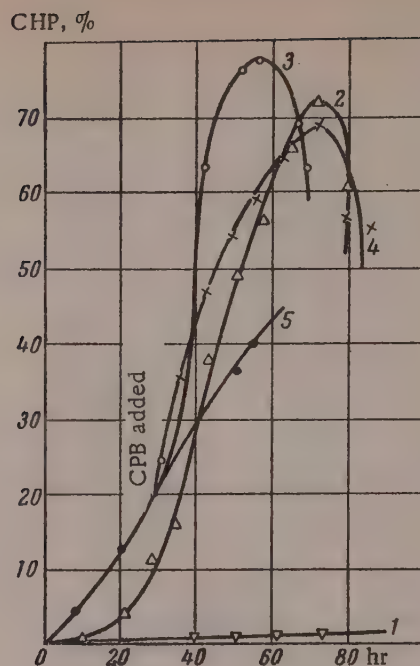


Fig. 5. Curves for the accumulation of CHP in emulsion oxidation of cumene with addition of CPB: 1) at the start of the reaction, 0.1%; 2) the same, 0.01%; 3) during the process, 0.1%; 4) the same, 0.01%; 5) without emulsifier.

and the maximum yields reach $\sim 70\%$ in both cases. These results show that the colloidchemical properties of the emulsifier (micelle formation, solubilization) have a significant influence on the oxidation rate. The emulsifier with the more pronounced colloidchemical properties (potassium palmitate), added even in low concentrations to the oxidation mixture, accelerates the process appreciably, assisting the reaction in the aqueous phase.

The emulsifiers form the following sequence in order of their accelerating effect on the oxidation of cumene: potassium palmitate > Nekal > Leukanol (Table 1); this is largely determined by their solubilizing power.

Kinetic curves representing the accumulation of CHP in the oil phase and in the oxidation system separately (Fig. 4) confirm this conclusion.

The crosshatched areas between the corresponding curves in Fig. 4 (1 and 1', 2 and 2', 3 and 3') represent the amount of hydroperoxide present in the aqueous phase during the oxidation process. This amount is greatest in presence of potassium palmitate because of solubilization of the hydroperoxide. In presence of an emulsifier an additional amount of hydroperoxide accumulates in the aqueous phase, and this, in turn, results in some increase of the total CHP yield. In presence of Nekal, and especially of Leukanol, the amount of CHP in the aqueous phase is less than in presence of potassium palmitate. Thus, the crosshatched areas increase with the use of more "active" emulsifiers, i.e., emulsifiers of higher solubilizing power.

The general results obtained in a study of the effects of anion-active emulsifiers on the emulsion oxidation of cumene are given in Table 2.

It follows from Table 2, that, if the optimum oxidation conditions (e.g., 0.5-1% potassium palmitate) are chosen, very considerable yields of CHP can be obtained at a high rate; this is quite impossible under other conditions.

In addition to the anion-active emulsifiers, we studied the effects of a cation-active emulsifier, cetylpyridinium bromide (CPB). This emulsifier has a very specific effect on the oxidation of cumene in emulsion. If added in the proportion of 0.1% or more relative to the aqueous phase at the start of the reaction, CHP inhibits accumulation of CHP almost completely (Curve 1, Fig. 5). After 80 hours of oxidation only traces of hydroperoxide are found in the system. The oil phase becomes yellow-brown in color and CO_2 is abundantly evolved. If 0.01% CPB is added, the process is again slower at first than in absence of emulsifier (Fig. 5, Curve 2). However, after an induction of 15-20 hours, the reaction develops. 70 hours after the start of the reaction the maximum amount of hydroperoxide (72%) accumulates, after which it decomposes rapidly. Thus, in this instance the amount of CPB added is very significant.

It is interesting to note that addition of 0.1% CPB 30 hours after the start of the process produces an unexpected and considerable stimulation of the reaction. An addition of 0.1% CPB is much more active than one-tenth of this amount (0.01%), and the CHP yield reaches almost 80% (Fig. 5).

This effect of cetylpyridinium bromide is primarily associated with its influence on the decomposition of CHP. Separate experiments [10] showed that the thermal decomposition of cumene hydroperoxide in an aqueous medium is accelerated considerably in presence of CPB. Moreover, if it is introduced at the start of the reaction there is an increase in the yields of products of more extensive oxidation (CO_2).

In accordance with Émanuel's views [11], the emulsion oxidation of cumene, analogously to the liquid-phase oxidation of hydrocarbons in a homogeneous medium, should be regarded as proceeding in several macroscopic stages, among which the initial period of the reaction is of special significance. CPB influences the initial macroscopic stage of the process and suppresses subsequent accumulation of CHP. Partial interaction may also take place between the free radicals formed by thermal activation of the hydrocarbon molecules and CPB molecules. The reaction is then directed toward formation of products of deeper oxidation, and the peroxide yield is slight. However, if cetylpyridinium bromide is introduced into the reaction mixture when some CHP is already present in it, decomposition of hydroperoxide in the aqueous phase is accelerated, and the development of the reaction is stimulated. Thus, introduction of CPB into the reaction system at the instant when the first macroscopic reaction stage has been completed is very favorable for the subsequent process.

Finally, it should be pointed out that cetylpyridinium bromide is a water-soluble emulsifier, and therefore, its significant influence on the oxidation kinetics of cumene in emulsion confirms once again our view that the aqueous phase is the principal location of the emulsion oxidation of hydrocarbons.

SUMMARY

1. The maximum rate of oxidation of cumene in emulsion, and the maximum yield of hydroperoxide, are obtained at potassium palmitate concentrations of 0.5-1%.

2. Sulfonated emulsifiers (Nekal and Leukanol) also accelerate the accumulation of hydroperoxide, but the process has a certain induction period. The influence of Nekal and of other colloidal electrolytes is largely associated with changes in the decomposition rate of hydroperoxide in their presence.

3. The influence of emulsifiers on the rate of emulsion oxidation of cumene depends considerably on their colloidal properties (micelle formation, solubilization). The induction period is shortened considerably after preliminary solubilization of the hydrocarbon in the aqueous phase.

4. Cation-active cetylpyridinium bromide, added at the start of the reaction, sharply suppresses the accumulation of CHP. Introduction of this emulsifier at a later stage in the reaction stimulates the emulsion oxidation of cumene.

LITERATURE CITED

- [1] B. D. Kruzhalov and P. G. Sergeev, *Chemical Science and Industry* 3, 1 (1956).
- [2] D. K. Tolopko, *Candidate's Dissertation* [In Russian] (L'vov, 1956).
- [3] K. I. Ivanov, *Intermediate Products and Intermediate Reactions in the Autoxidation of Hydrocarbons* [In Russian] (State Fuel Tech. Press, 1949).

- [4] N. N. Semenov, Problems of Hydrocarbon Oxidation [In Russian] (Izd. AN SSSR, Moscow, 1954).
- [5] M. S. Kharasch, W. Nudenberg and F. Arimoto, Science 113, 392 (1951).
- [6] D. G. Knorre, Z. K. Maizus and N. M. Émanuel, Proc. Acad. Sci. USSR 99, 415 (1954); 101, 895 (1955).
- [7] G. P. Armstrong, R. H. Hall and D. C. Quinn, J. Chem. Soc., 666 (1950); G. S. Serif, G. F. Hunt and A. N. Bourns, Canad. J. Chem., 31, 1229 (1953).
- [8] R. V. Kucher and A. I. Yurzhenko, Colloid J., 18, 555 (1956). *
- [9] R. V. Kucher, T. M. Polon'skii and M. O. Kovbuz, Proc. Acad. Sci. Ukrainian SSR 1, 42 (1957).
- [10] R. V. Kucher and S. D. Kaz'min, Colloid J., 19, 592 (1957). *
- [11] N. M. Émanuel, Proc. Acad. Sci. USSR 110, 245 (1956); R. V. Kucher, A. I. Yurzhenko and M. A. Kovbuz, Proc. Acad. Sci. USSR 117, 638 (1957). *

Received September 14, 1957

* Original Russian pagination. See C. B. Translation.

RELATIONSHIP BETWEEN THE STRUCTURE AND ADSORPTIONAL PROPERTIES OF SURFACE-ACTIVE SUBSTANCES

S. M. Levi and O. K. Smirnov

Scientific Research Institute for Motion Pictures and Photography

Surface-active substances (SAS) are widely used in photographic chemistry, especially for improving wetting when emulsions are applied to film base. The range of wetting agents used is restricted by the stringent requirements with regard to adsorptional and technological properties. These requirements include [1, 2]: a high rate of kinetic wetting, emulsifying or "anticomet" action [3], and low foaming power in gelatin solutions. Naturally, such emulsifiers must not have any detrimental effects on the photographic properties of the emulsion layer.

Despite the extensive uses of SAS, the relationship between their structure and adsorptional properties has been studied little. Dervichian and Lachampt [4] put forward some general considerations on the subject. Alexander and Posner [5] and Addison et al. [6] studied the effect of the length of the alkyl chain in a number of simple alcohols on their adsorption kinetics. We have studied the relationship between the structure, adsorption, and technological properties of wetting agents.

Test methods. When the emulsion is applied to the support, wetting takes place under kinetic, i.e., non-equilibrium conditions, with continuous formation of new emulsion — support and emulsion — air interfaces. At certain formation rates of these new interfaces wetting ceases [2, 7]. When a photographic emulsion is applied, the observed kinetic nonwetting is due to break of contact between the wetting liquid and the wetted support; the velocity at which this contact breaks down is defined as the critical velocity of kinetic wetting, U_c . It follows from the theory of kinetic wetting that breakdown of cohesive forces between the liquid and the support is determined by the magnitude of the kinetic potential difference at the interface, and by its kinetics, which depends on the kinetics of SAS adsorption. For maximum increase of U_c it is necessary that the adsorption of the wetting agent at the wetting solution — air interface should proceed at the maximum rate. A special apparatus [2, 7] was used for determination of the critical wetting velocity. In this apparatus the support with its emulsion layer moves at a certain gradually increasing velocity over the liquid in contact with it (Fig. 1); the instant is noted at which contact between the liquid and the support breaks down and wetting ceases (Fig. 2). A wetting agent is characterized by the critical wetting velocity at a wetting-agent concentration of $1 \cdot 10^{-4}$ M (U_{10}), and the difference between the critical wetting velocities at concentrations of $4 \cdot 10^{-4}$ and $1 \cdot 10^{-4}$ M (ΔU) [2, 7]. Wetting agents may be tested either in aqueous solution, or in 2 or 3% gelatin solutions.

The decrease of surface tension was determined by the capillary method. Foaming power was characterized by the lifetime of 500 ml of foam formed when a current of air at 80 mm pressure was blown at 40° through a 6% gelatin solution containing $1 \cdot 10^{-4}$ M of the wetting agent. The emulsifying (EE) and anticomet (AE) effects of wetting agents were determined by application, onto a moving support, of a layer of photographic emulsion containing oil-water emulsion and wetting agent; the wetting agent was introduced in amounts of $0.5 \cdot 10^{-4}$ or $1 \cdot 10^{-4}$ M; at one of these concentrations a uniform emulsion layer should be formed, without local comet-shaped faults known as "comets". If comets are not eliminated, the wetting agent has no AE.

Structure of the investigated surface-active substances. Several types of SAS were synthesized for the investigation — derivatives of alkylsuccinic and alkylphosphonic acids, in which the composition of the polar groups and the structure of the hydrocarbon chain were systematically varied. The following compounds were

TABLE 1

Effect of Structure of SAS on Decrease of Surface Tension $\Delta\sigma$ (dynes/cm) of Aqueous and Gelatin Solutions

Group	Decrease of surface tension $\Delta\sigma$ by derivatives of alkylenesuccinic acids, dynes/cm					
	aqueous solutions			gelatin solutions		
	$C_8 - C_{10}$	$C_8 - C_{10}$	$C_{12} - C_{16}$	$C_8 - C_{10}$	$C_8 - C_{10}$	$C_{12} - C_{16}$
I	5	—	10	8	—	20
II	—	—	26	—	—	27
IIa	—	28—30	29	—	28—30	30
IIb	38	37—38	39	31	30—31	31
IV	38—39	37—38	41	27—31	27—31	31—32
V	38—41	—	—	30—31	—	—
VI	39—42	38—40	43	27—31	28—32	31—32

Group	Decrease of surface tension $\Delta\sigma$ by derivatives of alkylphosphonic acids in gelatin solutions, dynes/cm				
	C_7	C_{10}	$C_8 - C_9^*$	$C_8 - C_9$	$C_{10} - C_{12}$
VIII	6	41	4	12	20
VII	5	41	13	18	32
IX	20	41	10—15	10—15	32—40
X ($m = 7$)	—	—	—	24	30

*Compounds of Groups VIIa and VIIb give $\Delta\sigma$ of 18-19 dynes/cm.

TABLE 2

Effect of Structure of Derivatives of Alkylenesuccinic Acids on Kinetic Wetting (U_c , cm/second)

Group	$C_8 - C_{10}$		$C_8 - C_{10}$		$C_{12} - C_{16}$	
	U_{10}	ΔU	U_{10}	ΔU	U_{10}	ΔU
IV $m = 1$	28	20	—	—	26	15
IV $m = 3$	35	20	18	32	30	15
IV $m = 5$	25	10	—	—	32	15
IV $m = 7$	24	5	—	—	34	18
IV $m = 9$	20	5	—	—	40	20
IIb	24	20	25	30	26	30
V	20—25	5—10	—	—	—	—
VI	20—25	5—10	18	20	20—25	5—10
I	16	6	—	—	10	3
IIa	15	22	—	—	15	23

TABLE 3

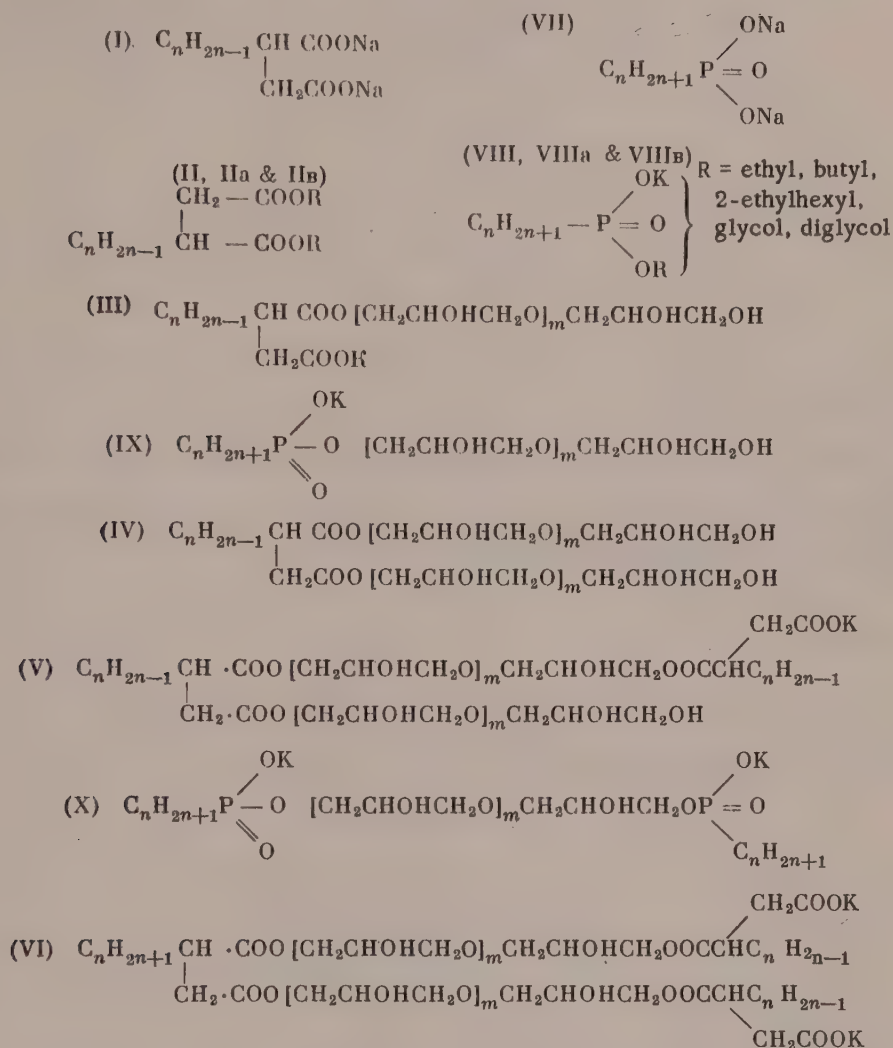
Effect of Structure of Alkylphosphonic Acid Derivatives on Kinetic Wetting (U_c , cm/second)

Group	C_7		C_{10}		$C_8 - C_9$		$C_{10} - C_{12}$	
	U_{10}	ΔU	U_{10}	ΔU	U_{10}	ΔU	U_{10}	ΔU
X	10	2	7	3	27	20	25	12
VII	20	7	21	7	21	9	21	9
IX $m < 20$	10	2	7	3	—	—	19—25*	8—10*
VIII	8,5	1,5	10	2	10	2	10	2

*For $m > 20$, $U_{10} = 19-25$ and $\Delta U = 10-12$ cm/second.

Investigated: 1) disodium salts (Groups I and VII) acid esters of monohydric alcohols (Groups II and VIII); 3) acid esters of dihydric alcohols (Groups IIa and VIIIa); 4) acid esters of trihydric alcohols (Groups IIb and VIIIb); 5) acid polyglycerides (Groups III and IX) with different contents of glyceryl residues (m); 6) neutral polyglycerides (Group IV) with different contents of glyceryl residues; 7) certain esters of the polyglycerides of alkylene-succinic (Groups V and VI) and alkylphosphonic (Group X) acids.

The structural formulas of these compounds are given below:



Alkylene groups were introduced into the wetting-agent molecules by condensation of olefins with maleic anhydride for synthesis of alkylene-succinic acids [8, 9], or by oxidation of paraffins in presence of phosphorus trichloride [10-14]. The hydrocarbon radicals of the alkylene-succinic acids were derived from polymerization products of propylene, butylene, and amylene, and reforming and cracking gases some of which were used in the form of mixtures of isoctylenes and isononylenes (C_8 - C_9) [15], nonylenes and decylenes (C_9 - C_{10}), dodecylenes and hexadecylenes (C_{12} - C_{16}), and octadecylene (C_{18}). For the alkylphosphonic acids, n-heptane, n-octadecane, and mixtures of hydrocarbons of normal structure with chain lengths C_6 - C_8 , C_6 - C_{10} , C_8 - C_9 , C_{10} - C_{12} (hydrogenated synthine fractions) were used. The SAS were made by saponification of the corresponding anhydrides (I and VII) [8, 9, 14], esterification (II, III, and VIII) [16], polyesterification with glycerol (IV and IX) [17, 18], and acylation of the acid polyglycerides with the original acid anhydrides (V, VI, and X) [18, 19].

The results of the determinations are given in Tables 1-5 and Fig. 3.

It follows from Table 4 that the length and structure of the hydrophobic hydrocarbon chains in SAS have a decisive influence on their emulsifying action. The best EE is found with substances from the group of

TABLE 4

Effect of Structure on Emulsifying Properties of SAS

Group	Derivatives of alkylsuccinic acids.								Group	Derivatives of alkylphosphonic acids			
	C ₈ - C ₁₀		C ₉ - C ₁₀		C ₁₂ - C ₁₆		C ₁₈			C ₈ - C ₉		C ₁₀ - C ₁₂	
	concentration × 10 ⁻³ , mmoles/liter									concentration × 10 ⁻³ , mmoles/liter			
	5	10	5	10	5	10	5	10		5	10	5	10
I	—	—	—		+	++	—	—	VII *	++	++	—	+
II	—	+			+	++	—	—	VIII	—	—		
IIa	—	—			++	++	—	—	VIIIa	—	—		
IIb	+	+	+	++	+	++	—	—	VIIIb	—	—	—	—
III	—	—			++	++	—	—	IX, <i>m</i> < 20	—	—	—	—
IV	—	—	++	++	+	++			IX, <i>m</i> > 20 **	—	—	++	++
V	+	++			+	++			X	—	—	+	++
VI	++	++	++	++	++	++							

Note. ++ is complete emulsification; + is incomplete emulsification; — is absence of emulsifying properties.

*Compounds of Group (VII) synthesized from individual hydrocarbons show maximum EE (++) with C₇ alkyl groups.

**Compounds of Group (IX) synthesized from individual hydrocarbons show maximum EE (++) with C₁₈ alkyl groups at $m > 20$.

TABLE 5

Effect of Structure of SAS on the Life of Foam Formed by 6% Gelatin Solution on Addition of $1 \cdot 10^{-4}$ Mole SAS per liter (Foam Life of Gelatin Solution Taken as 1)

Group	Alkylsuccinic acid derivatives			Group	Alkylphosphonic acid derivatives		
	C ₈ - C ₁₀	C ₁₂ - C ₁₆	C ₁₈		C ₈ - C ₉	C ₈ - C ₁₀	C ₁₀ - C ₁₂
I	0,1	1,2	—	VII	0,50	0,80	0,95
IIa	—	1	1*	VIIIa	1,5—1,8	—	—
IIb	20	30	—	VIIIb	0,60	7,5	7,5
III	10	15	—	IX	1,78—0,67**	8—2,6**	20,0—3,0***
II:							
R = C ₂ H ₅	1,0	1,7	0				
R = C ₄ H ₉	1,5	0	0				
R = C ₈ H ₁₇	0	0	0				
IV	20	30	—				
V и VI	25	35	—				

*Foam not formed with glycols; ** for m from 6 to 20; *** for m from 6 to 40.

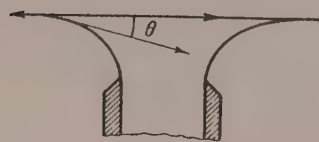


Fig. 1. Wetting of support at rest, when $U = 0$.

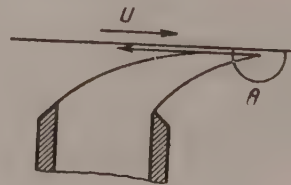


Fig. 2. Formation of an air gap, resulting in kinetic non-wetting at $U \rightarrow U_c$.

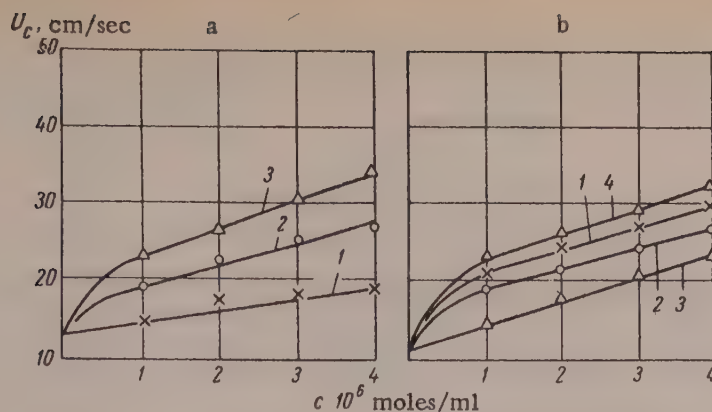


Fig. 3. Kinetic-wetting isotherms for Group VI wetting agents: a) in water; b) in 3% gelatin solution; 1) $n = 12-16$; 2) $n = n' = 12$; 3) $n = n' = 8-10$; 4) octaglyceride of alkylene-succinic acid; n from 12 to 16.

alkylenesuccinic acids containing from 10 to 16 carbon atoms in the molecule. On decrease of the length of the hydrocarbon chain in disodium salts (Group I) and polyglycerides (Group IV) of alkylenesuccinic acids from $C_{12}-C_{16}$ to C_8-C_9 they lose their EE almost completely. On the other hand, increase of chain length to C_{18} also results in decreases and even total loss of EE (acid esters of alkylenesuccinic acids, Groups II, IIa, and IIb).

The presence of ionogenic groups in the molecules of SAS has a significant influence on their EE. Thus, nonionogenic SAS of Group IV with radical containing 8-9 carbon atoms have almost no EE, although they have good static and kinetic wetting properties. The introduction of one or two ionogenic groups ($-\text{COOK}$) into the molecules of alkylenesuccinic acid polyglycerides confers good emulsifying properties on them (Groups V and VI), regardless of the length of the hydrocarbon radical. Acid esters of polyglycerides (Group III) have higher EE than neutral esters (Group IV).

The structure of the hydrophilic part of the molecules of SAS has a definite influence on EE, as is seen clearly in the case of acid esters (Groups II, IIa, IIb, VIII, VIIIa, VIIIb). In polyglycerides of alkylenesuccinic acids (Group IV), in contrast to the corresponding derivatives of alkylphosphonic acids (Group IX) the length of the polyhydric alcohol chain has no appreciable effect on the EE.

In the series of sodium salts of alkylphosphonic acids (Group VII) the best EE are found in compounds with alkyl chains containing from 7 to 9 carbon atoms. Shortening or lengthening of the hydrocarbon chain results in loss of EE. Monoglycerides (Group VIIIb) and acid polyglycerides with $C_{10}-C_{12}$ alkyl chains (Group IX) and polyglycerides chains containing from 6 to 20 glycerol molecules, irrespectively of the length of the alkyl chain, have no EE; if the glyceride chain is lengthened to above $m = 20$ the polyglycerides acquire EE; polyglycerides with alkyl chains up to C_{18} and glyceride chains with not less than 20 glycerol molecules have EE. Compounds formed by acylation of primary hydroxyl groups in polyglycerides by a second molecule of the same anhydride of an alkylphosphonic acid with alkyl chains from C_8-C_9 to $C_{10}-C_{12}$ (compounds of Group X) have high EE.

There is complete correlation between the foaming and emulsifying effects of SAS in gelatin solutions. Substances with small numbers of hydrophilic groups in their molecules (fewer than three hydroxyl groups) have weak EE, and sharply reduce and in some instances completely prevent foaming of gelatin solutions (compounds of Groups I, IIa, VII, and VIIIb). Conversely, substances with more developed and branched hydrocarbon chains, with high EE, increase foaming of gelatin solutions; for example, compounds of Groups IV, V, VI, and IX.

The influence of the structure of SAS on foaming of gelatin solutions and emulsifications may be represented by the following scheme:

Increase of foam-breaking action

Acid esters of monohydric
alcohols

Disodium salts

Acid esters of glycols
and glycerol

Polygly-
cerides

Increase of emulsifying action

Within a given homologous series, the critical wetting velocity is determined by the molecular weight of the compound. Thus, increase of the number of glyceride groups in compounds of Group IV, for the C_{12} - C_{16} range, and of Group IX, results in increases of U_c . In compounds of Groups IV and VIII lengthening of the hydrocarbon chain also increases U_c . On the one hand, in compounds of high molecular weight in Groups V, VI, IX, and X alteration of the chain length has almost no effect on the critical wetting velocity. The exceptions are polyglycerides of alkylsuccinic acid (Group IV) with C_8 - C_{10} hydrocarbon radicals, for which U_{10} has a maximum value with 8 glyceride groups. On the other hand, the critical wetting velocity depends on a combination of polar groups and a hydrocarbon radical in the molecule of the wetting agent. Neutral polyglycerides of alkylsuccinic acid (Groups IV) give higher critical velocities than their esters containing ionogenic groups (Groups IIb, V, and VI). Derivatives of alkylsuccinic acid give higher values of U_c than the analogous compounds of the alkylphosphonic series.

Optimum values of U_c are given by compounds of Groups V and VI. Increase of the hydrocarbon chain length results in some increase of U_c . Monoesters of octaglycerides of alkylphosphonic acids (Group X) with C_8 - C_9 and C_{10} - C_{12} alkyl chains give higher U_c than the corresponding derivatives of alkylsuccinic acids (Group V).

If the wetting agents are arranged in order of increasing U_c , the following series are obtained:

Alkylsuccinic Acids:

salts → polyglyceride esters → esters of trihydric alcohols → polyglycerides →
→ esters of mono- and dihydric alcohols

Alkylphosphonic Acids:

acid esters of glycerol → polyglycerides → salts → polyglyceride esters

The lowering of surface tension produced by SAS increases with increase of alkyl chain length in approximately the following sequence:

Alkylsuccinic Acids:

salts → acid esters of alcohols → polyglycerides → esters of polyglycerides

Alkylphosphonic Acids:

acid esters of glycerol → salts → polyglycerides → acid esters of mono-
and dihydric alcohols → polyglyceride esters

SUMMARY

1. The greatest emulsifying and foaming effects in gelatin solutions are produced by alkylsuccinic acid derivatives with C_{12} - C_{16} alkylene chains, in presence of ionogenic groups, and by alkylphosphonic acid polyglycerides with polyglyceride chains containing more than 20 glycerol molecules.

2. The critical wetting velocity increases to a certain maximum, highest for polyglycerides, with increase of molecular weight within a given homologous series.

3. The lowering of surface tension of aqueous and gelatin solutions of SAS increases with increase of the length of the alkyl radical.

In conclusion, it is our pleasant duty to offer our thanks to Corresponding Member (AN SSSR) B. V. Deryagin for much valuable advice, and to Academician P. A. Rebinder and Professor A. B. Taubman for reading the paper.

LITERATURE CITED

- [1] S. Levi and O. Smirnov, *Advances in Scientific Photography* [In Russian] No. 5 (1956).
- [2] B. Deryagin and S. Levi, *J. Sci. and Appl. Photography and Cinematography* 1, 354 (1956); Authors' Certif. No. 100824.
- [3] O. K. Smirnov and S. M. Levi, *J. Sci. and Appl. Photography and Cinematography* (in the press).
- [4] D. Dervichian and F. Lachampt, *Bull. Soc. chim. France*, 486 (1946).
- [5] A. E. Alexander and A. M. Posner, *J. Coll. Sci.* 8, 575 (1953).
- [6] L. Addison, *J. Amer. Chem. Soc.*, 930 (1948).
- [7] B. Deryagin and S. Levi, *Physical Chemistry of the Application of Thin Layers* [In Russian] (Izd. AN SSSR, 1959) [in the press].
- [8] F. N. Stepanov and O. K. Smirnov, Authors' Certif. No. 94321.
- [9] F. N. Stepanov and O. K. Smirnov, Authors' Certif. No. 81713.
- [10] O. K. Smirnov, Authors' Certif. No. 104890.
- [11] A. Z. Soborovskii, Yu. M. Zinov'ev, and M. A. Éngelin, *Proc. Acad. Sci. USSR* 67, 297 (1949).
- [12] J. O. Clayton and W. J. Jenson, *J. Amer. Chem. Soc.* 70, 3880 (1946).
- [13] R. Graf, *Ber.* 85, 9 (1952).
- [14] O. K. Smirnov, S. M. Levi and N. I. Grineva, Authors' Certif. No. 103162.
- [15] L. M. Paushkin, *Catalytic Polymerization of Olefins to Motor Fuel* [In Russian] (Izd. AN SSSR, 1942).
- [16] O. K. Smirnov, A. I. Rybnikova and S. M. Levi, Authors' Certif. No. 105345; O. K. Smirnov, S. M. Levi, N. I. Grineva and A. I. Rybnikova, Authors' Certif. No. 109067; O. K. Smirnov, S. M. Levi, N. I. Grineva and T. K. Stepanova, Authors' Certif. No. 107060.
- [17] O. K. Smirnov, and S. M. Levi, Authors' Certif. No. 102550.
- [18] O. K. Smirnov, S. M. Levi and A. I. Rybnikova, Authors' Certif. No. 108678.
- [19] O. K. Smirnov, A. I. Rybnikova, S. M. Levi and S. N. Kochneva, Authors' Certif. No. 105337.

Received December 30, 1957

USE OF AQUEOUS SOLUTIONS OF POLYVINYL ALCOHOL FOR STABILIZATION OF HIGHLY CONCENTRATED EMULSIONS

B. I. Losev and M. A. Troyanskaya

Institute of Combustible Minerals, Academy of Sciences, USSR, Moscow

Highly concentrated emulsions are widely used in the production of solidified motor fuels and other solidified organic liquids. The process of fuel solidification consists of the production of a highly concentrated emulsion in which the disperse phase is the fuel to be hardened (gasoline, kerosene, etc.) and the dispersion medium is an aqueous solution of polymeric emulsion stabilizers.

In the technological process the highly concentrated emulsion so formed is treated with solutions of appropriate hardening agents and then molded into briquets. In the preparation of solidified fuels the phase ratio in the emulsions reaches values of $V_d : c_m = 10 : 1$ and over; i.e., the fuel constitutes 90% and over of the total volume of emulsion.

The dispersion medium in such an emulsion is reduced to very thin adsorption layers separating the fuel droplets. The adsorption layers should form fairly strong coatings around the fuel droplets, with structuromechanical properties and capable of withstanding considerable deformations. Such coatings, which have been named surface or two-dimensional gels [1], can protect the fuel droplets against coalescence under conditions of constant direct contact, such as are found in highly concentrated emulsions.

The range of emulsifiers capable of stabilizing highly concentrated emulsions is fairly limited. Still smaller is the number of substances which can not form strong protective layers around the droplets in a highly concentrated emulsion, but can also be hardened by the action of suitable reagents so that the emulsion structure becomes fixed and the whole mass is transformed into the form of a solid.

We studied polyvinyl alcohol solutions among the emulsion stabilizers used in the production of solidified fuels. Polyvinyl alcohol is made from polyvinyl acetate by alkaline or acid hydrolysis, and is a white powder readily soluble in water and insoluble in alcohol, benzene, and other organic solvents. Polyvinyl alcohol films have good resistance to oil and hydrocarbons. Polyvinyl alcohol can be converted into totally insoluble products by the action of a number of substances: dicarboxylic and polycarboxylic acids, strong alkalies [2], and dimethylolurea [3].

The reaction of acetal formation with formaldehyde can also be used for cross linking and for conversion of polyvinyl alcohol into an insoluble form after formation of a highly concentrated emulsion. Aqueous solutions of polyvinyl alcohol have a weak alkaline reaction. Determinations of the hydrogen ion concentration by means of the glass electrode give pH values of 7.1-7.2.

The solubility of polyvinyl alcohol in water depends on its molecular weight and on the content of unsaponified acetate groups. We used polyvinyl alcohol containing not more than 5% acetate groups for the production of solidified gasoline.

Since the stability of an emulsion is determined by the structuromechanical properties of the protective adsorption layer, and, at the same time, by the mobility of the molecules or micelles of the adsorption layer [1], i.e., by the ability of this layer to recover its continuity, it is necessary to determine the most suitable viscosity and concentration of the emulsion stabilizer, which ensures its maximum emulsifying power and emul-

TABLE 1

Viscosities of Polyvinyl Alcohol Solutions Made by Acid and Alkaline Hydrolysis

Concentration, %	Viscosity of polyvinyl alcohol at 20°, centipoises		Concentration, %	Viscosity of polyvinyl alcohol at 20°, centipoises	
	acid hydrolysis M = 5000	alkaline hydrolysis, M = 13600		acid hydrolysis M = 5000	alkaline hydrolysis M = 13600
5	4.33	6.32	10	51.1	39.6
6	6.33	15.0	11	105.0	69.0
7	14.7	23.0	12	240.0	127.6
8	15.8	35.0	13	—	159.6
9	33.3	38.1	14	—	208.0

TABLE 2

Effect of Heating on the Viscosity of Solutions of Polyvinyl Alcohol of M = 5000 and M = 10000

Molecular weight M of polyvinyl alcohol	Heating temp., °C	Viscosity of polyvinyl alcohol solutions, centipoises		
		Solution concentration, %		
		5	7	10
5000	20	3,3	13,7	51,1
	40	2,8	10,7	45,0
	60	2,3	8,5	32,0
10000	Cooled again to 20°	3,3	13,7	51,1
	20	3,8	17,1	38,2
	40	3,11	13,5	31,1
	60	2,55	10,6	23,8
	Cooled again to 20°	3,8	17,1	38,2

sion stability. Polyvinyl alcohol solutions do not conform to the viscosity law. Table 1 contains values obtained by different methods for the viscosity of polyvinyl alcohol solutions.

The molecular weight (M) of polyvinyl alcohol was taken to be equal to the molecular weight of the polyvinyl acetate from which it was made, as it was assumed that the length of the molecule does not change during saponification of polyvinyl acetate.

In our estimations of the emulsifying properties of polyvinyl alcohol solutions we adopted the volumetric measure of emulsifying power [1], which is the maximum volume of the hydrocarbon phase (gasoline) emulsified in a given volume of the aqueous emulsifier solution: $V_{\max} = V_{ph}/V_m$.

The emulsifying power of polyvinyl alcohol solutions in the 3 to 10% concentration range is 4.5-5 for emulsification of gasoline. At solution concentrations above 10% and viscosities above 50 centipoises the emulsifying power of the solutions decreases. We used 10% solutions of polyvinyl alcohol, with viscosities of 40-50 centipoises, for preparation of solidified gasoline. Although the emulsifying power of more dilute solutions lies in the same range, they are unsuitable for use, as the excess water has an unfavorable effect on the quality of the briquets during drying.

The 10% solutions of polyvinyl alcohol recommended for fuel solidification have relatively low surface tension. The surface tension was determined by means of the Rebinder apparatus. The surface tensions (in ergs/cm²) of 10% polyvinyl alcohol solutions have the following values for different interfaces:

Polyvinyl alcohol solution - air	72.8 ergs/cm ²
Polyvinyl alcohol solution - isooctane	48.8 "
Polyvinyl alcohol solution - B-70 gasoline	56.6 "

The surface tension and viscosity generally decrease with increase of temperature; this has the ultimate effect of greatly facilitating and accelerating emulsion formation. However, it is not always possible to use increase of temperature for accelerating emulsification. Thus, in emulsification of butane, ethyl chloride, isooctane, and other hydrocarbons with high vapor pressures it is desirable to lower the temperature rather than to raise it, because of the large evaporation losses.

Emulsification in each individual case should be performed under definite temperature conditions which are the most suitable for the material. Gasoline is emulsified at 20°. The optimum emulsification temperature for kerosene and Diesel fuel is 40-50°. As Table 2 shows, the viscosity of polyvinyl alcohol solutions falls on heating, and retains its original values on cooling. It follows that the colloidal particles do not break down on heating, as is the case with starch solutions and oxygen-containing rubber solutions.

SUMMARY

1. Polyvinyl alcohol can be used as a stabilizer for highly concentrated emulsions in the production of solidified motor fuels.
2. A 10% aqueous solution of polyvinyl alcohol with viscosity of 40-50 centipoises and emulsifying power of 5 is recommended for emulsification.
3. Solutions of polyvinyl alcohol can be used in mixtures with other water-soluble stabilizers for improving the elasticity and gasoline resistance of films which form the multicellular structure in solidified fuel briquets.

LITERATURE CITED

- [1] P. A. Rebinder and K. A. Pospelova, introductory chapter to W. Clayton's Theory of Emulsions and Their Technical Treatment (IL, Moscow, 1950) [Russian translation].
- [2] V. V. Korshak and V. A. Zamyatina, Bull. Acad. Sci. USSR, Div. Chem. Sci. 106 (1949).
- [3] J. Jones, in High Polymers, Vol. 4 [Russian translation] (Goskhimizdat, 1945) p. 68.
- [4] A. A. Trapeznikov, in the book: Viscosity of Liquids and Colloidal Solutions, Vol. 2 [In Russian] (Izd. AN SSSR, 1943).

Received January 31, 1958

DEVELOPMENT OF CRYSTALLIZATION CENTERS IN A SUPERCOOLED ORGANIC LIQUID

G. L. Mikhnevich

Chair of Molecular Physics, University of Odessa

Development of crystallization centers which form during the latent period is a necessary procedure in determinations of the effect of temperature on the probability of nucleation in substances which crystallize very slowly (piperine, betol, etc.).

We denote by τ_e the temperature at which a preparation containing a drop of a melt is held for a time of τ_e minutes and at which crystallization centers should be formed (this is the "exposure" temperature, in Tammann's terminology). At the end of the time interval τ_e the crystals remain invisible under the microscope. Their growth must be accelerated to make them visible and to allow them to be counted. The preparation is therefore warmed rapidly and held for τ_p minutes at a temperature t_p° at which the probability of formation of new crystallization centers is negligibly small, and the growth rate is high. This warming process, introduced by Tammann and used by others in all subsequent investigations, has been given the name of development [1-4]. Tammann assumed that crystallization centers merely increase in size during development. It has been found, however, that the necessary condition — constancy of the number of centers formed at the exposure temperature — is not fulfilled: development reduces this number to an increasing extent with increase of the development temperature. As the result of development, the nucleation probability — temperature curve undergoes considerable distortion: the ordinates of the curve are lowered sharply, to an increasing extent, the lower the exposure temperature. As a result, the maximum on the curve is shifted in the direction of smaller supercooling [5].

In this paper, we present an interpretation of earlier results obtained in studies of development [5, 6], based on the theory of formation of crystallization centers on impurity particles which was put forward in the preceding paper [7]. It is assumed in this theory that nucleation is not spontaneous, but occurs on particles of active impurities. The surface of such a particle is covered by a crystalline layer of the substance in question or of a substance of allied structure. This crystalline layer is present on the particle even before supercooling, as its destruction by fusion requires a higher temperature than the usual phase-transition temperature [8]. In some cases the crystalline layer may cover the surface, and in others it may lie deep in cracks or scratches if these are present on the particle surface. The growth of such a "nucleus" consists of the formation of successive crystalline layers, but the growth mechanism depends on the particle size relative to the critical size r_c , given by Formula (1)

$$r_c = \frac{2MT_0\sigma}{q \cdot \rho \cdot \Delta T}, \quad (1)$$

where M is the molecular weight; T_0 is the melting point; σ is the interfacial energy; q is the heat of fusion; ρ is the density of the crystal nucleus; $\Delta T = T_0 - T$, is the supercooling.

At sufficiently low temperatures such "nuclei," containing foreign bodies, if larger than the critical size, are "ready" crystallization centers and grow steadily to reach a size visible under the microscope. In contrast, to this, if the temperature is so high that the critical size is greater than the initial size of the "nuclei", their conversion into crystallization centers can occur only as the result of fluctuations.

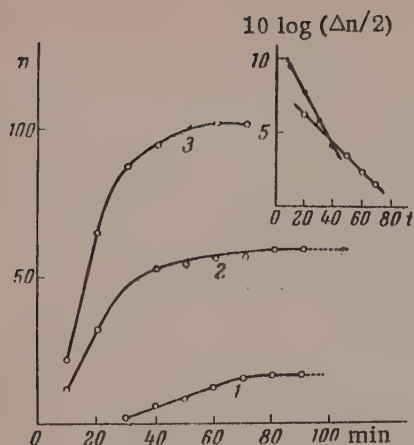


Fig. 1. Variations of the number of crystallization grains in piperine with time: 1) at 40°, without development; 2 and 3) after 24 and 48 hours at 15°; above — Curves 2 and 3 in semilogarithmic coordinates.

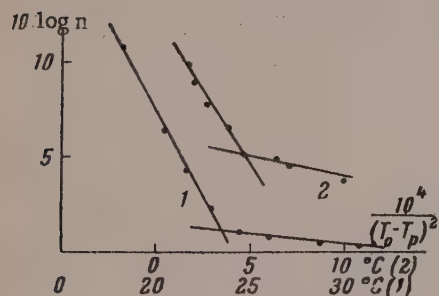


Fig. 2. Logarithm of the number of crystallization grains in betol as a function of the work of conversion of the impurity into crystallization centers at different development temperatures t_p : 1) at exposure temperature $t_e = 10.7^\circ$; 2) at $t_e = 6.4^\circ$.

Whereas in the former case ($r > r_c$) the number of centers observed under the microscope in the course of time is completely determined by the size-distribution function $\psi(r)$ of the nuclei, in the latter case only a part of the active particles present in the melt can reach the critical size r_c . This conversion of particle impurities occurs as the result of fluctuations. The gradual consumption of such "nuclei" and their conversion into crystallization centers in the course of time is represented by an equation of the first-order reaction type

$$n = n_\infty (1 - e^{-\alpha t}). \quad (2)$$

On the other hand, calculation shows that the same number \underline{n} represents the integral number of crystallization centers formed at time \underline{t}_i by the formula

$$n = \text{const} \cdot e^{-\beta r_c} \int_{r(t)}^m e^{\frac{\alpha}{c}(r-r_m)} dr, \quad (3)$$

where $\eta(t)$ is the radius of a nucleus at time t ; r_m is the largest "nucleus" at the initial instant; α is the rate of fluctuational growth, and the parameter β is defined by the equation

$$\beta = \frac{4\pi\sigma}{3kT}. \quad (4)$$

It was shown that the relationship between the number of crystallization centers and their conversion temperature t_e° is mainly determined by the factor $(-\beta r_c^2)$.

Thus, for a definite time instant \underline{t}_i or for a definite exposure time t_e , the dependence of the number of visible crystallization grains \underline{n} on the temperature is given by the expression

$$n = k_1 e^{-\beta r_c^2} \quad (5)$$

or, by Equation (1)

$$n = k_1 e^{-\frac{k_2}{(\Delta T)^2}}, \quad (6)$$

where $\Delta T = T_0 - T$ is the degree of supercooling, while $k_1 = \text{const} \int_{r(t)}^{r_m} e^{\frac{\alpha}{c}(r-r_m)} dr$ and $k_2 = \beta \left(\frac{2MT_0\sigma}{q\rho} \right)^2$

depend little on the temperature and may be regarded as constant.

We now consider the process of development of crystallization centers. In the light of the above theory we assume that conversion of "nuclei" into crystallization centers, i.e., their growth to the critical size corresponding to the development temperature t_p° , occurs only in the course of development and not at the exposure temperature. This conversion must always take place by fluctuations, as the development temperature used is always higher than the exposure temperature.

This assumption is confirmed by kinetic experiments [6]. A kinetic curve was first plotted for piperine without development at +40° (Curve 1, Fig. 1). The sample was then remelted and held at room temperature (15°) for t_c days. This time was initially 24 hours, considerably less than the total time required for conversion of all the "nuclei," which was usually 15-30 days. During the time the melt was kept at this temperature, the nuclei of size $r > r_c$ increased in size by $\Delta r = c_0 \tau_c$, where c_0 is their steady growth rate. Their initial distribution, characterized by the function $\psi(r)$, retained its original form, so that after the time interval τ_c the distribution function was represented by the expression $\psi(r + c_0 \tau_c)$. Immediately after this, the sample was placed in an air stream maintained at +40°, and the observations were continued; it was found that n increased further. This increase ceased when a new limiting value ($n_\infty = 60$) was reached. Curve 2 in Fig. 1 represents the second stage in the development of the "nuclei" which grew during time t_c and approached the critical size corresponding to the "development" temperature $t_p = 40^\circ$, i.e.

$$r_p = \frac{2MT_0\sigma}{q_p(T_0 - T_p)} \quad (7)$$

Curve 3 in Fig. 1 refers to longer exposure at t_c of 48 hours: it is evident that during the additional time (after the first exposure) new "nuclei" approached sufficiently in size to $(r_c)_p$; this gave a larger limiting value of $N_\infty = 105^\circ$. To confirm that at the development temperature at 40° the conversion took place as the result as the result of fluctuations, the applicability of the first-order equation (2) was tested, i.e., the relationship between $\log(n_\infty - n)$ and time t was determined. The graph at the top of Fig. 1 shows that this relationship, corresponding to Curves 1 and 2 respectively, is linear.

We now turn to the interpretation of earlier experiments on the development process [5]. These experiments were performed with betol, and involved determinations of the number of crystallization centers in relation to the development temperature t_p° . Each sample was held each time at the same exposure temperature t_e for $\tau_e = 2$ minutes, and then warmed rapidly to temperature t_p° during time $\tau_p \sim 40$ seconds. The temperature variations were recorded by the readings of a sensitive indicating galvanometer in the thermocouple circuit. The thermocouple was immersed in a control sample of the same size as the test sample. Both samples were subjected simultaneously to the same temperature variations. These experiments yielded the empirical relationship [5]: the number of crystallization centers decreases exponentially with increase of the temperature difference $(t_p^\circ - t_e)$.

Experiments were performed at low and high exposure temperatures, on each side of the maximum of the temperature curve.

It was assumed that at the development temperature nuclei are converted into crystallization centers, whereas during exposure at temperature t_e° only "formation" of the distribution function takes place. In a subsequent paper it will be shown that at temperatures above the maximum on the Tammann curve the nuclei are converted into crystallization centers as the result of fluctuations, whereas at temperatures below this maximum, they merely increase in size. It follows that in the former case development is accompanied by a second conversion of nuclei into crystallization centers of greater critical size.

Since in both cases the process has a fluctuation mechanism at the development temperature t_p , it should conform to the kinetic law (2). Since we are not concerned with the complete kinetic curves, but only with the temperature variations of the number \bar{n} of visible crystallization grains, we may apply Equation (6), where $\Delta T = T_0 - T_p$.

In Fig. 2, the abscissa axis represents quantities proportional to $(r_c)_p^2$, i.e., $10^4/(T_0 - T_p)^2$, and the ordinate axis shows $\log \bar{n}$, where \bar{n} is the number of grains corresponding to different temperatures t_p° . These temperatures are also marked along the abscissa axis. The lower graph corresponds to a high exposure temperature, 10.7°, and the upper to a low temperature $t_e = 6.4^\circ$.

Both cases give a good fit with Equation (6), but the experimental points yield not one straight line, but two, intersecting at an obtuse angle. Let us assume that the melt contains two types of impurity particles: in the first type the entire surface is coated with a crystalline layer, and in the second the crystalline material lies in deep cracks or scratches. Growth is much more rapid in the former than the latter, and therefore, particles of the second type are detected only at a sufficiently high development temperature [8]. The first portion of the broken line corresponds to particles of the first type, and the rest, of smaller slope, corresponds to the second type.

SUMMARY

1. After preliminary lengthy exposure of a sample at a lower constant temperature, a kinetic curve is obtained which conforms to an equation of the first-order reaction type. This confirms our earlier hypothesis [7] that crystallization centers consist of particles of active impurities covered by a crystalline layer of the substance.

2. The dependence of the logarithm of the number of crystallization centers on the temperature is a linear function of the work of conversion of an impurity particle into a crystallization center at the development temperature

$$\log n = k_1 - \frac{k_2}{(T_0 - T_p)^2}.$$

3. The linear plot of this function consists of two intersecting portions. The portion corresponding to high development temperatures represents formation of centers in micropores, where the conversion is slower than at lower temperatures, at which the mechanism indicated in Paragraph 1 operates.

LITERATURE CITED

- [1] G. Tammann, *Z. Phys. Chem.*, 25, 441 (1898).
- [2] M. M. Mazhul', Dissertation: The Cavitation Effect and Formation of Crystal Nuclei [In Russian] (Minsk, 1954).
- [3] M. E. Mikhlin, Dissertation: Effect of Pressure on Crystallization of a Supercooled Liquid [In Russian] (Minsk, 1954).
- [4] F. K. Gorski, *Bull. Acad. Sci. Belorussian SSR* No. 6, 117 (1950).
- [5] G. L. Mikhnevich and I. F. Browko, *Sov. Phys.*, 13, 113 (1938).
- [6] G. L. Mikhnevich and V. P. Efimova, *Trans. Odessa State Univ.*, 5, 115 (1954).
- [7] G. L. Mikhnevich, *Colloid J.*, 21, 69 (1959).*
- [8] V. I. Danilov, *Structure and Crystallization of Liquids* [In Russian] (Acad. Sci. Ukrainian SSR Press, 1956).

Received July 17, 1957

* Original Russian pagination. See C. B. Translation.

THE SPECIFIC SURFACE OF CELLULOSE

K. P. Mishchenko, S. L. Talmud and V. I. Yakimova

The Leningrad Technological Institute of the Cellulose and Paper Industry
Chair of Physical and Colloid Chemistry

A knowledge of the specific surface of cellulose is of great practical importance in relation to studies of the main technological processes in the pulp and paper industry.

Cellulose fibers are porous systems in which there are numerous free air-filled spaces between the cells, within the cell walls, and between the individual macromolecules. Most of the existing methods for determination of the specific surface of cellulose are based on the ability of cellulose to adsorb various substances. Isotherms for the adsorption of water vapor by cellulose at various temperatures have been investigated in detail by many workers [1-4]. All their results confirm that the adsorption isotherm is S-shaped and reveal the existence of a hysteresis effect in desorption. A detailed interpretation of the isotherms of adsorption of water vapor by cellulose has been published [1].

Many authors [5-10] consider that it is necessary to distinguish between the surfaces of fibrous materials in the dry and swollen states. By Kiselev's classification [11, 12], cellulose is included with the adsorbents which change their structure in the course of adsorption, especially in the adsorption of substances which swell cellulose fibers (water vapor). Therefore, values of specific surface determined for cellulose in the dry state cannot be identified with values found for fibers in the swollen state. Accordingly, all methods for determinations of the specific surface of cellulose can be divided into two types: determination of specific surface in the dry state (adsorption of nitrogen, argon, spectroscopic methods) and in the swollen state (adsorption of water vapor, adsorption of various substances from aqueous solutions, the ion-exchange method).

Assaff, Haass, and Purves [1], who studied the effects of swelling and drying on the specific surface of cellulose, noted that adsorption of 6-9% moisture increases the surface of strongly swelled cellulose by 70%, while in the case of unswollen cellulose the initial surface is increased 30-fold. They found that the surface of moist swollen cellulose is decreased by 98% as the result of drying.

Clark [13] proposed a method for determination of the specific surface of cellulose by deposition of metallic silver on the fiber surface.

Harris and Purves [14] determined the specific surface of cellulose by treatment with thallium ethylate in ether. It must be noted that their paper contains no data on the characteristics of the cellulose used, or on the method by which it was prepared.

Vickerstaff [15] studied the adsorption of phenol on fibrous materials and found a value of $350 \text{ m}^2/\text{g}$ for the specific surface of cellulose. He assumed that phenol is adsorbed at ester groups, and therefore, each glucose residue can interact with either one or two phenol molecules, dependent on whether one or both acetyl groups are outside the micelle surface. On the assumption that both groups are available for interaction with phenol, he calculated the specific surface of cellulose from the adsorption curve.

Assaff, Haass and Purves [1] studied high-quality defatted linters; they obtained an S-shaped isotherm for adsorption of nitrogen vapor, and used the Brunauer, Emmett, and Teller (BET) method to calculate the specific surface, which is $34.8 \text{ m}^2/\text{g}$ according to their data. They recommend this as a "standard" method for determination of the specific surface of cellulose. (In calculations of the surface the area occupied by one nitrogen molecule was assumed to be 17 \AA^2).

TABLE 1

Experimental and Calculated Data on the Adsorption of Nitrogen Vapor by Standard Cotton Cellulose and Bleached Sulfite RB Pulp

P/P_s		a		$\frac{P/P_s}{(1 - P/P_s) a}$	
Cotton cellulose	RB pulp	Cotton cellulose	RB pulp	Cotton cellulose	RB pulp
Adsorption					
0,072	0,095	0,039	0,010	1,964	10,362
0,131	0,120	0,066	0,011	2,286	12,231
0,159	0,144	0,079	0,012	2,394	14,003
0,229	0,167	0,113	0,014	2,625	15,760
0,290	0,344	0,144	0,026	2,824	20,455
Desorption					
0,246	0,290	0,127	0,021	2,552	18,774
0,193	0,221	0,089	0,017	2,412	16,304

Note. P/P_s is the pressure ratio; a is the amount of nitrogen adsorbed, in micromoles;

$\frac{P/P_s}{(1 - P/P_s) a}$ is the factor in the BET equation.

TABLE 2

Characteristics of the Cellulose Samples*

Cellulose	Ash, %	Moisture, %
Bleached sulfite, viscose	0.038	7.0
Bleached sulfite	0.045	7.8
Unbleached sulfite	0.055	7.4
Bleached sulfate	0.075	8.7
Unbleached sulfate	0.036	7.6

* The characteristics of standard cotton cellulose and of bleached sulfite RB pulp are given earlier in this paper.

Stamm [5] determined the specific surface of cellulose from the heat of wetting; he noted that in the equation

$$\alpha = \frac{-H}{A - \frac{A}{\sigma} \cdot T \cdot \frac{d\sigma}{dT}},$$

(where σ is the surface tension of the liquid; T is the absolute temperature; H is the heat of wetting; A is the adhesion pressure) the value of $\sigma = A$.

Yur'ev and his associates [16] developed a method for determination of the specific surface of cellulose, based on the ion-exchange capacity of fibrous materials, and showed that the exchange capacity of all types of cellulose depends on the pH of the medium and the concentration of the exchanged cation.

Yur'ev used the linear relationship between the amount of cations adsorbed and the solution pH to calculate the specific surface of cellulose by means of the formula:

$$S = b \frac{F^2}{2,303 \cdot CRT}$$

where S is the specific surface of the adsorbent; b is the slope of the straight line; F is the Faraday constant; C is the specific capacity of the electric double layer; R is the gas constant; T is the absolute temperature. By substituting the numerical values of the constants, Yur'ev et al. [16] found a very simple expression for calculation of the specific surface at 15°: $S = 85.10^4 b$, cm²/g.

TABLE 3

Experimental and Calculated Data for Different Celluloses, Determined by the Ion-Exchange Method

pH	Amount of Ca ²⁺ adsorbed, meq/100 g of bone-dry cellulose						
	cotton cellulose	sulfite pulp				sulfate pulp	
		bleached I	bleached viscose	un-bleached	bleached II	un-bleached	bleached
2,09	0,385	1,295	0,883	7,502	2,634	1,741	3,091
3,68	0,674	2,513	2,894	8,652	4,582	3,127	4,553
4,15	0,717	2,875	3,286	9,664	6,324	4,745	4,938
5,52	0,822	3,849	5,013	5,013	11,371	7,518	6,289
Slope factor	0,197	0,753	1,168	1,320	1,712	1,973	0,920
Specific surface, m ² /g	16,74	64,00	99,28	112,2	145,6	167,8	78,2

The purpose of the present investigation was to select the most reliable methods for determination of the specific surfaces of cellulose in the dry and swollen states, to test and compare existing methods experimentally, and to determine the most probable values for the specific surface of standard cotton cellulose and technical wood pulps made by different methods.

The specific surface of cellulose in the dry state was determined by the standard method of adsorption of nitrogen vapor at the boiling point of nitrogen (−195.7°) [17].

The experiments were performed at the boiling point of liquid nitrogen, when adsorption is purely physical in character. The nitrogen pressure did not rise above 1 atmosphere.

The ampoules were calibrated with nitrogen at room temperature.

The specific surface of two types of cellulose was determined: standard cotton cellulose and technical bleached sulfite wood pulp, RB grade.

Standard cotton cellulose was prepared by treatment of technical cotton with rosin soap, with subsequent bleaching by freshly prepared sodium hypochlorite solution and extraction with ether and acetone [18]. The cellulose so obtained had the following composition: α-cellulose, 99.8%; ash, 0.04%; moisture, 7.64%. Technical bleached sulfite RB pulp had the composition: α-cellulose, 94%; ash, 0.042%; moisture, 6.4%.

Table 1 contains the results of determination of the adsorption of nitrogen vapor by standard cotton cellulose and bleached sulfite RB pulp.

Fig. 1 shows experimental isotherms for adsorption of nitrogen vapor per g of bone-dry fiber. In Fig. 2, the adsorption isotherms are plotted in the coordinates of the BET equation. The specific surface of cellulose was calculated from the expression

$$S = N \cdot \omega \cdot a_m,$$

where N is the Avogadro number; ω is the area occupied by one nitrogen molecule, equal to 16.2 \AA^2 ; a_m is the number of nitrogen moles in a monolayer, calculated from the formula $a_m = 1/(a + b)$; a is the intercept cut off by the isotherm along the ordinate axis; b is the slope of the line.

Our value of the specific surface of standard cotton cellulose is $18.94 \text{ m}^2/\text{g}$, and for the specific surface of bleached sulfite RB pulp, $2.23 \text{ m}^2/\text{g}$. The result for standard cotton cellulose is of the same order as the values found previously [1, 7] by adsorption of nitrogen vapor at the boiling point. Technical pulps had not been previously investigated by this method.

In our opinion the most reliable method for determination of the specific surface of cellulose in the swollen state is Yur'ev's ion-exchange method [16]. The results obtained by this method are in good agreement with published values of the specific surface of sulfite pulp determined by other methods. For example, Stamm and Millett [5, 8] determined the specific surface of sulfite cellulose from the adsorption of water ($270 \text{ m}^2/\text{g}$) and from the heat of swelling ($180 \text{ m}^2/\text{g}$).

Yur'ev found the following values for the specific surface of different celluloses: cotton wool, $28.2 \text{ m}^2/\text{g}$; bleached sulfite viscose pulp, $129 \text{ m}^2/\text{g}$; unbleached sulfite pulp, $226 \text{ m}^2/\text{g}$; bleached sulfate pulp, $151 \text{ m}^2/\text{g}$. We used Yur'ev's ion-exchange method [16] to study the following celluloses: standard cotton, sulfite viscose, sulfite bleached RB, sulfite bleached, sulfite unbleached, sulfate bleached, sulfate unbleached. All the samples were treated before the experiments by threefold extraction with 0.1 N HCl solution to remove ash, and dried to the air-dry state (Table 2).

All the samples were kept in closely stoppered jars after demineralization.

Table 3 contains the measured and calculated values of the specific surface of the cellulose samples.

The values of the slope factor b necessary for calculation of the specific surface from the formula $S = 85 \cdot 10^4 b$ were obtained from the graphs in Fig. 3.

It follows from Table 3 that the values found for the specific surface of cellulose are of the same order as V. I. Yur'ev's values.

Of the methods considered above for determination of the specific surface of cellulose the most reliable, in our opinion, are the "standard" method of adsorption of nitrogen vapor, and Yur'ev's ion-exchange method [16].

Methods for determination of specific surface based on chemical reactions of the functional groups in cellulose [11, 12, 13] are of great interest, but the results obtained with them differ sharply from the results given by other methods; moreover, they are in sharp contradiction to many facts which indicate the high value of the specific surface of cellulose. For example, the specific surface of cellulose determined by the silver deposition method [13] is in the range of 0.64 to $1.8 \text{ m}^2/\text{g}$. The method based on the interaction of phenol with ester groups in cellulose [15], on the other hand, gives very high values for the specific surface ($350 \text{ m}^2/\text{g}$).

By our determination, the specific surface of standard cotton cellulose is $18.94 \text{ m}^2/\text{g}$ by the adsorption of nitrogen vapor and $16.74 \text{ m}^2/\text{g}$; i.e., the values obtained for the specific surface by two essentially different methods are in good agreement.

We conclude from this that the widely held view concerning the large difference between the values of the specific surface of cellulose in the dry and swollen states is incorrect in respect of native cellulose fibers.

Our viewpoint is fully consistent with the opinion of Nikitin [19], who considers that native fibers have a more ordered structure and closer packing of the chain molecules, and therefore, the water molecule dipoles cannot penetrate into the oriented regions.

The values obtained by different methods for the specific surface of wood celluloses differ sharply from our value for the specific surface of standard cotton cellulose.

Evidently, in the sulfite and sulfate cooking processes the bleaching and purification of cellulose is accompanied by intensive breakdown of the original fiber structure, loosening and disorientation, which influences the physicochemical properties and reactivity of the fibrous materials. When cellulose with a partially broken-

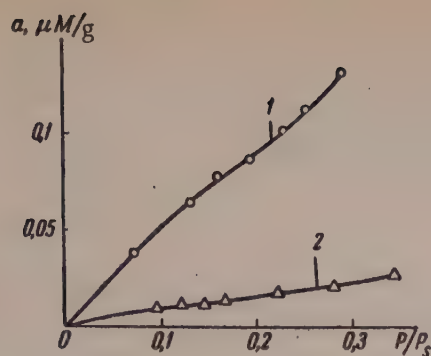


Fig. 1. Isotherms for adsorption of nitrogen vapor at the boiling point by cellulose samples: 1) standard cotton cellulose; 2) bleached sulfite RB pulp.

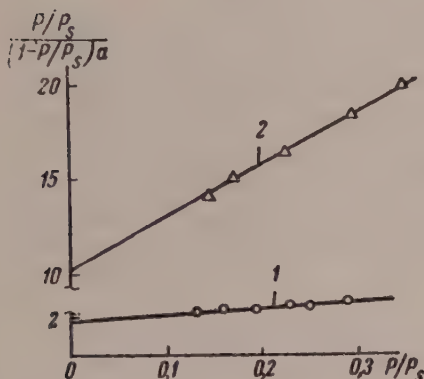


Fig. 2. Isotherms for adsorption of nitrogen vapor at the boiling point, in BET coordinates: 1) standard cotton cellulose; 2) bleached sulfite RB pulp.

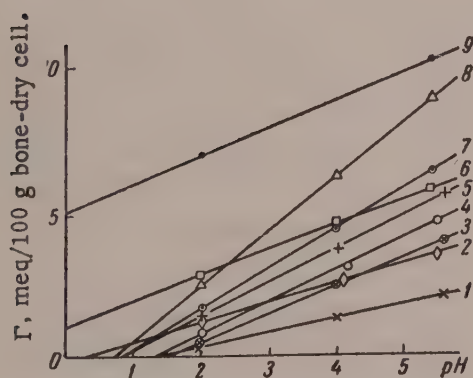


Fig. 3. Variation of the ion-exchange capacity (T, meq/100 g of bone-dry cellulose) with pH of 0.1 CaCl_2 solution, for different celluloses: 1, 2) bleached sulfite RB pulp; 3, 4) bleached sulfite, viscose; 5) unbleached sulfite I and II; 6) bleached sulfate; 7) unbleached sulfate.

down structure is dried, its density increases and porosity decreases; according to our data, the specific surface of bleached sulfite cellulose, determined by adsorption of nitrogen vapor, is $2.23 \text{ m}^2/\text{g}$.

When wood cellulose with partially broken-down structure swells, the internal active surface becomes considerably larger than in the native fibers.

The specific surface of technical wood pulps, determined by the ion-exchange method, varies between 100 and $200 \text{ m}^2/\text{g}$. The specific surface depends on the process and actual conditions used for the production of cellulose. Our data are in good agreement with Yur'ev's determinations.

Thus, the differences between the values of the specific surface of wood pulps determined in the dry state by adsorption of nitrogen vapor and in the swollen state by the ion-exchange method are caused not by swelling but by differences between the internal structure of wood pulp and that of the native fibers.

SUMMARY

1. Different methods for determination of the specific surface of cellulose were compared; the "standard" method of adsorption of nitrogen vapor and the ion-exchange method were found to be the most reliable.

2. The specific surface of standard cotton cellulose as determined by these methods is $16\text{--}19 \text{ m}^2/\text{g}$. The results obtained by the two methods are in good agreement.

3. Swelling in water does not influence the specific surface of plant fibers.

4. Wood pulps made by different processes differ sharply from native fibers in internal structure. The specific surface of wood pulps is $2\text{--}2.5 \text{ m}^2/\text{g}$, and in the swollen state it is $100\text{--}200 \text{ m}^2/\text{g}$.

The authors are deeply grateful to Professor A. V. Kiselev for the opportunity of carrying out determinations in the nitrogen adsorption apparatus and for his constant interest in the work.

LITERATURE CITED

- [1] A. G. Assaff, P. G. Haass and C. B. Purves, J. Amer. Chem. Soc., 66, 1, 66 (1944).
- [2] C. C. Houtz and D. A. McLean, J. Phys. Chem., 43, 309 (1939).
- [3] A. Stamm, Pulp and Paper Mag. Canada 51, 10, 90 (1950).
- [4] E. Filbu and O. Maass, Canad. J. Res., 13, 1 (1935).

- [5] J. Stamm, in the book: Wood Chemistry (edited by E. Wise) (1944) p. 449.
- [6] A. P. Zakoshchikov, Nitrocellulose [In Russian] (Defense Press, 1950), pp. 18, 275.
- [7] J. Escard, E. Girardy and A. Bisson, J. chim. phys. et phys.-chim. biol., 48 (1951).
- [8] J. Stamm and A. Millett, J. Phys. Chem., 45, 43 (1941).
- [9] H. Grotjahn and K. Hess, Kolloid-Z. 129, 128 (1952).
- [10] O. Howell and A. Jackson, J. Chem. Soc., 979 (1937).
- [11] A. V. Kiselev, Dissertation [In Russian] (Moscow, 1950).
- [12] A. V. Kiselev, J. Phys. Chem., 23, No. 9, 1018 (1949).
- [13] J. Clark, Paper Trade J., 115, 1, 32 (1942).
- [14] A. Harris and C. B. Purves, Paper Trade J., 110, 29 (1940).
- [15] T. Vickerstaff, The Physical Chemistry of Dyeing (1956) p. 366 [Russian translation].
- [16] V. I. Yur'ev, Trans. Central Sci. Res. Inst. Paper 37, 83 (1948).
- [17] A. V. Kiselev, J. Phys. Chem., 25, 10 (1951).
- [18] V. M. Nikitin, Chemistry of Wood and Cellulose [In Russian] (1951) p. 193.
- [19] N. I. Nikitin and N. I. Klenkova, J. Appl. Chem., 27, 171 (1954).*

Received October 3, 1957

*Original Russian pagination. See C. B. Translation.

EFFECT OF LOW TEMPERATURE ON THE VOLUME AND STABILITY OF FOAM

S. G. Mokrushin and L. G. Zhidkova

The S. M. Kirov Polytechnic Institute of the Urals, Sverdlovsk

Most investigations of foam properties have been concerned with the effects of the concentration or nature of the foaming agent on foam stability. There is little information in the literature on the effect of temperature on foam stability. Although there are data in the literature on the effect of high temperature on foam properties [1], there is very little on the influence of low temperatures on formation of foams in aqueous solutions, whereas foam formation and stability depend not only on the nature of the surface-active agent and the method of formation but also to a considerable extent on the temperature. Changes of temperature inevitably lead to changes of surface tension, which has a significant role in the formation of stable foams, and at low concentrations the variations of surface tension with temperature are complex in character, as both the surface tension and adsorption conditions alter [2, 3].

The majority of investigations have dealt with studies of foam formation in relation to temperature in systems consisting of organic liquids [1, 4], although the question of the influence of low temperatures on foam formation in solutions of inorganic substances is not less important, especially in fire fighting. The winter charges in foam-type extinguishers are designed for -18 and -23° [5], which is clearly unsuitable for the prevailing conditions in the northern regions of our country. Therefore, studies of the conditions of foam formation and stability at lower temperatures are of great practical importance.

The purpose of the present investigation was to study the formation and stability of foams formed from aqueous calcium chloride solution in the temperature range from $+23$ to -37° .

Before the investigations of foam stability it was necessary to select a vessel of suitable diameter. It has been shown by Rebinder and Savitskaya [6] that variations of the foam-air (vapor) interfacial area greatly influence foam stability. We prepared foams in vessels of different diameters. The kinetic curves representing the spontaneous collapse of foam, presented in Fig. 1, show that the greater the vessel diameter, the lower is the foam stability. A measuring cylinder 59 mm in diameter was used in our experiments for determinations of foam volume and stability.

Solutions of low freezing points were used for production of foams at low temperatures (see table).

The foams were formed in a one-liter cylinder contained in a thermostat with freezing mixture. The freezing mixtures used were: down to -20° , a mixture of snow and NaCl in definite weight proportions, and for temperatures below -20° , a mixture of $\text{CaCl}_2 \cdot 6\text{H}_2\text{O}$ and snow in definite weight proportions [7].

Chalk and finely ground malt (foaming agent) were added to CaCl_2 solution. The resultant suspension was stirred thoroughly and added to sulfuric acid. Before, they were mixed, the acid and the suspension of chalk and malt in calcium chloride solution were cooled to the required temperature in a thermostat with freezing mixture. The suspension was then added to the acid, and the foam temperature, volume, and stability were determined. In the first experiments spontaneous foaming (without the use of stirring) was observed. For this, a suspension of 3.6 g CaCO_3 (pure) and 1 g of malt in CaCl_2 solution (sp. gr. 1.28) was added to 3 ml H_2SO_4 (sp. gr. 1.58).

Characteristics of the Solutions Studied

Solutions studied	Density	Freezing point, °C
H ₂ SO ₄ [7]	1.58	below -40
HCl [8]	1.149 (30%)	below -50
CaCl ₂ [9]	1.28 (29%)	-50.1

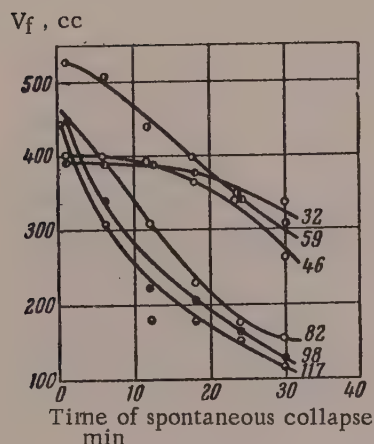


Fig. 1. Effect of vessel diameter on foam volume (V) and stability; the numbers on the curves represent vessel diameters in mm.

In spontaneous foaming, when the temperature is lowered from +18 to -35°, the volume of foam formed is decreased considerably, but its stability is appreciably increased, as is clear from the data in Fig. 2.

It is known [2] that increase of foam stability on decrease of temperature may be due to increased adsorption of the surface-active agent as the result of the salting-out effect. The foam formed at room temperature (18°), 375 cc in volume, collapsed in 90 minutes, whereas at -17°, the foam volume was slightly reduced to 350 cc and after 190 minutes only 150 cc of the foam was lost.

At temperatures below -20° foam is hardly formed at all if the suspensions are not stirred. Therefore, in the subsequent experiments after the suspension had been added to the acid the mixture was stirred until the maximum volume of foam had been formed. When sulfuric acid is mixed with a suspension of chalk (or pure CaCO₃) and foaming agent in CaCl₂ solution, heat is given out as the result of chemical reaction, and the temperature therefore rises by 7-10° above the temperature of the original solutions.

At low temperatures and with stirring foam is not formed at once [3], but some time after the components have been mixed; from 20 seconds for initial solutions at -25° to 90 seconds for initial solutions at -45°. The effect of temperature on foam volume is shown in Fig. 3.

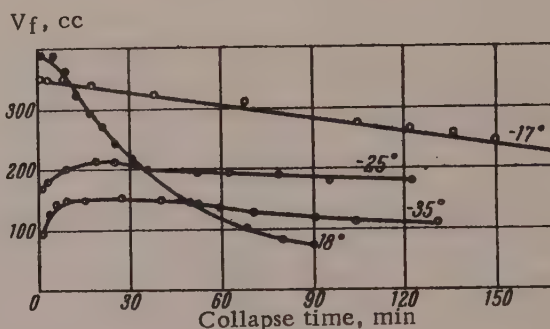


Fig. 2. Spontaneous collapse of foam with decrease of temperature.

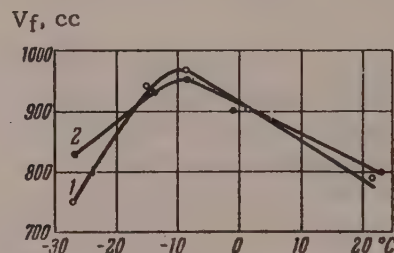


Fig. 3. Change of foam volume with decrease of temperature in the interaction of 6 ml of H₂SO₄ (sp. gr. 1.58) with suspensions formed from: 1) 8 g chalk and 2 g malt in 80 ml CaCl₂ solution (sp. gr. 1.28); 2) 9 g chalk and 2 g malt in 80 ml CaCl₂ solution.

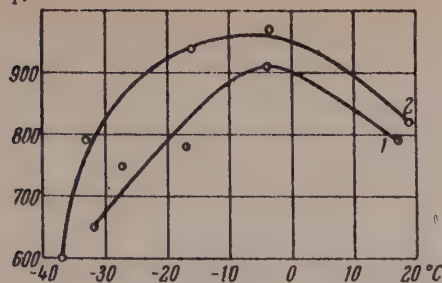


Fig. 4. Change of foam volume with decrease of temperature in the interaction of HCl with suspensions formed from: 1) 7.5 g chalk and 2 g malt in 80 ml CaCl_2 solution; 2) 8 g chalk and 2 g malt in 80 ml CaCl_2 solution.

The greatest foaming in the interaction of the suspension with sulfuric acid is observed in the temperature range from -5 to -14° . In our opinion, this is because when the temperature is lowered to -12 or -14° , the foam viscosity increases considerably; the films surrounding the foam-bubble cells acquire a mobile elastic structure and thus, the foam bubbles formed in this temperature range do not burst during foam formation. On further decrease of temperature the surface layers surrounding the bubbles become brittle and foam formation is accompanied by breakdown of a large number of bubbles, which accounts for the considerable decrease of volume at low temperatures. The foam column formed at a low temperature (below -15°) itself has considerable stability, which is greater at lower temperatures, but the slightest touch or agitation results in immediate collapse of the whole column of foam.

To reduce the time interval between the mixing of the components and the start of foaming at low temperatures, the more active hydrochloric acid of sp. gr. 1.149 (30%) was used. The results of experiments with foam prepared in this manner are presented in Fig. 4. The greatest foaming in this case was observed between -4 and -5° . The foam temperature rose by only $3-5^\circ$ over the temperature of the initial solutions; the time interval between the mixing of the components and foaming was shortened to 3 seconds at room temperature and to 25 seconds at low temperatures.

SUMMARY

1. When a suspension of chalk in calcium chloride solution containing a foaming agent is mixed with sulfuric or hydrochloric acid at low temperatures, there is virtually no foaming unless the mixture is stirred.
2. At low temperatures foam is not formed at once, but some time after the components have been mixed; this time interval is longer at lower foam-formation temperatures.
3. Foam stability increases with decrease of temperature.
4. At temperatures below -15° the surface layers surrounding the bubbles have brittle structure.

LITERATURE CITED

- [1] G. O. Erchikovskii, Formation of Flotation Foam [In Russian] (GONTI, 1939).
- [2] V. K. Semenchenko and A. F. Gracheva, J. Phys. Chem., 6, 49 (1935).
- [3] V. A. Naumov, Colloid Chemistry [In Russian] (State Chem. Tech. Press, 1932).
- [4] B. Ya. Teitel'baum, Colloid J., 12, 375 (1950).
- [5] Brief Rules for the Use and Charging of Manual Fire Extinguishers [In Russian] (Ministry of Municipal Economy, 1950).
- [6] E. M. Savitskaya and P. A. Rebinder, Colloid J., 13, 200 (1951).
- [7] Chemist's Handbook [In Russian] (Goskhimizdat, 1954) p. 449.
- [8] Landolt-Börnstein, Phys.-Chem. Tabellen 1, 490 (1920).
- [9] Yu. V. Karyakin, Pure Chemical Reagents [In Russian] (Goskhimizdat, 1947).

Received July 3, 1957

PREPARATION OF FERRIC HYDROXIDE GELS OF DIFFERENT PORE STRUCTURES, AND THEIR ADSORPTIONAL PROPERTIES

I. E. Neimark and I. B. Slinyakova

The L. V. Pisarzhevskii Institute of Physical Chemistry, Academy of Sciences
Ukrainian SSR, Kiev

Gels of hydrated iron oxides catalyze many chemical reactions [1]; they accelerate hydrogenation, cracking, oxidation, and other processes. In some instances ferric hydroxide gels may be used as adsorbents for gases, vapors, and dissolved substances [2-5]. Perry [2] found that acetone, chloroform, butyl alcohol, carbon tetrachloride, benzene, isobutyl alcohol, and sulfur dioxide were adsorbed to a considerable extent from their saturated vapors on ferric hydroxide. Adsorption of ammonia and carbon monoxide on ferric hydroxide gel was studied by Emmett and Love [3]; they found that if the gel is heated above 550° its adsorptive capacity falls sharply. Lambert and Clark [4] determined isotherms for the sorption of benzene on ferric hydroxide gel. Ferric hydroxide gel effectively adsorbs oxalic acid from solution [5]. Zaprometov and Virskaya [6] found that sorption of water and benzene vapor by coagulated $\text{Fe}(\text{OH})_3$ depends on the hydrophilic characteristics of the latter.

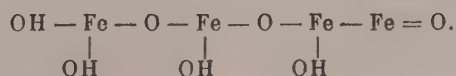
The adsorptional and catalytic properties of ferric hydroxide gels are determined to a considerable extent by the nature of their porosity, and therefore, it is very important to be able to prepare such gels with predetermined porosity. There have been very few investigations of this problem. We therefore undertook a study of the influence of the preparation conditions of ferric hydroxide gels on their structure and adsorptional properties.

In preparation of ferric hydroxide gels differing in pore structure we were guided by our theoretical concepts [7, 8] of the mechanism of structure formation in hydrophilic adsorbents. According to these concepts, structure formation in hydrophilic adsorbents is strongly influenced, on the one hand, by capillary forces, which depend on the surface tension of the intermicellar liquid and the wetting of the capillary walls by it, and on the other, by the degree of aggregation of the particles into chains and clusters during aging of the gel.

In the present investigation, we studied the influence of the precipitation medium, the aging temperature of the precipitate, and the nature of the intermicellar liquid on the pore structure and adsorptional properties of ferric hydroxide gels.

Methods for preparation and investigation of ferric hydroxide gels. Ferric hydroxide was prepared by Belotserkovskii's method [9, 10], by addition of ammonia solution to ferric chloride solution. The definite volume of ammonia solution necessary for precipitation of ferric hydroxide was added slowly, with stirring, to ferric chloride solution at room temperature. A flocculent precipitate of ferric hydroxide was formed as the ammonia was added.

According to Krause [11], primary ferric hydroxide particles are molecules consisting of groups of four iron atoms with the structure



These molecules polymerize to form groups containing 40-50 iron atoms (with orientation with respect to 40-50 iron atoms). Dumanskii [12] determined the molecular weight of colloidal ferric hydroxide, and found it to be 3122.

TABLE 1

Structural and Adsorptional Characteristics of Ferric Hydroxide Gels Prepared From Suspensions of Different pH

Series	Sample	pH of suspension	Apparent density, g/cc	Pore volume, cc/g		Specific surface, m ² /g
				total	sorptional	
I	1	10,0	1,60	0,38	0,39	
	2	9,6	1,87	0,28	0,30	
	3	6,8	2,15	0,22	0,15	
	4	5,3	2,34	0,17	0,19	
II	12	10,0	1,73	0,33	0,34	106
	13	9,6	2,0	0,25	0,27	75
	14	8,9	2,07	0,24	0,25	78
	5	6,3	2,20	0,21	0,20	32

TABLE 2

Effect of Aging Conditions of Hydrogel Precipitates on Total Porosity of Ferric Hydroxide Gels

Sample	pH of suspension	Aging temperature of precipitate, deg	Apparent density, g/cc	Total pore volume, cc/g
1a	10.0	20	1.74	0.32
1b	10.0	20.8	1.60	0.38
1c	10.0	100	1.57	0.39
2a	9.6	20	2.00	0.25
2b	9.6	20.8	1.87	0.29

TABLE 3

Effect of Replacement of the Intermicellar Liquid by Isobutyl Alcohol or Benzene on the Structural and Sorptional Characteristics of Ferric Hydroxide Gels

Series	Samples	Suspension pH	Intermicellar liquid in hydrogel	Apparent density, g/cc	Pore volume, cc/g			Specific surface from BET equation, m ² /g
					total	sorptional	macro-pores	
I	5	6,3	Water	2,20	0,21	0,20	—	32
	6	6,3	Isobutyl alcohol	0,71	1,16	0,83	0,33	—
	8	9,6	Water	2,06	0,24	0,24	—	—
II	11	9,6	Benzene	1,34	0,49	0,48	—	—
	12	9,6	Isobutyl alcohol(dried for 2 days)	0,65	1,31	1,22	0,10	—
	9	9,6	Isobutyl alcohol	0,47	1,88	1,27	0,41	—
	10	9,6	Isobutyl alcohol	0,47	1,88	1,28	0,40	185
III	12	10,0	Water	1,73	0,33	0,35	—	106
	12a	10,0	Isobutyl alcohol	0,52	1,66	1,08	0,58	—
IV	13	9,6	Water	2,00	0,25	0,27	—	75
	13a	9,6	Isobutyl alcohol	0,85	0,93	0,73	0,20	71
V	14	8,9	Water	2,07	0,24	0,25	—	78
	14a	8,9	Benzene	1,66	0,36	0,36	—	71
VI	15	5,7	Water	2,06	0,24	0,23	—	67
	15a	5,7	Benzene	1,39	0,47	0,44	—	85
	15b	5,7	Isobutyl alcohol	0,85	0,93	0,70	0,23	214

Levina and Ermolenko [13] found by observation under the electron microscope that at the instant of formation of ferric hydroxide hydrogel spherical particles are formed, which subsequently condense and crystallize.

Our suspension was aged for two days, after which the settled precipitate was washed by decantation with distilled water to a negative reaction for chloride in the wash waters. The washed precipitate was filtered off on a Büchner funnel, molded into cylinders, and dried at room temperature to 60-70% moisture content. The dehydration conditions were varied in accordance with the problem in hand. In some cases the hydroxide dehydrated at 100°, while in others the intermicellar liquid of the hydrogel was replaced by a liquid of low surface tension, as compared with water, with subsequent removal of both liquids at 150-200°.

The resultant gels were characterized by their total porosity, found from the difference of the reciprocals of the apparent and true densities and static activity for benzene vapor at $p/p_s = 1.0$; for the most typical samples, isotherms for sorption and desorption of methyl alcohol were determined by means of a vacuum apparatus with a spring balance.

Influence of precipitation medium on pore structure of ferric hydroxide gels. We found earlier [14] that the reaction of the medium in precipitation of chalky silica gels has a very strong influence on their pore structure. It seemed likely that differences in the precipitation medium should also influence pore structure in the preparation of ferric hydroxide gels. For investigation of this question, three series of samples were prepared differing in the pH of the suspension. The reaction of the precipitation medium was varied by additions of different amounts of 0.1 N hydrochloric acid to definite volumes of 0.55 N ferric chloride, the required volume of 20% ammonia being then added slowly. The pH of the suspensions was determined by means of the antimony electrode.

Attempts to prepare ferric hydroxide from an acid medium at $\text{pH} < 4$ were not successful, as the precipitate is peptized under such conditions.

The structural and sorptional characteristics of ferric hydroxide gels prepared from suspensions of different pH are given in Table 1.

It follows from Table 1 that when the pH of the precipitation medium is raised from 5.3 to 10, the total and sorptional pore volumes of ferric hydroxide gels are approximately doubled.

Fig. 1 shows that the isotherm for Sample 12, precipitated in an alkaline medium, lies higher at high values of p/p_s . Consequently, an alkaline medium favors formation of gels with a large volume of intermediate pores. The specific surface of these ferric hydroxide gels is not large.

Effect of aging temperature of the precipitate on the porosity of ferric hydroxide. It was shown [15, 16] that increase of the aging temperature of precipitated silicic acid hydrogels leads to formation of more coarsely-porous silica gels. It was of interest to determine how the aging temperature of a ferric hydroxide precipitate influences total porosity of the gel. Washed hydrogel Sample 1 (See Table 1) was divided into three portions: one portion was aged at room temperature ($20 \pm 1^\circ$); another was aged first at 20° for 24 hours and then at 80°, and the third portion was aged at 100°. Hydrogel Sample 2, was divided into two portions, one of which was aged at 20°, while the other was aged first at 20° and finally dried at 80°.

The aging conditions of the hydrogel precipitates and the total porosities of the gels are given in Table 2.

It is clear from Table 2 that increase of the aging temperature of the precipitate increases the total pore volume somewhat.

Effect of the nature of the intermicellar liquid in the hydrogel on pore structure of ferric hydroxide gels. Several series of ferric hydroxide samples were prepared for studying the influence of the nature of the intermicellar liquid on pore structure. The pH values of the suspensions were determined in the preparation of each series. The aged and washed precipitates were divided into several portions each, and dried at room temperature; one portion of each (the control samples) was dried at 100°, while in the other portions, the intermicellar liquid was replaced by isobutyl alcohol or benzene.

Table 3 contains details of preparation conditions and the structural and sorptional characteristics of ferric hydroxide samples in which the intermicellar liquid has been replaced by isobutyl alcohol or benzene. The structural characteristics of the control samples are also given, for comparison.

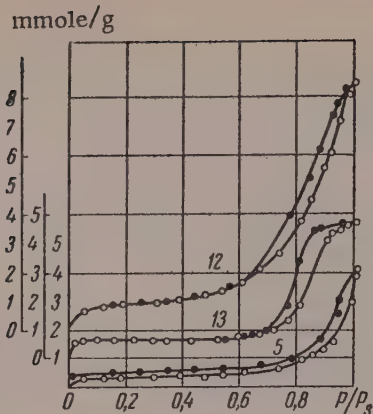


Fig. 1. Isotherms for sorption of methyl alcohol vapor by gels No. 5, 13, and 12, prepared from suspensions of pH 6.3, 9.6, and 10.0 respectively; black circles represent desorption.

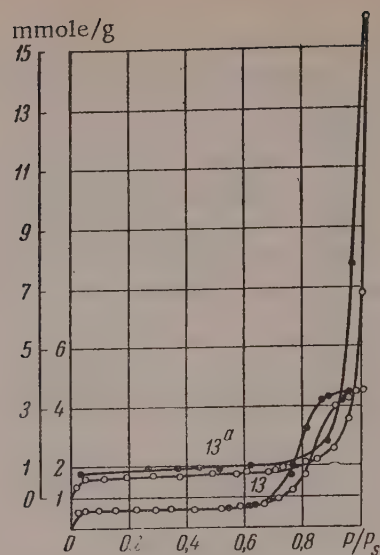


Fig. 2. Isotherms for sorption of methyl alcohol vapor on gel Samples No. 13 and 13 a; black circles represent desorption.

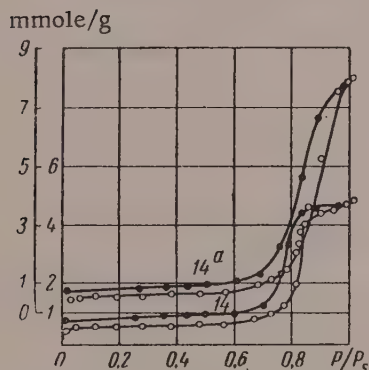


Fig. 3. Isotherms for sorption of methyl alcohol vapor on gel Samples No. 14 and 14 a; black circles represent desorption.

It follows from Table 3 that when the intermicellar liquid in the hydrogels is replaced by isobutyl alcohol, gels of a high total porosity are formed. The total pore volume increased 5 to 6-fold in comparison with the control samples, and the sorptional pore volume increased 2 to 3-fold; macropores also appeared, although their absolute volume was not large. The specific surface of these ferric hydroxide gels were not large.

When water in the hydrogels is replaced by benzene, the gels formed have approximately double the porosity and sorptional pore volume of the control samples (8 and 11; 14 and 14 a; 15 and 15 a). There were no macropores in these samples.

Thus, the total porosity of ferric hydroxide gels

can be increased severalfold by replacement of the intermicellar liquid in the hydrogels by isobutyl alcohol or benzene.

Isotherms for sorption and desorption of methyl alcohol vapor by these gels are given in Fig. 2, 3 and 4.

Examination of the sorption isotherms for control samples and for gels in which the intermicellar liquid was replaced by liquids of low surface tension as compared with water, leads to the conclusion that the resultant gels do not contain any fine pores (micropores), because all the isotherms lie close to the abscissa axis over almost the whole range of pressure ratios (up to 0.8). The curves begin to ascend steeply only at p/p_s from 0.8 to 1.0; the isotherms for samples treated with the surface-active substances rise to a much higher level than the isotherms for the control samples. This shows that the volume of the intermediate pores is large. Evidently, only the volume of the intermediate pores can be varied by this method.

It should be noted that in some instances the adsorption and desorption branches do not coincide. This is probably because of chemical interaction of methyl alcohol molecules with the gel surface.

These samples can be arranged in a series in order of increasing total pore volume.

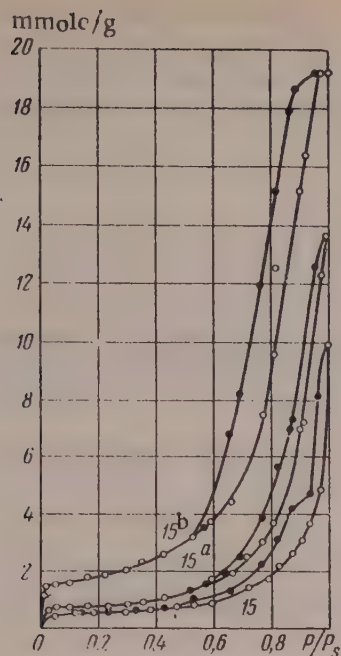


Fig. 4. Isotherms for sorption of methyl alcohol vapor on gel Samples No. 15, 15 a, and 15 b; black circles represent desorption.

A range of ferric hydroxide gels of different porosities is listed in Table 4.

Thus, a range of gels of total porosities from 0.17 to 1.88 cc/g was obtained.

Fig. 5 shows isotherms for the sorption of methyl alcohol vapor on some of the gel samples of this series. It follows from Fig. 5, that the variations of gel porosity are due mainly to increases in the number of intermediate pores.

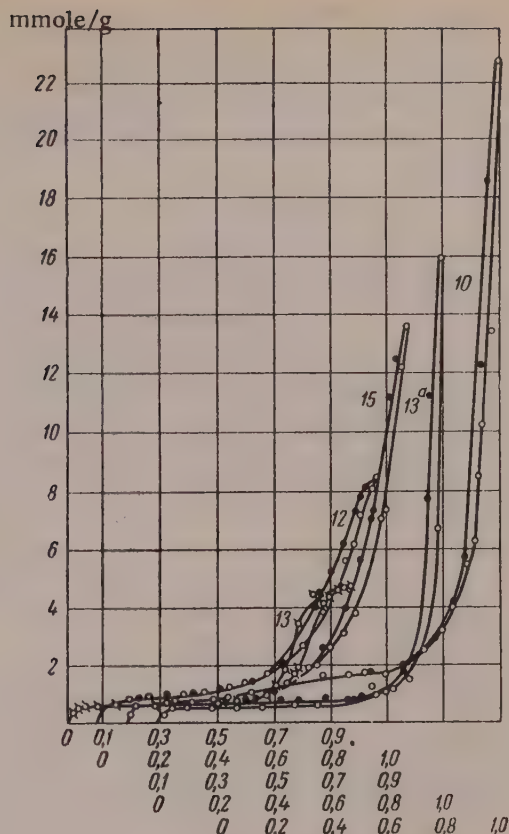


Fig. 5. Isotherms for sorption of methyl alcohol vapor on a number of ferric hydroxide gels; black circles represent desorption; values of P/P_s along the abscissa axis.

TABLE 4

Range of Ferric Hydroxide Gels of Different Porosities

Sample	Apparent density, g/cc	Pore volume, cc/g		Specific surface, m ² /g
		total	sorptional	
4	2,34	0,17	0,19	—
14	2,06	0,24	0,25	78
13	2,00	0,25	0,27	75
2	1,87	0,29	0,30	—
12	1,73	0,33	0,34	—
14a	1,66	0,36	0,36	71
1	1,60	0,39	0,39	—
15a	1,39	0,47	0,44	85
15b	0,85	0,93	0,73	214
6	0,72	1,16	0,79	—
12x	0,65	1,31	1,22	—
9,10	0,47	1,88	1,28	185

It follows from these results that the influence of principal factors (surface tension of the intermicellar liquid, aging temperature of the precipitate, pH of the suspension, etc.) on the pore structure of ferric hydroxide gels is analogous to the influence of the same factors on the structure of silica gels. It is probable that the main points of our theory of the formation of porous structures in hydrophilic adsorbents are also applicable to ferric hydroxide gels.

SUMMARY

1. The structure and sorptional properties of ferric hydroxide gels depend on the conditions of their preparation.

2. The influence of various factors on the nature of the porosity of silica gels and of ferric hydroxide gels respectively is analogous. It is shown that the fundamental concepts of our theory of the mechanism of structure formation in hydrophilic adsorbents are applicable to ferric hydroxide gels.

3. Methods have been worked out for preparation of a range of ferric hydroxide gels with total porosities from 0.17 to 1.88 cc/g.

LITERATURE CITED

- [1] S. Berkman, J. C. Morrell and G. Egloff, *Catalysis, Inorganic and Organic* (State Fuel Tech. Press, Moscow-Leningrad, 1949) [Russian translation].
- [2] J. H. Perry, *J. Phys. Chem.*, 29, 1462 (1925).
- [3] P. H. Emmett and K. S. Love, *J. Phys. Chem.*, 34, 54 (1930).
- [4] B. Lambert and A. Clark, *Proc. Roy. Soc.*, 117, 183 (1927); 122, 511 (1929).
- [5] A. S. Shakhov, *Colloid J.* 2, 215 (1936).
- [6] G. M. Virskaya, Author's Summary of Dissertation [In Russian] (1953); B. G. Zaprometov and G. M. Virskaya, *Colloid J.* 10, 339 (1948).
- [7] I. E. Neimark, *Progr. Chem.*, 25, 748, (1956).
- [8] I. E. Neimark and R. Yu. Sheinfain, *Colloid J.*, 15, 145 (1953).
- [9] E. V. Alekseevskii, *General Course of Defense Chemistry* [In Russian] Part 1 (Leningrad, 1935).*
- [10] E. V. Alekseevskii, G. M. Belotserkovskii and T. F. Plachenov, *Practical Work on Defense Chemistry* [In Russian] (Defense Press, Moscow, 1940).
- [11] S. Krause, *Z. anorgan. und. allgem. Chem.*, 204, 20 (1932).
- [12] A. V. Dumanskii, *J. Russ. Phys.-Chem. Soc.*, 43, 546 (1911).
- [13] S. A. Levina and N. F. Ermolenko, *Colloid J.* 17, 287 (1955).*
- [14] I. E. Neimark and I. B. Slinyakova, *Colloid J.* 15, 277 (1953). *
- [15] I. E. Neimark and F. I. Khatset, *Colloid J.* 9, 289 (1947).
- [16] V. S. Veselovskii and I. A. Selyaev, *J. Phys. Chem.*, 6, 1171 (1935).

Received November 15, 1957

*Original Russian pagination. See C. B. Translation.

VARIATIONS OF THE STRUCTURE AND ADSORPTION ACTIVITY OF ALUMINUM HYDROXIDE WITH THE CONDITIONS OF ITS FORMATION

M. A. Piontkovskaya, Ya. V. Zhigailo, L. A. Eremenko
and I. E. Neimark*

The L. V. Pisarzhevskii Institute of Physical Chemistry, Academy of Sciences
Ukrainian SSR, Kiev

Metal hydroxides are widely used in modern industry as catalysts and adsorbents. It is known that, with a constant chemical composition, the adsorption capacity, selectivity, and catalytic activity of a substance may vary within wide limits according to its origin. At the present time, most authors tend to believe that variations of selective action and catalytic and adsorption activity of different substances are caused mainly by changes of their pore structure in the course of their formation [1].

Noteworthy in this connection are investigations of the properties of metal hydroxides, the structure of which alters with the time of aging under the layer of mother liquor. The literature contains publications on variations of the chemical, catalytic, and other properties of metal hydroxides during aging [2]. However, there is little information in the literature on variations of the adsorption activity of metal hydroxides in relation to aging in the mother liquor [3].

In the present investigation, the adsorption and x-ray structural methods were used to study the adsorption activity, dispersity, and structure of aluminum hydroxide at the instant of its formation and after it had been left in contact with the mother liquor for different times.

Preparation of aluminum hydroxide and study of its structure and adsorption activity. Aluminum hydroxide gels were prepared by the mixing of equal volumes of 1 N solutions of aluminum sulfate and caustic soda. The aluminum hydroxide was left in contact with the mother liquor for different periods of time. The precipitates were then pressed out to remove mother liquor and washed thoroughly with distilled water to remove salts. The salt-free hydroxide was molded into cylinders and dried at room temperature. The structure of the adsorbents so formed was studied with the aid of isotherms for adsorption of benzene vapor, determined in an apparatus with a quartz spring balance. The specific surfaces of the samples and the predominant pore size were calculated from the data on adsorption of benzene vapor. The total pore volume was calculated from the differences between the reciprocals of the true and apparent densities, to characterize the pore structure.

Table 1 gives the aging time of the alumina gels, the total pore volume, adsorption capacity determined from data on adsorption from saturated vapor, specific surface, and the most probable pore radius for five alumina gel samples.

Isotherms for adsorption and desorption of benzene vapor by the same samples are presented in Fig. 1.

It follows from Fig. 1 and Table 1 that aging of aluminum hydroxide gel affects its adsorption activity. At the instant of its formation, aluminum hydroxide is a very active adsorbent; its adsorption capacity and effective pore radius decrease with progressive aging. It is probable that freshly-prepared aluminum hydroxide consists

*L. P. Shikina assisted in the adsorption determinations.

TABLE 1

Adsorption Characteristics of Alumina Gels

Sample no.	Aging time, days	Apparent density, g/cc	Volume of adsorbed benzene at $p/p_s = 1$, cc/g		Total pore volume, cc/g	Sp. surface, by BET, m^2/g	Effective pore radius, A
			in desiccator	from isotherm			
903	0	0.55	1.43	1.26	1.53	46	205
904	1	0.63	1.21	1.11	1.30	44	190
905	2	0.71	1.03	0.95	1.12	—	145
906	10	1.06	0.49	0.43	0.65	37	150
907	45	1.53	0.19	0.17	0.36	20	40

TABLE 2

Interplanar Spacings and Reflection Angles for Three Alumina Gel Samples.

Alumina gel sample No.	Line No.	$\sin \theta$	d exptl.	d from tables
907	1	0,3264	2,358	2,378
	2	0,4083	1,885	1,919
	3	0,5314	1,448	1,458
	4	0,6704	1,148	1,145
906	1	0,3239	2,376	2,378
	2	0,4115	1,870	1,919
	3	0,5348	1,440	1,458
905	1	0,3239	2,376	2,378
	2	0,4083	1,887	1,919
	3	0,5329	1,444	1,458

TABLE 3

Positions of Lines on the x-Ray Patterns of Corundum and of Alumina Gel Heated to 900°

Line No.	S for alumina gel heated to 900°	S for corundum	Line No.	S for alumina gel heated to 900°	S for corundum
1	29.35	29.35	6	62.25	64.85
2	40.20	20.00	7	69.30	69.05
3	42.80	43.03	8	75.55	74.90
4	49.40	49.25	9	77.30	76.95
5	59.90	59.50	10	87.20	86.60

of amorphous particles. The structural changes which take place in it during aging in the mother liquor are probably associated with condensation and crystallization of the gel in the course of aging. These changes are reflected especially clearly in the variations of the apparent density and sorption capacity with aging time: the apparent density of alumina gel (δ) increases during aging, whereas the sorption capacity (V_s) at $P/P_s = 1$ diminishes. (See Fig. 2).

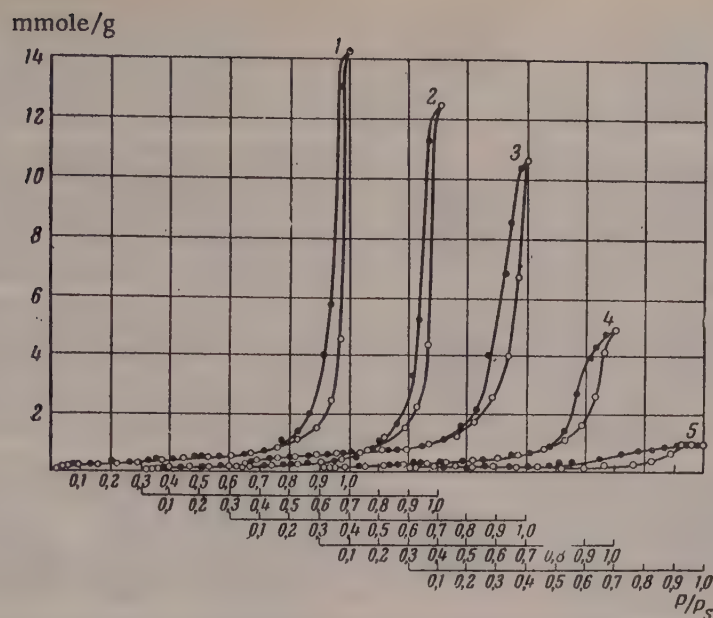


Fig. 1. Isotherms for adsorption of benzene vapor at 20° on alumina gels: 1) No. 903; 2) No. 904; 3) No. 905; 4) No. 906; 5) No. 907

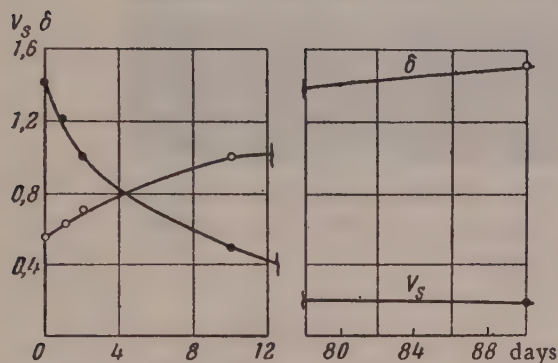


Fig. 2. Variations of apparent density (δ) and sorption capacity (V_s) of alumina gels with time of aging in the mother liquor.

patterns. The diffraction rings of the latter are so diffuse that they could not be indexed. These samples are practically amorphous.

Samples No. 905, 906, and 907 give fairly sharp diffraction rings, although the rings are somewhat broadened, indicating that these samples are microcrystalline. The half widths of the rings decrease appreciably from Sample No. 905 to Sample No. 907, i.e., the crystallites increase in size during aging. Table 2 gives values of $\sin \vartheta$ (ϑ is the Bragg reflection angle) and interplanar spacings for three alumina gel samples. It is seen that the angles of scattering remain constant for all the samples within the limits of experimental error, i.e., that all the samples have a similar crystal lattice. A comparison of the experimental values for the interplanar spacings for Samples No. 905, 906, and 907 with published data showed that these samples have the lattice of hydrargillite $\text{Al}_2\text{O}_3 \cdot 3\text{H}_2\text{O}$.

It follows from Table 3 that when these samples are heated to 900°, the crystal lattice changes and acquires the structure of corundum, Al_2O_3 .

Investigation of the alumina gels by x-ray diffraction provides good confirmation of this hypothesis. The x-ray patterns were taken by the Debye-Scherrer method with K_α radiation from a BSV-4 tube with a copper anticathode. Nickel foil was used as a filter to reduce K_β radiation. All the x-ray patterns were taken in the same camera 64.8 mm in diameter, under the same conditions (40 kv and 18 ma) with 7 hours' exposure. The x-ray patterns were analyzed photometrically by means of the MF-4 recording microphotometer.

Fig. 3, shows the x-ray patterns of five alumina gel samples aged for different times, and of alumina gel heated at 900°. Microphotometric curves of the same samples are given in Fig. 4. All the samples except No. 903 and No. 904 give fairly sharp diffraction

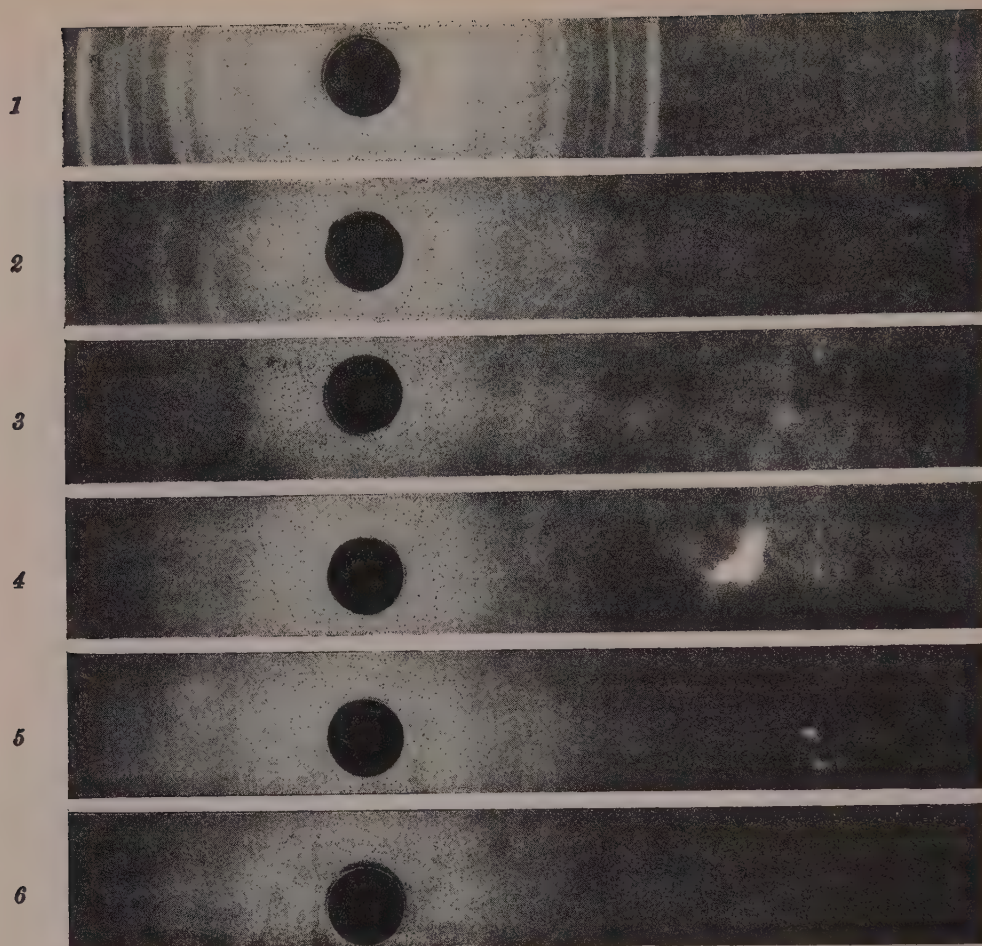


Fig. 3. The x-ray patterns of alumina gels formed after different aging times: 1) alumina gel heated to 900°; 2) Sample No. 907 (aging time 45 days); 3) No. 906 (10 days); 4) No. 905 (2 days); 5) No. 904 (1 day); 6) No. 903 (before aging).

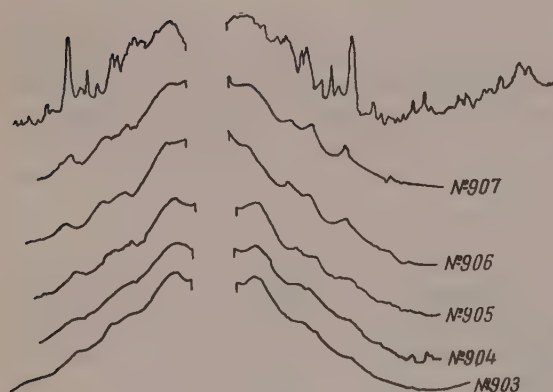


Fig. 4. Microphotometric curves of the x-ray patterns in Fig. 3.

SUMMARY

1. The effect of the time of aging of aluminum hydroxide gel in the mother liquor on its structure and adsorption activity was studied.

2. The pore structure of alumina gel alters during aging; the longer the aging time in the mother liquor, the more extensive are the structural changes in it.

3. It was shown by x-ray investigation that changes in the properties and pore structure of alumina gels during aging are due to conversion of the amorphous to the crystalline form.

LITERATURE CITED

- [1] A. V. Agafonov and M. A. Kaliko, *J. Gen. Chem.*, 1, 39 (1949);*G. K. Boreskov, *Heterogeneous Catalysis in Chemical Industry* [In Russian] (Goskhimizdat, 1955); V. A. Dziuk, *Heterogeneous Catalysis in Chemical Industry* [In Russian] (Goskhimizdat, 1955); D. P. Dobychin and T. F. Tselinskaya, *Proc. Acad. Sci. USSR* 109, 351 (1956);*G. K. Boreskov, *J. Phys. Chem.*, 31, 937 (1957); O. F. Sheheglov and G. K. Boreskov, *Proc. Acad. Sci. USSR* 105, 1, 123 (1955).

*Original Russian pagination. See C. B. Translation.

[2] W. Feitknecht, H. Studer and H. Meyer, *Kolloid.-Z.* 139, 3, 131 (1954); P. Howard and A. Roberts, *Trans. Brit. Ceramic Soc.*, 52, 7, 386 (1953); S. Gupta and S. Ghosh, *Z. Phys. Chem.*, 204, 1, 6 (1955); L. Greenstein, *J. Chem. Phys.*, 10, 4, 229 (1942); Narain Tewari Swarup and S. Ghosh, *Kolloid.-Z.* 130, 3, 169 (1953); Bagno Odette, *Compt. rend. Acad. Sci.*, 236, 12, 1275 (1953); Souza Santes P. et al., *Kolloid.-Z.* 133, 2/3, 101 (1953); S. Raychaudhuri et al., *J. Indian Chem. Soc.*, 20, 6, 195 (1943); G. Krige et al., *J. S. Afric. Chem. Inst.* 2, 61 (1948); Z. Ya. Berestneva and V. A. Kargin, *Colloid J.*, 12, No. 5, 338 (1950); 13, No. 5, 323 (1951); 14, No. 2, 73 (1952).*

[3] S. A. Levina and N. F. Ermolenko, *Bull. Acad. Sci. Belorussian SSR* 1, 107 (1954); *Colloid J.*, 17, No. 4, 287 (1955); B. Imelik and M. Mathieu, *J. chim. phys. et phys.-chim. biol.* 61, 11, 651 (1954); Y. Carteret, and B. Imelik, *Bull. Soc. chim. France* 1, 65 (1954); B. Imelik and M. Mathieu et al., *Compt. rend.* 242, 15, 1885 (1956).

Received November 6, 1957

* Original Russian pagination. See C. B. Translation.

INVESTIGATIONS OF ALUMINUM HYDROXIDE HYDROSOLS

5. EXPERIMENTS ON THE APPLICATION OF THERMOGRAPHY IN STUDIES OF THIXOTROPIC Al_2O_3 GELS

P. V. Rufimskii

The Ul'yanov-Lenin University of Kazan, Laboratory of Inorganic Chemistry

Thermography has extensive and diverse applications as one of the methods of physicochemical analysis. However, use of the thermographic method in colloid chemistry involves considerable difficulties because of the small magnitude of the heat effects in colloidal processes, and also of the possible breakdown of the internal structure of colloids in the course of thermal investigations. Nevertheless, the thermographic method has been used in investigations of some individual and particular problems of colloid chemistry. Lipatov, Stepanova and Fel'dman, in studying the course of cooling of a gelatin sol, found that heat is apparently liberated during the sol-gel transition. Nazarov and Nikolaev [2] attempted to study the formation of starch pastes and the influence of electrolytes on the process by the thermographic method. Kunzel and Docener [3] studied the same problem. Calvet, Boivinet, and Noel [4] used differential thermal analysis among other methods for studying Al_2O_3 gels. Krotov [5] used the thermographic method to demonstrate the existence of a thermostable form of aluminum hydroxide. It is known that Al_2O_3 in the colloidal state is widely used in technology. Plausible conclusions concerning the structure of alumina gels can be drawn from the results of experimental investigations, but the question cannot be regarded as finally solved, and there is no doubt that work in this field will continue.

In the present investigation an attempt was made to apply a physicochemical method, namely thermography, to investigation of thixotropic aluminum hydroxide gels.

Two modifications of aluminum hydroxide gel, prepared by Willstaetter's method [6], were used for the investigations. The first modification (A) was prepared by addition of aluminum sulfate solution, previously heated to boiling, to 20% ammonium hydroxide solution. The reaction mixture was then heated to 40-50° and a current of steam was passed through it for 5 hours. The precipitate was washed with distilled water by decantation and treated with 20% ammonium hydroxide solution on a water bath under reflux for 48 hours. At the end of the heating the aluminum hydroxide precipitate was washed several times with distilled water and separated off by decantation. The washed gel was filtered off on a Büchner funnel and dried in a desiccator over sulfuric acid, and then to constant weight at 60-65°.

The second modification of alumina gel (D) was prepared by dissolution of aluminum hydroxide in caustic soda solution, with subsequent filtration and dilution of the solution. A stream of carbon dioxide was then passed through this solution for 48 hours. The precipitate was washed 12-15 times with distilled water containing carbon dioxide. The precipitate was filtered off, dried in a desiccator over sulfuric acid, and then to constant weight at 60-65°.

Thermograms of the two gels are shown in Fig. 1 and 2. They were recorded by means of the PK-52 pyrometer, with Pt/Pt + Rh thermocouples and Al_2O_3 as the reference standard.*

The preliminary results so obtained can be interpreted on the basis of different forms of water-gel bonding.

*The author thanks E. F. Gubanov, laboratory assistant of the Kazan' Branch of the Academy of Sciences, who recorded the thermograms.

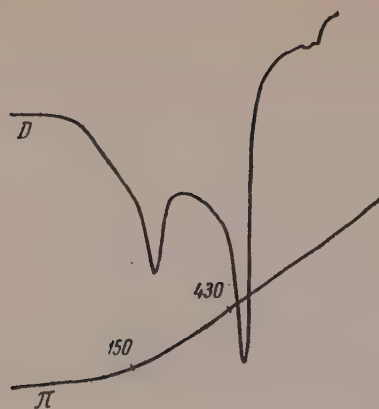


Fig. 1. Thermogram of Al_2O_3 gel; gel modification A.

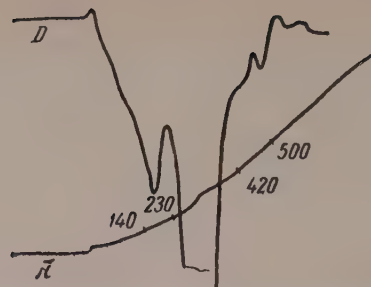
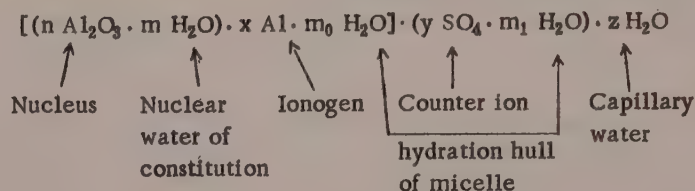


Fig. 2. Thermogram of Al_2O_3 gel; gel modification D.

The structure of the alumina gel micelle can be conventionally represented as follows:



Three endothermal effects may be expected in the thermal breakdown on the gel: caused by loss of capillary water, by loss of hydration water from the micelles, and by decomposition of the nuclei of the gel structure with loss of nuclear water of constitution:

Examination of the thermograms shows that both the gels studied give these three points. However, for gel A the third thermal effect is indistinct, while gel D gives an additional endothermal effect at 500°. A possible explanation of the latter is that the ionogenic group of gel D decomposes and liberates CO_2 . The smaller endothermal effect at 420° in the case of gel D suggests that gel A contains less capillary water than gel D, which may be caused by the higher dispersity of gel A. This hypothesis requires further detailed study.

The micelles of gel A form capillary water as the result of coalescence of their hydration hulls, since gel A does not give an endothermal effect at 230°, which in the case of gel D is probably due to loss of water from the hydration hulls. It follows from this hypothesis that gel A is less hydrated than gel D.

It follows from the thermogram (Fig. 1) that the endothermal effect at 430° for gel A is greater than the same effect at 420° for gel D; this may be attributed to the higher content of nuclear water of constitution in gel A. It follows from our interpretation of the thermal effect that the structure of the micelle nucleus of gel A corresponds to bauxite ($\text{Al}_2\text{O}_3 \cdot 2\text{H}_2\text{O}$), and that of gel D to diasporite ($\text{Al}_2\text{O}_3 \cdot \text{H}_2\text{O}$). This also, of course, requires additional proof.

The presence of an endothermal effect at 500° for gel D (Fig. 2) indicates separation of the counter ions (CO_3^{2-}) with their subsequent decomposition to CO_2 . This is not found for gel A, as its counter ions (SO_4^{2-}) are more stable.

The difference between the temperatures of the endothermal effects at 140° and 420° (10° in each case) may, in our opinion, be attributed to differences in the dispersity of the two gels.

SUMMARY

The results of thermographic investigations of Al_2O_3 gel samples suggest that at 140° these gels lose capillary water; at 230° the hydration hulls of their micelles are broken down; at 420° nuclear water of constitution is lost; and at 500°, the counter ions of the micelle are split off and decomposed.

I take this opportunity to thank Professor A. F. Bogoyavlenskii, Dr. Chem. Sci., for discussion of the results of this investigation.

LITERATURE CITED

- [1] S. M. Lipatov, N. V. Stepanova and R. I. Fel'dman, Colloid J. 3, 773 (1937).
- [2] V. I. Nazarov and A. V. Nikolaev, Proc. Acad. Sci. USSR 20, 537 (1938); 24, 262 (1939).
- [3] A. Kunzel and K. Docener, Kolloid.-Z. 80, 124, 130 (1939).
- [4] E. Calvet, P. Boivinnet and M. Noel, Bull. Soc. Chim. 1, 99 (1953).
- [5] I. V. Krotov, Proc. Acad. Sci. USSR 108, 263 (1956). *
- [6] Willstaetter, Ber. 57, 1082 (1924).

Received April 26, 1957

* Original Russian pagination. See C. B. Translation.

SEDIMENTOMETRIC ANALYSIS OF HIGHLY DISPERSE SUSPENSIONS BY MEANS OF THE CENTRIFUGAL BALANCE

N. A. Figurovskii and T. B. Gavrilova

The M. V. Lomonosov University, Moscow, Faculty of Chemistry

The usual methods of sedimentometric analysis in the Earth's gravitational field are applicable only within relatively narrow ranges of dispersity of the suspensions studied. For macrodisperse systems this range is limited by the physical conditions of applicability of Stokes' law (Reynolds number, etc.). In the microdisperse range, on the other hand, sedimentometric determinations depend on the practical possibility of performing the experiments and obtaining reliable results [1].

It is known that in studies of highly disperse and semicolloidal systems by the usual methods of sedimentometric analysis a number of difficulties are encountered, and it is far from always possible to overcome them. First of all, the settling time of an individual particle increases with increasing dispersity of a suspension, in accordance with the equation:

$$r^2 t = K,$$

where r is the particle radius; t is the time required for the particle to descend through 1 cm; K is the constant of the Stokes equation for the given disperse phase and dispersion medium. It is easy to calculate that quartz particles 0.2μ in size should settle at a rate of $3.7 \cdot 10^{-6}$ cm/second, i.e., they pass through a vertical distance of 1 cm in 75 hours.

The influence of various complicating factors on the sedimentation of the settling particles, especially convection currents in the suspension, particle hydration, and Brownian motion, increases sharply with increasing dispersity of the suspensions. Therefore, sedimentometric analysis in the Earth's gravitational field is not used for determinations of the dispersity of materials with particles $<1\mu$ in size. Nevertheless, powders and suspensions with particle sizes of the order of $0.1-1\mu$ are extensively used, and development of convenient methods for their investigations is becoming an urgent practical problem.

Methods based on various physical principles are used for studies of highly disperse systems; they include microscopical analysis, electron microscopy, adsorption methods, methods based on the rate of solution of particles, methods in which liquids and gases are forced through layers of powders of standard packing, diffusion methods, and certain others. With them may also be included slurry analysis, i.e., elutriation (fractionation) of suspensions, air-separation methods, the micro method of sedimentometric analysis, and various methods based on the use of centrifuges.

Without discussing the merits and applicability ranges of these methods, we may note that probably one of the most promising methods for studying dispersity in highly disperse materials is based on the use of centrifuges. This apparatus was first used by Dumanskii [2] for determinations of particle size in colloidal solutions. Various types of so-called supercentrifuges and ultracentrifuges were subsequently introduced for investigations of highly disperse and colloidal systems. Hauser and Lynn [3] have described a method for sedimentometric analysis of highly disperse materials by means of the Sharples ultracentrifuges. Svedberg [4], Nichols, and others designed a series of ultracentrifuges giving extremely powerful centrifugal fields, up to $9 \cdot 10^5$ g, and used them in polymer studies. The molecular weights of many high polymers were determined by means of these ultracentrifuges. Rinde [5] used one of the earliest models of the ultracentrifuge for sedimentometric determinations on colloidal

TABLE 1

Particle-Size Distribution in Quartz Suspensions

Method of analysis	Contents of fractions, wt. % (particle radii, μ)									
	0,4-0,5	0,5-0,6	0,6-0,7	0,7-0,8	0,8-0,9	0,9-1,0	1,0-1,1	1,1-1,2	1,2-1,5	1,5-2,0
Glass microbalance	5	25	11	8	5	4	3	2	3	34
Centrifugal balance	3	24	16	9	9	9	8	8	14	—

TABLE 2

Particle-Size Distribution in Gypsum Suspensions

Method of analysis	Contents of fractions, wt. % (particle radii, μ)									
	0,2-0,3	0,3-0,4	0,4-0,5	0,5-0,6	0,6-0,7	0,7-0,8	0,8-0,9	0,9-1,0	1,0-1,5	1,5-2,0
Glass microbalance	1	3	5	8	17	7	4	3	11	41
Centrifugal balance	1	4	8	11	16	13	12	11	24	—

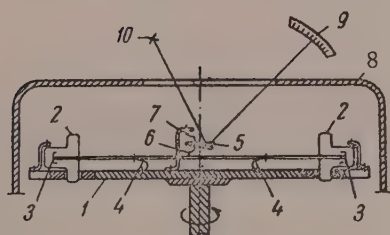


Fig. 1. Diagram of centrifugal sedimentation balance: 1) rotating disk; 2) shaped cell; 3) sedimentation cup; 4) spring connecting the rod to the disk; 5) moving mirror; 6) retaining spring for mirror; 7) support; 8) protective housing; 9) scale; 10) light source.

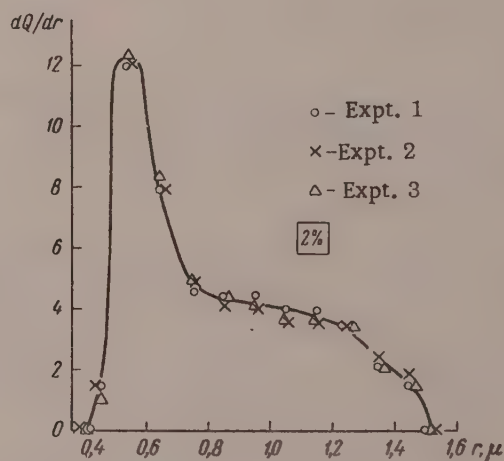


Fig. 2. Particle-size distribution curve for quartz suspension: an area of 1 cm^2 corresponds to 2% of the disperse phase by weight.

gold sols. Tube-type supercentrifuges [6-9], which give fairly high centrifugal accelerations (up to $4 \cdot 10^4 \text{ g}$) are now being used fairly widely for fractionation of suspensions. However, most of these instruments are generally used for special purposes only, and many of them are unique models.

There is no need at all to use centrifugal fields of high intensity for investigation and treatment of the coarser systems, with particles in the $0.1\text{--}2\mu$ range. Sedimentometric analysis of such systems is quite feasible with the aid of low-speed centrifuges, with rotating speeds of 1000 to 6000 rpm and centrifugal accelerations from 500 to 4000 g. The main difficulty in the use of low-speed centrifuges for sedimentometry lies in the choice of a principle and a practical method of continuous determination of the sedimentation rates of the particles in the centrifugal field. It seemed that this problem could be solved most simply with the aid of a

centrifugal sedimentometric balance, i.e., an instrument in which the settled particles are weighed either in the centrifugal field or by means of an ordinary balance linked by a special device to the rotating objects to be weighed [1].

Attempts to perform sedimentometric analysis of highly disperse suspensions with the aid of the first models of a centrifugal balance designed by one of us [10] were not successful. It was found that the friction in the hinges and rods connecting the pan to the weighing device was so high that the sensitivity of the instrument was greatly impaired. Completely reliable results cannot be obtained with such an instrument.

During recent years we have attempted to improve our original design of the centrifugal sedimentometric balance. Several instruments were designed, and one of them was constructed with the aid of specialists in the mechanical workshops of the Chemical Faculty of the Moscow State University. This instrument can be used for determination of distribution curves of highly disperse mineral suspensions with an adequate degree of reliability.

According to Svedberg [4] and Rinde [5], the radius of a settling particle can be calculated from the formula:

$$r = \sqrt{\frac{9\eta \ln \frac{x_2}{x_1}}{2(D-d)\omega^2(t_2-t_1)}} \quad (1)$$

where r is the equivalent particle radius; ω is the angular velocity of the centrifuge; x_1 is the distance from the center of rotation to the surface of the centrifuged suspension; x_2 is the distance from the center of rotation to the bottom of the cell; D is the density of the particle substance; d is the density of the medium; η is the viscosity of the medium.

According to Svedberg and Pedersen [4], the error in approximate calculation of particle size by the equation

$$r = \sqrt{\frac{9\eta(x_2-x_1)}{2(D-d)(x_1-x_2)\omega^2(t_2-t_1)}} \quad (2)$$

does not exceed 1% provided that $x_2/x_1 < 1.4$. The probable experimental error, estimated at about 2%, exceeds the calculation error.

Thus, in the design of centrifugal instruments for sedimentometric determinations it is more convenient to use large rotors, and the smallest possible sedimentation cells.

It may be noted that simple relationships may be used for calculating the acceleration developed in the centrifugal field and for comparing it with gravitational acceleration. It is known that $\omega = v/x$, where v is the linear velocity of a rotating point at a distance x from the center of rotation.

The centrifugal acceleration is:

$$c = \frac{v^2}{x} = \omega^2 x = \left(\frac{2\pi n}{60}\right)^2 x. \quad (3)$$

Hence, it is easy to calculate the ratio of centrifugal to gravitational acceleration.

Our instrument was based on a low-speed centrifuge of $n = 1500$ rpm. The centrifuge was driven by a stable direct-current motor. The distance x_2 from the center of rotation to the bottom of the cell containing the suspension was 27 cm; $x_1 = 22$ cm. The ratio $x_2/x_1 = 1.23$. The centrifugal acceleration developed in the centrifuge ($x_{av} = 25$ cm), calculated from Equation (3) was 628 g. The acceleration time of the centrifuge was 30 seconds.

The centrifugal balance (Fig. 1) was designed as follows: two cells, shaped for convenient filling and emptying, were fixed diametrically opposite each other on a rotating disk. One of the cells was filled with the suspension, and the other with pure dispersion medium. This served to balance the centrifuges during the experiments.

Two aluminum cups 3 of equal weight, fitting freely into the cells, were attached to the ends of a rod passing through the center of rotation. The rod carrying the cups were attached to the centrifuge disk by means of two springs 4 which allowed it to move along its own axis. When the suspension settles the weight of one of the cups increases; the rod moves in the direction of this cup and deflects the mirror 5 attached by means of the spring 6 to the support 7 near the center of the disk. The sedimentation curve is plotted from the displacement of the light spot reflected from the mirror. As in any balancing device with arms of equal length, the displacement of the light spot must be strictly proportional to the load. A special check experiment confirmed this proportionality. The instrument proved to be quite sensitive.

This centrifugal balance was used for sedimentometric studies of aqueous suspensions of highly disperse quartz and suspensions of gypsum in ethyl alcohol.

The 1% quartz suspension was prepared from a powder made by crushing of quartz glass with subsequent elutriation of the fine fractions settling a distance of 10 cm in 24 hours and over. The powder so prepared was purified by treatment with acids and subsequent prolonged washing with hot water.

Gypsum powder was prepared by grinding of fairly coarse material in a vibratory mill for 30 minutes. The two samples used for preparation of the suspensions were chosen in order to compare the results of particle-size distribution determinations with the aid of the centrifugal balance and by means of ordinary sedimentometric analysis with a glass sedimentometric balance. It was taken into account that in comparison of these results agreement can be approximate only, as sedimentometric analysis of such fine suspensions in the Earth's gravitational field involves the difficulties mentioned earlier in this paper.

The particle-size distribution of quartz suspensions determined by the two methods is given in Table 1. The ordinary sedimentometric analysis with a glass balance was carried out with a sedimentation height of 5.4 cm. The analysis lasted 45 hours. The results given by the two methods are very close. However, the low content of the coarse fractions given by the centrifugal sedimentometric balance cannot fail to be noticed. The explanation is that coarse fractions partially settle out even while the centrifuge is starting up.

Duplicate experiments with the centrifugal balance show good reproducibility, as is clear from Fig. 2.

Table 2 contains data on the particle-size distribution of gypsum suspensions in ethyl alcohol, determined by the two methods. Sedimentometric analysis with the glass balance took 192 hours with a sedimentation height of 5.5 cm.

As with the quartz suspension, sedimentometric analysis by means of the centrifugal balance gives a lower content of the coarse fractions for gypsum suspensions. However, the maxima on the distribution curves determined by the two methods coincided satisfactorily.

These determination results demonstrate the undoubted advantages of the use of the centrifugal balance for sedimentometric investigations of highly disperse suspensions. In all our experiments the analysis took 3-5 minutes, whereas the usual method of analysis required several days, and this inevitably introduced various errors.

In conclusion we may note that for mass analyses of various suspensions it would be desirable to have an instrument which can be used at different rotation speeds, for example, from 3000 to 300 rpm, so that the analysis should take from 5 to 10 minutes. In such cases the start-up time of the centrifuge may be disregarded altogether.

SUMMARY

1. An instrument for sedimentometric analysis of suspensions in a centrifugal field is described. Data on particle size and particle-size distribution of highly disperse materials can be easily obtained with this instrument.

2. Sedimentometric data are presented on highly disperse suspensions of quartz in water and of gypsum in ethyl alcohol, determined by means of the centrifugal balance and by ordinary sedimentometric analysis in the Earth's gravitational field. The results given by the two methods are in satisfactory agreement.

LITERATURE CITED

- [1] N. A. Figurovskii, Sedimentometric Analysis [In Russian] (Moscow-Leningrad, 1948).
- [2] A. V. Dumanskii, Kolloid.-Z, 12, 6 (1913).
- [3] E. Hauser and I. Lynn, Ind. Eng. Chem., 32, 659 (1940).
- [4] T. Svedberg and K. O. Pedersen, Die Ultrazentrifuge (Dresden und Leipzig, 1940).
- [5] H. Rinde, The Distribution of the Sizes of Particles in Gold Sols. Diss., (Upsala, 1928).
- [6] V. I. Sokolov, Centrifuges [In Russian] (Moscow State Press, 1950).
- [7] S. E. Bresler, Biochemistry 15, 198 (1950).
- [8] S. Ya. Frenkel', J. Tech. Phys. 25, 12 (1955).
- [9] D. S. Saminskii and N. L. Kayushina, Chem. Sci. and Ind. 2 (1956).
- [10] N. A. Figurovskii, Author's Certif. No. 58902.

Received October 22, 1957

INVESTIGATION OF THE COLLOIDAL NATURE OF POLYSACCHARIDES BY A HYDROLYSIS METHOD

V. I. Sharkov and V. P. Levanova

Scientific Research Institute of the Hydrolysis and Sulfite Alcohol Industry, Leningrad

In a series of earlier investigations it was shown by one of us [1] that the hydrolysis rate of cellulose depends to a considerable extent on whether the reaction is effected under homogeneous or heterogeneous conditions. The highest hydrolysis rate was observed with homogeneous solutions of cellulose, when there were no serious steric obstacles to the access of catalyst to each macromolecule. If the same reaction is conducted under heterogeneous conditions, access of catalyst into the depth of the cellulose macromolecules is hindered, and the reaction rate is accordingly lowered 60- to 100-fold. This effect was subsequently used in investigations of the colloidochemical nature of solutions and gels of various polysaccharides.

For example, it was found that the hydrolysis rate of cellulose in apparently homogeneous solutions in sulfuric acid varied according to the conditions used in the dissolving process [2], probably because of differences in the size of the colloidal particles of the solute. The same method was used for investigation of agar solutions and gels [3].

In the present investigation measurements of the hydrolysis rate were applied to a study of the colloidochemical nature of starch and wood hemicelluloses.

Starch. Potato starch, previously washed thoroughly with cold water and dried in air, was investigated. Quantitative hydrolysis of this starch by 10% sulfuric acid at 100° yielded 100% of glucose, which corresponds to a 99.01% polysaccharide content.

The hydrolysis rates of starch in heterogeneous and homogeneous conditions were compared by means of a series of experiments in which starch samples were first covered with water at 20°, then heated to 50-100°, and held at these temperatures for 1 hour with continuous stirring. Preliminary experiments showed that as the result of swelling in water the grains of potato starch increase 2.7-fold in diameter at 50°, and 1.6-fold at 40°, as compared with the diameter in water at 20°. Despite the 2.7-fold increase of the average grain diameter at 50°, the solubility of starch under these conditions was only 0.2%. At 60° and above, a homogeneous paste was formed. At the end of the heating each sample was cooled to 50°, and 25% sulfuric acid heated to 50° was added to it, with vigorous stirring, in an amount necessary to give a 10% solution of sulfuric acid with a polysaccharide concentration of 0.5%. The samples were then put in a thermostat for 24 hours at 50°. At the end of this time, glucose contents of the samples were determined by the ebullioscopic method. The glucose content was converted to polysaccharides by means of the conversion factor 0.9, and the result was used to calculate the hourly rate constant of polysaccharide hydrolysis (from the first-order equation).

The results are presented in Table 1.

The values of the coefficient β in Table 1 represent the ratio of the hydrolysis rate of a given sample of starch to the hydrolysis rate of a sample treated with water at 50°.

It follows from Table 1 that the hydrolysis rate of starch in grains swollen at 50° is about one-third of the hydrolysis rate in paste form. The temperature of paste formation, above the gelatinization temperature, has no significant influence on the rate of starch hydrolysis in solution.

TABLE 1

Hydrolysis at 50° of Starch Grains Treated with Water at Different Temperatures

Temperature of preliminary water treatment, °C	Amount of polysaccharides hydrolyzed, % of starch taken	Hydrolysis rate constant, $K \cdot 10^3, \text{hr}^{-1}$	Coefficient $\beta = K_t^\circ / K_{50}^\circ$
50	6.8	2.96	1.00
60	18.4	8.55	2.9
70	18.2	8.45	2.85
80	18.1	8.40	2.84
90	19.1	8.92	3.01
100	19.1	8.92	3.01

TABLE 2

Comparison of Hydrolysis of Starch at 40° in Grain and Paste Form

Hydrolysis time, hours	Starch treated with water at 40°		Starch treated with water at 100°	
	polysaccharides hydrolyzed, % of sample	$K \cdot 10^3, \text{hr}^{-1}$	polysaccharides hydrolyzed, % of sample	$K \cdot 10^3, \text{hr}^{-1}$
30	1.2	0.41	5.5	1.90
50	2.0	0.40	9.0	1.00
70	2.7	0.40	12.4	1.92
100	3.6	0.37	17.6	1.95
130	4.5	0.36	22.6	1.99
150	5.0	0.34	26.0	2.02
Average		0.38		1.95

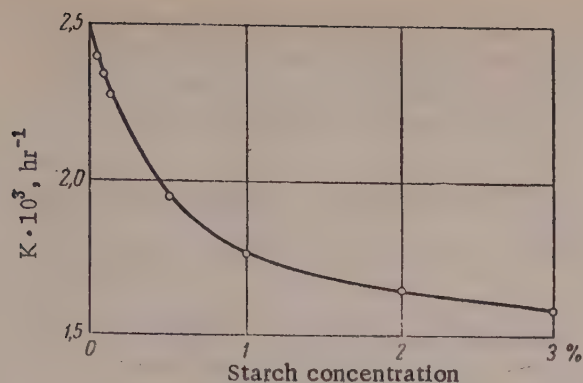
TABLE 3

Effect of Preliminary Treatment on the Hydrolysis Rate of Starch

Type of Starch	$K \cdot 10^3, \text{hr}^{-1}$	Coefficient β
Starch grains swollen in water at 40°	0.38	1.00
Paste made at 100°	1.95	5.1
Dried paste	1.56	4.1
Ground starch grains	1.44	3.8
Repeatedly-frozen starch grains	0.39	1.02

TABLE 4

Hemicellulose concentration, %	0.05	0.08	0.10	0.50	1.00	3.00
$K \cdot 10^3, \text{hr}^{-1}$	7.72	7.41	7.08	3.85	3.53	3.28



Variations of the hydrolysis rate constant of gelatinized starch with its concentration in solution.

vibratory ball mill, and starch grains frozen 15 times in water at -15° by Klenkova's method [4].

The average results are presented in Table 3.

It is clear from Table 3 that the rate of starch hydrolysis varies greatly with the conditions of preliminary treatment.

For example, if the temperature at which the starch is treated with water, is lowered from 50 to 40° , the difference between the hydrolysis rates of starch in grain and paste form increases. Thus, when the swelling and hydrolysis temperature is 50° , the coefficient β is 2.9-3.0, whereas at 40° the value of the coefficient is 5.1. At lower temperature the difference becomes even greater [5] and approaches values characteristic for cellulose.

Acceleration of the heterogeneous hydrolysis of starch grains with increase of temperature is probably the consequence of increased swelling at higher temperatures.

When starch grains are gelatinized their structure is changed, and is not restored by dehydration of the starch paste. A similar effect is observed in hydrolysis of starch grains after preliminary dry colloid milling. It seems that ground starch grains and dried paste swell and dissolve in water at lower temperatures than ordinary starch grains.

It is interesting to note that starch grains repeatedly frozen in water by Klenkova's method, which become capable of retaining considerable amounts of nonfreezing water, were not hydrolyzed at appreciably higher rates, which showed that this treatment does not produce appreciable changes in the starch grains.

In the light of the foregoing, it was of interest to investigate the hydrolysis rates of starch pastes of different concentrations. It was likely that with decreasing concentration of the starch its colloidal particles should break down into smaller ones, and this should result in an increase of hydrolysis rate.

To test this hypothesis, starch solutions of different concentrations were prepared by the action of heat in water at 100° for 60 minutes. The solutions were cooled to 40° and 25% sulfuric acid was added to give mixtures containing 10% sulfuric acid. These starch solutions were hydrolyzed at 40° by the method described above. The results are shown in the graph.

It follows from the graph that the hydrolysis rate of starch in pastes cooled to 40° depends on its concentration, increasing with decrease of concentration. This confirms the above hypothesis that the dispersity of starch in solution increases with decreasing concentration.

Hemicelluloses. Hemicelluloses insoluble in cold water were prepared by extraction in alkali from bleached spruce sulfite pulp, which was mercerized by the action of 18% caustic soda for 1 hour at 15° at 1:7 liquor ratio.

At the end of the mercerization the alkali was pressed out in a hydraulic press, filtered carefully through a No. 4 Schott filter, and mixed with double its own volume of ethyl alcohol. The precipitated alkali hemicellu-

It seemed likely that the rates of starch hydrolysis in homogeneous and heterogeneous conditions should differ even more if the hydrolysis is carried out at 40° . Two series of experiments were performed to test this hypothesis; in the first the starch was first swollen in water at 40° , and in the second, it was heated in water for 1 hour at 100° . Sulfuric acid was then added to samples of both series to an acid concentration of 10% and a polysaccharide concentration of 0.5%. After vigorous stirring the samples were placed for different times in a thermostat at 40° . The results were analyzed as before. The values of the constant are given in Table 2.

For comparison, hydrolysis experiments were performed under the same conditions on starch paste previously dried at 100° , dry starch grains ground dry in a

lose compound was filtered off, washed with alcohol, and decomposed by 10% alcoholic solution of acetic acid in the cold. The insoluble hemicellulose precipitate was washed with alcohol and ether, and dried in a thermostat at 60°. The resultant hemicellulose preparation was a fine white powder, insoluble in cold water; it consisted of easily-hydrolyzed polysaccharides which included 30.9% mannan, 41.5% pentosans, 9.3% uronic acids, and 17% glucosan.

The hydrolysis rate of these hemicelluloses was determined at 40° by the method described above for starch.

Table 4 gives the average values of the hydrolysis rate constant of hemicelluloses at different solution concentrations.

It follows from the data in Table 4 that the hydrolysis rate constant of hemicelluloses also depends on their concentration. This experiment also demonstrated that aqueous solutions and suspensions of hemicelluloses and starch at the concentrations generally used in investigations are not molecularly dispersed. Evidently for this reason, experiments on the fractionation of hemicelluloses into the individual components do not give satisfactory results.

These experiments show that measurements of the hydrolysis rates of polysaccharides can be used, equally with other investigation methods, for characterization of their structure and behavior in solution.

SUMMARY

1. The colloidal state of starch and wood hemicelluloses can be characterized by determinations of their hydrolysis rates.
2. Preliminary gelatinization or dry grinding increase the hydrolysis rate of starch at 40° 4- to 5-fold.
3. The hydrolysis rates of dissolved hemicelluloses and starch increase with decrease of concentration, indicating a decrease in the size of their colloidal micelles.

LITERATURE CITED

- [1] V. I. Sharkov, V. S. Muromtseva and G. D. Paramonova, *J. Appl. Chem.*, 21, 1037, 1073 (1948); V. I. Sharkov, *Hydrolysis Ind.*, 3, No. 4, 5 (1950); V. I. Sharkov, in the book: *Chemistry and Physical Chemistry of High Polymers* [In Russian] (Izd. AN SSSR, 1952) p. 132, etc.
- [2] I. I. Korol'kov, V. P. Levanova and V. I. Sharkov, *Colloid J.*, 17, No. 5, 353 (1955).*
- [3] V. I. Sharkov and R. K. Boyarskaya, *Proc. Acad. Sci. USSR* 108, No. 1, 99 (1956).*
- [4] N. I. Klenkova, *J. Appl. Chem.*, 27, No. 4, 433 (1954).*
- [5] V. I. Sharkov, *Trans. Inst. Forestry, Acad. Sci. Latvian SSR* No. 8, 23 (1955).

Received October 19, 1957

* Original Russian pagination. See C. B. Translation.

PREPARATION AND STUDY OF THE THIXOTROPIC PROPERTIES OF A SUSPENSION OF HIGHLY DISPERSE ASKANGEL FRACTIONS*

M. E. Shishniashvili and A. I. Avsarkisova

Laboratory of Colloid Chemistry, Institute of Chemistry, Georgian SSR, Tbilisi

Clay suspensions made from coarsely disperse clays, mainly of the kaolinite type, generally do not conform to drilling requirements. Because of the high concentration of the solid phase (30-40%) the thixotropy is low and the properties of these suspensions (viscosity, density, etc.) are difficult to control. The additives used in drilling practice (alkaline coal extract, sulfite waste liquor, carboxymethylcellulose, etc.) cannot confer adequate colloidal properties on coarsely disperse systems such as kaolinite clay suspensions [1].

Therefore, the production of highly colloidal clay suspensions for complicated deep oil-well drilling is a very topical problem. Such suspensions may be made from bentonites, of which the clay mineral montmorillonite is the principal component. Suspensions of alkaline montmorillonite are highly thixotropic at 4-6% concentrations.

One of the most characteristic representatives of the bentonite group found in the Soviet Union is askangel, the fine fractions of which are alkaline montmorillonite [2, 3]. The native form of askangel is polydisperse over a wide range of particle size.

The presence of coarse fractions (their content is $\sim 30\%$) has a very adverse effect on the colloidal properties of askangel suspensions. It therefore became necessary to isolate its fine fractions (particles $< 1\mu$). It must be pointed out that highly disperse askangel fractions are likely to find extensive uses in other branches of industry in addition to drilling [4-7].

The existing methods of evaporation or supercentrifugation of dilute suspensions of highly disperse askangel fractions (for preparation of "askancoll") [8] are very limited in their applicability.

The main purpose of this investigation was to find rational conditions for isolation of highly disperse fractions from askangel. Account was taken of the peculiarities in variations of the surface-chemical properties of aluminosilicate systems (gels, clays, etc.) under the influence of various electrolyte solutions [9, 10].

In accordance with the intensity of the coagulation process under the influence of hydrophobizing electrolytes, particles of askangel suspensions become more stably bonded and form compact aggregates, tending to visible coagulation. Chlorides of bi- and trivalent cations are the most active electrolytes [11]. Because of these properties, it is possible to bring about phase separation in highly disperse askangel suspensions with particles $< 1\mu$ at low electrolyte concentrations, with the aid of the ordinary types of industrial high-output centrifuges (2000-3000 rpm). The same high-output centrifuges were used for preliminary separation of coarse fractions ($> 1\mu$).

The hydrophobizing electrolyte used was BaCl_2 . Having the higher adsorption energy, Ba^{2+} displaced the Na^+ adsorbed on the askangel particles. The suspension became unstable and syneresis took place. After separation of the dispersion medium a paste consisting of highly disperse askangel fractions was obtained. We gave the name of coagulate paste to this intermediate product.

* Presented at the Fourth All-Union Conference on Colloid Chemistry, Tbilisi, 1958.

TABLE 1

Composition and Exchange Capacity of Askangel and Its Fractions

Samples	Contents of exchange cations and anions, meq/100 g						Total exchange capacity, meq/100 g askangel
	Na ⁺ (by difference)	Ca ²⁺	Ba ²⁺	Al ³⁺	SO ₄ ²⁻	Cl ⁻	
Askangel	37,8	49,1	—	—	6,0	Traces	86,9
Coarse fraction > 1 μ	26,6	39,5	—	—	4,2	»	66,1
Fine fraction << 1 μ	59,8	39,0	—	—	3,4	»	98,8

TABLE 2

Separation of Coarse Fractions from Askangel Suspensions by Means of Centrifugation

Concentration of suspension, %	Centrifuge speed, rpm	Capacity of model industrial centrifuge, kg/hr	Concentration of settled paste, %	Waste coarse fractions, %
2,3	1620	500	38,8	31,0
5,0	1340	750	37,5	14,0
4,3	1450	950	32,0	12,6

TABLE 3

Analysis of Filtrates of Coagulate Paste at Different BaCl₂ Contents

BaCl ₂ taken		pH of filtrate	meq/100 g of askangel		
% on askangel	meq/100 g of askangel		Ca ²⁺	Ba ²⁺	Cl ⁻
5	50	6,03	5,32	3,86	64,05
3,5	35	5,98	3,0	1,32	49,73
2,5	25	5,99	1,4	0,35	39,95
1,5	15	5,98	0,78	Not found	29,98

TABLE 4

Determinations of Exchange Ba²⁺ in Coagulate Paste by Analysis and by Conductometric Titration

BaCl ₂ taken for coagulation of highly disperse suspension, meq/100 g	Content of exchange Ba ²⁺ in KCl extract, meq/100 g	Determination of Ba ²⁺ by conductometric titration, meq/100 g
50	46,0	45,9
35	31,8	30,2-31,9
25	22,0	22,4
15	13,7	13,2

TABLE 5

Comparative Characteristics of Suspensions of Askangel, Askancoll, and Enriched Askangel

Suspension	Con- centra- tion, %	Sp. gr.	Viscosity, centi- poises	$\kappa \cdot 10^4$	pH	P_M , dynes/cm ²		K_T
						P_0	P_{max}	
Askangel	4,06	1,038	8,0	7,28	7,92	53	100	0,9
	5,08	1,050	16,1	8,53	7,97	57	225	3,0
	7,71	1,060	46,0	10,8	8,21	57	330	4,8
	8,01	1,064	140,0	11,9	8,25	66,5	424,5	5,4
Askancoll	4,01	1,026	68,0	8,83	8,07	61,8	294,5	3,8
	4,52	1,030	106,2	9,37	8,15	66,5	410,0	5,1
	4,95	1,032	556,8	10,2	8,25	223,3	537,3	1,4
Enriched askangel	4,01	1,026	7,0	5,92	8,29	53	220	2,8
	5,04	1,030	79,1	7,93	8,23	53	520	8,1
	5,97	1,040	120,0	8,75	8,21	50	615	11,3

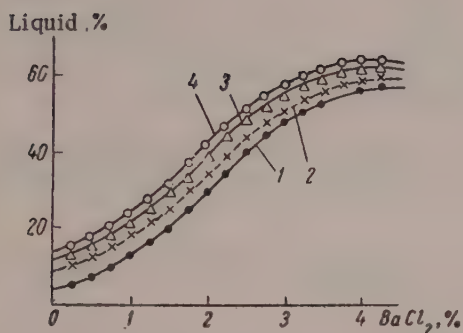


Fig. 1. Separation of dispersion medium (centrifugate liquid) from a coagulated 2% suspension of highly disperse askangel fractions as a function of the $BaCl_2$ concentration and pH: 1) pH 7.07; 2) pH 6.57; 3) pH 5.99; 4) pH 4.93.

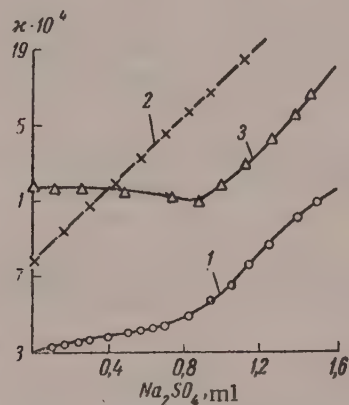


Fig. 2. Conductometric titration by 0.27 N Na_2SO_4 solution: 1) 25 ml of 4% suspension of coagulate paste; 2) 25 ml of 4% askancoll suspension; 3) 25 ml of aqueous $BaCl_2$ solution.

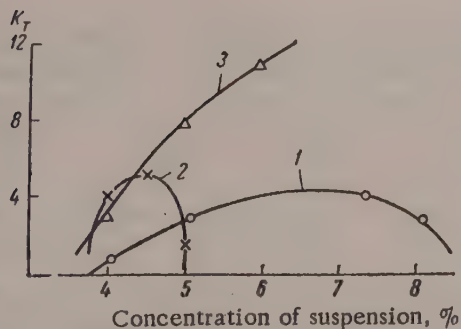


Fig. 3. Effect of suspension concentration on the coefficient of thixotropy (K_T): 1) askangel; 2) askancoll; 3) enriched askangel.

To bring back colloidal properties, the coagulate paste was peptized (reverse peptization) by means of sodium sulfate, when Na^+ displaced Ba^{2+} , and owing to the formation of insoluble $BaSO_4$ the exchange reaction went almost to completion. The product, similar to the American aquagel, was named enriched askangel.

The composition and exchange capacity of the askangel sample taken for the experiments and of its coarse and fine fractions are given in Table 1.

The composition of the exchange complex was determined by the Gedroits method, KCl and $(NH_4)_2SO_4$ extracts being obtained by repeated treatment (up to 20-25 times) with 1 N solutions of these salts. The total exchange capacity was also determined by the

Gedroits method by preparation of Ba^{2+} - substituted askangel. The absorbed Ba^{2+} was then displaced by the action of 1 N KCl solution [12].

To prepare the suspension, the askangel was first soaked in water in 1:5 ratio, and the swollen mass was ground in the doughlike state.

For separation of the coarse fractions, laboratory models of industrial centrifuges of the sedimentation type were tested at various rotor speeds*. The results of these experiments are given in Table 2.

It follows from Table 2 that the most complete removal of coarse fractions was achieved at a suspension concentration of 2.3% and a centrifuge rotor speed of 1620 rpm. Sedimentation analysis of the centrifugate showed a content of over 95% of particles of equivalent radius $< 2\mu$.

In subsequent experiments under laboratory conditions the coarse fractions were separated by sedimentation from 3.0-3.5% suspensions. The yield of coarse fractions was ~30%. The decanted suspension of highly disperse askangel fractions was treated with BaCl_2 solution after acidification with hydrochloric acid to pH 5.0-7.5. Experiments on the separation of the dispersion medium from hydrophobized suspensions were carried out in a tube-type laboratory centrifuge at rotation speeds of 1000-1500 rpm (Fig. 1).

It follows from the curves in Fig. 1, that decrease of pH does not lead to a sharp increase in the yield of coagulate paste. Therefore, in the subsequent experiments the suspension pH was 6, which corresponded to 14-15 meq of HCl per 100 g, or 0.4% on the askangel weight. Lower pH values may have caused chemisorptive changes on the surface of the askangel particles. The optimum BaCl_2 concentration is 2.5% on the weight of askangel in the suspension (25 meq/100 g of askangel). This amount of BaCl_2 corresponded to the start of syneresis. At higher BaCl_2 concentrations, the yield of coagulate paste increased only slightly.

In experiments under semiproduction conditions, with a vertical centrifuge of the sedimentation type, the concentration of the coagulate paste was not high enough, but phase separation was complete and losses of highly disperse fractions with the centrifuge were very low.

Under laboratory conditions a large amount of coagulate paste was prepared by means of vacuum filtration. Analytical data for the filtrates with different BaCl_2 contents are given in Table 3.

It follows from Table 3 that the Ca^{2+} contents of the filtrates are low. It seems that Ba^{2+} largely displaces the Na^+ adsorbed on the askangel particles. The losses of BaCl_2 with the filtrate are negligible. Chloride ions pass almost completely into the filtrate and are not adsorbed by the askangel particles.

The coagulate paste made by vacuum filtration, with the use of 2.5% BaCl_2 , consists of a concentrated paste of 25-30% of highly disperse fractions (particles $< 1\mu$) of askangel aggregated by the action of BaCl_2 and HCl.

The next stage in the preparation of enriched askangel is reverse peptization (as indicated earlier) by the action of sodium sulfate.

It is known from the work of Antipov-Karataev [13] that Ca^{2+} has selective exchange properties with respect to bentonite, with regard to its displacing power, when in competition with Ba^{2+} . Therefore, (with the higher solubility of CaSO_4 also taken into account) the replacement reaction in presence of Na_2SO_4 proceeds in the direction of displacement of Ba^{2+} and formation of BaSO_4 . This is clear from the results of conductometric titrations of a suspension of coagulate paste by Na_2SO_4 solution. The titration results were checked by determinations of Ba^{2+} in a KCl extract of the coagulate paste (Table 4).

Fig. 2 shows curves for variations of conductivity of a suspension of coagulate paste made with the use of 2.5% BaCl_2 (0.0010 g/ml), askancoll, and aqueous BaCl_2 solution (0.0010 g/ml), under the influence of Na_2SO_4 .

The inflection on the titration curve of the coagulate suspension paste almost corresponds to the stoichiometric amount of BaCl_2 (22 meq of Na_2SO_4 per 100 g of askangel) and virtually coincides with the inflection on the titration curve of an aqueous BaCl_2 solution (25 meq of Na_2SO_4) and with the results of analytical determinations of exchange Ba^{2+} (see Table 4). The change in the conductivity of askancoll suspension under the influence of Na_2SO_4 is represented by an ascending straight line.

* This part of the work was carried out with the assistance of L. M. Poleshchuk.

The suspensions of enriched askangel had relatively low pH values (6.7-6.8). It is known that the peptization optimum for clay in aqueous media corresponds to pH 8-9. It was found from the results of our experiments that maximum peptization of enriched askangel also corresponds to pH 8-9. Therefore, enriched askangel paste was treated with 0.1 NaOH solution to a pH value of 8.25 (equilibrium value). The amount of NaOH required for this was 0.13% on the weight of askangel in the suspension, or 3.2 meq/100 g of askangel.

Suspensions of natural askangel, askancoll, and enriched askangel of different concentrations were prepared for comparative tests (Table 5).

The structuromechanical properties of these suspensions were characterized by the kinetics of thixotropic buildup, yield value (in dynes/cm²), and the thixotropic coefficient [14].

$$K_T = \frac{P_m - P_0}{P_m}.$$

These parameters were determined by means of the Veller-Rebinder apparatus [15].

The pH and conductivity (κ) of the suspensions were determined by electrometric methods, and the viscosity by means of the Hoeppler ball-fall viscosimeter.

It follows from the structuromechanical properties in Table 4 that suspensions of enriched askangel are much more fluid and thixotropic than askancoll suspensions of the same concentrations. The thixotropic properties of askancoll suspensions reach a maximum at 4.5% concentration and then decrease sharply, while the viscosity increases considerably. Suspensions of enriched askangel, on the other hand, retain high fluidity and thixotropy up to 6% concentration.

Fig. 3 shows curves for the variations of K_T for suspensions of askangel, askancoll, and enriched askangel (22 meq Na₂SO₄ per 100 g of askangel) with concentration.

It follows from these results that the high fluidity, thixotropy, and stability of suspensions of enriched askangel make it a valuable material for production of highly colloidal drilling suspensions.

SUMMARY

1. The possibility was studied of isolating highly disperse askangel fractions (particles $< 1\mu$) by means of the hydrophobizing action of small amounts of BaCl₂ (25 meq/100 g, or 2.5% on the weight of askangel), which results in partial replacement of Na⁺ by Ba²⁺. The phases of such suspensions can be separated in the centrifuge (1500-3000 rpm) or by means of vacuum filtration (with production of coagulate paste).

2. Coarse fractions of askangel, which in its natural state contains ~30% of particles $> 1\mu$, can be separated from dilute suspensions (~2.5%) in a vertical centrifuge of the sedimentation type (at 1620 rpm) at a high rate of output.

3. The colloidal properties of the coagulate paste can be restored (by reverse peptization) by the action of Na₂SO₄ taken in an equivalent amount to the BaCl₂ used. Owing to the formation of BaSO₄, the reaction of replacement of Ba²⁺ by Na⁺ proceeds to completion. The resultant colloidal product (similar to the American aquagel), which is a fine fraction of true alkaline bentonite (askangel), has been named enriched askangel.

4. Suspensions of enriched askangel have high thixotropy and fluidity. Therefore, enriched askangel can be used for the production of highly disperse drilling muds and for other practical purposes.

LITERATURE CITED

- [1] N. I. Shatsov, Oil-Well Drilling [In Russian] (State Fuel Tech. Press, Moscow-Leningrad, 1950).
- [2] A. A. Tvalchrelidze, in the book: Bentonite Clays of Georgia and Their Applications in the National Economy [In Russian] (Acad. Sci. Georgian SSR Press, Tbilisi, 1953).
- [3] B. B. Zvyagin, E. L. Lapidus, and V. P. Petrov, Proc. Acad. Sci. USSR 62, No. 2, 379 (1949); B. B. Zvyagin, Proc. Acad. Sci. USSR 86, No. 1, 149 (1952).

- [4] M. L. Guliev, in the book: Bentonite Clays of the Georgian SSR [In Russian] ("Tekhnika da Shroma" Press, Tbilisi, 1941).
- [5] B. A. Dogadkin, K. E. Pechkovskaya and L. M. Chernikina, Colloid J. 8, 31 (1946).
- [6] N. I. Kutateladze, in the book: Bentonite Clays of Georgia and Their Applications in the National Economy [In Russian] (Acad. Sci. Georgian SSR Press, Tbilisi, 1953); N. E. Kakabadze, in the book: Bentonite Clays of Georgia and Their Applications in the National Economy [In Russian] (Acad. Sci. Georgian SSR Press, Tbilisi, 1953); M. S. Merabishvili, in the book: Bentonite Clays of Georgia and Their Applications in the National Economy [In Russian] (Acad. Sci. Georgian SSR Press, Tbilisi, 1953).
- [7] Yu. N. Novodranov, Colloid J. 8, No. 5, 381 (1946).
- [8] M. S. Merabishvili, S. S. Filatov and O. M. Mdivnishvili, in the book: Bentonite Clays of Georgia and Their Applications in the National Economy [In Russian] (Acad. Sci. Georgian SSR Press, Tbilisi, 1953).
- [9] M. E. Shishniashvili, V. A. Kargin and A. L. Batsanadze, Colloid J. 8, 269 (1946).
- [10] M. E. Shishniashvili, Bull. Acad. Sci. Belorussian SSR, Ser. Phys.-Tech. Sci. 3, 37 (1956).
- [11] N. N. Serb-Serbina, in the book: Viscosity of Liquids and Colloidal Solutions [In Russian] 1 (1941).
- [12] K. K. Gedroits, Chemical Analysis of Soil [In Russian] Agricultural Press, Moscow-Leningrad, 1935).
- [13] I. N. Antipov-Karataev and G. M. Kader, Colloid J. 9, No. 2, 81 (1947).
- [14] E. I. Kobakhidze and M. E. Shishniashvili, Colloid J. 19, 1, 60 (1957).*
- [15] S. Ya. Veiler and P. A. Rebinder, Proc. Acad. Sci. USSR 49, No. 5, 354 (1945).

Received October 9, 1957

*Original Russian pagination. See C. B. Translation.

CALCULATION OF THE NUMBER OF BRANCH POINTS IN THE SPATIAL NETWORKS OF RUBBERLIKE MATERIALS

L. A. Vishnitskaya

Scientific Research Institute of the Rubber Industry, Moscow

The theory of the deformation of spatial networks [1-6] leads to the extremely important practical conclusion that a mechanical method can be used for investigating the structure of the spatial network of a polymer and changes taking place in it under the influence of chemical processes in the polymer. The method essentially consists of determination of the equilibrium modulus E_{∞} , the value of which is a measure of the density of the spatial network, i.e., the number of chains N in unit volume (or the number of branch points, $N/2$).

For calculation of N , various theoretical formulas which connect this quantity with the stress, deformation, and temperature, can be used. Most of these formulas [1-4] yield the following relationship between the above quantities:

$$\sigma = 3kT (\lambda^2 - 1/\lambda) N, \quad (1)$$

where σ is the stress calculated for the true cross section of the deformed specimen; λ is the relative length, equal to the ratio of the length of the deformed specimen (between the marks) to its initial length; T is the absolute temperature; k is the Boltzmann constant.

The Bartenev formula [5] represents a weaker dependence of the stress on the number of chains per unit volume:

$$\sigma = \frac{1,26 kT}{l\alpha} (\lambda - 1) N^{2/3}, \quad (2)$$

where l is the statistical length of a segment of a rubber molecule; α is a coefficient equal to the ratio of the statistical length of a segment to its length along the chain contour.

The proportionality factor between stress and deformation in Equations (1) and (2) respectively is given by the expressions:

$$E_{\infty} = 0,43 \times 10^{-21} TN, \quad (3)$$

$$E_{\infty} = \frac{0,24 \times 10^{-21}}{l} TN^{2/3}, \quad (4)$$

where E_{∞} is in kg/cm^2 , T is in $^{\circ}\text{K}$, N is in $1/\text{cm}^3$ and l is in cm .

Thus, Equation (1) indicates that E_{∞} is proportional to N , whereas Equation (2) indicates that E_{∞} is proportional to $N^{2/3}$.

Equations (1) and (2) have been criticized on the grounds that the assumptions on which the theories are based cannot always be accepted without qualification. Our purpose was therefore, to use available experimental data for comparing the relationship between the equilibrium modulus and the number of branch points as given by Equations (3) and (4) and by experimental data.

	Natural rubber	SKS-30A	SKS-30	SKN-40	SKN-26	SKN-18	Butyl rubber	SKB
$l, \text{\AA}$	12.0	12.6	14.6	17.0	19.9	22.2	19.4	20.8
$C \times 10^{-21} [^\circ/\text{kg}]^{3/2}$	11	12	15	19	24	28	23	26

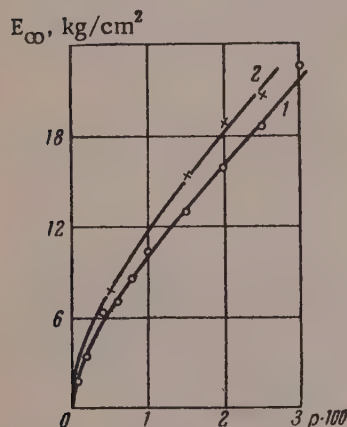


Fig. 1. Variations of the equilibrium modulus of natural (1) and butadiene-styrene (2) rubber vulcanizates with $\rho \times 100$.

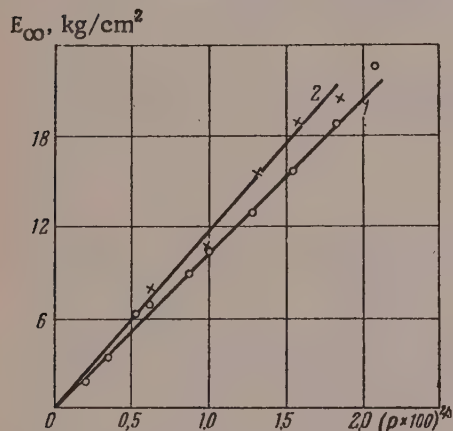


Fig. 2. Variations of the equilibrium modulus of natural (1) and butadiene-styrene (2) rubber vulcanizates with $(\rho \times 100)^{2/3}$.

To check the validity of these equations, it is necessary to determine N by an independent method. Such determinations have been performed in a number of studies. For example, in one investigation [7] the vulcanization agent used was decamethylenebis-*n*-decylazodicarboxylate, from the consumption of which the number of cross-links formed could be estimated. These results show [5, 8] that in $E_\infty - N$ coordinates [where $(\rho \times 100) \propto N$] curves are obtained (Fig. 1), whereas the relationship between E_∞ and $N^{2/3}$ is linear (Fig. 2).

Better agreement of Equation (2) with experimental data was demonstrated by other investigations [9, 10].

In one of these [9], it proved impossible to interpret the vulcanization mechanism of SKS-30A rubber fractions of different molecular weights on the assumption that $E_\infty \propto N$. The consequence of this assumption was that for all fractions with molecular weights from 100,000 to 1,170,000, the number of sulfur atoms in the cross links increased from 1 to 8 during vulcanization. However, if it was assumed that $E_\infty \propto N^{2/3}$ it could be shown that the number of sulfur atoms in the cross links does not alter during vulcanization, which was to be expected. The vulcanization accelerator used was mercapto-benzothiazole which leads to the predominant formation of disulfide bonds in presence of the usual ingredients of rubber mixes [11].

In the study [10] the relationship $E_\infty \propto N^{2/3}$ was used for finding the heat of formation of the cross links; the value found (6 kcal/mole) was consistent with the assumption that cross links are formed by hydrogen bonding. Further confirmation of the relationship $E_\infty \propto N^{2/3}$ was provided by Bucche [12], who studied the dependence of the modulus of polydimethylsiloxane on the radiation dose, which is proportional to N . Results for different polydimethylsiloxane fractions are presented in Fig. 3 and 4. These data lead to the same conclusions as Flory's experiments.

Thus, the available experimental facts indicate that the equilibrium modulus varies, not in proportion to the number of chains per unit volume, but more slowly; this is satisfactorily represented by the relationship $E_\infty \propto N^{2/3}$. We shall therefore,

use Equation (4) for determination of N , taking into account the approximate character of the theory on which this equation is based. The reason for the discrepancy between Equation (3) and experimental data is, in our opinion, the assumption of the statistical independence of the network chains; this is hardly valid for a block polymer. Moreover, Equation (3) does not take into account the chemical characteristics of rubber structure. Equation (4) takes these characteristics into account in terms of the statistical segment length l , which enters

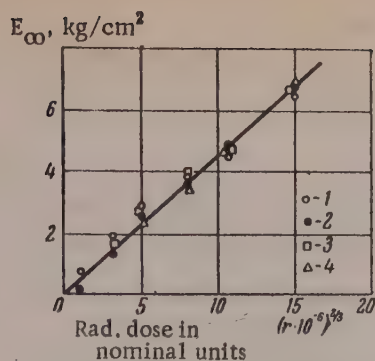
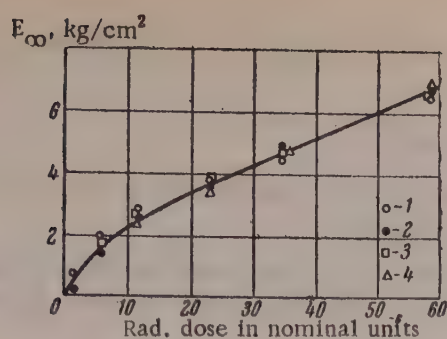


Fig. 3. Relationship between the equilibrium modulus of polydimethylsiloxane with the radiation dose (proportional to N), plotted in two different coordinate systems, for fractions of molecular weight: 1) 890,000; 2) 520,000; 3) 439,000; 4) 220,000.

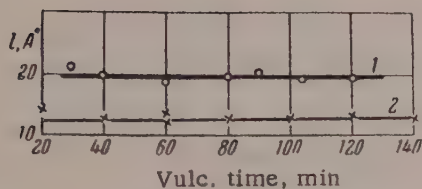


Fig. 4. Graph showing that the statistical segment length of butyl (1) and SKS-30 A (2) rubber molecules is independent of the vulcanization time.

the proportionality factor between E_∞ and $N^{2/3}$. Therefore, for calculation of the proportionality factor in Equation (4) it is necessary to determine l for different rubbers.

The statistical segment length is a structural characteristic of a rubber, and determines the flexibility of the rubber molecules. Calculation of the statistical segment length by means of Bartenev's equations [5] requires a knowledge of the structural characteristics of the rubber — the equilibrium modulus E_∞ and the limiting high-elastic deformation λ_∞ , equal to the ratio of the limiting high-elastic length L_∞ to the initial length of

the specimen L_0 . Both these quantities can be determined experimentally (the methods for their determination have been described [5, 8, 13, 14].

The statistical segment lengths for a number of rubbers are given in the table. The values were calculated from the formula [5]: $l = p/s$, where p is the effective volume of the segment; s is the effective chain cross section. Here $s = 3\mu / \rho N_A l_1$, where μ is the molecular weight of a monomer unit (for copolymers μ is calculated with the percentage contents of the copolymer constituents taken into account); ρ is the density of rubber in the vulcanizate [$\rho = \rho_0 (1 - a)$; ρ_0 is the density of the rubber; a is the fraction of nonrubber material in the vulcanizate]; N_A is the Avogadro number; l_1 is the length of a monomer unit (calculated from x-ray data for crystallizing rubbers, while for noncrystallizing rubbers, it is calculated from known interatomic distances and bond angles). The values so calculated for the statistical segment lengths of rubber molecules are in good agreement with literature values, found by other workers using other methods. Thus, Kuhn and Kuhn [15] found $l = 13$ Å for natural rubber from streaming birefringence data; in another study [16] the same method was used to find $l = 10$ -14 Å for the same rubber, which is in good agreement with our results.

The statistical segment length gives an indication of the flexibility of polymer molecules. For example, for polyisobutylene $l = 35.5$ Å [16], and for gutta-percha $l = 50$ Å [15]. The statistical segment length for different rubbers increases in the following sequence: natural rubber, SKS-30 A, SKS-30, SKN-40, SKN-26, SKN-18, butyl rubber, SKB*.

The statistical segment length, being a structural characteristic of the rubber, should not depend on the density of the spatial network of the rubber over a wide range. The results in Fig. 4 show that the statistical segment length is independent of the degree of vulcanization over a wide range of vulcanization times. Over

*When different rubbers are compared, the statistical segment length, which is an equilibrium value, should not be confused with nonequilibrium characteristics such as internal friction, values of which for different rubbers form a different series [17].

the same time range, the equilibrium modulus increases 1.5-fold for butyl rubber vulcanizates and 2.5-fold for SKS-30 A vulcanizates.

SUMMARY

1. Experimental data of different workers indicate that the equilibrium modulus is proportional to the number of chains per unit polymer volume raised to the power $2/3$.

2. Bartenev's equation was used to calculate statistical segment lengths for molecules of natural rubber, SKS-30 A, SKS-30, SKN-40, SKN-26, SKN-18, butyl rubber, and SKB; the results were in agreement with the experimental results of Kuhn, Stein, and Tobolsky.

3. Values of the constant C for these rubbers are given, for calculation of the number of chains per unit volume of a cross-linked polymer.

I offer my deep gratitude to Professor G. M. Bartenev for valuable advice and comments in the course of this work and discussions.

LITERATURE CITED

- [1] H. James and E. Guht, *J. Chem. Phys.* 11, 455 (1943); 15, 669 (1947); 21, 1039 (1953).
- [2] F. Wall, *J. Chem. Phys.* 10, 132, 485 (1942); 11, 527 (1943).
- [3] L. Treloar, *Trans. Faraday Soc.*, 39, 36, 341 (1943); 40, 59 (1944); 42, 83 (1946).
- [4] P. Flory and J. Rehner, *J. Chem. Phys.*, 11, 512 (1943); 35, 51 (1944).
- [5] G. M. Bartenev, *J. Tech. Phys.* 20, 461 (1950); 22, 1154 (1952).
- [6] M. V. Vol'kenshtein and O. B. Ptitsyn, *J. Tech. Phys.* 25, 662 (1955).
- [7] P. Flory, N. Rabjohn and M. Shaffer, *J. Polymer Sci.* 4, 225 (1949).
- [8] G. M. Bartenev, *Proc. Conference on Vulcanization [In Russian] (Goskhimizdat, 1954) p. 196.*
- [9] A. S. Novikov, G. M. Bartenev and F. A. Galil-Ogly, *Proc. Acad. Sci. USSR* 94, 253 (1954).
- [10] G. L. Slonimskii, V. A. Kargin and L. I. Golubenkova, *Proc. Acad. Sci. USSR* 93, 311 (1953).
- [11] B. A. Dogadkin and Z. N. Tarasova, *Proc. Acad. Sci. USSR* 85, 1069 (1952); *Colloid J.* 15, 347 (1953)*.
- [12] A. Bucche, *J. Polymer Sci.* 19, 297 (1956).
- [13] L. A. Vishnitskaya, *Trans. Sci. Res. Inst. Rubber Ind. No. 1 (Goskhimizdat, 1954) p. 53.*
- [14] G. M. Bartenev, *Colloid J.* 17, 18 (1955)*.
- [15] W. Kuhn and H. Kuhn, *Helv. chim. acta* 26, 1934 (1943).
- [16] R. Stein and A. Tobolsky, *J. Polymer Sci.* 11, 285 (1953).
- [17] G. M. Bartenev, M. M. Reznikovskii and M. K. Khromov, *Colloid J.* 18, 395 (1956)*.

Received April 8, 1957

* Original Russian pagination. See C. B. Translation.

LETTER TO THE EDITOR

THE EFFECTS OF CERTAIN ADDITIVES ON THE SYNERESIS AND STRENGTH OF LITHIUM GREASE, AND ON ITS SUBMICROSTRUCTURE

A. A. Trapeznikov and G. G. Shchegolev

Institute of Physical Chemistry, Academy of Sciences, USSR, Laboratory of Physical Oleocolloids and Monolayers, Moscow

Among the most important characteristics of lithium greases are their syneretic and strength properties. The effects of various organic polar substances added to the grease during its manufacture on these properties are of interest. We studied the effects of such additives with a model lithium grease, prepared under definite temperature conditions in a special cell with a narrow plane gap, which ensured that the cooling was fairly uniform across the thickness of the grease layer.

A 10% isotropic solution of lithium stearate in medicinal petrolatum was cooled in two stages. The first stage was from 230 to 70°, after which the grease was held at 70° for 30 minutes; in the second stage, it was cooled to 0° and held at 0° for 30 minutes. Under such cooling conditions, the soap fibers crystallize and grow under conditions of a strictly-defined temperature drop. The additives were nonylic and lauric acids, introduced into the system before the soap was dissolved. It follows from the curves in Fig. 1, that the structural strength P_r of the grease, determined in an apparatus with a tangentially displaced plate [1], and the oil loss S under pressure, determined by means of the KSA apparatus [2], greatly depend on the amounts of acids added. The value of P_r passes through a maximum and S through a minimum; the abscissas of these values coincide [3]. In the case of lauric acid, the positions of both extrema lie at a lower molar ratio of additive to soap than in the case of nonylic acid, while the absolute value of P_r is greater and that of S is less with nonylic acid. The opposing course of the P_r and S curves indicates that these properties are closely interrelated. The greater the structural strength, the less is the oil loss under pressure. Fig. 2, a, b, c are electron micrographs of soap fibers [4] in greases containing respectively 0; $1.8 \cdot 10^{-2}$; $18 \cdot 10^{-2}$ moles of nonylic acid per mole of Li stearate. Fig. 2, d shows microfibers of soap in a grease containing $18 \cdot 10^{-2}$ mole of nonylic acid per mole of Li stearate after storage during one year at room temperature. It is clear from the micrographs that when the additive concentration is $1.8 \cdot 10^{-2}$ the fibers decrease in size, while at a concentration of $18 \cdot 10^{-2}$ they greatly increase; this is especially noticeable after aging. Aging has a strong influence both on the decrease of structural strength and on the increase of oil loss under pressure.

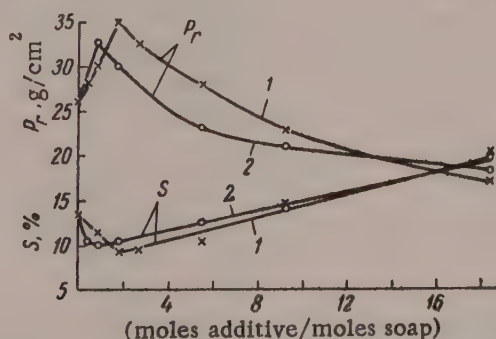


Fig. 1. Effects of added fatty acids on strength P_r and oil loss S under pressure, for a 10% lithium grease: 1) nonylic acid; 2) lauric acid.



Fig. 2. Electron micrographs of microfibrils of lithium soap in greases with additions of nonylic acid: a) no addition; b) with $1.8 \cdot 10^{-2}$ mole of nonylic acid per mole of Li stearate; c) with $18 \cdot 10^{-2}$ mole of nonylic acid per mole of Li stearate; d) the same, after one year of storage.

SUMMARY

A study has been made of the effect of the additions of nonylic and lauric acids on the synergetic and strength properties of lithium grease and on its submicrostructure. With increase in the amount of the addition the strength of the grease structure and amount of oil capable of being pressed out pass through a maximum and minimum respectively. The maximum and minimum for lauric acid are shifted in the direction of lower molecular ratios of the addition to the soap as compared with nonylic acid. It follows from electron microscopic photographs that the size and shape of the soap microfibrils of the grease containing nonylic acid depend upon the amount of the additive and on the time of storage of the grease.

LITERATURE CITED

- [1] G. G. Shchegolev, A. M. Tolmachev and A. A. Trapeznikov, *Industrial Lab.* 25, No. 5, 625 (1959).
- [2] GOST 7142-54.
- [3] A. A. Trapeznikov and G. G. Shchegolev, *Summaries of Papers at the 4th All-Union Conference on Colloid Chemistry* [In Russian] (Izd. AN SSSR, Moscow, 1958) p. 271.
- [4] A. A. Trapeznikov, G. G. Shchegolev and I. I. Astakhov, *2nd Conference on Electron Microscopy, Summaries of Papers* [In Russian] (Moscow, 1958) p. 35.

Received July 10, 1958

THEORY OF THERMAL PRECIPITATION OF HIGHLY DISPERSE AEROSOL SYSTEMS

S. P. Bakanov and B. V. Deryagin

Institute of Physical Chemistry, Academy of Sciences USSR, Moscow

The removal of suspended foreign particles from gases by passage of the gases through a chamber in which a temperature gradient $\text{grad } T$ is maintained (the thermal precipitation method) is a method widely used both in scientific research and in industrial practice. However, there is as yet no strict quantitative theory of this process. In the development of such a theory three cases must be distinguished, corresponding to different size σ_1 of the aerosol particles: 1) $\sigma_1 \ll \lambda$, where λ is the mean free path of the gas molecules; 2) $\sigma_1 \gg \lambda$ and 3) $\sigma_1 \sim \lambda$. The solution of the problem requires a different approach in each of these three cases.

In this paper we consider the problem of thermal precipitation of highly disperse aerosol systems (the first case). Quantitatively (under atmospheric pressure) this corresponds to aerosol particles 10^{-6} cm and less in size.

I. We consider a highly disperse aerosol system, in which a small temperature gradient is maintained, as a mixture of two gases – the gas itself, and dust. In this case, as in thermodiffusional separation of a mixture of two gases, the mixture undergoes separation. The velocity of the aerosol particles relative to the center of gravity of the sum of the gas molecules can be readily calculated from the Chapman-Enskog formula, obtained by solution of the Boltzmann kinetic equation:

$$\vec{u} = - \frac{n^2}{n_1 n_2} D_{12} k_T \text{grad } T, \quad (1)$$

where n_1 is the number of aerosol particles per cc; n_2 is the number of gas molecules per cc; $n = n_1 + n_2$; D_{12} is the coefficient of diffusion in this system; k_T is the thermal diffusion ratio; T is the absolute temperature.

In general, Equation (1) should contain an additive term proportional to the concentration gradient of the components of the mixture (only one, since the pressure is constant and consequently the molar concentration gradients of the two components are equal, but opposite in sign). However, at extremely low concentrations of the aerosol particles, or for the limiting case of low concentrations, or if we are concerned with the rate of separation at the initial instant when the concentration gradient has not yet appeared, the term as written is sufficient.

The unknown quantities D_{12} and k_T can be calculated by the Chapman-Enskog method; they are expressed in the form:

$$D_{12} = \frac{3kT}{2n} \frac{A_{00}}{A}; \quad (2)$$

$$k_T = (n_{10} m_0^{-1/2} A_{01} + n_{20} m_2^{-1/2} A_{0-1}) / A_{00}, \quad (3)$$

where k is the Boltzmann constant; $n_{10} = n_1 / n$, $n_{20} = n_2 / n$; m_1 and m_2 respectively are the masses of an aerosol particle and a gas molecule; A_{00} , A , A_{01} and A_{0-1} are certain determinants of infinite order.

In calculation of the velocity of thermal precipitation we confine ourselves to the first approximation. In this case the determinant A is of the form:

$$A = \begin{vmatrix} a_{-1-1} & a_{0-1} & a_{1-1} \\ a_{-10} & a_{00} & a_{10} \\ a_{-11} & a_{01} & a_{11} \end{vmatrix}, \quad (4)$$

and the determinants A_{00} , A_{01} , and A_{0-1} are minors to A , corresponding to the elements a_{00} , a_{01} and a_{0-1} . For calculation of a_{pq} it is necessary to start with the law for the interaction of the gas molecules with each other and with the aerosol particles (it is obvious that in all practical cases $n_1 \ll n_2$, and collisions between the aerosol particles may be disregarded). First, we consider the case when all the interactions conform to the law of collision between elastic spheres. Calculation of a_{pq} then presents no difficulty, and the values can be taken directly from Chapman and Cowling's book [1]. For the case $m_1 \gg m_2$ we have

$$\begin{aligned} a_{00} &= 4m_2 \left(\frac{2\pi kT}{m_2} \right)^{1/2} \sigma_{12}^2, \\ a_{01} &= -2m_1^{1/2} m_{21}^2 \left(\frac{2\pi kT}{m_2} \right)^{1/2} \sigma_{12}^2; \\ a_{0-1} &= 2m_2^{1/2} \left(\frac{2\pi kT}{m_2} \right)^{1/2} \sigma_{12}^2; \\ a_{1-1} &= -27m_{21}^2 \left(\frac{2\pi kT}{m_2} \right)^{1/2} \sigma_{12}^2; \\ a_{11} &= \left[m_{21} (30 + 13m_{21}^2 + 16m_{21}) + 4\sqrt{2} n_{12} \left(\frac{\sigma_1}{\sigma_{12}} \right)^2 m_{21}^{1/2} \right] \left(\frac{2\pi kT}{m_2} \right)^{1/2} \sigma_{12}^2; \\ a_{1-1} &= \left[30m_{21}^2 + 13 + 16m_{21} + 4\sqrt{2} n_{21} \left(\frac{\sigma_2}{\sigma_{12}} \right)^2 \right] \left(\frac{2\pi kT}{m_2} \right)^{1/2} \sigma_{12}^2. \end{aligned} \quad (5)$$

Here $m_{21} = m_2/m_1$; σ_2 is the average diameter of a gas molecule; $\sigma_{12} = \frac{1}{2}(\sigma_1 + \sigma_2)$.

Equations (5) can be simplified somewhat. When $\sigma_1 \sim 10^{-6} - 10^{-7}$ cm $\sigma_{12} \approx \frac{1}{2} \sigma_1$. The mass of an aerosol particle of this size is $m_1 \sim 10^{-17} - 10^{-20}$ g. Consequently, $m_{21} \sim 10^{-7} - 10^{-4}$. Finally, if it is assumed that $n_1 = 10^3$, then $n_{21} = 10^{16}$ $n_{20} \sim 1$. Hence we have:

$$\begin{aligned} a_{11} &= \frac{30m_{21}}{4} \left(\frac{2\pi kT}{m_2} \right)^{1/2} \sigma_{12}^2; \\ a_{-1-1} &= 4\sqrt{2} n_{21} m_{21}^{1/2} \left(\frac{\sigma_2}{\sigma_1} \right)^2 \left(\frac{2\pi kT}{m_2} \right)^{1/2} \sigma_{12}^2. \end{aligned} \quad (6)$$

Further, in this case

$$\begin{aligned} A &= 30m_2 m_{21} \cdot \sqrt{2} n_{21} \left(\frac{\sigma_2}{\sigma_1} \right)^2 \left(\frac{2\pi kT}{m_2} \right)^{1/2} \sigma_{12}^6, \\ A_{01} &= -2m_{21}^{1/2} m_1^{1/2} \sqrt{2} n_{21} \left(\frac{\sigma_2}{\sigma_1} \right)^2 \left(\frac{2\pi kT}{m_2} \right)^{1/2} \sigma_{12}^4; \\ A_{0-1} &= \frac{15}{4} m_2^{1/2} m_{21} \left(\frac{2\pi kT}{m_2} \right)^{1/2} \sigma_{12}^4. \end{aligned} \quad (7)$$

Hence

$$k_T = \frac{5}{2} \cdot \frac{15}{4} m_{21} \left(\frac{2\pi kT}{m_2} \right)^{1/2} \sigma_{12}^4 / A_{00}, \quad (8)$$

$$\vec{u} = -\frac{15}{8} \frac{1}{4\sqrt{2} n_{20} \sigma_2^2} \left(\frac{kT}{2\pi m_2} \right)^{1/2} \frac{\text{grad } T}{T}, \quad (9)$$

or, substituting into (9) the known expressions for the mean velocity of the gas molecules \bar{c}_2 and the free path λ

$$\bar{c}_2 = \left(\frac{8kT}{\pi m_2} \right)^{1/2}, \quad (10)$$

$$\lambda = \frac{1}{\sqrt{2} n_2 \pi \sigma_2^2}, \quad (11)$$

we finally have

$$\vec{u} = -\frac{15\pi}{128} \lambda \bar{c}_2 \frac{\text{grad } T}{T} \simeq -0,37 \frac{\lambda}{T} \bar{c}_2 \text{grad } T. \quad (12)$$

Thus, the velocity of thermal precipitation when $\sigma_1 \ll \lambda$ is independent of the particle size and is inversely proportional to the square root of the average temperature and pressure of the gas. The velocity \vec{u} at atmospheric pressure, $T = 300^\circ$, and $\text{grad } T = 30^\circ/\text{cm}$ for air is of the order of 0,25 mm/second.

It should be noted that Einstein [2] derived an equation of similar form for the velocity \vec{u} .

$$\vec{u} = -\frac{1}{8} \frac{\lambda}{T} \bar{c}_2 \text{grad } T = -0,125 \frac{\lambda}{T} \bar{c}_2 \text{grad } T, \quad (13)$$

with a numerical coefficient about one third of that in our equation.

II. For consideration of more general cases, of greater physical reality, of the interaction of gas molecules with the surfaces of aerosol particles it is more convenient to use another method, applied by us earlier [3] to solution of the problem of "diffusiophoresis" of small particles. This method consists of calculation of the resultant force with which a nonuniformly heated gas acts on an aerosol particle suspended in it.

Let a small constant temperature gradient be maintained in the gas. Then the distribution function for the gas molecule velocities can be written in the form:

$$f^{(1)} = f^{(0)} \left[1 + \left(\frac{2kT}{m_2} \right)^{1/2} \frac{1}{T n_2} \vec{B} \text{grad } T \right], \quad (14)$$

where

$$f^{(0)} = n_2 \left(\frac{m_2}{2\pi kT} \right)^{3/2} e^{-\frac{m_2 c_2^2}{2kT}};$$

$f^{(0)}$ is the equilibrium Maxwell distribution.

It can be shown (see [1]) that $\vec{B} = B(\vec{C}) \vec{C}$, where $\vec{C} = \left(\frac{m_2}{2kT} \right)^{1/2} \vec{c}$, and that B can be resolved into series by the Sonine polynomials:

$$\vec{B} = \sum_0^\infty a_r \vec{a}^{(r)}, \quad (15)$$

and $a_0 = 0$. Taking only the first term of the series, which is an adequate approximation of the same order as in the first section of this paper, we write B in the form:

$$\vec{B} = a_1 \vec{a}^{(1)} = a_1 S_{1/2}^{(1)}(C^2) \vec{C}. \quad (16)$$

The method described in [1] (see also [3]) can be used to calculate a_1 . On the assumption that the interaction of the gas molecule is elastic, a_1 has the value:

$$a_1 = \frac{15}{16} \left(\frac{\pi m_2}{2kT} \right)^{1/2} n_2 \lambda. \quad (17)$$

Hence Equation (14) may be written in the form:

$$f^{(1)} = f^{(0)} \left[1 + \frac{15\pi^{1/2}}{16} \frac{\lambda}{T} S_{1/2}^{(1)}(C^2) \vec{C} \cdot \text{grad } T \right]. \quad (14')$$

A small aerosol particle placed in a gas in which a temperature gradient is maintained, without affecting the distribution (14), acquires in addition to its random Brownian movement an ordered component of its velocity \vec{u} . The magnitude of this velocity that the average impulse per second transmits to the particle during collisions of the molecules is zero. For convenience in calculation, we adopt a system of coordinates moving together with the particle. The distribution Equation (14') is then transformed as follows (subsequently, the subscript 2 in the symbols n_2 , c_2 , and m_2 is omitted; it will be remembered that these quantities refer to gas molecules):

$$f^{(1)} = n \left(\frac{m}{2\pi kT} \right)^{3/2} e^{-(\vec{C} + \vec{U})^2} \left[1 + \frac{15\pi^{1/2}}{16} \frac{\lambda}{T} S_{1/2}^{(1)}(C^2) \vec{C} \cdot \text{grad } T \right], \quad (18)$$

where $\vec{U} = \left(\frac{m}{2\pi kT} \right)^{1/2} \vec{u}$. At sufficiently low values of $\text{grad } T$, $u \sim \text{grad } T \ll \bar{c}$. We, therefore, disregard terms containing u^2 and terms containing the product $u \cdot \text{grad } T$. We resolve the exponent in Equation (18) into a power series of the small ratio u/c ; taking only the first-degree term in this resolution we have

$$f^{(1)} = n \left(\frac{m}{2\pi kT} \right)^{3/2} e^{-C^2} (1 - 2\vec{C} \cdot \vec{U}) \left[1 + \frac{15\pi^{1/2}}{16} \frac{\lambda}{T} S_{1/2}^{(1)} \vec{C} \cdot \text{grad } T \right], \quad (18')$$

or

$$f^{(1)} = n \left(\frac{m}{2\pi kT} \right)^{3/2} e^{-C^2} \left[1 - 2\vec{C} \cdot \vec{U} + \frac{15\pi^{1/2}}{16} \frac{\lambda}{T} S_{1/2}^{(1)} \vec{C} \cdot \text{grad } T \right]. \quad (18'')$$

We first calculate the number of molecules colliding with an element dS of the surface of a spherical particle. For this we multiply $f^{(1)}$ by $-c \cos \psi$, where ψ is the angle between the velocity \vec{c} of the molecule and the normal \vec{n} to dS at the instant of impact, and integrate with respect to angles and velocities:

$$dN^{(1)} = - \int f^{(1)} c \cos \psi \sin \phi \, d\phi \, d\varphi \, c^2 \, dc \, dS. \quad (19)$$

If the angle between \vec{c} and \vec{u} is denoted by ϑ , we have from spherical trigonometry

$$\cos \vartheta = \cos \phi \cos \theta + \sin \phi \sin \theta \cos \varphi,$$

where θ is the angle between \vec{n} and \vec{u} , and φ is the azimuth of \vec{c} in the coordinate system associated with n . We denote the projection of the vector \vec{u} onto the direction of OZ (the direction of the OZ axis is opposite to the vector of $\text{grad } T$) by u_z . In expanded form Equation (19) becomes:

$$\begin{aligned} dN^{(1)} = & -n \left(\frac{m}{2\pi kT} \right)^{3/2} \int e^{-C^2} \left[1 - 2CU_z \cos \vartheta - \frac{15\pi^{1/2}}{16} \frac{\lambda}{T} S_{1/2}^{(1)} \times \right. \\ & \left. \times C |\text{grad } T| \cos \vartheta \right] c^3 dc \cos \phi \sin \phi \, d\phi \, d\varphi \, dS. \end{aligned}$$

Integration with respect to ψ between $\pi/2$ and π , and with respect to φ between 0 and 2π gives

$$dN_c^{(i)} = n \left(\frac{m}{2\pi kT} \right)^{3/2} e^{-C^2} c^3 dc dS \left[\pi + 2CU_z \cdot \frac{2\pi}{3} \cos \theta + \right. \\ \left. + \frac{5\pi^{3/2}}{8} \frac{\lambda}{T} S_{1/2}^{(1)} C |\text{grad } T| \cos \theta \right]. \quad (20)$$

Finally, integration with respect to absolute values of the velocity c between 0 and ∞ gives

$$dN^{(i)} = n \left(\frac{kT}{2\pi m} \right)^{1/2} \left[1 + \left(\frac{\pi m}{2kT} \right) u_z \cos \theta \right] dS. \quad (21)$$

The projection of the impulse of the molecule onto OZ is equal to $mc \cos \theta$. Hence, the impulse transmitted to the area dS by the molecules colliding with it per unit time in the direction OZ is

$$dW^{(i)} = -mn \left(\frac{m}{2\pi kT} \right)^{3/2} \int e^{-C^2} c^4 dc \cos \psi \sin \psi d\psi d\varphi \left[1 - \right. \\ \left. - 2CU_z \cos \theta - \frac{15\pi^{3/2}}{16} \frac{\lambda}{T} S_{1/2}^{(1)} C |\text{grad } T| \cos \theta \right] \cos \theta dS. \quad (22)$$

Integration with respect to the angles ψ between $\pi/2$ and π , and φ between 0 and 2π , and with respect to the absolute values of c between 0 and ∞ gives

$$dW^{(i)} = -kTn \left[\frac{\cos \theta}{2} + \left(\frac{m}{2\pi kT} \right)^{1/2} (\cos^2 \theta + 1) u_z - \frac{15}{64} \frac{\lambda}{T} |\text{grad } T| (\cos^2 \theta + 1) \right] dS. \quad (23)$$

The force due to the impact of the molecules can be found by integration for the whole sphere. If changes of gas concentration over a distance of the same order as the diameter of an aerosol particle are disregarded, we have

$$W^{(i)} = \frac{16\pi kTn}{3} \sigma_1^2 \left[\frac{15}{64} \frac{\lambda}{T} |\text{grad } T| - \left(\frac{m}{2\pi kT} \right)^{1/2} u_z \right]. \quad (24)$$

Next, we consider the recoil impulse transmitted to the sphere by the gas molecule on rebound (or evaporation) from its surface. The magnitude of this impulse differs in accordance with the nature of the interaction between the molecules and the surface.

Consider three thermodynamically admissible laws of rebound: 1) the mirror type (elastic rebound); 2) diffuse scattering (by the cosine law) with the absolute velocity unchanged; 3) diffuse evaporation of the molecules from the surface.

Case 1. The simplest case of interaction between a gas molecule and the particle surface is mirror rebound, when only the sign of the normal component of the velocity of the molecule (the sign of $\cos \psi$ in our notation) is changed. It is easily shown that reversal of the sign of $\cos \psi$ results in replacement of the term $(\cos^2 \theta + 1)$ in Equation (23) by the factor $(3 \cos^2 \theta - 1)$. On integration for the whole sphere the terms containing this factor become zero. Hence the total impulse in this case is

$$W_1 = \frac{16\pi kTn}{3} \sigma_1^2 \left[\frac{15}{64} \frac{\lambda}{T} |\text{grad } T| - \left(\frac{m}{2\pi kT} \right)^{1/2} u_z \right]. \quad (25)$$

Case 2. Interaction of this type presupposes that each molecule retains its previous velocity on rebounding from the surface, i.e., that the number of molecules rebounding from the surface at a velocity in the range $(c, c + dc)$ is given by Equation (20). The directions of the velocities of the rebounded molecules do not depend

on the directions before impact, and are distributed in space in conformity to the cosine law (similar to the Lambert cosine law of light reflection). Thus, the mean impulse transmitted to a rebounded molecule with a velocity in the range $(c; c + dc)$ in the OZ direction is

$$\frac{\int_0^{\pi/2} \int_0^{2\pi} mc \cos \vartheta \cos \psi \sin \psi d\psi d\varphi}{\int_0^{\pi/2} \int_0^{2\pi} \sin \psi \cos \psi d\psi d\varphi} = \frac{2}{3} mc \cos \vartheta. \quad (26)$$

Consequently, the impulse imparted to an element dS of the surface of an aerosol particle in the direction OZ by rebound of the gas molecules is in this case (with the negative sign of the whole expression taken into account):

$$dW_2^{(e)} = \frac{16}{9} kTn \cos \theta \left[\frac{15}{64} \frac{\lambda}{T} |\text{grad } T| \cos \theta - \frac{9}{32} - \left(\frac{m}{2\pi kT} \right)^{1/2} u_z \cos \theta \right] dS. \quad (27)$$

Integration of (27) for the whole sphere gives:

$$W_2^{(e)} = \frac{64\pi kTn\sigma_1^2}{27} \left[\frac{15}{64} \frac{\lambda}{T} |\text{grad } T| - \left(\frac{m}{2\pi kT} \right)^{1/2} u_z \right]. \quad (28)$$

The total impulse for this case is given by the expression:

$$W_2 = \frac{16\pi kTn\sigma_1^2}{3} \cdot \frac{13}{9} \left[\frac{15}{64} \frac{\lambda}{T} |\text{grad } T| - \left(\frac{m}{2\pi kT} \right)^{1/2} u_z \right]. \quad (29)$$

Case 3. In diffuse evaporation of molecules from the surface of an aerosol particle, in contrast to the cases already considered, the only condition to hold is equality of the number of molecules colliding with an element of the surface to the number evaporating from it. Let the number of molecules evaporating from a surface element dS per unit time at velocities in the $(c, c + dc)$ range be represented by an expression of the type of (19):

$$dN^{(e)} = \int Q e^{-C^2} c^3 \cos \phi \sin \phi d\phi d\varphi dc dS. \quad (30)$$

The value of the coefficient Q is found from the above-named equilibrium condition. We integrate (30) with respect to the velocity space:

$$dN^{(e)} = \int_0^\infty dc \int_0^{2\pi} d\varphi \int_0^{\pi/2} Q e^{-C^2} c^3 \cos \phi \sin \phi d\phi d\varphi dS = \left(\frac{2kT}{m} \right)^2 Q \frac{\pi}{2} dS. \quad (31)$$

Equating $dN^{(i)}$ (Equation 21) to $dN^{(e)}$ we have

$$Q = n \left(\frac{m}{2\pi kT} \right)^{1/2} \left[1 + \left(\frac{\pi m}{2kT} \right)^{1/2} u_z \cos \theta \right] dS. \quad (32)$$

The projection of the recoil impulse onto the direction OZ is found by multiplication of the distribution expression (30), in conjunction with (32), by $mc \cos \vartheta$ and integration with respect to the velocity space. This gives:

$$dW^{(e)} = -\frac{kTn}{2} \cos \theta \left[1 + \left(\frac{\pi m}{2kT} \right)^{1/2} u_z \cos \theta \right] dS. \quad (33)$$

Finally, integration for the whole sphere gives the total recoil impulse in this case:

$$W_3^{(e)} = -\frac{2\pi^2 k T n \sigma_1^2}{3} \left(\frac{m}{2\pi k T} \right)^{1/2} u_z, \quad (34)$$

Addition of (34) and (35)* gives the total impulse for this interaction:

$$W_3 = \frac{2\pi k T n \sigma_1^2}{3} \left[\frac{15}{8} \frac{\lambda}{T} |\text{grad } T| - \left(\frac{m}{2\pi k T} \right)^{1/2} (8 + \pi) u_z \right]. \quad (35)$$

Equating the force with which the gas molecules act on the aerosol particle to zero, we find the required velocity of thermophoresis; for all three cases considered it is given by an expression of the form:

$$\vec{u} = -\frac{15\pi}{16\mu} \frac{\lambda}{T} \text{grad } T, \quad (36)$$

here

$$\mu_1 = \mu_2 = 8; \mu_3 = 8 + \pi.$$

Hitherto, the thermophoresis velocity has been calculated in a calculation system rigidly linked to the center of mass of the gas (air). This velocity can be measured experimentally only under conditions when side walls (parallel to the heat flow) are absent, such as in the movement of an aerosol in the free and unequally heated terrestrial atmosphere.

However, in many cases of practical importance we are concerned with devices in which there are such walls. The unequally heated gas acts on the walls, and this causes slip of the gas along the latter. If the device is a pipe with open ends, the gas as a whole moves in it at a velocity equal to the sliding velocity [4]:

$$\vec{c}_0 = \frac{3}{4} \frac{\eta}{\rho T} \text{grad } T, \quad (37)$$

where η is the coefficient of viscosity and ρ is the density of the gas. The direction of the velocity coincides with the direction of grad T . Hence, the velocity of an aerosol particle relative to the walls is

$$\vec{u}' = \frac{3}{4} \frac{\text{grad } T}{T} \left(\frac{\eta}{\rho} - \frac{5\pi}{4\mu} \bar{c}\lambda \right). \quad (38)$$

According to the well-known kinetic gas equation (see [1])

$$\eta = \frac{5}{16\sigma_2^2} \sqrt{\frac{k T m}{\pi}}, \quad (39)$$

or, introducing λ and \bar{c} in accordance with (10) and (11), we have

$$\eta = \frac{5\pi}{32} \bar{c}\lambda\rho. \quad (40)$$

Equation (38) is rewritten in the form

$$\vec{u}' = \frac{15\pi}{16} \frac{\lambda}{T} \text{grad } T \left(\frac{1}{8} - \frac{1}{\mu} \right). \quad (41)$$

* As in original - Publisher's note.

If the action of the gas molecules conforms to cases 1 and 2 considered above, the particle is at rest relative to the walls. With diffuse scattering (case 3) the velocity \vec{u}' is given by the expression:

$$\vec{u}' = \frac{15\pi^2}{128(8+\pi)} \frac{\lambda}{c} \text{grad } T. \quad (42)$$

In practice case 3 is not found in the pure form: the molecules partially undergo elastic rebound. If this is taken into account the value of the numerical coefficient in Equation (42) is somewhat lowered. Finally, if an unequally heated gas is contained in a sealed tube, slip due to temperature near the walls results in a flow of gas in the opposite direction near the tube axis. This leads to a steady state such that the average gas flow over the tube section is zero. In this case, since the flow velocity of the gas depends on the distance from the wall, the velocity of thermophoresis relative to the tube wall must also depend on the distance; its sign may also change.

SUMMARY

1. A small aerosol particle (of diameter $\sigma_1 \ll \lambda$) suspended in a nonuniformly heated gas does not change the velocity distribution of the gas molecules to an appreciable extent but acquires, under the influence of impacts with the gas molecules, an ordered velocity component u in addition to its random Brownian motion. The direction of this velocity is opposite to the direction of grad T .

2. The value of u is proportional to grad T , inversely proportional to the gas pressure and the square root of the mean temperature and the molecular weight of the gas, and independent of the particle size.

3. The numerical value of the thermophoretic velocity depends, under given conditions, on the type of interaction between the gas molecules and the particle surfaces. This velocity is the same for elastic and diffuse rebound (at the same absolute velocity) of the molecules, and less by ~25% for diffuse scattering.

LITERATURE CITED

- [1] S. Chapman and J. G. Cowling, *The Mathematical Theory of Nonuniform Gases* (Cambridge, 1939).
- [2] A. Einstein, *Zs. Physik* 27, 1 (1924).
- [3] B. V. Deryagin and S. P. Bakanov, *Proc. Acad. Sci. USSR* 117, No. 6 (1957).*
- [4] P. Epstein, *Zs. Physik* 54, 537 (1929).

Received July 15, 1958

* Original Russian pagination. See C.B. Translation.

PRECIPITATION OF ARTIFICIAL MISTS

I. I. Belyaeva and N. S. Smirnov

Institute of Combustible Minerals, Academy of Sciences USSR, Moscow

Our previous communications [1, 2] were concerned with studies of mist formation by the action of ionizing radiations on highly disperse aerosols (ordinary air at relative humidity not above 100%). The present paper contains a brief account of the results obtained in a study of the precipitation of such mists.

The first series of experiments, with irradiation of ordinary moist air by α -particles, was performed by means of the apparatus described previously [2]. Small ($\sim 3 \text{ cm}^2$) thin (0.2 mm) glass plates, previously coated with a mixture of transformer oil and petrolatum, were placed on the floor of the chamber to protect the water droplets against evaporation when the photomicrographs were taken.*

When the radioactive source was introduced a mist was formed in the chamber, droplets settled on the glass plates, and photomicrographs of the precipitate were taken (see Fig. 1, micrographs 1, 2, 3).

Micrographs 1-3 show that when moist air was irradiated by α -particles a precipitate consisting of droplets up to 15μ in diameter was formed on the floor of the chamber; the number and size of these droplets depend on the irradiation time.

The second series of experiments was conducted in cylindrical glass chambers ($d = 11.0 \text{ cm}$; $h = 45.6 \text{ cm}$; $V = 4.4 \text{ liters}$), with irradiation of ordinary air by β -particles. Micrographs of the precipitates formed in these experiments are shown in Fig. 1, 4-6.

It is clear from Micrographs 1-6 that the precipitates formed by irradiation of a highly disperse aerosol (ordinary moist air) by α - and β -particles become more coarsely disperse with increase of irradiation time.

In the third series of experiments moist air was subjected to γ -radiation of varying intensities from Co^{60} ; photomicrographs of the precipitates were taken (No. 7-10, Fig. 1).

Micrographs 7-10 show that the dispersity of the precipitates depends on the radiation intensity, and the higher intensity the more numerous and larger the droplets. With weak irradiation (0.37 mcurie) the size and number of the precipitated droplets did not increase appreciably (in an airtight chamber) even after irradiation for 96 hours; sources of activity $\geq 3.7 \text{ mcurie}$ gave precipitates which increased with the irradiation time.

The usual method of microphotography used for studying precipitation cannot give an idea of the course of precipitation with time. We therefore devised a simple instrument for observing the course of precipitation in time. A quartz balance of type commonly used for sedimentation analysis of lyodisperse systems [3] was used; the only difference was that microscopic displacements of the depth of curvature were determined relative to a quartz rod (a fixed mark) directly connected with the elastic element of the quartz balance to form a single quartz system. The quartz balance is represented schematically in Fig. 2.

* If the sources of the ionizing radiations were not contained in the chambers, no droplets from the precipitated mist could be observed microscopically on the plates over a period of 7-10 days; this was confirmed by our optical observations, as a mist was not formed in the chamber in absence of the source during a period ≥ 100 hours. At the natural level of ionization visible mists are not formed under such conditions (at $\sim 100\%$ relative humidity).

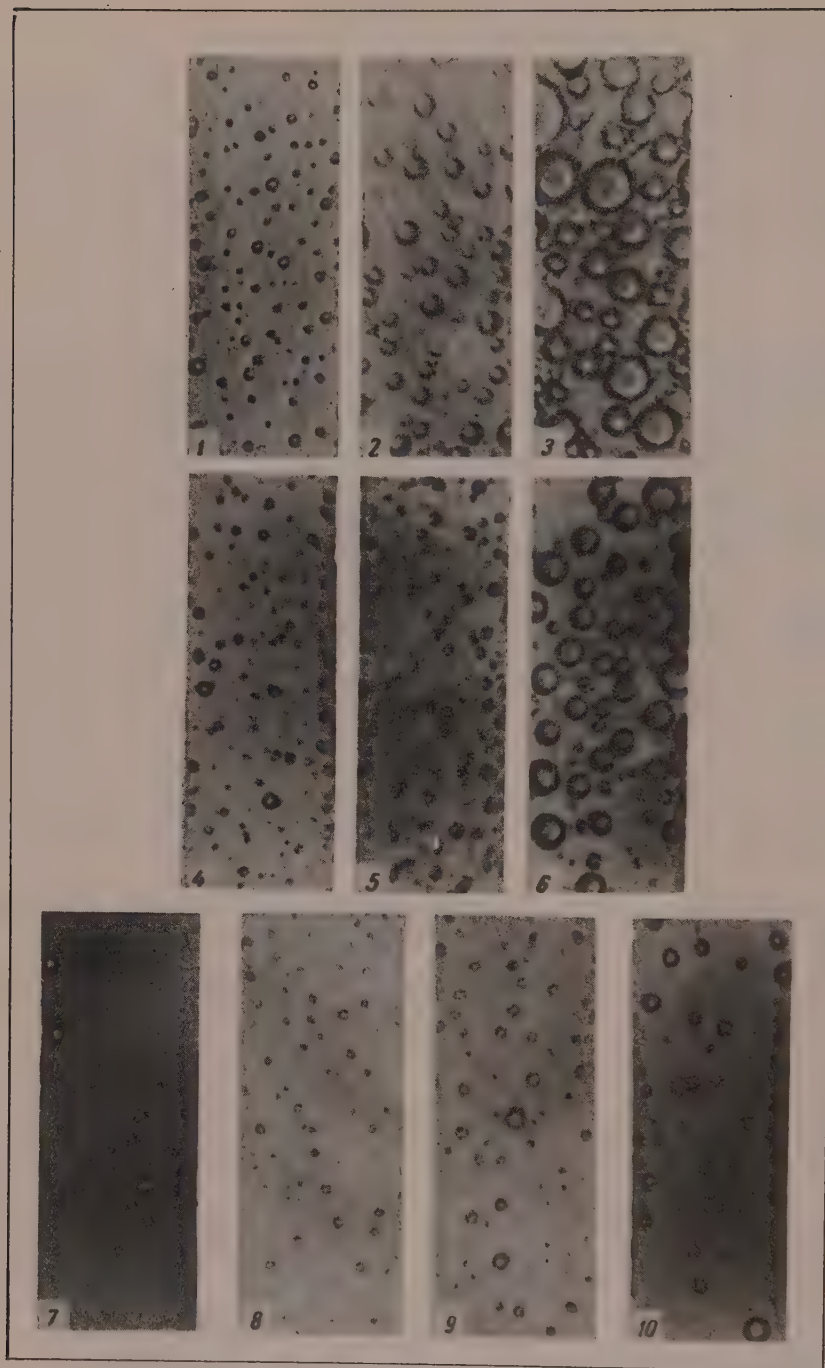


Fig. 1. Micrographs of precipitated water droplets after exposure to α - and β -particles and γ -radiation: α -particles: 1) 24 hours, 2) 48 hours, 3) 96 hours; β -particles: 4) 24 hours, 5) 48 hours, 6) 96 hours; γ -quanta: 7) 24 hours, activity 0.37 mcurie; 8) the same, 12 mcurie; 9) 27 hours, activity 3.7 mcurie; 10) 72 hours, activity 12 mcurie.

The elastic element of the microbalance is a thin thread 1 made of quartz glass, fused onto a quartz rod 2 which is the base of the elastic system. The free end of the thread 1 is fused to a thin horizontal quartz plate 3, onto which the aerosol particles settled. The fused-quartz plates used were 0.1-0.2 mm thick, 1 cm² in area, and 25-42 mg in weight. A thin quartz rod 4 was fused under the elastic thread for measurement of its deflection. The measurements were performed microscopically by means of the micrometer eyepiece 5, indicated conventionally in Fig. 2. By the theory of elasticity, the sensitivity of such a quartz microbalance is directly proportional to the cube of the thread length and inversely proportional to the fourth power of its diameter. Microbalances of roughly the same length (~10 cm) and with different thread thicknesses were used. The balances

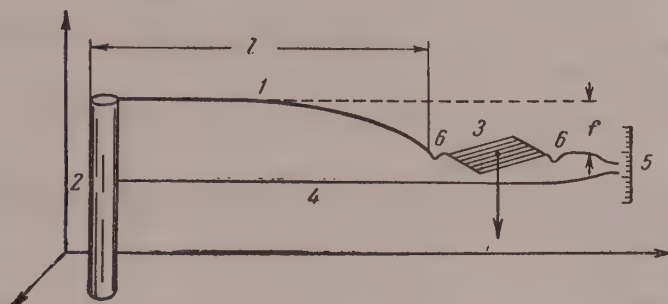


Fig. 2. Schematic diagram of quartz microbalance for observing precipitation of aerosols.

were calibrated by means of small weights made in the form of riders of platinum wire, 0.05 mm in diameter. These weights were placed successively at specially prepared points 6, and average values of two deflection determinations were taken. The sensitivity of the microbalances was $10^{-5} - 10^{-6}$ g.

The experiments on precipitation of aerosols formed after irradiation with α -particles were conducted in a cylindrical chamber. The apparatus is shown schematically in Fig. 3. The apparatus was kept in a basement room at constant temperature and relative humidity (the temperature fluctuations were $< \pm 1^\circ \text{C}$). There was no displacement of the quartz thread with the sedimentation plate for 72-100 hours before introduction of the radioactive source into the chamber. After the radioactive source had been introduced a mist was formed and began to settle on the plate. The results of the experiments are given in Fig. 4.

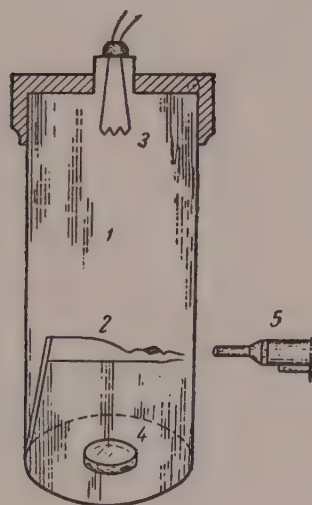


Fig. 3. Schematic diagram of apparatus used for observing the precipitation process: 1) cylindrical aerosol chamber, $d = 11$ cm, $h = 45.6$ cm, $V = 4.4$ liters; 2) quartz microbalance; 3) source of α -radiation; 4) basin of water to produce 100% relative humidity; 5) horizontal microscope.

Figure 4 shows that the mist is formed continuously, during the entire time of action of the ionizing

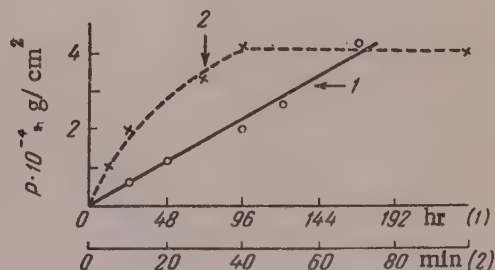


Fig. 4. Curves representing the course of aerosol precipitation: 1) mist formed by irradiation of ordinary moist air with α -particles; 2) smoke formed by combustion of red phosphorus in dry air.

radiations on the moist air. Visual confirmation of this is provided in Fig. 4 by Curve 2 for the precipitation of an ordinary aerosol, when a small electric heater in which a sample of red phosphorus was burned was introduced into the chamber instead of the radiation source. It is seen in Fig. 4 that Curve 1 for mist precipitation differs from Curve 2 for smoke formed by combustion of red phosphorus. Sedimentation of the red-phosphorus smoke cases after about 40 minutes, and the weight of the precipitate subsequently remains constant in the dry air of the chamber. Precipitation of the mist formed by irradiation of air with α -particles (Curve 1) occurs continuously during the whole irradiation period at a constant rate, which was $2.5 \cdot 10^{-5}$ g/ hour ($4.2 \cdot 10^{-7}$ g/ minute) per cm^2 of chamber floor area in our experiments.

SUMMARY

1. Exposure of ordinary moist air to ionizing radiations increases the number and size of the particles of its disperse phase. This results in mist formation.
2. Processes of formation and precipitation of the mist during irradiation occur continuously at constant rates.
3. The amount of mist precipitated and its dispersity depend on the intensity and duration of the irradiation to which the aerosol (ordinary moist air) is exposed.

LITERATURE CITED

- [1] K. M. Merzhanov, N. I. Petrimova, and N. S. Smirnov, *Colloid J.* 18, No. 5, 574 (1956).*
- [2] I. I. Belyaeva, A. E. Mikirov, and N. S. Smirnov, *Colloid J.* 19, No. 1, 24 (1957).*
- [3] N. A. Fugurovskii, *Industrial Lab.* 5, 829 (1936).

Received February 5, 1958

* Original Russian pagination. See C.B. Translation.

ULTRASONIC DISPERSION OF SILICIC ACID GEL IN ACID MEDIA

N. S. Bubyreva and B. P. Bindas

Dispersion by means of ultrasonics is widely used in production of fine suspensions, emulsions, and colloidal solutions. A problem of urgent importance is the question of the dispersing action of ultrasonics in the gel-sol transition in colloidal systems such as silicic acid in aqueous solution.

It is known that the presence of silicic acid gel in reagents and water causes considerable difficulties in the control of many technological processes. Moreover, precipitated silicic acid is often an undesirable impurity in the industrial products.

In the present investigation we considered the possibility of, and performed experiments on, the dispersion of silicic acid gels with complete homogenization of solutions containing various amounts of SiO_2 .

In accordance with the mechanism postulated by Rzhevkin [1], the dispersing action of ultrasonics is considered to involve the formation of differential accelerations in a particle when an ultrasonic wave passes through it. Most authors [2, 3] give preference to the cavitation mechanism of dispersion, and attribute not only mechanical but also chemical effects to cavitation.

When concentrated solutions of certain high polymers such as gelatin are exposed to ultrasonic vibrations, the viscosity of the system decreases considerably after a short time. It is suggested [4] that cavitation breaks down bonds between individual macromolecules which form a network and thereby confer high viscosity to the system. This is because molecular cohesion is determined by van der Waals forces, and breaks down readily under the action of ultrasonics. If the pressure is raised to 10 atmos, when cavitation is less, exposure of high polymers to ultrasonics has almost no effect on viscosity. These facts confirm the decisive influence of cavitation in dispersion.

It is known that silicic acid polymerizes in acid media. Si-O-Si linkages are formed in the process [5]. Dispersion of such polymers may be regarded as breakdown of Si-O bonds. It is convenient to compare the energy of the Si-O bond with the bond energies of carbon atoms after repeated breakdown under the influence of ultrasonics. Data on the bond energies of silicon and carbon [6] are presented in Table 1. The Si-O bond is the strongest in silicon compounds, but, as Table 1 shows, the other bond energies given are of the same order of magnitude.

This comparison suggests that silicic acid gel, like the high polymers in question, can be dispersed by means of ultrasonics.

A quartz-crystal ultrasonic generator was used for investigating dispersion of silicic acid gels.

The generator was operated at frequencies from 1 to 8 megacycles per second at an intensity of about 3 w/cm^2 . The liquid under investigation was contained in a vessel with a thin bottom ($20\text{--}30 \mu$ thick) which ensured complete transmission of the ultrasonic energy. The temperature in the vessel was kept constant by means of a liquid circulated from a thermostat through a tube within the vessel. Solution samples of about 5 ml were irradiated. The solution composition, irradiation time and ultrasonic frequency were varied in the experiments. Solutions containing silicic acid gels of different ages were investigated. For estimation of the results of irradiation, the amounts of silicic acid remaining in the solutions after irradiation were determined. The homogeneity of the material after irradiation was confirmed by the absence of a precipitate in a sample

centrifuged at 2000 revolutions / minute for 10 minutes. The frequency range from 1 to 8 megacycles/ second was studied.

For estimation of the possibility of dispersing SiO_2 gels, the total effect of ultrasonic irradiation was first determined. The degree of polymerization of the gel was not taken into account. Only the highest degree of dispersion, down to the monomeric form, was considered. Second, a study was made of the conditions for conversion of the whole coagulated form into a sol, i.e., for complete homogenization of the system. The silicic acid content was determined colorimetrically by the silicomolybdenum-blue reaction.

The ability of ultrasonics to convert polymerized silicic acid into the monomeric form was checked by a number of experiments, the results of which are given in Table 2. A solution containing 4 g SiO_2 per liter in 4 N HNO_3 was irradiated. Samples differing in the age of the silicic acid gel were tested.

Table 2 shows that on irradiation of acid solutions containing silicic acid gel the content of soluble SiO_2 increases roughly by one order of magnitude. Frequency variations between 6 and 3 Mc/ second and variations of the exposure time between 10 and 120 minutes have no practical effects on the final results. These results show that dispersion of coagulated silicic acid to the soluble form may reach a definite extent. It should be noted that the amount of the precipitate dispersed in this manner is very small. The degree of dispersion of the precipitate apparently depends on a number of factors: ultrasonic frequency, age of the gel, and composition (especially acidity) of the solution.

TABLE 2

Effects of the Age of Silicic Acid Gel, Frequency, and Irradiation Time on the Contents of Soluble SiO_2

Age of silicic acid, days	Ultrasonic frequency, Mc/ sec	Irradiation time, min	SiO ₂ content of solution, g	
			before irradiation	after irradiation
3	6	10	0,0090	0,030
3	5	60	0,0010	0,0071
4	5	30	0,0010	0,0086
4	3	120	0,010	0,066
10	3	20	0,038	0,20
10	3	15	0,038	0,30
12	3	35	0,010	0,13
12	3	20	0,021	0,26

The results of experiments on the extent of dispersion of silicic acid precipitated are summarized in Table 3.

Table 3 shows that the dispersion effect increases with decrease of ultrasonic frequency. Whereas at frequencies of 8-3 Mc/ second the precipitate largely remained undispersed, the dispersion increased considerably on decrease of frequency from 3 to 1.1 Mc/ second.

At a frequency of 1.1 Mc/ second the gel-sol conversion is complete and can be effected with good reproducibility.

The results show that the proportion of monomer formed by irradiation of these solutions is very small. The amount of monomer is certain measure of the proportion of ultrasonic energy expended in chemical action; in this case, for rupture of Si-O bonds.

Under given operating conditions of the generator the yield of soluble silicic acid should be proportional to the quantity of energy supplied, which is determined mainly by the irradiation intensity and time.

A rough calculation shows that for rupture of the Si-O bonds in 1 ml of the tested solutions containing 4 g of silicic acid per liter about 6 cal is required. The relatively small amount of energy is easily provided during a brief period of irradiation. However, neither brief nor prolonged irradiation result in formation of a con-

TABLE 3

Effects of Ultrasonic Frequency, Gel Age, and Solution Composition on the Extent of Dispersion of Silicic Acid Precipitate; Irradiation Time 30-60 minutes

Solution composition		Age of silicic acid, days	Ultrasonic frequency, Mc/sec	Amount of SiO ₂ in precipitate, g		Sol stability, days	Notes
SiO ₂ , g/liter	HNO ₃			before irradiation	after irradiation		
4	5N	4	8	0,080	0,28	—	Precipitate partially dispersed
2	2N	14	6	2,0	No precipitate	5	Total dispersion
4	4N	2	6	3,9	The same	4	The same
4*	4N	3	5	0,080	0,24	—	Partial dispersion
4*	4N	45	3	0,040	0,066	—	The same
5,1	4N	45	3	5,1	4,1	—	" "
6,5	4N	46	3	6,5	2,7	—	" "
4,4	4N	46	3	4,4	1,5	—	" "
2,5	4N	47	3	2,5	No precipitate	2	Total dispersion
4,2*	4N	48	3	0,038	0,30	—	Partial dispersion
4,2*	4N	48	3	4,2	1,7	—	The same
5,4	4N	49	3	0,038	0,10	—	" "
5,4	4N	49	3	5,4	1,7	—	" "
4	4N	49	3	Precipitate not analyzed	No precipitate	3	Total dispersion. Irradiation first at +20° then at +80°
4	4N	52	3	The same	The same	3	
4	5N	50	3	" "	" "	3	
4	5N	52	3	" "	" "	3	
4	4N	120	1,1	3,9	" "	5	Total dispersion
5,5	4N	120	1,1	5,5	" "	1	Liquid gelatinized after 24 hours

* SiO₂ determined in filtrate and not in the precipitate.

siderable proportion of the monomeric form. The amount of this form remains almost constant, and is only a few hundredths of the calculated amount. In our opinion, this low yield is the consequence of polymerization of silicic acid, competing with ultrasonic depolymerization, as the former is favored by the high acidity and the heat liberated during irradiation. The effect of irradiation can in all probability be increased by introduction of substances which bind soluble silicic acid into the solution.

SUMMARY

1. Silicic acid preprecipitated in gel form from highly acid solutions can be converted into the sol form by ultrasonic dispersion.
2. The degree of dispersion depends on the ultrasonic frequency. Total homogenization of the systems studied, containing up to 5 g SiO₂ per liter, can be effected by ultrasonic treatment at a frequency of 1 Mc/second.
3. The yields of soluble silicic acid obtained in the investigated systems were low; in the author's opinion, this may be caused by competition between processes of coagulation and ultrasonic dispersion of the silicic acid.

LITERATURE CITED

- [1] S. S. Rzhevkin, *Progr. Phys. Sci.* 9, 859 (1929).
- [2] D. W. Rayleigh, *Phil. Mag.* 34, 6 (1917).
- [3] N. Miller, *Radiation Chemistry* (IL, 1953) [Russian translation].
- [4] B. V. Kudryavtsev, *Use of Ultraacoustic Methods in Physicochemical Research Practice* [in Russian] (State Tech. Press, 1952).
- [5] L. Kh. Freidlin et al., *Bull. Acad. Sci. USSR, Div. Chem. Sci.* No. 4, 375 (1945).
- [6] *Brief Handbook of Physicochemical Data* [in Russian] (Goskhimizdat, 1955).

Received May 4, 1958

CHARACTERIZATION OF THE PROPERTIES OF PAINT AND LACQUER COATINGS BY THEIR ELECTRICAL RESISTANCE AND CAPACITANCE

P. I. Vasserman, Ya. M. Kolotyrkin, V. V. Chebotarevskii,
and A. A. Feoktistova

Moscow

The effectiveness of lacquer and paint coatings used to protect metals against corrosion depends on a number of properties of the films, including their lyophilicity, moisture permeability, adhesion to the surface of the protected metal, etc. A most important characteristic of protective coatings is their structure, which determines diffusion of moisture and electrolyte solutions, causing corrosive destruction of the metal, into the film.

Lacquer and paint films are dielectrics; when moisture penetrates into such a film the conductivity of the coating increases. Therefore, Wirth [1], Young [2], Bacon [3], and Wormell [4] suggested that the protective effect of coatings on steel can be expressed in terms of their resistance. It was found that a decrease of the protective action of a coating is accompanied by a decrease of film resistance and increase of capacity. Brasher [5] determined moisture absorption of films from changes of capacity.

In the present investigation the film structure and diffusion of moisture into the film were characterized by its electrical resistance and capacitance.

An alternating-current bridge was used for the resistance measurements. The bridge circuit is given in Fig. 1. The alternating-current source was a ZG-2A audio-frequency oscillator. Equal resistances R_1 and R_2 , of 10^2 , 10^3 , 10^4 , 10^5 and 10^6 ohms, were connected in two arms of the bridge. In the third arm, a resistance box with a range of 0.1 to 10^8 ohms and a capacitor box with a range of 0.00005 to 2 microfarads were connected in parallel. The null instrument was an EO-7 electronic oscillograph with a dual amplifier. The determinations were performed at 1 v.

The resistance of the coatings on metal was determined. However, as the results of such determinations may be distorted as the result of rupture of the films by metal corrosion products, resistance determinations were also performed on free films. The films were between 30 and 35 microns thick. The test cells were assembled as follows.

A glass cylinder 40 mm in diameter and 60 mm high was attached to the coated surface of the metal specimen by means of bitumen. The auxiliary electrode was a circular platinum plate attached to the cylinder lid at a distance of 15 mm from the test specimen. The cylinder was filled with electrolyte solution.

A free paint or lacquer film was fixed by means of BF-2 adhesive between two cylindrical vessels with side tubes with ground ends (the inner diameter of each side tube was 25 mm). The electrodes were two platinum plates placed on a level with the film. The cells are depicted in Fig. 1.

Results of determinations in 0.5 N NaCl solution. Figure 2 shows the results of determinations of the resistance of a nitrocellulose film and of capacitance of the system: platinum electrode-solution-film-solution-platinum electrode, determined at a frequency of 1 kc/second at various time intervals after immersion of the

film in 0.5 N NaCl solution. Immediately after immersion in the solution the film has very high resistance, which decreases appreciably as the film becomes wet. This decrease of resistance with a simultaneous increase in the capacitance of the system occurs primarily during the first 24 hours, and is determined by the kinetics of

absorption of the solution by the film. To determine the effect of the nature of the film former on film resistance and capacitance of the system, determinations were carried out with chlorinated polyvinyl chloride (PVC), nitrocellulose (NC), butyl methacrylate (BMA) and ethylcellulose (EC) films. In these experiments, in addition to film resistance and capacitance of the system, the swelling of the films in water and vapor permeability were determined. The results are summarized in the table, which also contains literature data on the dielectric constants (DC) of the investigated film formers.

It follows from the table that the investigated film formers have similar dielectric constants, and therefore the changes in the resistance observed in our experiments cannot be attributed to the nature of the film substance. At the same time there is a direct correlation between film structure, as characterized by vapor permeability, and resistance. For example, the polyvinyl chloride film, which has low vapor permeability, also has high resistance, $3.2 \cdot 10^8 \text{ ohm} \cdot \text{cm}^2$. Ethylcellulose film, which has high

vapor permeability, has low resistance. The data in the table also show that there is a direct correlation between changes in the capacitance with time and the swelling of the films. Thus, with polyvinyl chloride and butyl methacrylate films, which swell little in water (0.2-0.4% per 24 hours), the capacitance of the system changes little with time. On the other hand, with ethylcellulose and nitrocellulose films, which absorb water, the capacitance of the system increases considerably.

Influence of alternating-current frequency on the resistance of coating films. As is clear from Fig. 3, in most cases the resistance varies inversely with the frequency. However, the density of the film structure has a significant influence on this relationship. In films of less dense structure, such as ethylcellulose, the fall

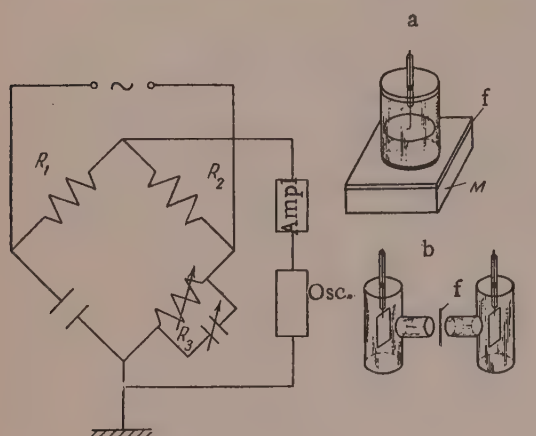


Fig. 1. Bridge circuit; a) cell for measurement of film (f) resistance on the metal (m); b) cell for measurement of resistance of free films (f).

Film	DC [6]	Vapor permeability per 24 hrs, mg/cm^2	Swelling in 24 hours, %	Resistance $10^{-7} \text{ ohm} \cdot \text{cm}^2$ at 1 kc/sec		Capacitance, $\mu\mu\text{f}/\text{cm}^2$ at 1 kc/sec	
				on im-mersion	after 24 hours	on im-mersion	after 24 hours
PVC	2,0	0,9	0,2	32	5,5	98	94
NC	2,7	8,6	2,3	4,4	1,1	150	190
BMA	2,0	7,6	0,4	1,6	0,7	74	81
EC	2,4	31,3	5,2	1,8	0,5	133	194

of resistance with frequency is much less, and occurs mainly at relatively low frequencies. On the other hand, nitrocellulose and especially polyvinyl chloride films, which are considerably denser in structure, show a much greater sensitivity of resistance to frequency changes. The results for butyl methacrylate film are somewhat different; despite the fact that its vapor permeability is about the same as that of nitrocellulose film, the relative decrease of resistance with increasing frequency is much less for the former. Similar results were obtained with coatings on metal.

The results of our experiments showed that the influence of frequency on film resistance decreases appreciably with increasing moisture content of the film (Fig. 4).

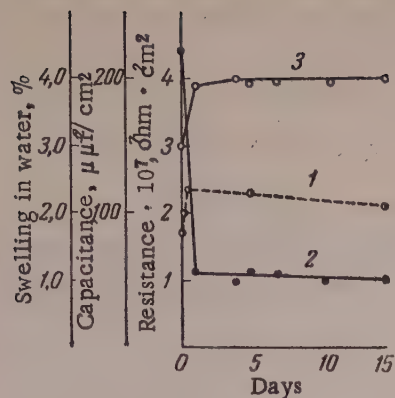


Fig. 2 Variations of swelling in water (1), resistance of nitrocellulose film (2), and capacitance (3) of the system in 0.5 N NaCl.

ter immersion in the solution must be determined by the conductivity of the electrolyte in its pores. In general, this concept is consistent with our experimental results, according to which films of denser structure have higher initial resistance, i.e., lower conductivity. Similar conclusions were reached by Brasher [5], Weinmann [7], and Wirth and Machu [8], who determined film structure and penetration of moisture by electrical and electro-osmotic methods.

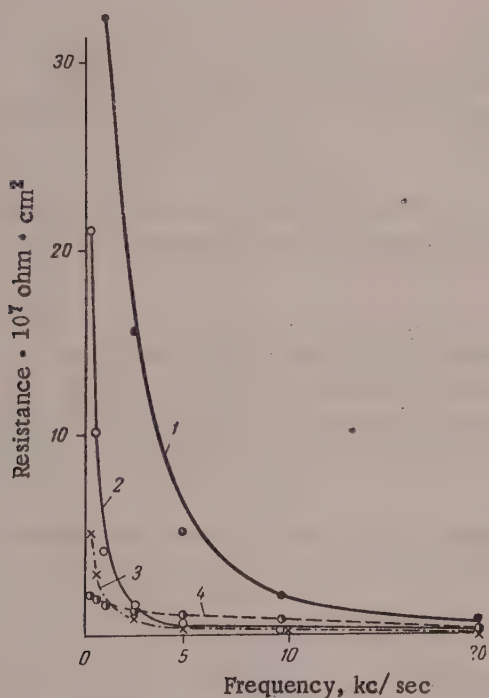


Fig. 3. Effect of frequency on resistance of films in 0.5 N NaCl: 1) polyvinyl chloride, 2) nitrocellulose, 3) ethylcellulose, 4) butyl methacrylate.

It was therefore natural to expect a direct correlation between electrolyte concentration and film structure on the one hand, and film conductivity on the other. However, comparison of the results obtained with 0.5 N NaCl and with distilled water shows that there is no such correlation even at the instant of immersion. To

Influence of the electrolyte on film resistance and capacitance of the system. Figures 5 and 6 show the results of resistance and capacitance determinations for ethylcellulose films at 1 kc/second in 0.5 N NaCl and in distilled water. The film resistance and the capacitance of the system are lower in distilled water than in NaCl solution. Similar results were obtained for the other films. The greater changes in the capacitance of the system in the transition from distilled water to 0.5 N NaCl are found for swelling films, while in the case of coatings which swell little, such as polyvinyl chloride film, the difference is less. Conversely, the increase of resistance with the use of 0.5 N NaCl is greater for coatings of low permeability and swelling, such as polyvinyl chloride films, and less for permeable and swelling coatings.

For interpretation of the experimental data it is necessary to take into account that a lacquer film is a dielectric and therefore its conductivity immediately af-

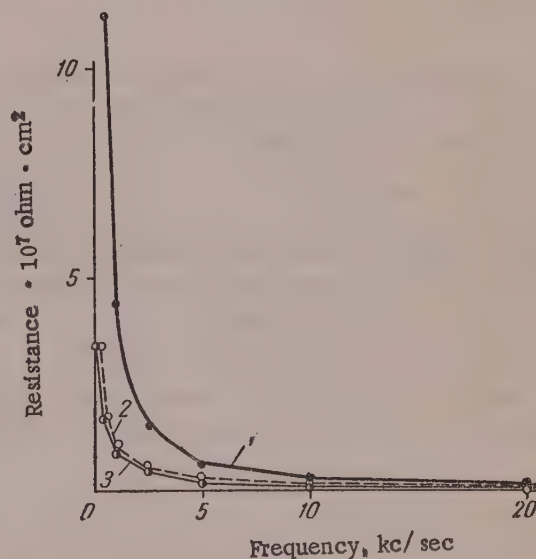


Fig. 4. Effect of frequency on resistance on nitrocellulose film in 0.5 N NaCl: 1) on immersion, 2) 1 day, 3) 15 days after immersion.

explain these results it must be assumed that the so-called surface conductivity [9] plays an important role in film conductivity. The total conductivity of a film immediately after immersion must then be determined by two components:

$$K_{\Sigma} = K_1 + K_2, \quad (1)$$

where K_1 is the conductivity of the electrolyte in the film pores, and K_2 is the surface conductivity.

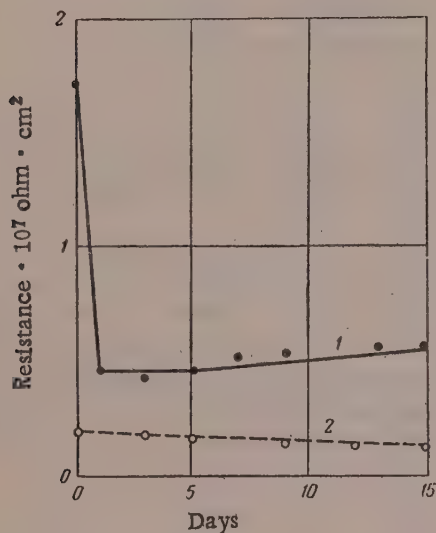


Fig. 5. Variations of the resistance of ethylcellulose films during soaking: 1) in 0.5 N NaCl; 2) in distilled water.

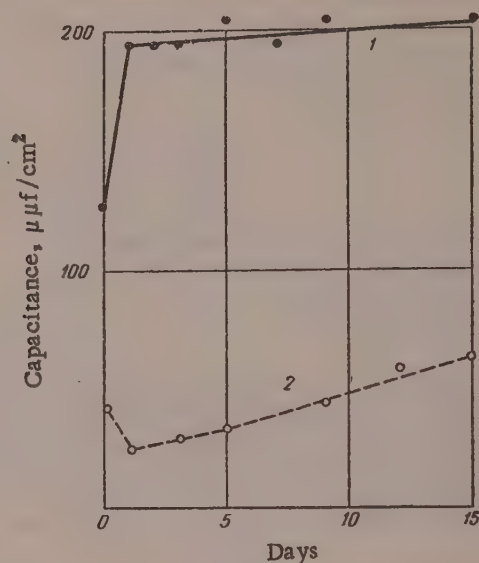


Fig. 6. Variations of the capacitance of the system during soaking of ethylcellulose films: 1) in 0.5 N NaCl; 2) in distilled water.

According to the work of numerous authors, and especially of Zhukov [10] and his school, the relative significance of surface conductivity in the total conductivity of a diaphragm increases appreciably with increasing pore size and decreasing electrolyte concentration.

Surface conductivity also explains the dependence of film resistance on alternating-current frequency. Although the conductivity of solutions also depends on the frequency, this dependence becomes apparent only at much higher frequencies, of the order of 10^8 – 10^9 cycles/second. Therefore it may be assumed that the decrease of film resistance with increasing frequency is caused mainly by changes of surface conductivity (K_2). This is confirmed by our observation that the frequency has a greater influence on the resistance of films with denser structure, such as polyvinyl chloride film.

As a film swells in the electrolyte, the conductivity acquires a third component, due to the conduction by the film material itself. The total conductivity K_{Σ} then becomes

$$K_{\Sigma} = |K_1 + K_2| + K_T, \quad (2)$$

where K_T is the conductivity of the film material. At the first instant after immersion the conductivity of the film material is low and the last term in the right-hand side of the equation may be ignored. This term gradually increases during swelling. As the film swells, the effect of frequency on resistance diminishes because the relative significance of surface conductivity in total conductivity of the film decreases.

SUMMARY

1. The relationship between electrical resistance, vapor permeability, and lyophilicity of lacquer coatings has been determined. Films with low vapor permeability and low swelling in water have higher resistance.

2. The conductivity of a coating film is made up of three components: conductivity of the electrolyte in the pores, surface conductivity in the pores, and conductivity of the film material.

3. The conductivity of a coating film depends on the alternating-current frequency, probably because of variations of the surface conductivity in the film pores.

LITERATURE CITED

- [1] J. K. Wirth, *Korrosion und Metallschutz* 16, 3, 116 (1940); 16, 11, 331 (1940).
- [2] G. H. Young and G. W. Gerhardt, *Ind. Eng. Chem. (Ind. Ed.)* 29, 1277 (1937).
- [3] R. G. Bacon, J. J. Smith, and F. M. Rugg, *Ind. Eng. Chem.* 40, 161 (1948).
- [4] F. M. Wormell and D. M. Brasher, *J. Iron and Steel Inst.* 164, 2, 141 (1952).
- [5] D. M. Brasher and A. H. Kingsbury, *J. Appl. Chem.* 4, 2, 62 (1954).
- [6] K. A. Andrianov and S. A. Yamanov, *Organic Dielectrics and Their Applications in the Communications Industry* [in Russian] (Moscow, 1949).
- [7] K. Weinmann, *Deutsche Farben, Z.* 12, 3, 4, 97, 136 (1958).
- [8] J. K. Wirth and W. Machu, *Werkstoffe und Korrosion* 3, 12, 444, 453 (1952).
- [9] I. I. Zhukov and D. A. Fridrikhsberg, *Colloid J.* 11, 163 (1949).
- [10] I. I. Zhukov, *Electrical Properties of Capillary Systems* [in Russian] (Izd. AN SSSR, Moscow-Leningrad, 1956).

Received February 7, 1958

RHEOLOGY OF BITUMENS AND THEIR FLOW THROUGH PIPES AT ELEVATED TEMPERATURES

B. V. Vedeneev and N. V. Mikhailov

The Gor'kii Institute of Engineering and Construction
The Scientific Research Institute for Construction, Moscow

The ever-extending uses of bitumen in construction work raise the problem of mechanization of the operations involved in applying or pouring bitumen into the structural elements. The most rational method for supplying hot bitumen to the working site is by pumping through pipes.

Petroleum bitumens are mixtures of liquid and solid hydrocarbons and their derivatives. Structurally, they are colloidal systems in which oils and tars are the dispersion medium and asphaltenes the disperse phase. These systems belong to the group of structurized liquids, the flow of which does not conform to Newton's law. At higher temperatures (above 140-170°) the bitumen structure breaks down as the result of thermal motion [1], and they become true viscous Newtonian liquids with viscosity η_m independent of the velocity gradient.

The principal laws governing the flow in pipes of such viscoplastic bodies as clay suspension, peat, slurry, sewage sludge, etc. have been investigated during recent years [2-4]. Investigations [1, 5-8] concerned with the rheological properties of petroleum bitumens have dealt with the relationships between the viscosity characteristics of bitumens and temperature, between the velocity gradient and the shear stress, and also with determinations of the power required to break down the structure, with the degree of structurization of the systems, and the influence of added fillers and diluents on the structural and mechanical properties at relatively low temperatures. The viscosimetric studies of bitumens were performed at temperatures not exceeding 90° with the elastoviscosimeter, and at a maximum temperature of 160° with the Volarovich instrument.

The flow of hot bitumen in pipes has not been studied as yet.

For determination of the hydraulic relationships and derivation of formulas for calculating pressure drop in the flow of hot bitumen in pipes of circular cross section, we carried out viscosimetric investigations on bitumen at high temperatures and performed tests in a special unit; this work is described in the present paper.

The work was performed with BN-IV bitumen from the Gor'kii plant, obtained from Artemovsk petroleum asphalt, with the following characteristics as determined in accordance with GOST 6617-53: penetration 40 mm; extensibility (ductility) at 25° 3.6 cm, softening temperature (Kraemer-Sarnow) 76°.

The rheological characteristics of the bitumen were determined by means of the NII-200 electronic selsyn elastoviscosimeter, the action of which depends on pure shear of the system in a narrow gap between two coaxial cylinders, with automatic recording of the stress and deformation curves. For investigations at 200° the instrument was additionally fitted with a TS-24 oil thermostat with automatic thermoregulation, and a thermal chamber heated by an electric coil.

The experimental unit for studying the flow of bitumen in pipes is depicted in Fig. 1.

The bitumen was heated and dehydrated in an induction-heated bitumen boiler 1, and was fed by means of the Sh-200 gear pump 2 into the header tank 3 at a height of 2.9 meters above floor level. From the header tank the hot bitumen passed into the measuring system consisting of standard steel gas pipes 5, 8.0 meters long

and 5.2, 4.02, and 2.05 cm in internal diameter. From the measuring system the bitumen was returned to the bitumen boiler, where it was heated and then pumped back into the header tank.

For measurement of pressure drop in pipes during flow of bitumen through them, holes 5.0 mm in diameter were drilled in the pipe walls at right angles to the pipe axis. Opposite these holes piezometer rings 6 with annular internal grooves and with glanded connecting tubes were welded onto the tubes; these rings were attached to piezometer tubes of Pyrex heat-resisting glass, 13.0 mm in diameter and 1.50 m long. Measuring scales with 1 mm divisions for recording the bitumen level in the tubes were placed alongside the piezometer tubes.

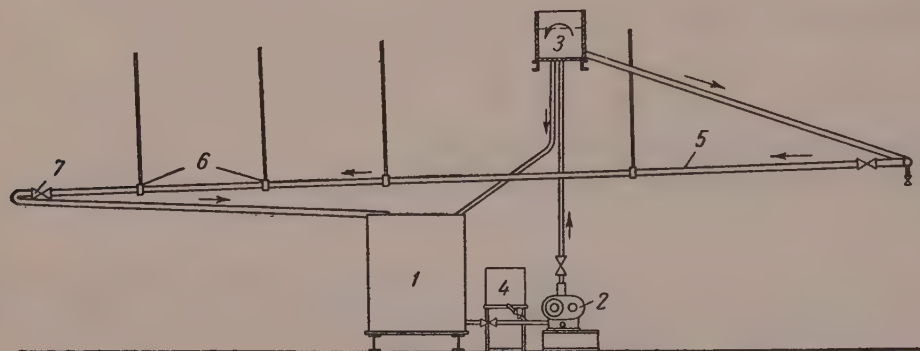


Fig. 1. Experimental unit.

The bitumen tank was connected to a tank 4 for solar oil, used for rinsing out the bitumen pipes.

The velocity of the bitumen in the measuring pipes was regulated by means of the cocks 7. The flow rate was measured volumetrically by means of a special measuring vessel.

To regulate the bitumen temperature and to ensure thermal stability, the bitumen boiler was equipped with three-stage heating, the header tank had double walls and an insulated bottom, and Nichrome heating coils were fitted onto the measuring pipes and the glass piezometer tubes.

The lengths of the entry and exit damping regions and of the working regions between the piezometer rings are given in Table 1.

TABLE 1

Principal Dimensions of the Pipes in the Experimental Unit

Internal diameter D, cm	Entry region		Exit region		Working region, m
	length l , m	$\frac{l}{D}$	length l , m	$\frac{l}{D}$	
5.2	2.2	42	0.80	15	5.0
4.02	2.0	50	1.98	49	4.0
2.04	1.83	89	2.25	110	5.0

The results of the rheological investigations are plotted in Fig. 2. At temperatures of 170 and 160° (and lower) the relationship between the velocity gradient ϵ and stress P for BN-IV bitumen is represented by an S-shaped curve, according to which the effective viscosity $\eta = P/\epsilon$ is not constant but decreases with increasing applied shear stress.

At temperatures of 180° and over, bitumen behaves as a Newtonian liquid of constant viscosity. When bitumen is heated from 100 to 200° its viscosity falls from 91.6 to 0.16 poises (Fig. 3), which is a 570-fold decrease.

The flow of BN-IV bitumen in pipes was studied at the temperature used in constructional practice, i.e., in the 160-200° range, at intervals of 10°. The structural and mechanical properties of bitumen are given in Table 2.

TABLE 2

Structural and Mechanical Properties of Bitumen at High Temperatures

Temperature, °C	γ , g/cc	η_m , poises	τ_0 , dynes/cm ²	C, kcal/kg
160°	0,943	1,45	150	0,505
170°	0,939	1,02	80	0,513
180°	0,933	0,69	0	0,522
190°	0,929	0,42	0	0,530
200°	0,923	0,16	0	0,540

Note. The values of C and γ are in agreement with the data of the B. E. Vedenev All-Union Scientific Research Institute of Hydraulic Engineering.

The experiments were performed only when the thermal and hydraulic conditions had become steady, i.e., when the temperature of the bitumen in the measuring pipes and its level in the piezometer tubes became constant with complete circulation of the bitumen in the closed system. The flow rates and pressures were determined simultaneously. A series of experiments was performed in each of three pipes simultaneously, and the bitumen flow rates decreased progressively from the highest to the lowest, close to a state of hydraulic equilibrium. At the end of experiments at a given temperature, bitumen was removed from the system through discharge devices and the hot pipes, header tank, and pump were washed out with solar oil. Residual bitumen and asphaltene deposits were removed from the pipe walls in the process. A total of about 200 experiments was carried out.

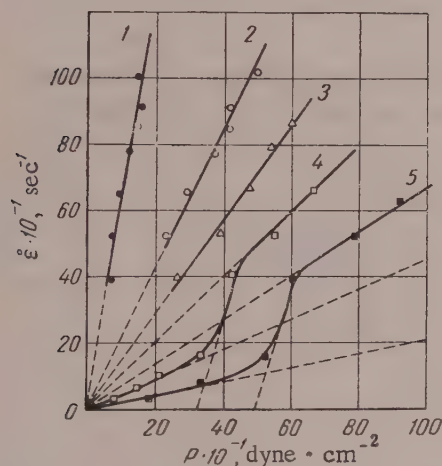


Fig. 2. Complete rheological $\dot{\epsilon}(P)$ curves for BN-IV bitumen: 1) $t = 200^\circ$, $\eta = 0.16$; 2) $t = 190^\circ$, $\eta = 0.42$; 3) $t = 180^\circ$, $\eta = 0.69$; 4) $t = 170^\circ$, $\eta_0 = 2.20$, $\eta_m = 1.02$; 5) $t = 160^\circ$, $\eta_0 = 4.74$, $\eta_m = 1.45$ poises.

where Q is the bitumen flow rate in cc/second; R is the internal pipe radius in cm; Δp is the pressure drop over the given pipe section, in dynes · cm⁻²; l is the length of the pipe section in cm.

The relationship $\tau_{\max} = F(v_{\max})$ is plotted in Fig. 4, from which it is clear that the determinations were performed with streamline flow.

The pressure losses in bitumen at 200, 190, and 180° are directly proportional to the flow rate and are represented by straight lines passing through the coordinate origin. The pressure losses at 170 and 160° are also proportional to the flow rate, but owing to the fact that the bitumen has a yield value and values of Δh_f are higher. For a given flow rate the pressure drop rises sharply with decrease of temperature; this indicates that structurization of bitumen increases at lower temperatures.

The fact that the experimental points in Fig. 4 are almost linear in streamline flow of bitumens at temperatures of 170° and lower indicates that under these conditions the Shvedov-Bingham equation is applicable:

$$\tau_{\max} = \Delta p R / 2l, \quad (1)$$

and the velocity gradient for a parabolic velocity distribution

$$V_{\max} = 4Q / \pi R^2, \quad (2)$$

$$\tau = \eta^* \frac{dv}{dr} + \tau_0, \quad (3)$$

here dv/dr is the velocity gradient; τ is the tangential stress in the bitumen; η^* is the plastic viscosity; τ_0 is the upper flow limit.

Formulas for Calculation of Hydraulic Losses in Bitumen Pipelines

The coefficient of hydraulic resistance was calculated by means of the Darcy-Weissbach equation:

$$h = \lambda \frac{v^2 l}{2gd}.$$

The experimental data can be used to find the hydraulic loss coefficient from the usual hydraulic relationship

$$\lambda = \frac{K}{Re^X}, \quad (4)$$

where K and X are empirical constants.

Values of the Reynolds number $Re = vd\rho/\eta$ and the Darcy-Weissbach coefficient $\lambda = \Delta h_l / 2gd/v^2$ were calculated for each experiment.

In the above equations d is the diameter of the bitumen pipe; ρ is the density of bitumen; η is the effective viscosity; g is the acceleration due to gravity; Δh_l is the pressure drop per meter of pipe length; v is the flow velocity of the bitumen, found from the expression $Q/\pi R^2$.

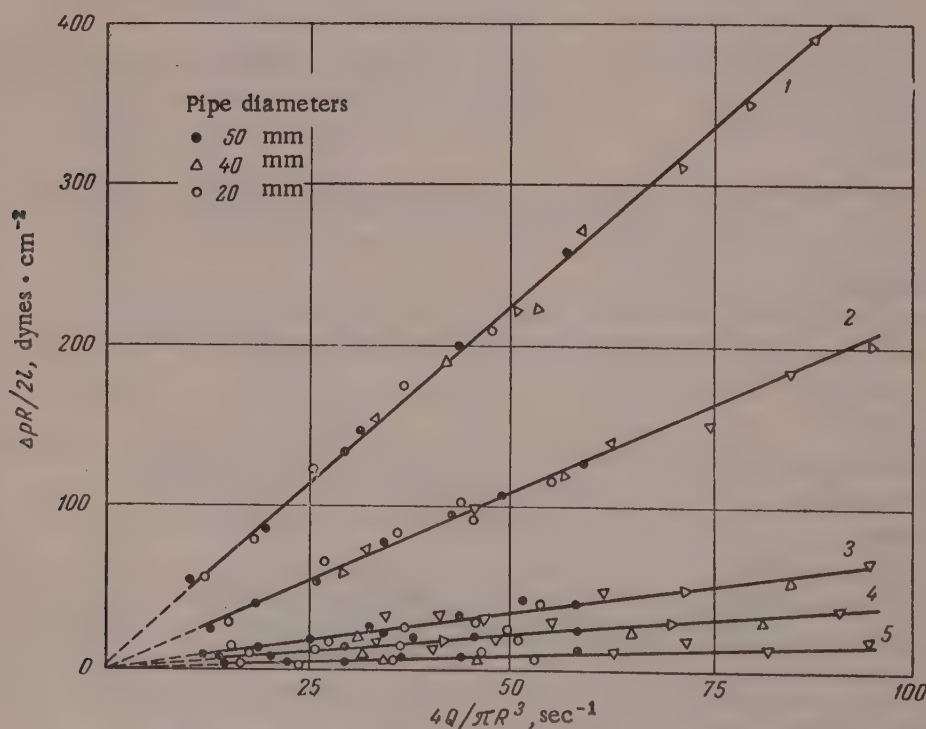


Fig. 4. Variations of maximum shear stress with the velocity gradient from results of measurements in pipes at: 1) 160°; 2) 170°; 3) 180°; 4) 190°; 5) 200°.

The values so found were used to plot the relationship $\lambda = f(\text{Re})$ in logarithmic coordinates (Fig. 5).

The experimental points form bands in Fig. 5, and the straight lines drawn along the centers of these bands are represented by Equation (4). Solution of these linear equations gives $K = 64$ and $X = 1$ for line a, and $K = 200$, $X = 1$ for line b. Hence, we find formulas for Newtonian and structured bitumens for determinations of the hydraulic resistance coefficients in streamline flow of BN-IV bitumen in pipes of circular cross section. For Newtonian bitumens at 200, 190, and 180°, we have:

$$\lambda = 64 / \text{Re} \quad (5)$$

And for structured bitumens at 170 and 160°:

$$\lambda = 200 / \text{Re} \quad (6)$$

The value of the Reynolds number in all cases includes the viscosity of the destructurized bitumen η_m , attained either by isotropic breakdown of structure as the result of thermal motion, or by the action of high velocity gradients.

Equation (5) is known in hydraulics as the Stokes equation.

The flow of bitumen at high temperatures, when it is a true viscous liquid, conforms to the usual hydraulic laws. The flow of bitumen at temperatures of 170° and lower, when it has a structure which has not been broken down isotropically, involves considerable hydraulic resistances and high velocity gradients are necessary to ensure flow.

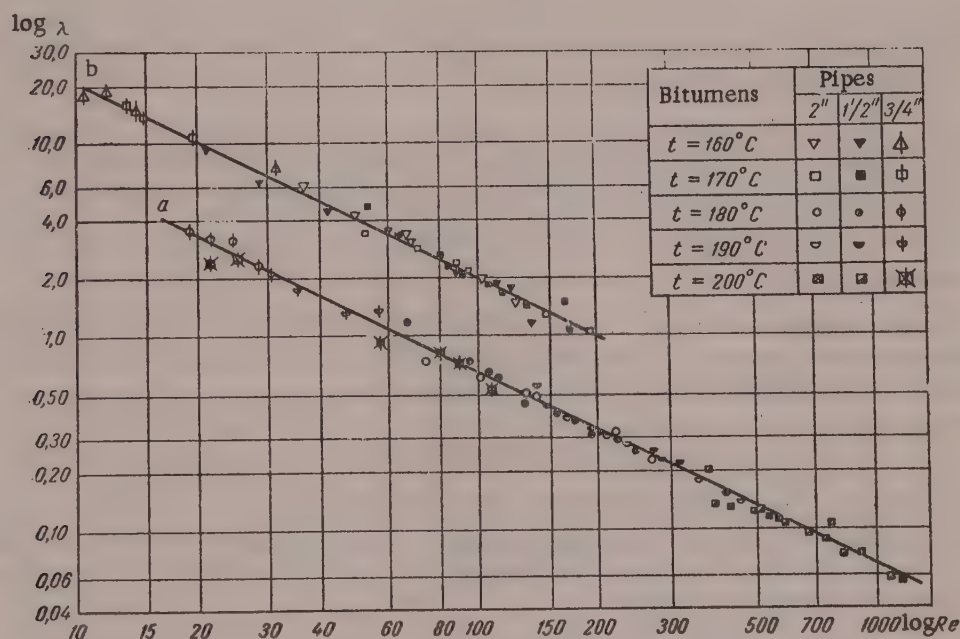


Fig. 5. Variations of the hydraulic resistance coefficient of BN-IV bitumen with Reynolds number Re : a) at 180, 190, 200°; b) at 160 and 170°.

A number of workers who studied the flow of viscoplastic systems have suggested that parameters characterizing the plastic properties of liquids should be introduced into the Reynolds number.

According to R. I. Shishchenko, the generalized Reynolds number can be represented by the expression:

$$\text{Re}' = \frac{\text{Re}}{1 + \frac{\tau_0 R}{\eta^* v}} \quad (7)$$

where η^* is the plastic (structural) viscosity; τ_0 is the yield stress; R is the pipe radius.

We determined the value of the generalized Reynolds number as given by Equation (7) from experimental data for BN-IV bitumen at 170 and 160°, when it is a structurized liquid and its flow through pipes conforms to the structural regime. The maximum value of the flow velocity of bitumen in streamline flow gave a value of Re^* below 10, which is meaningless.

The experimental results were analyzed on the basis of the original calculated viscosity η_m , which characterizes Newtonian flow of the bitumen. Therefore, the principal parameter determining the flow of hot bitumen through pipes is the usual Reynolds number, calculated from the equation

$$Re = \frac{vd\rho}{\eta_m}.$$

Hence our Equations (5) and (6) take fully into account the structural and mechanical properties of BN-IV bitumens and are suitable for technical calculations.

SUMMARY

1. The results of viscosimetric investigations yielded complete rheological curves for BN-IV bitumen at the high temperatures used when it is used for coating.
2. The experimental results fully confirm that it is technically possible and economically feasible to pump hot bitumen through the ordinary standard pipes over considerable horizontal and vertical distances. The pressure losses in pipes 50, 40, and 20 mm in diameter are relatively small at the average flow rates used industrially.
3. Bitumens should be pumped mainly in streamline flow, when lower pumping power is needed, the risk of hydraulic hammering is avoided, heat losses in pumping are lower, and the conditions are better for distribution of the hot bitumen from the pipeline.
4. The main factor which determines whether bitumen can be pumped through pipelines is the viscosity at ultimate structural breakdown, attained by the influence of heat or an appropriate velocity gradient. For a given bitumen velocity, the pressure drop in pipes increases sharply with fall of temperature.
5. The usual Darcy equation should be used for technical calculations relating to the flow of bitumens in pipes of circular cross section.

The hydraulic resistance coefficient in streamline flow must be determined by means of the following equations: a) for Newtonian bitumens, $\lambda = 64/Re$; b) for structurized bitumens, $\lambda = 200/Re$. These equations are applicable to all bitumens and also to bitumen mastics.

LITERATURE CITED

- [1] S. Y. Shalyt and N. V. Mikhailov, *Colloid J.* 18, 609 (1956).*
- [2] R. I. Shishchenko, *Hydraulics of Clay Suspensions* [in Russian] (1951).
- [3] B. S. Filatov, *Colloid J.* 16, 65 (1954).*
- [4] I. I. Orlov, *Colloid J.* 17, No. 6, 434 (1955).*
- [5] N. V. Mikhailov and A. M. Likhtgeim, *Colloid J.* 17, 344 (1955).*
- [6] S. Ya. Shalyt, N. V. Mikhailov, and P. A. Rebinder, *Colloid J.* 19, No. 2, 244 (1957).*
- [7] S. K. Noskov and N. V. Mikhailov, *Colloid J.* 18, No. 4, 461 (1956).*
- [8] N. V. Mikhailov, *Colloid J.* 17, No. 3, 242 (1955).*

Received September 3, 1958

*Original Russian pagination. See C.B. Translation.

KINETIC STUDIES OF THE TRANSITION OF CRYSTALS OF SOLID SOLUTIONS OF TWO-PHASE ALLOYS IN METALLIC SYSTEMS FROM THE COLLOIDAL TO THE TRUE HOMOGENEOUS STATE

V. N. Vigdorovich and V. M. Glazov

The M. I. Kalinin Institute of Nonferrous Metals

The A. A. Baikov Institute of Metallurgy, Academy of Sciences USSR, Moscow

It has been noted in investigations of microstructure and microhardness of crystals of solid solutions in two-phase alloys that the grains of the solid solution contain very thin layers of a second phase, giving rise to the so-called microheterogeneity [1]. Detailed investigations of the mechanism by which microheterogeneity originates in solid-solution crystals of metallic systems showed that it can arise in two ways during cooling of alloys: by disintegration of the melt by branches of growing dendrites in dendritic crystallization, and by decomposition of the solid solution because of differences in the solubility of the second component at high and low temperatures [2].

Analysis of experimental data on microhardness of solid-solution crystals and dark-ground microscope studies of solid-solution crystals in aluminum-copper, aluminum-silicon, and other two-phase alloys led us to the conclusion that the microheterogeneity regions consist of a colloidal solution of the second phase, formed in solid-solution crystals of two-phase alloys under definite crystallization and cooling conditions. In the light of these concepts the formation of microheterogeneous regions in two different ways is regarded as the dispersion and condensation mechanisms of formation of colloid solutions.

Investigations of a number of aluminum alloy systems showed that relatively brief (20-30 hours) and even fairly prolonged (100-150 hours) homogenization at elevated temperatures does not eliminate microheterogeneity. It was shown [2, 3] that a period of about 600 hours is needed for coagulation of a colloidal solution of CuAl_2 in solid-solution crystals of two-phase alloys in the aluminum-copper system.

The present investigation consisted of an experimental study of the kinetics and nature of the transition of quasi-homogeneous crystals of solid solutions into the true homogeneous state. A physical picture of the process is to be given as the result of analysis of the experimental data.

The materials chosen for the investigation were binary alloys of copper with titanium and zirconium, in which the presence of colloidal particles of the intermetallic compounds Cu_3Ti and Cu_3Zr in the crystals of solid solution has a considerable influence on the microhardness of the latter. Therefore microhardness determination was chosen as the principal method for investigating the kinetics of transition of quasi-homogeneous crystals of a solid solution into the true homogeneous state.

The kinetic studies were conducted at 850, 825, 800, 700, and 600° for alloys in the copper-titanium system, and at 850, 825, and 800° for alloys in the copper-zirconium system. The temperature was regulated to within $\pm 3^\circ$.

For saturation of their α -solid solutions the cast specimens were subjected to preliminary 50% deformation and heat treatment; the conditions are given in Table 1.

This treatment was followed by the first microhardness determinations. The method used for preparation of the specimen surface after quenching for microhardness testing is described elsewhere [4].

In nearly every case relatively brief homogenization for 16-20 hours at 800-850° and longer homogenization for 50-100 hours at 700-600° failed to cause coagulation of colloidal Cu_3Ti and Cu_3Zr solutions in the crystals of the α -solid solutions; this is indicated by the fact that the microhardness values of the α -crystals

TABLE 1

Conditions of Heat Treatment *

Heated to temperature, °C	850	825	800	700	600
Exposure time, hours	16	18	20	50	100

* The specimens were quenched in water in all cases.

were higher than the equilibrium values corresponding to absence of colloidal particles of the respective second phases. Longer exposures were required. This is illustrated by Figs. 1 and 2, which show variations of microhardness of solid-solution crystals with alloy composition in these binary systems, for two different treatment temperatures. It follows from the data in Figs. 1 and 2 that the microhardness of solid-solution crystals of a copper alloy containing 12% titanium after treatment for 20 hours at 850 and 800° exceeds the equilibrium values found after exposures of 100 and 500 hours respectively at these temperatures, by 10 and 70 kg/mm^2 . In copper alloys with 3.5% zirconium the microhardness of α -crystals after exposure for 20 hours at 850 and 825° is higher by 26 and 30 kg/mm^2 respectively than the equilibrium values after 500 hours.

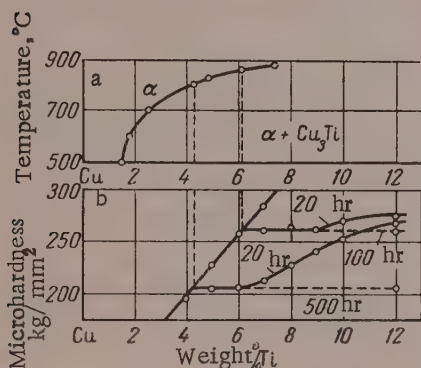


Fig. 1. Solubility of titanium in copper at different temperatures (a), and the corresponding microhardness isotherms for different times of homogenizing annealing (b).

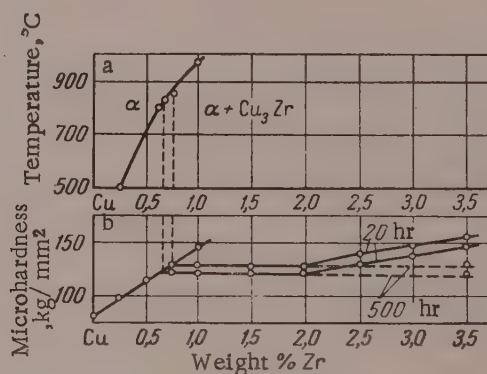


Fig. 2. Solubility of zirconium in copper at different temperatures (a), and the corresponding microhardness isotherms for different times of homogenizing annealing (b).

After determination of the initial points the subsequent annealing was performed in stages, in intervals between which the specimens were quenched and the microhardness determined. The specimens were held at the stated temperatures for two periods of 20 hours, then four periods of 40 hours, and finally five periods of 60 hours. Thus, the total duration of exposure was up to 600 hours. The results are presented in Fig. 3. It must be pointed out that despite these long exposures the influence of the particles, causing heterogeneity of the solid-solution grains, on microhardness of copper-titanium alloys treated at 700 and 600° was not completely eliminated.

In all other cases the microhardness of crystals of solid solutions of titanium in copper and zirconium in copper became, after prolonged homogenization, equal to the microhardness of the solid solutions of the alloys at maximum saturation for the given temperatures.

Analysis of the experimental results was difficult because of the lack of a common criterion of the degree of microheterogeneity in the two systems in question, so that specimens in the corresponding original states could not be investigated; but in view of the chemical analogy between zirconium and titanium it was likely that under the same conditions of preparation and treatment of copper-titanium and copper-zirconium alloys their original states were similar.

It should be noted that the accuracy to which the start and end of the transition of the solid solution from the colloidal into the true homogeneous state was in the region of 20 hours. Further, the instant at which this process is complete cannot be determined with absolute exactness from the microhardness, as the microhardness reaches values corresponding to that of crystals of a solution saturated at the given temperature before the last heterogenizing particles of the second phase have disappeared.

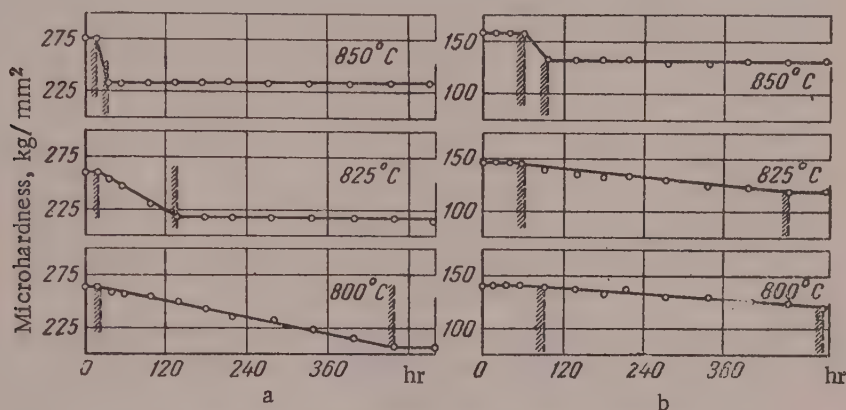


Fig. 3. Kinetic curves for transition of solid-solution crystals in alloys of copper with 12% titanium (a) and 3.5% zirconium (b) from the colloidal to the true homogeneous state.

In the light of the foregoing this investigation should be regarded as an approximate estimation of the influence of temperature and exposure time at a given temperature on the stability of a colloidal solution formed under the given conditions. However, such estimation is without doubt useful, as studies of the behavior of colloidal solutions formed by a second phase in the solid-solution grains of two-phase alloys are very difficult.

The graphs in Fig. 3 show that the relationships between microhardness and exposure time at different temperatures are of a strictly uniform character. These relationships conform to the general scheme shown in Fig. 4. It follows from this scheme that the stability of a colloidal solution at a given temperature can be estimated in terms of two quantities, one of which corresponds to the time interval (which we term the period of aggregative stability τ_{aggr}) during which the microhardness remains virtually constant, and the second corresponds to a period of rapid decrease of microhardness (which we term the kinetic stability τ_{kin}) down to the equilibrium value.

It seems that during the period of aggregative stability internal stresses are relaxed in the layers which surround the colloidal particles of the second phase and which arise in consequence of differences between the specific volumes of the coexisting phases. During the same period the least stable particles of the second phase, causing heterogeneity of the solid-solution grains, are dissolved.

During the period of kinetic stability, diffusional processes cause dissolution of particles of the second phase and disappearance of the interface with the solid-solution crystals. Since the transition of quasi-homogeneous solid-solution crystals into the true homogeneous state most probably occurs by a diffusional mechanism, the process in the two systems in question may be comparatively evaluated by known methods of chemical kinetics [5] and diffusion theory [6]. In this instance the diffusion rate may be estimated as the reciprocal of τ_{kin} .

In Fig. 5 the log of the reciprocal kinetic stability time ($\lg \frac{1}{\tau_{\text{kin}}}$) is plotted against the reciprocal absolute temperature ($1/T$). It follows from Fig. 5 that this relationship conforms satisfactorily to the equation

$$\lg \frac{1}{\tau_{\text{kin}}} = \frac{\Delta E}{RT} + \text{const},$$

where ΔE is the activation energy of transition of the quasi-homogeneous solid-solution crystals into the true homogeneous state; T is the temperature in $^{\circ}\text{K}$; R is the universal gas constant.

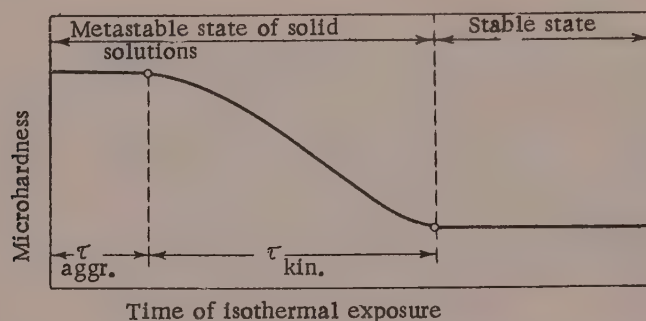


Fig. 4. Generalized scheme for the influence of the duration of isothermal homogenizing annealing on microhardness of solid solutions in two-phase alloys in the transition from the colloidal to the true homogeneous state.

From the slope of the function $\tau_{\text{kin}} = f(T)$ plotted in $\lg \frac{1}{\tau_{\text{kin}}} - \frac{10^3}{T}$ coordinates it is found that the activation energy of transition of quasi-homogeneous solid-solution crystals of two-phase alloys of copper with titanium and zirconium is -147500 and -261300 cal/g-atom respectively.

It would be instructive to compare these values with the activation energies for diffusion of titanium and zirconium into copper, and with the heats of solution of these metals in copper. However, there are no data in the literature on diffusion of titanium and zirconium in copper. However, it may be noted that the values found are 2-3 times as high as the values usually found for the activation energy in diffusion of one metal in another.

The heats of solution of titanium and zirconium in copper may be determined by mathematical analysis of the solubility-temperature relationships for these elements with the aid of the Schroder-Van't Hoff equation [7]

$$\ln x = \frac{Q}{RT} + \text{const},$$

where x is the atomic concentration of the dissolved component; Q is the molar heat of solution.

TABLE 2

Comparative Thermodynamic Characteristics of the Systems Cu-Ti and Cu-Zr

System	Temperature range, $^{\circ}\text{C}$	ΔE cal/g-atom	Temperature range, $^{\circ}\text{C}$	Q cal/g-atom	$\frac{\Delta E}{Q}$	$\frac{\Delta E_{\text{Ti}}}{\Delta E_{\text{Zr}}}$	$\frac{Q_{\text{Ti}}}{Q_{\text{Zr}}}$
Copper-titanium	800—850	—147 500	500—875	—4200	35,1	} 0,56	0,57
Copper-zirconium	800—850	—261 300	400—980	—7430	35,2		

Earlier data [8] on the solubility of titanium and zirconium in copper were used for this purpose. In Fig. 6 the log of the atomic concentration of the dissolved element is plotted against the reciprocal absolute temperature.

The heats of solution of titanium and zirconium in copper, determined from these data, are -4200 and -7430 cal/g-atom respectively.

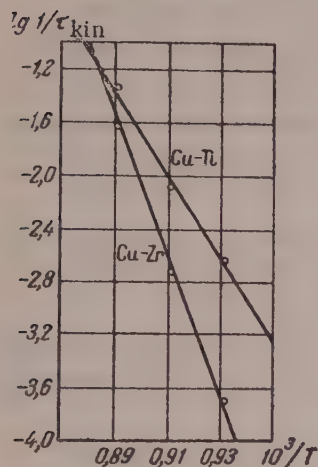


Fig. 5. Variations of $\lg \frac{1}{\tau_{kin}}$ with $1/T$ for colloidal solutions of Cu_3Ti and Cu_3Zr in crystals of α -solid solutions.

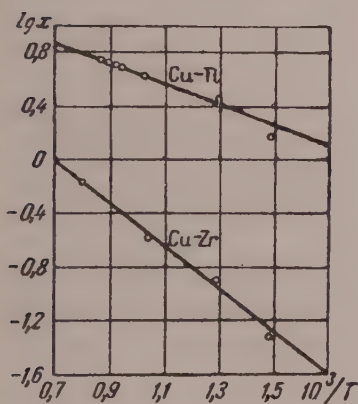


Fig. 6. Curves for the solubility of titanium and zirconium in copper in the solid state (Figs. 1,a and 2,a), in semilogarithmic coordinates.

second phase [10]. The finer the crystals of the heterogenizing phase, the greater the supersaturation of the solid solution surrounding it.

Accordingly it may be assumed that the presence of particles of different sizes in a solid-solution crystal gives rise to chemical heterogeneity, which leads to fluctuations of concentration in the vicinity of the surface of the disperse phase. Because of this at high temperatures spontaneous noncompensated diffusional transfer of

A comparison of the activation energies for transition of solid-solution crystals of titanium in copper and zirconium in copper from the colloidal into the true homogeneous state with the heats of solution of these elements in copper in the solid state (Table 2) reveals a definite correlation between the two sets of values for the two systems.

With some degree of approximation (possibly within the limits of binary alloys of any element with elements belonging to the same subgroup of the Mendeleev periodic system) the following relationship may be regarded as valid

$$\frac{\Delta E_1}{\Delta E_2} \simeq \frac{Q_1}{Q_2} = \text{const} \quad \text{or} \quad \frac{\Delta E_1}{Q_1} \simeq \frac{\Delta E_2}{Q_2} = \text{const},$$

i.e., the ratio of the activation energy for transition of solid-solution crystals from the colloidal into the true homogeneous state to the heat of solution is constant.

Mechanism of the process. It is quite evident that dispersed particles of the second phase, causing heterogeneity of the solid-solution crystals in a two-phase alloy, are unequal in size. Any size distribution of the inclusions is characterized by an appropriate distribution curve [9]. However, the maximum of the distribution curve must evidently be more "diffuse" for particles formed by the dispersional mechanism (the group of polydispersoid particles) and less "diffuse" for particles formed by the condensation mechanism (the group of the so-called monodispersoid particles). An explanation of this result was given by us earlier [3].

Thus, differences of particle size are associated both with differences in the formation mechanism of the particles and with statistical deviations of their sizes in each of the above-named groups. Accordingly, some of the particles must be more stable than others.

Moreover, particles of the second phase formed by the dispersional mechanism, i.e., in the course of dendritic crystallization, are more stable than particles formed by the condensation mechanism during decomposition of the solid solution, as evidently in the latter case diffusion processes in the regions adjoining the second-phase particles are facilitated by the absence of very thin layers of intercrystallite material, which is the consequence of crystallization from the liquid phase.

The size differences of the microdisperse inclusions of the second phase are decisive, and constitute the driving "force" of growth of larger particles from dissolving smaller ones. It is known that the solubilities of interacting components depend on the size of the inclusions of the dispersed

atoms takes place, which tends to equalize the chemical composition in the solid-solution crystal. In this process the regions in immediate proximity to the smaller particles become poorer in the second component and become unsaturated (with the influence of particle size on solubility taken into account) while the regions near the larger particles become supersaturated. The smaller particles dissolve in the impoverished surrounding regions, and as a result the surrounding layers of solid solutions reach a limiting concentration characteristic of the given particle size and temperature. On the other hand, supersaturation of the layers surrounding the larger particles leads to growth of these particles, so that the layers surrounding them become poorer in the second component and also reach a concentration characteristic of the given particle size and temperature. This concentration is lower than the concentration of the layers surrounding the smaller particles, and therefore the solid-solution crystal becomes chemically heterogeneous again.

Consequently, two processes take place in solid-solution crystals heterogenized by submicroscopic particles of the second phase: leveling of chemical heterogeneity by diffusion, and creation of this heterogeneity owing to differences in the solubility of the second component in the layers surrounding particles differing in size.

Both these processes lead to dissolution of the smaller and growth of the larger particles. Thus, the transition of quasi-homogeneous solid-solution crystals into the true homogeneous state is effected by diffusional redistribution of atoms of the second component by way of dissolution and precipitation processes.

The described process is thermodynamically spontaneous, as it occurs with a decrease of the surface energy of the system so that the system passes into a state characterized by a lower value of the isobaric-isothermal potential.

Kinetic studies of this process and the relationship found between its activation energy and the heat of solution confirm that it occurs by way of dissolution of atoms of the second component in some regions of the crystal, and their deposition on large inclusions of the second phase. Since this process is diffusional in character, it is evident that it can proceed intensively when the system has reached a certain temperature, and the start of the intensive process occurs after a definite latent period, represented by τ_{aggr} (Fig. 4) in this instance.

The latent period shortens with increase of temperature, and the transition of quasi-homogeneous solid-solution crystals into the true homogeneous state is more rapid (Fig. 3). Moreover, relatively small temperature variations have a very strong influence on the rate of this process; this also confirms that the process is diffusional in character [6].

SUMMARY

1. A kinetic study has been carried out of the transition of solid-solution crystals in two-phase copper-titanium and copper-zirconium alloys from the quasi-homogeneous into the true homogeneous state, and the activation energy of the process has been determined. The relationship between activation energy and heats of solution of titanium and zirconium in copper has been determined.

2. The transition of colloidal solutions formed by particles of the second phase in solid-solution crystals of two-phase alloys into true solutions is probably effected by coalescence of the particles causing microheterogeneity of the solid solutions, i.e., by dissolution of the smaller and growth of the larger particles.

LITERATURE CITED

- [1] A. A. Bochvar and O. S. Zhadaeva, *Bull. Acad. Sci. USSR, Div. Tech. Sci.*, No. 10-22, 108 (1945); V. M. Glazov, G. A. Korol'kov, and Yu. D. Chistyakov, *ibid.*, No. 10, 143 (1955); No. 12, 131 (1955); V. M. Glazov, V. N. Vigdorovich, and G. A. Korol'kov, *J. Phys. Chem.* No. 8, 1891 (1957).
- [2] V. M. Glazov and G. A. Korol'kov, *Metal Science and Treatment* No. 7, 18 (1957).
- [3] V. M. Glazov and V. N. Vigdorovich, *Colloid J.* 21, 18 (1959).*
- [4] V. M. Glazov, V. N. Vigdorovich, and G. A. Korol'kov, *Industrial Lab.* No. 11, 1343 (1956).
- [5] A. V. Rakovskii, *Introduction to Physical Chemistry* [in Russian] (GONTI NKTP USSR, Moscow, 1938).
- [6] R. M. Barrer, *Diffusion In and Through Solids* (IL, Moscow, 1948) [Russian translation].

* Original Russian pagination. See C.B. Translation.

[7] V. Ya. Anosov and S. A. Pogodin, Fundamentals of Physicochemical Analysis [in Russian] (Izd. AN SSSR, Moscow-Leningrad, 1947).

[8] V. N. Vigdorovich, A. N. Krestovnikov, and M. V. Mal'tsev, Bull. Acad. Sci. USSR, Div. Tech. Sci. 2 145 (1958); No. 3, 110 (1958); S. A. Pogodin, I. S. Shumova, and F. A. Kugucheva, Proc. Acad. Sci. USSR 27, No. 7, 1113 (1940).

[9] K. P. Bunin and Ya. N. Malinochka, Introduction to Metallography [in Russian] (Metallurgy Press, Moscow, 1954).

[10] S. T. Konobeevskii, in the book: Applications of x-Ray Crystallography to Investigations of Materials [in Russian] (ONTI, Moscow-Leningrad, 1936) p. 7; Bull. Acad. Sci. USSR, Chem. Ser., No. 5, 142 (1937); J. Exp. Theoret. Phys. 13, 418 (1943); B. N. Finkel'shtein, J. Exp. Theoret. Phys. 10, 341 (1940).

Received March 29, 1958

AMALGAM FOAMS

G. I. Volkov and D. Ya. Gusakova

Moscow

In work with sodium amalgam, light amalgam foams are frequently formed; these foams are even capable of floating on solution surfaces and are destroyed when the alkali metal is removed from the metallic phase. The literature contains only a few isolated references to the formation of amalgam foams [1-4]. We therefore carried out experiments on the effects of various metal impurities on the formation of amalgam foams.

A conical flask 0.5 liter in capacity contained 40 ml of 0.1-0.5% sodium amalgam and 0.5 liter of 1 N caustic soda solution containing an added metal salt. The sodium amalgam was prepared from purified metallic sodium and carefully purified mercury, and was allowed to settle before use. The caustic soda solution was treated with sodium amalgam to remove impurities. Chemically pure and analytical grade reagents were used in the experiments. The observations of the amalgam surface were continued for a whole day. The amounts of added salts were such that the amalgam did not decompose too rapidly.

The effects of the following additives were investigated (concentrations in terms of grams of metal per liter):

Ferric chloride	0.01	g/ liter	Palladous chloride	0.005	g/ liter
Copper sulfate	0.1	"	Potassium permanganate	0.1	"
Zinc sulfate	0.5	"	Titanous chloride	0.1	"
Cobalt nitrate	0.01	"	Arsenious acid	0.1	"
Barium chloride	1.0	"	Tellurium dioxide	1.0	"
Manganese sulfate	0.1	"	Germanium dioxide	0.0001	"
Stannous chloride	1.0	"	Antimony trioxide	1.0	"
Ammonium vanadate	0.00001	"	Lead acetate	1.0	"
Tungstic acid	0.1	"	Nickel chloride	0.0005	"
Ammonium molybdate	0.0001	"	Sodium chromate	0.00001 and 0.0001	"
Cadmium acetate	1.0	"	Chromium sulfate	0.0002	"

Amalgam foam was formed only in presence of chromium salt in the alkali solution. The foam was formed in the following manner: immediately after the start of the experiment numerous point sites of hydrogen evolution appeared on the amalgam surface; these moved over the surface and gradually coalesced into a large site. When the diameter of the hydrogen-evolution site had increased to about 0.5 cm the amalgam surface under it became convex. Gradually, the convexity increased and gave rise to a frothy mass which by the end of the experiment often covered the whole amalgam surface. The foam was readily destroyed by shaking. If the foam is left at rest after formation, it is destroyed after removal of sodium from the amalgam.

LITERATURE CITED

[1] Yu. V. Karyakin, Pure Chemical Reagents [in Russian] (Goskhimizdat, 1947) p. 35.

- [2] M. A. Rabinovich and A. P. Mashovets, Ukrain. Chem. J. 6, 1 (1931).
- [3] W. Hohn, Osterr. Chem. Zt. 49, 15, 60, 102 (1948).
- [4] W. Moldenhauer, K. F. A. Ewald, O. Roth, Z. angew. Chem. 42, 331 (1929).

Received November 4, 1957

ORIENTATION EFFECT IN LACQUER FILMS FILLED WITH CARBON BLACK

B. S. Gal'perin and L. P. Soldatova

Leningrad

Lacquer films filled with carbon black are widely used as conducting elements of resistors used in modern instrument construction. Uniformity of structure and properties in such films is of great importance in relation to the technical characteristics of the resistors.

Because of its high dispersity and tendency to structure formation, carbon black is preferred to other conducting powders. Carbon-black particles form a conducting network in a lacquer film, as shown in Fig. 1.

The conductivity of a film, under given conditions, is determined by the number of continuous conducting carbon chains per unit cross section of the film.

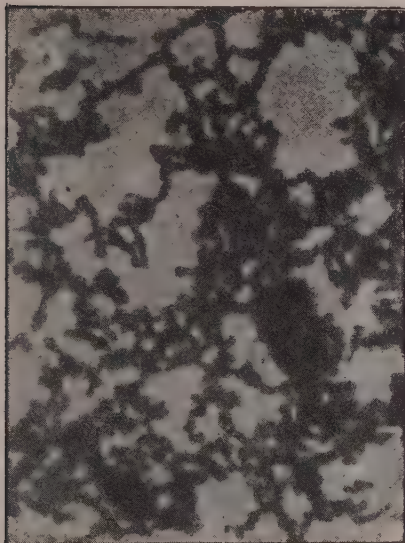


Fig. 1. Electron micrograph of a lacquer film containing 6% of carbon black (magnification 25000).

Figure 2 shows that if the volume concentration (F) of carbon black in the film is high enough the conductivity of the film, like the conductivity of pure carbon blacks, is almost independent of the type of carbon black. It may be assumed that in this case nearly all the carbon is involved in the formation of conducting chains, irrespectively of the tendency to structure formation.

With decrease of the volume concentration of carbon black the conductivity σ decreases more rapidly than F , as represented by the equation

$$\sigma = AF^{\underline{m}}, \quad (1)$$

where A and \underline{m} are constants which depend on the type of black; the value of \underline{m} ranges from 3 (from the most active acetylene black) to 15 and over. The structurizing power of carbon black becomes more significant with decreasing concentration. With structurizing carbons the conductivity decreases relatively slowly, so that there is appreciable conduction at low carbon concentrations, of the order of 2-3%.

Hence, it can be concluded that a relatively small proportion of the carbon particles is involved in formation of conducting chains in the film. The remaining portion, which relatively increases with decrease of F , is isolated in the form of individual particles or groups.

It is found in practice that with low concentrations of carbon black in the film, structure formation is greatly influenced by the method used for application of the suspension to the surface and by the hardening conditions. If the film is dried relatively rapidly, an appreciable orientational effect may be observed, and the films have higher conductivity in the direction of flow of the applied suspension.

In this investigation the orientation effect was studied in films applied by dipping onto porcelain rods 20 mm long and 4 mm in diameter. The rods were extracted vertically from the liquid, so that the suspension flowed down the rods. To obtain more uniform coatings, this operation was performed twice (with brief drying in air between), in opposite directions. The total thickness of the coating did not exceed 5-7 μ . The carbon concentration of the film varied from 8 to 15%.

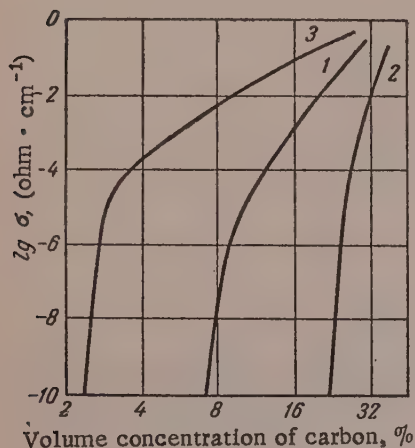


Fig. 2. Variation of film conductivity σ with the volume concentration of carbon black; 1) channel black, 2) thermal black, 3) acetylene black.

After air drying and appropriate polymerization of the films the rods were fitted with metal tips for effecting contact between the films and the measuring instruments.

The resistance was first measured in the direction of flow of the suspension - along the rod. A spiral was then cut in each rod by means of a special device. This converted the conducting film into a long thin strip (~ 1 mm wide) coiled around the rod. Therefore, a second resistance determination, performed after the cutting operation, made it possible to calculate film conductivity in a direction at right angles to the first.

The two resistances found, R' and R'' , were used to calculate the resistance per unit area R_s , with the length L and diameter D of the rod and the pitch t and width d of the spiral taken into account.

The surface resistivity along the rod is:

$$R'_s = R' \frac{\pi D}{L}, \quad (2)$$

and across the rod:

$$R''_s = R'' \frac{td}{\pi DL}. \quad (3)$$

The coefficient of anisotropy of conductivity (K_a) was found from the expression

$$K_a = \frac{R''_s}{R'_s} = \frac{R''}{R'} \frac{td}{(\pi D)^2}. \quad (4)$$

Values of K_a for films made from No. 211 resin dissolved in alcohol-toluene mixture with different carbon contents are given in Fig. 3. The strong dependence of K_a on the carbon concentration indicates that the

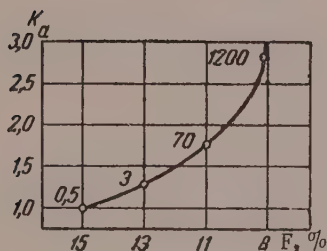


Fig. 3. Variation of the coefficient of anisotropy of conductivity K_a with volume concentration of of Ukhta channel black; (numbers on the curve represent the resistance in megohms); the top point should be 12000 megohms.

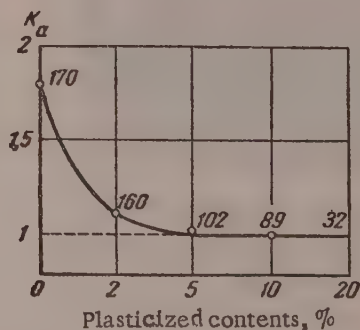


Fig. 4. Variation of the coefficient of anisotropy of conductivity K_a of a film containing 10% channel black with the amount of plasticizer (dibutyl phthalate); (numbers of the curve represent the resistance in megohms).

effect is due to anisotropic conductivity of the film and not to local heterogeneity caused by surface defects (such as thin or thick patches).

The higher conductivity of the film in the direction of the rod axis is caused by orientation of the carbon chains in the flow direction of the suspension, which persists in the film if it is rapidly dried. Difficulties in maintaining standard conditions of film drying in the production of resistors are among the causes of poor reproducibility of the electrical characteristics of resistors made by the dipping method.

If a plasticizer retarding film drying is added to the suspension, the orientation effect may be diminished considerably, as Fig. 4 shows. Introduction of 2-3% of plasticizer eliminates anisotropy of conductivity almost entirely, because during slow drying of the film the carbon chains, initially oriented, are able to distribute themselves more or less uniformly in all directions.

Figure 4 also shows that increase of the plasticizer content not only improves homogeneity but also increases conductivity, because of easier formation of carbon structure in the film.

In films based on oil varnishes, which dry relatively slowly, the orientation effect is almost absent. It is evident that the orientation effect can always be prevented if films are applied in a manner which excludes directional flow of the suspension (such as by spraying).

SUMMARY

1. Anisotropy of conductivity of lacquer films containing carbon black, applied by the dipping method, is due to orientation of carbon chains in the flow direction of the suspension.
2. Anisotropy of such films increases with increasing rate of drying and with decreasing carbon black content.
3. The orientation effect in films is eliminated by introduction of a small amount of plasticizer into the suspension.

Received March 1, 1958

BINDING OF WATER BY FINELY DISPERSED SEDIMENTS

2. DEPENDENCE OF THE AMOUNT OF BOUND WATER ON THE COMPOSITION AND CONCENTRATION OF EQUILIBRIUM SOLUTIONS

O. I. Dmitrenko and G. A. Pavlova

Institute of Oceanology, Academy of Sciences USSR, Moscow

The attention of research workers is now primarily concentrated on physical rather than chemical analysis of the structure of disperse systems.

In his x-ray diffraction studies of the role of water in monomineral crystalline substances, Bernal [1] distinguishes between two groups of water layers. In the first group the water molecules are bound by the cations of the anhydrous layers of the crystal lattice. In the second group the water molecules fill the spaces between the layers. He also showed that the water between layers in the lattice is not a liquid, and its molecules are in a fixed position, forming an ice structure. According to Bernal, the water molecules can give rise to local formations with extraneous atoms or ions stabilizing the ice structure, forming the class of tectohydrates. The charge on the molecules in solution is also a stabilizing factor which favors their agglomeration both in very dilute and in more concentrated (over 2%) solutions. According to Wooster [2], in most hydrates cleavage occurs along the line of bond cleavage between atoms and water molecules rather than at other bonds within the structure; this is consistent with the theory of the stabilizing effect of extraneous ions or molecules.

According to Bernal's observations, the stability of tectohydrates makes it possible to determine the position of ions and molecules "built into" the ice structure. In the case of particularly stable structures, the stability is retained even at relatively high temperatures, up to 65° (for example, in the case of $\text{Na}_2\text{SO}_4 \cdot 10\text{H}_2\text{O}$).

However, these ice structures in tectohydrates are deformed to a considerable extent, as the positive ions in them are always surrounded by coordination polyhedrons formed by water dipoles, the hydrogen atoms in which are directed outward. Freymann [3] in a study of the dielectric properties of solids and liquids by radio-frequency (Hertzian) spectroscopy showed that in all cases bound water continues to absorb short radio-frequency waves, and that this type of water originates in connection with lattice defects. As was noted earlier [4], these defects are the results of phase changes. In the light of the foregoing we concluded that layer "growth" of solid phase outside the lattice and formation of a liquid coagulum "completing" the lattice may occur at the boundary between the solid and liquid phases mainly owing to binding of the molecules. The direction of the lattice layers then determines quantitatively the predominant orientation of one of the two molecular components of the solution (water dipoles or electrolyte molecules). This logically leads to the concept that intermicellar solutions are structurized [5].

The purpose of the present investigation was to determine chemically, by the "indicator ion" method [5], the distribution of water dipoles and electrolyte molecules in the intermicellar solutions of finely dispersed sediments.

The presence of water molecules is a stabilizing factor in crystalline structures with sufficiently large voids. In Wiegner's classic terminology [6], these structures are characterized by exchange of the intermicellar type; in the modern terminology [1] they constitute the class of phyllohydrates, containing water in the form

of molecular layers. According to Bernal, the phyllohydrates are represented by two subgroups. In our experiments we studied phyllohydrates of the second subgroup, characterized by variable distances between the layers in the crystal lattice and variable water contents.

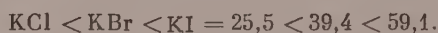
The absence of voids permeable to water molecules within crystalline adsorbents of the kaolin type, characterized by extramolecular exchange [6], suggests that in such cases surface reactions of molecular sorption predominate.

In the interaction of such adsorbents with aqueous electrolyte solutions the most probable type of molecular sorption reaction would be that characterized by direct dependence of the amount of electrolyte adsorbed on the concentration of the equilibrium solution. The water layers closest to the kaolin surface are stabilized by metal atoms, and the nature of such bonding depends on the chemical properties of these atoms.

In Bernal's view, in the case of alkali and alkaline-earth metals purely electrostatic forces operate, and the arrangement of the molecules is determined by their mutual repulsion, with formation of coordination tetrahedrons or octahedrons. In general, even univalent cations may change the structure of water appreciably at distances of the order of 8 Å. The presence of a large number of univalent and bivalent cations on the surface of a colloidal particle (or a crystallite of a monomineral clay) intensifies this effect and creates a layer of oriented water dipoles in the intermolecular solution.

It must also be taken into account that the extent of molecular sorption of the electrolyte is an inverse function of its solubility [7-10]. It is clear from the papers cited that increasing solubility (at 20°) in a series of halides of any alkali metal corresponds to decreasing molecular adsorption of these compounds.

This may be illustrated by the series of potassium halides in order of increasing solubility (in grams per 100 g H₂O):



When solutions of these electrolytes interact with a finely divided adsorbent of the kaolin type, molecular adsorption is "large" in the first case, "moderate" in the second, and "small" in the third. Since the total number of adsorbed molecules, i.e., the molecular capacity (Σm) is constant, the amount of adsorbed electrolyte must be inversely proportional to the amount of bound water. Therefore, in this series of potassium halides the amounts of water bound from solution must increase on adsorbents characterized by extramolecular exchange (such as kaolin), and decrease on adsorbents with exchange of the intramolecular type (montmorillonite, beidellite, etc.). The observed effect in the latter case can be regarded as the consequence of the occurrence of the reaction within the adsorbent. We verified this hypothesis experimentally.

The main task in the present investigation was to determine the relationship between the amount of water bound by the adsorbents, and the composition and concentration of the electrolyte.

The experiments were carried out with powdered samples sifted through a 0.5 mm screen. Samples of 50 g were washed on funnels with 0.125, 0.5, and 1.0 N solutions of sodium or potassium halides, and with sodium sulfate solutions of the same concentrations, until equilibrium was established. The preparatory operation was regarded as complete for practical purposes when about 2 liters of filtrate had been collected in a given experiment. The last portion of each filtrate (not more than 50 ml) was retained and the equilibrium electrolyte concentration in it was determined. For this, 0.3 ml samples of each solution were weighed and then either titrated with 0.02 N AgNO₃ by the Mohr method, or treated with 1 N BaCl₂ to precipitate sulfates. The equilibrium values (of Cl⁻, Br⁻, I⁻, and SO₄²⁻) were determined in this way. After the last portions of solution had been percolating for an hour, the sediments became spontaneously more compact. Each sediment prepared in this way was divided into two portions. The largest portion (~35 g) was again washed through with the solution (0.5 N KNO₃), about 1 liter of filtrate being collected in each case. The last filtrate portions were tested for absence of halides. Each filtrate was then made up to exactly 1 liter and the contents of eluted halide and sulfate ions were determined in 10.014 ml samples by titration by the Mohr method* and precipitation as barium sulfate.

* Iodide was determined by the Kolthoff "clear-point" method.

Simultaneously the second, smaller portion was dried to constant weight at a temperature not over 100-110°, for determination of the moisture content. It must be noted that the method used for calculation of bound water in these experiments was substantially different from that used for natural marine sediments.

The liquid phase remained unchanged in the systems studied in the previous investigation [5]. This simplified calculation of the amount of water bound by natural marine sediments. On the other hand, in the present investigation the liquid phase of the investigated systems was made artificially, and the concentration of the electrolytes in equilibrium with the monomineral clay samples, and in the subsequent series of experiments also with natural marine sediments, varied from 0.1 to 2 N, or 20-fold. Because of this, the following values were calculated: 1) moisture contents of the deposits as percentages relative to the natural salt-free material; 2) concentrations of the indicator anion (Cl^- , Br^- , I^- , and SO_4^{2-}) in the equilibrium solution, which were then expressed as grams of chlorine per kilogram of pure water, and 3) total amounts of the indicator anion (Cl^- , Br^- , I^- , and SO_4^{2-}) expressed as milligrams of chlorine.

The subsequent calculations of the contents of bound water in all the experiments with monomineral clays and marine sediments were made for a certain hypothetical "salt-free" material; this unified the data obtained in experiments with different indicator anions and for different concentrations of the eluting electrolytes.

Kaolin. The curves in Fig. 1 represent the contents of bound water in kaolin (from Prosyanyaya*) for equilibrium concentrations of the eluting solutions of halides and sodium sulfate in the range of 0.1 to 1 N.

Figure 1 shows that there is a direct relationship between the amount of water bound by kaolin and the concentration of the eluant. The solid phase predominantly retains water molecules from the more concentrated solutions, and the adsorption is greatest in such cases. The amounts of bound water pass from the negative into the positive region, to values not exceeding +15% of bound water per 100 g of dry kaolin.

The relative positions of the curves show that the amount of water bound by kaolin increases in the following electrolyte series:



This confirms the existence of a direct relationship between the amount of water bound by kaolin and electrolyte solubility, in the investigated range of equilibrium electrolyte concentrations. In the experiment with sodium sulfate the solubility should have less influence than its molecular charge on the adsorption of water from solutions. The amounts of free and fixed molecules of sodium sulfate distributed between the solid and liquid phases in this instance probably depends on the stability of the tectohydrate formed in solution. Since the tectohydrates of sodium sulfate are fairly stable [1], it may be concluded that the proportion of the kaolin surface occupied by Na_2SO_4 molecules must be relatively small, and therefore the adsorption of water molecules should be greatest.

Montmorillonite. Figure 2 shows the results of experiments with montmorillonite ("kil" clay, Crimea), samples of which were treated with solutions of three different sodium halides (chloride, bromide, and iodide) and of sodium sulfate, by the usual procedure. In this series of experiments there was found an inverse relationship between the percentage of water in the montmorillonite and the electrolyte concentration.

The amounts of water bound from aqueous solutions of electrolytes conform to the following series:



which is the reverse of the series found in the experiments with kaolin. It is probable that in this case a greater amount of bound water, with the ice structure, is contained within the montmorillonite lattice rather than on the surface. This suggests that molecular-exchange reactions should be hindered with electrolytes the molecules of which have large volumes. In our experiments changes of molecular volume corresponded to changes of the anion volume. The molecular volumes of nonhydrated sodium halides may be arranged in the sequence of the radii of their anions (determined in A experimentally by Goldschmidt), in the following series:

* The kaolin sample was obtained from the Karpinskii Mineralogical Museum, Academy of Sciences USSR, together with all the montmorillonite clay samples used in the present investigation.

$$\text{NaI} > \text{NaBr} > \text{NaCl} = \text{I}^- > \text{Br}^- > \text{Cl}^- \approx 2,20 > 1,56 > 1,81.$$

It is reasonable to suppose that access into the interlayer spaces of the montmorillonite lattice is more difficult for molecules of greater volume, and molecular exchange must be less intensive in such cases. Accordingly, the expected molecular exchange effect should be greatest in the experiment with NaCl solution and least with NaI solution; i.e., in order of decreasing intensity of molecular exchange the electrolyte can probably be arranged in the following series:

$$\text{NaCl} > \text{NaBr} > \text{NaI}.$$

In accordance with this series the amounts of molecularly bound water remaining within the montmorillonite lattice should be in the reverse sequence, i.e., least water (in the series of sodium halides) is bound from NaCl solutions, and most from NaI solutions.

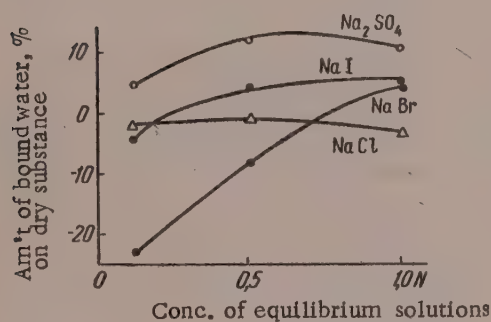


Fig. 1. Effects of solution composition and concentration on the amount of water bound by kaolin.

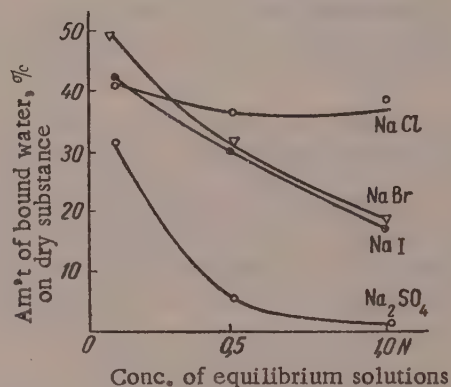


Fig. 2. Effects of solution composition and concentration on the amount of water bound by montmorillonite.

On the assumption that the molecular capacity is constant, an inverse relationship might be expected to exist between the amounts of electrolytes adsorbed molecularly by montmorillonite and of water bound from their solutions; i.e., less water should be bound from NaCl solution than from NaI solution, while in experiments with Na₂SO₄ the amounts of bound water should be greatest, as was already observed in experiments with kaolin.

However, the experimental results do not confirm this hypothesis. As was noted earlier, when montmorillonite was eluted with Na₂SO₄ solution particularly stable tectohydrates [1] were formed in the liquid phase. However, it is difficult to believe that in this case the greatest amounts of water would be bound within the solid phase of the adsorbent. Although the interlayer spaces of the montmorillonite lattice, already filled with layers of water in the solid state, might increase somewhat [11] by taking up some additional water molecules from the solutions, this effect should not be as significant as in the binding of water on the adsorbent surface. It follows that in the experiment with Na₂SO₄ the low solubility of the latter, which determines the structural state of the intermicellar solution, had a strong influence on the ultimate adsorption of its molecules within the adsorbent. Therefore, in subsequent displacement only the amounts of bound water which were previously contained in the montmorillonite lattice could be obtained. Therefore, in accordance with the hypotheses put forward above, the amounts of water should be greater if it is bound from solutions of nonhydrated halides than from sulfate solutions.

All the foregoing is valid only on the assumption that only the nonhydrated components of the solution take part in molecular exchange within the adsorbent, and that all the tectohydrates formed in the solutions of these electrolytes are stabilized to an equal degree by their molecules, which is hardly likely. This probably accounts for the fact that the positions of NaCl and NaI are interchanged in the experimental series of electrolytes in order of increasing volumes of water bound from their solutions.

Since molecular exchange is most intensive in concentrated electrolyte solutions, this same series of experiments should reveal an inverse relationship between the amount of bound water and the electrolyte concentration.

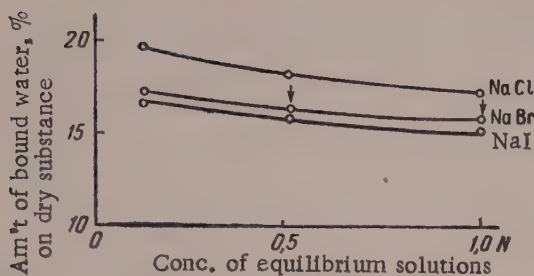


Fig. 3. Effects of eluant composition and concentration on the amount of water bound by beidellite.

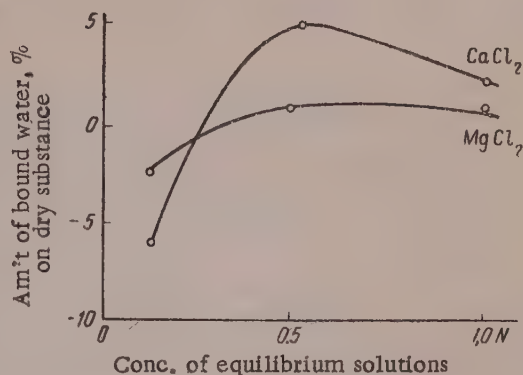


Fig. 4. Effect of accompanying cations on the molecular adsorption of water by beidellite.

It follows that molecular reactions within the adsorbent cannot be attributed solely to the effects of pure electrostatic intermolecular action, and they are determined to a considerable extent by the influence of the structure of the equilibrium solutions. Our results confirm this view. It is seen in Fig. 2 that the greatest amount of water (~40%) was bound by montmorillonite from sodium chloride solutions, followed by sodium iodide and bromide solutions (from 40 to 20%), and the least from sodium sulfate solutions (from 30 to 2%).

Beidellite. Experiments with beidellite (from Ufaei in the Urals) were performed as with the previous samples. The results are plotted in Fig. 3, which shows that the "nonsolvent" volumes of water, found by the indicator anion method, decrease in the series:



with an inverse relationship between the nonsolvent volume and the concentration of sodium halide. Thus, the distribution of electrolytes and water in the experiments with beidellite was similar to that in the experiments with montmorillonite. In addition to experiments with sodium halides, it was of some interest to deter-

mine the amounts of bound water in presence of different bivalent cations with a common anion; the electrolytes chosen for this purpose were CaCl₂ and MgCl₂. The experimental values of the radii of the Ca²⁺ and Mg²⁺ cations are 1.06 and 0.78 Å respectively. Therefore, the expected values of molecular adsorption should be less for CaCl₂ and greater for MgCl₂. Accordingly, more bound water should be obtained in experiments with the former than with the latter. In these experiments the influence of molecular volume on the course of the reaction within the absorbent is complicated by the fact that the solubilities of these two electrolytes change correspondingly. These considerations were fully confirmed by the experimental results. Figure 4 shows that the curve representing the amount of water bound by beidellite from CaCl₂ solution lies above the corresponding curve for MgCl₂ solution.

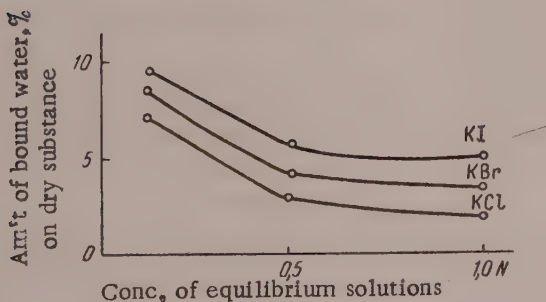


Fig. 5. Molecular binding of water by shallow marine sediments.

Both curves have a maximum in the region of 0.5 N. The adsorption of water from solutions of univalent chlorides is considerably greater than from solutions of bivalent chlorides. The amount of water bound by beidellite is ~20% in the former case, and 5% in the latter. This is due to the influence of the cation volume, which is

greater in the former case, so that in the former case, i.e., in experiments with univalent chlorides, water molecules are displaced less intensively from the beidellite lattice.

Fine sediments from the Bering Sea. Figures 5 and 6 show groups of curves which reveal a distinct inverse relationship between the amount of bound water and the equilibrium electrolyte concentration. This

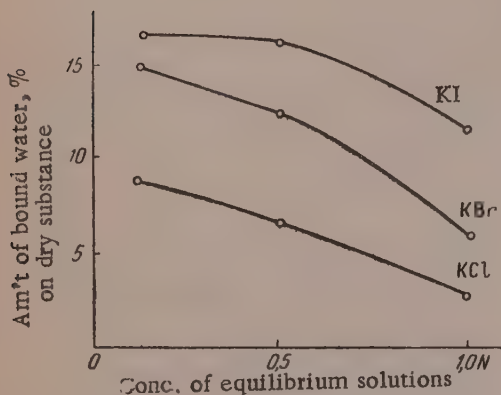


Fig. 6. Molecular binding of water by deep marine sediments.

relationship holds both for samples taken at shallow levels (Bering Sea, depth 95 meters, dark gray sediment; Fig. 5) and for deep samples of gray sediments (Bering Sea, depth 3400 meters, gray sediments; Fig. 6). The values of the nonsolvent volume of water determined in experiments with potassium halides form a series which is the reverse of that obtained in experiments with sodium halides and montmorillonite. Since in these experiments the radii of the anions (Cl^-) are the same, and only the cations differ by their experimental ionic radii (0.98 Å for Na and 1.33 Å for K), this result can be attributed to increased lattice parameters of the adsorbents constituting marine sediments [11, 12]. It is probable that during the prolonged existence of the sediments in the hydrosphere, conditions arise for swelling of the clay adsorbents and increase of the interlayer spaces in the lattices of the sediment components which are close to montmorillonite or beidellite [13]. In that case molecular displacement within the adsorbent is probably determined to a greater extent by solubility of potassium

halides than by the ionic radii. If Σm is constant, the greatest adsorbability of the least soluble potassium chloride must correspond to the smallest amount of water bound by the marine sediment. These views are confirmed by the results of the experiments discussed above.

SUMMARY

1. Molecular adsorption of water by adsorbents which exhibit extramolecular exchange is of a surface character. The concept of interchangeability of adsorbed water and electrolyte molecules [5] was used to explain the results.
2. There is a direct relationship between the adsorption of water dipoles by kaolin and the electrolyte concentration in solution; this can be attributed to the predominant influence of the structure of intermolecular solutions. There is also a direct relationship between the solubilities of halides (NaCl , NaBr , NaI) and the amounts of water bound from their solutions, for adsorbents exhibiting extramolecular exchange.
3. Molecular adsorption of water by adsorbents of the intramolecular exchange type occurs within the volume of such adsorbents, and surface adsorption is of subordinate significance.
4. In the case of two single clay minerals (montmorillonite and beidellite) the adsorption of water molecules was an inverse function of the electrolyte concentration in solution; this is due to intensive molecular exchange in concentrated solutions of electrolytes capable of displacing water dipoles within the adsorbent volume.

In the interaction of the same minerals with sodium halides the amount of bound water was an inverse function of halide solubility.

5. In a series of experiments with marine sediments there was found an interesting case of molecular exchange reactions within the volume of adsorbents with increased lattice parameters.

LITERATURE CITED

- [1] J. D. Bernal, *Progr. Chem.* 25, No. 5, 643 (1936).
- [2] W. A. Wooster, *J. chim. phys. et phys.-chim. biol.* 50, 19 (1953).

- [3] R. Freymann, J. chim. phys. et phys.-chim. biol. 50, 27 (1953).
- [4] I. Meinel, J. physique 5 (1953).
- [5] O. I. Dmitrenko, Colloid J. 20, 163 (1958)*
- [6] G. Wiegner, "Ionenumtausch und Struktur," Transactions of the Third International Congress of Soil Science, 8 (1936).
- [7] N. Shilov and L. Lepin', Journal of Lomonosov Phys.-Chem. Soc., Moscow (1919).
- [8] I. Kolthoff, J. Phys. Chem. 40, 8 (1936).
- [9] V. A. Kargin, P. S. Vasil'ev, and O. I. Dmitrenko, J. Phys. Chem. 14, No. 12, 1268 (1940).
- [10] S. S. Yarusev, Chemization of Socialist Agriculture No. 6, 49 (1940).
- [11] U. Hofmann, K. Endell, and D. Wilm, Angew. Chem. 47, 539(1934).
- [12] U. Hofmann and W. Bilke, Kolloid.-Z. 47, 238 (1936); J. W. Gruner, Amer. Mineralogist 20, 475 (1935); C. E. Marschall, J. Chem. Indus. 54, 393, (1953); C. W. Correns and M. Mehmel, Z. Kristallogr, 94, 337 (1936).
- [13] W. F. Bradley, R. E. Grim, and G. L. Clark, Z. Krist. (A) 97, 216 (1937); J. E. Gieseking and H. Jenny, Soil. Sci. 42, 273 (1936); J. E. Gieseking, Soil. Sci. 47, 1 (1939); L. E. Eusminger and J. E. Gieseking, Soil. Sci. 51, 125 (1946).

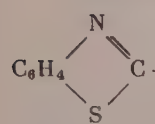
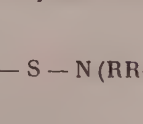
Received February 1, 1958

* Original Russian pagination. See C.B. Translation.

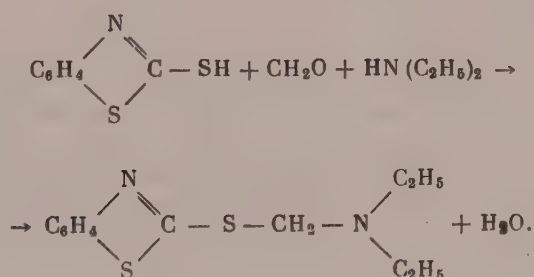
VULCANIZATION OF RUBBER IN PRESENCE OF AMINOMETHYL DERIVATIVES OF 2-MERCAPTOBENZOTHAZOLE AS ACCELERATORS

B. A. Dogadkin, I. I. Éitingon, M.S. Fel'dhstein, Z. N. Tarasova,
E. N. Gur'yanova, Lin Yang Ch'in, N. A. Klauzen, and D.M. Pevzner
Scientific Research Institute of the Tire Industry, Moscow

In recent years sulfenamide derivatives of 2-mercaptobenzothiazole, of the general formula

 C_6H_4  $\text{C} - \text{S} - \text{N}(\text{RR}_1)$, prepared by oxidative condensation of 2-mercaptobenzothiazole with various aliphatic and alicyclic amines and with heterocyclic oxazines, have been widely used as vulcanization accelerators for natural and synthetic rubber. In presence of these compounds vulcanization takes a peculiar course, with an induction period [1, 2].

It was desired to determine the influence of 2-mercaptobenzothiazole derivatives in which the $-\text{S}-\text{N}-$ sulfenamide group is replaced by the $-\text{S}-\text{C}(\text{H})_2-\text{N}-$ group on vulcanization kinetics. Diethylaminomethyl-2-thiobenzothiazole was synthesized for this purpose. This compound was prepared by condensation of 2-mercaptobenzothiazole and formaldehyde with diethylamine:



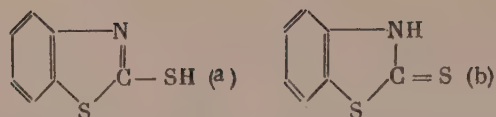
The product is a yellow crystalline powder of m. p. 86-87°.

The experimental value found for the molecular weight of this compound is 252, which coincides with the theoretical.

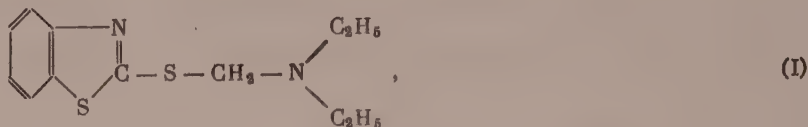
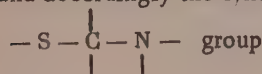
The elementary composition of the compound is:

Found %: C 57.25, H 6.66, N 11.01, S 25.02. $\text{C}_{12}\text{H}_{16}\text{N}_2\text{S}_2$. Calculated %: C 57.14, H 6.35, N 11.11, S 25.19.

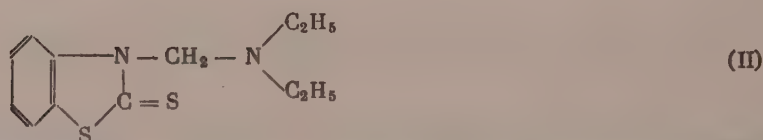
Two tautomeric forms of 2-mercaptobenzothiazole are known [3]:



and accordingly the synthesis could give rise to two entirely different substances, one containing the



and the other containing, in addition to the $-\text{C}=\text{S}$ group, the $-\text{N}-\underset{\text{|}}{\underset{\text{|}}{\text{C}}}-\text{N}-$ diamine group

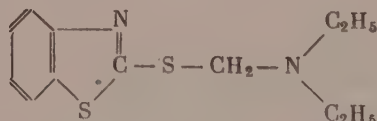


To determine the chemical nature of the product, it was investigated spectroscopically (by means of the IKS-11 infrared spectrograph). According to Bellamy [4], compounds containing the $-\text{N}-\underset{\text{|}}{\underset{\text{|}}{\text{C}}}=\text{S}$ group give an intense band at 6.7μ . This band is present in the spectrum of 2-mercaptobenzothiazole which, as stated earlier,

has the formula $\text{C}_6\text{H}_4\text{NH}-\text{C}(=\text{S})\text{S}$ in the solid state. This distinguishes the spectrum of 2-mercaptobenzothiazole from the spectrum of di-2-benzothiazolyl disulfide



which does not contain a $-\underset{\text{|}}{\underset{\text{|}}{\text{C}}}=\text{S}$ group. It is clear from Fig. 1 that a band at 6.7μ is found only for 2-mercaptobenzothiazole. No such band is present in the spectra of di-2-benzothiazolyl disulfide or of the synthesized product. This indicates that the condensation product of 2-mercaptobenzothiazole, formaldehyde, and diethylamine is diethylaminomethyl-2-thiobenzothiazole (or benzothiazole-2-thiomethylenediethylamine, BTMA) with the structural formula



The method described above was used for synthesizing analogous aminomethyl derivatives of 2-mercaptobenzothiazole, with the use of various aliphatic and alicyclic amines and a heterocyclic oxazine (Table 1). The vulcanization activities of these compounds were compared with those of the corresponding sulfenamide accelerators in natural and butadiene-styrene rubber stocks. The amounts of sulfur added were 3 weight parts in natural-rubber stocks and 2 weight parts in butadiene-styrene rubber stocks, per 100 weight parts of rubber. The compounds tested as vulcanization accelerators were added in the same molar proportions as the corresponding sulfenamide accelerators. The vulcanization was effected at 143° .

TABLE 1

Aminomethyl and Sulfenamide Derivatives of 2-Mercaptobenzothiazole

Compounds containing groups	Compounds containing groups
N,N-dimethyl-2-benzo- thiazolesulfenamide	Dimethylaminomethyl-2- thiobenzothiazole
N,N-diethyl-2-benzo- thiazolesulfenamide	Diethylaminomethyl-2- thiobenzothiazole
N,N-diisopropyl-2-benzo- thiazolesulfenamide	Diisopropylaminomethyl-2- thiobenzothiazole
N-cyclohexyl-2-benzo- thiazolesulfenamide	Cyclohexylaminomethyl-2- thiobenzothiazole
N-morpholyl-2-benzo- thiazolesulfenamide	Morpholyl-N-methyl-2- thiobenzothiazole

The data in Fig. 2 show that BTMA is an effective vulcanization accelerator. The vulcanizates obtained with the use of BTMA accelerator* are almost equivalent in physical and mechanical properties to vulcanizates

obtained with the use of sulfenamide accelerators - N,N-diethyl-2-benzothiazolesulfenamide and N-cyclohexyl-2-benzothiazolesulfenamide. The action of other derivatives in the investigated series of compounds is analogous; for example, cyclohexylaminomethyl-2-thiobenzothiazole and morpholyl-N-methyl-2-thiobenzothiazole give vulcanizates (Fig. 3) which are almost identical in strength characteristics with vulcanizates obtained with the use of N-cyclohexyl-2-benzothiazolesulfenamide and N-morpholyl-2-benzothiazolesulfenamide.

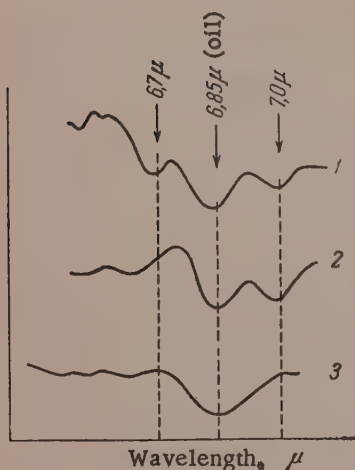


Fig. 1. Infrared spectra in the 6.5-7.2 μ region; 1) 2-mercaptobenzothiazole; 2) di-2-benzothiazolyl disulfide; 3) diethylaminomethyl-2-thiobenzothiazole.

The distinctive feature of the vulcanization kinetics of stocks containing the synthesized compounds as vulcanization accelerators is the more rapid vulcanization during the initial stage than is found with the corresponding sulfenamide accelerators. This is shown clearly by the data on addition of sulfur to rubber during vulcanization (Fig. 4). Whereas after 5 minutes of vulcanization the amount of bound sulfur in a natural-rubber stock containing N,N-diethyl-2-benzothiazolesulfenamide is 18%, in presence of diethylaminomethyl-2-thiobenzothiazole (BTMA) it is 62%. In agreement with this, maximum-swelling data (Fig. 5) indicate that vulcanizates with BTMA have a denser network at the initial vulcanization stage. At the next vulcanization stage, after 15-20 minutes, the amounts of bound sulfur are approximately the same in the two cases. However, vulcanizates with BTMA (Fig. 5) at this vulcanization stage have a somewhat less dense network.

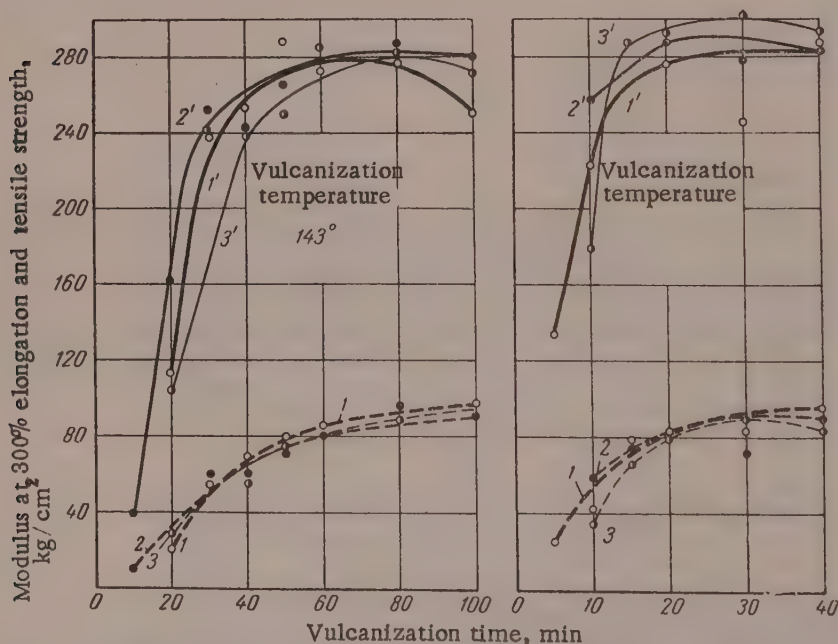


Fig. 2. Action of BTMA accelerator in SKS-30AM stocks, containing channel black: 1 and 1') N,N-diethyl-2-benzothiazolesulfenamide, 1.1 wt. parts; 2 and 2') BTMA accelerator, 1.2 wt. parts; 3 and 3') N-cyclohexyl-2-benzothiazolesulfenamide, 1.2 wt. parts; 1, 2, 3) modulus; 1', 2', 3') tensile strength.

* The action of BTMA accelerator in natural and butadiene-styrene rubber stocks is considered in greater detail in a separate communication [5].

The distinction between the vulcanization kinetics of rubber stocks containing the investigated accelerators and those with the corresponding sulfenamide accelerators is revealed more clearly in vulcanization of butadiene-styrene rubber, as Fig. 4,b shows. Addition of sulfur in presence of N,N-diethyl-2-benzothiazole-

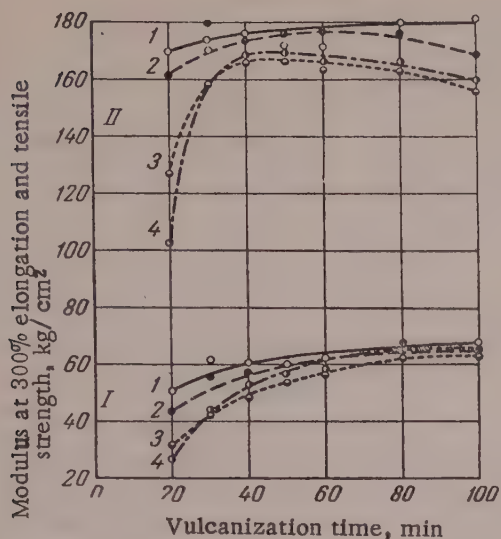


Fig. 3. Comparison of vulcanization activities of aminomethyl derivatives of 2-mercaptobenzothiazole and sulfenamide accelerators in SKS-30AM tread stocks: I) modulus; II) tensile strength; 1) cyclohexylaminomethyl-2-thiobenzothiazole, 1.3 wt. parts; 2) cyclohexyl-2-benzothiazolesulfenamide, 1.2 wt parts; 3) morpholyl-N-methyl-2-thiobenzothiazole, 1.3 wt. parts; 4) N-morpholyl-2-benzothiazole sulfenamide, 1.2 wt. parts.

sulfenamide is represented by an S-shaped curve with an initial period of retarded vulcanization, whereas there is no induction period on the curve for stocks containing diethylaminomethyl-2-thiobenzothiazole.

In order to determine the cause of this difference in vulcanization kinetics, the isotope exchange reaction of diethylamino-2-thiobenzothiazole was studied. It is known that the rate of isotope exchange between sulfur-containing accelerators and elemental sulfur can be used as a measure of their vulcanization activity.

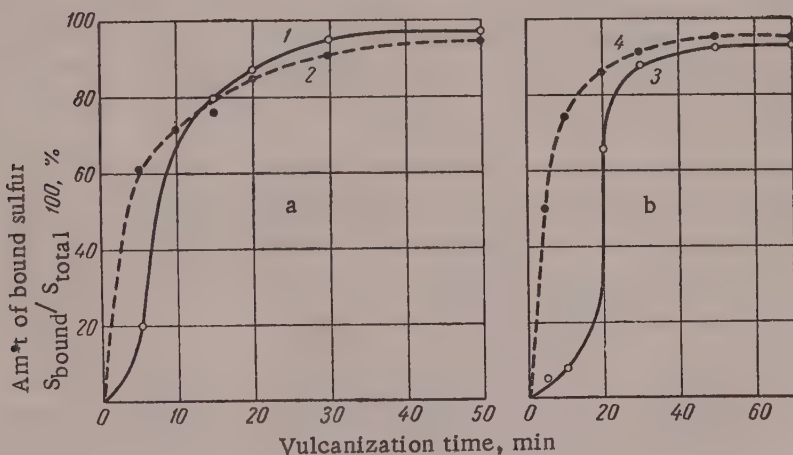


Fig. 4. Kinetics of sulfur addition in vulcanization of unfilled stocks: a) natural rubber; b) SKS-30A; 1 and 3) N,N-diethyl-2-benzothiazole-sulfenamide, 1.0 and 1.2 wt. parts respectively; 2 and 4) BTMA accelerator, 1.05 and 1.3 wt. parts respectively.

Studies of isotope exchange between diethylaminomethyl-2-thiobenzothiazole and radioactive sulfur proved impossible, as the accelerator was decomposed in the course of exchange even at a relatively low temperature (below 100°). For investigation of the strength of the -S-CH₂- linkage in diethylaminomethyl-2-thiobenzothiazole a study was made of exchange between benzothiazolyl groups and di-2-benzothiazolyl disulfide

tagged with S^{35} . The di-2-benzothiazolyl disulfide tagged at the disulfide linkage was prepared by exchange with radioactive sulfur [6].

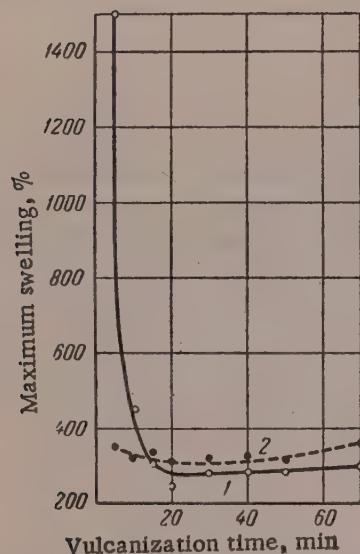


Fig. 5. Effect of vulcanization time on maximum swelling of unfilled natural-rubber stocks: 1) N,N-diethyl-2-benzothiazolesulfenamide, 1.0 wt. part; 2) BTMA accelerator, 1.05 wt. parts.

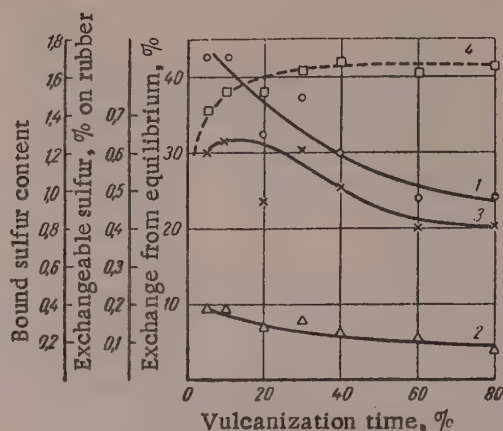


Fig. 6. Variations of exchangeability of SKS-30AM vulcanizates with BTMA accelerator with the vulcanization time: 1) exchange from equilibrium with sulfur, 2) exchange from equilibrium with di-2-benzothiazolyl disulfide; 3) contents of exchangeable sulfur; 4) contents of bound sulfur.

Experiments on isotope exchange of diethylaminomethyl-2-thiobenzothiazole with di-2-benzothiazolyl disulfide were carried out in benzene solution in sealed tubes. After the exchange reaction the solvent was evaporated in the cold (in a stream of nitrogen) and the residue was treated with acetone. Diethylaminomethyl-2-thiobenzothiazole dissolved in acetone, while di-2-benzothiazolyl disulfide remained in the residue. The residue was washed three times with benzene. Di-2-benzothiazolyl disulfide was then oxidized by the Carius method and precipitated by benzidine hydrochloride; the sulfur activity was determined in the precipitate.

TABLE 2

Results of Experiments on Isotope Exchange between the Studied Accelerators and Di-2-Benzothiazolyl Disulfide Tagged with S^{35}

Temperature °C	Time, hour	Activity of di-2-benzothiazolyl disulfide, pulses/min		Exchange, %
		before exchange	after exchange	
Diethylaminomethyl-2-thiobenzothiazole - di-2-benzothiazolyl disulfide				
30°	2,5	12056	11061	13,7
30	18	12056	8523	94
60	2	12056	7858	98
80	2	12056	7898	100
N-Cyclohexyl-2-benzothiazolesulfenamide - di-2-benzothiazolyl disulfide				
30°	18	12056	12348	0
60	2	12056	11851	0
80	2	12056	7835	96
100	2	12056	8557	100

Table 2 contains the results obtained in experiments on isotope exchange between diethylaminomethyl-2-thiobenzothiazole and di-2-benzothiazolyl disulfide, and also between N-cyclohexyl-2-benzothiazolesulfenamide and di-2-benzothiazolyl disulfide.

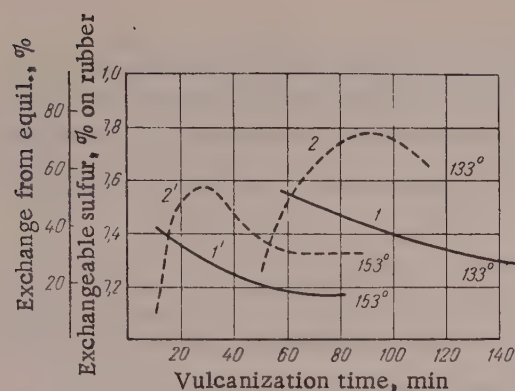
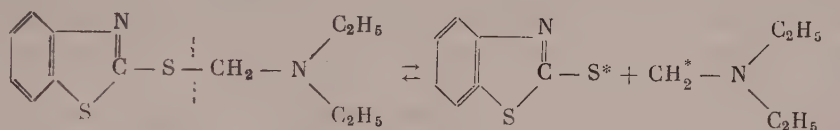


Fig. 7. S^{35} isotope exchange of vulcanizates from SKS-30AM, containing N,N-diethyl-2-benzothiazolesulfenamide: 1 and 1') exchange from equilibrium; 2 and 2') contents of exchangeable sulfur.

vulcanizates with elemental sulfur and with di-2-benzothiazolyl disulfide. The exchange was effected by a method described earlier [7] at 120° during 3 hours; it was found in special experiments that under these conditions the exchange proceeds to equilibrium.



Variations of exchangeability with vulcanization time are plotted in Fig. 6. It should be noted that the relative content of exchangeable sulfur in stocks with BTMA corresponds to its content in stocks with N,N-di-

TABLE 3

Variations of Maximum Swelling of Unfilled Mixes (without sulfur) of Natural Rubber during Heating at 143° (xylene solvent)

Accelerator	Maximum swelling, %							
	Heating time, min							
	70	90	120	150	180	210	240	300
N,N-diethyl-2-benzothiazole-sulfenamide	894	722	671	701	673	694	660	639
Diethylaminomethyl-2-thiobenzothiazole	Unlimited swelling							
N-cyclohexyl-2-benzothiazole-sulfenamide	2190	1512	1527	1504	1488	1442	1450	1410
Cyclohexylaminomethyl-2-thiobenzothiazole	Unlimited swelling							

Table 2 shows that exchange between diethylaminomethyl-2-thiobenzothiazole and di-2-benzothiazolyl disulfide takes place even at room temperature. Exchange between N-cyclohexyl-2-benzothiazolesulfenamide and di-2-benzothiazolyl disulfide begins at higher temperatures (about 60°). These data are in good agreement with the vulcanization kinetics (Figs. 4,5) of stocks with these accelerators. Stocks containing BTMA are characterized by a high vulcanization rate at the initial state, as compared with sulfenamide stocks.

The results of experiments on isotope exchange of BTMA accelerator with di-2-benzothiazolyl disulfide indicate that the BTMA molecule probably decomposes as shown below during vulcanization, and they also confirm the earlier conclusion concerning the structure of the BTMA molecule.

The vulcanization structure of vulcanizates made from SKS-30AM with BTMA accelerator was studied by observations of the kinetics of isotope exchange of these

ethyl-2-benzothiazolesulfenamide (sulfenamide BT) if equal amounts of these accelerators and sulfur are used. The relative change of exchangeability with vulcanization time is less pronounced in stocks with BTMA than in corresponding stocks with sulfenamide BT (Fig. 7). BTMA stocks contain a small amount of benzothiazolyl groups capable of exchanging with di-2-benzothiazolyl disulfide.

In contrast to sulfenamide BT [1], BTMA accelerator does not have an independent vulcanizing effect on rubber (see Table 3).

These results show that sulfenamide accelerators (in absence of sulfur as the vulcanization agent) have an appreciable cross-linking effect. This is indicated by the fact that rubber containing these accelerators acquires the property of limited swelling as the result of heat treatment at the vulcanization temperature. Vulcanization accelerators containing $\begin{array}{c} | \\ -S-C-N- \\ | \quad | \quad | \end{array}$ groups do not produce any appreciable cross-linking effect under such conditions.

SUMMARY

1. A series of condensation products of 2-mercaptobenzothiazole and formaldehyde has been synthesized. Spectrum analysis indicates that these derivatives of 2-mercaptobenzothiazole contain $\begin{array}{c} | \\ -S-C-N- \\ | \quad | \end{array}$ groups.
2. These aminomethyl derivatives of 2-mercaptobenzothiazole are effective vulcanization accelerators for synthetic and natural rubbers.
3. Vulcanization of rubber stocks proceeds at a higher rate at the initial stage in presence of these accelerators than in presence of sulfenamide accelerators.
4. Aminomethyl derivatives of 2-mercaptobenzothiazole enter isotope exchange with di-2-benzothiazolyl disulfide at lower temperatures than do sulfenamide compounds.
5. Aminomethyl derivatives of 2-mercaptobenzothiazole do not have an independent cross-linking (vulcanizing) effect on rubber.

LITERATURE CITED

- [1] B. Dogadkin, M. Fel'dhstein, and D. Pevzner, J. Appl. Chem. 28, No. 5, 533 (1955).*
- [2] M. Fel'dhstein, B. Dogadkin, I. Étingon, G. Shcherbachev, and N. Strel'nikova, J. Appl. Chem. 32, No. 4, 893 (1959).*
- [3] E. N. Gur'yanova, in the book: Vulcanization of Rubbers [in Russian] (Goskhimizdat, 1954) p. 101.
- [4] L. Bellamy, Infrared Spectra of Complex Molecules (IL, Moscow, 1957) p. 414 [Russian translation].
- [5] M. S. Fel'dshtein, I. I. Étingon, D. M. Pevzner, N. P. Strel'nikova, and B. A. Dogadkin, Caoutchouc and Rubber No. 1 (1959).
- [6] E. N. Gur'yanov and V. I. Vasil'eva, Proc. 1st Conference on the Peaceful Uses of Atomic Energy [in Russian] (Acad. Sci. USSR, Div. Chem. Sci. Moscow, 1955).
- [7] B. Dogadkin, Z. Tarasova, and M. Kaplunov, Proc. Acad. Sci. USSR 99, No. 5, 819 (1954).

Received December 23, 1958

* Original Russian pagination. See C.B. Translation.

INFLUENCE OF IONIZING RADIATIONS ON THE DISPERSITY OF AEROSOLS

V. F. Dunsii and N. S. Smirnov

Institute of Combustible Minerals, Academy of Sciences, USSR
Moscow Plant Protection Station

Our investigations [1] have shown that when highly disperse aerosols (ordinary moist air) are exposed to ionizing radiations, the size and concentration of the disperse phase particles are increased, with formation of visible mists.

In this investigation experiments on irradiation by ionizing radiations were performed in a laboratory aerosol unit shown schematically in Fig. 1.

Air passed from the compressor 1 into the cylinder 2, and then through the rheometers 3 into the coil 4 of the electric preheater 5, where it was heated to 400°. The heated air entered the beaker 6 filled with transformer oil. The mixture of heated air and vapor of the mist former passed out through the exit tube (4 mm internal diameter) at a velocity of 40.5 m/second, forming a turbulent stream in which a mist of the high-boiling fraction of transformer oil was produced. The aerosol stream entered a small aerodynamic tube of square cross section (18 × 18 cm), 70 cm long, in which a current of air with a velocity of 2.3 m/second is created by means of the fan 8. The velocity of the aerosol stream differs in different parts of the aerodynamic tube, but by our proposed method [2] it is possible to calculate the average velocity of the aerosol stream (U_{av}) over small ranges of distance (X) from the mist-former tube. The calculated results are given in Table 1.

TABLE 1

Average Velocity U_{av} and Residence Time ($\Delta \tau$) of the Aerosol in the Tube at Various Distances (X) from the Mist-Former Tube

X [cm]	2,5—7,5	12,5—17,5	22,5—27,5	35—45	55—70
U_{av} [cm/sec]	880	391	305	264	243
$\Delta \tau$ [sec]	$5,7 \cdot 10^{-3}$	$12,8 \cdot 10^{-3}$	$16,4 \cdot 10^{-3}$	$38 \cdot 10^{-3}$	$61,7 \cdot 10^{-3}$

Table 1 shows that the velocity of the aerosol stream in the aerodynamic tube varied from 8.8 to 2.4 m/second (average velocity 3.1 m/second). Each element of the aerosol volume remained in the aerodynamic tube for about 0.022 second.

The aerosol was made from a high-boiling ($\geq 320^\circ$) fraction of transformer oil by the condensation method, the hot (400°) mixture of oil vapor and air being mixed with air at 17°. The concentration of the disperse phase in the aerosol stream varied between $0.556 \cdot 10^{-1}$ and $3.328 \cdot 10^{-3}$ g/liter.

In each experiment the aerosol was blown into the aerodynamic tube for 8 minutes. The aerosol particle size was previously determined microscopically; the aerosol consisted mainly of droplets of radius $< 7.5 \cdot 10^{-5}$ cm. The approximate particle concentration of the aerosol in the aerodynamic tube varied between 10^8 and 10^6 per cubic centimeter.

The aerosol stream was irradiated by γ -quanta emitted by radioactive cobalt (Co^{60}). The radiation source was made from cobalt wires ($l = 1.5$ cm, $d = 0.05$ cm) situated at a distance of 0.5 cm from the mist-former tube (see Fig. 2). The total activity of the source was 1.85 microcurie.

Ionization of the air in the aerodynamic tube was calculated by the usual methods, widely used in dosimetric practice [3]. The results are given in Table 2.

TABLE 2

Dose Rate (P), Ionization Rate (q), and Equilibrium Ion Concentrate (c^\pm) at Different Distances (X) from the Source

X [cm]	0,5	5	15	30	70
P (r/sec)	$2,66 \cdot 10^{-2}$	$2,66 \cdot 10^{-4}$	$2,51 \cdot 10^{-5}$	$7,40 \cdot 10^{-6}$	$1,36 \cdot 10^{-6}$
q (i.p./cc.sec)*	$5,53 \cdot 10^7$	$5,53 \cdot 10^5$	$5,22 \cdot 10^4$	$1,5 \cdot 10^4$	$2,82 \cdot 10^3$
c^\pm (i.p./cc)*	$5,87 \cdot 10^6$	$5,90 \cdot 10^5$	$1,81 \cdot 10^5$	$9,84 \cdot 10^4$	$4,21 \cdot 10^4$

*i.p. = ion pairs.

Table 2 shows that ionization of air in the aerodynamic tube was 3-7 orders of magnitude greater than the natural ionization of air (q from 5 to 10 i.p./cc.^{second}, c^\pm from 2 to $5 \cdot 10^2$ i.p./cc).*

Changes in the disperse phase of the aerosol were observed by two methods. The usual method was used for the particles in the microscopic range. A glass slide 9 (Fig. 1) was placed at the tube outlet for sedimentation of particles from the stream of oil mist. After the experiment the slide was examined under the microscope at magnifications of $\times 120$ and $\times 600$, and the settled droplets were measured and counted.

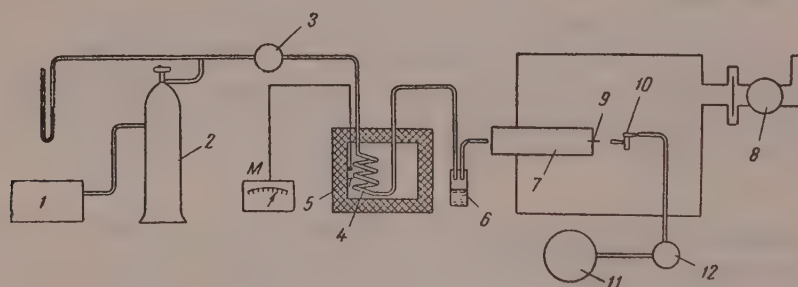


Fig. 1. Apparatus for formation of oil mists.

For observation of the fine aerosol fractions ($r < 7.5 \cdot 10^{-5}$ cm) a filter 10 of the cascade impactor type [4] was placed in the stream (Fig. 1). The aerosol was drawn through the cascade impactor and the rheometer 12 by means of the vacuum pump 11; all the coarse particles were retained on the plates of the first impactor stages, while the finer particles ($r < 7.5 \cdot 10^{-5}$ cm) were partially retained by a cotton-wool filter placed beyond the first stages. The weight of particles of this fraction retained by the filter was calculated per unit aerosol volume from the weight increase of the filter and the volume of aerosol which passed through the filter.**

The two methods did not give a complete characterization of all the disperse phase of the aerosol. However, they give an indication of changes in the dispersity of the mist and of filtration efficiency.

* The total radiation dose in 8 hours at 70 cm from the source is 0.039 r, which is below the permissible limit (0.050 r). At a distance of 1 m this dose is 0.019 r, which is just over one third of the permissible dose.

** In all experiments part of the fine fraction passed through the cotton-wool filter and entered the atmosphere. An oil mist was always visible at the outlet of the vacuum pump.

We have shown [5, 6] that aerosol particles formed by the condensation method are not electrically charged and can acquire charges only as the result of natural ionization of the air. The charging time of an aerosol under natural conditions was determined by the following experiments. A mist consisting of the principal component of technical oils (oleic acid) was produced by the condensation method in an aerosol chamber ($V = 1 \text{ m}^3$). The particle concentration of the aerosol was $\sim 10^6$ particles/cc, and the particle size was from $2.5 \cdot 10^{-5}$ to $7.5 \cdot 10^{-5}$ cm. After the aerosol had been mixed, samples were taken and variations of the contents of charged particles with time of existence of the mist were determined. The number of charged droplets was determined by the horizontal electric field method [7]. The results of the determinations are presented in Fig. 3, where the ordinates represent the total numbers of positive and negative particles as percentages of the total numbers of particles counted in the aerosol samples (from 400 to 200 particles in each sample).

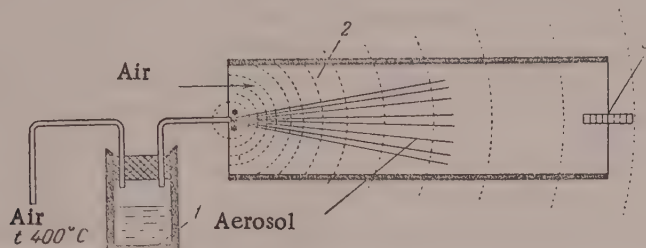


Fig. 2. Irradiation of aerosol stream by Co^{60} γ -quanta: 1) beaker; 2) aerodynamic tube; 3) glass slide; *) sources of γ -radiation.

It is known that natural ionization of air is determined by the ionization rate (q), and concentrations of small ions ($c \pm$) and medium and large ions ($N \pm$). The content of medium and large ions ($N \pm$) varies over a wide range and depends on the purity of the air. To determine the influence of air purity on the charging time of aerosols, freshly-prepared mist containing 10^4 - 10^5 particles/cc was introduced into the aerosol chamber ($V = 20$ liters). One series of experiments was carried out with ordinary unpurified air, and the others in the chamber containing previously -purified air. The results of these experiments are plotted in Fig. 4.

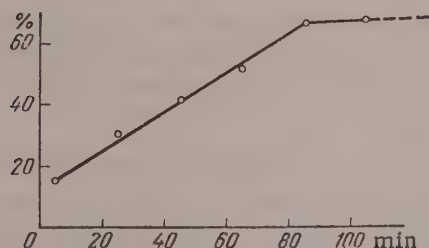


Fig. 3. Variation of relative contents of charged particles in oleic acid mist (%) with the age of the aerosol (minutes).

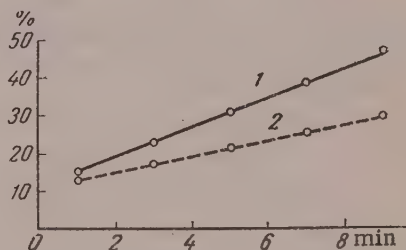


Fig. 4. Time variation of the relative contents (%) of charged particles in oleic acid mist: 1) unpurified air; 2) air previously purified.

It is clear from Figs. 3 and 4 that aerosol particles obtained by the condensation method are almost all uncharged (not more than 10% are charged); under natural ionization conditions the aerosol particles become charged slowly, especially in pure air.

Changes in the dispersity of microscopic droplets of a mist formed from a high-boiling ($\geq 320^\circ$) fraction of transformer oil after irradiation of the aerosol by Co^{60} γ -quanta can be expected in terms of the numbers of droplets precipitated per 1 cm^2 surface area. The results of such analyses are presented in Table 3.

Table 3 shows that irradiation of the mist stream by Co^{60} γ -quanta produces a coarse fraction ($r > 2 \mu$) which was not present in the aerosol before irradiation.

Changes in the amounts of ultramicroscopic and submicroscopic particles retained by the cotton-wool filter are presented in Table 4.

Table 4 shows that after irradiation of a stream of transformer-oil mist with Co^{60} γ -quanta the number of particles retained by the filter from the mist increases by $\sim 40\%$.

TABLE 3

Dispersity Changes of Microscopic Fractions as the Result of Irradiation of the Aerosol by Co^{60} γ -quanta *

Conditions	Number of particles deposited per cm^2 , with radii	
	$< 2 \mu$	$> 2 \mu$
Without irradiation**	$3.40 \cdot 10^6$	—
	$2.52 \cdot 10^6$	—
With irradiation	$1.15 \cdot 10^6$	$1.49 \cdot 10^8$
	$2.51 \cdot 10^6$	$0.63 \cdot 10^8$

* For greater clarity the particles are divided into two fractions with radii $< 2 \mu$ and $> 2 \mu$ respectively.

** More than 12 experiments were performed without irradiation and in none were any particles found with radius greater than 2μ .

TABLE 4

Change in the Amount of Aerosol Retained by the Filter as the Result of Irradiation by γ -quanta

Conditions	Amount of aerosol drawn through filter, g	Weight of aerosol retained by filter, g	Weight of retained particles per liter of aerosol filtered, g
Without irradiation	241	0.4206	$1.74 \cdot 10^{-3}$
	267	0.3740	$1.40 \cdot 10^{-3}$
With irradiation	238	0.5707	$2.39 \cdot 10^{-3}$
	262	0.5340	$2.04 \cdot 10^{-3}$

air mixture favors formation of ready condensation centers, and therefore condensation of the vapors of the components of technical oil at the instant of mixing of the vapor-air mixture with cold (also strongly ionized) air occurs preferentially on these centers. This may lead to increase in the size of the primary aerosol particles, as in aerosols formed without irradiation, primary particles arise on an enormous number of spontaneously formed condensation centers.

* Under laboratory conditions almost monodisperse aerosols are sometimes obtained with great difficulty.

The rapid processes which take place in practical production of aerosols by the condensation method are complex and have not been studied sufficiently. These processes probably take place as follows: 1) aerosol particles arise spontaneously owing to the enormous supersaturation of the vapors of the numerous chemical compounds present in technical oil; 2) droplets are formed on particles of different sizes, always present in ordinary air; 3) simultaneously with the formation of primary particles secondary particles are formed as the result of rapid coagulation of the primary ones, especially at the initial stages, when the concentration of primary particles reaches from 10^{10} to 10^9 per cc; 4) vapor distills continuously from the small to the large droplets. All these processes lead to the formation of a polydisperse mist; monodisperse aerosol systems do not exist in nature or in technical practice.*

Irradiation of a mist stream by ionizing radiations during formation and during the first instants of its existence complicates the above processes still further. However, ionizing radiations in general tend to increase the particle size in irradiated aerosols, for the following reasons.

1. When a vapor-air mixture is irradiated, even before it has left the outlet tube of the aerosol generator, high concentrations arise of ionized molecules and atoms of all the constituents of ordinary air and the vapors of the complex organic substances contained in technical oils.

High temperatures of the vapor-air mixture ($\sim 400^\circ$) and high radiation intensities at short distances (0.5 cm) from the source probably favor formation of ions bearing several unit charges.

2. In a very short time (10^{-6} seconds [8]) the elementary ions formed are converted into molecular complexes. Thus, irradiation of a hot-vapor-

3. The uncharged small droplets formed ($r = 10^{-7} - 10^{-6}$ cm), on becoming electrically charged, grow rapidly in size owing to condensational and coagulational growth of charged droplets. Usually uncharged droplets of this size become smaller as the result of evaporation as soon as they leave the narrow zone of enormous supersaturations.

It is well known from the theory of bipolar diffusional charging of aerosol particles [9] that the rate of charging of aerosol particles increases with decreasing particle size and concentration; it rises sharply with increasing ionization of the air. For example, at $q = 10^5$ i.p./cc · second, aerosols of concentration $N \leq 10^6$ particles/cc of $r = 10^{-4} - 10^{-6}$ cm reach a steady state of charge distribution in 10^4 to 10 seconds, according to the particle size and concentration. The same aerosols at $q = 10^7$ i.p./cc · second reach a steady state of charge distribution in time $\tau \leq 1$ second.

Consequently, in our experiments on irradiation of mist streams by γ -quanta the ionization rates q were from $5 \cdot 10^7$ to $3 \cdot 10^8$ i.p./cc · second; these mists in all probability contained more charged particles, by several orders of magnitude, than the same aerosols obtained under natural ionization conditions at q from 2 to 5 i.p./cc · second, as under our conditions of artificial ionization even the time required to reach equilibrium distribution of charges is less than one second.

SUMMARY

1. Mists obtained by the condensation method become charged very slowly under natural conditions of air ionization.
2. Irradiation of a stream of condensation mist by Co^{60} γ -quanta reduces the dispersity of its microscopic fractions, and the weight of finer particles ($r < 7.5 \cdot 10^{-5}$ cm) retained by the filter increases by 40-45%.
3. These results confirm our earlier experimental data concerning the influence of air ionization on the disperse phase of highly disperse aerosols.

LITERATURE CITED

- [1] K. M. Merzhanov, N. I. Peterimova, and N. S. Smirnov, Colloid J. 18, No. 5, 574 (1956)*; I. I. Belyaeva, A. E. Mikirov, and N. S. Smirnov, Colloid J. 19, No. 1, 24 (1957)*.
- [2] V. F. Dunsii, J. Tech. Phys. 25, 14, 2510-1 (1955).
- [3] V. Bochkarev, Keprim-Markus, M. L'vova, and Ya. Pruslin, Measurement of the Activity of β - and γ -Radiations [in Russian] (Izd. AN SSSR, Moscow, 1953).
- [4] V. F. Dunsii, Z. M. Yuzhnyi, and D. N. Khokhlov, Industrial Lab. No. 5, 575 (1955).
- [5] N. S. Smirnov, Colloid J. 10, No. 6, 448 (1948).
- [6] N. S. Smirnov, Proc. Acad. Sci. USSR 58, No. 7, 1357 (1947).
- [7] N. A. Fuks and I. V. Petryanov, J. Phys. Chem. 4, No. 5, 567 (1933).
- [8] L. Loeb, Fundamental Processes of Electrical Discharge in Gases (State Press, 1950) [Russian translation].
- [9] N. A. Fuks, Bull. Acad. Sci. USSR, Geogr.-Geophys. Ser. (1947).
- [10] P. V. Lisovskii, J. Phys. Chem. 14, 521 (1940).

Received February 5, 1958

* Original Russian pagination. See C.B. Translation.

INTERACTION OF CALCIUM HYDROXIDE AT ORDINARY TEMPERATURE WITH SAND OF DIFFERENT DISPERSITIES

G. I. Logginov, P. A. Rebinder, and V. F. Abrosenkova

Institute of Physical Chemistry, Academy of Sciences USSR, Moscow

The reaction between calcium hydroxide in aqueous solution and crystalline silica proceeds extremely slowly at room temperature. However, if the interaction continues for long enough the layer of new substance formed becomes sufficiently thick to be detected by means of x-ray structural analysis [1]. The appearance of a line characteristic of calcium monohydrosilicate, corresponding to an interplanar spacing of 3.01 Å, was observed by us in x-ray patterns for lime-sand blocks with sand of an average dispersity of 0.4 m²/g after two years of storage [2]. With the use of finer sand, ground down to a specific surface of 7 m²/g, the formation of calcium hydrosilicate was observed by Sominskii et al. [3] by x-ray analysis after only 7 days of storage of lime-sand blocks under moist conditions. In practice, the formation of hydrosilicate structures in such products as silicate bricks, beams, tiles, etc. is accelerated by hydrothermal treatment. The reaction between lime and sand under these conditions has been studied [4] sufficiently well to provide a basis for modern technological processes [5].

Our work on the physicochemical principles of wall-block production technology [6] shows that hydration hardening of the lime-sand mortar [7] is accompanied by the gradual development of a process in which calcium hydroxide is combined, with formation of a crystallizational calcium hydrosilicate structure at the surface of the sand grains [8].

The reaction between calcium hydroxide and sand was studied by means of the radioactive Ca⁴⁵ isotope, used in the form of Ca*(OH)₂. The kinetics of lime binding was studied by chemical determination of free lime. The material used was sand of Vol'sk origin, of different degrees of dispersity (specific surface S₁); in its natural state with S₁ = 0.11 m²/g, and ground down to S₁ of 0.62, 0.95, 2.6 and 5.4 m²/g.

In development of the determination techniques, measures were taken to restrict access of carbon dioxide and to account for the amount of lime combined as calcium carbonate. This correction did not exceed 5% of the total bound lime. In our experiments a sand sample varying in weight according to its fineness and reaction time (from 10 to 0.5 g) was placed in a 30 cc test tube. 20 cc of tagged Ca*(OH)₂ solution, filtered to remove any precipitate, the concentration of which was close to saturation was added into the test tube.

The experiments were performed at t° = 17° ± 1° with repeated shaking of the test tubes. During the first 24 hours the tubes were shaken vigorously 4-5 times, and subsequently once every 24 hours. It was found that because of the length of the experiments, which were continued for 6 months, the intensity and duration of the shaking had no practical effects on the results.

In these experiments the ratio of solid to liquid phase - sand to saturated solution of tagged calcium hydroxide - was between 0.02 to 0.8 in accordance with the interaction time and the fineness of the sand. Samples were taken after 7 days and 1, 2, 3, and 6 months, and the activity of the solution was determined in order to calculate the amount of calcium ions bound. In parallel experiments the kinetics of binding of lime from aqueous Ca(OH)₂ solutions by sand was studied by the usual chemical method. The solid-liquid ratio, sampling intervals, shaking of the tubes, their storage and thermostatic control, and corrections for carbonation were the same as in experiments with the tagged solution.

The amounts of bound lime were determined by titration of samples of the $\text{Ca}(\text{OH})_2$ solution with 0.01 N hydrochloric acid in presence of phenolphthalein. The amounts were found from the difference between the CaO contents of the original solution and the solutions sampled. The two methods gave results in good agreement.

The average results were used for plotting curves representing the kinetics of binding of lime by sand of different degrees of dispersity; these are shown in Fig. 1. Regardless of the fineness of the sand, the binding process always consists of two stages: chemisorptive, which is complete within 1 hour from the start, and very prolonged chemical binding of calcium hydroxide, which proceeds at a constant rate.

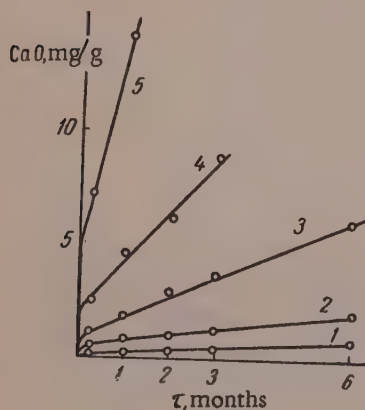


Fig. 1. Kinetics of binding of calcium ions from saturated aqueous $\text{Ca}(\text{OH})_2$ solution by sand with specific surface $S(\text{m}^2/\text{g})$: 1) 0.11 (not ground); 2) 0.62; 3) 0.95; 4) 2.6; 5) 5.4.

"Linearity", when the binding rate falls to a constant (steady) minimum value, is reached after 1 hour. Subsequently the steady rate of binding of lime by the given portion of sand remains constant for 6 months, and probably longer, and therefore it is independent of the lime concentration in solution over a fairly wide range. This was also confirmed by special experiments with lime solutions of initial concentrations from 1.2 to 0.3 g CaO/ liter.

The establishment of a constant rate of lime binding over a long period is evidently the result of calcium hydrosilicate formation - a process which takes place in solution by recrystallization of the new phase from the forming supersaturated solution [9].

According to K. G. Krasil'nikov, this process should evidently culminate in complete binding of the lime in the form of hydrosilicate, which corresponds to a residual concentration of ~ 0.006 g/ liter, i.e., hydrolytic equilibrium of calcium silicate in solution [10]. In concentrated suspensions this process leads to the development of a crystallization structure [11] of hydrosilicate hardening, as is the case in our experiments with compact specimens (blocks) of lime-sand mortar.

At the first stage of binding the principal process, which determines the initial highest binding rate, is chemisorptive formation of a thin layer of a surface chemical compound, calcium hydrosilicate, on the surface of the sand grains.

The amount of adsorbed calcium hydroxide (m_0/M , mg CaO per g sand) was determined at the end of the first hour, after the stirred suspension could be filtered easily. The value of m_0/M increases in proportion to the value of S_1 . The values found for m_0/M almost coincide with the intercepts cut off along the ordinate axis by the continuations of the linear regions of the kinetic curves for lime binding (Fig. 1).

The specific surface of fine sand was determined by the low-temperature adsorption method, and the area occupied by a nominal CaO molecule was calculated from the average values for each degree of dispersity (Table 1). The average value of this area.

$$S_0 = \frac{S_1 \mu \cdot 10^3}{(m_0/M) N},$$

where μ is the molecular weight of lime (CaO) and N is the Avogadro number, was $10.2 \text{ \AA}^2 (\pm 2.5\%)$. The average value of S_0 and the value for the sorption of lime were used to calculate S_1 for coarse sand, as this is almost impossible to determine by the nitrogen-adsorption method.

In addition, lime is bound by silicic acid which has passed into solution through the forming hydrosilicate film. The highest possible concentration of silicic acid in solution is determined by the maximum supersaturation of calcium hydrosilicate under the given conditions, and is always very low because of the low solubility of hydrosilicate. All the silicic acid passing into solution in excess of this binds lime in the form of solid calcium hydrosilicate which is deposited in a finely divided state from solution. The free lime

concentration in our solutions always corresponds to a large excess over the concentrations corresponding to the maximum supersaturations of calcium hydrosilicate in solution. Eventually, in addition to diffusion of silica from the surface of the sand grains into the solution, the film itself is dissolved and peptized by the solution, i.e., it undergoes colloidal dissolution (chemical dispersion). As the result of all these complex processes, which lead to the formation of supersaturated calcium hydrosilicate solutions in the medium surrounding the sand grains, a maximum thickness of the hydrosilicate film becomes established on the grains, and this subsequently remains unchanged. The steady rate of lime binding from solution, determined by us for different initial grain sizes of sand ground in a vibratory mill, is no longer proportional to the specific surface of the sand (as at the initial stage), but rises more steeply with S_1 in accordance with a semicubic parabolic law (Fig. 2).

$$\left(\frac{dm}{d\tau}\right)_m \frac{1}{M} = a S_1^{\frac{3}{2}}.$$

This is consistent with the determining role of the rate of dissolution of the sand grains, which should evidently increase with increasing solubility of the smaller particles (in accordance with the Kelvin law), and

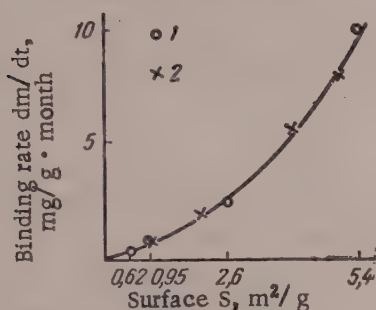


Fig. 2. Effect of specific surface of sand on the binding rate of calcium oxide: 1) experimental data; 2) calculated by formula.

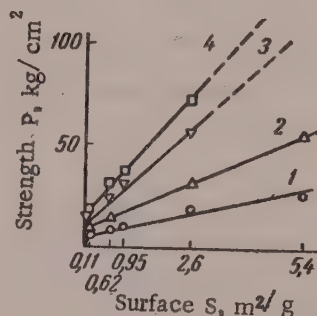


Fig. 3. Strength of 20 mm cubes containing 1 wt. part of calcium oxide to 4 wt. parts of sand as a function of specific surface, after storage times of: 1) 7 days; 2) 1 month; 3) 3 months; 4) 6 months.

with increasing imperfection (amorphousness) of the structure of the surface layer of quartz as the result of fine grinding, as was demonstrated by Khodakov [12].

We had shown earlier [13] that binding of $\text{Ca}(\text{OH})_2$ by sand is the direct cause of the prolonged increase in the strength and stability of lime-sand products made by hydration hardening of lime (without hydrothermal treatment). The quantitative relationship between the increase of mechanical strength and the specific surface

TABLE 1

Determination of the Area Occupied by a CaO Molecule Adsorbed on Sand

$S_1, \text{m}^2/\text{g}$	0.90	2.60	5.30
$m_0/M, \text{kg/g}$	0.80	2.40	4.92
$m_0/MS_1, \text{mg/m}^2$	0.90	0.92	0.90
$S_0, \text{\AA}^2$	10.35	10.14	10.14

TABLE 2

Comparative Data for Structural Strength Due to Hydration Hardening

Method	Strength, kg/cm at age			
	7 days	1 mo	3 mo	6 mo
Calculated	5.5	9.0	11.5	16.0
Experimental	3.3	7.0	12.1	—

of the sand was established experimentally. For these experiments 20 mm cubes containing 1 part by weight of quicklime to 4 parts by weight of ground sand were made, with sands of the different specific surfaces in question. The amount of water was chosen so that the plasticity of the mix was the same in each case. Before the

strength tests the specimens were kept in desiccators without access of carbon dioxide. The specimens were tested for compressive strength and the results were used to plot $p = f(S)$ curves (Fig. 3), showing the strength against the dispersity of the sand.

At each age the specimen strength increased rapidly with increase of the dispersity of the sand. Thus, by a 50-fold increase of the specific surface over the value for unground sand, the strength can be increased 7 to 8-fold.

The strength increase is caused by two forms of hardening — of the hydration and the hydrosilicate types. If the linear portions of the $p = f(S)$ curves in Fig. 3 are continued to their intersection with the ordinate axis, then the intercepts on the ordinate axis must evidently represent the numerical values of strength caused by hydration hardening, while the linear section of each curve represents the strength due to hydrosilicate hardening. The strength due to hydration hardening continues to increase for at least 6 months. This is explained by the influence of surface-active additives (sulfite alcohol liquor) which retard hydration hardening, and particularly by the lengthy recrystallization of the new substances formed.

To verify this hypothesis, cubes of the same size were made with quicklime containing an inert filler — chemically pure calcium carbonate — instead of sand. Results obtained in strength tests of these cubes are compared in Table 2 with the numerical values of the strength found from the ordinate intercepts.

Analysis of these results reveals a linear relationship between the structural strength due to hydrosilicate hardening and the dispersity of the sand, in the form of the equation

$$P = P_0 + pS,$$

where P is the total strength; P_0 is the structural strength due to hydration hardening; p is the "specific" strength due to hydrosilicate hardening, calculated per 1 m^2 of specific surface of the sand.

Thus, if the specific surface of the disperse phase (sand) is sufficiently large, it is possible in practice to produce products of predetermined strength from local materials without the use of cement. The adopted technological procedure [14] was used for production of hollow (slotted) blocks $390 \times 190 \times 190 \text{ mm}$, with different proportions of quicklime and sand. In all cases the mixing water contained plastifying retarders of hydration hardening, which also gave rise to a structure of greater stability to external influences.

Selected results of strength tests on these blocks, given in Table 3, give an idea of the extent of the slow strength increase.

TABLE 3

Compressive Strength of Hollow Lime-Sand Blocks Stored in Air

Mix composition, %				Strength, kg/cm ² , at age					
binder		unground sand	mixing water	7 days	1 mo	3 mo	6 mo	1 yr	2 yrs
quick-lime	ground sand								
12.5	12.5	75	7.5*	20	28	—	—	49	—
10	10	80	8.0**	12	20	28	36	—	48

* Coarse sand.

** Medium-grained sand.

The data in Table 3 are based on average values for many batches of blocks made in the No. 3 production unit of the All-Union Scientific Research Institute of Fine Grinding of New Constructional Materials [15]. All the batches showed a continuous increase of strength during air hardening, up to fourfold after 2 years.

A weak point in the technological process for production of cement-free blocks based on quicklime without subsequent hydrothermal treatment, is the low initial strength of the products, so that the blocks cannot be transported by the usual methods (in bulk).

To increase the initial strength of the blocks under the adopted production procedure it is necessary to activate the sand filler and to improve the mixing of the components. Both these aims can be achieved simultaneously if all the material is passed through a vibratory mill placed in the grinding unit before the mixer.

The above conclusion is confirmed by the results of investigations of activation of sand filler and improvement of mixing. For these experiments 70 mm cubes were made from quicklime and sand in different proportions by weight, and ground together in an M-10 laboratory mill to a specific surface of $1.2 \text{ m}^2/\text{g}$, corresponding to about 1% residue on a sieve with 10,000 holes per cm^2 . The ratio of binder to unground sand filler (medium-grained) was 1:3. As always, to retard hydration and to improve the properties of the product, 5% of calcium sulfate dihydrate was added (by weight) to the lime during grinding, and 0.3% of sulfite waste liquor, calculated as dry solids, (also on the weight of lime), was added to the mixing water.

One batch of blocks was made by the usual standard method, while for the other batch the binder and sand were mixed by passage through a vibratory mill for 1 minute. The mixing with water and molding were the same for both batches. During the first 24 hours the strength of the blocks made with activated sand was greater, in accordance with the data in Table 4, by 66%, and at subsequent ages (except at 6 months) it was double.

TABLE 4

Compressive Strength of 70 mm Cubes Made with Sand-Lime (1:1) Binder, with 1:3 Binder-Sand Ratio (aging in air; activity of lime 56%)

Filler - medium-grained sand	W/L*	Strength, kg/cm ² , at age				
		7 days	1 mo	2 mo	3 mo	6 mo
Not activated	0.75	25	31	36	39	73
Activated	0.90	34	62	89	92	108

*W/L = water-lime ratio.

In addition to the above-named factors - activation and improved mixing - the strength increase was influenced by increased fineness of the mix when passed through a vibratory mill. This increased the specific surface, determined by sorption of tagged Ca^{45} , from 1.2 to $1.3 \text{ m}^2/\text{g}$. There is also a distinct difference between the structures of activated and nonactivated specimens: specimens made from activated material are characterized by a more uniform and finer structure.

SUMMARY

1. A method was developed for investigation of binding of the calcium hydroxide by crystalline silica in an aqueous medium, with the aid of the Ca^{45} isotope and by determination of the effective specific surface of sand from chemisorption data for the same isotope. This method can be used for determinations of specific surface of sands of any degree of dispersity, whereas the method of low-temperature adsorption of nitrogen can be used only with highly disperse sands (specific surface greater than $1 \text{ m}^2/\text{g}$).

2. The rate of volume binding of lime remains constant with time for sand of given dispersity, and is independent of the residual lime concentration in solution. The relationship between the rate of binding of lime and the dispersity of the sand is represented by a semicubic parabolic equation.

3. The interaction of lime with sand occurs by way of the supersaturated solution, and its rate increases with degree of supersaturation.

4. The structural strength can be increased by 50% and over if the sand is activated by passage of the lime-sand mix through a vibratory mill.

5. Elucidation of the mechanism of lime binding opens up new technological possibilities for increasing the strength of lime-sand products by addition of substances which increase the rate of solution of silica in the aqueous medium.

LITERATURE CITED

- [1] R. H. Bogue, *Mag. of Concrete Res.*, No. 14, 90 (1953); H. F. Mc Murdie and E. P. Flint, *J. Res. Nat. Bur. Standards* 31, 225; 1943.
- [2] V. F. Abrosenkov, G. I. Logginov, and P. A. Rebinder, *Proc. Acad. Sci. USSR* 115, No. 3 (1957).*
- [3] D. S. Sominskii, G. G. Kornienko, and G. S. Khodakov, *Sci. Communication of the All-Union Sci. Res. Inst. Fine Grinding of Constr. Materials* No. 28, (1957).
- [4] Yu. M. Butt, and L. I. Rashkovich, *Col. Trans. Republican Sci. Res. Inst. of Local Constr. Materials RSFSR* No. 10 (1956).
- [5] P. P. Budnikov and L. G. Gulinova, *Colloid J.* 3, 195 (1937).
- [6] G. I. Logginov, N. E. Levina, and V. A. Abrosenkova, *Inf. Communication of the All-Union Sci. Res. Inst. of Fine Grinding of Constr. Materials* No. 6 (1956).
- [7] G. I. Logginov, P. A. Rebinder, and V. P. Sukhova, *Proc. Acad. Sci. USSR* 99, No. 4 (1954).
- [8] G. I. Logginov, *J. Acad. Sci. USSR*, No. 7 (1954).
- [9] E. E. Segalova and P. A. Rebinder, *Summaries of Papers at the 4th All-Union Conference on Colloid Chemistry [in Russian]* (1958) p. 130.
- [10] E. N. Segalova, V. N. Izmailova, and P. A. Rebinder, *Proc. Acad. Sci. USSR* 114, 3 (1957).*
- [11] K. G. Krasil'nikov, *Proc. Conference on Cement Chemistry [in Russian]* (Industrial Construction Press, 1956).
- [12] G. S. Khodakov, *Proc. Acad. Sci. USSR* 123, No. 4 (1958).*
- [13] G. I. Logginov, *Proc. Conference on the Use of Vibratory Grinding in the Building Materials Industry [in Russian]* (Industrial Construction Press, 1957).
- [14] Z. G. Gil'denberg, K. S. Zatsepin, G. I. Logginov, S. A. Krzheminskii, and L. V. Gurevich, *Registration Certificate* No. 9484 (1958).
- [15] S. G. Simonyan, *Vibratory Mills and their Industrial Uses [in Russian]* (Ministry of the Building Materials Industry USSR, 1956).

Received November 15, 1958

* See C.B. Translation.

CRYSTALLIZATION OF SUPERCOOLED ORGANIC LIQUIDS ON PARTICLES OF IMPURITIES AT VARIOUS TEMPERATURES

G. L. Mikhnevich

Odessa State University, Chair of Molecular Physics

Supercooled melted metals are characterized by a spontaneous mechanism of crystal "nucleus" formation from the liquid phase [1]. The organic compounds include a group (of which orthochlorobenzene is a representative) in which nucleation proceeds analogously [2].

However, the spontaneous-process theory does not make it possible to calculate the activation energy U and the interfacial energy σ in the equation for the nucleation probability I :

$$I = Ce^{-\frac{U}{RT} - \frac{A}{kT(\Delta T)^2}}, \quad (1)$$

where A is expressed in terms of the molecular weight M , the density ρ of the nucleus, the heat of fusion q , the melting point T_0 , and the surface energy σ ; k is the Boltzmann constant; R is the gas constant

$$A = \kappa \frac{M^2 T_0^2 \sigma^3}{q^2 \rho^2}, \quad (2)$$

where κ is the shape factor of a crystal nucleus of the critical size (crystallization center). Therefore, approximation of the experimental curve reduces to empirical selection of values of C , U , and σ from a comparison of the experimental data with the values calculated from Equation (1).

The organic compounds include a group of slowly crystallizing substances, classified by Tammann as Group IV, for which complete plots of the number of crystallization centers as a function of temperature can be determined [3]. Typical representatives of this group are piperine (an alkaloid related to piperic acid) and betol (β -naphthyl salicylate) [3,4]. This group is also included with the spontaneously crystallizing substances [2]. Some measure of agreement has been obtained for substances of the group between experimental data and calculated values based on the fluctuation theory, but only at the cost of a number of simplifying assumptions, among which is independence of C , U , and σ of the temperature. However, although for liquid metals the activation energy U may be regarded as constant [5], in the case of organic liquids such an assumption is at variance with results of determinations of viscosity, electrical conductivity, and relaxation time over wide ranges of supercooling [6, 7].

Although better agreement was obtained in our calculations for betol when the dependence of U and σ on temperature was taken into account, the theoretical curve was still flatter than the experimental [8]. In these calculations an attempt was also made to take into account the influence of development of the crystallization nuclei, which during the exposure time at constant temperature had not yet grown to dimensions visible under the microscope. To develop crystallization centers, the specimen is heated rapidly to a temperature at which the probability of formation of new centers is extremely low, while the growth rate of centers already formed is high.

The unsatisfactory results of the above-mentioned correlation and studies of the formation of crystallization centers over long periods of time at constant temperature [9] led to the conclusion that in the case of betol, piperine, and other substances of Tammann's group IV nucleation takes place on particles of active impurities which have not been removed during purification. In the present paper an attempt is made to interpret the experimental relationship between nucleation and temperature in the light of the kinetic laws derived in the previous investigations [9, 10].

The experiments were performed as follows. The specimen was either in a sealed tube or consisted of a drop of melt between two cover glasses, wetting both glasses. Preliminary purification of the substance by repeated crystallization from alcohol and filtration through a No. 4 glass filter did not completely remove all the solid impurity particles. Each prepared specimen was generally tested for reproducibility; it was taken through the whole cycle of operations under the same conditions. The number of crystallization centers decreased to a certain limiting value in the process. This means that some of the impurity particles became deactivated during repeated melting, which was always carried out at a temperature 5-10° above the melting point. The most stable particles remained in the specimen. The size distribution of these particles is characterized by the function $\psi(r)$.

The crystallized specimen, previously tested for reproducibility, was placed in a thermostat for fusion, and then transferred into another thermostat for exposure at temperature t_e^0 for time τ_e (usually 2-10 minutes). The specimen was then placed for 2-4 minutes in a bath at the development temperature t_p^0 . To count the number of grains which had grown to visible size, the specimen was usually cooled in order to diminish their subsequent growth rate. This cycle was repeated at different exposure temperatures. The exposure time τ_e , the temperature t_p^0 , and the development time τ_p were constant for all temperatures t_e^0 .

The resultant relationships between the number of crystal grains in unit volume of melt, per unit exposure time, and the absolute temperature of exposure are represented by curves known as Tammann curves. Tammann's own first experiments, performed with 5° intervals, revealed only single maxima on these curves [4]. Later, more thorough observations showed the existence of two adjacent maxima, first in the case of piperine [11], then in the case of betol and later for other substances [12]. The additional maximum, corresponding to a lower temperature, arises as the result of the influence of the glass surface in a thin wall layer ~0.05 mm thick [13]. Here the crystallization is slower than in the remaining volume [14]. The melt in this layer is considered to have a certain oriented structure of anomalously high viscosity as compared with the viscosity of the liquid outside this layer. Thus the experimental curve is formed by superposition of two curves: one relates to crystallization centers which arise in the two wall layers, and the other to centers formed beyond the range of influence of the glass surface.

It is significant for the subsequent discussion that the descending high-temperature branch of the resultant curve (Fig. 1, Region EKL) is the consequence of volume processes, while the low-temperature branch (Fig. 1, Region ABC) is determined by processes in surface layers. We have shown [9] that at high temperatures the kinetic process has a fluctuation mechanism, whereas at low temperatures the nuclei, initially of size $r > r_k$ (where r_k is the critical size) merely grow as "ready" crystallization centers; at moderate temperatures all particles of size $r > r_k$ are expended first, after which all particles of $r < r_k$ are converted into crystallization centers as the result of fluctuations. Since the temperature curve covers a wide range of temperatures, we assume that all three processes occur at different regions in it.

We now attempt to define more precisely the positions of these three regions by dividing the whole curve into three regions of supercooling. Region I in Fig. 1 contains the portion AB of the low-temperature region ABC, and terminates at the point of inflection B. Region III consists of the section KL of the high-temperature region EKL, and commences at the point of inflection K. Finally, Region II includes the whole region of the maxima, from the point of inflection B to the other point of inflection K. In studies of crystallization centers in all three regions it is necessary to perform "development" at t_p^0 , above the temperature of all these regions. At development temperature t_p^0 all the "nuclei," at any stages of supersaturation represented by the curve ABCDEKL, are smaller than the critical size $(r_k)_p$, corresponding to the temperature t_p^0 . Therefore, their conversion into crystallization centers should take place at this temperature as the result of fluctuations. At high temperatures the kinetics of formation of crystallization centers conforms to a first-order reaction equation [10]

$$n = n_{\infty} (1 - e^{-\alpha_p t}), \quad (3)$$

where α depends on the temperature. In this instance it corresponds to the temperature t_p^0 and we denote it as α_p .

The development time τ_p and the exposure time τ_e in all the experiments performed by the Tammann method were short (for betol $\tau_e \sim 4$ minutes, for piperine, ~ 10 minutes) in relation to the time required for complete exhaustion of all the active impurities (~ 1 hour). Therefore it may be assumed that the integral number of crystallization grains found experimentally refers only to the initial stage of the process, represented by Equation (3).

For these short development times τ_p we can confine ourselves to the first two terms in the resolution of Equation (3) into series:

$$n = n_{\infty} \alpha_p \tau_p. \quad (4)$$

We consider all three regions in detail.

Region I. According to our assumption, in this temperature range all the nuclei are of a size conforming to the condition

$$r > (r_k)_e(r_0, r_m).$$

The initial distribution function is the same for all temperatures in the region: during the exposure time τ_e it is merely shifted into the direction of large r and becomes the function

$\psi(r + \Delta r)$, where Δr is determined by the rate of growth

$$\Delta r = C_0 \tau_e. \quad (5)$$

In "development," the probability that the critical size $(r_k)_p$ is reached increases as the size of the largest nucleus r_m and those following it approach the critical size $(r_k)_p$. The extent of this approach is determined by the magnitude of Δr in Equation (5), and since the experimental value of τ_e was the same for all temperatures it is determined by the dependence of the rate C_0 on the temperature.

In Region I the factor $\left[-\frac{A}{kT(\Delta T)^3} \right]$ in Equation (1), which includes the work of formation of three-dimensional crystallization nuclei, is meaningless and should be disregarded, as will be shown below.

The dependence of the number of observed crystallization grains on temperature is determined by the temperature dependence of the growth rate C_0 . Let us assume that this latter dependence is determined by the activation energy U_2 , if it is expressed in terms of one of the equations of the fluctuation theory, either the Volmer equation

$$C_0 = k_1 \exp \left[-\frac{U_2}{RT} - \frac{D}{kT(\Delta T)} \right] \quad (6)$$

or the Stranskii equation

$$C_0 = \frac{k_2}{(\Delta T)^2} \exp \left[-\frac{U_2}{RT} - \frac{D}{kT(\Delta T)} \right], \quad (7)$$

where $D/\Delta T$ represents the work of formation of two-dimensional nuclei on the face of a three-dimensional crystal, and U_2 is the activation energy of this process.

The term containing the work of formation $D/\Delta T$ may be taken as equal to unity, as the whole range of the curve ABCDEKL lies at considerably greater degrees of supercooling than the main portion of the curve for the crystal growth rate against temperature, containing the maximum. Thus, for betol the curve ABCDEKL lies between -20 and $+20^\circ$, while the maximum growth rate is found at about $+63^\circ$ [3, 15]. Assume that the

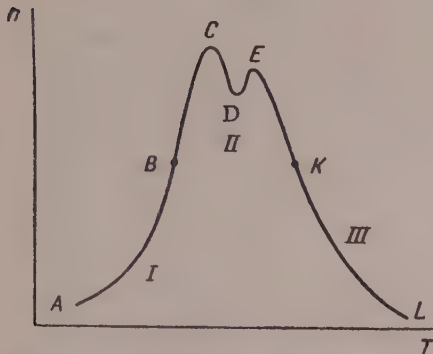


Fig. 1. Temperature dependence of the number of crystallization centers in a supercooled liquid (schematic).

dependence of the linear crystallization rate on the temperature is determined by the Volmer equation, namely by its first factor $\exp\left[-\frac{U_2}{RT}\right]$, as of the two Equations (6) and (7) for C_0 as a function of temperature the former gives a closer approximation to the experimental data for betol [15]. In these calculations for betol the activation energy was identified with the activation energy determined from the viscosity [16, 6], which we denote by U_η . Since in Region I the points on the curve refer to the growth of "nuclei" in the wall layer, the activation energy U_2 should be greater here than for the rest of the curve, especially Region III. In view of the fact that in the wall layer crystallization centers are formed at about half the rate for ordinary layers [14], the value of viscosity was doubled. Accordingly, the activation energy was increased by a constant value of 364 cal/mole [8].

Thereby it was implicitly assumed that the variation of viscosity with temperature is the same in the surface layer as within the volume, since this relationship has not yet been investigated experimentally. If we adopt the above assumptions concerning the mechanism of the growth of the nuclei at temperature t_e° and of their formation at t_p° , and if we also assume that U_2 and U_η depend similarly on the temperature, then the number of observed crystalline grains in Region I should conform to the equation

$$n = \text{const } e^{U_\eta/RT} \quad (8)$$

or

$$\lg n = -\gamma + \text{const}, \quad (9)$$

where

$$\gamma = \frac{U_\eta}{RT} \lg_{10} e.$$

In Fig. 2, γ is plotted against $\log n$; Line 1 for betol and Line 2 for piperine. In both cases there is a good fit with the linear Equation (9). This was confirmed for 20 curves for betol, and 10 curves for piperine, determined by different workers [10, 17, 18].

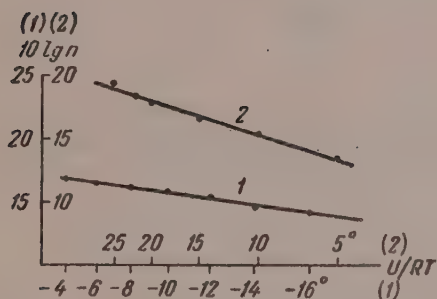


Fig. 2. Temperature dependence of the rate of conversion of impurity particles above the critical size for Region AB of the curve in Fig. 1: 1) for betol; 2) for piperine.

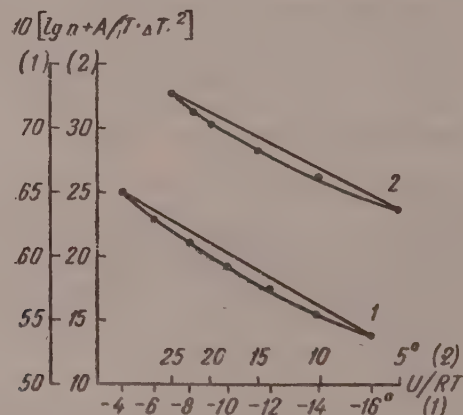


Fig. 3. Temperature dependence of the nucleation rate for Region AB of the curve in Fig. 1, in accordance with the spontaneous-mechanism theory: 1) for betol; 2) for piperine.

The following objection may be raised against the application of Equation (8): it is possible that Equation (1) for the spontaneous mechanism is valid rather than (8), but the influence of the term including the work of formation of three-dimensional nuclei $\frac{A}{kT (\Delta T)^2}$, is so small that it has no appreciable effect on linearity, as in Region I the exponent $\frac{A}{kT (\Delta T)^2}$ depends very slightly on temperature. To show that this is not the case the value of this term was calculated from data for Region III (see below). As before, γ is taken along the

abscissa axis in Fig. 3, and the sum $10 \left[\lg n + \frac{A}{T(\Delta T)^2} \right]$ is taken along the ordinate axis. The values of $\lg n$ were the same as in Fig. 2. There is found to be a systematic deviation from linearity.

For further refinement, the work of formation of two-dimensional nuclei D/kT was taken into account, but this correction did not alter the linear relationship, as it depends very little on the temperature in the region ABCDEKL, as this region is far from the maximum on the curve for the rate of crystal growth.

This confirms once again that the spontaneous mechanism is not applicable to Region I, as both the exponential terms must be taken into account in Equation (1).

However, the slope of the lines in Fig. 2 is considerably less than predicted by Equation (9), and therefore in reality the equation

$$\lg n = -k\gamma + \text{const}, \quad (10)$$

where $k < 1$ is valid, rather than Equation (9).

It follows that although our assumed temperature relationship for the activation energy holds satisfactorily, the absolute value of U_2 is less than U_η . Therefore quantitative agreement between experimental results and values calculated by means of Equations (6) or (7) cannot be expected.

Crystal growth in supercooled liquids [19, 15, 20] has not been studied sufficiently as yet, and therefore any further conclusions would be premature, especially as in this case we are concerned with the growth of micro- rather than macrocrystals.

Region III. In accordance with the assumption made earlier, the nuclei in this region (Region KL in Fig. 1) are smaller than the critical size

$$r < (r_k)_e, \quad (11)$$

corresponding to the exposure temperature. This size is reached only as the result of fluctuations. The number of nuclei converted at time t into crystallization centers of size $(r_k)_e$ during the exposure period should conform to Equation (3). In this case it is written in the form

$$\nu = \nu_\infty (1 - e^{-\alpha_e t}), \quad (12)$$

where α_e corresponds to the exposure temperature t_e° .

Since the exposure time τ_e is short, we have

$$\nu = \nu_\infty \alpha_e \tau_e. \quad (12a)$$

When the temperature is raised to t_p° all these crystallization centers are again converted into nuclei the sizes of which conform to the condition

$$r < (r_k)_p. \quad (13)$$

Therefore, they again undergo fluctuational conversion, this time a secondary process, into new crystallization centers. Their number should conform to conditions (3) or (4).

The dependence of the number of centers ν on the temperature t_e° in this region is not the same as in the first, and it is determined by their formation as the result of fluctuations and not by their growth during exposure. This process is represented by Equation (14), derived earlier [9]

$$\nu = \frac{\text{const}}{e^{\beta(r_k)_e^2}} \int_{r(t)}^{(r_k)_e} e^{-\frac{\alpha}{c}(r-r_m)} dr. \quad (14)$$

It had been shown [9] that the dependence of ν on temperature is determined by $\exp[-\beta(r_k)_e^2]$, and the number of centers n formed as the result of secondary conversion at the same "development" temperature also depends on their number.

Thus, the number n should depend as follows on the temperature:

$$\lg n = \text{const} - \beta (r_k)_e^3 \quad (15)$$

or, in another form

$$\lg n = \text{const} - \frac{A}{T_e (\Delta T)^2}, \quad (15a)$$

where

$$\Delta T = T_0 - T_e$$

or

$$\ln n = k_1 - \frac{k_2}{T (\Delta T)^2}. \quad (15b)$$

This is confirmed fairly accurately by the experimental data. In Fig. 4, values of $\frac{10^7}{T_e (\Delta T)^2}$ are taken along the abscissa axis, and the corresponding centigrade temperatures are also indicated, and multiples of $\lg n$ are taken along the ordinate axis. The linear relationship was confirmed for betol on the basis of more than 20 curves given by various authors [3, 4, 17], and for piperine on the basis of 10 curves [4, 11, 18]. One point of detail should be noted here. In Equation (15a), A is found from Equation (2).

The value of σ is taken to be independent of the temperature, as is generally assumed. However, variations of σ with temperature, which are to be expected on general theoretical grounds, may not have any appreciable influence on the slope of the lines in Fig. 4.

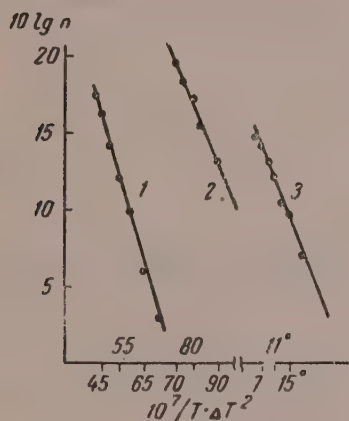


Fig. 4.

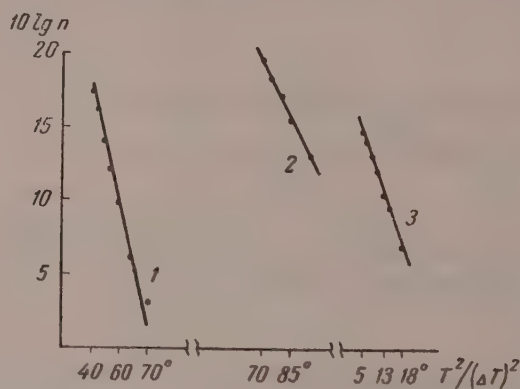


Fig. 5

Fig. 4. Effect of temperature on the rate of fluctuational conversion of impurity particles below the critical size in the temperature range corresponding to Region KL of the curve in Fig. 1: 1) for piperine; 2) quinic acid; 3) betol (interfacial energy σ is assumed constant).

Fig. 5. Effect of temperature on the rate of fluctuational conversion of impurity particles in the temperature range corresponding to Region KL of the curve in Fig. 1: 1) for piperine; 2) quinic acid; 3) betol; for constant $\beta = 4\pi\sigma/kT_e$.

It was assumed previously [9] that the variations of β , determined by the equation

$$\beta = \frac{r_4 \pi \sigma}{3kT_e}, \quad (16)$$

have so little influence on the accuracy of the calculated results that this influence may be ignored. This can be confirmed if Equation (15a) is verified, not at constant σ , but at constant β . It is sufficient for this purpose to express A in Equation (15a), based on Equation (2), as the constant $\sigma_0 \equiv \sigma / T$, when Equation (15a) becomes

$$\lg n = \text{const} - \left(\frac{\kappa M^2 T_0^2 \sigma_0^3}{q^2 \rho^2} \right) \frac{T^2}{(\Delta T)^2} \quad (17)$$

Figure 5 shows that the linear relationship in this case is no less satisfactory than at constant σ .

Our Equations (15a) or (17) can be used for calculating the interfacial energy from the slopes of the linear plots (Fig. 4 or 5), i.e., from the value of A. The remaining quantities q , ρ , T_0 may in the first approximation be given values determined experimentally for macrocrystals. However, for this it is necessary to determine accurate data for Region III, as the data available in the literature are generally restricted to Region II. A rough calculation based on published data [3] gives the value $\sigma \sim 10$ ergs/cm² for betol.

Region II contains both maxima of the temperature curve. On the high-temperature side this region should begin at temperature t_1^* , at which the radius of the largest crystallization center r_m coincides with the critical size r_k for the same temperature. If we imagine that the exposure temperature is reduced, starting from t_1 , then the first of the nuclei originating in time τ_e are larger than $(r_k)_e$, and the subsequent ones are smaller. The region terminates at a temperature at which all the centers relating to the interval τ_e are larger than $(r_k)_e$. Since the exposure is of finite duration, each of the maxima is diffuse. The question of the form of the maxima requires further experimental study.

Despite the fact that the results obtained by Tammann's method refer to crystallization on particles of accidental impurities, they can be used for determinations of surface energy at crystal-melt interfaces.

SUMMARY

1. The dependence of the number of crystallization centers in supercooled liquids on the temperature is examined. This relationship is represented by a curve which may be subdivided into three regions, corresponding to different growth mechanisms of the nuclei.

2. The low-temperature region of this curve corresponds to a stage at which the nuclei consist of impurity particles coated with a crystalline layer of the substance in the melt. At this stage, nuclei above the critical size grow monotonically. Crystallization centers are not formed at this stage.

3. The high-temperature region of the curve corresponds to conversion of the impurity particles into crystallization centers as the result of fluctuations, as in this case they are below the critical size.

4. At the "development" temperature all the impurity particles are below the critical size corresponding to this temperature, and are converted into crystallization centers as the result of fluctuations.

5. The relationship between the number of centers n and the temperature in the high-temperature region is represented by Equation (15b), where the constant k_2 can be used for determination of the interfacial energy σ .

LITERATURE CITED

- [1] D. Turnbull, J. Appl. Phys. 21, 1022 (1950).
- [2] V. I. Danilov, Structure and Crystallization of Liquids [in Russian] (Acad. Sci. Ukrainian SSR Press, 1956) p. 337.
- [3] M. E. Mikhlin, Dissertation: Influence of Pressure on Crystallization of Supercooled Liquids [in Russian] (Minsk, 1954).
- [4] G. Tammann, Z. phys. Chem. 25, 441 (1898).
- [5] J. H. Hollomon and D. Turnbull, Progr. Metal Physics 1, 316 (1956).

- [6] P. P. Kobeko, Amorphous Substances [in Russian] (Izd. AN SSSR, 1952).
- [7] N. I. Shishkin, J. Tech. Phys. 24, No. 7 (1956).
- [8] G. L. Mikhnevich, Trans. Odessa Univ., Phys. Ser. 67 (1957).
- [9] G. L. Mikhnevich, Colloid, J. 21, 69 (1959).*
- [10] G. L. Mikhnevich, Colloid J. 21, No. 3, 325 (1959).*
- [11] F. K. Gorskiĭ and G. L. Mikhnevich, J. Exp. Theoret. Phys. 2, 265 (1932).
- [12] L. O. Meleshko, Dissertation: Investigation of the Rate of Crystallization of a Single Grain as a Method for Determination of the Perimetric Energy [in Russian] (Odessa University, 1954).
- [13] G. L. Mikhnevich and I. F. Brovko, J. Exp. Theoret. Phys. 10, No. 3 (1940).
- [14] G. L. Mikhnevich and E. N. Ovchinnikova, Trans. Odessa Univ. Phys. Ser. 16, 57 (1952).
- [15] V. G. Zaremba, Trans. Odessa Univ., Young Scientists' Symposium, No. 2, 147 (1957).
- [16] Ya. I. Frenkel*, Theory of the Liquid State [in Russian] (Izd. AN SSSR, 1945).
- [17] M. M. Mazhul*, Dissertation: Cavitation and Formation of Crystal Nuclei [in Russian] (Odessa, 1954).
- [18] V. V. Kondoguri, J. Exp. Theoret. Phys. 11, 728 (1941).
- [19] F. C. Frank, Advances in Physics 1, 191 (1952).
- [20] O. Jantsch, Z. Kristallogr. 108, 185 (1956).

Received September 13, 1957

* Original Russian pagination. See C.B. Translation.

RELATIONSHIP BETWEEN FATIGUE RESISTANCE, STRENGTH, HYSTERESIS, AND CHEMICAL RESISTANCE OF RUBBERS

M. M. Resnikovskii, L. S. Priss, and M. K. Khromov

Scientific Research Institute of the Tire Industry, Moscow

In this communication an attempt is made to elucidate a number of relationships existing between the fatigue characteristics of rubbers and their other properties. Fatigue is taken to mean changes in the properties of a material under the influence of mechanical stresses, ultimately leading to destruction.

In addition to mechanical forces, other (nonmechanical) factors such as light, heat, chemically active media, etc., influence the fatigue process. However, the action of these factors is such that while it changes the properties of the material, usually in an unfavorable direction, it does not in itself (i.e., in absence of external forces) lead to destruction. Therefore, a clear distinction must be made between the concepts of "fatigue" and "aging", in view of the fact that the latter implies only changes in properties caused by the action of non-mechanical factors.

The aging of polymer materials, including rubbers, has been the subject of numerous investigations [1-3], the practical consequence of which has been that a number of substances, known as aging retarders, which protect the polymer against the action of light, oxygen, ozone, etc., have been recommended. In a number of cases these substances also have a substantial positive influence on fatigue resistance. This possibly explains why many authors [4] tend to regard fatigue as a special form of aging, accelerated and intensified by mechanical forces. The inadequacy of this approach to studies of fatigue is obvious, if only because attention is focused on changes in the properties of the material with time, while the actual strength, i.e., the resistance of the material to destruction, is not considered.

We believe that certain general and probably very important information on the nature of fatigue can be obtained by a more detailed consideration of the relationship between fatigue characteristics and certain other properties, relatively simpler and therefore better studied. These primarily include the strength, characterized by the tensile strength, and chemical resistance, characterized by resistance to various forms of aging.

The connection between fatigue strength, strength under a single loading (subsequently described as the tensile strength) and chemical resistance (or resistance to aging) is evident from a consideration of the fatigue stress corresponding to the minimum and maximum fatigue life.

It is evident that the greater the stress amplitude and the lower the fatigue life, the nearer is fatigue breakdown in character to ordinary physical rupture. At the limit, when the fatigue life decreases to a single cycle, the fatigue stress under alternating symmetrical load coincides with the tensile strength. It is equally obvious that in tests under asymmetric loading, which leads to rapid destruction, the tensile strength has the decisive influence on fatigue stress.

The time to failure increases with decrease of the applied stress. The factors which determine the fatigue life of the rubber at the limit are not mechanical stresses but other factors responsible for aging (light, heat, corrosive media, etc.).

In general, the proposition that the fatigue stress of a material increases with its tensile strength and chemical resistance as characterized by resistance to various forms of aging is so obvious that no special proof is necessary.

It is easy to show, however, that dynamic fatigue is not determined only by the strength characteristics and chemical resistance of the rubber. Indeed, it is known that the time to failure decreases sharply if static fatigue is replaced by dynamic (with the same maximum value of the deforming stress). This fact cannot be explained if it is assumed that fatigue stress depends only on the tensile strength and aging. Furthermore, our data on fatigue stress at a fatigue life of 10^6 cycles (data determined in the preceding investigation [5]) did not show any definite correlation with tensile strength or aging characteristics.

Finally, the fatigue life (the number of cycles to failure) at a given experimental temperature over a certain range depends little on the frequency [6, 7]; i.e., the time to failure falls sharply with increase of frequency, which is also inexplicable in the light of the above concept, as in that case the time to failure and not the number of cycles should be independent of frequency.

It is reported in a number of papers that the greater the mechanical losses associated with hysteresis the lower is the fatigue stress for rubbers. This fact is quite explicable if the temperature during the test is determined by the hysteresis properties of the specimen. However, there is reason to believe that even at the same temperature and under other equal conditions a rubber with the greater internal friction should have lower resistance to dynamic fatigue.

To test this hypothesis, we correlate the dynamic fatigue stress for vulcanizates of different rubbers, differing in degree of vulcanization, filler contents, etc., with the corresponding internal friction data. Data presented in the previous communication [5] are used for this purpose.

Since vulcanizates differing in internal friction usually also differ in strength which, as already stated, is one of the factors determining fatigue properties, it is reasonable to make use of dimensionless quantities representing the ratio of the dynamic fatigue stress f_{OF} (for a given fatigue life) to the tensile strength determined at the same temperature, or of other fatigue characteristics to the corresponding strength characteristics; for example, of the fatigue deformation ϵ_{OF} to the relative elongation at break.

Figures 1 and 2 represent variations of the ratios f_{OF}/P and ϵ_{OF}/ϵ_B (P is the tensile strength; ϵ_B is the relative elongation at break) with total sulfur and channel black contents. Whereas variations of the fatigue characteristics (the fatigue characteristics correspond to a fatigue life of 10^6 cycles, and were determined in alternating flex tests at 3000 cycles/minute and 100° [5]) differed in character (the fatigue deformation passed through a maximum with increasing contents of sulfur and carbon, while the fatigue stress increased steadily), as is clear from Fig. 5 in the earlier paper [5], the dimensionless quantities f_{OF}/P and ϵ_{OF}/P varied symmetrically, increasing with increase of vulcanization and decreasing with increase of carbon content. The general tendency to a decrease of fatigue resistance with increase of internal friction is clearly seen in Fig. 3, where f_{OF}/P is

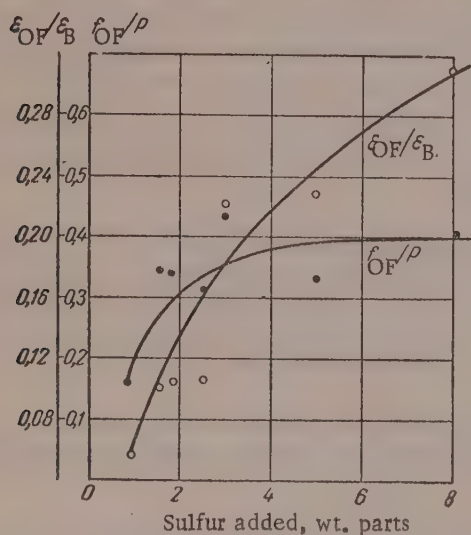


Fig. 1. Variations of f_{OF}/P and ϵ_{OF}/ϵ_B with the total sulfur content of SKS-30A vulcanizates without filler.

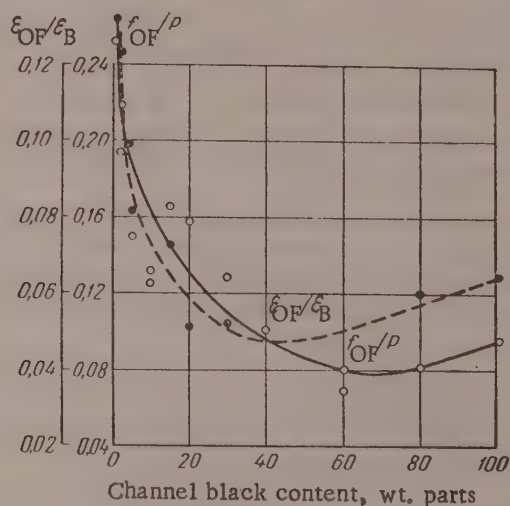


Fig. 2. Variations of f_{OF}/P and ϵ_{OF}/ϵ_B with the channel black content of SKS-30 vulcanizates.

plotted against the modulus of internal friction [8] for vulcanizates differing in the nature of the rubber polymer, carbon content, etc. The considerable scattering of the data is to be expected, as the compared vulcanizates differ in other characteristics as well as internal friction. It is evident that a similar dependence on the modulus of internal friction also holds ϵ_{OF}/ϵ_B , as this ratio varies symbatically with f_{OF}/P .

TABLE 1

Results of Comparative Tests on Breaker Vulcanizates Based on Butadiene-Styrene Rubber, with Different Moduli of Internal Friction*

Code	Total sulfur content, %	Carbon content, wt. parts per 100 wt. parts rubber	P, kg/cm ²	E, kg/cm ²	K, kg/cm ²	Fatigue life, 10 ³ cycles
A	3,0	55,0	167,6	53,0	14,3	160
B	3,5	49,5	158,5	51,2	11,5	310
C	4,0	44,0	174,7	52,0	9,65	440
D	4,5	38,5	150,0	52,5	8,8	580

*Determined by L. Pevzner, graduate student of the Lomonosov Institute of Fine Chemical Technology, Moscow.

A more definite conclusion concerning the dependence of the fatigue life of vulcanizates on their internal friction may be drawn from the results of the experiments described below; another object of these experiments was to determine the practical possibilities of increasing the fatigue resistance of rubber by lowering the internal friction by variations of the formulation and technological procedures.

The formulation of a standard breaker stock based on SKS-30A butadiene-styrene rubber (stock A in Table 1) was modified somewhat, with a higher sulfur content and a lower carbon content; these modifications were adjusted so as to keep the tensile strength and dynamic modulus E unchanged as far as possible. Four

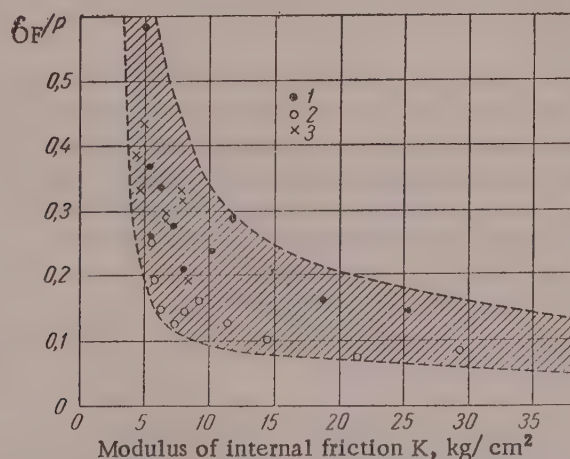


Fig. 3. Variations of f_{OF}/P with the modulus of internal friction K (alternating flex tests, $T = 100^\circ$): 1) with lamp black (SKS-30); 2) with channel black (SKS-30); 3) with different sulfur contents (SKS-30A).

vulcanizates were prepared, with progressively decreasing filler contents and consequently with decreasing values of the modulus of internal friction K (mixes given in Table 1). Alternating flex tests on these rubbers at 100° and 20% deformation amplitude showed that their fatigue life increases steadily with decrease of the modulus of the internal friction.

Since all the fatigue-life data were determined at 100°, this result can be regarded as direct confirmation of the inverse relationship between internal friction and fatigue endurance of a rubber. In practice, decrease of internal friction is a highly effective way of increasing the fatigue life for the further reason that the lower the internal friction, the lower the temperature which develops in a massive specimen as the result of hysteresis.

It is clear from the foregoing that under given conditions a rubber has a high fatigue stress if it has high tensile strength, high chemical resistance, and low internal friction. The relative role of these properties differs with the conditions of loading and the nature of the nonmechanical influences. A comparison of data for natural and polybutadiene rubber vulcanizates, presented in Table 2, serves to illustrate the effects of fatigue conditions on the relative significance of physical and chemical factors. In addition to data on tensile strength, aging, and modulus of internal friction, Table 2 contains values of fatigue stress corresponding to harsh mechanical conditions (asymmetric load cycle) and low temperature, and mild mechanical conditions (symmetrical load cycle) in conjunction with a high test temperature.

TABLE 2

Comparison of Vulcanizates of Natural Rubber (NR) and SKB with Regard to Tensile Strength, Aging, Internal Friction, and Fatigue Stress Corresponding to Different Fatigue Life and Temperatures

Vulcani- zates of	Tensile strength, kg/ cm ²		Aging coeffic- ient	Modulus of in- ternal friction, kg/ cm ²	Fatigue stress, kg/ cm ²		
	before aging	after ag- ing (72 hours) at 100°			fatigue life, asymmetric cycle, $\epsilon = 150\%$		symmetric cycle; fatigue life $5 \cdot 10^6$ cycles, $T =$ 120°
					10^6 cycles, $T = 23^\circ$	$4 \cdot 10^6$ cy- cle, $T = 80^\circ$	
NR	290	155	0,53	0,9	4,0	2,1	2,8
SKB	20	20	1,0	2,3	2,1	1,3	4,2

It follows from Table 2 that with increase of aging time and temperature, when the role of mechanical factors diminishes and that of nonmechanical factors (temperature) increases, NR vulcanizates gradually lose their superiority over SKB vulcanizates.

This comparison is of interest in principle, as it shows that the cause of the low fatigue life of SKB vulcanizates in many products, including tires, is their relatively low strength and high internal friction. With regard to chemical resistance, SKB vulcanizates are even superior to NR, although the latter give considerably better performance. It follows that for production of vulcanizates of high fatigue stress, attention must be devoted not only to ways of increasing their chemical stability, but also to methods of synthesis and technological procedures for production of elastomers of high strength and low internal friction.

SUMMARY

1. In tests under the same temperature and other conditions, vulcanizates of higher internal friction have lower fatigue life.
2. The fatigue resistance increases with increasing tensile strength and chemical resistance, and with decrease of internal friction, and the relative significance of each of these factors depends on the test conditions: loading procedure, temperature, surrounding medium, etc.

The authors thank Professor B. A. Dogadkin for his interest in the work and discussion of the results.

LITERATURE CITED

- [1] A. S. Kuz'minskii, Progr. Chem. 24, No. 7, 842 (1955).
- [2] A. S. Kuz'minskii, N. N. Lezhnev, and Yu. S. Zuev, Oxidation of Rubbers and Vulcanizates [in Russian] (Goskhimizdat, 1957).

- [3] Proc. Conference on the Aging of Rubber [in Russian] (Goskhimizdat, 1954).
- [4] Aging and Fatigue of Rubbers [in Russian] (Goskhimizdat, 1955).
- [5] M. M. Reznikovskii, L. S. Priss, and M. K. Khromov, Colloid J. 20, 368 (1958).*
- [6] J. Dillon, in the book: Fatigue of High Polymers (Goskhimizdat, 1957) [Russian translation].
- [7] G. M. Bartenev, Progr. Chem. 24, No. 7, 815 (1955).
- [8] M. M. Reznikovskii and B. A. Dogadkin, Chem. Ind. No. 4, 35 (1954).

Received February 25, 1958

* Original Russian pagination. See C.B. Translation.

INFLUENCE OF SIZE REDUCTION ON SOLUBILITY AND HEAT OF SOLUTION

P. P. Ryazantsev and L. M. Shcherbakov

The Tula Mechanical Institute

As long ago as 1900, W. Ostwald [1] noted that a finely divided substance has higher solubility, and gave a theoretical interpretation of this phenomenon. It is true that this interpretation contained a fairly crude thermodynamic error, subsequently corrected by Freundlich [2]. In subsequent years the influence of size reduction on solubility has been verified experimentally; the very careful experiments of Hullet [3], Glasstone [4], and Dundon [5] are worthy of special mention. The theory of this effect was subsequently expanded by Jones [6], who took into account the shape of the dissolving crystal. Among the later investigations, we may note the work of Lyalikov [7], concerned with an experimental verification of Ostwald's equation, and the theoretical papers by Semenchenko [8] and Rykov [9], in which this equation was developed further.

In 1927 Lipsett, Johnson, and Maass [10] showed experimentally that the heat of solution of finely divided common salt is lower. A theoretical explanation of this effect was given in 1945 by one of the present authors.* The formula derived for decrease of the heat of solution

$$\Delta L = -2\sigma v D \quad (1)$$

(where σ is the surface tension of a crystal; v is its molar volume; D is the dispersity) was subsequently deduced by Rykov [9]. However, in both these studies, as in most other investigations in this field, the derivation involved a number of simplifying assumptions (in particular, the assumption that the solutions are ideal), which could not fail to influence the results. A rigid thermodynamic examination, which gives more precise relationships, is given below.

It is first necessary to define more precisely the concept of surface tension of a solid. Strictly speaking, each crystal face has its own value for the surface tension σ_i , and the values of σ_i for different faces of an equilibrium crystal are interrelated as defined by Vulf's theorem [11]:

$$\sigma_1 : \sigma_2 : \sigma_3 : \dots = l_1 : l_2 : l_3 : \dots, \quad (2)$$

where l_i is the so-called Vulf distance for the i -th crystal face. However, in a thermodynamic discussion it is quite permissible to introduce a certain average value, characteristic for the crystal as a whole. For this we take the value of σ defined by the equation:

$$\sigma = \frac{\sum \sigma_i S_i}{\sum S_i} = \frac{\sum \sigma_i S_i}{S}, \quad (3)$$

which we shall term the surface tension of a solid. It should be pointed out that the methods described in the literature for experimental determination of surface energy do not give the surface tensions of individual faces, but a certain average value, corresponding to our σ .

The question of the dispersity of the crystal grains must also be defined. Dispersity is usually character-

* This work was not published because of war conditions.

ized in terms of effective radius \underline{r} , which is the radius of a sphere of equivalent volume. However, bodies of equal volume may vary greatly in surface area in accordance with their shape. Therefore, for complete characterization of dispersity it is also necessary to introduce a certain shape factor ξ . According to Strebeiko [12], this factor may be defined as the ratio of the surface area of the particle to the area of a sphere of equivalent volume. Accordingly, we adopt the following ratio as the measure of dispersity:

$$D = \xi / r. \quad (4)$$

It is easily seen that this measure of dispersity is related to the specific surface $s = S/V$ of a particle as follows:

$$D = \frac{1}{3} \frac{\xi 4\pi r^2}{\frac{4}{3} \pi r^3} = \frac{1}{3} \frac{S}{V} = \frac{1}{3} s, \quad (5)$$

In passing to the derivation of the required relationships, let us consider the two-component system "crystal-line grain (indicated') - saturated solution (indicated'').^a It is assumed that the grain consists of a single component (I), while the solution contains both components (solute I and solvent II). For the free energy of the system we have:

$$F = F' + F'' + \sigma S, \quad (6)$$

where σ is the average surface tension defined in Equation (3). The equilibrium conditions for the system can be found from the principle of minimum free energy. The following additional conditions of constant temperature and mechanical isolation must be applied to the system:

$$\left. \begin{aligned} T' &= T'' = T'' = \text{const} \\ V' + V'' &= \text{const} \\ n_1' + n_1'' &= \text{const} \\ n_2'' &= \text{const} \end{aligned} \right\} \quad (7)$$

Moreover, it is necessary to take into account the condition of shape-factor constancy which follows from Vulf's theorem and which can be represented mathematically as

$$\xi = \text{const}, \quad (7a)$$

where ξ is the shape factor.

Varying of Condition (6) with (7) and (7a) taken into account, and noting that

$$\left(\frac{\partial S}{\partial V} \right)_{\xi} = 2 \frac{\xi}{r} = 2D,$$

we have

$$\delta F = (\mu_1' - \mu_1'') \delta n_1 - (p' - p'') \delta V' + 2\sigma \cdot D \delta V'.$$

Hence, equating δF to zero, we have the equilibrium conditions for the system:

$$\left. \begin{aligned} \mu_1'(p', T) &= \mu_1''(p'', T) \\ p' &= p'' + 2\sigma D \end{aligned} \right\} \quad (8)$$

The first of these equations may be written in the form

$$\mu_1'(p'' + 2\sigma D, T) = \mu_1''(p'', T).$$

We now resolve the left-hand side into the Taylor series, taking the first two terms only. Then, remembering that

$$\frac{\partial \mu_1'}{\partial p} = v',$$

where v' is the molar volume of the crystalline phase, we have

$$\mu_1'(p'', T) + v' \cdot 2\sigma D = \mu_1''(p'', T).$$

By means of the known expression for the chemical potential of a solute

$$\mu = \mu^* + RT \ln fN$$

(where μ^* is the part of the chemical potential independent of the concentration: f is the activity coefficient; N is the concentration in mole fractions), we can rewrite the previous expression in the form

$$\mu_1'(p'', T) + 2\sigma v' D = \mu^*(p'', T) + RT \ln fN.$$

Analogously, for the substance before subdivision we have

$$\mu_1'(p'', T) = \mu^*(p'', T) + RT \ln f_0 N_0.$$

Subtracting the lower from the upper equation, we have, after simple transformations, the generalized Ostwald equation

$$fN = f_0 N_0 \cdot e^{\frac{2\sigma v'}{RT} \cdot D}, \quad (9)$$

which, in contrast to the usual Ostwald equation, is applicable to substances forming nonideal solutions.

For not very high dispersities ($D \leq 10^4 \text{ cm}^{-1}$, which corresponds to particles for radius $r \geq 1 \mu$) the difference between the activity coefficients f and f_0 may be disregarded, and Equation (9) then becomes

$$N = N_0 \cdot e^{\frac{2\sigma v'}{RT} \cdot D}. \quad (9a)$$

Hence, by resolution into the Taylor series, and taking only the first two terms, we have the following equation for the relative solubility increase due to subdivision

$$\frac{\Delta N}{N_0} = \frac{N - N_0}{N_0} \approx \frac{2\sigma v'}{RT} \cdot D. \quad (10)$$

According to Born and Stern [13] the surface tension of crystals of the NaCl type is given by the formula*

$$\sigma_i = k_i \frac{e^2}{a^3},$$

where e is the unit charge; a is the lattice constant, and k is a numerical factor the value of which differs for different faces. In particular, for the (100) face this factor is 0.016. Accordingly, for the average value of σ , we can write

$$\sigma = k \cdot \frac{e^2}{a^3}$$

(k is the average value of the factor). The molar volume of the crystal is $v' = N_A a^3$ (N_A is the Avogadro number).

* Strictly speaking, the crystal lattice theory makes it possible to calculate the total specific surface energy ϵ , but near absolute zero ϵ coincides with σ .

Hence

$$\sigma \cdot v' = k \cdot \frac{c^2}{a^3} N_A a^3 = k \cdot N_A c^2, \quad (11)$$

i.e., for salts of the NaCl type the product of surface tension and molar volume is constant. This result can apparently be extended to other types of crystals, although the numerical value of the constant in Equation (11) may differ.*

Using this result, we find from Equation (10) that for crystals of the same class at equal temperatures the relative solubility increase $\Delta N/N$ resulting at subdivision to a definite dispersity should be approximately the same.

For derivation of an equation for the effect of dispersity on heat of solution, we consider a solution volume which is so large that dissolution of a crystal does not alter the concentration. For the enthalpy change in the dissolution process, we have:

$$\Delta H = H - (H' + H_s + H'') = (H - H' - H'') - H_s = \Delta H_0 - H_s,$$

where ΔH_0 is the enthalpy change of the volume phases, and H_s is the surface enthalpy, equal to $\epsilon \cdot S$ (ϵ is the total specific surface energy). Differentiation of this expression with respect to the mass (in moles) of the dissolving crystal, we have the following expression for the molar differential heat of solution:

$$L = L_0 - \frac{\partial H_s}{\partial n'}.$$

Here $L_0 = \frac{\partial \Delta H_0}{\partial n'}$ is the molar differential heat of solution of the compact substance (before subdivision), and

$$\frac{\partial H_s}{\partial n'} = \epsilon \frac{\partial S}{\partial n'} = \epsilon \frac{\partial S}{\partial V'} \cdot \frac{\partial V'}{\partial n'} = \epsilon \cdot 2Dv'.$$

Substituting this value into the preceding expression, we have the following equation for the decrease of the differential heat of solution as the result of subdivision of the solute:

$$\Delta L = L - L_0 = -2\epsilon v' D. \quad (12)$$

This equation differs from Equation (1) by containing, not the surface tension σ of the crystal, but the specific total surface energy ϵ , related as follows to the surface tension:

$$\epsilon = \sigma - T \frac{\partial \sigma}{\partial T}. \quad (13)$$

With the aid of Equation (5), Equation (12) can be written in the form

$$\Delta L = -2\epsilon \cdot v' \frac{1}{3} \frac{S}{V'} = -\frac{2}{3} E_s, \quad (13a)$$

i.e., the decrease of the differential heat of solution is $2/3$ of the total surface energy of the comminuted solute.

Lipsett, Johnson, and Maass [10] carried out an experimental study of the effect of subdivision on heat of solution. They designed a special adiabatic calorimeter and developed a technique for preparation of fine NaCl powders of a definite particle size. These were prepared by precipitation from the vapor phase, so that the possibility of mechanical strains in the forming crystallites was eliminated. The fractionation of the powder was effected during the precipitation process itself, by means of special apparatus. The particle sizes of the individual fractions were determined by microphotography. The results of their experiments are given in the table.

* See also [14].

Decrease of the Heat of Solution of Finely Divided Common Salt from the Data of Lipsett et al, [10], and Values of Specific Total Surface Energy Calculated from the Decreased Heat of Solution

Average particle diameter, μ	Specific surface $\times 10^6$, cm^2/mole	Decrease of heat of solution, cal/mole	Heat of wetting Q , cal/mole	True decrease of heat of solution ΔL , cal/mole	Specific total surface energy ϵ , ergs/cm^2
1,30	1,25	12,3	9,0	3,3	166
1,16	1,40	13,6	10,1	3,5	156
1,00	1,62	15,3	11,6	3,7	143

Using these results and assuming ΔL equal simply to the total surface energy of the finely divided salt, Lipsett, Johnson, and Maass found the value of 386 ergs/cm² for the specific surface energy* of NaCl. In reality, however, ΔL is only $2/3 E_s$, so that this value must be multiplied by 1.5, and ϵ for NaCl must be taken as 580 ergs/cm². This is much higher than the values derived from the lattice theory [13, 15, 16, 17] or the values of ϵ for NaCl melts

Values of ϵ for crystalline NaCl from [13] 150	ergs/cm ²
" " " " " " " " " " " " " " " " " " " "	from [15]	164
" " " " " " " " " " " " " " " " " " " "	from [16]	210
" " " " " " " " " " " " " " " " " " " "	from [17]	130
" " " " " " " " " " " " " " " " " " " "	for NaCl melts from [18]	166

The cause of this discrepancy lies in the fact that Lipsett, Johnson, and Maass did not take into account the heat of wetting of the salt surface. Under the usual conditions this effect is of no significance. However, in experiments with fine powders, the specific surface of which reaches values of the order of $10^3 \text{ m}^2/\text{mole}$, it is absolutely essential to take the heat of wetting into account.

In this respect the earliest experiments of Lipsett, Johnson, and Maass must be regarded as more correct with regard to method; in these experiments no special steps were taken to prevent the action of water vapor on the salt before the dissolution. Under these conditions an adsorption layer of water was formed in the salt grains even before dissolution, so that it was possible to measure directly the lowering of the heat of solution. In the subsequent experiments there was no previous contact between water vapor and the salt surface. Therefore, the determinations gave an aggregate effect composed of the lowering of the heat of solution ΔL and the heat of wetting Q . The heat of wetting must be subtracted from the values found by Lipsett, Johnson, and Maass (see table) in order to find true values of ΔL .

The heat of wetting can be calculated from the data in the first paper of Lipsett, Johnson, and Maass. For salt of specific (molar) surface $s_0 = 1.25 \times 10^6 \text{ cm}^2/\text{mole}$, the value was found to be $Q_0 = 9 \text{ cal/mole}$. Hence for salt of specific surface s , we have

$$Q = \frac{Q_0}{s_0} s = Q_0 \frac{s}{s_0} \quad (14)$$

Equation (14) can be used to find true values of ΔL , and hence the specific total surface energy of NaCl. The calculation results are given in the table, according to which the average value of ϵ for NaCl is 155 ergs/cm². This value is in good agreement with the value given by the lattice theory and with the value of ϵ for NaCl melts.

* Lipsett, Johnson, and Maass make no distinction between the specific total surface energy ϵ and the surface tension σ .

SUMMARY

1. The lowering of the heat of solution of a substance with decrease of particle size is demonstrated theoretically.

2. It is shown that the reason why Lipsett, Johnson, and Maass obtained high values of ϵ_{NaCl} is that the heat of wetting of the salt surface was not taken into account. With the appropriate correction the value $\epsilon_{\text{NaCl}} = 155 \text{ ergs/cm}^2$ was obtained for the specific total surface energy of crystalline NaCl.

The authors are deeply grateful to Corresponding Member (AN SSSR) B. V. Deryagin for valuable discussions.

LITERATURE CITED

- [1] W. Ostwald, Z. phys. Chem. 34, 495 (1900).
- [2] H. Freundlich, Kapillarchemie, B. I, Leipzig, (1930) S. 268.
- [3] A. Hullet, Z. phys. Chem. 37, 385 (1901); 47, 357 (1904).
- [4] S. Glasstone, J. Chem. Soc. 119, 1589 (1922).
- [5] M. L. Dundon, J. Amer. Chem. Soc. 45, 2658 (1923).
- [6] W. J. Jones, Ann. phys. 41, 441 (1913).
- [7] K. S. Lyalikov, Proc. Acad. Sci. USSR 31, 586 (1941).
- [8] V. K. Semenchenko, J. Phys. Chem. 19, 298 (1945).
- [9] V. I. Rykov, Sci. Mem. Kishinev Univ. 1, 37, (1949).
- [10] S. G. Lipsett, F. M. Johnson, and C. Maass, J. Amer. Chem. Soc. 49, 925 (1927); 49, 1940 (1927); 50, 2701 (1928).
- [11] Yu. V. Vul'f, Selected Papers on Crystal Physics and Crystallography [in Russian] (Moscow-Leningrad, 1952) p. 96.
- [12] P. É. Strebeiko, Dissertation: Influence of Subdivision on Transition Temperatures [in Russian] (Moscow, 1939).
- [13] M. Born and O. Stern, Sitzungsberichte der preussischen Akademie der Wissenschaften 33, 901 (1919).
- [14] V. K. Semenchenko, Surface Effects in Metals and Alloys [in Russian] (Moscow, 1957) p. 299.
- [15] Ya. I. Frenkel', Electrical Theory of Solids [in Russian] (Moscow, 1924).
- [16] V. D. Kuznetsov, Physics of Solids, Vol. 1, 2nd edn. [in Russian] (Tomsk, 1937) chapter 4.
- [17] A. E. Glauberman, J. Phys. Chem. 23, 124 (1949).
- [18] C. D. Hodgman, Handbook of Chem. and Phys., Ed. 33 (1951-1952).

Received April 4, 1958

SORPTION OF IONS BY CARBOXYLIC RESINS IN THE HYDROGEN FORM

G. V. Samsonov, Yu. B. Boltaks, N. P. Kuznetsova,

A. P. Bashkovich, and R. B. Ponomareva

Institute of High Polymers, Academy of Sciences USSR, Leningrad

The sorption of ions by carboxylic resins in the hydrogen form has attracted attention in recent years in connection with reports of successful sorption of proteins from neutral solutions by such resins [1]. Before this it was regarded as obvious and conclusively proved that carboxylic resins in the acid (or hydrogen) form can take up ions only from alkaline solutions, because of the low degree of dissociation of the hydrogen. In order to explain the sorption of proteins and a number of other experimental facts it was necessary to carry out systematic studies of the conditions for ion sorption by carboxylic resins in the hydrogen form. For example, it follows from the potentiometric titration curves of carboxylic resins (Fig. 1) that at solution pH of about 7 a considerable amount of sodium ions is present in the adsorbed equilibrium state in the resin. Nevertheless it is not possible to take up sodium ions from neutral chloride or sulfate solutions either under static or under dynamic conditions at an appreciable rate, equal to the rate of cation sorption by carboxylic resins in the salt form. Under static conditions, i.e., in a stirred vessel, sorption of cations by carboxylic resins should evidently occur on neutralization of the desorbed hydrogen ions, for example by means of basic anion exchangers [2]. Thus, the low degree of sorption of cations by carboxylic resins in the hydrogen form from neutral solutions is inconsistent with the potentiometric titration curves, and can only be accounted for by the presence of kinetic obstacles to the process. There is reason to believe that sorption of proteins by carboxylic resins in the hydrogen form proceeds successfully because of elimination of the slowest step in the sorption of H ions by carboxylic resins.

Two hypotheses may be advanced to account for the low sorbability (low sorption rate) of ions on the resins under consideration:

1. Diffusion of desorbed hydrogen ions from the resin grains into the solution is slow, probably because of the low equilibrium concentration of hydrogen ions in the resin. The equilibrium hydrogen-ion concentration is indeed extremely low, as is shown by the potentiometric titration curves for carboxylic resins (Fig. 1). Accordingly, the rate of diffusion of hydrogen ions from the resin grains into the solution should be low, by Fick's law:

$$G = D \frac{\partial c}{\partial x}$$

(where G is the ion-diffusion rate and D is the coefficient of diffusion), as the concentration gradient $\partial c / \partial x$ is small in this case.

2. In experiments on the sorption of streptomycin [2] the slow diffusion of streptomycin into the grains of the carboxylic cation exchanger in the hydrogen form was regarded as the slowest stage of the process. Indeed, carboxylic resins in the hydrogen form are usually of low porosity and swell little and, in any event, a carboxylic cation exchanger in the hydrogen form swells less than the same resin in the salt form. However, conclusions of this sort are extremely dubious in the light of the above-mentioned low sorption of sodium ions and the sorption

of large protein ions by carboxylic resins in the hydrogen form. Nevertheless, the problem of the causes of low sorption in a particular case (that of streptomycin) can be solved conclusively only after a direct analysis of such causes, and not as the result of indirect reasoning as in earlier publications [2].

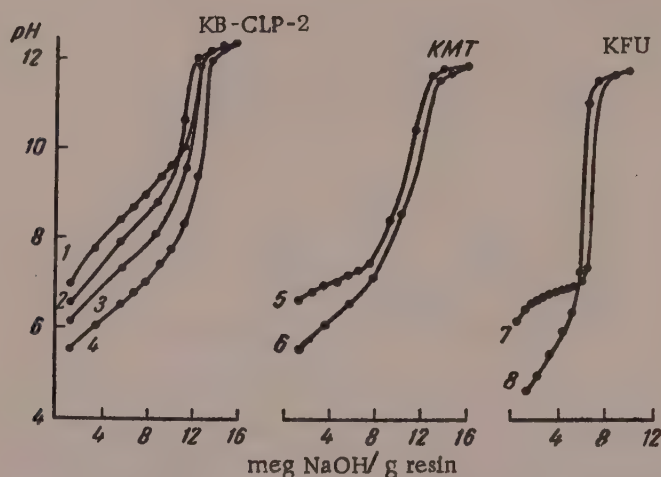


Fig. 1. Potentiometric titration curves for carboxylic resins: 1, 5, 7—0.1 N NaOH; 2) 0.1 N NaOH + 0.001 N NaCl; 3) 0.1 N NaOH + 0.01 N NaCl; 4, 6, 8—0.1 N NaOH + 0.1 N NaCl.

First we consider a possible second explanation of the low degree of sorption of ions by carboxylic resins in the hydrogen form. To obtain a direct answer to the problem, we studied the sorption of streptomycin by two samples of KMT carboxylic resin, synthesized by A. A. Vansheidt, A. V. Okhrimenko, and A. V. Tunik. The first resin sample was formed with a very small amount of cross-linking agent, and in the hydrogen form its swelling coefficient K_{sw} (ratio of the volume of the resin swollen in water to the volume of dry resin) was 4.4,

TABLE 1

Sorption Capacity of KMT Carboxylic Resin in the Hydrogen (H) and Sodium (Na) Forms for Streptomycin Under Dynamic Conditions

Resin form	K_{sw}	Sorption capacity, mg/g
H form	4.4	60
Na form	1.5	440

whereas the second sample, formed with a larger amount of cross-linking agent had a swelling coefficient of only 1.5 in the sodium form. Thus, the resin in the hydrogen form had considerably greater porosity than the second sample, which was used in the sodium form. Nevertheless, as is clear from Table 1, the dynamic sorption capacity of the hydrogen resin for streptomycin was considerably lower than the sorption capacity for streptomycin of the sodium form of the carboxylic resin under the same conditions (feed flow rate 60 ml/cm² · hour, streptomycin concentration 2 mg/ml); thus it is quite impossible to attribute the low sorption of streptomycin by carboxylic resins in the hydrogen form to low porosity and obstacles to diffusion of streptomycin ions into the resin grains.

If we return to the first viewpoint that diffusion of desorbed hydrogen ions is the slowest state of the process, it is possible to check experimentally a number of consequences of this hypothesis. First, the sorption of cations of different properties and different ionic radii should proceed at comparable rates, within certain limits, from solutions of equal normality. Figure 2 shows that the kinetic curves for sorption of streptomycin and sodium by the carboxylic cation exchanger in the hydrogen form from solutions of equivalent concentration in presence of a hydroxylic cation exchanger coincide almost completely. Of course, this resemblance between the kinetic curves disappears at very low ion concentrations or with resins of very low porosity, when only a small proportion of carboxyl groups is accessible to the large streptomycin ions.

The character of sorption of cations by carboxylic resins in the hydrogen form should change sharply on increase of the diffusion rate of hydrogen ions from the resin into the solution. It was therefore to be expected that sorption of cations by carboxylic resins in the hydrogen form should be more rapid from buffer solutions.

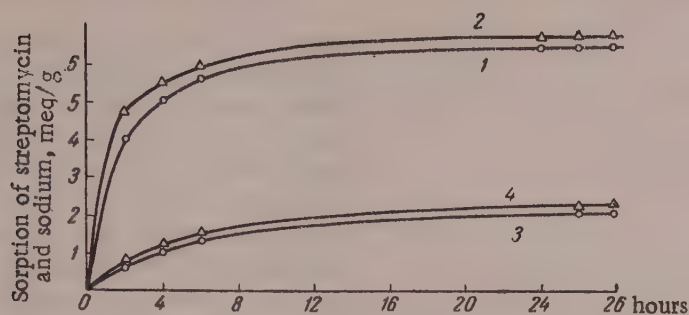


Fig. 2. Sorption of streptomycin and sodium by carboxylic cation exchanger in presence of ÉDÉ anion exchanger in the basic form (c_0 = initial concentration): 1) streptomycin ($c_0 = 0.25$ N); 2) sodium ($c_0 = 0.25$ N); 3) streptomycin ($c_0 = 0.025$ N); 4) sodium ($c_0 = 0.025$ N).

Indeed, as Table 2 shows, the dynamic capacity for streptomycin from buffer solutions is high even at pH 4-6. Under the same conditions streptomycin is not adsorbed at all by KMT resin in the hydrogen form from neutral aqueous solutions.

It follows from Table 2 that the introduction of limited amounts of neutral salts increases the sorption of streptomycin. This effect is easily explained as being due to increase of the equilibrium hydrogen-ion concentration in the resin grains on increase of the ionic strength of the solution, in accordance with the potentiometric titration curves (Fig. 1), which leads to an increase of the concentration gradient of the hydrogen ions between

TABLE 2

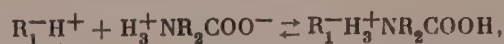
Sorption Capacity of KMT Resin in the Hydrogen Form for Streptomycin from Buffer Solutions and From Solutions Containing Na_2SO_4

pH of acetate buffer solution (0.3 M)	Sorption capacity of streptomycin, mg/g	Na_2SO_4 concentration, M	Sorption capacity of streptomycin, mg/g
3.19	89	0	0
4.02	110	0.3	37.6
5.09	302	1.6	3.6
6.22	750	1.2	0

the resin and solution and thus accelerates cation sorption, in harmony with the considerations presented above. Moreover, shift of equilibrium in three-component systems may play a certain part here. The significance of the dimensions of the adsorbed ions in this effect is to some extent limited, and consequently a similar effect should be observed in sorption of metal ions. It is seen in Fig. 3 that the rate of sorption of lanthanum also increases sharply on addition of a sodium salt (1.11 g NaCl per 380 ml solution). Increase of the sorption of ions by carboxylic resins in the hydrogen form on addition of competing ions is possible only if selective sorption takes place.

Next we must consider the sorption of proteins by carboxylic resins in the hydrogen form. We had shown earlier [3] that sorption of dipolar ions by sulfonic resins in the hydrogen form is accompanied by transfer of hydrogen ions to the carboxyl groups and conversion of dipolar ions into cations. Sorption of dipolar ions by

carboxylic ions in the hydrogen form also proceeds without acidification of the solution, and therefore it can be represented as follows:



where R_1 is the resin polymer radical; $H_3^+NR_2COO^-$ is the dipolar ion in solution. According to this reaction, sorption of dipolar ions occurs under conditions such that transfer of hydrogen ions from the resin grains into solution is excluded, and this excludes the slowest stage in the sorption of ions by carboxylic resins in the hydrogen form. It is therefore quite clear that dipolar ions, in contrast to cations, are adsorbed by carboxylic resins from neutral solutions. For example, the antibiotic albomycin, which is present in neutral solutions in the form of dipolar ions [4], is adsorbed by KMT carboxylic resin in the hydrogen form ($K_{sw} = 2.15$), the capacity of which is tens of times as great as that of the same resin in the sodium form, because adsorption of dipolar ions by cation exchangers in the salt form is hindered [3]. A similar situation is seen in the sorption of proteins by KMT resin. For investigation of this effect a series of resin specimens was synthesized, and two were selected, of which one had a swelling coefficient of 3.6 in the hydrogen form and the other had the same swelling coefficient in the sodium form. The experiments were performed under static conditions with finely ground resins, settling through water in 15-30 minutes from a height of 20-30 cm. Table 3 shows that most proteins are adsorbed considerably better by carboxylic resins in the hydrogen form than by the corresponding resins in the sodium form.

The above experimental results suggest that the combination of peculiar phenomena observed in the sorption of ions by carboxylic resins in the hydrogen form is primarily associated with retarded diffusion of hydrogen ions from the resin grains into the solution.

SUMMARY

1. The low sorption of cations by carboxylic resins in the hydrogen form is due to the low rate of hydrogen-ion diffusion from the resin into the solution.
2. The specific characteristics of sorption of cations by carboxylic resins apply both to metal ions and to ions of large size.
3. Dipolar ions can be adsorbed by carboxyl resins in the hydrogen form, as this process does not involve transfer of hydrogen ions into solution.

LITERATURE CITED

- [1] H. B. F. Dixon and M. P. Stack-Dunne, *Biochem. J.* 61, 483 (1955).

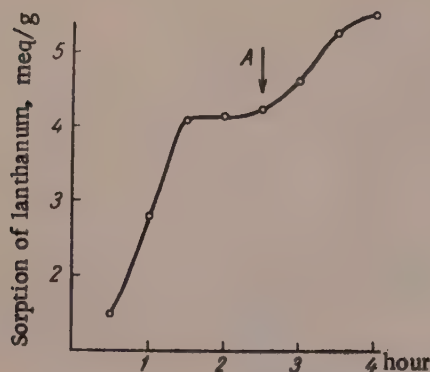


Fig. 3. Sorption of lanthanum by KB-4P-2 carboxylic resin in the hydrogen form: A is the instant of NaCl addition.

TABLE 3

Sorption Capacity for Proteins of Carboxylic Resins in the Hydrogen and Sodium Forms

Protein	Sorption capacity, mg/ g	
	H form of resin	Na form of resin
Serum albumin	120	0
Insulin	156	16
γ -Globulin	140	40
Adrenocorticotropin	160	77
Chymotrypsinogen	284	136

gen form is primarily associated with retarded diffusion of hydrogen ions from the resin grains into the solution.

[2] L. F. Yakhontova, E. M. Savitskaya, and B. P. Bruns, *Proc. Acad. Sci. USSR* 110, 249 (1956);^{*} 111, 338, (1956);^{*} L. F. Yakhontova, in the book: *Investigations in the Field of Ion-Exchange Chromatography* [in Russian] (Izd. AN SSSR, 1957), p. 179.

[3] G. V. Samsonov and N. P. Kuznetsova, *Proc. Acad. Sci. USSR* 115, 351 (1957).^{*}

[4] G. V. Samsonov, L. V. Dmitrenko, A. G. Sirota, M. P. Shesterikova, and S. F. Klikh, *Biochemistry* 23, 220 (1958).

Received April 8, 1958

^{*} Original Russian pagination. See C.B. Translation.

INVESTIGATION OF THE STRUCTUROMECHANICAL AND RHEOLOGICAL PROPERTIES OF UNMODIFIED THICKENERS

A. V. Senakhov and F. I. Sadov

The Moscow Textile Institute

The basic principles of fabric printing have been studied very little as yet. This is especially true of the deformation properties of printing pastes. The general purpose of this investigation was to study the principal deformation characteristics of thickeners and simple model substances, as they determine the corresponding properties of printing pastes.

The existing publications in this field [1-3, etc.] are mainly concerned with viscosimetric studies of the flow of printing pastes and thickeners under different stresses. A common and fundamental defect of the results is that they all apply only to certain arbitrary stress regions, i.e., they correspond only to definite portions of the corresponding-flow curves. The structuromechanical properties of thickeners and printing pastes used in the textile industry have never been studied before.

The investigation of the structuromechanical properties of thickener solutions was based on Rebinder's system of elasticoplasticoviscous properties [4]. This system has been used in a number of investigations in which structuromechanical properties were studied by various methods, including the tangential displacement of a plate in a plane gap [5], and the use of the Shvedov type of rotational instrument [6].

The plate method [7] was used in the present study. The model characteristics E_1 , E_2 , η_1 , η_2 , P_k , and the values of P_{lim} were determined by the plate method with the aid of a disk pulley and weights, described earlier [5]; P_s was measured by the plate method with the aid of calibrated steel dynamometer springs [7]. Aqueous solutions of thickeners were prepared by special techniques which differed for each thickener. The time during which the solutions were kept in cells before the start of the determinations, necessary for complete structuration, also differed for different thickeners, but was not less than 3-4 hours.

Ordinary technical samples of thickeners were used for the investigation.

The sections of the flow curves required for construction of the complete rheological curves were determined by means of a modified Stormer viscosimeter [8].

First, the deformation kinetics of thickener solutions was studied; for this, the shear deformation (ϵ) was plotted against the time (τ) of action of the load (P) at various $P = \text{const} = P_c$.

The kinetic deformation curves $\epsilon(\tau)$ are of a similar character both for a number of high polymers in the condensed state [9] and for their gels and solutions [6] and other disperse systems [5]. The relationship may be represented by the following equation:

$$\epsilon(\tau)_{P_c} = \underbrace{\frac{P_c}{E_1} + \frac{P_c - P_k}{\eta_1}}_{\text{Sh}} \tau + \underbrace{\frac{P_c}{E_2}}_K (1 - e^{-\frac{\tau}{\theta_2}}). \quad (1)$$

Thus equation is valid only for the region of intact internal structure, and it includes all five structuromechanical model characteristics (E_1 , E_2 , η_1 , η_2 and P_k) of Rebinder's system [4] of elasticoplasticoviscous

properties. The first term of Equation (1) describes the deformation component due to the nominal-instantaneous elasticity of the system, the third term represents the component due to elastic aftereffect, and the second term, the component due to plastic flow (relaxation creep) of the system and the corresponding residual deformation.

It should be noted, however, that actually the experimental $\epsilon(\tau)$ curves for real systems represent in each particular instance a definite statistical range of theoretical $\epsilon(\tau)$ curves, characteristic only of the given system [9], and corresponding to a definite number of moduli E and viscosities η . Hence, Equation (1), applied to real systems, is only of an approximate semiquantitative character, and gives the least number of structuro-mechanical characteristics.

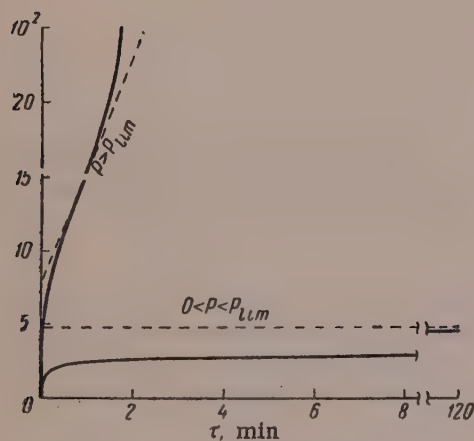


Fig. 1. Deformation $\epsilon(\tau)$ curves for starch gels: ($c = 12\%$, $P_{lim} = 24.7 \cdot 10^3$ dynes \cdot cm^{-2}).

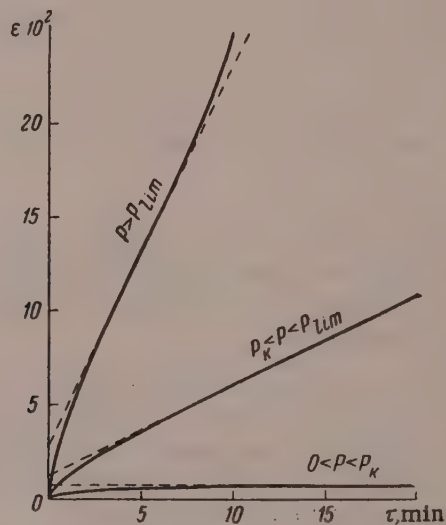


Fig. 2. Deformation $\epsilon(\tau)$ curves for tragacanth gels: ($c = 8\%$, $P_k = 0.429 \cdot 10^3$ dynes \cdot cm^{-2} ; $P_{lim} = 2.07 \cdot 10^3$ dynes \cdot cm^{-2}).

Our $\epsilon(\tau)$ curves may be divided into two main groups. The first includes the curves for starch (Fig. 1) and the second, curves for the other thickeners (Figs. 2 and 3). The main distinction between these groups of curves is that in the case of starch the curve has no inclined linear region corresponding to relaxational creep or plastic flow at constant viscosity η_1 , whereas the curves for all the other thickeners have such regions, commencing at a definite stress $P = P_k$ for each thickener. In the case of starch gels at stresses $P \geq P_{lim}$ the $\epsilon(\tau)$ curves bend upward, to an increasing extent with increases of P . The bends represent regions of rapid breakdown of the gel structure, while the absence of a sloping region on the $\epsilon(\tau)$ curve is indicative of brittle breakdown of structure. The curves for solutions of the other thickeners usually have inclined regions preceding the bends, indicating plastic breakdown of structure.

The presence of inclined linear regions on the $\epsilon(\tau)$ curves, corresponding to relaxational creep* in the stress $P_k < P < P_{lim}$ in the case of solutions of these thickeners, and the absence of such regions in the case of starch gels, indicates that in the former solutions the structure has thixotropic properties, whereas in the case of starch gels the existence of a rigid structural nonthixotropic skeleton must be postulated.

Therefore, whereas in the former case $P_k < P_{lim}$, i.e., breakdown of structure is preceded by plastic deformation, in the second case either P_k is absent altogether, or $P_{lim} < P_k$, i.e., structural breakdown precedes plastic deformation. It follows that plastic deformation of starch gels can be achieved only by irreversible breakdown of the structure. This explains why pure starch gels cannot be used as thickeners. It also follows that the existence of thixotropic properties in solutions of a particular substance may be regarded as one

* The mechanism of which is based on thixotropic buildup of structure in the flow process [4, 5].

criterion of its suitability as a thickener. The structuromechanical characteristics determined by analysis of the $\epsilon(\tau)$ kinetic curves are given in the table.

Dynamometric investigations of the relationship between deformation (ϵ) and stress (P) can give an idea of the elastic properties and the nature of structural breakdown in gels. The values of the "apparent" modulus of elasticity E , determined from the $P(\epsilon)$ curves for the thickener solutions in question, were in all cases intermediate between the values of the corresponding model moduli E_1 and E' (see below). The explanation is that in general the value of the apparent modulus E depends on the loading rate $\dot{\nu} = dP/d\tau$, the value of which in

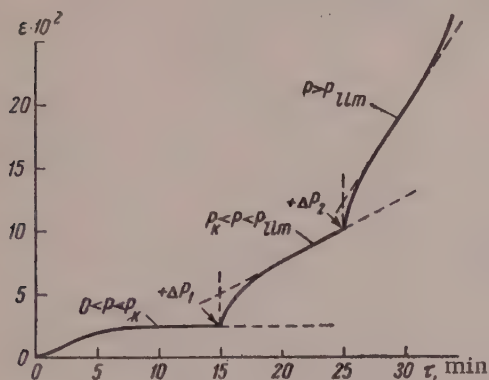


Fig. 3. Deformation $\epsilon(\tau)$ curves for highly concentrated dextrin solutions: ($c = 77\%$, $P_K = 0.672 \cdot 10^3$ dynes \cdot cm $^{-2}$, $P_{lim} = 3.73 \cdot 10^3$ dynes \cdot cm $^{-2}$).

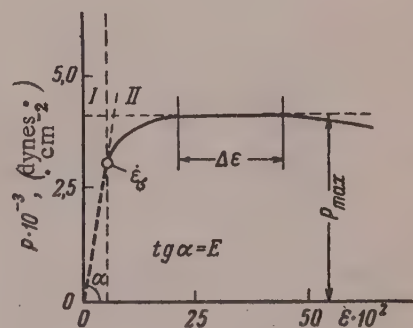


Fig. 4. $P(\epsilon)$ curve for sodium alginate gel: ($c = 18\%$, $E = 2.06 \cdot 10^5$ dynes \cdot cm $^{-2}$, $\epsilon_\sigma = 1.25 \cdot 10^{-3}$ sec $^{-1}$, $P_{max} = 4.34 \cdot 10^3$ dynes \cdot cm $^{-2}$, $\Delta\epsilon = 0.25$).

our case is determined by the rate of lowering of the instrument stage and the modulus of the dynamometer spring used. If $\dot{\nu}$ is so large that only the elastic element E_1 of the structuromechanical model in Fig. 6 has time to react, then $E = E_1$; if $\dot{\nu}$ is so small that both elastic elements E_1 and E_2 have time to react, then $E = E'$. In our case, however, the magnitude of $\dot{\nu}$ is such that element E_1 reacts completely and E_2 only partially, so that $E_1 > E > E'$.

Our $P(\epsilon)$ curves can be divided* into two regions (see Fig. 4; here the form of the $P(\epsilon)$ curve is typical for a number of the investigated gels). The initial, almost linear region apparently corresponds to an undestroyed structure and determines the value of the apparent modulus E . The linear character of this region also represents only a slight variation of the deformation rate $\dot{\epsilon} = d\epsilon/d\tau$, and for all the studied systems $\dot{\epsilon}_\sigma < 1/\theta_2$. Hence, the deformation rate is less than the rate of development of the elastic aftereffects, which corresponds to only partial relaxation of the elastic element E_2 , as mentioned above. Starting at a certain load, the $P(\epsilon)$ curves show a considerable inflection. This second region of the $P(\epsilon)$ curves corresponds to the process of structural breakdown, leading at the break in the curve at $P = P_{max}$ to total breakdown in the structural continuity in the shear plane. This region corresponds to the bends in the $\epsilon(\tau)$ curves.

Thus, the initial region of the experimental $P(\epsilon)$ curve is characterized by a relatively small change of the deformation rate $\dot{\epsilon}$ (as in the $\epsilon(\tau)$ curves, where $\dot{\epsilon}_\infty = \text{const}$ for the region corresponding to the undestroyed structure), while the second region corresponds to abrupt increases of the rate (analogously to the bends in the $\epsilon(\tau)$ curves, where $\dot{\epsilon}$ also increases sharply) and, accordingly, the transition point may be characterized by a certain limiting rate $\dot{\epsilon}$.

The flow plateau $\Delta\epsilon$ for our systems increases with decreasing thickener concentration, while the dynamic yield stress P_s (corresponding to $P = P_{max}$) falls sharply (Fig. 5). The same cause is responsible for these changes of $\Delta\epsilon$ and P_s . The table shows that the index n in Equation (2) (see below) is considerably greater than 2/3.

* This paper contains only a simplified presentation of the results obtained by analysis of the $P(\epsilon)$ dynamometric curves.

This indicates that the degree of structurization of the disperse system should increase with its concentration [10]. Hence, it follows that increase of thickener concentration is accompanied by increase of the structural strength P_s on the one hand, and by increasingly abrupt breakdown of structure on the other. This leads to decrease of fluidity on breakdown of the structure, i.e., decrease of $\Delta \epsilon$.

Influence of Concentration on the Structuromechanical Properties of Aqueous Solutions of Thickeners

Thickener	$c_2, \%$	$E_r \cdot 10^{-5},$ dynes \cdot cm $^{-2}$	$E_s \cdot 10^{-1},$ dynes \cdot cm $^{-2}$	$\eta, 10^{-1},$ poises	$\eta_2 \cdot 10^{-6},$ poises	$P_k \cdot 10^{-3},$ dynes \cdot cm $^{-2}$	$P_{lim} \cdot 10^{-3},$ dynes \cdot cm $^{-2}$	$P_s \cdot 10^{-3},$ dynes \cdot cm $^{-2}$	n
Corn starch	6,0	0,782	0,291	—	1,73	—	5,61	6,08	2,3
	9,0	1,79	0,647	—	4,88	—	12,4	14,9	
	12,0	3,53	1,33	—	10,3	—	24,7	28,5	
	15,0	5,82	2,46	—	16,9	—	40,6	48,0	
	18,0	9,04	3,49	—	27,2	—	61,5	69,7	
Tragacanth	6,0	1,50	0,325	1,79	0,728	0,203	1,02	1,615	2,7
	8,0	2,98	0,702	4,32	1,77	0,429	2,07	3,27	
	10,0	5,15	1,185	7,82	3,25	0,784	3,92	5,86	
	12,0	7,94	1,96	13,75	5,68	1,405	6,62	9,42	
Sodium alginate	12,0	0,513	0,095	0,376	0,112	0,054	0,204	0,248	6,4
	15,0	1,87	0,345	1,76	0,469	0,229	1,05	1,20	
	18,0	5,42	1,02	4,92	1,475	0,745	3,38	4,34	
	21,0	15,45	3,07	15,6	3,52	2,31	10,3	13,7	
Fruit gum	17,0	1,99	0,249	1,07	0,448	0,162	0,408	0,905	4,2
	20,0	3,73	0,499	2,21	0,887	0,342	0,852	1,56	
	23,0	6,70	1,015	3,74	1,765	0,594	1,45	3,04	
	26,0	11,15	1,63	6,38	2,74	0,973	2,35	4,52	
Na-CMC**	24,0	4,72	1,03	2,48	1,49	0,0036	0,043	—	9,1
	27,0	12,2	2,83	7,54	3,89	0,011	0,129	—	
	30,0	29,4	7,28	21,5	11,25	0,028	0,337	—	
	32,5	64,4	15,4	46,9	23,3	0,061	0,737	—	
	35,0	137,0	33,8	113,5	49,6	0,137	1,45	—	
Dextrin***	68,0	0,989	0,070	1,025	0,236	0,089	0,472	—	14,9
	71,0	1,78	0,149	2,13	0,522	0,194	0,946	—	
	74,0	3,77	0,295	4,48	0,973	0,354	1,88	—	
	77,0	7,03	0,566	8,07	1,99	0,672	3,73	—	

* The values of c_2 are concentrations of the air-dry substances in solution, with the following moisture contents: starch 12.6%, tragacanth 11.9%, sodium alginate 14.4%, CMC 12.2%, dextrin 9.18%. It is easy to show that the value of n is not changed if c_2 is expressed as bone-dry substance rather than air-dry.

** Sodium carboxymethylcellulose.

*** The structuromechanical characteristics of dextrin solutions were determined by stepwise loading (see Fig. 3).

Fluidity at rupture may be regarded as a process of plastic rupture in the flow regime, or ductility [11]. Pezold [12], Shikher [1] and others have studied ductility as a characteristic of the plastic properties of thickener solutions. The maximum length of a thread of thickener solution, which they took as the measure of ductility probably corresponds in our case to the flow of plateau $\Delta \epsilon$. Since P_s decreases and $\Delta \epsilon$ increases with falling concentration, while the reverse effects are observed with increasing concentration, it is to be expected that the maximum ductility would be found at a certain definite ratio of P_s to $\Delta \epsilon$, corresponding to a definite degree of structurization of the system, i.e., at a certain optimum concentration of the thickener.

All the investigated thickeners can be divided into three groups in accordance with the extent of the plateau $\Delta \epsilon$. In the case of starch gels this plateau is virtually absent, which indicates a brittle type of rupture (without ductility). For solutions of sodium alginate, fruit gum, and tragacanth the plateau $\Delta \epsilon$ is appreciable

but finite, which indicates plastic rupture (i.e., the existence of definite ductility). For CMC and dextrin solutions the limits of the $\Delta\epsilon$ plateau could not be determined with the instrument used; this indicates that solutions of these thickeners have high ductility.

It has been shown for a number of disperse systems [13, 14] that variations of strength and apparent modulus of elasticity with concentration conform to a parabolic equation over a fairly wide concentration range.

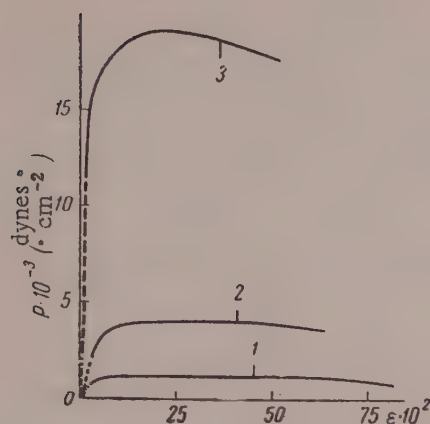


Fig. 5. $P(\epsilon)$ curves for sodium alginate gels: 1) $c = 15\%$, $E = 0.58 \cdot 10^5$ dynes \cdot cm^{-2} , $\dot{\epsilon}_\sigma = 0.81 \cdot 10^{-3}$ sec^{-1} ; 2) $c = 18\%$, $E = 2.06 \cdot 10^5$ dynes \cdot cm^{-2} , $\dot{\epsilon}_\sigma = 1.25 \cdot 10^{-3}$ sec^{-1} ; 3) $c = 21\%$, $E = 6.83 \cdot 10^5$ dynes \cdot cm^{-2} , $\dot{\epsilon}_\sigma = 1.12 \cdot 10^{-3}$ sec^{-1} .

All our thickener solutions conform to this equation over the concentration ranges studied. The results indicate that the parabolic equations for the different structuromechanical characteristics all have a common index. Its values for solutions of the investigated thickeners are given in the table.

Thus, we may write for solutions of each of the investigated thickeners:

$$X = X' c_2^{\underline{n}}, \quad (2)$$

where X' is a structuromechanical characteristic (E_1 , E_2 , η_1 , η_2 , P_K , P_{lim} , P_s); X' is the corresponding proportionality factor; \underline{n} is the index common for all X ; c_2 is the thickener concentration in the gel.

The value of the index \underline{n} in Equation (2) is a measure of the number of elementary particles in the system capable of coming in contact with each other under the given conditions with formation of a continuous structural network [10]. The values of X are, in general, probably associated with the activation energy of the gelation process [14]. The latter may be regarded as the activation energy of synergetic reinforcement of the structural network, which ultimately leads to syneresis of the gel.

Our characteristics of the mechanical properties of the structure in solutions of various thickeners can be represented with the aid of appropriate structuromechanical models [9, 15]. Two different types of model are applicable in our case: for starch gels (Fig. 6, 1) and for solutions of the other thickener (Fig. 6, 2). The presence of element Pl indicates that the internal structure of the system has thixotropic properties, and the system as a whole is plastic. The part of the model denoted by Sh corresponds to the model of a Shvedov body,* and

* The element Sh in the model is only a part of the Shvedov type model [16]. This also applies to the corresponding terms in Equation (1).

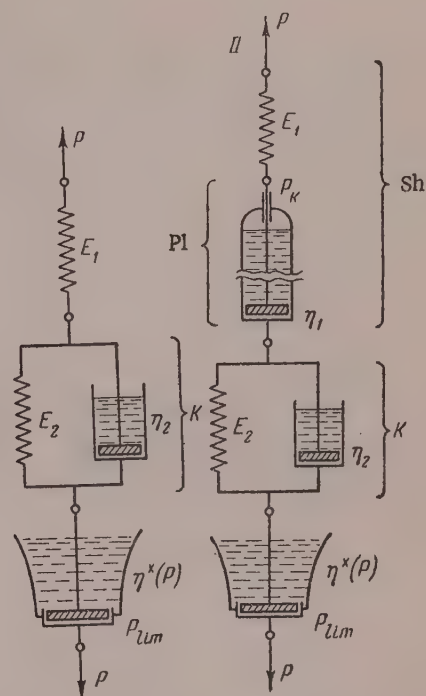


Fig. 6. Structuromechanical models of: 1) starch gels; 2) gel solutions of the investigated thickeners.

is represented by the part of Equation (1) marked similarly; the other part of the same model, denoted by K, corresponds to the model of a Kelvin-Voigt body and is represented by the part of Equation (1) marked K. Here E_1 represents the modulus of nominally instantaneous elasticity; E_2 and η_2 are the modulus and viscosity of elastic aftereffects; η_1 is the relaxational creep viscosity; P_k is the upper elastic limit or true fluidity limit, corresponding to Shvedov's residual stress [16]; P_{lim} is the static yield value; $\eta^*(P)$ corresponds to the region of structural breakdown accompanied by decrease of viscosity.

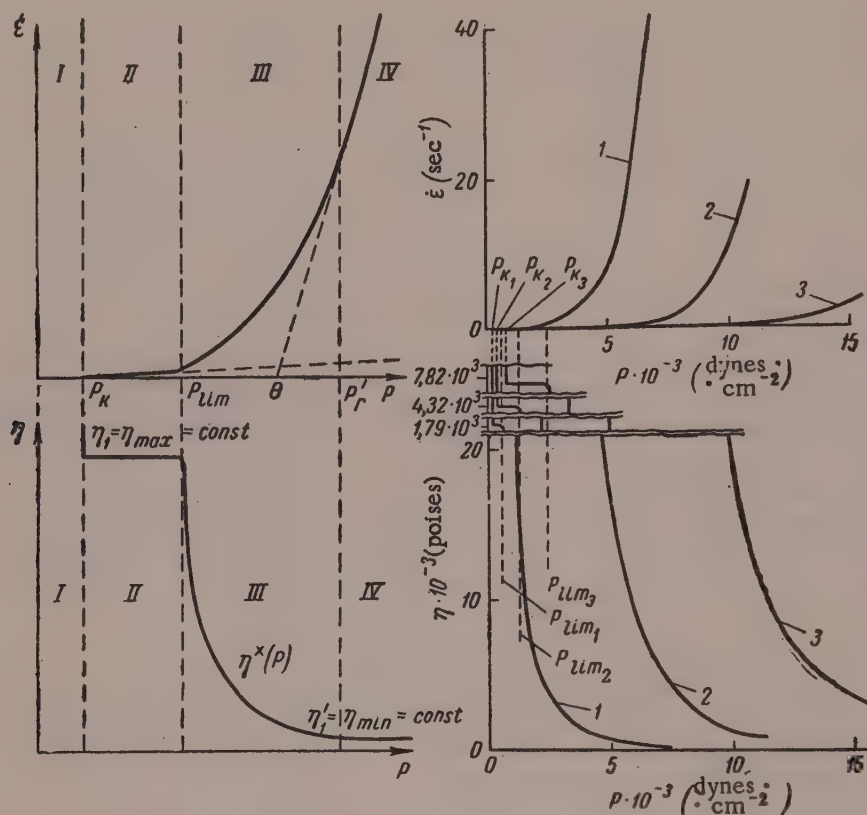


Fig. 7. Schematic typical rheological curves for the thickener solutions studied (a) and rheological curves for tragacanth gels (b) at concentrations: 1) 6%; 2) 8%; 3) 10%.

The values of P_k and P_{lim} establish the boundaries between relaxation regions of different type. Since the values of the indices \underline{n} in Equation (2) for solutions of different thickeners were the same for different structuromechanical characteristics, it follows that various relationships between the latter, such as the lag time $\vartheta_2 = \eta_2 / E_2$, the periods of elastic and true relaxation $\vartheta^* = \eta_2 / (E_1 + E_2)$ and $\vartheta^1 = \eta_1 / E^1$ (where E^1 is the effective modulus, equal to $\frac{1}{1/E_1 + 1/E_2}$ and corresponding to maximum extension of both springs, E_1 and E_2), the elasticity $\lambda = E_1 / (E_1 + E_2)$, and the ratio P_{lim} / P_k which determines the relative magnitude of the region of relaxational creep, are independent of the concentration of a given thickener and are characteristic quantities for it.

The rheological curves for all the thickener solutions with the exception of starch are all of the same type and their common features may be represented by means of the schematic $\dot{\epsilon}(P)$ and $\eta(P)$ curves in Fig. 7, a.

It follows from Fig. 7, a that the entire load region can be divided into three regions separated by the limiting stresses P_k and P_{lim} .

Region I for $0 < P < P_k$ corresponds to elastic deformation, i.e., $\dot{\epsilon}(P) = 0$, $\eta(P) = \infty$.

Region II for $P_k < P < P_{lim}$ corresponds to plastic deformation taking place as the result of relaxational creep at constant maximum viscosity $\eta = \eta_1$. This region of the flow curve conforms to the Bingham equation: $P - P_k = \eta_1 \dot{\epsilon}$ and corresponds to the inclined linear regions of the $\epsilon(\tau)$ curves. In this case the value of P_k must be taken into account because the corresponding energy is not dissipated in the course of viscous flow, but is expended in maintaining certain limiting elastic stresses in the structural network, which ensure the creep process. Therefore, such flow must be regarded as true plastic flow.

Region III for $P_{lim} < P < P_r$ characterizes the breakdown of the coherent structure and its fragments in flow, which corresponds to a sharp drop of viscosity $\eta^*(P)$. Since the coherent structure is broken down here (when the steady state is reached), there should be no expenditure of energy for maintenance of elastic stresses in the structural network, corresponding to P_k , and therefore this region of the flow curve should conform to the equation: $P = \eta^* \dot{\epsilon}$, where the viscosity $\eta = \eta^*$ is variable. In Region III the flow curve corresponds to the bends on the $\epsilon(\tau)$ curves.

Region IV for $P > P_r$, corresponding to plasticoviscous flow at constant and least viscosity $\eta = \eta_1'$, when all the structural elements should be ultimately broken down, and where flow conforms to the Bingham equation in the form $P - \theta = \eta_1' \dot{\epsilon}$, was never attained in our experiments.

The rheological curve for starch gels differs from the curves for the other thickeners by absence of P_k , i.e., absence of a region of plastic flow, and a considerably sharper fall of viscosity in Region III.

In accordance with these structuromechanical models and the nature of the rheological curves, all the systems studied may be qualitatively divided into elasticobrittle, described by the characteristics: E_1, E_2, η_2 and P_{lim} (starch gels), and elasticoplastic, described by the characteristics: $E_1, E_2, \eta_1, \eta_2, P_k$ and P_{lim} (solutions of the other thickeners).

SUMMARY

1. The structuromechanical and rheological properties of solutions of a number of thickeners have been investigated, the structuromechanical characteristics and the corresponding models for the thickener solutions have been determined, and their rheological curves have been plotted.
2. In contrast to the other thickeners studied, plastic deformation of nonmodified starch gels can be effected only by irreversible breakdown of their internal structure. This explains why pure starch gels cannot be used as thickeners.
3. The existence of thixotropic properties in a solution of a given thickener may be regarded as one of the main criteria of its suitability for thickening. In the present instance the main factor determining the plasticity of a system is its degree of thixotropy.
4. For solutions of each thickener there is a definite optimum concentration, corresponding to a definite degree of structurization of the system at which the system has maximum ductility.
5. All the structuromechanical characteristics of the investigated solutions increase with concentration in accordance with a parabolic law. For each of the thickeners investigated the index \underline{n} in the equation $X = X^* C_2^{\underline{n}}$ is common for the different structuromechanical characteristics X , which shows that the various relationships between the structuromechanical characteristics do not change with concentration, and are therefore characteristic values for each thickener.
6. Since the index \underline{n} in the equation $X = X^* C_2^{\underline{n}}$ is the same for the different structuromechanical characteristics X , and since in all cases studied \underline{n} is greater than $2/3$, for comparison of solutions of the same or of different thickeners it is permissible to use the concept of "degree of structurization", which corresponds to the relative proportion of particles forming the structural network at the given thickener concentration in solution.
7. Thickeners suitable for practical use have a common structuromechanical model and similar rheological properties. They differ only in the values of the characteristics.

LITERATURE CITED

- [1] M. G. Shikher, J. Appl. Chem. 18, 329 (1945); 19, 542 (1946).
- [2] S. N. Glarum, Amer. Dyestuff Reporter 23, 175 (1934); 25, 150 (1936); 26, 33 (1937); 26, 124, 437 (1937); 27, 303 (1938).
- [3] A. I. Maklashin, Bull. Higher Educ. Establishments - Text. Technology No. 1, 155 (1957).
- [4] P. A. Rebinder and E. A. Segalova, Proc. Acad. Sci. USSR 71, 85 (1950).
- [5] P. A. Rebinder and E. E. Segalova, Colloid J. 10, 223 (1948).
- [6] P. A. Rebinder and A. S. Kolbanovskaya, Colloid J. 12, 194, 208 (1950).
- [7] P. A. Rebinder and S. Ya. Veiler, Proc. Acad. Sci. USSR 49, 354 (1945).
- [8] Stormer, Trans. Amer. Ceram. Soc. 11, 597 (1909).
- [9] T. Alfrey, Mechanical Behavior of High Polymers (IL, Moscow, 1952) [Russian translation].
- [10] Yu. S. Zuev, Colloid J. 12, 36 (1950).
- [11] W. Reif, Melland Textilber 33, 532 (1952).
- [12] E. W. Pezold, Melland Textilber 17, 222, 330 (1936).
- [13] E. W. Mardless, Trans. Faraday Soc. 19, 118 (1923); H. I. Poole, Trans. Faraday Soc. 21, 114, (1925); L. H. Lampitt and R. W. Money, J. Soc. Chem. Ind. 55, 88 (1936); 56, 290 (1937); 58, 29 (1939), etc.
- [14] H. Braune and I. Richter, Koll.-Z. 113, 20 (1949).
- [15] J. M. Burgers, in the Book: First Report on Viscosity and Plasticity, 2nd edn. (Amsterdam, 1939); M. Reiner, Ten Lectures on Theoretical Rheology (GITTL, Moscow-Leningrad, 1947) [Russian translation].
- [16] F. N. Shvedov, J. de phys. theor. et appl. 2, 8, 341 (1889).

Received December 24, 1957

STRESS-STRAIN, HIGH-ELASTIC, AND VISCOUS PROPERTIES OF RUBBER SOLUTIONS

A. A. Trapeznikov and T. V. Assonova

Institute of Physical Chemistry, Academy of Sciences, USSR
Laboratory of Oleocolloids and Monolayers, Moscow

The structure of high-polymer particles, their flexibility, and interaction among themselves and with the solvent, have a pronounced influence on solution viscosity, which has been studied fairly extensively [1]. The high-elastic properties of polymer solutions have been studied much less, and the experiments in such cases were performed at relatively low shear stresses and small deformations [2, 3]. Methods used in investigations of solid polymers involve deformation to failure of the specimen [4, 5]. As reported earlier [6], a new feature is a study of analogous relationships for solutions and gels of high polymers and other fluid colloidal systems, and determination of the maximum deformations for them.

Fluid solutions of high polymers are distinguished by high rates of relaxation. Therefore, investigations of the strength characteristics of such systems must be conducted at high rates of deformation $\dot{\epsilon}$, exceeding the relaxation velocity of the system v_{rel} or, more precisely, the condition $\dot{\epsilon} > v_{rel} \cdot \epsilon_{ki}$, where ϵ_{ki} is the critical elastic deformation for the i -th element of the structure [7], must be satisfied. Under such conditions, and if the range of structural elements lies within fairly narrow limits of ϵ_{ki} and $\Phi_i = 1/v_{rel}$, the strength is revealed in the form of the maximum $P = P_r$ on the stress-strain $P(\epsilon)$ curves, which is found at the breaking strain $\epsilon = \epsilon_r$.

Much interest attaches to direct measurement of the maximum elastic (reversible) deformation in polymer solutions and gels over the entire $P(\epsilon)$ curve. It is known that molecules of linear polymers in the unstressed state consist of tangled coils which assume a threadlike shape on deformation. Determination by a direct method of the maximum reversible deformability of the molecular network in solutions and gels gives an indication of the degree of uncoiling of the molecules or chains in the network, their effective length, and degree of asymmetry.

Our investigations of the stress-strain characteristics of rubber solutions were performed with the aid of specially designed instruments; a multiple elastoviscosimeter with oscillographic recording [8] and an elastorelaxometer (model 2) designed for direct measurement of large elastic deformations [9]

It was found that $P(\epsilon)$ curves for rubber solutions have much in common with $P(\epsilon)$ curves for solid rubbers [4, 5], although they differ in the magnitude of the stresses and breaking strains.

Figure 1 shows $P(\epsilon)$ curves for 4% solution of natural rubber (pale crepe), in decalin,* recorded by means of the oscillographic elastoviscosimeter. It is seen in Fig. 1 that both P_r and ϵ_r increase with $\dot{\epsilon}$, and at $\dot{\epsilon} = 4762 \text{ sec}^{-1}$, ϵ_r is 9600%. This is in agreement with the results of earlier investigations on rubber and polyisobutylene [6, 10].

* In this and in all the preceding investigations [6-10] decalin supplied by Kommunalwirtschaftsunternehmen der Stadt Eisenach - Chemische Fabrik, was used, of $d = 0.877$, and b. p. 188° . This decalin was not subjected to additional purification.

In order to obtain $P(\epsilon)$ curves of the correct shape and correct values of ϵ_r and P_r it is important that the deformation rate of the system $\dot{\epsilon}$ should reach a constant value almost as soon as the outer cylinder begins to rotate, i.e., from the instant the electromagnetic starter is switched on. Oscillographic traces of the angle of rotation of the outer cylinder relative to the inner cylinder, as a function of time, show that at $\dot{\epsilon} < 1400 \text{ sec}^{-1}$ the rotation rate may be assumed constant almost from the start of the curve, i.e., it becomes steady within a few degrees or fractions of a degree. At higher rates $\dot{\epsilon} = 3000\text{--}5000 \text{ sec}^{-1}$ during the first instants after the magnetic clutch is connected the rate lags somewhat behind the steady rate, owing to inertia of the outer cylinder and the lid of the magnetic clutch, and slippage of the latter. The lag increases with increase of $\dot{\epsilon}$.

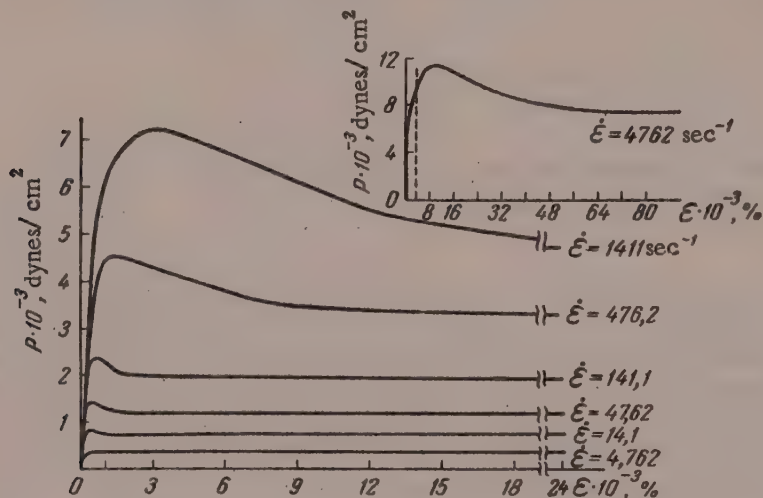


Fig. 1. $P(\epsilon)$ curves for different values of ϵ for 4% rubber solution in decalin.

However, at a high enough $\dot{\epsilon} = 4762 \text{ sec}^{-1}$ a constant value of $\dot{\epsilon}$ is reached starting from $\epsilon = 3800\%$ (in Fig. 1 this boundary is indicated by a dash line), i.e., long before $\epsilon_r = 9600\%$, and at $\epsilon = 2100\%$ the value of $\dot{\epsilon}$ is only 25% below the steady value. Thus, the form of the $P(\epsilon)$ curve and the values found for ϵ_r and P_r differ relatively little from the true values.

$P(\epsilon)$ curves for natural-rubber solutions, after passing through a maximum $P = P_r$, fall to $P = P_s$, which corresponds to steady flow of the system as a viscous liquid. At the initial stage of deformation the system behaves like a "solid" body [11]. However, this behavior of the system as a "solid" can occur at $\dot{\epsilon} > \dot{\epsilon}_k$ [6, 7].

A feature of great interest is the correspondence in the positions of $\epsilon_r(P_s)$ and $\dot{\epsilon}(P_s)$ curves for rubber solutions (Fig. 2), analogous to that found earlier [6, 7]; it follows that transition into the region of rapidly increasing ϵ (anomalous viscosity) is due not so much to particle orientation in steady flow as to stretching of the particles and breakdown of structure before the transition to steady flow, as a result of which the viscosity $\eta = P_s / \dot{\epsilon}$ decreases (Fig. 3). Figure 2 also shows $P_r(\dot{\epsilon})$ curves. The region between the $P_r(\epsilon)$ and $P_s(\dot{\epsilon})$ curves gives an indication of the thixotropic properties (strength thixotropy) of rubber solutions [6, 12]. The degree of thixotropic breakdown increases with increase of rubber concentration in the solution.

In Fig. 4 the function $\epsilon_r(\dot{\epsilon})$ is plotted for three concentrations of rubber solutions. The values of ϵ_r for these solutions are similar, and therefore a single common curve is drawn. Approximately it may be assumed that the function $\epsilon_r(\dot{\epsilon})$ for rubber solutions is the same for all concentrations in the range of 4–10%, which is a matter of definite interest. From earlier data on aluminum naphthenate [13] an appreciable decrease of ϵ_r with increase of solution concentration (c) might be expected. Evidently the difference between the $\epsilon_r(c)$ relationship for naphthenate and rubber solutions respectively is associated with differences in their structures. In the former case fairly stable cross links, i.e., resistant to relaxation, are formed, while in the latter they are relatively unstable and less numerous. Intertwining does not play an important part in this case, as the molecules are not branched and slide relatively easily among each other. Therefore, the observed $\epsilon_r(\dot{\epsilon})$ relationship for rubber solutions is probably determined mainly by the relaxational properties of the chains

themselves and not relaxational breakdown of cross links at low $\dot{\epsilon}$. However, it is difficult to give a more detailed explanation of this relationship at present, as there are not enough experimental data as yet.

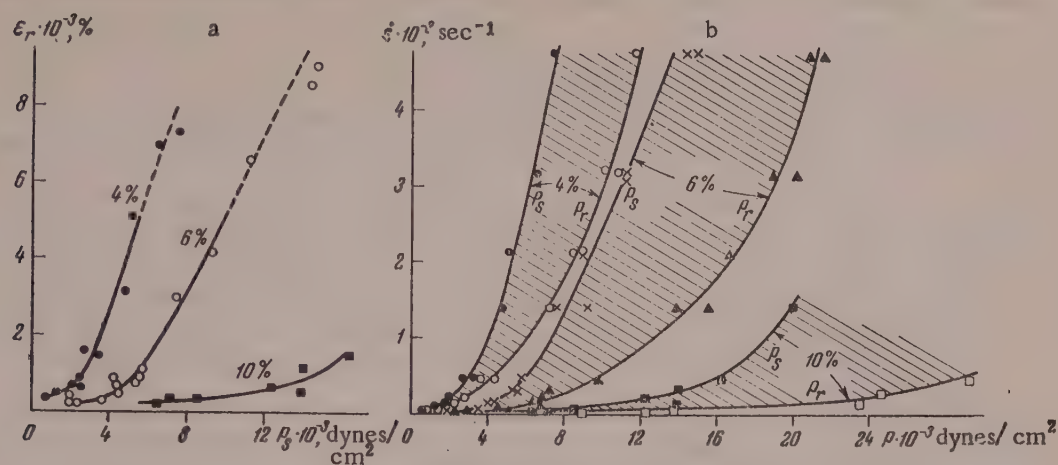


Fig. 2. $\epsilon(P_s)$ curves (a) and $P_s(\dot{\epsilon})$ and $P_r(\dot{\epsilon})$ curves for 4, 6, and 10% solutions of rubber in decalin (b).

It is important in principle to clarify the nature of the breaking strain ϵ_r , or its subdivision into the reversible (high-elastic) ϵ_e and residual ϵ_v portions. This was done with the aid of the elastorelaxometer, in which ϵ_e could be varied with automatic stopping of the outer and release of the inner cylinders in the

range up to $\epsilon = 1100 \text{ sec}^{-1}$. The relationship $\epsilon_e(\epsilon)$ for 4% solution at two values of $\dot{\epsilon}$, equal to 143 and 1142 sec^{-1} respectively, is plotted in Fig. 5. The existence of maxima on the curves and the decrease of elastic deformation prove that the structure of the solution is broken down. If only particle orientation took place, to which the decrease of viscosity in such solutions is commonly attributed, then the elastic deformation (recoil) should increase to a limit corresponding to maximum orientation in steady flow and the greatest possible contraction of the particles during coiling on removal of the load.

It is clear from Fig. 5 that at $\dot{\epsilon} = 143 \text{ sec}^{-1}$ the value of $\epsilon_{e \text{ max}} = 770\%$ and at $\dot{\epsilon} = 1142 \text{ sec}^{-1}$ $\epsilon_{e \text{ max}} = 1100\%$. Here the deformations ϵ_m are 4000 and 5400% respectively. It follows that at these values of $\dot{\epsilon}$ the residual deformations $\epsilon_v = \epsilon_r - \epsilon_e$ are 3230 and 4300% respectively.

Comparison of the data in Figs. 1 and 5 shows that $\epsilon_r \ll \epsilon_m$, for both deformation rates, although ϵ_r increases much more rapidly than ϵ_m with increase of (see Fig. 4). Therefore, the deformations ϵ_m at which the maximum recoils $\epsilon_{e \text{ max}}$ are

attained (in these cases) exceed considerably the deformations ϵ_r corresponding to the maximum stresses P_r which determine the strength of the structure. This result is in agreement with the result obtained for naphthenates with incompletely restored structure [14].

In accordance with the earlier concept of the range of structural elements in a system characterized by different ϵ_{kl} and Φ_1 , and corresponding, largely independent, distribution functions, it may be assumed that the maxima P_r correspond to a certain group of structural elements corresponding to a given ϵ_r at a given $\dot{\epsilon}$. A stress equal to the maximum $P = P_r$ is required to overcome the resistance to deformation and breakdown of the bonds belonging to the given group of structural elements. However, the fact that after this yield point of structure has been passed the recoil does not fall but continues to rise shows that longer,

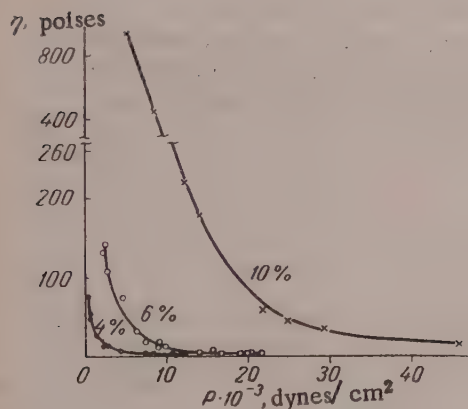


Fig. 3. Variations of viscosity with shear stress for 4, 6, and 10% solutions of rubber in decalin.

elastically deformed structural elements remain undestroyed in the system. However, the number of such longer structural elements (at a given $\dot{\epsilon}$) is probably relatively small, and therefore the total stress P which develops in their deformation to $\epsilon = \epsilon_m$ is less than P_r . The increase of the absolute value of $\epsilon_{e \max}$ on increase of $\dot{\epsilon}$ is due to the fact that the more mobile and longer structural elements no longer have time to relax irreversibly and lose a greater proportion of their deformation in the elastic form. At the same time the relative role of

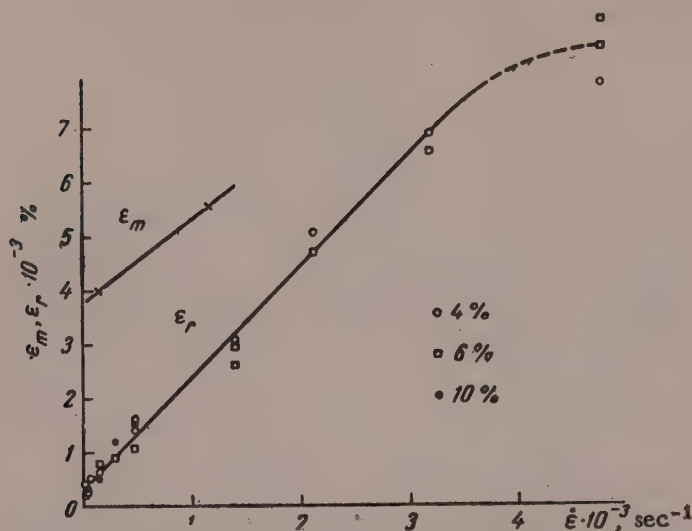


Fig. 4. The $\epsilon_r(\dot{\epsilon})$ relationship for 4, 6, and 10% solutions of rubber in decalin, and $\epsilon_m(\dot{\epsilon})$ for 4% solution of rubber in decalin.

these long structural elements in the total magnitude of the breaking stress evidently increases, as this strain not only increases, which might have been due to the usual influence of $\dot{\epsilon}$, but is displaced toward higher $\epsilon = \epsilon_r$, i.e., the stress maximum is transferred to the longer structural elements, which are broken down in

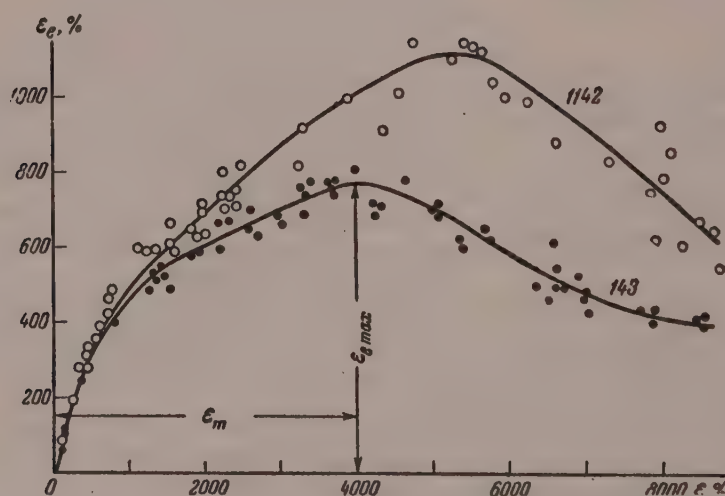


Fig. 5. $\epsilon_e(\epsilon)$ curves for 4% solutions of rubber in decalin at $\dot{\epsilon}$ of 143 and 1142 sec^{-1} .

larger numbers. With increase of $\dot{\epsilon}$ relaxational flow and residual deformation ϵ_v (which arises before the transition to $P = P_g$) should diminish, and therefore the relative proportion of ϵ_e in the total value of ϵ_m increases.

At the same time it should be remembered that actual detection of such large recoils as the values of ϵ_r or ϵ_m at high $\dot{\epsilon}$ may involve difficulties in principle. Contraction of elastically deformed "long" structural elements occurs in a medium of shorter structural elements, formed partially as the result of breakdown of the structure and having a definite viscosity. The overcome viscous resistance takes time, during which irreversible relaxation may take place, and in consequence the recoil determined by the long structural elements greatly decreases. Therefore ϵ_e in such systems, even at the highest $\dot{\epsilon}$, may prove considerably less than ϵ_r .

The need for very high $\dot{\epsilon}$ in order to extend the coiled rubber molecules and to reveal large breaking and elastic deformations is attributable to weakness of the van der Waals forces acting between the rubber molecules in solution, which ensure easy relaxation. On the other hand, the existence of P_r conclusively confirms the presence of such interaction in solutions of linear polymers. The stronger interaction in the network consisting of threadlike particles in aluminum naphthenate gels, due to the polar character of the bonds, leads to relaxation rates which, although are not very low, are considerably lower than in rubber solutions.

Indeed, vulcanization of rubber, which leads to the formation of very strong cross links and a fairly stable network, greatly increases the relaxation time of the system and consequently increases the recoil ϵ_e up to values of the order of ϵ_m or to values of ϵ_r characteristic of a nonvulcanized solution at the highest $\dot{\epsilon}$ [10].

SUMMARY

1. The stress-strain and viscosity characteristics of 4, 6, and 10% solutions of natural rubber in decalin (not subjected to special purification) have been studied with the aid of stress-strain curves determined by means of an elastoviscosimeter with an oscillographic recording device, in the range of deformation rates from 14 to 5000 sec^{-1} .

2. The stress-strain curves for rubber solutions pass through maxima corresponding to the strength of the structure before the stage of steady flow is reached; they are analogous in form to stress-strain curves for solid rubber.

3. Reversible (high-elastic) deformation at deformation rates of 143 and 1142 sec^{-1} has been measured in 4% rubber solution by means of the elastorelaxometer. The maximum values of the recoil are 770 and 1100% respectively and are found at deformations ϵ_m considerably exceeding the breaking strains ϵ_r corresponding to the stress maximum P_r .

4. For rubber solutions of different concentrations ϵ_r increases linearly with the deformation rate $\dot{\epsilon}$. This relationship may be represented by a common curve.

These properties reflect the existence of a structure and its breakdown in rubber solutions, determined by van der Waals forces, and the formation of weak relaxing network cross links. At the same time, Point 4 above indicates that the relaxational properties of the rubber chains themselves play the predominant role.

LITERATURE CITED

- [1] W. Philippoff, *Viscosität der Kolloide*, (Dresden, 1942).
- [2] A. S. Kolbanovskaya and P. A. Rebinder, *Colloid J.* 12, 194 (1950).
- [3] M. P. Volarovich and L. Ya. Ginzburg, *Colloid J.* 14, 20 (1952).*
- [4] T. Alfrey, *Mechanical Behavior of High Polymers* (IL, 1952) [Russian translation].
- [5] Yu. S. Lazurkin and R. L. Fogel'son, *J. Tech. Phys.* 21, 267 (1951).
- [6] A. A. Trapeznikov, *Colloid J.* 12, 67 (1950); *Proc. All-Union Conf. on Colloid Chem.* [in Russian] (Kiev, 1952) p. 175; A. A. Trapeznikov and V. A. Fedotova, *Proc. 3rd All-Union Conf. on Colloid Chem.* [in Russian] (1956) p. 65; V. A. Fedotova, *Candidate's Dissertation* [in Russian] (Inst. Phys. Chem. Acad. Sci. USSR, Moscow, 1957).

* Original Russian pagination. See C.B. Translation.

- [7] A. A. Trapeznikov, Proc. Acad. Sci. USSR 102, 1177 (1955); Colloid J. 18, 496 (1956).*
- [8] T. G. Shalopalkina and A. A. Trapeznikov, Proc. Acad. Sci. USSR 118, 994 (1958).*
- [9] A. A. Trapeznikov, Colloid J. 21, 108 (1959);* Instruments and Tech. Expt. No. 3, 994 (1958).
- [10] A. A. Trapeznikov and T. V. Assonova, Colloid J. 20, 398 (1958).*
- [11] A. A. Trapeznikov and T. G. Shalopalkina, Colloid J. 17, 471 (1955).*
- [12] A. A. Trapeznikov and V. A. Fedotova, Proc. Acad. Sci. USSR 95, 595 (1954).
- [13] V. A. Fedotova and A. A. Trapeznikov, Proc. Acad. Sci. USSR 120, 841 (1958).*
- [14] A. A. Trapeznikov, Colloid J. 20, 476 (1958).*

Received March 15, 1958

* Original Russian Pagination. See C.B. Translation.

ELECTROCHEMICAL STUDIES OF BENTONITE SUSPENSIONS

4. POTENTIOMETRIC TITRATION OF DIFFERENT ACID FORMS OF ASKANGEL*

I. A. Uskov and E. T. Uskova

The T. G. Shevchenko University, Kiev
Ukrainian Academy of Agricultural Sciences

There have been numerous studies of the acid forms of bentonite [1]. However, the existing data on the nature of the acid-determining ions adsorbed by montmorillonite are far from adequate for definite conclusions. The main reason is that the methods generally used for preparation of acid forms of clays (electrodialysis and, less often, leaching of clays by dilute solutions of mineral acids) do not yield clays with cations replaced by hydrogen only [2].

In such acid forms of bentonite most of the adsorbed ions are Al ions [1, 2]; this, as we showed earlier [4, 5] is the cause of the anomalous results obtained in titration of such bentonites. For example, the cation-exchange capacity, determined from the titration curves, varies with the time of interaction with the base and with the nature of the base.

Such deviations should not occur in titration of bentonites containing mainly hydrogen ions as the acid-determining ions.

Two different methods can be used for preparation of H-bentonite: treatment of the bentonite by concentrated mineral acid, followed by rapid washing out of excess acid, and treatment in a column containing a resin in the H form [3].

In the present investigation, acid forms of bentonite prepared by these two methods were studied by means of potentiometric titration.

For comparison of the results with data for electrodialed askangel we studied the influence of suspension concentration on the form of the titration curves.

Influence of Suspension Concentration on the Nature of the Titration Curves for Electrodialyzed Askangel

The investigations were performed with electrodialed askangel samples kept for 4 months after electro-dialysis. The capacity of these samples was 830 microequiv/g. The pH was determined by the method described previously [4].

The titration results are plotted in Fig. 1. It is clear from Fig. 1 that as the suspension concentration increases the initial region of the titration curve is lowered and the final region raised. All the curves have the same characteristic inflection point in the weakly alkaline pH region; its position depends on the suspension concentration: it is displaced into the regions of smaller amount of bound base with increase of concentration. At the same time the inflection becomes more distinct and steeper.

* Presented at the 4th All-Union Conference on Colloid Chemistry in Tbilisi, 1958.

Increase of the suspension concentration leads to an abrupt increase of pH on addition of the first portions of alkali, and to a steeper rise of the first flat portion of the curve.

The concentration of the potential-determining ions increases with increase of the suspension concentration. In the case of electrolyzed bentonite these are evidently aluminum and hydrogen ions. Increase of their concentration results in a sharp rise of pH near the equivalence point. This rise of pH becomes even more prominent as the alkali concentration is also higher in titration of more highly concentrated suspensions (the abscissa axis shows the amounts of alkali added to the suspension, calculated per g of dry substance, and not the volume of alkali added). Increase of alkali concentration intensifies the influence of the excess reagent on dissociation of the sodium salt of bentonite. Therefore, in titration of more highly concentrated suspensions the rise of pH near the equivalence point becomes greater and the titration curve has a sharper inflection.

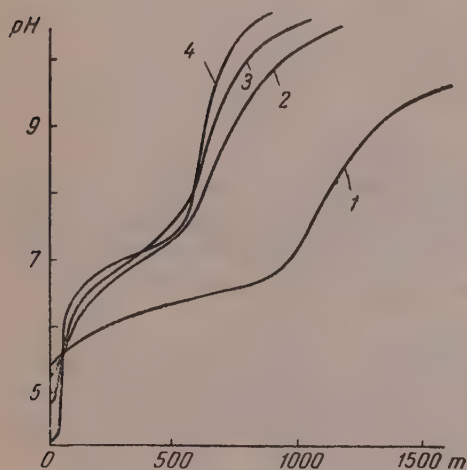


Fig. 1. Potentiometric titration of a suspension of electrolyzed askangel by caustic soda (m is the amount of NaOH in meq added per g of bentonite): suspension concentration: 1) 0.029%; 2) 0.19%; 3) 0.29%; 4) 2.7%.

Therefore, potentiometric curves can be compared within a definite concentration range of the suspensions, namely from 0.5 to 3%.

Investigation of Hydrogen Askangel

The high content of water-soluble salts in native askangel, in addition to the chlorides formed from the calcium and magnesium carbonates present in the mineral by the action of hydrochloric acid, may account for the incomplete replacement of the adsorbed cations by hydrogen. Therefore, we preferred to use electrolyzed bentonite, free from these salt impurities.

The hydrogen-substituted sample was prepared as follows. A 5% suspension of electrolyzed bentonite was diluted with an equal volume of 2 N HCl and immediately centrifuged in a continuous supercentrifuge at the maximum feed rate. The residue from the supercentrifuge cylinder was transferred to a vessel and diluted with water to an approximately 0.5% suspension. The centrifuging process was repeated to remove free hydrochloric acid completely. The degree of acid removal was checked by conductometric titration of the suspension with caustic soda. Preliminary experiments showed that three washings are sufficient. The last centrifugation was performed at a lower feed rate in order to avoid loss of the fine fractions in the suspension. The whole process of H-bentonite preparation took 30-45 minutes.

Displacement of the inflection points on the potentiometric curves with changes of suspension concentration cannot be explained in the light of electrochemical concepts. The colloidchemical properties of electrolyzed askangel suspensions are evidently operative here.

Increase of the suspension concentration first produces a sharp decrease in the amount of bound alkali (Fig. 2), probably because of intensified hydrolysis of mobile aluminum groups in the montmorillonite lattice at high dilutions. As a result, hydrogen ions replace aluminum ions at the exchange sites in the bentonite, and colloidal aluminum hydroxide is formed in the intermicellar liquid. The amount formed is greater than in suspensions of higher concentration. This aluminum hydroxide, in contrast to the hydroxide formed in the interlayer spaces of montmorillonite when alkali acts on electrolyzed bentonite, readily interacts with alkali to form aluminate. Thus, when a dilute suspension of electrolyzed bentonite is titrated the alkali reacts both with the active ions in the particle surfaces and with colloidal aluminum hydroxide. As a result there is an increase in the amount of base taken up with decrease of the suspension concentration. In the concentration range of 0.5-3% this amount is almost constant.

To retard the exchange by hydrogen ions for aluminum ions in the montmorillonite lattice, the temperature was kept at 3-5° during preparation of the hydrogen bentonite, dilution of the suspension to the required concentration, storage, and titration.

Figure 3 shows the results of potentiometric titration of 0.5% H-bentonite suspension by different alkalis. To detect any possible changes in the nature of the H-bentonite during the experiment, the titration with caustic soda was performed twice: suspensions aged 27 minutes and 3 hours respectively were titrated. Suspensions aged 4.5-105 minutes were used in the titrations by lithium, potassium, rubidium, and cesium hydroxides. The experimental points for these latter ions all fit virtually on the same curve. The resultant titration curve is typical for titration of a strong acid by a strong base. Its initial region is almost parallel to the abscissa axis, then the pH rises abruptly in the neutralization region, and this is followed by a final less steep portion in the alkaline region. The low pH of the suspension (2.94) indicates that it is strongly acidic.

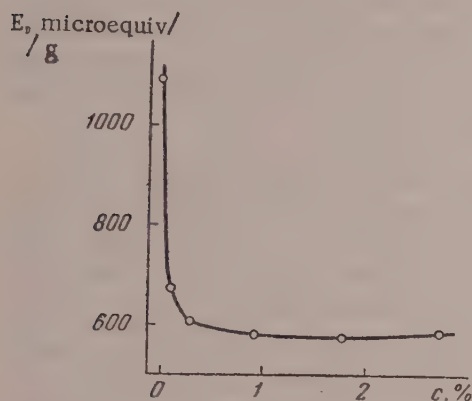


Fig. 2. Effect of concentration of electro-dialyzed-askangel suspensions (c) on the position of the inflection point on the potentiometric titration curves.

The form of the titration curve indicates that the acid-determining ions in the bentonite preparation are very mobile and readily accessible to the action of alkalis. H-bentonite is strongly dissociated: the hydrogen-ion activity of its 0.5% suspensions is 0.0012, which corresponds to a degree of dissociation of 0.26.

Treatment of a dilute suspension of electro-dialyzed bentonite with 1 N HCl in the cold, followed by rapid elution of the free acid, results in complete replacement of the adsorbed cations by hydrogen ions. Potentiometric titration of a dilute hydrogen-bentonite suspension by strong alkalis gives the total cation-exchange capacity.

It follows from these results that when hydrogen bentonite is titrated with different bases there are no differences in the cation-exchange capacity, such as were found in the case of electro-dialyzed bentonite [5]. The value found for the exchange capacity is greater than that found after two weeks of interaction of electro-dialyzed bentonite with the most favorable base - lithium hydroxide. This is probably a consequence

of the high degree of dissociation of hydrogen bentonite and the high mobility of the protons. Neutralization of hydrogen bentonite by strong bases is rapid and complete, and therefore differences in the nature of the cations are not apparent.

The different values of the cation-exchange capacity calculated from the titration curves of acid bentonites by different bases, observed by a number of workers [6] can be ascribed to the fact that the substance titrated was not hydrogen bentonite, but other acid forms, in which exchangeable aluminum was inevitably present in various amounts. When such acid forms interact with bases the aluminum hydroxide formed creates steric obstacles; the difficulty with which these can be overcome depends on the dimensions and polarizability of the nonhydrated ions. This also applies to a certain extent to values of sorption capacity determined by substitution methods.

Investigation of Resin-Treated Askangel Suspensions

A cation-exchange resin in the H form was used for the treatment. A highly disperse suspension of native askangel was first treated in a continuous supercentrifuge to remove soluble electrolytes.

The resin used was Espatit-1, a sulfonated resin with a cation-exchange capacity of 0.85 meq/g [7]. Fractions with particle diameters in the range of 0.85-1.5 mm were obtained from the commercial product by sieving. The diameter of the column was 3.5 cm, and the height 80 cm. The eluants and suspension were fed upward through the column. The dead space, including communicating tubes, did not exceed 30 ml with a working volume of 200 ml.

Directly before passage of the suspension the column with the resin in the H form was eluted by freshly-boiled water until an eluate of constant conductivity was obtained. This conductivity generally did not exceed $1.5 \cdot 10^{-5} \text{ ohm}^{-1}$ under static conditions during 24 hours the conductivity of the liquid in the column rose to $6 \cdot 10^{-5} \text{ ohm}^{-1}$.

The suspension was passed through the column at different rates, which were checked immediately before sampling, the first 100-120 ml of suspension being discarded. The contact time of the suspension with the resin was taken to be the time from the instant the suspension began to pass through the column until it left the column, which is the time for flow of 200 ml of suspension at the given rate. The weight concentration of the suspension was determined in all samples.

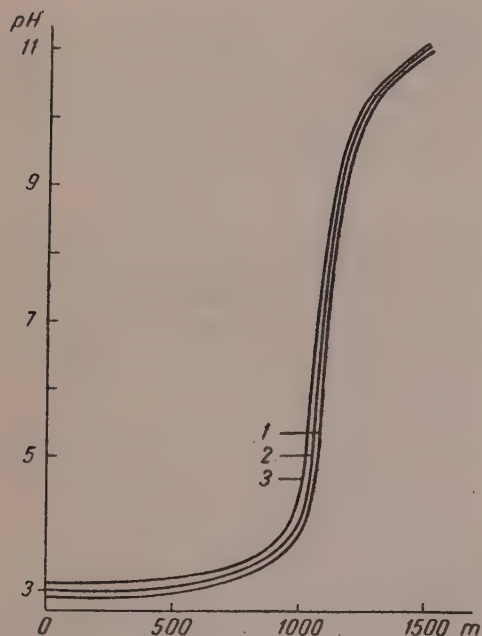


Fig. 3. Potentiometric titration of 0.5% H-askangel suspensions by caustic alkalis (m is the amount of alkali in meq added per g of bentonite); 1) caustic soda, age of suspension 27 minutes; 2) lithium, potassium, rubidium, and cesium hydroxides, age 45-105 minutes; 3) caustic soda, age 3 hours.

If a native-askangel suspension is washed thoroughly to remove electrolytes, some acidity may arise in the askangel as the result of hydrolysis. Therefore, the resultant native-askangel suspensions, almost free of electrolyte impurities, were titrated potentiometrically by a dilute caustic soda solution. It was found that the suspensions were almost free of acidity (Fig. 4, Curve 1).

If 0.5% highly disperse native-askangel suspension is passed fairly rapidly through the column, considerable acidity appears in the suspension. The titration curve (Fig. 4, Curve 2) shows two distinct inflections: one in the acid and the other in the alkaline pH region.

Very slow percolation of the same suspension results in an increase of the total acidity of the suspension, but the titration curve (Fig. 4, Curve 3) retains its general form. The position of the inflection point in the acid region of pH remains almost unchanged. With the shortest contact time (90 minutes) the total acidity is 460 microequiv/g, and with the longest (12 hours), it is 780 microequiv/g.

Analysis of the titration curves shows that the acid form of the sample is not a pure hydrogen form. The two inflections on the curves, one in the acid and the other in the alkaline region, shows that the acidity in this case is caused by the presence of hydrogen and aluminum exchange ions. The amount of exchangeable hydrogen does not increase with increasing contact time between the suspension and the resin, but even diminishes somewhat.

Treatment of native-askangel suspension in a column with a cation exchanger in the H form gave H-Al-bentonite and not H-bentonite. This is evidently because of the low cation-exchange capacity and inadequate activity of the resin used. The relatively rapid appearance of exchangeable aluminum instead of hydrogen ions acquired by the bentonite from the cation exchanger in the H form indicates a high rate of replacement of hydrogen ions by aluminum ions from the montmorillonite lattice. It was reported earlier that electro dialyzed bentonite is also H-Al-substituted [5]. If this is so, then percolation of this substance through a cation exchanger in the H form should produce some changes in the shape of the titration curve as the result of additional replacement of some of the exchangeable aluminum ions by hydrogen ions.

Figure 5 shows curves for titration of electro dialyzed-askangel suspensions before and after percolation through the resin in the H form. As expected, resin treatment results in the appearance of an inflection in the acid region of the titration curve, which is only faintly indicated in the case of electro dialyzed bentonite. Relatively to the curve for electro dialyzed bentonite, the curve for the treated sample descends by more than one pH unit and is shifted in the direction of greater sorption of base.

The appearance of an inflection in the acid region indicates that the surface of the bentonite particles carries strongly dissociated acidic groups, which evidently arise as the result of adsorption of hydrogen ions on contact with the resin in the H form. The inflection in the alkaline region indicates that acidic groups characteristic of electrodialed bentonite persist on the particle surfaces

The equivalence point in the alkaline region is shifted to the right after column treatment. This shift is approximately equivalent to the amount of hydrogen ions which have additionally appeared on the bentonite. Evidently, the most accessible aluminum ions present on the surface of the electrodialed bentonite are replaced by H ions. This replacement makes the more deeply lying exchangeable aluminum ions accessible to the base. As a result the amount of alkali combined by the Al ions remains virtually unchanged. The total acidity of the bentonite increases to an extent corresponding to the amount of new hydrogen ions. The results of percolation of an electrodialed bentonite suspension through resin in the H form indicate that this suspension contains ions which can be replaced by hydrogen. As already stated, these are probably aluminum ions.

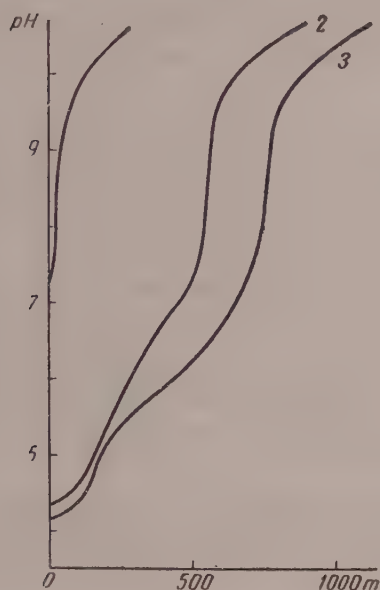


Fig. 4. Potentiometric titration of native-askangel suspension by caustic soda (m is the amount of NaOH in microequivalents per g of bentonite): 1) original suspension; 2) percolated through H resin, contact time 1.5 hours; 3) the same, contact time 12 hours.

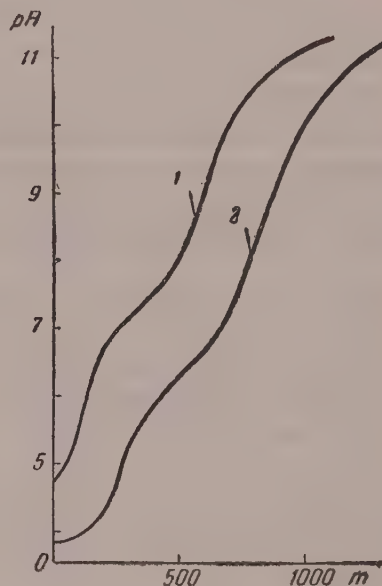


Fig. 5. Potentiometric titration of electrodialed-askangel suspension (m is the amount of NaOH in microequivalents per g of bentonite): 1) original suspension; 2) percolated through H resin, contact time 2.5 hours.

The question may arise whether electrodialed bentonite might not be completely Al-substituted. In that case percolation through a cation exchanger in the Al form should not produce any changes in the shape of the titration curves. To clarify this point, we passed a suspension of electrodialed bentonite through a column containing resin in the Al form.

In contrast to the results with resin in the H form, when the bentonite suspension comes into contact with the Al resin it coagulates in the capillaries and its concentration therefore falls sharply. Repeated percolation leads to further coagulation and almost complete filtration of the intermicellar liquid.

Because of these large changes of concentration, the titration results are difficult to interpret, and are therefore not given here.

The observed complete coagulation of the suspension when electrodialed bentonite is passed through the resin in the Al form indicates the formation of aggregatively unstable bentonite, distinct from the electrodialed form, completely substituted with aluminum ions. Some of the adsorbed ions in the electrodialed askangel are replaced by aluminum ions in the process. These can only be hydrogen ions.

Thus, comparison of the results obtained by percolation of electrodialed-bentonite suspensions through resins in the H and Al forms confirms once again that its acidity is caused by the simultaneous presence of aluminum and hydrogen ions in equilibrium proportions, and not by only one of these types of ions.

SUMMARY

1. In contrast to electrodialed bentonite, which is Al-H-bentonite, the cation-exchange capacity of H-bentonite has the same value in titration by different alkalis. The true maximum cation-exchange capacity of bentonite can be determined by potentiometric titration of a dilute (0.5-1%) suspension of H-bentonite by a strong base.

2. Percolation of native askangel through a cation exchanger in the H form leads to the formation of an acid form of bentonite, the acidity of which is caused partly by hydrogen and partly by aluminum ions. Incomplete replacement of the exchange cations by hydrogen is due to the relatively low exchange capacity of the resin and its comparatively low activity.

3. Potentiometric titration of electrodialed askangel after percolation through resin in the H form shows that the suspension has a considerable content of adsorbed H ions.

4. Percolation of electrodialed askangel through resin in the Al form leads to formation of Al-bentonite, which coagulates on the surface of the resin grains and clogs the column.

5. Comparison of the results obtained in treatment of electrodialed-bentonite suspensions with resins in the H and Al forms confirms that its acidity is due to the simultaneous presence of adsorbed H and Al ions.

6. The jump of potential in the saturation region of the potentiometric curves becomes greater with increasing concentration of the electrodialed-askangel suspensions. The amount of base neutralized by the bentonite, calculated per gram of the bentonite, first falls sharply and then remains almost constant over a wide concentration range.

7. Determinations of the cation-exchange capacity from the inflection points on the potentiometric titration curves should be performed with H-bentonite suspensions in a definite concentration range (0.5-2% in the case of askangel).

LITERATURE CITED

- [1] V. A. Chernov, The Nature of Soil Acidity [in Russian] (Izd. AN SSSR, Moscow, 1947).
- [2] M. E. Harward and N. T. Coleman, Soil Sci. 78, 181 (1954).
- [3] W. H. Slabaugh, J. Amer. Chem. Soc. 74, 4462 (1952).
- [4] I. A. Uskov and E. T. Uskova, Colloid J. 20, 487 (1958).*
- [5] I. A. Uskov and E. T. Uskova, Colloid J. 19, 361 (1957).*
- [6] J. N. Mukherjee, R. P. Mitra, and D. K. Mitra, J. Phys. Chem. 47, 543 (1943); R. P. Mitra, S. N. Bagchi and S. P. Ray, *ibid.*, p. 549.
- [7] V. A. Chernov, N. I. Belyaeva, and V. S. Maksimova, Proc. Sci. USSR 110, 849 (1956).*

Received March 4, 1958

*Original Russian pagination. See C.B. Translation.

THE STATES OF AGGREGATION OF HIGH POLYMERS

4. COLLAGEN, GELATIN, AND SILK FIBROIN

R. I. Fel'dman

The N. K. Krupskaya Moscow Regional Pedagogic Institute

In the previous communications [1-3] it was shown for various high polymers that the dilatometric method, and in particular linear dilatometry, under conditions of uniform heating and cooling of samples after different pretreatments, can give useful information with regard to the behavior and states of aggregation of the materials provided that the sensitivity is adequate. The heating and cooling curves can be used for finding transition points and regions, and for observing the kinetics of phase change with characteristic hysteresis effects.

The results so obtained, in conjunction with data provided by other methods, provide more extensive and detailed information on the behavior both of individual high polymers and of their groups or types. Moreover, the experimental values of shrinkages and expansion coefficients, determined under nonequilibrium conditions, are of practical interest. Such data are indicative of the behavior of materials during storage and of changes in their dimensions under the influence of variable external conditions.

It was observed in studies of nonhygroscopic hydrophobic materials [1-2] that their linear dimensions alter in a characteristic manner with change of temperature. The behavior of a specimen is influenced by its state, which is determined by previous heat treatment (quenching and annealing), mechanical treatment (such as stretching, causing orientation of the structural elements), etc. In the case of polyamides, which are also slightly hygroscopic, variations of moisture content were also shown to exert an influence in addition to the above-named factors [3]. However, this influence is apparent, at the heating and cooling rates used, only in specimens of large specific surface, such as threads and thin films, because the rate of loss and absorption of moisture greatly depends on the surface area. Massive polyamide specimens in rod form were completely similar to hydrophobic materials in their behavior.

The purpose of the present investigation was to extend these test methods to hydrophilic and hygroscopic materials, which include natural substances of the protein type. Their moisture absorption and loss under conditions approaching equilibrium have been frequently studied. Therefore, other aims are pursued and other problems solved in the present investigation. On the assumption that the change in the linear dimensions of a specimen is a complex result, indicating changes not only of the physical state but also to some extent of composition, we considered it useful to compare the behavior of hydrophobic and hydrophilic materials under completely analogous heating and cooling conditions. Attention was mainly focused on the behavior of specimens under real conditions, with all the hysteresis effects in the change of state. For comparison, variations of the specimen weight with the moisture content were observed under the same conditions. The results obtained with this procedure cannot be regarded as true constants for the various materials; other conditions and investigation methods would be required for this.

The results of our investigations can be used for comparing the behavior of materials of different hydrophilic properties under definite kinetic conditions, and for predicting the behavior of the material in an article under real conditions of variable temperatures and corresponding variable humidity.

The results in this communication relate to collagen, gelatin, and silk fibroin.

Collagen. The different kinds of collagen are important representatives of fibrous proteins in which, according to x-ray data [4, 5], there is relatively perfect orientation of the long molecular chains along the fiber axis.

The oriented structure of collagen is completely fixed at room temperature and in the air-dry state, owing to strong intermolecular forces and the presence of covalent and electrovalent bonds between the side branches

of the chains. Hydrogen bonding plays an important part in intermolecular action of protein chains. The relatively high hygroscopicity of collagen is due to the presence of functional groups capable of forming hydrogen bonds. Therefore, collagen, like any other protein, may in a certain sense be regarded as a binary system in which the second component is water. The quantitative collagen-water ratio varies greatly with the temperature. The ratio of different forms of protein-water bonding evidently varies also. The structure of collagen, with the influence of moisture taken into account, has been studied by x-ray and electron diffraction and by electron microscopy [4-13]. According to electron microscope data [11], the distance along the fiber axis between the bands of collagen fibrils exhibiting cross banding varies with the moisture content from 522 to 902 Å, while the regular identity period of ~640 Å in the direction of the fiber axis, calculated from low-angle x-ray data [12] increases to 672 Å if the relative humidity of the air reaches 100% [11]. When collagen is heated in water to ~65° it undergoes irreversible supercontraction to 33% of the initial length. The x-ray pattern of supercontracted

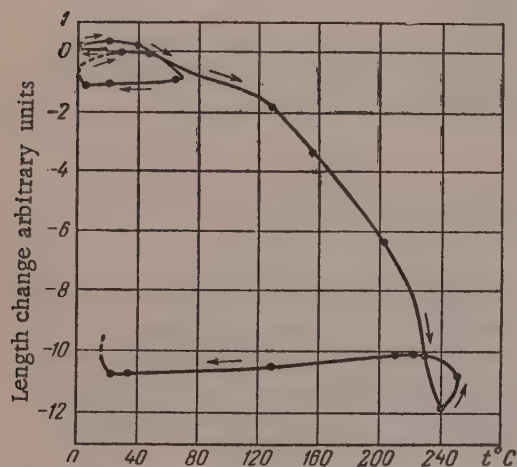


Fig. 1. Variation of the length of a collagen specimen with temperature.

(shrunk) collagen changes sharply, as the longitudinally oriented peptide chains become randomly coiled.

Collagen in the form of strips cut from semifinished hides made by the standard technological procedure was used for the dilatometric investigations. The collagen strips were carefully neutralized, electrodialyzed, and dried in air in the stretched state at 25-30°. The resultant specimens were compact, hard plates without

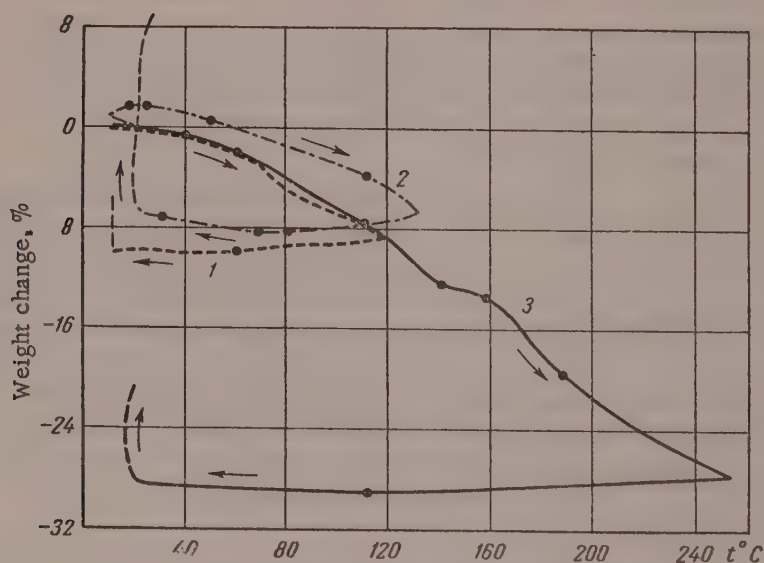


Fig. 2. Weight changes of collagen specimens on heating and cooling; 1) 13°→120°→12°→14°; 2) 22°→11.5°→131°→23°; 3) 15°→250.5°→18°.

signs of coarse porosity, as the fibers are glued together by this method of preparation. The average cross-sectional area of the specimens was 15.5 mm^2 and the thickness, 1.1 mm. Because the specimens were relatively massive and rigid, the length measurements were performed under relatively low load ($P = 0.23 \text{ g/mm}^2$). The results of two series of dilatometric determinations are given in Fig. 1. In the first series the temperature changes were $17^\circ \rightarrow 1^\circ \rightarrow 70^\circ \rightarrow 1^\circ \rightarrow 18^\circ$, and in the second series, 36 hours after the first, $18^\circ \rightarrow 252.5^\circ \rightarrow 15^\circ$. Changes in the linear dimensions of collagen under the influence of heat can be estimated from the fact that when the specimen was heated from 22 to 70° in the first series the length decreased by 2.13%. The coefficient of linear expansion was $\alpha_{65-22^\circ} = 0.75 \cdot 10^{-4} [\text{cm/cm} \cdot \text{degree}]$ in the first series, and $\alpha_{210-130^\circ} = 0.75 \cdot 10^{-4}$, $\alpha_{130-33^\circ} = 0.70 \cdot 10^{-4}$ in the second series.

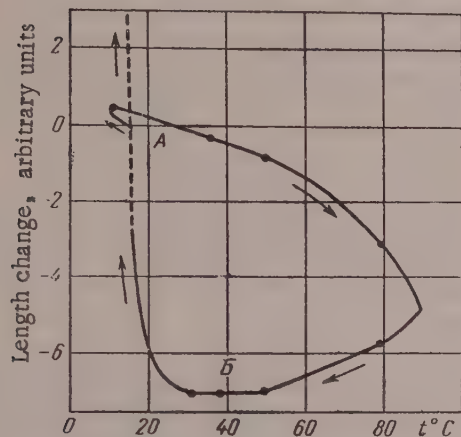


Fig. 3. Variations of the length of a gelatin specimen with temperature.

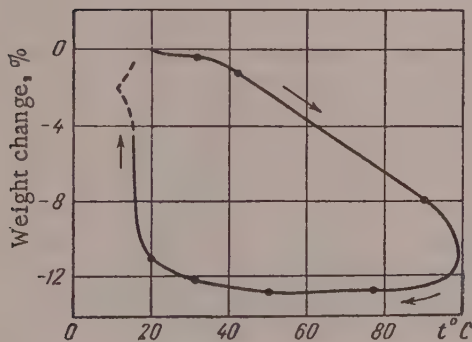


Fig. 4. Weight changes of a gelatin specimen on heating and cooling.

chains are in the extended state [17]. Our tests were performed on fibers of cross-sectional area from $4.41 \cdot 10^{-5}$ to $5.16 \cdot 10^{-5} \text{ cm}^2$, isolated from natural silk fibers washed free of sericin [18]. In illustration, Fig. 5 shows the results of two series of tests, performed with an interval of 12 hours, at a load $P = 434 \text{ g/mm}^2$ (the first series: $22.5^\circ \rightarrow 2^\circ \rightarrow 93^\circ \rightarrow 10.5^\circ \rightarrow 23^\circ$, and the second, $23^\circ \rightarrow 22.5^\circ \rightarrow 25^\circ$). The elongation of the specimen in the first series in the temperature range $22.5^\circ \rightarrow 2^\circ \rightarrow 13^\circ$ was 0.36%. The shrinkage when the specimen was heated from 13 to 93° was 0.76%. The thermal treatment in the first series decreased the shrinkage caused by heating from 23 to 95° to 0.57% in the second series. Similar results were reported earlier for hydrophobic polymers and weakly hygroscopic polyamides [1-3]. The changes of fiber length calculated from the minimum point (Fig. 3) at 93° (A) to the maximum point at 22.3° (B) was approximately 1.15%. The coefficient of

In illustration, Fig. 2 shows the results of three series of experiments on variations of the weight of collagen specimens with temperature. A spring microbalance [3] was used for weight determinations. The principal weighings were followed by determinations of the specimen weight at constant or slightly changing temperature, for a long time, such as 38 days (Curve 2, Fig. 2). The influence of the sequence of the heating and cooling operations and the maximum heating temperature on the form and magnitude of the hysteresis loop is clear from a comparison of Curves 1, 2, and 3 in Fig. 2. The principal determinations of specimen length and weight were performed at intervals of 1° every 3-5 minutes. The additional determinations, performed over a long period at constant temperature or at a temperature which varied very slowly, are indicated by dash lines.

Gelatin. Gelatin is a derivative of collagen and has often been used as a more convenient material for investigations yielding information on various physicochemical properties of collagen [4,5,14,15]. It was, therefore, considered necessary to compare the results obtained for collagen with results for gelatin. Oriented strips of dialyzed photographic gelatin, dried in the stretched state, were used for the tests. The average cross-sectional area of the specimens was 2.3 mm^2 , and thickness, 0.45 mm. Figure 3 shows the results of one series of dilatometric measurements, performed on a specimen previously heated to 40° , at $P = 0.2 \text{ g/mm}^2$. The maximum length shrinkage of the specimen, from the start of the measurements at 16.5° to the minimum point on the curve, at 37° (from A to B) was 0.83%, $\alpha_{80-48^\circ} = 0.46 \cdot 10^{-4}$. Variations in the weight of gelatin during heating and cooling are plotted in Fig. 4.

Silk fibroin. Silk fibroin at room temperature is a highly concentrated protein gel, in the glassy state [16], although with strong axial orientation. The x-ray pattern of silk fibroin resembles that of β -keratin and shows that its molecular

linear expansion, calculated for the linear region between 19.5 and 80°, was $0.15 \cdot 10^{-4}$. If the fiber length is measured at a smaller load, the shrinkage is greater. It should be noted that measurements of the lengths of fine fibers and threads under small loads present practical difficulties.

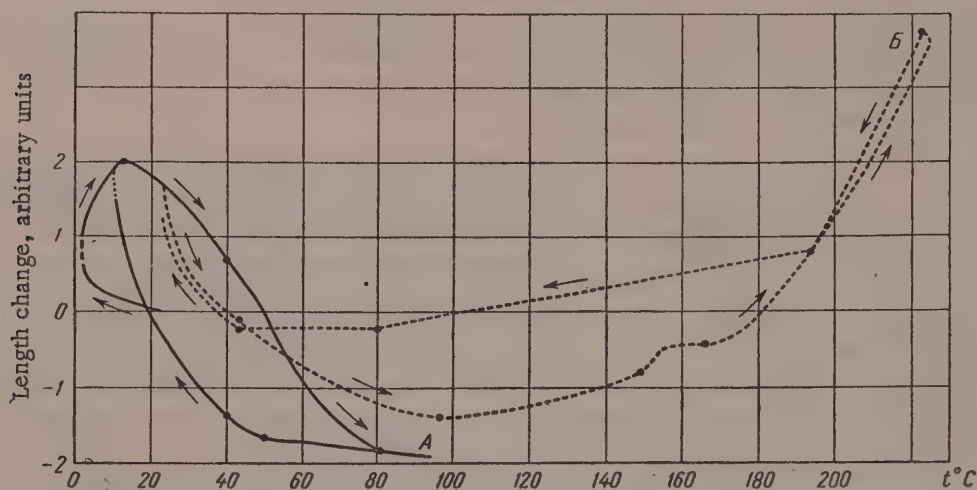


Fig. 5. Variations of the length of a silk-fibroin fiber with temperature.

Before the tests all the collagen, gelatin, and silk fibroin specimens were kept at the initial experimental temperature until the weight and length became virtually constant. The length variations shown in Figs. 1, 3, 5, and 6 are given in arbitrary units and cannot be used for comparing absolute magnitudes.

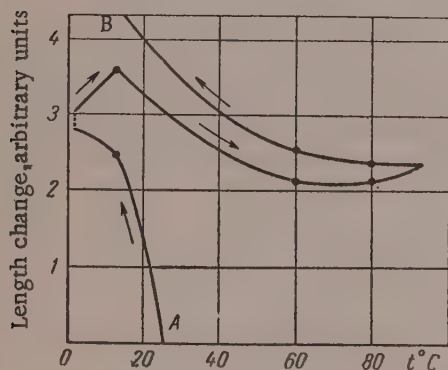


Fig. 6. Variations of the length of a silk-fibroin fiber with temperature in additionally humidified air.

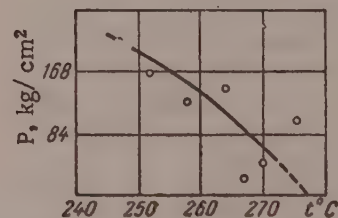


Fig. 7. Dependence of the temperature of mechanical breakdown of silk-fibroin fibers on the applied load.

DISCUSSION OF RESULTS

Comparison of the effects of temperature on specimen length (Figs. 1, 3, 5, and 6) and on weight (Figs. 2 and 4) shows that the effects are interrelated. It follows that dimensional changes in collagen, gelatin, and silk fibroin specimens, as in other hygroscopic polymers such as polyamides [3], under the influence of temperature changes depend not only on thermal expansion, changes in the degree of orientation, and transition of the system from the nonequilibrium and unstable state (with regard to molecular packing) to a more stable state, but also to a considerable extent on changes of moisture content. The rates of these processes differ, and vary with temperature. The behavior of a "massive" lump of collagen is similar, with regard to the properties studied, to that of thinner specimens of gelatin film and silk-fibroin threads. In earlier experiments with polyamides [3] a difference was found between the behavior of massive rods and of films and threads with a larger specific surface. This difference is probably due to the fact that moisture, the content of which under normal

conditions reaches $\sim 18\%$, plays a more important part in the proteins studied, and its removal from a massive specimen is less difficult because of the specific structure of collagen. The difference lies not only in the amount of water present in the protein system, but in the forms of its bonding. In fibrous proteins, in contrast to polyamides, some of the water (such as water condensed in the capillaries) is less firmly bound and is easier to remove from the system.

The regions of constant length with varying temperature, observed on the dilatometric curves, indicate that in these temperature ranges the simultaneous increases and decreases of linear dimensions, which are components of the observed complex effect [3], proceed at equal rates. The direction and dimensions of the hysteresis loops depend on the maximum heating temperature. This is illustrated in Figs. 1 and 5. The specimen length may alter under isothermal conditions, as in the case of synthetic polyamides [3], with changes of moisture content until equilibrium is attained under the given conditions. Dilatometric measurements performed in additionally humidified air showed that shrinkages decrease and elongations increase in the corresponding temperature ranges. The form of the relationship does not change essentially, but the direction of the hysteresis loop may alter.

Figure 6 shows the effect of temperature on the length of silk fibroin fibers in conditions of high humidity (in presence of liquid water in the dilatometer chamber), determined at $P = 434 \text{ g/mm}^2$. The change of fiber length under these conditions from the start of the tests (25° , Point A) to the end (15° , Point B) was about 1.4% . It follows that the behavior of hygroscopic materials depends on many factors and is a complex effect which appears both under the influence of heat treatment and under isothermal conditions.

In addition to the experiments described, the temperatures at which silk-fibroin fibers undergo mechanical breakdown under different loads were determined by visual observations (Fig. 7). The temperature at which the fiber breaks can be regarded, in a certain sense, as the point at which flow commences under the applied load (P). The temperature at $P = 0$, determined by extrapolation, could be regarded as the transition point of the material into the viscofluid state in absence of external mechanical forces, if appreciable thermal degradation did not occur at that temperature. Analysis of variations of specimen length and weight with temperature reveals points on the curves corresponding to temperatures at which their steady course alters. The positions of these points may vary somewhat with the previous history of the specimen, the heating or cooling rate, and other factors. These points (with variations in their positions taken into account) were found in the following approximate temperature ranges: from 20 to 60° , from 90 to 130° , from 150 to 160° , and from 190 to 220° . Changes in the systems observed at $\sim 40^\circ$ are associated with the very high mobility of a certain portion of the moisture. This fact may be correlated with literature data on the character of hydrogen bonds [19], which have a decisive influence on these phenomena. Another and stronger form of bonding is represented on the curves by transition points around 100° . The change in the course of the dilatometric curves at $\sim 190^\circ$ is probably associated with transition of the protein component into the high-elastic state. The viscofluid state is reached above 200° . In the case of collagen there is a special temperature point, close to 240° , where the course of the curve changes sharply; this is the softening point above which fluidity appears. However, material taken to this temperature shows surface signs of thermal degradation. In this instance this may be regarded as a side process, which complicates the normal changes of aggregation states to only a small extent. An interesting fact is that this softening point of dry collagen, and also of silk fibroin, is close to the corresponding point for synthetic polyamides. In the case of collagen two temperature points were found: at 210 and 225° , determined from measurements of specimen length on heating in Wood's alloy. For collagen tanned by vegetable tannins and chromium salts the second point is shifted to 250 and 260° respectively [20].

Thus, the dilatometric method can be used together with others for investigation of the state of fibrous proteins and determination of characteristic transition temperatures. Moreover, these results are of direct practical interest, as they give an indication of the causes and extent of shrinkage in protein fibers and films with changes of temperature, and under natural atmospheric conditions.

The conditions of hydrothermal and mechanical treatment of articles made from silk, collagen, and other fibrous proteins, intended for relative stabilization of the form and dimensions of the articles, can be chosen on the basis of dilatometric measurements in accordance with the end use.

In numerous products made from collagen and fibroin fibers or layers of gelatin, extensively used in technology and the home dimensional changes and sometimes the associated stresses may have a decisive influence on their successful utilization. The hysteresis effects revealed by the dilatometric method also play an important part.

SUMMARY

1. With collagen, gelatin, and silk fibroin as samples, it is shown that the dilatometric method can be successfully used for studying the behavior of fibrous proteins at varying temperatures.
2. Variations of the moisture content sorbed or desorbed by the material play a significant role in the complex causes of linear expansion and contraction of protein materials.
3. The changes of state revealed by the dilatometric method in the system studied, as in other polymer materials, are characterized by transition points, shrinkages, and typical hysteresis effects.

I offer my deep gratitude to Professor S. I. Sokolov for his constant interest and discussions.

LITERATURE CITED

- [1] R. I. Fel'dman, *Colloid J.* 20, No. 2, 220 (1958).*
- [2] R. I. Fel'dman and S. I. Sokolov, *Colloid J.* 20, No. 3, 388 (1958).*
- [3] R. I. Fel'dman, *Colloid J.* 21, No. 2, 238 (1959).*
- [4] S. I. Sokolov (editor), *Physical Chemistry of Collagen, Tannins, and Tanning Processes* [in Russian], Collected Papers, Central Scientific Research Institute of the Leather Industry (State Light Industry Press, 1941).
- [5] S. I. Sokolov, *Physical Chemistry of Collagen and Its Derivatives* [in Russian] (State Light Industry Press, 1937); *Proc. of the 1st and 2nd Conference on High Polymers* [in Russian] (Izd. AN SSSR, 1945) p. 111.
- [6] A. L. Zaides and S. A. Pupko, *Proc. Acad. Sci. USSR* 65, 227 (1949).
- [7] A. L. Zaides and A. N. Mikhailov, *Proc. Acad. Sci. USSR* 65, 227 (1949).
- [8] F. O. Schmitt, C. E. Hall, and M. A. Jakus, *J. Cellular Comp. Physiol.* 20, 11, (1942).
- [9] C. E. Hall, M. A. Jakus, and F. O. Schmitt, *J. Amer. Chem. Soc.* 64, 1234 (1943).
- [10] N. Andreeva, *Candidate's Dissertation* [in Russian] (Moscow, 1954).
- [11] B. Wright, *Nature* 162, 23 (1948).
- [12] O. Kratky, *J. Polymer Sci.* 3, 195 (1948).
- [13] A. L. Zaides, *Colloid J.* 12, 114, 447 (1950).
- [14] S. I. Sokolov and R. I. Fel'dman, *Colloid J.* 8, No. 5, 367 (1946); *Light Industry* No. 6, 19 (1943); No. 6, 20 (1944).
- [15] R. I. Fel'dman and S. I. Sokolov, *Light. Ind.* 18, (1943).
- [16] A. G. Pasynskii and V. P. Blokhina, *Chemistry and Physical Chemistry of High Polymers* [in Russian] (Izd. AN SSSR, 1952) p. 291.
- [17] W. T. Astbury, *Advances in Enzymol.* 3, 63 (1943).
- [18] F. Haurowitz, *Chemistry and Biology of Proteins* (IL, 1953) [Russian translation].
- [19] Ya. K. Syrkin and M. E. Dyatkina, *The Chemical Bond and the Structure of Molecules* [in Russian] (Goskhimizdat, 1946).
- [20] G. I. Kutyanin, *Proc. Acad. Sci. USSR* 82, 405 (1952).

Received January 29, 1958

* Original Russian pagination. See C.B. Translation.

BOOK REVIEW

COLLOID CHEMISTRY (TEXT BOOK FOR STUDENTS OF COMMODITY AND TECHNOLOGICAL FACULTIES)

A. P. Pisarenko, K. A. Pospelova, and A. G. Yakovlev

Institute of Soviet Trade Press, 1956, 245 pp.

During recent years many branches of colloid chemistry have acquired a new content, and the subject has become transformed to a considerable extent into the science of molecular surface phenomena and disperse systems.

However, many textbooks of colloid chemistry, including some published recently, do not reflect these changes in due measure, and the book under review differs favorably from them in this respect, as it gives an adequately full presentation of the most important aspects of modern colloid science.

In addition to colloidal systems proper, much attention is devoted in the book to microheterogeneous (coarsely disperse) systems - suspensions, emulsions, and foams. Two chapters deal with compounds of high molecular weight - polymers and their solutions - and these are especially important, not only from the scientific but also from the practical standpoint.

Considerable space is devoted to descriptions of the mechanical properties of polymers and structuro-mechanical properties of disperse systems. Fundamental information on surface effects and adsorption at various interfaces is presented in adequate detail.

The presentation is strictly scientific, and the text contains much data in illustration of the diverse applications of colloid chemistry in technology and everyday life.

Another merit of the book is the clarity of presentation, which enables the nonspecialist reader to become acquainted with all branches of colloid chemistry.

In addition to these meritorious features, certain defects must also be pointed out.

First, attention must be drawn to the somewhat inapt presentation of one of the most important problems of colloid chemistry - the stability of disperse systems. It is known that the principal factor in their strong stabilization is the structuromechanical barrier which is the consequence of formation of mechanically strong structured adsorption layers on the surface of the stabilized particles of the disperse phase, or of volume structuration of the dispersion medium.

However, the presentation of this problem in various parts of the book suffers from lack of clarity. Thus, in Chapter 6 (p. 136) the term "structuromechanical stabilization" of colloids with the aid of soaps is used for the first time, without an explanation of the nature of the effects. In Chapter 7 the structuromechanical factor is not considered in a discussion of the stabilization of suspensions, on p. 148 an emulsifier is referred to as the "third component" of the system and, finally, on p. 151 there is a more detailed discussion of the structuro-mechanical factor, again in relation to the stabilizing action of soaps. Soaps themselves are described in the last (10th) chapter, on p. 237; and they are referred to as semicolloids, forming micelles of definite structure in solutions, and not as strongly surface-active substances the structured adsorption layers of which have a high stabilizing effect on all disperse systems.

As a result the reader gains an incorrect impression of the difference between mechanisms determining the stability of different disperse systems and of the role played in them by structure-forming surface-active substances. The role of another stabilizing factor – the ionic double layer – also remains somewhat obscure.

It is therefore desirable to present this problem differently, to concentrate it in one chapter and with reference to all disperse systems, regardless of their state of aggregation and dispersity.

Another defect is the fact that the authors devote very little attention to the properties of proteins and their solutions. Such a section would be particularly important, as the book is intended for commodity students, future specialists on the properties of food products, in which proteins constitute a fundamental material.

In Chapter 1, in the classification of colloidal and disperse systems, the existence should have been noted of the class of lyophilic systems – soaps and spontaneously forming emulsions – in accordance with modern concepts (P. A. Rebinder). A distinction should also be drawn between emulsions of gases in liquids, and foams, which are cellular film structures.

It should have been pointed out in Chapter 4 that the coefficient K in the equation $A = KS$ (p. 85) is proportional to the surface energy, with a reference to the work of Rebinder and his associates on hardness lowering. In the same chapter the method of electrical pulverization of metals should be included with dispersion methods.

In Chapter 6, B. V. Deryagin's coagulation theory should have been presented in greater detail. In Chapter 7 the question of stabilization of suspensions in different media should be correlated with the problem of selective wetting.

In the classification of gels in Chapter 10, attention should have been drawn to the role of condensational and coagulative structurization in their formation.

On the whole, this book is a valuable educational aid for students of nonchemical universities and colleges, and especially for correspondence and evening classes.

With suitable corrections and additions the book should be republished for a wider circle of readers studying colloid chemistry.

There is no doubt that this book should be useful not only to students, but to practical workers for improving their qualifications in this field.

A. B. Taubman

CURRENT EVENTS

PROBLEMS OF COLLOID CHEMISTRY AT THE 8th MENDELEEV CONGRESS

The 8th Mendeleev Congress on general and applied chemistry was held in Moscow from March 16 to 23. Considerable attention was devoted at the Congress to problems of colloid chemistry. It included a Section of Colloid Chemistry, and a number of problems closely related to colloid chemistry was discussed in certain other sections. In particular, in the Section of Electrochemistry papers were presented on solvation of ions and molecules and the structure of the double layer of adsorbed ions; in the Section of Polymer Chemistry and Technology, on the mechanical properties of polymers containing fillers; in the Section of Silicate Chemistry and Technology, on the properties of clay suspensions; the "Catalysis and Adsorption" subsection of the Physical Chemistry Section devoted one of its meetings (11 papers) to problems of physical adsorption and ion exchange.

The Section of Colloid Chemistry held 6 meetings (one jointly with the Section of Silicate Chemistry), at which 57 papers and communications were read. From 70 to 250 delegates were present at the different meetings, and over 600 attended the joint meeting. Despite the fact that all published papers were excluded from the agenda, and the time allowed to the speakers was short and sometimes obviously inadequate, the sections were overloaded and the discussions were therefore restricted.

The papers presented to the Section were centered around the following problems: 1) surface layers and thin films; adhesion (10 papers); 2) adsorption and adsorptional interactions (11 papers); 3) emulsions and foams (7 papers); 4) formation, stability, and coagulation of colloids (11 papers); 5) physicochemical mechanics and processes of structure formation (11 papers); 6) semicolloids and disperse systems in polymers (7 papers). Each of these problems was discussed at a separate meeting of the section.

Adhesion was discussed in the paper by V. P. Smilga and B. V. Deryagin on electronic concepts in the theory of adhesion, and by N. A. Krotova and L. P. Morozova on adhesion bonding and methods for its investigation. The theory of adhesion was developed further in these papers by consideration of electrostatic interaction forces. Yu. F. Deinega, A. V. Dumanskii, G. V. Vinogradov, and I. E. Neimark reported in their paper on the influence of surfaces and surface modification on the dielectric properties of certain disperse systems. They showed that measurements of the dielectric constant and the tangent of the dielectric loss angle constitute a valuable method for investigating surface changes in powders and suspensions of solid particles. The paper by V. V. Karasev and B. V. Deryagin contained new viscosity data on thin wall layers of liquid, determined by the viscosimetric "blow-off" method. G. I. Fuks reported the results of model studies of elementary acts of particle interaction in electrolyte solutions and showed how this effect is influenced by electrostatic repulsion of diffuse layers, ion hydration, and surface properties of the particles in relation to the distances between them. M. S. Ostrikov reported on his method for visual investigation of the development and "self-healing" of cracks in a transparent material under a varying load. This method was used to model and study drying and humidification processes in disperse and polymer systems. The problem of surface layers and thin films was also discussed in the papers by S. I. Popel' on interfacial tension between iron and a silicate melt (measurements of drop shape), and by N. V. Pertsov on the surface activity of liquid metallic coatings and their influence on metal strength.

The group of papers on adsorption and adsorptional interactions was concerned with theoretical and practical aspects of the problem. Deep-bitumenization coals, which are becoming increasingly significant in the national economy of Belorussia and adjoining regions, were discussed in detail in the paper by N. F. Ermolenko and Z. A. Krivchik, who described the structure and adsorptional activity of these coals. A. B. Taubman and S. A. Nikitina discussed the role of the kinetic factor in adsorption and wetting, and showed that when wetting agents are used in practice for dust removal their effectiveness depends on their ability to form equilibrium adsorption layers rapidly rather than on their high surface activity under static conditions. The use of solutions of

surface-active substances for dust collection was also the subject of the paper by P. I. Ermilov, who studied the relationship between the structure and effectiveness of polyethylene glycol ethers of alkyl phenols. I. E. Neimark presented the results of his investigations of the influence of chemical modification of the surface of mineral sorbents on their adsorptional properties. Four papers were concerned with the theory and technology of dyeing. P. V. Moryganov considered the thermodynamics of dyeing of cellulose fibers; B. N. Mel'nikov presented equations for the kinetics of fiber dyeing; V. F. Androsov described the influence of various factors on the selectivity of vat dyes with respect to synthetic fibers (capron and nitron); A. A. Kharkharov described his researches on dyeing of synthetic fibers (nitron and lavsan) by soluble and insoluble dyes. The papers by A. A. Morozov, R. M. Dranitskaya, and E. K. Tsugui on the separation of the green and violet modifications of chromium sulfate, and by G. V. Nemirov on the sorption of certain salts from solution by cellulose, were concerned with particular problems of electrolyte adsorption and properties of adsorbents. Among the papers on adsorptional interactions was one by E. M. Kazakov and G. A. Kitaev on electron-microscope studies of the mechanism of formation of copper hydroxide films on a solid surface.

Although, for formal reasons, the meeting of the section on "Emulsions and Foams" was opened by a paper presented by V. F. Boiko; his researches lie outside the scope of this problem and are concerned with methods for construction of composition--state--property diagrams for multicomponent disperse systems. E. M. Aleksandrova, V. N. Tsveikov, and N. S. Razumikhina reported on their work on nonelectrolytic coagulation of polystyrene latexes. Coagulation was effected by stirring of concentrated latexes in an apparatus designed by the authors. The paper by A. I. Yurzhenko and R. V. Kucher was concerned with certain characteristics in the course of chain reactions in hydrocarbon emulsions stabilized by surface-active emulsifiers. In the authors' opinion these characteristics are associated with the presence of hydrocarbons of three degrees of dispersity in the system. A. B. Taubman and A. F. Koretskii discussed the role of the structuromechanical properties of adsorbed layers in the stabilizing action of solid emulsifiers. In the light of the results the action mechanism of solid emulsifiers was considered and methods of emulsifier selection indicated. M. A. Kovbuz presented a paper entitled "The role of the emulsifier as a kinetic factor in the oxidation of hydrocarbons in emulsion form." S. M. Levi reported on his investigations of the structuromechanical properties of gelatin and photographic emulsions, which gave rise to a series of relationships necessary in relation to the application of photosensitive emulsions into supports. M. B. Radvinskii discussed the action mechanism of chemical antifoaming agents and proposed a new process for production of an effective antifoaming agent for systems boiling under pressure.

Considerable interest was aroused by the paper presented by the leader of the Dutch school of colloid chemistry, H. Kruyt, who opened the discussion on colloid formation and stability. In his paper on "Motion of molecules", Kruyt showed that the distinction between simple and polymeric molecules is a nominal one. At the same meeting the Yugoslav chemist B. Tezak described researches in relation to the construction of plane and space models of disperse systems in the course of precipitation. Z. Ya. Berestneva and V. A. Kargin presented a paper on the crystallization mechanism of colloidal titanium dioxide. This work was a continuation of the series of electron-microscope investigations of the formation mechanism of colloidal particles. B. V. Deryagin read two papers. In the first he described original instruments for investigation of disperse systems or particle surfaces in flow (flow ultramicroscope, flow counter of condensation nuclei, etc.). These instruments are among the few available for kinetic studies of rapid changes in colloidal solutions and aerosols. In his second paper B. V. Deryagin discussed the specific characteristics of heterocoagulation and the elementary theory of this effect, and described model experiments which confirm the theoretical principles. Yu. M. Glazman and D. N. Strazhesko gave a paper entitled "Significance of adsorption effects in the mechanism of coagulation of lyophobic sols by electrolytes," which included the results obtained with the use of a radiometric method (perfected by the authors) for studying adsorption of ions by colloids. In his paper on the production and properties of concentrated sols, E. M. Natanson generalized his researches of many years in this field, and discussed a series of practical application of metal sols. S. G. Teletov's paper was concerned with the results of a study of the reversibility of the Fe_2O_3 hydrosol-dry gel transition, and the influence of copper acetate on this process. S. E. Kharin discussed the applicability of thermodynamic methods for describing the stability of equilibrium (or, more correctly, quasi-equilibrium) colloidal systems, with resin sols and transformer-oil emulsions as examples. K. S. Lyalikov described a study of the recrystallization of polydisperse systems stabilized against aggregation. P. M. Silin, in his paper, generalized his theoretical and experimental work on the crystallization of sucrose.

Problems of physicochemical mechanics and structurization processes were discussed at a joint meeting of the Colloid Chemistry and Silicate Chemistry Sections. The discussion was opened with P. A. Rebinder's paper entitled: "Fundamental problems of the physicochemical mechanics of disperse and polymer structures." This paper consisted of a summary of the principal laws of this new branch of science, developed by the author and his school. E. E. Segalova reported on her work on the kinetics of the development of crystallizational structures and demonstrated the significance of these processes in relation to cements. The first two papers were associated with communications by O. I. Luk'yanova on the structurochemical conditions of hydration hardening of sulfates, and E. B. Andreeva on crystallizational structure formation in calcium hydrochloro-aluminate. M. P. Volarovich and I. V. Churaev described their investigations of the physicochemical properties and structure of peat with the aid of radioactive isotopes. A number of original methods of general interest was developed by the authors for these investigations.

The physicochemical theory of concrete and some of its individual applications was developed further, and the structure-forming function of aggregates in cement pastes was elucidated in papers by N. V. Mikhailov with E. E. Kalmykova and N. V. Mikhailov. N. V. Mikhailov's colloidchemical theory of concrete has yielded valuable practical results. O. P. Mchedlov-Petrosyan, F. A. Latyshev, A. G. Bunakov, and N. A. Levchuk presented a paper entitled "Thermochemical investigation of vibratory activation of cements," in which the hardening mechanism of cements of different compositions was examined. G. I. Logginov discussed the binding of calcium oxide by quartz sand. The paper by G. V. Tsitsishvili, D. N. Barnabishvili, and K. E. Avallani was concerned with the adsorptive properties and structure of montmorillonites. V. N. Eremenko's paper dealt with the physicochemical principles of formation of sintered-metal compacts.

The papers on semicolloids and disperse systems in polymers touched upon particular, but important practical or theoretical aspects of these problems. They included a paper by V. I. Akimova, S. L. Talmud, and K. P. Mishchenko on interaction of cellulose with liquids, a communication by M. I. Knyaginichev and Yu. R. Bolkhovitina on the properties of starch in salt solutions, and a paper by A. A. Morozov and S. N. Stavrov on the results of a study of cation-substituted samples of Black-Sea agaroid and White-Sea agar. L. I. Belen'kii, M. E. Kazanskaya, and T. V. Bromberg reported on their work on the absorption spectra of dyes. Molecular interactions in semicolloid systems could be estimated from shifts in these spectra. É. V. Frisman reported on the use of a birefringence method for determination of the shape of macromolecules in solution. A. P. Demchenko read a paper entitled "Lyophily and some questions of the theory of directed synthesis of detergents," in which he considered the influence of structure on the wetting and detergent action of surface-active substances.

The work of the Colloid Chemistry Section was summarized in a final address by its chairman, P. A. Rebinder.

In its decisions, the section welcomed the successful development of applied and theoretical colloid chemistry in the Soviet Union. Indeed, the Colloid Chemistry Section of the 8th Mendeleev Congress was only a little inferior in the number and significance of the papers to the regular conferences on colloid chemistry, although less than a year had passed since the last one of these had been held in Tbilisi. The volume of "Colloid Journal" is not adequate to keep up with this development of colloid science, so that there are considerable delays in publication. The section requested the Academy of Sciences USSR to increase the volume of Colloid Journal by at least 50%. In welcoming the appearance of a new branch of knowledge - physicochemical mechanics - the section requested the Academy of Sciences USSR to speed up the organization of an institute of physicochemical mechanics. The decisions of the section also raised the question of the organization of a permanent colloquium on colloid chemistry, and drew attention to the fact that the next regular conference on colloid chemistry is due to take place in 1961.

G. I. Fuks

THE 60TH BIRTHDAY AND 35 YEARS OF SCIENTIFIC ACTIVITY
OF PROFESSOR S. M. LIPATOV, ACADEMICIAN OF THE ACADEMY
OF SCIENCES BELORUSSIAN SSR

Z. A. Rogovin, V. A. Kargin, and P. I. Zubov

October 12, 1959 was the sixtieth birthday and marked the completion of thirty five years of scientific activity of one of the most eminent representatives of colloid science, the outstanding Soviet scientist and social worker, Academician of the Belorussian SSR Sergei Mikhailovich Lipatov.

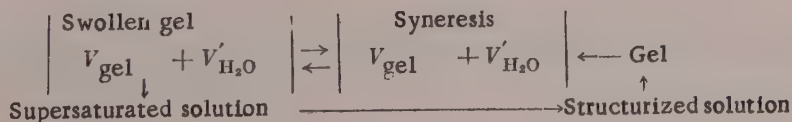
His scientific work began in 1924 in the chemical laboratory of the First Moscow Cotton-Printing Works, where he carried out a series of investigations concerned with the adsorption of electrolytes on cellulose and insoluble dyes and showed for the first time that because of selective sorption of ions these processes may be regarded as chemical ion-exchange reactions. As the result of his experimental investigations Lipatov derived in 1926 the isotherm for ion exchange between adsorbent and solution, in the form accepted at the present time.

In 1927 he became the head of the scientific section of the Central Laboratory of the Ivanovo - Voznesensk Combine. The researches performed during this period - on viscosity of dye solutions, characteristics of dye solvation, and coagulation of dye solutions - enabled him to formulate the general theory of syneresis which has been universally accepted, is given in all monographs and textbooks on colloid chemistry, and has retained its significance to the present day. For this work Lipatov was awarded the Mendeleev Prize by the Russian Physico-chemical Society. In 1927, while he was a lecturer of the Ivanovo-Voznesensk Polytechnic Institute, he organized a special course of lectures on the theory of dyeing, and in 1929 he published them in the form of a monograph entitled "Colloidochemical Principles of Dyeing", which until recently was the only handbook on the theory of dyeing by a Soviet author. In view of the great significance of artificial fibers in the development of the national economy, Lipatov organized in 1929 the first laboratory of artificial fibers in the USSR, in the Karpov Physico-chemical Institute, and when in charge of this laboratory he initiated extensive investigations of high polymers, which were of both theoretical and applied significance. During this period he did work on the theory of the viscous process.

As long ago as 1925 he worked out in detail the physicochemical aspects of cellulose mercerization, and on the basis of the law of mass action, he demonstrated the formation of a compound with the limiting composition $C_6H_7O_2(ONa)_3$. A detailed study of viscose production led him to conclude that the aging stage is not essential; this was somewhat later applied in practice. In studies of celluloses of different structures it was shown that the kinetics of cellulose hydrolysis differs for different cellulose modifications and is determined by the intermolecular action of OH groups which are responsible for the structure of these modifications.

Continuing his work on syneresis of polymer solutions, Lipatov established that syneresis is phase separation of a thermodynamically unstable solution into a gel and a molecular solution, and substantiated the hypothesis that the swollen gel is the only equilibrium state of polymers which do not dissolve spontaneously.

Lipatov represented the spontaneous transition of a nonequilibrium solution into a swollen gel schematically as follows:





Sergei Mikhailovich Lipatov

which explains the effect of solution aging, somewhat confused at that time, as a transition into an equilibrium state. A series of investigations concerned with gel formation is closely associated with this work.

It is evident from this scheme that a gel is not an equilibrium system but merely an intermediate link in the general chain of continuous changes taking place during aging. Accordingly Lipatov describes gelation as microsyneresis. If it is remembered that at that time Kryut's theories, in which lyophilic colloids were regarded as lyophobic colloids with strong surface hydration and gelation was considered to be dehydration of the particles, were dominant, it is clear that the theory of gelation advanced by Lipatov was a new step forward. As the result of careful determinations of the heats of interaction of various high polymers (acetylcellulose, agar, gelatin, etc.) with different liquids Lipatov showed in 1932 for the first time that these systems are not especially highly solvated and that one polar group in a polymer molecule is shielded by one molecule of liquid. From this a new calorimetric method for titration of free polar groups in solid polymers was developed and it was shown for the first time that the so-called lyophilic colloids are hydrated quantitatively to the same extent as molecules or ions of sample substances. Kryut's theory was subjected to serious criticism from this essentially new standpoint and was shown to be unjustifiable. In 1932 Lipatov wrote: "At the present time we certainly cannot regard a solvated particle of a lyophilic substance as a spherical nucleus uniformly covered by a solvation layer. The lyophilic particles have a chain structure, and a solvent interacts only with the lyophilic groups of such a molecule or micelle, and not with its entire surface. The presence of free unprotected hydrocarbon groups in the chain is sufficient for definite interaction to appear between the chains".

Applying Langmuir's principle of independent surface action for the first time in this field, Lipatov showed that polar groups occupied by solvent molecules are prevented from mutual interaction, and that interparticle bonding can be effected only by means of the free field of force of CH_2 groups.

At the end of 1931 Lipatov, who up to that time had been giving a course of colloid chemistry at the Moscow Higher Technical School, was appointed to the chair of physical and colloid chemistry in the All-Union Institute of the Leather Industry, where he organized the first polymer laboratory in the USSR and gave the first course on high polymers to be given in the USSR. These courses formed the basis of two books: "Colloid Science", published in 1934, and "High Polymers", published in 1936. In 1934 he was given the title of professor, and in 1936 he was awarded the degree of doctor of chemical sciences without a dissertation.

In 1938 he started work in the Colloidal and Electrochemical Institute of the Academy of Sciences USSR as head of the laboratory of the physical chemistry of colloids, where he continued his research in the field of high polymers. During his work in the Colloidal and Electrochemical Institute he was also, until the end of 1939, the head of the scientific program section of the Presidium of the Academy of Sciences USSR.

During this period he developed a theory of swelling of high polymers, based on concepts of diphilic structure of macromolecules and the principle of independent surface action. He regards swelling as a complex process which occurs in two stages: 1) solvation, which breaks the most stable bonds between polar groups, accompanied by liberation of heat and slight changes of polymer volume, and 2) swelling proper, without a heat effect, purely an osmotic entropy process. It was only by means of this theory that the fact could be explained that the temperature coefficient of swelling is positive although the process is exothermic.

In his detailed investigations of aggregation effects in polymer solutions, regarded as being among the causes of the anomalous behavior of such solutions, he has, since 1936, carried out systematic studies of the influence of temperature on the properties of polymer solutions, such as viscosity, osmotic pressure, swelling, and gelation, and showed that on increase of temperature heat is expended for "fusion" of bonds at the non-solvated groups.

Many of Lipatov's investigations are concerned with modification of the properties of individual polymers by introduction or removal of low-molecular fractions and surface-active substances.

In 1940 Lipatov was elected Academician and Vice-President of the Academy of Sciences Belorussian SSR, and did extensive organizing work in relation to the establishment of a polymer laboratory in Minsk and the training of scientific workers.

During the Great Patriotic War Lipatov was sent to Tashkent to organize the work of Belorussian Academy of Sciences; there, in addition to his work in the Academy, he was professor in the University of Central Asia and consultant to VIKhI of the Red Army.

From 1944 to the present day Lipatov has been head of the Department of Physical and Colloid Chemistry of the Moscow Textile Institute. During this period his scientific activity was marked by development of research on thermodynamic properties of polymer solutions and polymer thermochemistry. A series of investigations by Lipatov and his associates demonstrated the influence of temperature on the heats of solution and swelling of polymers; this made possible the development of an essentially new method for studying polymer structure. New fundamental data of great scientific importance were obtained in the course of these studies.

In addition to his work of general theoretical significance, Lipatov carried out work of great importance to industry; this includes a method, developed jointly with his associates, for production of alcohol from dispersed raw materials containing starch and cellulose, and a new vacuum method of dyeing which accelerates the process 3 to 4-fold. The origin and development of these investigations are closely associated with the general theoretical trend of Lipatov's work.

Lipatov's work is carried out in close contact with the scientific research institutes, and he does extensive consultant work.

Lipatov and his school have published more than 200 scientific papers and seven monographs and textbooks. The large manual on the physical chemistry of colloids, published in 1948, is widely used in the countries of the peoples' democracies (China, Czechoslovakia, Hungary, German Democratic Republic).

For 30 years he has done a great deal of teaching work, and has devoted much effort and care to the training of young scientists, including those from the national republics. During this time he has trained 25 candidates of sciences and 6 doctors; his pupils hold leading positions in scientific research institutes and headships of departments in higher educational establishments.

For a number of years Lipatov was a member of the scientific and technical council of the Ministry of the Food Industry and a member of the expert commission attached to the Higher Certification Commission.

He has been a member of the editorial board of Colloid Journal since its foundation and has participated actively in a number of conferences on colloid chemistry.

The work of Lipatov and his associates has furthered the development of colloid chemistry and the physical chemistry of polymers; his varied and prolonged scientific, teaching, and social activity has deservedly won for him the authority of an outstanding Soviet communist scientist among the scientific community.

With all our hearts we wish our dear Sergei Mikhailovich many years of life, health, and creative success in his varied activities for the good of our great country.

PHASE SEPARATION ON POLYMER - POLYMER - SOLVENT SYSTEMS

S. M. Lipatov and G. V. Lipatova

Moscow Textile Institute

Thermodynamically unstable polymer solutions (agar, gelatin, cellulose derivatives, etc.) can be stabilized by introduction of low-molecular fractions of these substances or of surface-active substances [1]. Zhigach and Rebinder [2] demonstrated the stabilizing effect of alcohols on gelatin solutions. Thus, these investigations laid the foundations of methods for modifying the properties of individual polymers in various liquids. It is now well known that many synthetic polymers, such as polyvinyl chloride, polyethylene, and others, form predominantly unstable solutions which separate out after a definite time. The general principle of formation of such a solution of any polymer lies in the selection of a liquid or mixture of liquids which act as solvents only above the critical solution temperature. Below this temperature metastable solutions are formed, which can pass spontaneously in the course of time into colloidal solutions (microseparation) or form two phases (macroseparation). Such solutions can be stabilized by low-molecular additives, the molecules of which can become attached at the interphase boundary and smooth out sharp differences between the phases. The form of the molecules is of great importance in this respect. For a given concentration, solutions of flexible macro- molecules may be regarded as being far from saturation if the macromolecules are coiled and the surface density of the polar groups is high, and as super-saturated solutions if the macromolecules are uncoiled and the surface density of CH_2 groups is considerable (in a polar medium). In the latter case the conditions are fully favorable for separation. For solutions of molecules with rigid uncoiled chains in presence of numerous CH_2 groups the stable region is represented by an aggregated solution ($\Delta F_s > \Delta F_{\text{agg. s}}$ where F is the change of free energy because, as the result of aggregation through CH_2 groups, their force fields are balanced by mutual interaction of these groups. If the chains are coiled the region of highest stability in a polar medium is represented by a macromolecular solution because $\Delta F_s > \Delta F_{\text{agg. s}}$.

Phase separation occurs quite analogously, although in a more complex manner, in polymer - polymer - solvent systems. Such systems are characterized by complete miscibility of the polymers taken separately in a given liquid, and lack of miscibility when the polymers are mixed in the same liquid. It should be emphasized that one polymer may act as both a stabilizer and as a precipitant with respect to the other. Such systems have been studied for a long time.

In studies of mixtures of starch and gelatin, de Jong showed that at a quite definite concentration this system separates out into two solutions, each of which contains the dissolved polymers in different proportions. This effect was termed coacervation. Dobry [3], who studied a number of such systems, concluded that phase separation in polymers is the rule rather than the exception, and that the concentration at which it occurs depends not only on the chemical nature of the components but on their molecular weight and the form of their macromolecules. It was held that the basic condition for compatibility is the presence of common quasicrystalline structural elements in the macromolecules. Kern [4], who studied phase separation in solutions of vinyl polymers, stressed that interaction is stronger between similar than between dissimilar molecules, and that separation of polymer solutions can be attributed to very low values of the entropy of mixing or positive values of the free energy of mixing. Scott [5], in a study of polymer compatibility, showed that mixing is possible if the heat content $\Delta H < 0$. Slonimskii and Struminskii [6], who investigated the same problem also considered that complete compatibility occurs when $\Delta H < 0$. They emphasized that with increase of the molecular weights of the two polymers the role of the entropy change (ΔS) in the value of ΔF diminishes considerably. Indeed, if we assume that two compatible polymers have macromolecules of the same size and flexibility, we may also assume that when such macromole-

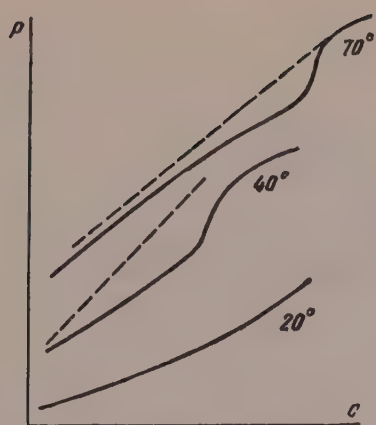


Fig. 1. Variation of osmotic pressure (P) with concentration (c) in starch - gelatin systems at various temperatures.

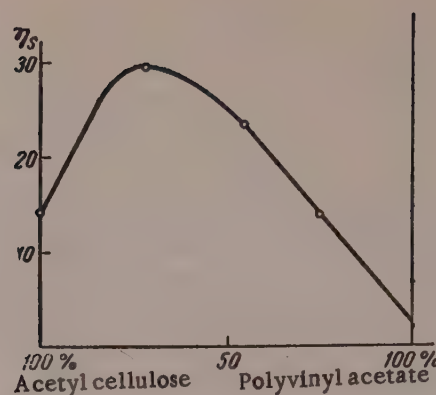


Fig. 2. Variation of specific viscosity (η_s) with composition (N) of mixtures of 1% solutions of acetylcellulose and polyvinyl acetate.

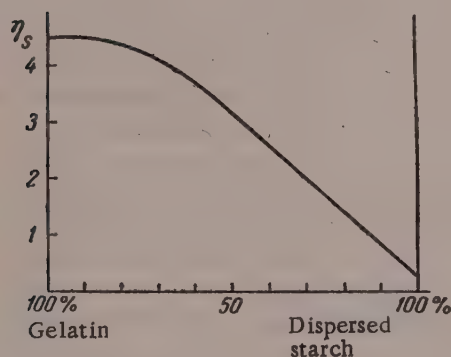


Fig. 3. Variation of specific viscosity (η_s) with composition of mixtures of 0.5% aqueous solutions of gelatin and dispersed starch.

cules are mixed no additional configurations arise. The entropy of mixing of such polymers per g of mixture is very small and the sign of the free energy is determined by the sign of ΔH ; i.e., mixing occurs only when $\Delta H < 0$ and even a small negative heat of mixing corresponds to phase separation. Recently Mikhailov [7], in studies of mixtures of polyvinyl chloride with acetylcellulose and of polyacrylonitrile with acetylcellulose, found that both true and colloidal solutions may be formed, in accordance with concentration, and the former may pass into the latter in the 2-5% concentration range. Mikhailov considers that such colloidal solutions are thermodynamically unstable, and that their kinetic stability is high only because of the high viscosity.

In that publication the criterion of thermodynamic compatibility of polymers in the solid phase is taken to be the expression $\Delta H \neq 0$.

Recently the question of compatibility has been receiving increased attention, as studies of compatibility provide means of modifying the properties of different polymers with the aid of a common solvent.

Vigelow and Kraagg [8] studied a number of systems by the viscosity method and showed that if a common solvent for two polymers is a good solvent for one and a bad solvent for the other then the viscosity - concentration curves exhibit peaks or depressions which are not found if the solvent can be regarded as a good one for both polymers. In a very interesting paper, Hungar and Wiesner [9] considered processes of transition from true solutions to colloidal systems in solutions of polymer mixtures; it was shown that additions of small amounts of other liquids to such solutions raises polymer compatibility sharply.

Dogadkin [10] also showed that mixtures of natural rubber and SKB synthetic rubber in a common solvent do not separate out if the total concentration is less than 5%, but the experimental viscosity - composition curves are not additive. They become additive if polar substances are added to the mixtures or if the temperature is raised.

It follows from all the foregoing that there are many different explanations for phase separation of solutions of pairs of polymers, and different ways of inducing compatibility have been suggested. In our opinion the compatibility of polymers both in the solid state and in solution with a common solvent is determined by the same

factor as the compatibility of substances of low molecular weight – a negative value of the free energy. Spontaneous mixing of polymers in the solid state is improbable because the macromolecules are bound by intermolecular forces which must be overcome on mixing. Such mixing is more possible in the high-elastic than in the solid state, and it readily occurs spontaneously in the viscofluid state. The free energy ΔF may have a negative sign either when $\Delta H < 0$, or when $\Delta S > 0$, or as the result of both factors together. We cannot agree with the view that there is no gain of ΔS when polymers are mixed, such as is the case when a polymer is mixed with a liquid of low molecular weight. Everything depends on the packing density when the polymers are mixed. If the packing density was greater in the original state than after mixing ΔS increases considerably and the sign of ΔF is to a considerable extent determined by the sign of ΔS , as this is equivalent to conversion of rigid into flexible molecules. The assumption that mixing is determined only by a negative value of ΔH is equivalent to the assumption that only polar polymers are miscible.

Therefore the first way of achieving mixing is by rolling or a similar operation which converts the polymer into the viscofluid state. This condition for mixing is satisfied if the macromolecules to be mixed are of similar structure or contain groups capable of interacting with each other. It is quite obvious that two nonpolar polymers of similar structure must be miscible, mainly owing to increase of ΔS , as in this case $\Delta H = 0$ or is very small. Another way of mixing two polymers is in solution with a common solvent. In such cases there are not many solvents that give complete miscibility, as molecules of one solvent may interact differently with the molecules of the two polymers. If the two polymers are nonpolar and dissolve in a nonpolar solvent, they are deposited as a mixture when precipitated from solution. In this case

$$\sum Q = Q_{11} + Q_{12} + Q_{13} + Q_{22} + Q_{23} + Q_{33},$$

where Q is the heat of mixing, the subscript 1 refers to the solvent, and the subscripts 2 and 3 to the two polymers.

If the solvent eliminates the field of force of the macromolecules completely and they exist in isolation from each other in solution, then in the case of polar polymers they can also be mixed in the solid state on precipitation. If the solvent does not eliminate the field of force of the macromolecules of the two polymers, then if the polymers contain certain groups, interaction between them may occur even in the dissolved state. In that case:

$$Q_{23} = \sum Q - (Q_{11} + Q_{12} + Q_{13} + Q_{22} + Q_{33})$$

If such a mixture in the solid state is dissolved in a more active solvent or at a higher temperature the complex present breaks down into isolated molecules with rupture of Q_{23} bonds.

Of course, all the foregoing is highly simplified, because polymer miscibility may be determined by entropy as well as energy factors. Steric factors, form and flexibility of the macromolecules, and presence of functional groups are of great significance in this respect. Unfortunately, these aspects have not been studied as yet, so that it can only be stated that mixing of a rigid and a flexible, a linear and a branched, or a linear and a globular polymer, etc., would differ from the mixing, say, of two linear polymers. Since the solubilities of polymers in the same liquid differ and the critical concentration is very high for some and very low for others, and the critical concentration of one polymer may diminish sharply in presence of another, as is the case in presence of a nonsolvent, it follows that the problem of mixing is highly complex and its study is of great practical and theoretical interest.

Consider first the mixing of two solutions, of gelatin and starch respectively in water, neither of which has been formed spontaneously; it may be seen that these solutions are supersaturated and the critical concentrations of the two polymers are very low; these same polymers in the dispersed state, when the critical concentration of each is increased sharply, form macromolecular solutions which are completely miscible without separation.

It should be noted that mixing of supersaturated solutions of starch and gelatin does not lead to phase separation in the region of low concentrations. However, a mixture of the same polymers loses its stability at higher concentrations. We may assume that separation may occur in latent and visible forms: latent separation can be observed by means of methods which reveal absence of additivity of properties in the mixtures; the more

pronounced the anomalies, the greater the tendency to visible separation of the mixture. Viscosimetric, osmotic, and colorimetric methods, which may reveal structural and thermodynamic peculiarities in separating systems, may be utilized with polymer mixtures. Figure 1 represents results obtained in determinations of the osmotic pressure of starch and gelatin solutions at different polymer concentrations. It is seen that the osmotic pressures of the mixtures are lower than the additive values; at higher polymer concentrations there are inflection points, which indicate considerable microseparation of the system. If the temperature is raised to 40° the point of inflection is shifted toward higher concentrations, which may be due to the fact that one of the mixture components, gelatin, forms a true solution at 40° and the tendency to phase separation can be caused only by aggregation of starch macromolecules. At 80° anomalous behavior of the mixture ceases entirely. Starch and gelatin in the dispersed state are miscible without appreciable separation. It may be assumed that because of the presence of acidic OH groups in gelatin and basic NH₂ groups in starch these groups interact by hydrogen bonding in polymers in the native state. Such interaction is hindered in dispersed polymers because of the globular state of the gelatin. The curves presented here are in good agreement with the heats of swelling and solution of the mixtures, experimental data on which will be presented in the next communication.

The results of viscosity determinations for the same systems are given in Fig. 3; these indicate that deviations from additivity are very slight if one of the components is in the dispersed state. Mixtures of polyvinyl acetate with acetylcellulose and polystyrene* respectively exhibit very pronounced anomalies. The viscosity curve for the first pair of substances is presented in Fig. 2. The very pronounced anomalies found for this mixture do not, however, denote lack of compatibility of these polymers in a common solvent — acetone.

SUMMARY

1. Conditions for separation of mixtures of polymer solutions in a common solvent have been considered in relation to the surface density of polar and hydrocarbon groups in the polymer molecules.
2. The criterion for miscibility of polymers, as of substances of low molecular weight, is decrease of free energy, due to both enthalpy and entropy factors.
3. Miscibility of polymer solutions is significantly correlated with the general structure and form of the macromolecules: for example, starch and gelatin, which do not mix under normal conditions, can be mixed if one of the components is in a more soluble (e.g., dispersed) state.

LITERATURE CITED

- [1] S. M. Lipatov, Zhur. Obshchei Khim. 3, 685, 694 (1933).
- [2] K. F. Zhigach and P. A. Rebinder, Zhur. Fiz. Khim. 13, 94 (1939).
- [3] A. Dobry, J. Polymer Sci. 2, 90, (1947).
- [4] R. J. Kern, J. Polymer Sci. 15, 183, (1955).
- [5] R. Scott, J. Chem. Phys. 17, 279 (1949).
- [6] G. V. Struminskiĭ and G. L. Slonimskii, Zhur. Fiz. Khim. 32, 100 (1958).
- [7] N. V. Mikhailov, Summaries of Papers at the 4th All-Union Conference on Colloid Chemistry in Tbilisi [in Russian] (Izd. AN SSSR, 1958) p. 243.
- [8] Vigelaw and Kraagg, Canad. J. Chem. 36, 199 (1958).
- [9] A. Hungar and E. Wiesner, J. Polymer Sci. 30, 121 (1958).
- [10] B. A. Dogadkin, Summaries of Papers at the 4th All-Union Conference on Colloid Chemistry in Tbilisi [in Russian] (Izd. AN SSSR, 1958) p. 229.

Received July 8, 1959

*The results of these determinations will be reported separately in Proc. Acad. Sci. Belorussian SSR.

HEATS OF SOLUTION OF DYES IN WATER AND THE DYEING PROBLEM

S. M. Lipatov and I. M. Movshovich

Moscow Textile Institute

Problems relating to the dyeing of polymer materials are at the center of attention at the present time. The problem of dyeing (mechanism of formation of colored material) can be solved only if the properties of both the fibers and the dyes are taken into consideration. In the existing thermodynamic theory of dyeing the measure of dye - fiber affinity is taken to be the change of standard chemical potential μ :

$$\Delta\mu^0 = RT \ln \frac{|Na|_f^z |D|_f}{V^{z-1}} - RT \ln |Na|_\sigma^z |D|_\sigma,$$

where $|Na|$ is the sodium-ion concentration; $|D|$ is the dye-ion concentration; V is the effective volume; the subscripts f and σ refer to the fiber and solution respectively.

Unfortunately, no investigations in this field have revealed the equilibrium constant, and therefore the mechanism of dyeing remains obscure. As a consequence of this, $\Delta\mu^0$ retains a constant value for a large group of dyes which differ in chemical composition, degree of aggregation, and solubility, and therefore it does not represent either the individual properties of the dyes or the characteristics of the dyeing process (see table).

The table shows that $\Delta\mu^0$ varies over a very narrow range, from 5.11 to 5.83 kcal/mole. Since it is related to $-\Delta H$ and $-\Delta S^0$ ($\Delta\mu^0 = -T\Delta S^0$), the table contains calculated values of $-\Delta H$ and $-\Delta S^0$, which give a more precise characterization of the individual properties of the dyes. It seems that dye and fiber reactivity can be better expressed in terms of the heat of dyeing ΔH^0 or the entropy change ΔS^0 . It is important to note that ΔH^0 depends not only on the reactivity of the active groups in the fiber and dye, but also to a considerable extent on the bonding energy between the dye molecule and water, i.e., on hydration of the dye. As the heat of hydration cannot be determined separately, we may assume that ΔH^0 is connected with the heat of solution of the dye in water, and therefore determinations of the heats of solution of dyes in relation to temperature are of interest not only for providing insight into dye properties, but in relation to the mechanism of dyeing as a whole.

One of the most characteristic properties of direct dyes is their tendency to form fairly stable supersaturated solutions. This characteristic may be attributed to lack of compensation of the field of force of the nonpolar groups of the dye molecule in water.

Apparently in an aqueous medium all the polar groups of a dye molecule are completely hydrated, and aggregation can be caused only by mutual interaction of nonpolar groups. In general it may be assumed that aggregation in dye solutions may occur in different ways, as shown schematically below:



As the temperature increases, aggregates of type I and II break up into individual ions or molecules, and the heat of such dissociation can be found especially easily by determinations of the heats of solution at different temperatures. It is interesting to note that the heats of solution of most dyes at room temperature are positive. Therefore in the equation $Q = q - c$ the value $q > c$, which indicates that the heat of solvation predominates over

Dyes	$-\Delta\mu^\circ$, kcal/mole		$-\Delta\mu^\circ$, kcal/mole	$-\Delta S^\circ$, kcal/mole · degree	Number of SC_3Na groups
	80°	100°			
Direct Pure Sky-Blue	5.83	4.88	22.5	48.6	4
Direct Black K	5.64	4.75	21.5	46.2	2
Direct Dark Green	5.56	4.86	17.9	35.0	2
Direct Black 3	5.58	4.89	17.6	36.0	2
Direct Blue Light-Fast K	5.17	4.49	12.0	20.4	2
Direct Diazo Blue K	5.34	4.97	11.9	19.1	3
Direct Violet	5.28	4.91	11.9	18.7	2
Direct Gray S	5.11	4.76	11.3	17.5	5

* Calculated from Moryganov's data [1].

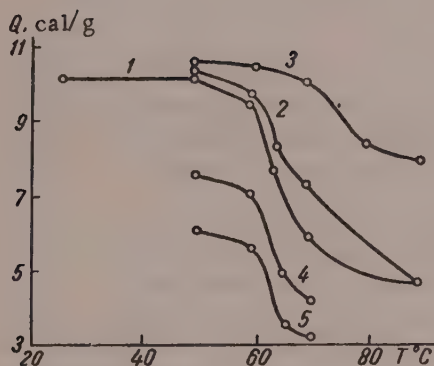


Fig. 1. Heats of solution of Congo Red in various solvents: 1) water; 2) NaCl, 10 g/liter; 3) 20% pyridine solution; 4) 10% ethyl alcohol solution; 5) 20% ethyl alcohol solution.

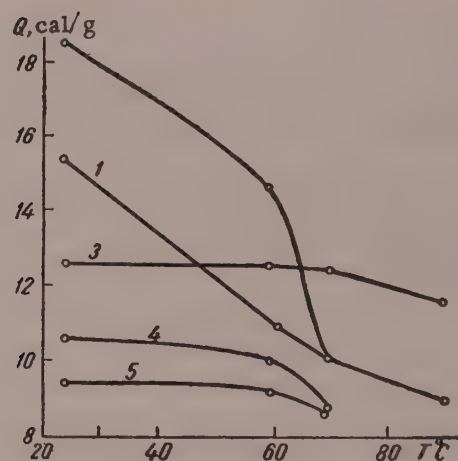


Fig. 2. Heats of solution of Direct Pure Sky-Blue in various solvents: 1) water; 2) NaCl, 10 g/liter; 3) 20% pyridine solution; 4) 20% ethyl alcohol solution; 5) 80% ethyl alcohol solution.

the heat of bond breakdown between any particular groups. In this connection it is interesting to note that the solubility of a dye rises sharply with rise of temperature instead of decreasing; this may be attributed in the first instance to breakdown of bonds between nonhydrated polar groups. In studies of heats of solution of dyes in relation to temperature [2] it was found for a number of polymers, soaps, and dyes that the heat of solution depends sharply on the temperature, and the relationship is of the nature of fusion and conforms to the Kirchhoff law. However, not all substances conform to this relationship, which varies appreciably with the nature of the solvent; therefore, in accordance with the results of osmotic determinations, it was assumed that the sharp decrease of the heat effect with increase of temperature is due to formation of aggregated solutions at low temperatures, and of molecular or ionic solutions at high temperatures. That is why in such systems the partial solubilities and heats of solutions of individual groups must be taken into account. The heat of solution Q_L may be regarded as the sum:

$$Q_L = q_p - c_p - c_n$$

where q_p is the heat of solvation of the polar groups; c_p is the heat expended in cleavage of the bonds between polar groups; and c_n is the bond energy for the nonpolar groups and the energy characteristics of the bonds between the nonsolvated groups in general. For this investigation two dyes were chosen, differing in the number of SO_3Na groups and therefore in solubility: Congo Red (two SO_3Na groups), with a tendency to form aggregated solutions, and Direct Pure Sky-Blue, which dissolves without appreciable aggregation. In addition to water, the solvents used were aqueous alcohol, aqueous pyridine, and NaCl solutions.

Congo Red. Determinations of the heat of solution of Congo Red in water at various temperatures (Fig. 1) showed that the heat of solution is positive over the entire investigated range from 20 to 90°, and over a fairly wide temperature range (20-60 and 75-90°) the heat of solution is independent of the temperature.

Thus, over an interval of about 15° (between 60 and 75°) there is a sharp drop in the heat effect, involving absorption of ~ 5 calories of heat. It is interesting to note that the heat of solution of Congo Red is somewhat higher in NaCl solution than in water, although it is well known that common salt suppresses the electrolytic dissociation of this dye. The heat of solution - temperature curve for aqueous pyridine solution lies consequently higher; the upper point of the inflection corresponds to 72° and the lower to 80°, and only ~2 calories of heat is absorbed. This is quite consistent with the solvent properties of pyridine. On the other hand, the heats of solution in alcohol, which is an effective precipitant, are considerably lower, and the higher the alcohol concentration the lower does the heat-effect curve lie. These results are fully consistent with the adsorption properties of Congo Red. Congo Red is taken up in greater amounts from aqueous alcohol solutions than from solutions in water. The influence of common salt, in presence of which dyeing is more intensive and the heat of solution even increases somewhat, is probably associated with electrostatic phenomena.

Direct Pure Sky-Blue differs sharply in its behavior from Congo Red, not only in pure water but also in the above-mentioned solutions. The heat of solution of Direct Pure Sky-Blue decreases steadily with increase of temperature in the 25-90° range (Fig. 2). The curves in Fig. 2 do not have the sharp breaks characteristic of Congo Red, and there is a fairly considerable decrease of the heat effect, possibly owing to the polydisperse character of this dye. Possible confirmation of this assumption is provided by the fact that, in presence of aggregating agents such as common salt and alcohol, the plateaus and drops in the curves become more pronounced (as in fusion). Comparison of the absolute heats of solution of Congo Red and Direct Pure Sky-Blue shows that at both low and high temperatures the heat of solution of Direct Pure Sky-Blue is approximately 1.5-2 times that of Congo Red.

These preliminary determinations show that heats of solution and sorption provide a more accurate measure of dye - fiber interaction than the chemical potential.

SUMMARY

1. It is shown that the enthalpy ΔH° and entropy ΔS° are a better measure of fiber and dye reactivity than the standard chemical potential $\Delta \mu^\circ$.
2. The heats of solution of dyes have been studied in relation to temperature and the connection between the heat of solution and the sorption of the dye by fibers is demonstrated.

LITERATURE CITED

- [1] T. Vickerstaff, Physical Chemistry of Dyeing (Moscow, 1958) [Russian translation]; P. V. Moryganov, Doctorate Dissertation [in Russian] (Moscow, 1958).
- [2] S. M. Lipatov, Colloidochemical Principles of Dyeing [in Russian] (Ivanovo, "Osnova" Press, 1929); Zhur, Obshchei. Khim. 3, 695 (1933).

Received May 26, 1959

THE PHASE STATE OF DIFFERENT CELLULOSE MODIFICATIONS

S. M. Lipatov, D. V. Zharkovskii, and I. M. Zagraevskaya

Moscow Textile Institute

The question of the structure of different cellulose modifications is of great interest because of the exceptional position of cellulose among the other polymers.

We showed in 1932 [1] that different modifications of cellulose (native, depolymerized, and hydrate cellulose) differ from each other by their contents of free OH groups, i.e., by the numbers of OH groups involved in intermolecular bonding.

The rate of hydrolysis of such modifications increases with decrease in the number of intermolecular bonds between the chains, i.e., with decrease in the number of free OH groups; this has been confirmed by a number of investigations [2, 3]. Kargin and Mikhailov [4] showed that structural changes need not be correlated with mutual interaction of OH groups, as is the case in mechanical stretching of hydrate cellulose fibers which acquire additional strength but retain the activity of the original material. If such cellulose is heated in water or glycerol it loses its orientation completely; this is regarded as return to the equilibrium amorphous state.

Discussions of this subject [5, 6] led to the conclusion that the x-ray and electron diffraction methods, which had been regarded as convincing, do not solve the problem of the phase state of cellulose and other polymers. Mikhailov [7] considers that these methods "indicate the high orientation of cellulose but do not touch upon the question of its phase state". Further investigations in this field may therefore shed more light on the problem.

The Role of CH_2 and OH Groups in Formation of Cellulose Structure. In discussion of cellulose structure the role of CH_2 groups, which do not receive due attention in recent publications, must not be ignored. Cellulose is easily wetted by hydrocarbons; this is shown by the results of determinations of the heats of wetting of native cellulose (11.8 cal/g) and hydrated cellulose (20.0 cal/g) by benzene. The higher heat of wetting of hydrated cellulose by benzene can be attributed only to the looser structure of hydrate cellulose and the greater accessibility of its CH_2 groups. The fact that hydrocarbons do not act as plasticizers indicates that their bond energy with CH_2 groups is very low, but the value of the heat of wetting gives reason to believe that under favorable conditions bonding of the macromolecules may be effected by means of CH_2 groups also. When cellulose is wetted by water the latter interacts with weakly-bound and free OH groups in cellulose. The heats of wetting of native cellulose (10.5 cal/g) and hydrated cellulose (16 cal/g) by water indicate that water does not overcome all the bond energy between OH groups and interacts only with free OH groups. Evidently, investigation of the heat of wetting is a means of determining the numbers of free and bound OH groups in cellulose if the heat of wetting of one OH group by water is known.

It has been shown [8] that all the OH groups in starch, irrespectively of its structure, are accessible to interaction with water. The heat of wetting of starch is the same for different structural modifications of starch, and is 28 cal/g or 4536 calories per glucose residue, which corresponds to the heat of wetting of three OH groups. Hence the heat of wetting (Q) of one OH group by water is $(28 \times 162)/3 = 1512$ calories.

From this value and the results of determinations for different cellulose modifications [9] we have the

following data:

	cal per OH Group	Number of Bound OH Groups
Native	561	2
Hydrate cellulose	800	1.4
Dispersed during 1 hour	1165	0.5

Temperature, t °C	Native	Hydrate cellulose	Dispersed	Recrystallized
14	43.6	53.0	---	---
25	34.0	43.6	58.0	40.0
35	25.0	34.0	---	---
60	17.3	26.8	---	---

The calorimetric method is the most accurate method for determination of the numbers of free and bound OH groups. If the maximum heat of wetting (Q) of starch containing three free OH groups [8] is 28.1 cal/g (4536 cal per $C_6H_{10}O_5$ group or three OH groups) whereas for dispersed cellulose $Q = 20.9$ cal/g, the number of free OH groups is $c_{OH} = [20.9/28.1] \cdot 100 = 74\%$. It follows that dispersed cellulose contains 74% free and only 26% bound OH groups. Native cellulose contains 27% free and 63% bound OH groups, and hydrate cellulose has 55% free and 45% bound OH groups. These values are in good agreement with data on "crystalline" and "amorphous" regions determined by the x-ray method, from density data, and by other methods. The number of bound OH groups determines the magnitude of the oriented regions in cellulose, and therefore it is not possible to alter the cellulose structure (packing density) without affecting the bonds between OH groups.

In most cases stability of the structure is determined by the orienting field of the OH groups. Therefore if certain properties of a sample are changed as the result of some influence (such as stretching), such changes cannot be regarded as being at all stable until the structure, determined by the chain orientation, becomes fixed as the result of intermolecular interaction through OH groups. Such an unstable structure breaks down readily when warmed in water, and such breakdown indicates merely instability of the packing, and not a tendency of oriented cellulose to return to the amorphous state as one nearer to equilibrium.

We consider that the structure of cellulose is primarily determined by the ability of the chains to assume a configuration which ensures maximum mutual approach of the OH groups (see [1]). Only in such cases can artificially induced orientation be expected to be stable; i.e., ΔF is negative if $\Delta H < 0$ and $\Delta H > T \Delta S$.

Recrystallization. Cellulose subjected to vigorous mechanical dispersion has a predominantly amorphous structure (as shown by x-ray diffraction) and a high content of free OH groups. However, this amorphous structure of cellulose does not represent an equilibrium state. Numerous attempts have been made to influence the structure of hydrated cellulose in various ways, and the contradictions between the results are due to the unsuitable methods used for recrystallization. Heating of cellulose in water and in glycerol at 250° cannot be regarded as suitable, because even at that temperature the OH groups in cellulose are hydrated by water or solvated by glycerol, and cannot interact with each other.

The method recently suggested by Mikhailov [7] for fiber formation with stretching in alkaline salt solutions at 140-160° is more successful. This method gave the α -modification of cellulose with bounding between OH groups, with a consequent decrease of equilibrium sorption and the appearance of new interference spots on the x-ray fiber patterns.

We showed by the x-ray method [9] that amorphous cellulose passes spontaneously into the crystalline form on recrystallization, as indicated by the appearance of new interference spots not found for amorphous cellulose. Accordingly the transition of dispersed cellulose into the native state may be regarded as a phase transition of amorphous to crystalline cellulose.

Recrystallization, both of starch and of cellulose, was effected by the action of steam on the samples at 100-140° for 1-2 hours. The heats of wetting (Q) of different cellulose samples in water show that as the result of more prolonged heating Q decreases to 12 cal/g; this may be regarded as almost complete restoration of the native cellulose structure. The macromolecules must have some freedom of movement for orientation. This is achieved if the OH groups are hydrated as the result of wetting and are not interlinked by hydrogen bonds.

	Q, cal/g
Native cellulose	10.4
Hydrate cellulose	15.5
Cellulose dispersed during 2 hours	21.6
Cellulose recrystallized at 100°	17.2
Same, at 140°	12.0

However, when the sample is heated, not only is the thermal motion of the macromolecules and their structural units increased, but the water taken up by the cellulose evaporates, and therefore as soon as OH groups become released from water they interact with each other and reinforce the structure formed. Thus at 120° this process occurs spontaneously ($\Delta F < 0$, $\Delta H < 0$ and $\Delta S < 0$), and the decrease of ΔS is determined by a more ordered arrangement of the macromolecules. This means that in the general thermodynamic equation $\Delta F = \Delta H - T\Delta S$ the term ΔF can have a negative sign only if ΔH ($\Delta H > T\Delta S$), is negative, i.e., if bonds are formed. The packing density then increases not only because of flexibility, but primarily as the result of hydrogen bonding, i.e., owing to a change of enthalpy.

Dissolution of Cellulose. It is very often emphasized that the heat of wetting cannot be used in solving problems of structure, since it refers to the state of the surface only, and that only the heat of solution can provide the answer to the question of the phase state of a polymer. However, the heat of solution of cellulose $Q_L \neq q_{OH} - c_{OH}$, where q_{OH} is the heat of hydration of OH groups and c_{OH} is the energy of rupture of the bonds between them. Since some OH groups are free even in native cellulose, Q_L is for the most part positive and in reality $Q_L = q''_{OH} + q'_{OH} - c_{OH}$, where q'_{OH} and q''_{OH} are the heat of hydration of the free and bound groups respectively. The value of q'_{OH} is higher for hydrate cellulose than for native cellulose, and higher for dispersed cellulose than for hydrate cellulose. Consequently the heat of wetting enters into the heat of solution and if the heats of solution of samples of different degrees of orientation are found experimentally to be constant, the true heat of solution $Q_0 = Q_L - q_{OH} = q''_{OH} - c_{OH}$ can be found. The true heats of solution Q_0 may be equal if q'_{OH} is also equal for all the samples, i.e., if mechanical orientation does not lead to formation of new bonds between OH groups and if the orientation is of a purely mechanical, unstable character.

To provide a more precise solution to this problem, we determined the heats of solution of different cellulose samples in the $[(C_2H_5)_3C_6H_5N]OH$ base at different temperatures.

The results of these determinations are presented in the table.

These results show that Q_0 has different values for different cellulose samples and that recrystallization has a significant influence on the number of OH groups involved in bond formation. If it is taken into account that bond formation is accompanied by artificial orientation and that such orientation conforms to the general equation $\Delta F_{or} = \Delta H_{or} - T\Delta S_{or}$, it follows that the expenditure of energy to overcome the kinetic forces of macromolecular flexibility, which tend to disperse individual portions of the macromolecules, leads to a negative value of ΔS , and the orientation may be stable if the signs of ΔF and ΔH are negative.

Only intermolecular forces can make any given cellulose groupings stable; therefore the stable form of cellulose is not the amorphous but the orientated modification; in the limit, the crystalline modification.

SUMMARY

1. The heats of wetting of various cellulose modifications by water and benzene were determined, and the role of CH_2 and OH groups in structure formation was demonstrated.
2. The stable modifications of cellulose are those with the greatest orientation.
3. Conditions for recrystallization of cellulose are considered and a new method for effecting it is proposed.
4. Different cellulose modifications have different heats of wetting and of solution; the structure of cellulose is determined by interaction of the molecules and not by their flexibility.

LITERATURE CITED

- [1] S. M. Lipatov, Zhur. Priklad. Khim. 3, 1091 (1930); High Polymers [in Russian] (State Light Industry Press, 1936) p. 132.
- [2] Z. A. Rogovin, Cellulose Chemistry [in Russian] (Goskhimizdat, 1953).
- [3] A. A. Konkin, Doctorate Dissertation [in Russian] (Moscow, 1957).
- [4] V. A. Kargin and N. V. Mikhailov, Zhur. Fiz. Khim. 14, 195 (1940).
- [5] A. L. Zaides, Doklady Akad. Nauk SSSR 80, 213 (1951); Kolloid. Zhur. 18 (1956).*
- [6] G. L. Slonimskii, Mechanical Properties of Polymers and Properties of Polymer Solutions [in Russian] (State Light Industry Press, 1951).
- [7] N. V. Mikhailov, Doklady Akad. Nauk SSSR 109, 1160 (1956).
- [8] S. M. Lipatov and M. S. Shul'man, Kolloid Zhur. 12, 207 (1950).
- [9] D. B. Zharkovskii and S. M. Lipatov, Izv. AN BSSR 2, 170 (1952).
- [10] N. V. Mikhailov, Summaries of Papers at the 8th Mendeleev Congress, No. 6 [in Russian] (Izd. AN SSSR, 1959).

Received May 26, 1959

*Original Russian pagination. See C. B. Translation.

EFFECT OF TEMPERATURE ON THE HEAT OF SOLUTION AND PACKING DENSITY OF POLYSTYRENE

S. I. Meerson and S. M. Lipatov

Moscow Textile Institute

Studies of the effects of temperature on the heats of solution of polymers reveal the changes undergone by the polymer in the pure and dissolved states on change of temperature, and make it possible to establish the relationship between the heat of solution of a polymer and its physical and phase states. Therefore our method for determination of heats of solution at various temperatures is very important as a "structural" method of studying polymers.

In recent years numerous publications have appeared in which the physicochemical properties of polymers are correlated with their packing density; accordingly, the question of methods for determining the packing density has arisen. Gatovskaya, Kargin, and Tager [1] noted that determinations of heats of solution and sorption isotherms are the main methods by which the packing density of polymer chains can be estimated. However, it has been pointed out [2] that "in estimations of packing density the sorption and calorimetric methods are not equivalent: changes of intermolecular forces can be assessed from determinations of heat effects, whereas sorption is determined by the configuration range as well as by looseness of packing". In the discussion of this question we shall consider the calorimetric method for determination of packing density.

We showed that different fractions of a given polymer, with limited swelling in the range of relatively low temperatures, have the same heat effects of interaction with the liquid at these temperatures, but at higher temperatures the heats of solution of the fractions differ from each other. We correlated these differences with differences in the structure of the fractions, in the looseness of their packing, and in the energy of intermolecular bonding [3]. Similar investigations were carried out on fractions and certain structural modifications of gelatin [3, 4], agar [5], starch [6], and polyvinyl chloride [7]. In all these cases, except that of agar, the heats of solution of the fractions at high temperatures were lower for fractions of higher molecular weights, in contrast to polystyrene, the heat of solution of which was found by Schulz [8] to diminish with decrease of molecular weight. It was shown for these polymers that structural characteristics of polymers and polymer fractions which exhibit limited swelling can be revealed only in the temperature range in which all intermolecular bonds are overcome and complete dissolution occurs [9]. Studies of the heat of interaction with liquids at low temperatures in such cases only give the heats of solvation of free or weakly interbonded active groups, and are therefore inadequate for estimation of intermolecular bond energies or polymer packing densities. Despite the existence of publications concerned with studies of the influence of polymer structure on heat of solution, in a publication [10] concerned with the relationships between thermodynamic functions, packing density, and molecular flexibility the conclusion is drawn that packing density has never been taken into consideration in thermochemical investigations of polymer dissolution. This is not so, because packing density is primarily related to the energy of intermolecular bonding of a polymer (ΔH_{22}), and this quantity, which characterized the polymer microstructure, has always been taken into consideration in calorimetric investigations, since

$$\Delta H = \Delta H_{11} + \Delta H_{22} - \Delta H_{12},$$

where ΔH is the total change of enthalpy during dissolution; ΔH_{11} is the change of enthalpy on interaction of solvent molecules; ΔH_{12} is the change of enthalpy on solvation.

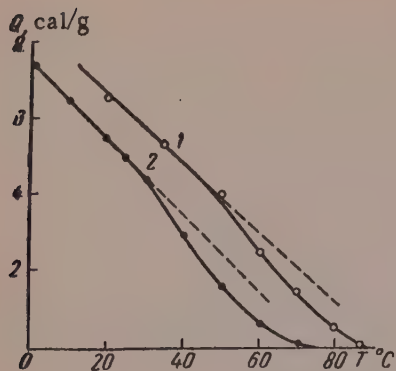


Fig. 1. Effect of temperature on the heat of solution of polystyrene in toluene: 1) our data; 2) data of A. A. Tager and N. M. Gur'yanova.

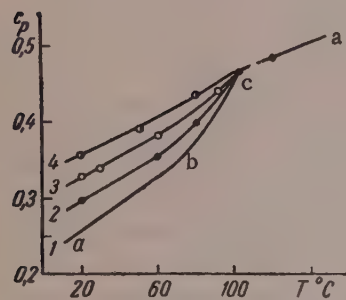


Fig. 2. Heat capacity of polystyrene as a function of temperature: 1) pure polystyrene [7]; 2) 49% solution of polystyrene in toluene; 3) the same, 24% solution; 4) the same, 7% solution.

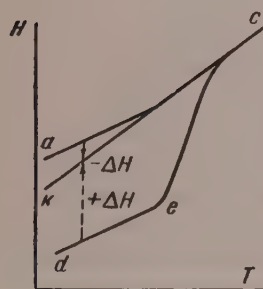


Fig. 3. Enthalpy-temperature relationship for a glassy polymer (abc), a crystalline polymer (dec), and an "equilibrium melt" (kbc).

1. Studies of the heats of solution of polymers can yield definite information on changes of their packing density under various influences only if the chemical composition of the polymer is unchanged.

Examples of this are provided by variations of the heat of solution of rubber with the degree of stretching [11], differences between the heats of solution of crystalline and amorphous polymers, changes in the heat of solution as the result of thermal relaxation of quenched polymers, etc. If other functional groups are introduced into the polymer chain (as in saponification of polyvinyl acetate or changes in copolymer composition) definite conclusions concerning changes in the packing density cannot be drawn from the heats of solution, because the chemical composition has been changed. In such cases it is not always possible to find a solvent such that ΔH_{12} is zero or, at least, the same for all copolymers of different composition. Thus, in work on saponified polyvinyl acetates [12] the solvent chosen was acetone, in which polyvinyl acetate dissolves readily, but polyvinyl alcohol does not even swell. It is clear that no conclusions can be drawn concerning changes of packing density in the series polyvinyl acetate — partially saponified polyvinyl acetates — polyvinyl alcohol. In another study [13] with the same series of polymers the solvents used were ethyl acetate, mixtures of ethyl acetate and alcohol corresponding in composition to the composition of the saponified polyvinyl acetates, and pure ethyl alcohol. In this case when pure liquids are replaced by solutions of various compositions the heats of interaction of the two liquids, the values of which depend on the composition, must be considered; moreover, it is necessary to take into account the possibility of interaction of the polymer with the second liquid, which is not its hydrogenated monomer. These effects must be taken into account because of the very small differences between the heats of solutions of the copolymers.

Thermochemical investigations in which such changes are not taken into consideration do not give correct estimates of variations of packing density in a copolymer series. It follows that definite conclusions concerning variations of packing density of polymers can be drawn from heats of solution only if the chemical composition of the polymer remains unchanged during the treatment and if the same solvent is used.

On the assumption that the heat of solution of a polymer depends on the energy of intermolecular bonding and the packing density, we considered [14] the possibility of accounting for the decrease of heats of solution of polymers by increase of their packing density on heating, and drew attention to the fact that the experimental data needed for convincing conclusions of this nature are lacking.

Recently Tager and Gur'yanova [15] repeated the experiments performed by Schulz and by ourselves on determinations of the heats of solution of polystyrene in toluene over a wide temperature range, and obtained similar results. An interesting fact is that the heat of solution of polystyrene in ethylbenzene is the same as in benzene and toluene, despite the fact that ethylbenzene

TABLE 1

Effect of the Duration of Heating of Polystyrene on Its Heat of Solution at 60°

Heating time, hours	1	3	8	12
Q, cal/g	3.2	3.1	2.8	2.8

TABLE 2

Effect of Preliminary Heating of Polystyrene on the Heat of Solution (Q) in Benzene at 25°

Heating temperature, °C	Time of heating, hours	Cooling conditions	Q, cal/g
—	—	—	6.0
80	4	Slow	5.3
90	2	Rapid	6.5
80	8	Slow	5.5

is the hydrogenated monomer of polystyrene. In their paper the decrease of the heat of solution of polystyrene with temperature is ascribed conclusively to increase of the packing density of polystyrene which takes place, in the author's opinion, when the polymer is heated under the conditions of the calorimetric experiments (during 8-12 hours) because of the decrease of the relaxation time and increase of macromolecular flexibility. On these grounds the authors consider that they established the general relationship between polymer packing density and temperature. This conclusion is inconsistent with experimental data. Let us consider how the time of heating of a tube containing the substance under the conditions of the calorimetric experiment influences the heat of solution. Our published data on the effects of temperature on the heats of solution of polystyrene in various solvents were obtained under conditions such that the tubes with the substances were not held in the calorimeter for 10 hours. Nevertheless, we observed a decrease of the heat of solution from 7 cal/g to zero as the temperature was increased from 10 to 80°. Our data and those from the paper cited [15] are plotted in Fig. 1. As the specimens of polystyrene used in the experiments may have been different, the experimental points show some differences. The discrepancy is least in the region

of low temperatures. It is also possible that these discrepancies are associated with the effect of the duration of heating on the heat of solution. It must be pointed out, however, that despite the different conditions of heating in both cases the heat of solution decreases by 6.5-7 cal/g on increase of temperature. According to the views of the authors of the paper cited there should not be such a considerable decrease of the heat effect with increase of temperature without prolonged heating.

It follows that either preliminary heating does not have any significant influence on the heat of solution and its variations with temperature, or relaxation processes are more rapid when polystyrene is heated than when the tubes are kept in the calorimeter. It has been shown [16] that the time of volume relaxation of polystyrene depends on temperature: at 73° volume relaxation is completed after about 1.5 hours, and at 60°, after 3 hours. With these data taken into consideration in determination of the influence of the heating time on the heat of solution of polystyrene, we carried out experiments at 60°. The tubes with polystyrene were kept in a calorimeter previously heated at 60° for different times, and the heat of solution in benzene was then determined. The results are presented in Table 1.

Table 1 shows that the duration of preliminary heating has no significant influence on the heat of solution of polystyrene.

This result may be confirmed by other experiments. If the observed considerable decrease of the heat of solution of polystyrene with increase of temperature (~7 cal/g) was due to increase of its packing density on heating, then preliminary heating of polystyrene at high temperatures ($\geq T_g$) and subsequent cooling to room temperature should influence the heat of solution at room temperature. If this view is correct, the heat of solution should be less after heating than before. The results of determinations of the heat of solution of polystyrene after preliminary heating are given in Table 2.

Table 2 shows that preliminary prolonged heating of polystyrene has very little effect on the heat of solution. Similar results were obtained earlier [17], when it was shown that isotropic polystyrene film dried under vacuum dissolves with liberation of 5.5 cal/g; oriented film stretched 2000% and heated at 120° under the same tension for 10 hours dissolves with a very similar heat effect, 5.1 cal/g. It is evident from this that heating even under these conditions does not result in a substantial decrease of the heat of solution. From the fact that the heat of solution is decreased by 0.5 cal/g it is concluded [17] that the packing density of oriented polystyrene increases as the result of heating. Therefore it follows from these data and Table 2 that the change of intermolecular

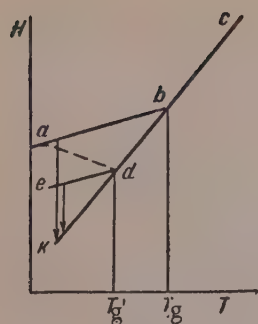


Fig. 4. Enthalpy - temperature relationship for a rapidly-chilled polymer (abc), slowly-chilled polymer (edc), and an "equilibrium melt" (kdc).

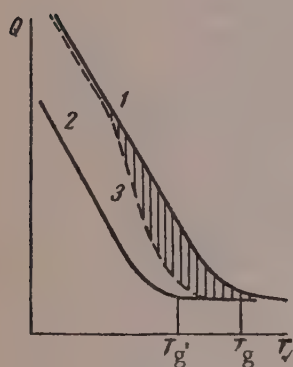


Fig. 5. Heat of solution - temperature relationships for: 1) rapidly-chilled glassy polymer (for the abc - kbc transition, Fig. 4); 2) slowly-chilled polymer (for the edc - kde transition, Fig. 4); 3) on increase of the polymer packing density under conditions of the calorimetric experiment (for the adc - kde transition, Fig. 4).

zero), it follows that as the temperature increases the decrease of the heat of solution of polystyrene is due to decrease of the heat of glass transition.

It follows that the effect of temperature on the heat of solution and the magnitude of the heat of solution of polystyrene at a given temperature are determined by the value of Δc and its dependence on the temperature, i.e.,

$$Q_d = -\Delta H_g = \int_{T_1}^{T_2} \Delta c dT.$$

bonding energy in polystyrene heated at temperatures close to T_g does not exceed 0.5-0.6 cal/g. It is clear from this that when polystyrene is heated there is some increase of the packing density, but the decrease of the heat of solution with increase of temperature should not be ascribed to this change.

We showed earlier [18], in agreement with the results of Schulz [19], that when polystyrene dissolves the heat liberated is equal to the difference between the enthalpies of glassy (H_g) and dissolved (H_d) polystyrene

$$-\frac{dQ}{dT} = \Delta c = \frac{d(H_d - H_g)}{dT}.$$

The heat capacity - temperature relationships of pure and dissolved polystyrene are plotted in Fig. 2. Data for pure polystyrene are taken from the Schulz paper [19], while the heat capacities of polystyrene solutions were determined by us. Figure 2 shows that the heat capacity of dissolved polystyrene ($c_d = dH_d/dT$) is greater than that of glassy polystyrene ($c_g = dH_g/dT$) at temperatures below T_g , while the two are equal above T_g . This means that as the temperature rises the enthalpy difference diminishes and ΔH tends to zero or to a constant value as T_g is approached. It follows that the heat of solution of polystyrene should also decrease with rise of temperature, because

$$\Delta H = H_d - H_g$$

It is well known that the integral heat of solution calculated for the solute (second component) when $H_2 \rightarrow 0$ is equal, for crystalline substances, to the sum of the heat of fusion and the integral heat of melt - solvent interaction. In the case of glassy substances it must be taken into account that their enthalpy is not equal to the enthalpy of a supercooled melt ("equilibrium melt"). Figure 3 represents the enthalpy-temperature relationships of a substance in the glassy (abc), crystalline (dec), or "equilibrium melt" (kbc) states. It is clear from Fig. 3 that the enthalpy of a glassy substance is greater than the enthalpy of an "equilibrium melt".

If it is assumed that the enthalpy of a dissolved substance varies linearly to correspond to the line kc for an equilibrium melt, then it follows that when a glassy substance dissolves heat would be evolved which was not liberated in the course of the glass transition, the "heat of glass transition".

Therefore the integral heat of solution of polystyrene is the sum of the "heat of glass transition" and the integral heat of mixing of the "equilibrium melt" with the solvent. If the heat of mixing of an equilibrium melt of polystyrene with toluene and ethylbenzene is taken as zero (since the heats of solution of polystyrene in these two solvents are the same, and ethylbenzene is the hydrogenated monomer, the heat of interaction for which is

On the assumption that in the 20-81° temperature range the change of heat capacity is approximately 0.1, we find the heat of solution of polystyrene at 20°

$$Q_{20^{\circ}} = -\Delta H_g \approx 0,1 (81 - 20) = 6,1 \text{ cal/g}$$

This coincides with the experimental value found for the heat of solution.

We now consider, in the light of the foregoing, how the change of enthalpy of polystyrene due to increase of its packing density on heating should influence the heat of solution - temperature relationship. Figure 4 shows changes in the enthalpy of glassy polystyrene on rapid (abc) and relatively slow (edc) cooling. The straight line kb, which is the continuation of the straight line for the enthalpy change of the melt, may be regarded with some degree of approximation as the line for the enthalpy change of dissolved polystyrene. It is clear from Fig. 4 that as the glassy polymer passes into solution (indicated by arrows) the positive heat of solution decreases with increase of temperature, because $\Delta H_g = H_d - H_g$ decreases. However, in the case of an annealed polymer (edc) the $Q = f(T)$ curve lies somewhat lower than in the transition from ab to kb. It follows from Table 2 and our earlier work [17] that the $Q = f(T)$ curves lie close to each other. If it is assumed that when polystyrene is heated under the conditions of the calorimetric experiments its packing density increases, and as a result the enthalpy of polystyrene varied in accordance with the line ad, then this variation should be reflected in the $Q = f(T)$ curve as shown in Fig. 5 (curve 3). At some temperatures curves 1 and 3 (Fig. 5) coalesce, and then as the packing density increases, a small deflection associated with absorption of heat appears in curve 3. This somewhat diminishes the heat of glass transition liberated during dissolution. It follows that the hatched portion of the graph in Fig. 5 represents the decrease of the heat of solution owing to increase of packing density on heating. As was shown earlier, this value does not exceed 0.5-0.6 cal/g for polystyrene. Careful analysis of the data in Fig. 1 shows that the $Q = f(T)$ relationship is of the nature of curve 3 in Fig. 5. By continuing the linear portion of the curve we can find the decrease of the heat of solution due to increase of the packing density. This value is very small in both cases.

Thus, when polystyrene is dissolved in toluene, benzene, or ethylbenzene, heat of glass transition is liberated. The decrease of 7 cal/g in the heat of solution with increase of temperature is due to the decrease of the heat of glass transition with increase of temperature. The closer the temperature to T_g , the lower the heat of glass transition. The effect of the increased packing density of polystyrene when it is heated in the conditions of the calorimetric experiments is manifested in a certain decrease of the heat of solution, especially as the glass-transition region is approached.

Hence the conclusion that the decrease of the heat of solution of polystyrene is due entirely to increase of its packing density on heating is incorrect, and cannot be automatically applied to all polymers. Every concrete instance requires independent investigation with the physical and phase states of the polymer and their changes over a wide range of temperatures taken into account. In addition, the solution state of the polymer must also be considered. For example, when amorphous polyvinyl alcohol is dissolved in water, or amorphous polyvinyl chloride is dissolved in various solvents, heat is absorbed and not liberated. This indicates that the packing density is higher and that intermolecular forces play a greater role in the glass transition of these polymers than in that of polystyrene.

2. It is known [20] that the sorption of ethylbenzene by polystyrene has high values in the region of low relative vapor pressures, and the higher the molecular weight of polystyrene the more ethylbenzene is absorbed per gram of polystyrene. Sorption data were used to calculate values of $\Delta \bar{z}_1$, and the method of intercepts was applied to calculate values of ΔH_1 from the heats of solution of polystyrene in ethylbenzene [21], and it was shown that $\Delta \bar{S}_1 < 0$. It was concluded from this that sorption of ethylbenzene in the region of low relative vapor pressures may be regarded as true adsorption and that the packing density can be estimated from the values of ΔS_1 . However, as heat of glass transition is liberated when polystyrene is dissolved, a different approach is needed for evaluation of the results obtained in studies of the sorption of ethylbenzene by polystyrene.

It was noted by Jenckel [21] that if the heat of glass transition of polystyrene is taken into account in calculation of partial thermodynamic values, the partial heat of dilution $\Delta \bar{H}_1$ becomes zero over the entire composition range. In that case $\Delta \bar{z}_1 = -T\Delta \bar{S}_1$ is greater than zero for all polystyrene samples of various molecular weights. Accordingly, data [20] on the sorption of ethylbenzene by polystyrene in the region of low vapor pressures are subject to a different interpretation, consistent with the views of Kargin and Gatovskaya [22] according

to whom, in the case of polystyrene, sorption of very small amounts of monomer is sufficient to give rise to high-elastic properties and diffusional sorption. Therefore in sorption of the hydrogenated monomer by polystyrene the degree of sorption is determined by the flexibility of the polymer chains, as in the case of sorption by a polymer with flexible chains, and not by the packing density. In this case $\Delta\bar{S}_1$ represents the partial entropy of dilution, independent of the packing density and the phase state of the polymer. It follows that the packing density cannot be estimated either from this value or from $\Delta\bar{H}_1$, which is the partial enthalpy of dilution. That is not the case for the partial heat of solution of polystyrene, $\Delta\bar{H}_2$. It is clear from the foregoing considerations that the partial heat of solution is equal to the sum of the heat of glass transition (or fusion) and the partial heat of mixing of the melt with the solvent. This value gives an indication of changes in the packing density of the polymer on interaction with the liquid, in contrast with $\Delta\bar{H}_1$, which is the heat of dilution. The same value of $\Delta\bar{H}_1$ may correspond to several values of $\Delta\bar{H}_2$, in accordance with the packing density of the pure polymer. Similar reasoning is valid in relation to the partial entropy of solution of polystyrene, $\Delta\bar{S}_2$.

It follows that the packing density of polystyrene cannot be estimated from the isotherms of sorption of ethylbenzene by polystyrene or from values of $\Delta\bar{S}_1$ and $\Delta\bar{H}_1$. This also follows from the contradiction between calorimetric and sorption data which arises from the paper [12] in which it is shown that in the region of low relative vapor pressures the sorption of ethylbenzene is greater by chilled than by annealed polystyrene, while their heats of solution are equal.

It has been shown [23] that the sorption of n-heptane by crystalline and amorphous rubber is the same, and that the presence of the crystalline phase does not influence the sorptive capacity of rubber. However, it is well known that the phase state of a polymer influences its packing density, specific volume, and heat of solution. The heat of solution is lower for crystalline than for amorphous polymers, as in the solution process more heat must be expended to break down intermolecular bonds formed in the course of close packing. It follows that in this case also the sorption and calorimetric methods give contradictory results: sorption does not depend on the phase state, but the heat of solution does.

It follows that in all cases when there is no true adsorption of the vapor from the liquid by active groups in the polymer, and the sorption process is accompanied by solvation with breakdown for intermolecular bonds between the solvated groups, swelling, and dissolution, the magnitude of the sorption depends not so much on the packing density as on the concentration of the swollen polymer and the configuration range (flexibility). In such cases sorption provides an approach to determination of flexibility of the macromolecules and not of the actual packing density.

Thus the calorimetric method for evaluation of the structural characteristics of polymers (packing density) gives more reliable information than sorption studies in the cases under consideration.

SUMMARY

1. The increase of packing density of polystyrene when it is heated in calorimetric determinations is very slight, and therefore it has very little influence on the heat of solution.
2. The negative temperature coefficient of the heat of solution of polystyrene is attributable to decrease of the "heat of glass transition" with increase of temperature, and not to increase of packing density.
3. Studies of the sorption of ethylbenzene by polystyrene make it possible to estimate flexibility of the macromolecules rather than the packing density of polystyrene, as there is no true sorption in this case, and the sorptional process is diffusional in character.

LITERATURE CITED

- [1] T. V. Gatovskaya, V. A. Kargin, and A. A. Tager, *Zhur. Fiz. Khim.* **29**, 833 (1955).
- [2] V. A. Kargin and Yu. S. Lipatov, *Zhur. Fiz. Khim.* **32**, 327 (1958).
- [3] S. M. Lipatov, Problems of the Science of Lyophilic Colloids [in Russian] (Minsk, 1941); S. M. Lipatov, *Kolloid Zhur.* **8**, 84 (1946); S. M. Lipatov and S. I. Meerson, in the book: Colloids in Processes of the Food Industry [in Russian] (Food Industry Press, 1946).

- [4] S. I. Meerson, Candidate's Dissertation [in Russian] (Moscow, 1945); S. M. Lipatov and S. I. Meerson, *Kolloid Zhur.* 12, 122 (1950).
- [5] S. M. Lipatov and A. A. Morozov, *Zhur. Obshchei Khim* 5, 1120 (1935).
- [6] S. M. Lipatov, B. A. Kartovnik, and M. S. Shul'man, *Kolloid Zhur.* 12, 286, 343 (1950).
- [7] K. S. Akhmedov and S. M. Lipatov, *Kolloid Zhur.* 19, 257 (1957).*
- [8] K. Günner and G. V. Schulz, *Naturwissenschaften* 40, 164 (1950).
- [9] S. M. Lipatov and S. I. Meerson, Report on the Scientific Work of Members of the D. I. Mendeleev All-Union Chemical Society [in Russian] 3, 31 (1953).
- [10] A. A. Tager, Doctorate Dissertation [in Russian] (Moscow, 1956).
- [11] S. M. Lipatov and S. I. Meerson, *Kolloid Zhur.* 8, 233 (1946).
- [12] A. A. Tager and M. Iovleva, *Zhur. Fiz. Khim.* 32, 1774 (1958).
- [13] A. A. Tager and V. A. Kargin, *Zhur. Fiz. Khim.* 32, 1362 (1958).
- [14] S. I. Meerson and S. M. Lipatov, *Kolloid Zhur.* 18, 447 (1956).*
- [15] A. A. Tager and N. M. Gur'yanova, *Zhur. Fiz. Khim.* 10, 9 (1958).
- [16] P. P. Kobeko, Amorphous Substances [in Russian] (Izd. AN SSSR, 1952) p. 171.
- [17] Yu. S. Lipatov, V. A. Kargin, and G. L. Slonimskii, *Zhur. Fiz. Khim.* 30, 1075 (1956).
- [18] S. I. Meerson and S. M. Lipatov, *Kolloid Zhur.* 20, 353 (1958).*
- [19] G. W. Schulz, K. Günner and H. Gerrens, *Z. phys. Chem.* 4, 192 (1955).
- [20] A. A. Tager and Zh. Dombek, *Kolloid Zhur.* 15, 69 (1953).*
- [21] E. Jenckel and K. Gorke, *Z. Elektrochem.* 60, 6 (1956).
- [22] V. A. Kargin and T. V. Gatovskaya, *Doklady Akad. Nauk SSSR* 99, 1037 (1954).
- [23] V. A. Kargin and T. V. Gatovskaya, *Zhur. Fiz. Khim.* 30, 2051 (1956).

Received April 6, 1959

*Original Russian pagination. See C. B. Translation.

DISPERSION OF CELLULOSE

M. S. Shul'man and S. M. Lipatov

Scientific Research Institute of the Alcohol, Liqueur, and Vodka Industry

After fine dispersion in a ball or vibratory mill, starch becomes soluble in the cold and can react actively with amylase without preliminary boiling or conversion into paste [1, 2]. It was shown by x-ray diffraction that the molecular chains in dispersed starch completely lost their spatial orientation. Viscosimetric investigation of solutions of dispersed starch showed that $(\eta_{av}/c = f(c))$ is constant over a wide concentration range. It was found [3, 4] that for polymers with a tendency to aggregation the heat of solution changes considerably with temperature, but if a polymer dissolves molecularly in a liquid its heat of solution is independent of temperature.

We showed [2] that the heat of solution of dispersed starch of the maximum solubility is likewise independent of temperature and less heat is required to bring such starch modification into molecular solution than is needed in the case of native starch. The heat of solution of starch at the maximum degree of dispersion is 25 cal/g. The explanation of the fact that the heat of solution of starch of the maximum degree of dispersion is independent of the temperature may be that intermolecular forces between the starch macromolecules are overcome during dispersion, possibly with simultaneous disintegration of aggregates and changes in their form. The possibility is not excluded that mechanical dispersion also leads to breakdown of ester bridge linkages and formation of free radicals, but in this case these changes were reversible. If dispersed starch is heated in steam at 100° it returns almost entirely to its original state (recrystallization occurs). It follows that the amorphous state of starch is not an equilibrium state.

It should be noted that although the molecular weight of dispersed starch is about one half that of native starch, their copper numbers are the same, so that it may be assumed that the oxygen bridges in the starch macromolecules remain virtually intact. This formed the basis of a new method of alcohol production without boiling of starch. We showed [1, 6] that if starch-containing raw materials are dispersed they can be saccharified without preliminary boiling. This method [1, 6] gives 5-7% more alcohol than is obtained from boiled raw materials because it does not involve the losses which occur during boiling and by dispersion of unhulled grains, when certain amounts of fermenting substances are formed from the dispersed hemicellulose of the cereal hulls (Table 1).

TABLE 1

Alcohol Yields From Starch Materials

Raw material	Yield of alcohol		Raw material	Yield of alcohol	
	% of theoretical	in deca-liters/ton		% of theoretical	in deca-liters/ton
Dispersed hulled oats	85.45	61.13	Dispersed unhulled oats and barley	96.56	69.00
Dispersed unhulled oats	88.20	64.90	Boiled unhulled oats (control experiment)	84.73	60.62

TABLE 2

Effects of Dispersion and of Acid Concentration on the Sugar Yield in Hydrolysis During 1 Hour

Acid concentration, %	Sugar formed, %		Hydrolysis conditions
	original sawdust	dispersed sawdust	
3	1.85	4.62	In the cold
5	2.25	6.26	The same
3	12.35	17.5	Heated on water bath
10	13.50	27.5	The same

The data in Table 1 indicate that dispersion results in formation of some fermentable sugars from the cereal hemicellulose, and this increases the yield of alcohol formed by fermentation.

Different cellulose modifications differ in their susceptibility to hydrolysis owing to differences in the intermolecular forces [5]. Our investigations with dispersed cellulose (sawdust) confirmed this and showed that fine dispersion of cellulose raises the yield of sugars as the result of enzyme action by 2%. Undispersed sawdust yielded 8.6% glucose, whereas the dispersed material gave 10.8%; thus, dispersion breaks down intermolecular bonds in the same manner as in starch.

It was found in hydrolysis of native and dispersed cellulose in presence of sulfuric acid that fine dispersion of cellulose considerably facilitates acid hydrolysis (Table 2).

It is clear from Table 2 that fine mechanical dispersion of cellulose modifies its microstructure by disintegration of the molecular bundles, and thereby facilitates hydrolysis.

SUMMARY

Fine mechanical dispersion of cellulose, leading to breakdown of its molecules, favors an increase of sugar yields after enzymatic and acid hydrolysis.

LITERATURE CITED

- [1] S. M. Lipatov and M. S. Shul'man, Proc. All-Union Conference on Colloid Chemistry [in Russian] (Kiev, 1950) p. 272.
- [2] S. M. Lipatov, B. A. Kartsovnik, and M. S. Shul'man, Kolloid Zhur. 12, 286 (1950).
- [3] S. M. Lipatov, Kolloid Zhur. 8, 74 (1946).
- [4] S. I. Meerson and S. M. Lipatov, Kolloid Zhur. 18, 447 (1956).
- [5] S. M. Lipatov, High Polymers [in Russian] (Moscow, 1936).
- [6] S. M. Lipatov and M. S. Shul'man, Authors' Certif. No. 83381 and 86626 (1948).

Received May 19, 1959

PREPARATION OF EMULSIONS BY ADDITION OF ELECTROLYTES AND NONELECTROLYTES FROM MUTUALLY SOLUBLE LIQUIDS AFTER PHASE SEPARATION*

A. I. Al'tov

Yaroslav Technological Institute

It is usually considered that two immiscible liquids, i.e., liquids differing in polarity, are required for the formation of an emulsion [1]. The experiments described below show that this is not a necessary condition. It is possible to obtain emulsions from liquids miscible in any proportions. For this, in addition to the three components (oil, water, emulsifier) required for any emulsion, it is necessary to have a fourth component, which decreases the mutual solubility of the liquids and causes the system to separate into two layers.

If to a system of two mutually-soluble liquids a third substance, soluble in only one of them, is added, the system separates out; this is illustrated by the systems ethyl alcohol - water + K_2CO_3 or propyl alcohol - water + KCl [2].

Evidently in such cases one liquid phase can be emulsified in the other; for example, ethyl alcohol in aqueous potassium carbonate solution (Table 1).

It follows from Table 1 and certain other data that propyl alcohol and pyridine are salted out more easily from aqueous solutions than ethyl alcohol or acetone, and that the greater the solubility of a salt in water the stronger its salting-out effect.

The two-phase liquid systems listed in Table 1 were taken for preparation of emulsions. Emulsification was effected by intermittent shaking in presence of an emulsifier [3]. The chief difficulty lay in the choice of emulsifiers which would make the emulsions stable in presence of considerable amounts of electrolyte. Many emulsifiers used in formation of ordinary emulsions (as of benzene in water) fail to stabilize the investigated emulsions in presence of the electrolyte. Water-soluble surface-active substances (sodium oleate, Nekal, gelatin, etc.) were salted out by the electrolytes, and stable emulsions could not be obtained in their presence. Gold and ferric hydroxide hydrosols and latex also proved ineffective, as they were coagulated and precipitated when added to systems containing considerable amounts of salts.

Good results were obtained with solid powdered emulsifiers. Concentrated stable emulsions of propyl alcohol, ethyl alcohol, acetone, and pyridine in 4N aqueous K_2CO_3 could be obtained with kaolin as emulsifier. The optimum proportions of the components were: 10 ml of salt solution, 5 ml of the second liquid, and 3 g of kaolin** (Table 2).

The stability of the emulsions was decreased if these proportions were altered. Emulsions of the following composition were less stable: 5 ml of pyridine, 10 ml of aqueous 4N NaH_2PO_4 solution, and 10 g of kaolin, and 5 ml of propyl alcohol, 10 ml of 20% aqueous KCl solution, and 2 g of wheat flour.

Increase of the amount of kaolin to 3 g in emulsions of pyridine in sodium dihydrogen phosphate solution resulted in rapid breakdown of the system. The stability of the system was raised considerably by increase of the NaH_2PO_4 concentration (to 35%). The stabilizing effect of increase of the concentration of the electrolyte solutions was confirmed for other emulsions.

* Presented at the 4th Colloid Conference, Tbilisi, May 1958.

** Prosyanyaya kaolin, GOST 6138-52.

TABLE 1

Separation of Aqueous Solutions of Ethyl and Propyl Alcohols, Acetone, and Pyridine by Addition of Salts (organic liquid — salt solution taken in 1 : 2 ratio)

Organic liquid	Aqueous salt solution			
	KCl, 20%	NaCl, 4N	K ₂ CO ₃ , 4N	NaH ₂ PO ₄ , 4N
Propyl alcohol	Two layers	Two layers	Two layers	Two layers
Pyridine	Same	Same	Same	Same
Ethyl alcohol	One layer	One layer	Same	Same
Acetone	Same	Same	Same	Same

Thus, direct emulsions of the "oil" — water type can be obtained from miscible liquids separated by salting out, with the use of solid emulsifiers taken in large quantities. Solid emulsifiers do not have any significant effect on interfacial tension between liquid phases [4], but they form spatial structures of a quasisolid character at such interfaces.

The emulsion type was determined under the microscope in presence of methyl red, insoluble in water and soluble in organic solvents. Experiments on separation of kaolin and charcoal powders by means of two-layer systems showed that kaolin remained in the aqueous solution while the charcoal was floated into the layer of the second liquid (alcohol, acetone, pyridine). It follows that polar compounds such as alcohols, pyridine, and acetone behaved like "oils" in relation to layers of salt solutions immiscible with them.

A series of experiments was performed on formation of emulsions of the inverse type. When the sulfides of iron, copper, and zinc were used as emulsifiers, rapidly-separating emulsions of the water — oil type were obtained. Attempts to change the type of emulsion formed in presence of kaolin by variations of the phase proportions and by replacement of the glass test tubes by plastic vessels were unsuccessful. There was no phase reversal in the emulsions.

When a direct current was passed through emulsions of alcohol, pyridine, and acetone in aqueous salt solutions the emulsions were broken with liberation of kaolin at the positive electrode. Other methods of breaking the emulsions were also tested. If they were shaken with excess water the dispersity of the droplets first decreased and the emulsions were then broken. If an excess of the second liquid was added to an emulsion, this liquid soon separated out when shaking was discontinued, and a layer of concentrated emulsion formed in the lower part of the vessel. If the emulsions were boiled they were destroyed with liberation of kaolin. Centrifugation also resulted in complete breakdown of the emulsions with separation into three phases (two liquid and one solid).

Nonelectrolytes as well as salts were found to be suitable for inducing phase separation of mutually soluble liquids. The two-layer liquid systems so obtained were emulsified by the same method of intermittent shaking.

Two pairs of the mutually-soluble liquids used in the first part of this investigation were taken: water with propyl alcohol, and water with acetone. The third substances used to induce separation were sucrose, which is soluble in water and insoluble in acetone and propyl alcohol, and camphor, which is soluble in acetone and propyl alcohol and insoluble in water. The solutions separated out when equal volumes of 40% aqueous sucrose solution and propyl alcohol or acetone were mixed, or when an equal volume of water was mixed with 25% solution of camphor in acetone or propyl alcohol. To avoid precipitation of the demixing agent, pure liquid should be added gradually with shaking to the solution; for example, water to a solution of camphor in acetone.

During the preparation of these systems in a number of cases fairly stable emulsions were formed without addition of emulsifier. Examples of these are emulsions of the W/O type: a) water in a solution of camphor in propyl alcohol; b) aqueous sucrose solution in propyl alcohol (Table 3). The breakdown of these emulsions and separation of the system took 2-3 hours.

TABLE 2

Composition of Stable Emulsions of Mutually-Soluble Liquids in Presence of Electrolytes and Powdered Emulsifiers

Aqueous electrolyte solution (10 ml)	Organic liquid (5 ml)	Emulsifier	
		name	amount, g
4 N K_2CO_3	Propyl alcohol	Kaolin	3
4 N K_2CO_3	Ethyl alcohol	Kaolin	3
4 N K_2CO_3	Acetone	Kaolin	3
4 N K_2CO_3	Pyridine	Kaolin	3
4 N NaH_2PO_4	Pyridine	Kaolin	2
35% NaH_2PO_4	Pyridine	Kaolin	2
20% KCl	Propyl alcohol	Flour	2

TABLE 3

Composition of the Investigated Emulsions of Mutually-Soluble Liquids in Presence of Nonelectrolytes and Organic Emulsifiers

System No.	First liquid		Second liquid		Emulsifier	
	name	amount, ml	name	amount, ml	name	amount
1	40% sucrose solution in water	5	Propyl alcohol	5	—	—
2	25% camphor solution in propyl alcohol	5	Water	5	—	—
3	40% sucrose solution in water	10	Propyl alcohol	5	Agar in water	0.1%
4	Same	10	Same	5	OP-4	5 drops
5	25% camphor solution in propyl alcohol	5	Water	10	Agar in water	0.1%
6	Same	5	Same	10	Gelatin in water	0.5%
7	Same	5	Same	10	OP-4	5 drops
8	Same	5	40% sucrose solution in water		OP-4	10 drops
9	25% camphor solution in acetone	5	Water	10	Agar in water	0.1%
10	Same	5	Same	10	Gelatin in water	0.5%
11	Same	5	Same	10	OP-4	5 drops

For preparation of more stable emulsions from mutually-soluble liquids separated by nonelectrolytes, kaolin was tested as the emulsifier as before. However, in these systems kaolin did not have a stabilizing effect and the emulsions separated out rapidly. Better results were obtained with emulsifiers of high molecular weight: agar, gelatin, and OP-4 emulsifier (octyl phenol polyether with four ethylene glycol groups).

Of a number of oil - water type emulsions obtained, the most stable were systems No. 5, 8, and 9 given in Table 3; these separated out only after 24 hours. The other emulsions began to separate out gradually after a few hours (from 2 to 6). Benzene - water emulsions containing the emulsifiers listed in Table 3 had similar stability.

Emulsions containing nonelectrolyte additives were broken by the same methods as emulsions prepared in presence of salts.

SUMMARY

1. A series of emulsions has been prepared from mutually-soluble liquids separated into two layers by dissolution of an electrolyte or nonelectrolyte at a high concentration in one of the liquids.

2. Only emulsions prepared in presence of a solid powdered emulsifier (kaolin) had high stability, but not emulsions with soluble emulsifiers.

3. Emulsions prepared in presence of dissolved nonelectrolytes with agar, gelatin, or OP-4 as emulsifiers were stable for several hours.

LITERATURE CITED

[1] N. P. Peskov and E. M. Aleksandrova-Preis, Course of Colloid Chemistry [in Russian] (Goskhimizdat, 1948); I. L. Zhukov, Colloid Chemistry [in Russian] (Izd. LGU, 1949); P. P. Mitrofanov and S. E. Severin, Textbook of Physical and Colloid Chemistry [in Russian] (State Medical Press, 1948).

[2] A. V. Rakovskii, Introduction to Physical Chemistry [in Russian] (ONTI, 1938); E. F. Zhuravlev, Uch. Zap. Permskogo gos. un-ta 2, 233 (1936).

[3] W. Clayton, Emulsions [Russian translation] (IL, Moscow, 1950).

[4] P. A. Rebinder and K. A. Pospelova, Introductory Chapter to the Russian Translation of W. Clayton's Emulsions (IL, Moscow, 1950); L. Ya. Kremnev, K. P. Mishchenko, and A. I. Feklinov, Zhur. Priklad, Khim. 19, 363 (1946).

Received May 26, 1958

X-RAY STRUCTURAL ANALYSIS OF INTERACTION BETWEEN PAPER AND BINDERS IN PRINTING INKS

M. P. Volarovich, V. T. Ivanova, E. M. Afanas'eva,
and K. F. Gusev

The Gosznak Scientific Research Institute and the Kalinin Peat Institute

The purpose of the present investigation was to elucidate the interaction of paper with binders in printing inks. The material used for the tests was ashless filter paper previously treated with benzene. The binders used were soluble potato starch, gelatin, drying oil, and petrolatum. Drying oils differing in activity were used: drying oil III, oxidized, of high activity, and drying oil VI, polymerized, of low activity. The paper was impregnated with the drying oils, petrolatum, and starch, and sized with gelatin. The starch-impregnated paper contained 10-30% of starch by weight. After being dried at room temperature, the paper samples (except those impregnated with petrolatum) were studied by x-ray analysis. In addition, the following were investigated separately for comparison: unsized and unimpregnated paper, dried oil films, petrolatum, starch in paste and dried form, and air-dry gelatin. Petrolatum, a nondrying liquid, was applied in the form of a drop to a wire ring where it was held by surface tension.

The investigation was carried out with x-ray cameras of high resolving power using flat film, with 80 mm distance between the specimen and the film. These cameras were used earlier for studies of the structure of peat and other disperse systems [1-4]. The photographs were taken with unfiltered K_{α} and K_{β} copper radiation; $\lambda_{K_{\alpha}} = 1.539 \text{ \AA}$ and $\lambda_{K_{\beta}} = 1.389 \text{ \AA}$. A nickel filter was used in a few instances only. In order to obtain a sharp interference picture the exposure time was 6 hours with 25 ma tube current at 20 kv. All the patterns were analyzed by means of the MF-2 microphotometer and the results were plotted in the form of microphotometric curves.

Untreated filter paper. It was shown earlier [1] that filter paper has the structure of native cellulose. A number of investigations [5, 6] have shown that native cellulose — ramie, cotton, etc. — has monoclinic symmetry with the angle $\beta = 84^{\circ}$ and cell constants $a = 8.35 \text{ \AA}$, $b = 10.3 \text{ \AA}$ and $c = 7.95 \text{ \AA}$ [7]. However, detailed indexing of the x-ray pattern of filter paper (Fig. 1, a and Table 1) leads to the conclusion that in addition to the three reflecting planes of the lattice there is a fourth plane. This plane corresponds to the interference ring A_3 in Fig. 1 and Table 1; the ring A_3 is the result of superposition of K_{α} interferences from the (200) plane and K_{β} from the (002) plane. In previous publications [1, 5-7] this ring was attributed entirely to K_{β} radiation of the tube from the A_4 (002) plane. The necessity to postulate the A_3 plane arose owing to the impossibility of indexing the other reflections in accordance with the cell constants given above. To confirm this, an x-ray pattern of the filter paper was obtained with a standard nickel filter in the form of foil 0.007 mm thick in order to exclude β -radiation of the tube. The A_3 interference ring was retained, although its intensity diminished somewhat because of the loss of β -radiation from the tube.

The calculations are presented in Table 1. Column 1 contains the interplanar spacings and values of $\sin^2\theta$ calculated from the measured diameters of the interference rings on the x-ray patterns. Column II contains the quadratic forms of the monoclinic lattice for each reflecting plane separately. Columns III and IV contain calculated data on the quadratic form for native cellulose [7] and for filter paper from our experiments. The values of $\sin^2\theta$ and the interplanar spacings d given in columns I and III respectively differ somewhat. This is because the lattice parameters of filter paper and native cellulose are not identical. If the lattice of filter paper is

TABLE 1

Indexing of X-ray Pattern of Filter Paper, With Modified Constants for the Monoclinic Crystal Lattice of Native Cellulose

inter- ference	I Found from X-ray pattern of filter paper, $\tan 2\theta = \frac{1}{A}$, r = radius of ring, $A = 80$ mm camera radius, $2d = \frac{\lambda}{\sin \theta}$			II Quadratic form of monoclinic lattice for (101), (101), (200), and (002)	III Calculated for monoclinic lattice of native cellulose [7]. Constants: $a = 8.35$ A, $b = 10.3$ A and $c = 7.90$ A, angle $\beta = 84^\circ$			IV Calculated for filter paper. Constants: $a = 8.78$ A, $b = 10.3$ A and $c = 7.96$ A; angle $\beta = 84^\circ$	
	diameters of interference rings, mm	$\sin^2 \theta$	d , A		hkl	$\sin^2 \theta$	d , A	hkl	$\sin^2 \theta$
A_1	40, 2	0,0151	6,25	$\sin^2 \theta_{101} = \frac{\lambda^2}{4} \left(\frac{1}{a^2} + \frac{1}{c^2} + \frac{1}{c^2} - \frac{2}{ac} \cos \beta \right) \frac{1}{\sin^2 \beta}$	101	0,0172	6,05	101	0,0152
A_2	45, 2	0,0188	5,60	$\sin^2 \theta_{101} = \frac{\lambda^2}{4} \left(\frac{1}{a^2} + \frac{1}{c^2} + \frac{1}{c^2} + \frac{2}{ac} \cos \beta \right) \frac{1}{\sin^2 \beta}$	101	0,0195	5,45	101	0,0188
A_3	59, 2	0,0310	4,37 + β	$\sin^2 \theta_{200} = \frac{\lambda^2}{4} \left(\frac{4}{a^2} \cdot \frac{1}{\sin^2 \beta} \right)$	200	0,0343	β	200	0,0311
A_4	66, 0	0,0377	3,96	$\sin^2 \theta_{002} = \frac{\lambda^2}{4} \left(\frac{4}{c^2} \cdot \frac{1}{\sin^2 \beta} \right)$	002	0,0384	3,92	002	0,0378

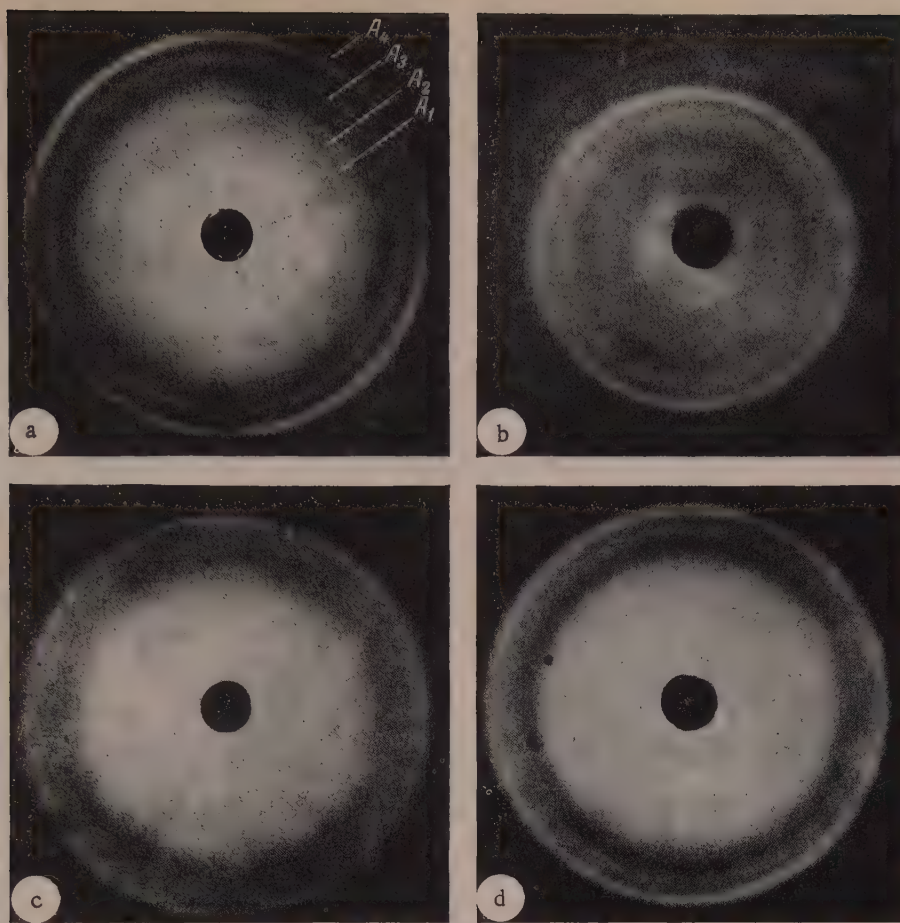


Fig. 1. X-ray patterns: a) original filter paper; b) dried starch paste; c) filter paper impregnated with starch (10% starch); d) same, 30% starch.

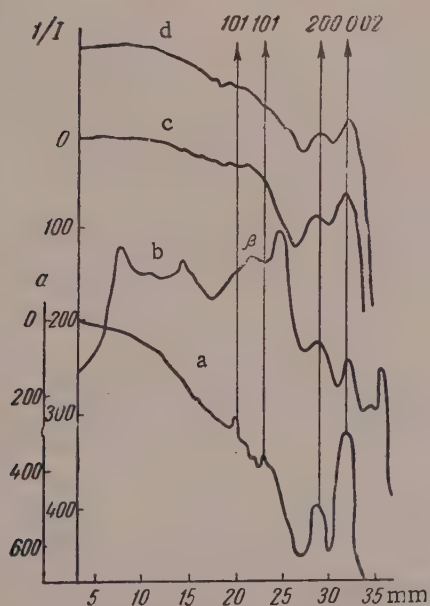


Fig. 2. Photometric curves from x-ray patterns: a) filter paper; b) dried starch paste; c) filter paper impregnated with starch (10% starch); d) same, 30% starch.

regarded as being somewhat broadened along the a axis (8.78 Å instead of 8.35 Å) the X-ray pattern is indexed satisfactorily in the monoclinic form. It follows that the technological conversion of cellulose into filter paper and the associated mechanical degradation may modify the original cellulose structure and weaken the bonds between individual molecular chains; this is manifested in broadening of the lattice.

Paper impregnated with starch. Figure 1, b, c and d shows the x-ray patterns of starch converted to paste and dried at room temperature, and of filter paper impregnated with starch. Figure 2 shows the corresponding photometric curves, where the distances from the centers of the patterns (ring radii) are taken along the abscissa axis, and the reciprocal of the intensity of the light transmitted by the pattern is taken along the ordinate axis. Figure 1, c and d, and curves c and d in Fig. 2 show complete disappearance of two interference maxima of the cellulose lattice, (101) and (10 $\bar{1}$). It seems that starch, with zigzag-shaped molecules, can penetrate into the "intermolecular space" of cellulose with large interplanar spacings only, i.e., into space with weakened bonds. It becomes embedded between the layers and disorients

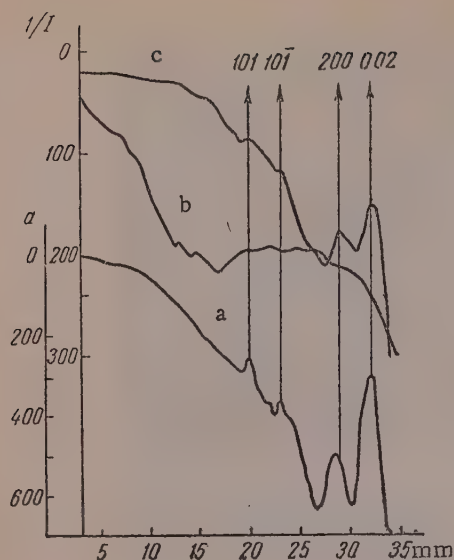


Fig. 3. Photometric curves from X-ray patterns: a) filter paper; b) air-dry gelatin; c) gelatin-sized filter paper.

Paper sized with gelatin. Fig. 3 shows photometric curves based on x-ray patterns of gelatin and of gelatin-sized paper. In contrast to the results of starch impregnation, complete disappearance of the (101) and (10 $\bar{1}$) interference maxima of the cellulose lattice is not observed in curve c, Fig. 3. The gelatin which penetrates into the cellulose lattice produces only partial disorientation of the molecular chains and, as in starch impregnation, penetrates into the "intermolecular space" formed by the large interplanar spacings of the lattice. The (101) and (10 $\bar{1}$) interference rings are very diffuse. As in starch impregnation, there is a slight displacement of the (002) interference ring in the direction of smaller glancing angles, i.e., the (002) interplanar spacing increases by approximately the same amount as for paper impregnated with starch (1.5-2%). Air-dry gelatin has amorphous structure and Fig. 3, curve b, indicates a diffuse, very broad halo.

Paper impregnated with drying oils. Fig. 4 shows the x-ray patterns of drying oil VI and of filter paper impregnated with this oil; the corresponding photometric curves are given in Fig. 5. Fig. 6 shows photometric curves based on x-ray patterns of drying oil III and of paper impregnated with this oil. It is clear from Fig. 4 that the x-ray patterns present a totally different interference picture in this case from that found for paper impregnated with starch or sized with gelatin; impregnation of paper with drying oils does not cause distortion or broadening of the cellulose lattice. The (101) and (10 $\bar{1}$) interference rings are not diffuse and can be observed quite distinctly in the x-ray patterns (Fig. 4,b); however, there is a redistribution of intensity between the (200) and (002) interference rings. In the x-ray pattern for unimpregnated paper the (200) interference ring is much less intense than the (002) ring. On the other hand, in the x-ray patterns of paper impregnated with drying oils the (200) interference ring is considerably more intense than the (002) ring. Moreover, these photometric curves reveal, near the (200) interference ring in the direction of smaller glancing angles, an interference maximum of very low intensity, caused by β -radiation of the x-ray tube from the (200) reflecting plane. This fact indicates once again that the (200) interference ring, A_3 in Table 1, owes its origin to α -radiation from the x-ray tube and that it is masked by β -radiation of the tube from the (002) reflecting plane. Because of the low intensity of the (200) ring for unimpregnated paper the interference from β -radiation of the tube does not appear on the x-ray patterns and photometric curves.

It seems that drying oils enter into a chemical reaction with cellulose, similar to the mercerization reaction which occurs when cellulose is treated with aqueous alkali solutions of definite concentrations. It was demonstrated in the case of cotton wool [8] that an interference pattern similar to that given by paper impregnated with drying oils is obtained at the intermediate stage of cellulose mercerization, when aqueous alkali of definite concentration is incapable of converting the cellulose completely into the mercerized modification. The sample then contains both forms of cellulose. This state may be regarded as an independent phase [5].

them; other planes of the cellulose lattice also undergo partial disorientation. Measurement of the (002) interference ring for starch-impregnated paper showed that its diameter was smaller than that of the corresponding ring for paper not impregnated with starch. It follows that the (002) interplanar spacing, according to our calculations, increased somewhat (by 1.5-2%) and there was additional broadening of the cellulose lattice. It should be noted that Sponsler and Dore [6] established as long ago as 1926 that when hemp fibers swell in water there is some broadening of the lattice; namely, 2% in the (002) plane.

It is noteworthy that pure starch without paper, after being converted to paste and dried, returns to the native state and crystallizes during drying (Fig. 2, curve b). When starch is introduced into paper it is unable to crystallize and is apparently present there in the amorphous state. Otherwise a mixed x-ray pattern with interferences both for starch and for cellulose should be obtained. Variations of the starch content in paper (10 and 30%) do not produce any appreciable change in the appearance of the x-ray pattern (Fig. 1,c and d).

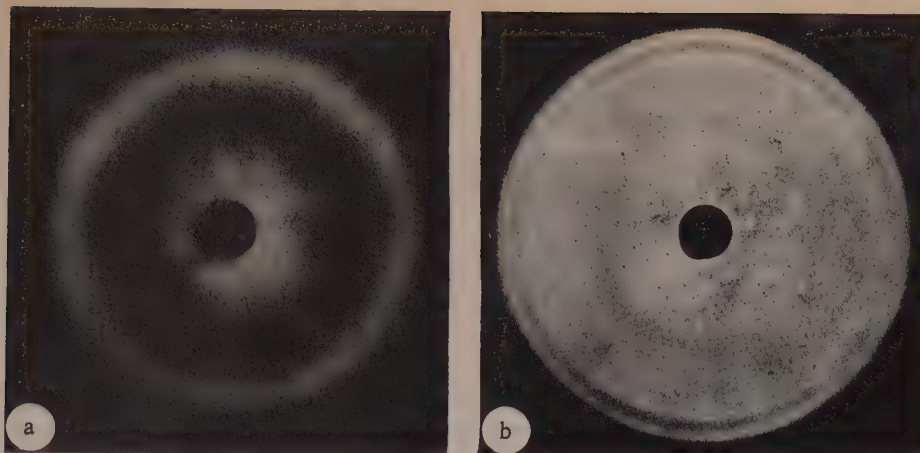


Fig. 4. X-ray patterns: a) dry No. VI polymerized drying oil; b) filter paper impregnated with No. VI polymerized drying oil.

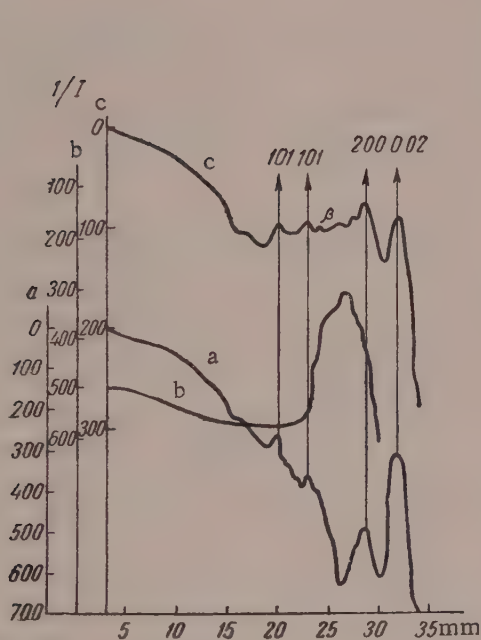


Fig. 5. Photometric curves from X-ray patterns: a) filter paper; b) dry polymerized drying oil VI; c) filter paper impregnated with polymerized drying oil VI.

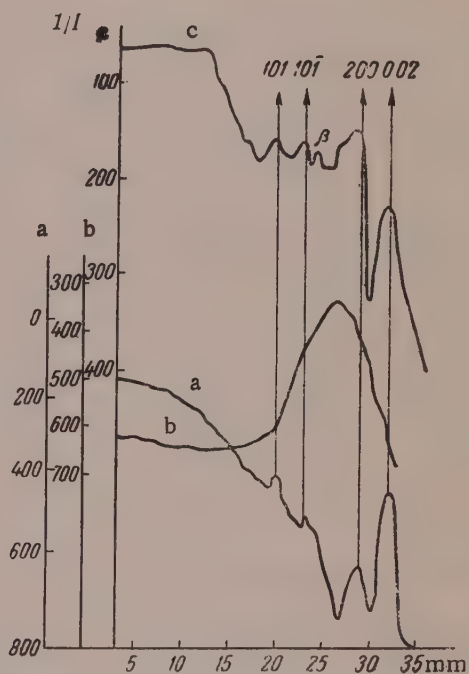


Fig. 6. Photometric curves from X-ray patterns: a) filter paper; b) dry oxidized drying oil III; c) filter paper impregnated with oxidized drying oil III.

The (200) interference rings in curves c of Fig. 5 and 6 differ from each other in intensity. This ring has much higher intensity for paper impregnated with oxidized drying oil III than for paper impregnated with polymerized drying oil VI. However, in both cases the intensity of the (200) interference rings is higher than that of the (002) rings. In our opinion this is to be explained by the degrees of activity of the two drying oils: the oxidized oil is the more active. To test these conclusions, filter paper was impregnated with petrolatum, which is known not to contain active groups.

Paper impregnated with petrolatum. Figure 7 shows photometric curves based on the x-ray patterns of petrolatum and paper impregnated with petrolatum. Curve c in Fig. 7 indicates that the (101) and (10 $\bar{1}$) interference rings are diffuse. Impregnation with petrolatum (like impregnation with starch and sizing with gelatin) can cause

TABLE 2

Interaction of Filter Paper with Binders

Binder	Amount of alkali taken for titration of solutions after treatment, mg*			
	pure paper	pure binder	pure paper and pure binder	oiled paper
Drying oil VI, polymerized	198.8	59.8	258.4	228.1
Drying oil III, oxidized	198.8	65.9	265.1	172.3
Petrolatum	198.8	28.2	227.0	227.0

* Mean of three determinations.

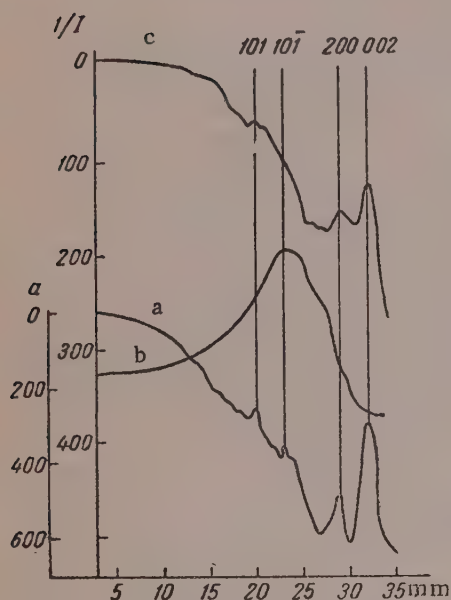


Fig. 7. Photometric curves from X-ray patterns: a) filter paper; b) petrolatum; c) filter paper impregnated with petrolatum.

partial disorientation of the molecular chains in the cellulose lattice, in the "intermolecular space" with large interplanar spacings as before. However, there is no broadening of the lattice or redistribution of intensity between the (200) and (002) interference maxima. It follows that there is no chemical reaction between paper and petrolatum, such as occurs between paper and drying oils.

Physicochemical investigations. The saponification numbers of pure paper, drying oils, and paper impregnated with the drying oils (oiled paper) were determined to confirm the existence of interaction between papers and binders in printing inks. It was assumed that in absence of chemical action between the paper and the drying oils the amount of 0.1 N acid expressed in terms of milligrams of alkali required for titration of the solution after treatment of the oiled paper should be equal to the total amount of alkali required for titration of the solutions after treatment of the pure paper and pure binder. However, experiments showed (see Table 2) that in reality the amount of alkali required for titration of the solutions after treatment of pure filter paper and pure drying oil is considerably greater than the amount taken in titration of solutions after treatment of oiled paper. In determinations of the saponification number of paper treated with petrolatum, on the other hand, the amount of alkali taken for titration of the solutions after treatment of the oiled paper was equal to the total alkali taken for titration after treatment of pure paper and pure petrolatum.

The amount of alkali required for titration of the solutions after treatment of oiled paper is less than the total amount of alkali required for titration of solutions after treatment of pure paper and pure drying oil because some of the active groups in cellulose and the drying oil interact. When paper is treated with petrolatum, which does not contain active groups, there is no interaction between the paper and the petrolatum and the amount of alkali required for titration of solutions after treatment of the oiled paper is equal to the total amount of alkali taken for titration of solutions after treatment of the pure paper and pure petrolatum. The results of this investigation indicate that chemical action takes place when paper is treated with drying oils.

SUMMARY

1. Ashless filter paper has the monoclinic cellulose unit cell with parameters somewhat different from those of native cellulose, namely: $a = 8.78 \text{ \AA}$; $b = 10.3 \text{ \AA}$; $c = 7.96 \text{ \AA}$; angle $\beta = 84^\circ$.

2. The A_3 interference maximum, formerly regarded as the consequence of β -radiation of the tube from the (002) reflecting plane, is in fact the total interference maximum due to α -radiation of the tube from the (200) reflecting plane and β -radiation of the tube from the (002) reflecting plane.

3. Impregnation of filter paper with starch and sizing with gelatin results in disorientation of the cellulose molecular chains in the (101) and (10 $\bar{1}$) reflecting planes and additional broadening of the lattice by 1.5-2% in the (002) plane.

4. Impregnation of filter paper with drying oils results in redistribution of the intensities of the (200) and (002) interference maxima and in formation of an intermediate form of cellulose structure, similar to the intermediate form in mercerization. Thus there is chemical action between cellulose in filter paper and drying oils.

5. There is no chemical action between filter-paper cellulose and petrolatum, which does not contain active groups; when paper is impregnated with petrolatum there is no broadening of the lattice in the (002) plane.

6. The existence of chemical action between filter-paper cellulose and drying oils, and absence of such action between filter-paper cellulose and petrolatum, has also been demonstrated by chemical methods.

LITERATURE CITED

[1] M. P. Volarovich and K. F. Gusev, Tr. Mosk. Torf. in-ta 2, 97 (1953); Kolloid Zhur. 18, 6, 643 (1956);* Tr. Mosk. Torf. in-ta 5, 3 (1957); 6, 53 (1957).

[2] K. F. Gusev, Kolloid Zhur. 4, 4, 377 (1938); Zavodskaya Lab. 4, 477 (1953).

[3] M. P. Volarovich, L. Ya. Ginzburg, and K. F. Gusev, Proc. 3rd All-Union Conf. Colloid Chem. [in Russian] (Minsk, 1953) p. 155.

[4] M. P. Volarovich, K. F. Gusev, S. N. Markov, and V. P. Tropin, Kolloid Zhur. 19, 4, 401 (1957).*

[5] K. H. Meyer and H. Mark, Structure of Natural Organic High Polymers [Russian translation] (State Chem. Tech. Press, Leningrad, 1932).

[6] J. F. Katz, Radiography of Colloids and Tissues [Russian translation] (ONTI, 1937).

[7] A. I. Kitaigorodskii, X-ray Structural Analysis of Microcrystalline and Amorphous Substances [in Russian] (State Tech. Press, 1953).

[8] M. P. Volarovich and K. F. Gusev, Tr. Mosk. Torf. in-ta, in the press.

Received March 10, 1959

*Original Russian pagination. See C. B. Translation.

INVESTIGATION OF THE MECHANISM OF FILM FORMATION FROM VULCANIZED LATEX

1. FORMATION OF FILMS FROM NATURAL LATEX

S. S. Voyutskii, D. M. Sandomirskii, N. M. Fodiman,
and R. M. Panich

Moscow Institute of Fine Chemical Technology, Elastomer Laboratory

Despite the fact that the question of the mechanism of film formation from vulcanized latexes ("vultexes") has been discussed repeatedly in the literature [1-7], it still remains obscure. The most justified view [7] seems to be that film formation during drying of vulcanized latexes consists of diffusion of free ends of the rubber chain molecules from one globule to another, resulting in the formation of fairly stable bonds.

It is known from practical experience that the strength of vultex films increases during storage. The probable explanation is that chemical bonds may form between the rubber molecules in different globules, either as the result of continuing vulcanization or migration of sulfur bridges already present, or by formation of oxygen bridges as the result of oxidation reactions. In addition, film strength depends on the protein emulsifier which, remaining between the globules, forms a network structure [8] and may join the globules together.

The present investigation is concerned with experimental confirmation of this hypothesis, advanced earlier on theoretical grounds.

The experiments were performed with films made from natural latex preserved by ammonia and containing 32.4% solids. The following films were made from this latex:

1. Unvulcanized films, made in the usual way by drying of latex at room temperature in glass cells.
2. Films from vulcanized latex (vultex) made from a mixture of the following composition:

Rubber in latex form	100 wt. parts
Sulfur	2 wt. parts
Zinc oxide	2 wt. parts
Sodium diethyldithiocarbamate	1 wt. part

This mixture was heated in a thermostat for 45 minutes to 70°, and the heating was then continued for 30 minutes at that temperature. Films were then made from the mixture by the usual method.

3. Films made from latex, vulcanized after they had been prepared to the same extent as the vultex films. These films were made by the usual method from the latex mixture of the composition given in (2) above. The dried films were vulcanized at 90° in a thermostat for one hour. It was found that films vulcanized by this procedure were similar to vultex films in their degree of swelling in benzene, which is a measure of the degree of vulcanization.

4. Films made from latex vulcanized under the usual conditions for rubber stocks. These films were prepared as described in (3) above, but were vulcanized at 125° for one hour.

For determination of the degree of cross linking of the molecules during vulcanization the swelling of the films in benzene was estimated and the molecular weight M_s of segments between the branch points was

TABLE 1

Swelling of Films in Benzene

Film	Maximum swelling, %	Content of soluble fraction, %	M _s
Vultex	665	8.5	75,200
Vulcanized in the dry state at 125°	472	3.5	21,500

TABLE 2

Characteristics of Various Latex Films Before and After Swelling in Water Vapor

Films	Swelling, % on initial weight	Amount of water-soluble substances removed, % of specimen weight	Tensile strength	
			before swelling	after swelling
Unvulcanized latex	5,4	6,2	35,8	10,8
Vultex	6,3	5,6	132	59,6
Vulcanized in the dry state at 90°	7,2	4,8	146	157,9
Same, at 125°	10,1	3,4	148	159

calculated. This treatment weakened the films made from unvulcanized latex so much that the degree of swelling could not be determined. It is clear from the results in Table 1 that the degree of cross linking is considerably lower in the vultex film than in the film vulcanized in the dry state. It should be pointed out that these data characterize the vulcanizate network as a whole and give no indication of the presence of chemical inter-globular bonds.

Effect of swelling in water vapor on film properties. The hydrophilic protein which cements the individual globules together swells to the greatest extent in water vapor. Accordingly, the film strength should decrease on swelling. In these experiments six weighed spade-shaped specimens prepared for dynamometer tests were placed for 24 hours in an atmosphere of 100% humidity. The specimens were then taken out, condensed surface moisture was carefully removed by means of filter paper, and the specimens were weighed; the degree of swelling was thus determined. The specimens were then subjected to tensile tests on an ordinary dynamometer with the lower jaw moving at 500 mm/minute.

Control specimens were dried to constant weight, so that the weight loss after swelling could be determined.

Table 2 contains data on the amount of water absorbed by the specimens during swelling, the amounts of water-soluble substances removed together with water when the specimens were dried by filter paper, and the average tensile strengths of the swollen films.

The strength of films from unvulcanized latex and vultex falls sharply as the result of swelling in water vapor. This shows that the strength of these films is significantly influenced by the native protein present between the globules, which forms a network structure and acts as a cement for the globules in the unswollen film. Moreover, swelling of the protein in the spaces between the globules probably causes the globules to be pushed apart. This, of course, should also weaken the system.

The strength of latex films vulcanized in the dry state does not decrease on swelling, but even increases somewhat. Evidently in this case interaction between globules is effected by means of chemical bonds and the presence of a certain amount of moisture in the film does not weaken it. It is known that the strength of high polymers is increased by introduction of small amounts of water or other solvent which serves as a plasticizer [9].

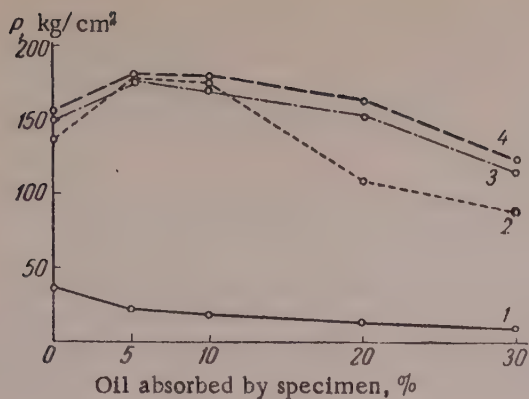


Fig. 1. Effect of swelling in petrolatum on tensile strength of latex films: 1) unvulcanized film; 2) vultex film; 3) film vulcanized in the dry state at 90°; 4) same, at 125°.

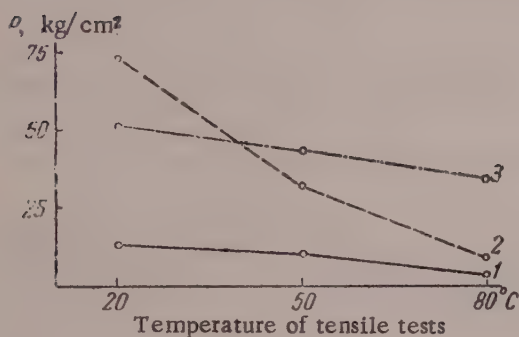


Fig. 2. Effect of test temperature on the tensile strength of latex films: 1) unvulcanized film; 2) vultex film; 3) film vulcanized in the dry state at 90°.

Figure 1 shows that the tensile strength of films from natural latex fell sharply with increased swelling. The strength was reduced to less than one third as the result of 30% swelling. The strength of the other films first increased somewhat on swelling, and then decreased at high swelling values (20-30%).

It must be pointed out that at high swelling values the vultex film shows the most pronounced fall in strength. This indicates that the strength of this film, as of film from unvulcanized latex, depends to a considerable extent on intermolecular forces. Films vulcanized in the dry state do not show this sharp loss of strength as the result of swelling in petrolatum, evidently because the strength of such films is largely determined by the presence of continuous molecular networks characteristic of vulcanizates.

Effect of test temperature on film strength. Since increase of temperature in the range studied usually leads to a sharp weakening of intermolecular forces but has hardly any effect on the strength of chemical bonds, it was of interest to study the influence of temperature during the tensile tests on the strength of different latex films.

The tensile-strength determinations were performed in a special Schopper dynamometer fitted with a thermostat in which the clamped specimens were immersed. Before the determination each specimen was kept in the thermostat for 5 minutes to allow it to reach the required temperature.

Another interesting fact is that as the degree of vulcanization increases swelling increases, while the amount of water-soluble substances removed from the film decreases. The explanation is that a larger amount of water-soluble substance which cause swelling remains in highly vulcanized films with extensive vulcanization networks.

A similar effect was observed by one of us in comparative swelling tests, in water vapor, on films made from latexes and from solutions of the corresponding rubbers [10]. Films made from solutions swelled more than films from latex, because the former do not contain continuous networks of hydrophilic substances whereby they can be washed out. Such networks are destroyed if the films are swollen or dissolved, or heated at the vulcanization temperature.

Effect of swelling in hydrocarbons on film strength. Hydrocarbons, which have a plasticizing effect, might be expected to assist slippage of the ends of the rubber molecules, intertwined as the result of diffusion, in the zones of contact between individual globules. This should lower the film strength considerably if the latter is determined only by intertwining of ends of molecules which have diffused from one globule to another.

Petrolatum was chosen as the hydrocarbon. The reason for its choice was that rubber swells well in it and it is nonvolatile. Spade-shaped specimens of different films were weighed and immersed in a vessel with petrolatum. After a definite time they were withdrawn, excess oil was carefully removed by means of filter paper, and weighed. To ensure uniform distribution of the oil in the films the specimens were kept between sheets of filter paper for 5 days after the end of swelling. Specimens containing 5, 10, 20, and 30% of petrolatum were obtained in this way. They were tested in an ordinary dynamometer. The results are plotted in Fig. 1.

The results are plotted in Fig. 2. Because of the different test conditions the results in Fig. 2 cannot be compared with the data in Table 1 and Fig. 1. However, it is clear from Fig. 2 that the strength of all the films decreases with increase of the test temperature. Films made from unvulcanized latex and from vultex show especially sharp drops of strength. The strength of films from unvulcanized latex falls by 80% in the 20-80° range, and the strength of vultex films by 88%. Films vulcanized in the dry state at 90° lose only 33% strength under the same conditions.

This undoubtedly indicates that the bonds in films made from unvulcanized natural latex or vultex are intermolecular.

It is quite understandable that when the films are heated their strength decreases more than when they swell in water or oil, because in the former case bonds between the rubber molecules and between the protein molecules are weakened simultaneously, whereas swelling in water vapor or oil loosens either the bonds between the protein molecules only, or the bonds between the rubber molecules only.

However, increase of temperature does not lead to total loss of strength in vultex films. To some extent the film strength also depends on the presence of chemical bonds between molecules in adjacent globules, formed either as the result of continuing vulcanization or migration of sulfur bridges, or as the result of oxidation processes.

Effect of mechanical treatment on film strength. The above data on the effects of swelling and temperature on the strength of vultex films show that bonds caused by van der Waals forces form between the globules during formation of films from vultex and unvulcanized latex. If the film is vulcanized in the dry state a network of chemical bonds is formed in it. It was desired to find how this difference in the nature of the forces influences film behavior in mechanical treatment.

Accordingly the films were milled at room temperature on microrolls for 5 minutes with a 2 mm gap and for 5 minutes with a 1 mm gap.

It was found that latex and vultex films form good continuous skins, whereas films vulcanized at 125° do not form a skin but are crumbled.

In the first case absence of interglobular chemical bonds enables the globules to slide relatively to each other during milling so that their rubber contents can coalesce into a continuous mass. The presence of a spatial molecular network in the second case makes plastic deformation impossible.

Thus, the fact that the strength of vultex films depends on the degree of swelling in water and hydrocarbons and the temperature, and their behavior in mechanical treatment, confirms that the strength of these films is caused mainly by van der Waals forces between the globules.

In conclusion, we must point out that our view on the causes of the strength of vultex films is not inconsistent with the fact that vultex films are always much stronger than films made from nonvulcanized latexes, although the bonding between the globules is effected by forces of the same nature in both cases. It is quite reasonable to assume that films made from unvulcanized latex are ruptured in the rubber substance in the globules themselves rather than along the very strong protein interlayers between the globules or at the protein - rubber interface. In vultex films such rupture is greatly hindered by formation of a spatial vulcanization structure in the globules, so that the vultex films are considerably stronger than films from unvulcanized latex.

SUMMARY

1. The effects of swelling in water and petrolatum and of the testing temperature on the strength of rubber films made from natural latex, vultex, and latex films vulcanized in the dry state have been tested.
2. The behavior of the films in mechanical treatment (milling) has been investigated.
3. The strength of films from unvulcanized natural latex and vultex is due mainly to intermolecular forces, and the strength of films vulcanized in the dry state to the presence of a continuous molecular network characteristic of vulcanizates.
4. It is likely that latex films are generally ruptured in the rubber material in the globules rather than along the very strong protein interlayers between the globules or at the protein - rubber interface.

LITERATURE CITED

- [1] E. Hauser, Latex [Russian translation] (Moscow-Leningrad, 1932) p. 87.
- [2] E. A. Hauser, India-Rubb. J. 68, 726 (1924).
- [3] I. W. Van Dalfsen, Rubber Chem. and Technol. 16, 318 (1943).
- [4] N. C. Humphreys and W. C. Wake, IRI Trans. 25, 334 (1950).
- [5] S. D. Sutton, IRI Trans. 27, 193 (1952).
- [6] W. Bowler, Ind. Eng. Chem. 44, 748 (1952).
- [7] S. S. Voyutskii and B. A. Shtrakh, Physical Chemistry of Film Formation from Dispersions of High Polymers [In Russian] (State Light Ind. Press, 1954).
- [8] D. Sandomirskii and K. Gagina, Kolloid. Zhur. 15, 448 (1953).*
- [9] S. S. Voyutskii, N. A. Volokitina, and A. D. Zaionchkovskii, Coll. Trans. Central Sci. Res. Inst. Leather Substitutes [In Russian] 4, 22 (State Light Ind. Press, 1952).
- [10] D. Sandomirskii, in the book: Production and Use of Synthetic Latexes [In Russian] (Moscow-Leningrad, 1953) p. 23.

Received April 11, 1958

*Original Russian pagination. See C. B. Translation.

INVESTIGATION OF ADHESION EFFECTS IN BONDING RUBBER TO METAL BY LEUKONAT ADHESIVE

2. BONDING OF UNFILLED RUBBERS TO METALS

B. V. Deryagin, S. K. Zherebkov, and A. M. Medvedeva

Scientific Research Institute of the Rubber Industry, Moscow

It was shown in the previous communication [1] that the strength of bonding of filled rubbers to metal by means of Leukonat adhesive is high when the intensity of interaction of the adhesive film with the rubber is approximately the same as with the metal. Experiments showed that the interaction of the adhesive film with metal and rubber is influenced by such factors as the surface treatment of the metal and the type of filler in the rubber, so that the strength of bonding of rubber to metal may be varied. The present paper is concerned with studies of adhesion effects in bonding of unfilled rubbers to metal by Leukonat adhesive.

By the electrical theory of adhesion [2] the reason why the work of peeling of polymer films from solid substrates has high values is that an electrical double layer, which acts as a kind of capacitor, is formed at the boundary of contact between the polymer and the substrate. The work expended in peeling the film from the substrate is used to overcome the attraction forces between the oppositely-charged layers of the capacitor. As the layers move further apart the potential difference increases. Occurrence of electric discharge sets the limit to the increase of potential difference. It follows that the work of peeling the film from the substrate depends on the charge density of the electric double layer. The charge density, in its turn, is directly related to the surface and volume properties of the contacting materials. The formation of the electric double layer may be attributed to the following processes: a) chemical interaction between the film and the substrate with transition of electrons from one phase to the other owing to their donor and acceptor properties; b) differences in the electron affinity between the two contacting surfaces; c) oriented adsorption of dipolar molecules in the film; the formation of a dipolar potential difference at the interphase boundary causes redistribution of electrons between them which is equivalent to formation of an electric double layer with its layers in the two phases; these layers should become separated when contact is broken, or, in other words, the dipolar adsorption monolayer induces or intensifies differences in electron affinity of the two contacting bodies.

The process of bond formation at adhesive - polymer and adhesive - metal interfaces may occur by various mechanisms in accordance with the composition, structure, and properties of the contacting substances and with the conditions of bond formation (temperature, pressure). If rubber is bonded to metal by means of an adhesive layer a high value of adhesion at the adhesive - rubber boundary would depend mainly on the composition and structure of the rubber present in the stock. It seems that the higher the polarity of the rubber the greater generally are its adhesive properties. The cause of the high bond strength at the interface between a polar rubber and a substrate is oriented adsorption of the rubber molecules at this interface. It is evident that in bond formation between a nonpolar rubber and a substrate the role of oriented adsorption is negligible. In such cases the causes of formation of the electric double layer are forces of chemical interaction between the nonpolar rubber and the substance which forms the basis of the substrate (adhesive).

In the light of the foregoing it was of interest to determine the character of the forces causing bond formation in different rubbers when attached to metal by means of Leukonat adhesive, widely used as a bonding agent.

TABLE 1

Compounding Formulas of the Rubber Stocks in Parts by Weight

Ingredients	Rubber code marks						
	A-1 NR	A-2, naitrit	A-3, SKS-30	A-4, SKN-18	A-5, SKN-26	A-6, SKN-40	A-7, butyl rubber
Rubber	100,0	100,0	100,0	100,0	100,0	100,0	100,0
Magnesium oxide	—	7,0	—	—	—	—	—
Zinc oxide	5,0	5,0	5,0	5,0	5,0	5,0	5,0
Stearic acid	0,5	—	2,0	0,5	0,5	0,5	3,0
Mercaptobenzothiazole	0,7	—	0,6	0,8	0,8	0,8	0,65
Tetramethylthiuram disulfide	—	—	0,1	—	—	—	1,30
Sulfur	3,0	—	2,0	1,5	1,5	1,5	2,0
Total	109,2	112,0	109,7	107,8	107,8	107,8	111,95
Vulcanization time at 143°, min.	20	30	60	50	50	50	50

The experiments were performed with unfilled vulcanizates based on different rubbers. The formulations are given in Table 1.

The rubbers were bonded by means of Leukonat adhesive to smooth steel plates (cleaned with No. 100 emery paper) in the course of curing. The bond strength was measured in terms of the force required to peel the rubber from the metal and was expressed in kilograms per running centimeter of specimen width (in work units per unit area, ergs/cm²).

The results of preliminary tests showed that in a number of cases the bond strength exceeds the strength of the rubbers themselves, and the bond failure is cohesive in character. In order that the bond failure should be adhesive in character in all cases, the thickness of the adhesive film was reduced. It was found, however, that decrease of the adhesive film has different effects on the bond strengths for different types of rubbers.

The test results, presented in Table 2 and Fig. 1, show that Leukonat adhesive, based on triphenylmethane trisocyanate, can be used for bonding vulcanizates of both polar and nonpolar rubbers to metal. Considered in order of increasing polarity of the rubbers, the situation is as follows: butyl rubber does not contain polar groups, its chemical activity is also low, and therefore when its vulcanizates are attached to metal by means of Leukonat the bond strength is negligible. When the rubber is peeled off the metal all the adhesive remains on the metal. Natural rubber has a negligible content of polar groups, but it is much more active chemically than butyl rubber. Unfilled vulcanizates of natural rubber are bonded very well to metal by means of Leukonat. However, when the rubber is peeled off the adhesive remains on the metal, so that the bond strength between the adhesive film and the metal is greater than between the film and the rubber. Unfilled butadiene-styrene vulcanizates are also bonded very satisfactorily to metal by Leukonat, so that the bond strength is greater than the strength of the rubber itself. However, as the strength of the rubber itself is low, the absolute value of the work of peeling, which is a measure of the strength of bonding of this rubber to metal is not high (1.47 kg/cm); it was observed in the tests that the adhesive remains on the metal. Unfilled SKN-18 vulcanizate contains a definite amount of polar groups and is bonded well to metal by means of Leukonat (but not quite as well as natural-rubber vulcanizates). When the rubber is peeled off the metal some of the adhesive passes from the metal to the rubber. Vulcanizates based on SKN-26 have a higher content of polar acrylonitrile group than those based on SKN-18. These vulcanizates are attached fairly well to metal by Leukonat, but the bond is weaker than with SKN-18 vulcanizates. When the rubber is peeled off part of the adhesive remains on the metal, but most passes to the rubber. Naitrit rubber is similar to SKN-26. Vulcanizates based on SKN-40, with the highest content of polar groups, are bonded weakly to metal by Leukonat and when peeled off the metal all the adhesive stays on the rubber.

Thus, as the chemical activity and polarity of rubbers increase, the interaction of the adhesive film with vulcanizates of these rubbers also increases while the interaction between the adhesive film and the metal remains

TABLE 2

Effect of Thickness of Adhesive Film (in μ) on the Nature of Failure and Resistance to Peeling (kg/cm) of Rubbers From Metal

Rubber code mark	Film thickness, μ									
	3.2*		1.6		0.4		0.2		0.1	
	kg/cm	type of failure	kg/cm	type of failure	kg/cm	type of failure	kg/cm	type of failure	kg/cm	type of failure
A-7 (butyl rubber)	0.4	Adhesive remains on metal	0.1	Adhesive remains on metal	—	—	0.1	Adhesive remains on metal	—	—
A-1 (natural rubber)	4.68	Same	0.25	Same	0.16	Adhesive remains on metal	—	—	—	—
A-3 (SKS-30)	1.46	Rupture of rubber	0.65	»	0.24	Same	—	—	—	—
A-4 (SKN-18)	3.94	Most adhesive remains on metal	3.07	»	2.66	»	2.24	Adhesive remains on metal	2.20	Adhesive remains on metal
A-2 (nairit)	3.12	Same	2.98	»	2.73	»	—	—	1.49	—
A-5 (SKN-26)	2.93	Part of adhesive on rubber, part on metal	2.97	Most adhesive remains on metal	1.80	»	—	—	1.46	—
A-6 (SKN-40)	0.82	Adhesive remains on rubber	1.02	Part of adhesive on rubber, part on metal	1.03	Most adhesive remains on metal	—	—	1.01	»
									0.68	Adhesive remains on metal

* An adhesive film 3.2 μ thick corresponds to Leukonat adhesive of 20% concentration.

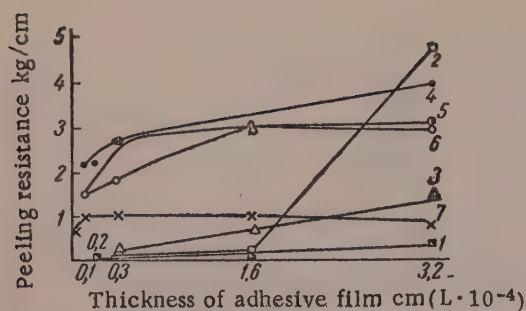


Fig. 1. Effect of thickness of Leukonat adhesive film on the strength of bonding of different unfilled vulcanizates to metal: 1) butyl rubber; 2) natural rubber; 3) butadiene - styrene rubber; 4) SKN-18; 5) nairit; 6) SKN-26; 7) SKN-40.

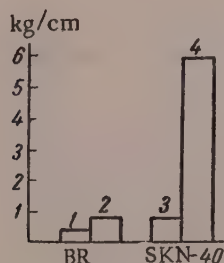


Fig. 2. Effect of metal surface treatment on the strength of bonding of SKN-40 and butyl rubber (BR) vulcanizates to it: 1 and 3) metal cleaned with No. 100 emery paper; 2 and 4) metal sandblasted.

strength of bonding of these two rubbers to it (see Fig. 2). Whereas the strength of bonding of butyl rubber to metal is almost unchanged after sandblasting (some increase of bond strength may occur perhaps as the result of an increase of the contact area caused by sandblasting) the bond strength with SKN-40 vulcanizate is increased roughly 10-fold; any further increase of the bond strength is limited by the strength of the rubber itself, as the failure of the joints occurs in the rubber.

The test results in Table 2 and Fig. 1 show that decrease of the adhesive film thickness has different effects on the bond strengths for vulcanizates of different rubbers.

An examination of the variations of the nature of the failure, presented in Table 2, shows that as the thickness of the adhesive film decreases, the interaction between the adhesive and the rubber usually diminishes because of the decreasing concentration of the adhesive. This influences the course of the curve representing the rubber - metal bond strength as a function of the adhesive film thickness. If A_1 is the interaction of a film of the undiluted adhesive with rubber; A'_1 is the interaction of a film of diluted adhesive with rubber; and A_2 is the interaction of the adhesive film with the metal, then it follows from the experimental data that if the adhesive is diluted $A'_1 < A_1$ (this is a general rule).

constant. However, as the results show, the bond strength does not increase continuously with chemical activity and polarity of the rubbers; it increases at first, passes through a maximum, and then diminishes. If we denote the interaction between the adhesive film and rubber by A_1 and the interaction between the adhesive film and the metal by A_2 , then we have:

1) if $A_1 < A_2$ the rubber - metal bonding is poor. This is the case when a chemically inert, nonpolar rubber vulcanizate (butyl rubber) is attached to metal by Luekonat adhesive.

2) if $A_1 \approx A_2$, the rubber - metal bonding is good. This is the case when a chemically-active rubber or a rubber of moderate polarity (natural rubber, SKS-30, SKN-18, nairit, SKN-26) is attached to metal.

3) if $A_1 > A_2$ the rubber - metal bonding is poor. This is the case when a vulcanized rubber with a high content of polar groups (SKN-40) is attached to metal.

It is thus seen that rubber - metal bond strength is high only if the interaction at the adhesive - metal and adhesive - rubber interfaces is of approximately the same intensity. If the interaction is considerably greater with one of the surfaces in contact with the adhesive film the rubber - metal bond strength is low.

It has been shown [1] that if the metal surface is sandblasted the interaction of the adhesive film with the surface is increased. Therefore the situation is different if the same vulcanizates are bonded to sandblasted metal surfaces.

The two most typical cases were chosen: bonding of unfilled vulcanizates of butyl and SKN-40 rubbers. Both these unfilled vulcanizates are bonded weakly to smooth metal surfaces by Leukonat adhesive; however, the bond with butyl rubber is weak because of weak adhesion at the adhesive - rubber interface, while with SKN-40 rubber the adhesion at the adhesive - metal interface is weak. Sandblasting of the metal surface has different effects on the

For Nonpolar Rubber Vulcanizates

For undiluted adhesive $A_1 \leq A_2$. For diluted adhesive $A'_1 \ll A_2$ (the bond strength falls sharply with dilution of the adhesive).

For Vulcanizates of SKN-18, Nairit, and SKN-26 (rubbers of moderate polarity)

For undiluted adhesive $A_1 \geq A_2$. For diluted adhesive $A'_1 \approx A_2$ (the bond strength falls very slowly with dilution of the adhesive).

For Vulcanizates of SKN-40 (highly polar rubber)

For undiluted adhesive $A_1 \gg A_2$. For a diluted adhesive $A'_1 \geq A_2$ (the bond strength increases somewhat with dilution of the adhesive).

Leukonat adhesive can be used for fixing metal fairly firmly to vulcanizates based on both polar rubbers and nonpolar rubbers which are chemically active (natural rubber, SKS-30). Polar groups take active part in bond formation at the adhesive - rubber interface, as is exemplified by the bonding of unfilled rubbers (SKN-18, SKN-26, and SKN-40). The higher the nitrile group content of the rubber, the greater the interaction between the adhesive film and the vulcanized rubber. When mixes based on nonpolar rubbers are bonded to metal by means of Leukonat adhesive in the course of vulcanization, chemical interaction can apparently take place between the rubber and the adhesive film.

Since triphenylmethane triisocyanate, which is the basis of Leukonat adhesive, is polyfunctional in character, it may interact simultaneously with several rubber molecules and not only with one, with formation of a structural network as in vulcanization. To test this hypothesis it was of interest to study the interaction of rubber with isocyanate in solution, and the action of isocyanate as a vulcanization agent.

SUMMARY

1. The strength of the bond between rubber and metal effected by an adhesive film depends on the ratio of the intensities of interaction of the adhesive film with the contacting surfaces at the adhesive - rubber and adhesive - metal interfaces. The bond strength is greatest if they are approximately equal. If they differ considerably the bond strength is lower.
2. One of the factors influencing the interaction between the adhesive film and rubber is the thickness of the adhesive film; as the film thickness decreases its interaction with rubber diminishes, and this influences the rubber - metal bond strength differently for different rubber vulcanizates, causing in some cases a decrease and in others a certain increase in the strength of the rubber - metal bond.
3. Leukonat isocyanate adhesive gives a fairly high bond strength between metal and unfilled vulcanizates based on most polar and nonpolar rubbers.
4. The interaction of the adhesive film with a vulcanizate increases with increasing content of polar groups in the rubber.

LITERATURE CITED

- [1] A. M. Medvedev, B. V. Deryagin, and S. K. Zhrebkov, *Kolloid. Zhur.* **19**, 412 (1957).*
- [2] B. V. Deryagin and N. A. Krotova, *Adhesion* [in Russian] (Izd. AN SSSR, 1949).

Received October 2, 1958

*Original Russian pagination. See C. B. Translation.

INVESTIGATION OF THE STRUCTURE AND ADSORPTIVE AND CATALYTIC ACTIVITY OF THE HYDROXIDES OF IRON, CHROMIUM, AND ALUMINUM IN RELATION TO THE PRECIPITATION METHOD AND TEMPERATURE

N. F. Ermolenko and S. A. Levina

Institute of Chemistry, Academy of Sciences Belorussian SSR, Minsk

During recent years numerous papers have been published on the structure and adsorptive and catalytic properties of the hydroxides and oxides of aluminum, chromium, and iron. The interest in these compounds is due to their extensive applications as adsorbents and catalysts. It is known that adsorptive and catalytic activity depends on the structure of the adsorbent, and the latter depends to a considerable extent on the conditions in which the adsorbent was prepared. Naturally, much attention has been devoted to this problem. Studies of the effects of preparation conditions on the structure and adsorptive and catalytic properties of the hydroxides of aluminum [1-6], chromium [7-11], and iron [12-15] have been reported. Our earlier studies were concerned with the effects of the medium, aging time, and temperature on the adsorptive properties and structure of gels of aluminum, chromium, and iron hydroxides at the instant of formation in the mother liquors [16-18], of the pure, dialyzed gels in the air-dry state [19-21], and after appropriate heat treatment [22].

In the present investigation we studied the effects of the sequence and rate of precipitation and of temperature on the structure, specific surface, and the adsorptive and catalytic activity of the hydroxides of iron, chromium, and aluminum.

The adsorbents (hydroxides of iron, chromium, and aluminum) were prepared from solutions of their sulfates by precipitation by ammonia (from chrome alum in the case of chromium hydroxide) by the following four methods:

1. The equivalent amount of ammonia solution was added dropwise to the salt solution during 30 minutes with continuous stirring.
2. The equivalent amount of ammonia was added at once to the salt solution.
3. The salt solution was added at once to ammonia solution.
4. The salt solution was added dropwise to the ammonia solution during 30 minutes with constant stirring.

The pH of the medium after precipitation was 7-7.2. The temperature of the solutions before precipitation was 19°. In addition, precipitation by methods 1 and 2 was carried out at -10 and +50°.

A total of 24 hydroxide samples was prepared. The samples were washed with distilled water to a negative reaction for SO_4^{2-} with BaCl_2 , dried in air, ground in a mortar, and passed through a 52 mesh screen.

The specific surface and structure of the samples were determined from the absorption of CCl_4 vapor in a vacuum apparatus with the McBain quartz balance. The adsorptive activity was determined from the adsorption of Congo Red dye, the concentration of which was found by means of a photocolormeter. The catalytic activity was estimated from the rate of condensation of acetone to diacetone alcohol. The concentration of diacetone alcohol was determined with the aid of an interferometer by means of a calibration curve plotted from data for solutions of diacetone alcohol in acetone [20-23].

TABLE 1

Contents of Moisture and SO_4^{2-} in $\text{Fe}(\text{OH})_3$ Samples

$\text{Fe}(\text{OH})_3$ sample*	Moisture, %	SO_4^{2-} content, %	Color shade
1	10.08	3.29	Brown
2	19.81	0.08	Red-brown
3	15.04	9.60	Yellow-brown
4	22.80	2.56	Brown

* The nos. correspond to preparation methods (p. 543).

Table 1 shows that the yellow-brown sample 3 had the highest impurity content, and the red-brown sample 2 was the purest hydroxide. The dye Congo Red, of large particle size, was not adsorbed by any of the hydroxide samples. Moreover, the color of the dye solution changed from red to blue-violet with samples 1 and 3. The probable cause of this color change is that in an aqueous medium SO_4^{2-} ions are exchanged for OH^- ions, and the medium becomes acidified (the pH was 3.0-5.2). It has been shown by Shishniashvili and Kargin [30] that highly purified gels do not take part in such exchange.

Since the $\text{Fe}(\text{OH})_3$ samples did not adsorb the dye, we assumed that they were microporous in structure. The microporous structure of the samples was confirmed by adsorption of CCl_4 vapor.

Figure 1 shows isotherms for adsorption and desorption of CCl_4 vapor on samples 1, 2, and 4 of $\text{Fe}(\text{OH})_3$ gel. Sample 3 was completely inactive and its isotherms are not given. In accordance with Kiselev's classification [31], the isotherms in Fig. 1 are of the third type, i.e., characteristic of homogeneous microporous adsorbents. The adsorption isotherms were used for calculations of the specific surface of the samples, and the effective pore radius was calculated from the desorption branch of the curve (the pore-size characteristics are given). Since the $\text{Fe}(\text{OH})_3$ samples were microporous, with a relatively large specific surface, we used them as catalysts in preparation of diacetone alcohol from acetone [20-23]. Ferric hydroxide had not been used previously for this purpose. It was found that some of our samples were more active than the calcium and barium hydroxides used in industry. Table 2 contains data on the specific surface, porosity characteristics, rate constants for the reaction of diacetone alcohol formation, and variations in the structure of samples 1 and 2 with the precipitation temperature.

It follows from Table 2 that the hydroxide of the highest catalytic activity was that prepared by rapid addition of ammonia to the ferric salt solution at an initial solution temperature of -10° , and the least active was that prepared by the reverse procedure (sample 3). The active sample (2_{-10°) had high specific surface and the greatest pore volume. Calculations showed that the effective pore radius in this case was 20 Å. The adsorption isotherms and data in Table 2 indicate that less active gels are formed at 19° than at -10 or $+50^\circ$.

Structure and adsorptive and catalytic activity of chromium hydroxide. The air-dry samples of chromium hydroxide gel were analyzed for moisture and SO_4^{2-} (Table 3). Table 3 shows that the SO_4^{2-} contents decrease in the sequence from sample 1 to sample 4. It is well known that basic salts are formed in precipitation of chromium hydroxide [32].

In studies of the adsorption of Congo Red by chromium hydroxide we did not observe changes in the color of the dye solution such as were found with samples 1 and 2 of ferric hydroxide gel. The adsorption isotherms for the dye were plotted and used to calculate the maximum amounts of dye which saturate the adsorbent surface. The results, also given in Table 3, show that the chromium hydroxide samples had large numbers of medium and large pores, so that these large amounts of the dye could be adsorbed.

Investigation of the adsorption of CCl_4 vapor showed that the $\text{Cr}(\text{OH})_3$ samples did in fact have very extensive porosity. Figure 2 shows isotherms for adsorption and desorption of CCl_4 vapor on samples of chromium hydroxide gel, and adsorption isotherms for samples 1 and 2 precipitated at -10 , 19 , and 50° . They differ sharply

Structure and adsorptive and catalytic activity of ferric hydroxide. Our samples of ferric hydroxide differed slightly in color shade. It has been reported in the literature that catalytic activity, as in decomposition of hydrogen peroxide, differs for differently-colored samples of ferric hydroxide [24, 25]. Gupta and Ghosh [26] found that hydroxide prepared at different pH values of the medium and in presence of different electrolytes varied in color from red to yellow. Like several other authors [27-29], they consider that the color of ferric hydroxide depends more on its composition than on the size of the colloidal gel particles. Our analyses showed that the ferric hydroxide samples contained moisture and certain amounts of accompanying ions (Table 1).

TABLE 2

Specific Surface, Rate Constant of Diacetone Alcohol Formation, and Pore-Size Characteristics of the Samples

Fe(OH) ₃ * sample	Specific surface, m ² /g	Rate constant × 10 ⁴	Pore volume, cc/g		
			total	fine	intermediate
1 _{-10°}	200	5,04	0,1738	0,1640	0,0098
1 _{10°}	64	1,98	0,1167	0,1020	0,0147
1 _{50°}	189	3,71	0,1911	0,1800	0,0111
2 _{-10°}	197	8,23	0,2193	0,1350	0,0783
2 _{10°}	145	5,66	0,1686	0,1160	0,0300
2 _{50°}	153	6,03	0,1807	0,1800	—
3	9	0,06	—	—	—
4	140	2,03	0,1470	0,1000	0,0470

*The numbers correspond to the preparation methods. The subscripts represent the temperatures at which the samples were prepared.

TABLE 3

Contents of Moisture and SO₄²⁻ and Maximum Adsorption of Dye by Samples of Chromium Hydroxide Gel

Cr(OH) ₃ sample*	Moisture, %	SO ₄ ²⁻ content, %	Dye adsorp- tion, mg/g
1	15.0	10.24	666
2	21.6	9.24	666
3	26.3	6.00	454
4	27.2	3.03	666

*The numbers correspond to the preparation methods.

in appearance from the isotherms for ferric hydroxide, and may be classified as belonging to the fourth type [31], i.e., isotherms characteristic of adsorbents with mixed porosity, containing moderate and large pores in addition to fine pores, although the isotherms for samples 3 and 4 approach to the type characteristic of coarsely-porous adsorbents. The adsorption isotherms were used for calculating the specific surface by the BET method, and the pore sizes were estimated (Table 4). Since the samples of chromium hydroxide gel had relatively large specific surface and contained fine pores, we attempted to use them for synthesis of diacetone alcohol. It was found that diacetone alcohol is formed from acetone in presence of chromium hydroxide too, but, despite the fairly large specific surface, the reaction rate constant was lower than with the use of ferric hydroxide. This is evidently the consequence of specific catalytic activity.

It follows from Table 4 that, as with ferric hydroxide, the most active hydroxide is formed when ammonia solution is added rapidly to the salt solution at -10°. Similar results were obtained by other workers in studies of chromic oxide catalysts, prepared by the bisulfate method, used for catalytic oxidation of SO₂ [11].

Table 4 shows that increase of the precipitation temperature results in formation of less-porous hydroxides. This is seen especially clearly in the case of sample 2 (Fig. 2), the adsorption isotherm for which lies much lower at 50°, and the total pore volume is almost halved.

Structure and adsorptive and catalytic activity of aluminum hydroxide. Analysis of the aluminum hydroxide samples showed them to contain considerable amounts of SO₄²⁻. The tendency to formation of basic salts during precipitation of the hydroxide has been reported more than once [33, 34]. Table 5 contains data on moisture content, SO₄²⁻ content, and maximum adsorption of dye for the aluminum hydroxide samples.

Table 5 shows that the Al(OH)₃ samples contained up to 35% of SO₄²⁻ ions. This is considerably more than was found in the hydroxides of chromium and iron. However, acidification of the medium during adsorption of Congo Red was not observed. Congo Red is adsorbed considerably less by aluminum hydroxide gel than by chromium hydroxide. The data on dye adsorption suggest that sample 4 contained most medium and large pores, whereas sample 2 contained fine pores.

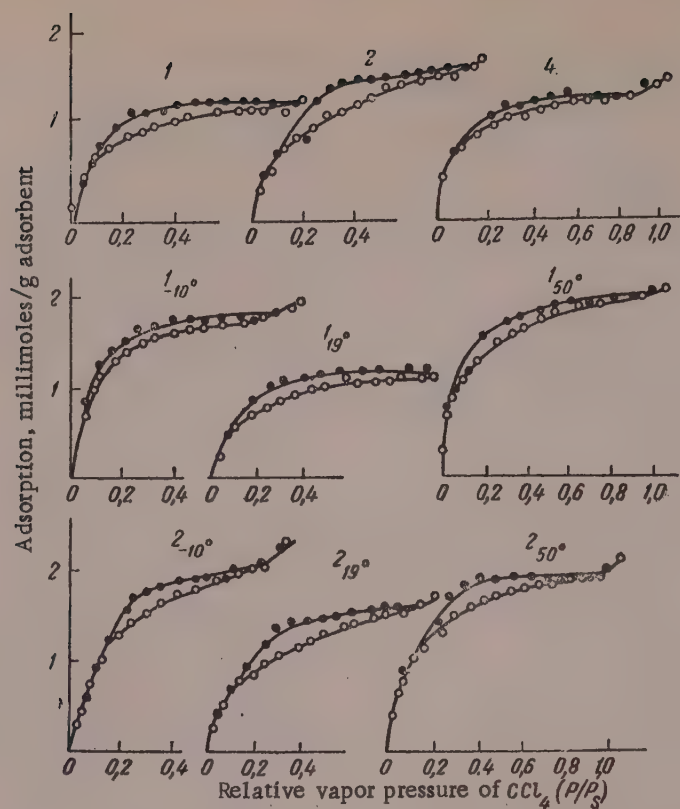


Fig. 1. Isotherms for adsorption of CCl_4 vapor on $\text{Fe}(\text{OH})_3$ samples: 1, 2, and 4) samples prepared by methods 1, 2, and 4; 1 $_{-10^\circ}$, 1 $_{19^\circ}$, and 1 $_{50^\circ}$ samples prepared by the first method at -10 , 19 , and 50° ; 2 $_{-10^\circ}$, 2 $_{19^\circ}$, 2 $_{50^\circ}$ samples prepared by the second method at -10 , 19 , and 50° .

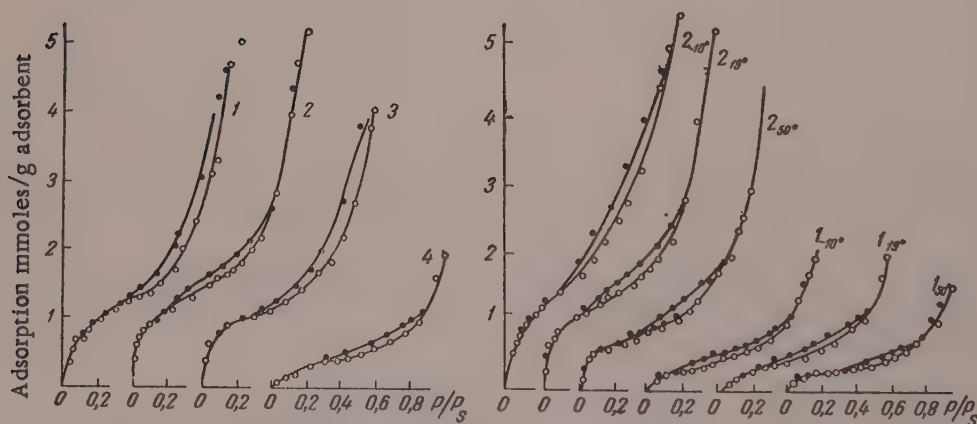


Fig. 2. Isotherms for adsorption of CCl_4 vapor on $\text{Cr}(\text{OH})_3$ samples: 1, 2, 3, and 4) samples prepared by methods 1, 2, 3, and 4; 1 $_{-10^\circ}$, 1 $_{19^\circ}$, 1 $_{50^\circ}$ samples prepared by the first method at -10 , 19 , 50° ; 2 $_{-10^\circ}$, 2 $_{19^\circ}$, 2 $_{50^\circ}$ samples prepared by the second method at -10 , 19 , and 50° .

Study of the structure of $\text{Al}(\text{OH})_3$ samples based on adsorption of CCl_4 vapor showed that the method of precipitation has a very strong influence on the structure of the hydroxide. Table 6 contains data on the specific surface and porosity of $\text{Al}(\text{OH})_3$ gel samples.

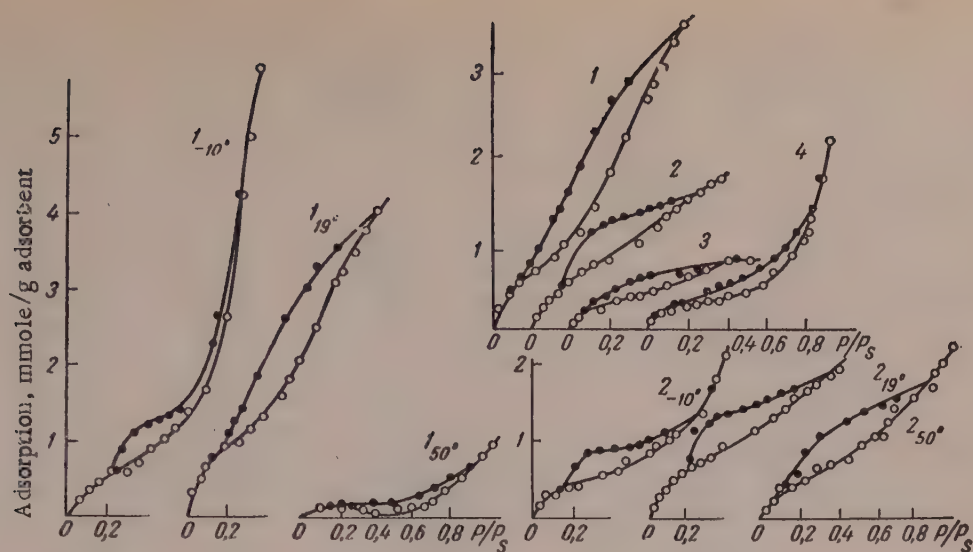


Fig. 3. Isotherms for adsorption of CCl_4 vapor on $\text{Al}(\text{OH})_3$ samples: 1, 2, 3 and 4) samples prepared by methods 1, 2, 3, and 4; 1_{-10°}, 1_{19°}, 1_{50°} samples prepared by the first method at -10, 19 and 50°; 2_{-10°}, 2_{19°}, 2_{50°} samples prepared by the second method at -10, 19, and 50°.

TABLE 4

Specific Surface, Rate Constant of Diacetone Alcohol Formation, and Pore-Size Characteristics of Chromium Hydroxide Samples

$\text{Cr}(\text{OH})_3$ sample*	Reaction rate constant $\times 10^{-4}$	Specific surface, m^2/g	Pore volume, cc/g			
			total	fine	intermediate	coarse
1 _{-10°}	2,21	54	0,1931	0,036	0,030	0,067
1 _{19°}	1,64	64	0,1931	0,030	0,060	0,103
1 _{50°}	2,16	45	0,1293	0,024	0,094	0,011
2 _{-10°}	4,23	224	0,5310	0,130	0,320	0,080
2 _{19°}	4,20	200	0,5060	0,120	0,280	0,106
2 _{50°}	2,95	121	0,2915	0,070	0,118	0,102
3	2,86	168	0,5000	0,012	0,310	0,090
4	2,52	158	0,4441	0,100	0,295	0,049

*The numbers correspond to the preparation methods. The subscripts represent the temperatures at which the samples were prepared.

Table 6 shows that, in contrast to the results for ferric and chromium hydroxides, rapid precipitation of aluminum hydroxide does not give the most active samples. Sample 1 had the greatest pore volume and the greatest specific surface. Increase of the precipitation temperature has an especially strong effect on the structure of the adsorbent (sample 1).

On increase of the temperature to 50° the total pore volume of sample 1 fell from 0.57 to 0.11 cc/g, whereas at 19° the number of fine pores increased, so that the specific surface rose from 104 to 148 m^2/g . As already noted, at 50° the total pore volume and the specific surface were considerably less. Change of temperature did not have such a pronounced effect in the case of sample 2. This is clearly seen in Fig. 3, which shows isotherms for adsorption and desorption of CCl_4 vapor; they are different in form for each sample. Whereas the isotherm for sample 1 can be classified with adsorbents of the second type (coarsely porous) [31], samples 2 and 3 occupy an intermediate position between the second and third types, while the isotherm for sample 4 is characteristic of samples with mixed porosity (the fourth type). The shape of the hysteresis loop in the isotherm of sample 2

TABLE 5

Moisture Contents and Maximum Adsorption of Dye by Aluminum Hydroxide Samples

Al(OH) ₃ sample*	Moisture, %	SO ₄ ²⁻ content, %	Dye adsorption, mg/g
1	25.0	26.3	304
2	29.0	23.8	153
3	10.5	35.5	303
4	20.9	34.7	952

*The numbers correspond to the preparation methods (p. 543).

isorption branch of the isotherm give 20 Å for sample 2_(-10°) and 10 Å for sample 2_(19°), which apparently corresponds to the narrow necks of the bottle-shaped pores. The presence of bottle-shaped pores in sample 2 is confirmed by adsorption data for Congo Red. Sample 2 has the lowest adsorption of this dye. Evidently the narrow necks of the bottle-shaped pores are too small for the large dye particles to penetrate. Our samples also proved inactive as catalysts in condensation of acetone to diacetone alcohol, although it has been reported that diacetone alcohol is formed during prolonged contact of acetone with active alumina [36]. The absence of catalytic activity is evidence against a microporous structure in the aluminum hydroxide gel samples.

Electron-microscopic investigation of the samples. Electron micrographs of our samples were taken in order to obtain a clearer idea of the structure of the ferric, chromium, and aluminum hydroxide gels. For this drops of very dilute suspensions of the samples were placed on nitrocellulose films. The dried specimens were then examined in the electron microscope. Unfortunately, we were only able to obtain relatively low magnifications of 7000-11,000 ×. It was found that many samples had a system of open macropores of 500 Å and over in size; most of the pores were at the edges of the particles. Micrographs 1, 2, and 3 show particles of ferric hydroxide gel (samples 1, 2, and 3) at 7000 × magnification. Micrograph 1 shows that particles of sample 1 had fairly numerous open pores between 170 and 500 Å in radius; sample 2 (micrograph 2) had pores between 140 and 250 Å, and finally, the particles in sample 3 were compact and quite lacking in large pores. As has already been shown, the effective pore radius of the ferric hydroxide gel specimens does not exceed 20 Å, and even if these pores were open we could not observe them at the magnification used.

TABLE 6

Specific Surface and Porosity Characteristics of Samples of Al(OH)₃ Gel

Al(OH) ₃ sample*	Specific surface, m ² /g	Pore volume, cc/g			
		total	fine	intermediate	coarse
1 _{-10°}	104	0,5793	0,0750	0,3500	0,1780
1 _{19°}	148	0,3616	0,1100	0,2500	0,0016
1 _{50°}	33	0,1158	0,0070	0,0845	0,0243
2 _{-10°}	95	0,2122	0,0800	0,0700	0,0622
2 _{19°}	121	0,1834	0,0700	0,0960	0,0174
2 _{50°}	104	0,2239	0,09400	0,0860	0,0439
3	51	0,0868	0,0380	0,0320	0,0168
4	55	0,2896	0,0180	0,1080	0,1816

*The numbers correspond to the preparation methods. The subscripts represent the temperature at which the samples were prepared.

is striking. The whole isotherm resembles the isotherms obtained by Zhdanov [35] for adsorption of water vapor by porous glasses of a peculiar structure, described as the bottle type. If open pores are of cylindrical or nearly cylindrical shape, the following relationship should be valid: $(P/P_S)_{des} < (P/P_S)_{ads}^2$. In Zhdanov's view, if pores of the bottle type are present, in which the radius of the wide part is greater than $2r$, the following relationship should hold: $(P/P_S)_{des} < (P/P_S)_{ads}^2$. The hysteresis loop should then be anomalously wide. Examination of the isotherms for adsorption of CCl₄ vapor on samples 2_(-10°) and 2_(19°) showed that in the relative-pressure range of 0.5-0.6 for sample 2_(-10°) and 0.6-0.75 for sample 2_(19°), the relationship $(P/P_S)_{des} < (P/P_S)_{ads}^2$ is valid. In this range of relative pressures pores from 40-60 Å and 45-75 Å are filled. It may be assumed that in this case the pores are bottle-shaped. Calculations of the effective pore radius from the de-

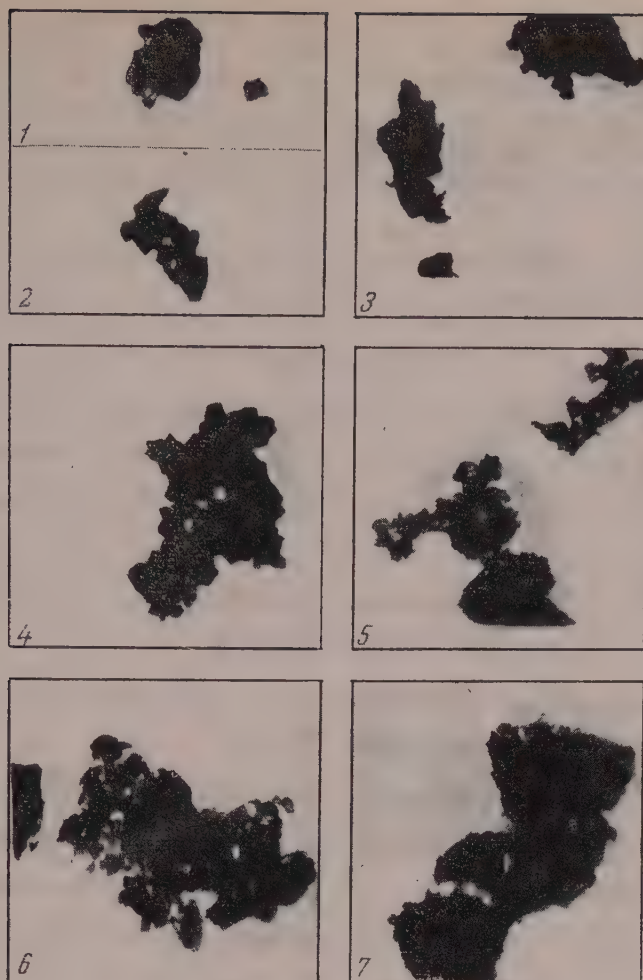


Fig. 4. Electron micrographs: 1) sample 1 $\text{Fe}(\text{OH})_3$ ($\times 7000$); 2) sample 2 $\text{Fe}(\text{OH})_3$ ($\times 7000$); 3) sample 3 $\text{Fe}(\text{OH})_3$ ($\times 7000$); 4) sample 1 $\text{Cr}(\text{OH})_3$ ($\times 11000$); 5) sample 2 $\text{Cr}(\text{OH})_3$ ($\times 10000$); 6) sample 1 $\text{Al}(\text{OH})_3$ ($\times 11000$); 7) sample 2 $\text{Al}(\text{OH})_3$ ($\times 7000$).

Figure 4 shows sample 1 of chromium hydroxide gel (micrograph 4) at $\times 11,000$ magnification. Pores with radii from 200 to 450 Å can be clearly seen. Sample 2 of the same gel is shown in micrograph 5. This sample was very porous, with pore radii from 50 to 250 Å. Sample 1 of aluminum hydroxide gel (micrograph 2) had numerous larger pores, with many open pores from 50 to 500 Å in size. This confirms that its structure is coarsely porous, as was found from the form of its isotherm. Sample 2 of $\text{Al}(\text{OH})_3$ gel was compact, with only very large pores, greater than 500 Å in radius, visible (micrograph 7). If, as we believe, this sample had bottle-shaped pores, the narrow necks of the pores are invisible at $\times 7000$ magnification even if the pores were open.

Thus the electron micrographs confirm our experimental data on the structure of ferric, chromium, and aluminum hydroxide gels.

SUMMARY

1. The sequence and the rate at which the solutions are mixed and the temperature have significant effects on the structure and the adsorptive and catalytic properties of hydroxides.

2. In the case of ferric and chromium hydroxides the samples formed by rapid addition of ammonia solution to ferric or chromium sulfate at -10° are the most active.

3. All the hydroxide samples studied differed from each other in structure. Ferric hydroxide was uniformly microporous; chromic hydroxide had mixed porosity. The form of the isotherms is not changed sharply if the sequence and rate of precipitation are varied. In the case of aluminum hydroxide the form of the isotherms varies in accordance with the sequence and rate of precipitation: sample 1 gives isotherms of the 2nd type (characteristic of coarsely-porous adsorbents), samples 2 and 3 give isotherms of a type intermediate between those characteristic of coarsely-porous and microporous adsorbents, and sample 4 gives isotherms characteristic of adsorbents with mixed porosity.

4. Chromium and ferric hydroxides were used for the first time as catalysts for synthesis of diacetone alcohol from acetone.

LITERATURE CITED

- [1] K. Z. Elmore, C. M. Mason, and J. D. Hatfield, *J. Amer. Chem. Soc.* 64, 1449 (1945).
- [2] I. I. Iskol'dskii, *Chemistry of Solutions in the Aluminum Industry* [in Russian] (ONTI, 1937).
- [3] H. B. Weiser, W. Milligan, and Purcell, *Ind. Engng. Chem.* 32, 1487 (1940).
- [4] H. B. Weiser, W. Milligan, and Purcell, *Ind. Engng. Chem.* 33, 669 (1941).
- [5] N. M. Osmolovskii, *Candidate's Dissertation* [in Russian] (Leningrad, 1953).
- [6] E. I. Amezola, *Rev. Fac. cienegium* 1952 (1955) 27, 65.
- [7] N. V. Alekseevskaya, *Tr. Leningr. tekhnol. in-ta im. Lensovet* 27, 46 (1953).
- [8] S. Tewari and S. Ghosh, *Koll.-Z.* 138, (2), 87 (1954).
- [9] W. Weller and S. Voltz, *Z. Phys. Chem.* 5, (1-2), 100 (1955).
- [10] M. S. Belen'kii and M. M. Gurevich, *Tr. In-ta khimii AN Azerbaidzh. SSR* 7 (1949).
- [11] M. S. Belen'kii and M. M. Gurevich, *Tr. In-ta khimii AN Azerbaidzh. SSR* 8, 5 (1952).
- [12] A. Michel, C. Lilin, and M. Lensen, *Bull. Soc. chem. France* No. 2, 283; No. 3, 453 (1956).
- [13] Sabatier and Mailhe, *Ann. Chim. Phys.* 20, 313 (1910).
- [14] G. Virskaya, *Author's Summary of Dissertation* [in Russian] (Tashkent, SAGU Press, 1953).
- [15] S. Gupta and S. Ghosh, *Proc. Nat. Acad. Sci. Ind.* 21A, 3 (1952); *Koll.-Z.* 132, 141 (1953).
- [16] N. F. Ermolenko and S. A. Levina, *Izv. AN Beloruss. SSR* 1, 107 (1954).
- [17] N. F. Ermolenko and S. A. Levina, *Authors' Certif. No.* 13877 (1953).
- [18] N. F. Ermolenko and S. A. Levina, *Proc. 3rd All-Union Conf. on Colloid Chemistry* [in Russian] (1956) p. 276.
- [19] S. A. Levina and N. F. Ermolenko, *Kolloid. Zhur.* 19, 673 (1957).*
- [20] S. A. Levina, N. F. Ermolenko, and V. I. Pansevich-Kolyada, *Zhur. Obshchei Khim.* 29, 1920 (1959).
- [21] N. F. Ermolenko and S. A. Levina, *Coll. Trans. Inst. Chem. Acad. Sci. Belorussian SSR* [in Russian] (1959) 7, (3) (in the press).
- [22] S. A. Levina and N. F. Ermolenko, *Coll. Trans. Inst. Chem. Acad. Sci. Belorussian SSR* [in Russian] (1957) 6, (2).
- [23] S. A. Levina, N. F. Ermolenko, and V. I. Pansevich-Kolyada, *Authors' Certif. No.* 11060 (1957).
- [24] Hüttig and Zorner, *Z. anorg. allgem. Chem.* 184, 180 (1929).
- [25] S. Gupta and S. Ghosh, *Z. Phys. Chem.* No. 1-2, 204 (1955).
- [26] S. Gupta and S. Ghosh, *Koll.-Z.* 29, 10 (1956).

*Original Russian pagination. See C. B. Translation.

- [27] L. N. Uspenskaya, A. Kh. Girenko and M. S. Ostrikov, Zhur. Priklad. Khim. 29, 10, 1601 (1956).*
- [28] L. N. Uspenskaya and A. Kh. Girenko, Zhur. Priklad. Khim. 29, 8, 1142 (1956).*
- [29] L. N. Uspenskaya and A. Kh. Girenko, Zhur. Priklad. Khim. 29, 7, 1040 (1956).*
- [30] M. E. Shishniashvili, V. A. Kargin, and A. A. Batsanadze, Kolloid. Zhur. 8, 4 (1946).
- [31] A. V. Kiselev, Vestn. MGU 11, 111 (1949).
- [32] Amelin-Kraut (1912) 3, 1, 401.
- [33] V. A. Kargin and N. A. Ogadzhanova, Zhur. Fiz. Khim. 10, 78 (1937).
- [34] Z. Ya. Berestneva and V. A. Kargin, Zhur. Fiz. Khim. 10, 593 (1937).
- [35] S. P. Zhdanov, in the book: Methods of Investigating the Structures of Highly Disperse and Porous Bodies [in Russian] (Izd. AN SSSR, 1953) p. 114.
- [36] R. Furhmann, J. rech. Centr. nat. rech. scient. No. 25, 257(1933).

Received July 2, 1958

* Original Russian pagination. See C. B. Translation.

PREPARATION OF MIXED ALUMINUM HYDROXIDE AND HYDROXY-SULFATE FILMS AND INVESTIGATION OF THEIR STRUCTURE

I. A. Istomina, Z. Ya. Berestneva, and V. A. Kargin

The L. Ya. Karpov Physicochemical Institute, Moscow

It is known that metal sulfides and hydroxides obtained in the form of films on the surfaces of their salts are used as stabilizers for emulsion systems consisting of various oils and water. Mixed films of aluminum hydroxide and hydroxysulfate are more indifferent than films of other compounds, and may be widely used as stabilizers for emulsions.

There are several papers dealing with preparation of metal sulfide and hydroxide films [1-3]. However, the methods described are suitable only for preparation of small amounts of films for laboratory research work.

The aim of the present investigation was to find a more productive method for preparation of mixed aluminum oxide and hydroxysulfate films and to investigate their structure.

For preparation of the films an apparatus was devised (Fig. 1) consisting of a drum 1 rotating on a shaft, enclosed in a hermetic chamber 2. In the upper part of the chamber there is a slot 3 through which the surface of the rotating drum is uniformly moistened with salt solution. A mixture of ammonia and air, formed by the passage of a current of air through ammonia solution, is blown into the lower part of the chamber through the tube 4 by means of a fan. The spent mixture of ammonia and air is drawn out by the same fan through the tube 5 in the upper part of the chamber and passes to a vessel containing ammonia solution; there it is enriched with ammonia, and after passing through a cleaning chamber it returns to the apparatus.

A mixed film of aluminum hydroxide and hydroxysulfate is formed on the drum surface when the salt solution reacts with the ammonia which is fed into the chamber. The film is removed from the drum surface by the scraper 6 and falls to the chamber floor 7.

Potash alum, ammonium alum, and aluminum sulfate may be used as the aluminum salts for film preparation. Experiments showed that the yield of film depends on the concentration of the salt solution.

Of the above-named salts, aluminum sulfate has the highest solubility. Therefore its solutions are the most suitable for preparation of mixed films of aluminum hydroxide and hydroxysulfate. It was found by experience that 30% aluminum sulfate solution should be used for film preparation, as the productivity of the apparatus decreases at lower concentrations, while the use of solutions of higher concentrations (close to saturation) proved inconvenient because temperature fluctuations caused precipitation of salt crystals.

The films were separated from aluminum sulfate solution on a vacuum filter and washed with distilled water by repeated decantation followed by filtration. Washing may be accelerated by the use of hot distilled water (60-70°), when the consumption of distilled water is almost halved.

The prepared films were examined in the electron microscope at $\times 10,000$ - $12,000$ direct electron-optical magnification, and then studied by electron diffraction.

Freshly prepared films washed either with hot water or water at room temperature present almost the same picture under the electron microscope.

Section
along BB

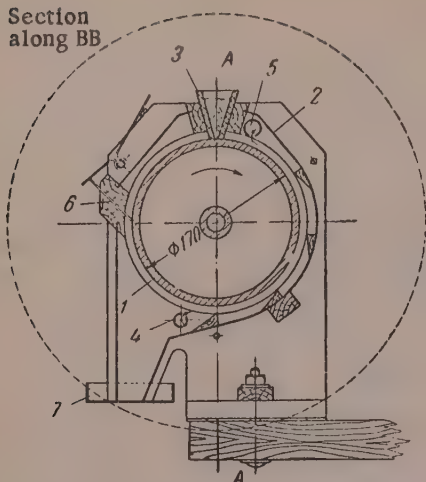


Fig. 1. Apparatus for preparation of aluminum hydroxide and hydroxysulfate films.

of aluminum hydroxide does not penetrate right across the thickness of the layer of aluminum sulfate solution.

During the first instant a very thin film of aluminum hydroxide, which prevents interaction of the components, is formed on the surface of the layer of aqueous aluminum sulfate solution, and further formation of aluminum hydroxide is determined by diffusion processes only. Therefore, in the deeper regions the amount of ammonia is insufficient for formation of aluminum hydroxide. It was shown by one of us [5] that in this case aluminum hydroxysulfate, which is sparingly soluble in water, is formed. Aluminum hydroxide is probably formed at the same time as the hydroxysulfate, so that mixed films of aluminum hydroxide and hydroxysulfate are obtained.

If a mixture of aluminum hydroxide and hydroxysulfate is prepared in bulk, when 70-75% of the equivalent amount of aqueous ammonia is added to aqueous aluminum sulfate with vigorous stirring, a precipitate consisting of a mixture of aluminum hydroxide and hydroxysulfate is formed. However, it differs from the films in having a much looser structure. The presence of aluminum hydroxysulfate in the films can be confirmed by the following experiment: if a film of aluminum hydroxide is washed free of SO_4 ions, converted into an aqueous suspension, and boiled for 10-15 minutes, and filtered, addition of barium chloride to the filtrate produces considerable turbidity. The turbidity indicates that barium sulfate is formed. Evidently when the suspension is boiled, hydrolysis of aluminum hydroxysulfate takes place.

If ammonia is added to an aqueous suspension of the film at room temperature, the film is converted into thin, scarcely visible platelets which gradually disappear, and the liquid becomes opalescent.

Films treated with ammonia appear as globular particles in the electron microscope (Fig. 3). In such cases crystallization is considerably slower than with pure aluminum hydroxide made by the usual method, but more rapid than with films.

Electron-diffraction data indicate that crystallization of the particles begins about 4-5 weeks after preparation. The probable explanation of the low rate of crystallization in this case is that not all the aluminum hydroxysulfate is converted into hydroxide at room temperature.

A similar result is obtained if a mixture of aluminum hydroxide and hydroxysulfate is prepared in bulk.

Thus, if a mixture of aluminum hydroxide and hydroxysulfate is prepared from aluminum sulfate in bulk, or if mixed films of aluminum hydroxide and hydroxysulfate are treated with ammonia, crystallization begins 4-5 weeks after preparation. If, on the other hand, films of aluminum hydroxide and hydroxysulfate are prepared by the method described above, crystallization does not begin until 5-6 months have elapsed. The explanation is that a mixture of aluminum hydroxide and hydroxysulfate prepared by the film method has considerably greater density than a similar mixture prepared in bulk. Therefore, because of steric conditions, crystallization in films is slow.

Films made from dilute (1-3%) aluminum sulfate solutions consist of globules joined into chains and small clusters with large gaps between them (Fig. 2,2).

In films made from concentrated (20-30%) solutions the globules are packed more closely (Fig. 2,3).

The microphotographs show that the globular particles which constitute the films vary in density; some are darker and others lighter. This shows that the globular particles comprise mixtures of at least two substances differing in density. The presence of a mixture of substances is also confirmed by the fact that crystallization processes in the films are exceedingly slow.

Whereas in pure aluminum hydroxide crystallization begins 1-2 days after preparation [4], aluminum hydroxide in film form remained amorphous after 4-4.5 months (Fig. 2,5).

Apart from aluminum hydroxide, the films can contain only aluminum hydroxysulfate, the solubility of which in water is very low. During preparation of the films formation

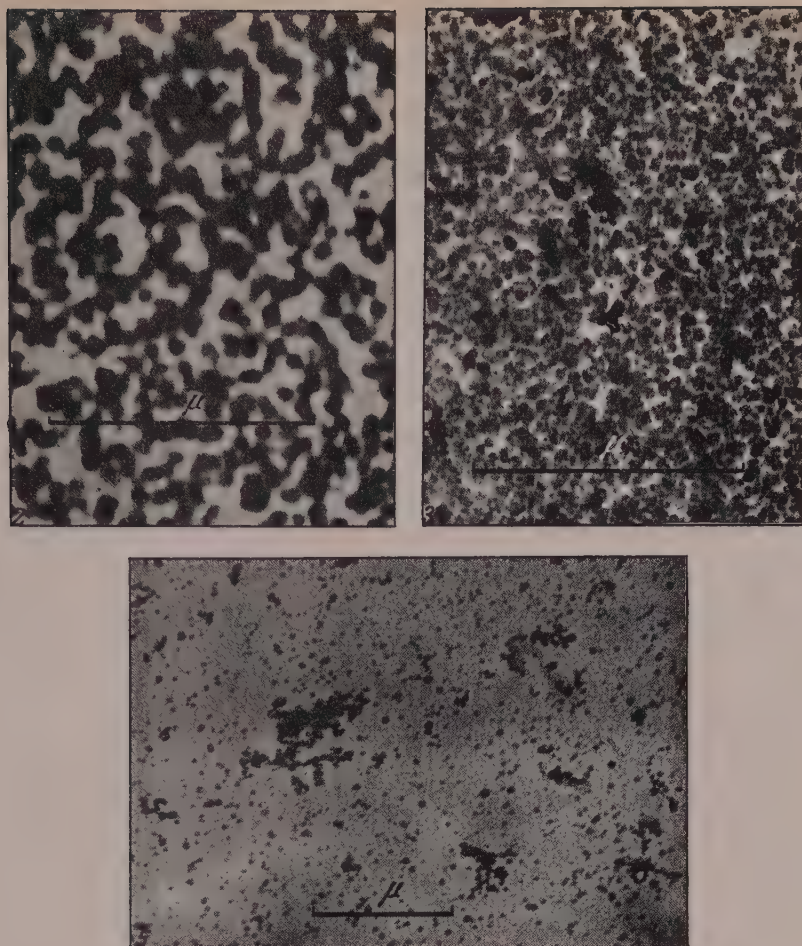


Fig. 2. Microphotographs (2, 3, 5): 2) of films made from dilute (1-3%) aluminum sulfate solution; 3) same, from concentrated (20-30%) solution; 5) aluminum hydroxide made by dissolution of the films in ammonia.

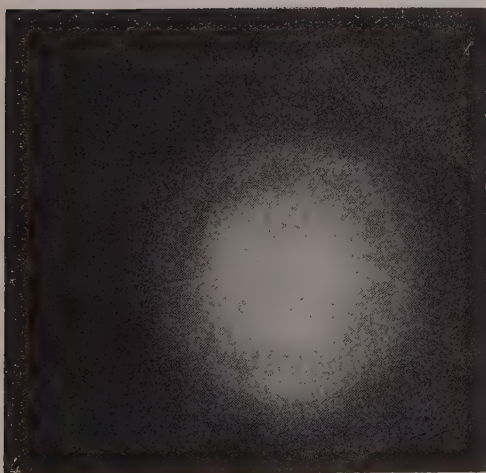


Fig. 3. Electron diffraction pattern (4) of a film made from aluminum sulfate solution.

A mixture of aluminum hydroxide and hydroxysulfate, prepared either in bulk or by the film method, may be used as emulsifier in preparation of oil - water emulsions. However, it is better to use a mixture of aluminum hydroxide and hydroxysulfate prepared in film form, as a denser precipitate, which can be washed free from salts much more easily and rapidly, is obtained in this way.

SUMMARY

1. A method has been worked out for preparation of mixed films of aluminum hydroxide and hydroxysulfate, which stabilize oil - water emulsions.

2. It was shown by electron microscopy and electron diffraction that the freshly-prepared films consist of globular particles grouped in chains. Crystallization in films occurs 5-6 months after preparation.

LITERATURE CITED

- [1] S. G. Mokrushin, Zhur. Fiz. Khim. 5, 1082 (1934).
- [2] M. Faraday, Phil. Trans. 147, 154 (1857).
- [3] N. G. Koltashev, Kolloid. Zhur. 7, 23 (1941).
- [4] Z. Ya. Berestneva, G. A. Koretskaya, and V. A. Kargin, Kolloid. Zhur. 13, 323 (1951). *
- [5] V. A. Kargin, M. E. Shishniashvili, and A. L. Batsanadze, Zhur. Fiz. Khim. 21, 391 (1947).

Received March 21, 1959

* Original Russian pagination. See C. B. Translation.

ANALYSIS OF THE FORMS OF BONDING OF WATER BY CLAYS AND SOILS BY MEANS OF DRYING THERMOGRAMS

M. F. Kazanskii

The A. M. Gor'kii Pedagogic Institute, Kiev, Laboratory of Molecular Physics

Our earlier investigations demonstrated that the forms of bonding of water by artificial adsorbents (silica gels and activated carbon) [1, 2] and certain natural sorbents (Pobiyankov and Pyzh bentonites) [3] can be analyzed by studies of their drying kinetics with the aid of drying thermograms and weight-loss curves obtained by means of a simultaneous recording apparatus [3].

This paper contains the results of a study of the hydrophilic properties of clays containing different minerals, and of certain types of soils. The materials chosen for the investigation comprised five clays: Zhabye, Pobiyankov, and Pyzh bentonites, containing up to 99% montmorillonite, Chasov Yar clay, containing 90.5% monothermite, and a kaolin polymineral clay from Poltava [4]. Four soils were also investigated: a turfy weakly podzolized gley soil of a sandy loam composition, a chernozem meadow solonetz soil, thick low-humus chernozem of a dusty moderate loam composition, and a turfy weakly podzolized soil of a sandy light loam composition.

The clay samples were kindly supplied by the Laboratory of Clay Minerals of the Institute of General and Inorganic Chemistry, Academy of Sciences Ukrainian SSR, where their physicochemical and colloidophysical properties have been studied for a number of years [4]. The soils are typical samples of soils from the Rzhishchev region of the Kiev province of the Ukrainian SSR; the soils were analyzed and classified by type in the Department of Pedology of the Kiev Pedagogic Institute.

In accordance with the method described earlier [3] for analysis of the forms of bonding of moisture by adsorbents, thin (not greater than 1 mm thick) samples of the clays and soils were first humidified to their total moisture capacity and then dried; the temperature of the surrounding air was constant in each experiment but differed in different experiments. The drying-kinetics curves — thermograms and drying curves — were recorded automatically during the drying.

Typical thermograms and drying curves of the clays and soils are given in Fig. 1-3. Each thermogram is recorded in terms of the temperature difference between the dried sample and the surrounding air. It therefore indicates how much lower the temperature of the dried sample is below the constant temperature of the surrounding air at any given instant.

It is clear from Fig. 1-3 that, regardless of the temperature, the drying thermograms of clays and soils retain the general form typical for drying thermograms of colloidal capillary-porous bodies [5]. In each thermogram three critical points may be distinguished; these divide the thermogram and therefore the whole drying period of a clay or soil into four regions.

The first region, which is the initial horizontal portion of the thermogram and ends at the first critical point *b*, corresponds to the period of drying at constant temperature of the drying sample. During this period capillary-porous bodies lose osmotic moisture which evaporates from their water-saturated surfaces [5, 6]. On the drying curve this period is represented by a portion of linear rate of weight loss, indicating that drying proceeds at a constant rate.

The region of the thermogram beyond the first critical point is a convex curve terminating at the second critical point *c*, past which the thermogram passes into a sloping straight line. Beyond the third critical point

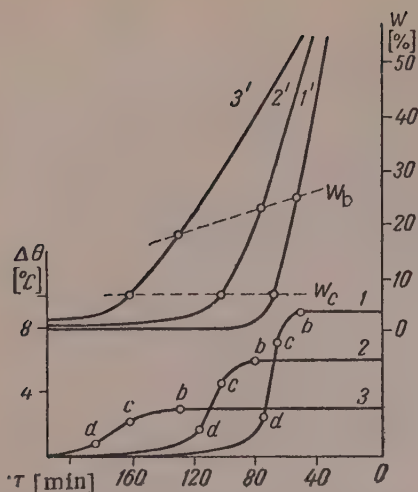


Fig. 1. Thermograms (1-3) and drying curves (1'-3') of Chasov Yar clay at temperatures: 1 and 1') 71.0°; 2 and 2') 61.2°; 3 and 3') 35.0°.

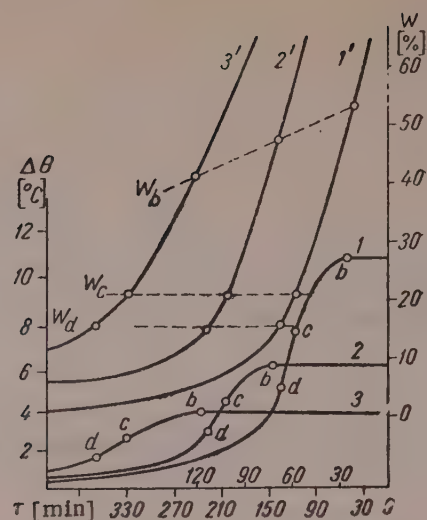


Fig. 2. Thermograms (1-3) and drying curves (1'-3') of Pobiyankov bentonite at temperatures: 1 and 1') 81.0°; 2 and 2') 54.0°; 3 and 3') 40.2°.

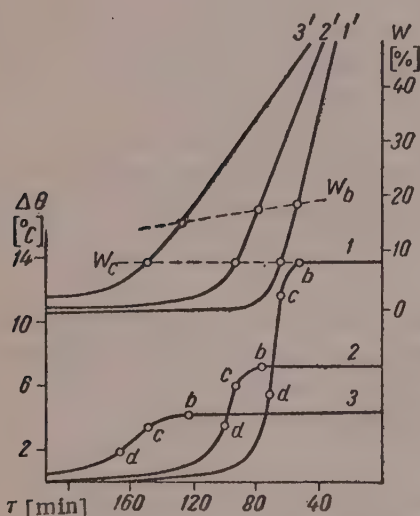


Fig. 3. Thermograms (1-3) and drying curves (1'-3') of turfey gley soil at temperatures: 1 and 1') 98.0°; 2 and 2') 61.5°; 3 and 3') 41.0°.

the thermogram becomes a concave curve. In accordance with the theory of drying [6] and experimental data [5], when thin samples of colloidal capillary-porous bodies are dried, hygroscopic moisture is removed, starting from the first critical point b , at a relative water-vapor pressure less than unity in the surrounding air. The convex portion of the thermogram, between the first and second critical points, corresponds to removal of capillary moisture from pores less than 10^{-5} cm in radius. Between the second and third critical points loosely-bound moisture adsorbed in the multimolecular layers is removed, and then, past the third critical point, moisture which is most firmly bound to the solid phase in clays and soils is removed — adsorbed moisture from the monomolecular layers.

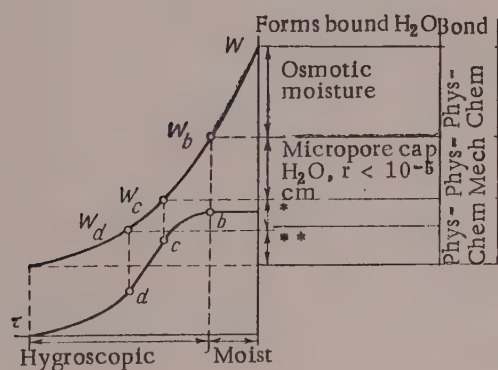
The schematic diagram in Fig. 4 represents the different stages in the drying of thin samples of colloidal capillary-porous bodies in relation to different forms and bonding types of the water removed. By projection of each critical point on the thermogram onto the drying curve recorded simultaneously during the same experiment it is possible to determine the amount of water of a particular bonding type.

This schematic representation of stages in the drying process is satisfactorily confirmed by comparison of the moisture contents of clays and soils found from the values of the critical points and by other independent methods (see table), and by the general kinetics of heat and mass transfer during drying of colloidal capillary-porous bodies [6].

The suggested method of analysis of the forms of bonding of water was used for determining the influence of temperature on the hydrophilic properties of clays and soils. For this, the moisture contents and temperatures of all the clay and soil samples were determined at the second critical point on the thermograms (recorded at

Differential Moisture Contents of the Investigated Clays and Soils (as % of the dry substance at 20-25°)

Material studied	Hygroscopic moisture, %		Adsorbed moisture, from results of determinations by different methods, %						
	from adsorption isotherms	from point b in thermogram	from heat of wetting	by indicator method	from the dielectric constant	hygroscopic point [4]	mean value	from point c in thermogram	from point d in thermogram
Clays									
Zhabye bentonite	41.4	42.5	22.7	—	—	19.7	21.2	21.9	14.9
Pyzl bentonite	28.8	31.0	20.1	20.7	—	19.2	20.0	21.4	14.0
Pobiyankov bentonite	30.1	31.5	21.0	—	—	18.0	19.5	21.6	14.5
Chasov Yar clay	16.0	14.8	5.4-7.0	7.1	6.7	6.5	6.4	6.8	3.5
Poltava clay	17.1	18.0	6.0	6.8	6.5	7.0	6.6	6.0	3.8
Soils									
Turfy gley	13.5	13.0	—	8.4-10.0	—	9.1-7.5	8.7	8.0	5.0
Meadow chernozem	8.9	10.7	—	7.3-7.5	—	5.4-5.0	6.3	5.8	3.8
Thick chernozem	6.8	8.7	—	5.8-6.1	—	4.5-3.4	4.9	5.2	2.8
Turfy, weakly podzolic	6.0	7.0	—	3.7-4.7	—	3.5-2.6	3.6	3.3	1.8



- * Moisture of multimolecular adsorption.
- ** Moisture of monomolecular adsorption.

Fig. 4. Line diagram representing kinetics of consecutive removal of moisture of different forms and bonding types during drying of thin samples of colloidal capillary-porous bodies.

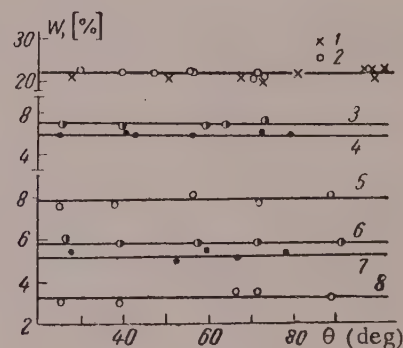


Fig. 5. Amounts of water held by adsorption by clays and soils at different temperatures: 1) Pobiyankov bentonite; 2) Pyzh bentonite; 3) Chasov Yar clay; 4) Poltava clay; 5) turfey gley soil; 6) chernozem meadow soil; 7) thick chernozem; 8) turfey weakly podzolic soil.

different drying temperatures). Naturally, the higher the temperature of drying the higher was the temperature of the drying sample at the given critical point.

The moisture contents of the samples were determined from the drying curves, and the temperatures were found from the thermograms and the temperatures of the surrounding air. These data were used to plot Fig. 5,

which shows the effect of the temperature of the drying samples on the moisture contents of clays and soils at the critical point of the thermogram. Since the moisture content at the critical point is equal to the total amount of moisture held by adsorption, this graph also shows how the hydrophilic property of the clays and soils depends on the temperature. The total amount of moisture held by adsorption in clays and soils remains constant over the 25-100° temperature range. This is in good agreement with the results of Ovcharenko's experiments [4] which showed that the heats of wetting of the clays used are also independent of the temperature.

SUMMARY

1. Curves of drying kinetics (thermograms and drying curves for thin samples) were used to analyze the water-holding properties of clays and soils in relation to different forms of moisture.
2. The results obtained by this method agree, within the limits of experimental error, with results given by other mutually independent methods.
3. Analysis of drying thermograms for different temperatures of the surrounding air showed that the total amount of moisture adsorbed by clays and soils is independent of their temperature.

LITERATURE CITED

- [1] M. F. Kazanskii, *Kolloid. Zhur.* 19, 663 (1957).*
- [2] M. F. Kazanskii, *Coll. MTIPP: Heat and Mass Transfer in Capillary-Porous Bodies* [in Russian] (State Power Press, 1957) 8, 180.
- [3] M. F. Kazanskii, in the book: *Bentonite Clays of the Ukraine* [in Russian] (Academy of Sciences Ukrainian SSR Press, 1957) 2, 76.
- [4] F. D. Ovcharenko, *Dissertation: The Hydrophilic Nature of Clays* [in Russian] (Kiev, 1955).
- [5] M. F. Kazanskii, *Naukovi Zapiski* 25, fizika (Kiev Pedagogic Inst. 1957) p. 37.
- [6] A. V. Lykov, *Theory of Drying* [in Russian] (State Power Press, 1957).
- [7] O. F. Miglyachenko, *Naukovi Zapiski* 25, fizika (Kiev Pedagogic Inst. 1957) p. 42.
- [8] V. P. Dushchenko, *Dissertation: Investigation of the Physical Meaning of the Critical Points on Drying-Rate Curves of Colloidal Capillary-Porous Substances* [in Russian] (Kiev, 1952).

Received March 12, 1958

* Original Russian pagination. See C. B. Translation.

INFRARED ABSORPTION SPECTRA AND STRUCTURE OF THE HYDROXYL LAYERS ON SILICAS OF DIFFERENT DEGREES OF HYDRATION

A. V. Kiselev and V. I. Lygin

The M. V. Lomonosov University, Moscow, Faculty of Chemistry, Adsorption Laboratory

A knowledge of the characteristics of chemical surface structure of many highly-disperse substances, including silicas, is needed for understanding of their adsorption and catalytic properties and for regulated chemical modification of their surfaces.

A series of researches in our laboratory and also carried out by S. P. Zhdanov demonstrated the considerable influence of the degree of dehydration of silica surfaces on their adsorption properties, not only in relation to polar substances containing hydroxyl groups [1-8], but also to aromatic and unsaturated hydrocarbons [4, 5, 8-14] and nitrogen [15], the molecules of which are nonpolar as a whole but have sharply nonuniform charge distribution [14]. Studies of these effects by adsorption methods only are not sufficient; they must be augmented by investigations of isotope exchange, spectroscopy, and studies of nuclear magnetic resonance. Such multiple approach to studies of the chemistry of surfaces is important in relation to chemical modification of adsorbent and catalyst surfaces [16, 17].

It is known that silica gel which has been dried and heated under vacuum at temperatures up to 150-200° contains up to 5-6% of chemically bound hydroxyl groups [18, 19]. The existence of surface hydroxyl groups has also been detected spectroscopically [20]. The spectra of porous glass [21-25], silica gel [26], aerogel [27], and Aerosil [28] indicate the presence of hydroxyl groups, the absorption band for the valence oscillations of which is shifted slightly relatively to the absorption band for water vapor. The narrowness of the absorption band and its shift under the influence of even weakly-adsorbed substances [20, 28, 29] led to the conclusion that the hydroxyl groups, isolated from each other, are "freely" disposed over the surface of the silicon-oxygen skeleton [21, 22, 28]. However, this conclusion refers to specimens the hydroxyl coating of which has been considerably impoverished as the result of vacuum treatment at 450-500° [22-27], or because of the method used for preparation of the silica [28]. None of the spectroscopic publications contain any information on the surface concentration of the hydroxyl groups and the adsorption properties of the specimens, and the question of the state of the hydroxyl groups on the surface is answered on the basis of studies of their valence oscillations only. It is therefore of interest to study the infrared spectra of silicas with known surface hydroxyl concentrations, and to correlate the results with the adsorption properties.

Silica gel KSK-2, studied previously by adsorption methods [6, 8, 11], was taken for this investigation. The structural characteristics and degree of surface hydration of this silica gel, as found in the earlier studies, are presented in Table 1.

For the spectroscopic studies the silica gel was prepared in the form of a fine powder by sedimentation from an aqueous medium. A thin layer of the powder was spread uniformly between two NaCl plates and placed in a vacuum optical cell, similar to that described earlier [22], consisting of a sealed glass tube with NaCl windows attached by means of shellac adhesive. For heat treatment of the specimen the cell was connected to vacuum and the specimen was moved to its sealed end. For determination of the spectrum the specimen was moved to the end of the cell with windows, the cell was disconnected from the vacuum source, and fixed in front

TABLE 1

Structural Characteristics and Degree of Hydration of Silica Gel Surface

Evacuation temperature, (°C)	Pore diameter, A	Specific surface, m ² /g	Surface hydroxyl groups, $\mu\text{moles/m}^2$	Average distance between hydroxyls, A
200	105	340	10.8	~4
400	105	340	7	~5

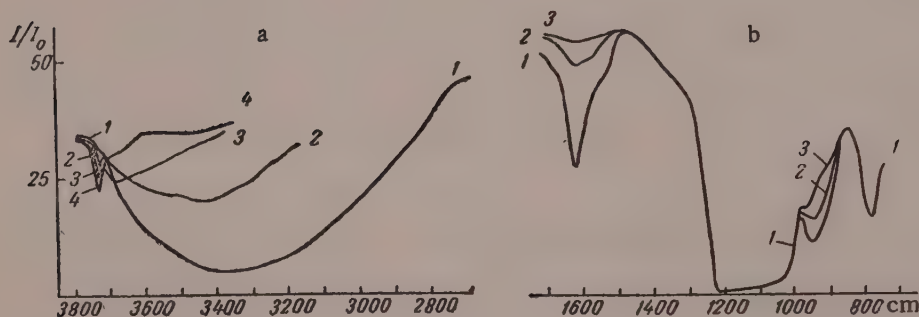


Fig. 1. Infrared absorption spectra of silica gel with surface OH groups, after adsorption of water at $p/p_s \approx 0.6$ (1), and after evacuation for 4 hours at 20° (2), at 200° (3), and at 300°, (4): a) with LiF prism; b) with NaCl prism.

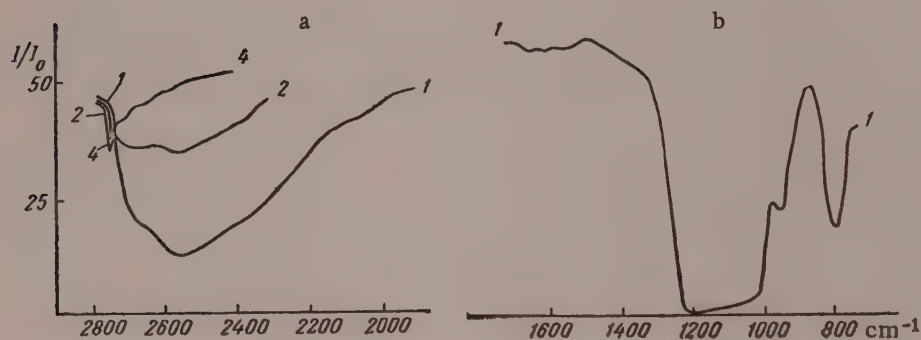


Fig. 2. Infrared absorption spectra of silica gel containing surface OD groups, after adsorption of D₂O at $p/p_s \approx 0.6$ (1); after evacuation for 4 hours at 20° (2); at 300° (4): a) with LiF prism; b) with NaCl prism.

of the spectrometer slit. The specimens were evacuated for four hours at 10^{-5} mm pressure in the cell, water vapor being frozen out by liquid nitrogen*.

The surface was deuterated by repeated filling of the cell with D₂O vapor and evacuation at 300°. The degree of substitution of OH by OD was estimated spectroscopically. Single-beam infrared spectrometers, type IKS-11 and IKS-12, with LiF prisms for the 3800-1800 cm⁻¹ region and NaCl prisms for the 1800-700 cm⁻¹ region

* Heat treatment above 300° was not possible with the use of NaCl plates for fixing the silica gel powder, because appreciable evaporation of NaCl begins at 350°.

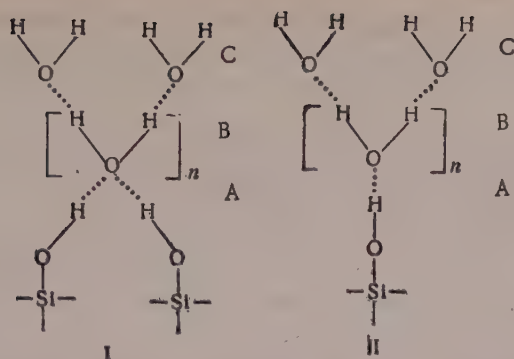


Fig. 3. Adsorption of water on surface hydroxyl groups of silica gel: I) bond with two OH groups; II) bond with one OH group; A) surface groups of silica gel, B) complex of n associated molecules of adsorbed water; C) end molecules of this complex.

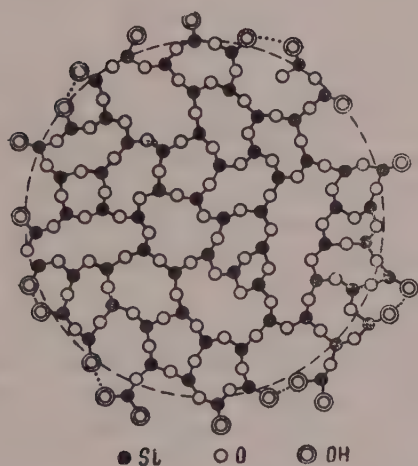


Fig. 4. Schematic structure of a globule of silica gel (free from adsorbed water molecules) with a surface layer of free and associated (joined by a dash line) hydroxyl groups.

As in the case of the deuterium exchange studied earlier [22, 23], threefold treatment with D_2O vapor with subsequent evacuation at 300° eliminates absorption in the region of valence oscillations of the OH groups (3749 cm^{-1}) and leads to the appearance of a band at 2761 cm^{-1} corresponding to valence oscillations of OD groups (Fig. 2,a). Changes in the spectrum of valence oscillations of hydroxyl groups in deuterated silica gel are of the same nature as in the original silica gel. The spectrum of deuterated silica gel after adsorption of D_2O vapor at $p/p_s = 0.6$ has a broad band with a maximum at $\sim 2550\text{ cm}^{-1}$ (Fig. 2,a, curve 1). Evacuation at 20° diminishes absorption considerably and leaves two broad overlapping bands at 2550 and 2660 cm^{-1} (Fig. 2,a, curve 2). A narrow band appears simultaneously at 2761 cm^{-1} . The spectrum of valence oscillations of deuterated silica gel treated in vacuum at 300° (Fig. 2,a, curve 4) contains only an intense narrow band at 2761 cm^{-1} with asymmetric absorption in the long-wave direction.

The spectra of the original (Fig. 1,b, curve 1) and deuterated (Fig. 2,b, curve 1) specimens also contain a broad band at $1000\text{--}1200\text{ cm}^{-1}$ and a band at 785 cm^{-1} , observed in the spectra of quartz and ascribed to oscillations of the silicon-oxygen framework [30]. The absorption band of deformation oscillations of D_2O

were used. To prevent absorption of atmospheric moisture, nitrogen dried by phosphorus pentoxide was blown through the jacket of the monochromator and lamp. Powdered silica gel strongly scatters infrared radiation, so that transmission in the 3700 cm^{-1} region was less than 30%.

Figures 1 and 2 show the absorption spectra of the original and deuterated silica gel after different vacuum treatments.

A broad absorption band with a maximum at $\sim 3400\text{ cm}^{-1}$ is found in the region of valence oscillations of hydroxyl groups of the spectrum of the original silica gel which adsorbed water at $p/p_s \approx 0.6$ (Fig. 1,a, curve 1). Vacuum treatment at 20° for one hour results in a considerable decrease of absorption in the long-wave region on the band and in the appearance of a narrow band at 3749 cm^{-1} (Fig. 1,a, curve 2). Vacuum treatment at 200° increases the intensity of the 3749 cm^{-1} band and leads to the appearance of a band with a maximum at $\sim 3660\text{ cm}^{-1}$ (Fig. 1,a, curve 3). A narrow band at 3749 cm^{-1} with asymmetric absorption in the long-wave direction remains in the spectrum of silica gel treated under vacuum at 300° (Fig. 1,a, curve 4).

An intensive band with a maximum at 1640 cm^{-1} (Fig. 1,b, curve 1) is observed in the region of deformation oscillations of the hydroxyl groups in the spectrum of silica gel after adsorption of water at $p/p_s \approx 0.6$. After vacuum treatment at 20° the intensity of this band decreases considerably (Fig. 1,b, curve 2). After vacuum treatment at 200° only traces of absorption remain in this region (Fig. 1,b, curve 3).

Vacuum treatment of silica gel produces considerable changes in the $900\text{--}1000\text{ cm}^{-1}$ region. The diffuse band at 950 cm^{-1} observed in the spectrum of silica gel which adsorbed water at $p/p_s \approx 0.6$ diminishes in intensity after vacuum treatment at 20° and 200° , and the absorption maximum is shifted to 970 cm^{-1} (Fig. 1,b, curves 1-3).

TABLE 2

Characteristics of OH and OD Groups

Type of surface group	ν , cm^{-1}	2ν , cm^{-1} * [22]	ω	x
Si - OH	3749	7325	3921	0.022
Si - OD	2761	5431	2852	0.016

molecules and structural hydroxyl groups of silica gel in surface complexes of types I and II (Fig. 3). In the spectrum of silica gel which adsorbed water at high p/p_s , absorption is due mainly to hydroxyl groups of water molecules (Fig. 3) linked by hydrogen bonds and giving a broad band with a maximum at 3400 cm^{-1} . Evacuation at 20° removes most of the adsorbed water. If the evacuation is not too prolonged, structural hydroxyl groups of type A and a part of the water molecules adsorbed on the hydroxyl groups remain on the surface (Fig. 3). The appearance of a distinct band due to free OH groups at 3749 cm^{-1} (Fig. 1,a, curve 2) and at 2761 cm^{-1} (Fig. 2,a, curve 2) in the spectrum of silica gel evacuated at 20° apparently indicates that adsorbed water has been removed from most of the surface hydroxyl groups on the silica gel. Evacuation at 200 and 300° leads to liberation of even more surface hydroxyl groups. However, some residual absorption can still be observed in direct proximity to the narrow band due to free hydroxyls in the spectrum of silica gel treated at 200 and 300° (Fig. 1,a, curves 3 and 4, and Fig. 2,a, curve 4).

It was also reported earlier [21] that increase of the treatment temperature of porous glass leads not only to a change of intensity but also to narrowing of the absorption band due to valence oscillations of hydroxyl groups in the region of higher harmonics. In the fundamental region of the spectrum of valence oscillations of the hydroxyl groups, absorption was observed in the 3660 cm^{-1} region in addition to a narrow absorption band at 3749 cm^{-1} even after evacuation at 450° [23]. The diffuse character of the absorption band for valence oscillations of hydroxyl groups in porous glass at moderate temperatures of vacuum treatment (up to 300°) was observed in more distinct form in another investigation [32].

It must be emphasized that this absorption in the long-wave region of the spectrum of valence oscillations of hydroxyl groups in silicas treated under vacuum at temperatures above 200° cannot be attributed to absorption by water molecules remaining on the surface, since thermal analysis [33, 34], data on heats of wetting [18], and dehydration kinetics [7] all indicate that adsorbed water is removed below 200° . The almost total absence of absorption in the region of deformation oscillations of hydroxyl groups of adsorbed water on silica gel evacuated at 200° (Fig. 1,b, curve 3) also indicates that adsorbed water is completely removed.

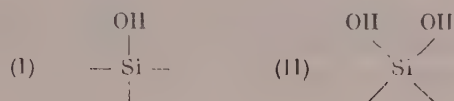
The observed form and position of the absorption band may help to reveal the structural characteristics of the hydroxyl layer on silicas, since the position of the band depends on the geometrical arrangement and mutual interaction of the hydroxyl groups [35]. To interpret the observed spectral data it is necessary to know the concentration of hydroxyl groups on the silicas and their geometrical arrangement on the surface. Whereas quantitative data on the average concentration of surface hydroxyl groups may be obtained from the loss of weight on calcination or from data on deuterium exchange, the local distribution of the hydroxyl groups over the surface remains uncertain in most cases. Because of the amorphous character of the investigated silicas the structure of the hydroxyl layer is determined by the disordered packing of the silicon - oxygen tetrahedrons and therefore to a considerable extent by the random orientation of the corners and edges of the surface silicon - oxygen tetrahedrons carrying the hydroxyl groups. Table 1 shows that the average distance between hydroxyl groups in hydrated silica gel is $\sim 4\text{ \AA}$. The disordered distribution leads to appearance of hydroxyl groups at shorter distances apart, which may be $< 3\text{ \AA}$. Analysis of possible bond ruptures on the cleavage planes of quartz [36] also indicates that such closely adjacent hydroxyl groups exist in the surface layer. Numerous examples are known of formation of hydrogen bonds and the consequent shift of the absorption bands of hydroxyl groups at distances of $< 3\text{ \AA}$ apart [35, 37]. Intramolecular hydrogen bonds may be formed between neighboring hydroxyls of the same molecule if these hydroxyls are suitably oriented and are at a distance favorable for bond formation [38].

molecules at $\sim 1220\text{ cm}^{-1}$ [31] in the spectrum of deuterated silica gel is superposed on the broad absorption band of the silicon - oxygen framework at $1000\text{--}1200\text{ cm}^{-1}$ and does not appear in the spectrum (Fig. 2,b, curve 1). The 950 cm^{-1} absorption band in the spectrum of deuterated silica gel (Fig. 2,b, curve 1) does not differ significantly from the corresponding band for the original silica gel (Fig. 1,b, curve 1).

The absorption bands due to OH and OD valence vibrations seen in Fig. 1,a and 2,a (curve 1) are the result of absorption by disturbed hydroxyl groups of water

On these grounds, and in accordance with Terenin's interpretation [20], we attributed the narrow bands observed in the spectra of valence oscillations of hydroxyl groups (in silicas which are still fully hydrated but already devoid of adsorbed water) to hydroxyl groups which are fairly far apart and do not interact with each other [24, 13].

In our opinion, absorption in the longer-wave region of the spectrum of valence oscillations of structural hydroxyl groups is due to hydroxyl groups in close proximity, which influence each other [24, 25]. The observed shift of absorption due to interaction of surface hydroxyl groups ($\sim 100 \text{ cm}^{-1}$) is not large in comparison with the shift caused by hydrogen bonding in liquid (325 cm^{-1}) [39] or solid (450 cm^{-1}) [40] silanols. This indicates that the mutual influence of some of the hydroxyl groups is weaker than in the formation of strong hydrogen bonds; this suggests rather the formation of intramolecular hydrogen bonds similar to the intramolecular bonds in hydroxylic organic compounds [38]. The formation of stable hydrogen bonds is evidently prevented by the rigid surface orientation of the hydroxyl groups and by the fact that on the average they are fairly far apart. The scheme below



represents the most probable hydroxyl groupings (I) and (II) on the surface of strongly-hydrated silica [4, 13]. It seems that interaction occurs between hydroxyls of type (II) groupings and between neighboring hydroxyls of type (I) and (II) groupings, since the spatial orientation of these hydroxyls is the most favorable for this. On the surfaces of silica gel globules, observed in the electron microscope [41] and represented schematically in Fig. 4, various combinations of these groupings can probably arise, with formation of intramolecular hydrogen bonds between some of their hydroxyls.

It is believed that a shift of the absorption band of hydroxyl groups into the short-wave region is evidence of bond weakening [42]. It is natural to suppose that dehydration is accompanied in the first instance by joining of such closely-situated hydroxyl groups of type (II) and (I) + (II), so that scattered and more uniformly distributed hydroxyl groups of type (I) will in the main be left on the surface. This form of dehydration corresponds to the observed decrease of absorption in the long-wave region, so that the spectra of silicas treated in vacuum above 200° retain only a narrow absorption band due to these "free" hydroxyl groups. The presence of groups of type (I) only on the surface of silica after heat treatment has been reported elsewhere [19]. Table 1 shows that the average distance between the hydroxyl groups increases with increase of the temperature of vacuum treatment, and becomes $>5\text{\AA}$, even at 400° ; this is considerably greater than the distance favorable for hydrogen bonding.

The concept of "free" hydroxyl groups as anharmonic oscillators [20] is useful for interpretation of the spectral characteristics caused by interaction of surface hydroxyl groups with adsorbed molecules. The oscillation frequency (ω) and anharmonicity coefficient (x) of such oscillators may be calculated in accordance with the classical theory [43] from the fundamental oscillation frequencies ν of the hydroxyl group (0 - 1 transition) and its 2ν harmonic (0 - 2 transition) (Table 2).

The frequency ratio found from the reduced masses (μ) of the oscillators $\frac{\omega_{\text{OH}}}{\omega_{\text{OD}}} = \sqrt{\frac{\mu_{\text{OD}}}{\mu_{\text{OH}}}} = 1,374$ is very close to the value found from the data in Table 2 (1.375).

Conclusions as to the structure of the hydroxyl layer are usually based on analysis of the absorption band for valence oscillations of hydroxyl groups. Additional information on the state of surface hydroxyl groups may be expected from investigation of other oscillations in which these groups take part. Attention should be drawn to the absorption bands in the $900\text{--}1000 \text{ cm}^{-1}$ region, observed in the spectra of the original and deuterated silica gels (Fig. 1 and 2) and sensitive to the degree of surface hydration. These bands are usually attributed to hydroxyl groups in silicas [30]. It is not possible as yet to assign the absorption bands in this region to any definite type of oscillation. It is possible that they are due to deformation oscillations of surface hydroxyl groups. The possibility is not excluded that these bands may be assigned to oscillations of the whole hydroxyl group relative to the silicon atom. It is to be hoped that further investigations will provide new information on the interaction

of surface hydroxyl groups both with each other and with adsorbed molecules, since it is known that analogous bands in the spectra of organosilicon compounds containing hydroxyl groups are sensitive to the degree of association [44].

The surface layer of hydroxyl groups, rigidly bound to the silicon - oxygen framework, is exceptionally suitable for spectroscopic studies of hydrogen bonding between these groups and molecules capable of forming hydrogen bonds. Spectroscopic investigation of interaction between water molecules and the silica surface is of the greatest significance for elucidation of the mechanism of formation of the hydroxyl layer and of the adsorption mechanism. Strongly dehydrated silicas were used in the reported spectroscopic investigations [22, 23]. Water is attached to such materials by chemisorption [1-8, 19] with regeneration of the hydroxyl layer, favoring further physical sorption of water, which proceeds by at least two mechanisms (see Fig. 3) with subsequent growth of surface complexes from molecules held together by hydrogen bonds. As a result, the spectra of silicas with hydrated surfaces after physical sorption of water should show absorption bands both for surface structural hydroxyl groups disturbed by interaction with each other and with adsorbed water molecules (type A, Fig. 3) and for disturbed hydroxyl groups of the adsorbed water molecules themselves (types B and C, Fig. 3). Interpretation of this spectroscopic picture is difficult, and can be achieved only with the aid of parallel investigation of activated and physical adsorption of water, the differential heats of these processes, enthalpies and entropies of the complexes formed, and their other physical properties.

In further investigations of the hydroxyl layer on silicas by the spectroscopic method we hope to photograph under vacuum the spectra of samples with known and gradually changing concentrations of surface hydroxyl groups, with subsequent addition of water attached by chemisorption and physical sorption and evaluation of the number of molecules held by physical adsorption per one hydroxyl group of the surface. For clarification of the characteristics of activated and physical adsorption of water it is very necessary to study changes both in the absorption bands due to valence oscillations of the hydroxyl groups and in the absorption bands due to deformation oscillations of hydroxyl groups of adsorbed water and surface hydroxyl groups in the silicas.

SUMMARY

1. The infrared absorption spectra of original and deuterated silica gels with different known degrees of surface hydration were studied in the regions of valence and deformation oscillations of OH and OD groups.
2. The spectra corresponding to valence oscillations of the hydroxyl groups of silica gel with a fully hydrated surface indicate the formation of intramolecular hydrogen bonds between some of the hydroxyl groups which are located closely enough together and are in suitable orientation.
3. The spectrum of substantially dehydrated silica gel contains, in the main, a narrow absorption band corresponding to "free" hydroxyl groups which are less numerous and more uniformly distributed over the surface.
4. In spectroscopic studies of interaction between water molecules and silica surfaces in addition to valence oscillations, it is also necessary to investigate deformation oscillations both due to hydroxyl groups of adsorbed water and to structural hydroxyl groups in the silica surfaces.

The authors thank A. N. Terenin and A. N. Sidorov for discussion of this work.

LITERATURE CITED

- [1] S. P. Zhdanov, *Doklady Akad. Nauk SSSR* **68**, 99 (1949).
- [2] S. P. Zhdanov, in the book: *Chemical Surface Compounds and Their Role in Adsorption Phenomena* [in Russian] (Izd. MGU, 1957) p. 129.
- [3] S. P. Zhdanov, *Doklady Akad. Nauk SSSR* **120**, 103 (1958)*; *Zhur. Fiz. Khim.* **32**, 699 (1958).
- [4] A. V. Kiselev, in the book: *Chemical Surface Compounds and Their Role in Adsorption Phenomena* [in Russian] (Izd. MGU, 1957) p. 90, 199.
- [5] A. V. Kiselev, K. G. Krasil'nikov, and L. N. Soboleva, *Doklady Akad. Nauk SSSR* **94**, 85 (1954).
- [6] L. D. Belyakova, O. M. Dzhigit, and A. V. Kiselev, *Zhur. Fiz. Khim.* **31**, 1577 (1957).

*Original Russian pagination. See C. B. Translation.

- [7] A. V. Kiselev and G. G. Muttik, *Kolloid Zhur.* 19, 562 (1957).
- [8] L. D. Belyakova and A. V. Kiselev, *Doklady Akad. Nauk SSSR* 119, 298 (1958)*; *Zhur. Fiz. Khim.* 33, 1534 (1959).
- [9] A. V. Kiselev, *Doklady Akad. Nauk SSSR* 106, 1046 (1956).
- [10] A. V. Kiselev, *Uspekhi Khim.* 25, 705 (1956).
- [11] A. A. Isrikyan and A. V. Kiselev, *Doklady Akad. Nauk SSSR* 115, 393 (1957)*.
- [12] A. V. Kiselev, *Proc. Second Intern. Congress on Surface Activity (London, 1957)* 2, 179.
- [13] A. V. Kiselev, in the book: *The Structure and Properties of Porous Materials (London, 1958)* p. 195.
- [14] A. V. Kiselev and D. P. Poshkus, *Doklady Akad. Nauk SSSR* 120, 834 (1958)*.
- [15] A. V. Kiselev and E. V. Khrapova, *Kolloid. Zhur.* 19, 572 (1957)*.
- [16] K. D. Shcherbakova and K. I. Slovetskaya, *Doklady Akad. Nauk SSSR* 111, 855 (1956).
- [17] A. V. Kiselev, N. V. Kovaleva, A. Ya. Korolev, and K. D. Shcherbakova, *Doklady Akad. Nauk SSSR* 124, 617 (1959)*.
- [18] A. V. Kiselev, *Kolloid Zhur.* 2, 17 (1936).
- [19] I. H. de Boer and I. M. Fleeskens, *Koninkl. nederl. Academie van wetenschappen Amsterdam. Ser.* 701, 1 (1958).
- [20] A. N. Terenin, in the book: *Chemical Surface Compounds and Their Role in Adsorption Phenomena [in Russian] (Izd. MGU, 1957)* pp 206, 271.
- [21] N. G. Yaroslavskii, *Zhur. Fiz. Khim.* 24, 68 (1950).
- [22] V. A. Nikitin, A. N. Sidorov, and A. V. Karyakin, *Zhur. Fiz. Khim.* 30, 117 (1956).
- [23] A. N. Sidorov, *Zhur. Fiz. Khim.* 30, 995 (1956).
- [24] A. V. Kiselev and V. I. Lygin, *Proc. Second Intern. Congress on Surface Activity (London, 1957)* 2, 204.
- [25] V. I. Lygin, *Vestnik Moskovskogo un-ta* 1, 223 (1958).
- [26] V. N. Filimonov, *Optika i Spektroskopiya* 1, 490 (1956).
- [27] L. N. Kurbatov and G. G. Neuimin, *Doklady Akad. Nauk SSSR* 68, 341 (1949).
- [28] R. S. McDonald, *J. Amer. Chem. Soc.* 79, 850 (1957).
- [29] A. N. Sidorov, *Doklady Akad. Nauk SSSR* 95, 1235 (1954).
- [30] V. A. Florinskaya and R. S. Pechenkina, in the book: *The Structure of Glass [in Russian] (Izd. AN SSSR, 1953)*; N. A. Savchenko and V. A. Florinskaya, *Optika i Spektroskopiya* 5, 23 (1958).
- [31] P. A. Gignere and K. B. Harvey, *Canad. J. Chem.* 34, 798 (1956).
- [32] D. J. C. Jates, N. Sheppard and C. L. Angel, *J. Chem. Phys.* 23, 1980 (1955).
- [33] E. A. Hauser and D. S. Le-Beau, *J. Phys. Chem.* 56, 136 (1952).
- [34] C. J. Yong, *J. Coll. Sci.* 13, 67 (1958).
- [35] E. Harter and O. Glemser, *Naturwiss.* 40, 19 (1953).
- [36] S. P. Zhdanov and A. V. Kiselev, *Zhur. Fiz. Khim.* 31, 2213 (1957).
- [37] R. E. Rundl and M. Parasol, *J. Chem. Phys.* 20, 1487 (1952); G. C. Pimentel and C. H. Sederholm, *J. Chem. Phys.* 24, 639 (1956).
- [38] L. P. Kuhn, *J. Amer. Chem. Soc.* 74, 2492 (1952).

*Original Russian pagination. See C. B. Translation.

- [39] V. I. Kasatochkin, M. F. Shostakovskii, O. I. Zil'ber, and L. A. Kochkin, *Izvestiya Akad. Nauk SSSR, ser. fiz.* 18, 726 (1954).
- [40] R. E. Richards and H. W. Thompson, *J. Chem. Soc.* 124 (1949).
- [41] A. V. Kiselev, V. I. Lygin, I. E. Niemark, I. B. Slinyakova, and Chen' Wen'-hang, *Kolloid Zhur.* 20, 52 (1958).*
- [42] M. I. Batuev, *Zhur. Fiz. Khim.* 23, 1405 (1949).
- [43] G. Herzberg, *Spectra and Structure of Diatomic Molecules* [Russian translation] (IL, 1949) p. 73; C. Cabannes-Ott, *Compt. rend.* 242, 355 (1956).
- [44] Ya. I. Ryskin and M. G. Voronkov, *Zhur. Fiz. Khim.* 30, 2275 (1956); Ya. I. Ryskin, *Optika i Spektroskopiya* 4, 532 (1958).

Received August 23, 1958

*Original Russian pagination. See C. B. Translation.

ISOTHERMS OF ADSORPTION OF BENZENE AND *n*-HEXANE VAPORS ON MAGNESIUM OXIDE

A. V. Kiselev and D. P. Poshkus

The M. V. Lomonosov University, Moscow, Faculty of Chemistry, Adsorption Laboratory;
The Institute of Physical Chemistry, Academy of Sciences USSR, Laboratory of Sorption
Processes

The preceding communications [1-3] dealt with the geometric structure of magnesium oxide samples prepared from uniformly coarse-pored magnesium hydroxide by vacuum heat treatment at different temperatures. Further publications [4, 5] contained calculations of the energy of adsorption of hydrocarbons on the (100) face of magnesium oxide and the heats of adsorption for one of these samples were calculated. The present paper contains the results of a study of the isotherms for adsorption of benzene and *n*-hexane vapors in the initial region on these magnesium oxide samples and on a sample prepared by thermal decomposition of magnesium carbonate. In the subsequent investigation the corresponding results were obtained for magnesium hydroxide.

Comparison of the adsorption of benzene and hexane is interesting because these hydrocarbons, which contain equal numbers of carbon atoms in their respective molecules, are adsorbed quite reversibly but differently owing to specific features of their structures. In the case of adsorption due to dispersional forces only (on graphite) the adsorption and heat of adsorption of hexane are greater than those of benzene [5-7], whereas in the case of silica gel with a hydrated surface the adsorption and heat of adsorption of benzene are greater than those of hexane, and dehydration of the silica gel surface lowers these values sharply for benzene but has only a slight effect for hexane [3, 8, 9]. Decrease of the heat of adsorption of benzene on dehydration of the silica gel surface is mainly due to a decrease in the energy of the Coulomb forces of interaction between the benzene molecule and the electric field of the silica gel surface, due mainly to the hydroxyl groups of the latter [10]. Theoretical and experimental studies of the adsorption of these hydrocarbons on different oxides and hydroxides are therefore of great interest.

The adsorbents used were samples of magnesium oxide made from coarse-pored magnesium hydroxide by vacuum treatment at 350, 500, 1000 and 1400° [1] and from magnesium carbonate by calcination at 1000°. The method of preparation of the original coarse-pored magnesium hydroxide, denoted here as $\text{Mg}(\text{OH})_2 - 1$, the conditions of the vacuum heat treatment, the water contents, and the structural characteristics of the magnesium oxide samples were given previously [1]. Samples of magnesium oxide made from $\text{Mg}(\text{OH})_2 - 1$ by vacuum heat treatment at 350 and 500° (denoted by $\text{MgO} - 1 - 350^\circ$ and $\text{MgO} - 1 - 500^\circ$ respectively) had a bidisperse porous structure: they retained the coarse-pored structure of the original $\text{Mg}(\text{OH})_2 - 1$ skeleton, but its primary platelets were penetrated by fine pores (cracks) formed during thermal decomposition of the hydroxide. The magnesia samples $\text{MgO} - 1 - 1000^\circ$ and $\text{MgO} - 1 - 1400^\circ$ contained predominantly coarse pores. Electron microscope investigations of the pore structure of the original $\text{Mg}(\text{OH})_2 - 1$ sample and of samples calcined at 1000 and 1400° confirmed the conclusions drawn from adsorption data [2]. Determinations of the differential heats of adsorption of benzene and hexane on $\text{MgO} - 1 - 1000^\circ$ [5] showed that its surface is in the main homogeneous.

Figure 1,a shows one of our [1] adsorption isotherms for benzene vapor (on $\text{MgO} - 1 - 1000^\circ$) and the corresponding pore volume distribution curve, which indicate that the pores of this sample have a uniform structure. Figure 1,b shows the adsorption isotherm for benzene vapor and the distribution curve for a sample

TABLE 1

Constants of the Hydrocarbons Used

Hydrocarbons [*]	Temperature, (°C)	p_s , mm	d_4^{20}	n_D^{20}
Benzene	10	45.8	0.8790	1.5012
	20	75.4		
	30	119.8		
n-Hexane	10	76.2	0.6595	1.3749
	20	121.8		
	30	188.3		

* Highly pure benzene and hexane for adsorption were kindly provided by E. A. Mikhailova from the Institute of Organic Chemistry of the Academy of Sciences USSR.

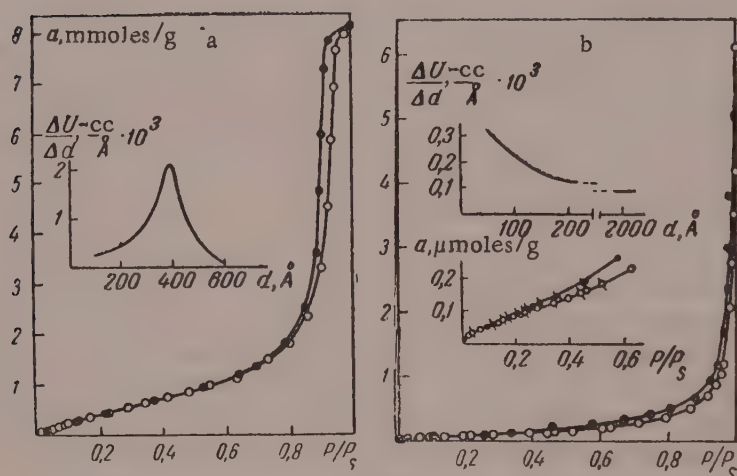


Fig. 1. Isotherms for adsorption of benzene vapor and curves for pore volume distribution by effective diameters for samples MgO — 1 — 1000° (a) and MgO — 2 — 1000° (b): black points here and subsequently represent desorption.

prepared from magnesium carbonate (sample MgO — 2 — 1000°). Capillary-condensation hysteresis begins for this sample at $p/p_s \approx 0.2$, and the two branches of the isotherm, in contrast to that for sample MgO — 1 — 1000°, asymptotically approach $p/p_s = 1$. The distribution curve indicates that the porosity of this magnesia sample is not uniform.

The specific surface of the skeleton of sample MgO — 2 — 1000° determined from adsorption of nitrogen vapor, was $s = 23 \text{ m}^2/\text{g}$, whereas the area of the adsorbed benzene film formed at the start of hysteresis was $s' = 30 \text{ m}^2/\text{g}$, so that $s'/s > 1$, evidently owing to the nature of the porosity of this sample. For samples of nonuniform porosity, in calculations of s' the work of multimolecular adsorption cannot be disregarded by comparison with the work of capillary condensation proper, as this would give high values of s' . The question of calculation of the surface area of adsorption films for adsorbents of the fourth structural type (heterogeneously porous) [11] therefore needs further examination.

Certain constants of the hydrocarbons used are given in Table 1. The vapor pressures p_s were determined in the adsorption apparatus.

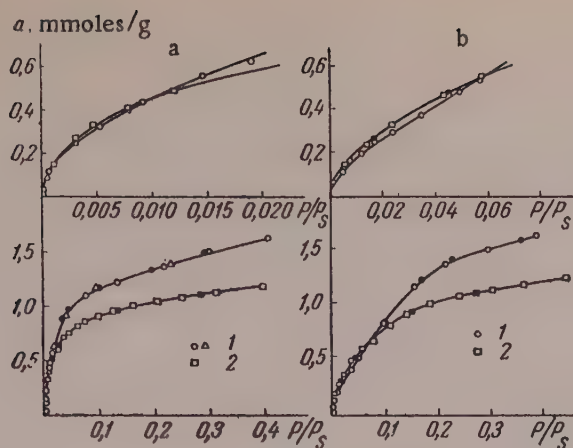


Fig. 2. Isotherms for adsorption of benzene (1) and n-hexane (2) vapors on samples MgO - 1 - 350° (a) and MgO - 1 - 500° (b).

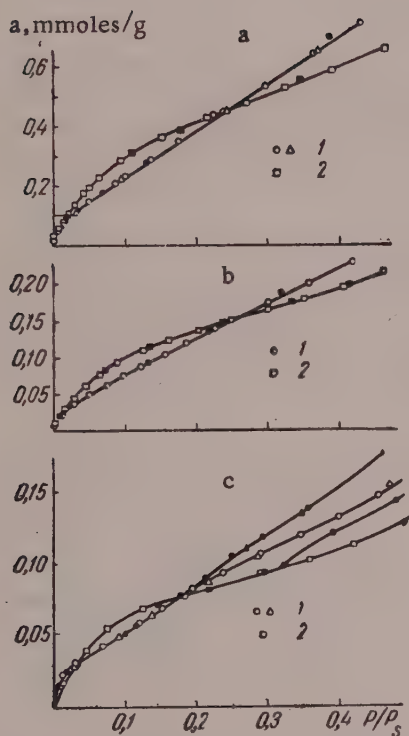


Fig. 3. Isotherms for adsorption of benzene (1) and hexane (2) vapors on samples MgO - 1 - 1000° (a), MgO - 1 - 1400° (b), and MgO - 2 - 1000° (c).

Adsorption was determined by means of vacuum liquid microburets [1] with an accuracy of about ± 1 micromole/g in the initial region of the adsorption isotherm, and about ± 10 micromoles/g in the region of high p/p_s values.

The adsorption isotherms for benzene vapor were determined up to $p/p_s = 1$ (see [1] and Fig. 1). Adsorption isotherms for hexane vapor were determined up to $p/p_s = 0.4-0.9$. For comparison, only the initial portions of these curves are given below.

It is clear from Fig. 2,a that the isotherms for adsorption of benzene and n-hexane on sample MgO - 1 - 350° are markedly convex, and initially (the upper part of Fig. 2,a) the isotherm for n-hexane lies somewhat above the isotherm for benzene; then they intersect, and after this the isotherm for benzene lies above that for n-hexane. The isotherms for adsorption of benzene and n-hexane on sample MgO - 1 - 500° (Fig. 2,b) are both convex, and in the initial region (upper portion of Fig. 2,b) the isotherm for n-hexane is appreciably above the isotherm for benzene.

For samples MgO - 1 - 1000° (Fig. 3,a) and MgO - 1 - 1400° (Fig. 3,b) the isotherms for adsorption of benzene are almost linear, with the exception of the earliest region, while the isotherms for n-hexane are convex, and the isotherm for n-hexane is considerably above that for benzene in the initial region.

The adsorption isotherms of benzene and n-hexane vapors on sample MgO - 2 - 1000° (Fig. 3,c) intersect twice: at first the isotherm for benzene is markedly convex and lies

above the isotherm for n-hexane, then they intersect and the hexane isotherm lies above the benzene isotherm, and in this region the isotherm for n-hexane is convex and that for benzene is almost linear. At even higher p/p_s the isotherms intersect again and, as with other samples of magnesium oxide, the isotherm for benzene lies above that for n-hexane. In view of the fact that the sample MgO - 2 - 1000° contains numerous fine pores, capillary-condensational hysteresis begins at lower values of p/p_s than for MgO - 1 - 1000°. The start of hysteresis

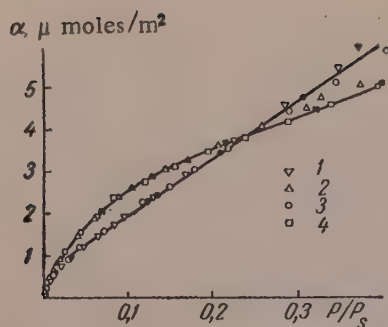


Fig. 4. Absolute isotherms for adsorption of benzene (1) and hexane (2) vapors on sample MgO-1-1000°, and benzene (3) and hexane (4) vapors on sample MgO-1-1400°.

higher sensitivity of benzene molecules than of hexane molecules to heterogeneity of the adsorbent surface [6, 12]. As a result the isotherm for adsorption of benzene on magnesium oxide obtained from magnesium carbonate initially lies even higher than the isotherm for hexane adsorption (Fig. 3,c).

Figure 5 shows adsorption isotherms of benzene and hexane on the finely porous samples MgO-1-350° and MgO-1-500°, reduced to the corresponding absolute isotherms for adsorption on coarsely-porous magnesium oxide (Fig. 4) by division of the relative adsorption α in millimoles/g by the corresponding specific surfaces of these adsorbents, formally determined by the BET method from isotherms for low-temperature adsorption of nitrogen vapor. The explanation of the steep slope of the isotherms for adsorption of benzene and hexane on MgO-1-350°, and the decrease of the slope for MgO-1-500° is probably that the adsorption potential is increased in the fine cracks formed in the platelets of magnesium hydroxide during volume dehydration at 350°, and some sintering, as was demonstrated by us earlier [1], of magnesium oxide (predominantly in the fine cracks) at 500°. Thus, the high adsorptive capacity of magnesium oxide made from magnesium hydroxide by heat treatment at 300-500° is due not only to its large specific surface but also to an increase of the adsorption potential in the fine pores present in such samples. Magnesium oxide obtained at low temperatures has been described as the active form [13].

Application of equations for isotherms of multimolecular adsorption. Application of the theoretical equation for the adsorption isotherm to the experimental isotherm is reasonable only if the real adsorption system is close to the ideal model on which the derivation of the equation is based. Often a particular equation which can represent an experimental adsorption isotherm is purely formal, and the constants so determined have no physical meaning [14, 3]. Therefore isotherm equations based on a homogeneous-surface model, the BET [15] and Kiselev and Poshkus [16-18] equations for multimolecular adsorption, were applied only to isotherms for adsorption of benzene and hexane vapors on magnesium oxide samples with the most uniform surface, namely MgO-1-1400°.

The experimental adsorption isotherms plotted in linear coordinates of the BET equation are given in Fig. 6,a. The limits of applicability of the BET equation to the experimental adsorption isotherms and the constants of this equation found from the graphs are given in Table 2, where C is the energy constant; a_m is the capacity of the monolayer; and ω_0 are the areas occupied by benzene and hexane molecules in a dense monolayer. Values of ω_0 were calculated from the expression $\omega_0 = s/N_A a_m$, where s is the specific surface of the adsorbent, determined from the isotherm for low-temperature adsorption of nitrogen by the BET method (ω_0 for nitrogen was taken to be 16.2 \AA^2) and N_A is the Avogadro number.

It follows from Fig. 6 and Table 2 that the BET equation is satisfactorily applicable in these cases. The energy constant C is small for adsorption of both benzene and hexane on magnesium oxide; its value does not exceed 20, because of the relatively low values of the heat of pure adsorption on magnesium oxide (in contrast to adsorption on graphitized carbon black [6, 7, 19] when $C_{C_6H_6} = 56$ and $C_{C_6H_{14}} = 500$).

for sample MgO-2-1000° corresponds to effective radii of 15-20 Å, as calculated by the Thomson equation with a correction for the thickness of the adsorption film.

Absolute and reduced isotherms for adsorption of benzene and n-hexane on magnesium oxide. Absolute isotherms (referred to unit surface area) for adsorption of benzene and hexane on uniformly-porous samples MgO-1-1000° and MgO-1-1400° are given in Fig. 4. The respective isotherms almost coincide; this means that the adsorptive capacities per unit area of these uniformly-porous samples are almost the same, although their specific surfaces differ almost by a factor of 3 [1].

Comparison of the adsorption isotherms for the heterogeneously porous sample MgO-2-1000° with the isotherms for adsorption of benzene and hexane on magnesium oxide with more uniform and larger pores (MgO-1-1000° and MgO-1-1400°) shows that for the sample obtained from carbonate the isotherm for benzene adsorption is more steep at first. The probable explanation is the

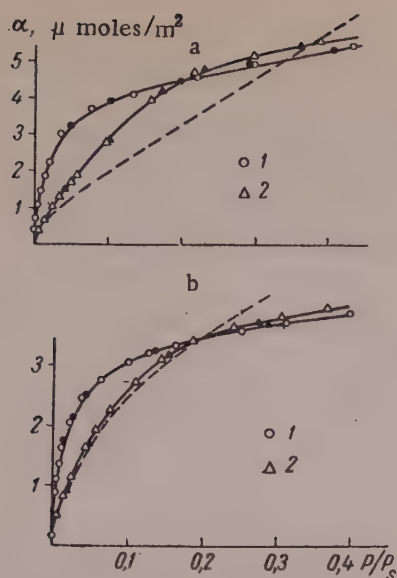


Fig. 5. Isotherms for adsorption of benzene (a) and hexane (b) vapors on samples MgO - 1 - 350° (1) and MgO - 1 - 500° (2), reduced to the corresponding absolute adsorption isotherms on magnesium oxide (dash lines, see Fig. 4).

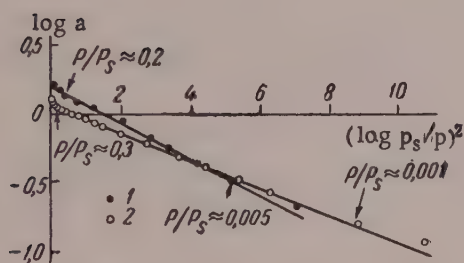


Fig. 7. Isotherms for adsorption of benzene (1) and hexane (2) vapors on MgO - 1 - 350° sample, in linear coordinates of the Dubinin-Radushkevich equation; arrows indicate the corresponding values of p/p_s .

is too low in the case of adsorption on magnesium oxide. Thus, in an investigation [21] where it was assumed that nitrogen molecules are adsorbed on the (100) face of magnesium oxide only in certain definite positions, the value of 17.67 \AA^2 was found for ω_0 . This value gives 40.3 and 54 \AA^2 for ω_0 of benzene and hexane molecules respectively on MgO - 1 - 1400°, which are more probable values.

The equation derived by A. Kiselev and Poshkus [16-18] for the isotherm of multimolecular adsorption, with interaction between adsorbed molecules in the first layer taken into account, is:

$$\frac{0(1-h)^2}{[1-0(1-h)]h} = K'_1 + K'_1 K_n 0(1-h), \quad (1)$$

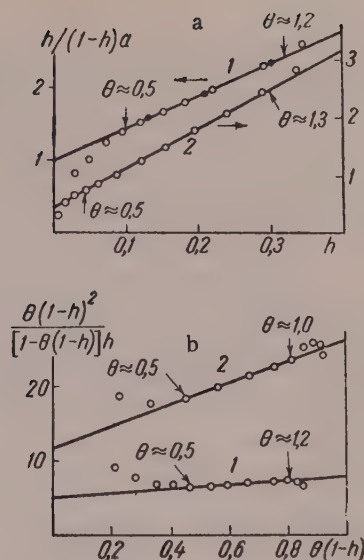


Fig. 6. Isotherms for adsorption of benzene (a) and hexane (b) vapors on sample MgO - 1 - 1400° in linear coordinates of the BET equation (a) and equation (1) (b).

The values of ω_0 found for adsorption of benzene and hexane molecules on magnesium oxide are lower than those for adsorption on graphitized carbon black ($\sim 40 \text{ \AA}^2$ [6] and $\sim 51 \text{ \AA}^2$ [19] respectively). This contradicts the relationship established earlier [20], according to which ω_0 increases with decrease of C for a given molecule. However, at low values of the constant C (at low values of the heat of pure adsorption) the BET equation can only formally valid, as in such cases there are more pronounced deviations of the real adsorption system from the ideal system on which the BET equation is based. It follows that the low values of ω_0 obtained from this equation for benzene and hexane on magnesium oxide samples do not have a definite physical meaning. On the other hand, it is possible that the area taken for the area of a nitrogen molecule in a dense monolayer $\omega_0 = 16.2 \text{ \AA}^2$

TABLE 2

Applicability Limits and Constants for Equations of Isotherms for Multimolecular Adsorption of Benzene and Hexane Vapors on MgO-1-1400° Sample of Magnesium Oxide

Adsorbate	BET equation					Equation (1)				
	applicability limits		C	a _m , milli-mole/g	ω ₀ , Å ²	Value of ω ₀ taken in Å ²	applica- bility limits for θ	K ₁ '	K _n	$\frac{K_n}{K_1'}$
	for p/p _s	for θ								
Benzene	0,1—0,35	0,5—1,2	6	0,18	37	40	0,5—1,2	5	0,7	0,14
Hexane	0,05—0,3	0,5—1,3	19	0,135	49,5	51,5	0,5—1,0	11	1,4	0,13

TABLE 3

Constants of Equation (2) for Isotherms for Adsorption of Benzene and Hexane on Sample MgO-1-350°

Adsorbate	w ₀ , cc/g	$\frac{B}{\beta^2} \cdot 10^6$	β
Benzene	0.14	3.52	1.00
Hexane	0.15	2.95	1.09

51.5 Å² for hexane. These values were found from the isotherms for adsorption of these vapors on graphitized carbon black [6, 19] when K₁' >> K_n and Eq. (1) approximates to the BET equation.

It is clear from Table 2 that the applicability limits of Eq. (1) and the BET equation in relation to experimental isotherms for adsorption of benzene and hexane on magnesium oxide are approximately the same, probably because in these cases the values of the constants K_n are low, so that the BET equation is still a close approximation to Eq. (1).

The heterogeneous sample MgO-1-350° contains fine pores or cracks which become filled with the liquid adsorbate as the result of the primary process, which is still one of pure adsorption. The first type of the Dubinin-Radushkevich equation [23] for adsorption of vapors on fine-pore adsorbents, was convenient to apply to the isotherms for adsorption of benzene and hexane vapors on this sample. In the linear form this equation is written:

$$\log a = \log \frac{w_0}{v_m} - B \frac{T^2}{2,33^2} (\log p_s/p)^2, \quad (2)$$

where ω₀ is the volume of micropores filled by condensed vapor as the result of the pure adsorption process, v_m is the molal volume of the liquid adsorbate; B is a constant related to the pore size; β is the affinity coefficient. The experimental isotherms for adsorption of benzene and hexane on sample MgO-1-350°, plotted in the coordinates of equation (2), are given in Fig. 7. The equation is valid in the p/p_s range from 0.005 to 0.2. The constants w₀, B, and β (in the case of benzene β is taken as unity) found from the graphs are given in Table 3.

Table 3 shows that the isotherms for adsorption of benzene and hexane give almost the same value, about 0.15 cc/g, for the volume w₀ of the micro-pores of sample MgO-1-350°. The affinity coefficient β for hexane is lower than on active carbon, when β = 1.35 [24]; this is probably because the heats of adsorption of benzene and hexane on magnesium oxide are similar.

SUMMARY

1. The isotherms for adsorption of benzene and n-hexane vapors on a series of magnesium oxide samples made by thermal decomposition of magnesium hydroxide and carbonate have been determined.
2. In the region of relative vapor pressures corresponding to predominant filling of a monolayer the adsorption of hexane on magnesium oxide is greater than adsorption of benzene.
3. Absolute isotherms for adsorption of benzene and hexane vapors on magnesium oxide were determined and studied.

LITERATURE CITED

- [1] A. V. Kiselev, I. E. Niemark, D. P. Poshkus, and M. A. Piontkovskaya, *Izvestiya Akad. Nauk SSSR, Otd. khim. nauk* **232** (1959).
- [2] A. V. Kiselev and V. I. Lygin, *Izvestiya Akad. Nauk SSSR, Otd. khim. nauk* **412** (1959).
- [3] A. V. Kiselev, *The Structure and Properties of Porous Materials*, Ed. Everett, Stone (London, 1958) p. 195 — *Proc. of the Symposium in the Structure and Properties of Porous Materials, Colston Papers X*, (Bristol, 1958).
- [4] A. V. Kiselev and D. P. Poshkus, *Zhur. Fiz. Khim.* **32**, 2824 (1958).
- [5] N. N. Avgul', A. A. Isirikyan, A. V. Kiselev, I. A. Lygina, and D. P. Poshkus, *Izvestiya Akad. Nauk SSSR, Otd. khim. nauk* **1314** (1957).
- [6] N. N. Avgul', G. I. Berezin, A. V. Kiselev, and I. A. Lygina, *Izvestiya Akad. Nauk SSSR, Otd. Khim. nauk* **1304** (1956).
- [7] N. N. Avgul', G. I. Berezin, A. V. Kiselev, I. A. Lygina, and G. G. Muttik, *J. Chim. Phys.* **197** (1958).
- [8] A. A. Isirikyan and A. V. Kiselev, *Doklady Akad. Nauk SSSR* **115**, 343 (1957).*
- [9] L. D. Belyakova and A. V. Kiselev, *Doklady Akad. Nauk SSSR* **119**, 298 (1958).*
- [10] A. V. Kiselev and D. P. Poshkus, *Doklady Akad. Nauk SSSR* **120**, 834 (1958).*
- [11] A. V. Kiselev, *Zhur. Fiz. Khim.* **23**, 452 (1949).
- [12] N. N. Avgul', G. I. Berezin, A. V. Kiselev, and A. Ya. Korolev, *Kolloid Zhur.* **20**, 298 (1958).*
- [13] A. C. Zettlemoyer and W. C. Walker, *Ind. Eng. Chem.* **39**, 69 (1947).
- [14] A. A. Isirikyan and A. V. Kiselev, *Zhur. Fiz. Khim.* **31**, 2127 (1957).
- [15] S. Brunauer, P. H. Emmett and E. Teller, *J. Amer. Chem. Soc.* **60**, 306 (1938).
- [16] A. V. Kiselev, *Doklady Akad. Nauk SSSR* **117**, 1023 (1957).
- [17] A. V. Kiselev and D. P. Poshkus, *Izvestiya Akad. Nauk SSSR, Otd. Khim. nauk* **520** (1958).
- [18] A. V. Kiselev, *Kolloid Zhur.* **20**, 338 (1958).*
- [19] N. N. Avgul', G. I. Berezin, A. V. Kiselev, and I. A. Lygina, *Zhur. Fiz. Khim.* **30**, 2106 (1956).
- [20] A. V. Kiselev and Yu. A. Él'tekov, *Zhur. Fiz. Khim.* **31**, 250 (1957).
- [21] W. C. Walker and A. C. Zettlemoyer, *J. Phys. Chem.* **57**, 182, (1953).
- [22] A. V. Kiselev, N. V. Kovaleva, V. A. Sinitsyn, and E. V. Khrapova, *Kolloid Zhur.* **20**, 444 (1958).*
- [23] M. M. Dubinin, in the book: *Methods for Investigating the Structure of Highly Disperse and Porous Bodies* [in Russian] (Izd. AN SSSR, 1953) p. 72.
- [24] M. M. Dubinin, E. D. Zaverina, and D. P. Timofeev, *Izv. A. N. SSSR, Otd. Khim. nauk* **670** (1957).

* Original Russian pagination. See C. B. Translation.

Received October 3, 1958

CHARACTERISTICS OF STRUCTURE FORMATION IN CONCENTRATED SOLUTIONS OF POLYMETHACRYLIC ACID

Yu. S. Lipatov, P. I. Zubov, and E. A. Andryushchenko

The L. Ya. Karpov Physicochemical Institute, Moscow

It may be regarded as established by the large number of investigations concerned with gel formation in polymer solutions that the principal condition for gel formation is the formation of stable bonds between the macromolecules; it is caused by partial decrease in the solubility of certain groups of the polymer molecule in a given solvent [1, 2]. It has been deduced from a number of properties of polymer gels that gel structure is determined by formation of a spatial network of macromolecules which are, to a certain degree, of elongated form; this applies especially to gels of rigid polymers in poor solvents. Chain flexibility, which determines the chain configuration, influences in many ways both the variation of viscosity with the nature of the solvent and the concentration, and the character of structure formation [3]. Special interest attaches from this viewpoint to studies of the rheological properties of solutions of synthetic polyelectrolytes in which changes in the degree of ionization result in sharp changes in the form of the chain molecules and in consequent changes of rheological properties. However, the literature contains hardly any information on the behavior of concentrated solutions of synthetic polyelectrolytes in relation to the presence of extraneous electrolytes, to the degree of neutralization of the polyelectrolyte in solution, and to the temperature.

It was desired to carry out such an investigation of the rheological characteristics of concentrated solutions of polymethacrylic acid. There have been numerous publications concerned with studies of the properties of dilute solutions of this electrolyte in relation to various factors, including temperature and the nature of the solvent. Our purpose was to determine the possible conditions of structure formation in systems in which the form of the chain may alter with the degree of ionization of the molecules.

Viscosities of solutions of polymethacrylic acid [4] in various solvents were determined at polymer concentrations from 1 to 12%. Aqueous solutions of polymethacrylic acid neutralized to different extents by NaOH solutions were investigated. Viscosity was determined by means of the Ostwald and Ubbelohde (variable-pressure) viscosimeter and the rotational viscosimeter [5]. The FEK-M photocolormeter was used to determine the effects of temperature on turbidity of a number of solutions of polymethacrylic acid in different solvents.

Figure 1 shows variations of the specific viscosity of aqueous solutions of polymethacrylic acid with concentration at 20 and 60°, at a velocity gradient of 500 sec⁻¹. Figure 1 clearly reveals a characteristic feature of solutions of this polymer, which is that the temperature coefficient of viscosity depends sharply on the concentration and changes sign in the transition from less to more highly concentrated solutions. Appreciable gel formation already occurs in 8% solutions of polymethacrylic acid at 60°. Thus, here we are concerned with a system in which, in contrast to most polymers (with the exception of nitrocellulose solutions in ethanol [6] and of butyl rubber in benzene [7]), the viscosity increases sharply with temperature in concentrated solutions above a certain concentration. This concentration at which gel formation begins is relatively high in comparison, say, with the concentrations at which gelatin solutions form gels on cooling. It is evident that it is only at these concentrations that a sufficient number of intermolecular bonds, capable of withstanding thermal motion and leading to viscosity increase and gel formation, can be formed on increase of temperature.

Similar results are found for solutions of polymethacrylic acid in 0.1 N HCl. The table contains values of the average temperature coefficient of viscosity for solution of polymethacrylic acid in water and HCl in relation to the concentration, $(\eta_{t_1} - \eta_{t_2}) / (t_1 - t_2)$ when $t_1 < t_2$.

Mean Temperature Coefficient of Viscosity of Polymethacrylic Acid Solutions at Different Concentrations

Concentration, %	Temperature coefficient of viscosity		Concentration, %	Temperature coefficient of viscosity	
	solutions in water	solutions in HCl		solutions in water	solutions in HCl
1	-0.01	-0.08	5	-0.045	-0.062
2	-0.015	—	6	+0.03	-0.1
3	-0.018	-0.02	7	—	+1.3
4	-0.036	-0.04	8	$\gg +1$	—

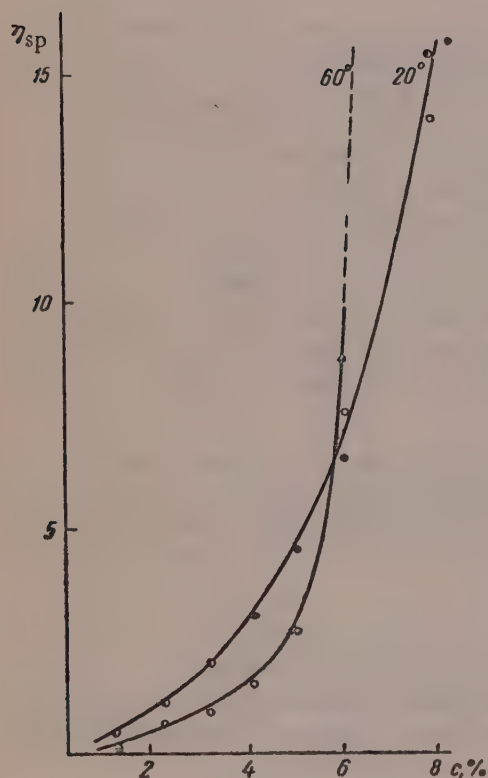


Fig. 1. Variations of the specific viscosity of aqueous polymethacrylic acid solutions with concentration at 20 and 60°.

It is seen in the table that the sign of the temperature coefficient changes abruptly when the concentration of polymethacrylic acid solutions is $\sim 6\%$. Comparison of the values of this coefficient with the corresponding temperature for water shows that up to $\sim 6\%$ concentration the fall in the viscosity of polymethacrylic acid solutions with increase of temperature exceeds the fall in the viscosity of water over the same temperature range; above this concentration the viscosity rises sharply with temperature.

We believe that the observed effects are caused by a decrease of the solubility of polymethacrylic acid with rise of temperature. This hypothesis is consistent with the results of certain thermodynamic investigations of polymethacrylic acid solutions [8] and of investigations of infrared and Raman spectra [9].

As a consequence of the decreased solubility of polymethacrylic acid on heating, certain coiling of the molecules due to formation of additional intramolecular bonds takes place in solutions of relatively low concentration owing to weakened interaction between the polymer molecules and the solvent. At higher concentrations intermolecular bonding becomes more probable, and this causes structure formation in the solutions on heating. In fact, our data on variations of the specific viscosity of the solutions with the rate of shear show that in the range of shear rates from 100 to 1000 sec^{-1} the viscosity begins to depend appreciably on the rate of shear only at the concentrations at which structure formation begins in the solutions on heating.

Available data on the shape of polymethacrylic acid molecules in dilute aqueous solutions show that these molecules have a coiled configuration because of the presence of fairly numerous intramolecular hydrogen bonds. It is evident that with increase in the solution concentration the molecules retain their coiled form, although the molecular coils probably become considerably smaller. We consider that the structure formation in polymethacrylic acid solutions which we observed on heating is caused by intensified interaction between molecules in a coiled configuration. If intramolecular bonds were broken down on heating, the viscosity would increase with temperature even at low concentrations; this is not the case in fact. Addition of urea (which can break down hydrogen bonds) to 1% solution of polymethacrylic acid does not increase the viscosity, but lowers it somewhat. This indicates that the intramolecular bonds are fairly stable. When 1% polymethacrylic acid solutions

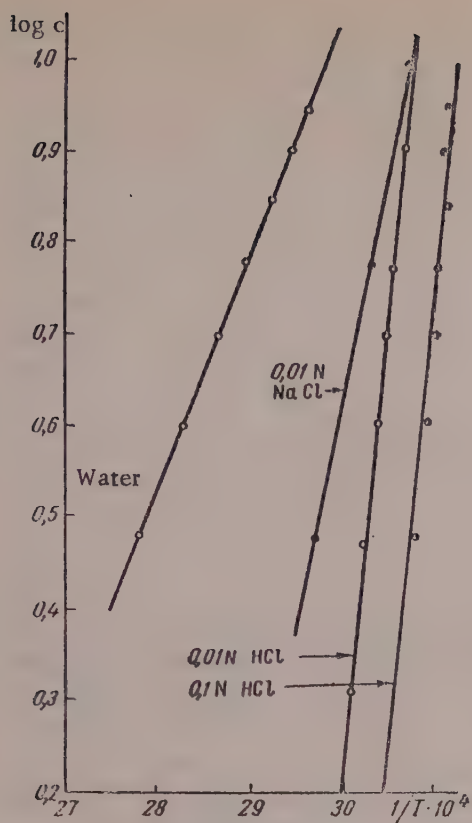


Fig. 2. Variations of $\log c$ with $1/T$, where T is the temperature at which the turbidity of a solution of concentration c is 100%.

In water are heated in absence of urea the viscosity falls, whereas in presence of urea the viscosity remains unchanged; this may indicate that the intramolecular bonds are broken down to some extent in presence of urea only when the solutions are heated. We thus correlate structure formation in concentrated solutions of polymethacrylic acid on increase of temperature with a decrease in the solubility of the polymer in water which leads, at sufficiently high solution concentration, to intensified intermolecular action.

A distinguishing feature of gel formation in this system, as compared with other well-known cases of gel formation, such as in gelatin, is that in the present instance the bonds are formed between molecules in the coiled, globular form. Such gels should approximate in properties to gels formed in solutions of hydrophobic colloids.

Gel formation in aqueous solutions of polymethacrylic acid was also studied nephelometrically. This was possible because increase of temperature in the investigated systems resulted in an appreciable increase of turbidity, evidently caused by aggregation processes. Studies of effects of temperature on turbidity of aqueous and hydrochloric acid solutions of polymethacrylic acid at concentrations from 3 to 9% showed that above a definite temperature the turbidity begins to increase appreciably. There is a linear relationship between the reciprocal of the temperature at which the turbidity of the solution reaches 100% and the logarithm of the concentration. These results are plotted in Fig. 2. From these data we determined the heat of gelation by means of the equation

$$\ln c = -\Delta H/RT + \text{const.}$$

used in other publications [10, 11] for a similar purpose. We found that in aqueous solutions the heat of aggregation of polymethacrylic acid is 11.4 kcal/mole, and in solutions of 0.1 N HCl it is 45.5 kcal/mole. These values are considerably lower than the heats of gelation in gelatin solutions; according to the publications cited, these are 60-90 kcal/mole.

This is probably because in solutions of polymethacrylic acid intermolecular hydrogen bonds are formed; their number, in contrast to the number in a gelatin gel, is relatively small because of the coiled configuration of the molecules in solution. If the energy of hydrogen bonding is taken to be ~ 5 kcal/mole, our data correspond to the formation of 2-8 bonds per molecule, as compared with 12-20 bonds for gelatin. This is understandable, because the more open form of the gelatin chains favors formation of a larger number of intermolecular bonds.

The considerable difference between the heats of aggregation in aqueous and hydrochloric acid solutions of polymethacrylic acid is of great interest. We attribute this difference to the fact that in hydrochloric acid solutions the conditions are favorable for formation of a larger number of stabler bonds; in aqueous solutions, where polymethacrylic acid is dissociated, although only to a slight extent, electrostatic repulsion of the chains prevents formation of sufficiently stable intermolecular bonds. This hypothesis is confirmed by data on heats of aggregation in aqueous solutions in presence of NaCl. Addition of NaCl increases the ionic strength of the solution and thereby lowers the degree of dissociation of methacrylic acid, although not as much as addition of HCl does. Therefore, in solutions with added NaCl the heat of aggregation has the intermediate value of 19.7 kcal/mole. It follows that conditions of structure formation depend to a significant extent on the degree of ionization of the molecules. The fact that intermolecular bonds are numerous in hydrochloric acid solutions is confirmed by the higher viscosities of these solutions as compared with viscosities in absence of HCl, and by the greater stability of the structures formed when solutions in hydrochloric acid are heated. This is clear from the data in Fig. 3 on the development of shearing deformation at 53° for aqueous and hydrochloric acid solutions.

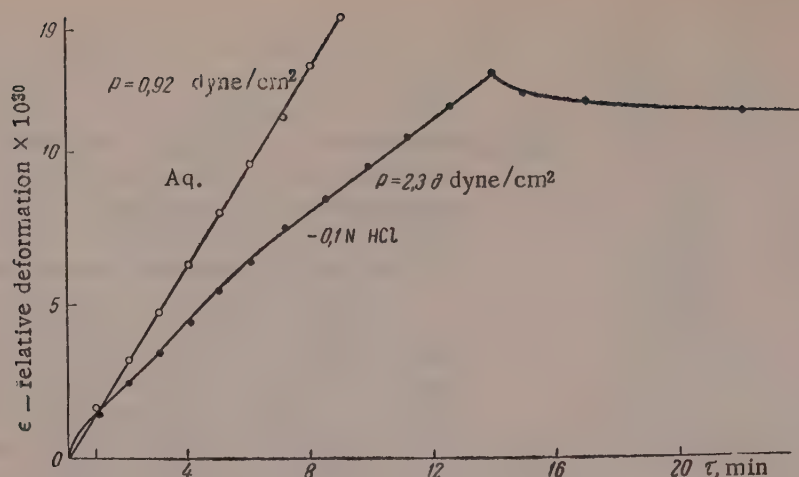


Fig. 3. Variations of relative deformation with time for solutions of poly-methacrylic acid in water and in HCl at 53°.

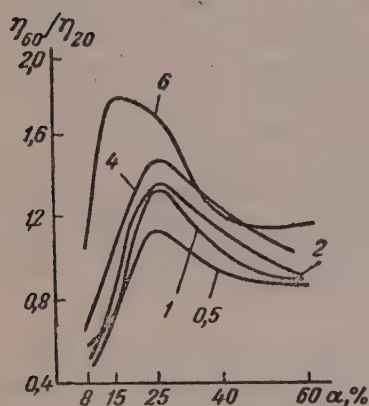


Fig. 4. Effect of degree of neutralization on the ratio of specific viscosities at 20 and 60° for aqueous solutions of polymethacrylic acid of different concentrations.

Fig. 3 shows that in presence of HCl the system has properties characteristic of a gel, i.e., it exhibits slight elastic deformation, whereas in absence of HCl the properties of a gel do not appear at this temperature and a shearing stress produces only irreversible deformation (these results were obtained by means of a rotational viscosimeter by the method described earlier [5]). The following fact confirms that intermolecular hydrogen bonds are formed during gelation. If urea is added to solutions of polymethacrylic acid, the turbidity of the solutions does not alter with increase of temperature and gel formation does not take place. Earlier we drew attention to specific characteristics of structure formation in aqueous solutions of methacrylic acid, associated with globular configuration of the macromolecules. It was of interest to find, however, whether structure formation takes place in aqueous solutions of the partially-neutralized acid, i.e., when the shape of the macromolecules determined by their ionization alters. The effects of temperature on the specific viscosity of aqueous solutions of polymethacrylic acid of 5, 15, 25, 40 and 60% neutralization were therefore investigated. The results [4] show that as the degree of neutralization of polymethacrylic acid in solution increases, with uncoiling of the molecules and increase of viscosity, the tempera-

ture coefficient of viscosity also undergoes characteristic changes. Whereas in aqueous solutions the viscosity increases with temperature above a certain concentration, in the case of solutions of partially-neutralized polymethacrylic acid this effect appears, above a definite degree of neutralization, even in relatively dilute solutions. Figure 4 shows variations of the ratio of specific viscosities at 20 and 60° with the degree of neutralization for solutions of different concentrations. It is seen in Fig. 4 that the viscosity may either decrease or increase on heating, depending on the degree of neutralization. The maximum increase of viscosity with temperature is found for 25% neutralization. Figure 5 shows that above a certain concentration the solution viscosities begin to rise sharply. Concepts concerning the behavior of polyelectrolytes in dilute solutions cannot be extended to concentrated solutions. In general this is because, for a given degree of neutralization, the degree of ionization of the macromolecules is lower in a concentrated than in a dilute solution, because the ionic strength is higher; therefore the change in the shape of the chain on neutralization is also less pronounced. At the same time, because of the lower degree of dissociation in concentrated solutions the polymer chains in these solutions contain fairly numerous undissociated carboxyl groups, capable of forming intermolecular bonds in concentrated solutions. The presence of COONa groups with firmly-bound sodium ions is also possible. Under certain conditions these

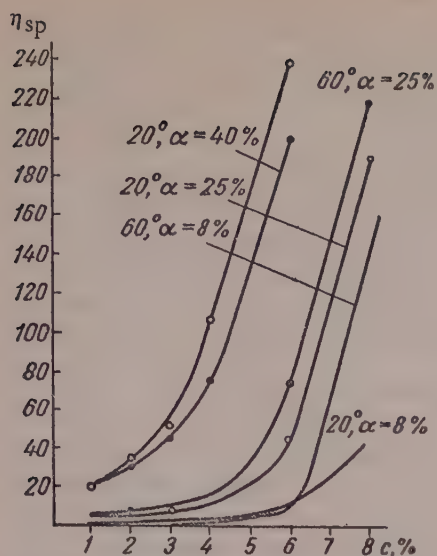


Fig. 5. Variations of specific viscosity of aqueous solutions of methacrylic acid at different degrees of neutralization with the concentration of the acid.

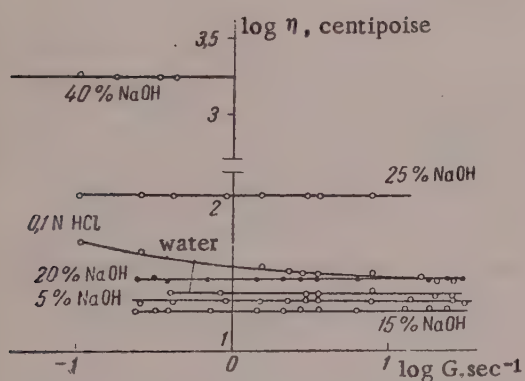


Fig. 6. Variations of the viscosity of 9% aqueous solutions of polymethacrylic acid with the rate of shear at 20° .

degrees of neutralization, as a function of the shear rate (Fig. 6). Figure 7 shows variations of the viscosity of a 9% solution with the degree of neutralization at a shear rate of 0.33 sec^{-1} ; the straight line represents the viscosity of a solution of polymethacrylic acid in 0.1 N HCl . Figure 8 shows variations of viscosity with rate of shear for some 12% solutions of polymethacrylic acid. The data in Fig. 8 indicate that in a concentrated solution viscosity increases with decrease of solubility, and hence with increase of coiling of the molecular chains. This shows that in the present instance the effects associated with decreased solubility and increased intermolecular action have a much greater influence on viscosity than any possible effects due to changes in the shape of the chains on neutralization of the polymeric-acid molecules, accompanied by an increase of solubility. The effects of changed configuration become appreciable only when the degree of neutralization reaches $\sim 25\%$. It follows that structure formation in concentrated solutions largely depends on the degree of intermolecular interaction, determined by the nature of the polymer and solvent, rather than on the configuration of the polymer chains.

factors would favor structure formation in solutions. Our results indicate that structure formation in solutions increases with rise of temperature although no gel formation takes place. Increase of structure formation may be attributed to decrease of the solubility of partially-neutralized polymethacrylic acid with increase of temperature; this, in particular, is indicated by the greater increase of viscosity with concentration at high concentrations. Absence of gel formation may be due both to the higher solubility of the salt as compared with pure polymethacrylic acid, and to the presence of similarly-charged groups which prevents mutual approach of the polymer chains in solution and formation of stable intermolecular bonds. According to our nephelometric data [12], when the sodium content reaches only 2% on the carboxyl groups heating no longer produces changes in the turbidity of polymethacrylic acid solutions or gel formation. The foregoing is supported by data which show that the greatest viscosity changes on heating of partially-neutralized solutions of polymethacrylic acid take place at an intermediate degree of neutralization, when the molecules are already uncoiled but their mutual repulsion is not yet very strong and the effect of solubility increase due to conversion into salt is also not very pronounced. The increase of viscosity with temperature begins at lower concentrations in solutions of partially-neutralized polymethacrylic acid than in solutions of the unneutralized acid; this is because structure formation occurs more easily on decrease of solubility with molecules in extended configuration than with coiled molecules.

The hypothesis that solubility decrease is the cause of the observed increase of viscosity with rise of temperature in solutions of partially-neutralized polymethacrylic acid is also confirmed by the following data. We found for the first time for concentrated solutions of methacrylic acid that the relationships which hold for dilute polyelectrolyte solutions are not valid for concentrated solutions. We showed that even for 8% solutions the lower the degree of neutralization the higher the viscosity (at degrees of neutralization up to 25%) [13]. Further, the viscosity of an 8% solution is higher in presence of HCl than the viscosity of an aqueous solution. These results were confirmed in our studies of the viscosity of 9% solutions of polymethacrylic acid in water and in 0.1 N HCl and NaOH at different de-

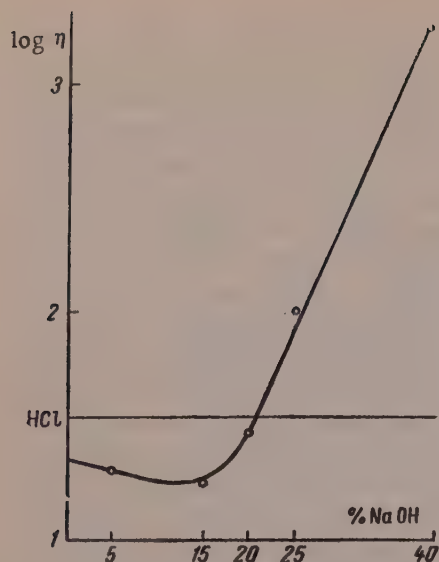


Fig. 7. Variations of the viscosity of 9% solutions of methacrylic acid with the degree of neutralization.

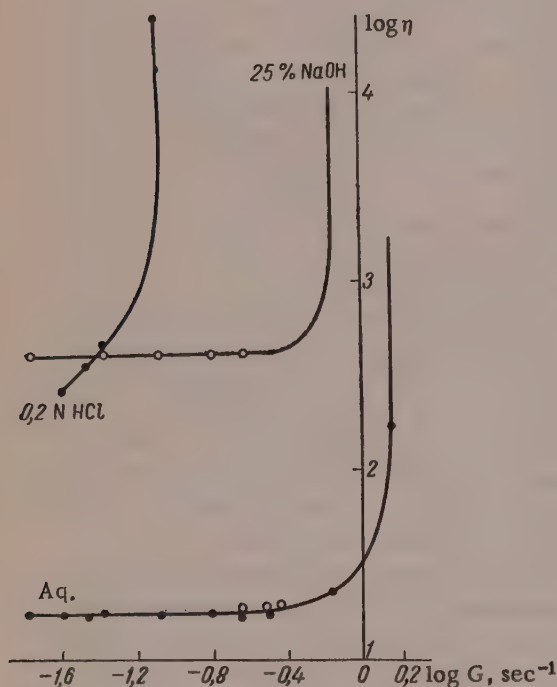


Fig. 8. Effect of rate of shear on the viscosity of 12% solutions of polymethacrylic acid.

An interesting characteristic of concentrated solutions of polymethacrylic acid is that, above a certain concentration (12% in the present instance), the viscosity — shear rate relationship differs from that found for most other polymer systems.

From a definite value of the rate of shear the viscosity increases sharply with time. This is evidently associated with effects of negative thixotropy and more detailed study of this effect is needed. In the light of our results it was of interest to study the behavior of polymethacrylic acid in a less polar solvent, methanol.

The results of determinations of specific viscosity at different temperatures, plotted in Fig. 9, show that the specific viscosities are considerably higher in methanol than in aqueous solutions of the corresponding concentrations. According to literature data the viscosities of polymethacrylic acid in dilute methanol solutions are lower than in aqueous solutions of the corresponding concentrations; this indicates that the macromolecules are more coiled in methanol, which is the "poorer" solvent in the thermodynamic sense. However, in concentrated solutions the viscosities of methanol solutions are higher; this is consistent with the general nature of the viscosity — concentration relationship for solutions of flexible molecules in good and poor solvents [14].

Here, in contrast to aqueous solutions, the viscosity falls instead of rising when solutions of polymethacrylic acid of up to 15% concentration are heated.

This indicates that either the solubility of methacrylic acid in methanol increases with temperature, or that intramolecular bonding predominates over intermolecular if solubility decreases with rise of temperature. We believe that the more probable cause of the observed effects is decrease of the solubility of polymethacrylic acid in methanol, because solution viscosity also decreases when a precipitant is added to methanol solutions, i.e., when the quality of the solvent becomes even worse. The solubility of polymethacrylic acid in a mixture of methanol and precipitant (methyl ethyl ketone) also falls on increase of temperature, as is shown by the increased turbidity of such solutions when they are heated. The predominance of intramolecular over intermolecular bonding on decrease of solubility indicates, in our opinion, that the flexibility of the polymer chains in this solvent alters with rise of temperature. Increase of flexibility favors chain coiling. Evidently the change in the chain flexibility in this mixed solvent also accounts for the fact that the relationship between the temperature at which the turbidity reaches 100%

and the solution concentration is nonlinear. Lower temperatures correspond to a smaller slope and consequently to a lower heat of bond formation. If this relationship (Fig. 10) is plotted in the form of two straight lines, they are found to correspond to heats of aggregation of 7.4 and 28.5 kcal/mole respectively. Since these values, as in the case of aqueous solutions, are greater than the heat of formation of one hydrogen bond per molecule it

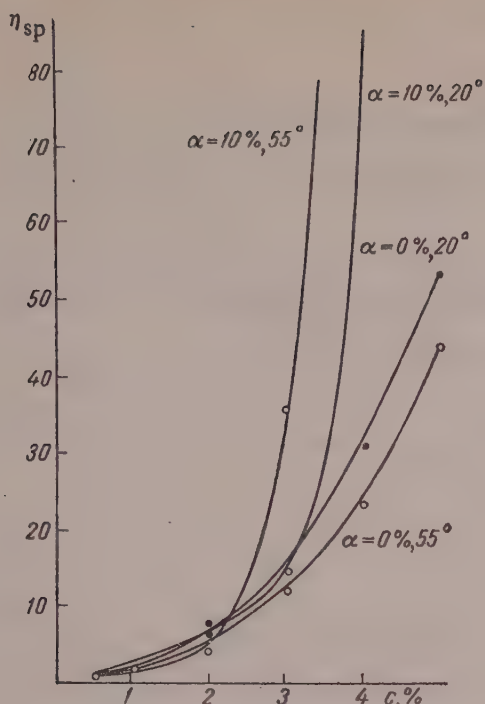


Fig. 9. Variations of the specific viscosity with concentration of solutions of polymethacrylic acid in methanol.

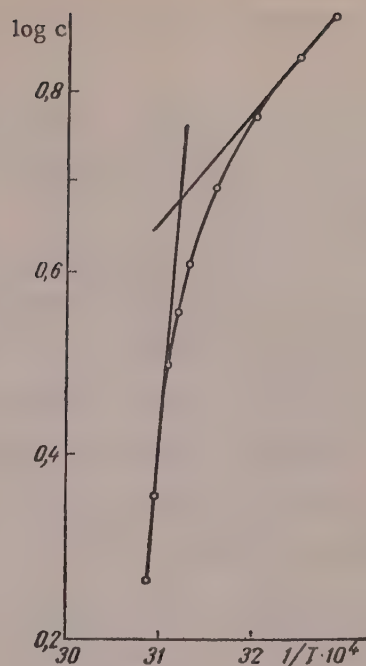


Fig. 10. Variation of $\log c$ with $1/T$ for solutions of polymethacrylic acid in methanol-methyl ethyl ketone mixture (1:1).

may be assumed that the ratio of intermolecular to intramolecular bonds changes with change of temperature and the associated change of flexibility; the number of intermolecular bonds increases with rise of temperature, because the solubility is lower at higher temperatures.

Addition of NaOH in amounts corresponding to 10% neutralization of the acid to methanol solutions of polymethacrylic acid results, in relatively dilute solutions, in a decrease of viscosity, which we ascribe to a decrease of the solubility of the partially neutralized acid in methanol. The behavior of such solutions on changes of concentration and temperature is analogous to the behavior of aqueous solutions (Fig. 9); above a certain concentration the viscosity rises sharply with increase of temperature and gel formation begins.

Evidently in this case, as for aqueous solutions, decrease of solubility and chain coiling leads at certain concentrations to formation of gels from molecules in the coiled, globular form. The heat of aggregation, determined as indicated above, is 20,000 cal/mole.

Thus, both in aqueous solutions of polymethacrylic acid and in methanol solutions of the partially-neutralized acid increase of temperature may result in gelation processes associated with partial decrease of the solubility of the polymer in the given solvent on heating. Evidently in both cases the gel network is built up of molecules in the coiled configuration. Partial loss of solubility of certain groups contained in the polymer is therefore a necessary condition for gel formation. This conclusion is in harmony with Lipatov's views[2] concerning the significance of partial solubilities of different groups in a polymer for gel formation.

SUMMARY

1. The viscosity-temperature relationships of solutions of polymethacrylic acid in methanol and water have been studied for different degrees of neutralization of the acid.
2. Under certain conditions gel formation may occur in these systems, due to partial decrease of the solubility of the polymer in a given solvent.
3. The gels so formed are spatial networks made of polymer macromolecules in a coiled configuration.

4. The relationships between viscosity and degree of neutralization which are valid for dilute solutions do not hold for concentrated aqueous solutions of polymethacrylic acid.

LITERATURE CITED

- [1] P. Hermans, in the book: Colloid Science, vol. II, Reversible Systems (edited by H. Kruyt) (1949).
- [2] S. M. Lipatov, Abstracts of Papers at the 4th All-Union Conference on Colloid Chemistry (Tbilisi, Izd. AN SSSR, 1958) [in Russian].
- [3] A. A. Tager, *Uspekhi Khimii* 27, 481 (1958).
- [4] Yu. S. Lipatov and P. I. Zubov, *Vysokomolekulyar Soedineniya* 1, 1, 88 (1959).
- [5] L. V. Ivanova-Chumakova and P. A. Rebinder, *Kolloid. Zhur.* 18, 429 (1956).
- [6] S. Newman, *J. Phys. Chem.* 5, 648 (1956).
- [7] T. V. Dorokhina, Candidate's Dissertation [in Russian] (Moscow, 1958).
- [8] A. Silberberg, *J. Polymer Sci.* 23, 259 (1957).
- [9] A. Simon, *J. Polymer Sci.* 30, 201, (1958).
- [10] J. Eldridge and J. Ferry, *J. Phys. Chem.* 58, 992 (1954).
- [11] S. I. Meerson and S. M. Lipatov, *Kolloid. Zhur.* 20, 3, 353 (1957).*
- [12] Yu. S. Lipatov, P. I. Zubov, and E. A. Andryushchenko, *Vysokomolekulyar Soedineniya* 1, 3 (1959).
- [13] Yu. S. Lipatov and P. I. Zubov, *Vysokomolekulyar Soedineniya* 1, 2 (1959).
- [14] F. Billmeyer, Textbook of Polymer Chemistry [Russian translation] (1958) p. 91.

Received May 25, 1959

*Original Russian pagination. See C. B. Translation.

CHANGES IN THE COLLOIDAL PROPERTIES OF WHEAT FLOUR DURING DRY HEATING ABOVE 100°

D. N. Lobanov and L. V. Babichenko

The G. V. Plekhanov Institute of National Economy, Moscow

Flour is heated in the dry state at temperatures above 100° in some branches of the food industry and in communal feeding.

The literature contains some information on the effects of dry heating on the nutrient substances present in flour, but hardly any data are available on changes in its colloidal properties. This problem is of considerable practical interest, because dry-heated flour is added to certain products in order to make them richer in colloids.

The material used for the investigation was air-dry first-grade wheat flour, heated at 120 and 150°. The changes produced by the heating in the filtration rates of suspensions, water-binding capacity, and viscosities of standard suspensions were determined.

The method of filtration analysis [1, 2] was used for determinations of the relative hydrophilic nature of the flour. The method is based on the sensitivity of the filtration rate of a sol prepared under standard conditions to the degree of dispersion and hydration of the colloid particles.

Differences in the rates of filtration of aqueous suspensions of the samples became apparent even at the start of the process (Fig. 1). The filtration time of 20 cc of sol was specially significant: for air-dry flour it was 24 minutes 32 seconds, for flour heated at 120°, 40.5 seconds, and for flour heated at 150°, 9 seconds. These differences between the filtration rates of suspensions of the flour samples are the result of decreased hydrophily, mainly owing to protein denaturation [3].

The water-binding capacity of the flour was determined from the heat of wetting. The amount of bound water was calculated by Dumanskii's formula [4]:

$$A = \frac{Q}{80},$$

where A is the water-binding capacity of 1 g of the substance, in grams; Q is the heat of wetting, in calories per gram. The values of Q were found from calorimetric determinations of the increase of temperature as the result of wetting in a variable-temperature calorimeter with an isothermal jacket [5], and were calculated from the formula

$$Q = \frac{(\Delta t + x_t) [(m + m_1) \cdot C + K]}{m},$$

where Δt is the rise of temperature caused by wetting of the flour by water; x_t is a temperature correction for heat transfer to the surroundings during the wetting; m is the weight of the sample in grams; m_1 is the weight of water taken for the wetting, in grams; C is the specific heat of an aqueous flour suspension (assumed arbitrarily to be unity [6]); K is the water equivalent of the calorimetric unit, representing the quantity of heat required to raise the temperature of the whole system by 1°. In our experiments the water equivalent was 23.41 cal with the first calorimeter and 21.93 cal with the second.

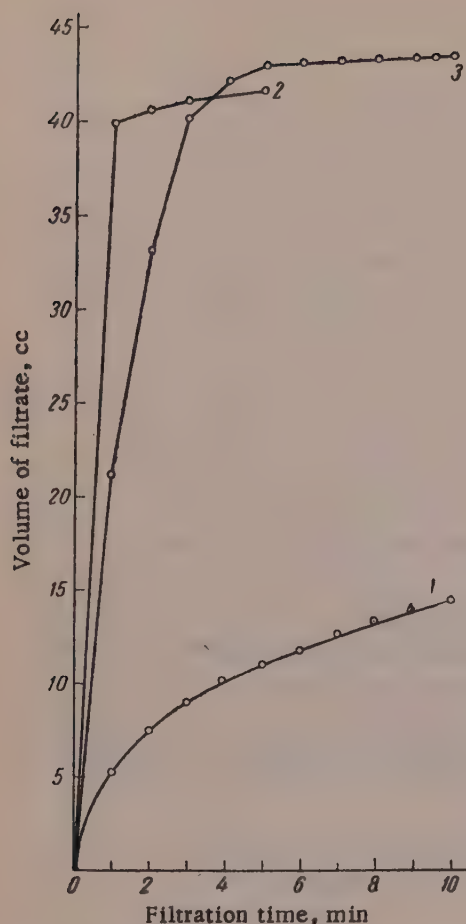


Fig. 1. Filtration rates of flour suspensions: 1) air-dry flour; 2) heated to 150°; 3) heated to 120°.

The graph representing the temperature rise during wetting of the flour samples, shown in Fig. 3, gives a clear idea of the course of wetting of the flour in the calorimeter.

An attempt was made to derive a mathematical expression for this temperature change. If Δt represents the temperature difference as the result of the reaction in time τ (minutes), the following three equations can be obtained with the aid of Newton's formula of divided differences:

1) For air-dry flour:

$$\Delta t = -0,1086 + 0,2415 \tau - 0,0129 \tau^2;$$

2) For flour heated to 120°:

$$\Delta t = -0,1300 + 0,2150 \tau - 0,0100 \tau^2;$$

3) For flour heated at 150°:

$$\Delta t = -0,0810 + 0,1330 \tau - 0,0020 \tau^2,$$

The calorimetric vessel (Fig. 2) was designed so that the test substance and the calorimetric liquid (distilled water) could be brought into contact without introduction of any auxiliary devices into the calorimetric vessel.

The temperature change (Δt) as the result of the reaction was found from the difference between two thermometer readings: the highest at the end of the reaction and the last before the start. The temperature correction for heat transfer to the surroundings during the reaction (x_t) was calculated from the formula [7]:

$$x_t = \frac{x_1 + x_2}{2} n,$$

where x_1 and x_2 are the approximate values of the mean temperature fluctuations before and after the reaction, and n is the number of temperature readings during the reaction; x_1 and x_2 , found by division of the difference between the first and eleventh thermometer readings by the number of 30-second intervals did not exceed 0.005°, which shows that the thermal operation of the calorimeter was normal.

We were unable to determine the water-binding capacity of air-dry flour, as its wetting was not complete with the type of stirrer used in the calorimeter. Accordingly, the water-binding capacity of flour dried to constant weight at 105° was determined (see table).

According to Dumanskii [4], flour dried at 80-90° under vacuum can bind 34% of water. Therefore even such mild heat treatment as drying at 105° decreases the water-binding capacity of flour by not less than 30%. If flour is heated to 120 and 150°, the water-binding capacity is lowered by at least 46 and 50% respectively.

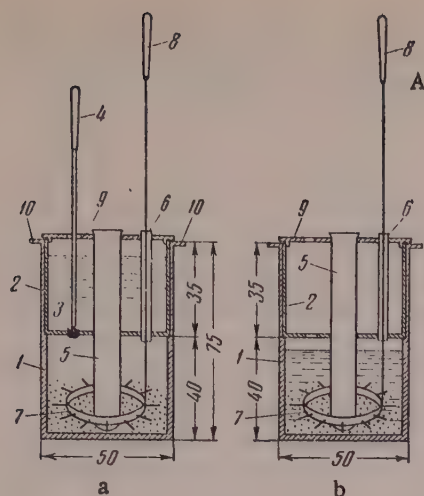


Fig. 2. Calorimetric vessel: a) position before reaction; b) position during reaction; 1) main cylinder; 2) second brass cylinder; 3) cork with handle 4; 5) thin sheet-steel tube for Beckmann thermometers; 6) tube for stirrer; 7) stirrer with handle 8 made from a good insulator; 9) brass cover for calorimetric vessel; 10) projecting edges by which the calorimeters are held in the protecting container.

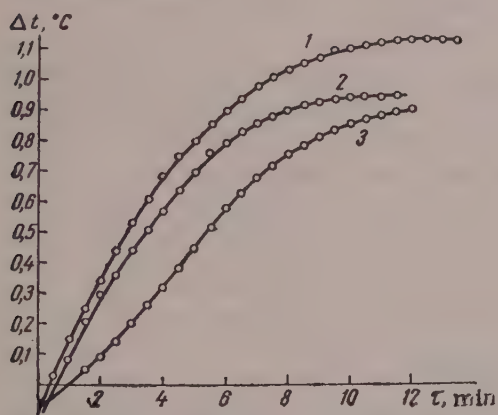


Fig. 3. Rise of temperature in the action of water on flour: 1) dried at 105°; 2) heated to 120°; 3) heated to 150°.

These equations were tested for all values of τ from 0.5 to 16 minutes. They were found to be applicable during the first 11 minutes of the experiment. During this period the calculated and experimental values of Δt coincided exactly. These formulas can be used to check the accuracy of the experimental data and to simplify experimental procedure in determination of heats of wetting of flour and similar materials in a calorimeter.

The presence of soluble substances does not have any significant influence on the results of the determinations. The total contents of water-soluble substances were 7.0% for flour heated to 120° and 6.4% for flour heated to 150° (calculated on the dry substance); these are lower values than those found for wheat flour (9.4-12.0%) investigated earlier by Dumanskii [4], in whose experiments 20-30% of the total amount of water-soluble substances in flour went into solution.

In view of the conditions in which heated flour is used, it was of interest to find how the viscosity of flour suspensions varies when they are heated from 20 to 100°.

The viscosities of 4.5% suspensions of air-dry and heat-treated flour were determined in an Ostwald viscosimeter ($\tau_{H_2O} = 3.8$ seconds at 20°) by the method [12] recommended for suspensions. The results are presented in the form of graphs in which τ (the efflux time in the viscosimeter) is plotted against the suspension temperature t (Fig. 4).

It is known that suspensions of starch in cold water have very low viscosity, which increases in direct proportion to the concentration. On increase of temperature the viscosity falls at first and then begins to rise (usually at about 60°). This increase of viscosity at higher temperature is due to paste formation.

The viscosity of an aqueous suspension of air-dried flour is so high even at 50-60° that it cannot be determined in the Ostwald viscosimeter.

Aqueous suspensions of flour previously heated to 120 and 150° respectively behave differently on increase of temperature (Fig. 4). In the first of these, starch is converted into paste, as is shown by a temperature range corresponding to a viscosity minimum followed by a steep rise of viscosity at 80-90°. The viscosity of the second suspension falls somewhat with increase of temperature and remains constant in the 80-90° range.

Heating temperature, °C	Heat of wetting, cal/g	Amount of bound water, %	Moisture content, % on dry substance
120	14,8	18,56	2,16
150	13,51	16,89	2,95
105 (dried to constant weight)	18,63	23,29	0

This large difference between the viscosity changes with temperature in the investigated suspensions is the result of differences in the state of the starch grains in them after the flour has been heated to 120 and 150° respectively [13-14]. Heat treatment at 150° breaks down the native structure of the starch grains to such an extent that they all lose their capacity to form a paste.

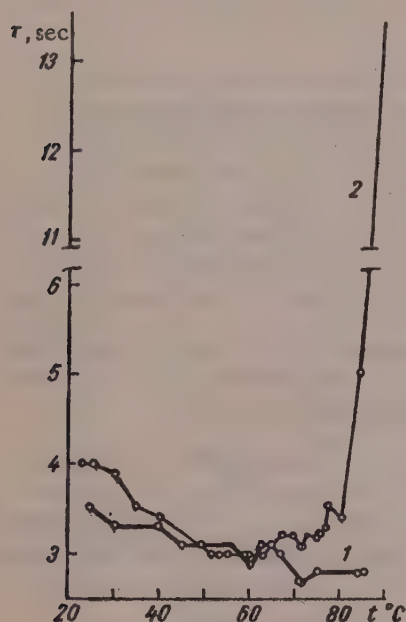


Fig. 4. Viscosity variations of 4.5% suspensions of heat-treated flour when heated from 20 to 100°: 1) flour heated to 150°; 2) flour heated to 120°.

SUMMARY

If first-grade wheat flour is heated to 120 and 150° respectively the hydrophilic property is lowered to almost the same extent, but the native structure of the starch grains is broken down to different degrees. In the former case starch grains capable of paste formation remain, whereas flour heated to 150° does not contain such grains. In consequence of this the viscosity of suspensions of flour heated to 120° rises sharply in the 80-90° range whereas the viscosity of suspensions of flour heated to 150° remains unchanged.

LITERATURE CITED

- [1] A. G. Kul'man, Colloids in Bread Baking [in Russian] (1941).
- [2] A. G. Kul'man, Soviet Flour Milling and Bread Baking [in Russian] (1936) p. 39.
- [3] A. G. Kul'man and E. P. Strukova, Proc. 2nd Conference on Colloid Chemistry [in Russian] (Acad. Sci. Ukrainian SSR Press, Kiev, 1950).
- [4] A. V. Dumanskii and E. F. Nekrvach, Kolloid Zhur. 13, 20 (1951); 17, 168 (1955).*
- [5] V. A. Koltygin, Dissertation [in Russian] (Moscow, 1951).
- [6] S. M. Skuratov, Kolloid Zhur. 13, 396 (1951); 9, 133 (1947).
- [7] M. M. Popov, Thermometry and Calorimetry [in Russian] (Izd. MGU, 1954) p. 356.
- [8] Ya. S. Bezikovich, Approximate Calculations [in Russian] (State Trade Press, 1949) p. 107.
- [9] S. M. Lipatov, Physical Chemistry of Colloids [in Russian] (Goskhimizdat, 1948) p. 79.
- [10] S. M. Lipatov, B. Sh. Kartsovnik, and L. V. Babich, Kolloid Zhur. 10, 349 (1948).
- [11] S. M. Lipatov, Science of Lyophilic Colloids [in Russian] (Minsk, 1941).
- [12] I. N. Putilova, Handbook of Practical Colloid Chemistry [in Russian] (Goskhimizdat, 1943) p. 143.
- [13] V. I. Nazarov, N. P. Silina, and T. P. Tikhomirova Kolloid Zhur. 20, 465 (1958).*
- [14] V. Katz and Weidinger, Z. phys. Chem. 184, 188 (1939).

Received April 14, 1958

* Original Russian pagination. See C. B. Translation.

DILATOMETRIC INVESTIGATIONS OF GELATIN GELS

S. I. Meerson and N. N. Puchkova

The Moscow Textile Institute

Thermochemical investigations of the liquefaction of gelatin gels over a wide range of temperatures [1] show that transition of a gel into the liquid state occurs in a fairly narrow temperature range and is accompanied by absorption of heat which may be regarded as heat of fusion. Dilatometric studies of 60% gelatin gel [1] confirm the thermochemical data and demonstrate the existence of a volume effect in the fusion of the gel.

This paper contains more detailed results of dilatometric investigations on gelatin gels of different concentrations*.

The determinations were performed in glass dilatometers without stoppers and with ground-glass stoppers. The dilatometer without a stopper was a cylindrical vessel with a measuring capillary sealed to the top end. The dilatometer was filled with the substance through the lower orifice, which was then sealed. It was then connected to a vacuum pump and a mercury reservoir by means of a two-way cock. After evacuation the dilatometer was gradually filled with mercury. These dilatometers are convenient for use with gelatin either in the dry state or containing small amounts of water. The distinguishing feature of the dilatometers with the ground-glass stoppers was that the measuring capillary was sealed to the lower end of the cylindrical vessel and curved upward. The radii of the measuring capillaries did not exceed 0.2-0.3 mm. The capillaries had been previously calibrated. The mercury level in the capillaries was read off to the nearest 0.2 mm. The filled dilatometers were kept in a thermostat at the given temperature ($\pm 0.05^\circ$) until the equilibrium volume was reached. The height of the mercury in the capillary was measured continuously, starting at 14° , for each $1-2^\circ$ rise of temperature. Because of the long time of volume relaxation of the gel, at low temperatures control experiments were carried out in which the dilatometers were kept at the given temperature for 5-6 hours.

It was observed that a second heating of a cooled gel does not alter the form of the volume - temperature curve, but the whole curve lies lower, i.e., the system contracts. Cooling after a second heating again leads to contraction. An equilibrium curve can be obtained only after several consecutive heatings. The gelation and fusion processes are reversible, but the time required to reach equilibrium on gelation increases. All the results presented below refer to equilibrium experimental conditions.

Gels of 12.5, 20, 40, 60 and 66% concentration and air-dry gelatin were studied. In calculations of the volume expansion, given by the height of the mercury level in the capillary, corrections were applied for the volume expansion of free water in the gel, the glass, and mercury.

Since 1 g of gelatin binds 0.30 g of water with liberation of heat, if the weight and concentration of the gel in the dilatometer is known the amount of free water in the gel and its coefficient of volume expansion can be calculated.

Thus, the changes in the height of the mercury in the dilatometer capillary were calculated for the hydrated gelatin in the gel and not for the gel.

* These results were presented together with the earlier data [1] at the Scientific Conference of the Moscow Textile Institute in October 1957, and at the All-Union Conference on Colloid Chemistry in May 1958 (in Tbilisi).

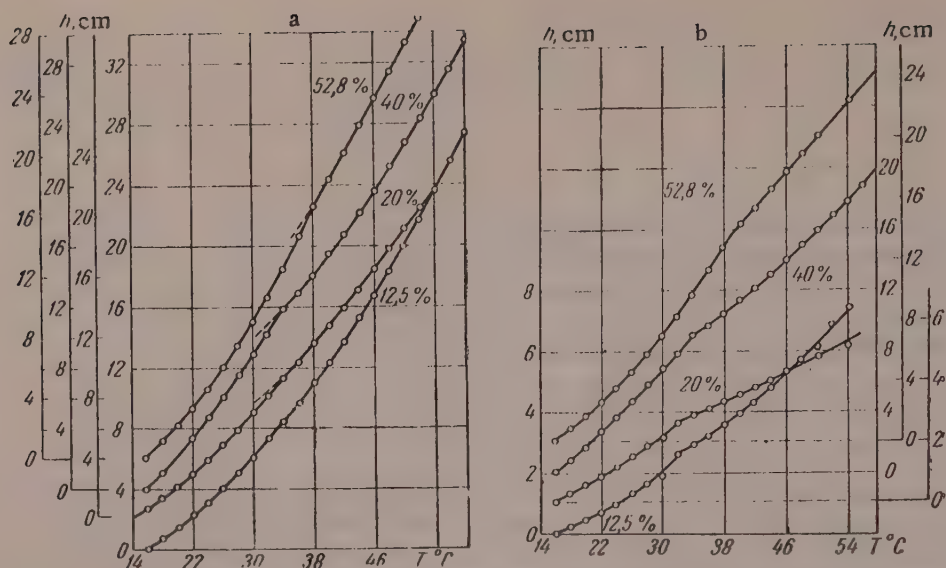


Fig. 1. Volume - temperature relationships for gelatin gels of different concentrations (in %) without a correction (a) and with a correction (b) for volume expansion of water.

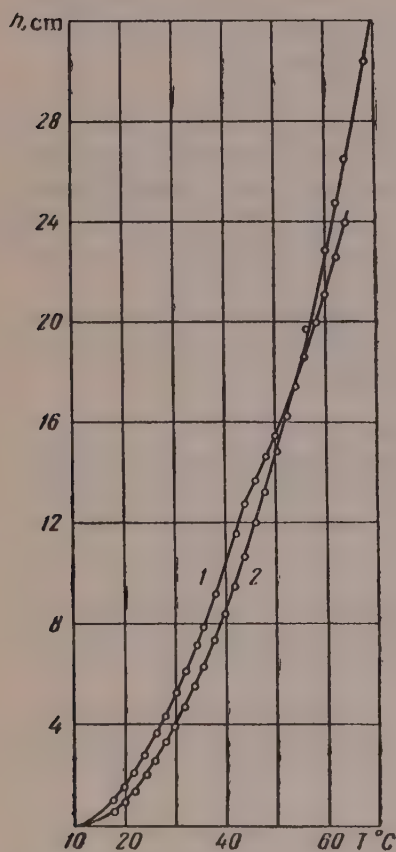


Fig. 2. Volume - temperature relationships: 1) 66% gelatin; 2) air-dry gelatin.

Figure 1,a shows variations of the height of the mercury level in the capillary with the temperature for 12.5, 20, 40, and 52.8% gels without a correction for the volume expansion of water; Fig. 1,b shows the corresponding curves with the appropriate correction. It follows from Fig. 1 that this correction is especially important in experiments with 12-20% gels. For example, correct graphical interpretation of the curve for 12.5% gel is impossible without this correction. This accounts for the erroneous nature of the $V = f(T)$ graph in our earlier paper [2]. On further dilution of the gels ($c < 12\%$) the correction for the volume expansion of water becomes so large that nearly all the volume expansion of the system is due to non-linear expansion of water, so that the volume changes corresponding to the hydrated polymer lie within the limits of experimental error. It follows that dilatometric data for relatively dilute gels, determined by the method described, cannot give a correct picture of the volume changes in the structural network of the gel during fusion.

The volume - temperature curves are of the form characteristic for polymer fusion, but the volumetric effect of melting is very small. The breaks on the curves correspond to the melting temperatures of the gels, T_m , determined both visually and from $Q = f(T)$ curves where Q is the heat of solution of the gel in urea solution [1]. The higher the gel concentration, the higher the melting temperature. The volume - temperature curve for air-dry gelatin does not have any characteristic points in the investigated temperature range (Fig. 2). It follows that to melt gelatin it is necessary to introduce a certain amount of water in order to overcome the more stable bonds. This is in agreement with the results of our thermochemical investigations, which showed that dry gelatin and

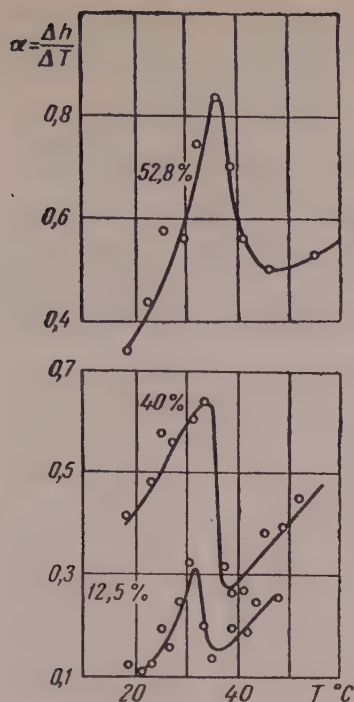


Fig. 3. $\alpha = f(T)$ relationships for gelatin gels of different concentrations (%).

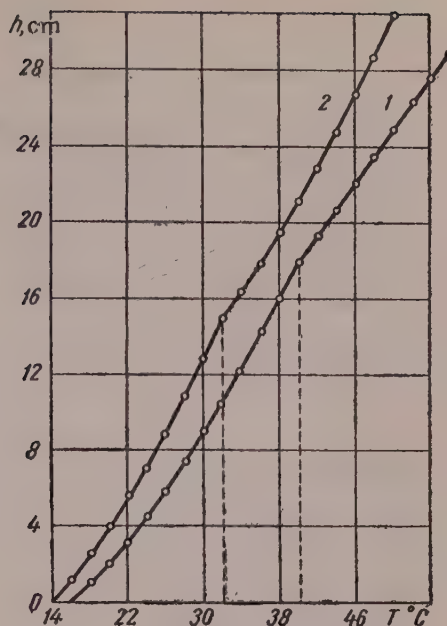


Fig. 4. Volume - temperature relationship: 1) for 60% gelatin gel in water; 2) same gel in 8M urea solution.

hydrated gelatin containing less than 30% water have negative temperature coefficients of their heats of solution in urea solution, whereas for gels $dQ/dT > 0$.

The results were used to calculate the temperature coefficients of volume expansion of the gels $\alpha = dh/dT$; these are plotted against the temperature in Fig. 3. Figure 3 shows that α passes through a small maximum which corresponds to the melting range of the gels. This maximum is found at lower temperatures with decrease of the gel concentration.

The volume effect of melting becomes more pronounced with decrease of the temperature at which the gel is formed and of the initial measurement temperature. Therefore with relatively dilute gels (15 and 20%) the measurements should not be started at 20° and higher, as was done in an earlier investigation [3]; this error led to incorrect graphical interpretation of the volume - temperature curve, and absence of corrections for the volume expansion of glass, mercury, and free water also contributed to this.

In the paper cited the volume - temperature relationship is represented in the form of two intersecting straight lines, the first of which has a less steep slope than the second. Variations of α are plotted in the form of a curve with a maximum, although clearly this cannot be true if the volume - temperature relationship is in fact represented by two intersecting straight lines. These data led the author to the erroneous conclusion that there is no volume effect of gelation. Neiman [4] found that addition of urea to gelatin gels does not influence the nature of the $\alpha = f(T)$ curve and that the maximum value of α is found at the same temperature. However, this is contrary to experimental data on the effect of urea on the properties of gelatin gels. To check these results we prepared a 60% gelatin gel in water and in 8 M urea solution. The resultant variations of the mercury level in the capillary and of α with the temperature, plotted in Fig. 4 and 5, showed that in presence of urea the melting temperature of the gel fell from 40° to 32°. Calculation of the heats of fusion of the gels by the equation

$$\log c = -\frac{\Delta H}{2,3RT} + \text{const}$$

(where c is the concentration of the gel and T is the fusion temperature) showed that urea has a significant effect on the heat of fusion of gels, lowering it almost 10-fold (see table).

Effects of Urea on Heat of Fusion and Temperature of Fusion of 60% Gelatin Gels

Gelatin gel in water			Gelatin gel in 8 M urea solution		
c, %	T _m , °C	ΔH, kcal/mole	c, %	T _m , °C	ΔH, kcal/mole
5.0	300.0	~50	30.2	290.7	~5
10.0	302.0		37.2	297.3	
20.0	305.2		44.7	304.0	
40.0	307.3		53.0	305.3	

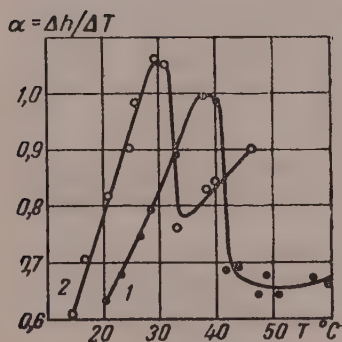


Fig. 5. $\alpha = f(T)$ relationship:
1) for 60% gelatin gel in water;
2) same gel in 8M urea solution.

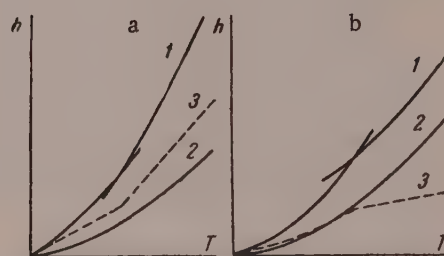


Fig. 6. Effect of volume expansion of water on the volume - temperature relationship; schematic curves: 1) for gel; 2) for water; 3) for gel after correction for volume expansion of water.

Graphical analysis of volume - temperature curves for gelatin gels shows that this relationship cannot be represented either by a straight line or by two intersecting straight lines. This follows from the fact that introduction of a correction for volume expansion of free water would in such cases lead to absurd volume - temperature curves calculated for 1 g of hydrated polymer. In the former case this relationship is represented by a curve convex toward the temperature axis and tending to cut the latter; in the latter case there are two intersecting curves convex toward the same axis.

If the volume - temperature relationship for a gel is represented by a convex curve, then introduction of a correction for expansion of free water would not result in any breaks in the curve. Introduction of a correction for volume expansion of water in the volume - temperature curves given in Fig. 6,a and 6,b, curves 1, gives volume changes observed in second-order transition or fusion of polymers (curves 3). Our experimental data correspond to fusion curves (Fig. 6,b).

SUMMARY

1. In analysis of dilatometric data on gelatin gels over a wide range of temperatures and concentrations (especially in the case of dilute gels) a correction for expansion of free water should be introduced in addition to corrections for volume expansion of glass and mercury.
2. Introduction of urea into gelatin gels lowers the melting temperature and the heat of fusion of the gels, and shifts the maximum of the temperature coefficient of volume expansion of the gels toward lower temperatures.
3. The form of the volume - temperature curves indicates that melting of gels is accompanied by a volume effect.

The authors thank Member of the Academy of Sciences Belorussian SSR Prof. S. M. Lipatov for his constant interest in the work and for discussion of the results.

LITERATURE CITED

- [1] S. I. Meerson and S. M. Lipatov, *Kolloid. Zhur.* 20, 353 (1958).*
- [2] S. M. Lipatov and S. I. Meerson, *Kolloid. Zhur.* 19, 390 (1957).*
- [3] R. É. Neiman, *Kolloid. Zhur.* 14, 107 (1952).*
- [4] R. É. Neiman, *Kolloid. Zhur.* 16, 201 (1954).*

Received November 11, 1958

* Original Russian pagination. See C. B. Translation.

INFLUENCE OF ORGANIC SOLVENTS ON THE SOLUTION STATE OF DIRECT DYES AND ON THEIR RATE OF DIFFUSION IN CELLOPHANE FILM

B. N. Mel'nikov and P. V. Moryganov

The Ivanovo Institute of Chemical Technology, Department of the Chemical Technology
of Fibrous Materials

Addition of hydrophilic organic solvents such as pyridine and triethanolamine to dyebaths has a significant influence on the solution state of direct dyes. It was shown in a series of our earlier investigations [1-3] that such addition causes changes in the degree of dispersion of the dyes and of their affinity for the fiber. Changes of these properties influence the rates of diffusion of the dyes in cellulosic materials and the rates of dyeing as a whole, so that they are of great practical significance. However, because of the restricted range of organic solvents and of the lack of clarity in regard to the influence of solvent concentration on the solution state of direct dyes it was not possible to make definite generalizations concerning use of organic solvents as effective means for regulation of the dyeing process. The main purpose of the present investigation was to fill this gap. It was concerned with a study of the effects of various organic solvents on the solution state of direct dyes and on the diffusion rates of these dyes in cellophane film.

To determine the influence of organic solvents on association or disaggregation of the dye particles the coefficients of diffusion of their solutions through porous glass plates were determined. The rate of penetration of dyes into cellulosic materials in presence of various organic solvents in the dyebath was estimated from the coefficients of diffusion of the dyes in cellophane film. The experimental procedure was described previously [2, 3]. The coefficients of diffusion in solution were found from the equation:

$$\bar{D} \cdot \alpha = \frac{2\lambda}{(\lambda + 1) \tau} \cdot \log \frac{c_1}{c_1 - (\lambda + 1) c_2}, \quad (1)$$

where α is the calibration constant of the apparatus; τ is time; λ is the ratio of the solution volumes on the two sides of the plate; c_1 is the dye concentration (inner vessel) at the start (when the dye concentration in the outer vessel = 0); c_2 is the dye concentration in the outer vessel after time τ .

The coefficients of diffusion of dyes in cellophane film were calculated from the expression

$$\frac{ds}{dt} = -DA \frac{dc}{dx} \quad \text{or} \quad D = \frac{bP}{A(c_2 - c_1)}, \quad (2)$$

where $P = \frac{ds}{dt}$ is dye quantity diffused through the film in unit time (in mg/min.); b is film thickness (cm); A is film area (cm²); c_1 and c_2 are the dye concentrations on each side of the film (mg/cc).

All the experiments were performed with three direct dyes: Direct Sky-Blue K, Direct Diazo Black S, and Direct Pure Sky-Blue. The dyes were purified and analyzed by the methods described earlier [4]. The dye and electrolyte (common salt) concentrations were the same in all the experiments, 0.1 and 10 g per liter respectively. The only exceptions were experiments in which pyridine was used as the dispersing agent. In this case the sodium chloride concentration in solution was 70 g/liter with Direct Sky-Blue K and Direct Pure Sky-Blue, and 50 g/liter with Direct Diazo Black S. The following organic solvents were used as additives to the dye solutions: pyridine, monoethanolamine, diethylamine, and polyvinylpyrrolidone. All the solvents used were chemically pure. Polyvinylpyrrolidone was used in the form of 30% aqueous solution. The diffusion coefficients of the dyes in aqueous solutions were determined at 25°. This temperature was chosen because the experiments are more convenient to perform under such conditions and the accuracy of the determinations themselves is somewhat higher. In all probability, at higher temperatures the influence of organic solvents on the dispersion state of dyes is similar but less pronounced. Diffusion of dyes in cellophane film was studied at 40°, as at 25° in absence of organic solvents direct dyes do not diffuse at all, so that the results cannot be compared.

Average Coefficients of Diffusion of Direct Dyes Through Cellophane Film Under Equilibrium Conditions in Presence of Organic Solvents in Solution

Dye	Coefficients of diffusion in film $D \times 10^7, \text{cm}^2/\text{min}$ in presence of monoethanolamine, g/liter					
	0	5	10	25	50	100
	0,24	1,30	2,16	2,70	3,22	2,19
Direct Pure Sky-Blue	0,57	1,40	1,48	2,30	2,93	2,26
Direct Sky-Blue K	0,48	0,73	0,96	1,09	1,23	2,07
Direct Diazo Black S	in presence of diethylamine, g/liter					
	0	1	5	10	15	
Direct Pure Sky-Blue	0,24	1,32	2,95	5,44	3,74	
Direct Sky-Blue K	0,57	1,68	2,91	3,74	3,08	
Direct Diazo Black S	0,48	0,52	1,60	1,83	1,32	
	in presence of polyvinylpyrrolidone, g/liter					
	0	0,1	0,25	1,0		
Direct Pure Sky-Blue	0,24	0,51	0,71	0,13		
Direct Sky-Blue K	0,57	1,25	1,97	0,65		
Direct Diazo Black S	0,48	1,30	1,65	0,15		

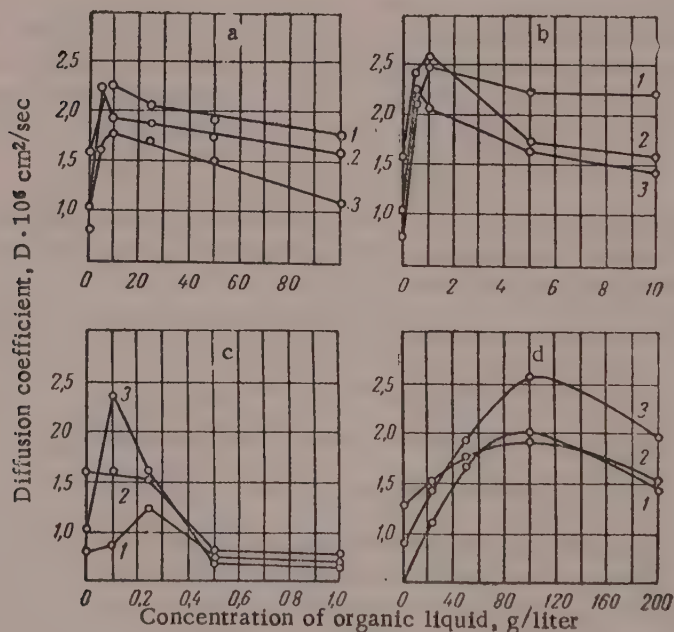


Fig. 1. Effects of monoethanolamine (a), diethylamine (b), polyvinylpyrrolidone (c), and pyridine (d) on the diffusion coefficients of direct dyes in solution: 1) Direct Pure Sky-Blue; 2) Direct Sky-Blue K; 3) Direct Diazo Black S.

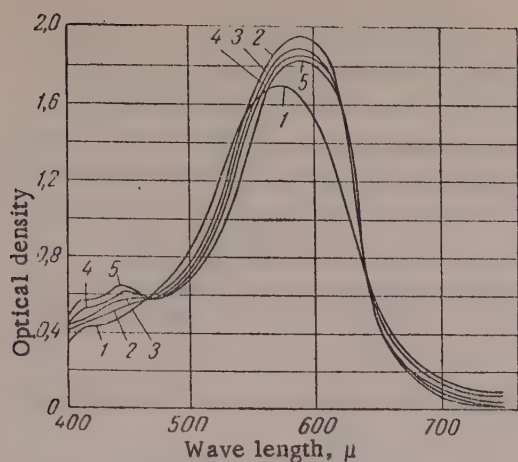


Fig. 2. Spectrophotometric curves for Direct Diazo Black S: 1) aqueous solution; 2, 3, 4, and 5) with pyridine at concentrations of 10, 25, 50, and 75% respectively.

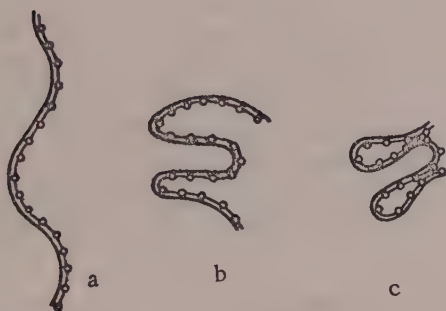


Fig. 3. Schematic representation of the formation of complexes of polyvinylpyrrolidone with direct dyes: a) at low concentrations of polyvinylpyrrolidone; b) at moderate concentrations; c) at high concentrations.

to the results of physicochemical investigations, lead to increased association of the dyes in solution. With decrease of the degree of association of the dye molecules the number of absorbing centers increases, and this leads to a relative increase of the long-wave maximum.

Thus, variations of the ratio between the absorptions in the long- and short-wave regions of the spectrum reflect changes in the degree of association in the dye solution and can therefore serve as a measure of such changes [6]. It may be seen in Fig. 6 that the absorption curve for the aqueous solution of the dye has a subsidiary, although weak maximum in the short-wave region of the spectrum. With 10% pyridine this maximum is entirely absent, but it reappears on increase of the pyridine concentration from 25 to 75%. In the long-wave region of the spectrum the absorption maxima become more pronounced with 10% pyridine, but as the pyridine concentration in solution is increased they approach in magnitude to the absorption maximum for aqueous solutions of the dye. This, like the results of diffusion determinations, indicates that when organic solvents are introduced into the dye solutions the dyes are first dispersed and then aggregated.

The bathochromic shift of the absorption maxima for direct dyes in presence of organic solvents in solution also indicates that interaction occurs between the substances in question. This view is confirmed by the results of investigations [7-10] in which it was shown convincingly that interaction of direct dyes with a number of substances is associated with bathochromic shifts of the absorption maxima.

The results are presented in Fig. 1 and 2 for diffusion in solution, and in the table for diffusion in cellophane film.

It follows from the data in Fig. 1 that introduction of organic solvents into the solutions increases the coefficients of diffusion. In each case there is an optimum addition of organic solvent at which the coefficient of diffusion of the dye in solution is highest. This means that above and below this concentration the size of the diffusing particles increases.

In our opinion, this type of variation of the diffusion coefficients in solutions indicates that interaction occurs between the direct dyes and organic solvents. Incorporation of organic solvent molecules in large aggregates of dye anions and formation of solvation layers around the latter increases the degree of dispersion of the dye particles. However, with increase of the organic solvent concentration the thickness of the solvation layers around the dye anions gradually increases. This leads to a decrease of the diffusion coefficients of the dyes in solution.

The above views are confirmed to some extent by data on the absorption spectra of direct dyes in pyridine solution and in water. As an example, Fig. 2 shows spectrophotometric curves for Direct Diazo Black S. The curves for all the other dyes are of a similar character and relative configuration. The determinations were performed in the SF-2M recording spectrophotometer at dye concentrations of 30 mg/liter. Each spectroscopic curve has one or several maxima in the regions of visible light. One of the maxima is very pronounced, while the others, in the short-wave region, are weaker or may be entirely absent. Variations of concentration, temperature, and certain other conditions influence the ratio of the absorption maxima in the fundamental and subsidiary bands [5]. A relative increase of the short-wave maximum occurs as the result of changes which, according

The data presented in Fig. 1,a,b, and c indicate that the maximum dispersing effect of organic solvents is found at relatively low concentrations in solution. Fig. 1,d and 2 indicate that this is not true of pyridine. However, this is not because pyridine has a weaker dispersing effect on direct dyes, but because the dye solutions in this case were less stable owing to the much higher electrolyte concentrations (from 50 to 70 g/liter). It is obvious that under such conditions the dyes are much more highly aggregated and a higher concentration of pyridine in solution is required to disperse them. It follows that the optimum concentrations of organic solvents vary in accordance with the degree of aggregation of the dyes in solution.

In contrast to all the other organic solvents, polyvinylpyrrolidone accelerates the diffusion of direct dyes in solution over a very narrow concentration range only. This is because polyvinylpyrrolidone molecules are large and can form network structures [11] in which the dye molecules act as bridges, as shown schematically in Fig. 3.

These more complex formations evidently have very low mobility. Therefore the coefficients of diffusion of the dyes in solution decrease on increase of the polyvinylpyrrolidone concentration.

The somewhat peculiar effect of polyvinylpyrrolidone on Direct Sky-Blue K is probably due to the fact that in solutions free from organic solvents this dye is more finely dispersed than the others. This is also indicated by the coefficients of diffusion. Therefore addition of polyvinylpyrrolidone, even in very small amounts, to solutions of this dye does not favor dispersion but, on the contrary, leads to formation of particles larger than those present initially.

The presence of thick solvation layers around the dye anions hinders mutual attraction of the solvated particles, increases their affinity for the solvent, and lowers their affinity for the fiber. All this has a strong influence on the rates of diffusion of direct dyes in cellophane film (see table). Comparison of data on diffusion of direct dyes in solution and in cellophane film shows that a maximum increase of the diffusion rate of a dye in the film does not always correspond to the greatest effect of dye dispersion in solution. For example, the maximum coefficients of diffusion of Direct Pure Sky-Blue, Direct Sky-Blue K, and Direct Diazo Black S in solution are found at monoethanolamine concentrations of 5 and 10 g/liter respectively, whereas in diffusion in cellophane film this solvent has the greatest influence at a concentration of 50 g/liter for Direct Pure Sky-Blue and Direct Sky-Blue K, and at 100 g/liter for Direct Diazo Black S. Similar results are found for other organic solvents such as diethylamine.

The explanation of this peculiar influence of organic solvents is that migration of a dye in a cellulosic material is influenced considerably by the affinity of the dye for the active centers of the fiber, in addition to the particle size. It is natural to expect that the rate of diffusion should increase if the delay of the dye near the active centers of the fiber is diminished; in other words, if the affinity of the dye for cellulose is less. If this is taken into account it becomes understandable why the maximum increase of the diffusion coefficients of direct dyes in the film does not coincide with the most pronounced dispersing effect of organic solvents on the dyes. Evidently in some instances the retarding effect of the affinity of the dye for cellulose on diffusion in the film becomes very considerable, and therefore the coefficients of diffusion in the film increase greatly not at the instant of maximum dispersion of the dyes in solution but only after the rather thick solvation layers formed around the dye particles have greatly lowered the affinity of the dye to the fiber.

The increase, although very slight, of the coefficients of diffusion of direct dyes in cellophane film in presence of polyvinylpyrrolidone in solution is evidently due to the fact that the large aggregates of dye anions break down into separate smaller particles or even anions. The attachment of these anions to the chain molecules of polyvinylpyrrolidone is fairly labile, so that they are able to leave the latter and diffuse through the cellophane film. At the same time, at high concentrations of polyvinylpyrrolidone the concentration of free dye anions capable of diffusing through the film falls sharply, thereby lowering the coefficient of diffusion of the dye in the film. However, the uniformity of dyeing of the film nevertheless improves.

Intensification of dye diffusion within the fiber should be accompanied by an increase of the over-all dyeing rate. Preliminary experiments confirm this hypothesis. In all cases the rate of dyeing increases in presence of organic solvents in solution. This is especially prominent at low temperatures and short dyeing times. Moreover, addition of organic solvents to the dyebath increases uniformity of dyeing and improves through-dyeing of the cellulose material.

SUMMARY

1. The coefficients of free diffusion of three direct dyes in presence of pyridine, monoethanolamine, diethylamine and polyvinylpyrrolidone have been determined at 25°. The concentrations of the solvents were varied over a wide range.

2. When organic solvents are added to dye solutions the first effect is dispersion of the dyes owing to splitting of large aggregates and formation of solvation layers around the dye molecules. With subsequent increase of the organic solvent concentration the thickness of the solvation layers increases and thereby the particles as a whole become larger.

3. An attempt is made to explain the results obtained on the changes in the state of aggregation of direct dyes by the use of absorption spectra of the dyes dissolved in water and in aqueous pyridine mixtures.

4. The coefficients of diffusion of these dyes in cellophane film under equilibrium conditions and in presence of monoethanolamine, diethylamine, and polyvinylpyrrolidone in solution were determined at 40°.

5. The observed influence of organic solvents on the solution state of dyes also affects their diffusion in cellophane film. The diffusion coefficients are increased, on the average, 3 to 5-fold, but in some instances the decrease is more considerable (11 to 25-fold).

LITERATURE CITED

- [1] B. N. Mel'nikov and P. V. Moryganov, *Kolloid. Zhur.* 17, 99 (1955).*
- [2] B. N. Mel'nikov and P. V. Moryganov, *Trudy Ivanovskogo khimiko-tekhrol. in-ta* 8 (1958).
- [3] B. N. Mel'nikov and P. V. Moryganov, *Kolloid. Zhur.* 19, 689 (1957).*
- [4] B. N. Mel'nikov and P. V. Moryganov, *Trudy Ivanovskogo khimiko-tekhrol. in-ta* 5 (1956).
- [5] V. L. Levshin, *Photoluminescence of Liquids and Solids* [in Russian] (1951) p. 177.
- [6] Kh. L. Arvan, *Some Aspects of Dye Synthesis and Application*, Conference Proceedings [in Russian] (Goskhimizdat, 1956) p. 127.
- [7] G. Centola, *Bull. Inst. Text. France*, No. 63, 45 (1956).
- [8] G. Centola, *Review Textile* 54, 545 (1956).
- [9] G. Centola, D. Borrus and G. Prati, *Gazz. Chim. Ital.* 85, 1468 (1955).
- [10] T. Martin and H. A. Standing, *J. Textile Inst.* 40, T. 671 (1949).
- [11] H. P. Frank, S. Barkin and F. R. Elrich, *J. Phys. Chem.* 61, 1375 (1957).

Received September 29, 1959

*Original Russian pagination. See C. B. Translation.

INVESTIGATION OF THE STRUCTURE OF IRRADIATED POLYSTYRENE BY LIGHT-SCATTERING, OSMOMETRIC, AND VISCOSIMETRIC METHODS

I. G. Soboleva, N. V. Makletsova, and S. S. Medvedev

The L. Ya. Karpov Physicochemical Scientific Research Institute

It has been shown [1-3] that polymer branching can be estimated from determinations of molecular characteristics. We used a model branched polystyrene [4] to demonstrate that the structure of the molecular chains can be studied by correlation of the molecular weight and size of the molecules in solution as determined by light scattering. In the present investigation we were concerned with application of the light-scattering method to investigations of the structure of molecular chains of polymers subjected to γ -radiation.

It is known [5-8] that the action of γ -radiation on polymers results in extensive changes in the polymer chain structure owing to rupture of C-C and C-H chemical bonds. Either degradation of the molecular chains or formation of nonlinear molecules and spatial networks prevails, depending on the irradiation conditions and the nature of the radicals formed. When γ -radiation acts on polymer solutions, the products formed by decomposition of the solvents also take part in these processes.

For the purposes of the present investigation the polymer had to be completely or partially soluble after irradiation, with molecules in solution not smaller than 500 Å.

As the result of preliminary experiments polystyrene was chosen for the investigation, as it is one of the polymers which are most resistant to radiations.

In contrast to polystyrene, such polymers as polyisoprene and polymethylmethacrylate decomposed with a considerable decrease of molecular weight (Table 1) when acted upon by relatively small doses of radiation ($\sim 3 \cdot 10^6$ r) in 1% solution, so that the molecular size in solution could not be determined by the light-scattering method.

The molecular weight (from light scattering) and viscosity of polystyrene solutions were determined in toluene after twofold reprecipitation of the irradiated polymer. The results of experiments on which the choice of the irradiation conditions (radiation dose and solvent) for polystyrene were based are given in Fig. 1 and 2.

It follows from Fig. 1 and 2 that a radiation dose of $7 \cdot 10^6$ r produces only slight changes in the molecular characteristics of polystyrene. However, irradiation in dichloroethane greatly lowers the viscosity of polystyrene, probably because of incorporation of chlorine in the molecule. Increase of the radiation dose produced an increase of the average molecular weight in all solvents, with a simultaneous decrease of viscosity; this was especially prominent in dichloroethane.

It is known that the average molecular weight determined from light scattering is the weight-average value while \bar{z} is the average value. It follows that if the distribution function is unknown these values can be compared only for monodisperse systems. Therefore the subsequent investigations were performed with narrow polystyrene fractions. Polystyrene was irradiated in benzene solution at room temperature in absence of oxygen; the integral dose was $35 \cdot 10^6$ r. The polymer consisted of an average fraction (bulk polymerization at 20° in presence of 0.01 mole of benzoyl peroxide per liter) which could be separated into narrower fractions by fractionation from solutions containing 0.05 g/100 ml. The need for such high dilution was demonstrated by special experiments on fractionation of a solution made by mixing of two fractions ($M = 2.6 \cdot 10^6$ and $M = 0.36 \cdot 10^6$) one of which (with the lower molecular weight) contained labeled carbon, C^{14} .

TABLE 1

Changes of the Molecular Characteristics of Polyisobutylene and Polymethylmethacrylate Under the Influence of γ -Radiation

Polymer	Solvent (irradiation conditions)	Integral dose, $r \cdot 10^{-6}$	Molecular weight from light scattering, $M \cdot 10^{-6}$	Dissymmetry coefficient q	Intrinsic viscosity $[\eta]$, 100 ml/g
Polyisobutylene	-----	0	1080	1,42	7,6
	Hexane	0,72	260	1,10	1,15
	Heptane	1,44	180	1,00	—
Polymethylmethacrylate	---	0	3000	1,70	7,2
	Film	2,88	2000	1,58	2,7
	Benzene	2,88	990	1,27	1,55
	Dichloroethane	1,44	710	1,19	1,30

TABLE 2

Control Fractionation of a Mixture of Two Polystyrene Fractions

Fractions studied	Number of pulses per 3 minutes	Contents of polymer of low m. wt, %
Original mixture	1650*	16.9
Fraction of high molecular weight after first reprecipitation from solution, $c = 0.05$ g/100 ml	195	1.64
Fraction of high molecular weight after third reprecipitation from solution, $c = 0.05$ g/100 ml	0	0

* Calculated from the activity of the portion of low molecular weight.

The fractionation results are presented in Table 2. Complete separation was achieved after the third reprecipitation.

The irradiated polystyrene was fractionated as described above. The results of determinations of the molecular characteristics of narrow fractions isolated from 1% polystyrene solution in benzene before and after irradiation are given in Table 3.

The molecular-weight distribution curves (Fig. 3 and 4) show that irradiation results in a considerable broadening of the distribution. Fractions of lower molecular weight are predominant. The root mean square radius of the molecules in solution decreases somewhat after irradiation. The intrinsic viscosity of irradiated polystyrene fractions is also somewhat lower than that of the original polystyrene fractions. The decrease in the size of the molecules in solution, as indicated by direct determinations of light scattering and by the viscosity decrease, is evidence of molecular chain branching. The ratio of the radius of a linear polystyrene molecule to the radius of an irradiated molecule of the same molecular weight varies from 1.2 to 1.6, possibly owing to different degrees of branching. However, the interpretation of these data may be ambiguous because of the anomalously high polydispersity of the fractions (such as fractions 5 and 7, Table 3) found despite the careful fractionation. The simultaneous precipitation of molecules of different molecular weights from solution serves as indirect evidence of differences in their structure.

The explanation that the polystyrene fractions have a higher content of products of low molecular weight (40%) than of high (15%) after irradiation may be that the polymeric radicals formed as the result of rupture of

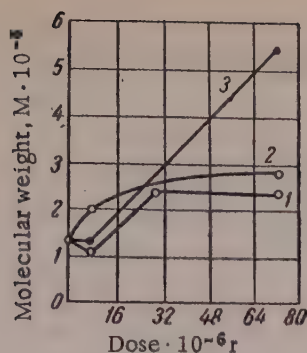


Fig. 1. Effect of radiation dose on the molecular weight of polystyrene, irradiated in 1% solution: 1) in dichloroethane; 2) in cyclohexane + 4% benzene; 3) in dichloroethane.

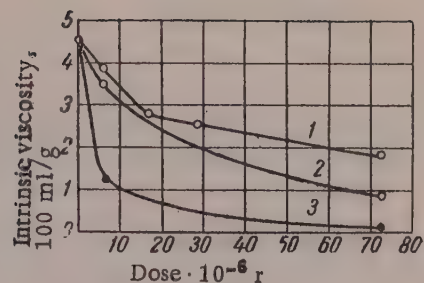


Fig. 2. Effect of radiation dose on intrinsic viscosity of toluene solutions of polystyrene, irradiated in 1% solution: 1) in benzene; 2) in cyclohexane + 4% benzene; 3) in dichloroethane.

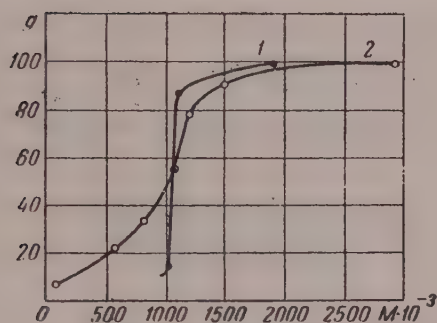


Fig. 3. Integral molecular weight distribution curves for polystyrene: 1) original polystyrene; 2) irradiated polystyrene.

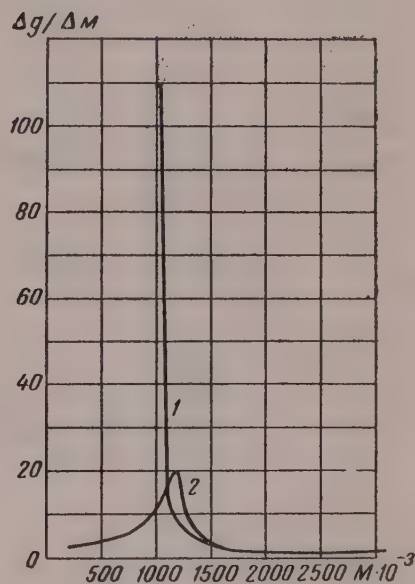


Fig. 4. Differential molecular weight distribution curves for polystyrene: 1) original polystyrene; 2) irradiated polystyrene.

C-C bonds are mainly lost under these conditions by interaction with the solvent and with the degradation products of low molecular weight. Branched molecules are formed in solution under the influence of γ -radiation as the result of recombination of polymeric radicals.

Recombination of polymeric radicals occurs to a slight extent even in highly dilute solutions. The proportion of polymer of low molecular weight which entered into molecules of high molecular weight as the result of recombination was estimated in special experiments with radioactive polystyrene. A mixture of equal amounts of polystyrene fractions with molecular weights of $1.5 \cdot 10^6$ and $0.3 \cdot 10^6$ was irradiated in film form (dose $18.2 \cdot 10^6 r$) and in benzene solution containing 0.3 g/100 ml (dose $29.0 \cdot 10^6 r$). The polystyrene of low molecular weight contained labeled carbon (C^{14}), and it was thus possible to follow the fractional distribution of this component of the original polymer. The fractional composition, in weight percentages, of the original polymer and the polymer after irradiation in film form and in solution is given in Table 4.

Table 4 also shows the fractional distribution of the low molecular weight portion of the original polymer ($M = 0.3 \cdot 10^6$) after irradiation.

TABLE 3

Molecular Characteristics of Fractions Isolated From Polystyrene Before and After Irradiation

Polystyrene fractions	Contents, %	Molecular weight, $M \cdot 10^{-3}$		Root mean square radius in toluene, $r, \text{\AA}$	Intrinsic viscosity $[\eta]$, 100 ml/g
		by light scattering	osmotic method		
Not irradiated					
1	11,6	2300	—	600	5,2
2	4,0	1500	—	—	4,5
3	70,0	1360	—	390	3,6
4	14,4	1000	—	390	3,2
Irradiated					
1	7,6	2900	—	450	4,80
2	12,5	1450	—	420	2,90
3	24,1	1200	—	370	3,50
4	9,8	1050	—	—	2,70
5	11,1	1000	400	360	2,25
6	12,0	820	785	—	2,45
7	15,0	570	275	—	1,90
8	7,2	—	80	—	1,33
9	0,7	—	67	—	—

TABLE 4

Fractional Distribution of Radioactive Polystyrene of Low Molecular Weight in Accordance With Irradiation Conditions

Fraction No.	Molecular weight $M \cdot 10^{-3}$	Original polystyrene			Polystyrene irradiated in film form			Polystyrene irradiated in benzene solution ($c = 0.3 \text{ g/100 ml}$)		
		fractional composition, %	number of pulses	content of radioactive polymer, %	fractional composition, %***	number of pulses*	content of radioactive polymer, %	fractional composition, %***	number of pulses*	content of radioactive polymer, %
1	4000	—	—	—	38,5	1524	32,0	—	—	—
2	2500	—	—	—	—	—	—	17,1	390	8,2
3	1500	50	0	0	—	—	—	—	—	—
4	300**	50	4756	100	—	—	—	—	—	—
5	200	—	—	—	43,2	3272	68,8	—	—	—
6	80	—	—	—	—	—	—	40,1	2654	55,6
7	50	—	—	—	4,7	3058	64,0	37,8	1898	39,8
Losses		—	—	—	3,6	—	—	5,0	—	—

* Pulse counts for 2 minutes.

** Radioactivity of the fraction taken as 100.

*** The polymer contained 10% of insoluble material.

Thus, the amount of polystyrene of low molecular weight which entered as a component of molecules of molecular weight $2.5 \cdot 10^6$ on irradiation in dilute solution was 1.4% of the original mixture or 2.8% of the component of low molecular weight.

An interesting feature is the presence of an appreciable amount (4.7%) of polymer of low molecular weight in polystyrene irradiated in film form. This is probably mainly due to interaction of hydrogen split off with the polymeric radicals.

SUMMARY

1. When γ -radiation acts on a narrow fraction of linear polystyrene dissolved in benzene ($c = 1.0$ g/100 ml) the molecular weight distribution is broadened considerably and the molecular chains lose their linear structure.

2. Labeled polystyrene (with C^{14}) was used to demonstrate the extent of the participation of polystyrene of low molecular weight in formation of large molecules in dilute solutions (by recombination of polymeric radicals) under the influence of γ -radiation.

LITERATURE CITED

- [1] B. Zimm and W. Stockmayer, *J. Chem. Phys.* 17, 1301 (1949).
- [2] V. N. Tsvetkov, *Doklady Akad. Nauk SSSR* 78, 1123 (1951).
- [3] H. Benoit, *Compt. rend.* 240, 533 (1955).
- [4] I. G. Soboleva, N. V. Makletsova, and S. S. Medvedev, *Kolloid Zhur.* 19, 619 (1957).*
- [5] A. Charlesby, *Research* 8, 288 (1955).
- [6] E. J. Lawton, A. M. Beuche, and J. S. Balwit, *Nature* 172, 76 (1953).
- [7] A. Henglein, M. Boysen, and W. Schnabel, *Z. phys. Chem.* 10, 137 (1957).
- [8] E. D. Kunst, *Recueil. trav. chim.* 69, 125 (1950).

Received August 13, 1958

*Original Russian pagination. See C. B. Translation.

THE STATES OF AGGREGATION OF HIGH POLYMERS

5. TYPES OF PACKING OF MACROMOLECULES IN CONDENSED PHASES

S. I. Sokolov and R. I. Fel'dman

The Moscow Institute of Chemical Equipment Construction

The N. K. Krupskaya Moscow Regional Pedagogic Institute

The states of aggregation [1, 2] of high polymers are characterized not only by the coordination and packing of the individual chain segments or primary structural elements, but also by what may be termed chain packing. This term is taken to mean the mutual spatial orientation of large regions of the chains in a particular configuration. Most of the schematic representations of chain arrangement in systems with a polycrystalline structure or in amorphous systems which have signs of order in individual microregions, given by various authors, show parallel chain orientation in some regions and random arrangement in others. In general, if the chain packing is to some extent ordered, a segmentary character of chain packing is postulated. In our present state of knowledge these general concepts may be regarded as acceptable. However, here we wish to focus attention on one aspect which is usually avoided and is discussed only in a few special cases as a matter of independent interest. The point is that ordered regions may be composed either of segments of different chains or of segments of the same chain if this is long enough. We consider that either situation may arise in practice. Therefore two main types of chain packing may be recognized: in the first type each chain passes through a series of ordered and random regions, roughly in the same direction, and if the direction does change this occurs without sharp turns leading to return. This may be named the rectile type of chain packing (rectus, straight). In the second type of packing the chains turn in the reverse direction at individual points, forming folds of various extents; this may be named the flexural type of chain packing (flexuralis, folded).

The ability of chain molecules to form folds with parallel arrangement of the individual portions under favorable conditions can hardly be doubted. For example, it is known that the molecule of oleic acid in a saturated monomolecular adsorption layer occupies twice the area occupied by a molecule of a saturated fatty acid [3]. The explanation is that the oleic acid molecule is folded in half lengthwise.

The presence of folds in crystallizing high polymers was established, on the basis of structural investigations, by Storks for gutta-percha [4] and by Keller [5] for polyethylene. In these cases we have a well-defined flexural type of chain packing in the crystalline regions. Numerous observations of the behavior of chain polymers, especially in the stretched state, provide what in our view is very convincing, even if indirect, evidence of the existence of flexural packing in many other polymeric systems.

It must be pointed out that ordered regular folds, which constitute the most typical and interesting case, may be of two different types: microperiodic and macroperiodic. We apply the term microperiodic to folds consisting of a small number of monomer units each. Their main feature is that as the result of unfolding under the influence of any factor, such as mechanical stretching, a new structure is formed, which gives a different pattern in x-ray and electron-diffraction analysis. Macroperiodic folds, with the same arrangement of segments along their length as in extended and parallel chains, do not give rise to structures differing in their diffraction patterns from those found in their absence.

The formation of folds with a short-range period was postulated in many instances if the materials under investigation gave different x-ray patterns after definite treatments in conjunction with mechanical stretching.

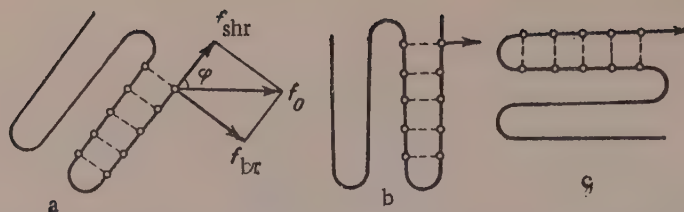


Fig. 1. Action of a tensile force with different fold orientations

The classic example of this is the natural protein material keratin, studied in detail by Astbury [6]. Keratin can exist in three modifications which differ in their x-ray diffraction characteristics. Astbury postulated that they differ in the configuration of the polypeptide chains. The β -modification is considered to consist of fully extended chains, the α -modification has chains with small regular folds, and supercontracted chains have somewhat deeper folds. Similar views have been advanced with regard to other polypeptides [7].

When one modification of gutta-percha passes into the other, a similar unfolding of microperiodic folds apparently takes place, with a change in the x-ray pattern.

If we do not confine ourselves only to consideration of highly-ordered regular folds in polymers, then we can find indirect evidence that elements of a flexural type of chain packing can also be found in polymers which do not crystallize but have many features in common with crystallizing polymers. For example, some amorphous polymers such as polystyrene exhibit under certain conditions the effect of "neck formation" during extension, typical of crystallizing polymers, and when in the glassy state have the so-called "enforced" elasticity [8], strongly reminiscent of "cold drawing" in polyamides and similar polymers.

Finally, the concept of folds of an even lower degree of order, mobile, and constantly varying under the influence of thermal motion, has long been used to account for the structure of polymers in the high-elastic state, when they have rubberlike properties. In such cases chain coiling with formation of random folds and the ability of the chains to uncoil under the influence of external tensile forces is associated with the important role of thermal motion. Coiling is considered as an entropy effect, i.e., transition of the chains into a more probable state under the influence of thermal motion.

However, as is clear from the foregoing, the present discussion is concerned with formation of folds with some measure of order, mainly macroperiodic. This effect should be regarded as the result of the action of forces of attraction between monomer units of neighboring segments of the same chain, i.e., as an energy effect. Formation of folds of this type is accompanied by a decrease of entropy. Most probably random folds formed as the result of thermal motion form the basis for formation of a set of organized folds (a flexural aggregate).

The presence of a macroperiodic flexural type of chain packing, not detected directly by X-ray or electron diffraction, may be revealed by a number of particularly "sensitive" properties which reflect structures of this type. Foremost in this respect is the behavior of such materials during deformation. It is known that certain polymers, when in the glassy or partly crystalline state, can increase their linear dimensions severalfold in the direction of the extension axis without destruction.

The extension λ , which is the ratio of the length l of the extended specimen to the initial length l_0 , can be as much as 4-5, and in some instances reaches values of 10 and over. This effect can be attributed only to uncoiling of chains which are strongly coiled with fold formation.

An unoriented specimen of a material such as a polyamide before it is stretched may be imagined to contain folds in the form of packets oriented in a great variety of directions (Fig. 1).

A tensile force applied at a certain angle φ to the direction of the segments in an aggregate can be resolved into two component forces, directed along and normally to the segment lengths (Fig. 1,a). The normal component acts as a breaking force against the single intermolecular bonds between the individual units in the segments; its value is

$$f_{\text{shr}} = f_0 \sin \varphi,$$

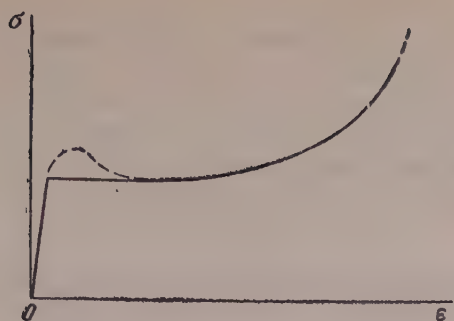


Fig. 2. Schematic course of an extension curve with opening of folds.

where f_0 is the total tensile force applied to the specimen; f_{br} is the breaking component; φ is the angle between the direction of the segment and the total force.

The longitudinal component is a shearing force acting against the sum of all the bonds along the segment; its value is

$$f_{shr} = f_0 \cos \varphi$$

The breaking force has the maximum value, equal to the total force, if the orientation of the fold is at right angles to the force applied to the specimen (Fig. 1,b). The action of this force should lead to consecutive opening of the folds as the result of rupture of the bonds between consecutive units.

Consequently, folds situated at an angle of 90° should be the first to open, as this requires the least total force. This should be followed by opening of folds (or packets of folds) situated at smaller angles. Folds situated with their axes in the direction of the applied force can be opened only by shear of the segment as a whole with simultaneous displacement of the bend (Fig. 1,b). This should require a considerable force and it is possible that if the force is great enough chain rupture leading to failure of the specimen may occur instead of shear.

The general form of the extension (ϵ) - stress (σ) curve, when there is no general structural orientation in the specimen, is shown in Fig. 2.

The presumed form of the extension curve is generally confirmed by experience. The maximum denoted by the dash line in Fig. 2, frequently found in practice, may be due to the presence of a certain number of chains in the rectile configuration, without folds, in the mass of the specimen. Such chains offer additional resistance which must be overcome by rupture of these chains or in the course of irreversible flow.

Simple consideration of the process of fold opening leads to the conclusion that when a packet of folds (an individual flexural aggregate) is opened the total elongation depends on the depth of the folds, i.e., their length between two flexure points. If the folds were opened by a shearing mechanism, which is unlikely, elongation would be determined by the number of folds in an aggregate.

The possible elongations which may occur in presence of folds of different lengths may be estimated by simple calculations. For example, in polypeptide chains of fibrous proteins we have monomer units ~ 3 Å in length along the chain. The equilibrium distance between the chains is ~ 4.5 Å. Therefore when a fold 3 units long, with a total length of 9 Å, is opened, the distance in the direction of the acting force increases from 4.5 Å to 9 Å, which is equivalent to elongation $\lambda = 2$. Fourfold elongation is obtained with folds 6 units long, and $\lambda = 10$ is obtained with 15 units in the fold.

It may be assumed that with folds 5-6 units and more in length the elongation effect may be regarded as corresponding to folds of a macroperiodic character.

In all probability, the determining role in all the situations described above is played by packets of folds on minimum depth, as after they have been opened further elongation may occur either by shear of the straightened chains, or by chain rupture.

In crystallizing polymers the uncoiled chains, oriented in one direction, may naturally form new crystallites, oriented along the extension axis; i.e., some of the crystallites undergo recrystallization in the course of deformation. The rest of the crystallites apparently remain unchanged.

We have considered only a part of the effects which may be associated with flexural chain packing. Many other known facts concerning states and processes in the field of chain polymers can be understood better in the light of the foregoing concepts. These include characteristic behavior of films and threads of polyamides, polyesters, polyethylene, and other substances in the course of preparation, processing, and testing; formation of different types of crystalline regions; numerous observations made with the aid of the electron microscope, etc. In a broader aspect, we may refer to the connection between concepts of chain folds, fixed and stabilized to a

certain degree, and problems of protein structure, such as coiling of chain macromolecules not only in the condensed but also in the dissolved state. The concepts of the structure of flexural aggregates must themselves be detailed more closely; for example, in relation to the structure of the flexural points of the chains in certain concrete examples, classification of aggregates in accordance with the number and length of the folds, regularity, and structure of plane and volume aggregates. Of great importance in this connection is the question of the general flexibility of chains of different structures and of the possible presence in the chains of regions of especially high flexibility, such as are assumed in protein molecular chains. Instances of rigid chains or individual regions (segments) of low flexibility are equally important.

We consider that the problem of formation of folds, with a certain degree of order, is closely associated with the problem of formation of periodic structures with long identity periods. Periodic structures are observed in a number of natural and artificial substances by means of low-angle x-ray scattering and of the electron microscope.

Special forms of flexural packing of chain macromolecules with a high degree of order, fixed by systems of specific bonds (hydrogen bonds, salt bonds, coordination bonds involving complex-forming metal atoms, etc.) are of undoubted significance in biological formations involving high polymers.

The above concepts of a folded (flexural) type of polymer chain packing, which in the first instance is confirmed by only a limited number of examples [4, 5] are advanced by us as a working hypothesis. It is important not only because it provides an explanation of certain observations, but also because it raises a number of problems for further investigation. The results of such investigations may give an indication of the extent to which structures of the flexural type or structures of an allied intermediate character are to be found.

SUMMARY

1. The existence of two extreme types of packing of chain molecules in polymeric systems is postulated; these are: a) the rectile type, with parallel coordination of different macromolecules only, and b) the flexural type with parallel coordination of segments in the same chain, forming more or less regular folds with turns through 180° .

2. It is pointed out that the presence of folded formations (flexural aggregates) in polymeric systems is reflected in their texture and behavior, especially in deformation processes.

Some characteristic features of the behavior of polymers in the crystalline and glassy states (cold flow, enforced elasticity) are considered to be directly associated with opening of folds with definite orientation.

3. Attention is drawn briefly to a number of problems relating to properties of polymer systems, which may be approached and studied in a new manner by suitable experiments with the possibility of formation of more or less regular folds in the chain molecules being taken into account.

LITERATURE CITED

- [1] R. I. Fel'dman, *Kolloid. Zhur.* 20, 2, 220 (1958)*; 21, 238, 499 (1959).*
- [2] R. I. Fel'dman and S. I. Sokolov, *Kolloid. Zhur.* 20, 3, 338 (1958).*
- [3] N. P. Peskov, *Physicochemical Principles of Colloid Science* [in Russian] (Chem. Tech. Press, 1932).
- [4] K. H. Storks, *J. Amer. Chem. Soc.* 60, 1753 (1938).
- [5] A. Keller, *Phil. Mag.* 2, 1171 (1957).
- [6] W. T. Astbury, *Advances in Enzymology* 3, 63 (1943).
- [7] S. Mizushima, *Molecular Structure and Internal Rotation* [Russian translation] (IL, 1957) p. 161; F. Billmeyer, *Introduction to Polymer Chemistry and Technology* [Russian translation] (IL, 1958) p. 70.
- [8] Yu. S. Lazurkin and R. L. Fogel'son, *Zhur. Tekh. Fiz.* 21, 3, 267 (1951).

Received March 2, 1958

* Original Russian pagination. See C. B. Translation.

THE STRUCTURE OF GELS

18. INFRARED SPECTRA OF GLOBULAR CASEIN

D. N. Shigorin and P. I. Zubov

The L. Ya. Karpov Physicochemical Institute

Casein was obtained earlier [1] in a globular form; investigations of its physicochemical properties showed that on interaction with water at room temperature it dissolves and gives solutions of low viscosity. After removal of the solvent, globular casein forms films which are considerably weaker than films of fibrous casein. Under the influence of alkalis, globular casein can undergo denaturation (a precipitate is formed). Electrochemical investigation with the aid of a glass electrode showed that globular casein contains fewer alkaline groups than fibrous.

The infrared absorption spectra of both forms of casein were studied in the present investigation. The spectra were determined by means of the IKS-II spectrometer with a lithium fluoride prism. The infrared absorption spectra of casein films are given in Fig. 1; it is seen that in the spectrum of globular casein (curve 1) the N-H bonds in peptide groups ($=\text{HN}-\text{C}=\text{O}$) give rise to three bands at frequencies of 3080 cm^{-1} , 3200 cm^{-1} , and about 3300 cm^{-1} , whereas in the spectrum of ordinary (fibrous) casein (curve 2) there is no band at 3200 cm^{-1} , and only the ~ 3080 and 3300 cm^{-1} bands are present.

It should be noted that the infrared spectrum of globular casein in the investigated region bears a great similarity to the spectra of α -keratin or wool fibers (Fig. 2), whereas the spectrum of fibrous casein is analogous to the spectrum of fibroin or natural silk fibers.

In investigations of the infrared spectra of α -keratin, wool fibers, fibroin, and natural silk fibers [2, 3] it was shown that the 3200 cm^{-1} band is due to valence vibrations of $\text{N-H}\cdots$ groups in coiled α -peptide chains

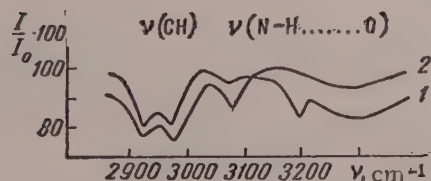


Fig. 1. Infrared absorption spectra of globular (1) and fibrous (2) casein.

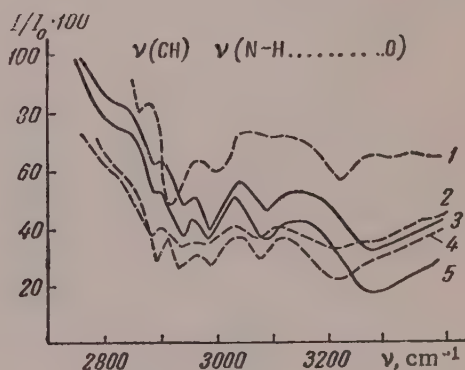


Fig. 2. Infrared absorption spectra of polyamides: 1) α -keratin; 2 and 4) wool fibers; 3) pure fibroin; 4) natural silk.

within which hydrogen bonds are formed with the aid of these groups. The 3300 cm^{-1} and 3080 cm^{-1} bands are assigned to valence vibrations of N-H groups in the peptide chains, where they form two types of hydrogen bonds corresponding to cis and trans positions of the NH- and C=O groups. In extended (β) polypeptide chains the latter frequencies are fundamental. In coiled (α) chains a band at 3200 cm^{-1} is observed in all cases in addition to the 3080 and 3300 cm^{-1} bands. This distribution of the bands due to valence vibrations of the groups agrees with x-ray structural data for α -keratin and fibroin.

Comparison of the infrared absorption spectra of globular and fibrous casein with the spectra of α -keratin and fibroin leads to the conclusion that the peptide chains are coiled (the α -form) in globular casein, and extended (the β -form) in fibrous casein.

We consider that the specific characteristics of globular casein, and in particular its solubility in water, are primarily due to the fact that in conversion into the globular form the polypeptide chains pass from the β - into the α -form.

SUMMARY

1. The infrared absorption spectra of globular and fibrous protein have been studied.
2. The polypeptide chains are of the α -form in globular and of the β -form in fibrous casein.

LITERATURE CITED

- [1] P. I. Zubov, Z. N. Zhurkina, and V. A. Kargin, *Kolloid. Zhur.* 16, 107 (1954).*
- [2] D. N. Shigorin, N. V. Mikhailov, and O. A. Klyueva, *Zhur. Fiz. Khim.* 30, 1951 (1956).
- [3] D. N. Shigorin, N. V. Mikhailov, and S. P. Makar'eva, *Doklady Akad. Nauk SSSR* 94, 714 (1954); 97, 71 (1954).

Received September 10, 1958

* Original Russian pagination. See C. B. Translation.

LETTERS TO THE EDITOR

THE ADSORBABILITY OF CARBOHYDRATES

M. S. Shul'man

Scientific Research Institute of the Alcohol, Liqueur, and Vodka Industry, Moscow

It was shown [1] that at the concentrations studied (up to 0.2%) arabinose, sucrose, and glucose have little effect on the height of the polarographic oxygen maximum, whereas maltose has an appreciable lowering effect on this maximum.

It was desired to determine the limiting concentrations of the sugars at which the oxygen maximum is completely suppressed.

Since the adsorbability of sugars is low, these investigations were conducted with 20% solutions of the sugars in 0.02 N KCl solution (to give a constant concentration of potassium chloride on addition of considerable amounts of the sugar solutions).

The results of these investigations (see table) showed that the sugars studied form the following series in order of their activity in suppressing the oxygen maximum: maltose > arabinose > glucose > fructose > sucrose.

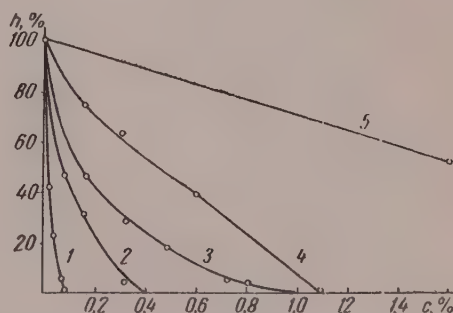
Suppression of the oxygen maximum by sugar solutions is represented graphically in the figure. The difference between the maximum and the residual current corresponding to 0.02 N KCl was taken as 100%, and the corresponding differences after additions of the sugars were calculated in percentages relative to the original KCl solution.

Suppression of the polarographic oxygen maximum by sugar solutions is associated with an adsorption process on the surface of the mercury drops, discussed in detail earlier [2-3].

Our investigations [4] showed that the sugars in question form the following series in order of the activity of their reduction at a dropping mercury electrode: fructose > arabinose > xylose > maltose > glucose (sucrose is not reduced).

Suppression of Oxygen Maximum by Sugar
Concentration in 2 N HCl

Sugar	Concentration of sugar solution		
	%	g/liter	M per liter
Maltose	0.08	0.8	$2.3 \cdot 10^{-3}$
Arabinose	0.40	4.0	$2.7 \cdot 10^{-2}$
Glucose	1.0	10	$5.6 \cdot 10^{-2}$
Fructose	1.1	11	$6.1 \cdot 10^{-2}$
Sucrose	11.5	115	$33.6 \cdot 10^{-2}$



Effect of sugars on the polarographic wave height of oxygen: 1) maltose; 2) arabinose; 3) glucose; 4) fructose; 5) sucrose.

An error was recently discovered in the earlier paper [1]; in studies of suppression of the oxygen maximum in the sugar solutions (glucose, maltose, sucrose, and arabinose) were prepared, as stated in the paper, in 1% concentrations, whereas the concentration of the starch and dextrin solutions was 0.1% and not 1%.

Accordingly, the limiting adsorption (complete suppression of the oxygen maximum) occurs at 0.006% and not 0.06%.

Therefore the concentrations of the solutions of polymeric carbohydrates given in the table in the article [1] must be divided by 10.

This error was detected during development of a polarographic method for determination of oxygen in media used in yeast production [5].

The results of additional investigations showed that the limiting adsorption of solutions of starch pastes and dispersed starch, at which complete suppression of the oxygen maximum occurs, is in the 0.0045-0.0060% range.

LITERATURE CITED

- [1] M. S. Shul'man, *Kolloid. Zhur.* 19, 3, 384 (1957).*
- [2] A. N. Frumkin and V. G. Levich, *Zhur. Fiz. Khim.* 21, 1183 (1947).
- [3] T. A. Kryukova and A. N. Frumkin, *Zhur. Fiz. Khim.* 23, 819 (1949).
- [4] M. S. Shul'man, *Sakhar. Prom.* 1 (1958).
- [5] M. S. Shul'man and L. A. Samokhvalov, *Gidroliz. i Lesokhim. Prom.* 8 (1958).

Received July 14, 1959

*Original Russian pagination. See C. B. Translation.

September 9 of this year was the 60th birthday and marked the completion of 35 years of scientific, teaching, and social activity of the President of the Academy of Sciences USSR, Academician Aleksandr Nikolaevich Nesmeyanov.

A. N. Nesmeyanov's scientific and teaching activity embraces a wide range of problems in theoretical and applied chemistry. He was the originator of a most important trend in the chemistry of metallororganic compounds, and recently he has been studying telomerization reactions with outstanding success; in the course of this work he has solved the problem of production of a new type of polyamide fiber.

Thus, A. N. Nesmeyanov's researches have penetrated into the field of colloid chemistry of high polymers.

The Editorial Board of Kolloidnyi Zhurnal offers him jubilee greetings and the best wishes for health and further successes in scientific and social activity.

Editorial Board of Kolloidnyi Zhurnal

GENERALIZATION OF THE THEORY OF G. V. TROITSKII'S METHOD FOR OPTICAL RECORDING OF MIXTURE COMPOSITIONS

Ya. M. Bikson

The Borisoglebsk Pedagogic Institute

Troitskii [1-3] proposed a new method for optical recording of the concentration gradient of mixture components, arising as the result of electrophoresis. In the previous paper [4] we presented the theory of this method in relation to one variant of the optical system. It was shown that if the parameters of the optical system are suitably chosen the Troitskii method gives a higher resolving power than the corresponding variant of the Svensson method [5]. However, since Svensson's theory was presented by him in the most general form and is applicable to any variant of his optical system, a corresponding generalization of our proposed theory of the Troitskii method is desirable.

Figure 1 represents certain variants of the recording optical system conforming to the Troitskii method. The systems shown here differ from the corresponding systems given by Troitskii [2] by the presence of a small-aperture diaphragm used as a point source of light. By restricting the light beam which passes through the optical system the diaphragm diminishes the intensity of the rays forming the electrophoretic diagram but, as follows from the theory [4], it confers higher resolving power on the system.*

The principle of focusing of the light rays is the same in all the different arrangements of the optical system. The light source A is projected by means of the short-focus lens B onto the small aperture of the diaphragm C. The lens system (or single lens) D, F gives an image of the small aperture C in the plane G. The system of lenses (or single lens) F, H gives an image of the electrophoresis vessel E on the photographic plate K. ** The inclined cylindrical lens J, which introduces astigmatism into the optical system, is placed between G and K in such a manner so that the foci of the sagittal beams from the plane G and the foci of the meridional beams from the cell C coincide on the plate.

For the first of the variants of the optical system shown in Fig. 1 a basic equation was derived connecting the area S covered by the electrophoretic diagram, the concentration c of a component of the mixture, and the angle θ between the lens J and the vertical:

$$S = \frac{1}{2} a m l K_2 \Delta c \sin 2\theta, \quad (1)$$

where a is the thickness of the electrophoretic cell; \underline{m} is the constant in the equation of proportionality between the refractive index of the solution and the concentration of the solute; \underline{l} is the distance between the planes G and K; K_2 is the magnifying power of the cylindrical lens; Δc is the difference between the maximum and minimum concentrations of the component; this is in practice equal to the concentration of the component in solution.

*In the Svensson apparatus the combination of two crossed slits restricts the light beam to almost the same extent.

** In absence of the lens J (one of the cell faces is meant; the front face, for the sake of definiteness).

Another important result of the theory is estimation of the minimum concentration Δc_i of the component detectable by the apparatus

$$\Delta c_i = \frac{KK_1\epsilon}{aml} (1 + \cot \theta) \Delta z, \quad (2)$$

where K is the magnifying power of the lens system D, F ; K_1 is the magnifying power of lens F ; ϵ is the diameter of the small aperture in the diaphragm; Δz is the boundary layer in which the concentration gradient of the given component arises after electrophoresis.

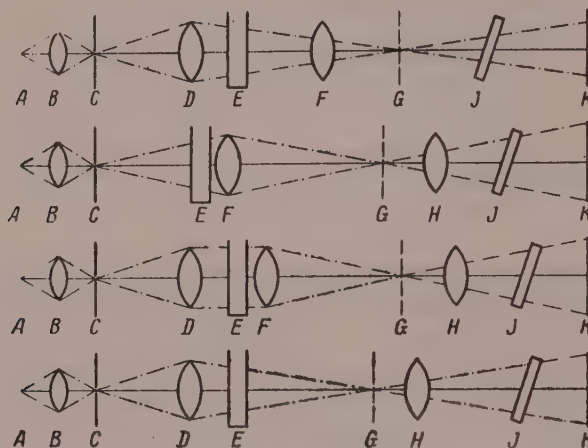


Fig. 1. Different arrangements of the components of the optical system.

The most rational method for generalization of these results is by the use of Svensson's concept of active distance [5].

Suppose that between the planes P and Q there is a system of lenses which gives images of points in plane P on plane P' with magnification K_P , and of points in plane Q on plane Q' with magnification K_Q . The distances between the respective planes denoted by PQ' , $P'Q$, $P'Q'$. Then the effective path \overline{PQ} between planes P and Q is the quantity PQ'/K_Q . If the magnification K is taken as positive for an upright image and negative for an inverted image, the following definitions of the effective path may be shown to be identical:

$$\overline{PQ} = \frac{PQ'}{K_Q} = \frac{P'Q}{K_P} = \frac{P'Q'}{K_P K_Q}. \quad (3)$$

Figure 2 (from Svensson's monograph) illustrates the application of the active-distance concept. The planes P and Q are on the two sides of the lens; P' is the image of the plane P (real in Fig. 2, a and virtual in Fig. 2, b). Two rays enclosing the angle $\Delta \varphi$ from plane P are refracted by the lens and converge at a certain point in plane P' . They cut plane Q at points Q_1 and Q_2 . The distance $Q_1 Q_2$ is the product of $P'Q$ and the angle $Q_1 P' Q_2$, which is equal to $\Delta \varphi / K_P$. Therefore

$$Q_1 Q_2 = \frac{P'Q}{K_P} \Delta \varphi = \overline{PQ} \Delta \varphi. \quad (4)$$

In particular if $\Delta \varphi$ is the angle of deviation of the rays in the electrophoretic cell (due to the existence of a concentration gradient), then the displacement Z of the image of the diaphragm C in plane G (Fig. 1) caused by this deviation can be found from the expression

$$Z = \bar{l} \Delta \varphi, \quad (5)$$

where \bar{l} is the active distance between planes E and G .

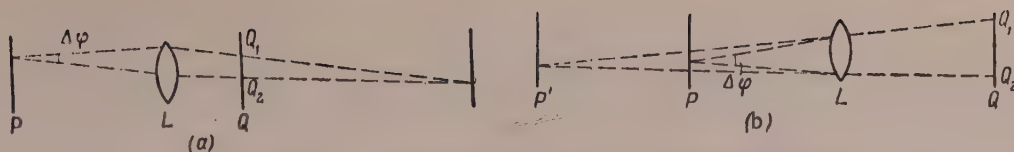


Fig. 2. Application of the active-distance concept.

Equation (5) is the general form of Equation (6) in our preceding paper [4]. By using this equation and performing consecutively all the calculations indicated earlier for the possible different arrangements of the optical system we find general expressions for the area S covered by the electrophoretic diagram.

$$S = \frac{1}{2} \bar{a} \bar{l} m K_{II} K_{III} \Delta c \sin 2\theta, \quad (6)$$

and for the resolving power of the optical system

$$\Delta c_i = K_I \frac{\epsilon}{\bar{a} \bar{l} m} (1 + \cot \theta) \Delta z, \quad (7)$$

where K_I is the magnification of the image of the diaphragm; K_{II} is the magnification of the image of the vessel (for the meridional rays); K_{III} is the magnification of objects in plane G (for sagittal rays).

For comparison, we give Svensson's equation for estimating the resolving power in the crossed-slit method:

$$\Delta c_I = K_I \frac{\epsilon}{\bar{a} \bar{l} m} \Delta z + \Phi(\lambda), \quad (8)$$

where ϵ is the width of the horizontal slit; Φ is a function of the wave length of the light λ ; the other symbols have the same meaning as in Equation (7).

Svensson [5] showed that in the right-hand side of Equation (8) the second term, which depends on the wave length, is considerably greater than the first. Therefore comparison of Equations (7) and (8) shows that Troitskii's method, in which diffraction effects are virtually absent, may give higher resolution than Svensson's method.

SUMMARY

1. The theory of optical recording of mixture composition by the inclined cylindrical lens method, advanced earlier by the author, has been generalized. In its generalized form the theory covers all possible arrangements of the optical system.

2. The conclusion drawn earlier for a particular case, that the inclined cylindrical lens method can give higher resolution by the optical system than the crossed slit method, has been confirmed.

LITERATURE CITED

- [1] G. V. Troitskii, Dissertation [in Russian] (Moscow, 1950).
- [2] G. V. Troitskii, *Biokhimiya* 16, 592 (1951).
- [3] G. V. Troitskii and I. I. Rodionov, *Biokhimiya* 20, 431 (1955).
- [4] Ya. M. Bikson, *Kolloid. Zhur.* 20, 129 (1958). *
- [5] H. Svensson, *Electrophoresis by the Moving Boundary Method*, (Stockholm, 1946).

Received May 31, 1958

*Original Russian pagination. See C. B. Translation.

AN X-RAY STUDY OF THE CRYSTALLIZATION OF SORBED WATER

V. S. Brzhan

The Voronezh Agricultural Institute, Department of Physics

Zhilentov [1] found that the activation energy of polarization of water molecules sorbed by silica gel, which remains unchanged in the transition through 0° , undergoes an abrupt change at about -100° . Accordingly, in the light of literature data [2] on the special position of water in the hydride series and of the idea advanced in an earlier publication [3], it has been suggested that adsorbed water remains in the liquid state down to -100° .

As the sudden change in the activation energy tends to increase with increased adsorption [1], it may be assumed that this change occurs if the silica gel is completely saturated with water vapor. If the pores of some types of silica gel are completely filled with water, the conditions should be favorable (with regard to the possible crystal size) for direct verification of the crystallization of capillary-condensed water by means of x-ray structural analysis. This hypothesis has been confirmed by a number of investigations, including the work of Radzievskii and Shekhtman [4].

The present communication contains the first results of an x-ray study of the crystallization of water, present in a state of capillary condensation, sorbed by silica gel.

Experimental procedure. The lid of the usual x-ray camera with the mechanism for rotation of the specimen was replaced by a close-fitting aluminum block. The block contained two deep drilled cavities for the cooling liquid; liquid oxygen was generally used for this purpose.

Oxygen was put into both cavities when the camera was cooled to the required temperature. Nevertheless, because of the large mass of metal the average cooling rate was only 3° per minute. Subsequently, in order to maintain the established temperature, the cooling liquid was fed intermittently into one of the cavities by means of a specially constructed device which was switched on automatically by an ERM-47 electronic regulator with a thermocouple; a control thermometer was put in the other cavity. The camera was fixed on a textolite support and enclosed in an insulated box. The temperature was maintained to within $\pm 1^{\circ}$.

The material chosen for investigation was KSK-2 silica gel with an average pore size of 104 Å. The x-ray pattern on the dry silica gel contains no lines. Humidification of the gel to saturation at 20° corresponded to sorption of about 50 millimoles of water vapor per gram of dry silica gel. The earlier specimens were sealed thin-walled capillaries made of molybdenum glass, about 1 mm in diameter. The capillaries were filled with silica gel saturated with water vapor, and with helium at low pressure. Subsequently, in order to obtain better x-ray patterns, celluloid capillaries 0.60 mm in internal diameter with walls ~ 0.01 mm thick were used instead of glass. Silica gel was saturated with water vapor in presence of air in a desiccator at $14-16^{\circ}$. To prevent condensation of water vapor from the air on the specimens at low temperatures the camera was hermetically closed. All the joints were smeared with petrolatum. Absence of any appreciable condensation of vapor from inside the camera was confirmed by control photographs.

The time of preparation of the camera, from extraction of the specimens from the desiccator to transition through 0° , was reduced to 13-15 minutes. The investigations were performed with copper radiation without a filter in the URS-70 x-ray unit. The operating conditions were: 10 ma, 30 kv. The exposure time was 2 hours.

1

2

3

The x-ray patterns given at -8° (1) and -20° (2) by KSK-2 silica gel; x-ray pattern of another powdered silica gel sample at -8° (3).

Data from typical patterns are presented in Table 1. The x-ray diagram (2) shows sharp interference maxima on a diffuse background due to the microporous structure of the adsorbent. This indicates that water sorbed by KSK-2 silica gel forms ice with a well-defined if not the usual crystal structure. Additional control experiments showed that these lines were definitely due to ice formed from the sorbed water.

The small total number of diffraction maxima is noteworthy. The x-ray pattern appears to be cut off beyond $\theta > 24^{\circ}$.

The x-ray patterns determined at different temperatures between -1° and -70° indicate that water adsorbed on KSK-2 silica gel, contrary to expectation, crystallizes at about -9° . The lines do not appear at higher temperatures, under the same exposure conditions (x-ray diagram 1). Small variations of the cooling rate, which reached 10 degrees/minute in the first (preliminary) variant of the experiment, had no appreciable influence either on the freezing point or the form of the x-ray pattern. None of the x-ray patterns taken below -9° differ to any appreciable extent from each other either in the positions or the intensities of the lines.

Since the operating conditions of the x-ray tube were stable and the exposures constant, these results show that the capillary water, at least the part of it which is responsible for the appearance of the lines, apparently has a quite definite freezing point.

Whatever the reason, the freezing point of the water in a state of capillary condensation in KSK-2 silica gel was considerably higher than expected. In our experiments ice at -100° showed no special features with regard to x-ray structural analysis.

The x-ray patterns of KSK-2 silica gel, saturated with moisture and frozen, were compared with the patterns given, under similar conditions, by another adsorbent (powdered silica gel) with much coarser pores. In the latter case ordinary ice was formed (x-ray diagram 3). It follows that pore size is the most important factor determining the appearance of the unusual form of ice.

TABLE 1

Calculated Data from the x-Ray Pattern of Ice Formed from Water Sorbed by KSK-2 Silica Gel

Intensity	$l_{\text{det}}, \text{mm}$	$l_{\text{corr}}, \text{mm}$	θ	d
Strong	23.2	22.63	$11^{\circ} 21'$	3.95
Very strong	24.8	24.2	$11^{\circ} 99'$	3.70
Strong	40.7	40.17	$19^{\circ} 90'$	2.26
Moderate	48.0	47.5	$23^{\circ} 53'$	1.92

Despite the fact that the adsorptive capacity of the second sample of powdered silica gel was considerably lower than that of KSK-2, the total intensity of all the lines in its x-ray pattern is many times greater than in that of KSK-2. This is to be regarded as definite evidence that in KSK-2 far from all the sorbed water is involved

TABLE 2

Comparative x-Ray Data for Ice I of Different Structures

Hexagonal ice [7]			Ice from sorbed water ("semicrystalline")		Cubic ice [6]		
$d, \text{\AA}$	I^{**}	hkl^{***}	d	I	d	I	hkl
3,92	10 (w)	(10 $\bar{1}$ 0)	3,95	s	—	—	—
3,67	100 (vvs)	(0001) [2]	3,70	vs	3,66	(vvs)	(111)
3,44	20 (m)	(10 $\bar{1}$ 1)	—	—	—	—	—
2,68	15 (m)	(10 $\bar{1}$ 2)	—	—	—	—	—
2,26	10 (w)	(11 $\bar{2}$ 0)	2,26	s	2,25	(s)	(220)
2,065	50 (vs)	(10 $\bar{1}$ 3)	—	—	—	—	—
1,92	10 (w)	(11 $\bar{2}$ 2)	1,92	m	1,92	(m)	(311)
1,516	15 (w)	(20 $\bar{2}$ 3)	—	—	1,59	(w)	(400)
1,368	20 (m)	(10 $\bar{1}$ 5)	—	—	1,46	(m)	(331)
		(12 $\bar{3}$ 2)	—	—	—	—	—
1,30	2,5 (vw)	(10 $\bar{1}$ 6)	—	—	1,30	(m)	(422)
1,25	2,5 (vw)	(12 $\bar{3}$ 3)	—	—	1,22	(w)	(333)
							(511)
1,167	5 (vw)	(20 $\bar{2}$ 5)	—	—	1,12	(w)	(440)
					1,07	(m)	(531)
					1,00	(vw)	(620)
					0,97	(vw)	(533)
					0,92	(vw)	(444)
					0,89	(vw)	(551)
							(711)
					0,85	(w)	(642)

*d = interplanar spacing.

** I = intensity: w = weak, vvs = very, very strong, m = moderate, vs = very strong, vw = very weak.

*** hkl = indices of the reflecting plane.

in formation of crystals which are large enough to give distinct interference maxima. At the same time, as the outlines of the observed lines are not diffuse the formation of very small crystals is doubtful. It follows that even if the water does freeze in the very fine pores, most probably it does not enter the crystalline state. Other results [4] are in favor of this too. Unfortunately, the x-ray pattern of the observed ice lacks lines corresponding to large values of Θ . If they were present it would be possible to draw more definite conclusions concerning the state of the remaining water.

The structure of our "capillary" ice coincides with that reported by Burton and Oliver [5] for ice formed by low-pressure condensation of water vapor on a cooled metal surface. They consider that this is an unstable form of ice I, which exists at pressures below 2000 atmos. In contrast to our results, the ice which was observed in this investigation [5] and which was described as "semicrystalline" is found only at temperatures below -90° . On increase of temperature it begins to recrystallize at a finite rate into ordinary ice. When the temperature is lowered again, the return conversion does not occur at temperatures down to -183° .

In the light of the above results and those of Konig [6], recrystallization of ice formed from sorbed water is improbable on decrease of temperature, and the absence of such recrystallization at -100° in Zhilenkov's investigation [1], as established by us, is quite understandable.

It must be noted that the recrystallization temperature (T_{recr}) of ice, estimated in the publications cited at -90° , is in good agreement with the general concepts with regard to crystallization according to which $T_{\text{recr}} = 2/3 T_m = 182^\circ \text{K} = 91^\circ \text{C}$. In our case recrystallization was not observed at all. This is doubtlessly due to the specific conditions which influence the water molecules in a manner analogous to a decrease of their thermal mobility.

Attempts to correlate our results with the data cited suggest that in the earlier work [5] the vapor passed on condensation through a state analogous to adsorption.

With regard to the structure of the unusual form of ice described above, Burton and Oliver [5] consider that this is ordinary ice with incomplete atomic order in which order is observed, in their view, only "along certain planes". We regard this as not fully convincing; like Konig's explanation of "semicrystalline ice," in which the first line of the x-ray diagram was simply disregarded.

In Table 2 that x-ray patterns of our ice are compared with those of ordinary ice [7] and the cubic modification of ice of the cristobalite type [6]. As the x-ray pattern of the unusual or "semicrystalline" ice does not have the relatively intense $(10\bar{1}1)$, $(10\bar{1}2)$ and $(10\bar{1}3)$, lines of hexagonal ice, and the relative intensities of the lines common to both modifications are different, it follows that the x-ray pattern of "semicrystalline" ice is not simply a part of the pattern of hexagonal ice. Thus, Table 2 shows that these ice forms are structurally different.

There is much more in common between the unusual ice and cubic ice. However, since semicrystalline ice has an interference maximum corresponding to $d = 3.95 \text{ \AA}$ [this line for hexagonal ice has the indices $(10\bar{1}0)$] it cannot be identified with that modification. It seems that ice formed from sorbed water is a crystallographical-independent phase with an imperfect structure intermediate between hexagonal and cubic ice.

Unfortunately, the specific experimental conditions are such that the finer methods of x-ray structural analysis cannot be used.

SUMMARY

1. It has been shown by x-ray structural analysis that water sorbed by KSK-2 silica gel crystallizes at least partially at low temperature, forming ice I of unusual structure, "semicrystalline" ice. Pore size is one of the most important factors in the formation of this ice.

2. The temperature at which semicrystalline ice is formed from water sorbed by KSK-2 silica gel is about -9° .

3. "Semicrystalline" ice may be formed not only on condensation of water vapor [6], but also by freezing of water in a state of capillary condensation. It can then exist over a much wider range of temperatures: from -9° to -170° , and probably lower.

4. Semicrystalline ice formed from water in a state of capillary condensation shows no signs of instability and does not undergo any phase transitions at temperatures below -9° , at least during exposures lasting two hours.

5. The abrupt change of the activation energy of polarization[1] is apparently unrelated to the crystal structure of sorbed water.

I thank candidate of physicomathematical sciences I. V. Zhilenkov for the idea of the present investigation and for his constant interest.

LITERATURE CITED

- [1] I. V. Zhilenkov, *Izvestiya Akad. Nauk SSSR, Otdel Khim. Nauk.* 2, 232 (1957). *
- [2] A. F. Wells, *Structural Inorganic Chemistry* [Russian translation] (1948) p. 291.
- [3] M. Freumann and R. Freumann, *Comp. Rend.* 232, 1096 (1951).
- [4] G. B. Radzievskii and Ya. L. Shekhtman, *Kolloid. Zhur.* 18, 77 (1956). *
- [5] E. F. Burton and W. F. Oliver, *Proc. Roy Soc. (L)* A153, 166 (1935).
- [6] H. Konig, *Z. Kristallographie (A)* 105, 4, 279 (1944).
- [7] D. M. Dennison, *Phys. Rev.* 17, 1, 20 (1927).

Received March 5, 1958

*Original Russian pagination. See C. B. Translation.

SEDIMENTATION VOLUMES OF POLYDISPERSE KAOLIN SUSPENSIONS IN SOLUTIONS OF NONELECTROLYTES

G. G. Kandilarov

Chair of Inorganic, Analytical, Colloid, and Physical Chemistry, VIKhVPROM Plovdiv, Bulgaria

Our earlier investigations were concerned with sedimentation volumes and internal friction of polydisperse kaolin suspensions in electrolyte solutions [1]. It was desired to find how the volume of the precipitates formed in kaolin suspensions is influenced by certain nonelectrolytes, and in particular by solutions of ethyl alcohol.

It is known that kaolin suspensions have pronounced hydrophilic properties. Since the dielectric constant of ethyl alcohol is considerable (although less than that of water), it is to be expected that alcoholic kaolin suspensions would also be lyophilic [2], which would have a certain influence on their sedimentation volumes.

The methods used for preparation of the kaolin suspensions* and determination of sedimentation volumes are described elsewhere. In most cases the surface of the precipitates was smooth enough to allow the volume to be measured accurately. It was only when the water content was 20,000 millimoles/liter that the surface of the precipitates was very strongly concave, so that the volume was difficult to read off accurately.

The graph shows that the volume of the kaolin precipitate tends to increase slightly with increase in the concentration of water added to the ethyl alcohol, and a maximum appears on the curve when the water content is $\sim 20,000$ millimoles/liter.

The reverse effect is observed in aqueous kaolin suspensions. In this case the volume of the precipitate does not initially show any substantial change with increasing concentration of added ethyl alcohol, but at high alcohol concentrations (50,000 millimoles/liter and in pure alcohol) the volume decreases, although only slightly.

These observations are associated with formation of more or less stable turbidity which persists over the precipitates for 24 hours after sedimentation of the suspensions.

Thus, 24 hours after sedimentation of suspensions in alcohol or in alcohol with a low water content the supernatant liquid remained quite clear. It should be noted that in such cases the suspensions were coarse-grained (coagulated**) while the sedimentation volume was at a minimum.

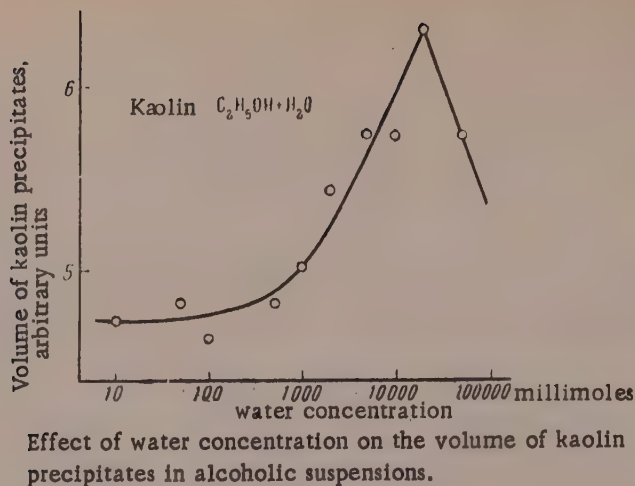
With increasing concentration of water the supernatant liquid after 24 hours was opalescent or slightly turbid. This was accompanied by a small increase in the volume of the kaolin precipitate. The turbidity was most persistent at high concentrations of water (in pure water or with 50,000 millimoles of water per liter).

In the system water-ethyl alcohol the turbidity of the supernatant liquid was greatest when the concentration of ethyl alcohol was 100 and 500 millimoles/liter, while at ethyl alcohol concentrations of 5,000 and 10,000 millimoles/liter and in pure ethyl alcohol the liquid was quite clear.

It is assumed for suspensions of the quartz type that the maximum sedimentation volume corresponds to coagulated suspensions, and the minimum to stable suspensions [3]. This applies also to suspensions of CaC_2O_4

*Kaolin from Senovo (Bulgaria, Rusenskii province) and alcohol of analytical-grade purity were used for this purpose.

** This effect was probably due to the dehydrating action of ethyl alcohol.



in electrolyte solutions [4]. In that case, with cations of higher valence (Ca^{2+} and Al^{3+}) the liquid above the precipitate showed persistent turbidity after 24 hours; this corresponded to the minimum volume of the CaC_2O_4 precipitate.

However, in experiments with lyophilic kaolin suspensions in aqueous ethyl alcohol the reverse effect was observed: the volume of the precipitate was least in coagulated suspensions in pure alcohol or in alcohol at high concentrations, and not in stable suspensions, whereas the maximum volume was obtained in solvated stable suspensions such as are formed at high concentrations of water. These observations may be explained on the following hypothesis. It is known that the dielectric constant of the solvation layers on the particles increases with increasing amount of water, so that their electric charge also increases. This probably results in an increase in the size of the solvation layers and greater stability of the suspension. As the experiments showed that the volume of the kaolin precipitates varies in the same sense, it may be assumed that its variation is related to changes in the thickness of the solvation layer.

Since the solvation layer in coagulated suspensions (in alcohol or at high alcohol concentrations) is composed of relatively few alcohol molecules, the added molecules of water, being more strongly polar, form a thicker layer and probably replace alcohol molecules in the outside layer; the total volume of the particles (and, accordingly, the volume of the precipitate) increases to a maximum. With further increase of the amount of water (in water with a low alcohol content or in pure water) the water molecules gradually displace the remaining, less polar alcohol molecules from solution, and finally the entire solvation layer is composed predominantly of water molecules. The latter have a smaller volume than the displaced alcohol molecules, so that the volume of the kaolin precipitate diminishes somewhat.

SUMMARY

Water molecules are strongly polar, and therefore as the water concentration in alcoholic kaolin suspensions increases the solvation layer becomes thicker, the suspensions become more stable, and the volume of the precipitate increases (although only slightly) to a definite maximum. The maximum can probably be ascribed to the additive solvating effects of water and ethyl alcohol.

LITERATURE CITED

- [1] G. G. Kandilarov, *Kolloid. Z* 90, 320 (1940); 91, 56 (1940); *Kolloid. Zhur.* 13, 357 (1951); 18, 293 (1956); *Izv. Bolgarskoi A. N. Khim. Institut* 4, 289 (1956); *Doklady Bolgarskoi A. N.* 6, 23, 29, 33 (1953).
- [2] A. Dumanskii, *Kolloid.-Z.* 65, 179 (1933).
- [3] H. R. Kruyt, *Colloid Science [Russian Translation]* (Moscow, 1955) p. 495.
- [4] G. G. Kandilarov, *Kolloid. Zhur.* 20, 713 (1958).*

Received August 14, 1958

*Original Russian pagination. See C. B. Translation.

ADSORPTION OF BENZENE AND n-HEXANE VAPORS ON MAGNESIUM HYDROXIDE

A. V. Kiselev and D. P. Poshkus

The M. V. Lomonosov University, Moscow, Faculty of Chemistry, Adsorption Laboratory

Institute of Physical Chemistry, Academy of Sciences USSR, Laboratory of Sorption Processes

Recent work in our laboratory has demonstrated the exceptionally important influence of surface hydroxyl groups on adsorption, not only of polar molecules capable of ordinary hydrogen bonding, but also of aromatic and unsaturated hydrocarbons, the molecules of which are, as a whole, nonpolar. Studies of the adsorption of such hydrocarbons on various hydroxides and on products formed by surface and volume dehydration of the latter are therefore of special interest.

In the preceding paper we considered the isotherms of adsorption of benzene and hexane vapors on different samples of magnesium oxide [1]. In the present investigation the isotherms for adsorption of these vapors on different samples of magnesium hydroxide were determined.

Method. It was very important to prepare a sample of magnesium hydroxide with a hydrated surface but without adsorbed water. This task is especially difficult in the case of hydroxides which decompose readily on relatively gentle heating.

The adsorbents used were four samples of magnesium hydroxide, evacuated at 20, 30, 100, and 200°. The method for preparation of coarse-pored magnesium oxide, which was designated as $\text{Mg}(\text{OH})_2$ -1, in the previous paper [1], was described in the first paper of this series [2].

Sample $\text{Mg}(\text{OH})_2$ -2 was prepared by hydration of sample $\text{Mg}(\text{OH})_2$ -2, calcined at 1000° (MgO -1-1000°), in deaerated distilled water for 10 days. In order to avoid any possible dehydration of magnesium oxide during evacuation, in this case liquid and adsorbed water was pumped off at 20° in the adsorption apparatus down to $\sim 10^{-4}$ mm water-vapor pressure, and for several hours further. When the evacuation was stopped a pressure of 10^{-2} mm became established in a few minutes over the adsorbent at 20°, and this remained almost unchanged for several days. After a second evacuation to 10^{-4} mm approximately the same water-vapor pressure ($\sim 10^{-2}$ mm) became established over the magnesium hydroxide*.

*It seems that the equilibrium pressure of water vapor over magnesium hydroxide at 20° has not been determined. Values of ~ 8 and 67 mm were found for the pressure of water vapor over magnesium hydroxide at 35 and 66° [3]; this gives 2.7 mm at 20°, which is much higher than our value. However, these values for the vapor pressure of water over magnesium hydroxide correspond to an improbably low heat of formation of magnesium hydroxide [4], ~ 13.1 kcal/mole. In that investigation [4] experimental values of the heat of formation of magnesium hydroxide were used to estimate, by means of the approximate Nernst equation, the equilibrium pressure of water vapor over magnesium hydroxide at 20°; the value found was $\sim 10^{-4}$ – 10^{-6} mm, which is considerably less than the value for

TABLE 1

Conditions of Vacuum Heat Treatment, Weight Loss at 1000-1100°, and Structural Characteristics of Samples $\text{Mg}(\text{OH})_2$ -1;-2;- 3;-4 and MgO -1-1000°

Sample	Vacuum heat treatment		Weight loss, %	Surface area			Pore diameter d, Å	Total pore volume V_s , cc/g	Porosity type
	temperature t_{max} , degree	time at t_{max} , hours		skeleton, s , m ² /g	adsorption film, s' , m ² /g	s/s'			
$\text{Mg}(\text{OH})_2$ -1	200	4	31,9	69	66	0,96	450	0,71	Coarse
$\text{Mg}(\text{OH})_2$ -2	30	Prolonged, repeated	30,3	41,7	45,6	1,1	450	0,53	Homogeneously coarse
$\text{Mg}(\text{OH})_2$ -3	20	10	—	—	—	—	—	—	Same
Same	100	6	31,0	40,5	—	—	—	—	»
$\text{Mg}(\text{OH})_2$ -4	20	10	—	—	—	—	—	—	Heterogeneous
Same	100	4	—	—	—	—	—	—	Same
»	200	4	31,7	16	13	1,2	—	0,34	»
MgO -1-1000°	1000	8	—	80*	43*	0,54	400	0,48*	Coarse, with remains of fine structure of active magnesium oxide [2]

* Reduced to magnesium hydroxide.

Sample $\text{Mg}(\text{OH})_2$ -4 was prepared by precipitation from dilute (0.1 M) boiling magnesium chloride solution by the action of gaseous ammonia; the precipitate was filtered off, washed with water to a negative reaction for chloride, and water was pumped off as for sample $\text{Mg}(\text{OH})_2$ -3.

The adsorption isotherms for this sample evacuated at different temperatures were determined with the same portion of material. The treatment conditions (temperature, time) and losses on calcination to constant weight at 1000-1100° are given in Table 1. The weight losses were determined with the same portions of magnesium hydroxide as were used for determination of the isotherms; the value found for most of the specimens is somewhat higher than the theoretical content of water in magnesium hydroxide (30.88%), probably because of slight condensation of mercury vapor on the adsorbent during determination of the adsorption isotherms and also owing to adsorption of water vapor while the samples were transferred from the bulbs to the crucible for calcination.

The adsorbates and the method used for determination of the adsorption isotherms were the same as previously [1].

Pore structure of the adsorbents. The pore structure was determined by the adsorption method, as before [2].

The structure of sample $\text{Mg}(\text{OH})_2$ -1, evacuated at 200° ($\text{Mg}(\text{OH})_2$ -1-200°), was considered earlier [2]; its main structural characteristics are given in Table 1.

The pore structure of sample $\text{Mg}(\text{OH})_2$ -2 may be deduced from the adsorption isotherm for benzene vapor, given in Fig. 1. The adsorption on this and the other adsorbents is expressed in millimoles per g of sample.

our sample ($\sim 10^{-2}$ mm). It is therefore difficult to decide from literature data which is the true equilibrium pressure of water vapor over magnesium hydroxide at 20°. However, even if our observed value for the pressure of water vapor over magnesium hydroxide at 20° is the consequence of incomplete removal of adsorbed water from the magnesium hydroxide, the degree of surface cover at this low relative vapor pressure ($p/p_s \approx 0.5 \cdot 10^{-3}$), is probably small. No exact data are available on adsorption of water vapor on magnesium hydroxide, but in the

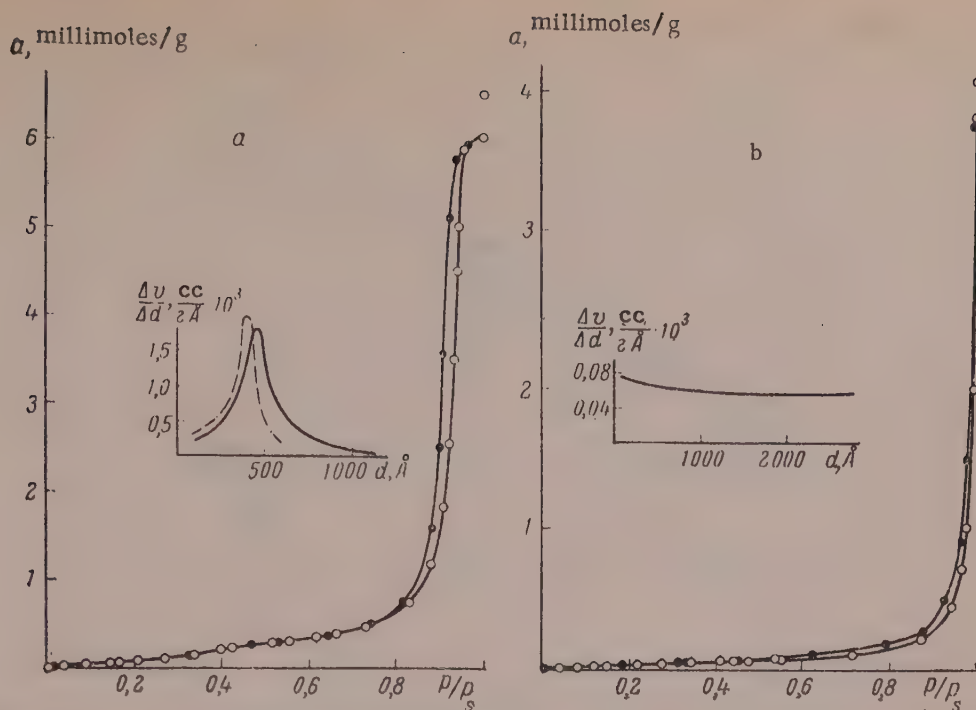


Fig. 1. Adsorption isotherms for benzene vapor and curves for distribution of pore volume by effective diameters (in middle of diagram): a) on Mg(OH)₂-2; the dash line represents the distribution curve for MgO-1-1000°, from an earlier paper [2]; b) on Mg(OH)₂-4; black points here and subsequently represent desorption.

Fig. 1, a, shows that in the region of high relative pressures the isotherm for Mg(OH)₂-2 has a well-defined hysteresis loop indicating capillary condensation; it commences at $p/p_s \approx 0.8$, rises sharply over a narrow range of p/p_s , and near the end of the isotherm the adsorption flattens out considerably. This course of the hysteresis loop indicates that the porosity of the sample is uniform.

The middle of Fig. 1, a, shows curves for pore volume distribution by effective diameter for sample Mg(OH)₂-2 (continuous line) and the original sample Mg(OH)₂-1, calcined at 1000° (dash line); the distribution curves are reduced to 1 g of magnesium hydroxide (see [2]). Comparison of the distribution curves shows that the coarse pores in sample MgO-1-1000° became somewhat larger after hydration. Values of the specific surface of the skeleton (s), the adsorption film formed at the start of hysteresis (s^*), and the ratio s^*/s for sample Mg(OH)₂-2 are given in Table 1. Comparison of the corresponding values for samples MgO-1-1000° and Mg(OH)₂-2 (Table 1) shows that the values of v_s and s^* remained virtually unchanged by hydration of sample MgO-1-1000°, whereas the surface s was approximately halved and the ratio s^*/s became close to unity. This shows that hydration of sample MgO-1-1000° caused disappearance of fine pores (cracks) present in this sample, without any significant changes in the coarse pores.

Repeated hydration of sample Mg(OH)₂-2 sample Mg(OH)₂-3, resulted in only a slight decrease of the specific surface, as Table 1 shows. Therefore the pore structure of sample Mg(OH)₂-3 was not studied specially, and it was assumed to be just as uniformly coarse-pored as sample Mg(OH)₂-2.

The pore structure of sample Mg(OH)₂-4 may be deduced from the adsorption isotherm for benzene vapor, shown in Fig. 1, b. Hysteresis in the isotherm for this sample begins at a fairly low relative pressure $p/p_s \approx 0.25$ (see further Fig. 3, b) while at high p/p_s it approaches almost asymptotically to the axis $p/p_s = 1$.

case of adsorption of water on hydrated silica gel, which is very considerable, the silica gel surface is only 10-20% covered by water molecules at the same relative pressure [5].

It would be very important to work out methods for direct determination both of adsorbed water molecules and of structural hydroxyl groups on hydroxide surface.

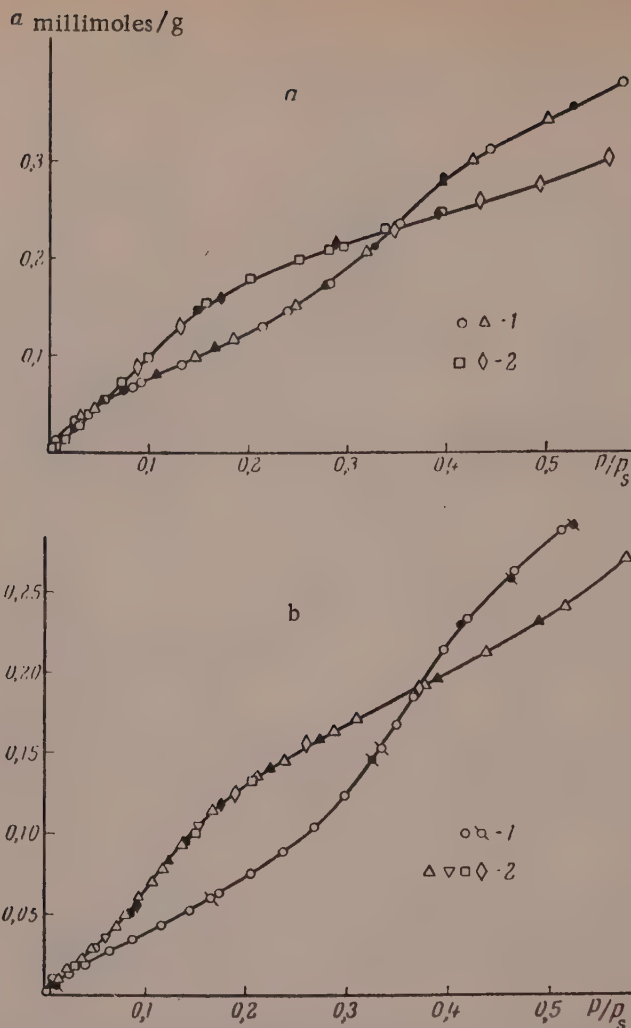


Fig. 2. Isotherms for adsorption of benzene (1) and hexane (2) vapors on samples: a) $\text{Mg}(\text{OH})_2-1-200^\circ$; b) $\text{Mg}(\text{OH})_2-2$. Different points for the same vapor correspond to different series of determinations.

The curve for pore volume distribution by effective diameters shows that the porosity is quite heterogeneous (Table 1*).

Isotherms for adsorption of benzene and hexane vapors on $\text{Mg}(\text{OH})_2-1$ evacuated at 200° are given in Fig. 2, a. The isotherm for adsorption of benzene vapor on sample $\text{Mg}(\text{OH})_2-1-200^\circ$ is wave-shaped. The isotherm for adsorption of hexane is approximately linear at first, and then becomes S-shaped. The isotherms for adsorption of benzene and hexane on this sample intersect twice, and initially the isotherm for benzene is more convex and lies above the isotherm for hexane.

Isotherms for adsorption of benzene and hexane vapors on sample $\text{Mg}(\text{OH})_2-2$ are given in Fig. 2, b. The isotherm for benzene is wave-shaped and somewhat convex at first. The isotherm for hexane is initially concave, and then has two bends.

The adsorption of benzene up to $p/p_s \approx 0.4$ is less than that of hexane.

* The ratio s^*/s for sample $\text{Mg}(\text{OH})_2-2$, and especially for $\text{Mg}(\text{OH})_2-4$, is greater than unity, although the latter contains some fine pores. This is probably because in determinations of s^* by the method of capillary condensation it is necessary to take into account the multimolecular adsorption which also occurs, and which plays an important role in samples of nonuniform porosity and with very coarse pores [1].

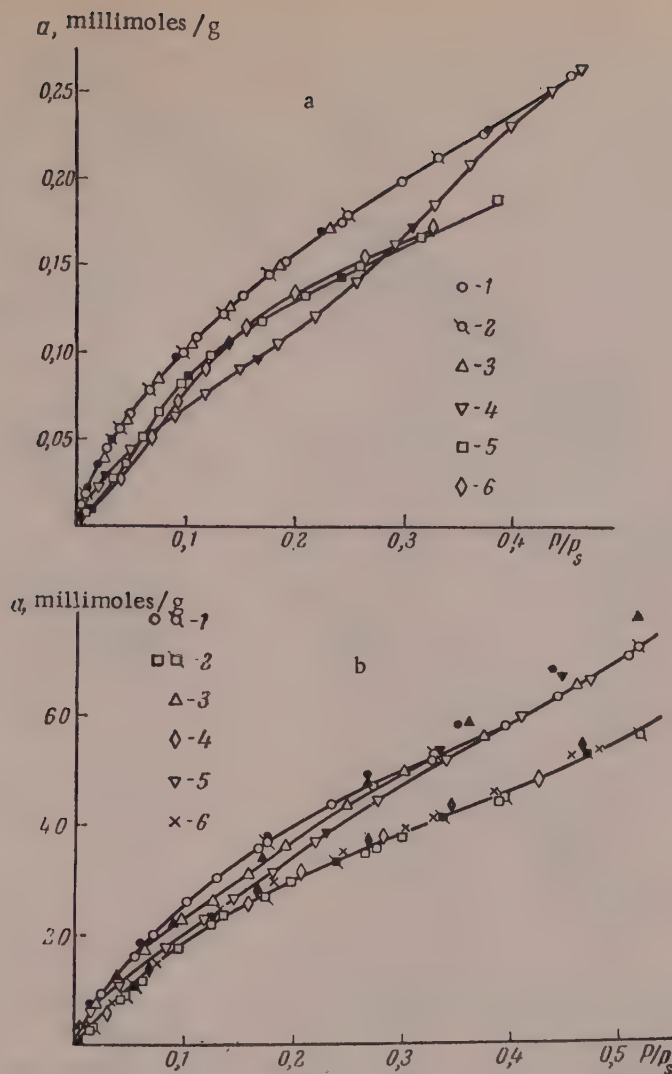


Fig. 3. Adsorption isotherms: a) benzene vapor on $Mg(OH)_2-3$ evacuated at 20° for 10 hours (1), 17 hours (2), and 32 hours (3), and evacuated at 100° (4); hexane vapor on $Mg(OH)_2-3$ evacuated at 20° (5) and 100° (6); b) benzene and hexane vapors on $Mg(OH)_2-4$ evacuated at 20° (1, 2), at 100° (3, 4) and at 200° (5, 6); only the adsorption branches of the isotherms are given.

Isotherms for adsorption of benzene and hexane vapors on sample $Mg(OH)_2-3$ are given in Fig. 3, a. The isotherm for adsorption of benzene on a sample evacuated at 20° (Curve 1) is convex and initially lies above the concave isotherm for hexane (Curve 5). A repeated evacuation of sample $Mg(OH)_2-3$ at 20° for 7 hours (Curve 2) and for 15 more hours (Curve 3) did not result in any appreciable change in the adsorption of benzene.

The isotherm for adsorption of benzene on sample $Mg(OH)_2-3$, evacuated at 100° (Curve 4) is wave-shaped. The isotherm for adsorption of hexane (Curve 6) is initially concave. As in the case of adsorption on sample $Mg(OH)_2-1-200^\circ$ (Fig. 2, a) these isotherms intersect twice in the initial region.

Isotherms for adsorption of benzene and hexane vapors on sample $Mg(OH)_2-4$, evacuated at 20, 100, and 200° are given in Fig. 3, b. The isotherm for adsorption of benzene on this sample, evacuated at 20° (Curve 1) is convex and lies above the isotherm for hexane (Curve 2). Increase of the evacuation temperature of sample $Mg(OH)_2-4$ resulted in decreased adsorption of benzene in the central region of the isotherm (Curves 3 and 5); with increase of the evacuation temperature the decrease of adsorption becomes greater and extends toward both lower and higher values of p/p_s , the isotherm becomes wave-shaped instead of convex. At $p/p_s > 0.4$ all

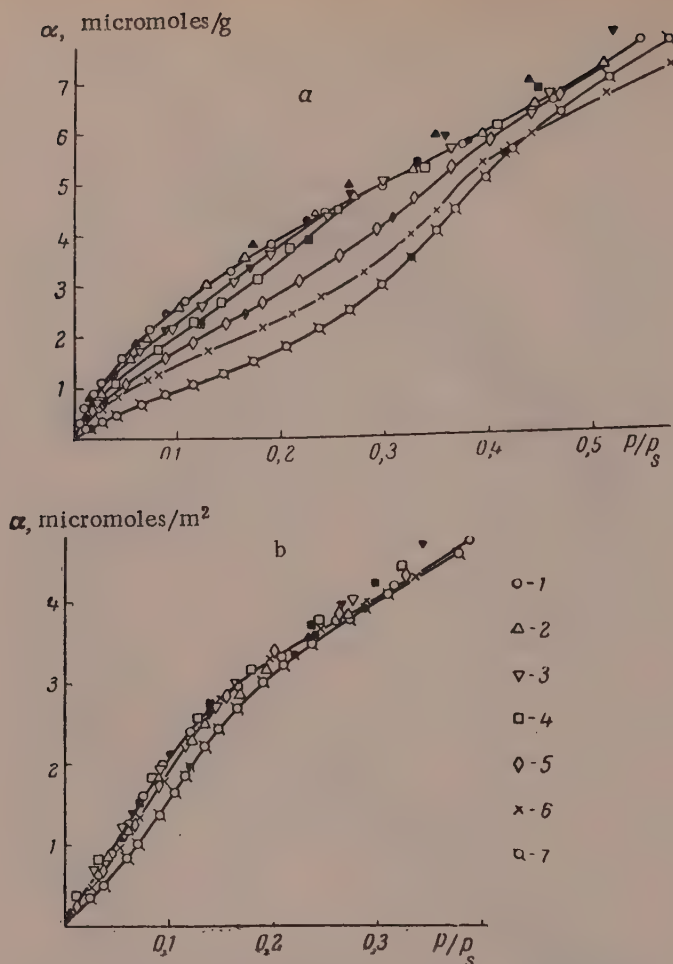


Fig. 4. Absolute isotherms for adsorption of benzene (a) and hexane (b) on $\text{Mg}(\text{OH})_2$ -3-20° (1), $\text{Mg}(\text{OH})_2$ -3-100° (5), $\text{Mg}(\text{OH})_2$ -2 (7), and reduced isotherms for adsorption on $\text{Mg}(\text{OH})_2$ -4 evacuated at 20° (2), 100° (3), and 300° (4), and $\text{Mg}(\text{OH})_2$ -1-200° (6).

these isotherms for benzene virtually coalesce. Adsorption of hexane remained almost unchanged with increase of the evacuation temperature of $\text{Mg}(\text{OH})_2$ -4 curves 2, 4, and 6).

Absolute and reduced isotherms for adsorption of benzene and hexane vapors on magnesium hydroxide.

Fig. 4 shows absolute isotherms for adsorption of benzene and hexane on $\text{Mg}(\text{OH})_2$ -2 evacuated at 30° and $\text{Mg}(\text{OH})_2$ -3, evacuated at 20 and 100°. Values for adsorption of benzene and hexane per g of samples $\text{Mg}(\text{OH})_2$ -1-200° and $\text{Mg}(\text{OH})_2$ -4, divided by their respective specific surfaces determined by the BET method from adsorption of nitrogen vapor, lie appreciably below the absolute isotherms for adsorption on samples $\text{Mg}(\text{OH})_2$ -2 and $\text{Mg}(\text{OH})_2$ -3, probably because of the presence of micropores, not only in the monolayer region, but for filling of the second adsorption layer. We therefore used reduced isotherms for comparing the isotherms for adsorption of benzene and hexane vapors on $\text{Mg}(\text{OH})_2$ -1-200° and $\text{Mg}(\text{OH})_2$ -4 with the absolute isotherms for $\text{Mg}(\text{OH})_2$ -2 and $\text{Mg}(\text{OH})_2$ -3. In Fig. 4a, the isotherm for adsorption of hexane on sample $\text{Mg}(\text{OH})_2$ -1-200° is reduced to the absolute isotherms for adsorption on sample $\text{Mg}(\text{OH})_2$ -3-20° at $p/p_s = 0.2$. The same reduction factor was used for the isotherm for adsorption of benzene on sample $\text{Mg}(\text{OH})_2$ -1-200°. Isotherms for adsorption of benzene and hexane on sample $\text{Mg}(\text{OH})_2$ -4-20° are reduced to the corresponding absolute isotherms for sample $\text{Mg}(\text{OH})_2$ -3-20°, also at $p/p_s = 0.2$. The same reduction factors were used for isotherms for adsorption of benzene and hexane on sample $\text{Mg}(\text{OH})_2$ -4, evacuated at 100 and 200°.

It is clear from Fig. 4,a that adsorption of benzene per unit area of magnesium hydroxide in the monolayer region at the given p/p_s depends very strongly on the conditions used for the vacuum heat treatment of magnesium hydroxide.

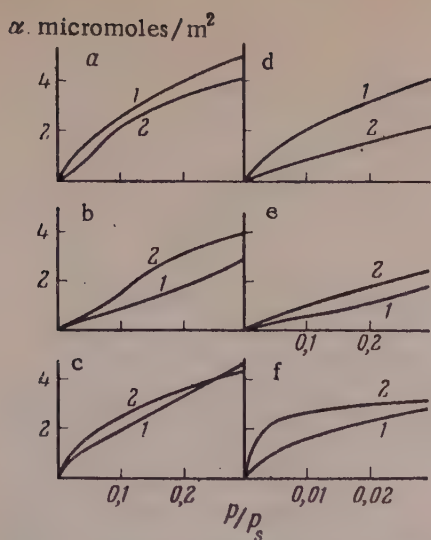


Fig. 5. Absolute isotherms for adsorption of benzene (1) and hexane (2) vapors on samples of $\text{Mg}(\text{OH})_2$ -3-20° (a), $\text{Mg}(\text{OH})_2$ -2 (b), hydrated (d) and dehydrated (e) silica gels; magnesium oxide (c); graphitized carbon black (f).

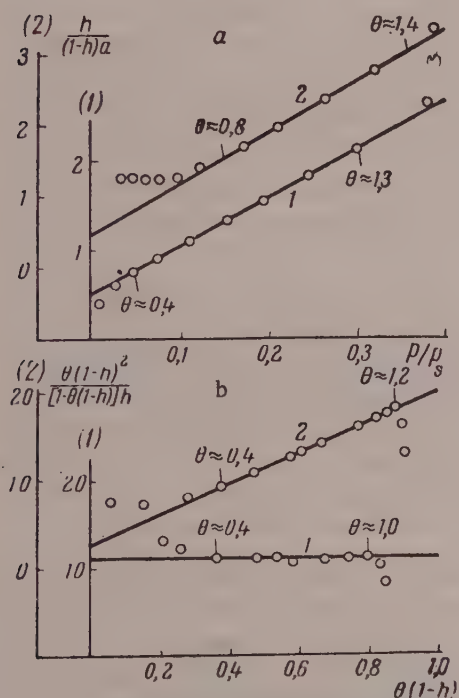


Fig. 6. Isotherms for adsorption of benzene (1) and hexane (2) in linear coordinates of the BET equation (a) and of Equation (1) (b).

by hydration of magnesium oxide [9]. It is therefore possible that the presumed extensive dehydration of the surface of $\text{Mg}(\text{OH})_2$ -2 is due to a considerable extent to deformation of its crystal lattice which occurred when it was prepared by hydration of magnesium oxide.

Fig. 4, b, shows that adsorption of hexane on magnesium hydroxide in the monolayer region decreases somewhat with intensification of the vacuum heat treatment up to 200°, but this decrease is much less pronounced than in the case of benzene. The relative positions of the isotherms for adsorption of hexane on different samples of magnesium hydroxide, evacuated at different temperatures, are approximately the same as in adsorption of benzene. In the region of multimolecular adsorption (at $p/p_s > 0.2$) the adsorption of hexane remains almost unchanged.

Further increase of the evacuation temperature of magnesium hydroxide to 350° results in a sharp increase of adsorption and makes the isotherms much steeper both for benzene and for hexane, owing to formation of fine pores in the primary platelets of magnesium hydroxide during volume dehydration [1].

The decrease in the adsorption of benzene and hexane vapors per unit surface of magnesium hydroxide due to vacuum treatment at 200° is probably caused by dehydration of the magnesium hydroxide, mainly on the surface. Since the water-vapor pressure over magnesium hydroxide at 20° is appreciable, it should decompose under high vacuum even at room temperature. However, appreciable volume dehydration of magnesium hydroxide under vacuum, during evacuation lasting several hours, occurs only at temperatures above 200° [6, 7]; this indicates that the dehydration process at lower temperatures is slow. Thermal decomposition of magnesium hydroxide probably begins at the surface of the magnesium hydroxide platelets and gradually spreads inward [8]. Therefore in the case of our sample of magnesium hydroxide: $\text{Mg}(\text{OH})_2$ -1, evacuated at 200° for 4 hours, $\text{Mg}(\text{OH})_2$ -2, after prolonged and repeated evacuation at 30°, $\text{Mg}(\text{OH})_2$ -3 evacuated at 100° for 6 hours, and $\text{Mg}(\text{OH})_2$ -4 evacuated at 100 and 200° for 4 hours, we also had different degrees of surface hydration. Considerable decomposition within the particles could not have taken place yet, as the water contents of these samples (Table 1) were still close to the theoretical water content of magnesium hydroxide. The surface of samples $\text{Mg}(\text{OH})_2$ -3 and $\text{Mg}(\text{OH})_2$ -4 carefully evacuated at 20° was apparently only slightly hydrated.

The water-vapor pressure over magnesium hydroxide at a given temperature greatly depends on the energy state of magnesium hydroxide [4], which in its turn depends on the preparation conditions [9]. This should also influence the degree of dehydration of magnesium hydroxide under the same conditions of vacuum heat treatment. Magnesium hydroxide with a very high energy content is formed

TABLE 2

Applicability Limits and Constants in the Equations for Isotherms of Multimolecular Adsorption of Benzene and Hexane Vapors on Magnesium Hydroxide

Adsorbate	BET equation					Equation (1)				
	applicability limit ^d		C	a _m , milli-moles/g	ω _m , Å ²	value taken for ω _m , Å ²	applicability limits for θ	K ₁	K _n	$\frac{K_n}{K'_1}$
	for p/p _s	for degree of coverage θ								
Benzene	0,05—0,3	0,4—1,3	11	0,17	39,5	40	0,4—1,0	11	0,1	0,01
n-Hexane	0,15—0,35	0,8—1,4	18	0,43	52	51,5	0,4—1,2	3	6,7	2,2

As was pointed out earlier, the surface of magnesium hydroxide is apparently dehydrated to different extents in accordance with the intensity of vacuum heat treatment up to 200°; magnesium hydroxide subjected to vacuum heat treatment up to 200° is, in a sense, a mixed adsorbent consisting in part of undehydrated magnesium hydroxide and in part of magnesium hydroxide with a dehydrated surface. The consequent dualism in the properties of the surface of magnesium hydroxide after vacuum heat treatment is manifested in changes in the degree of adsorption and the form of the adsorption isotherms for benzene and hexane (Fig. 2, a and 3). The probable explanation is that at low p/p_s benzene is adsorbed predominantly on the undehydrated part of the magnesium hydroxide surface (in regions more advantageous from the energy aspect), when the isotherm for adsorption of benzene vapor is convex and lies above the isotherm for hexane (see Fig. 3, a). At higher p/p_s after a considerable proportion of the hydrated part of the surface has been filled, benzene is adsorbed predominantly on the dehydrated part, when the isotherm for benzene adsorption lies below the isotherm for hexane and is concave. Consequently, as p/p_s increases, in the transition from adsorption on the hydrated to adsorption on the dehydrated part of the magnesium hydroxide surface the isotherms for adsorption of benzene and hexane should intersect and the isotherm for benzene should change from convex to concave; this is seen to be the case in Fig. 2, a and 3, a (Curves 4 and 6).

The second intersection of the isotherms for adsorption of benzene and hexane, as in the case of adsorption on graphite [10, 11], occurs because of the difference in the areas occupied by these molecules in a compact monolayer, and is directly associated with the nature of the surface.

Comparison of the absolute isotherms for adsorption of benzene and hexane on sample Mg(OH)₂-3 evacuated at 20°, the surface of which is apparently only very slightly dehydrated, and on sample Mg(OH)₂-2 evacuated repeatedly for a long time at 30°, the surface of which is strongly dehydrated, with the isotherms for adsorption of these vapors on dehydrated and on undehydrated silica gel [12] shows that the effects of dehydration on these adsorbents are very similar (Fig. 5). Thus, for undehydrated magnesium hydroxide and undehydrated silica gel the isotherm for benzene lies above the isotherm for hexane, whereas dehydration of the surface both of magnesium hydroxide and of silica gel alters the relative positions of the adsorption isotherms for these substances: in the initial region the isotherms for hexane lies above those for benzene.

Fig. 5 also shows the absolute isotherms for adsorption of benzene and hexane vapors on magnesium oxide [1] and on graphitized carbon black [10, 11]. It is clear from Fig. 5 that magnesium hydroxide and oxide differ qualitatively in their adsorption properties with respect to benzene and hexane vapors: in the monolayer region the adsorption of benzene on magnesium hydroxide is greater than adsorption of hexane, whereas on magnesium oxide and on graphitized carbon black the adsorption of hexane is greater than that of benzene.*

*Thus, benzene is adsorbed more than hexane on an undecomposed magnesium hydroxide surface. Initially, in work with a hydroxide sample evacuated at 200° (Mg(OH)₂-1-200°), we concluded that dehydration of magnesium hydroxide, unlike dehydration of silicon hydroxide, increases adsorption of benzene [13]. However, it is clear from the present investigation that the sample of hydroxide evacuated at 200° already had a very dehydrated surface.

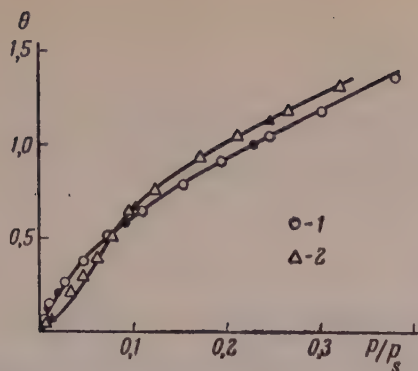


Fig. 7. Absolute isotherm of the adsorption of benzene (1) and hexane (2) on $\text{Mg}(\text{OH})_2\text{-3-20}^\circ$. The points were determined experimentally and the curves on an approximation.

much less so to adsorption of hexane. The energy constant C for adsorption of benzene and hexane is low, because of the low heats of pure adsorption of these vapors on magnesium hydroxide. The values found for ω_m for benzene and hexane on magnesium hydroxide are close to the corresponding values of ω_m on graphitized carbon black ($\sim 40 \text{ \AA}^2$ [10] and $\sim 51.5 \text{ \AA}^2$ [18] respectively).

In Fig. 6, b the experimental isotherms for adsorption of benzene and hexane on $\text{Mg}(\text{OH})_2\text{-3-20}^\circ$ are plotted in the linear coordinates of our equation

$$\frac{\Theta(1-h)^2}{h[1-\Theta(1-h)]} = K'_1 + K'_1 K_n \Theta(1-h), \quad (1)$$

where Θ is the degree of surface cover; $h = p/p_s$ is the relative vapor pressure; K'_1 and K_n are constants which give an approximate measure of the relative significance of adsorbate-adsorbent and adsorbate-adsorbate interaction. As in the previous paper [1], in determination Θ the values of ω_m were taken to be 40 \AA^2 for benzene and 51.5 \AA^2 for hexane, which are the values found for adsorption on graphitized carbon black. The applicability limits of the equation to the experimental isotherms and values of the constants K'_1 and K_n determined from the graphs are given in Table 2. In Fig. 7 the absolute values found for adsorption of benzene and hexane on the least dehydrated sample of magnesium hydroxide ($\text{Mg}(\text{OH})_2\text{-3-20}^\circ$) are compared with the values calculated from Equation (1) with the constants given above. It is clear from Table 2 and Fig. 7 that the adsorption isotherm for hexane, which has two bends, is represented satisfactorily by this equation, as is the case for isotherms of similar form for graphitized carbon black [19]. Because of residual surface heterogeneity, the experimental points of the initial region lie somewhat above the calculated curve. The BET equation does not fit the isotherm with two bends.

SUMMARY

1. The isotherms for adsorption of benzene and hexane vapors on a series of samples of magnesium hydroxide with a partially dehydrated surface have been determined.
2. The adsorption of benzene is greater than that of hexane on a sample with a slightly dehydrated surface. The isotherm for hexane in the monolayer region is initially concave, is wave-shaped, and is satisfactorily represented by the equation for multimolecular adsorption in which adsorbate-adsorbate interaction in the first layer is taken approximately into account.
3. Dehydration of the magnesium hydroxide surface decreases adsorption of these vapors, especially of benzene.

LITERATURE CITED

- [1] A. V. Kiselev and D. P. Poshkus, *Kolloid. Zhur.* 21, 590 (1959).*
- [2] A. V. Kiselev, I. E. Neimark, D. P. Poshkus, and M. A. Piontkovskaya, *Izvestiya Akad. Nauk SSSR, Otdel Khim. Nauk* 232 (1959).*

*Original Russian pagination. See C. B. Translation.

Application of equations for adsorption isotherms. We applied the BET equation for multimolecular adsorption [14] and our equation [15-17] to isotherms for adsorption of benzene and hexane vapors on the magnesium hydroxide sample with the most uniform surface [$\text{Mg}(\text{OH})_2\text{-3}$], evacuated at 20° .

The experimental adsorption isotherms are plotted in linear coordinates of the BET equation in Fig. 6, a. Table 2 gives the applicability limits of the equation and the constants found from the graphs: the energy constants C , the capacity of the monolayer a_m , and the areas occupied by benzene and hexane molecules in a dense monolayer ω_0 .

Figure 6, a and Table 2 show that the BET equation is satisfactorily applicable to adsorption of benzene, and

- [3] J. Johnston, Z. Phys. Chem. 62, 341 (1908).
- [4] R. Fricke and J. Lucke, Z. Electrochem. 41, 174 (1935).
- [5] L. D. Belyakova, O. M. Dzhigit, and A. V. Kiselev, Zhur. Fiz. Khim. 31, 1577 (1957).
- [6] G. K. Boreskov, V. A. Dzis'ko, and M. S. Borisova, Zhur. Fiz. Khim. 27, 1176 (1953).
- [7] S. J. Gregg and R. K. Packer, J. Chem. Soc. 51 (1955).
- [8] S. J. Gregg and R. J. Razouk, J. Chem. Soc. S1, 36 (1949).
- [9] R. Fricke, R. Schnabel, and K. Beck, Z. Electrochem. 42, 881, (1936).
- [10] N. N. Avgul*, G. I. Berezin, A. V. Kiselev, and I. A. Lygina, Izvestiya Akad. Nauk SSSR, Otdel Khim.* Nauk 1304 (1956).
- [11] N. N. Avgul*, G. I. Berezin, A. V. Kiselev, I. A. Lygina, and G. G. Muttik, J. Chim. Phys. 197 (1958).
- [12] L. D. Belyakova and A. V. Kiselev, Doklady Akad. Nauk SSSR 119, 298 (1958).*
- [13] L. D. Belyakova, A. V. Kiselev, D. P. Poshkus, and E. V. Khrapova, Proc. of the Second International Congress on Surface Activity, vol. 2, (Butterworth, London, 1957) p. 213.
- [14] S. Brunauer, P. H. Emmett and E. Teller, J. Amer. Chem. Soc. 60, 306, (1938).
- [15] A. V. Kiselev, Doklady Akad. Nauk 117, 1023 (1957). *
- [16] A. V. Kiselev and D. P. Poshkus, Izvestiya Akad. Nauk SSSR, Otdel Khim. Nauk 520 (1958).*
- [17] A. V. Kiselev, Kolloid. Zhur. 20, 338 (1958).*
- [18] N. N. Avgul*, G. I. Berezin, A. V. Kiselev, and I. A. Lygina, Zhur. Fiz. Khim. 30, 2106 (1956).
- [19] A. V. Kiselev, N. V. Kovaleva, V. A. Sinitsyn, and E. V. Khrapova, Kolloid. Zhur. 20, 444 (1958).*

Received September 3, 1958

*Original Russian pagination. See C. B. Translation.

INFLUENCE OF IONS IN SOLUTION ON PRECIPITATION OF A SPARINGLY SOLUBLE SALT

N. Kusheva-Markova

Chemical Institute of the Physicomathematical Faculty, Sofia State University

In studies of the relationship between the dispersity of precipitates and the concentration of dilute reacting solutions, Weimarn [1] found that for solutions of moderate and high concentrations the plot of particles size of the precipitate against concentration passes through a maximum [2]. This maximum corresponds to solutions of moderate concentration; the precipitated particles are finer with solutions of lower and higher concentrations.

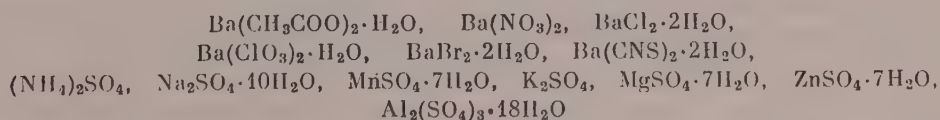
To account for this relationship, Weimarn [3] advanced a theory which, although not quantitative, makes it possible to control formation of colloidal systems of different degrees of dispersion. The relationship has been explained by Overbeek [4].

Weimarn [1, 5] and other authors [6] have given evidence for the existence of intermediate colloidal phases in precipitate formation. The concept that studies of formation of precipitates of different degrees of dispersion can be applied in the preparation of sols has been accepted in the literature [4].

Hofmeister, in a study of the effects of electrolytes on coagulation of hydrophilic colloids, showed that coagulation is influenced more by anions and less by cations. Anions can be arranged in definite series in order of their coagulating powers, in accordance with the pH of the medium; for example, the following series of anions applies to alkali-metal salts in coagulation of acid sols: citrate > tartrate > SO_4^{2-} > CH_3COO^- > ClO_3^- > Cl^- > NO_3^- > Br^- > I^- > CNS^- [7].

Such series, which are known as lyotropic, are also applicable to other effects, such as changes in the internal friction and surface tension of water, anomalies of freezing-point depression [8], catalytic decomposition of H_2O_2 in presence of a solid catalyst [9], changes of crystal habit of NH_4Cl [10], and variations of the stability of supersaturated salt solutions [11]. Such series also exist if anions are included in sparingly soluble [12] and highly soluble [13] crystalline ionic systems. It has been shown in relation to these last cases that at a given pH [14] the Hofmeister series are reversed, i.e., the relationship derived for typical colloid systems (protein substances) is applicable to typically macrocrystalline ionic salts.

In relation to the foregoing and to the problem of precipitate contamination we undertook a study of the influence of ions present in solution on precipitation of sparingly soluble salts. Variations of the sedimentation rate of BaSO_4 were studied in relation to the concentration of the original solutions and excess of component ions. BaSO_4 was the salt chosen because its precipitation conditions have been studied thoroughly and because it has a very pronounced tendency to occlude extraneous ions. The following highly soluble barium and sulfate salts were used for precipitation:



Equivalent solutions of the soluble sulfates and Ba salts were prepared at 20°. A definite solution pH was used, because this value influences the order of the ions in the lyotropic series [14]. The experiments were

TABLE 1

Sedimentation Rates of BaSO₄ Prepared by Mixing of (NH₄)₂SO₄ and BaBr₂ Solutions, with Excess of Ba²⁺ and Br⁻ (Sample 1) or of SO₄²⁻ and NH₄⁺ (Sample 2)

Normality of original solutions	2,5		1,25		0,63		0,32	
Sample numbers	2	1	2	1	2	1	2	1
Ions present in excess	NH ₄ ⁺ SO ₄ ²⁻	Ba ²⁺ Br ⁻	NH ₄ ⁺ SO ₄ ²⁻	Ba ²⁺ Br ⁻	NH ₄ ⁺ SO ₄ ²⁻	Ba ²⁺ Br ⁻	NH ₄ ⁺ SO ₄ ²⁻	Ba ²⁺ Br ⁻
Height of clear liquid layer above precipitate after 30 minutes, mm	0,5	4	18	2	83	0	124	0
Same, after 60 minutes	1	13	37	7	100	0	124	0

conducted at pH 5.7 and 10.2, because, according to Kolarow [15], the isoelectric point of BaSO₄ in crystallization from supersaturated solutions is close to pH 12.3. Solutions of the corresponding acids and bases were used for adjusting the pH of the original solutions to the required values. For example, with solutions of Ba(CH₃COO)₂ and (NH₄)₂SO₄, solutions of CH₃COOH and H₂SO₄, respectively, were used for the acid pH region, and Ba(OH)₂ and NH₄OH for the alkaline region. The ratio of the volumes of the original solutions was kept constant (11 : 8) in all cases. BaSO₄ precipitates were obtained under two different precipitation conditions: with excess of barium ions and with excess of sulfate ions, respectively, in solution. For example, with original solutions of (NH₄)₂SO₄ and BaBr₂, the BaSO₄ precipitate was prepared by two methods.

Sample 1: To 11 ml of BaBr₂ solution of definite concentration and pH, 8 ml of sulfate solution [(NH₄)₂SO₄] of the same concentration and pH, excess of Ba ions) was added at once with vigorous shaking.

Sample 2: To 11 ml of ammonium sulfate solution 8 ml of BaBr₂ solution (excess of sulfate ions) was added under the same conditions.

The white BaSO₄ suspensions formed in both cases were transferred one minute after mixing of the solutions into long narrow test tubes so that the heights of the suspension columns were equal. At equal time intervals, read off by means of a stopwatch, the clear layers of liquid over the precipitates were measured (the time was measured in minutes and the height in millimeters). The height of the transparent liquid layer after a definite time in each case was taken as a qualitative indication of the sedimentation rate. The measurements were accurate to within ± 1 mm. The reproducibility of the experiments was within the error limits.

Two series of experiments were carried out.

First series of experiments. The effect of concentrations of the original solutions on the rate of precipitation of BaSO₄ in presence of excess of one of the ions was studied. Salts of relatively high solubility at 20° were used. The barium salts: BaBr₂; BaCl₂; Ba(CNS)₂ and (NH₄)₂SO₄ were used to prepare solutions of different concentrations; these were used as the original solutions for preparation of samples 1 and 2 of BaSO₄ as described above. The results of some of the experiments, with original solutions of (NH₄)₂SO₄ and BaBr₂ at concentrations of 2.5; 1.25; 0.63 and 0.32 N, are given in Table 1.

It follows from the data in Table 1 and from results obtained with other salt pairs that with more highly concentrated solutions (2.5 N) the BaSO₄ precipitates formed with excess of Ba²⁺ have higher sedimentation rates than samples 2, formed with excess of SO₄²⁻. With more dilute solutions the sedimentation rate falls for samples 1 and rises for samples 2; with very dilute solutions (0.32 N) the sedimentation rate of samples 2 becomes very high and the process is completed after 30 minutes, whereas for samples 1 it does not even commence after 2 hours.

Second series of experiments. The influence of the nature of the ion present in excess on the sedimentation rate of BaSO₄ was investigated. The influence of anions was studied with solutions of (NH₄)₂SO₄ and Ba(CNS)₂; BaCl₂; Ba(ClO₃)₂; Ba(CH₃COO)₂ and Ba(NO₃)₂ at concentrations of 2, 1.6, 1.2, and 0.7 N. Because of the low solubility of Ba(NO₃)₂ at 20°, only a 0.7 solution of this salt was used.

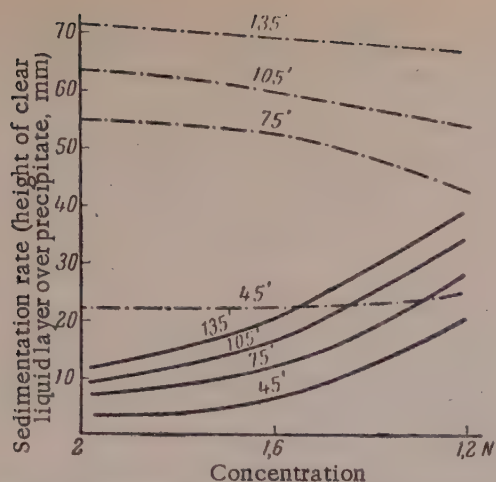


Fig. 1. Influence of ions in the sedimentation rate of precipitate from $(\text{NH}_4)_2\text{SO}_4\text{--Ba}(\text{CNS})_2$ solutions: (numbers on the curves represent the time in minutes): — = excess SO_4^{2-} , sample 2; --- = excess CNS^- , sample 1.

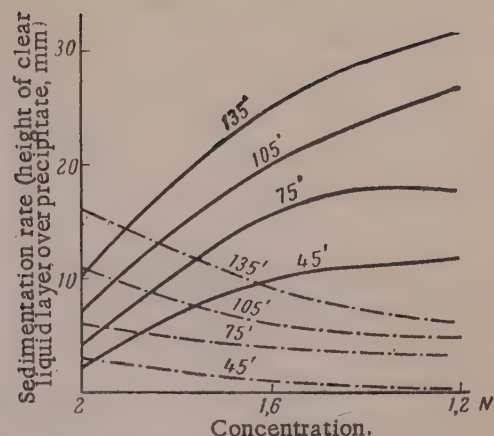


Fig. 2. Influence of ions in the sedimentation rates of BaSO_4 precipitated from $(\text{NH}_4)_2\text{SO}_4\text{--BaCl}_2$ solutions: (numbers on the curves represent the time in minutes): --- = excess SO_4^{2-} , sample 2; — = excess Cl^- , sample 1.

The results of the experiments are presented in Table 2, where samples 1 with different anions are compared. Fig. 1 and 2 show the comparative results of experiments with samples 1 and 2 for the systems $(\text{NH}_4)_2\text{SO}_4\text{--BaCl}_2$ and $(\text{NH}_4)_2\text{SO}_4\text{--Ba}(\text{CNS})_2$.

Comparison of the sedimentation rates for sample 1 (Table 2) for the same length of time (45 or 105 minutes) for the same excess of CNS^- , CH_3COO^- , ClO_3^- and Cl^- anions and at the same equivalent concentration of the original solutions shows that the anions form the following series in order of their lowering effect on the sedimentation rate:



With 0.7 N original solutions NO_3^- can also be included in this series:



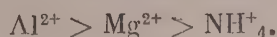
This series of anions corresponds to the Hofmeister lyotropic series.

It follows from Fig. 1 and 2 that at higher concentrations of the original solutions the sedimentation rate of sample 2 of BaSO_4 is lower than that of sample 1.

At 1.2 N (Fig. 1) and 2 N (Fig. 2) concentrations the sedimentation rate of sample 2 approaches that of sample 1. In all other cases the sedimentation rate of sample 2 is higher than that of sample 1, and increases with dilution.

These experiments were conducted at pH 5.7. The sedimentation rates of both samples are higher at pH 10.2, because this pH value is close to the isoelectric points of the samples (pH 12.3) [15].

The investigations of the influence of the nature of cations of equal valence on sedimentation rate showed that this influence is not characteristic. Therefore we studied the effects of cations of different valences: $\text{Ba}(\text{ClO}_3)_2$, $(\text{NH}_4)_2\text{SO}_4$, MgSO_4 and $\text{Al}_2(\text{SO}_4)_3$, on sedimentation at pH 5.7 and concentrations of 2 N and lower. The sedimentation proceeds at the highest rate in presence of excess $\text{Al}_2(\text{SO}_4)_3$, and at the lowest in presence of excess $(\text{NH}_4)_2\text{SO}_4$. Therefore the cations form the following series in order of their influence on the sedimentation rate:



The fact that $\text{Al}_2(\text{SO}_4)_3$ is strongly hydrolyzed in water whereas $(\text{NH}_4)_2\text{SO}_4$ and MgSO_4 are virtually unhydrolyzed was probably also significant in these experiments. On the other hand, in the pH range used $\text{Al}(\text{OH})_3$ of a colloidal degree of dispersion is precipitated [16], and this probably also influences the sedimentation rate.

The experimental data on the influence of excess ions on the sedimentation rate can be explained on the assumption that under the chosen experimental conditions the systems formed are analogous to hydrophobic colloids [11, 15] which conform to the relationships established for stability and coagulation of colloids of this type.

TABLE 2

Sedimentation Rates of Sample 1 of BaSO_4 with Excess of Different Barium Salts in Solution

Normality of original solution	Ions present in excess	Height of clear liquid layer above precipitate, mm, after				
		45 min	75 min	105 min	135 min	165 min
2,0	Ba^{2+} , CNS^-	22	55	64	72	72
	Ba^{2+} , Cl^-	3	6	11	16	20
	Ba^{2+} , ClO_3^-	1	1	2	3,5	5
	Ba^{2+} , CH_3COO^-	0	0	0	0	0
1,6	Ba^{2+} , CNS^-	23	53	60	65	70
	Ba^{2+} , Cl^-	1	4	6	9	12
	Ba^{2+} , ClO_3^-	1	1,5	2,5	4	6
	Ba^{2+} , CH_3COO^-	0	0	0	0	0
1,2	Ba^{2+} , CNS^-	25	43	55	67	73
	Ba^{2+} , Cl^-	0	3	5	8	11
	Ba^{2+} , ClO_3^-	0	0	0	0	0
	Ba^{2+} , CH_3COO^-	0	0	0	0	0
0,7	Ba^{2+} , CNS^-	27	38	50	—	—
	Ba^{2+} , Cl^-	0	0	0	0	0
	Ba^{2+} , ClO_3^-	0	0	0	0	0
	Ba^{2+} , CH_3COO^-	0	0	0	0	0
	Ba^{2+} , NO_3^-	20	34	46	51	55

On the question of the charge of the particles in BaSO_4 precipitates, the investigations of a number of workers [17-19] relating to adsorption effects in precipitation of BaSO_4 should be taken into consideration. The crystals of this salt have a heteropolar surface which may adsorb ions in conformity to the rule of Ba^{2+} [20]; in presence of excess of soluble Ba^{2+} salt the particles are positively charged (samples 1 in our experiments), whereas in presence of excess soluble SO_4^{2-} they are negatively charged (samples 2).

This primary adsorption of their own Ba^{2+} [19] or SO_4^{2-} ions, respectively, is likely to influence adsorption of extraneous ions by the particles from solution.

Although as yet there is no general theory of coagulation of hydrophobic colloids by the action of electrolytes [21], the fact that they form a series analogous to the Hofmeister series in their influence on the sedimentation rate can probably be ascribed to specific adsorption on positively-charged BaSO_4 particles. This is consistent with the fact that in coagulation of hydrophobic sols under the influence of electrolytes, ions of the opposite charge are preferentially adsorbed rather than ions of the same charge as the colloidal particles [21]. In our experiments electrolytes were present in considerable excess; therefore in explanations of coagulation and stability of hydrophobic colloids it is necessary to consider specific adsorption and size of the ions [4, 24] as well as the diffuse electric double layer [22, 23].

Since in our experiments BaSO_4 was precipitated from supersaturated solutions in presence of the same excess of soluble Ba salts, it seems likely that adsorption of these ions should influence the maximum rates of spontaneous and linear crystallization, so that coarse-grained precipitates or sols of different stabilities are obtained; this can be seen in a comparison of corresponding samples 1 and 2 formed at the same concentrations of the original solutions.

Similar effects of ionic or colloidally-dissolved impurities in solution on crystallization rates have been reported and investigated by a number of workers [25, 26], who also attributed them to adsorption phenomena.

SUMMARY

1. Changes in the concentration of the original solutions have different effects on the sedimentation rate of BaSO_4 .
2. At a definite dilution and in presence of excess Ba^{2+} ions a stable BaSO_4 sol is formed in an aqueous medium.
3. Under the experimental conditions used, anions have a more characteristic effect than cations on the sedimentation rate. Anions present in equal excess can be arranged in a series analogous to the Hofmeister series in their influence on the sedimentation rate of BaSO_4 at a given concentration of the respective original solutions.
4. The Weimarn rule is modified: not only the concentrations of the original solutions but also the nature of the ions, especially anions, present in excess in the solution must be taken into account in the application of this rule.

LITERATURE CITED

- [1] P. P. Weimarn, *Kolloides und Kristalloides Losen und Niederschlagen*, (Steinkopff, 1925).
- [2] W. Ostwald, *Die Welt der vernachlassigten Dimensionen*, 10 Aufl., (1927).
- [3] P. P. Weimarn, H. E. Buckley, *Crystal Growth* [Russian translation] (1954) p. 33.
- [4] Cited through H. R. Kruyt, *Colloid Science* [Russian translation] (Moscow, 1955).
- [5] P. P. Weimarn, *Kolloid.-Z.*, 5, 221 (1909).
- [6] Kato-Menr, *Coll. Sci. and Eng.* 2, 187 (Kyoto 1909/10); B. Lambert, W. Hume-Rothery, *J. Chem. Soc.* 2637 (1926).
- [7] R. Zsigmondy, (*Kolloidchemie*, 1912) p. 240.
- [8] A. Kuhn, *Worterbuch der Kolloidchemie*, (Dresden, 1932).
- [9] N. Kolyarov, *Izvestiya Geol. Geogr. Khim. in-ta Bulgar. A. N.* 185 (1951).
- [10] Yu. Ya. Til'mans, *Zhur. Obshechi Khim.* 18, 1754 (1948).
- [11] M. V. Tovbin and S. I. Krasnova, *Zhur. Fiz. Khim.* 25, 165 (1951).
- [12] D. Balarew, *Z. Analyt. Chem.* 120, 393 (1940).
- [13] D. Balarew, *Z. Analyt. Chem.* 122, 289 (1941).
- [14] D. Balarew, N. Kuschewa, *Jahrb. der Univ., Sofia, Phys.-math. Fak.* 2, 48, 53, (1953/54).
- [15] N. Kolarow, *Compt. Rend. de l'Academie Bulgare des Sciences* 3, 21 (1950).
- [16] G. Charlot, *Theorie et Method Nouvelle d'Analyse Qualitative* (1949), p. 155.
- [17] L. De Brouckere, *J. Phys. Chem.* 26, 250 (1929); 27, 543, (1930).
- [18] J. M. Kolthoff, W. M. McNevin, *J. Amer. Chem. Soc.* 58, 1543 (1936).
- [19] D. Balarew, *Kolloid. Z.* 67, 203, (1934).
- [20] O. Hahn, *Z. Phys. Chem.* 144, 161 (1929).
- [21] Yu. M. Glazman, D. N. Strazhesko, and B. E. Tartakovskaya, *Kolloid. Zhur.* 15, 161 (1953).*
- [22] G. Gouy, *J. Phys.* (4) 9, 457 (1910); *Ann. Phys.* (9) 7, 129 (1917).
- [23] D. L. Chapman, *Philos. Mag.* (6) 25, 475 (1913).

*Original Russian pagination. See C. B. Translation.

[24] O. Stern, Z. Elektrochem. 30, 508, (1924).

[25] R. F. Reitemeier and T. F. Buehrer, J. Phys. Chem. 44, 553 (1940).

[26] H. Freundlich and E. Oppenheimer, Ber. Deut. Chem. Ges. 58, 143 (1925).

Received July 7, 1958

APPLICATION OF THE REPLICA METHOD TO STUDIES OF ICE CRYSTALS

A. D. Malkina

Central Aerological Laboratory, Moscow

The results of microstructure observations are of great importance in studies of cloud formation and precipitation [1]. However, such observations involve considerable experimental difficulties, especially in studies of ice particles [2, 3]. For investigation of the latter it is necessary to obtain the most accurate copies of the crystals—imprints (replicas) on special supports. Replicas of ice crystals and snowflakes can be kept indefinitely and can be used for microscopic exposures of any duration.

The literature contains data on applications of the replica method for studying the surface structure of solid specimens in the electron microscope [4, 5], for electron microscope studies of ice-crystal nuclei [6, 7], and of the structure of ice [8], and for other purposes. Schaefer [9, 10] was the first to prepare replicas of ice crystals and snowflakes from winter atmospheric precipitates on films made from Formvar, a solution of polyvinyl formal resin in dichloroethane. A later paper by Schaefer [11] refers to formation of replicas by spraying of plastics. However, in this case satisfactory replicas are obtained only if the crystals are caught extremely rapidly, before the solvent can evaporate. Isono [7] used the replica technique for electron microscope investigations of formation of ice crystals in a cooling chamber by the action of silver iodide on a supercooled mist. The replicas gave an indication of the shape of the ice crystals, and crystallization nuclei were then studied in the electron microscope. Hibi [5] used methyl methacrylate for production of high-resolution replicas to be used in electron microscope studies. Attempts were made by Weickmann [12] to obtain replicas of ice crystals in clouds during aerial flights. A solution of celluloid in amyl acetate was used as the replica material. As the author himself pointed out, the results are random and not reproducible.

In view of the great practical importance of studying the ice phase in the atmosphere in meteorological investigations, the author developed a technique for preparing replicas of ice crystals; the replica-forming films were prepared from solutions of chlorinated polyvinyl chloride in dichloroethane, celluloid in amyl acetate, polyvinyl formal in dichloroethane, nitrocellulose varnish in acetone, GIPI-4 varnish, adhesive No. 227, methyl methacrylate, and solutions of polymethyl methacrylate in dichloroethane. The present paper contains a description of a method for preparation of replicas of ice crystals from films of prepolymerized methyl methacrylate and of polymethyl methacrylate dissolved in dichloroethane; these were selected from the materials tried because they gave good reproducibility of the shape, dimensions, and surface structure of the ice crystals. The replica is formed by hardening of a liquid film of the substance with an included ice crystal. After melting of the crystal and evaporation of water the remaining solid film retains an imprint of the ice particle which reproduces its surface structure as well as its shape and size.

Two methods for replica preparation were used.

1. The laboratory method, in crystallization of ice from supercooled mist in a cooling chamber. Elements of the crystalline mist were collected by sedimentation on a glass plate coated with a layer of the replica former (Fig. 1); if the crystals were very small and not numerous, a special diffusor [13] was used. After a given time (definite for each replica former) at a low temperature, the specimen was examined under the microscope and photographed. Simultaneously with replica preparation, the crystals were observed directly in a small cooling

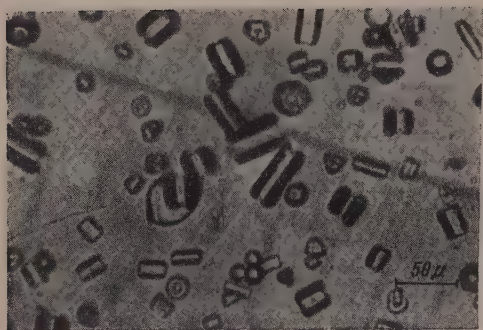


Fig. 1. Replicas of ice crystals from mist, on a film made from prepolymerized methyl methacrylate.



Fig. 2. Replica of a snowflake, on a film of prepolymerized methyl methacrylate.

chamber, on a piece of optical glass fixed inside the chamber in the focal plane of the observation microscope. This made it possible to control the quality of the replicas formed.

2. The field method, intended for preparation of replicas of ice crystals and snowflakes in natural snow-falls (Fig. 2).

The tens of thousands of replicas of crystals and snowflakes from 5 to 2000 microns in size obtained in these experiments in the temperature range from -2° to -26° on films of various substances showed that prepolymerized methyl methacrylate and a solution of polymethyl methacrylate in dichloroethane are the most suitable replica formers; their films are optically homogeneous, fairly transparent to visible light, and do not interact with water or ice. A very important advantage of these substances is that they give replicas which correspond accurately to ice crystals. The discrepancy between the linear dimensions of a replica and a crystal > 30 microns in size does not exceed 3 microns.

Before use 0.01% of benzoyl peroxide by weight is added to methyl methacrylate monomer and the mixture is heated on a boiling water bath for 25 minutes. The viscosity of the replica former is taken to 3.2 poises. The average exposure time of the film is 5 minutes. If the film was exposed to wind, the useful exposure time was shortened considerably in accordance with the wind velocity because of the increased evaporation rate of the solvent. At a velocity of 20 meters/second the useful exposure time was 10-15 seconds. During heavy falls of snow the exposure time must be shortened 2 to 3-fold to avoid multilayer deposition of crystals.

Since the physicochemical properties of prepolymerized methyl methacrylate alter with time owing to polymerization, if the substance has to be kept for more than two months it is recommended to use a 2% solution (by weight) of polymethyl methacrylate in dichloroethane. Chemically pure materials must be used for preparation of the solutions, as impurities lower the replica quality.

Samples of ice crystals are collected on glass slides, previously washed thoroughly and coated with films of the replica former from 50 to 100 microns thick immediately before exposure. With thicker films examinations of the replicas by transmitted light is difficult, while if the films are too thin the surface relief of large ice crystals is not reproduced.

Under field conditions the place of exposure of the slides for collection of ice crystals from snow or crystalline mist must be shielded from the wind and open to free access of falling ice crystals. The slides are laid horizontally at snow level.

To prevent melting of the collected crystals, the replica former and glass slides are kept at a temperature below 0° before application of the films. In order to fix the replicas throughout the film volume the slides are held at a low temperature for 20-30 minutes after the crystal samples have been taken.

This replica technique makes it possible to carry out microstructure investigations of crystalline mists and precipitations during the cold seasons of the year, and it can be applied to surface investigations of microstructure of mists when acted upon artificially from ground level and from aircraft.

SUMMARY

1. A technique has been developed for preparation of replicas of ice crystals, whereby it is possible to study the dimensions, shape, and surface structural characteristics of crystalline phases in the atmosphere over a wide range of crystal sizes.

2. This replica technique opens up possibilities for investigation of ice crystals and ice-forming nuclei in the electron microscope, and aids microstructure investigations of the crystalline phases in clouds and mists exposed to artificial influences.

LITERATURE CITED

- [1] E. G. Zak, *Metodicheskie Ukazaniya* 9 (1950).
- [2] A. M. Borovikov, *Trudy Tsentr. Aerol. Observ.* 10 (1953).
- [3] A. D. Zamroskii, *Trudy Glav. Geofiz. Observ.* 13 (1948).
- [4] E. Leont'ev and V. Luk'yanovich, *Doklady Akad. Nauk SSSR* 103 (1955).
- [5] F. Hibi and K. Jada, *J. Appl. Phys.* 25 (1953).
- [6] A. M. Borovikov, *Trudy Tsentr. Aerol. Observ.* 3 (1947).
- [7] N. Isono, *J. Meteorol Soc. Japan.* 31 (1953).
- [8] E. Truby, *J. Appl. Phys.* 26 (1955).
- [9] V. Schaefer, *Science* 93, 239 (1941).
- [10] V. Schaefer, *Nature*, 149 (1942).
- [11] V. Schaefer, *Compendium of Meteorol.* 222 (1951).
- [12] H. Weickmann, *Die Eisphase in der Atmosph.* (1952).
- [13] A. M. Borovikov, *Tr. Tsentr. Aerol. Observ.* 3 (1947).

Received July 11, 1958

INCREASE OF THE SURFACE ACTIVITY OF SULFONIC ACIDS AND SULFONATES

E. A. Myshkin

Scientific Research Institute for Oil and Gas Processing and Production
of Synthetic Liquid Fuel, Moscow

The effectiveness of surface-active agents is based upon surface tension. The surface activity required in a particular product may vary over a wide range in accordance with its purpose. For example, emulsion breakers should have the highest possible surface activity at low concentrations (to 0.01%). In such cases their surface tension at saturation concentrations of the surface layer does not appear to be of great importance. In the case of emulsifiers, on the other hand, the surface activity may be moderate but the surface film should be as strong as possible. Detergents should evidently occupy an intermediate position between emulsion breakers and emulsifiers, approaching the former, with regard to surface activity. It is therefore important to be able to regulate the surface activity of such products in the desired direction.

The surface activity of water-soluble substances increases with molecular weight, in accordance with the Traube rule. However, this relationship holds only up to a certain limit. On further increase of molecular weight the surface activity falls, to such an extent for certain substances (such as sodium cerotate) that they do not alter the surface tension of water [1].

The cause of this is that the solubility of soaps falls with increase of molecular weight and surface tension increases when colloidal micelles appear in solution. The same may occur with increasing concentration of the solution. The surface-tension isotherm changes direction and turns upward at the concentration of micelle formation.

Thus, if the solubility can be increased sufficiently, a substance of high molecular weight can exhibit surface activity. The solubility of surface-activity sulfonic acids was increased in this investigation by replacement of the cations and by the use of combinations of substances of high and low molecular weights.

It is known that ammonium soaps of organic acids are more soluble in water than the corresponding potassium or sodium soaps. Therefore the surface activity of the former is higher than of the latter. This is confirmed by the isotherms in Fig. 1 for surface tension of aqueous solutions of sodium and ammonium sulfonates prepared from the acid tar obtained in purification of spindle oil by oleum.

Figure 1 shows that in the case of the sodium sulfonate the surface tension falls up to 0.06% concentration, and then rises. Ammonium sulfate has higher surface activity without a tendency to decrease in the investigated concentration range.

Because of this higher surface activity of the ammonium sulfonate it was recommended as a more efficient emulsion breaker than the sodium compound [2]. The production and use of ammonium emulsion breakers (NChK) has been adopted in the oil industry. Evidently the same can be done with regard to other analogous surface-active agents if the introduction of an ammonium group does not adversely affect their other properties.

Sulfonic acids of different molecular weights were used for studying the effectiveness of mixing substances of high and low molecular weight. Surface tension was determined by the capillary method in neutral solutions (after neutralization with caustic soda).

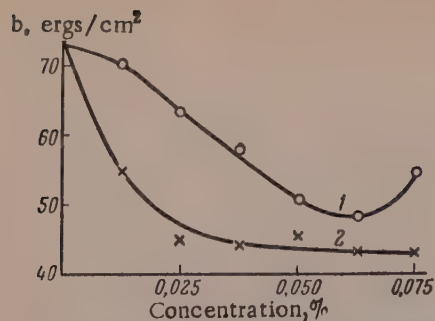


Fig. 1. Surface-tension isotherms of aqueous solutions of sodium (1) and ammonium (2) sulfonates.

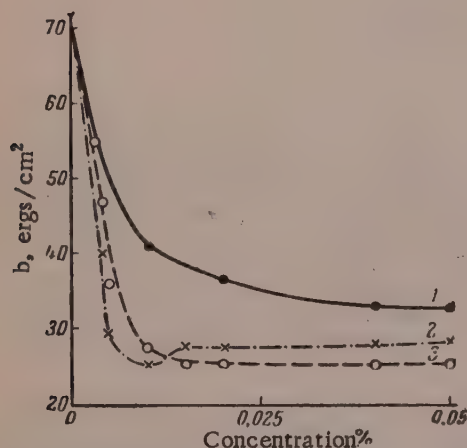


Fig. 2. Surface-tension isotherms of solutions of sulfonic acids from purification of pyrolytic toluene (1), their mixtures with 40% sulfonic acids from kerosene purification (2), and Mersolat (3).

When sulfonic acids of low molecular weight are added to sparingly-soluble sulfonic acids of high molecular weight the solubility of the latter is increased considerably. The surface activity of the mixture alters accordingly. However, the surface tension of a solution of a mixture decreases only up to a certain optimum amount of the low-molecular weight additive. The surface activity falls with further increase in the amount of the latter. Table 2 gives the results of surface-tension determinations on mixtures of sulfonic acids formed in purification of oil and kerosene. Sulfonic acids of high molecular weight were obtained from alkaline wastes after purification of spindle oil by oleum, containing 24% sulfonic acids and 50% oil. Extraction (oil removal) was effected by addition of sulfonic acids from kerosene purification; the minimum amount of the latter was 12%. Table 1 shows that increase of the amount of sulfonic acids from kerosene purification improves the surface activity of the mixture up to the optimum ratio of the components, 70:30. Further increase of the amount of sulfonic acids of low molecular weight lowers surface activity sharply.

The next series of experiments was performed with mixtures of sulfonic acids contained in the first wash liquors from purification of pyrolytic toluene and sulfonic acids from kerosene purification. During purification of the toluene fraction the unsaturated hydrocarbons present are polymerized and sulfonated to form compounds of relatively high molecular weight.

Table 2 shows that in this case the optimum amount of the component of lower molecular weight is 40%. This mixture has high surface activity in dilute solutions and low surface tension on saturation of the surface layer, which occurs at 0.015% concentration.

Sulfonic acids from kerosene purification have considerably lower surface activity than sulfonic acids from toluene wastes. This is evidently why an excess (above the optimum) lowers the surface activity of the mixture.

It follows from the surface-tension isotherms in Fig. 2 that the surface activity of the best mixtures of sulfonic acids from toluene wastes and from kerosene purification is not inferior to that of the synthetic product Mersolat, and is even better at low solution concentrations.

A similar increase of surface activity was obtained with other sulfonic acids of high molecular weight, isolated from waste products in the purification of transformer, cylinder, and white oils and of gas oil.

Interesting results were obtained by combination of three types of sulfonic acids, extracted from waste in the purification of spindle oil, toluene, and kerosene. Values of the surface tension of solutions of these mixtures and of Tergitol * solutions are compared in Table 3. According to the literature, Tergitol has very high surface activity and is used as a wetting agent in dust removal.

Table 3 shows that No. 2 mixture of sulfonic acids is close to Tergitol in surface activity, while mixture No. 1 is even better.

*Tergitol [3] is a synthetic anionic agent (molecular weight 715) of the composition:

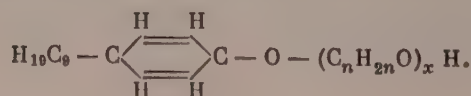


TABLE 1

Surface Tension (ergs/cm²) of Aqueous Solutions of Mixtures of Sulfonic Acids of Molecular Weight 370 and 280

Concentration of sodium sulfonates in water %	Surface tension, ergs/cm ² , of sulfonic acids of m.w. 370 in presence of sulfonic acids of m.w. 280 (kerosene purification), % of mixture			
	12	20	30	35
0,0125	69	63,3	65,5	71,3
0,0250	59	56	55,1	65,7
0,0375	57	50,3	47,5	57,5
0,05	51,5	47,3	44,0	50,8
0,075	47,4	41,5	42,9	49,2
0,10	47,0	40,6	40,0	46,7
0,15	42,0	44,0	36,0	42,0

TABLE 2

Surface Tension (ergs/cm²) of Aqueous Solutions of Sulfonic Acids from Purification of Pyrolytic Toluene and Their Mixtures with Sulfonic Acids from Kerosene Purification

Concentration of sodium sulfonate in water, %	Surface tension, ergs/cm ² , of sulfonic acids from kerosene purification mixed with sulfonic acid from toluene purification %				
	0	20	40	45	100
0,003	72,7	72,7	55	72,7	72,7
0,004	72,7	72,7	47,5	72,7	72,7
0,005	72,7	70,0	36,0	43,0	72,7
0,01	72,7	65,0	27,5	39,0	72,7
0,015	41,2	43,7	25,6	35,0	67
0,04	33,7	40,0	25,6	32,5	58
0,10	33,7	35,0	25,6	—	48,7
0,30	36,8	35,0	26,9	—	31

TABLE 3

Surface Tension (ergs/cm²) of Aqueous Solutions of Ternary Mixtures of Sulfonic Acids and of Tergitol

Concentration in water, %	Surface tension, ergs/cm ²				Concen- tration in water, %	Surface tension, ergs/cm ²			
	mix. of sulfonic acid			tergitol		mix. of sulfonic acids			tergitol
	№ 1	№ 2	№ 3			№ 1	№ 2	№ 3	
0,0005	70,0	62,1	—	—	0,003	33,7	48,5	41,6	38,5
0,001	40,6	53,4	—	—	0,004	31,3	42,7	—	34,5
0,0013	39,6	52,8	—	44,2	0,005	31,2	42,6	40,6	34,3
0,0022	36,5	49,3	—	40,5	0,01	30,0	38,8	30,8	—
0,0025	35,0	48,8	—	39,5	0,02	33,0	37,8	30,0	—

* The sulfonic acid mixtures No. 1 and No. 2 had the following composition: sulfonic acids from wastes of spindle oil purification 55.6%; from purification of pyrolytic toluene 15.8%; from kerosene purification, 28.6%. Mixture No. 1 was prepared in 1952, and mixture No. 3 in 1957. Mixture No. 3 consisted of the following sulfonic acids: from purification of solar oil, 63%; from kerosene purification, 24.6%; from purification of pyrolytic toluene, 12.4%.

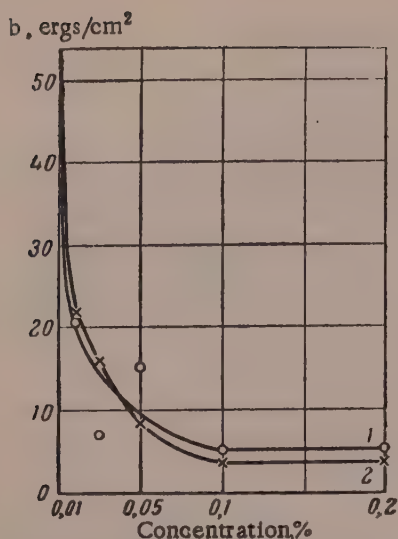


Fig. 3. Interfacial-tension isotherms for calcium sulfonates containing 12% (1) and 30% (2) of low-molecular weight sulfonic acids in white oil at the water interface.

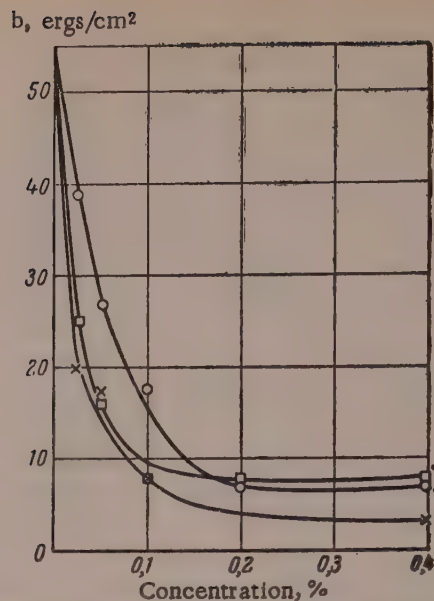


Fig. 4. Interfacial-tension isotherms for aluminum sulfonates in petrolatum, containing 30% (1), 12% (2), and 35% (3) of low-molecular weight sulfonic acids at the water interface.

Thus, by using sulfonic acids of high and low molecular weight in different proportions, we can obtain mixtures with various surface activities. The most active of these can be used as emulsion breakers or additives for dust wetting and silicosis control.

Combinations with lower contents of the lighter components, the adsorption films of which are stronger, are suitable for preparation of emulsifiers and dispersing agents. They should have an alkaline reaction for higher activity.

The selection of the most active three-component mixtures is made difficult because a large number of samples must be prepared and tested.

In this method for raising the surface activity, the component of low molecular weight must evidently be a substance allied to the component of high molecular weight, (wastes from kerosene purification in this case); attempts to replace it by acetic, isovaleric, and isobutyric acids were unsuccessful.

Increase of the surface activity of sulfonic acids makes it possible to prepare highly effective calcium and aluminum sulfonates soluble in hydrocarbons from them. Fig. 3 and 4 show interfacial-tension isotherms (determined by Rebinder's method) for solutions of these sulfonates in medicinal oil at the water interface. The sulfonates were prepared from mixtures of sulfonic acids obtained in purification of spindle oil and kerosene; their surface tensions are given in Table 1. It is seen that sulfonates obtained from mixtures of highest surface activity at the air interface have the highest activity at the water interface [4]. This fact enabled the author to obtain highly effective demulsifiers for dewatering and desalting petroleum [5].

The foregoing data suggests that the method described should have extensive applications for raising and regulating the surface activity of various surface-active agents, both water-soluble and soluble in hydrocarbons.

SUMMARY

1. Methods have been worked out for raising the surface activity of sulfonic acids and sulfonates, by introduction of the ammonium cation and by the combined use of sulfonic acids of high and low molecular weight.

2. These methods can be used for increasing sharply and regulating the surface activity of sulfonic acids and sulfonates soluble in water and in hydrocarbons.

LITERATURE CITED

- [1] P. A. Rebinder, Physical Chemistry of Detergent Action [in Russian] (Food Industry Press, 1934).
- [2] E. A. Myshkin, Neftyanoe Khozyaistvo 8 (1950).
- [3] P. L. Walker et al., Ind. Eng. Chem. 44, 2389 (1952).
- [4] E. A. Myshkin, Use of Oil-Soluble Demulsifiers for Demulsification and Desalting of Oils [in Russian] (Dissertation, Moscow, 1952).
- [5] E. A. Myshkin, Authors' Certif. TP-6710 (1937).

Received August 1, 1958

INVESTIGATION OF LATEX FOAMS

I. FOAMING POWER OF RUBBER LATEX

D. M. Sandomirskii and A. A. Korotkova

Scientific Research Institute of Rubber and Latex Goods, Moscow

The process for production of sponge rubber from rubber latex is being increasingly widely used. One of the most important stages in this process is foaming of the latex mix, i.e., its conversion into a form which yields spongy rubber after gelation (coagulation) and vulcanization. The latex foam should have a number of definite properties; primarily, it should be stable enough not to break down under the influence of electrolytes during coagulation and of elevated temperatures during vulcanization.

The literature contains a very large number of publications dealing with foams of molecular and colloidal solutions of surface-active substances, but analogous studies of latex foams are entirely lacking. Publications dealing with the production of sponge rubber from latexes are concerned with descriptions of the technological process, equipment, and properties of the finished product [4]. Only very recently a paper concerned with the stability of latex foams has been published [5].

Rubber latex is a polydisperse system in which the dispersion medium is a solution of colloidal, semicolloidal, and molecularly-soluble substances, and the disperse phase consists of rubber globules with adsorbed layers of surface-active substances. In the case of latex mixes the system also contains particles of the other ingredients. Foaming in such a complex system and the properties of the foam formed should differ considerably from those of solutions of surface-active substances.

This work was concerned with an investigation of the stability and other properties of latex foams. The present communication contains some results obtained in a study of the foaming power of butadiene-styrene latexes. Similar data were obtained for a number of other synthetic latexes, so that the results are of a fairly general character.

Initially, the criterion of foaming power of latex was taken to be the "limiting" height h_0 of a foam column attained before destruction begins, as proposed by Dumanskii [2]. If the life of one foam bubble is τ ; then with air entering the liquid through the capillary at velocity u foam will build up until the height of the foam column becomes

$$h_0 = u\tau.$$

Evidently h_0 depends on the properties of the system and may serve as a measure of foaming power.

The apparatus used for foam formation in latex until the start of foam collapse is shown in Fig. 1.

Water flows at a definite rate, regulated by the stopcock 2, from the 250 ml measuring cylinder 1 filled above the top mark through the open cock 3 into the bottle 4 and displaces air from it. The air velocity is measured by means of the flowmeter 5, and the pressure by the manometer 6. The cock 7 is used to adjust the apparatus to a definite air velocity. The stopper of the cock 8 has two orifices at right angles to each other, corresponding to the two branches. The left branch of the cock, terminating in a capillary, leads to the stopper of the foaming vessel 9, and the right branch communicates with the atmosphere.

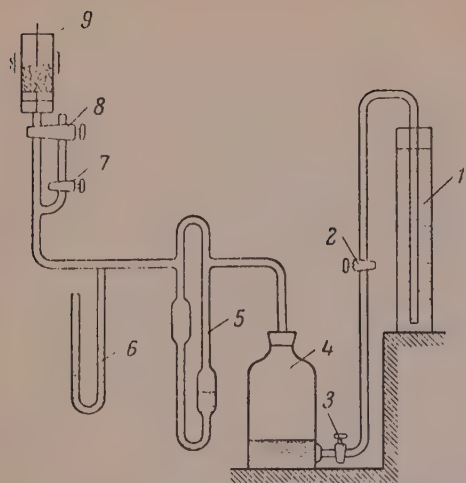


Fig. 1. Apparatus for studying foaming power of latex.

To adjust the apparatus to the required air velocity the stopper of the cock 8 is turned so that the left orifice is closed and the right is open. By regulation of the rate of water flow from the measuring cylinder 1 into the bottle 4 and by adjustment of the regulating cock 7 it is possible to obtain the required air velocity in the apparatus, with the aid of the flowmeter 5, with the pressure in the apparatus corresponding to the resistance of the investigated liquid layer in the vessel 9.

As a preliminary stage in the experiment, while water in the measuring cylinder is falling to the upper mark, the required air velocity is established in the apparatus. At the instant when the water in the cylinder 1 has reached the mark the stopper of the cock 8 is quickly turned and air is directed into the foaming vessel 9. The stopwatch is started at this instant. Foaming then begins, and ends when the first 2-3 bubbles in the surface layer of the foam have burst. At that instant the cock 3 is

closed and the stopwatch is stopped. This gives the foaming time to the start of collapse, as measured by the stopwatch, and the volume of the foam formed during this time as given by the volume of water flowing out of the measuring cylinder.

Clearly, the volume of the foam formed is equivalent to the "limiting" height h_0 .

Experiments on foaming of different latexes at different air velocities showed that the "limiting" volume of foam is not characteristic of a given system, as it depends considerably on the air velocity. The higher the air velocity, the greater the volume of foam which can be obtained before the start of collapse, and the more rapid the collapse.

Table 1 contains results obtained in experiments on foaming of SKS-30 butadiene-styrene latexes of different concentrations and of Nekal solution (used as the emulsifier in this latex) at different air velocities.

TABLE 1

Limiting Foam Volumes for Butadiene-Styrene Latex and Nekal Solution

SKS-30 latex						Nekal solution		
30%			25%			3,25%		
Limiting volume V, cc	Foaming time t, sec	Vt, cc. sec	limiting volume V, cc	foaming time t, sec	Vt, cc. sec	limiting volume V, cc	foaming time t, sec	Vt, cc. sec
64	18	1150	12	18	216	84	30	2520
60	25	1500	13	16	208	83	29	2400
42	24	1010	11	16	176	78	29	2260
45	26	1170	15	11	165	76	34	2580
43	31	1330	13	11	143	68	31	2100
40	44	1760	18	9	162	64	31	1980
25	43	1070	26	8	208	61	36	2200
25	50	1250	23	7	161	60	43	2580
23	55	1260	23	8	184	48	56	2680
Average		1280	Average		180	Average		2370

Table 1 shows that the product of the "limiting" foam volume V and time t (Vt) taken to reach this volume (equal to the life of a single bubble) is independent of the air supply rate, and may serve as the measure of the foaming power of a given system.

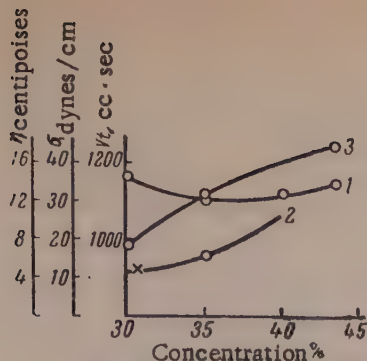


Fig. 2. Variations of the properties of SKS-50N latex with concentration: 1) surface tension; 2) viscosity; 3) foaming power.

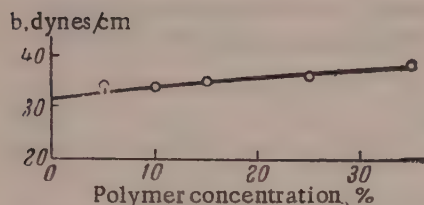


Fig. 3. Effect of polymer content on the surface tension of 4.3% Nekal solution.

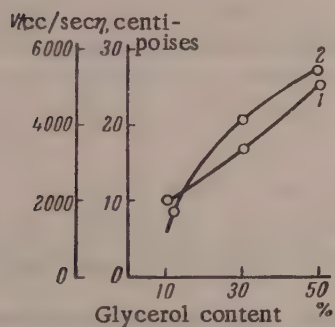


Fig. 4. Effect of glycerol content on properties of SKS-30 latex: 1) viscosity; 2) foaming power.

It can be shown that the value of V_t is determined by the physicochemical properties of the foamed liquid. It was observed during pneumatic foaming of latexes that the volume V_1 of a single foam bubble increases with the air velocity. Assuming that the "limiting" foam volume is

$$V = V_1 n,$$

where n is the number of bubbles in the foam, assumed approximately to be constant, we can write

$$Vt = V_1 nt = \text{const.} \quad (1)$$

or

$$V_1 t = \text{const.} \quad (2)$$

It follows from Equation (2) that for a given system the life of a single bubble, or its stability, decreases with increase of its volume (this was observed experimentally in qualitative form), and that for a given bubble stability the greater the bubble volume the higher the foaming power of the system.

The following forces act on a bubble formed at the tip of a capillary when air is blown slowly through the layer of foaming liquid:

1) the buoyancy force which tends to detach the bubble from the capillary

$$F_1 = V_1 (D - d) g, \quad (3)$$

where D is the density of the liquid, d is the density of air, and g is the acceleration due to gravity;

2) the vertical component of surface tension, tending to hold the bubble at the capillary

$$F_2 = 2\pi r \sigma \sin \alpha = 2\pi \sigma \frac{r^2}{R}, \quad (4)$$

where r is the capillary radius; σ is the surface tension at the liquid-air interface; α is the angle formed between the tangent to the bubble surface and the perpendicular to the capillary axis at the base of the bubble; R is the bubble radius.

Calculations show that under our experimental conditions F_2 is negligible in comparison with F_1 . Therefore there must be some other force which prevents separation of the bubble from the capillary. This may be the force of viscous resistance of the liquid. When the bubble forms and grows the liquid layers in contact with its surface are displaced. The higher the liquid viscosity, the greater the resistance offered by the movement of these layers to increase of the bubble volume and separation from the capillary. In the general form this resistance may be expressed by the Newton equation

$$F_3 = \eta S \frac{du}{dz}, \quad (5)$$

TABLE 2

Effects of Surface-Active Substances on Foaming Power of Dialyzed Latex

SKS-50N latex					Solution of surface-active agent		
additive	amt. added, %	σ , dynes/cm	η	Vt, cc. sec	concent- ration %	σ dynes/cm	Vt, cc. sec
—	—	45,4	4,7	83	—	—	—
Nekal	1	40,4	4,4	282	0,5	33,8	396
Same	2	37,6	4,3	360	1,0	32,9	380
»	3	33,7	4,4	680	1,5	32,9	414
Sodium oleate	1	39,0	4,2	53	0,5	35,0	372
Same	2	36,0	4,2	85	1,0	27,2	705
»	3	34,2	4,2	140	1,5	29,0	520

where η is the viscosity of the liquid; S is the area of contact between the bubble and the liquid; du/dz is the velocity gradient of the liquid layers. At the instant when the bubble is detached from the capillary the forces F_1 , F_2 , and F_3 are balanced, i.e.

$$F_1 = F_2 + F_3 \quad \text{or} \quad V_1(D-d)g = 2\pi\sigma \frac{r^2}{R} + \eta S \frac{du}{dz}. \quad (6)$$

Hence the volume of the bubble at the instant of separation from the capillary is:

$$V_1 = \frac{2\pi\sigma \frac{r^2}{R} + \eta S \frac{du}{dz}}{(D-d)g}. \quad (7)$$

Substituting this expression for V_1 into Equation (1) we have the following expression for the foaming power of the system:

$$Vt = V_1 nt = \frac{2\pi\sigma \frac{r^2}{R} + \eta S \frac{du}{dz}}{(D-d)g} nt, \quad (8)$$

which connects the foaming power with such properties of the foamed liquid as the surface tension and viscosity.

In studies of latex foaming Vt was taken to be the measure of foaming power. The foaming experiments were conducted in the apparatus described above, with the same capillary and at the same air velocity in each case, and average values from 5-10 experiments were taken for Vt . The surface tension of the latex was measured by the maximum bubble pressure method, and viscosity by the Hoepler method.

Variations of the surface tension, viscosity, and foaming power of the latex with concentration are plotted in Fig. 2. The original latex was diluted with distilled water. The surface tension varies only slightly with dilution, but viscosity and foaming power depend strongly and approximately equally on concentration.

For a more detailed investigation of the influence of surface tension on foaming power SKS-50N butadiene-styrene latex was dialyzed. This raised the surface tension by 10-12 units. Nekal and potassium oleate were added to the dialyzed latex in the proportions of 1, 2, and 3% on the dry substance. The latex concentration remained constant (34%). Solutions of these substances at the concentrations found in latex serum were also investigated. The results are given in Table 2.

It follows from Table 2 that addition of surface-active agents has almost no effect on the viscosity of the latex and therefore the observed change in the foaming power is due to changes of surface tension. The surface tension of latex is always somewhat higher than that of a surface-active agent of the corresponding concentration.

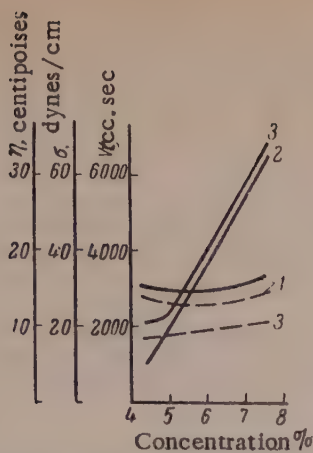


Fig. 5. Comparison of properties of SKS-50N latex (continuous line) and Nekal solutions (dash line): 1) surface tension; 2) viscosity; 3) foaming power.

increase in the foaming power of latex is small when potassium oleate is added, whereas it is considerable after addition of Nekal. This is probably because mixed adsorption layers of lower stability are formed at the liquid-air interface when the soap is added.

To determine the effect of viscosity, foaming experiments were performed with latex the viscosity of which was varied by addition of glycerol. The surface tension remained unchanged. The results, plotted in Fig. 4, show that foaming power increases appreciably with rise of viscosity. The symbatic variation of foaming power and viscosity is clearly seen. Similar relationships were observed on comparison of viscosity, surface tension, and foaming power of latex (not dialyzed) containing different amounts of Nekal, and of Nekal solutions of the same concentrations. The results are presented in Fig. 5 (data on the viscosity of Nekal solutions are not given in Fig. 5; the value is about 1 centipoise and depends little on concentration). Increase of Nekal concentration has little effect on the surface tension either of the original undialyzed latex or of the solution, but produces a considerable increase in the structural viscosity of the latex. The foaming power of the latex also increases sharply. The foaming power of Nekal solutions varies little, in accordance with the slight changes in their surface tension and viscosity.

The results therefore show that, in contrast to solutions of surface-active agents, the foaming power of latex depends not only on surface tension but also on viscosity, especially if the latter becomes of the structural type, as in the case of concentrated latex or on addition of thickening agents if this does not cause destabilization of the latex.

The foaming power of latexes of relatively low concentration (25-30%) and low viscosity the foaming power is determined by their surface tension, increasing with decrease of the latter. In Equation (8) the foaming power Vt increases primarily owing to the value of t , representing the stability of a foam bubble, which increases with decrease of surface tension σ .

At a certain sufficiently low value of the surface tension, which is characteristic of commercial butadiene-styrene latex, the foaming power rises sharply with increase of viscosity. In this case Vt in Equation (8) increases both owing to the viscosity of the system η and to t , which increases with the viscosity.

The experiments show that the rate of draining of the liquid from the foam films decreases with increase of viscosity; this slows down attenuation of the films and therefore raises the foam stability. Moreover, the strength of the foam films should increase with thickening, and this also leads to increased foam stability and foaming power of the system.

SUMMARY

1. The foaming of rubber latex was studied at different velocities of air blown through it. The product of the foam volume V and the time of foam formation to the start of collapse t is independent of the air velocity and is a measure of the foaming power of the latex.

This is because part of the surface-active agent added to the dialyzed latex is adsorbed by the globules so that its concentration in the serum decreases. However, the globules may also have a direct influence on this surface tension of the latex. To test this hypothesis, SKS-50N latex was diluted, not with distilled water, but with solution of emulsifier of the same concentration as in the latex serum. Fig. 3 shows that in this case the surface tension increases with the latex concentration although the concentration of surface-active agent remains constant. The globules make the surface tension of the latex higher than that of a solution of the surface-active agent of the same concentration.

Table 2 shows that the foaming power of the latex increases with decrease of surface tension on addition of Nekal or potassium oleate, but the nature of the increase depends on the surface-active agent added. Thus, the

2. The effects of latex concentration, surface tension, and viscosity on foaming power were investigated.
3. In a fairly concentrated latex the principal factor determining foam stability is the viscosity.

LITERATURE CITED

- [1] P. A. Rebinder, Zhur. Russ. Fiz.-Khim. Obschestva, Ch.Fiz. 58, 517 (1926); Physical Chemistry of Detergent Action, Collected Research Papers [in Russian] (Moscow-Leningrad, 1935); Bartsch, Kolloid.-Z. 38, 177 (1926); D. T. Talmud and S. D. Sukhoval'skaya, Zhur. Fiz. Khim. 11, 31 (1931); B. Tyutyunnikov and N. Kas'yanov, Masloboino-Zhirovoe Delo 2, 40 (1930).
- [2] A. V. Dumanskii, T. A. Granskaya, and N. V. Novikov, Trudy Tsentr. N.-I. Biokhim. In-ta Pishchevoi Prom. 3, 361 (1933).
- [3] K. N. Arbuzov and B. N. Grebenshchikov, Zhur. Fiz. Khim. 10, 32 (1937); J. Bikerman, Trans. Faraday Soc. 34, 634 (1938); A. M. Rozenfel'd, Physical Chemistry of Stable Mechanical Air Foams Used in Fire Fighting [in Russian] (Moscow, 1941); E. M. Savitskaya and P. A. Rebinder, Kolloid. Zhur. 13, 200 (1951); B. V. Deryagin and A. S. Titievskaya, Kolloid. Zhur. 15, 416 (1953).
- [4] Mc. C. H. Fadden, Ind. Rubber World 121, 419 (1950); E. C. Crocker, Rubber Age 67, 305 (1950); L. Talalay, A. Talalay, Ind. Eng. Chem. 44, 791 (1952); R. Noble, Latex in Industry, 4 (1953); C. F. Flint, Natural Latex and its applications (Leningrad, 1954) [Russian translation]; E. A. Murphy, Trans. Proc. Instn. Rubber Ind. 31, 90 (1955).
- [5] A. J. de Vries, Rec. Trav. Chim. 77, 81, 209, 283 (1957).

Received May 27, 1958

AGGLOMERATION OF LATEX PARTICLES BY THE ACTION OF SODIUM CHLORIDE

S. A. Selivanovskii and N. M. Ershova

The S. V. Lebedev Scientific Research Institute of Synthetic Rubber, Leningrad

It is known [1, 2] that fluid concentrates with high polymer contents, which are of practical importance in a number of cases, can be obtained only from latexes containing large polymer particles. Such latexes can be obtained either in the course of synthesis by suitable modification of the polymerization conditions (decrease of the amount of emulsifier, etc.) or by increase of the particle size in the finished latexes, which may be achieved by addition of electrolytes [3] or solvents [1].

The first way inevitably slows down the reaction and lowers the output of the equipment, as the rate of polymerization in emulsion depends on the number of particles per unit volume [4] or their total surface [5]. In the second case polymerization may be effected at a high rate, but a special operation—agglomeration of the latex particles—must be performed. The purpose of the present investigation was to determine the basic conditions for increasing the particle size in latexes, prepared by polymerization of various monomers with different emulsifiers, by the action of electrolytes (sodium chloride). The results obtained may at the same time help in understanding the processes taking place at the early stages of latex coagulation.

The following latexes were synthesized for the investigation: 1) butadiene—styrene latex SKS-30, with the sodium soap of synthetic fatty acids ("sodium paraffinate") as emulsifier; 2) chloroprene latexes with sodium oleate, Nekal, and OP-10 wetting agent as emulsifiers; 3) polystyrene latex with sodium oleate as emulsifier. The synthetic fatty ("paraffinic") acids comprised a technical mixture of saturated fatty acids with between 10 and 16 carbon atoms in the chain, acid number 252, and average molecular weight 222. Nekal (sodium di-sec-butyl-naphthalene sulfonate) was the technical product carefully purified to remove mineral salts (sodium sulfate and sodium chloride) by repeated solution in butyl alcohol followed by evaporation of the butyl alcohol and vacuum drying; it contained 98.5% surface-active material (the rest was water). Wetting agent OP-10 was the technical product of condensation of alkyl phenols with ethylene oxide [6], containing 11.25% water; the average molecular weight was 690* [7]. The latexes were stabilized by 1% of hydroquinone (used as 3% aqueous solution calculated on the monomers taken). Unchanged monomers were removed from the butadiene—styrene and polystyrene latexes by steam distillation under vacuum. Brief details of the latexes are given in Table 1.

The average volume—surface radius of the latex particles was determined by adsorption titration with a solution of the emulsifier used in the production of the given latex, until the start of formation of soap micelles in the aqueous phase as found from changes in the surface tension at the latex—air interface determined by means of the du Nouy tensiometer [7].

The use of this method with agglomerated latexes is justified by the fact that, as was demonstrated by Schmidt and Kalsey [3], compact spherical particles rather than loose aggregates coalesced at separate points are formed in agglomeration.

The areas occupied by molecules of different emulsifiers in the adsorption layer were determined by parallel titrations of the latexes with solutions of the emulsifiers and sodium oleate, the area occupied by a sodium oleate molecule being taken as $28.2 \cdot 10^{-16} \text{ cm}^2$, as given by Maron [8]. The results, used in subsequent calculations, are given in Table 2.

*Found from the hydroxyl content by phthalation.

TABLE 1

Main Properties of Latexes

Latex	Emulsifier	Conversion %	Solids content, %	pH of latex	Particle radius, m μ
SKS-30 latex	Sodium paraffinate	79,0	30,7	9,3	17,4
Polystyrene latex	Sodium oleate	92,7	33,9	10,1	38,6
Chloroprene latex	Same	99,6	37,3	11,4	39,0
Same	Nekal	99,9	37,4	12,0	44,5
	OP-10	98,9	37,0	11,8	32,2

TABLE 2

Areas Occupied by Molecules of Different Emulsifiers in the Adsorption Layer

Emulsifier	Adsorption area of molecule $\times 10^{16}$, cm ²
Sodium oleate	28.2
Potassium paraffinate	34.5
Nekal	45.1
OP-10	74.5

TABLE 3

Variations of Particle Size in Polystyrene Latex and SKS-30 Latex with Sodium Chloride Concentration in the Aqueous Phase after 9 Days

NaCl content of aqueous phase, %	0	0.2	0.5	0.75	0.9	1.5	1.9	2.0
Particle radius in SKS-30 latex, m μ	17.4	17.5	18.4	23.2	—	50.4	56.5	Latex coagulates
Particle radius of polystyrene latex, m μ	38.7	—	38.3	38.2	Latex coagulates			

The determinations of particle size were accompanied by determinations of the degree of saturation of the adsorption layers on the latex particles by the emulsifiers, i.e., the ratio, expressed as a percentage, of the amount of emulsifier in the layers before titration to the amount present at the instant of micelle formation in the aqueous phase [9].

To investigate the agglomerating action of sodium chloride, equal weights of aqueous sodium chloride solutions of different concentrations were added to weighed portions of latex in which the particle size had been previously determined, and the liquids were mixed thoroughly. The mixed liquids were kept for 9 days at room temperature (preliminary experiments showed that particle agglomeration is almost complete at the end of this time) and those which did not undergo phase separation or coagulation were then diluted with an equal quantity

TABLE 4

Variations of Particle Size in Chloroprene Latex with Sodium Chloride Concentration in the Aqueous Phase after 9 Days

NaCl content of aqueous phase, %	Particle radii of chloroprene latexes, m μ , in presence of emulsifiers		
	sodium oleate	nekal	OP-10
—	39,0	44,5	32,2
0,5	39,4	—	—
0,6	39,5	—	—
0,8	42,4	—	—
1,0	46,6	46,2	33,0
1,4	100,4	—	—
1,5	Separation	48,6	—
2,0	»	54,3	—
2,2	»	Separation	—
12,3	»	»	33,9

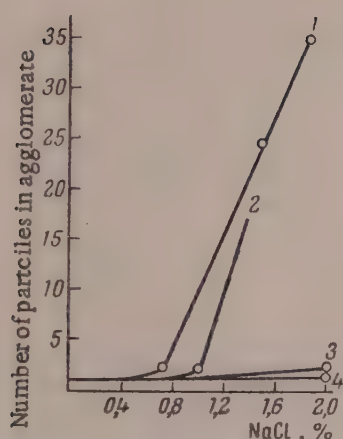


Fig. 1. Average number of particles in an agglomerate as a function of sodium chloride concentration in the aqueous phase, after 9 days of storage:
1) latex SKS-30 with sodium paraffinate;
2) chloroprene latex with sodium oleate;
3) same, with Nekal; 4) same, with OP-10.

of water (pH \sim 11) to lower the salt concentration below the critical value* and to stop further agglomeration of the particle. The average volume-surface radius of the particles in the diluted samples was determined. To determine variations of particle size with time, samples were prepared containing the maximum amount of salt which does not cause phase separation and coagulation of the latex, and portions were taken out after 3, 6, and 9 days for determination of the particle size (after the appropriate dilution). The results are given in Tables 3-6 and Fig. 1-6.

It follows from these results that the effects of added sodium chloride differ in accordance with the nature of the emulsifier and polymer. In butadiene-styrene and chloroprene latexes made with fatty acid soaps as emulsifiers addition of sodium chloride in amounts to give over 0.7% (the critical concentration) in the aqueous phase results in appreciable agglomeration of the latex particles; the extent of this agglomeration increases with the salt concentration until the latex loses its stability. At the limit the average volume-surface radius of the particles can be increased more than three fold in the case of butadiene-styrene latex (Table 3) and 2.5-fold in the case of chloro-

prene latex (Table 4). In chloroprene latex with Nekal as emulsifier particle agglomeration is considerably less: the maximum increase of particle size attained in this case was only 122% (Table 4). This is probably because dibutyl-naphthalene-sulfonic acid is a considerably stronger acid than oleic and the saturated fatty acids. In chloroprene latex, prepared with the nonionic emulsifier OP-10, stability is due to the high mechanical strength of the protective layer on the particles, which are virtually uncharged,** and therefore addition even of very large amounts of sodium chloride (12.3% in the aqueous phase) does not cause particle growth.

Addition of sodium chloride in an amount sufficient to give 0.75% in the aqueous phase to deodorized polystyrene latex made with sodium oleate did not cause either lowering of surface tension or increase of particle

* Here the critical concentration is taken to mean the minimum salt concentration at which particle agglomeration begins.

** In this case the zeta potential is very small and is of the induced type.

TABLE 5

Variations of Particle Size with Time in Butadiene—Styrene and Chloroprene Latexes on Addition of Sodium Chloride

Latex	Emulsifier	NaCl content of aqueous phase, %	Particle radius, m μ , after storage time in days			
			0	3	6	9
SKS-30	Sosium paraffinate	1,5	17,4	37,6	47,5	50,4
Chloroprene	Sodium oleate	1,4	39,0	83,1	95,1	100,4
Same	Nekal	2,0	44,5	53,8	—	54,3

TABLE 6

Variations of the Degree of Saturation of the Protective Layers with Emulsifier (%) after 9 Days with the Concentration of Added Sodium Chloride in the Aqueous Phase

NaCl content of aqueous phase, %	SKS-30 latex with sodium paraffinate %	Chloroprene latexes %		NaCl content of aqueous phase, %	SKS-30 latex with sodium paraffinate %	Chloroprene latexes, %	
		with sodium oleate	with nekai			with sodium oleate	with nekai
0,00	18,1	34,6	33,7	1,00	—	41,5	40,7
0,50	18,3	—	—	1,40	—	88,5	—
0,60	—	34,6	—	1,50	55,9	—	43,9
0,75	24,3	—	—	1,90	66,5	—	—
0,80	—	36,8	—	2,00	—	—	47,9

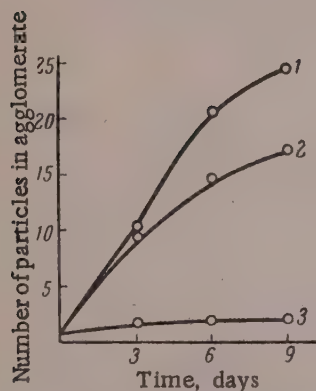


Fig. 2. Effect of storage time on the number of particles in agglomerates formed after addition of sodium chloride: 1) SKS-30 latex with sodium paraffinate; 2) chloroprene latex with sodium oleate; 3) the same, with Nekal.

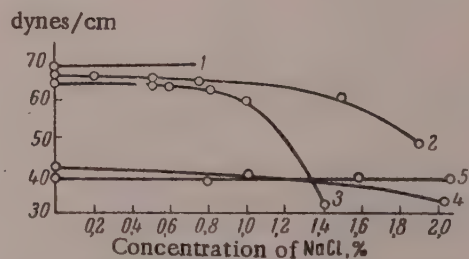


Fig. 3. Surface tension variations of different latexes with concentration of sodium chloride in the aqueous phase, after 9 days of storage: 1) polystyrene latex with sodium oleate; 2) SKS-30 latex with sodium paraffinate; 3) chloroprene latex with sodium oleate; 4) same, with Nekal; 5) same, with OP-10.

size. This may be because solid particles of polystyrene do not tend to cohere [10], or because the salt concentration used was below the critical value; higher concentrations could not be used because this latex sample was not sufficiently stable to electrolytes.

It follows from the data in Table 5 and Fig. 2 that in butadiene—styrene and especially in chloroprene latexes prepared with fatty acid soaps as emulsifiers particle growth on addition of sodium chloride was rapid during 3 days and then slowed down appreciably (Fig. 3).

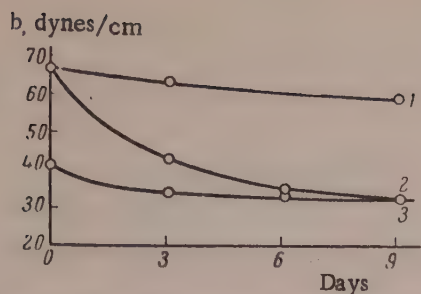


Fig. 4. Effect of storage time on the surface tension of different latexes with added sodium chloride: 1) SKS-30 latex with sodium paraffinate; 2) chloroprene latex with sodium oleate; 3) same, with sodium paraffinate.

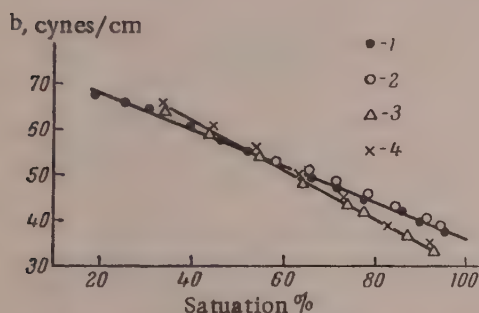


Fig. 6. Variations of the surface tension of latexes with the degree of saturation of the layers with emulsifier: 1) original SKS-30 latex; 2) same, with 1.5% NaCl; 3) original chloroprene latex made with sodium oleate; 4) same, with 0.5% NaCl.

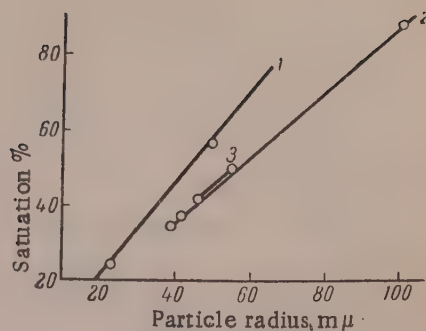


Fig. 5. Variation of the degree of saturation in different latexes with changes of particle radius on agglomeration: 1) SKS-30 latex with sodium paraffinate; 2) chloroprene latex with sodium oleate; 3) same, with Neka1.

The degree of saturation of the adsorption layers of the latex particles with emulsifier during growth under the influence of added sodium chloride (Table 6 and Fig. 4 and 5) increases in direct proportion to the particle radius, while variations of the surface tension of the latex with the degree of saturation of the layers on the polymer particles before and after agglomeration are represented by curves which are almost identical (within the accuracy limits of the methods used) (Fig. 6). These facts show convincingly that the distribution of the emulsifier (in the adsorbed state and dissolved in the liquid phase) is approximately the same in presence of the electrolyte as in its absence.* Additions of sodium chloride do not cause desorption of the emulsifier, apart from that due to its redistribution owing to increases saturation of the layers; this is contrary to previous suggestions [3, 8].

SUMMARY

1. Particle agglomeration under the influence of added sodium chloride was studied in latexes prepared by emulsion polymerization of styrene, butadiene with styrene, and chloroprene, in presence of various emulsifiers (fatty acid soaps, Neka1, OP-10). The degree of agglomeration depends on the nature of the emulsifier and polymer. Particle agglomeration does not occur in polystyrene latexes and latexes made in presence of nonionic emulsifiers.

2. The relationship between surface tension of latexes and the degree of saturation of the protective layers is approximately the same before as after agglomeration of the particles by addition of sodium chloride.

We thank N. A. Fermor for help in the course of this investigation and in its presentation.

* For a given degree of saturation of the layers the concentration of dissolved emulsifier in the aqueous phase may even be somewhat less in presence of electrolytes, since in this case the same surface tension is attained by increase of the emulsifier concentration at the latex-air interface with a corresponding decrease in the volume phase.

LITERATURE CITED

- [1] R. W. Brown and L. H. Howland, *Rubber World* 132, 471 (1955).
- [2] A. V. Lebedev and N. A. Fermor, *Khimicheskaya Promyshlennost* 2, 339 (1957).
- [3] E. Schmidt and R. H. Kalsey, *Ind. Eng. Chem.* 43, 406 (1951).
- [4] W. V. Smith, *J. Amer. Chem. Soc.* 70, 3695 (1948); W. V. Smith and R. H. Ewart, *J. Chem. Phys.* 16, 592 (1948).
- [5] E. V. Zabolotskaya, N. G. Soboleva, N. V. Makletskova, and S. S. Medvedev, *Kolloid Zhur.* 18, 420 (1956).*
- [6] P. N. Chatskii and N. P. Ivanova-Tolmacheva, *Exchange of Technical Experience* 86, [in Russian] (State Light Industry Press, 1952).
- [7] N. V. Garmonov (editor), *Analysis of Materials in the Production of Synthetic Ethyl Alcohol and Synthetic Rubbers* [in Russian] (Goskhimizdat, Leningrad, 1957) p. 150.
- [8] S. M. Maron, M. E. Elder, and I. N. Ulevitch. *J. Colloid Sci.* 9, 89 (1954).
- [9] B. Jakobi, *Angew. Chemie* 64, 539 (1952).
- [10] C. E. Rhines and J. Mc Gavack, *Rubber Age* 63, 599 (New York, 1948).

Received May 15, 1958

*Original Russian pagination. See C. B. Translation.

CHANGES IN THE STRUCTUROMECHANICAL AND RHEOLOGICAL PROPERTIES OF STARCH GELS PRODUCED BY THE ACTION OF ACIDS

A. V. Senakhov and F. I. Sadov

The Moscow Textile Institute

The hydrolysis of starch has already been thoroughly studied. However, until now there have not been any papers dealing with changes in the structuromechanical properties of starch gels under the influence of acids. We have investigated variations of the structuromechanical properties of starch gels in relation to the nature and concentration of the acids, duration and temperature of hydrolysis, and starch concentration in the gel. The methods used for determination of the structuromechanical and rheological properties of starch gels were described in the preceding paper [1]. Comparison of different technical samples of nonmodified maize starch revealed considerable variations (by factors of 2-3 and over) in the structuromechanical data for gels of equal concentrations. The subsequent investigation was confined to one starch sample, containing 12.6% moisture and 0.189% ash.

A preliminary study of the action of acid (HCl) on starch gels* showed that in the region of low acid concentrations all the structuromechanical characteristics of the gels (E_1 , E_2 , η_2 and P_{lim} , subsequently denoted by X) exhibited a more complex relationship than the expected decrease.

It was found in a more detailed study in the region of low acid concentrations c_1'' by measurements of the dynamic yield value P_s that at any of the investigated concentrations of starch in the gel c_2 the values of P_s corresponding to ranges of c_1'' from zero to a certain value $c_1'' = c_1'$, do not show any variations with c_1'' and there is a certain boundary curve $P_{sb}(c_1')$ ** which separates the regions of constant and variable P_s . Therefore values of $P_s = P_{sb}$ which lie on this curve are equal to values of P_{s_0} for gels from nonmodified starch, while the curve $P_{sb}(c_1')$, itself, as is clear from Fig. 1, is parabolic in character. Comparison of the c' intercepts (cut off along the c_1'' axis in Fig. 1 by the points O_1 , O_2 , O_3 and O_4) for different values of c_2 showed that in reality the values of c_1' and the corresponding values of $P_{sb} = P_{s_0}$ correspond to the same quantity of acid expressed in percentages on the weight of bone-dry starch. This fact may be attributed to binding of the acid at the initial stage of the process, corresponding to the initial regions of the $P_s(c_1'')$, curves cut off by the $P_{sb}(c_1')$ curve and parallel to the abscissa axis. This hypothesis was confirmed by parallel determinations of the iodine numbers (q)*.

(q).*** The relationships between $y = \lg \frac{q_\infty - q_0}{q_\infty - q_\tau}$ **** and the acid concentrations are represented by straight lines cutting the abscissa axis in direct proximity to the values of c_1' corresponding to the points O_1 , O_2 , O_3 and O_4 on the c_1'' axis (Fig. 1).

*The time of action of the acid on the starch during boiling of the pastes up to the instant of neutralization was constant (1 hour).

**The position of the $P_{sb}(c_1')$, curve shown in Fig. 1 was also checked by determinations of P_s corresponding to the points O_1 , O_2 , O_3 and O_4 on the c_1'' axis, while the positions of these points were determined by potentiometric titration [4].

***The iodine numbers (q) of hydrolyzed starch in the gels were determined by the ferrocyanide method [2].

****Here q_∞ is the iodine number of glucose; q_0 is the iodine number of the original starch; q_τ is the iodine number corresponding to a definite degree of hydrolysis of the starch.

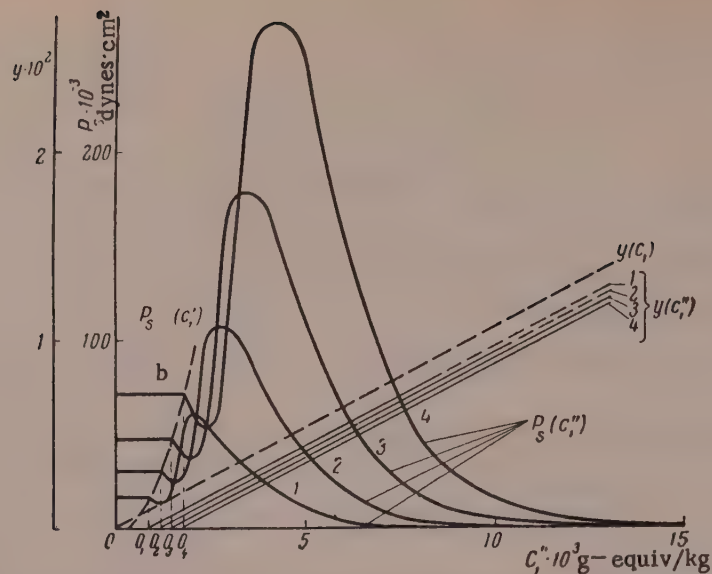


Fig. 1. The functions $P_s(c_1^*)$ and $y(c_1^*)$ for starch gels of different concentrations (c_2): 1) 9%; 2) 12%; 3) 15%; 4) 18%.

Binding of acid by starch has been studied previously [3, 4]. It was shown by Smirnov [4] that binding of acid by starch is due to a considerable extent to various impurities bound in different ways to the starch. The fact that during the entire binding process there is no appreciable change in the original values of $P_s = P_{s_0}$, which correspond to gels from nonmodified starch, and therefore no appreciable changes in the structural network of the gels, indicates that the functional groups in the molecules of the impurities reacting with the acid are not involved in formation of the structural network of the gel.

On further increase of the acid concentration c_1^* binding is replaced by hydrolysis, and P_s decreases in consequence. Therefore in studies of starch hydrolysis use should be made of the concept of free (active) acid

$$c_1 = c_1^* - c_1',$$

where c_1 is the concentration of free acid acting as catalyst; c_1^* is the total acid concentration in the gel; c_1' is the decrease of the total acid concentration c_1^* as the result of binding of a part of it by starch (in Fig. 3-5 it lies in the negative region, to the left of the ordinate axis).

The complex form of the $P_s(c_1^*)$ relationships for different values of c_2 , found in the initial stages of hydrolysis, cannot, to judge by the character of the corresponding $y(c_1^*)$ relationships, be attributed to any peculiarities in the course of starch hydrolysis at these stages; it is more correctly explained by characteristic structural changes in the starch gels, which are a consequence of hydrolysis of starch occurring in the usual manner (i.e., in accordance with a first-order reaction equation).

After the nature of the variations of P_s at the boundary between acid binding and hydrolysis had been established, changes in the structuromechanical characteristics X of the starch gels during hydrolysis were investigated. Starch gels of a definite degree of hydrolysis were prepared by two different methods: by preliminary hydrolysis of starch in suspension at 18-19° followed by conversion into paste, and by hydrolysis of starch previously converted into paste in solution at 91-92°.

The hydrolysis of starch in suspension was carried out at constant acid concentration $c_1 = 1.0$ g-equiv/kg, but during different times τ . A preliminary study of the function $P_s(\tau)$ at $c_1 = \text{const.}$ showed that the resultant $P_s(\tau)$ curves were similar to the $P_s(c_1^*)$ curves shown in Fig. 1 if these were plotted in $P_s - c_1$ coordinates. The ranges of τ for the subsequent investigations of the other characteristics X were confined to regions of steady descent of the $P_s(\tau)$ curves, which correspond to the similar regions of the $X(c_1)$ curves (see below) lying in the Π_2 region to the right of the $X(c_1, c_2)$ curve (Fig. 3-5).

TABLE 1

Main Values Characterizing Variations of X^* and q for Starch Gels as the Result of Hydrolysis of Maize Starch in Solution and in Suspension in Presence of HCl

Quantity for which values of A and E* are determined	T, °K	$k(X^*, y)$ (hr $\frac{g\text{-equiv}}{kg}$)	$A^*(x', y) \cdot 10^{-17}$ (sec $\frac{g\text{-equiv}}{kg}$) ⁻¹	$L_{X^*} \cdot 10^{-3}$	$E^* \cdot 10^{-3}$ cal/mole	$\Delta H^\ddagger \cdot 10^{-3}$ cal/mole	ΔS^\ddagger cal/mole·deg
E'_1	291,5 364,5	$4,23 \cdot 10^{-2}$ $1,39 \cdot 10^3$	5,23	5,76			
E'_2	291,5 364,5	$4,35 \cdot 10^{-2}$ $1,43 \cdot 10^3$	5,38	5,93			
η'_1	291,5 364,5	$4,54 \cdot 10^{-2}$ $1,49 \cdot 10^3$	5,61	6,18			
η'_2	291,5 364,5	$4,40 \cdot 10^{-2}$ $1,45 \cdot 10^3$	5,46	6,01	30,2	+29,6	+7,73
P'_k	291,5 364,5	$4,49 \cdot 10^{-2}$ $1,49 \cdot 10^3$	5,57	6,13			
P'_{lim}	291,5 364,5	$4,28 \cdot 10^{-2}$ $1,44 \cdot 10^3$	5,36	5,90			
q	291,5 364,5	$7,28 \cdot 10^{-5}$ 2,45	$9,08 \cdot 10^{-3}$	0,01			

* Values of $A(X^*, y)$ were calculated from average values of $\lg k(X^*, y)$ for the given range of hydrolysis temperatures.

Hydrolysis of starch in suspension form in these ranges of τ yielded samples of different degrees of hydrolysis, which could be regarded as individual thickeners of different properties. For each such sample there was its own $X(c_2)$ concentration curve, represented by an equation of the type:

$$X = X'c_2^n, \quad (1)$$

already discussed in our previous communication [1]. The average value of \bar{n} (n_{av}) for all values of X was taken. It was found that with increase of the degree of hydrolysis (with increase of the hydrolysis time t in this instance) the constants X^* decreased sharply and the index \bar{n} in Equations (1) increased appreciably. The $\lg X^*(t)$ relationships can be represented by the straight lines in Fig. 2, so that the rate constants k_{X^*} for variations of the corresponding values of X^* in the course of hydrolysis can be found (Table 1). The function $\lg (n - n_N) = f(\lg \tau)$ is also close to linear in character, and is found by rectification of the $\lg n = f(\lg \tau)$ curve, by selection of a suitable value for n_N .

The effect of acid concentration on the structuromechanical characteristics of the gels was studied by hydrolysis of starch in solution for constant time $t = 1$ hour. The results are presented in Fig. 3-5, where the $X(c_1)$ relationships are plotted. The ordinate axes used for E_1 , E_2 , η_2 and P_{lim} were the corresponding $X_b(c_1)$, boundary curves the positions of which, like the position of the $P_{sb}(c_1)$ curve, were determined from potentiometric titration data.

P_k and η_1 , which characterize the plastic properties of a system and which do not exist for gels of non-hydrolyzed starch, are likewise absent at the earliest stages of hydrolysis; on further hydrolysis they indicate the appearance of a region of plastic flow, corresponding to the ranges $P_k < P < P_{lim}$, for the gels. Moreover, as is shown later in this paper, the regions of steady descent of the $X(c_1)$ curves, which commence to the right of the maxima on these curves, conform to Equation (4) (see below) for all X characteristics. Because of these two facts it is convenient to divide the $X(c_1)$ curves for E_1 , E_2 , η_2 and P_{lim} into three consecutive regions, and the

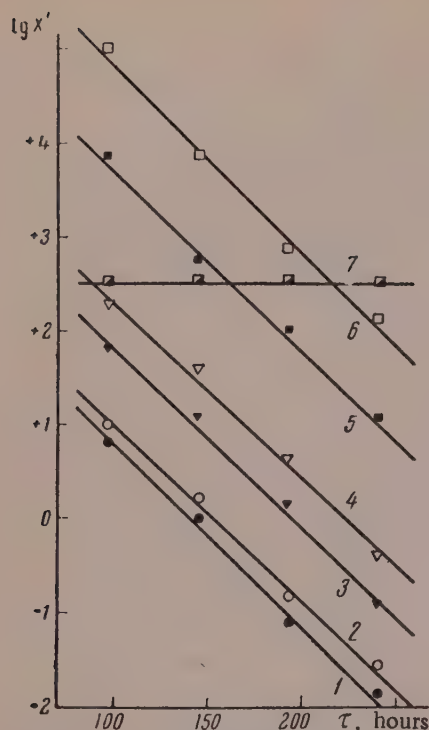


Fig. 2. $\lg X^*(t)$ relationships for gels of hydrolyzed starch: 1) $\lg P_k^*$; 2) $\lg P_{lim}^*$; 3) $\lg E_2^*$; 4) $\lg E_1^*$; 5) $\lg \eta_2^*$; 6) $\lg \eta_1^*$; 7) $\lg(q_\infty - q_t)$.

with the corresponding $X_{cr1}(c_1, c_2)$ curve. The subregions II_1 and II_2 respectively are regions in which the given X value conforms and does not conform to Equation (4).

Fig. 3. shows that in the case of hydrolyzed starch gels plastic flow is possible at yield (P_{lim}) and flow (P_k) values considerably higher than the corresponding values of P_{lim} for gels of the same concentration from nonmodified starch, P_{lim0} . This may be attributed to a considerable increase of the number of bonds forming a network skeleton in the gel which occurs at definite stages of hydrolysis.

This effect, and the nature of the curves in Fig. 3-5, may be explained schematically by the diagram in Fig. 6. Hydrolysis of starch gels may be regarded as consisting of at least two simultaneous processes: hydrolytic breakdown of the original structural network (network A), and formation with subsequent breakdown of an additional network (network B). Networks A and B are superposed to form an aggregate network C, which determines the structuromechanical characteristics X of the starch gels. The continuous line in Fig. 6 represents one experimental $X(c_1)$ curve at a constant c_2 , denoted by the letter \underline{d} and reflecting the changes of X corresponding to network C. The dash lines in the same diagram indicate the possible form of curves \underline{a} and \underline{b} for variations of the structuromechanical properties of networks A and B in the course of hydrolysis. Network A is similar to the networks in gels from nonhydrolyzed starch which have, as has already been noted, brittle properties. Our experimental data on the action of salts on starch gels* indicate that the bonds involved in the formation of the structural network are not all the same. Some of them are weaker and may possibly have thixotropic properties, as they can break down at very low salt concentrations in certain ranges of c_2 . This leads to the suggestion that the brittle properties of network A are determined only by the part of the bonds which do not have thixotropic properties, i.e., that network A consists of a nonthixotropic skeleton and a thixotropic network mutually superposed. Hydrolysis results in an increase in the number of thixotropic bonds at the expense of the nonthixotropic,

$P_k(c_1)$ and $\eta_1(c_1)$, curves into two regions. If the points on the $X(c_1)$ curves for E_1 , E_2 , η_2 and P_{lim} , corresponding to transitions from one region to another on the $X(c_1)$ curves, are denoted by X_{cr2} and X_{cr2} respectively, then evidently in the transition from one value of c_2 to another, these points form certain boundary curves $X_{cr1}(c_1, c_2)$ and $X_{cr1}(c_1, c_2)$, shown by dash lines in Fig. 3-5. The (c_1, c_2) curve for a given X divides all the regions of starch hydrolysis into two main regions (I and II), while the $X_{cr1}(c_1, c_2)$ curve additionally divides the region II into two subregions II_1 and II_2 (see Fig. 3 and 5). It is evident that for P_k and η_1 the points X_{cr1} on the $X(c_1)$ curves coincide with the initial points X_0 of these curves, i.e., the $X_{cr1}(c_1, c_2)$ boundary curves in this case coincide with the $X_0(c_1, c_2)$ curves, and there is no region I for the $P_k(c_1)$ and $\eta_1(c_1)$ curves. Region I corresponds to absence of a plasticity element (II), composed of the quantities P_k and η_1 , in the structuromechanical gel model [1], and it may be regarded as the brittle region for hydrolyzed starch gels, corresponding to the presence of a nonthixotropic skeleton in addition to a thixotropic structural network. Region II corresponds to the presence of a plasticity element [1] in the structuromechanical gel model, and may be regarded as the plastic region for hydrolyzed gels, corresponding to the presence of a thixotropic network only. The stage at which the plastic element appears, corresponding to disappearance of the nonthixotropic skeleton from the gels, virtually coincides for each X

* $\lg = \log$ —Publisher.

**The data on the action of salts on starch gels are to be presented in a future communication.

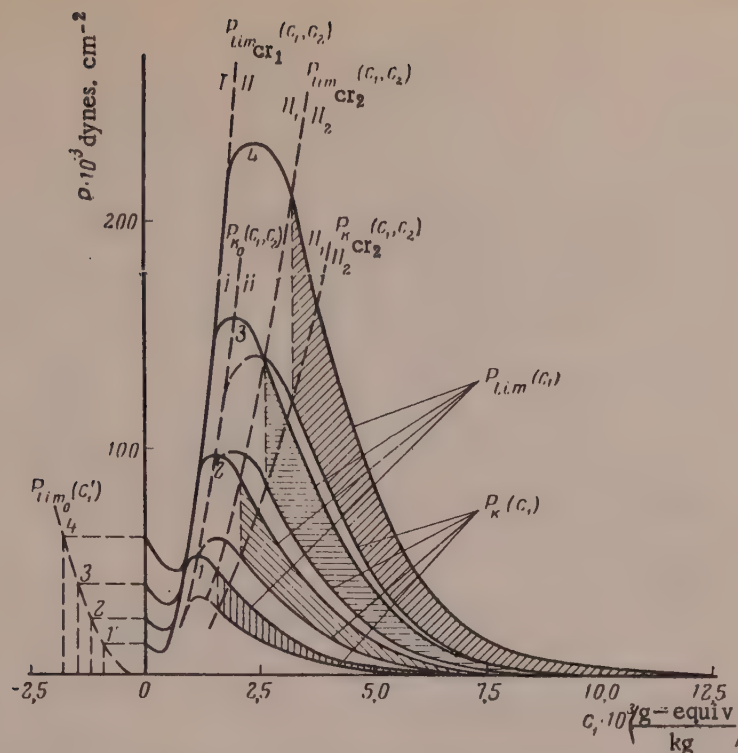


Fig. 3. $P_k, \lim(c_1)$ curves for gels of hydrolyzed starch of different concentrations (c_2): 1) 9%; 2) 12%; 3) 15%; 4) 18%.

and in increased thixotropy of the former. This leads to weakening of the nonthixotropic skeleton. At a certain stage of hydrolysis the number of nonthixotropic bonds in the system decreases so much as to be insufficient to form a coherent skeleton and from this instant the mechanical properties of the structure are determined by the thixotropic network only. This instant (the point a_{cr} in Curve a, Fig. 6) corresponds to transition from the initial region of Curve a to the succeeding region for the characteristics E_1 , E_2 , η_2 and P_{lim} , which already exist in the original network A, and to appearance of the characteristics P_k and η_1 in network A. If it is further assumed that network B is completely thixotropic, i.e., that only network A is responsible for brittle properties in the aggregate network C, then the position of the point a_{cr} also determines the instant (or stage) at which network C loses its brittle properties, i.e., the position of the point X_{cr1} or of the corresponding intercept on the $X_{cr1}(c_1, c_2)$ curve.

At the initial instant of hydrolysis, when network B is absent, network A represents the primary gel structure, i.e., the structure of a gel of nonhydrolyzed starch. The smooth descent of the earliest regions of the $X(c_1)$ curves for E_1 , E_2 , η_2 and P_{lim} indicates that the gel structure at the corresponding hydrolysis stages resembles the primary structure. The regions of the $X(c_1)$ curves to the right of the X_{cr} points correspond to the secondary gel structure. The intermediate regions of the $X(c_1)$ curves, each including a minimum and a maximum, correspond to some intermediate type of structure. The primary (more complex) gel structure may be imagined as consisting of dense accumulations (aggregates) of starch macromolecules bound by a relatively small number of bonds. Hydrolysis of the starch results in a decrease in the size of the original aggregates or their breakdown into smaller aggregates, accompanied by an increase of the number of bonds between them. These new bonds lead to the formation of the additional network B, which raises the values of the quantities X at the corresponding hydrolysis stages. When the limiting degree of aggregate breakdown, corresponding to the points X_{cr2} , is reached, hydrolytic formation of the secondary structure ends and further hydrolysis leads only to hydrolytic breakdown of the secondary structure in accordance with Equation (4). It is possible that breakdown of network A in some way facilitates formation of network B. It is evident that formation of network B is also a complex process, consisting of at least two competing processes: hydrolytic weakening and breakdown of bonds formed previously, and simultaneous formation of new bonds. The aggregate result of these two processes determines the form of Curve b. At the initial region of Curve b formation of new bonds predominates, and after the maximum has been reached the breakdown process begins to prevail. From a certain point b_{cr} (the inflection of Curve b) bond breakdown in network B reaches a steady

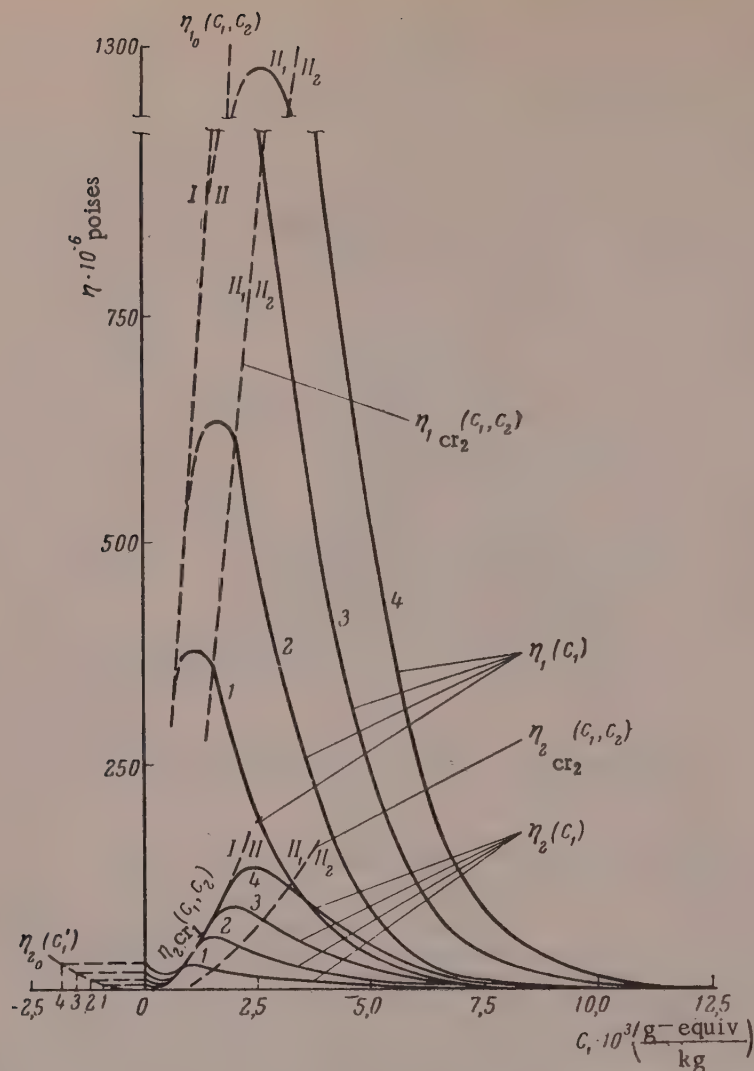


Fig. 4. $\eta_{1,2}(c_1)$ curves for gels of hydrolyzed starch of different concentrations (c_2): 1) 9%; 2) 12%; 3) 15%; 4) 18%.

state and from this point Curve \underline{b} begins to descend monotonically. The position of the point b_{cr} on Curve \underline{b} evidently determines the position of the point X_{cr_2} on Curve \underline{b} , which establishes the upper limit of conformity of Curve \underline{b} to Equation (4).

Fig. 3 shows that with equal absolute values of the stress ranges $P_k < P < P_{lim}$ for gels of different concentrations the relative magnitude of these ranges increases with increase of starch concentration in the gels. This is accompanied by corresponding increases in the concentration of active acid. If it is assumed that the plasticity of the system increases with increase of the relative magnitude of the region of relaxational creep (see [1]), it may be concluded that with equal absolute values of the stress ranges $P_k < P < P_{lim}$ the plasticity of the gels increases with increase of their concentration, accompanied by corresponding increases in the degree of hydrolysis. This probably explains why an increase of the starch concentration in a thickener paste with corresponding increase of its degree of hydrolysis is accompanied by an appreciable improvement of its printing properties. There is probably a definite limit of starch concentration in the thickener below which the printing properties deteriorate so much that the thickener is practically useless. This may be due to the existence of a very narrow stress range $P_k < P < P_{lim}$ in such cases.

On the other hand, however, there may be a certain upper limit of starch concentration (and, correspondingly, of degree of hydrolysis) above which the purely viscous gel properties become prominent and the plasticity

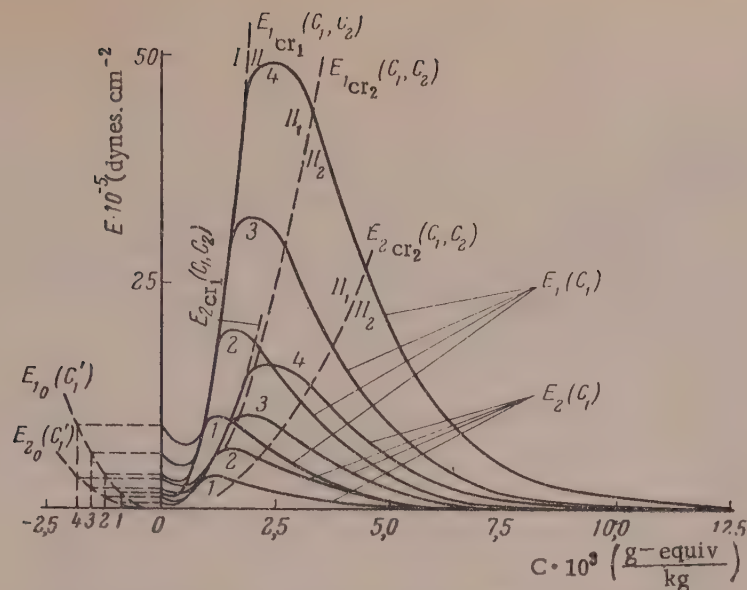


Fig. 5. $E_{1,2}(c_1)$ curves for gels of hydrolyzed starch of different concentrations (c_2): 1) 9%; 2) 12%; 3) 15%; 4) 18%.

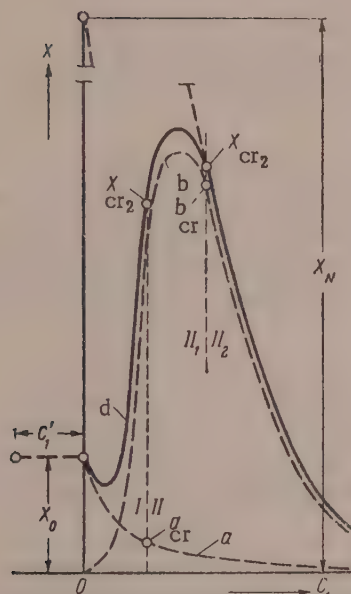


Fig. 6. Explanatory diagram for analysis of the experimental $X(c_1)$ curve for a constant value of c_2 .

c_1 in this instance). The increase of \underline{n} is a sign of a decrease of the relative number of particles involved in the formation of a structural network in starch gels of equal concentrations but different degrees of hydrolysis [1].

* This is confirmed, in particular, by the nature of their $E(\tau)$ kinetics curves (see [1]).

** The degree of structurization ρ in this instance might be determined directly from the formula:

$\rho = K' \cdot c_2^{n-1}$, where K' is a constant connected with the constant K in Equation (6) by the equation

$$K' = K^{2/3}; \quad c_2 =$$

c_2 is the concentration of the thickener; \underline{n} is the index in Equation (1); K and \underline{n} have different values

accordingly decreases. It is possible that dextrin thickeners are above this limit, as their rheological behavior is determined to a considerable extent by purely viscous properties,* so that excessively high concentrations must be used.

It follows from the foregoing that in comparison of different thickeners the criterion is not the degree of structurization but the character and properties of their internal structure. Since for all the thickeners studied the numerical value of \underline{n} in Equation (1) is considerably greater than $2/3$, the degree of structurization of their solutions must rise sharply with the concentration. Of two thickeners, solutions of which have similar printing properties at different concentrations, the better one is the one which has the higher degree of structurization in solutions at lower concentrations, i.e., for which the value of \underline{n} in Equation (1) is less than the corresponding value of \underline{n} for the other thickener.**

The $X(c_1)$ curves in Fig. 3-5 may be represented as a series of concentration curves corresponding to Equation (1), from which the respective constants X^* and \underline{n} can be found. It is then found that X^* falls sharply and \underline{n} increases in the course of hydrolysis (with increase of

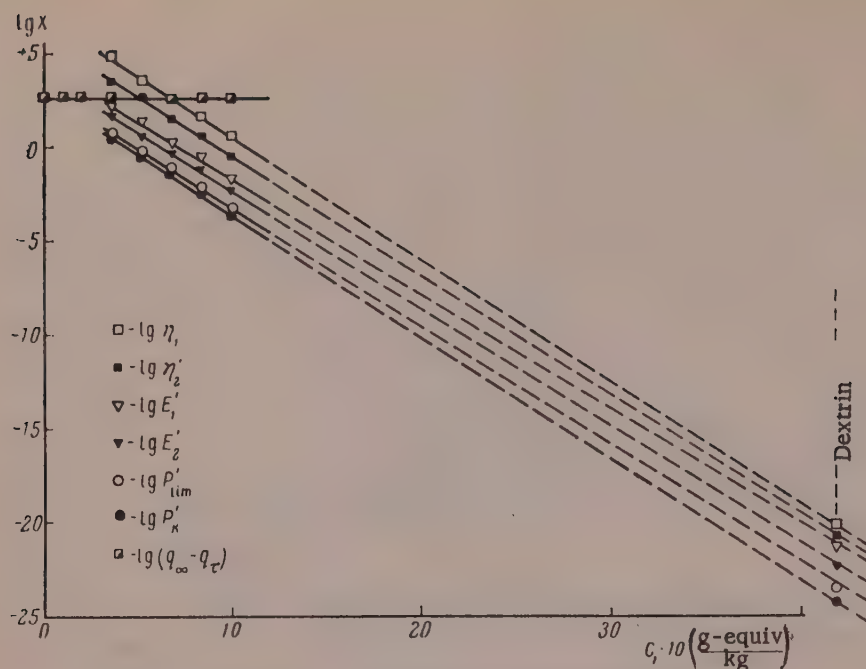


Fig. 7. The $\lg X'(c_1)$ relationships for hydrolyzed starch gels.

The $\lg X'(c_1)$ relationships are represented by the straight lines in Fig. 7, so that the values of k_X , in Table 1 can be found. The $\lg(n-n_N) = f(\lg c_1)$ relationship is also nearly linear in character; it is obtained by rectification of the $\lg n = f(\lg c_1)$ curve with a suitable value of n_N .

According to Kryachkov [5] and Sadov [6], who studied the acid hydrolysis of starch in the 80-120° and 119-143° ranges, the $\lg k = f(t)$ relationship is linear, i.e., variations of the hydrolysis rate τ with temperature τ conform to the Arrhenius equation. Although we determined the rate constants k_{X1} and k_Y for only two different temperatures, since there are no data which might indicate the possibility of appreciable deviations from the Arrhenius Equation (2) for the hydrolysis of starch at lower temperatures, the equation may be used for determining the constants A and E^* .

$$k = Ae^{-\frac{E^*}{RT}} \quad (2)$$

The values of E^* , determining the activation energy of starch hydrolysis, were almost the same in all cases, but there were variations in the value of A .

On the basis of the activated-complex [7] or transition-state [8] theories, and on the assumption that all hydrolysis reactions may be regarded as adiabatic in the quantum-mechanical sense (this means that in Equation (3) $_{\kappa} = 1$), we can find the values of the heat (ΔH^\ddagger) and entropy (ΔS^\ddagger) of activation of starch hydrolysis from the equations:

$$k_{Yav} = \alpha A e^{-\frac{E^*}{RT_{av}}} = \underbrace{\left(e^{\frac{\Delta S^\ddagger}{R}} e^{-\frac{E^\ddagger}{RT_{av}}} \right)}_{\alpha} \underbrace{\times e^{\frac{kT_{av}}{h}} e^{\frac{\Delta S^\ddagger}{R}} e^{-\frac{E^*}{RT_{av}}}}_{A} \quad (3)$$

$$\Delta H^\ddagger = E^* - RT_{av}$$

for different thickeners. However, the difficulty lies in exact determination of K^* , and therefore comparative estimations of the degree of structurization ρ for different thickeners are best done by simple comparison of the corresponding values of \underline{n} in Equation (1).

and

where k_{yav} is the average value of the rate constant for change in the amount of reducing substances, determined from the iodine numbers; α is the activity coefficient of the catalyst (assumed to be 1 for HCl); κ is the quantum-mechanical transition coefficient; k and h are the Boltzmann and Planck constants; T_{av} is the average value for the hydrolysis temperature range studied. Investigations of the comparative effects of HCl and H_2SO_4 at 91-92° showed that if the activity coefficient for HCl is taken to be 1, for H_2SO_4 we have $\alpha = 0.62$. The relative corresponding change of free energy in activation of hydrolysis for the change from HCl to H_2SO_4 is only 1.3% at that temperature.

The values found for ΔH^\ddagger , ΔS^\ddagger and E^* are the same for all k_{X^*} , as they all characterize the same hydrolysis process. This explains the experimental relationships:

$$L_{X'} = \frac{k_{X'}}{k_y} = \frac{A_{X'}}{A_y},$$

where $L_{X'}$ are constants different for different X and independent of the starch hydrolysis conditions. As has been pointed out, the present investigation was confined to only one starch sample and it may be that for the same value of k_y different starch samples may have different values of L_{X^*} .

The values of k_{X^*} , k_y , A_{X^*} , A_y , E^* , ΔH^\ddagger , ΔS^\ddagger , and L_{X^*} , are given in Table 1.

Our data as a whole may be represented by the general equation:

$$X = X'_N e^{-k_{X'} c_1 \tau} c_2^{n_N + \lambda_n c_1^{\frac{1}{a}} \tau^{\frac{1}{b}}}, \quad (4)$$

which expresses the dependence of a particular structuromechanical value X on the hydrolysis conditions (time τ catalyst concentration c_1 , and hydrolysis temperature), on the nature of the catalyst, and on the concentration of starch in the gel (c_2). *

The following symbols are used: X'_N is the coefficient in Equation (1) for maximum binding of acid by starch [this corresponds to the particular X_N in Fig. 6, and is found by extrapolation of the $\lg X^*(c_1)$ and $\lg X^*(t)$ linear functions to zero concentrations ($c_1=0$) (Fig. 7) or to zero time ($\tau=0$) (Fig. 2)]; n is the index of Equation (1) for the case in question [this is found by plotting of the linear functions $\lg(n-n_N) = f(\lg c_1)$ and $\lg(n-n_N) = f(\log \tau)$]; a and b are constants, greater than unity; λ_n is a temperature coefficient.

Equation (4) indicates, in particular, that X^* in Equation (1) conforms to a first-order reaction equation.

The relationship between any structuromechanical quantity X and the thickener concentration may be represented, either empirically by Equation (1), or theoretically (if it is assumed, as was done by Zuev [9] for P_s , that the value of a structuromechanical characteristic X is proportional to the number of contacting particles) by the equation:

$$X = X'_T c_{2k}^{\frac{2}{k}}, \quad (5)$$

when in Equation (1) X^* and n are empirical constants and c_2 is the total concentration of the solid-phase particles in the gel (thickener concentration), and in Equation (5) c_{2k} is the concentration of the solid-phase contacting particles in the gel; X'_T are coefficients determined by the structural characteristics of the solid-phase

*Fig. 1, 3-5 give values of c_2 calculated for air-dry starch containing 12.6% moisture. For analysis of the data corresponding to Fig. 1 and 3-5 the values were converted to the bone-dry material.

particles which directly influence the nature of mutual interaction of these particles, such as the ratio $\eta_{1T}^0/E_{1T}^0 = \Theta_1$, determined by the dimensions, shape, and deformability of the solid-phase particle (in the present instance macromolecules or macromolecular aggregates of starch), or $\eta_{2T}^0/E_2^0 = \Theta_2$, determined by the dimensions, shape, and deformability of the mobile elements ("segments") of such particles (in the present instance these may be interacting portions of macromolecular starch chains in the structural network of the gel, and in particular the external branches of amylopectin macromolecules), or, finally, P_{kT}^0 , the coefficient of particle cohesion in relation to shear and P_{1unT}^0/P_{kT}^0 , a quantity which determines the extent of the region of relaxational creep. The last two quantities are determined by the above-named structural characteristics of the solid-phase particles, associated with values of Θ_1 and Θ_2 , and by the type of the functional groups present (in the present instance OH groups). * The value of $2/3$ for the exponent in Equation (5) takes into account the fact that X in Equation (1) represents structuromechanical characteristics in shear.

It follows from Equation (1) and (5) that

$$X(c_2) = X'c_2^n = X'_T c_{2k}^{2/3}$$

or

$$c_{2k}^{2/3}(c_2) = (X'/X'_T)c_2^n = Kc_2^n.$$

Substituting the expression found for

$$X = X'_T(Kc_2^n) = X'_T[(c_{2k})^{2/3}c_2^n], \quad (6)$$

where $K = (c_{2k}^{2/3})^{2/3}$ is a constant representing the number of solid-phase particles in contact with specific area in the shear plane at $c_2 = 1$.

It follows from our experimental Equation (4) that

$$X' = X'_N e^{-k_{X'}c_1\tau}.$$

From Equation (6) we have $X^* = X'_T K$ and $X_N^* = X'_{TN} K_N$, and substituting these values of X^* and X_N^* into the equation for the rate constant

$$k_{X'} = \frac{\ln(X'_N/X')}{c_1\tau},$$

we find

$$k_{X'} = \frac{\ln\left(\frac{X'_{TN}K_N}{X'_TK}\right)}{c_1\tau} = \frac{\ln(X'_{TN}/X'_T)}{c_1\tau} + \frac{\ln(K_N/K)}{c_1\tau} = k_{X'_T} + k_K, \quad (7)$$

where $K_{X'_T}$ represents the rate constants for variations of the values of X'_T in the course of hydrolysis; k_K is the rate constant for variation of K in the course of hydrolysis.

Since one of the terms in the total rate constant k_{X^*} in Equation (7) (the quantity k_K) is the same for all X^* , the experimental differences between the values of k_{X^*} (Table 2) must be attributed only to corresponding

* Values of X^* , n , c_{2k} and X'_T are taken for a long gelation time, when they become close to constant.

TABLE 2

Values of X'_{2N}/X'_{1N} and $\Delta k_{X'}$, Representing Variations of Different X_2/X_1 with Concentration of Active Acid (HCl) c_1 and Hydrolysis Time in Acid Hydrolysis of Maize Starch in Solution and in Suspension

$\frac{X_2}{X_1}$	(τ=1.0 hour; (t=91-92°)		(c ₁ =1.0 g-equiv/kg; t=18-19°)	
	$\frac{X'_{2N}}{X'_{1N}}$	(hr $\frac{\text{g-equiv}}{\text{kg}}$) ⁻¹	$\frac{X'_{2N}}{X'_{1N}}$	(hr $\frac{\text{g-equiv}}{\text{kg}}$) ⁻¹
P_{lim}/P_k	1,48	-0,5	1,26	-2,1
η_1/η_2	14,1	+0,4	15,5	+1,4
E_1/E_2	2,88	-0,4	2,62	-1,2
η_1/E_1	4,27·10 ²	+1,0	4,68·10 ²	+3,1
η_2/E_2	87,2	+0,2	79,3	+0,5

differences in the values of $k_{X',T}$. Accordingly, our experimental values of

$$k_{\eta_1} = k_{\eta_1'} - k_{E_1'} = k_{\eta_{1T}'} - k_{E_{1T}'} > 0 \quad \text{and} \quad k_{\eta_2} = k_{\eta_2'} - k_{E_2'} = k_{\eta_{2T}'} - k_{E_{2T}'} > 0$$

may indicate, in the former case, a decrease in the size of the starch macromolecules (or aggregates which may be formed in the gel) as the result of hydrolysis, and in the latter a decrease in the size of the macromolecular chain segments between the branch points in formation of the structural network of the gel. The same effect, and consequently an increased thixotropy of the contacts between the particles, is indicated also by the experimental value of $k_{P_{lim}'} - k_{P_T'} < 0$ (since the nature of the functional groups, OH, cannot change in the course of hydrolysis).

The main defect of Equation (4) is the clearly empirical nature of the factor $\left(\frac{n_N + \lambda_n c_1^{1/a} \tau^{1/b}}{c_2}\right)$ and its somewhat indeterminate character due to the fact that n_N cannot be found by direct experiment but only by trial and error. Therefore only tentative data can be obtained from Equation (4). Equation (4) is applicable to all the structuromechanical characteristics of starch gels studied in this investigation, from certain critical values $X \approx X_{Cr2}$ indicated in Fig. 3-5.

Equation(4) can also be expressed numerically in terms of iodine numbers:

$$X = N_{X'}(q_{\infty} - q_0) e^{-L_{X'} k_y c_1 \tau} \left(\frac{n_N + \lambda_n c_1^{1/a} \tau^{1/b}}{c_2}\right), \quad (4a)$$

where $N_{X'}$ and $L_{X'}$ are constants different for different X , lying in the following limits: $N_{X'} \approx 1.28/1.04 \cdot 10^4$; $L_{X'} \approx 5.7 \cdot 10^2/6.18 \cdot 10^2$; k_y is the rate constant for accumulation of reducing substances in the course of hydrolysis; q_{∞} and q_0 are the iodine numbers of glucose and the original starch respectively.

Since the value of the exponent $n = n_N + \lambda_n c_1^{1/a} \tau^{1/b}$ in Equation (4) is common for all the structuromechanical quantities X , the following expression may be derived for ratios of different X :

$$\frac{X_2}{X_1} = \frac{X'_{2N}}{X'_{1N}} e^{-\Delta k_{X'} c_1 \tau}, \quad (8)$$

where $\Delta k_{X'} = k_{X'_2} - k_{X'_1}$; X_2 and X_1 are the respective structuromechanical quantities; X'_{2N} and X'_{1N} are their

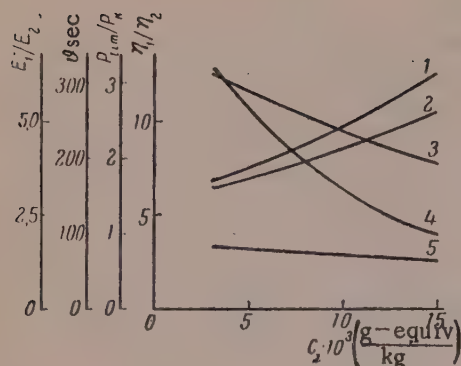


Fig. 8. Calculated $(X_2/X_1)(c_1)$ curves for hydrolyzed starch gels: 1) P_{lim}/P_k ; 2) E_1/E_2 ; 3) η_1/η_2 ; 4) $\theta_1 = \eta_1/E_1$; 5) $\theta_2 = \eta_2/E_2$.

respective values for maximum binding of acid by starch, referred to the secondary structure and extrapolated to unit concentration; k_{X_2} and k_{X_1} are the respective rate constants for variations of X_2 and X_1 in the course of hydrolysis.

Equation (8) can be used for calculating curves for variation of the ratios of different structuromechanical quantities in the course of hydrolysis. The numerical values of X_2/X_1 and Δk_{X^*} , required for such calculations are given in Table 2. Fig. 8 shows calculated curves for the ratios E_1/E_2 , η_1/η_2 , $\theta_1 = \eta_1/E_1$, $\theta_2 = \eta_2/E_2$ and P_{lim}/P_k . It follows from the increase of P_{lim}/P_k and decrease of η_1/η_2 that as hydrolysis proceeds the relative extent of the region of relaxational creep (see [1]) increased, while the relative value of its viscosity falls. Increase of E_1/E_2 and decrease of η_1/η_2 are such that the ratio θ'/θ^* decreases in accordance with the equation,

$$\frac{\theta'}{\theta^*} = \frac{\eta_{1N}}{\eta_{2N}} \left(2e^{-0.4 \cdot 10^3 c_1 \tau} + \frac{E'_{2N}}{E'_{1N}} e^{-0.8 \cdot 10^3 c_1 \tau} + \frac{E'_{1N}}{E'_{2N}} \right)^{**},$$

which leads to the conclusion that the relative proportion of relaxation due to relaxational creep increases as the result of hydrolysis.

Transition from gels of nonmodified starch to gels of hydrolyzed starch is accompanied by a corresponding change of the structuromechanical model and of the type of rheological curve. For hydrolyzed starch gels these correspond to the structuromechanical model and type of rheological curve which we found for solutions of other thickeners [1]. This may explain why hydrolyzed starch is suitable as a thickener.

Hydrolyzed starch gels may be classified with elasticoplastic systems described by the following characteristics: E_1 , E_2 , η_1 , η_2 , P_k and P_{lim} .

SUMMARY

1. Variations of the structuromechanical and rheological properties of starch gels during hydrolysis of starch have been studied.
2. The values of the structuromechanical characteristics of the gels at low acid concentrations, when acid is bound by starch, were found to be constant; the explanation is that the functional groups of the molecules of extraneous substances reacting with the acid do not take part in formation of the structural network of the gel.
3. Variations of all the structuromechanical characteristics of the gels are complex at the early stages of hydrolysis; variations of the iodine numbers during the same stages indicate that this complexity cannot be attributed to any peculiarities in the course of starch hydrolysis but must be attributed to structural transformations in the starch gels.
4. Starch gels contain two types of bonds involved in formation of the structural network. The presence of nonthixotropic bonds leads to formation of a skeleton superposed on the thixotropic structural network and

* Here

$$\theta' = \eta_1 \left(\frac{1}{E_1} + \frac{1}{E_2} \right) \text{ and } \theta^* = \frac{\eta_2}{E_1 + E_2}.$$

** The equation applies to 91-92°.

responsible for the brittle character of the aggregate structural network. The gradual decrease in the number of nonthixotropic bonds as the result of hydrolysis makes the formation of a brittle skeleton with their aid impossible at a certain stage, and the gels begin to exhibit plastic properties, while retaining fairly high values for the strength and other structuromechanical characteristics.

5. Variations of values of X^* in the $X = X^* \cdot c_2^n$ concentration equations for different structuromechanical characteristics X in the course of hydrolysis conform to a first-order reaction equation.

6. In the course of hydrolysis the exponent n increases and different values are obtained for the rate constants k_X^* for variations of the proportionality coefficients X^* in the concentration equation $X = X^* \cdot c_2^n$ for starch gels. Increase of n indicates a decrease in the relative number of particles involved in formation of a structural network in starch gels of the same concentration but different degrees of hydrolysis, while the differences in k_X^* may indicate a decrease in the average size both of the external branches of the macromolecules (in the case of amylopectin) and of the macromolecules as a whole.

7. A general equation has been derived for variations of different structuromechanical characteristics of starch gels in the course of hydrolysis, which includes the main parameters of acid hydrolysis and which represents the influence of hydrolysis conditions on the mechanical properties of a certain "secondary" structure, the formation which terminates at a certain stage of starch hydrolysis. The deviations of the values of the structuromechanical characteristics from this equation, observed at the initial stages of hydrolysis, may be attributed to conversion of the primary structure, present in nonhydrolyzed starch gels, to the secondary.

8. The transition from gels of nonmodified starch to hydrolyzed starch gels is accompanied by corresponding changes of the structuromechanical model and the rheological curve. The latter, for gels of hydrolyzed starch, correspond to the structuromechanical model and type of rheological curve found earlier for solutions of other thickeners. This accounts for the suitability of hydrolyzed starch as a thickener.

LITERATURE CITED

- [1] A. V. Senakhov and F. I. Sadov, *Kolloid. Zhur.* 21, 476 (1959).*
- [2] H. C. Gore and H. K. Steele, *Ind. Eng. Chem. Anal. Ed.* 7, 324 (1935).
- [3] P. M. Silin, *Izv. Tomskogo Tekhnol. in-ta* 45, 3, 56 (1924).
- [4] V. A. Smirnov, *Trudy Voronezh. Khimiko-Tekhnol. in-ta Pishchevoi Promyshlennosti* 3-4, 99 (1939).
- [5] N. N. Kryachkov, *Trudy Leningrad Tekhnol. in-ta Pishchevoi Promyshlennosti* 1 (9), 57 (1949).
- [6] I. E. Sadovyi, *Trudy Voronezh. Khimiko-Tekhnol. in-ta Pischevoi Promyshlennosti* 3-4, 89 (1939).
- [7] H. Eyring, *J. Chem. Phys.* 3, 107 (1935); W. K. Wynne-Jones and H. Eyring, *J. Chem. Phys.* 3, 492 (1935).
- [8] M. G. Evans and M. Polanyi, *Trans. Faraday Soc.* 31, 875 (1935); 33, 448 (1937); M. Polanyi, *J. Chem. Soc.* 629 (1937).
- [9] Yu. S. Zuev, *Kolloid. Zhur.* 12, 36 (1950).

Received December 24, 1957

*Original Russian Pagination. See C. B. Translation.

TWO TYPES OF CONTACTS DETERMINING THE STRENGTH OF CRYSTALLIZATION STRUCTURES IN CALCIUM SULFATE DIHYDRATE

E. Stoklosa, Z. N. Markina, and E. E. Segalova

The M. V. Lomonosov University, Moscow, Faculty of Chemistry,
Department of Colloid Chemistry

The basis of the concepts of a crystallization mechanism of hardening in mineral cements, put forward by Rebinder and his associates, is that the strength of the forming crystallization structures is determined only by the strength of the crystals forming the structure and of the points of their direct concretion, i.e., of the crystallization contacts.

However, our investigations of a monomineral cement, plaster of Paris, indicate that the strength of real hardened structures is determined, in addition to direct concretion contacts, by bonds of another type, which are to be regarded rather as coagulation bonds; they are regions in intertwining of elongated crystals in concretions, or of direct superposition. We shall refer provisionally to these bonds as coagulation contacts, although it must be remembered that they undoubtedly differ from coagulation bonds in the ordinary sense of the term [2]. These bonds serve as steric obstacles, i.e., they give rise to considerable resistance to uniaxial compression of the contacting intertwined crystals. The tensile strength of such a steric bond may be zero, in contrast to concretion points, the strength of which in respect of any type of deformation may be very considerable. Steric bonds, or superposition bonds, may produce appreciable shearing strength owing to formation of a true (direct) contact in absence of an aqueous medium. When the material is moistened the shearing strength of such bonds should fall almost to zero owing to inclusion of an adsorbed (hydration) interlayer which acts as a boundary lubricant film between the crystals and prevents direct contact and cohesion between them. This sharp decrease of strength under the influence of a liquid medium with respect to which the solid phase in lyophilic is quite analogous to the behavior of coagulation structures in thickening of the liquid interlayers at the points of contact, i.e., on stabilization of the particles forming these structures.

Thus, the distinction between coagulation and crystallization structures is revealed most easily when these structures are moistened. Coagulation structures then exhibit pronounced plasticity while their strength falls almost to zero. Although the strength of crystallization structures falls on moistening, it is retained to a very considerable extent. We utilized this difference and the results of direct determinations of compressive (R_{cm}) and tensile (R_t) strengths of dry and moist specimens of hardened plaster in an attempt to determine the relative role of crystallization contacts in the strength of the hardened structure and to elucidate certain strength characteristics of hardened plaster which have long been known but are not yet adequately explained.

It should be noted that a serious obstacle to solution of this problem is the decrease of strength of the plaster crystals themselves under the influence of the external medium. This effect, adsorptional strength lowering, greatly obscures the picture, as it is difficult to determine its role in the general strength decrease of hardened moistened plaster. Nevertheless, by variation of different factors and by artificial increase of the role of the coagulation structure in the test specimens we partially eliminated this difficulty.

It is known that the effect of adsorbed water, causing a strength decrease in a porous body, becomes very pronounced even at small water contents in the specimens [3], and therefore in studies of dry structures all adsorbed water must be very carefully removed, because even a very small increase of its content has a strong influence on the strength characteristics of the hardened plaster.

The dry specimens were humidified under vacuum in order to remove completely the air present in the porous material, because measurements of plaster strength in the intermediate state, i.e., incompletely humidified, obscure the picture because of the action of capillary forces which come into effect in the solid-liquid-gas three-phase system. The influence of this last factor can be seen by comparison of the compressive strengths of hardened plaster containing capillaries incompletely filled with water and plaster entirely free of the action of capillary forces. Thus, the compressive strength of specimens made from β -gypsum at $W/S = 1$ (W/S is the ratio of water to solid) directly after the end of hardening was 14 kg/cm^2 , while the strength of specimens dried and then moistened under vacuum, at the same W/S ratio, was 11 kg/cm^2 , so that the action of capillary forces raised the compressive strength of the plaster by 27%.

The measure used for the decrease in the strength of plaster as the result of moistening was the ratio R_w/R_d where R_w is the strength in the completely moist state, and R_d is the strength in the dry state.

For a coagulation structure this ratio is almost zero under our experimental conditions. If the strength did not decrease it would be unity.

Effect of Water - Plaster (W/P) Ratio on the Strength Characteristics of

Hardened Plaster

The results of strength determinations of hardened plaster at different water-plaster ratios can be interpreted more conveniently if the variable factor which directly determines the structure of the hardened plaster is taken to be the porosity, and not the water-plaster ratio, which characterizes only the initial conditions of structure formation.

The initial W/P ratio really predetermines the volume of the crystallization structure formed, because the expansion in the hardening of plaster is so small that it can be disregarded. With a knowledge of the initial W/P ratio and of the densities of calcium sulfate hemihydrate and dihydrate it is easy to calculate the final porosity of the hardened plaster formed at a given W/P ratio. However, such calculations disregard the fact that when the suspension is mixed it always entrains a certain amount of air, which increases the porosity of the hardened plaster. Therefore the porosity of the final hardened plaster was determined experimentally from the weight difference between dried and completely moistened specimens. The results of these determinations are presented in Fig. 1, where the porosity, i.e., the percentage of voids in the total volume of the plaster, is presented as a function of the W/P ratio.

The dash line represents porosity values calculated from the W/P ratio. The difference between the ordinates of the two curves indicates the increase of final porosity due to entrainment of air; it is seen in Fig. 1 that this is greater at lower initial W/P ratios.

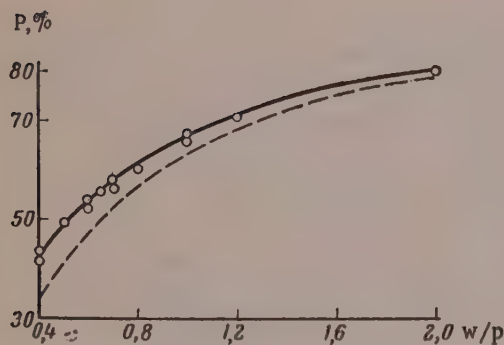


Fig. 1. Variations of porosity (P) of hardened plaster with the water-plaster ratio (W/P).

Figure 1 also shows that the porosity of our specimens varied from 43% ($W/P = 0.4$) to 80% ($W/P = 2.0$).

Because of the large part played by adsorptional strength lowering in polycrystalline structures of high porosity, it was also necessary to determine the internal surface area of the hardened plaster. This value, together with the porosity, may provide certain information on the shape of the pores and crystals in hardened plaster. The results of determinations of the internal surface by low-temperature adsorption of nitrogen are presented in Table 1.

Table 1 shows that as the porosity increases the specific surface first decreases and then begins to increase again. The order of magnitude of the internal surface indicates that the pores are very small, and that therefore surface effects should play an important role in such plaster. It follows from Table 1 that the internal surface of low-porosity plaster is greater than that of plaster of considerable porosity. This is related to the size of the crystals formed in suspension.

TABLE 1

Internal Surface of Hardened Plaster Specimens Formed at Different W/P Ratios

Porosity, %	42	60	63	70	80
Specific internal surface, m^2/g	2.60	1.26	0.83	1.70	1.45

Crystallization out of a fairly concentrated suspension is very rapid, supersaturation is maintained for a relatively long time, and numerous crystallization centers are formed per unit volume, favoring the formation of large numbers of small crystals. Under such conditions crystal anisometry is relatively slight.

The specific internal surface greatly decreases (by about 2/3 for 60-65% porosity) with increase of W/P ratio (and of porosity). This is due to increase of crystal size. At the same time there is another effect, acting in the opposite direction—the crystals become increasingly anisometric [4]. The second effect plays a minor role at first, but it increases rapidly with porosity until it begins to predominate at about 60-65% porosity. From that instant the role of anisometry is so great that it produces the reverse effect—increase of the internal specific surface.

It was of interest to determine the separate effects of increased porosity and of changed conditions of structure formation, which follow inevitably with changes in the concentration of the suspension, on the decrease in the strength of hardened cement (with increase of W/P ratio) (Fig. 2).

It is evident that in a solid, the strength of which in the homogeneous (nonporous) state is always constant, the formation of uniformly-distributed porosity should result in a linear decrease of strength in accordance with the decrease of the true cross section.

If the experimental strength is divided by the bulk density of the material, the values for the specific strength so found are independent of the porosity and are determined only by the strength characteristics of the solid, nonporous material. Fig. 3 shows values of the specific strength (R_{sp}) calculated for hardened plaster by division of R_{cm} by the bulk density of the specimen.

The specific strength does not remain constant with increase of W/P ratio, but falls sharply. This shows that the decrease of strength with increase of W/P ratio is due not only to increase of the porosity but also to changes in conditions of structure formation, leading to decreased strength of the crystalline concretions themselves. The time during which supersaturations high enough for formation of crystallization contacts decreases

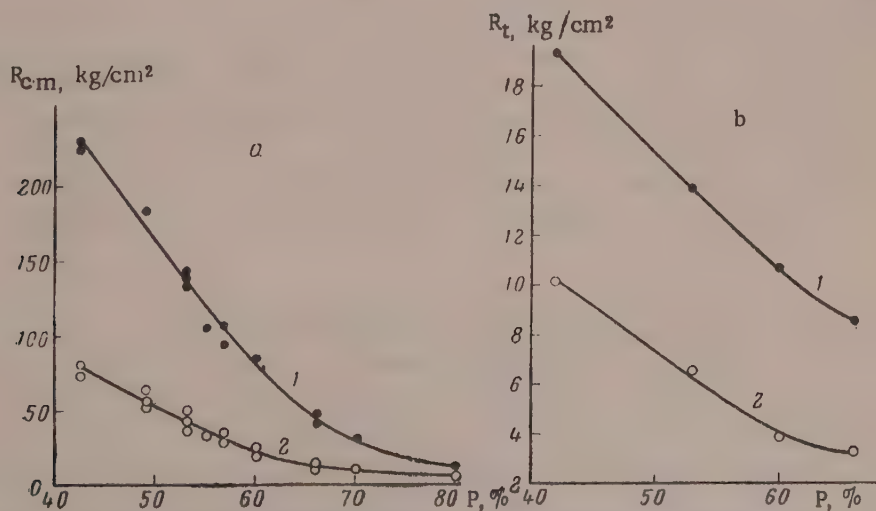


Fig. 2. Variations of the strength of dry (1) and moist (water-saturated, 2) specimens of hardened plaster with the porosity (P): a) compressive strength; b) tensile strength.

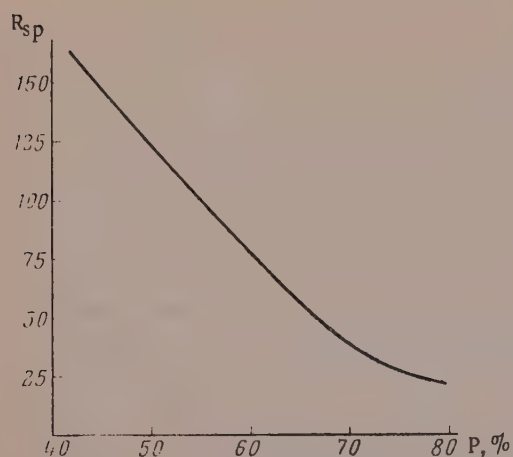


Fig. 3. Variation of specific strength (R_{sp}) of hardened plaster with the porosity (P).

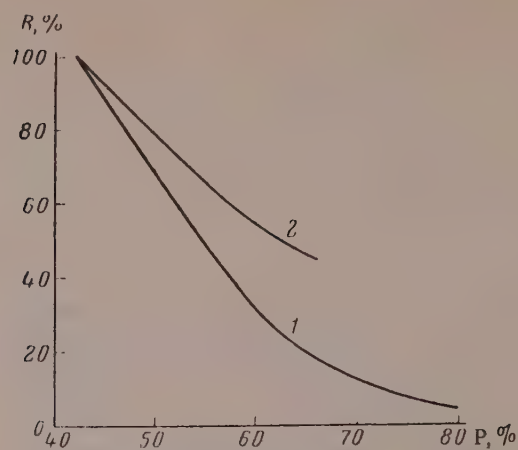


Fig. 4. Variations of compressive (1) and tensile (2) strength of plaster stone with porosity (P). The strength of the densest specimen at $P = 42\%$ is taken as 100%.

with increase of the original W/P ratio. Therefore the number of crystallization contacts falls with increase of W/P ratio, and this in itself results in a considerable decrease of strength. Moreover, at low W/P ratios an important part in formation of the hardened structure is played by contacts of the coagulation type, involving intertwining and superposition of calcium sulfate dihydrate crystals. The role of contacts of this type should diminish sharply with increase of the original W/P ratio. At high porosities the decrease of specific strength is somewhat less, probably because the crystals become increasingly anisometric, and this favors formation of additional coagulation bonds.

It follows from Fig. 2 that compressive strength decreases more than tensile strength with increased porosity of hardened plaster. This is shown especially clearly in Fig. 4, where the strength of the plaster is expressed as a percentage of the strength of the densest specimens. The sharp fall of R_{cm} with increase of original W/P ratio shows that this quantity is more sensitive than tensile strength to a decrease in the number of coagulation bonds in the hardened plaster structure. During deformation of the specimen in a compressive-strength test the individual crystals of calcium sulfate dihydrate are brought closer together, and this tends to increase the cohesion forces in the plaster.

When the specimens are moistened the compressive strength decreases more than the tensile strength (Fig. 5). This confirms the hypothesis that coagulation bonds play an important role in compressive strength, and their significance is reduced to a minimum on moistening. Since coagulation bonds are more prominent at low W/G, the difference between the decreases of compressive and tensile strengths on moistening is more pronounced at these W/G ratios. It must be pointed out that the observed decrease of the strength of hardened plaster in these experiments was a direct result of adsorptional strength decrease. The partial dissolution of crystallization contacts which takes place on moistening is so slight under these conditions that it has no practical effect on the strength. This is confirmed by the fact that specimens which have been dried again after single or twofold moistening do not lose strength but in some instances even show strength increases, probably

TABLE 2

Variations of Compressive (R_{cm}) and Tensile (R_t) Strength of Dry Specimens of Calcium Sulfate Dihydrate with the Number of Alternate Moistening and Drying Cycles (W/P = 0.7)

Number of cycles	0	1	2	3	4
R_{cm} , kg/cm ²	100	105	108	100	80
R_t , kg/cm ²	12.0	17.7	16.0	15.1	14.8

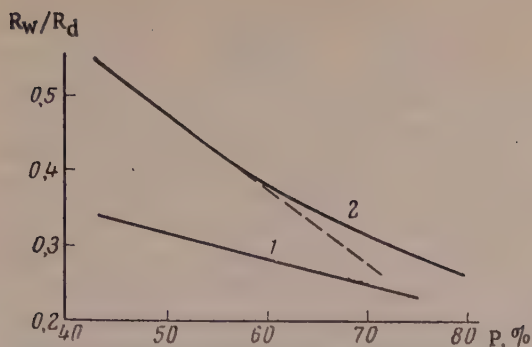


Fig. 5. Effect of porosity of hardened plaster on the R_w/R_d ratio for compressive (1) and tensile (2) strengths.

W/P ratio. It is known that adsorptional strength decrease is more pronounced for larger crystals, because of their greater defectiveness [5].

Investigation of the Strength Characteristics of Structures with Different

Proportions of Coagulation and Crystallization Bonds

For elucidation of the relative importance of crystallization and coagulation contacts in the development of strength in hardened plaster we investigated the strength characteristics of structure in which the amounts of coagulation or crystallization bonds were artificially varied.

The number of crystallization contacts formed in the hardened structure can be reduced by introduction of dihydrate crystals into the original suspension of calcium sulfate hemihydrate. This increases the rate at which the plaster crystallizes out and reduces the time during which high supersaturations are maintained in the suspension, thus decreasing the amount of crystallization bonds formed. For these experiments mixtures of previously dried calcium sulfate hemihydrate and dihydrate were prepared by means of shaking for an hour. The dihydrate was prepared previously from the same original hemihydrate. The specimens, made from these mixtures at $W/P = 0.7$, were dried to constant weight; some were moistened under vacuum after being dried.

TABLE 3

Variations of Compressive (R_{cm}) and Tensile (R_t) Strengths of Hardened Plaster Specimens with the Content of Dihydrate in the Original Mixture ($W/P = 0.7$)

Specimens	Dihydrate content, %				Specimens	Dihydrate content, %			
	0	20	40	60		0	20	40	60
Compressive strength, kg/cm ²					Tensile strength, kg/cm ²				
Dry	93	60	28	21	Dry	12,1	6,5	4,3	3,1
Fully moistened	30	3	—	—	Fully moistened	4,9	1,8	0,6	0,3

Introduction of dihydrate into the suspensions greatly accelerated hardening, as it completely eliminated the induction period associated with nucleation of the new phase.

It follows from Table 3 that the strength of hardened plaster falls rapidly with increase of calcium sulfate dihydrate in the original mixture, both for moist and for dry specimens. As has already been stated, this is because the number of contacts of the crystallization type decreases sharply with increase of dihydrate in the original mixture, and above a certain dihydrate content they are not formed at all. The limiting content of calcium sulfate dihydrate above which a crystallization structure is not formed is difficult to determine, because both the hardening time and the strength of the structure formed decrease with increase of the dihydrate

because the recrystallization which occurs releases excessive stresses in the crystallization structure. An appreciable strength decrease is observed only after 3 to 4-fold moistening and drying of the specimens (Table 2). The experiments on moistening were conducted in such a manner that leaching of the calcium sulfate was entirely prevented.

In a porous structure adsorptional strength decrease should be more pronounced with increase of the internal specific surface. However, as Fig. 5 shows, the strength decrease on moistening becomes greater with increased porosity of the hardened plaster, although the internal surface first falls fairly sharply, and then rises somewhat (Table 5). This is probably due to increase in the size of the calcium sulfate dihydrate crystals with increase of

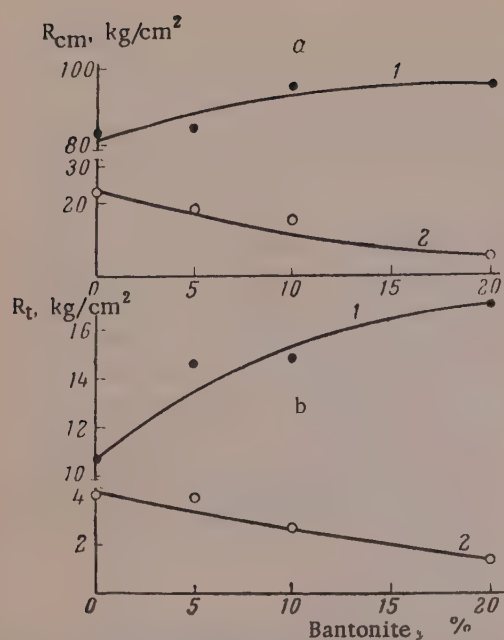


Fig. 6. Effect of bentonite additions on the strength of dry (1) and moist (2) specimens of hardened plaster. The abscissa axis indicates the amount of bentonite mixed with dry hemihydrate; $W/S = 0.8$ a) compressive strength; b) tensile strength.

causes a sharp increase of strength, which reaches 96 kg/cm^2 in compressive and 19.2 kg/cm^2 in tensile tests. The porosity of the resultant specimen is 44%, whereas the porosity of a specimen with a crystallization structure (at the same W/P ratio) is 58%. This shows that although the strength of coagulation bonds after drying is considerably less than the strength caused by crystallizational concretion of dihydrate, it is still fairly high. This explains why calcium sulfate dihydrate has been suggested as an unfired cement [6, 7].

The main defect of such structure is that they have no water resistance at all, as their strength falls virtually to zero on moistening. Moreover, the measurement results for these dried coagulation structures were very variable, probably because of inhomogeneity of the structure which becomes more compact during drying, and of internal stresses and even cracks which may result from nonuniform drying.

It is interesting to note that comparisons of specimens of equal porosity, but formed by crystallizational structure formation in hemihydrate in one case, and by drying of a coagulation structure in the other, shows that their compressive strengths differ sharply (235 and 96 kg/cm^2 respectively) whereas the tensile strength is virtually the same, 19 kg/cm^2 in both cases.

For determination of the influence of coagulation bonds on the strength of hardened plaster, two inert fillers—clay and quartz sand—were added to suspensions of the hemihydrate. The first of these fillers has a pronounced tendency to form coagulation structures whereas the second, because of the symmetrical shape of its particles, is quite incapable of forming loose coagulation structures. The compact coagulation structures of sand, formed in concentrated suspensions, have such low strength when dried (because of the very small area of contact between the particles) that they break down under their own weight.

All the specimens of plaster with added bentonite were prepared at 0.8 W/S ratio. Addition of bentonite to the original hemihydrate raises the strength of dry and lowers the strength of wet specimens (Fig. 6). On the one hand, bentonite "dilutes" the plaster and decreases the number of crystallization contacts in the ultimate structure of the hardened plaster, thereby reducing its strength, but on the other hand it increases strength by increasing the number of coagulation bonds; this particularly affects the strength of dry specimens. As coagulation structures can have high strength in the dry state, the strength of dry plaster specimens is higher in presence

content. It is impossible in practice to obtain this weak limiting structure, as it is broken down almost immediately after addition of water. Although the number of contacts decreases considerably on introduction of dihydrate and the structure becomes progressively weaker, a continuous crystallizational framework is nevertheless formed in specimens containing 40 and even 60% dihydrate. This is shown by the fact that after these specimens were dried they did not differ in size from specimens made from pure hemihydrate. However, when they are moistened their strength falls so much that it cannot be measured in practice. It follows that in these structures the predominant role is played by coagulation bonds, which confer high strength on the dry specimens.

The significance of coagulation bonds which may arise in presence of calcium sulfate dihydrate is demonstrated especially clearly in investigations of purely coagulation structures formed by prolonged grinding of the original hemihydrate. For example, if a suspension of calcium sulfate hemihydrate formed at $W/P = 0.7$ is ground for 30–40 minutes the possibility of formation of a crystallization structure in it is eliminated and a coagulation structure of free crystals of dihydrate is formed in the suspension. Such a structure in the moist state does not have compressive strength which is measurable in the ordinary press tester, but if it is dried the considerable shrinkage, bringing the crystals closer together,

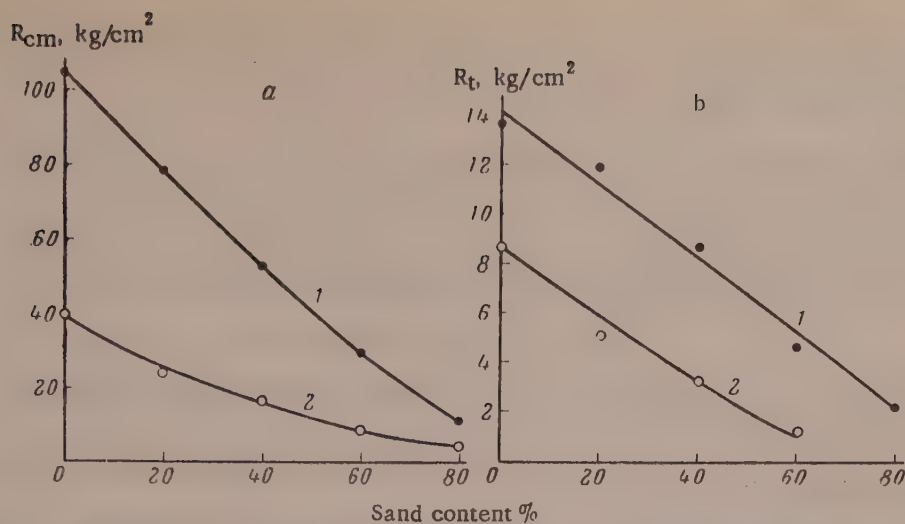


Fig. 7. Variations of the strength of dry (1) and moist (2) specimens of hardened plaster with the amount of quartz sand mixed with dry hemihydrate ($W/S = 0.7$): a) compressive strength; b) tensile strength.

TABLE 4

Effect of the Amount of Quartz sand ($S = 17000 \text{ cm}^2$) in the Original Mixture on the Compressive (R_{cm}) and Tensile (R_t) Strength of Dried Specimens of Calcium Sulfate Dihydrate after Breakdown of the Crystallization Structure

Sand content (by weight), %	20	50	80
R_{cm} , kg/cm ²	130	74	30
R_t , kg/cm ²	18	8.5	4.5

of bentonite although the number of crystallization bonds is less. In the case of moist specimens the explanation of the fall of strength with increase of the bentonite content is that with the great weakening of interaction between the crystals of the bentonite minerals, owing to the presence of water interlayers, the contribution of coagulation contacts to the total strength is negligibly small. Naturally the more bentonite is contained in the specimen the greater is the strength decrease on moistening.

Increase of the amount of quartz sand in hardened plaster considerably reduces the strength of both dry and moist specimens (Fig. 7). Sand acts as an inert filler which lowers strength by reducing the amount of structure-forming material per unit volume of the hardened plaster. It has the same effect on the strength of dried coagulation structure in calcium sulfate dihydrate (Table 4). These specimens were made by prolonged grinding of a concentrated aqueous suspension of hemihydrate and sand, with subsequent drying of the resultant coagulation structure. These specimens completely lose their strength when moistened.

SUMMARY

1. The tensile and compressive strengths of plaster specimens, formed at different water-plaster (W/P) ratios, in the dry and water-saturated states have been compared; the porosities and internal specific surfaces were measured.

2. Apart from direct-concretion contacts, the strength of hardened plaster is also determined by bonds of the coagulation type, which are regions of intertwining and direct superposition of elongated crystals in the concretions.

3. The relative significance of contacts of the coagulation type increases with increasing density of the hardened plaster (with decrease of W/P); the compressive strength is more influenced than the tensile strength by variations in the number of coagulation bonds in the plaster structure.

4. Addition of dihydrate results in a sharp fall in the plaster strength owing to a decrease in the number of crystal concretions in the course of crystallization. Additions of bentonite clay, which tends to form coagulation structures, increase the strength of dry specimens but lower it in the moist state, when the strength of coagulation structures is reduced to a minimum. Addition of quartz sand, which does not give rise to coagulation structures of any appreciable strength, lowers the strength of both dry and moist specimens.

LITERATURE CITED

- [1] E. E. Segalova, B. N. Izmailova, and P. A. Rebinder, *Doklady Akad. Nauk SSSR* 110, 808 (1956)*114, 594 (1957).
- [2] P. Rebinder and E. Segalova, *Preprints Proc. 2 Internat. Congress of Surface Activity* (London, April, 1957).
- [3] V. B. Ratinov Ya. L. Zabezhinskiĭ, and T. I. Rozenberg, *Coll. Trans. All-Union Sci. Res. Inst. Reinforced Concrete* [in Russian] (1957) 1, 3.
- [4] N. L. Sirotkina and N. V. Mikhailov, *Summaries of Papers at the 4th All-Union Conference on Colloid Chemistry, Tbilisi, May 1958* [in Russian] (Izd. AN SSSR, 1958) p. 153.
- [5] L. A. Shreiner, *Brittleness of Solids* [in Russian] (Izd. AN SSSR, 1949).
- [6] L. G. Gul'nova and V. A. Ipat'eva, *Unfired Gypsum Cement and Articles from It* [in Russian] (Kiev, 1954).
- [7] I. I. Rivlin and L. P. Papkova, *Trudy Kharkov Politekh. in-ta im. V. I. Lenina* 8, 3, 219 (1956).

Received July 19, 1958

* Original Russian pagination. See C. B. Translation.

INVESTIGATION OF BOUNDARY FRICTION AND ADHESION IN RELATION TO STUDIES OF THE INTERACTION OF FINELY DISPERSED PARTICLES

2. INFLUENCE OF CATIONS ON ADHESION OF GLASS DISKS

G. I. Fuks and N. I. Kaverina

Scientific Research Institute of the Watch Industry

It can now be regarded as proved that coagulation of disperse systems by electrolytes is determined by the balance of attraction and repulsion forces acting between the particles. In the modern theory [1-3] the principal forces of the first type are taken to be van der Waals-London forces, and the second type consists of electrostatic repulsion forces between interacting diffuse layers of adsorbed ions. The decrease of these forces with distance conforms to different laws, so that zones of repulsion and attraction are formed near the particle surfaces.

Relatively recently Deryagin and Abrikosova [4]* measured van der Waals forces as a function of distance from the surface. Experiments on adhesion of gas bubbles [7], investigations of disjoining pressure [8], and measurements of adhesion of microscopic particles [9, 10] and threads [11] show that the repulsion force must depend on the nature and concentration of the ions in solution, and therefore on the composition and thickness of the diffuse layer. However, there have been few direct determinations of the influence of electrolytes on surface interaction between solid particles in liquids, and in most of them the distance between the interacting surfaces was not found. Therefore the method of potential curves, which is the basis of the theory of coagulation and stability, could not be experimentally verified or developed.

Methods and objects of investigation. Possibilities of such investigations are provided by the method for determination of the kinetics of adhesion and separation of plane-parallel disks, developed by one of us for model experiments on the interaction of highly disperse particles [13, 14]. This method can be used for measuring the distance between mirror-polished plane-parallel disks immersed in a liquid, in the range of 0.02 to 20μ to an accuracy of $\pm 0.01\mu$. The gap between the disks pressed together under a given load in air is taken as zero. The disks in the liquid are brought together or separated by forces from 0.04 to 10.0 kg/cm^2 . The rate of change of the distance between them is measured to an accuracy of ± 0.005 seconds. Methods for cleaning the disks and removing dust and air bubbles, and procedures for eliminating or allowing for other sources of experimental error are described in the literature cited above.

It was demonstrated by this method that in liquids such as benzene, isooctane, cyclohexane, and highly-purified low-viscosity mineral oil the kinetics of adhesion and separation of steel and quartz disks conforms to the laws of hydrodynamics of viscous liquids, and in particular to the Stefan-Reynolds equation. In contrast to such liquids, mineral oils of the ordinary degree of purity, hydrocarbon solutions of fatty acids, and aqueous solutions of electrolytes in layers less than $0.2\text{--}0.3\mu$ thick exhibit significant deviations from the Stefan-Reynolds equation [13-15], indicating that in narrow plane gaps there may be formed multimolecular layers of surface-active substances and electrolytes which offer static resistance to attenuation and which have increased viscosity.

*A similar attempt was made by Overbeek [5], but objections have been raised to his results [6].

In the present investigation the chlorides of alkali and alkaline-earth metals and aluminum and thorium nitrate were used for studying the influence of cation valence and size, solution concentration, and temperature on the properties, as recorded by this method, of the boundary layers of electrolyte solutions in gaps between fused-quartz disks. The disk diameter was 12 ± 0.25 mm; the working surfaces were polished to Class 14 finish (GOST 2789-51) and ground against each other. The following quantities were measured:

1. The thickness h_b of the boundary layer, equal to half of the distance between the approaching disks at which the Stefan-Reynolds law begins to break down.*

2. The thickness h_{\min} of the residual layer, equal to half of the layer of solution not pressed out of the gap by the given load during the time of determination (up to 6-9 hours).

3. The disjoining pressure [8], corresponding to the equilibrium portion of the residual layer.**

4. The resistance of the residual layer to attenuation, measured in terms of $\bar{E} = \frac{h'_{\min}(\sigma'_n - \sigma''_n)}{h'_{\min} - h''_{\min}}$,

where h'_{\min} and h''_{\min} are the thicknesses of the residual layer under specific loads σ'_n and σ''_n .

5. The ratio of the boundary viscosity, given by the rate of disk separation, to the volume viscosity η_0/n .

6. The dimensionless coefficient of thickening $\psi = \frac{t_{sp}\sigma_{sp}}{\eta}$, where t_{sp} is the time of separation of the disk under a normal specific separating force σ_{sp} .

Since the disks serve as models for interaction between plane particles in disperse systems [13, 14], the first four of these quantities and partly the fifth characterize the ability of electrolytes to protect these particles against cohesion, while the fifth and especially the sixth characterize the kinetic relationship of the plane particles, the nature of which was considered earlier [13].

The Protective Role of Electrolytes

Figure 1 represents typical kinetics of the approach of disks in electrolyte solutions. In accordance with theory, initially the width of the graph is inversely proportional to the square root of the contact time t . During this period the curves for solutions and for water are close together or coincide, because their viscosities are, in the first approximation, equal. Subsequently the rate of displacement of the solutions from the gap decreases, which represents an increase of viscosity, different for different solutions. Ultimately the velocity of approach of the disks falls to zero and a layer of solution remains between them; the thickness of this layer does not alter during the experiment within the sensitivity limits of the method.

Water of conductivity $\chi_{20} = 1.2 \cdot 10^{-6} \Omega^{-1} \text{cm}^{-1}$, made by combustion of hydrogen in oxygen, retains a linear relationship between h and \sqrt{t} for a longer period, but in narrow gaps it also shows some deviations from this law; this may possibly be due to inadequate purification or to experimental errors, which reach 25-35% when the distance between the disks is less than 0.04 - 0.05μ . However, in contrast to electrolyte solutions, highly-purified water does not form a residual layer (Curve 1, Fig. 1).

The thickness of the boundary layer in the gap between quartz disks does not exceed 0.35μ and diminishes with increasing load, i.e. with increase of maximum pressure between the disks and of the rate of shear of the liquid in the gap (for fuller details, see [14]). At a constant and not too high load h_b diminishes with increase of cation radius and charge (Table 1).

The thickness of the residual layer of solution is a function of the load and, for different solutions under the same external conditions, a function of the cation charge and size (Fig. 2). At 20° and 1 kg/cm^2 pressure, h_{\min}

*It was shown [14] that the thickness of the residual layer of electrolyte solution under alternate loading and unloading is partially reversible. It was assumed that the specific load compressing the equilibrium portion of the residual layer is equal to the disjoining pressure.

**This definition of the boundary layer, which follows from the experimental data presented here, differs from the concept of the boundary layer introduced by B. V. Deryagin, as the former does not necessarily postulate an ordered structure across the entire layer. It will be shown that the boundary layer of an electrolyte solution has no sharp boundary.

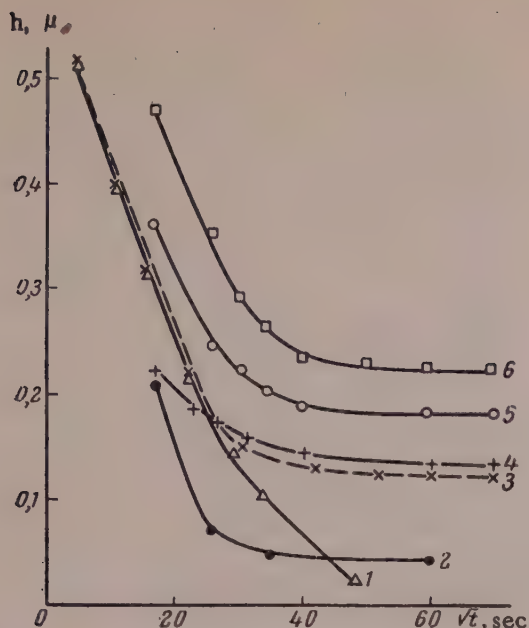


Fig. 1. Variation of the width of the gap between plane-parallel quartz disks with the time in contact in electrolyte solutions: 1) H_2O ; 2,3) 0.005 N NaCl; 4) 0.001 N CaCl_2 ; 5) 0.1 N LiCl; 6) 0.01 N LiCl (Curve 5 at 40° , the rest at 20° ; Curve 2 represents contact pressure of 4 kg/cm^2 , the rest, 0.2 kg/cm^2).

temperature. The temperature coefficient increases with decrease of cation radius, i.e., with increase of cation hydration, and also with decrease of pressure. At high temperatures or pressures the influence of cation radius on the residual layer becomes imperceptibly small. Above 60° the greatest differences between h_{\min} for solutions containing alkali-metal ions do not exceed 0.02μ which is near the sensitivity limit of the method.

TABLE 1

Effects of Cation Charge and Radius on the Thickness of the Boundary Layers on 0.01 N Electrolyte Solutions; Temperature 20° ; Pressure 1 kg/cm^2

Electrolytes	h_b, μ	Electrolytes	h_b, μ
LiCl	0.27	MgCl_2	0.14
NaCl	0.16	CaCl_2	0.11
KCl	0.12	BaCl_2	0.10
RbCl	0.12	AlCl_3	0.08
		$\text{Th}(\text{NO}_3)_4$	0.04

Under small loads the resistance of the residual layer to attenuation depends little on the ionic charge on radius (Table 2). In contrast to this, at pressures above $1\text{--}2 \text{ kg/cm}^2$ it is seen distinctly that the thickness of the residual layer decreases and its "strength" correspondingly increases with increase of the valence of the ions. The concentration of alkaline-earth salt solutions above 5-10 meq/liter has no effect on $\bar{E}_{0.2-2.0}$. In the series of univalent cations this quantity increases with ionic radius (Fig. 5). As the thickness of the residual layer decreases simultaneously, here again the thinner residual layers are the "stronger".

for 0.001 N solutions of NaCl, CaCl_2 , AlCl_3 and $\text{Th}(\text{NO}_3)_4$ is 0.14; 0.09; 0.08 and 0.04μ respectively. The radius has little influence in the case of bivalent ions, whereas the difference between the values of h_{\min} for LiCl and CsCl solutions is greater than the corresponding difference for NaCl and CaCl_2 solution (Fig. 2).

The influence of cation radius (r_k) decreases with increasing load, and the mathematical expression for the relationship between the thickness of the residual layer and cation radius approximate to the simple equation:

$$h_{\min} = K_1 - K_2 r_k,$$

where K_1 is a constant which decreases with increase of ion valence, load, and temperature; K_2 is a constant which is close to zero at high loads.

Increase of the solution concentration from 1 to 50-100 meq/liter reduces the thickness of the residual layer (Fig. 3). Subsequently h_{\min} remains unchanged or even increases somewhat. Experiments were not carried out at solution concentrations $< 0.5 \text{ meq/liter}$, but as highly purified water does not form a residual layer, decrease of concentration for very dilute solutions should probably result in a decrease of h_{\min} .

Figure 4 shows that h_{\min} decreases with rise of

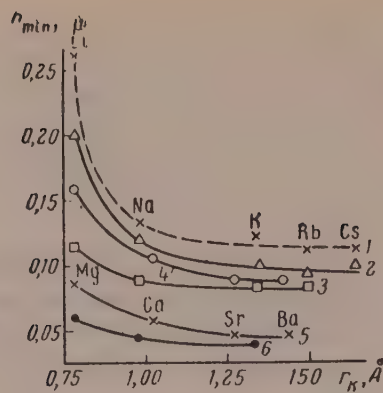


Fig. 2

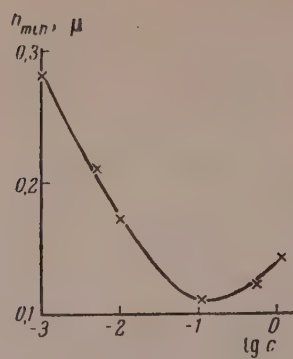


Fig. 3

Fig. 2. Variations of the thickness of residual layers of 0.01 N electrolyte solutions with the crystallochemical cation radius and load: Curve 6 at 60°, the rest at 20°: 1) Univalent cations, $\sigma_n = 0.2 \text{ kg/cm}^2$; 2) same, $\sigma_n = 1 \text{ kg/cm}^2$; 3) same, $\sigma_n = 2 \text{ kg/cm}^2$; 4) bivalent cations, $\sigma_n = 0.2 \text{ kg/cm}^2$, 5) same, $\sigma_n = 2 \text{ kg/cm}^2$; 6) univalent cations, $\sigma_n = 1 \text{ kg/cm}^2$.

Fig. 3. Variation of the thickness of the residual layer of NaCl solution with concentration at contact pressure of 0.2 kg/cm^2 and 20°.

The resistance to attenuation of the residual layers of solutions increases with increasing load and decreasing gap between the disks, and consequently with approach of the solid to the surface (Table 2). Comparison of the experimental results for different solutions shows that the composition of the ions plays a subordinate role to the initial h_{\min} , but nevertheless for a given thickness of the residual layer $E_{\sigma'_n - \sigma''_n}$ generally increases with increase of the cationic charge.

The disjoining pressure determines the equilibrium component of the attenuation resistance of the residual layer; for the solutions studied (as for other substances [8]) this pressure is a function of the distance between the interfaces. The pressure is higher in boundary layers of univalent-cation solutions than in corresponding layers containing bivalent cations, and in the former case it increases with decrease of ionic radius (Fig. 6). Thus the influence of ions on the attenuation resistance of residual layers and on the disjoining pressure is not of the same nature.

TABLE 2

Variation of the Resistance to Attenuation of Residual Layers of 0.01 N Electrolyte Solutions with the Thickness of these Layers (at 20°)

Electro- lyte	Load range, kg/cm ²	Initial h _{min} , μ	$E_{\sigma'_n - \sigma''_n}$ kg/cm ²	Electro- lyte	Load range kg/cm ²	Initial h _{min} , μ	$\bar{E}_{\sigma'_n - \sigma''_n}$ kg/cm ²
LiCl	0,2—2,0	0,24	4,3	MgCl ₂	0,2—2,0	0,16	4,1
	1,0—4,0	0,20	4,6		2,0—4,0	0,09	11,3
	2,0—4,0	0,11	5,5		0,2—2,0	0,11	4,0
NaCl	0,2—2,0	0,14	5,3	CaCl ₂	1,0—4,0	0,07	7,0
	1,0—4,0	0,12	6,0		2,0—4,0	0,06	15,0
	2,0—4,0	0,09	6,7		0,2—2,0	0,08	4,8
KCl	0,2—2,0	0,13	4,7	AlCl ₃	2,0—4,0	0,05	12,0
	1,0—4,0	0,10	9,0		0,2—2,0	0,06	5,4
	2,0—4,0	0,08	10,6		2,0—4,0	0,04	18,0
				Th(NO ₃) ₄	2,0—4,0	0,04	

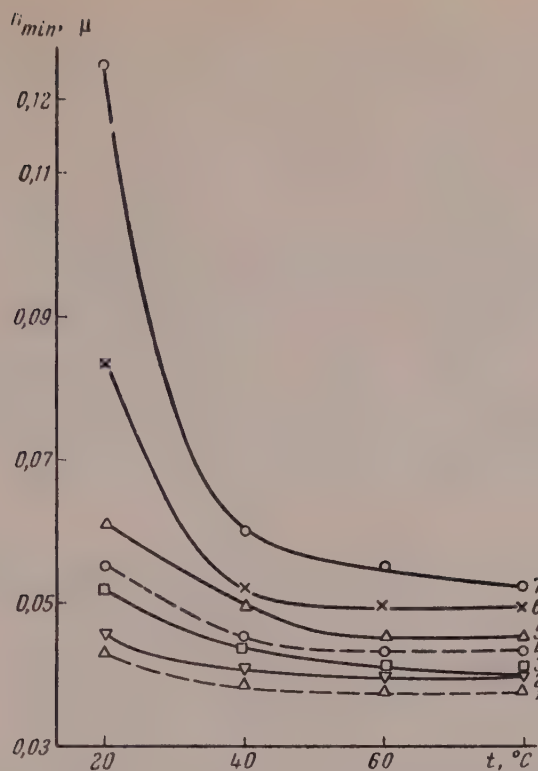


Fig. 4. Effect of temperature on the thickness of residual layers of electrolyte solutions in the gap between quartz disks at pressures of: 1.0 kg/cm², Curves 5 and 7; 2.0 kg/cm², the remaining curves; 1) 0.01 N BaCl₂; 2) 0.01N KCl; 3) 0.01 N NaCl; 4) 0.01 N LiCl; 5) 0.01 N NaCl; 6) 0.1 N LiCl; 7) 0.1 N LiCl.

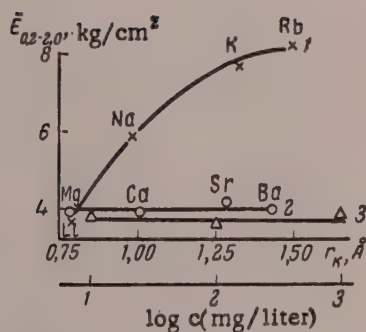


Fig. 5

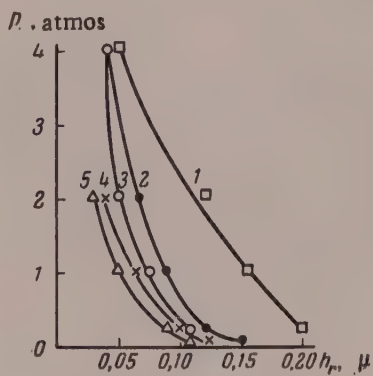


Fig. 6

Fig. 5. Variation of the resistance to attenuation of residual layers of electrolyte solutions with the crystallochemical radius of the cations (at 25°): 1 and 2) 0.01 N solutions, of salts with univalent and bivalent cations; 3) LiCl of different concentrations.

Fig. 6. Disjoining pressure of electrolyte solutions in the plane gaps between quartz surfaces at 20°; h_r is one half of the equilibrium gap: 1) 0.01 N LiCl; 2) 0.01 N NaCl; 3) 0.01 N KCl; 4) 0.01 N NaCl; 5) 0.01 N CaCl₂.

In mutual approach of quartz disks in water and aqueous electrolyte solutions to distances down to 0.02μ a static adhesion force in excess of 40 g/cm^2 (the minimum separating force in the method) was not observed, but electrolytes have a significant influence on the time required for separation of the disks, i.e., on the kinetic bond between them. This bond arises as the result of the hydrodynamic effect produced by the liquid flowing into the gap between the separating disks [13].

It has been shown that increase of the contact time between solid surfaces in liquids increases the static adhesion force [10, 11]. It follows from the data in Fig. 7 that this factor also influences the time required for separation of the disks. Comparison of the data in Fig. 7 and Fig. 1 indicates that increase of t_{sp} is a consequence of the decrease in the thickness of the boundary layer of liquid between the disks.

If the contact pressure is not large and the time of contact between the disks is less than 15-20 seconds, then the composition of the solution does not have any appreciable influence on the time of separation, but if the contact time is considerable, then the time of separation may vary by a factor of 10 or more in accordance with the nature and concentration of the electrolyte (Table 3).

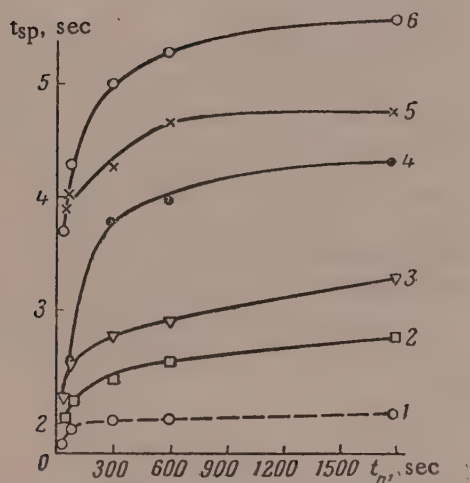


Fig. 7. Effect of contact time (t_n) on the time of separation (t_{sp}) of quartz disks in electrolyte solutions: (Curve 4 for pressure of 4 kg/cm^2 , the rest for 1 kg/cm^2): 1) 0.001 N NaCl ; 2) 0.01 N NaCl ; 3) 0.01 N KCl ; 4) 0.01 N NaCl ; 5) 0.01 N CaCl_2 ; 6) 0.1 N NaCl .

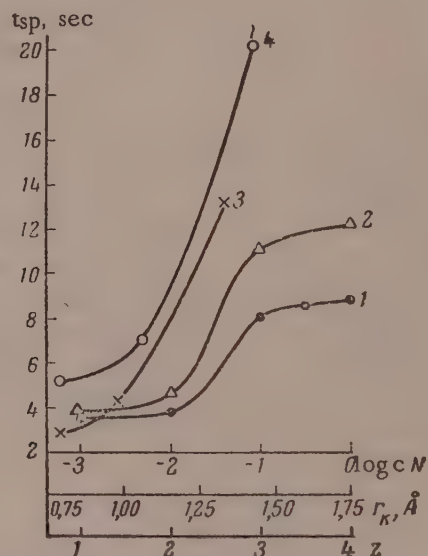


Fig. 8. Effect of composition of electrolyte solutions on the separation time (t_{sp}) of quartz disks immersed in them: 1) $t_{sp} = f(c_{Na})$, $\sigma_n = 4\text{ kg/cm}^2$; 2) $t_{sp} = f(z)$, $c = 0.01\text{ N}$, $\sigma_n = 1\text{ kg/cm}^2$; 3) $t_{sp} = f(r_k)$, univalent cations, $\sigma_n = 1\text{ kg/cm}^2$; 4) $t_{sp} = f(r_k)$, bivalent cations, $\sigma_n = 1\text{ kg/cm}^2$.

The increase of t_{sp} is in good agreement with the effects of solution concentration and the charge and size of the ions on the thickness of the residual layer (Fig. 8).

The boundary viscosity of electrolyte solutions is a function of the thickness of the boundary layer. * Thus, at 20° for 0.1 N solution of NaCl $\eta_\sigma/\eta = 1.4$ if the gap h between the disks is 0.24μ , and $\eta_\sigma/\eta = 2$, at $h = 0.14\mu$. In a gap close to $2h_{\min}$ the boundary viscosity decreases with increase of the cationic charge and radius and increases with increasing concentration. At 20° η_σ/η for 0.01 N solutions of LiCl , NaCl , KCl , MgCl_2 and CaCl_2 in a gap of $2h_{\min} + 0.02 \pm 0.02\mu$ have the values of 4.4; 4.1; 3.4; 2.6; 2.4 respectively. In the concentration series of 0.0001 , 0.01 , and 0.1 N NaCl solutions, with a gap between the disks $2h_{\min} + 0.03 \pm 0.02\mu$, the values of η_σ/η are 3.1, 4.0, and 4.7.

* In determinations of boundary viscosity by the method of disk separation a similar relationship applies to other liquids which form boundary layers [12, 14].

TABLE 3

Effect of Solution Composition on the Time of Separation of Quartz Disks; Temperature 20°; Compressive Force on Disks 4 kg/cm²; Separating Force 0.08 kg/cm²

Electrolytes	Concentration meq/liter	t _n , min	t _{sp} , sec	Electrolytes	Concentration meq/liter	t _n , min	t _{sp} , sec
LiCl	10	30	2,9	CaCl ₂	10	1	7,0
NaCl	1	30	3,7		10	30	15,5
	10	1	2,8		10	120	26,2
	10	30	4,3	BaCl ₂	5	30	30,0
	10	120	5,2		10	1	10,5
	1000	30	9,3		10	30	34,0
KCl	10	1	5,0	AlCl ₃	10	120	42,0
	10	30	13,0		10	30	43,0
	10	120	16,5	Th(NO ₃) ₄	10	30	45,4

The effect of temperature on η_{σ}/η is variable. With increase of temperature the boundary viscosity in the peripheral part of the boundary layer falls more rapidly than the volume viscosity, and η_{σ}/η decreases accordingly; for example, for 0.005 N CaCl₂ solution with a gap 0.3 μ thick between the disks this ratio is 2.1 at 20° and 1.0 at 80°. When the gap between the disks approaches $2h_{\min}$, η_{σ}/η is either independent of the temperature or increases with rise of temperature; for example, it is almost doubled with increase of temperature from 20 to 90° for 0.01 N LiCl solution with a gap of $2h_{\min} + 0.04 \mu$. The boundary viscosity, measured after the disks have been in prolonged contact, also increases with rise of temperature.

Figure 9 shows that the coefficient of boundary thickening of the investigated solutions is a function of the same factors as the boundary viscosity. An interesting fact is that ψ is very sensitive to electrolytes (Curves 5 and 6, Fig. 9). The effect of temperature on the coefficient of boundary thickening becomes more pronounced with increase of the solution concentration.

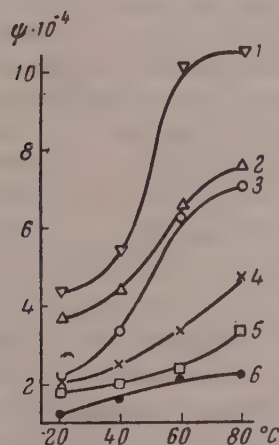


Fig. 9. Effect of temperature on the coefficient of boundary thickening of electrolyte solutions in the gap between quartz surfaces; $t_n = 30$ minutes, $\sigma_n = 1 \text{ kg/cm}^2$, $\sigma_{sp} = 0.08 \text{ kg/cm}^2$; 1) 100 meq NaCl per liter; 2) 10 meq CaCl₂ per liter; 3) 10 meq LiCl per liter; 4) 10 meq NaCl per liter; 5) 1 meq NaCl per liter; 6) H₂O.

The results of this investigation confirm the earlier hypothesis [13] that kinetic bonding should play a considerable role in interaction between particles in disperse systems if plane or nearly plane gaps are formed between the particles and if their contact and area, and consequently the hydrodynamic aggregation factor, are large. The kinetic bonding between such particles increases with increases of contact time and contact pressure, concentration of electrolyte solutions, and the valence and radius of ions with charges of opposite sign to the charges on the particles.

DISCUSSION OF RESULTS

These results show that the thickness of the diffuse layer and of the residual layer depend in the same manner on the composition of the electrolyte solutions. This justifies an experimental verification of the theory of interaction of diffuse layers.

In the case of the investigated strongly-charged disk surfaces separated by distances greater than double the theoretical thickness of the diffuse layer*, i.e., in the case of weak interaction, the quantitative theory of

* There have been no direct determinations of the thickness of diffuse ionic layers and the values used in the literature have been derived theoretically or from electrokinetic determinations (see reviews [16, 17]).

repulsion of these layers yields an exponential expression of the general form

$$F_r = j(e^{-\chi d}),$$

where F_r is the repulsion force; d is the distance between the surfaces; $\chi = \sqrt{\frac{8\pi c z^2 e^2}{\epsilon k T}}$ (here c is the concentration, z is the valence, e is the unit ionic charge, and ϵ is the dielectric constant). This expression follows from the distribution of potential in the double layer, in accordance with the Gouy-Chapman theory, by which the potential φ_x at a distance x from a surface with a potential φ_0 (not large) is given by the approximate equation: $\varphi_x = \varphi_0 e^{-\chi x}$. In the Debye-Huckel-Gouy theory $1/\chi$ is taken to be the thickness of the diffuse layer (the ionic atmosphere). For solutions of univalent ions at concentrations from 0.001 to 0.1 N $1/\chi$ is in the range of 0.01 to 0.001 μ .

The theoretical equations representing weak interaction (repulsion) of plane-parallel surfaces in electrolyte solutions, derived by Deryagin [18], Frumkin and Gorodetskaya [7], Deryagin and Landau, and Verwey and Overbeek [3], have a common basis. When $\varphi_0 \ll RT/F$ the first two of these equations coincide and may be written $F_r = K \frac{e^{-\chi h}}{x^2}$ where K is a constant.

If χ is expressed as $Kz\sqrt{c}$ this equation assumes a form convenient for experimental verification, the results of which are presented in Fig. 10*. At high loads and low solution concentrations there is quite satisfactory agreement between the theoretical and experimental relationships between F_r for z and c respectively, on the one hand, and between F_r and h on the other. Solutions containing more than 10 meq of salt per liter do not conform to this equation. However, purely electrostatic concepts of interaction between diffuse layers, based on the Gouy-Chapman theory, cannot account for all the properties of boundary layers of electrolyte solutions. The greatest thickness of the residual layer is almost ten times that of the diffuse layer in accordance with the Debye-Huckel-Gouy theory; with increase of temperature the thickness of the residual layer does not increase, as might be expected, but decreases; the thickness of residual layers with univalent cations at small loads depends significantly on their position in the lyotropic series; the resistance of the residual layer to attenuation is determined not only by its thickness but also by the radius of the ions forming this layer; and finally the disjoining pressure of solutions decreases more rapidly with increased radius of univalent cations than with increase of ionic charge.

It is known that the theory of Stern and its recent modifications [19-21] make it possible, within certain limits, to take into account the influence of ionic size and interaction between the ions of the inner and outer layers of the double layer. This theory gives thicker diffuse layers, the external portions of which should conform to the above relationship between F_r and χd ; it should bring the theoretical and experimental relationships closer together. However, no quantitative concepts of interaction between diffuse layers, which could be verified experimentally, have yet been derived from Stern's theory. A purely qualitative consideration shows that if the ionic radius is taken into account the theoretical thickness of the diffuse layer is not brought up to the experimental values for the thickness of the residual layer,** and the influence of temperature on the effects in question is not explained; nor does this account for the effect of concentration on h_{\min} and for solutions containing more than 10 meq of salt per liter. These and certain other phenomena can be understood only by introduction of the concept of hydration of ions in the diffuse layer.

It is known that very different hydration values are obtained by studies of different solution properties (transference numbers, compressibility, salting out, etc.).*** These discrepancies are due not so much to differences in the methods as to the ability of the ions to involve different numbers of water molecules in the given

*The values of \sqrt{c} arranged in an arithmetical progression (common difference 0.71 for verification of the equation $F_r = K(Vc)^2 \cdot e^{-K Vc}$, were calculated by interpolation from experimental values of F_r for c of 0.5; 1; 2.5;

5; 10; 50 and 100 meq/liter.

**The thickness of the residual layer of 0.01 N NaCl solution is from 120 to 600 times the diameter of Na^+ in solution [22], depending on the contact pressure.

***One sodium ion in solution binds 66 molecules of water according to Ramy [23], 6-7 molecules according to Pasynskii [24], and 1 molecule according to Darmon [25]. Even greater differences are found for the hydration of Li^+ (from 4 to 160).

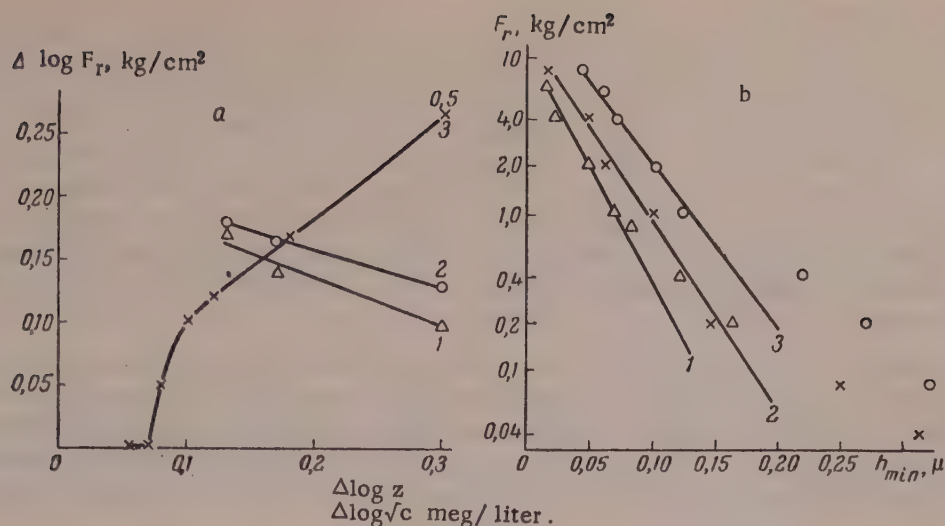


Fig. 10. Test of the applicability of the equation $F_r = kz^2ce^{-kz\sqrt{ch}}$ by the smoothing method: a) $F_r = f(z, c)$ when $h_{\min} = \text{const}$: 1) $F_r = f(z)$; $h = 0.06 \pm 0.01 \mu$; 2) $F_r = f(z)$; $h = 0.04 \pm 0.01 \mu$; 3) $F_r = f(\sqrt{ch})KCl$; $h = 0.10 \pm 0.01 \mu$; 0.5 and 8) values of c in meq/liter; the linear region corresponds to solution concentration from 0.5 to 8 meq/liter; b) $F_r = f(h)$ when $x = \text{const}$: 1) 5) meq $CaCl_2$ per liter; 2) 2.5 meq KCl per liter; 3) 1 meq $NaCl$ per liter.

effects [26, 27]. The concept of ion hydration becomes more definite if primary or near and secondary or remote hydration* are considered separately; the former comprises water molecules which have lost their translational degree of freedom and move together with the ions, and the second, water molecules polarized in the field of force of the ions.

According to Bockris [26], the primary ion hydration number does not exceed 10 (with the possible exception of Mg^{2+} , which, according to certain data, may have a hydration number as high as 13). On the basis of Bernal and Fowler's model [28] of the water molecule and its nearest environment, Kapustinskii [22, 29] and Samoilov [27, 30] developed a theory of the structure of electrolyte solutions in accordance with which an ion occupies a central position in a tetrahedron formed by four water molecules. If it is assumed that this structure persists in the diffuse layer,** then this model can be used for calculating, in the first approximation, the effective diameter of a kinetic unit consisting of an ion and its close hydration molecules. Calculations based on published values for radii of hydrated ions [22] and water molecules [28, 31] show that the experimental values of the thickness of the residual layers formed by the corresponding ions are 50 to 600 times as high as the calculated values.

It is quite probable that the diffuse layer extends to a distance of some tens of ionic diameters, and therefore structural concepts in which near hydration is taken into account show, in full agreement with the results of verification of the Deryagin-Frumkin equation, that residual layers of electrolyte solutions in narrow gaps between solid surfaces owe their existence to interaction between diffuse layers of primarily-hydrated ions.

However, this effect cannot provide an explanation for the static resistance to attenuation of a layer of solution several hundreds of ionic diameters thick, because thermal motion must destroy or greatly weaken the diffuse layer at such a large distance from the surface. The irreversibility of the "thick" residual layers on

* There are differences between the concepts of primary and secondary hydration as introduced by Bockris [26] and of near and remote hydration as introduced by Samoilov [27] in relation to the problem of structure of electrolyte solutions, but they are not of great importance in relation to the questions considered here.

**Grahame [20] showed that in the case of a double layer on a mercury surface only the ions of the inner layer are adsorbed and partially dehydrated, whereas ions of the diffuse layer apparently remain fully hydrated. The heats of ion adsorption also indicate that ions of the diffuse layer are hydrated.

removal of load, and the fact that their properties do not conform to the theoretical equation in question (Fig. 10), also show that this explanation is inapplicable.

Some peculiarities in the properties of these layers give an indication of the causes of their formation. First, the dependence of the thickness of the residual layer (and also of the boundary layer) on the position of the ions in the lyotropic series is most pronounced at small contacts pressures (Fig. 2). It is known that the lyotropic series of ions is based on the heats of solution and heats of hydration of ions, which in their turn depend mainly on remote hydration [32]. It is therefore quite natural to attribute the static resistance to approach between surfaces at large distances mainly to remote hydration of ions in the diffuse layer. This is consistent with the strong influence of temperature on "thick" and the relatively slight influence on "thin" residual layers (Fig. 4), as the temperature coefficient of remote hydration is considerably greater than the corresponding coefficient of near hydration.

The energy of remote hydration is not large (about 90% of the energy of an ion is expended in binding the nearest water molecules [33]), and it is not enough to cause the reversibility, detected by our method, of the peripheral part of the residual layer on removal of load. It is detected as a static mechanical resistance only as the result of summation of energies of weak interaction in the plane diffuse layer. It is therefore possible that the thickness of the residual and boundary layers, associated with remote hydration, depends on the scale factor and the shape of the surface.

Evidently a certain role in these effects must be played not only by water molecules far from the ions outside the diffuse layer, but also by such molecules within it. The dependence of resistance to attenuation and of disjoining pressure on the ionic radius (Table 2 and Fig. 5 and 6) may be associated with this. There is no doubt that increased interaction between water molecules and ions in strongly compressed diffuse layers causes increase of the thickness of the residual layers of concentrated solutions (Fig. 3) and accounts for the deviations in the behavior of these layers from the Deryagin-Frumkin equation (Fig. 10).

Three a priori explanations may be offered for the increased kinetic resistance to disk separation: 1) decrease of the effective gap owing to partial filling by a quasisolid residual layer; 2) the electroviscous effect; 3) increased viscosity owing to polarization of water molecules in the field of stationary ions or ions of low mobility. Despite the fact that the rate of disk separation depends very much on the width of the gap between the disks, it was shown in the first communication of the present series ([14], Fig. 2) that geometrical factors, even with a correction for the residual layer, cannot account fully for the observed deviations from the Stefan-Reynolds equation. According to modern theoretical [34, 35] and experimental [36] studies, the magnitude and role of the electroviscous effect have been greatly overestimated. Retarded flow of solutions in and out of "wide" gaps (of thickness near to double the thickness of the boundary layer) cannot be ascribed to the electroviscous effect, as according to the theory of this effect its magnitude is proportional to the square of the zeta potential, whereas η_0/η increases with increase of the solution concentration and with decrease of ionic radius (see earlier). This is demonstrated particularly clearly by determinations of the rate of disk separation at a constant initial gap between the disks ([14] Fig. 7). In such gaps the solution viscosity increases, at least partially, because of further hydration. This hypothesis is supported both by the dependence of η_0/η on the position of the ions in the lyotropic series, and by the high temperature coefficient of boundary viscosity for the investigated solutions. At the same time, boundary viscosity determined after prolonged contact of the disks under high contact pressure depends little on the nature of the ions or the temperature [37]. Therefore it may be supposed that in narrow gaps, close to the thickness of the diffuse layer in width, the main cause of boundary viscosity is the resistance to shear of the ions in the diffuse layer, which is the cause of the electroviscous effect. Finally, the effective viscosity of solutions in narrow gaps may be higher than the volume viscosity because of the higher concentration of ions.

It is noteworthy that the boundary layers of electrolyte solutions offer much greater resistance to normal loads than to tangential shearing forces. As was shown by one of us, mechanical anisotropy of a boundary liquid layer is a characteristic sign of its lubricating power, and the ratio of normal and tangential resistances to stress may serve as a measure of this effect [38]. In the most general form, this effect is explained by differences in the scattering of energy in the motion of water molecules or ions along and across the field of force of the surface and its associated ions of the double layer or adsorbed molecules.

In conclusion it must be pointed out that in discussion of the experimental data we disregarded the surface microrelief of the disks. Although the disks were so thoroughly polished and ground against each other that their roughness does not influence the qualitative aspects of the observed effects [12-14], this factor may have a certain quantitative influence which increases with decrease of the gap width.

SUMMARY

1. Model experiments on the kinetics of adhesion and separation of plane-parallel quartz disks in electrolyte solutions yielded data on the influence of solution concentration, cation valence and radius, and temperature on the interaction of plane particles in disperse systems. This method was used for studying the influence of contact pressure and duration of contact on the width of the gap between the particles and on kinetic bonding between them.

2. Boundary layers of electrolyte solutions in plane gaps between quartz surfaces have static (equilibrium and nonequilibrium) resistance to attenuation and higher viscosity than in the solution volume. The boundary layers of electrolyte solutions oppose cohesion of the particles on the one hand, and increase kinetic bonding between them on the other.

3. Formation and properties of the peripheral part of the boundary layer of an electrolyte solution are associated mainly with remote hydration of ions in the diffuse layer. Because of the small energy of hydration the resistance to attenuation of this part of the boundary layer is low; its thickness depends significantly on the ionic radius and temperature.

4. The resistance to mutual approach of quartz surfaces separated by thin boundary layers of electrolyte solutions is caused mainly by electrostatic repulsion of diffuse layers of adsorbed ions with bound near molecules of water. Water molecules remote from the ions, within the diffuse layer, also apparently have a certain influence. The repulsion force is a negative exponential function of the ion valence and the square root of the solution concentration.

5. Kinetic bonding between plane quartz particles increases with the time of contact, contact pressure, solution concentration, cation valence and radius, and rise of temperature; i.e., with the effects of factors which diminish the gap between the particles. Boundary viscosity increases also increases the time of separation of the particles.

LITERATURE CITED

- [1] B. V. Deryagin, Proc. 3rd All-Union Conference on Colloid Chemistry [in Russian] (Izd. AN SSSR, 1956) p. 225; B. V. Deryagin and D. L. Landau, *Zhur. Eksptl. Teoret. Fiz.* 15 (1945).
- [2] H. Hamaker, *Recueil Trav. Chim.* 55, 1015 (1936); 56, 8 (1937); 57, 61 (1938).
- [3] F. Verwey and J. Overbeek, *Theory of the Stability of Lyophobic Colloids* (New York and London, 1948).
- [4] B. V. Deryagin and I. I. Abrikosova, *Zhur. Eksptl. Teoret. Fiz.* 21, 945 (1951); 30, 993 (1956); 31, 3 (1956); *Doklady Akad. Nauk SSSR* 90, 1055 (1953).
- [5] J. Overbeek, "Discussion on Coagulation and Flocculation" *Trans. Faraday Soc.* 18, 12 (1954).
- [6] B. V. Deryagin, I. I. Abrikosova, and E. M. Livshits, *Uspekhi Fiz. Nauk* 64, 493 (1959).
- [7] A. N. Frumkin and A. V. Gorodetskaya, *Acta Physicochim. URSS* 9, 327 (1938).
- [8] B. V. Deryagin and E. B. Obukhov, *Kolloid. Zhur.* 1, 385 (1935); B. V. Deryagin and M. M. Kusakov, *Izvest. Akad. Nauk SSSR, Ser. Khim.* 5, 471 (1936); *ibid.*, 5, 1119 (1937); *Zhur. Fiz. Khim.* 26, 586 (1952); B. V. Deryagin, *Kolloid. Zhur.* 17, 207 (1955).*
- [9] A. Buzagh, *Kolloid.-Z.* 47, 370 (1929); 51, 105, 230 (1930); *J. Phys. Chem.* 43, 1003 (1939).
- [10] G. I. Fuks, V. I. Klychnikov, and E. V. Tsyganova, *Doklady Akad. Nauk SSSR* 65, 307 (1949); G. I. Fuks and V. I. Klychnikov, *Trans. All-Union Inst. Fertilizers, Soil Science, and Agricultural Engineering* 28, 215 (1948) [in Russian]; G. I. Fuks and E. V. Tsyganova, in the book: *Investigation and Uses of Petroleum Products* (1948) 1, 171 [in Russian].

*Original Russian pagination. See C. B. Translation.

- [11] A. D. Malkina and B. V. Deryagin, *Kolloid. Zhur.* 12, 431 (1950).
- [12] G. I. Fuks, *Zavodskaya Lab.* 21, 1455 (1955).
- [13] G. I. Fuks, *Proc. 3rd All-Union Conference on Colloid Chemistry* (Izd. AN SSSR, 1956) p. 301 [in Russian].
- [14] G. I. Fuks, *Kolloid Zhur.* 20, 748 (1958). *
- [15] G. I. Fuks, *Doklady Akad. Nauk SSSR* 103, 635 (1957). *
- [16] A. I. Rabinerson, *Problems of Colloid Chemistry* [in Russian] (Chem. Theoret. Press, Leningrad, 1937), Ch. 1.
- [17] H. R. Kruyt (ed.) *Colloid Science* (IL, 1955), 1, 4 [in Russian].
- [18] B. V. Deryagin, *Izvest. Akad. Nauk SSSR, OMEN, Ser. Khim.* 5, 1153 (1937); *Trans. Faraday Soc.* 36, 203 (1940).
- [19] A. N. Frumkin, *Trans. Faraday Soc.* 36, 117, (1940) *Acta Physicochim. URSS* 18, 473 (1943).
- [20] D. C. Grahame, *Chem. Rev.* 41, 441 (1947); *J. Chem. Phys.* 18, 903 (1950).
- [21] O. Esin and V. Shikov, *Zhur. Fiz. Khim.* 17, 236 (1943); B. V. Eershler, 20, 679 (1946).
- [22] A. F. Kapustinskii, *Zhur. Fiz. Khim.* 32, 1648 (1958).
- [23] H. Ramy, *Z. Phys. Chem.* 126, 161 (1927); *Trans. Faraday Soc.* 23, 381 (1927).
- [24] A. G. Pasyanskii, *Zhur. Fiz. Khim.* 11, 606 (1938).
- [25] E. Darmon, *J. Phys. et Rad.* 2, 2 (1941); *La Solvatisation des Ions*, (Paris, 1945).
- [26] J. Bockris, *Quart. Rev. Chem. Soc. London* 3, 173 (1949); *Modern Aspects of Electrochemistry* (ed. J. Bockris) [Russian translation] (IL, 1958), Ch. 2.
- [27] O. Ya. Samoilov, *Structure of Aqueous Electrolyte Solutions and Hydration of Ions* [in Russian] (Izd. AN SSSR, 1957); *Zhur. Fiz. Khim.* 31, 537 (1957).
- [28] J. Bernal, and R. Fowler, *J. Chem. Phys.* 1, 515 (1933); *Uspekhi Fiz. Nauk* 14, 586 (1934).
- [29] A. F. Kapustinskii, *Summaries of Papers at the Conference on Thermodynamics and Structure of Solutions, Moscow, 1958* (Izd. AN SSSR, 1957) [in Russian] p. 29.
- [30] A. F. Kapustinskii and O. Ya. Samoilov, *Zhur. Fiz. Khim.* 26, 918 (1952).
- [31] J. Morgan and B. Warren, *J. Chem. Phys.* 6, 666 (1938).
- [32] O. Ya. Samoilov, *Izvest. Akad. Nauk SSSR, Otdel. Khim. Nauk* 2, 242 (1953);* E. A. Moelwyn-Hughes, *Proc. Cambridge Phil. Soc.* 45, 477 (1949).
- [33] K. P. Mishchenko, *Zhur. Fiz. Khim.* 26, 1376 (1952); K. P. Mishchenko and A. I. Sukhotin, *Zhur. Fiz. Kim.* 27, 26 (1953); K. P. Mishchenko and E. I. Kvyat, *Zhur. Fiz. Khim.* 28, 1451 (1954).
- [34] B. N. Finkel'shtein and M. P. Chursin, *Proc. Conference on Viscosity of Liquids and Colloidal Solutions* (Izd. AN SSSR, 1944) 2, 43 [in Russian].
- [35] F. Booth, *Nature* 161, 83 (1948); *Proc. Roy. Soc. A* 203, 533 (1950).
- [36] H. B. Bull, *Trans. Faraday Soc.* 36, 80 (1940); D. R. Briggs and M. Hanig, *J. Phys. Chem.* 48, 1 (1944).
- [37] G. I. Fuks, *Doklady Akad. Nauk SSSR* 121, 322 (1958).*
- [38] G. I. Fuks, in the book: *Wear Mechanisms* (Mashgiz, 1955) 1, 186 [in Russian]. *Summaries of Papers at the 3rd All-Union Conference on Friction and Wear in Machines* [in Russian] (Institute of Machine Science, Acad. Sci. USSR, 1957) p. 75.

Received December 2, 1958

*Original Russian pagination. See C. B. Translation.

DIELECTRIC CONSTANTS OF PETROLEUM EMULSIONS

S. F. Khmunin

The S. Ordzhonikidze Aviation Institute, Moscow Department of Physics

Investigations of the relationship between the dielectric constants (DC) of petroleum emulsions and their volume contents f of moisture with different salt concentrations are important in relation to practical applications of the dielectric method for determinations of moisture in petroleum products (fuels and oils).

Because of the large difference between the dielectric constants of dispersed water ($\epsilon = 81$) and petroleum products which form the dispersion medium in such emulsions ($\epsilon = 2.25$ -2.4), a slight increase of the moisture content in an emulsion changes its DC appreciably. This makes the method sufficiently sensitive.

Available data on the DC of water containing petroleum products (heavy oils and natural petroleum) and emulsions of water in oil [1-3] containing up to 10% of moisture by volume indicate that differences in the values of DC of the original dehydrated petroleum products, in their viscosities, or in their sulfur contents should not give rise to any particular difficulties in application of the dielectric method of moisture determination to them. However, there is no agreed opinion on the influence of the concentration of salts or other electrolytes present in petroleum products and oils on their DC. The effects of the frequencies used in investigations by the dielectric method on the results of the determinations have not been finally determined. Nevertheless, this is an especially important problem in relation to the design of suitable equipment for wide applications of the method.

In the investigations cited the measurements of DC of emulsions were confined to relatively low moisture contents ($f \leq 10\%$). Therefore the nature of the relationship between DC and f was itself not fully elucidated. The purpose of the present investigation was to fill this gap by establishing the relationship between DC of emulsions and their moisture contents f up to relatively high values of the latter.

These investigations are also important for experimental tests of the theories of disperse systems which predict the dependence of DC on the volume contents of the components. Emulsions provide examples of disperse systems with randomly distributed spherical inclusions. Because of this it is not necessary to introduce corrections for particle shape or aggregate structure into the theory.

Dielectric constants of slow-settling highly viscous petroleum emulsions. The dispersion medium in the investigated emulsions was a highly viscous petroleum fuel, mazut (sp. gr. 0.952). The disperse phase was water or 2N aqueous NaCl solution. The emulsions were prepared with the aid of a high-speed glass propeller stirrer (2000-2200 r.p.m.) which gave fairly homogeneous but nevertheless polydisperse emulsions. The water droplets in the emulsions were about 1-4 μ in diameter. With the evaporation of moisture during stirring taken into account, the volume composition could be determined with the necessary accuracy (relative error 0.2-0.3%). The volume content of water varied from $f = 0$ to $f = 36\%$.

The determinations were performed by the Drude-Coolidge method at wave lengths $\lambda = 1.66$ m ($\nu = 180$ megacycles/second), $\lambda = 0.99$ m, and $\lambda = 0.28$ m, and by the method of beats with a dielectric-constant meter at $\lambda = 300$ m ($\nu = 1$ megacycle/second). In determinations by the Drude-Coolidge method there was virtually no increase in the DC of the emulsions in time at any of the wave lengths used. Thus, the variations of DC with time reported previously by us [4] for emulsions with lubricating oil as the dispersion medium were not observed in this case. This may be attributed not only to the relatively high density of mazut but also to the fact that more stable emulsions could be obtained from mazut containing petroleum tars, which are good natural

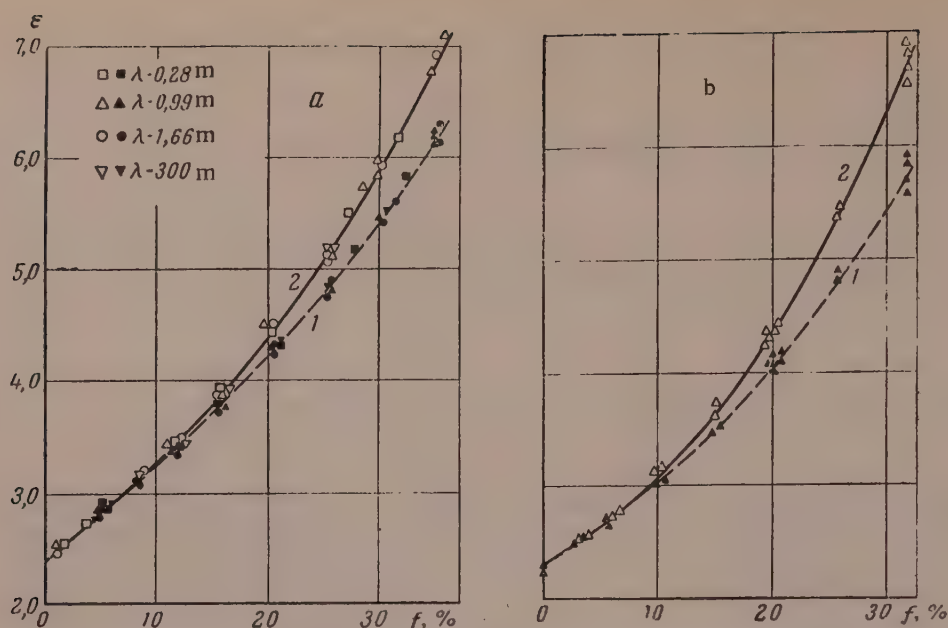


Fig. 1. Dielectric constants ϵ of emulsions as a function of the volume content of moisture f : a) mazut + water (1) and mazut + 2N aqueous NaCl (2); b) oil + water (1) and oil + 2N aqueous NaCl (2).

emulsifiers [5]. In determinations by the method of beats the required DC of an emulsion was found by extrapolation of the observed variations with time [4] to the initial time instant, when there was a uniformly random distribution of the droplets of the disperse phase in the emulsion.

The results of determinations of DC (ϵ) of emulsions with mazut as the dispersion medium at all the above-mentioned wave lengths are plotted in Fig. 1,a.

Figure 1, a, shows that the experimental points fit fairly well on smooth curves which show a nonlinear variation of ϵ with f at $f > 10\%$. When $f < 10\%$ this relationship may be regarded as linear; deviations from linearity lie completely within the limits of experimental error.

The average deviations of the individual determinations, calculated for the corresponding points on the curves, are 0.8% both for water-mazut emulsions and for emulsions with NaCl solution.

The fact that all the values of DC found in our determinations fit on the same curves shows that the results are independent of frequency over a wide range of wave lengths, from 0.28 to 300 m.

This makes it much easier to select a method and to design apparatus for dielectric determination of moisture in petroleum products and emulsions.

At moisture contents above 10% the values of ϵ for emulsions with salt solution are higher than for emulsions with distilled water at the same contents of the disperse phase. This difference increases for emulsions of higher values of f . At $f = 35\%$ the value of ϵ for an emulsion with salt solution is almost 12% higher than value of ϵ for an emulsion with pure water.

Dielectric constants of settling oil emulsions. Because of the stability of emulsions with mazut as the dispersion medium the values of ϵ determined at high frequencies remained almost unchanged with time. However, this stability was due to a considerable extent to the presence of petroleum tars in the mazut. The presence of these emulsifiers, which lower the surface tension at the interfaces, introduces new factors which are not taken into account in any of the theories presented below relating to the DC of disperse systems. To exclude these factors, determinations of DC were performed with emulsions in which the dispersion medium was lubricating oil (MK) of a high degree of purity. Since in this case the DC varied with time even in high-frequency determinations by the Drude-Coolidge method, because of settling of the emulsions, as was shown in our earlier paper [4],

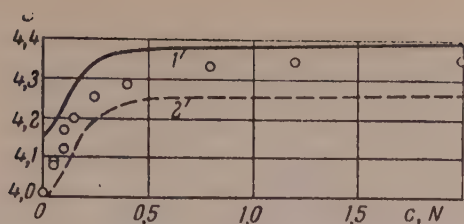


Fig. 2. Variations of DC of emulsions of oil + aqueous NaCl with the salt concentration in the disperse phase: 1) by the Bruggeman equation, 2) by the Fradkina equation.

the true DC of an emulsion for the initial uniformly random distribution of the disperse phase was determined by extrapolation of the DC-time curve to the initial time instant, corresponding to the moment when stirring of the emulsion was stopped. To overcome the difficulties which arise in preparation of emulsions without emulsifiers in the dispersion medium the stirrer speed was increased (to 2600 revolutions/minute). Emulsions containing up to 30% of the disperse phase were prepared. The determinations were performed at wave length $\lambda = 0.99 \text{ m}$, and by the method of beats at wave length $\lambda = 300 \text{ m}$.

The results obtained in determinations of DC (ϵ) of oil emulsions are plotted in Fig. 1, b.

Up to $f = 8\%$ the variation of ϵ with f is nearly linear; as for the mazut emulsions, the values of DC for emulsions with 2 N salt solutions are higher than for emulsions with water at $f > 8\%$. The difference increases continuously with increasing content of the disperse phase; it is appreciably greater than the corresponding difference for mazut emulsions. To explain this fact DC determinations were performed with similar oil emulsions with iron naphthenate which acted as an emulsifier added to the dispersion medium. The addition of the emulsifier produced virtually no change in the DC of the oil itself but resulted in an appreciable decrease of the DC

Comparison of the Author's Results of DC Determinations of Oil Emulsions with the Results of Other Workers

Determinations performed by	Type of emulsion	DC of dispersion medium	Dielectric constants of emulsions for different contents of disperse phase, vol. %			
			2.5	3.0	5.0	10
Dumanskii and Kuridenko	0.5 N NaOH solution in transformer oil	2,25	2,40	—	2,56	3,00
Vargaftik, Golubtsov, and Stepanenko	15% NaCl solution in transformer oil	2,25	—	2,46	2,625	2,97
Present author	2 N NaCl solution in transformer oil	2,30	—	2,52	2,66	3,07
Vargaftik, Golubtsov and Stepanenko	Distilled water in transformer oil	2,25	—	2,45	2,615	2,98
Present author	Distilled water in lubricating oil	2,30	—	2,52	2,66	3,02

of the emulsions in comparison with emulsions with such a relatively pure medium as lubricating oil. It seems likely that this is the reason why in the case of mazut emulsions the difference between DC of emulsions with 2N aqueous NaCl solution and of emulsions with pure water at the same content of the disperse phase is less. Thus, at $f = 25\%$ the difference between the values of DC for the two types of emulsions was 12% (relative to the DC of an emulsion with pure water) for oil emulsions, 8.6% for similar emulsions with iron naphthenate added to the oil, and $\sim 6.5\%$ for mazut emulsions.

To determine the influence of salt concentration in the disperse phase, DC determinations were performed on emulsions with NaCl solutions at the same value of f ($\sim 20\%$) but at different electrolyte concentrations. The results are plotted in Fig. 2.

The experimental results show that nearly all the increase in the DC of emulsions with increasing electrolyte concentration occurs over a small region at low values of the latter (from 0 to 0.5 N). Further increase of concentration no longer has any significant influence on the DC increase.

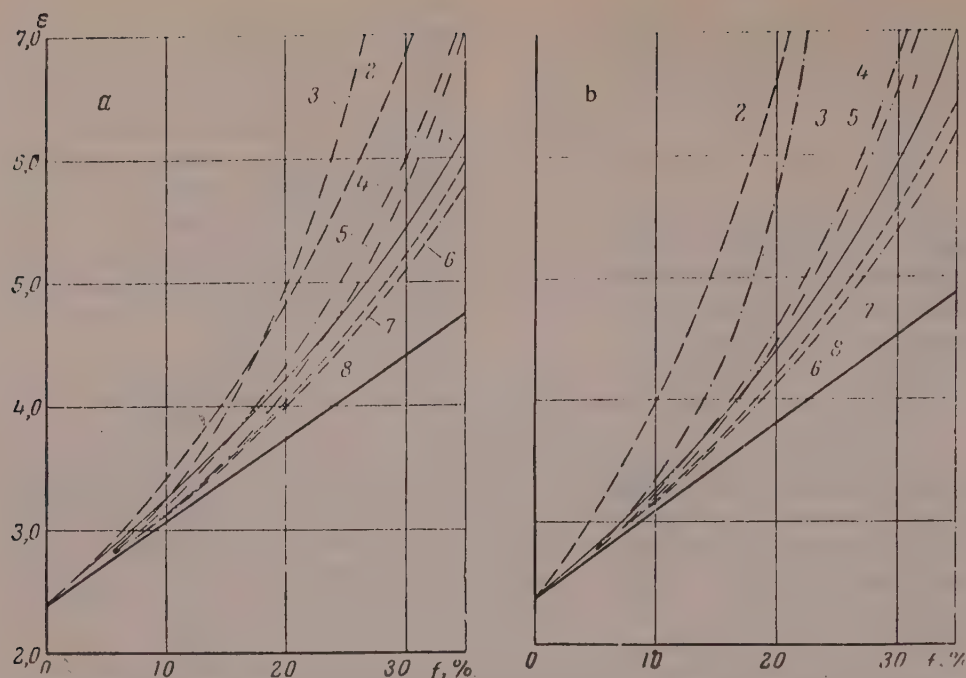


Fig. 3. Effect of moisture content on the DC of emulsions; mazut + water (a), and mazut + 2N aqueous NaCl solution (b): 1) experimental data; by the equations of 2) Lichtenecker; 3) Odelevskii; 4) Bruggeman; 5) Fradkina; 6) Plekara; 7) Wiener; 8) Wagner.

For comparison, curves for ϵ as a function of the salt concentration in solution, plotted in accordance with the Bruggeman and Fradkina equations, are also shown in Fig. 2; the values of DC for the solution were taken from Fradkina's data [6].

Our values for DC of highly viscous petroleum and oil emulsions are in fairly good quantitative agreement with results reported earlier [2], and are also close to the results obtained in determinations of DC of emulsions of salt solutions in transformer oil [3] (see table).

Correlation of the experimental data with theoretical equations. It is of interest to correlate the experimental data for variations of ϵ for emulsions with f with theoretical formulas derived by a number of workers [6-12].

In calculations by these formulas the following values of DC were used: for pure water $\epsilon = 81$, and for 2N aqueous NaCl solution $\epsilon = 386$, which is the value found by Fradkina [6].

The theoretical $\epsilon - f$ curves for emulsions with mazut as the dispersion medium are given in Fig. 3, and for emulsions with oil in Fig. 4.

Wiener's equation [7] for disperse systems with spherical inclusions, analogous to the Lorentz-Lorenz formula, is:

$$\frac{\epsilon - \epsilon_2}{\epsilon + 2\epsilon_2} = f \frac{\epsilon_1 - \epsilon_2}{\epsilon_1 + 2\epsilon_2}, \quad (1)$$

where ϵ , ϵ_1 , ϵ_2 respectively, are the DC of the disperse system, the disperse phase, and the dispersion medium, and f is the content of the dispersed component by volume. The equation was derived for relatively low values of f . It can be applied quite justifiably for any values of f if the disperse system has a regular cubic structure with inclusions of approximately the same size.

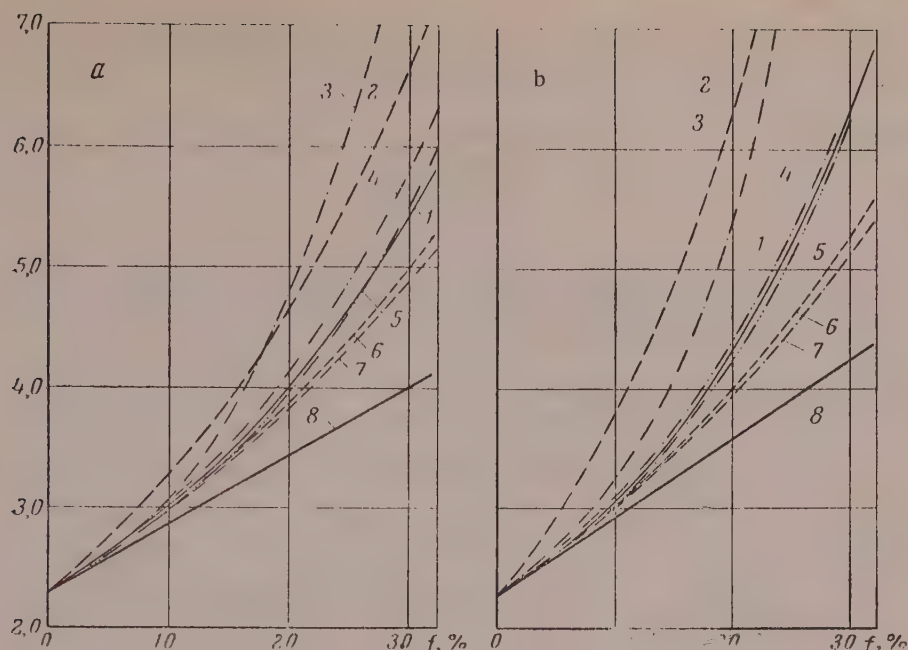


Fig. 4. Effect of moisture content on the DC of emulsions: oil + water (a) and oil + 2N aqueous NaCl solution: 1) experimental data; by the equations of 2) Lichtenecker; 3) Odelevskii; 4) Bruggeman; 5) Fradkina; 6) Piekara; 7) Wiener; 8) Wagner.

At low contents of the disperse phase ($f \leq 5-6\%$) Wiener's equation is simplified and passes into Wagner's equation [8]:

$$\epsilon = \epsilon_2 \left(1 + 3f \frac{\epsilon_1 - \epsilon_2}{\epsilon_1 + 2\epsilon_2} \right), \quad (1a)$$

which gives a linear relationship between ϵ and f .

Odelevskii [13] attempted to extend the applicability limits of Wiener's equation to disperse systems of the emulsion or suspension types ("matrix systems") with any values of f . However, his reasoning, in many respects analogous to the reasoning of Wachholz and Franzeson [14], is not particularly strict; moreover, by introducing the conditions that the film surrounding the inclusion is of approximately uniform thickness the author made the results less general.

Piekara's equation [9]:

$$\frac{\epsilon - \epsilon_2}{\epsilon + 2\epsilon_2} = fx + 0,1x^3f^2, \quad (2)$$

where $\frac{\epsilon_1 - \epsilon_2}{\epsilon_2 + 2\epsilon_2}$, is also an attempt to extend the Lorentz-Lorenz formula to systems with high values of f ; however, the correction introduced by Piekara is small.

Bruggeman's equation [6]:

$$1 - f = \frac{\epsilon_1 - \epsilon}{\epsilon - \epsilon_2} \sqrt[3]{\frac{\epsilon_2}{\epsilon}} \quad (3)$$

for his "porphyritic" disperse system (i.e., systems of the emulsion and suspension types) with spherical particles may be regarded as strictly justified on the basis of a number of a priori postulates which he regards as not

provable but "highly probable". It must be pointed out that Guillen's data [15] on the DC of emulsions of mercury in oils give very good agreement with this equation up to $f = 40\%$.

Fradkina's formula:

$$\epsilon = \epsilon_2 \frac{(1-f)^{2/3} + 2fAx}{(1-f)^{2/3} - fAx}, \quad (4)$$

where $A = x = \frac{\epsilon_1 - \epsilon_2}{\epsilon_1 + 2\epsilon_2}$, like the Bruggeman equation in the region of $f < 20\%$, gives values of ϵ which are the closest to ours.

The equations derived by Lichtenecker [9]

$$\lg \epsilon = f_1 \lg \epsilon_1 + f_2 \lg \epsilon_2 \quad (5)$$

and Odelevskii [12]:

$$\epsilon = \frac{(3f_1 - 1)\epsilon_1 + (3f_2 - 1)\epsilon_2}{4} + \sqrt{\frac{[(3f_1 - 1)\epsilon_1 + (3f_2 - 1)\epsilon_2]^2}{16} + \frac{\epsilon_1\epsilon_2}{2}}, \quad (6)$$

where f_1 and f_2 are the volume concentrations of the disperse phase and dispersion medium for his "statistical mixtures" assume that the components of the mixture are of the same sign; Odelevskii's equation is identical with the Bruggeman equation for "pure" mixtures [11].

Figure 3 shows that the experimental curves for both types of emulsions with mazut at $f > 10\%$ lie between the curves plotted from the equations of Wiener and Piekara on the one side, and of Bruggeman and Fradkina on the other.

The experimental curves for oil emulsions (Fig. 4) are closest to the curves plotted from the Bruggeman and Fradkina equations. Particularly good agreement is found for oil emulsions with 2N NaCl solution as the disperse phase (the deviation of the experimental from the theoretical curves does not exceed 1.2% in this case). For water-oil emulsions the experimental curve gives somewhat lower values than the Bruggeman equation, but the curve is of the same character as the theoretical one.

It is quite understandable that the experimental curves lie between the curves based on the Wiener equation, applicable to any contents of the disperse phase provided that the particles are at least approximately of equal size and of regular cubic distribution, and the curves given by Bruggeman and Odelevskii for "statistical" mixtures. The emulsions studied are better included with the former of these categories, but the Wiener equation cannot be regarded as completely applicable to them, because they are not monodisperse and moreover the dispersion medium in them does not (and cannot) form films of equal thickness around each included spherical particle; according to Odelevskii, this is another condition for applicability of the Wiener equation to such systems.

SUMMARY

1. The values of the dielectric constant (DC) of highly viscous petroleum and oil emulsions containing pure water or salt solution as the disperse phase are independent of the frequency used in the determinations, over a wide range of wave lengths from 0.28 to 300 m.
2. With over 10% of moisture in the emulsions the DC becomes appreciably dependent on the salt concentration in the dispersed water. This dependence becomes more pronounced with increase of the volume content of water f . The values of DC change sharply in the salt concentration range from 0 to 0.5 N; further increase of concentration has very little effect on DC.
3. Addition of an emulsifier to the dispersion medium (oil or mazut) apparently lowers the DC of the emulsions; this is manifested only at fairly high moisture contents (above 10%).

4. Of the theoretical equations for DC of emulsions as a function of f the formulas of Fradkina and Bruggeman give best agreement with the experimental results (up to $f = 30\%$).

This investigation was performed under the guidance of E. M. Fradkina, to whom I offer my sincere thanks.

I am also very grateful to Prof. B. A. Dogadkin and Prof. N. B. Vargaftik for extremely valuable discussions.

LITERATURE CITED

- [1] I. A. Mukhtarov, Doklady Akad. Nauk Azerbaidzhan SSSR 4, 3 (1948).
- [2] N. B. Vargaftik, V. A. Golubtsov, and N. N. Stepanenko, Electrical Method for Moisture Determination in Petroleum Products [in Russian] (State Tech. Press, 1947).
- [3] Yu. F. Deinega, A. V. Dumanskii, and O. D. Kurilenko, Kolloid. Zhur. 15, 5, 361 (1953).*
- [4] E. M. Fradkina and S. F. Khmunin, Kolloid. Zhur. 18, 5, 604 (1956)*.
- [5] B. P. Tonkoshkurov, N. N. Serb-Serbina, and A. M. Smirnova, Principles of Chemical Demulsification of Petroleums [in Russian] (State Fuel Tech. Press, 1946).
- [6] E. M. Fradkina, Kolloid. Zhur. 18, 4, 480 (1956).*
- [7] O. Wiener, Abhandl. Sachsish Gesellsch. Wiss. Math.-Phys. 32, 509 (1912).
- [8] K. W. Wagner, Arch. Elektrotechnik 2, 371 (1914).
- [9] K. Lichteneker, Phys. Z. 27, 115 (1926).
- [10] A. Piekara, Kolloid.-Z. 58, 283 (1932); Phys. Z. 31, 579 (1930).
- [11] A. G. Bruggeman, Leitfahig. Misch. Substanzen. Ann. Phys. 24, 636 (1935).
- [12] V. A. Odelevskii, Zhur. Tekh. Fiz. 21, 6, 679 (1951).
- [13] V. A. Odelevskii, Zhur. Tekh. Fiz. 21, 6, 662 (1951).
- [14] F. Wachholz, Franzeson, Kolloid-ZB. 92, Juli H. 1, 75 and H. 2, 158 (1940).
- [15] R. Guillen, Ann. Phys. 16, Oktobre-Decembre (1941).

Received June 6, 1958

*Original Russian pagination. See C. B. Translation.

AN AIR-DRIVEN ULTRACENTRIFUGE AND AEROSOL GENERATOR AND ITS USES IN SCIENCE AND PRACTICE

B. Cizinsky and J. Kolousek

Institute of Biophysics, Faculty of Hygiene and Medicine, Karlov University, Prague

High-speed ultracentrifuges are finding increasing uses in research work; they are used most extensively in physical chemistry, macromolecular chemistry, and biochemistry [1]; in particular, for investigations of protein macromolecules, biochemical fluids, tissues, and metabolites. The ultracentrifuge is widely used in biochemistry and in histological chemistry.

However, the ultracentrifuge is used relatively seldom in routine laboratory or clinical practice, because of the complexity and high cost of modern high-speed ultracentrifuges. These instruments give centrifugal forces up to 300,000 g and are unsuitable for routine laboratory work. For studies of tissue proteins and for ultracentrifuge histochemical investigations the biochemist needs a simple, cheap, manageable instrument which gives a strong gravitational field.

An instrument of this type was designed as long ago as 1925-1927 by Henriot and Huguenard [2] on the principle of the air turbine; the initial design underwent many modifications, and only Beams [3] succeeded in improving it considerably and obtaining a high speed. In addition to Beams, others worked on designs of this type [4]. Girard and Chukri [4] attempted to eliminate vibration of the stator by mounting it on a rubber air-blast tube. They emphasize that the ratio of rotor and stator weights must be 1 : 1 for steady operation. They reached centrifugal forces of up to 1,000,000 g at the periphery of a rotor 13 mm in diameter in their instrument. However, its applicability to experimental work is very limited.

Further attempts to improve equipment of this type were made by Garman [5]; he studied the shape and angle of the nozzles, and separation of the grooves on the rotor, in order to eliminate air turbulence. Bauer and Pickels [4] used an ultracentrifuge based on the same principle, with a rotor 20 cm in diameter, which could contain 8 test tubes, 7 ml in volume. Under these conditions accelerations of 20,000 g in the center of the tubes were reached. Despite all these efforts, ultracentrifuge rotors remained rather unstable and tended to fly out of the stator cone. Recently May [6] partially eliminated this fault, and his instrument has a number of advantages. However, the instrument must be placed in a strictly horizontal position and the rotor readily loses stability; this prevents extensive utilization of this apparatus.

Design and Uses of the Ultracentrifuge

On the basis of the above-mentioned investigations Cizinsky designed an ultracentrifuge driven by compressed air, intended for extensive use in laboratory practice.

Chizhinskii's air-driven high-speed ultracentrifuge is free from most of the defects of its predecessors [7]. It subsequently underwent further improvements until it received its present form.

The apparatus (Fig. 1 and 2) consists of a body in the form of a hollow cone with air nozzles. The body also acts as the stator; it contains a conical rotor with grooves into which air is driven from the nozzles. The support, in contrast to other types of centrifuges, is very simple. The instrument, fixed on rubber supports, stands on a metallic board with two screws by means of which the base of the instrument is brought into an almost horizontal position. However, this position is not obligatory for normal operation, as the instrument can work even

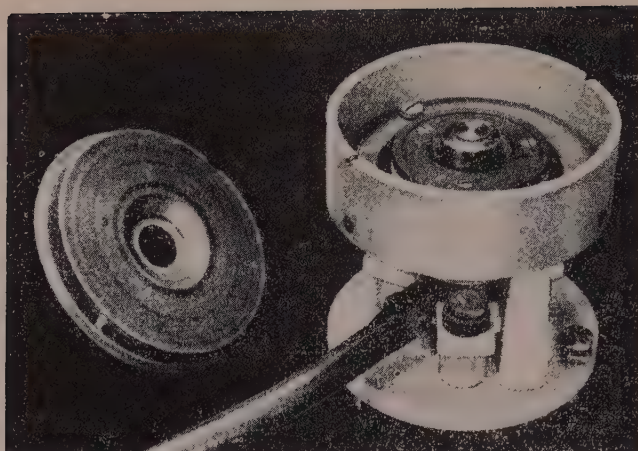


Fig. 1. General view of Cizinsky's ultracentrifuge.

when turned through 180° . The air is fed into the apparatus through rubber vacuum tubing fixed by screws emerging from the centrifuge body. One of the main causes of rotor vibration—eddying and impacts of air on the directing surfaces—is eliminated by a simple device. By comparison with the older types of centrifuge the rotor operates quite uniformly at all speeds. Steady starting and stopping of the rotor are much better than in the older types.

The rotor is made of stainless steel, and has a drilled cavity 3 ml in volume, closed by a screw stopper. The cavity is in the shape of a squat cylinder 11.5 mm in radius. The rotor speed depends on the pressure of the incoming air. At 10 atmos pressure a speed of 200,000 r.p.m. was reached in one of the early models of this centrifuge.

The rotor speed was determined by a photoelectric method based on measurement of the vibration frequency of light reflected from the centrifuge rotor, half of which is black and half bright. The frequency corresponds to the rotor speed. The rotor was illuminated by nonflickering light from an electric lamp fed by direct current. The vibrating light entered a photoelectric cell the current from which, after amplification, passed to the vertical part of the kinescope of an oscillograph. Current from a regulated vibration source at a known frequency passed to the horizontal part of the kinescope. Combination of the vibration frequencies in both parts of the kinescope gave a simple closed curve (circle or ellipse). The frequency of the regulated vibration source at which this curve appeared was equal to the centrifuge speed.

This method was used to obtain the curve in Fig. 3, which represents the speed as a function of air pressure. It is not necessary to measure the speed by the above method when the centrifuge is used for ordinary laboratory purposes. It is sufficient to determine the pressure of the air entering the ultracentrifuge and to find the speed from the graph.

The small air-driven ultracentrifuges described previously were used for investigations of various biological material. Exhaustive information on such work up to 1951 has been given by Beams [8]. Ruben and his associates [9] measured the radioactivity of sedimenting substances labeled with radioactive isotopes; Waisman et al [10] used the instrument in serological studies of luetic serums; Dalcq [11] studied oocytes; finally, Bessis [12] used the instrument for studying the influence of ultracentrifugation on leukocytes.

Konopik [13] used Cizinsky's first centrifuge for a serological investigation of luetic serums and found that after ultracentrifugation of some serologically positive serums their reaction became much less positive with a deviation of the component. Nejtek [14] studied the behavior of agglutinins and plasma proteins in a strong gravitational field. Kolousek and Kutacek [15] studied the effect of a strong gravitational field on horse serum proteins; they found that the refractive index increases after ultracentrifugation in all serums from healthy horses, the residual nitrogen content in the serum increases, and the percentage nitrogen of the total proteins decreases. One of the present authors, jointly with Turek [16], applied ultracentrifugation to the Brdicka filtrate polarographic reaction and showed that the process has a strong influence on this reaction of serums from human cancer patients. The sensitivity of the Brdicka reaction for cancer was increased considerably in this way.

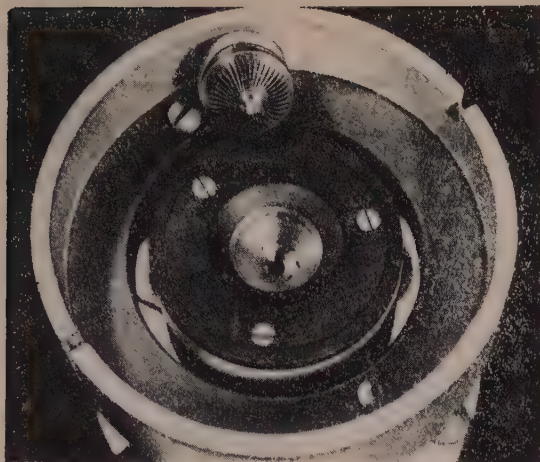


Fig. 2. Stator and withdrawn rotor of Cizinsky's ultracentrifuge.

Cizinsky has developed a new method for determination of microorganisms in fluids, based on the ultracentrifuge. A sterile strip of filter paper is placed in a sterile cylindrical cell of the centrifuge in such a manner as to form a ring around the inside of the cell. A known volume of the fluid flows into the middle of the rotating cell. Under the influence of the strong centrifugal field the microorganisms are separated from the fluid and are embedded in the paper strip. The liquid free from microorganisms flows out of the cell into an annular receiver. After the ultracentrifugation the paper strip is placed in a Petri dish and cultures are grown by the usual microbiological methods. This method is of importance for investigation of microorganisms present in water.

McDonald, Beams, and King [17] used an ultracentrifuge of this type for investigating cellular elements. No changes were observed in cells of chick embryo tissues after exposure to a centrifugal field of the order of 150,000–400,000 g for 30 minutes. Eggs of *Ascaris suum* were not killed in a field of 400,000 g, and the authors consider that protoplasm is capable of withstanding the greatest centrifugal forces. They suggest that endurance of the protoplasm is assisted by electrostatic forces which prevent splitting of its structure. These findings are contrary to the results of Smetana [18], who used a prototype of the Cizinsky instrument for investigating changes in the nuclei of neutrophil leukocytes after ultracentrifugation at 425,000 g. It was found that changes in the cytoplasm are accompanied by changes in the structure of the nuclei and a decrease of the Ginek number, which may be attributed to breakdown of leukocytes (in small numbers) and combination of nuclear segments.

Several workers have used centrifuges for investigation of other biological materials [19–24].

Cizinsky's ultracentrifuge proved suitable for investigation of amino acids and peptides of animal tissues. With the use of this instrument prolonged extraction of such substances from tissues was avoided [25]. Kolousek developed a method whereby it is possible to investigate (for example, by paper chromatography or electrophoresis) extracts containing amino acids and peptides 15 minutes after a sample of living tissue has been taken. By accelerating extraction with the aid of ultracentrifuge Kolousek and Jirack [26] were able to determine free ammonia and glutamine in animal tissues without decomposition by trichloroacetic acid.

This ultracentrifuge was used successfully by Konopik [27] for the so-called ultracentrifugational histochemistry; by means of a strong centrifugal field he succeeded in weakening glycidic and lipid bonds in the skin of psoriatic patients. He demonstrated by means of histochemistry that ultracentrifugation of the skin of psoriatic patients releases large amounts of lipids and glycidic. Ultracentrifugation of serum from psoriatic patients with a considerable rash splits off lipids. This test may be used for diagnostic purposes, especially for determination of the stage of the disease.

This type of ultracentrifuge is of great importance in ultracentrifuge techniques, as it permits regulation of the temperature of the tissue in the rotor by means of the compressed air. The apparatus can easily be contained in a refrigerator.

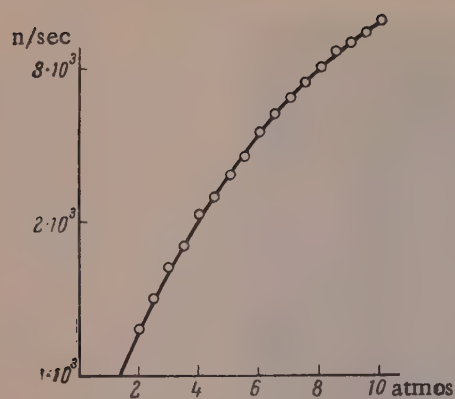


Fig. 3. Variation of centrifuge rotor speed with the air pressure.



Fig. 4. Chizhinskii's aerosol generator.

Another advantage of the instrument is the short time required for starting and stopping the rotor; it does not exceed a few minutes. A strong centrifugal field is therefore attained rapidly and easily.

It follows from the foregoing that this small ultracentrifuge may have extensive applications. A new type of ultracentrifuge operating on the same principle is now being tested. The potentialities of the instrument are extended by the use of several interchangeable rotors. For example, a rotor 26 mm in diameter can give a centrifugal field of the order of 800,000 g. Another rotor, of large diameter, can be used for determinations of sedimentation constants and for preparative work.

The Ultracentrifuge as an Aerosol Generator

This ultracentrifuge may be used as an aerosol generator of the rotary nozzle type. Aerosol generators based on this principle have already been in use for several years for air humidification. May [6] used them for studies of aerosols.

The ultracentrifuge described above was modified considerably for use as an aerosol generator (Fig. 4). The upper side of the rotor was converted into a polished surface with liquid flowing at a definite rate onto its center; when the liquid comes into contact with the rotating surface it is converted into an aerosol. The size of the aerosol particles can be regulated by variations of the rotor speed. This apparatus was used to prepare an aerosol with a very narrow range of droplet size; the smallest droplets were $\sim 0.2 \mu$ in diameter.

Tests showed that this aerosol generator can be recommended for air disinfection*, spraying of suspensions of microorganisms (for drying), and preparation of aerosols of medicinal substances. This last field of application proved very effective in treatment of certain diseases of the respiratory tract, as demonstrated by recent experiments carried out by Cizinsky et al.

Of the available methods for preparation of aerosols the rotary nozzle method is considered to be the best [28]. This method is used most often in chemical industry and is suitable for production of homogeneous aerosols. However, this principle has not until recently been applied to medical inhalation, as no completely suitable apparatus was available.

The micelles of aerosols for medical purposes must be able to penetrate into the bronchioles and alveoli. According to Findeisen [29] the optimum micelle size is 0.6μ . Such particles have Brownian motion and are able to penetrate into the alveoli, which is very important, as there is very little air motion in these spaces. Herbst and Philipp [30] demonstrated in inhalation of aerosols that the electric charge on micelles hinders their penetration into the lungs; this shows that aerosols, the micelles of which carry static electric charges, are unsuitable.

*It was shown that 40 ml of 2% ayatin solution disinfects a room 60 m^3 in volume, strongly contaminated with microorganisms, within 45 minutes.

Some authors [31] consider that the effectiveness of aerosols (for example, of antibiotics) in inhalation is indicated by their presence in the blood of the patient after the treatment. However, Dauterband [32] asserts that the presence of antibiotics in the blood is a consequence of absorption of large drops in the respiratory tract.

On the basis of experience in development work on aerosol generators and of the characteristics required in aerosols for inhalation, Cizinsky designed an apparatus which produces homogeneous aerosols of satisfactory quality. The main part of the apparatus is a disk 26 mm in diameter, rotating at 75,000 r.p.m. The medical solution flows onto the disk at a rate of 2 ml per minute. The particles sprayed by the disk are drawn into a distributing channel situated at the disk periphery. Large drops settle while the homogeneous small droplets are carried along by the air stream. The particle size is being measured at the present time. However, this operation is difficult because of the rapid evaporation of the finely-divided liquid. The bacteriological test is more informative. 1,000,000 units of penicillin was sprayed in a room 55 m³ in volume; after this the sensitive Oxford staphylococcus failed to grow on media in different parts of the room for 3 minutes during operation of the apparatus, and for 10 minutes when 2 hours had elapsed after the apparatus had been stopped. Yellow coloration of a previously colorless gas flame indicated uniform distribution of sodium ions in this room 14 hours after the generator had sprayed 20 ml of physiological saline in it.

The Cizinsky inhalator with a rotary nozzle was used in a number of investigations. It was used for inhalation treatment of patients with bronchial asthma [33]. Sea water in aerosol form is inhaled by the patient for a definite time in a closed room. The administration of certain drugs in the form of aerosols also proved useful. In comparison with intravenous injection of the same drugs, the results obtained were astounding. The inhalation dose used for 10 patients was equal to a single injection dose.

This generator is also used for inhalation of antibiotics (penicillin, streptomycin, bacitracin, etc.) with good results in preparative and postoperative treatment in lung surgery [34]. The generator was also used with good results in clinical practice.

The apparatus was used for inhalation treatment of costly laboratory animals, including monkeys, suffering from respiratory diseases [35].

Experience in inhalation treatment shows that the rotary nozzle inhalator may be recommended for extensive use in clinical practice. It must be taken into account, however, that a dose of a drug which is harmless when administered intravenously may be dangerous in aerosol form.

This generator may be used with success not only in clinical practice but also prophylactically for prevention of occupational diseases of the respiratory organs exposed to harmful vapors and dust. Our apparatus was used with good results for inhalation treatment of workers in a sulfuric-acid plant. Alkaline mineral waters ("Vintsentka" from Lubacovice in Moravia) were sprayed in this case. Inhalation of suitable aerosols makes the lungs capable of clearing themselves continuously, and it may therefore be recommended for workers in dusty atmospheres.

SUMMARY

1. A portable ultracentrifuge and an aerosol generator, driven by compressed air, are described. Their fields of application are listed, described, and discussed.
2. The ultracentrifuge can be used in biochemical investigations; the aerosol generator (with a rotary nozzle) has been used in therapy and prophylactics of lung diseases.

LITERATURE CITED

[1] T. Svedberg, *The Ultracentrifuge* (Oxford, 1940); A. S. Mc. Farlane, *Nature* 141, 1000 (1938); S. E. Bresler, V. V. Korshak, S. A. Pavlova, and P. A. Finogenov, *Izvest. Akad. Nauk SSSR Otdel. Khim. Nauk* 2, 354 (1954);* S. E. Bresler and S. Ya. Frenkel*, *Zhur. Tekh. Fiz.* 23, 1502 (1953); S. Ya. Frenkel*, *Zhur. Tekh. Fiz.* 23, 1502 (1953); 24, 2169 (1954); P. L. Kirk and E. L. Duggan, *Anal. Chem.* 24, 124 (1952); K. Borgin, *K'jem. Bergwes, Metall.* 12, 166 (1952).

[2] E. Henriot and E. Huguenard, *Compt. Rend.* 180, 1389 (1925); *J. Phys. Radium* 8, 433 (1927).

[3] J. W. Beams, *Rev. Sci. Instr.* I, 667 (1930); J. W. Beams and A. J. Weed, *Science* 74, 44 (1931); J. W. Beams and E. G. Pickels, *Rev. Sci. Instruments* 6, 299 (1955).

*Original Russian pagination. See C. B. Translation.

[4] E. N. Harvey, *Science* 75, 268 (1932); *Biol. Bull.* 66, 48 (1934); J. H. Bauer, and E. G. Pickels, *J. Bacter.* 31, 53 (1935); J. Mc Intosh, *J. of Path.* 41, 215 (1935); J. W. Mc Bain and O. Sullivan, *J. Am. Chem. Soc.* 57, 780, 2631 (1935); E. G. Pickels, *Science* 83, 471 (1936); J. W. Mc Bain and C. A. Tostado, *Nature* 139, 1066 (1937); *J. Am. Chem. Soc.* 59, 2489 (1937); J. W. Mc Bain and F. A. Leyda, *Nature* 141, 913 (1938); *J. Am. Chem. Soc.* 60, 2998 (1938); J. W. Mc Bain, *Chem. Rev.* 24, 289 (1939); J. W. Mc Bain and A. H. Levis, *J. Phys. Chem.* 43, 1197 (1939); *Science* 89, 611, (1939); K. G. Stern, *Science* 96, 561 (1942); P. Girard and C. Chukrl, *Soc. Biol. Paris*, 113, 1344 (1938).

[5] W. Garman *Rev. Sci. Instr.* 4, 450 (1933).

[6] K. R. May, *J. Appl. Phys.* 20, 932 (1949).

[7] B. Cizinsky, *Cas. Lek. Ces.* 93, 10 (1954).

[8] H. W. Beams, *Ann. NY Acad. Sci.* 51, 1349 (1951).

[9] S. Ruben, M. D. Kamen and L. H. Perry, *J. Am. Chem. Soc.* 62, 3450 (1940).

[10] A. Waisman and A. Hamelin, *Compt. Rend. Soc. Biol.* 146, 52 (1952).

[11] A. Dalcq, *Arch. de Biologie* 64, 311 (1953).

[12] M. Bessis, *Compt. Rend. Soc. Biol.* 144, 44 (1950); *Cytologie Sanguine Normale et Pathologique* (Masson, Paris, 1954).

[13] J. Konopik, *Cas. Lek. Ces.* 93, 13 (1954).

[14] U. Nejtek, *Cas. Lek. Ces.* 93, 14 (1954).

[15] J. Kolousek and C. Kutacek, *Cas. Lek. Ces.* 93, 16 (1954).

[16] S. Turek and B. Cizinsky, *Csl. Onkologia* 2, 335 (1955).

[17] T. J. Mc. Dougald, H. W. Beams, and R. L. King, *Proc. Soc. Exptl. Biol. Med.* 37, 234 (1937).

[18] K. Smetana, *Csl. Morphologiem* (in press).

[19] M. F. Guyer and P. E. Claus, *Biol. Bull.* 71, 462 (1936); *Cancer Research* 2, 16 (1942).

[20] E. B. Harvey and G. J. Lavin, *Biol. Bull.* 86, 163 (1944).

[21] E. J. Dornfeld, *Anat. Rec.* 65, 403 (1936); *Marquette Med. Rev.* 3, 51 (1939).

[22] A. Claude, *Science* 91, 77 (1940).

[23] E. V. Cowdry and F. X. Paletta, *Am. J. Path.* 17, 335 (1941).

[24] J. Brachet, *Experientia* 3, 329 (1947).

[25] J. Koloucek, First State Congress of Czechoslovak Biochemists [in Czech] Prague (September, 1957).

[26] J. Koloucek and Jiracek VI (in press).

[27] J. Konopik (in press).

[28] R. P. Fraser and P. Eisenklam, *Trans. Inst. Chem. Engrs.* 34, 294 (1956).

[29] W. Findeisen, *Arch. Ges. Physiol (Pflugers)* 236, 367 (1935).

[30] W. Herbst and K. Philipp, *Z. Aerosol-Forsch.* 1, 43 (1951).

[31] I. I. Elkin and Ts. I. Eidel'shtein, *Preparation and Clinical Uses of Antibiotic Aerosols* [in Russian] (Moscow, 1955).

[32] W. Dauterband, *Physiol. Rev.* 32, 214 (1952).

[33] B. Cizinsky and B. Hodek, *Cas. Lek. Ces.* 95, 1251 (1956).

[34] B. Dvoracek, J. Lorenc, and B. Cizinsky, *Zentralbl. Chirurgie*, 28, 1414 (1958).

[35] J. Simon and B. Cizinsky (in press).

Received May 15, 1959

ELECTROPHORESIS OF DYES IN THE GELATIN LAYER OF A PHOTOGRAPHIC FILM

A. Sheludko, G. Konstantinov, and K. Tsvetanov

Institute of Physical Chemistry, Sofia State University

The main disadvantage of zone electrophoresis on paper is that the spots of the investigated substances spread over the paper and acquire indistinct and irregular outlines. Moreover, exact photometric evaluation of the electrophoresis diagrams is hindered by inhomogeneity of the paper. All this lowers the resolving power of this very convenient method. To avoid these disadvantages attempts have recently been made to replace paper in zone electrophoresis by a more homogeneous and transparent medium. For example, Bussard and Perrin [1] recommend the use of agar films on glass. The electrophoregrams obtained on such films are more distinct and more suitable for photometry than those on paper, but preparation of these films is a somewhat laborious operation and the films are not of very consistent quality. Grabar and Williams [2] attempted to replace agar by gelatin in a similar method of film preparation. They used this medium for electrophoresis of serums, with the aid of immunochemical reactions for developing. However, they did not reach any definite conclusions concerning the possibility of using gelatin as a medium for zone electrophoresis.

The purpose of the present investigation was to study the properties of a gelatin layer of photographic film as a medium for zone electrophoresis. The photosensitive material is removed from the gelatin layer of the photographic film by the action of fixing agents and thorough washing with water. The films so obtained are very consistent in properties, homogeneous, and transparent. The flexible celluloid base makes such films convenient to use in any apparatus for paper electrophoresis, while the perforations along the edges can be used for fixing and stretching the films on suitable glass frames with pins.

The chief disadvantage of gelatin as a medium for zone electrophoresis is that it is colored by the same dyes as other proteins. Therefore the usual development methods cannot be used with electrophoregrams of protein materials, and specific indicators are required (for example, immunochemical reactions, tagging of proteins with radioactive isotopes, etc.). Because of these difficulties it was decided to study electrophoresis in the gelatin layer of a photographic film with the aid of water-soluble dyes which do not require development. A direct consequence of this investigation is the possible application of the method to dye analysis.

Film preparation and application of dye solution. The film is freed from photosensitive material, dried, and cut into pieces of suitable length. Because of the high resolving power of the method a relatively short strip, with a working length of less than 10 cm, can be used for electrophoresis. A transverse line is scratched with a needle on the celluloid side of the film, and the dye is then applied opposite it. The film is immersed for half an hour in a buffer solution at the pH used for electrophoresis. The film, with the gelatin layer swollen in the buffer, is taken out of the solution and free solution is removed. This operation is very important, because the film must be dry enough for application of the dye without spreading, but at the same time its moisture content must always be the same. This is checked from the current strength when a voltage is applied to the film. We were able to achieve good results by the following procedure: the film is placed celluloid side down on filter paper and pressed down by damp chamois. Under these conditions the resistance of the partially dried film was usually reproducible to within 2-3%. The dye, dissolved in the same buffer, is applied in the form of a line 0.3-0.5 mm wide, the film is stretched on a frame, and placed in a humid (closed) electrophoresis chamber. Under

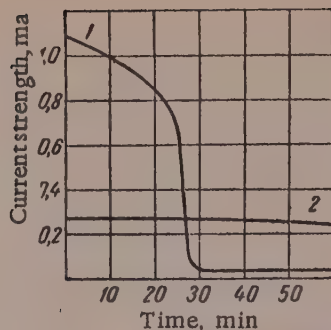


Fig. 1. Variations of current strength with time, with a concentrated (1) and dilute (2) buffer solution.

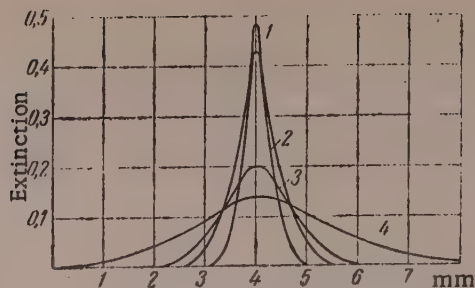


Fig. 2. Spreading of a band of Bromophenol Blue by diffusion: 1) in 1 hour; 2) in 2 hours; 3) in 4 hours; 4) in 24 hours.

such conditions the swollen gelatin layer retains constant resistance for several hours if a current is not passed through it. However, current causes "drying" of the gelatin layer, and the film resistance gradually increases. This is very disadvantageous, as the rate of migration of a dye in electrophoresis decreases with increase of the film resistance. With a veronal buffer at pH 8.6 containing 17.5 g of veronal sodium and 2.75 g of veronal per liter this "drying" was very considerable (Curve 1, Fig. 1, potential 190 v). It is decreased considerably when the buffer was used at fourfold dilution (Curve 2, Fig. 1). This method for decreasing the heating of the film by the current is more convenient than reduction of the electrophoretic potential, because high rates of electrophoresis are retained. It is probable that further work (for example, on decrease of the chamber temperature) may make it possible to make the current still more constant.

Spreading and diffusion of dye in the gelatin film. The maximum time of electrophoresis depends on spreading and diffusion of the applied substance in the given medium. Our observations with 1% Bromophenol Blue at pH 8.6 showed that spreading and diffusion in the gelatin layer are very slow. The observations were made in a closed vessel, containing saturated water vapor, at $\sim 18^\circ$. Fig. 2 shows the distribution curves for this dye, obtained by means of a microspectrophotometer with a filter suitable for Bromophenol Blue. These curves show that electrophoresis may be successfully continued for several hours, with diffusional spreading of a few millimeters in the bands of the individual fractions.

Distribution of dye during electrophoresis. Our observations showed that the dye distribution in the direction of electrophoresis differs considerably from symmetrical distribution by diffusion. On the side of the "starting" line the dye band has a relatively well-defined concentration maximum (peak), while on the opposite side, further from the start, the spreading is considerably greater than spreading caused by diffusion. This type of distribution was observed for all the electrophoretically active dyes studied. The asymmetry of distribution decreases with decrease of dye concentration, the concentration maximum shifts toward the center of the band, and the width of the spread portion decreases, approaching to the width caused by diffusion. Fig. 3 shows extinction curves for bands of Bromophenol Blue of different concentrations, for one hour of electrophoresis. The coordinate origin corresponds to the "starting" line.

As the distribution curves for different dyes are similar, it is improbable that this effect can be attributed to distribution of the dyes according to their electrophoretic activity. The observed distribution of a dye during electrophoresis is explained most simply by inhomogeneity of the electrical field due to the presence of the dye. Since the dye is electrophoretically active, the film resistance is lower in regions where it is applied than in free regions, and the higher its concentration the greater the decrease of resistance. As the rate of electrophoresis is proportional to the field strength, and the latter is proportional to the resistance, a dye spread by diffusion moves more rapidly from the starting side than the dye in the region of maximum concentration; it catches up the concentrated part of the band and enters it, forming a concentration peak on that side. The diffused dye on the opposite side, on the other hand, "runs away" from the peak, extending the diffuse region of the band. If v_c represents the velocity of electrophoretic migration of the peak and v_0 the velocity of the diffuse end of the band, where the dye concentration approaches zero, then

$$\frac{v_0}{v_c} = \frac{(dE/dl)_0}{(dE/dl)_c}, \quad (1)$$

where $(dE/dl)_0$ and $(dE/dl)_c$ are the electric field strengths at zero and maximum concentrations c in the peak. On the other hand, $dE/dl \sim 1/\kappa$ where κ is the conductivity of the layer. Hence

$$\frac{v_0}{v_c} = \frac{\kappa_0 + \kappa_c}{\kappa_0} \quad \text{or} \quad \frac{v_0 - v_c}{v_c} = \frac{\kappa_c}{\kappa_0}, \quad (2)$$

where κ_c is the conductivity of the dye at concentration c , and κ_0 is the conductivity of the buffer, both in the gelatin layer. The rates of migration of the peak v_c and of the diffuse end v_0 are approximately proportional to the corresponding displacements l_c and l_0 , so that

$$\frac{l_0 - l_c}{l_c} = \frac{\kappa_c}{\kappa_0}. \quad (3)$$

Finally, κ_c may be taken as proportional to the dye concentration c in the peak or also to the extinction of the peak ϵ . Hence the above hypothesis concerning the causes of the unsymmetrical distribution of the dye in electrophoresis leads to the relationship (see Fig. 4)

$$\frac{l_0 - l_c}{l_c} \sim \epsilon. \quad (4)$$

Experimental results are in good agreement with (4), which confirms our hypothesis*.

The unsymmetrical distribution of a dye in electrophoresis may be used as an additional method for its identification. On the basis of Equation (3) it is possible to determine κ_c/κ_0 for each component of a mixture of several dyes, and since κ_0 is the same for all components, it is possible ultimately to find the ratios λ_c ($\lambda_c = \kappa_0/c$) for different components. For this, of course, electrophoresis must be continued to complete separation of all the components and the mutual influence of the components on their migration must be taken into account.

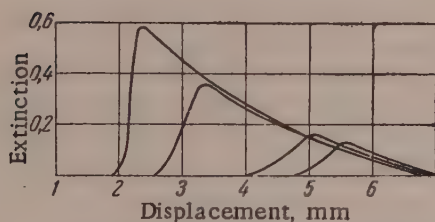


Fig. 3. Spreading of Bromophenol Blue at different concentrations in the same time of electrophoresis.

Another conclusion to be drawn from the foregoing is that if the resolving power of the method has to be increased (by decrease of band width) it is necessary to have the smallest possible values of κ/κ_0 either by decrease of dye concentration or by increase of the ionic strength of the buffer. The first alternative is inconvenient, because dilution of the dye reduces the density of the bands. Small impurities then become indistinguishable. Under our experimental conditions the second alternative is also impracticable, as increase of the ionic strength of the buffer leads to increase of current strength and "drying" of the film. If the electrophoresis apparatus is improved, with the use of cooling and removal of Joule heat from the film, "drying" can probably be reduced, ionic strength of the buffer increased, and the resolving power thereby raised.

The foregoing considerations and approximate calculations were based on the assumption that displacement of a dye from the starting line completely corresponds to its electrophoretic migration. However, it is known that in microelectrophoresis and paper electrophoresis the observed displacement of the migrating substance is the sum

*After this paper had gone to press D. N. Platikanov in our laboratory demonstrated by direct measurements the inhomogeneity of the electric field in the region of the film where the dye is present. By measuring the potential between two platinum microelectrodes immersed in the gelatin layer to a distance of several tenths of a millimeter along the film he found a drop of potential during the time when the dye passed along the electrodes. The variations of potential with time corresponded to the unsymmetrical distribution of the dye in the band.

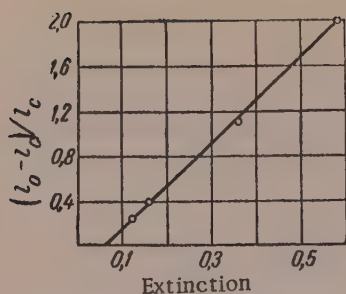


Fig. 4. Relation of $(l_0 - l_e)l_c$ to extinction peaks given in Fig. 3.

swollen in the buffer solution does not spread by diffusion in the gelatin and does not become unsymmetrically distributed after electrophoresis; it retains completely the form in which it was applied. Measurements showed that a band of Congo Red does not move from the starting line in electrophoresis; this shows that the gelatin is firmly held by the support. It is possible that this immobility of the gelatin layer on the support is the result of the special methods used in the production of photosensitive materials for attaching the gelatin layer on the film.

Further investigations showed that the buffer solution migrates relative to the gelatin. Thus, after a dextrin solution, which is generally used as a marker of solution migration, had been applied, the solution migrated at 2-3 mm per hour from the starting line (the investigation was carried out with the above-named buffer solution and at the same field strength; dextrin was developed by means of iodine vapor after electrophoresis). Nevertheless, we are inclined to think that this movement of the solution does not influence displacement of the dye. The reason is that dyes in general are adsorbed by gelatin and proteins and therefore it is most likely that in electrophoresis they migrate along the gelatin and not in the buffer solution. These conjectures cannot, of course, be regarded as proof of this mechanism, but only this hypothesis avoids the contradictions which otherwise arise in verification of the relationship (4). If this view is confirmed by further investigations, it would also be advisable to revise the usual method for taking into account the influence of electroosmosis on migration in paper electrophoresis, especially if the substance is readily adsorbed on the support (paper).

It was also observed in paper electrophoresis that the solution migrates from the ends of the paper strip dipped in the solution toward its middle, owing to evaporation of the solution heated by the current [3]. Such migration does not occur in electrophoresis in a gelatin layer; this can easily be demonstrated if the same dye is applied at the center of the film and near the ends immersed in the solution. If the solution migrated as the result of evaporation and the dye was carried by the migrating solution, the dye applied at the ends should migrate to the center even if an alternating current instead of a direct current is passed through the film. Determinations showed that no such transference of dye takes place, probably because of the very low mobility of the solution in the gelatin layer. This greatly simplifies electrophoresis in a gelatin layer by comparison with paper electrophoresis because, first, it is not necessary to take into account the position of the dye relative to the middle of the film in evaluation of mobilities from the electrophoretic displacement and second, exact equalization of the liquid levels in the electrode compartments is not necessary.

Electrophoresis of certain dyes. Zone electrophoresis in the gelatin layer of a photographic film was tested with several water soluble dyes of a relatively high degree of purity (indicators). The buffer solution used in all cases contained 3.50 g of veronal sodium and 0.55 g of veronal per liter, of pH 8.6. The electrophoresis was conducted at 250 v, at a field strength of 12.2 v/cm in the dye free film. The strength of the current flowing through the film was ~ 0.275 ma, and fell by 5 to 15% during one hour of electrophoresis. The dyes were previously neutralized and dissolved at 1% concentration in the same buffer solution. The electrophoresis was conducted at room temperature.

These experiments showed that Congo Red, Water Blue and Crystal Violet are bound so firmly by gelatin that they do not diffuse in it, do not migrate, and do not spread in electrophoresis. The last of these dyes is apparently also bound firmly by paper in paper electrophoresis [4]. Dyes of this type cannot be investigated by the described method, but may be used as additions to mixtures under investigation for marking the starting line.

of its displacement in the solvent and displacement of the latter relative to the capillary system (paper) in which electrophoresis takes place.

In the present instance of electrophoresis of a dye in a gelatin layer on a nonconducting support, electrophoretic displacement of the gelatin layer relative to the support and displacement of the dye solution in the buffer relative to the gelatin layer are possible.

We were able to show that the gelatin layer is not displaced relative to the support. The marker for migration of the gelatin layer was Congo Red, which is bound stably and irreversibly with gelatin and is not absorbed by the support. A band of this dye applied to a gelatin layer



Fig. 5. Electrophoregrams of dyes in the gelatin layer of a photographic film: 1) Bromophenol Red, 60 minutes; 2) Phenol Red, 95 minutes; 3) Cresol Red 60 minutes; 4) Bromophenol Blue, 60 minutes; 5) Bromocresol Green, 95 minutes; 6) eosin 120 minutes; 7a) Bromocresol Purple, 60 minutes; 7b) same, on paper; 8a) a mixture of 0.25% Bromophenol Blue, 0.38% Bromocresol Purple, 0.25% Phenol Red, 0.12% Congo Red (60 minutes); 8b) same, without Congo Red, in paper. (For technical reasons the original color plate has been reproduced in black and white, therefore, some detail has been lost.)

Bromophenol Red (Chemapol), Phenol Red (Merck) and Cresol Red (Merck) were found to be free of impurities. Each gave a single band (Fig. 5, photographs 1, 2, 3). There is some doubt about the purity of Phenol Red as it gave an unusually wide band. The mobilities of these three dyes at pH 8.6 were found to be $3.65 \cdot 10^{-5}$, $3.95 \cdot 10^{-5}$ and $2.85 \cdot 10^{-5}$ cm/v · second respectively.

Dye	Mobility in gelatin, $\times 10^5$	Mobility on paper, $\times 10^5$	Dye	Mobility in gelatin, $\times 10^5$	Mobility on paper, $\times 10^5$
Bromocresol Blue	1.60	13.5	Cresol Red	2.85	12.2
Bromophenol Blue	1.35	12.8	Bromophenol Red	3.65	13.8
Phenol Red	3.95	13.8	Bromocresol Purple	2.30	13.4

The other dyes investigated showed the presence of impurities. Thus, Bromophenol Blue (Ciba) (Photograph 4) revealed the presence of two additional components, giving a very pale violet and a pink band, which were scarcely distinguishable in paper electrophoresis. This is possibly the reason why other workers [5] failed to detect this impurity although, of course, it must be remembered that they used a product made by a different firm. The mobility of bromophenol blue was found to be $1.35 \cdot 10^{-5}$, and of the impurities approximately $1.7 \cdot 10^{-5}$ and $2.2 \cdot 10^{-5}$ cm/v · second.

Bromocresol Green (Merck) (Photograph 5) with a mobility of $1.60 \cdot 10^{-5}$ contained a clearly distinguishable component with a mobility of $\sim 2.2 \cdot 10^{-5}$ Bromocresol Purple (Merck) (Photograph 7a) revealed very clearly the presence of two additional components, which had also been detected in paper electrophoresis in a product of a different firm [5] (Photograph 7b). The mobility of the main component was $2.30 \cdot 10^{-5}$; the mobility of one impurity was $0.5 \cdot 10^{-5}$ while the second was not displaced in electrophoresis. Finally, eosin (Ciba) (Photograph 6) revealed the presence of two components in visible light: one very weak with very low mobility, and the other in the form of a bright and very wide band. The width of this band suggested that it is formed by several components. In fact, it was found under ultraviolet illumination that this wide and brightly fluorescent band consists of at least four separate bands.

The table gives the mobilities of the principal components of the investigated dyes in a gelatin layer, and also their mobilities determined in paper electrophoresis at the same pH [5]. It is seen that the mobilities in the gelatin layer are less by a factor of 10 than in paper electrophoresis. Moreover, there is no correlation between the mobilities in these two media. The lower mobility in gelatin cannot be attributed to the higher viscosity of the gelatin layer in comparison with the free buffer solution, as the viscosity of the gelatin layer is many orders of magnitude greater than that of water. This fact, and the absence of any correlation between mobilities in gelatin and on paper (Photographs 8a and 8b) indicate that the mechanism of electrophoresis in gelatin is not the same as in free solution. This is consistent with our hypothesis that electrophoretic displacement of a dye is independent of displacement of the buffer solution.

Thus, electrophoretic mobilities in gelatin are relative in character and cannot be directly correlated with electrophoretic mobilities in free solution.

Finally, it must be pointed out that despite the fact that the mobility in gelatin is lower by a factor of 10 than on paper, the sharpness of the bands is such that the resolving power in electrophoresis on gelatin is higher than in paper electrophoresis.

SUMMARY

1. The gelatin layer of a photographic film, freed of photosensitive material, is a suitable medium for zone electrophoresis of dyes.
2. Diffusion of dyes under electrophoresis conditions does not cause extensive spreading.
3. The specific asymmetrical spreading of dyes in electrophoresis is due to inhomogeneity of the electric field in the regions where the dyes are present.
4. Migration of gelatin and buffer solution during electrophoresis, and migration of the solution under the influence of evaporation, do not have any significant influence in electrophoresis in a gelatin layer.

5. Several dyes have been subjected to zone electrophoresis in a gelatin layer. It was found that there is no correlation between electrophoretic mobility in gelatin and on paper, and that the former is lower by a factor of ten than the latter.

LITERATURE CITED

- [1] Bussard and Perrin, J. Lab. and Clin. Med. 46, 689 (1955).
- [2] Grabar and Williams, Biochem. et Biophys. Acta 17, 67 (1955).
- [3] Macheboeuf, Rebeyrotte, and Dubert, Bull. Soc. Chim. Biol. 35, 334 (1953).
- [4] Evans and Walls, J. Bacteriol. 63, 422 (1952).
- [5] Franglen, Nature 175, 134 (1955).

Received February 3, 1958

A STUDY OF BOND CHARACTERISTICS IN THE SYSTEM RUBBER - CARBON BLACK

V. G. Epshtein and Z. V. Chernykh

The Yaroslav' Technological Institute

Reinforcement of rubbers, i.e., increase of their strength under single and repeated deformations, which results from introduction of fillers (especially carbon blacks) is one of the fundamental problems of modern rubber technology. Reinforcement is due mainly to adsorption of the flexible polymer molecules on the loading agent. Carbon black particles form branch points of a molecular network and cause redistribution and equalization of stresses in deformation [1]. Kobeko [2] considers that the effect of reinforcement by carbon blacks is similar to crystallization of rubbers and points out that the reinforcing effect of carbon black also involves a change in the strength-temperature relationship.

Certain investigators [3, 4] devoted much attention to the formation of the so-called carbon-black structures, or continuous chains composed of carbon particles. The formation of a carbon-black structure should lead to a more uniform stress distribution, orientation of the rubber molecules along the filler chains, and decreased spreading of sites of damage [5].

Rubber-carbon black interaction has been studied by means of determination of elastic modulus of vulcanizates under repeated extension [6-9].

It is considered that the decrease in the modulus caused by deformation is due mainly to breakdown of weak secondary bonds formed by forces of adsorption [10]. Some authors consider that the decrease of the modulus is due to breakdown of carbon-black structures under repeated deformation [11, 12].

Test method. The best vulcanizates (vulcanized at 143°) of noncrystallizing SKB (50a.v.) and SKS-30A (thermally milled, plasticity 0.50) rubber were chosen for the tests. The mixes were prepared in accordance with the standard formulations, containing channel, furnace, and lamp blacks in the proportions of 20, 40, 60, 80, and 100 parts by weight per 100 parts by weight of rubber. The test specimen were in the form of strips 10 mm wide and 2 ± 0.1 mm thick. The length of the working part of the specimen was 40 mm, and was determined by the distance between the jaws of thermostatically-controlled tensile testing machines types TsMG and T (Schopper). The specimens were stretched at 100 mm/minute to 200% elongation. This was followed by contraction at the same rate. The deformation cycles were repeated four times. The load-extension curves were obtained by means of a recording instrument.

The value of the deformation in the tests was calculated relative to the initial length of the working region (residual deformation was disregarded).

The change of modulus in repeated deformation was determined at + 20, + 40, + 70 and + 100°.

Effect of repeated deformation on the modulus of vulcanizates. Table 1 gives the decrease of $M_{100\%}$ * after fourfold extension for SKB and SKS-30A vulcanizates with different contents of carbon blacks.

The absolute and relative decrease of the modulus becomes greater with increased carbon content, but not in direct proportion; the decrease is much more rapid than the increase of carbon-black content.

* Modulus at 100% elongation.

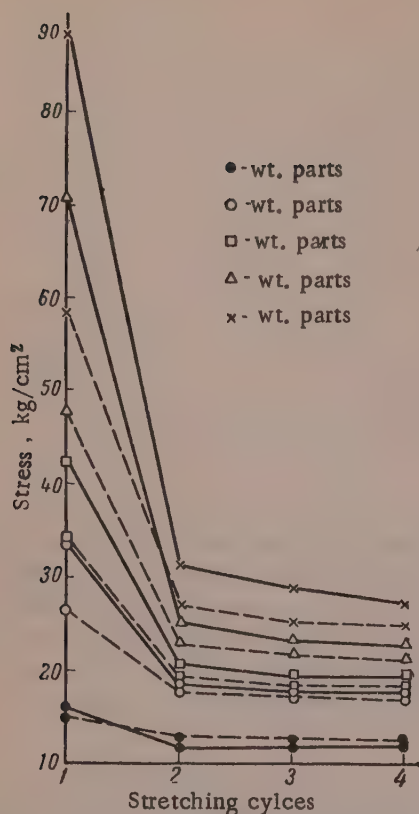


Fig. 1. Variation of modulus at 100% elongation with the number of stretching cycles for SKS-30A vulcanizates with lamp black at 20° (continuous curves) and at 100° (dash lines).

The greatest decrease of modulus on repeated deformation is found for SKB and SKS-30A vulcanizates with lamp black; the decrease is somewhat less with channel black, and last with furnace black.

SKS-30A vulcanizates show greater decreases of modulus than SKB vulcanizates with all carbon black contents. The effect of the number of deformation cycles on modulus of SKS-30A vulcanizates is shown in Fig. 1. The greatest decrease in the modulus takes place during the first stretching cycle, as has already been reported in a number of papers [6-8]. At low contents of carbon black there is no appreciable change of modulus after repeated deformations. In the case of vulcanizates with high carbon contents each successive extension leads to a considerable decrease of modulus. In such cases equilibrium values of the modulus are not reached after four stretching cycles.

The form of the stress-elongation curves for vulcanizates with carbon black after repeated extensions differs from that of curves after the first extension (Fig. 2, a and 2, b). Whereas in the first stretching the vulcanizate conforms approximately to Hooke's law, the curves for repeated stretching are S-shaped, similar to the curves for crystallizing rubbers.

Effect of the test temperature. Fig. 3 shows variations of modulus in the first and second stretching in relation to the test temperature for SKS-30A vulcanizates with lamp black and SKB with channel black.

At low carbon contents increase of temperature results in only a very small decrease of modulus in the first stretching. The effect of increased temperature is more pronounced at higher contents of carbon black.

TABLE 1

Changes (ΔM) of Modulus at 100% Elongation Caused by Four Stretching Cycles for Different Types and Contents of Carbon Black at 20°

Carbon content, wt. parts per 100 wt. parts rubber	Channel black			Furnace black			Lamp black		
	m_1^* kg/cm²	m kg/cm²	$\frac{\Delta M}{M_1}$ %	M_1 kg/cm²	M kg/cm²	$\frac{\Delta M}{M_1}$ %	M_1 kg/cm²	M kg/cm²	$\frac{\Delta M}{M_1}$ %
SKB									
20	8,21	2,25	27,4	6,75	1,66	24,6	7,34	2,13	29,0
40	12,31	4,39	35,6	9,04	2,83	31,3	11,98	4,86	40,7
60	19,82	9,59	48,3	13,13	5,55	42,2	21,1	11,33	53,7
80	30,17	18,74	61,9	13,87	6,79	48,8	44,4	30,9	69,9
100	41,03	27,78	67,6	21,53	11,92	55,5	51,0	—	—
SKB-30A									
20	14,1	3,4	24,1	12,6	2,6	20,6	15,8	4,6	29,1
40	24,0	10,6	44,2	17,67	4,37	24,7	33,5	16,2	48,2
60	27,8	12,2	43,9	23,7	7,7	32,5	42,5	23,5	55,3
80	35,0	16,8	48,0	33,3	16,2	48,7	71,0	48,5	68,3
100	51,8	29,1	56,1	31,8	14,0	44,1	88,67	61,9	69,7

* M_1 is the modulus in the first stretching.

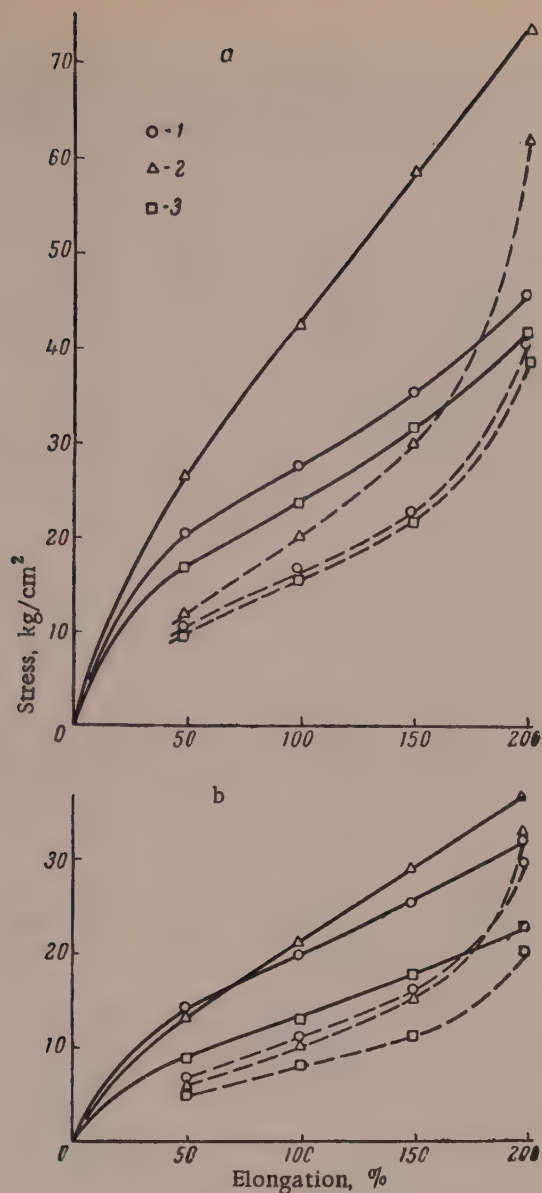


Fig. 2. Stress—elongation curves for vulcanizates of SKS-30A (a) and SKB (b) with different carbon blacks (60 wt. parts per 100 wt. parts rubber) at 20°: Continuous curves—first stretching; dash lines—second stretching; 1) channel black, 2) lamp black, 3) furnace black.

On repeated stretching of vulcanizates, containing 20 parts of carbon black by weight, increase of temperature leads to some increase of the modulus. At high carbon contents the modulus decreases with increase of temperature, but not so much as in the first stretching.

Table 2 gives the decreases of modulus at 100% elongation, caused by increase of temperature from 20 to 100°. In SKB vulcanizates with low contents of lamp black increase of temperature results in some increase of modulus; vulcanizates of SKB and SKS-30A with channel black have greater decreases of modulus than vulcanizates with other types of carbon black; vulcanizates with furnace black show the least decreases of modulus with increase of temperature.

Figure 1 shows changes of modulus at 100% elongation in relation to the number of stretching cycles at 20 and 100°. At high temperatures repeated deformations produce smaller changes in the modulus than at 20°. This also follows from a comparison of Tables 1 and 3.

TABLE 2

Changes (ΔM) of Modulus of Vulcanizates of SKB and SKS-30A Rubbers at 100% Elongation, Determined at the First Stretching, Caused by Increase of Temperature from 20 to 100°

Carbon content, wt. parts per 100 wt. parts rubber	SKB						SKS-30A					
	channel		furnace		lamp		channel		furnace		lamp	
	ΔM , kg/cm ²	$\Delta M/M_{20}$ %	ΔM , kg/cm ²	$\Delta M/M_{20}$ %	ΔM , kg/cm ²	$\Delta M/M_{20}$ %	ΔM , kg/cm ²	$\Delta M/M_{20}$ %	ΔM , kg/cm ²	$\Delta M/M_{20}$ %	ΔM , kg/cm ²	$\Delta M/M_{20}$ %
	ΔM , kg/cm ²	$\Delta M/M_{20}$ %	ΔM , kg/cm ²	$\Delta M/M_{20}$ %	ΔM , kg/cm ²	$\Delta M/M_{20}$ %	ΔM , kg/cm ²	$\Delta M/M_{20}$ %	ΔM , kg/cm ²	$\Delta M/M_{20}$ %	ΔM , kg/cm ²	$\Delta M/M_{20}$ %
20	0,32	3,89	0,1	1,4	-0,26	-30,55	1,73	12,28	-0,26	2,06	0,98	6,2
40	1,68	13,8	0,14	1,55	-0,22	-1,83	9,03	37,6	0,47	2,66	7,28	21,7
60	4,89	24,6	0,23	1,75	1,3	6,15	9,48	34,1	0,55	2,32	8,98	21,1
80	11,34	37,7	0,57	4,11	—	—	12,43	35,6	7,91	23,8	23,04	32,5
100	18,56	45,2	4,13	19,2	—	—	18,24	35,2	—	—	30,17	34,2

* M_{20} is the modulus at 20°.

TABLE 3

Changes (ΔM) of Modulus at 100% Elongation Caused by Four Stretching Cycles for Different Types and Contents of Carbon Black in SKS-30A Vulcanizates at 100°

Carbon content, wt. parts 100 wt. parts rubber	Channel			Furnace			Lamp		
	M_1 , kg/cm ²	ΔM , kg/cm ²	$\frac{\Delta M}{M_1}$ %	M_1 , kg/cm ²	ΔM , kg/cm ²	$\frac{\Delta M}{M_1}$ %	M_1 , kg/cm ²	ΔM , kg/cm ²	$\frac{\Delta M}{M_1}$ %
20	12,37	2,05	16,5	12,86	1,93	15,0	14,82	3,06	20,6
40	14,97	3,35	22,4	17,2	4,42	25,7	26,22	9,57	36,5
60	18,32	5,62	30,7	23,15	7,25	31,4	33,52	15,77	47,1
80	22,57	8,52	37,7	25,39	9,14	36,0	47,96	26,9	56,2
100	33,56	16,84	50,3	26,67	9,87	36,9	58,5	34,1	58,3

* M_1 is the modulus in the first stretching.

The carbon content has the same influence at 100° as at 20°, and the main decrease of the modulus takes place in the first stretching. Thus, increase of the test temperature produces changes in the modulus of vulcanizates which depend both on the type of rubber and on the type and contents of carbon black; this provides possibilities for successful use of this method for studying reinforcement effects.

The increase in the modulus of a loaded vulcanizate depends mainly on the degree of rubber-carbon interaction. The corresponding change of tensile strength depends on a number of other factors (uniformity of structure, manner of growth of the damaged places, etc.) in addition to rubber-carbon interaction. Therefore rubber reinforcement is manifested most clearly by changes in the modulus of vulcanizates, and it can be studied more precisely by comparison of moduli than of tensile strengths. Accordingly, particular characteristics of the reinforcing action of fillers were estimated from changes in the modulus under repeated deformations and under the influence of elevated temperatures.

Adsorption of segments of the rubber molecules on the carbon-black surface increases the number of bonds between the molecules and reduces the mobility of the molecular chains, thereby increasing the modulus of the vulcanizate. Deformation or heating decreases the modulus, probably owing to desorption of the rubber molecules. It has been reported that after deformation the modulus of a loaded rubber approaches that of the rubber without

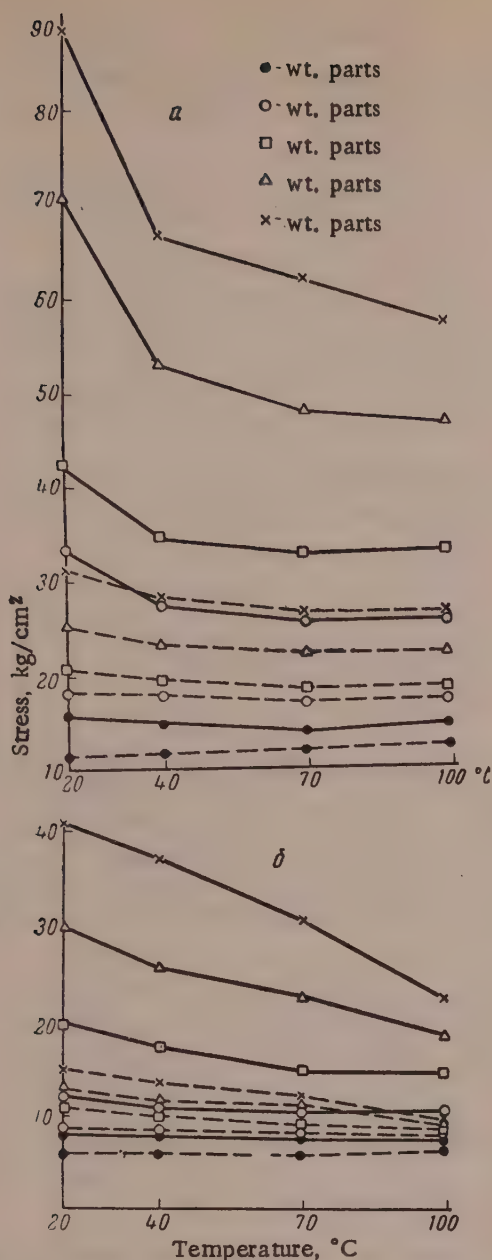


Fig. 3. Effect of test temperature on modulus at 100% elongation for vulcanizates of: SKS-30A with lamp black (a) and SKB with channel black (b): Carbon contents in weight parts per 100 weight parts of rubber; continuous curves - first stretching; dash lines - second stretching.

black interaction on repeated deformation is so weak owing to desorption of most of the rubber that the modulus increases with rise of temperature (this is known to occur in the case of equilibrium modulus if intermolecular action does not exert an influence).

*Formation of a secondary carbon-black structure.

**Formation of a primary carbon-black structure.

filler [8]. This indicates breakdown of most of the bonds between the carbon and rubber. Therefore the forces of interaction between the rubber and the carbon can be estimated from the changes of modulus.

The decrease of modulus does not correspond to the specific surface of the carbon blacks. It is known that channel black has the greatest specific surface, that of furnace black is less, and of lamp black is less still. These blacks form a different sequence in order of decreasing modulus on repeated deformation: the greatest decrease is found for vulcanizates with lamp black, then with channel black, and the least is found with furnace black.

It is generally believed that lamp black yields vulcanizates of high modulus. However, this effect becomes less pronounced after repeated deformations. This must evidently be taken into account in formulations of stocks for rubber products.

The decrease of modulus rises nonlinearly with increase of the carbon content. This shows that the decrease of modulus depends not only on the specific surface of the carbon black, which increases linearly with its content, but also possibly on the formation of a carbon structure.

The decrease of modulus observed in repeated stretchings is more pronounced at higher carbon contents, whereas at low contents the decrease of modulus is slight and occurs mainly during the first stretching.

These results indicate that interaction of molecular rubber chains with carbon black is more pronounced when the carbon particles join to form a structure. This may occur either as the result of considerable interaction between the carbon particles (channel black)* [4] or by joining of the particles during production of the carbon black (which is characteristic for lamp black)** [13].

Formation of a branched carbon-black structure probably favors steric trapping of the molecular chains, with an increase in the amount of rubber adsorbed. This explanation is consistent with data on the amount of carbon-rubber gel and increase of the amount of bound rubber in the gel on formation of a carbon-black structure [14].

At low contents of carbon black rubber-carbon

TABLE 4

Changes of Modulus at 100% Elongation ($M_{100\%}$) Caused by Repeated Deformations and Increase of Temperature in Vulcanizates of Different Rubbers (kg/cm^2) (60 weight parts of carbon per 100 of rubber)

Vulcanizates of type of carbon black	SKB			SKS-30A			NR [15]* without carbon
	chan- nel	fur- nace	lamp	chan- nel	fur- nace	lamp	
$M_{100\%}$, first stretching at 20°	19,82	13,13	21,1	27,8	23,7	42,5	31,9
$M_{100\%}$, fourth stretching at 20°	10,23	7,58	9,77	15,6	16,0	19,0	28,6
$M_{100\%}$, first stretching at 100°	14,93	12,9	19,8	18,32	23,15	33,52	17,6
Change of $M_{100\%}$ caused by fourfold deformation	9,59	5,55	11,33	12,2	7,7	23,5	3,3
Change of $M_{100\%}$ caused by rise of temperature from 20 to 100°	4,89	0,23	1,3	9,48	0,55	8,98	14,3

*For vulcanizates of natural rubber (NR) the change of modulus at 500% elongation (in the crystallization zone) was determined after twofold extension.

Increase of the test temperature reduces the modulus, but the decrease is appreciably less than that caused by repeated deformations (compare Tables 1 and 2). For example, for SKS-30A vulcanizates containing 20 and 40 parts of lamp black by weight rise of temperature from 20 to 100° reduces the modulus by 0.98 and 7.28 kg/cm^2 , while repeated deformations reduce it by 4.0 and 16.2 kg/cm^2 respectively. The decrease of modulus with rise of temperature becomes greater at higher contents of carbon black, especially in vulcanizates with lamp black. The difference between the decreases of modulus caused by repeated deformations and by rise of temperature becomes greater with increase of carbon content.

All these results indicate that the presence of a carbon-black structure, which does not hinder desorption under the influence of mechanical energy in deformation, appreciably hinders desorption of rubber under the influence of heat. The presence of joined carbon particles probably hinders sterically the desorption of molecules on increase of thermal motion.

The greater stability of the modulus on heating in vulcanizates with low contents of lamp black as compared with vulcanizates with the same contents of channel black is probably due to the presence of interconnected particles of lamp black and the absence of a channel-black structure in such cases.

There is an important difference between vulcanizates with carbon black and vulcanizates of crystallizing rubbers with regard to the influence of heat and deformation on the modulus. In the case of crystallizing vulcanizates of natural rubber, rise of temperature produces a considerable decrease of the modulus, whereas deformation has less effect (Table 4). The reverse is true in reinforcement by carbon black. Possibly the high stability of rubber-carbon bonds to the action of heat accounts to some extent for the increase of the resistance to heat produced by introduction of carbon black.

SUMMARY

1. The decrease in the modulus of vulcanizates containing rubber black on repeated extension depends on the type of rubber and on the type and content of carbon black. The presence of extensive carbon-black structures decreases the modulus considerably.

2. A method is proposed for estimating rubber-carbon black interaction by the change in the modulus of vulcanizates with increase of temperature. This change depends on the type of rubber and is related to the type and content of the carbon black.

3. The decrease of modulus caused by deformation is greater in vulcanizates with carbon black than the decrease caused by rise of temperature; this may be attributed to steric hindrance caused by the carbon chains in desorption of the rubber molecules in the course of heating.

4. Reinforcement by carbon blacks is shown to differ from reinforcement by crystallites in that the rubber-carbon bonds are more stable than the crystallites to the action of heat.

LITERATURE CITED

- [1] A. P. Aleksandrov and Yu. S. Lazurkin, *Doklady Akad. Nauk SSSR* 7, 308 (1944).
- [2] P. P. Kobeko, *Amorphous Substances* [in Russian] (Izd. AN SSSR, 1952).
- [3] B. A. Dogadkin and K. A. Pechkovskaya, *Proc. 3rd All-Union Conference on Colloid Chemistry* [in Russian] (Izd. AN SSR, 1956) p. 371.
- [4] B. Dogadkin, K. Pechkovskaya, and M. Dashevskii, *Kolloid. Zhur.* 10, 357 (1948); K. Pechkovskaya, Ts. Mil'man, and B. Dogadkin, *Kolloid. Zhur.* 14, 250 (1952).*
- [5] B. A. Dogadkin and A. I. Lukomskaya, *Proc. 3rd All-Union Conference on Colloid Chemistry* [in Russian] (Izd. AN SSSR, 1956) p. 363.
- [6] S. I. Vol'fkovich (editor), *General Chemical Technology* [in Russian] (Goskhimizdat, 1946) 2, chapter 12.
- [7] L. Mullins, *J. Rubber Res.* 16, 275 (1947); *Trans. Inst. Rubber Ind.* 23, 6 (1948); 26, 27 (1950).
- [8] A. B. Kusov and N. I. Voronovich, *Kauchuk i Rezina* 2, (1958).
- [9] M. M. Reznikovskii, L. S. Priss, and B. A. Dogadkin, *Kolloid Zhur.* 16, 211 (1954). *
- [10] D. Parkinson, and A. F. Blanchard, *Ind. Eng. Chem.* 44, 799 (1952).
- [11] R. G. Newton, *India Rubber J.* 117, 10, 354 (1949).
- [12] E. M. Dannenberg, M. E. Jordan, and A. Stokes, *Trans. Inst. Rubber. Ind.* 122, 6, 663 (1950).
- [13] K. A. Pechkovskaya, N. A. Shedid-Khuzemi, P. N. Orlovskii, F. B. Livshits, I. S. Novikova, and I. I. Bryushkova, *Kauchuk i Rezina* 6 (1958).
- [14] Z. V. Chernykh and V. G. Epshtein, *Kolloid. Zhur.* 19, 644 (1957). *
- [15] V. G. Epshtein and V. G. Tret'yakov, *Uchen. Zapiski Yaroslav. Tekhnol. in-ta* (Yaroslav1*, 1957) 2, 191.

Received June 18, 1958

*Original Russian pagination. See C. B. Translation.

LETTER TO THE EDITOR

In 1939 I proposed a method for determination of swelling, based on measurement of the volume V_1 of liquid remaining free after swelling of the specimen in a certain initial volume V_0 of the liquid. The difference $V = V_0 - V_1$ gives the amount of liquid absorbed by the swelling specimen. I designed two instruments for application of this method; the first was described in the journal *Kauchuk i Rezina*, No. 2, 10 (1941). It consists of a glass vessel with two widened portions connected by a graduated measuring tube (Fig. 1). The vessel is closed by a ground-glass stopper with a hook from which the specimen is suspended. At the start of the experiment a volume V_0 of liquid is poured into the apparatus up to the upper mark; the apparatus is then inverted or placed at a suitable angle so that the specimen in the bulb a is covered with the liquid. After the required time the apparatus is placed vertically and the volume V_1 of liquid is read off (the dimensions of the apparatus and details of the method are given in the article cited above).

The second apparatus was described in my paper in *Kolloid. Zhur.* 8, 32 (1946). It consists of a U-shaped vessel with bulbs at the lower and upper ends (Fig. 2). The specimen is again put in the upper bulb a , which is filled with a definite volume V_0 of liquid forced by air pressure through the tube with a stopcock g . To determine the volume V_1 the liquid is allowed to descend with the stopcock g open.

The method and both pieces of apparatus are widely used in scientific, industrial, and teaching laboratories owing to their simplicity and reasonable accuracy. However, for reasons which I do not understand, this method and apparatus are attributed to others in certain manuals of colloid chemistry. For example, in the book by I. A. Volzhinskii, V. N. L'vov, and V. O. Reikhsfel'd: *Manual of Practical Work in Laboratories for Synthetic Rubbers* [in Russian] (Goskhimizdat, 1955) p. 172 the first apparatus is described as "Fedotov's apparatus". In the book by O. N. Grigorov et al.: *Practical Manual of Colloid Chemistry* [in Russian] (Leningrad University Press, 1955) p. 91, the same apparatus (but with a stopper in the side of one of the bulbs) is described as "designed in the colloid chemistry laboratory". In S. A. Balezin's book: *Practical Manual of Physical and Colloid Chemistry* [in Russian] (State Science Teaching Press, 1959) p. 218, the method is again attributed to Leningrad University.

I hope that this letter will restore the true origin of my proposed method and apparatus for swelling determinations.

B. A. Dogadkin

— INDEX —

Volume 21, 1960

COLLOID JOURNAL

Abrosenkova, V. F.	- 429	Edelman, L. I.	- 115	Kazanskii, M. F.	- 557
Afanas'eva, E. M.	- 523	Eitingon, L. I.	- 415	Khmulin, S. F.	- 699
Al'tov, A. I.	- 519	Epshtein, E. G.	- 721	Khromov, M. K.	- 443
Andryushchenko, E. A.	- 567	Eremeeva, A. S.	- 235	Kiselev, A. V.	- 559
Antipov-Karataev, I. N.	- 129	Eremenko, L. A.	- 333	Kiselev, A. V.	- 561
Apukhtina, N. P.	- 41	Ermolenko, N. F.	- 543	Kiselev, A. V.	- 627
Apukhtina, N. P.	- 167	Ershova, N. M.	- 659	Kitaev, G. A.	- 71
Assonova, T. V.	- 469	Fel'dhtein, M. S.	- 415	Klyukina, N. G.	- 275
Avsarkisova, A. I.	- 353	Fel'dman, R. I.	- 223	Kolotyrkhin, Ya. M.	- 381
Azarov, K. P.	- 133	Fel'dman, R. I.	- 481	Koloushek, Ya.	- 707
Babichenko, L. V.	- 575	Fel'dman, R. I.	- 597	Komarov, V. S.	- 281
Bakanov, S. P.	- 365	Feoktistova, A. A.	- 381	Komarova, N. A.	- 175
Bartenev, G. M.	- 1	Figurovskii, N. A.	- 343	Konstantinov, G.	- 713
Bartenev, G. M.	- 235	Fodiman, N. M.	- 531	Korotkova, A. A.	- 653
Bashkovich, A. P.	- 455	Fuks, G. I.	- 687	Kovbuz, M. A.	- 295
Belyaeva, I. I.	- 373	Fuks, N. A.	- 123	Kozlova, V. F.	- 201
Berestneva, Z. Ya.	- 553	Gal'perin, B. S.	- 403	Kravchenko, L. V.	- 7
Bikson, Ya. M.	- 617	Gamayunov, N. I.	- 243	Kryukov, P. A.	- 175
Bindas, B. P.	- 377	Gavrilova, T. B.	- 343	Kuadzhe, M. I.	- 285
Boltaks, Yu. B.	- 455	Glazman, Yu. M.	- 249	Kucher, R. V.	- 295
Brzhan, V. S.	- 621	Glazov, V. M.	- 15	Kudryavtsev, B. B.	- 49
Bubyreva, N. S.	- 377	Glazov, V. M.	- 393	Kulzenev, V. N.	- 161
Budnikov, P. P.	- 7	Glikman, S. A.	- 21	Kurdobov, Yu. F.	- 291
Chebotarevskii, V. V.	- 381	Gol'dshtein, M. N.	- 25	Kurilenko, O. D.	- 181
Chernykh, Z. V.	- 721	Gol'dshtein, M. N.	- 257	Kusheva, Markova, N.	- 637
Chervyatsova, L. L.	- 249	Gorina, A. A.	- 261	Kut'in, V. A.	- 53
Chizhinskii, V.	- 707	Grechanova, S. B.	- 133	Kuznetsova, N. P.	- 455
Churaev, N. V.	- 145	Gul', V. E.	- 267	Levanova, V. P.	- 349
Churaev, N. V.	- 243	Gurvich, M. M.	- 151	Levi, S. M.	- 301
Deinaga, Yu. F.	- 157	Gur'yanova, E. N.	- 415	Levina, S. A.	- 543
Deryagin, B. V.	- 31	Gusakova, D. Ya.	- 401	Lin, Yang Ch'in	- 415
Deryagin, B. V.	- 365	Gusev, K. F.	- 523	Lipatov, S. M.	- 497
Deryagin, B. V.	- 537	Gutman, E. M.	- 257	Lipatov, S. M.	- 501
Dibrov, G. D.	- 87	Iatomina, I. A.	- 553	Lipatov, S. M.	- 505
Dlauzen, N. A.	- 418	Ivanova, V. T.	- 523	Lipatov, S. M.	- 509
Dmitrenko, O. I.	- 407	Kader, G. M.	- 129	Lipatov, S. M.	- 517
Dogadkin, B. A.	- 161	Kandilarov, G. G.	- 625	Lipatov, Yu. S.	- 567
Dogadkin, B. A.	- 229	Kapustin, A. P.	- 273	Lipatova, G. V.	- 497
Dogadkin, B. A.	- 415	Kargin, V. A.	- 261	Lobanov, D. N.	- 575
Dukhin, S. S.	- 31	Kargin, V. A.	- 493	Lobastova, A. V.	- 157
Dumanskii, A. V.	- 157	Kargin, V. A.	- 553	Logginov, G. I.	- 429
Dunskii, V. F.	- 423	Kaverina, N. I.	- 687	Losev, B. I.	- 309

Lushcheikin, Yu. G.	- 267	Pospelova, K. A.	- 487	Talmud, S. L.	- 317
Lygin, V. I.	- 561	Priss, L. S.	- 443	Tarasova, Z. N.	- 415
Maiboroda, V. I.	- 231	Pryakhina, S. F.	- 161	Teletov, S. G.	- 93
Makletsova, N. V.	- 591	Puchkova, N. N.	- 579	Trapeznikov, A. A.	- 99
Malkina, A. D.	- 643	Rebinder, P. A.	- 429	Trapeznikov, A. A.	- 363
Mamaeva, L. Ya.	- 185	Resnikovskii, M. M.	- 443	Trapeznikov, A. A.	- 469
Mamakov, A. A.	- 193	Rogovin, Z. A.	- 493	Troyanskaya, M. A.	- 309
Markina, Z. N.	- 677	Rubina, S. I.	- 291	Tsvetanov, K.	- 713
Medvedev, S. S.	- 591	Rufimskii, P. V.	- 339	Tsyperovich, A. S.	- 109
Medvedeva, A. M.	- 537	Ryazantsev, P. P.	- 449	Tyabin, N. V.	- 193
Meerson, S. I.	- 509	Sadov, F. I.	- 461	Uskow, I. A.	- 217
Meerson, S. I.	- 579	Sadov, F. I.	- 665	Uskow, I. A.	- 475
Mel'nikov, B. N.	- 77	Samsonov, G. V.	- 455	Uskova, E. T.	- 217
Mel'nikov, B. N.	- 585	Sandomirskii, D. M.	- 121	Uskova, E. T.	- 475
Mikhailov, N. V.	- 387	Sandomirskii, D. M.	- 531	Vasil'ev, S. S.	- 137
Mishchenko, K. P.	- 317	Sandomirskii, D. M.	- 653	Vasil'eva, V. V.	- 139
Mokrushin, S. G.	- 71	Segalova, E. E.	- 677	Vasserman, P. I.	- 381
Mokrushin, S. G.	- 323	Selivanovskii, S. A.	- 659	Vdovchenkova, M. K.	- 121
Mikhnevich, G. L.	- 61	Senakhov, A. V.	- 461	Vedeneev, B. V.	- 387
Mikhnevich, G. L.	- 313	Senakhov, A. V.	- 665	Vigdorovich, V. N.	- 15
Mikhnevich, G. L.	- 435	Sharkov, V. I.	- 349	Vigdorovich, V. N.	- 393
Mikhalyuk, R. V.	- 181	Shchegolev, G. G.	- 363	Vinogradov, G. V.	- 193
Moryganov, P. V.	- 77	Shcherbakov, L. M.	- 449	Vishnitskaya, L. A.	- 359
Movshovich, I. M.	- 501	Sheludko, A.	- 713	Volarovich, M. P.	- 145
Myshkin, E. A.	- 647	Shershnev, V. A.	- 229	Volarovich, M. P.	- 243
Neimark, I. E.	- 327	Shifrin, K. S.	- 125	Volarovich, M. P.	- 523
Neimark, I. E.	- 333	Shigorin, D. N.	- 603	Volkov, G. I.	- 401
Nikolaeva, S. S.	- 231	Shishniashvili, M. E.	- 353	Voyutskii, S. S.	- 531
Novikova, E. N.	- 81	Shtarkh, E. V.	- 291	Yakimova, V. I.	- 317
Novikova, N. M.	- 1	Shubtsova, I. G.	- 21	Yakovlev, A. G.	- 487
Onusaitis, B. A.	- 201	Shul'man, M. S.	- 517	Yankovskii, S. S.	- 123
Ostrikov, M. S.	- 87	Shul'man, M. S.	- 603	Yurzhenko, A. I.	- 295
Panich, R. M.	- 531	Slinyakova, I. B.	- 327	Yushina, V. V.	- 137
Pavlova, G. A.	- 407	Smirnov, N. S.	- 373	Zagraevskaya, I. M.	- 505
Perepelkin, K. E.	- 211	Smirnov, N. S.	- 423	Zharkovskii, D. V.	- 505
Pevzner, D. M.	- 415	Smirnov, O. K.	- 301	Zhel'vis, E. F.	- 249
Plontkovskaya, M. A.	- 333	Soboleva, I. G.	- 591	Zherebkov, S. K.	- 537
Pisarenko, A. P.	- 291	Sokolov, S. I.	- 597	Zhidkova, L. G.	- 323
Pisarenko, A. P.	- 487	Soldatova, L. P.	- 403	Zhigailo, Ya. V.	- 333
Polyakov, Yu. A.	- 205	Sominskii, D. S.	- 115	Zimina, M. G.	- 41
Ponomareva, R. B.	- 455	Starikova, Z. A.	- 243	Zimina, M. G.	- 167
Poshkus, D. P.	- 559	Stoklosa, E.	- 677	Zubov, P. I.	- 493
Poshkus, D. P.	- 627	Strazhesko, D. N.	- 249	Zubov, P. I.	- 567
				Zubov, P. I.	- 603

CONTENTS

	PAGE	RUSS. PAGE
Impact Deformation of Rubber. <u>G. M. Bartenev and N. M. Novikova</u>	1	3
Investigation of the Hydration Processes of Calcium Monoaluminate. <u>P. P. Budnikov and I. V. Kravchenko</u>	7	9
The Colloidal State of Solid Solutions in Two-Phase Metallic Alloy Systems. <u>V. M. Glazov and V. N. Vigdorovich</u>	15	18
Investigations of the Physical Chemistry of Agar. 3. Factors Determining the Elastico-viscous Properties of Agar Gels. <u>S. A. Glikman and I. G. Shubtsova</u>	21	25
Thermodynamics of Irreversible Processes and Electroosmotic Transfer in Disperse Systems. <u>M. N. Gol'dshtein</u>	25	30
The Electrical Field on a Moving Drop. 1. The Theory of the Electrical Field of a Drop Containing an Ionogenic Surface-Active Substance. <u>S. S. Dukhin and B. V. Deryagin</u>	31	37
Relationship Between the Structure of Emulsifiers of the Alkyl Aryl Sulfonate Type and the Polymerization of Unsaturated Compounds. 5. Colloidochemical Properties of Sodium Alkyl Aryl Sulfonates. <u>M. G. Zimina and N. P. Apukhtina</u>	41	50
The Dispersing Action of Cavitation. <u>B. B. Kudryavtsev</u>	49	58
Properties of the Products Formed by "Melting Out" of Proteins from the Derma of Animal Hides. <u>V. A. Kut'in</u>	53	62
Kinetics of the Formation of Crystallization Centers of Supercooled Organic Liquids on Particles of Impurities. <u>G. L. Mikhnevich</u>	61	69
Experimental Investigations of Laminar Systems. 24. Kinetics of the Formation of Hydroxide Films on the Surface of Cobalt and Nickel Ammine Solutions. <u>S. G. Mokrushin and G. A. Kitaev</u>	71	80
Interaction of Direct Dyes with Cellotriose. <u>P. V. Moryganov and B. N. Mel'nikov</u>	77	86
Swelling of Vulcanized Rubber in Acetyl Hydroperoxide Solution. <u>E. N. Novikova</u>	81	91
Formation Mechanism of Porous Structures. <u>M. S. Ostrikov and G. D. Dibrov</u>	87	97
The Influence of Accompanying Ions on Coagulator Ions. <u>S. G. Teletov</u>	93	102
A New Instrument (The Elastorelaxometer) for Studies of Large Reversible Deformations, Strength, and Relaxation of High-Elastic Colloid Systems and Polymer Solutions. <u>A. A. Trapeznikov</u>	99	108
Nature of "Denaturation Stabilization" of Globular Proteins. <u>A. S. Tsyperovich</u>	109	119

CONTENTS (continued)

	PAGE	RUSS. PAGE
Estimation of the Aggregative Stability of Suspensions. <u>L. I. Édelman and D. S. Sominskii</u>	115	126
Letters to the Editor		
Effect of the Viscosity of Rubber Latex on the Gelation Rate. <u>D. M. Sandomirskii and M. K. Vdovchenkova</u>	121	132
Method for Precipitation of Aerosols in a Thermal Precipitator for Electron Microscopy. <u>N. A. Fuks and S. S. Yankovskii</u>	123	133
Book Review. <u>K. S. Shifrin</u>	125	134

CONTENTS

	PAGE	RUSS. PAGE
On the Seventieth Birthday of Ivan Nikolaevich Antipov-Karataev	127	137
Investigation of Exchange Reactions in Soils with the Aid of a Calcium Isotope. <u>I. N. Antipov-Karataev and G. M. Kader</u>	129	139
Viscosity of Enamels for Steel. <u>K. P. Azarov and S. B. Grechanova</u>	133	144
The Stabilizing Action of Silver Ions on Albumin. <u>S. S. Vasil'ev and V. V. Yushina</u>	137	148
Investigation of the Viscoplastic Properties of Building Materials. <u>V. V. Vasil'eva</u>	139	151
Study of the Hydration Properties and Structure of Peat by Means of Radioactive Isotopes. I. Hydration Properties and Structure of Peat. <u>M. P. Volarovich and N. V. Churaev</u>	145	157
Use of the RV-4 Rotational Viscosimeter for Rheological Studies of Systems with Rapidly Changing Structural Properties. <u>M. M. Gurvich</u>	151	164
A Dielectric Study of the Formation of Soap - Hydrocarbon Solutions. <u>Yu. F. Deinega, A. V. Dumanskiĭ and A. V. Lobastova</u>	157	170
The Compatibility of Polymers in Solution. <u>B. A. Dogadkin, V. N. Kuleznev, and S. F. Pryakhina</u>	161	174
Relationship Between the Structure of Emulsifiers of the Alkyl Aryl Sulfonate Type and the Polymerization of Unsaturated Compounds. 6. Effect of Sodium Alkyl Aryl Sulfonates on the Polymerization Process. <u>M. G. Zimina and N. P. Apukhtina</u>	167	181
Determination of the Activity of Sodium Ions in Disperse Systems. <u>N. A. Komarova and P. A. Kryukov</u>	175	189
Adsorption of Aliphatic Amines on Bentonite From Aqueous Solutions. <u>O. D. Kurilenko and R. V. Mikhalyuk</u>	181	195
Effect of Exchange Cations on the Structural and Mechanical Properties of Soils. <u>L. Ya. Mamaeva</u>	185	200
Application of the Similarity Theory in Calculations of the Flow of Plastic Greases in Pipes. <u>A. A. Mamakov, N. V. Tyabin and G. V. Vinogradov</u>	193	208
Mechanism of the Contraction of Coke Material Causing Its Packing and Cracking. 1. Contraction and Shrinkage of Coke Material. <u>B. A. Onusaitis and V. F. Kozlova</u>	201	216

CONTENTS (continued)

	PAGE	RUSS. PAGE
Sorption of Strontium and Calcium Ions by Soils. <u>Yu. A. Polyakov</u>	205	221
Causes of Formation, and Certain Properties, of Air Dispersions in Viscose. <u>K. E. Perepelkin</u>	211	226
Electrochemical Studies of Bentonite Suspensions. 3. Potentiometric and Conductometric Titration of Electrodialyzed Askangel Suspensions By Alkali Metal Hydroxides. <u>I. A. Uskov and E. T. Uskova</u>	217	231
States of Aggregation of High Polymers. 3. Synthetic Polyamides. <u>R. I. Fel'dman</u>	223	238
Letters to the Editor		
The Interaction of Tetramethylthiuram Disulfide and Tetramethylthiuram Monosulfide with Rubber. <u>B. A. Dogadkin and V. A. Shershnev</u>	229	244
Preparation and Certain Properties of Lyophobic Colloidal Dispersions of Fiber-Forming Polymers. <u>N. V. Mikhailov, V. I. Maiboroda, and S. S. Nikolaeva</u>	231	246

CONTENTS

	PAGE	RUSS. PAGE
The Structure and Structuromechanical Properties of Inorganic Glasses. <u>G. M. Bartenev</u> and <u>A. S. Ereemeeva</u>	235	249
Study of the Hydration Properties and Structure of Peat by Means of Radioactive Isotopes. 2. Changes of Hydration Properties and Structure on Dispersion and Compression of Peat. <u>M. P. Volarovich, N. I. Gamayunov, Z. A. Starikova, and N. V. Churaev</u>	243	257
Changes in the Adsorption of Potential-Determining Ions during Coagulation of Lyophobic Sols by Indifferent Electrolytes. <u>Yu. M. Glazman, D. N. Strazhesko, E. F. Zhel'vis,</u> and <u>L. L. Chervyatsova</u>	249	263
Effect of a High-Frequency Ultrasonic Field on Plastic Pastes. <u>M. N. Gol'dshtein and</u> <u>É. M. Gutman</u>	257	272
Study of the Sintering Mechanism of Ftoroplast-4 (Polytetrafluoroethylene) Preforms. 1. Investigation of the Sorption Process. <u>A. S. Gorina and V. A. Kargin</u>	261	276
Influence of Molecular Interaction of the Dielectric Strength of Vulcanizates. <u>V. E.</u> <u>Gul'</u> and <u>Yu. G. Lushcheikin</u>	267	283
Preparation of Highly-Concentrated Lithium, Potassium, and Sodium Suspensions in an Ultrasonic Field. <u>A. P. Kapustin</u>	273	289
Adsorption of Electrolytes by Nickel Hydroxide. <u>N. G. Klyukina</u>	275	292
Effect of Pressure on Swelling Isotherms and Equilibrium Curves. <u>V. S. Komarov</u>	281	298
Electron Microscope Studies of Colloids. 2. Minerals of the Montmorillonite Group. <u>M. I.</u> <u>Kuadzhe</u>	285	301
Lignin as a Reinforcing Agent for SKS-30 Rubber. <u>Yu. F. Kurdubov, A. P. Pisarenko, S. I.</u> <u>Rubina, and E. V. Shtarkh</u>	291	306
Certain Emulsifiers as Kinetic Factors in the Oxidation of Cumene in Emulsions. <u>R. V.</u> <u>Kucher, A. I. Yurzhenko, and M. A. Kovbuz</u>	295	309
Relationship Between the Structure and Adsorptional Properties of Surface-Active Substances. <u>S. M. Levi and O. K. Smirnov</u>	301	315
Use of Aqueous Solutions of Polyvinyl Alcohol for Stabilization of Highly Concentrated Emulsions. <u>B. I. Losev and M. A. Troyanskaya</u>	309	322
Development of Crystallization Centers in a Supercooled Organic Liquid. <u>G. L.</u> <u>Mikhnevich</u>	313	325
The Specific Surface of Cellulose. <u>K. P. Mishchenko, S. L. Talmud, and V. I. Yakimova</u> . .	317	330
Effect of Low Temperature on the Volume and Stability of Foam. <u>S. G. Mokrushin and</u> <u>L. G. Zhidkova</u>	323	336

CONTENTS (continued)

	PAGE	RUSS. PAGE
Preparation of Ferric Hydroxide Gels of Different Pore Structures, and their Adsorptional Properties. <u>I. E. Neimark and I. B. Slinyakova</u>	327	340
Variations of the Structure and Adsorption Activity of Aluminum Hydroxide with the Conditions of its Formation. <u>M. A. Piontkovskaya, Ya. V. Zhigailo, L. A. Eremenko, and I. E. Neimark</u>	333	347
Investigations of Aluminum Hydroxide Hydrosols. 5. Experiments on the Application of Thermography in Studies of Thixotropic Al_2O_3 Gels. <u>P. V. Rufimiskii</u>	339	351
Sedimentometric Analysis of Highly Disperse Suspensions by Means of the Centrifugal Balance. <u>N. A. Figurovskii and T. B. Gavrilova</u>	343	354
Investigation of the Colloidal Nature of Polysaccharides by a Hydrolysis Method. <u>V. I. Sharkov and V. P. Levanova</u>	349	359
Preparation and Study of the Thixotropic Properties of a Suspension of Highly Disperse Askangel Fractions. <u>M. E. Shishniashvili and A. I. Avsarkisova</u>	353	364
Calculation of the Number of Branch Points in the Spatial Networks of Rubberlike Materials. <u>L. A. Vishnitskaya</u>	359	370
Letter to the Editor		
The Effects of Certain Additives on the Syneresis and Strength of Lithium Grease, and on its Submicrostructure. <u>A. A. Trapeznikov and G. G. Shchegolev</u>	363	374

CONTENTS

	PAGE	RUSS. PAGE
Theory of Thermal Precipitation of Highly Disperse Aerosol Systems. <u>S. P. Bakanov and B. V. Deryagin</u>	365	377
Precipitation of Artificial Mists. <u>I. I. Belyaeva and N. S. Smirnov</u>	373	385
Ultrasonic Dispersion of Silicic Acid Gel in Acid Media. <u>N. S. Bubyreva and B. P. Bindas</u>	377	388
Characterization of the Properties of Paint and Lacquer Coatings by Their Electrical Resistance and Capacitance. <u>P. I. Vasserman, Ya. M. Kolotyrlkin, V. V. Chebotarevskii, and A. A. Feoktistova</u>	381	392
Rheology of Bitumens and Their Flow Through Pipes at Elevated Temperatures. <u>B. V. Vedenev and N. V. Mikhailov</u>	387	398
Kinetic Studies of the Transition of Crystals of Solid Solutions of Two-Phase Alloys in Metallic Systems from the Colloidal to the True Homogeneous State. <u>V. N. Vigdorovich and V. M. Glazov</u>	393	405
Amalgam Foams. <u>G. I. Volkov and D. Ya. Gusakova</u>	401	413
Orientation Effect in Lacquer Films Filled with Carbon Black. <u>B. S. Gal'perin and L. P. Soldatova</u>	403	415
Binding of Water by Finely Dispersed Sediments. 2. Dependence of the Amount of Bound Water on the Composition and Concentration of Equilibrium Solutions. <u>O. I. Dmitrenko and G. A. Pavlova</u>	407	419
Vulcanization of Rubber in Presence of Aminomethyl Derivatives of 2-Mercaptobenzothiazole as Accelerators. <u>B. A. Dogadkin, I. I. Étingon, M. S. Fel'dshtein, Z. N. Tarasova, E. N. Gur'yanova, Lin Yang Ch'in, N. A. Klauzen, and D. M. Pevzner</u>	415	427
Influence of Ionizing Radiations on the Dispersity of Aerosols. <u>V. F. Dunsii and N. S. Smirnov</u>	423	436
Interaction of Calcium Hydroxide at Ordinary Temperatures with Sand of Different Dispersities. <u>G. I. Logginov, P. A. Rebinder, and V. F. Abrosenkova</u> ...	429	442
Crystallization of Supercooled Organic Liquids on Particles of Impurities at Various Temperatures. <u>G. L. Mikhnevich</u>	435	449
Relationship between Fatigue Resistance, Strength, Hysteresis, and Chemical Resistance of Rubbers. <u>M. M. Resnikovskii, L. S. Priss, and M. K. Khromov</u> ...	443	458
Influence of Size Reduction on Solubility and Heat of Solution. <u>P. P. Ryazantsev and L. M. Shcherbakov</u>	449	464

CONTENTS (continued)

	PAGE	RUSS. PAGE
Sorption of Ions by Carboxylic Resins in the Hydrogen Form. <u>G. V. Samsonov, Yu. B. Boltaks, N. P. Kuznetsova, A. P. Bashkovich, and R.B. Ponomareva</u>	455	471
Investigation of the Structuromechanical and Rheological Properties of Unmodified Thickness. <u>A. V. Senakhov and F. L. Sadov</u>	461	476
Stress-Strain, High-Elastic, and Viscous Properties of Rubber Solutions. <u>A. A. Trapeznikov and T. V. Assonova</u>	469	485
Electrochemical Studies of Bentonite Suspensions. 4. Potentiometric Titration of Different Acid Forms of Askangel. <u>I. A. Uskov and E. T. Uskova</u>	475	492
The States of Aggregation of High Polymers. 4. Collagen, Gelatin, and Silk Fibroin. <u>R. L. Feldman</u>	481	499
Book Review		
Colloid Chemistry (Textbook for Students of Commodity and Technological Faculties). <u>A. P. Pisarenko, K. A. Pospelova, and A. G. Yakovlev</u>	487	507
Current Events		
Problems of Colloid Chemistry at the 8th Mendelev Congress	489	509

CONTENTS

	PAGE	RUSS. PAGE
The 60th Birthday and 35 Years of Scientific Activity of Professor S. M. Lipatov, Academician of the Academy of Sciences Belorussian SSR. <u>Z. A. Rogovin, V. A. Kargin, and P. I. Zubov</u>	493	513
Phase Separation of Polymer - Polymer - Solvent Systems. <u>S. M. Lipatov and G. V. Lipatova</u>	497	517
Heats of Solution of Dyes in Water and the Dyeing Problem. <u>S. M. Lipatov and I. M. Movshovich</u>	501	522
The Phase State of Different Cellulose Modifications. <u>S. M. Lipatov, D. V. Zharkovskii, and I. M. Zagraevskaya</u>	505	526
Effect of Temperature on the Heat of Solution and Packing Density of Polystyrene. <u>S. I. Meerson and S. M. Lipatov</u>	509	530
Dispersion of Cellulose. <u>M. S. Shul'man and S. M. Lipatov</u>	517	538
Preparation of Emulsions by Addition of Electrolytes and Nonelectrolytes From Mutually Soluble Liquids After Phase Separation. <u>A. I. Al'tov</u>	519	540
X-Ray Structural Analysis of Interaction Between Paper and Binders in Printing Inks. <u>M. P. Volarovich, V. T. Ivanova, E. M. Afanas'eva, and K. F. Gusev</u>	523	544
Investigation of the Mechanism of Film Formation From Vulcanized Latex. 1. Formation of Films From Natural Latex. <u>S. S. Voyutskii, D. M. Sandomirskii, N. M. Fodiman, and R. M. Panich</u>	531	552
Investigation of Adhesion Effects in Bonding Rubber to Metal by Leukonat Adhesive. 2. Bonding of Unfilled Rubbers to Metals. <u>B. V. Deryagin, S. K. Zherebkov, and A. M. Medvedeva</u>	537	558
Investigation of the Structure and Adsorptive and Catalytic Activity of the Hydroxides of Iron, Chromium, and Aluminum in Relation to the Precipitation Method and Temperature. <u>N. F. Ermolenko and S. A. Levina</u>	543	564
Preparation of Mixed Aluminum Hydroxide and Hydroxysulfate Films and Investigation of Their Structure. <u>I. A. Istomina, Z. Ya. Berestneva, and V. A. Kargin</u>	553	574
Analysis of the Forms of Bonding of Water by Clays and Soils by Means of Drying Thermograms. <u>M. F. Kazanskii</u>	557	577
Infrared Absorption Spectra and Structure of the Hydroxyl Layers on Silicas of Different Degrees of Hydration. <u>A. V. Kiselev and V. I. Lygin</u>	561	581

	PAGE	RUSS. PAGE
Isotherms of Adsorption of Benzene and n-Hexane Vapors on Magnesium Oxide. <u>A. V. Kiselev and D. P. Poshkus</u>	569	590
Characteristics of Structure Formation in Concentrated Solutions of Polymethacrylic Acid. <u>Yu. S. Lipatov, P. I. Zubov, and E. A. Andryushchenko</u>	577	598
Changes in the Colloidal Properties of Wheat Flour During Dry Heating Above 100°. <u>D. N. Lobanov and L. V. Babichenko</u>	585	608
Dilatometric Investigations of Gelatin Gels. <u>S. I. Meerson and N. N. Puchkova.</u>	589	613
Influence of Organic Solvents on the Solution State of Direct Dyes and on Their Rate of Diffusion in Cellophane Film. <u>B. N. Mel'nikov and P. V. Moryganov</u>	595	618
Investigation of the Structure of Irradiated Polystyrene by Light-Scattering, Osmometric, and Viscosimetric Methods. <u>I. G. Soboleva, N. V. Makletsova, and S. S. Medvedev.</u>	601	625
The States of Aggregation of High Polymers. 5. Types of Packing of Macromolecules in Condensed Phases. <u>S. I. Sokolov and R. I. Fel'dman</u>	607	630
The Structure of Gels. 18. Infrared Spectra of Globular Casein. <u>D. N. Shigorin and P. I. Zubov.</u>	611	636
Letters to the Editor		
The Adsorbability of Carbohydrates. <u>M. S. Shul'man</u>	613	638

CONTENTS

	PAGE	RUSS. PAGE
Generalization of the Theory of G. V. Troitskii's Method for Optical Recording of Mixture Compositions. <u>Ya. M. Biksón</u>	617	642
An X-Ray Study of the Crystallization of Sorbed Water. <u>V. S. Brzhan</u>	621	645
Sedimentation Volumes of Polydisperse Kaolin Suspensions in Solutions of Nonelectrolytes <u>G. G. Kandilarov</u>	625	650
Adsorption of Benzene and n-Hexane Vapors on Magnesium Hydroxide. <u>A. V. Kiselev and D. P. Poshkus</u>	627	653
Influence of Ions in Solution on Precipitation of a Sparingly Soluble Salt. <u>N. Kusheva-Markova</u>	637	664
Application of the Replica Method to Studies of Ice Crystals. <u>A. D. Malkina</u>	643	670
Increase of the Surface Activity of Sulfonic Acids and Sulfonates. <u>E. A. Myshkin</u>	647	673
Investigation of Latex foams. I. Foaming Power of Rubber Latex. <u>D. M. Sandomirskii and A. A. Korotkova</u>	653	679
Agglomeration of Latex Particles by the Action of Sodium Chloride. <u>S. A. Selivanovskii and N. M. Ershova</u>	659	686
Changes in the Structuromechanical and Rheological Properties of Starch Gels Produced by The Action of Acids. <u>A. V. Senakhov and F. I. Sadov</u>	665	692
Two Types of Contacts Determining the Strength of Crystallization Structures in Calcium Sulfate Dihydrate. <u>E. Stoklosa, Z. N. Markina, and E. E. Segalova</u>	677	708
Investigation of Boundary Friction and Adhesion in Relation to Studies of the Interaction of Finely Dispersed Particles. 2. Influence of Cations on Adhesion of Glass Disks <u>G. I. Fuks and N. I. Kaverina</u>	687	718
Dielectric Constants of Petroleum Emulsions. <u>S. F. Khmunin</u>	699	731
An Air-Driven Ultracentrifuge and Aerosol Generator and its Uses in Science and Practice <u>V. Chizhinskii and Ya. Koloushek</u>	707	739
Electrophoresis of Dyes in the Gelatin Layer of a Photographic Film. <u>A. Sheludko, G. Konstantinov, and K. Tsvetanov</u>	713	747
A Study of Bond Characteristics in the System Rubber-Carbon Black. <u>E. G. Épshtein and Z. V. Chernykh</u>	721	754
Letters to the Editor	729	761
Author index, Vol. 21, 1960	733	
Tables of Contents, Vol. 21, 1960	735	

SIGNIFICANCE OF ABBREVIATIONS MOST FREQUENTLY
ENCOUNTERED IN SOVIET PERIODICALS

FIAN	Phys. Inst. Acad. Sci. USSR.
GDI	Water Power Inst.
GITI	State Sci.-Tech. Press
GITTLL	State Tech. and Theor. Lit. Press
GONTI	State United Sci.-Tech. Press
Gosenergoizdat	State Power Press
Goskhimizdat	State Chem. Press
GOST	All-Union State Standard
GTTI	State Tech. and Theor. Lit. Press
IL	Foreign Lit. Press
ISN (Izd. Sov. Nauk)	Soviet Science Press
Izd. AN SSSR	Acad. Sci. USSR Press
Izd. MGU	Moscow State Univ. Press
LEIIZhT	Leningrad Power Inst. of Railroad Engineering
LET	Leningrad Elec. Engr. School
LETI	Leningrad Electrotechnical Inst.
LETIIZhT	Leningrad Electrical Engineering Research Inst. of Railroad Engr.
Mashgiz	State Sci.-Tech. Press for Machine Construction Lit.
MEP	Ministry of Electrical Industry
MES	Ministry of Electrical Power Plants
MESEP	Ministry of Electrical Power Plants and the Electrical Industry
MGU	Moscow State Univ.
MKhTI	Moscow Inst. Chem. Tech.
MOPI	Moscow Regional Pedagogical Inst.
MSP	Ministry of Industrial Construction
NII ZVUKSZAPIOI	Scientific Research Inst. of Sound Recording
NIKFI	Sci. Inst. of Modern Motion Picture Photography
ONTI	United Sci.-Tech. Press
OTI	Division of Technical Information
OTN	Div. Tech. Sci.
Stroiizdat	Construction Press
TOE	Association of Power Engineers
TsKTI	Central Research Inst. for Boilers and Turbines
TsNIEL	Central Scientific Research Elec. Engr. Lab.
TsNIEL-MES	Central Scientific Research Elec. Engr. Lab.- Ministry of Electric Power Plants
TsVTI	Central Office of Economic Information
UF	Ural Branch
VIESKh	All-Union Inst. of Rural Elec. Power Stations
VNIIM	All-Union Scientific Research Inst. of Meteorology
VNIIZhDT	All-Union Scientific Research Inst. of Railroad Engineering
VTI	All-Union Thermotech. Inst.
VZEI	All-Union Power Correspondence Inst.

Note: Abbreviations not on this list and not explained in the translation have been transliterated, no further information about their significance being available to us. — Publisher.

